



**FRIEDRICH-SCHILLER-  
UNIVERSITÄT  
JENA**

**STRATEGIES TO OPTIMIZE CATIONIC  
POLYMERS FOR GENE DELIVERY *VIA*  
ENDOSOMAL ESCAPE**

**Dissertation**

**(kumulativ)**

zur Erlangung des akademischen Grades doctor rerum naturalium

(Dr. rer. nat.)

vorgelegt dem Rat der Chemisch-Geowissenschaftlichen Fakultät der  
Friedrich-Schiller-Universität Jena

von M. Sc. Friederike Richter  
geboren am 28.09.1991 in Berlin

## **Gutachter**

1. Dr. Anja Träger, Friedrich-Schiller-Universität Jena
2. Prof. Dr. Ulrich S. Schubert, Friedrich-Schiller-Universität Jena

Tag der Verteidigung: 09.11.2022

## Table of contents

Table of contents .....	I
Documentation of authorship .....	II
1. Introduction.....	1
2. The calcein release assay to study endosomal escape .....	6
3. Influence of cationic moieties on endosomal escape.....	13
4. Increasing gene delivery by introducing hydrophobic monomers.....	20
5. Optimizing gene delivery with hydrophilic/anionic monomers .....	32
6. Summary.....	44
7. Zusammenfassung .....	48
8. References.....	52
List of abbreviations .....	A
Description of unpublished methods .....	C
Curriculum vitae.....	E
Publication List.....	F
Acknowledgement/Danksagung.....	H
Declaration of authorship/Selbstständigkeitserklärung.....	J
Publications Pub1 to Pub8.....	K

## Documentation of authorship

This section contains a list of individual authors' contributions to the publications reprinted in this thesis. ‡ Equal contribution of both authors.

Pub1					
F. Hausig, <sup>1,‡</sup> F. Richter, <sup>2,‡</sup> M. Hoernke, <sup>3</sup> J. C. Brendel, <sup>4</sup> A. Traeger, <sup>5</sup> Tracking the endosomal escape: A closer look at calcein and related reporters, <i>J. Mater. Chem. B</i> <b>2022</b> , submitted.					
Author	1	2	3	4	5
Conceptual development	×	×		×	×
Preparation of the manuscript –					
Introduction					×
Chemical background of calcein		×			
Calcein leakage from model vesicles		×	×		
Calcein release studied in cells					
Release of encapsulated calcein		×			
Simultaneous and sequential addition	×				
Analytical Methods	×				
Potential pitfalls of the calcein release assay		×			
Complementary methods	×				
Conclusion & perspectives				×	
Correction of the manuscript	×	×	×	×	×
Supervision of F. Hausig				×	
Supervision of F. Richter					×
Proposed publication equivalent		0.5			

Pub2							
F. Richter, <sup>1</sup> L. Martin, <sup>2</sup> K. Leer, <sup>3</sup> E. Moek, <sup>4</sup> F. Hausig, <sup>5</sup> J. C. Brendel, <sup>6</sup> A. Traeger, <sup>7</sup> Tuning of endosomal escape and gene expression by functional groups, molecular weight and transfection medium: A structure–activity relationship study, <i>J. Mater. Chem. B</i> <b>2020</b> , <i>8</i> , 5026-5041.							
Author	1	2	3	4	5	6	7
Conceptual development	×	×					×
Polymer synthesis & characterization		×	×				
Polyplex characterization	×						
<i>In vitro</i> method development	×				×		
<i>In vitro</i> biological investigations	×			×			
Preparation of the manuscript	×	×					
Correction of the manuscript					×	×	×
Supervision of F. Richter							×
Proposed publication equivalent	1.0						

## DOCUMENTATION OF AUTHORSHIP

<b>Pub3</b> F. Hausig, <sup>1</sup> F. H. Sobotta, <sup>2</sup> D. O. Harz, <sup>3</sup> F. Richter, <sup>4</sup> A. Traeger, <sup>5</sup> J. C. Brendel, <sup>6</sup> Correlation between protonation of tailor-made polypiperazines and endosomal escape for cytosolic protein delivery, <i>ACS Appl. Mater. Interfaces</i> <b>2021</b> , 13, 35233-35247.						
Author	1	2	3	4	5	6
Conceptual development	×					×
Polymer synthesis & characterization	×	×	×			
<i>In vitro</i> method development	×			×		
<i>In vitro</i> biological investigations	×					
Preparation of the manuscript	×					
Correction of the manuscript		×	×	×	×	×
Supervision of F. Hausig						×
Supervision of F. Richter					×	
Proposed publication equivalent				0.5		

<b>Pub4</b> F. Richter, <sup>1,‡</sup> K. Leer, <sup>2,‡</sup> L. Martin, <sup>3</sup> P. Mapfumo, <sup>4</sup> J. I. Solomun, <sup>5</sup> Maren T. Kuchenbrod, <sup>6</sup> S. Hoepfener, <sup>7</sup> J. C. Brendel, <sup>8</sup> A. Traeger, <sup>9</sup> The impact of anionic polymers on gene delivery: How composition and assembly help evading the toxicity-efficiency dilemma, <i>J. Nanobiotechnol.</i> <b>2021</b> , 19, 292.									
Author	1	2	3	4	5	6	7	8	9
Conceptual development	×	×						×	×
Polymer synthesis & characterization		×	×	×					
Micelle formation & characterization	×	×				×			
Polyplex characterization	×								
<i>In vitro</i> method development	×				×				
<i>In vitro</i> biological investigations	×								
Preparation of the manuscript	×	×							
Correction of the manuscript			×	×	×	×	×	×	×
Supervision of K. Leer									×
Supervision of F. Richter									×
Proposed publication equivalent	1.0								

## DOCUMENTATION OF AUTHORSHIP

<b>Pub5</b> F. Richter, <sup>1, ‡</sup> P. Mapfumo, <sup>2, ‡</sup> L. Martin, <sup>3</sup> J. I. Solomun, <sup>4</sup> F. Hausig, <sup>5</sup> J. J. Frietsch, <sup>6</sup> T. Ernst, <sup>7</sup> S. Hoepfener, <sup>8</sup> J. C. Brendel, <sup>9</sup> A. Traeger, <sup>10</sup> Improved gene delivery to K-562 leukemia cells by lipoic acid modified block copolymer micelles, <i>J. Nanobiotechnol.</i> <b>2021</b> , 19, 70.										
<b>Author</b>	<b>1</b>	<b>2</b>	<b>3</b>	<b>4</b>	<b>5</b>	<b>6</b>	<b>7</b>	<b>8</b>	<b>9</b>	<b>10</b>
Conceptual development	×	×	×							×
Polymer synthesis & characterization		×	×							
Micelle formation & characterization		×						×		
Polyplex characterization	×									
<i>In vitro</i> method development	×			×	×					
<i>In vitro</i> biological investigations	×									
Preparation of the manuscript	×	×								
Correction of the manuscript			×	×	×	×	×	×	×	×
Supervision of P. Mapfumo										×
Supervision of F. Richter										×
Proposed publication equivalent	1.0									

<b>Pub6</b> J. I. Solomun, <sup>1</sup> G. Cinar, <sup>2</sup> P. Mapfumo, <sup>3</sup> F. Richter, <sup>4</sup> E. Moek, <sup>5</sup> F. Hausig, <sup>6</sup> L. Martin, <sup>7</sup> S. Hoepfener, <sup>8</sup> I. Nischang, <sup>9</sup> A. Traeger, <sup>10</sup> Solely aqueous formulation of hydrophobic cationic polymers for efficient gene delivery, <i>Int. J. Pharm.</i> <b>2021</b> , 593, 120080.										
<b>Author</b>	<b>1</b>	<b>2</b>	<b>3</b>	<b>4</b>	<b>5</b>	<b>6</b>	<b>7</b>	<b>8</b>	<b>9</b>	<b>10</b>
Conceptual development	×									×
Polymer synthesis & characterization			×			×	×			
Nanoparticle formulation	×									
Characterization of nanostructures	×	×						×	×	
<i>In vitro</i> method development	×			×		×				
<i>In vitro</i> biological investigations	×				×					
Preparation of the manuscript	×									
Correction of the manuscript		×	×	×	×	×	×	×	×	×
Supervision of J. I. Solomun										×
Supervision of F. Richter										×
Proposed publication equivalent				0.5						

## DOCUMENTATION OF AUTHORSHIP

**Pub7** M. N. Leiske,<sup>1</sup> F. H. Sobotta,<sup>2</sup> F. Richter,<sup>3</sup> S. Hoepfner,<sup>4</sup> J. C. Brendel,<sup>5</sup> A. Traeger,<sup>6</sup> U. S. Schubert,<sup>7</sup> How to tune the gene delivery and biocompatibility of poly(2-(4-aminobutyl)-2-oxazoline) by self- and coassembly, *Biomacromolecules* **2018**, 19, 748-760.

Author	1	2	3	4	5	6	7
Polymer synthesis	×	×					
Polymer characterization	×	×					
Self-assembly	×	×					
Characterization of nanostructures	×			×			
<i>In vitro</i> experiments			×			×	
Development of concept	×				×	×	
Preparation of the manuscript	×					×	
Correction of the manuscript		×	×	×	×		×
Supervision of M. N. Leiske						×	×
Supervision of F. Richter						×	
Proposed publication equivalent			0.5				

**Pub8** C. Chen,<sup>1</sup> F. Richter,<sup>2</sup> C. Guerrero-Sanchez,<sup>3</sup> A. Traeger,<sup>4</sup> U. S. Schubert,<sup>5</sup> A. Feng,<sup>6</sup> S. H. Thang,<sup>7</sup> Cell-penetrating, peptide-based RAFT agent for constructing penetration enhancers, *ACS Macro Lett.* **2020**, 9, 260-265.

Author	1	2	3	4	5	6	7
Conceptual development	×		×			×	×
Polymer synthesis & characterization	×						
<i>In vitro</i> biological investigations		×		×			
Preparation of the manuscript	×						
Correction of the manuscript	×	×	×	×	×	×	×
Supervision of C. Chen			×			×	×
Supervision of F. Richter				×			
Proposed publication equivalent		0.5					

**Erklärung zu den Eigenanteilen der Promovendin sowie der weiteren Doktorandinnen/Doktoranden als Co-Autorinnen/-Autoren an den Publikationen und Zweitpublikationsrechten bei einer kumulativen Dissertation**

Für alle in dieser kumulativen Dissertation verwendeten Manuskripte liegen die notwendigen Genehmigungen der Verlage („Reprint permissions“) für die Zweitpublikation vor.

Die Co-Autorinnen/-Autoren der in dieser kumulativen Dissertation verwendeten Manuskripte sind sowohl über die Nutzung als auch über die oben angegebenen Eigenanteile der weiteren Doktorandinnen/Doktoranden als Co-Autorinnen/-Autoren an den Publikationen und Zweitpublikationsrechten bei einer kumulativen Dissertation informiert und stimmen dem zu.

Die Anteile der Promovendin sowie der weiteren Doktorandinnen/Doktoranden als Co-Autorinnen/Co-Autoren an den Publikationen und Zweitpublikationsrechten bei einer kumulativen Dissertation sind in der Anlage aufgeführt.

Friederike Richter \_\_\_\_\_ Jena, \_\_\_\_\_

Ich bin mit der Abfassung der Dissertation als publikationsbasierte Dissertation, d.h. kumulativ, einverstanden und bestätige die vorstehenden Angaben.

Dr. Anja Träger \_\_\_\_\_ Jena, \_\_\_\_\_



“Just as GFP and other fluorescent molecules absorb light of one wavelength and convert it to light of a different wavelength, we, too, take in what others have learned about the world, add our observations and insights, and produce additional gains in human knowledge.”

(Martin Chalfie, Nobel Lecture, December 8, 2008)



# 1. Introduction

Gene therapy represents a powerful tool to correct genetic defects by the introduction of different exogenous nucleic acids. Already since the 1970s, it has been increasingly investigated not only for treating inherited genetic disorders, but also for fighting acquired afflictions such as cancer, diabetes or neurodegenerative diseases.<sup>[1-3]</sup> Moreover, infectious diseases can be countered by vaccines that contain nucleic acids encoding for virus-specific antigens. Currently, this is being successfully demonstrated by four of the five European Medicines Agency (EMA)-approved vaccines against the severe acute respiratory syndrome coronavirus 2 (SARS-CoV-2).<sup>[4]</sup> For an efficient arrival of the genes (*e.g.*, in form of plasmid DNA, pDNA) or other nucleic acids (*e.g.*, messenger RNA (mRNA), silencing RNA (siRNA)) at their respective site of action inside the cell, specialized nanomaterials are required due to the instability of naked nucleic acids against nucleases, their rapid renal clearance and their inefficient uptake into the target cells.<sup>[5-6]</sup> Optimally, these materials should be non-toxic, form stable complexes with the genetic material, exhibit low interaction with serum proteins, avoid recognition by the immune system and mediate the uptake by the desired cells (**Figure 1.1**). Following an endocytic uptake, they should further provide the intracellular escape of the nucleic acids from the endolysosomal compartment and release them intracellularly to ensure their activity inside the cells.<sup>[3, 7-9]</sup>

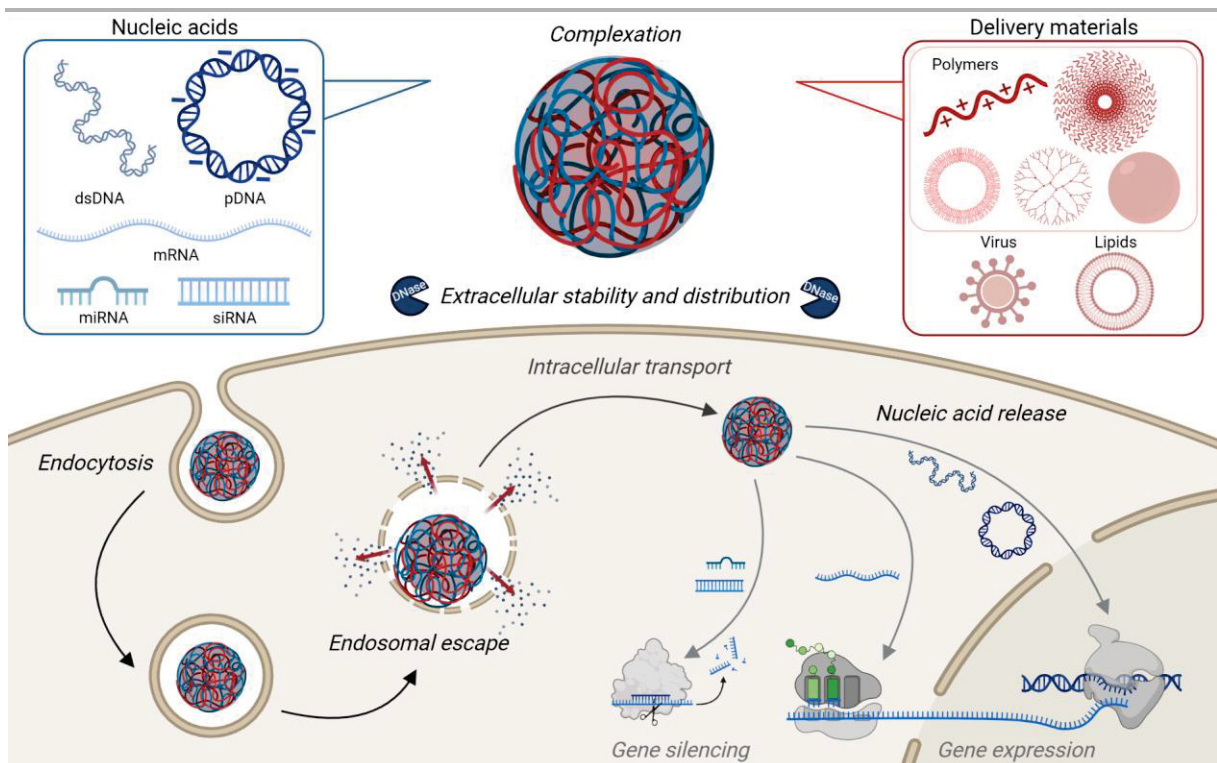


**Figure 1.1.** The (non-viral) delivery of nucleic acids and its barriers. Created with BioRender.com.

To date, the most prominent delivery strategy in clinical trials and on the market are different forms of (inactivated) viruses since they are naturally designed for the transport of genes, have already been investigated for a long time and are highly efficient.<sup>[10-11]</sup> Nevertheless, they also bear the risk of random recombination, immunogenicity and inflammatory reactions, are difficult to modify and limited in their upscaling as well as their cargo capacity.<sup>[5, 12-14]</sup> Therefore, alternative non-viral strategies for the delivery of nucleic acids are investigated, including lipid- or polymer-based nanocarriers.<sup>[15-16]</sup> Due to their application in SARS-CoV-2 vaccines, lipid formulations in particular have gained increasing attention within the last two years, but also had to face stability issues.<sup>[17]</sup> Although only a few polymeric nanomaterials have reached clinical trials for nucleic acids so far,<sup>[9, 18-20]</sup> the number of papers on polymers for gene delivery is constantly increasing due to several advantages such as an easy and cost-effective upscaling and the ability to transport nucleic acids of higher molecular weight (**Figure 1.2**). More importantly, the development of controlled polymerization techniques such as reversible deactivation radical polymerizations (RDRP) or cationic ring opening polymerization (CROP) enabled the preparation of well-defined macromolecules with controlled architectures and sizes. They further allow for the preparation of polymers tailored to their respective area of application due to the facile and variable combination of monomers with functionalities such as positive charges, hydrophobicity, hydrophilicity, or responsivity to different stimuli (pH, temperature, redox state).<sup>[9, 21-25]</sup>

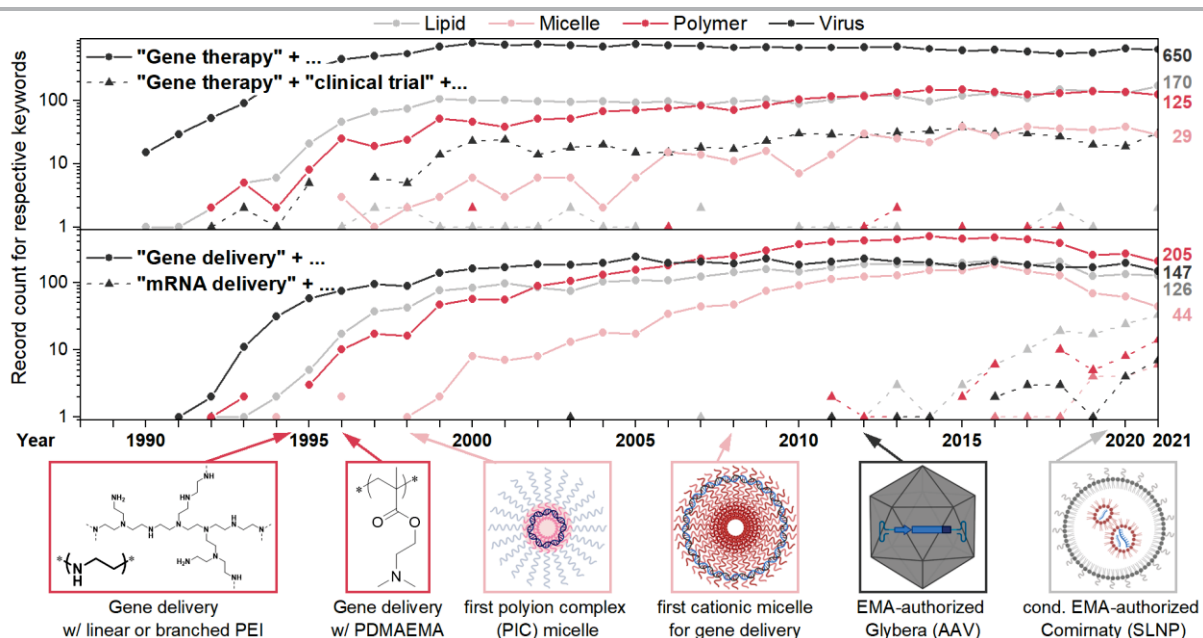


**Figure 1.2. Number of publications per year (only articles) for indicated keywords in combination with selected delivery materials.** Data were derived from Clarivate Web of Science. © Copyright Clarivate 2021. All rights reserved. Numbers to the right of the graph refer to 2021. Partially created with BioRender.com.

The most important functionality is represented by cationic moieties, which are usually different types of amines and only rarely polysulfonium or -phosphonium ions.<sup>[26-27]</sup> They condense the nucleic acids due to electrostatic interaction between positively charged amines of the polymers and the negatively charged phosphates of the nucleic acid. Similarly, they provide electrostatic interaction with the negatively charged phosphates of the cell membrane, thereby enhancing the uptake of the polymer-nucleic acid-complexes (polyplexes). Moreover, these amines exhibit different buffer capacities at physiological pH values, that assist in escaping the acidification along the endolysosomal pathway.<sup>[27-28]</sup> The endosomal escape represents one of the most crucial steps for cationic polymers in the gene delivery process. While the recycling or enzymatic degradation of the nucleic acids within the lysosome must be prevented, the genetic material, especially pDNA, should be transported as close to its site of action (the nucleus) as possible.<sup>[9, 29-31]</sup> Therefore, the endolysosomal maturation will be described in more detail in **Chapter 2** and the common calcein release assay will be elucidated for the investigation of the endosomal escape of different gene delivery materials.

Various cationic polymer classes have been investigated so far with the first generation being polycations based on natural molecules, such as spermine, diethylaminoethyl (DEAE) dextran or cationic poly(amino acids), in particular poly-*L*-lysine (PLL) or poly-*L*-arginine.<sup>[32-33]</sup> In the 1990s, these polymers were followed by polyamidoamine (PAMAM) dendrimers and polyethyleneimine (PEI), which is still the most prominent and commercially available cationic homopolymer (besides PLL).<sup>[34-35]</sup> Its superior transfection efficiency compared to the other systems can be related to the high amine to carbon ratio (charge density), and the buffer capacity leading to increased endosomal escape.<sup>[13, 20, 35-36]</sup> These properties have led to its abundant use as a commercial standard for comparison and made it (slightly modified) a research object in different (pre)clinical trials, *e.g.*, against cancer, as a HIV vaccine or as an immune adjuvant material.<sup>[2, 18, 37-38]</sup> Nevertheless, the search for alternative cationic polymers did not end at this point due to the low biocompatibility of PEI, and the need for even higher efficiency.<sup>[19, 36, 39-41]</sup> In general, cationic polymers can differ not only in their charge density, but also in their architecture (linear *vs.* branched), the position of the cation (backbone *vs.* side chain) or in the type of the amine (primary *vs.* secondary *vs.* tertiary).<sup>[9]</sup> In **Chapter 3**, new insights into the influence of these different types of amines on the endosomal escape are described considering not only pH responsive types of amines but also the pH independently charged guanidinium moiety as well as different hydrophobic modifications of tertiary amines resulting in finely tuned  $pK_a$  values within the physiological pH range. Polyacrylamides with amino alkyl or piperazine side chains have been utilized for these studies because the type of amine can easily be varied due to its presence in the side chain and their synthesis route being flexible for various

monomers.<sup>[22]</sup> They belong to the vinyl polymers, which are commonly synthesized *via* RDRP methods and of which poly(2-(dimethylamino)ethyl methacrylate) (PDMAEMA) is the most prominent representative. It was discovered for gene delivery shortly after PEI and its higher molecular weight variants (> 20 kDa) are well-known for the buffering capacity of the tertiary amine, high endosomal escape, and transfection efficiency within the range of PEI.<sup>[42-44]</sup>

Beside the positive charge, the architecture of the polymeric nanocarriers has a great impact on the efficiency of nucleic acid delivery. In addition to a branched or star-shaped linkage of the monomers within the polymer chains, the (3D-) architecture can also be influenced by altering the hydrophobicity. For instance, hydrophobic monomers with alkyl, or lipidic side chains can be combined with the cationic monomers to form amphiphilic block, gradient, or statistical copolymers. Following different assembly methods, these copolymers assemble into 3D-structures such as micelles, worms, polymersomes or polymeric nanoparticle dispersions depending on their topologies.<sup>[9, 23, 45-50]</sup> How hydrophobic monomers can be used to enhance the efficiency of cationic polymers for pDNA delivery is elucidated in **Chapter 4** using the example of two new micelles which are further compared to an amphiphilic polyplex nanoparticle. Thereby, the cationic monomers are based again on vinylic tertiary amine monomers, whereas butyl (meth)acrylate monomers are utilized to introduce the hydrophobic property. Furthermore, the impact of a hydrophobic methacrylate with a fatty acid side chain is considered, which, due to its disulfide bond, introduces redox-responsivity as a further stimuli-responsive property in addition to the pH sensitivity of the cations.<sup>[51-52]</sup>

Whereas cationic and hydrophobic moieties are predominantly applied to enhance the gene delivery efficiency, they also involve the risk of cytotoxicity which is often proportional to the efficiency up to a certain point.<sup>[48, 53-54]</sup> To prevent this side effect, either the cellular conditions (concentration, incubation time) or the polymeric nanocarriers can be optimized. On the polymeric side, the degree of polymerization/molar mass can be reduced,<sup>[53, 55-56]</sup> and the cationic charges can be shielded or neutralized by hydrophilic<sup>[57-58]</sup> or anionic moieties,<sup>[59-60]</sup> respectively. However, these modifications often also compromise the efficiency resulting in the toxicity-efficiency dilemma, which, therefore, requires a fine-tuning of the balance between critical cationic and counteracting moieties. Therefore, **Chapter 5** illustrates three different strategies to combine cationic micelles with hydrophilic and/or anionic functionalities and how they can be used to optimize the balance between pDNA delivery efficiency and toxicity. In addition to the polyvinylic micelles, also poly(oxazoline) (POx) micelles and a cell penetrating peptide (CPP) containing vinylic copolymer are investigated.

The overall scope of this thesis is the biological characterization of different polymeric cationic nanocarriers with regard to their performance at different steps of the gene delivery process, most importantly the endosomal escape and transfection efficiency. Starting with simple cationic homopolymers in Chapter 3, the complexity of the nanocarriers increases with each chapter due to the addition of different functionalities leading to different architectures. Thereby, this thesis covers optimization not only of the polymeric material, but also of the biological incubation conditions to achieve optimal results for the delivery of genetic material.

## 2. The calcein release assay to study endosomal escape

Parts of this chapter have been published in

**Pub1** F. Hausig,<sup>‡</sup> F. Richter,<sup>‡</sup> M. Hoernke, J. C. Brendel, A. Traeger, Tracking the endosomal escape: A closer look at calcein and related reporters, *J. Mater. Chem. B* **2022**, submitted.

On their way to deliver the nucleic acids to their site of action, polymeric nanocarriers have to overcome several different hurdles, of which the endosomal escape is very critical. Due to the size of the polymeric nanocarriers being commonly around 100 nm, they enter the cells *via* active uptake mechanisms, *i.e.*, endocytosis and therefore find themselves inside endocytic vesicles within the cells.<sup>[27, 61-62]</sup> These vesicles fuse with early endosomes and further vesicles while moving along microtubules towards the perinuclear region, thereby changing in their size, lipid composition, intraluminal pH value as well as surface proteins (**Figure 2.1**). Finally, lysosomes are formed, which provide the degradation and, thus, the disposal of non-required or harmful molecules due to their acidic pH and different enzymes.<sup>[63-66]</sup> Since this would represent a dead end for the nanocarriers, they must be designed to escape the endolysosomal pathway beforehand. To date, the most common strategy is the utilization of pH dependent cationic amine functionalities within polymers or lipids. Upon endolysosomal acidification, more amines are protonated. According to the “proton-sponge” theory, this leads to an increased chloride ion influx inducing an osmotic imbalance, followed by endolysosomal swelling and membrane rupture or lysis.<sup>[27]</sup> However, this theory is highly debated and other mechanisms describe the interaction of the cationic polyplexes with or the intercalation of free polymer into the endolysosomal membrane, whereby the endolysosome remains intact.<sup>[27, 67-68]</sup>



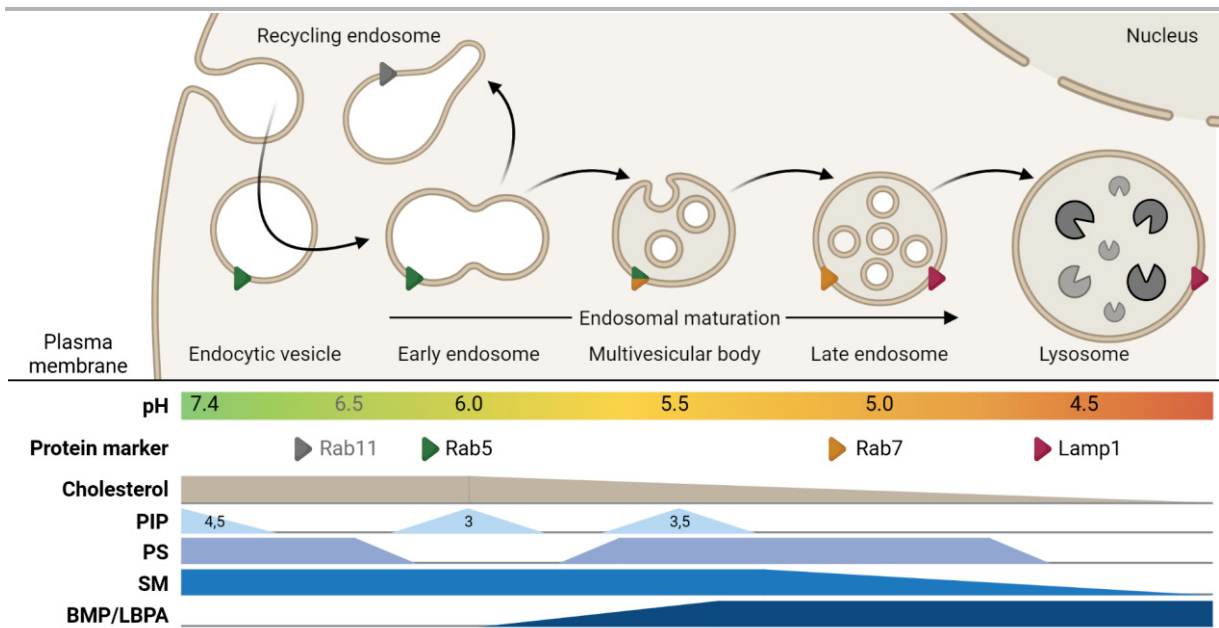


**Figure 2.1. Schematic illustration of the changes in pH value, proteins, and lipid composition during endosomal maturation.** PIP – phosphoinositides (numbers indicate phosphate positions on the inositol ring), PS – phosphatidylserine, SM – sphingomyelin, BMP/LBPA – bis(monoacylglycerol)phosphate/lysobisphosphatidic acid. Adapted from [69] and created with BioRender.com.

Different techniques can be utilized to determine the endosomal escape properties of nanocarriers with the most straightforward method being the measurement of reporter protein expression induced by the delivery of model nucleic acids, *e.g.*, mRNAs or pDNAs, through the nanocarriers (**Figure 2.2A**). Since the nucleic acids have to reach the cytosol or even the nucleus for the expression of the fluorescent protein, *e.g.*, the green fluorescent protein (GFP), this can be an indirect and qualitative method with positive results revealing that endosomal escape must have occurred.<sup>[70]</sup> Another indirect strategy is their influence on the cellular membrane which can be assessed by different cytotoxicity assays such as the lactate dehydrogenase (LDH) assay or the hemolysis assay with erythrocytes. In contrast to other toxicity assays, determining the metabolic activity of the cells, these two assays measure the release of molecules (LDH or hemoglobin, respectively) into the supernatant as a result of damage to the cellular membrane by the nanocarrier (**Figure 2.2B, C**).<sup>[39, 71-72]</sup> Although the hemolysis assay can even be performed at different pH values to mimic endolysosomal acidification,<sup>[73-74]</sup> these assays only involve the lipid composition of the plasma membrane. Therefore, they can be rather used to determine the ability of a nanocarrier to escape the endolysosome.

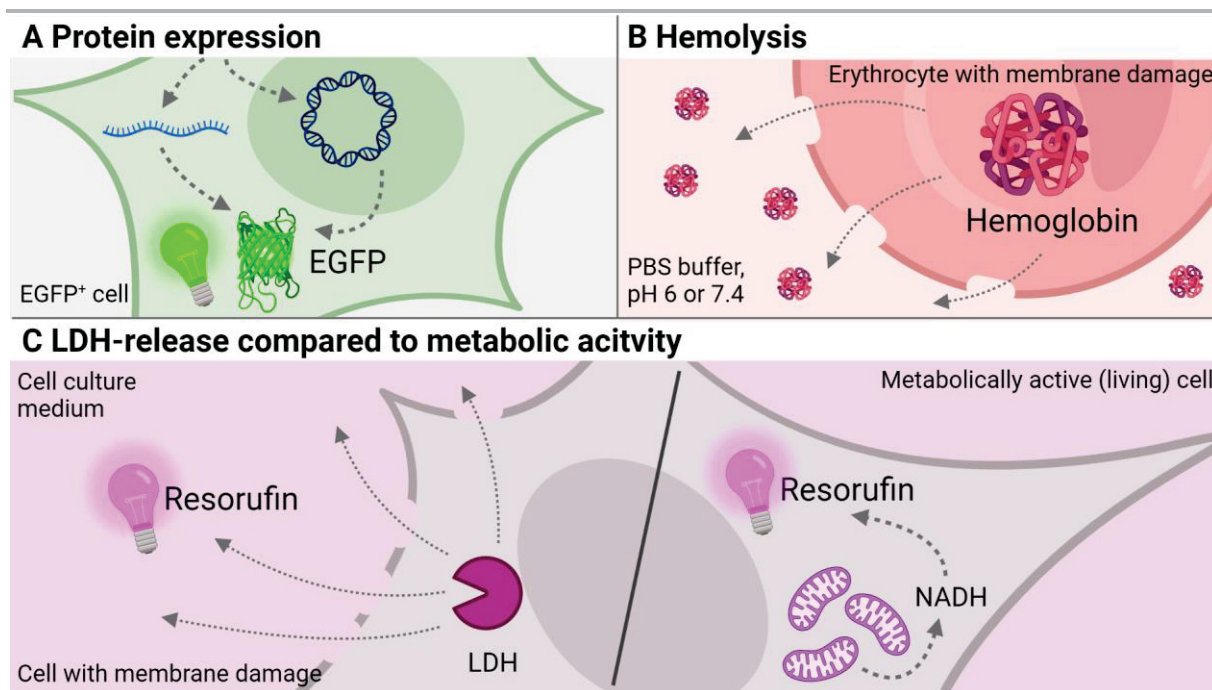


**Figure 2.2. Methods indirectly indicating or pointing towards the nanocarrier's ability to escape the endolysosomal pathway.** GFP – green fluorescent protein, NADH – nicotinamide adenine dinucleotide. LDH – lactate dehydrogenase. Created with BioRender.com.

A more direct strategy to analyze the endosomal escape of nanocarriers is the application of fluorescent molecules such as dyes or labeled proteins that change their fluorescence properties or patterns upon their release from the endolysosome. A very common tracer molecule for that is calcein, which is easily synthesized *via* Mannich-type condensation of fluorescein, formaldehyde, and iminodiacetic acid (**Figure 2.3A**).<sup>[75-76]</sup> Calcein exhibits the strong fluorescence intensity of fluorescein and the ion chelation ability of ethylenediaminetetraacetic acid (EDTA). As a consequence, its fluorescence intensity is influenced by the pH value and the presence of differently valent cations (**Figure 2.3B**).<sup>[77]</sup> However, due to its six protonatable carboxy groups, calcein fluoresces more within the biologically relevant pH range including endolysosomal pH values,<sup>[78-80]</sup> which is important for the analysis of endosomal escape. These carboxy groups are also responsible for the higher polarity and lower hydrophobicity of calcein compared to fluorescein which makes it less membrane permeable at low pH values.<sup>[81-83]</sup> Furthermore, the fluorescence self-quenches at high calcein concentrations which has been exploited to investigate the stability of liposomes encapsulating calcein. Upon damage of the liposomal membrane by the investigated release material (polymers, lipids, peptides), the dye is diluted which results in an increase in its fluorescence intensity.<sup>[84-85]</sup> These liposomes can be utilized as model vesicles to mimic different stages of the endolysosomal pathway for the investigation of the influence of specific parameters on the endosomal escape such as the membrane lipid composition, the decreasing pH value or different salt concentrations separately

(Pub1-Figure 4). In combination with fluorescence life-time measurements,<sup>[86-89]</sup> the incubation with different release materials can further provide more details regarding their endosomal escape mechanism (*e.g.*, graded, or all-or-none).

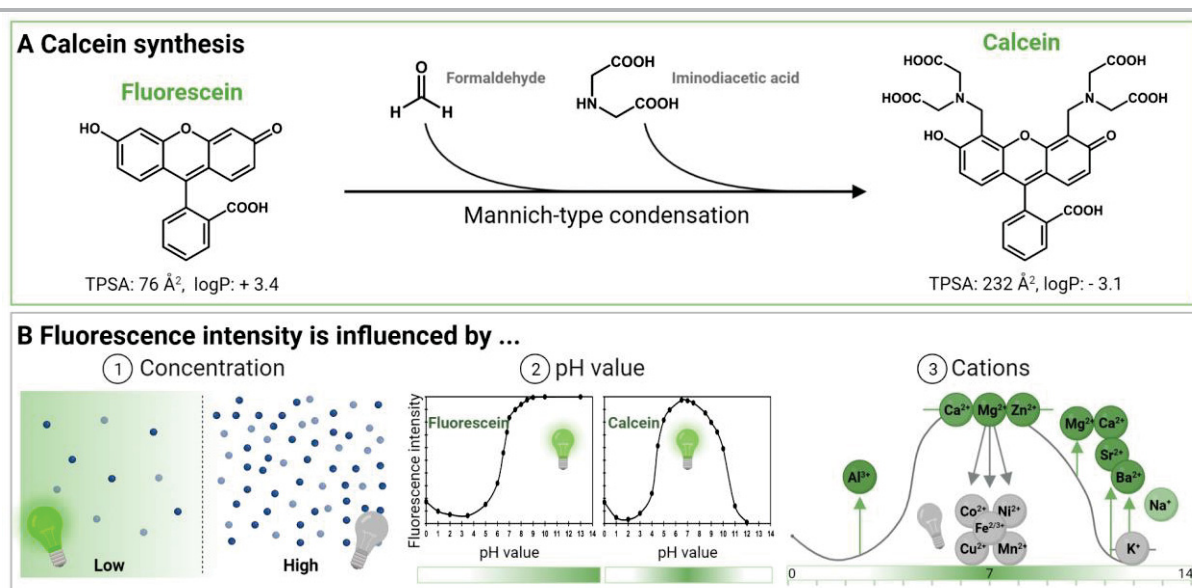


**Figure 2.3. Synthesis and factors influencing the fluorescence of calcein.** Polarity and hydrophobicity of fluorescein and calcein are indicated by their TPSA (topological polar surface area) and logP values, respectively. Created with BioRender.com.

Nevertheless, liposomes are only models of the complex intracellular situation and mimicking the exact endolysosomal conditions can be very complex. Therefore, the analysis within cells is inevitable, also to consider the uptake of the release material and the continuous exchange and fusion of the endolysosomal compartments. The *in vitro* calcein release assay comprises the incubation of different cells with calcein and the release material of interest. Control cells treated with the calcein alone exhibit a punctate fluorescence pattern resulting from the calcein located within endocytic organelles, whereas cells treated additionally with materials escaping from endolysosomal compartments display a broad cytosolic fluorescence. This difference in the fluorescence pattern can be detected using epifluorescence microscopy (**Pub1-Figure 7A**).<sup>[44]</sup> It is the most frequent analysis method and provides qualitative information on the endosomal escape which can further be quantified using (high-throughput) image analysis.<sup>[90-97]</sup> Using confocal microscopy, even a more detailed investigation with regard to the subcellular distribution of calcein and the release material and possibly also the leakage mechanism can be performed.<sup>[92, 98-99]</sup> For quantitative and high-throughput analyses, flow cytometry has been applied measuring the endosomal escape as an increase in fluorescence intensity upon incubation with the release materials (**Pub1-Figure 7B**).<sup>[64, 100-107]</sup> Nevertheless, the results should be treated with caution as an increase in fluorescence intensity could also

indicate an increased uptake of calcein. Exemplary microscopy images could help in this case to validate the flow cytometry results.<sup>[102, 108-109]</sup>

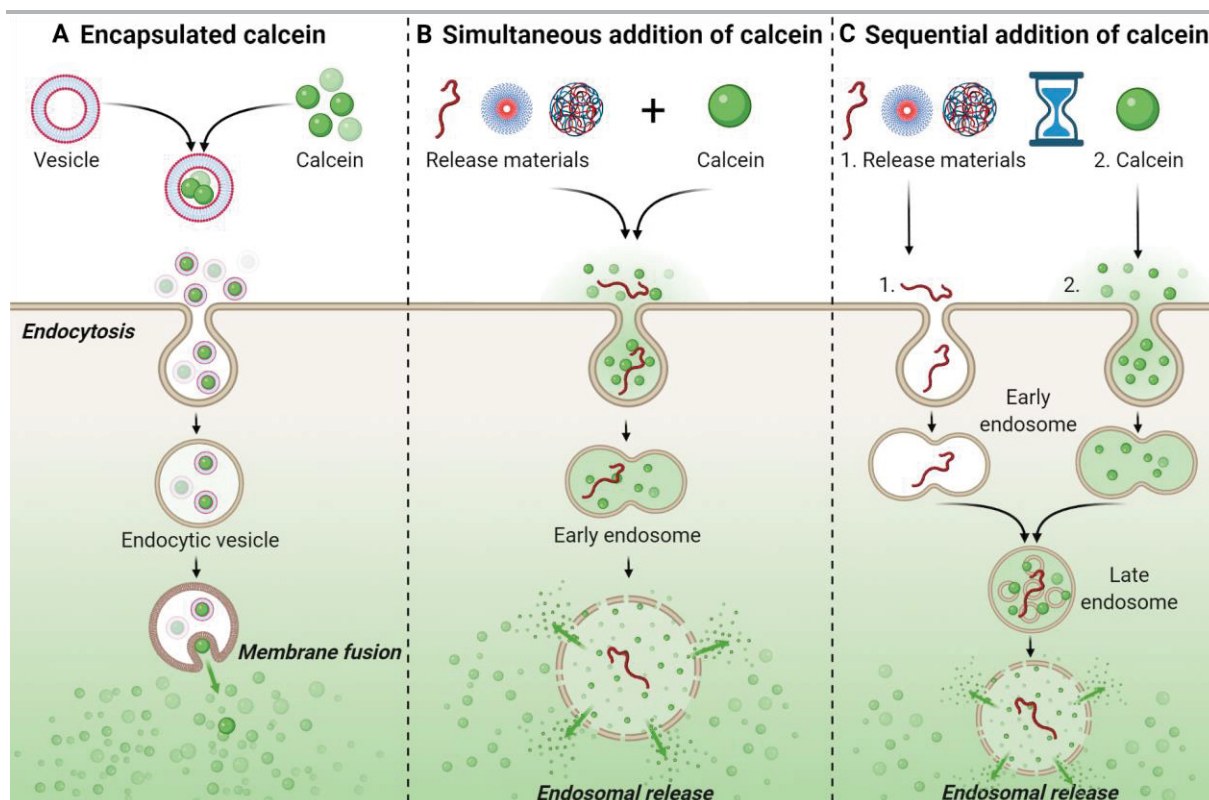


**Figure 2.4.** The different types of calcein addition determined by the release material of interest and their respective progress towards endosomal escape. Created with BioRender.com.

There are three ways to incubate the cells with calcein, depending mainly on the type of material to be examined (**Figure 2.4**). Calcein can be added i) encapsulated within the investigated release material,<sup>[95-97, 103-107, 110-118]</sup> ii) simultaneously with the release material,<sup>[44, 90-93, 98-102, 108-109, 119-125]</sup> or iii) sequentially, after incubating the cells with the release material.<sup>[64, 94, 126-130]</sup> For cationic polymers and micelles, mostly the simultaneous incubation with calcein has been applied and the method details differed widely with regard to the utilized cell types, calcein concentration (25-3214  $\mu\text{M}$ ), incubation time (0.5-48 h) and analysis method (**Pub1-Table 4**).<sup>[44, 90-93, 98-101, 109, 120-122]</sup> Therefore, a closer look was taken at factors influencing the performance of calcein as a tracer molecule for endosomal escape, which should be considered when planning the calcein release assay (**Figure 2.5**). Regarding the incubation solution, mainly the different properties of the calcein fluorescence are of importance. The pH value should be chosen high enough to dissolve the calcein,<sup>[79]</sup> and the calcein concentration should be chosen high enough to also visualize the release of small amounts of released calcein, *e.g.*, if the formation of small pores was expected. This could be addressed with a concentration-dependent calcein release assay. As polymers or micelles containing cationic moieties are investigated with this assay, an interaction between calcein and polymer might be possible which could be avoided by not

mixing both components before the incubation or by a sequential addition of both. Thereby, the optimal incubation time also depends on the endosomal escape mechanism of the investigated material and its cellular uptake kinetics. Moreover, the cellular kinetics for calcein such as endocytosis or exocytosis/export rates can also have an impact on the incubation time and can be specific for different cell types (**Pub1-Figure 9**). While studies on endocytosis and exocytosis rates have not been published so far, cytosolic calcein has been shown to be exported *via* the multidrug resistance protein (MRP),<sup>[131-132]</sup> and different efflux rates have been demonstrated for different prostate cancer and bone marrow endothelial cells.<sup>[133]</sup> The issue that cytosolic calcein released from the endosome can exit the cell could be addressed by performing a time-dependent calcein release assay. Furthermore, shorter incubation times could avoid this problem but should still be long enough to allow for i) a sufficiently high uptake of calcein and release material into the cell and ii) the intracellular fusion of the endolysosomal compartments if both components were taken up by different organelles.

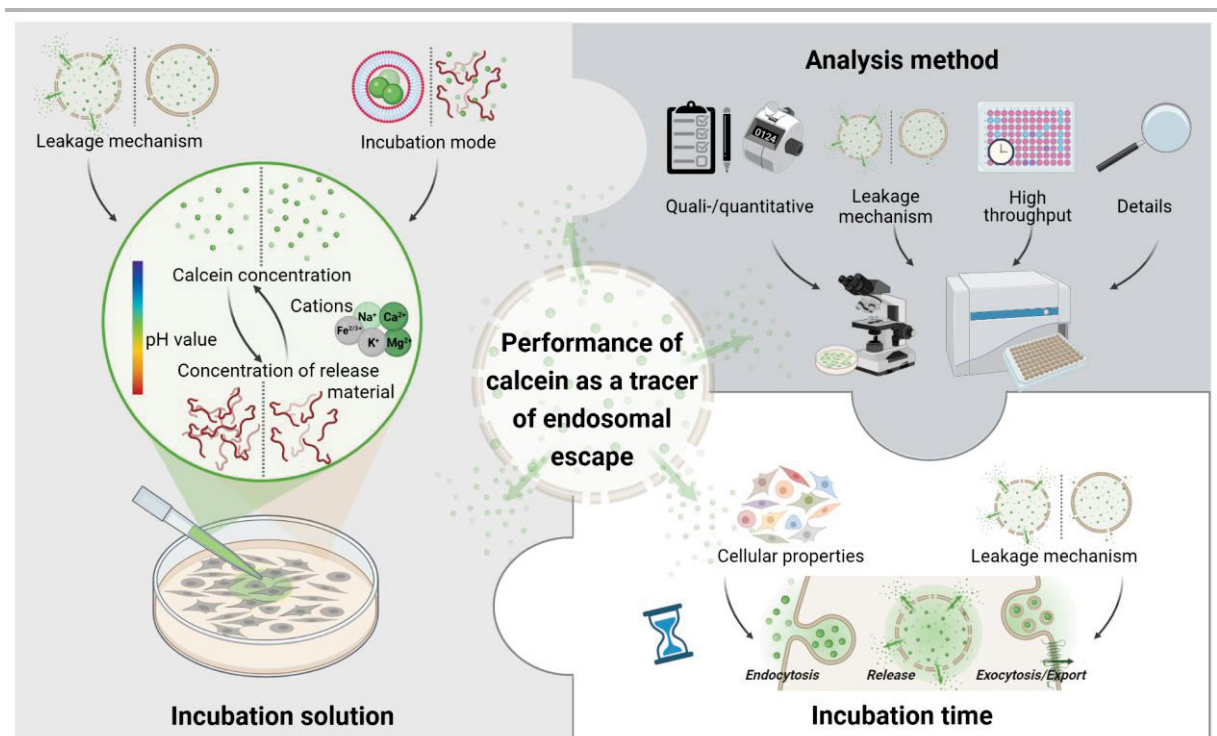


**Figure 2.5.** Factors influencing the performance of calcein as a tracer of endosomal escape with regard to the composition of the incubation solution, the incubation time, and the analysis method. Created with BioRender.com.

All in all, the advantages of the calcein release assay are its simplicity, cost-effectiveness, and rapidity. However, the factors influencing its fluorescence such as cellular properties and the requirements of the analysis technique need to be considered. While the various conditions utilized to investigate the endosomal escape demonstrate the robustness of calcein as a tracer molecule to these changes, they also show the difficulty of comparing results obtained by different methods. This could be addressed by including controls of commercially available release materials or measuring the calcein release time- and/or concentration dependently. Nevertheless, the assay is a powerful tool to investigate the endosomal escape and nicely complements the general biological investigation of different nanocarriers for gene delivery.

### 3. Influence of cationic moieties on endosomal escape

Parts of this chapter have been published in

**Pub2** F. Richter, L. Martin, K. Leer, E. Moek, F. Hausig, J. C. Brendel, A. Traeger, Tuning of endosomal escape and gene expression by functional groups, molecular weight and transfection medium: A structure–activity relationship study, *J. Mater. Chem. B* **2020**, 8, 5026-5041 and in

**Pub3** F. Hausig, F. H. Sobotta, D. O. Harz, F. Richter, A. Traeger, J. C. Brendel, Correlation between protonation of tailor-made polypiperazines and endosomal escape for cytosolic protein delivery, *ACS App. Mater. Inter.* **2021**, 13, 35233-35247.

The cationic moiety is of crucial importance for polymeric gene delivery since it is a vital feature for DNA binding, membrane interaction, cellular uptake, endosomal escape, and DNA release, but also involves the risk of high cytotoxicity. Polymers based on vinyl backbones can possess a broad range of functional pendant groups and may be readily synthesized by RDRP techniques such as reversible addition–fragmentation chain transfer (RAFT) polymerization.<sup>[134-138]</sup> Therefore, this polymer classes can be used for structure-property studies to investigate the influence of the cationic moiety within the side chain on the gene delivery efficiency.<sup>[44, 139]</sup> Among the vinyl polymers, polyacrylamides are hydrolytically more stable and considered to possess more hydrophilic polymeric backbones than their acrylate, methacrylate and methacrylamide counterparts.<sup>[140-142]</sup> Moreover, polyacrylamides with tertiary<sup>[143-146]</sup> and primary<sup>[147-149]</sup> amines have been investigated showing promising transfection efficiency in different cell lines. However, there are only few systematic studies focusing on the investigation of the correlation between the nature of the cationic moiety and the transfection mechanism. These were mainly conducted with polymethacrylamides<sup>[150-151]</sup> or polymethacrylates.<sup>[44]</sup> Most studies focused on pH responsive polymers, that were partially protonated at physiological pH values and became increasingly charged with decreasing pH during endolysosomal maturation, therefore supporting endosomal escape.<sup>[44, 139, 152]</sup> Beside pH dependent moieties, also pH independent ones were investigated, *e.g.*, the guanidinium group, that is not pH dependent in a physiological context ( $pK_a > 12$ ) and occurs in many different biomolecules as part of the amino acid arginine. Moreover, it exhibited promising efficiency and endosomal escape as part of many cell penetrating peptides which are rich in arginine residues, such as the TAT peptide.<sup>[153-154]</sup> Therefore, guanidinium is frequently exploited for the development of synthetic vectors.<sup>[155-161]</sup>

In this chapter, a homopolymer library of poly(amino acrylamide)s (**PAAm**) with different amine moieties and spacer lengths resulting in different  $pK_a$  values was investigated regarding the performance in endosomal escape (**Figure 3.1, Pub2**). The library comprised a polymer with a primary amine and an ethyl spacer (**PAEAm**) as well as two polymers with a tertiary

amine and an ethyl (**PDMAEAm**) and a propyl spacer (**PDMAPAm**), respectively. It also contained a polyacrylamide with a guanidinium group, poly(3-guanidinopropyl acrylamide) (**PGPAm**), to examine pH independent effects as well. Moreover, these polymers were compared to results of a study by Hausig *et al.* (**Pub3**) investigating a homopolymer library of poly(*N*-acryloyl piperazines) (**PNAP**) comprising tertiary amines with different alkyl groups from methyl (**PNAMP**) and ethyl (**PNAEP**) to *iso*-propyl (**PNAiPP**) and *tert*-butyl (**PNA*t*BP**). Although these polymers have not been studied for biomedical applications so far, favorable  $pK_a$  values have been reported, which can be fine-tuned closer to the physiological relevant pH range by the respective substituent.<sup>[162-163]</sup>

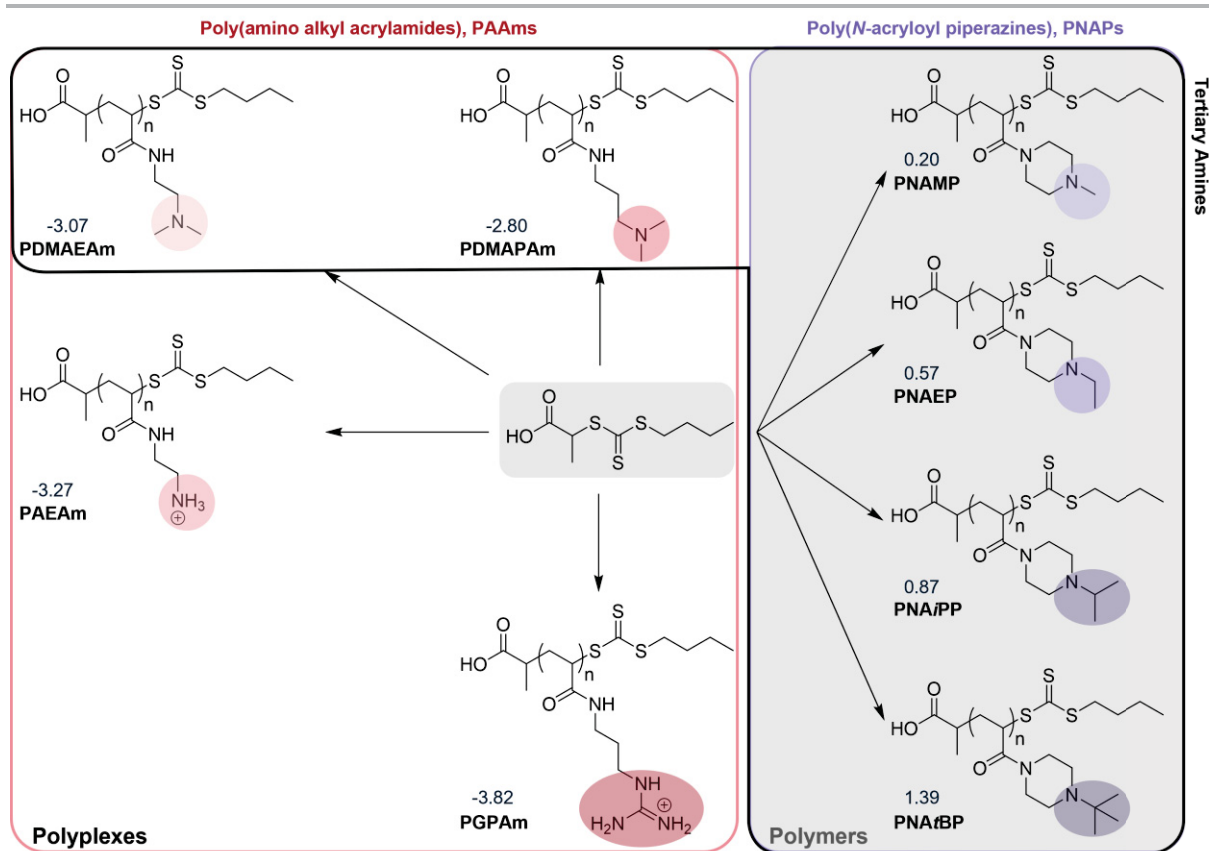


**Figure 3.1. Schematic overview of the polyacrylamides investigated within this chapter.** Numbers indicate logP values of the respective monomers calculated using the Molinspiration Cheminformatics website.<sup>[164]</sup>

The polymers were synthesized *via* RAFT polymerization resulting in well-defined polymers with molar masses of about 10 kDa (PAAms, DP  $\approx$  100) and 60 kDa (PNAPs, DP  $\approx$  500) as determined *via* size exclusion chromatography (SEC) (Table 3.1).



**Table 3.1. Polyacrylamide libraries with selected characterization data.**

PAAMs	DP [a]	$M_{n,SEC}$ [b] kg mol <sup>-1</sup>	$\bar{D}$ [b]	$pK_a$ [c]	PNAPs	DP	$M_{n,SEC}$ [d] kg mol <sup>-1</sup>	$\bar{D}$ [d]	$pK_a$ [c]
PDMAEAm	88	10.0	1.48	7.8	PNAMP	500	53.5	1.22	6.2
PAEAm	96	10.0	1.17	8.3	PNAEP	500	55.8	1.29	6.5
PDMAPAm	71	9.7	1.26	8.7	PNA/PP	500	65.0	1.23	6.7
PGPAm	94	8.5	1.27	> 12	PNA/BP	500	62.5	1.30	7.1

[a] Determined via <sup>1</sup>H NMR spectroscopy.

[b] Determined via SEC, eluent: 0.1 M NaCl + 0.1 % TFA, P2VP standard.

[c] Calculated using the Henderson-Hasselbalch equation following potentiometric titration of acidified polymer solutions in 125 mM (PAAMs) or 150 mM NaCl (PNAPs) against 0.1 M NaOH (0.5 M for PGPAm).

[d] Determined via SEC, eluent: DMAc + 0.21 % LiCl, PS standard.

To compare the influence of the pH value on the charge of the homopolymers, their  $pK_a$  values were determined by titrating acidified solutions of the polymers against NaOH (Table 3.1), and the theoretical degree of charge was calculated (Figure 3.2). The PAAMs possessed  $pK_a$  values above 7.8, with the one for PGPAm being assumed to be around 12 since the  $pK_a$  could not be determined with the available system. Therefore, all PAAMs were already mainly positively charged outside the cell and within the cytosol (pH 7.4). By contrast, the PNAPs exhibited  $pK_a$  values between 6.2 and 7.1 and were, therefore, only slightly positively charged at pH 7.4 with a steep increase upon pH decrease to pH 5.0 (endolysosome).

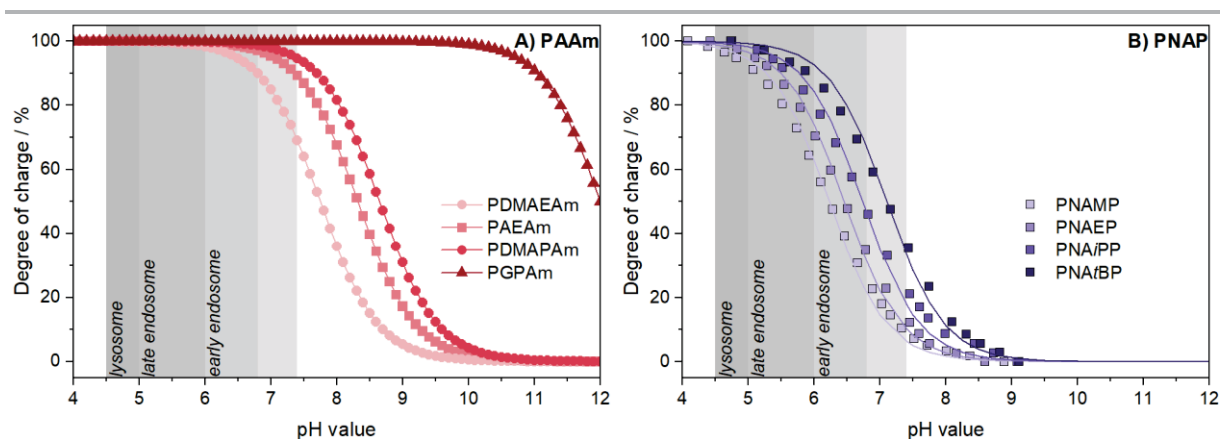


**Figure 3.2. Theoretical determination of the degree of charge** of the (A) poly(alkyl acrylamide) (PAAM) library and (B) the poly(*N*-acryloyl piperazine) (PNAP) library.

As polycations are known for their interaction with cell membranes,<sup>[39]</sup> hemolysis and aggregation assays were performed with human erythrocytes following incubation with polymers at different pH values and without serum (Figure 3.3). In general, all polymers were non-hemolytic (< 2 % hemolysis) but slight increases with increasing  $pK_a$  values were observed. The PAAMs exhibited slightly higher hemolytic activity at pH 7.4 (0.5-2.3 %) compared to the

**PNAPs** (0.2-2.0 %) which can be related to the different amounts of positive charges present. The difference between the libraries was also observed with standard toxicity assays (see **Pub2-Figure S9, Pub3-Figure S6**). Correlating well with the degrees of charge, the **PAAMs** showed only slight pH dependency, whereas the membrane interaction of the **PNAPs** increased drastically at pH 6 with regard to both, hemolysis, and aggregation. Although the results demonstrate the influence of the type of cation and the degree of charge within each library, they cannot be directly compared, since they differ in more factors such as molecular weight, polymer concentration or hydrophobicity of the side chain (see logP values, **Figure 3.1**). These apparently influence the membrane interaction/destruction as well and could be the reason for the increased hemolysis/ aggregation values of the **PNAP** library at comparatively lower degree of charge values. Nevertheless, the results point towards the potential of these polymers to escape the endosome.

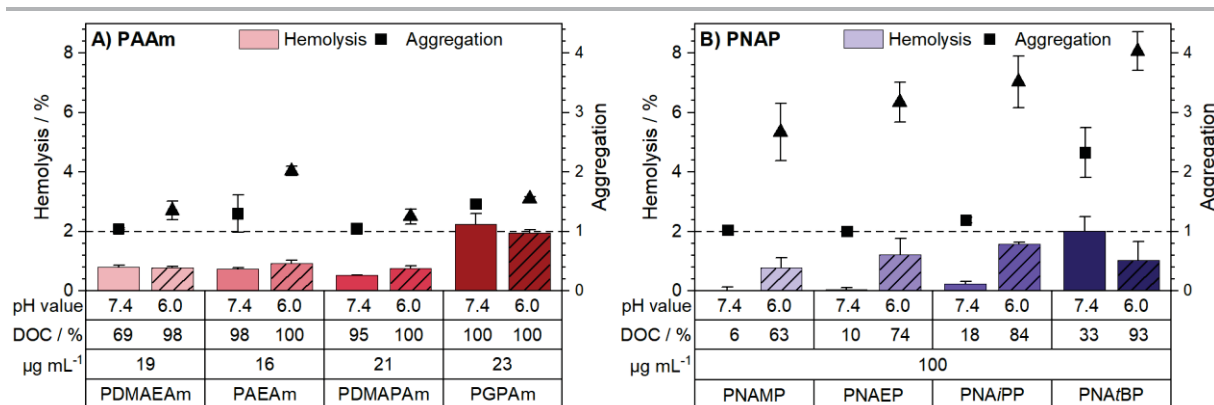


**Figure 3.3. Membrane interaction of (A) PAAMs and (B) PNAPs with human erythrocytes** determined by hemolysis and aggregation assays following incubation with polymers without serum for 1 and 2 h, respectively. Values represent mean  $\pm$  SD (n = 3). Lines indicate thresholds for slightly hemolytic activity (> 2 %) and aggregation (> 1), respectively. DOC: degree of charge at respective pH values.

Therefore, the calcein release assay was utilized to investigate the two libraries regarding their endosomal escape (**Figure 3.4**). HEK293T cells were incubated simultaneously with calcein and PAAM-polyplexes (N\*/P 30) or PNAPs for 4 h or 16 h, respectively, in serum-free Opti-MEM. Subsequently acquired CLSM images of HEK293T cells showed cytosolic fluorescence to different extents for all polymers indicating endosomal escape of calcein. Remarkably, the incubation with polyplexes of guanidinium functional polymers caused a very bright fluorescence inside the cells which was also reflected in flow cytometry measurements by high relative mean fluorescence intensity (rMFI) values. This high level of calcein release with **PGPAm** polyplexes was not shown for guanidinium functional polymers before and points towards an efficient and pH independent endosomal release for this polymer class.

The calcein release by the remaining polymers was in the same range for all of them (rMFI: 1.2 to 3.2). While the different molar masses used for both libraries seem to be negligible in this assay due to similar results for lower molar mass **PNAPs** (**Pub3-Figure 4k**), the increased incubation time and concentration of the **PNAP** library should be considered. They could indicate a lower efficiency compared to the **PAAs** which again might be linked to the different degrees of charge of both libraries. Nevertheless, the calcein release of the **PNAPs** was nearly unaffected by serum-containing growth medium (**Pub3-Figure S17**), whereas the **PAAs** exhibited much lower values in this medium (**Pub2-Figure 6A**), which could be explained by interaction with serum proteins due to the higher degree of charge. Within the **PNAP** library, again a correlation of endosomal release of calcein with increased  $pK_a$  values was observed with **PNAiPP** emerging to be the best performer of this library due to toxic side-effects of **PNAiBP**. Regarding the **PAAs**, the primary amine polymer **PAEAm** was better than the tertiary amine polymers confirming the results of a study with polymethacrylates showing that primary amines are slightly more efficient.<sup>[44]</sup> Moreover, the results of the **PAAm** library correlated well with their transfection efficiency in the different media (**Pub2-Figure 2A**), further supporting the results of the calcein release assay.

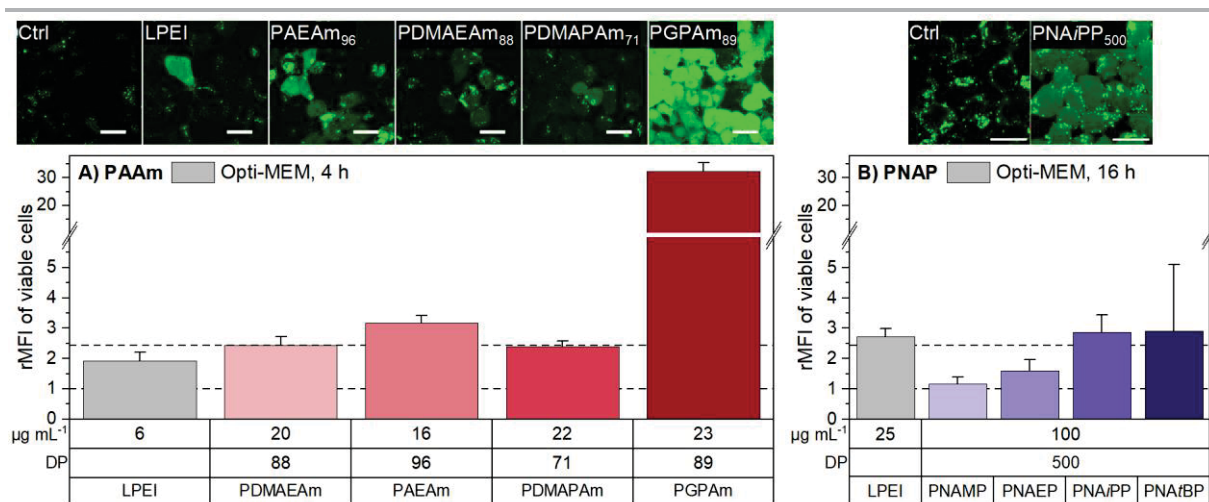


**Figure 3.4. Endosomal escape investigated using the calcein release assay.** HEK293T cells were incubated with (A) PAAm library at N\*/P 30 in Opti-MEM for 4 h or (B) with the PNAPs in Opti-MEM for 16 h. The cells were washed and analyzed *via* CLSM (images) or flow cytometry (graphs). Scale bars in images represent 20  $\mu\text{m}$ . Values in graphs represent mean  $\pm$  SD ( $n = 3$ ). rMFI: relative mean fluorescence intensity referred to calcein control. Since the images of the PAAs were not published so far, a detailed method description and further images can be found in the appendix section “Description of unpublished methods”.

Regarding the mechanism of endosomal escape, the proton sponge theory could be adopted for the **PNAPs** since the polymers become protonated only upon the pH decrease during endosomal

maturation leading to an increasing membrane interaction. Also the rather fast calcein release by **PNAiPP** and its ability to release other differently sized molecules indicate a proton sponge-like mechanism rather than membrane destabilization or pore formation (**Pub3-Figures 5, 6**). By contrast, the **PAAm**s are already mainly protonated when entering the cells with **PGPAm** being even unresponsive to any pH change within the physiological range. Since this indicates a different endosomal escape mechanism for this polymer, the **PAAm** library was further characterized regarding the polyplex uptake to exclude a non-endocytotic uptake. HEK293T cells were incubated with polyplexes of YOYO-1 labeled pDNA and the respective polymers at N\*/P 30 for 4 h followed by CLSM analysis (**Figure 3.5 A**). The incubation with the different **PAAm** polyplexes led to a punctate pattern within the cells in all cases which is known from endolysosomal organelle staining and could point towards YOYO-1 fluorescence trapped within organelles. Furthermore, flow cytometry measurements of HEK293T cells showed almost no YOYO-1 fluorescence when incubated with the polyplexes at 4 °C to inhibit energy-dependent processes, *i.e.*, endocytosis (**Pub1-Figure 4B**). Therefore, an endocytotic uptake mechanism for the polymers can be assumed.

Secondly, the mechanism of endosomal escape for guanidinium containing CPPs was considered to also play a role for guanidinium containing polymers. The endosomal release of CPPs was proposed to occur *via* binding to bis(monoacryloyl glycerol)phosphate (BMP), a lipid present in the membranes of intra late endosomal vesicles (ILEV) and barely in the limiting membrane of late endosomes or lysosomes.<sup>[165-169]</sup> Therefore, a lipid-polymer binding assay was conducted to investigate the interaction of the **PAAm**s with this lipid (**Figure 3.5 B**). DY635-labeled **PAAm** polymers in acetate buffer (pH 5.7) were mixed thoroughly with different concentrations of BMP in hexane and allowed for phase separation followed by fluorescence intensity measurement of the aqueous phase. A decrease in fluorescence intensity indicated the removal of the polymer from the aqueous phase and therefore interaction with the lipid in the hexane phase. Phosphatidyl choline (PC) and phosphatidyl ethanolamine (PE) were used as also phosphate-containing but neutral control lipids. The incubation of the polymers with PC or PE caused a negligible decrease in relative fluorescence intensity (rFI), indicating almost no interaction. By contrast, the rFI decreased substantially upon polymer incubation with BMP with increasing P/N ratio (lipid-phosphate to polymer-amine) and results comparable to those obtained for a tetramethylrhodamine (TMR)-labeled TAT dimer.<sup>[165]</sup> **PGPAm** exhibited the highest decrease in rFI, but the remaining polymers also showed BMP-binding properties, albeit not as strong as **PGPAm**. The investigations therefore point towards a multifactorial endosomal escape of **PGPAm**.

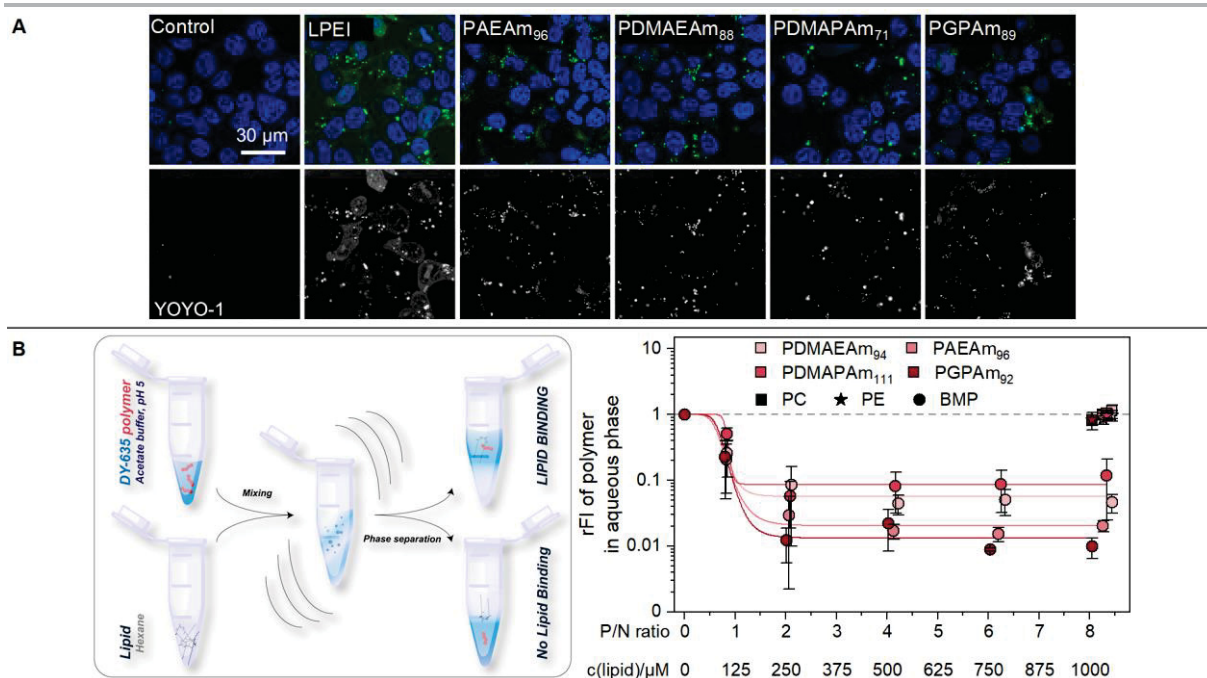


**Figure 3.5. Endosomal escape mechanism of PAAs.** (A) Representative images of polyplex uptake with alkyl acrylamide polymers investigated *via* CLSM in HEK293T cells incubated with polyplexes containing YOYO-1 (green) labeled pDNA and PAAs at N\*/P 30 in Opti-MEM for 4 h. Nuclei were stained with Hoechst 33342 and fluorescence outside the cells was quenched with trypan blue. (B) Procedure and results of the lipid polymer interaction assay performed with DY635-labeled PAAs in acetate buffer (pH 5.7) and indicated lipids in hexane. A decrease in rFI of the aqueous phase indicated partitioning of the DY635-labeled polymer into the hexane phase. Dots represent mean  $\pm$  SD ( $n = 3$ ). Lines represent a logistic equation fitted to the values of each replicate. P/N ratio: lipid-phosphate to polymer-amine, PC: phosphatidyl choline, PE: phosphatidyl ethanolamine, BMP: bis(monoacryloyl glycerol)phosphate.

To conclude, it was shown that membrane interaction as well as endosomal escape strongly depend on the degree of cationic charges present within the polymers which again depends on the polymers'  $pK_a$ . Polyacrylamides with increased  $pK_a$  values due to lower substituted amines (**PAEAm**, **PGPAm**) or due to an increase in hydrophobicity of the substituent (**PNAiBP**, **PNAiPP**) tended to interact more with cellular membranes and exhibited an increased endosomal escape. Furthermore, the superior release by **PGPAm** demonstrated that also pH independent mechanisms such as interaction with membrane lipids are responsible for endosomal escape. However, also the mainly uncharged (pH 7.4) **PNAPs** achieved a remarkable calcein release, when their conditions were adjusted towards higher molar masses, longer incubation times and higher polymer concentrations, illustrating optimization as a useful tool to increase the efficacy of previously not very promising structures.

## 4. Increasing gene delivery by introducing hydrophobic monomers

Parts of this chapter have been published in

**Pub4** F. Richter,<sup>‡</sup> K. Leer,<sup>‡</sup> L. Martin, P. Mapfumo, J. I. Solomun, Maren T. Kuchenbrod, S. Hoepfener, J. C. Brendel, A. Traeger, The impact of anionic polymers on gene delivery: How composition and assembly help evading the toxicity-efficiency dilemma, *J. Nanobiotechnol.* **2021**, 19, 292, in

**Pub5** F. Richter,<sup>‡</sup> P. Mapfumo,<sup>‡</sup> L. Martin, J. I. Solomun, F. Hausig, J. J. Frietsch, T. Ernst, S. Hoepfener, J. C. Brendel, A. Traeger, Improved gene delivery to K-562 leukemia cells by lipoic acid modified block copolymer micelles, *J. Nanobiotechnol.* **2021**, 19, 70, and in

**Pub6** J. I. Solomun, G. Cinar, P. Mapfumo, F. Richter, E. Moek, F. Hausig, L. Martin, S. Hoepfener, I. Nischang, A. Traeger, Solely aqueous formulation of hydrophobic cationic polymers for efficient gene delivery, *Int. J. Pharm.* **2021**, 593, 120080.

One major advantage of using polymers for gene delivery is the abundance of functionalized monomers which can be combined in various ways generating new nanocarriers with different characteristics. A very common modification is the addition of hydrophobic moieties to cationic polymers resulting in amphiphilic copolymers which can self-assemble into higher ordered structures such as micelles or vesicles in aqueous solutions.<sup>[49, 170-172]</sup> Different compositions of these polymeric micelles have been investigated for gene delivery. Whereas one approach uses cationic-hydrophilic block copolymers to incorporate the genetic material within the core of a polyion complex (PIC) micelle with a neutral shell,<sup>[49, 173]</sup> another one uses pre-assembled micelles from hydrophobic-cationic block copolymers to form complexes with genetic material (micelleplexes).<sup>[45-46]</sup> The hydrophobic segment induces not only the self-assembly in water but potentially also contributes to efficient transfection as it can facilitate interaction with the lipophilic cell membranes promoting cellular uptake and release from endosomes.<sup>[48, 60, 174-175]</sup>

Among others, *n*-butyl methacrylate (*n*BMA) and *n*-butyl acrylate (*n*BA) have been shown to form a stable hydrophobic core and, as such, been included for hydrophobic modifications of polymers and formation of micelles.<sup>[175-178]</sup> In this chapter, both monomers have been utilized in different architectures to combine hydrophobic properties with cationic tertiary amine polymers and were investigated regarding their effect on the gene delivery efficiency (**Figure 4.1**).

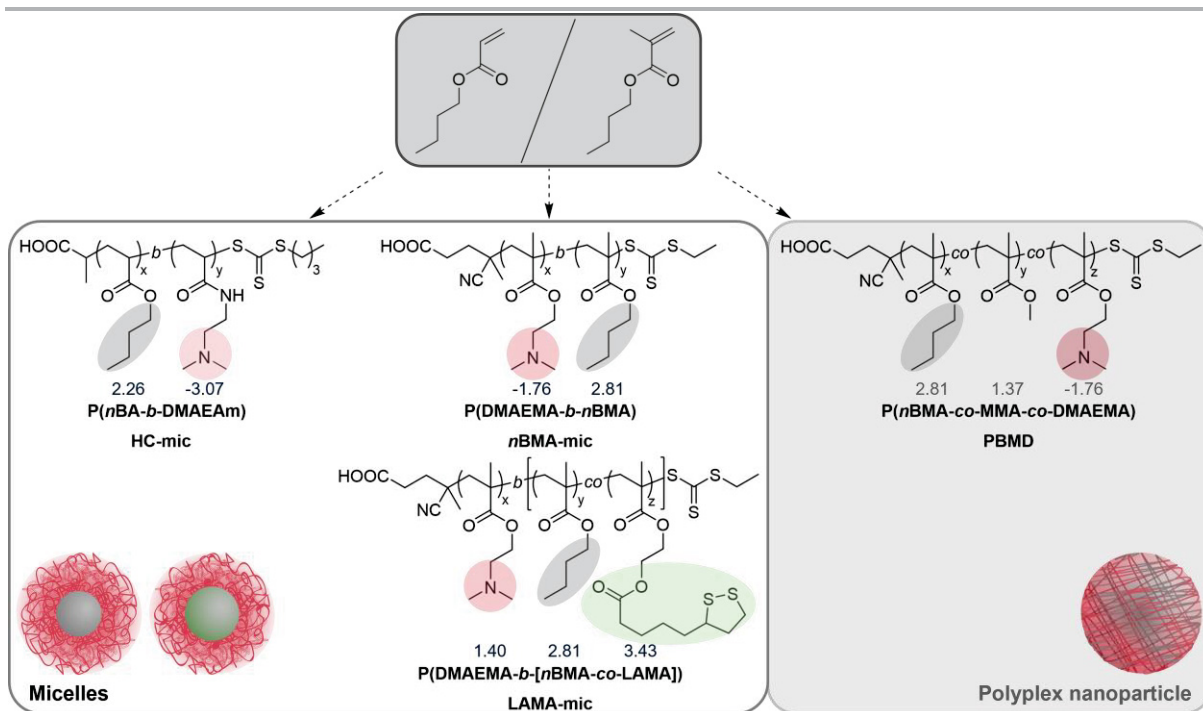


**Figure 4.1. Schematic overview of the cationic-hydrophobic polymers investigated within this chapter.**

The polymers were based on either *n*-butyl acrylate (*n*BA) or *n*-butyl methacrylate (*n*BMA). Numbers indicate log*P* values of the respective monomers calculated using the Molinspiration Cheminformatics website.<sup>[164]</sup>

The first example is the combination of *n*BA with the pH responsive DMAEAm described already in **Chapter 3**. Its low transfection efficiency in combination with the moderate toxicity as a homopolymer (**Pub2-Figure 2A**) made it an ideal candidate for optimization in a micellar assembly. The diblock copolymer was synthesized *via* sequential RAFT polymerization starting with *n*BA and was purified after each block synthesis step. Characterization with DMAc-SEC showed a monomodal dispersed polymer ( $D = 1.37$ ) with a molar mass of  $28.4 \text{ kg mol}^{-1}$  (Table 4.1). The DPs of both blocks were nearly of equal length with the cationic block matching the length of the PDMAEAm homopolymer from Chapter 3 ( $DP = 90$ ). Subsequently, HC-Micelles (**HC-mic**) were prepared using the solvent exchange method by gradually adding 150 mM NaCl solution as selective solvent to the polymer dissolved in THF/MeOH. During this process, the block copolymers underwent microphase separation with P*n*BA forming the hydrophobic (H) core and PDMAEAm the hydrophilic cationic (C) shell. The formation of micelles was confirmed *via* cryo transmission electron microscopy (cryo-TEM) (**Pub4-Figure 3A**).

**Table 4.1. Characterization data for the HC-mic.**

Polymer/ Micelle	DP [a]		$M_{n,SEC}$ [b]	$\bar{D}$ [b]
	DMAEAm	<i>n</i> BA		
PDMAEAm	82	-	11.9	1.67
HC-mic	90	80	28.4	1.37

[a] Determined *via*  $^1\text{H}$  NMR spectroscopy.

[b] Determined *via* SEC, eluent: DMAc + 0.21 % LiCl, PMMA standard.

Following combination with pDNA, the **HC-mic micelleplex** exhibited a hydrodynamic diameter (z-Average) of  $68 \pm 3$  nm and was, therefore, only slightly smaller compared to  $83 \pm 10$  nm of the cationic homopolymer polyplex (**Figure 4.2A**). The interaction with pDNA was further investigated using the combined ethidium bromide quenching (EBA) and heparin release assays (HRA). They revealed a slightly higher binding efficiency and the formation of more stable micelleplexes for the **HC-mic** compared to the linear **PDMAEAm** as indicated by slightly lower rFI values and higher heparin concentrations, respectively (**Figure 4.2B**). Together with the dynamic light scattering (DLS) results, this indicates a slightly stronger complexation of pDNA by the micelle.

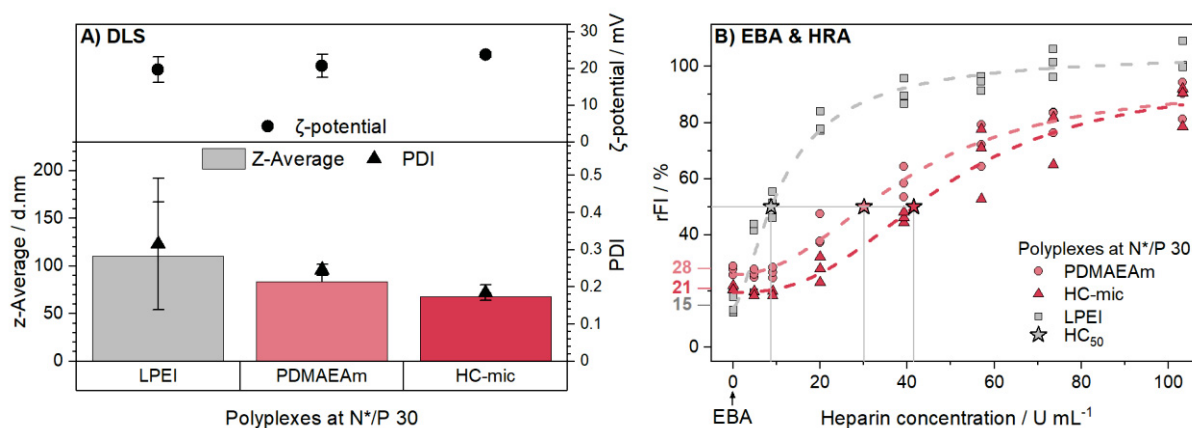


**Figure 4.2. Micelleplex formation by HC-micelles.** (A) DLS and ELS measurement of poly-/micelleplexes at N\*/P 30 in HBG buffer. Values represent mean  $\pm$  SD ( $n = 2$ ) of z-average (columns), PDI (triangles) or  $\zeta$ -potential (dots). (B) Combined EBA and HRA of poly-/micelleplexes at N\*/P 30 in HBG buffer. Values represent mean  $\pm$  SD ( $n = 3$ ). HC<sub>50</sub> indicates heparin concentration required to release 50 % of pDNA and was calculated using logistic fit functions (represented by the dashed lines). Additional numbers on y-axis indicate rFI values of pure polymer/micelle-pDNA complexes and represent EBA results.

Since both, micelle and homopolymer, exhibited good pDNA binding properties, the transfection efficiency was determined *via* flow cytometry as the expression of EGFP in HEK293T cells following incubation with micelleplexes at N\*/P 30 in growth medium



containing serum for 24 or 48 h (**Figure 4.3A**). Consistent with previous studies with different polymers,<sup>[60, 179]</sup> the incorporation of a hydrophobic monomer led to superior transfection efficiency of the **HC-mic** with up to  $95 \pm 4$  % cells showing EGFP expression which was even higher than the commercial control LPEI (up to  $39 \pm 8$  % EGFP-positive cells). Moreover, increasing the pDNA concentration only led to an increase in EGFP-positive cells for LPEI but not for the **HC-mic** pointing towards a more efficient transport by the latter one allowing for the saving of genetic material. By contrast, incubation with the **PDMAEAm** polyplex hardly resulted in transfected cells ( $2 \pm 0$  % EGFP positive cells) which could be due to a less efficient endosomal escape as reported in Chapter 3. However, the hydrophobic modification also led to a severe increase in metabolism related cytotoxicity as determined by the PrestoBlue assay in L-929 cells following incubation with the polymers at different concentrations for 24 h (**Figure 4.3B**). For the **HC-mic**, the concentration leading to 50 % viable cells ( $CC_{50}$ ) was the same as for LPEI ( $23 \mu\text{g mL}^{-1}$ ) which is renowned for its toxicity, whereas the  $CC_{50}$  value of the homopolymer was about four times as high.

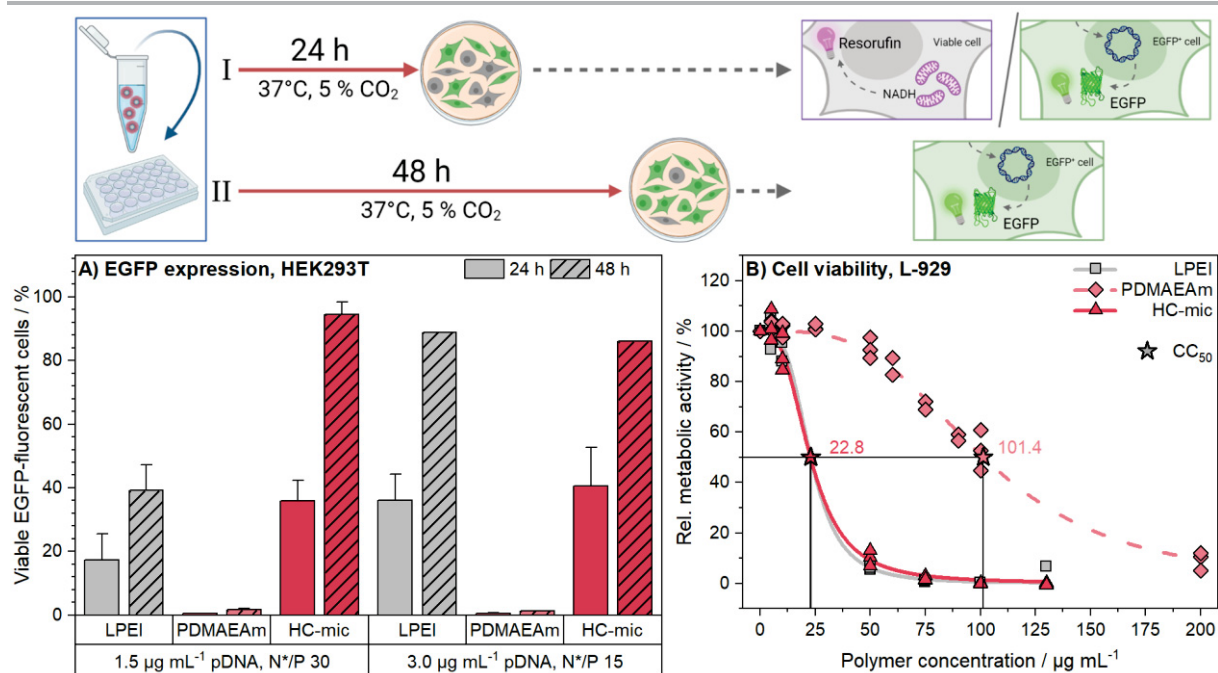


**Figure 4.3. Transfection efficiency and cytotoxicity of HC-micelles.** (A) Transfection efficiency determined *via* flow cytometry as EGFP expression in HEK293T cells following incubation with poly-/micelleplexes for indicated time periods. Values represent mean  $\pm$  SD ( $n \geq 1$ ). (B) Viability of L-929 cells using the PrestoBlue assay following incubation with polymers at indicated concentrations for 24 h. Dots represent values of single repetitions and lines represent logistic functions fitted to the single measurements ( $n = 3$ ). Stars with numbers indicate polymer concentrations resulting in 50 % viable cells.

To further investigate the impact of hydrophobic moieties, methacrylates were utilized for the backbone of block copolymers comprising the pH sensitive DMAEMA and *n*BMA. Moreover,

the monomer lipoic acid methacrylate (2-(methacryloyloxy)ethyl 5-(1,2-dithiolan-3-yl)pentanoate, LAMA) synthesized by a DCC/DMAP coupling reaction was incorporated into the hydrophobic block. Lipoic acid is an essential fatty acid and was investigated as a potential therapeutic.<sup>[180-181]</sup> Due to its redox-sensitivity, it is also capable of forming disulfide linkages in the micellar core,<sup>[182]</sup> which has been utilized for different lipoic acid conjugated drug delivery systems exhibiting superior stability in the extracellular environment and undergoing rapid de-crosslinking/disassembly under reductive conditions.<sup>[183-186]</sup> Moreover, beneficial effects were observed for siRNA or pDNA transfection when lipoic acid was incorporated into nanogels,<sup>[187]</sup> used for hydrophobic modification of LPEI,<sup>[188]</sup> or as amphiphiles.<sup>[189-190]</sup> Therefore, the effect of lipoic acid within micelles was also investigated for gene delivery in **Pub5**.

Again, sequential RAFT polymerization was performed to synthesize the block copolymer and solvent exchange was used to assemble the micelle (**LAMA-mic**) followed by dialysis against water. The synthesis and assembly steps had to be performed twice for sufficient material for all tests resulting in slightly different but still comparable monomer compositions of both batches (**Table 4.2**). A diblock copolymer consisting of only DMAEMA and *n*BMA was synthesized and assembled similarly (**BMA-mic**) for the use as a control for the transfection assays. The formation of micelles was confirmed *via* cryo-TEM (**Pub5-Figure S5**). At similar concentrations, DLS measurements revealed similar hydrodynamic diameters of about 50 nm for the micelles with the batches of the **LAMA-mic** being slightly larger. Upon complex formation with pDNA (micelleplex), the size increased slightly by 4-10 nm.

**Table 4.2. Characterization data for polymers and micelles of the LAMA library.**

Polymer/ Micelle	DP [a]			$M_{n,SEC}$ [b]	$\bar{D}$ [b]	Micelle		Poly-/Micelleplex	
	DMAEMA	<i>n</i> BMA	LAMA			Size [c]	PDI [c]	Size [d]	PDI [d]
				kg mol <sup>-1</sup>		nm		nm	
PDMAEMA I	101	-	-	13.8	1.17	-	-	56.1*	0.25*
PDMAEMA II	89	-	-	14.0	1.15	-	-	42.6*	0.23*
BMA-mic	89	68	-	21.0	1.18	46.6	0.10	56.8	0.21
LAMA-mic I	101	120	22	30.0	1.19	53.4	0.15	58.2*	0.14*
LAMA-mic II	89	101	19	23.1	1.32	54.2	0.12	61.1	0.14

[a] Determined *via* <sup>1</sup>H NMR spectroscopy.

[b] Determined *via* SEC, eluent: CHCl<sub>3</sub> + 2 % IPA + 4 % NEt<sub>3</sub> or DMAc + 0.21 % LiCl, PMMA standard.

[c] Hydrodynamic diameter (z-average) and polydispersity index (PDI) determined *via* DLS at equal amine concentrations (N\*/P 30, 371-549 μg mL<sup>-1</sup>).

[d] Hydrodynamic diameter (z-average) and polydispersity index (PDI) determined *via* DLS following complexation with pDNA at N\*/P 30 (221-549 μg mL<sup>-1</sup>).

\* Data are not published and were obtained as described in Pub5-SI p.9. Further information can be found in the appendix section "Description of unpublished methods".

The pDNA binding capability of the micelle was investigated using the combined EBA/HRA assays (**Figure 4.4**). Strikingly, the methacrylate version of the tertiary amine, **PDMAEMA** (rFI:  $50 \pm 16$ ), did not displace as much ethidium bromide as the acrylamide version **PDMAEAm** (rFI:  $27 \pm 2$ , **Figure 4.2B**), pointing towards only 50 % of bound pDNA for **PDMAEMA**. However, the difference could also be due to the slightly more hydrophobic backbone of the methacrylate (logP values of the monomers: **Figure 4.1**) or a different packing of the pDNA within the methacrylate polyplex since the ethidium bromide fluorescence intensity is based not only on the intercalation between the base pairs of the double helix but also on their hydrophobicity.<sup>[191-192]</sup> Moreover, a gel migration assay revealed the complete retardation of the pDNA by the polymers (**Pub5-Figure S6**). The micellization/addition of hydrophobic monomers affected the binding capability only slightly, whereas the influence was more pronounced for the poly-/micelleplex stability against heparin. Indicated by the lower heparin concentration required to release the pDNA, the complexation of the pDNA by the **LAMA-mic I** was slightly less stable compared to the homopolymer (**Figure 4.4B**).

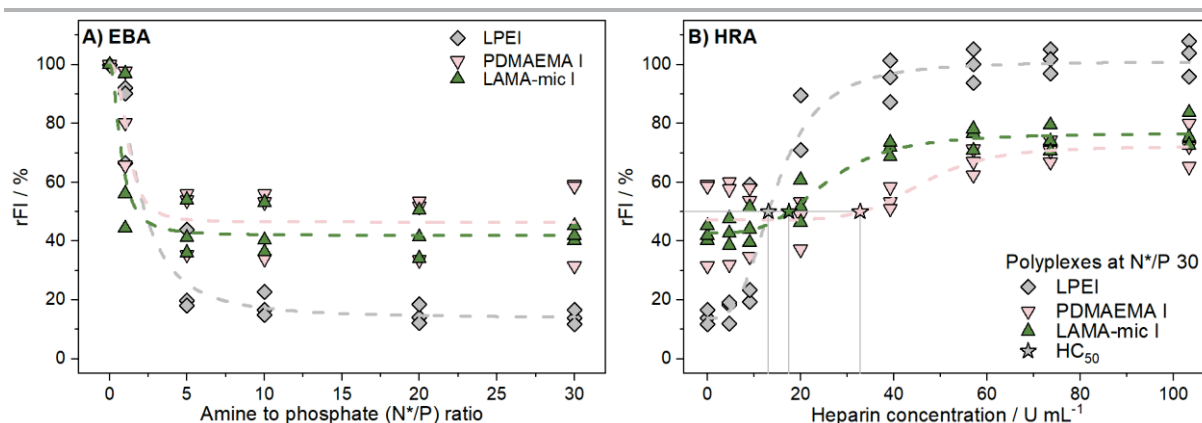


**Figure 4.4. Poly-/Micelleplex formation by methacrylate polymers.** (A) EBA at different N\*/P ratios in HBG buffer pH 7.4. (B) HRA of poly-/micelleplexes at N\*/P 30 in HBG buffer pH 7.4. HC<sub>50</sub> indicates heparin concentration required to release 50 % of pDNA and was calculated with logistic fit functions. (A+B) Dots represent individual replicates and lines represent the logistic fit to the respective data points (n = 3).

The cytotoxicity of **LAMA-mic I** was determined as its influence on the metabolic activity in the standard cell line L-929 following incubation with the polymers at different concentrations for 24 h (**Figure 4.5A**). Again, the micelle was more toxic than the cationic homopolymer, but this time only slightly, and it was less harmful than the commercial LPEI. At concentrations applied in transfection assays, all polymers led to cell viabilities above 70 %. This was also confirmed for the second batch of **LAMA-mic** when measuring transfection efficiency in HEK293T cells *via* flow cytometry, simultaneously analyzing cell viability in the FSC:SSC plot (**Figure 4.5B**, squares/dots). The addition of hydrophobic monomers led to superior transfection efficiency compared to the homopolymer especially following longer incubation

times when the amount of EGFP positive cells exceeded even LPEI (**Figure 4.5B**, columns). However, the addition of lipoic acid, led only to a slight increase in transfection efficiency compared to the control micelle **BMA-mic**.

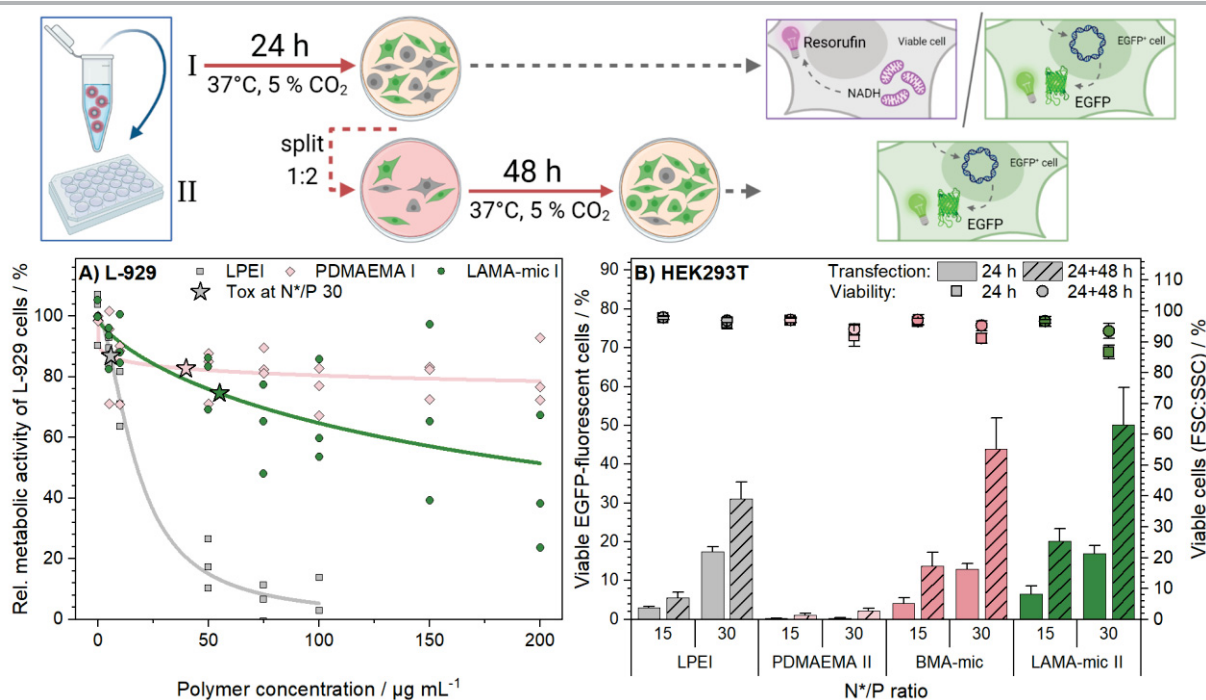


**Figure 4.5. Cytotoxicity and transfection efficiency of methacrylate micelles in standard cell lines.** (A) PrestoBlue assay in L-929 cells following incubation with polymers at indicated concentrations for 24 h. Dots represent values of single repetitions and lines represent logistic fit functions ( $n = 3$ ). Stars indicate polymer/micelle concentrations used for N\*/P 30 in transfection assays. (B) EGFP expression (columns) of viable HEK293T cells was analyzed *via* flow cytometry following incubation with poly-/micelleplexes of pDNA ( $1.5 \mu\text{g mL}^{-1}$ ) and polymers in growth medium either for 24 h (I) or for 24 h followed by splitting of cells and medium and further incubation for 48 h (II, also see scheme above). Viability (dots/squares) was determined according to the FSC:SSC plot of flow cytometry. Values represent mean  $\pm$  SD ( $n = 3$ ).

Subsequently, the transfection efficiency was tested in K-562 suspension cells, which are derived from chronic myeloid leukemia (CML) cells and precursors to erythrocytes. They express a *BCR-ABL* oncogene encoding for the BCR-ABL fusion protein which leads to an altered metabolism within these cells.<sup>[193-194]</sup> In general, suspension/immune cells are considered difficult to transfect, but polymeric nanocarriers could be a promising strategy to interact more efficiently with the cells and enhance the intracellular concentration of active agents to counteract mechanisms such as drug resistance or poor response to treatment.<sup>[195-196]</sup> Moreover, hydrophobic moieties have already been shown to be beneficial for transfecting K-562 cells.<sup>[197-199]</sup>

In the K-562 cells, the addition of *n*BMA to PDMAEMA also led to an increased transfection efficiency whereas the commercial LPEI proved the difficult-to-transfect property of this cell

line (**Figure 4.6A**). By contrast, the efficiency of the **BMA-mic** was even surpassed by the addition of lipoic acid resulting in  $64 \pm 10\%$  transfected cells after incubation for 24+48 h. Remarkably, the **LAMA-mic II** performed even better at a lower N\*/P ratio and thus lower polymer concentration indicating a better efficacy in pDNA binding. Due to these results, the transfection of **LAMA-mic I** was measured in further leukemia cell lines also expressing the *BCR-ABL* oncogene (KCL-22, LAMA-84) and in an acute myeloid leukemia cell line without the oncogene (M07p210, **Figure 4.6B**). Unfortunately, only very few transfected cells and high cytotoxicity were measured pointing towards a non-participation of BCR-ABL in the transfection mechanism of the **LAMA-mic**.

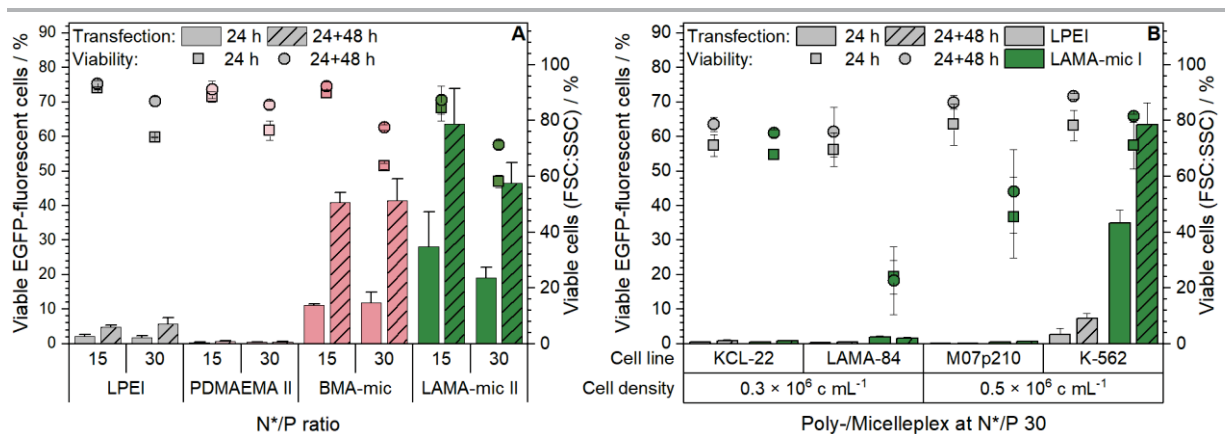


**Figure 4.6. Transfection efficiency of LAMA-mic in leukemia cell lines.** EGFP expression of viable cells was analyzed *via* flow cytometry following incubation of (A) K-562, or (B) further leukemia cells with poly-/micelleplexes of mEGFP-N1 pDNA and polymers in respective growth medium either for 24 h or for 24 h followed by splitting of cells and medium and further incubation for 48 h. Values represent mean  $\pm$  SD ( $n = 3$  for A,  $n \geq 1$  for B). Squares/dots indicate cell viability according to the FSC:SSC plot of flow cytometry.

Therefore, the transfection mechanism of **LAMA-mic** was analyzed regarding the cellular uptake and the endosomal release. To assess the polyplex uptake, K-562 and HEK293T cells were incubated with YOYO-1 labelled polyplexes at N\*/P 30 for different time periods and analyzed *via* flow cytometry regarding the rMFI of all viable single cells (**Figure 4.7A**). Remarkably, no significant differences were observed between the polymers. To the contrary, the uptake patterns of the cell lines were found to be different. In HEK293T cells, a time-dependent uptake was found for all polyplexes, whereas in K-562 cells the uptake reached a constant level after 4 h. The low endocytosis rate by suspension cells was also observed in other studies.<sup>[198, 200]</sup> It may be associated with increased exocytosis, where the polyplexes are removed at a rate comparable to the rate they are taken up.

The endosomal escape was investigated using the calcein release assay (**Figure 4.7B**). The cells were incubated with calcein and polyplexes at N\*/P 30 for different periods of time and were

analyzed *via* flow cytometry. In contrast to the pDNA uptake, the endosomal release showed almost no dependence on the cell line but on the polymer used. In both cell lines the **LAMA-mic** exhibited a significantly better release of calcein ( $p < 0.01$ ), in particular during the first hours (1-4 h) which could be due to an increased membrane interaction of the hydrophobic moieties with the endolysosomal membrane. As these results correlate more with the observed transfection efficiencies than the uptake results, the endosomal escape might be the critical point for the **LAMA-mic**'s efficiency in K-562 cells.

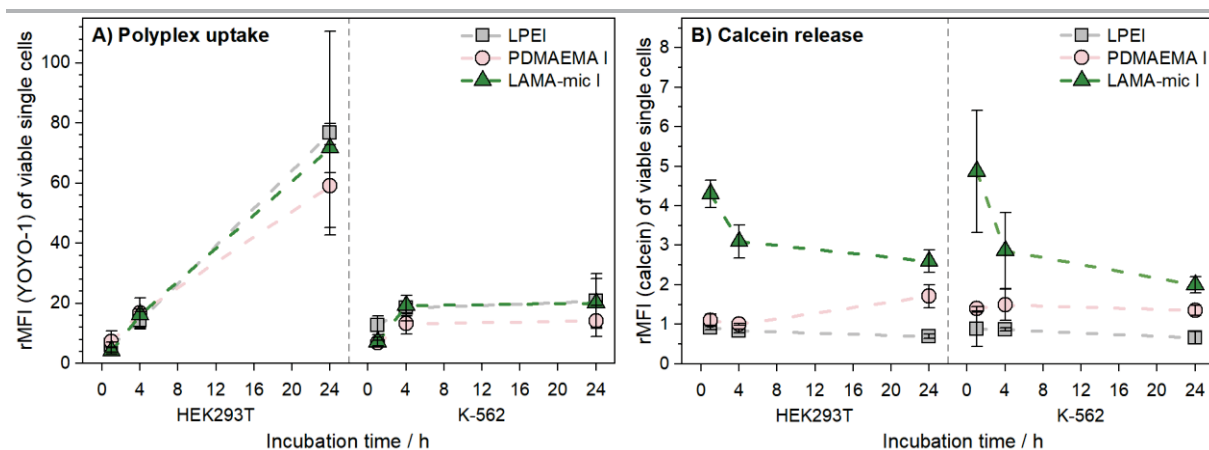


**Figure 4.7. Gene delivery mechanism of LAMA-mic.** (A) Cellular internalization analyzed *via* flow cytometry following incubation of different cell lines with LAMA-mic micelleplexes containing YOYO-1-labeled pDNA at N\*/P 30 in growth medium. Cells incubated with labeled pDNA served as control (rMFI = 1). Values represent mean  $\pm$  SD ( $n = 3$ ). (B) Endosomal escape of LAMA-mic micelleplexes was detected by the non-permeable dye calcein and analyzed *via* flow cytometry relative to the calcein control (rMFI = 1). Values represent mean  $\pm$  SD ( $n = 3$ ).

Additionally to the combination of hydrophobic monomers within block copolymers, cationic and hydrophobic monomers can be copolymerized simultaneously with the result of a random distribution of both moieties throughout the polymer chain. These copolymers can be assembled to spherical 3D-structures (nanoparticles) *via* different formulation methods, such as emulsion/solvent evaporation or nanoprecipitation.<sup>[201]</sup> A well-known example is the Eudragit® E(PO/100), a commercial copolymer of DMAEMA, *n*BMA and methyl methacrylate (MMA). Besides being approved by the Food and Drug Administration (FDA) and the European Medicines Agency (EMA) for the coating of orally administered drugs, it has been studied for the encapsulation of essential oils, drugs and genetic material.<sup>[202-207]</sup> In the study of Solomun *et al.* (**Pub6**), a copolymer with a monomer composition similar to that of Eudragit® E(PO/100) (DMAEMA:*n*BMA:MMA = 2:1:1, PBMD) was used to develop a new green formulation method for the complexation of pDNA without organic solvents. The well-defined **PBMD** polymer with narrow molar mass distribution was synthesized *via* RAFT polymerization and

exhibited a molar mass comparable to the commercial Eudragit® E(PO/100) and to the micelles of the **LAMA-mic** project (Table 4.3, Table 4.2). In contrast to the formulations involving organic solvents (Pub6-Figure 4), narrowly dispersed **PBMD-pDNA complexes** with sizes of about 100 nm were obtained by dissolving the polymer in acetate buffer (0.2 M, pH 5) followed by dilution and mixing with pDNA in HBG buffer (pH 7.4).

**Table 4.3. Characterization data of PBMD.**

Polymer/ Micelle	DP [a]			$M_{n,SEC}$ [b] kg mol <sup>-1</sup>	$\bar{D}$ [b]	Polyplex	
	DMAEMA	nBMA	MMA			Size [c] nm	PDI [d]
<b>PDMAEMA</b>	101	-	-	13.8	1.17	-	-
<b>PBMD</b>	90	45	46	25.1	1.13	98.9	0.22

[a] Determined *via* <sup>1</sup>H NMR spectroscopy.

[b] Determined *via* SEC, eluent: DMAc + 0.21 % LiCl, PMMA standard.

[c] Determination of the hydrodynamic diameter as the z-average *via* DLS at 15 µg mL<sup>-1</sup> pDNA and N\*/P 20 in HBG, pH 7.4.

[d] Determined *via* DLS at 15 µg mL<sup>-1</sup> pDNA and N\*/P 20 in HBG, pH 7.4.

In the combined EBA/HRA assay, the **PBMD** hardly seemed to interact with the pDNA as indicated by the low decrease in the rFI values and only slight changes in the rFI values upon heparin addition (Figure 4.8). But comparable to the results of the previously described methacrylate project, this was disproved by the gel migration assay which demonstrated a complete retention of the pDNA at N\*/P ratios greater than one (Pub6-Figure 2a). This discrepancy illustrates that data obtained by EBA/HRA have to be used with caution but can also provide additional information when combined with the gel migration assay: The high rFI values for the **PBMD-pDNA complexes** despite a strong retention of pDNA point towards an increased hydrophobicity of these complexes, even higher compared to the **LAMA-mic**. Since the **LAMA-mic** contained more hydrophobic monomer units with slightly higher logP values (Figure 4.1), this could be attributed to the different arrangement of the monomers, a different packing of the polymer chains within the complex or a different interaction between the micelle and pDNA.

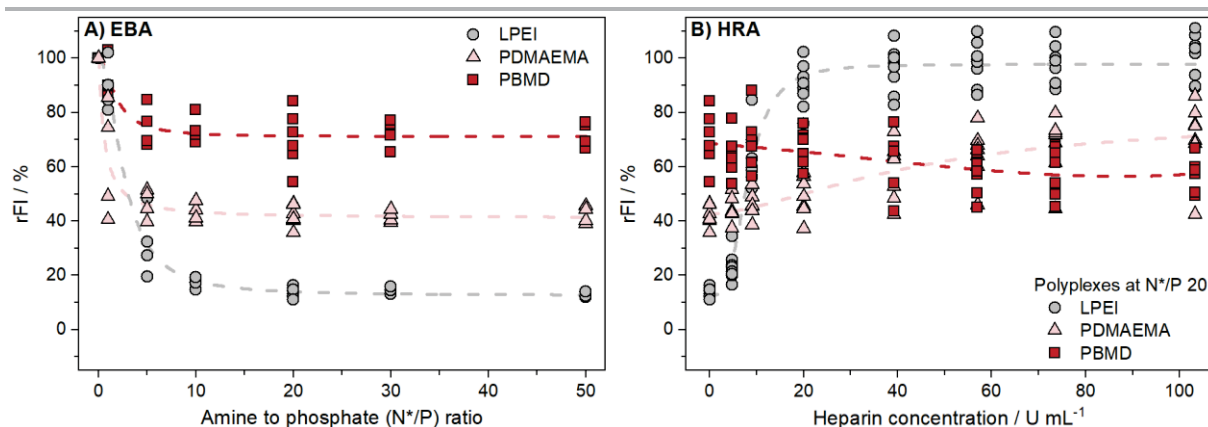


**Figure 4.8. Polyplex formation by PBMD.** (A) EBA at different N\*/P ratios in HBG buffer pH 7.4. (B) HRA of polyplexes at N\*/P 20 in HBG buffer pH 7.4. (A+B) Dots represent individual replicates and lines represent the logistic or exponential fits to the respective data points ( $n \geq 7$ ).

An increased hydrophobicity could also be the reason for the high cytotoxicity of the **PBMD** polymer which was observed in L-929 cells using the PrestoBlue assay (**Figure 4.9A**). Already following incubation for 1 h, the pure polymer was more toxic than the commercial LPEI and a lot more toxic than the **LAMA-mic** measured in the studies above. This could be due to the presence of the hydrophobic moieties throughout the whole polymer solution in contrast to the localization/hiding within the hydrophobic core of the micelle. Hence, they are better accessible for membrane interaction leading to increased cytotoxicity as it was also shown for random and block copolymers of BMA and DMAEMA.<sup>[208]</sup> On the other hand, the **PBMD-pDNA complexes** were also much more efficient compared to LPEI in transfecting HEK293T cells with pDNA encoding for EGFP as indicated by the low pDNA concentration and short incubation times required to obtain high numbers of transfected cells (**Figure 4.9B**). Taking the cytotoxicity measured by the PrestoBlue assay at higher pDNA concentrations and N\*/P ratios into account, the optimal conditions for **PBMD** were  $0.5 \mu\text{g mL}^{-1}$  pDNA at N\*/P 20 for 4+20 h resulting in  $41 \pm 3 \%$  viable transfected cells and more than 75 % viable cells. This is about a fifth of the pDNA concentration required for LPEI to achieve similar transfection efficiency demonstrating the high potential of hydrophobic monomers for transection.



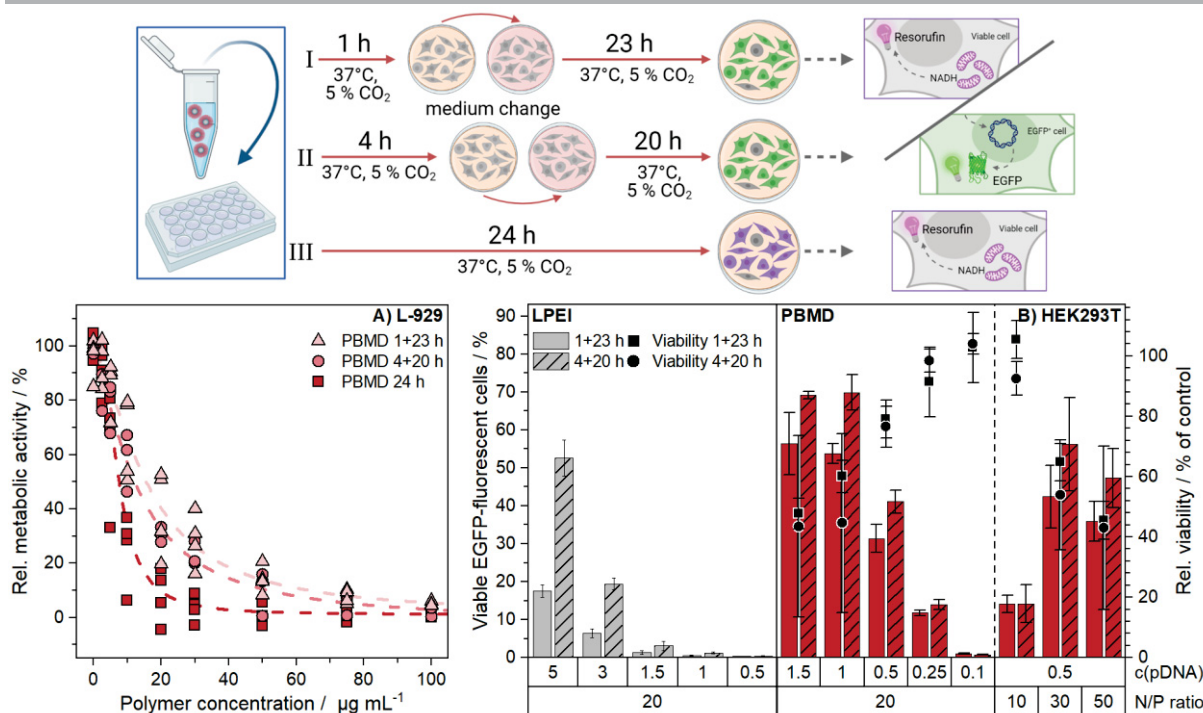


**Figure 4.9. Cytotoxicity and transfection efficiency of PBMD in standard cell lines.** (A) PrestoBlue assay in L-929 cells following incubation with PBMD dissolved in acetate buffer at indicated concentrations for 1, 4 or 24 h followed by medium change and further incubation until 24 h for the shorter incubation periods. Dots represent values of single repetitions and lines represent logistic fit functions ( $n \geq 3$ ). (B) EGFP expression (columns) of viable HEK293T cells was analyzed *via* flow cytometry following incubation with complexes of pDNA at indicated concentrations (in  $\mu\text{g mL}^{-1}$ ) and polymers in growth medium either for 1 h (I) or for 4 h (II) followed by medium change and further incubation until 24 h (see scheme above). Viability of PBMD (dots/squares) was determined by the PrestoBlue assay in HEK293T cells at the same conditions used for transfection assays. Values represent mean  $\pm$  SD ( $n = 3$ ).

All in all, the combination of cationic with hydrophobic monomers to obtain higher ordered 3D structures resulted in two main but contrary effects: increased cytotoxicity and transfection efficiency, which is also called the toxicity-efficiency-dilemma. By using different hydrophobic monomers (LAMA) or a different arrangement of the monomers within the polymer chain (random *vs.* block), the transfection efficiency was additionally tuned for difficult-to-transfect suspension cells (**LAMA-mic**) or for saving costly material (**PBMD**), respectively. It should also be kept in mind that the change in hydrophobicity can influence the results of certain assays (EBA). However, due to the increase in cytotoxicity, the nanocarriers have to be further improved and a more efficient balance between toxicity and efficiency has to be found, *e.g.*, by the incorporation of monomers counteracting the cationic charges which will be discussed in the next chapter.

## 5. Optimizing gene delivery with hydrophilic/anionic monomers

Parts of this chapter have been published in

**Pub7** M. N. Leiske, F. H. Sobotta, F. Richter, S. Hoepfner, J. C. Brendel, A. Traeger, U. S. Schubert, How to tune the gene delivery and biocompatibility of poly(2-(4aminobutyl)-2-oxazoline) by self- and coassembly, *Biomacromolecules* **2018**, 19, 748-760, in

**Pub8** C. Chen, F. Richter, C. Guerrero-Sanchez, A. Traeger, U. S. Schubert, A. Feng, S. H. Thang, A cell penetrating peptide based RAFT agent for constructing penetration enhancers, *ACS Macro Lett* **2020**, 9, 260-265 and in

**Pub4** F. Richter,<sup>‡</sup> K. Leer,<sup>‡</sup> L. Martin, P. Mapfumo, J. I. Solomun, Maren T. Kuchenbrod, S. Hoepfner, J. C. Brendel, A. Traeger, The impact of anionic polymers on gene delivery: how composition and assembly help evading the toxicity-efficiency dilemma, *J. Nanobiotechnol.* **2021**, 19, 292.

Since the addition of hydrophobic to cationic monomers increased not only their transfection efficiency (**Chapter 4**) but also their already high cytotoxicity potential (**Chapter 3**), strategies need to be developed to mitigate toxic side effects without reducing the efficiency. One strategy is the utilization of hydrophilic polymers for the generation of a steric hydration barrier around the micelle to shield the cationic charges and to decrease the interaction with serum proteins, therefore, prolonging circulation times within the blood.<sup>[57-58]</sup> The most prominent and an FDA approved representative is poly(ethylene glycol) (PEG) which has been utilized as a so-called stealth polymer for the delivery of different cargos since the late 1970's.<sup>[57, 209-210]</sup> Thereby, it has been combined not only with polymers but also with proteins and lipids as recently demonstrated in the liposomal mRNA vaccines against SARS-CoV-2.<sup>[211]</sup> However, PEG-containing nanocarriers also have to overcome the toxicity-efficiency dilemma due to a decelerated uptake and an impeded endosomal escape.<sup>[31, 212-213]</sup> Moreover, PEG can cause the formation of anti-PEG antibodies leading to an accelerated blood clearance upon re-administration which could result in the occurrence of allergic reactions or even worse side effects.<sup>[214-218]</sup> Therefore, the search for alternative stealth polymers, such as poly(oxazoline)s (**POx**), poly(oligo(ethylene glycol) methyl ether methacrylate) (**POEGMA**) or **PNAM** has increased within the past years.<sup>[71-72, 210, 217, 219-220]</sup> In this chapter, the combination of cationic-hydrophobic polymers with hydrophilic monomers in different compositions and architectures has been investigated focusing on cytotoxicity, cellular uptake and transfection efficiency (**Figure 5.1**).

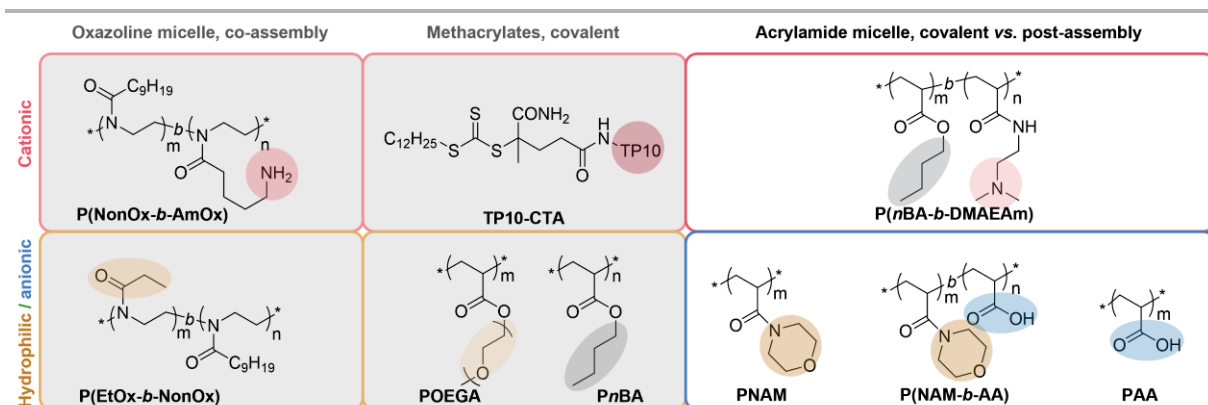


**Figure 5.1.** Schematic overview of the hydrophilic/anionic polymers investigated within this chapter.

In the study of Leiske *et al.* (**Pub7**), the hydrophilic stealth character was introduced by co-assembling hydrophobic-cationic with hydrophobic-hydrophilic **POx** block copolymers. The hydrophobic block was formed by 2-nonyl-2-oxazoline (**NonOx**), whereas 2-ethyl-2-oxazoline (**EtOx**) and 2-(4-aminobutyl)-2-oxazoline (**AmOx**) were utilized for the hydrophilic and cationic blocks, respectively. **P(EtOx<sub>3</sub>-b-AmOx<sub>157</sub>)** was synthesized additionally as a control for a cationic and completely hydrophilic polymer. The well-defined polymers were obtained using the CROP method (**Table 5.1**). For the assembly of mixed micelles, the solvent exchange method was applied after mixing the two hydrophobic-hydrophilic block copolymers at different weight ratios (**Figure 5.2**, scheme). Following dialysis against water, all assemblies exhibited hydrodynamic diameters below 100 nm with higher values for increasing **P(EtOx<sub>155</sub>-b-NonOx<sub>76</sub>)** contents as well as upon complexation with pDNA (**Pub7-Figures 1A, 4D**).

**Table 5.1.** Characterization data of polymers for the POx micelles.

Polymer	DP [a]			$M_{n,SEC}$ [b] kg mol <sup>-1</sup>	$\bar{D}$ [b]
	EtOx	NonOx	AmOx		
<b>P(EtOx<sub>155</sub>-b-NonOx<sub>76</sub>)</b>	155	76	-	38.3	1.14
<b>P(NonOx<sub>52</sub>-b-AmOx<sub>184</sub>)</b>	-	52	184	24.3	1.26
<b>P(EtOx<sub>3</sub>-b-AmOx<sub>157</sub>)</b>	3	-	167	13.5 <sup>[c]</sup>	1.56 <sup>[c]</sup>

[a] Determined *via* <sup>1</sup>H NMR spectroscopy.

[b] Determined *via* SEC, eluent: DMAc + 0.21 % LiCl, PS standard. [c] Eluent: 0.1 M NaCl + 0.3 % TFA, P2VP standard.

Since neither the incorporation of the hydrophobic NonOx nor the hydrophilic EtOx had considerable influence on the interaction between the cationic AmOx and the pDNA (**Pub7-Figure 4A**), the assemblies were tested regarding their cytotoxicity in L-929 cells following incubation for 24 h (**Figure 5.2A**). In this project, the linear cationic polymer **P(EtOx<sub>3</sub>-b-AmOx<sub>157</sub>)** ( $CC_{50} \approx 40 \mu\text{g mL}^{-1}$ ) was about twice as toxic as the cationic micelle **P(NonOx<sub>52</sub>-b-AmOx<sub>184</sub>)** ( $CC_{50} \approx 80 \mu\text{g mL}^{-1}$ ) which contradicts the results described in **Chapter 4**. It can be

explained by the cationic block being about twice as long compared to those in the previous chapter, as it has been shown both in own (**Pub2**, **Pub3**) and in other projects<sup>[53,221]</sup> that toxicity increases with increasing DP of the cationic moiety. Therefore, a higher viability was also observed for cells treated with assemblies containing lower ratios of the cationic micelle **P(NonOx<sub>52</sub>-b-AmOx<sub>184</sub>)**. The CC<sub>50</sub> values were already more than doubled by incorporation of only **20 wt% P(EtOx<sub>155</sub>-b-NonOx<sub>76</sub>)**. This corroborates the shielding effect of the incorporated EtOx observed in previous studies.<sup>[71, 152]</sup> However, incorporation of the hydrophilic EtOx also influenced the transfection efficiency in HEK293T cells (**Figure 5.2B**). Whereas the incubation with micelleplexes of the cationic **P(NonOx<sub>52</sub>-b-AmOx<sub>184</sub>)** demonstrated that the incorporation of only 22 % hydrophobic units (compared to about 50 % in **Chapter 4**) can be enough to achieve about 60 % transfected cells, the mixing with higher ratios of **P(EtOx<sub>155</sub>-b-NonOx<sub>76</sub>)** led to a decrease up to almost no transfection efficiency with **80 wt% P(EtOx<sub>155</sub>-b-NonOx<sub>76</sub>)**. This was further supported by uptake studies following incubation with YOYO-1 labeled micelleplexes for 4 h (**Figure 5.2C**). They showed similar high proportions of YOYO-1 positive cells for nearly all micellar assemblies (> 85 % compared to 60 % transfected cells for linear polymers) but decreasing MFI values with increasing ratios of **P(EtOx<sub>155</sub>-b-NonOx<sub>76</sub>)**. It indicates a lower amount of pDNA present per cell, which could be caused by either fewer micelles entering the cells or less pDNA being transported per micelle due to the incorporation of EtOx. Furthermore, this could be the reason for the decreasing transfection efficiency with increasing amounts of EtOx moieties.

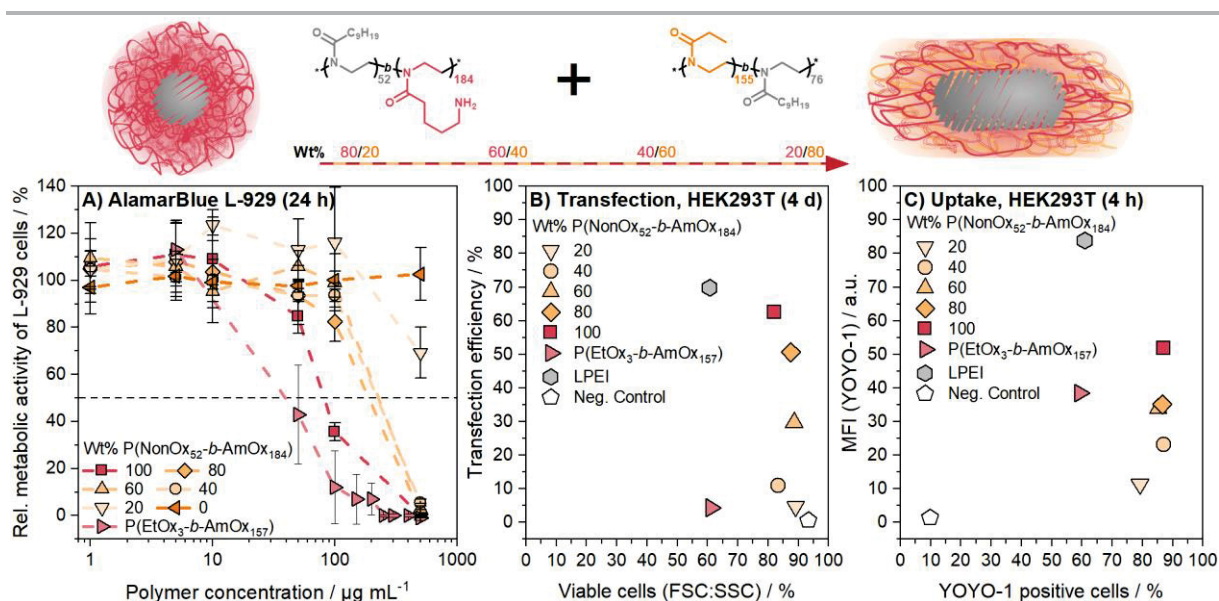


**Figure 5.2. Cytotoxicity and efficiency of POx micelles.** (A) Viability of L-929 cells using the AlamarBlue assay following incubation with polymers at indicated concentrations for 24 h. Values represent mean  $\pm$  SD (n = 3). (B) Transfection efficiency (EGFP expression) vs. cell viability determined via flow cytometry in HEK293T cells following incubation with micelleplexes at N\*/P 50 in growth medium for 4 d. Values represent mean  $\pm$  SD (n = 3). (C) Uptake of YOYO-1 labeled micelleplexes in HEK293T cells following incubation for 4 h. Values represent mean  $\pm$  SD (n = 3).

represent mean  $\pm$  SD (n = 3). (C) Cellular internalization analyzed *via* flow cytometry following incubation of HEK293T cells with micelleplexes containing YOYO-1-labeled pDNA at N\*/P 50 in growth medium for 4 h. Cells incubated with labeled pDNA (YOYO-1) served as control. Values represent mean  $\pm$  SD (n = 3).

Nevertheless, the overall performance (efficiency-toxicity ratio) of the polymers was still improved by combining hydrophobic and hydrophilic moieties with the cationic **PO<sub>x</sub>**, as the transfection efficiency of **20 wt% P(EtOx<sub>155</sub>-*b*-NonOx<sub>76</sub>)** ( $51 \pm 19$  % transfected cells) was still about 80 % of the only cationic micelleplexes' transfection efficiency while the CC<sub>50</sub> values were doubled, hence, the efficiency-toxicity ratio increased (Table 5.2). However, if more than **60 wt% of P(EtOx<sub>155</sub>-*b*-NonOx<sub>76</sub>)** were incorporated, the uptake and the transfection efficiency were rather low indicating that a certain amount of cationic moieties is still needed for a successful transfection process.

**Table 5.2. Hydrophilic to cationic moiety ratios and relative results for PO<sub>x</sub> micelles.**

wt% P(NonOx <sub>52</sub> - <i>b</i> -AmOx <sub>184</sub> )	mass ratio [a]	molar ratio [b]	moiety ratio [c]	% TE [d]	% Tox [e]	TE/Tox ratio [f]
100	-	-	-	100	0	3.5
80	0.25	0.3	0.25	81	-6.7	4.1
60	0.67	0.8	0.67	47	-8.1	2.6
40	1.50	1.8	1.52	18	-1.5	0.7
20	4.05	4.8	4.05	7	-8.7	0.4

[a] Values were calculated: m(mitigating)/m(cationic) polymers.

[b] Values were calculated: n(mitigating)/n(cationic) polymer.

[c] Values were calculated: n(hydrophilic)/n(NH<sub>x</sub>) moieties.

[d] Difference to cationic micelle (100 wt% P(NonOx<sub>52</sub>-*b*-AmOx<sub>184</sub>)) after 4 d was calculated: %EGFP-positive cells(assembly)/%EGFP-positive cells(cationic micelle)\*100.

[e] Difference to cationic micelle (100 wt% P(NonOx<sub>52</sub>-*b*-AmOx<sub>184</sub>)) after 4 d was calculated: 100-(%viable cells<sub>FSC,SSC</sub>(assembly)/%viable cells<sub>FSC,SSC</sub>(cationic micelle)\*100).

[f] Values were calculated: %EGFP-positive cells/(100-%viable cells<sub>FSC,SSC</sub>), TE/Tox for cationic homopolymer was 0.11

The requirement of cationic moieties for successful cellular uptake was also observed in the study of Chen *et al.* (**Pub8**) investigating a new chain transfer agent (CTA) for RAFT synthesis based on the CPP Transportan 10 (TP10), which is well-known for increasing cellular uptake due to the primary amines of its lysine moieties and its  $\alpha$ -helical 3D structure.<sup>[222-224]</sup> The TP10-CTA was utilized for the sequential polymerization of oligo (ethylene glycol) methyl ether acrylate (OEGA) and *n*BA resulting in the block copolymer **TP10-P(OEGA-*b*-*n*BA)**, which was compared to the same block copolymer without TP10. Both polymers were not toxic within the tested concentration range, but the uncharged block copolymer **P(OEGA-*b*-*n*BA)** was slightly more biocompatible (**Figure 5.3A**). However, uptake measurements of cells incubated with rhodamine B labeled polymers showed a lower uptake efficiency into HEK293T cells for

the uncharged block copolymer (< 40 % rhodamine B-positive cells, **Figure 5.3B**). This illustrates the high shielding effect of the hydrophilic OEGA making it suitable for long circulation *in vivo* tests, but it also shows that if higher efficiencies are required, the right balance of hydrophilic and cationic charges must be determined.

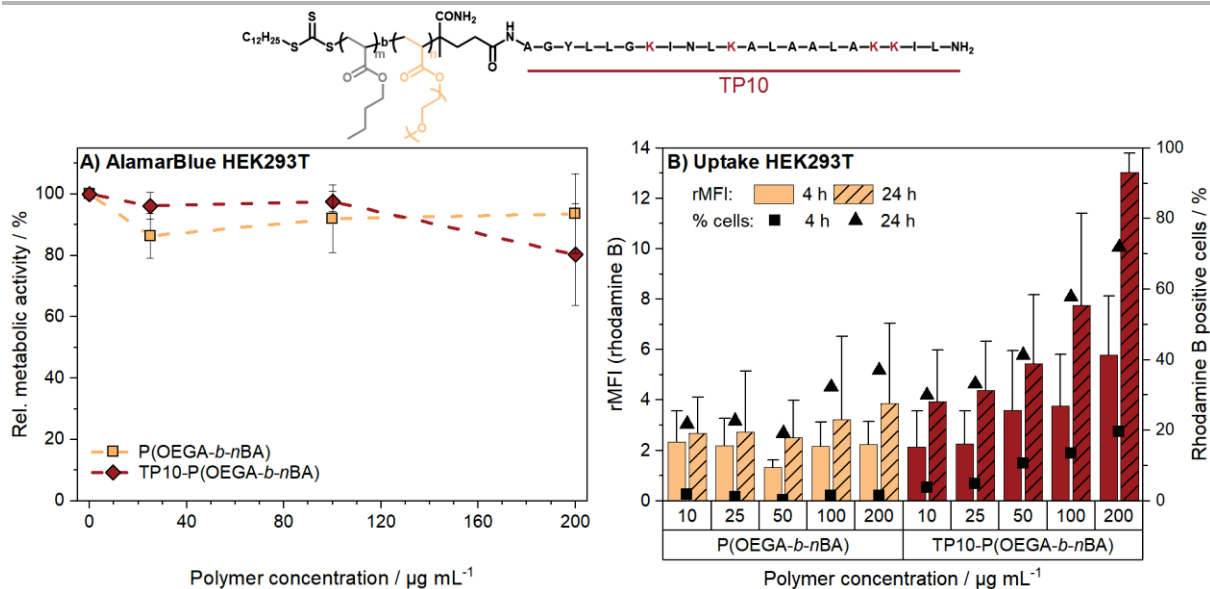


**Figure 5.3. Cytotoxicity and uptake of (TP10) block copolymers.** (A) Viability of HEK293T cells using the AlamarBlue assay following incubation with polymers at indicated concentrations for 24 h. Values represent mean  $\pm$  SD ( $n = 3$ ). (B) Cellular uptake determined *via* flow cytometry in HEK293T cells following incubation with rhodamine B labeled polymers in growth medium. Values represent mean  $\pm$  SD ( $n = 3$ ).

Instead of hydrophilic uncharged moieties, also negatively charged anions can be included within the polymer structure to reduce cytotoxic side effects *via* electrostatic interaction with the cationic moieties. For example, polycarboxylates such as poly(methacrylic acid) (PMAA) have been combined within different nanocarriers, *e.g.*, multicompart ment micelles with a molar mass of  $100,000 \text{ g mol}^{-1}$  resulting in superior performances while maintaining high viability.<sup>[59, 225-227]</sup> The neutralization of cationic charges was also utilized in terms of intra- and interpolyelectrolyte complexes as well as layer-by-layer assembly.<sup>[228-229]</sup> Moreover, both strategies, *i.e.*, uncharged and anionic moieties, can be combined within entirely hydrophilic block copolymers for the application as layer polymers,<sup>[230-231]</sup> which has not been investigated with cationic micelleplexes so far. Therefore, the cationic micelle **HC-mic** (assembled from P(*n*BA-*b*-DMAEAm)) described in **Chapter 4** was utilized to identify the best shielding strategy among four slightly different approaches. Different hydrophilic/anionic polymers, *i.e.*, PNAM (**S**), poly(acrylic acid) (PAA, **A**) or the block copolymer combining both (P(NAM-*b*-AA), **AS**), were added as layer polymers to the **HC-mic** following assembly (or micelleplex formation). Their performance was compared to a triblock terpolymer micelle containing the

anionic PAA as the middle block (P(*n*BA-*b*-AA-*b*-DMAEAm), **HAC-mic** see also scheme in **Figure 5.4A**). Except for the commercial PAA, all polymers were synthesized *via* (sequential) RAFT polymerization resulting in relatively narrow molar mass distributions followed by deprotection of PAA-containing block copolymers with TFA (**Table 5.3**).

**Table 5.3. Characterization data of (protected) polymers for the (layered) PAAm micelles.**

Polymer [a]	$M_{n,th}$ [b] kg mol <sup>-1</sup>	$M_{n,SEC}$ [c]	$\bar{D}$ [c]	Assembly code [d]
P( <i>n</i> BA <sub>80</sub> - <i>b</i> -DMAEAm <sub>90</sub> )	23.3	28.4	1.37	HC
P( <i>n</i> BA <sub>86</sub> - <i>b</i> - <i>t</i> BA <sub>43</sub> - <i>b</i> -DMAEAm <sub>88</sub> )	29.3	34.6	1.26	HAC
PNAM <sub>72</sub> (S)	10.4	8.8	1.12	HC <sup>S</sup>
P(NAM <sub>74</sub> - <i>b</i> - <i>t</i> BA <sub>42</sub> )	16.0	15.2	1.20	HC <sup>AS</sup>
P(NAM <sub>74</sub> - <i>b</i> -AA <sub>42</sub> ) (AS)		17.7 <sup>[f]</sup>	1.26 <sup>[f]</sup>	
PAA (A)	2.0 <sup>[e]</sup>	1.0 <sup>[f]</sup>	1.27 <sup>[f]</sup>	HC <sup>A</sup>

[a] Subscripts indicate degree of polymerization as determined *via* <sup>1</sup>H NMR spectroscopy (before deprotection of *tert*-butyl acrylate (*t*BA) to AA).

[b] Calculated based on  $([M]_0 \times \text{monomer conversion} \times \text{monomer molar mass}) / [\text{CTA}]_0 + \text{CTA molar mass}$

[c] Determined *via* SEC, eluent: DMAc + 0.21 % LiCl, PMMA standard.

[d] Superscripts indicate addition of (deprotected) shielding polymers as a layer following micelle formation.

[e] According to the distributor.

[f] Determined *via* SEC, eluent: 0.08 M Na<sub>2</sub>HPO<sub>4</sub> + 0.05 % NaN<sub>3</sub> (pH 9), PEG standard.

The micelles were assembled *via* the solvent exchange method followed by dialysis against 50 mM sodium acetate buffer (pH 5.0) and their formation was confirmed by cryo-TEM showing a size of  $35 \pm 4$  nm for the **HC-mic** (**Figure 5.4A**). Only a slight increase up to  $43 \pm 6$  nm was observed with the addition of the hydrophilic polymers **A** or **AS** to the **HC-mic** (**HC<sup>AS</sup>**, **HC<sup>A</sup>**) pointing towards negligible interaction between both sides at pH 5. Beyond the increase in total size, an increase in the core size was observed for the **HAC-mic**. This could be attributed to the **PAA**-block being less charged at pH 5 (**Pub4- Figure 2**), and therefore contributing more to the hydrophobic core. DLS/ELS measurements of the different assemblies in acetate-HEPES buffer of pH 5.0 supported the cryo-TEM results (**Figure 5.4B-D**). However, measurements in the same buffer at pH 7.4 led to decreased  $\zeta$ -potential values for **PAA**-containing assemblies which indicates an increased degree of negative charge of the **PAA** block which could hence interact with the cationic charges of the **PDMAEAm** block. Apparently, this interaction also increased the hydrophobicity, possibly through neutralization of the **PDMAEAm** block (60 % charged at pH 7.4 minus 50 % anionic charges at a COOH/NH ratio of 0.5, **Pub4- Figure 2**) leading to the formation of aggregates. Interestingly, this could be avoided in the **HC<sup>AS</sup>** assembly by adding another uncharged hydrophilic block resulting in stable micelles even at neutral  $\zeta$ -potential. Furthermore, the successful complexation with

pDNA before the addition of the layer polymers also resulted in an increase in hydrophilicity and thus no formation of aggregates (**Pub4- Figure 4**).

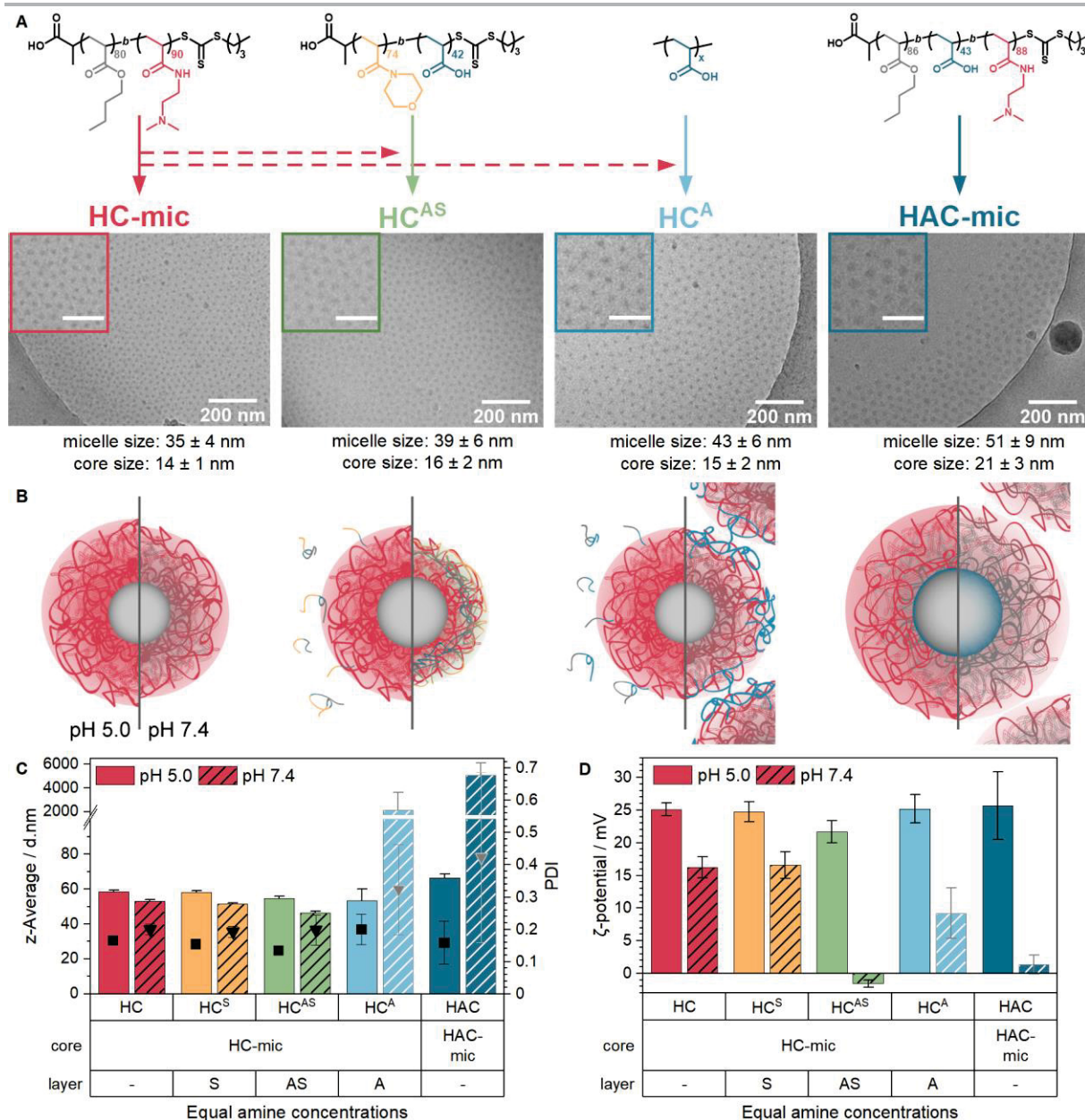


**Figure 5.4. Characterization of (layered) micelles at different pH values.** (A) Polymer structures and cryo-TEM images of HAC-mic, HC-mic and HC-mic layered with PAA (A) or P(NAM-*b*-AA) (AS) at pH 5. Scale bars in insets represent 100 nm. (B) Schematic representation of (layered) micelles at pH 5.0 and 7.4 (left and right side, respectively) (C+D) DLS (C) and ELS (D) measurements of (layered) micelles at equal amine content in acetate-HEPES buffer of pH 5.0 or 7.4. Values represent mean  $\pm$  SD ( $n = 2$ ) of z-average (columns), PDI (triangles) or  $\zeta$ -potential (columns). Bright/gray shades indicate formation of aggregates.

In the standard PrestoBlue assay measuring the metabolic activity of HEK293T cells (**Figure 5.5A**), the addition/incorporation of PAA led to a reduction of the HC-mic's cytotoxicity and a complete restoration of cell viability when NAM was added. Interestingly, the cells were more viable when the anionic block was incorporated into the micelle (HAC-mic) compared to the



addition after micelleplex formation (**HC<sup>A</sup>**) pointing towards a weaker interaction between **HC-mic** and **PAA**. Nevertheless, the anionic charge of **PAA** seems to be required for the reduction in cytotoxicity, since the addition of pure PNAM (**HC<sup>S</sup>**) did not show any effect on the **HC-mic**'s performance and could, therefore, be considered as a co-incubation rather than a layering of the micelle. Although the same trends were also observed in other assays measuring membrane integrity (LDH-release) or cell morphology (flow cytometry), the differences were not as great (**Figure 5.5B, C**). This indicates that the cytotoxicity of the **HC-mic** affects the vitality inside the cells rather than through the plasma membrane.

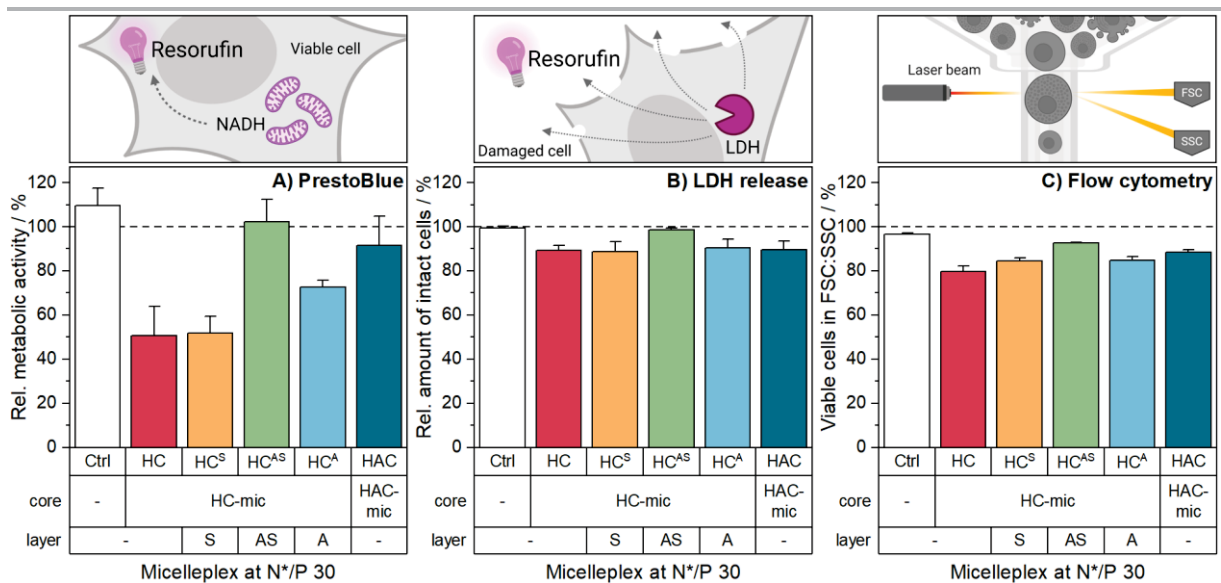


**Figure 5.5. Cytotoxicity of (layered) micelleplexes (N\*/P 30, 24 h) in HEK293T cells.** The viability of the cells was investigated using (A) the PrestoBlue assay for metabolic activity, (B) the LDH release assay, or (C) flow cytometry with gating for viable cells in the FSC:SSC plot. Cells treated with pDNA only served as control. Values represent mean  $\pm$  SD (n = 3).

Due to the toxicity-efficiency dilemma, an increase in cell viability usually correlates with a loss in efficiency. Strikingly, the high amount of EGFP-expressing HEK293T cells observed for the **HC-mic** (up to  $95 \pm 4$  % cells) was only slightly affected by the incorporation/addition of purely anionic blocks (**HC<sup>A</sup>**, **HAC-mic**) or pure PNAM (**HC<sup>S</sup>**), especially following longer incubation times (**Figure 5.6A**). Furthermore, the difference in the amount of EGFP-positive cells between **HC<sup>A</sup>** and **HAC-mic** also decreased with increasing incubation time from 30 to 1 percent points. A slightly higher influence of the anionic blocks on the efficiency was only observed for the rMFI values of the viable single cells pointing towards a slightly lower amount of EGFP protein present within the cells compared to the **HC-mic** (**Figure 5.6B**).

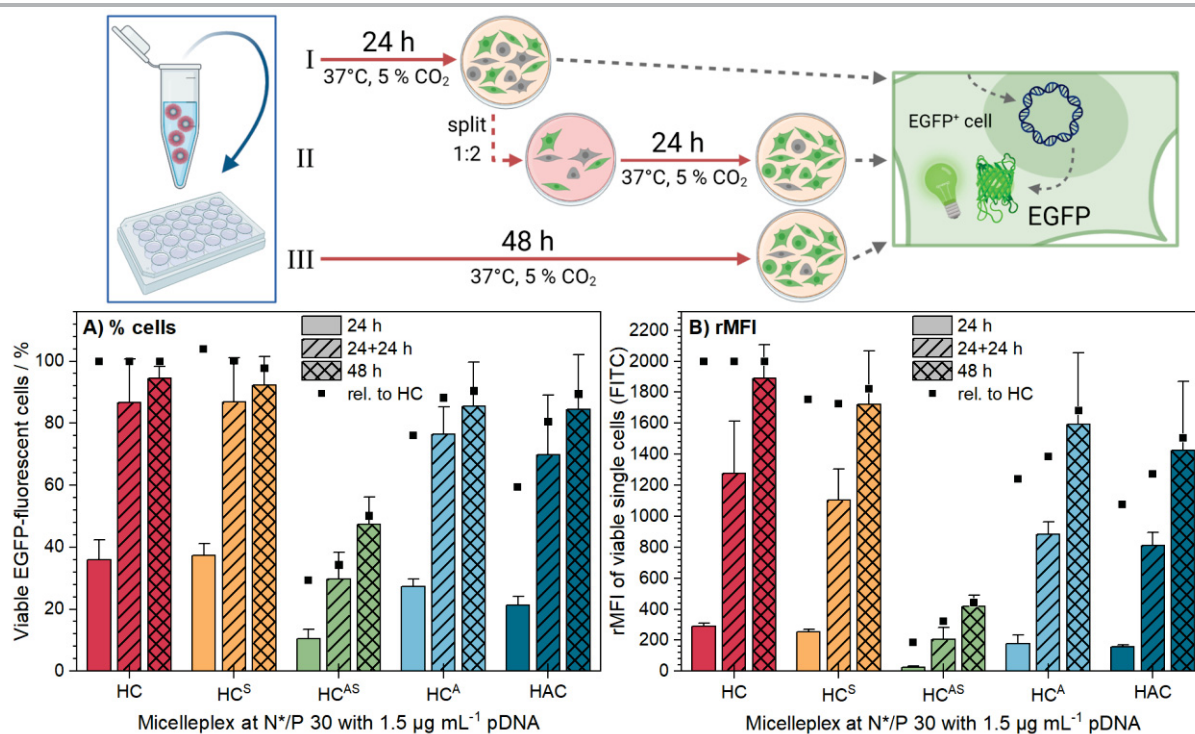


**Figure 5.6. Transfection efficiency of (layered) micelleplexes.** EGFP expression was determined *via* flow cytometry in HEK293T cells following incubation in growth medium for 24 h (I), for 24 h followed by splitting of cells and medium and further incubation for 24 h (II), or for 48 h (III). Values represent mean  $\pm$  SD ( $n = 3$ ) of (A) viable, single EGFP positive cells, and (B) rMFI of all viable single cells relative to cells treated with polyplexes of pKMyC pDNA and polymers. Squares indicate values calculated relative to the HC-mic treatment of the respective time point to illustrate the differences more clearly.

For the **HC<sup>AS</sup>** assembly combining both shielding blocks a sharp decrease by about 50 percent points of the **HC-mic**'s transfection efficiency was observed. With the highest ratio of mitigating (anionic and hydrophilic stealth) to amine moieties, the **HC<sup>AS</sup>** was also the only assembly of the PAAm micelles decreasing the efficiency-toxicity ratio of the **HC-mic** (Table 5.4). Although the **HC<sup>S</sup>** assembly had the second highest ratio of hydrophilic uncharged to amine moieties which was also well in the range of some POx micelles (see Table 5.2), its effect on transfection efficiency and toxicity of the **HC-mic** was negligible. Intriguingly, the anion containing assemblies **HC<sup>A</sup>** and **HAC-mic** could increase or nearly double the efficiency-toxicity ratio compared to the **HC-mic**, although their ratio of mitigating to amine moieties is also comparable to some POx micelles. This could be due to the anionic charge being pH dependent and partially removed inside the endolysosome, thereby releasing the cationic charges. Therefore, in addition to the amount of mitigating moieties, two further parameters might affect the shielding performance: i) the combination method of shielding and cationic moiety and ii) the type of the mitigating moiety. Concerning the first, simple co-incubation as it is assumed for the **HC<sup>S</sup>** assembly is apparently not sufficient to hide the cationic charges.

Instead, the required spatial proximity can be achieved by coassembly of hydrophobic-cationic and hydrophobic-hydrophilic block copolymers (POx mixed micelles), by electrostatic interaction (AS- or A-layered HC micelles) or by incorporation within the same polymer chain (HAC-mic). Regarding the type of the mitigating moiety, the still high transfection efficiency of the anion containing assemblies compared to the POx-micelles might be due the anionic charge being pH dependent providing further functionality inside the endolysosome.

**Table 5.4. Hydrophilic/anionic to cationic moieties and relative results for PAAm micelles.**

PAAm-mic	mass ratio [a]	molar ratio [b]	moiety ratio [c]	% TE [d]	% Tox [e]	TE/Tox ratio [f]
HC	-	-	-	100	0	7.5
HC <sup>S</sup>	0.45	1	0.8	98	-1.3	8.1
HC <sup>AS</sup>	0.63	1.07	0.5+0.9	50	-6.7	7.1
HC <sup>A</sup>	0.14	1.61	0.5	90	-4.4	9.8
HAC-mic	1	1	0.5	89	-6.7	12.6

[a] Values were calculated: m(mitigating)/m(cationic) polymers.

[b] Values were calculated: n(mitigating)/n(cationic) polymer.

[c] Values were calculated: n(COOH)/n(NH<sub>x</sub>) or n(hydrophilic)/n(NH<sub>x</sub>) moieties. HC<sup>AS</sup>: values for AA+NAM monomers.

[d] Difference to cationic micelle (HC-mic) after 48 h was calculated:

%EGFP-positive cells(assembly)/%EGFP-positive cells(cationic micelle)\*100.

[e] Difference to cationic micelle (HC-mic) after 48 h was calculated:

100-(%viable cells<sub>FSC:SSC</sub>(assembly)/%viable cells<sub>FSC:SSC</sub>(cationic micelle)\*100).

[f] Values were calculated: %EGFP-positive cells/(100-%viable cells<sub>FSC:SSC</sub>), TE/Tox for cationic homopolymer was 0.11

Hence, the uptake of YOYO-1 labeled micelleplexes and their endosomal release of calcein within the cell were investigated to elucidate the transfection process in more detail. Again, pure PNAM (HC<sup>S</sup>) had no or only slight influence on the HC-mic's performance supporting the hypothesis of lacking interaction between both polymers. Interestingly, different uptake trends were observed after different incubation times (**Figure 5.7B**). Following incubation for 1 h, the HC-mic was taken up by a higher number of cells ( $35 \pm 7\%$  YOYO-1 positive cells) than the PAA containing assemblies (about 20 % YOYO-1 positive cells). However, the similar rMFI values point towards a higher amount of pDNA present per cell for the latter assemblies. Interestingly, after 24 h, only a difference in the rMFI values was observed between the HC-mic and the PAA containing assemblies. Taken together, this indicates a moderate retardation of the uptake process by the incorporation/addition of PAA but at the same time a similarly or even more efficient transport of pDNA per micelle compared to the HC-mic. It was further supported by CLSM studies showing a slightly higher number of polyplexes per cell for the HAC-mic following incubation for 1 h already (**Figure 5.7A, Pub4- Figure S20B**). Therefore,

the uptake process might not be the reason for the slightly decreased EGFP fluorescence of cells treated with  $\text{HC}^{\text{A}}$  or the  $\text{HAC-mic}$ .

By contrast, the  $\text{HC}^{\text{AS}}$  assembly led to decreased values for both parameters which was also supported by the CLSM studies (Figure 5.7A). The % cells values of the other assemblies were only approached by the  $\text{HC}^{\text{AS}}$  assembly following the 24 h incubation rendering the  $\text{HC}^{\text{AS}}$  assembly a promising candidate for applications requiring prolonged circulation times. Similarly to the results for the mixed  $\text{POx}$  micelles (Figure 5.2C), the decreased rMFI values for the  $\text{HC}^{\text{AS}}$  assembly could indicate a less efficient transport of pDNA per micelle or less micelles per cell. With the CLSM images showing not only less polyplexes per cell for the  $\text{HC}^{\text{AS}}$  assembly but also a smaller diameter of the YOYO-1 fluorescent dots which could point towards a lower amount of pDNA in this spot, a combination of both reasons could be conceivable.

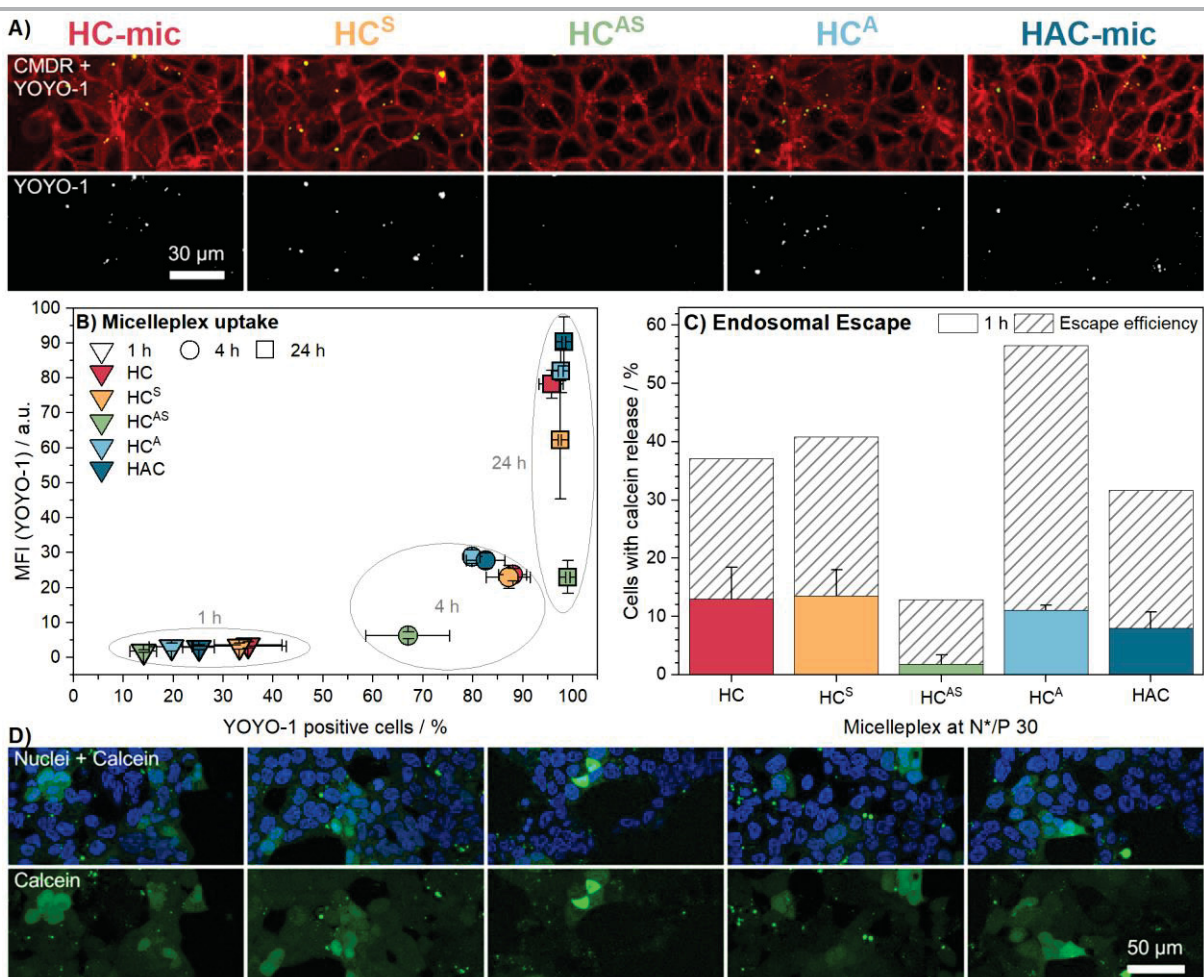


**Figure 5.7. Gene delivery process of (layered) micelleplexes.** (A+B) Cellular uptake of polyplexes in HEK293T cells, incubated with (layered) micelleplexes containing YOYO-1-labeled pDNA (green) and analyzed *via* CLSM (A) or flow cytometry (B). For CLSM, incubation time was 1 h followed by co-staining of plasma membrane and membrane associated organelles with CellMask Deep Red (CMDR, red). Cells incubated with labeled pDNA served as control (rMFI = 1). Values represent mean  $\pm$  SD. (C+D) Endosomal

escape was analyzed *via* CLSM following simultaneous incubation with the non-permeable dye calcein (green) and (layered) micelleplexes for 1 h. Cell nuclei were stained with Hoechst 33342 (blue). Values in (B) were obtained by image analysis of all acquired images using ImageJ and represent mean  $\pm$  SD ( $n = 3$ ). Shaded columns represent the proportion of cells with calcein release divided by the proportion of YOYO-1 positive cells at the same time point (in percent).

---

The decrease of the **HC-mic**'s efficiency due to the addition of the **AS** block copolymer was further observed in the calcein release assay (**Figure 5.7B, C**), whereas the **PAA** containing assemblies only slightly decreased the calcein release. To consider different uptake efficiencies of the assemblies, the escape efficiency was calculated by normalization of the calcein release assay results to the uptake efficiency at the same incubation time. Thereby, the difference between **HC-mic** and **HAC-mic** could be decreased to about 25 percent points, whereas the **HC<sup>A</sup>** assembly was by about 50 percent points better than the **HC-mic**. This could be due to the presence of the **PAA** outside the micelleplex in the **HC<sup>A</sup>** assembly leading to an easier unmasking of the cationic charges and an increase in molecule concentration upon endolysosomal pH decrease which in turn results in slightly higher transfection efficiency compared to the **HAC-mic**.

In conclusion, the three projects showed that incorporation of mitigating (hydrophilic uncharged or negatively charged) monomers inevitably leads to the confrontation with the toxicity-efficiency dilemma and that a certain amount of cationic moieties is required for higher efficiencies (**TP10-P(OEGA-*b-n*BA)**). But it was also demonstrated that different settings can be optimized to still obtain efficient assemblies for gene delivery and to fine-tune the performance for the respective application. One prominent parameter is certainly the ratio of the cationic and the anionic/hydrophilic moieties. If this balance is optimized, the toxicity can be shifted to higher concentrations and high transfection efficiencies can be maintained as it was the case for **POx** mixed micelles containing only **20 wt% P(EtOx<sub>155</sub>-*b*-NonOx<sub>76</sub>)** or the **HAC-mic** and **HC<sup>A</sup>** assembly. Furthermore, the combination method of shielding and cationic moiety (mixed micelles, covalent or electrostatic interaction), and the type of the mitigating moiety (hydrophilic or anionic) can be optimized to achieve high efficiency-toxicity ratios. Regarding the latter, the shielding effect by hydrophilic uncharged moieties seemed to be stronger and also affected the transfection efficiency whereas the anionic shielding still led to high transfection values, probably due to the pH dependent anionic charge releasing the cationic charges inside the endolysosome. Eventually, the stealth effect of mitigating monomers could even purposefully be exploited for applications requiring long circulation times or a targeted transport of the cargo to particular organs.

## 6. Summary

The targeted delivery of nucleic acids is a powerful tool for the treatment of health issues, such as genetic disorders and cancer, or for the prevention of viral infections through vaccination. Since naked nucleic acids are readily accessible to enzymatic degradation and only inefficiently reach their point of destination, protective materials are required for their successful delivery. The optimal gene delivery material should show low cytotoxicity, form stable complexes with nucleic acids, exhibit low interaction with serum proteins, transfer their cargo to the desired cells, enable endosomal escape and finally ensure its activity inside the cells.

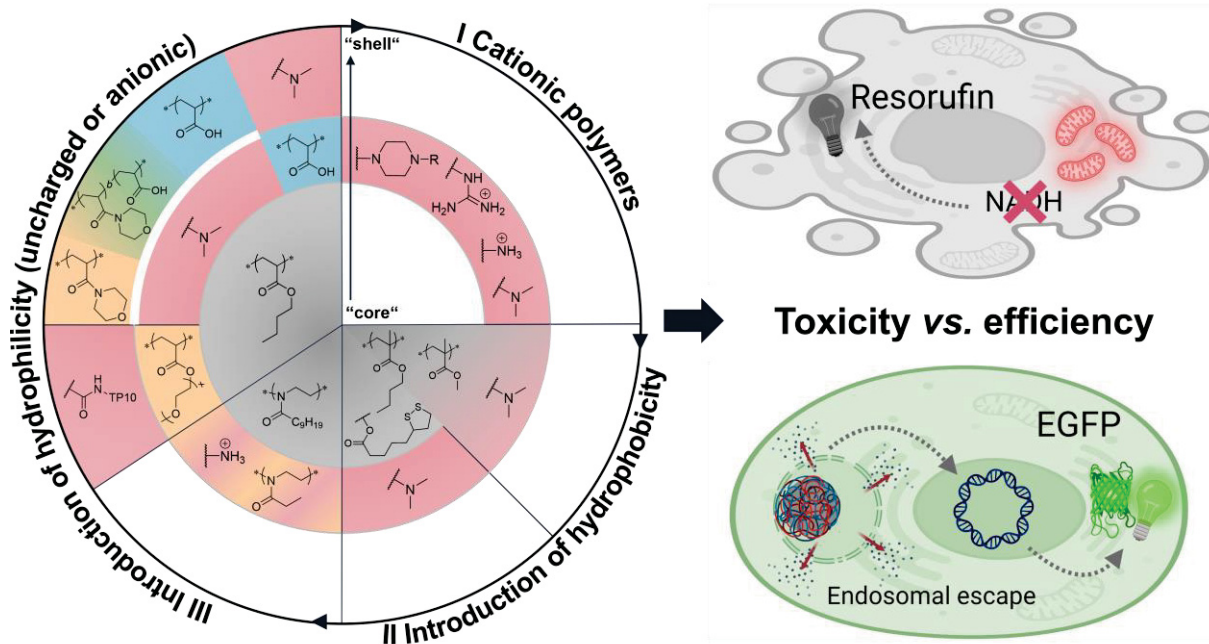


**Figure 6.1.** Schematic depiction of the monomer composition of polymers investigated in this work regarding their gene delivery efficiency. Partially created with BioRender.com.

Polymeric delivery materials represent a promising approach due to their controlled synthesis, increased stability and simple combinability of different components allowing for the introduction of responsiveness to different stimuli. The most prominent representatives of cationic polymers used for gene delivery are polyethyleneimine (PEI) and poly(2-(dimethylamino)ethyl methacrylate) (PDMAEMA), whose different types of cationic amines facilitate not only the complex formation with pDNA (polyplexes) through electrostatic interaction with the anionic phosphate backbone of the nucleic acids but also mediate the endosomal escape following endocytic uptake due to their increased buffer capacity within the physiological pH range leading to high transfection efficiencies. Nevertheless, cationic polymers also face cytotoxicity issues due to the cationic charges interacting with and/or disrupting the cellular membrane. Therefore, this thesis aims at finding strategies to optimize

the efficiency-toxicity ratio of cationic polymers with a special focus on their endosomal escape as the most crucial barrier of the transfection process (**Figure 6.1**).

Due to the flexibility for different functional pendant groups and the controlled synthesis, vinyl polymers obtained by reversible addition-fragmentation chain transfer (RAFT) polymerization are well-suited for structure-property-relationship studies. As there are only few studies examining the influence of different types of cationic moieties on the gene delivery process, poly(amino alkyl acrylamides) (PAAm) were utilized for the first time to comparatively screen primary and tertiary amines as well as the pH independent guanidinium moiety well-known from the amino acid arginine and cell penetrating peptides (CPP). The tertiary amines were further compared to a poly(*N*-acryloyl piperazine) (PNAP) library whose amines were hydrophobically modified by different alkyl groups. Due to the different amine functionalities, the homopolymers possessed different  $pK_a$  values leading to different degrees of charge within the physiologically relevant pH range. The PAAms were nearly completely positively charged at pH 7.4 with the exception of poly(dimethylaminoethyl acrylamide) (PDMAEAm). By contrast, the PNAPs reached only a maximum of 30 % of positively charged amines at pH 7.4 which increased up to 100 % upon a decrease to pH 5.0, indicating a stronger pH sensitivity for the PNAPs compared to the PAAms. These differences were also reflected in the subsequent cellular studies showing a positive correlation of increased cytotoxicity, membrane interaction and endosomal escape in serum-reduced medium with a high degree of charge at the respective pH value (pH 7.4: cytosol, toxicity/membrane interaction; pH 5-6: endosome). With the highest  $pK_a$  ( $> 12$ ), the guanidinium functional poly(guanidinopropyl acrylamide) (GPAm) exhibited the highest endosomal escape, followed by the primary and tertiary amine functional PAAms. Remarkably, the endosomal escape of the PNAPs was comparable or even slightly higher compared to the tertiary amine PAAms which can be explained by the increased polymer concentration utilized for the PNAPs compensating their decreased degree of charge. Regarding the escape mechanism, the “proton-sponge” theory can be assumed for the PNAPs but not for all PAAms, since they are not as pH sensitive. In a lipid binding assay, all PAAms were shown to interact with bis(monoacryloylglycerol) phosphate (BMP), a lipid found in intra late endosomal vesicles (ILEVs), with PGPAm showing the highest levels. As this has also been shown for arginine containing CPPs but not for polymers before, the disruption of the endolysosomal membrane *via* interaction with BMP, hence, represents a possible escape mechanism. Nevertheless, further studies are required to confirm this hypothesis, *e.g.*, regarding the influence on the integrity of BMP containing liposomes, the colocalization of PGPAm with endo- or lysosomes or a proof of the PGPAm-BMP interaction within cells.

Although all cationic homopolymers have been shown to escape the endolysosomal pathway in the calcein release assay, their efficiency was still improvable, in particular in serum containing medium. To increase the efficiency of cationic polymers, their combination with hydrophobic moieties either random or in form of block copolymers is a common alternative resulting in the formation of different 3D architectures. Herein, the low efficiency tertiary amines containing homopolymers PDMAEAm and PDMAEMA (at DP 100) were combined with the well-known *n*-butyl acrylate (*n*BA) or *n*-butyl methacrylate (*n*BMA), respectively, either as block or as random copolymers. Furthermore, the monomer lipoic acid methacrylate (LAMA) containing the redox-sensitive essential fatty acid lipoic acid was incorporated additionally since its benefit has been shown before, *i.a.*, in micelles for drug delivery or as hydrophobic modification of PEI for pDNA delivery. While the block copolymers P(*n*BA-*b*-DMAEAm) and P(DMAEMA-*b*-[*n*BMA-*co*-LAMA]) were assembled *via* solvent exchange into micelles with diameters of about 50 nm (HC-mic, LAMA-mic), the random copolymer P(*n*BMA-*co*-MMA-*co*-DMAEMA) formed polyplex nanoparticles (PBMD) of about 100 nm upon aqueous complexation with pDNA. The different assemblies were investigated regarding their micelle-/polyplex formation, cytotoxicity, and transfection efficiency. In all cases, the incorporation of hydrophobic moieties had negligible influence on pDNA complexation, but substantially increased the transfection efficiency in HEK-293T cells even in serum containing medium. Especially the PBMD polyplex convinced with higher efficiencies than LPEI at very low pDNA and polymer concentrations as well as shorter incubation times, hence, saving costly time and material. Moreover, the LAMA-mic also transfected difficult-to-transfect K-562 suspension cells derived from chronic myeloid leukemia (CML), particularly following longer incubation times, whereas LPEI and the cationic homopolymer elicited only few transfected cells. The transfection mechanism was shown to be independent of the expression of the oncogene *BCR-ABL* and the micelleplex uptake but could be promoted by a higher and faster endosomal escape as shown in the calcein release assay. Also, the lipoic acid was beneficial but apparently not the only factor responsible for the high transfection efficiency in K-562 cells, as demonstrated by comparison with a similar micelle without the LAMA monomer (BMA-mic).

Nevertheless, the addition of hydrophobic to cationic monomers increased not only their transfection efficiency but also their already high cytotoxicity potential, requiring further strategies to mitigate the toxic side effects and increase the efficiency-toxicity ratio. Commonly, hydrophilic “stealth” polymers such as poly(ethylene glycol) (PEG) and its alternatives poly(oxazoline)s (POx), poly(oligo(ethylene glycol) methyl ether acrylate) (POEGA) or poly(*N*-acryloylmorpholine) (PNAM) are utilized to provide a steric hydration barrier around the toxic moieties. Furthermore, negatively charged anions such as polycarboxylates have been

46



included to reduce cytotoxic side effects *via* electrostatic interaction with the cationic moieties. Herein, mixed micelles assembled from POx block copolymers of 2-nonyl-2-oxazoline (NonOx) and either the cationic 2-(4-aminobutyl)-2-oxazoline (AmOx) or the hydrophilic 2-ethyl-2-oxazoline (EtOx) were utilized to determine the optimal amount of P(EtOx-*b*-NonOx) for the best efficiency-toxicity ratio. Furthermore, a block copolymer of the hydrophilic OEGA and *n*BA was utilized to investigate the performance of a Transportan 10 (TP10)-containing chain transfer agent (CTA). Finally, the already described HC-mic was utilized to investigate the influence of hydrophilic, anionic or both moieties on the efficiency-toxicity ratio using PNAM (HC<sup>S</sup>), poly(acrylic acid) (PAA, HC<sup>A</sup>), and P(NAM-*b*-AA) (HC<sup>AS</sup>), respectively, as layer polymers which were further compared to a triblock terpolymer micelle containing PAA as the middle block (HAC-mic). The three projects showed that three different factors influence the effect of mitigating moieties on the efficiency-toxicity ratio of cationic polymers: i) the ratio of the cationic and the anionic/hydrophilic moieties, ii) the combination method of shielding and cationic moiety (mixed micelles, covalent or electrostatic interaction), and iii) the type of the mitigating moiety (hydrophilic uncharged or anionic). If these factors are optimized, the toxicity can be shifted to higher concentrations while high transfection efficiencies are maintained as it was the case for POx mixed micelles containing only 20 wt% P(EtOx<sub>155</sub>-*b*-NonOx<sub>76</sub>) or the HAC-mic and HC<sup>A</sup> assembly. Intriguingly, in contrast to hydrophilic uncharged moieties, the anionic moieties still allow for superior transfection efficiencies while reducing the cytotoxicity. Nevertheless, strongly shielding polymers such as P(NAM-*b*-AA) could be applied for long circulation times or targeted gene delivery.

All in all, the presented work illustrates the high suitability of cationic polymers for gene delivery with special emphasis on preformed cationic micelles. The high potential of polymers has been demonstrated in structure-activity-relationship studies regarding their performance at different barriers of the gene delivery process such as the endosomal escape. Moreover, due to their straightforward synthesis and easy combinability of different functional moieties, it was shown that polymers can be optimized in different parameters towards high cell viability (mitigating moieties) while maintaining superior gene delivery efficiency (hydrophobic moieties). Hence, they represent promising tools for future gene therapy and further (*in vivo*) studies are now required to transfer these results to humans. Methods such as artificial intelligence and high-throughput synthesis/characterization can support this in the future by facilitating the transfer of knowledge towards other polymers, more substantial comparisons of different polymers, and faster development of suitable gene delivery materials for different diseases.

## 7. Zusammenfassung

Der zielgerichtete Transfer von Nukleinsäuren ist eine vielversprechende Technologie für die Behandlung verschiedenster genetischer, Immun-, oder Krebserkrankungen. Da Nukleinsäuren für den enzymatischen Abbau leicht zugänglich sind und dadurch nur ineffizient ihren Bestimmungsort erreichen, müssen sie für einen erfolgreichen Transfer mit schützenden Materialien komplexiert werden. Optimale Materialien für den Gentransport sollten dabei nicht toxisch sein, stabile Komplexe mit den Nukleinsäuren bilden, eine geringe Wechselwirkung mit Serumproteinen aufweisen, den Transport zu den gewünschten Zellen sowie die endosomale Freisetzung ermöglichen und schließlich die Aktivität der Nukleinsäuren innerhalb der Zellen gewährleisten.

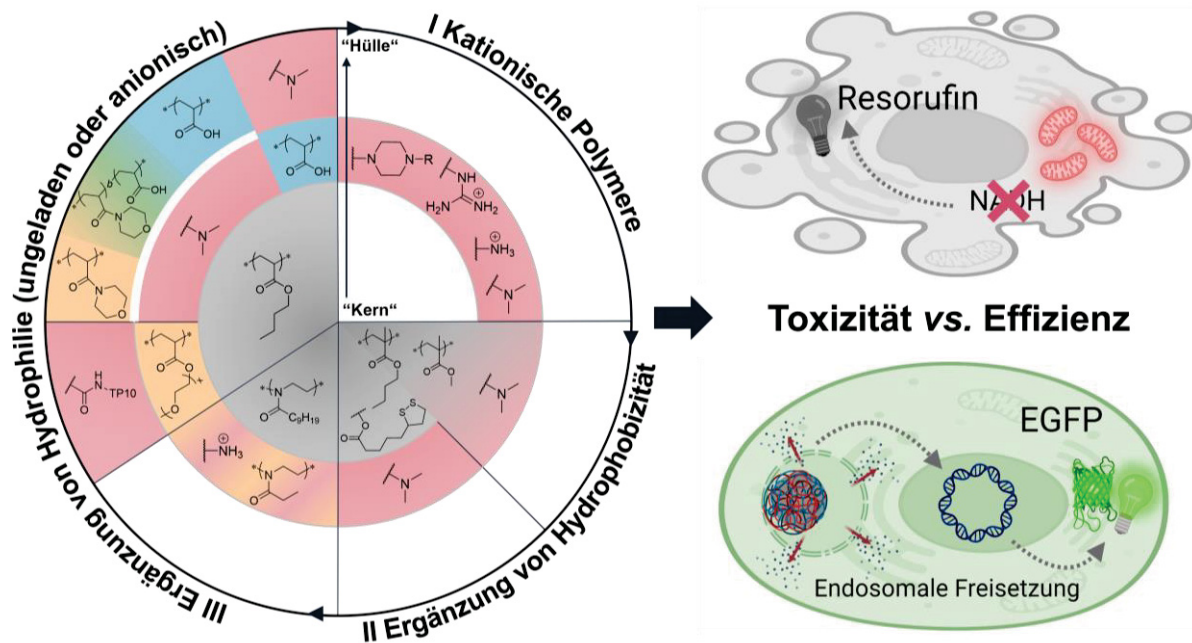


Abbildung 7.1. Schematische Darstellung der Monomerzusammensetzung der in dieser Arbeit auf ihre Effizienz bei der Genübertragung untersuchten (Co)Polymere. Teilweise erstellt mit BioRender.com.

Polymermaterialien stellen aufgrund ihrer kontrollierten Synthese, ihrer erhöhten Stabilität und der einfachen Kombinierbarkeit verschieden funktioneller Einheiten einen vielversprechenden Ansatz dar. Die bekanntesten Vertreter der kationischen Polymere für den Gentransfer sind Polyethylenimin (PEI) und Poly(2-(dimethylamino)ethylmethacrylat) (PDMAEMA), deren verschiedene kationische Amine die Komplexbildung mit pDNA durch elektrostatische Wechselwirkung mit dem anionischen Phosphatrückgrat der Nukleinsäuren erleichtern. Aufgrund ihrer erhöhten Pufferkapazität im physiologischen pH-Bereich vermitteln sie zudem die endosomale Freisetzung, wodurch hohe Transfektionseffizienzen erreicht werden können. Kationische Polymere erhöhen jedoch auch die Zytotoxizität, da die kationischen Ladungen mit

der Zellmembran interagieren und diese zerstören. Ziel dieser Arbeit war daher die Untersuchung von Strategien zur Optimierung des Effizienz-Toxizitäts-Verhältnisses kationischer Polymere unter besonderer Beachtung der endosomalen Freisetzung (Abbildung 7.1).

Aufgrund der Flexibilität für verschiedene funktionelle Seitengruppen und der kontrollierten Synthese über reversible Additions-Fragmentierungs-Kettentransfer (RAFT)-Polymerisation sind Vinylpolymere gut für Studien zu Struktur-Eigenschafts-Beziehungen geeignet. Erstmals wurden hier Poly(aminoalkylacrylamide) (PAAm) verwendet, um primäre und tertiäre Amine sowie die pH-unabhängige Guanidinium-Einheit, bekannt aus der Aminosäure Arginin und zelldurchdringenden Peptiden (CPP), vergleichend zu untersuchen. Des Weiteren wurden die tertiären Amine mit einer Poly(*N*-acryloyl piperazine) (PNAP)-Bibliothek verglichen, deren Amine durch verschiedene Alkylgruppen hydrophob modifiziert wurden. Durch die verschiedenen Aminfunktionalitäten besaßen die Homopolymere unterschiedliche  $pK_a$ -Werte, wodurch unterschiedliche Ladungsgrade innerhalb des physiologisch relevanten pH-Bereichs erreicht wurden. Während die PAAms bei pH 7,4 mit Ausnahme von Poly(dimethylaminoethylacrylamid) (PDMAEAm) fast vollständig positiv geladen waren, erreichten die PNAPs nur maximal 30 % positiv geladene Amine, bei pH 5 jedoch ebenfalls 100 %, was auf eine stärkere pH-Sensitivität der PNAPs hindeutet. Diese Unterschiede spiegelten sich auch in anschließenden *in vitro*-Studien wider. Dabei korrelierten erhöhte Zytotoxizität, Membraninteraktion und endosomale Freisetzung in serumreduziertem Medium positiv mit einem hohen Ladungsgrad bei dem jeweiligen pH-Wert. Mit dem höchsten  $pK_a$  ( $> 12$ ) erzielte Poly(guanidinopropylacrylamid) (GPAm) die höchste endosomale Freisetzung, gefolgt von den primären und tertiären Amin-haltigen PAAms. Die endosomale Freisetzung der PNAPs war vergleichbar oder etwas höher als bei den PAAms mit tertiären Aminen, was durch die höhere Polymerkonzentration erklärt werden kann, die für die PNAPs verwendet wurde, um deren geringeren Ladungsgrad zu kompensieren. Bei der endosomalen Freisetzung kann die "proton sponge"-Theorie für die PNAPs, aber nicht für alle PAAms, als Mechanismus angenommen werden, da letztere eher pH-unempfindlich sind. In einem Lipidbindungsassay wurde gezeigt, dass alle PAAms mit dem Lipid Bis(monoacryloyl-glycerol)phosphat (BMP) interagieren, das in Vesikeln innerhalb von späten Endosomen vorkommt, wobei PGPAm die höchste Interaktion aufwies. Dies könnte daher einen möglichen Freisetzungsmechanismus darstellen. Dennoch sind weitere Studien erforderlich, um diese Hypothese zu bestätigen, z. B. hinsichtlich des Einflusses von PGPAm auf die Integrität von BMP-haltigen Liposomen, der Colokalisierung von PGPAm mit Endo- oder Lysosomen oder der PGPAm-BMP-Interaktion innerhalb von Zellen.

Obwohl alle kationischen Homopolymere im Calcein-Assay eine endosomale Freisetzung zeigten, war ihre Effizienz noch steigerungsfähig, insbesondere in serumhaltigem Medium. Um die Effizienz kationischer Polymere zu erhöhen, ist die Kombination mit hydrophoben Einheiten bekannt, wobei verschiedene 3D-Architekturen gebildet werden können. Hier wurden die weniger effizienten Homopolymere PDMAEAm und PDMAEMA (DP 100) mit *n*-Butylacrylat (*n*BA) bzw. *n*-Butylmethacrylat (*n*BMA) entweder als Block- oder als Copolymere mit zufälliger Verteilung der Monomere kombiniert. Darüber hinaus wurde zusätzlich das Monomer Liponsäuremethacrylat (LAMA), das die redoxsensitive essenzielle Fettsäure Liponsäure enthält, eingebracht. Dessen Nutzen wurde bspw. in Mizellen für den Wirkstofftransport oder als hydrophobe Modifikation von PEI für den pDNA-Transfer nachgewiesen. Während die Blockcopolymere P(*n*BA-*b*-DMAEAm) und P(DMAEMA-*b*-[*n*BMA-*co*-LAMA]) durch Lösungsmittelaustausch zu Mizellen (HC-mic, LAMA-mic) assembliert wurden, bildete das statistische Copolymer P(*n*BMA-*co*-MMA-*co*-DMAEMA) mit pDNA Polyplex-Nanopartikel (PBMD). Die verschiedenen Assemblierungen wurden hinsichtlich Mizell-/Polyplex-bildung, Zytotoxizität und Transfektionseffizienz untersucht. In allen Fällen hatten die hydrophoben Einheiten einen vernachlässigbaren Einfluss auf die pDNA-Komplexierung, erhöhten aber sogar in serumhaltigem Medium die Transfektionseffizienz in HEK-293T-Zellen erheblich. Insbesondere das PBMD überzeugte mit höheren Effizienzen als LPEI bei sehr niedrigen pDNA- und Polymerkonzentrationen sowie kürzeren Inkubationszeiten wodurch kostbare Zeit und Material gespart werden können. Darüber hinaus transfizierte die LAMA-mic auch die schwer zu transfizierenden K-562 Suspensionszellen (chronische myeloische Leukämie), v. a. nach längeren Inkubationszeiten, während LPEI und das kationische Homopolymer nur wenige Zellen transfizierten. Der Transfektionsmechanismus erwies sich als unabhängig von der Expression des Onkogens *BCR-ABL* und der Aufnahme des Mizellplexes, könnte aber durch eine höhere und schnellere endosomale Freisetzung gefördert werden, wie der Calcein-Assay zeigte. Darüber hinaus war die Liponsäure zwar von Vorteil, aber nicht entscheidend für die hohe Transfektionseffizienz, wie ein Vergleich mit der ähnlichen Mizelle ohne das LAMA-Monomer (BMA-mic) zeigte.

Die Kombination von hydrophoben mit kationischen Monomeren erhöhte nicht nur deren Transfektionseffizienz, sondern auch ihr bereits hohes Zytotoxizitätspotenzial, was weitere Strategien zur Abmilderung der toxischen Nebenwirkungen und zur Optimierung des Effizienz-Toxizitäts-Verhältnisses erforderte. Üblicherweise werden hydrophile "Stealth"-Polymere wie Poly(ethylenglykol) (PEG) und seine Alternativen Poly(oxazoline) (POx), Poly(oligo(ethylenglykol)methyletheracrylat) (POEGA) oder Poly(*N*-acryloylmorpholin) (PNAM) verwendet, um eine sterische Hydrathülle um die toxischen Komponenten zu schaffen. Auch negativ

geladene Anionen wie Polycarboxylate werden genutzt, um zytotoxische Nebenwirkungen durch elektrostatische Wechselwirkung mit den kationischen Einheiten zu verringern. Hier wurden gemischte Mizellen aus POx-Blockcopolymeren von 2-Nonyl-2-oxazolin (NonOx) und entweder 2-(4-Aminobutyl)-2-oxazolin (AmOx) oder 2-Ethyl-2-oxazolin (EtOx) verwendet, um die optimale Menge an P(EtOx-*b*-NonOx) für das beste Effizienz-Toxizitäts-Verhältnis zu bestimmen. Darüber hinaus wurde ein Blockcopolymer aus dem hydrophilen OEGA und nBA verwendet, um die Effizienz eines neuen Transportan 10 (TP10)-haltigen Kettenübertragungsreagenz (CTA) zu untersuchen. Schließlich wurde die bereits beschriebene HC-mic verwendet, um den Einfluss hydrophiler, anionischer oder beider Komponenten auf das Effizienz-Toxizitäts-Verhältnis zu untersuchen, wobei PNAM (HC<sup>S</sup>), Poly(acrylsäure) (PAA, HC<sup>A</sup>) bzw. P(NAM-*b*-AA) (HC<sup>AS</sup>) als Layerpolymere verwendet wurden, die mit einer Triblock-Terpolymer-Mizelle mit PAA als Mittelblock (HAC-mic) verglichen wurden. Die drei Projekte zeigten, dass drei verschiedene Faktoren das Effizienz-Toxizitäts-Verhältnis kationischer Polymere beeinflussen: i) das Verhältnis zwischen kationischen und anionischen/hydrophilen Einheiten, ii) die Kombinationsmethode von mildernden und kationischen Einheiten und iii) die Art der mildernden Einheit. Wenn diese Faktoren optimiert werden, kann die Toxizität zu höheren Konzentrationen verschoben und hohe Transfektionseffizienzen beibehalten werden, wie z. B. bei POx-Mischmizellen mit nur 20 wt.% P(EtOx<sub>155</sub>-*b*-NonOx<sub>76</sub>) oder der HAC-mic und HC<sup>A</sup>-Assemblierung. Die anionischen Einheiten ermöglichen dabei trotz geringerer Zytotoxizität eine höhere Transfektionseffizienz. Auch stark abschirmende Polymere wie P(NAM-*b*-AA) können für Anwendungen mit langen Zirkulationszeiten oder zellspezifischen Gentransfer eingesetzt werden.

Alles in allem veranschaulicht die vorliegende Arbeit die sehr gute Eignung kationischer Polymere (Mizellen) für den Gentransfer. Das herausragende Potenzial der Polymere wurde in Studien zur Struktur-Aktivitäts-Beziehung bezogen auf ihr Verhalten während des Transfektionsprozesses (endosomalen Freisetzung) nachgewiesen. Darüber hinaus wurde gezeigt, dass Polymere aufgrund ihrer einfachen Synthese und Kombinierbarkeit in Hinblick auf eine hohe Zellviabilität bei gleichzeitiger ausgezeichneter Gentransfereffizienz optimiert werden können. Polymere stellen daher eine vielversprechende Technologie für die zukünftige Gentherapie dar, und weitere (*in vivo*-) Studien sind nun erforderlich, um diese Ergebnisse auf den Menschen zu übertragen. Methoden wie künstliche Intelligenz und Hochdurchsatztechniken können dies in Zukunft aufgrund der Erleichterung des Wissenstransfers auf andere Polymere, des umfassenderen Vergleichs verschiedener Polymere und der schnelleren Entwicklung geeigneter Gentransportmaterialien für verschiedene Krankheiten unterstützen.

## 8. References

- [1] C.-C. Ma, Z.-L. Wang, T. Xu, Z.-Y. He, Y.-Q. Wei, *Biotechnol. Adv.* **2020**, *40*, 107502.
- [2] G. Shim, D. Kim, Q. V. Le, G. T. Park, T. Kwon, Y. K. Oh, *Curr. Gene Ther.* **2018**, *18*, 3-20.
- [3] N. A. Helal, A. Osami, A. Helmy, T. McDonald, L. A. Shaaban, M. I. Nounou, *Pharmazie* **2017**, *72*, 627-693.
- [4] European Medicines Agency, "COVID-19 vaccines: authorised", can be found under <https://www.ema.europa.eu/en/human-regulatory/overview/public-health-threats/coronavirus-disease-covid-19/treatments-vaccines/vaccines-covid-19/covid-19-vaccines-authorized#authorized-covid-19-vaccines-section>, last accessed: March **2022**.
- [5] H. Chen, Z. Gu, H. An, C. Chen, J. Chen, R. Cui, S. Chen, W. Chen, X. Chen, X. Chen, *Sci. China Chem.* **2018**, *61*, 1503-1552.
- [6] D. Lechardeur, K. Sohn, M. Haardt, P. Joshi, M. Monck, R. Graham, B. Beatty, J. Squire, H. O'brodovich, G. Lukacs, *Gene Ther.* **1999**, *6*, 482.
- [7] M. Durymanov, J. Reineke, *Front. Pharmacol.* **2018**, *9*, 971.
- [8] A. M. Jhaveri, V. P. Torchilin, *Front. Pharmacol.* **2014**, *5*, 77.
- [9] R. Kumar, C. F. Santa Chalarca, M. R. Bockman, C. V. Bruggen, C. J. Grimme, R. J. Dalal, M. G. Hanson, J. K. Hexum, T. M. Reineke, *Chem. Rev.* **2021**, *121*, 11527-11652.
- [10] K. Lundstrom, *Diseases* **2018**, *6*, 42.
- [11] S. L. Ginn, A. K. Amaya, I. E. Alexander, M. Edelstein, M. R. Abedi, *J. Gene Med.* **2018**, *20*, e3015.
- [12] I. Lostalé-Seijo, J. Montenegro, *Nat. Rev. Chem.* **2018**, *2*, 258-277.
- [13] N. Bono, F. Ponti, D. Mantovani, G. Candiani, *Pharmaceutics* **2020**, *12*, 183.
- [14] B. Kealy, A. Liew, J. M. McMahon, T. Ritter, A. O'Doherty, M. Hoare, U. Greiser, E. E. Vaughan, M. Maenz, C. O'Shea, *Tissue Eng., Part C* **2009**, *15*, 223-231.
- [15] M. K. Riley, W. Vermerris, *Nanomaterials (Basel)* **2017**, *7*.
- [16] N. Pardi, M. J. Hogan, F. W. Porter, D. Weissman, *Nat. Rev. Drug Discov.* **2018**, *17*, 261-279.
- [17] L. Schoenmaker, D. Witzigmann, J. A. Kulkarni, R. Verbeke, G. Kersten, W. Jiskoot, D. J. A. Crommelin, *Int. J. Pharm.* **2021**, *601*, 120586.
- [18] C. Englert, J. C. Brendel, T. C. Majdanski, T. Yildirim, S. Schubert, M. Gottschaldt, N. Windhab, U. S. Schubert, *Prog. Polym. Sci.* **2018**, *87*, 107-164.
- [19] L. Tortajada, C. Felip-León, M. J. Vicent, *Polym. Chem.* **2022**.
- [20] A. Wahane, A. Waghmode, A. Kapphahn, K. Dhuri, A. Gupta, R. Bahal, *Molecules* **2020**, *25*, 2866.
- [21] D. S. H. Chu, J. G. Schellinger, J. Shi, A. J. Convertine, P. S. Stayton, S. H. Pun, *Acc. Chem. Res.* **2012**, *45*, 1089-1099.
- [22] N. Corrigan, K. Jung, G. Moad, C. J. Hawker, K. Matyjaszewski, C. Boyer, *Prog. Polym. Sci.* **2020**, *111*, 101311.
- [23] A. C. Rinkenauer, S. Schubert, A. Traeger, U. S. Schubert, *J. Mater. Chem. B* **2015**, *3*, 7477-7493.
- [24] K. Muhammad, J. Zhao, B. Gao, Y. Feng, *J. Mater. Chem. B* **2020**.
- [25] R. Hoogenboom, *Angew. Chem. Int. Ed.* **2009**, *48*, 7978-7994.
- [26] D. Zhu, H. Yan, X. Liu, J. Xiang, Z. Zhou, J. Tang, X. Liu, Y. Shen, *Adv. Funct. Mater.* **2017**, *27*, 1606826.
- [27] T. Bus, A. Traeger, U. S. Schubert, *J. Mater. Chem. B* **2018**, *6*, 6904-6918.
- [28] J. Chen, K. Wang, J. Wu, H. Tian, X. Chen, *Bioconj. Chem.* **2019**, *30*, 338-349.
- [29] R. J. Christie, N. Nishiyama, K. Kataoka, *Endocrinology* **2010**, *151*, 466-473.
- [30] U. Lächelt, E. Wagner, *Chem. Rev.* **2015**, *115*, 11043-11078.

- [31] Z. Zhou, X. Liu, D. Zhu, Y. Wang, Z. Zhang, X. Zhou, N. Qiu, X. Chen, Y. Shen, *Adv. Drug. Deliv. Rev.* **2017**, *115*, 115-154.
- [32] C. Xu, H. Tian, X. Chen, *Sci. China Chem.* **2017**, *60*, 319-328.
- [33] A. I. S. van den Berg, C.-O. Yun, R. M. Schiffelers, W. E. Hennink, *J. Control. Release* **2021**, *331*, 121-141.
- [34] B. Surekha, N. S. Kommana, S. K. Dubey, A. V. P. Kumar, R. Shukla, P. Kesharwani, *Colloids Surf. B Biointerfaces* **2021**, *204*, 111837.
- [35] O. Boussif, Lezoualc, F. h, M. A. Zanta, M. D. Mergny, D. Scherman, B. Demeneix, J. P. Behr, *Proc. Natl. Acad. Sci. U.S.A.* **1995**, *92*, 7297.
- [36] A. P. Pandey, K. K. Sawant, *Mater. Sci. Eng. C* **2016**, *68*, 904-918.
- [37] N. C. Sheppard, S. A. Brinckmann, K. H. Gartlan, M. Puthia, C. Svanborg, G. Krashias, S. C. Eisenbarth, R. A. Flavell, Q. J. Sattentau, F. Wegmann, *Int. Immunol.* **2014**, *26*, 531-538.
- [38] T. Qin, Y. Yin, L. Huang, Q. Yu, Q. Yang, *Clin. Vaccine Immunol.* **2015**, *22*, 421-429.
- [39] D. Fischer, Y. Li, B. Ahlemeyer, J. Kriegelstein, T. Kissel, *Biomaterials* **2003**, *24*, 1121-1131.
- [40] H. K. de Wolf, J. Luten, C. J. Snel, G. Storm, W. E. Hennink, *Mol. Pharm.* **2008**, *5*, 349-357.
- [41] M. Neu, D. Fischer, T. Kissel, *J. Gene Med.* **2005**, *7*, 992-1009.
- [42] S. Agarwal, Y. Zhang, S. Maji, A. Greiner, *Mater. Today* **2012**, *15*, 388-393.
- [43] C. V. Synatschke, A. Schallon, V. Jerome, R. Freitag, A. H. Muller, *Biomacromolecules* **2011**, *12*, 4247-4255.
- [44] A. K. Trutzschler, T. Bus, M. Reifarth, J. C. Brendel, S. Hoepfener, A. Traeger, U. S. Schubert, *Bioconj. Chem.* **2018**, *29*, 2181-2194.
- [45] G. Navarro, J. Pan, V. P. Torchilin, *Mol. Pharm.* **2015**, *12*, 301-313.
- [46] H. Wang, S. Ding, Z. Zhang, L. Wang, Y. You, *J. Gene Med.* **2019**, *21*, e3101.
- [47] M. Yousefpour Marzbali, A. Yari Khosroushahi, *Cancer Chemother. Pharmacol.* **2017**, *79*, 637-649.
- [48] Z. H. Liu, Z. Y. Zhang, C. R. Zhou, Y. P. Jiao, *Prog. Polym. Sci.* **2010**, *35*, 1144-1162.
- [49] H. Cabral, K. Miyata, K. Osada, K. Kataoka, *Chem. Rev.* **2018**, *118*, 6844-6892.
- [50] J. P. Rao, K. E. Geckeler, *Prog. Polym. Sci.* **2011**, *36*, 887-913.
- [51] M. S. Shim, Y. J. Kwon, *Adv. Drug Deliv. Rev.* **2012**, *64*, 1046-1059.
- [52] M. Sun, K. Wang, D. Oupický, *Adv. Healthc. Mater.* **2018**, *7*, 1701070.
- [53] B. D. Monnery, M. Wright, R. Cavill, R. Hoogenboom, S. Shaunak, J. H. G. Steinke, M. Thanou, *Int. J. Pharm.* **2017**, *521*, 249-258.
- [54] H. Lv, S. Zhang, B. Wang, S. Cui, J. Yan, *J. Control. Release* **2006**, *114*, 100-109.
- [55] W. T. Godbey, K. K. Wu, A. G. Mikos, *J. Biomed. Mater. Res.* **1999**, *45*, 268-275.
- [56] J. M. Layman, S. M. Ramirez, M. D. Green, T. E. Long, *Biomacromolecules* **2009**, *10*, 1244-1252.
- [57] C. M. Hu, R. H. Fang, B. T. Luk, L. Zhang, *Nanoscale* **2014**, *6*, 65-75.
- [58] J. L. Yang, X. C. Zhang, C. Liu, Z. Wang, L. F. Deng, C. Feng, W. Tao, X. Y. Xu, W. G. Cui, *Prog. Mater. Sci.* **2021**, *118*, 100768.
- [59] A. E. Felber, M. H. Dufresne, J. C. Leroux, *Adv. Drug Deliv. Rev.* **2012**, *64*, 979-992.
- [60] A. J. Convertine, D. S. Benoit, C. L. Duvall, A. S. Hoffman, P. S. Stayton, *J. Control. Release* **2009**, *133*, 221-229.
- [61] P. Midoux, G. Breuzard, J. P. Gomez, C. Pichon, *Curr. Gene Ther.* **2008**, *8*, 335-352.
- [62] S. Prabha, G. Arya, R. Chandra, B. Ahmed, S. Nimesh, *Artif. Cells, Nanomed., Biotechnol.* **2016**, *44*, 83-91.
- [63] J. Huotari, A. Helenius, *EMBO J.* **2011**, *30*, 3481-3500.
- [64] L. M. P. Vermeulen, T. Brans, S. K. Samal, P. Dubruel, J. Demeester, S. C. De Smedt, K. Remaut, K. Braeckmans, *ACS Nano* **2018**, *12*, 2332-2345.

## REFERENCES

- [65] M. E. G. de Araujo, G. Liebscher, M. W. Hess, L. A. Huber, *Traffic* **2020**, *21*, 60-75.
- [66] A. El-Sayed, H. Harashima, *Mol. Ther.* **2013**, *21*, 1118-1130.
- [67] R. V. Benjaminsen, M. A. Matthebjerg, J. R. Henriksen, S. M. Moghimi, T. L. Andresen, *Mol. Ther.* **2013**, *21*, 149-157.
- [68] L. M. P. Vermeulen, S. C. De Smedt, K. Remaut, K. Braeckmans, *Eur. J. Pharm. Biopharm.* **2018**, *129*, 184-190.
- [69] F. Hullin-Matsuda, T. Taguchi, P. Greimel, T. Kobayashi, *Semin. Cell. Dev. Biol.* **2014**, *31*, 48-56.
- [70] T. F. Martens, K. Remaut, J. Demeester, S. C. De Smedt, K. Braeckmans, *Nano Today* **2014**, *9*, 344-364.
- [71] M. Bauer, C. Lautenschlaeger, K. Kempe, L. Tauhardt, U. S. Schubert, D. Fischer, *Macromol. Biosci.* **2012**, *12*, 986-998.
- [72] A. C. Rinkenauer, L. Tauhardt, F. Wendler, K. Kempe, M. Gottschaldt, A. Traeger, U. S. Schubert, *Macromol. Biosci.* **2015**, *15*, 414-425.
- [73] N. Murthy, J. R. Robichaud, D. A. Tirrell, P. S. Stayton, A. S. Hoffman, *J. Control. Release* **1999**, *61*, 137-143.
- [74] A. J. Convertine, C. Diab, M. Prieve, A. Paschal, A. S. Hoffman, P. H. Johnson, P. S. Stayton, *Biomacromolecules* **2010**, *11*, 2904-2911.
- [75] H. Diehl, J. L. Ellingboe, *Anal. Chem.* **1956**, *28*, 882-884.
- [76] H. Diehl, *Anal. Chem.* **1967**, *39*, 30A-43A.
- [77] Richard Markuszewski, Iowa State University (Ames, Iowa), **1976**.
- [78] A. J. Hefley, Iowa State University (Ames, Iowa), **1967**.
- [79] J. W. Furry, Iowa State University (Ames, Iowa), **1985**.
- [80] D. F. H. Wallach, T. L. Steck, *Anal. Chem.* **1963**, *35*, 1035-1044.
- [81] J. Weinstein, S. Yoshikami, P. Henkart, R. Blumenthal, W. Hagins, *Science* **1977**, *195*, 489-492.
- [82] R. M. Straubinger, K. Hong, D. S. Friend, D. Papahadjopoulos, *Cell* **1983**, *32*, 1069-1079.
- [83] F. C. Szoka, K. Jacobson, D. Papahadjopoulos, *Biochim. Biophys. Acta Biomembr.* **1979**, *551*, 295-303.
- [84] T. M. Allen, L. G. Cleland, *Biochim. Biophys. Acta Biomembr.* **1980**, *597*, 418-426.
- [85] D. A. Kendall, R. C. MacDonald, *Anal. Biochem.* **1983**, *134*, 26-33.
- [86] H. Patel, C. Tscheka, H. Heerklotz, *Soft Matter* **2009**, *5*, 2849-2851.
- [87] H. Patel, C. Tscheka, K. Edwards, G. Karlsson, H. Heerklotz, *Biochim. Biophys. Acta Biomembr.* **2011**, *1808*, 2000-2008.
- [88] S. Braun, Š. Pokorná, R. Šachl, M. Hof, H. Heerklotz, M. Hoernke, *ACS Nano* **2018**, *12*, 813-819.
- [89] B. Apellániz, J. L. Nieva, P. Schwille, A. J. García-Sáez, *Biophys. J.* **2010**, *99*, 3619-3628.
- [90] D. K. Bonner, X. Zhao, H. Buss, R. Langer, P. T. Hammond, *J. Control. Release* **2013**, *167*, 101-107.
- [91] D. K. Bonner, C. Leung, J. Chen-Liang, L. Chingozha, R. Langer, P. T. Hammond, *Bioconjug. Chem.* **2011**, *22*, 1519-1525.
- [92] S. Deshpande, S. Patil, N. Singh, *ACS Omega* **2018**, *3*, 8042-8049.
- [93] Y. Hu, T. Litwin, A. R. Nagaraja, B. Kwong, J. Katz, N. Watson, D. J. Irvine, *Nano Lett.* **2007**, *7*, 3056-3064.
- [94] A. S. Wong, S. K. Mann, E. Czuba, A. Sahut, H. Liu, T. C. Suckama, T. Bickerton, A. P. Johnston, G. K. Such, *Soft Matter* **2015**, *11*, 2993-3002.
- [95] N. Brkovic, L. Zhang, J. N. Peters, S. Kleine-Doepke, W. J. Parak, D. Zhu, *Small* **2020**, *16*, e2003639.
- [96] J. Connor, L. Huang, *J. Cell Biol.* **1985**, *101*, 582-589.



- [97] B. Illes, P. Hirschle, S. Barnert, V. Cauda, S. Wuttke, H. Engelke, *Chem. Mater.* **2017**, *29*, 8042-8046.
- [98] X. Zhan, K. K. Tran, L. Wang, H. Shen, *Pharm. Res.* **2015**, *32*, 2280-2291.
- [99] K. K. Tran, X. Zhan, H. Shen, *Advanced healthcare materials* **2014**, *3*, 690-702.
- [100] F. Richter, P. Mapfumo, L. Martin, J. I. Solomun, F. Hausig, J. J. Frietsch, T. Ernst, S. Hoepfener, J. C. Brendel, A. Traeger, *J. Nanobiotechnology* **2021**, *19*, 70.
- [101] F. Richter, L. Martin, K. Leer, E. Moek, F. Hausig, J. C. Brendel, A. Traeger, *J. Mater. Chem. B* **2020**, *8*, 5026-5041.
- [102] F. Salomone, F. Cardarelli, M. Di Luca, C. Boccardi, R. Nifosi, G. Bardi, L. Di Bari, M. Serresi, F. Beltram, *J. Control. Release* **2012**, *163*, 293-303.
- [103] E. Ducat, J. Deprez, A. Gillet, A. Noel, B. Evrard, O. Peulen, G. Piel, *Int. J. Pharm.* **2011**, *420*, 319-332.
- [104] Z. Li, B. li, M. Wang, M. Xie, H. Shen, S. Shen, X. Wang, X. Guo, M. Yao, Y. Jin, *J. Mater. Chem. B* **2013**, *1*, 1466-1474.
- [105] H. Xu, W. Zhang, Y. Li, F. F. Ye, P. P. Yin, X. Yu, M. N. Hu, Y. S. Fu, C. Wang, J. Shang de, *Pharm. Res.* **2014**, *31*, 3038-3050.
- [106] S. Simoes, V. Slepishkin, N. Duzgunes, M. C. Pedroso de Lima, *Biochim. Biophys. Acta* **2001**, *1515*, 23-37.
- [107] V. A. Slepishkin, S. Simoes, P. Dazin, M. S. Newman, L. S. Guo, M. C. Pedroso de Lima, N. Duzgunes, *J. Biol. Chem.* **1997**, *272*, 2382-2388.
- [108] R. A. Jones, C. Y. Cheung, F. E. Black, J. K. Zia, P. S. Stayton, A. S. Hoffman, M. R. Wilson, *Biochem. J.* **2003**, *372*, 65-75.
- [109] F. Hausig, F. H. Sobotta, F. Richter, D. O. Harz, A. Traeger, J. C. Brendel, *ACS Appl. Mater. Interfaces* **2021**, *13*, 35233-35247.
- [110] C. J. Chu, J. Dijkstra, M. Z. Lai, K. Hong, F. C. Szoka, *Pharm. Res.* **1990**, *7*, 824-834.
- [111] M. Kanamala, B. D. Palmer, H. Ghandehari, W. R. Wilson, Z. Wu, *Pharm. Res.* **2018**, *35*, 154.
- [112] P. Enzian, C. Schell, A. Link, C. Malich, R. Pries, B. Wollenberg, R. Rahmzadeh, *Mol. Pharm.* **2020**, *17*, 2779-2788.
- [113] S. Cerritelli, D. Velluto, J. A. Hubbell, *Biomacromolecules* **2007**, *8*, 1966-1972.
- [114] E. A. Scott, A. Stano, M. Gillard, A. C. Maio-Liu, M. A. Swartz, J. A. Hubbell, *Biomaterials* **2012**, *33*, 6211-6219.
- [115] A. E. Vasdekis, E. A. Scott, C. P. O'Neil, D. Psaltis, J. A. Hubbell, *ACS Nano* **2012**, *6*, 7850-7857.
- [116] K. Kono, T. Igawa, T. Takagishi, *Biochim. Biophys. Acta* **1997**, *1325*, 143-154.
- [117] Y. Nishimura, K. Takeda, R. Ezawa, J. Ishii, C. Ogino, A. Kondo, *J. Nanobiotechnology* **2014**, *12*, 11.
- [118] S. Niedermayer, V. Weiss, A. Herrmann, A. Schmidt, S. Datz, K. Muller, E. Wagner, T. Bein, C. Brauchle, *Nanoscale* **2015**, *7*, 7953-7964.
- [119] U. Lächelt, P. Kos, F. M. Mickler, A. Herrmann, E. E. Salcher, W. Rödl, N. Badgajar, C. Bräuchle, E. Wagner, *Nanomedicine* **2014**, *10*, 35-44.
- [120] R. A. Jones, M. H. Poniris, M. R. Wilson, *J. Control. Release* **2004**, *96*, 379-391.
- [121] F. Richter, K. Leer, L. Martin, P. Mapfumo, J. I. Solomun, M. T. Kuchenbrod, S. Hoepfener, J. C. Brendel, A. Traeger, *J. Nanobiotechnology* **2021**, *19*, 292.
- [122] X. Su, J. Fricke, D. G. Kavanagh, D. J. Irvine, *Mol. Pharm.* **2011**, *8*, 774-787.
- [123] S. Wannasarit, S. Q. Wang, P. Figueiredo, C. Trujillo, F. Eburnea, L. Simon-Gracia, A. Correia, Y. P. Ding, T. Teesalu, D. F. Liu, R. Wiwattanapatapee, H. A. Santos, W. Li, *Adv. Funct. Mater.* **2019**, *29*, 1905352.
- [124] J. Chen, J. Li, J. Zhou, Z. Lin, F. Cavalieri, E. Czuba-Wojnilowicz, Y. Hu, A. Glab, Y. Ju, J. J. Richardson, F. Caruso, *ACS Nano* **2019**, *13*, 11653-11664.
- [125] J. R. Clegg, J. A. Sun, J. Gu, A. K. Venkataraman, N. A. Peppas, *J. Control. Release* **2021**, *329*, 1162-1171.

## REFERENCES

---

- [126] N. Kongkatigumjorn, C. Cortez-Jugo, E. Czuba, A. S. Wong, R. Y. Hodgetts, A. P. Johnston, G. K. Such, *Macromol. Biosci.* **2017**, *17*, 1600248.
- [127] N. Kongkatigumjorn, S. A. Smith, M. Chen, K. T. Fang, S. L. Yang, E. R. Gillies, A. P. R. Johnston, G. K. Such, *ACS Appl. Nano Mater.* **2018**, *1*, 3164-3173.
- [128] M. Galliani, C. Tremolanti, G. Signore, *Nanomaterials (Basel)* **2019**, *9*, 652.
- [129] J. S. Kim, D. K. Choi, J. Y. Shin, S. M. Shin, S. W. Park, H. S. Cho, Y. S. Kim, *J. Control. Release* **2016**, *235*, 165-175.
- [130] J. C. Brendel, J. Sanchis, S. Catrouillet, E. Czuba, M. Z. Chen, B. M. Long, C. Nowell, A. Johnston, K. A. Jolliffe, S. Perrier, *Angew. Chem. Int. Ed. Engl.* **2018**, *57*, 16678-16682.
- [131] M. Essodaigui, H. J. Broxterman, A. Garnier-Suillerot, *Biochemistry* **1998**, *37*, 2243-2250.
- [132] N. Feller, H. J. Broxterman, D. C. R. Währer, H. M. Pinedo, *FEBS Letters* **1995**, *368*, 385-388.
- [133] F. Miles, J. Lynch, R. Sikes, *J. Biol. Methods* **2015**, *2*, e29.
- [134] A. Gregory, M. H. Stenzel, *Prog. Polym. Sci.* **2012**, *37*, 38-105.
- [135] K. Matyjaszewski, *Macromolecules* **2012**, *45*, 4015-4039.
- [136] D. J. Siegwart, J. K. Oh, K. Matyjaszewski, *Prog. Polym. Sci.* **2012**, *37*, 18-37.
- [137] C. L. Moad, G. Moad, *Chem. Teach. Int.* **2021**, *3*, 3-17.
- [138] M. Ahmed, R. Narain, *Prog. Polym. Sci.* **2013**, *38*, 767-790.
- [139] P. van de Wetering, E. E. Moret, N. M. Schuurmans-Nieuwenbroek, M. J. van Steenbergen, W. E. Hennink, *Bioconjug. Chem.* **1999**, *10*, 589-597.
- [140] G. Gody, T. Maschmeyer, P. B. Zetterlund, S. Perrier, *Macromolecules* **2014**, *47*, 639-649.
- [141] L. Martin, G. Gody, S. Perrier, *Polym. Chem.* **2015**, *6*, 4875-4886.
- [142] J. Schrooten, I. Lacík, M. Stach, P. Hesse, M. Buback, *Macromol. Chem. Phys.* **2013**, *214*, 2283-2294.
- [143] I. Mizoguchi, Y. Ooe, S. Hoshino, M. Shimura, T. Kasahara, S. Kano, T. Ohta, F. Takaku, Y. Nakayama, Y. Ishizaka, *Biochem. Biophys. Res. Commun.* **2005**, *338*, 1499-1506.
- [144] Y. Nakayama, C. Kakei, A. Ishikawa, Y.-M. Zhou, Y. Nemoto, K. Uchida, *Bioconjugate Chem.* **2007**, *18*, 2037-2044.
- [145] Y. Nemoto, A. Borovkov, Y.-M. Zhou, Y. Takewa, E. Tatsumi, Y. Nakayama, *Bioconjugate Chem.* **2009**, *20*, 2293-2299.
- [146] N. Yasuhide, M. Takeshi, N. Makoto, H. Michiko, O. Moto, H.-S. Mariko, *Curr. Drug Deliv.* **2005**, *2*, 53-57.
- [147] J.-H. Ke, M.-F. Wei, M.-J. Shieh, T.-H. Young, *J. Biomater. Sci., Polym. Ed.* **2011**, *22*, 1215-1236.
- [148] J.-H. Ke, M.-F. Wei, M.-J. Shieh, T.-H. Young, *J. Biomater. Sci., Polym. Ed.* **2011**, *22*, 1753-1775.
- [149] J.-H. Ke, T.-H. Young, *Biomaterials* **2010**, *31*, 9366-9372.
- [150] H. Li, M. A. Cortez, H. R. Phillips, Y. Wu, T. M. Reineke, *ACS Macro Lett.* **2013**, *2*, 230-235.
- [151] D. Sprouse, T. M. Reineke, *Biomacromolecules* **2014**, *15*, 2616-2628.
- [152] T. Bus, C. Englert, M. Reifarth, P. Borchers, M. Hartlieb, A. Vollrath, S. Hoepfener, A. Traeger, U. S. Schubert, *J. Mater. Chem. B* **2017**, *5*, 1258-1274.
- [153] C. Bechara, S. Sagan, *FEBS Lett.* **2013**, *587*, 1693-1702.
- [154] J. K. Allen, D. J. Brock, H. M. Kondow-McConaghy, J.-P. Pellois, *Biomolecules* **2018**, *8*, 50.
- [155] K. J. Abd Karim, R. H. Utama, H. Lu, M. H. Stenzel, *Polym. Chem.* **2014**, *5*, 6600-6610.
- [156] M. Ahmed, *Biomater. Sci.* **2017**, *5*, 2188-2211.

- [157] C. Cokca, L. Zartner, I. Tabujew, D. Fischer, K. Peneva, *Macromol. Rapid Commun.* **2020**, *41*, 1900668.
- [158] Y. Kim, S. Binauld, M. H. Stenzel, *Biomacromolecules* **2012**, *13*, 3418-3426.
- [159] J. D. Ramsey, N. H. Flynn, *Pharmacol. Ther.* **2015**, *154*, 78-86.
- [160] N. Schmidt, A. Mishra, G. H. Lai, G. C. Wong, *FEBS Lett.* **2010**, *584*, 1806-1813.
- [161] A. M. Funhoff, C. F. van Nostrum, M. C. Lok, M. M. Fretz, D. J. A. Crommelin, W. E. Hennink, *Bioconj. Chem.* **2004**, *15*, 1212-1220.
- [162] L. H. Gan, Y. Y. Gan, G. R. Deen, *Macromolecules* **2000**, *33*, 7893-7897.
- [163] G. Roshan Deen, L. H. Gan, *J. Appl. Polym. Sci.* **2008**, *107*, 1449-1458.
- [164] Molinspiration Cheminformatics, "Molinspiration Property Calculation Service", can be found under <https://www.molinspiration.com/cgi-bin/properties>, last accessed: February **2022**.
- [165] A. Erazo-Oliveras, K. Najjar, D. Truong, T. Y. Wang, D. J. Brock, A. R. Prater, J. P. Pellois, *Cell Chem. Biol.* **2016**, *23*, 598-607.
- [166] S.-T. Yang, E. Zaitseva, L. V. Chernomordik, K. Melikov, *Biophys. J.* **2010**, *99*, 2525-2533.
- [167] T. Kobayashi, E. Stang, K. S. Fang, P. de Moerloose, R. G. Parton, J. Gruenberg, *Nature* **1998**, *392*, 193-197.
- [168] W. Mobius, E. van Donselaar, Y. Ohno-Iwashita, Y. Shimada, H. F. Heijnen, J. W. Slot, H. J. Geuze, *Traffic* **2003**, *4*, 222-231.
- [169] T. Kobayashi, M.-H. Beuchat, J. Chevallier, A. Makino, N. Mayran, J.-M. Escola, C. Lebrand, P. Cosson, T. Kobayashi, J. Gruenberg, *J. Biol. Chem.* **2002**, *277*, 32157-32164.
- [170] K. Letchford, H. Burt, *Eur. J. Pharm. Biopharm.* **2007**, *65*, 259-269.
- [171] S. R. Mane, A. Sathyan, R. Shunmugam, *Acs Applied Nano Materials* **2020**, *3*, 2104-2117.
- [172] C. Oerlemans, W. Bult, M. Bos, G. Storm, J. F. Nijsen, W. E. Hennink, *Pharm. Res.* **2010**, *27*, 2569-2589.
- [173] S. Uchida, K. Kataoka, *J. Biomed. Mater. Res. A* **2019**, *107*, 978-990.
- [174] D. H. Wakefield, J. J. Klein, J. A. Wolff, D. B. Rozema, *Bioconj. Chem.* **2005**, *16*, 1204-1208.
- [175] V. Incani, A. Lavasanifar, H. Uludag, *Soft Matter* **2010**, *6*, 2124-2138.
- [176] O. Colombani, M. Ruppel, M. Burkhardt, M. Drechsler, M. Schumacher, M. Gradzielski, R. Schweins, A. H. E. Muller, *Macromolecules* **2007**, *40*, 4351-4362.
- [177] E. Gardey, F. H. Sobotta, S. Hoepfener, T. Bruns, A. Stallmach, J. C. Brendel, *Biomacromolecules* **2020**, *21*, 1393-1406.
- [178] D. Sprouse, Y. Jiang, J. E. Laaser, T. P. Lodge, T. M. Reineke, *Biomacromolecules* **2016**, *17*, 2849-2859.
- [179] Z. Tan, Y. Jiang, W. Zhang, L. Karls, T. P. Lodge, T. M. Reineke, *J. Am. Chem. Soc.* **2019**, *141*, 15804-15817.
- [180] A. Bast, G. R. M. M. Haenen, *Environ. Toxicol. Phar.* **2002**, *11*, 251-258.
- [181] M. B. Gomes, C. A. Negrato, *Diabetol. Metab. Syndr.* **2014**, *6*, 80.
- [182] M. Talelli, M. Barz, C. J. Rijcken, F. Kiessling, W. E. Hennink, T. Lammers, *Nano Today* **2015**, *10*, 93-117.
- [183] Y. L. Li, L. Zhu, Z. Liu, R. Cheng, F. Meng, J. H. Cui, S. J. Ji, Z. Zhong, *Angew. Chem. Int. Ed. Engl.* **2009**, *48*, 9914-9918.
- [184] R. Wei, L. Cheng, M. Zheng, R. Cheng, F. Meng, C. Deng, Z. Zhong, *Biomacromolecules* **2012**, *13*, 2429-2438.
- [185] L. Wu, Y. Zou, C. Deng, R. Cheng, F. Meng, Z. Zhong, *Biomaterials* **2013**, *34*, 5262-5272.
- [186] Y. Xu, F. Meng, R. Cheng, Z. Zhong, *Macromol. Biosci.* **2009**, *9*, 1254-1261.

REFERENCES

- [187] R. Q. Li, W. Wu, H. Q. Song, Y. Ren, M. Yang, J. Li, F. J. Xu, *Acta Biomater.* **2016**, *41*, 282-292.
- [188] M. Zheng, Y. Zhong, F. Meng, R. Peng, Z. Zhong, *Mol. Pharm.* **2011**, *8*, 2434-2443.
- [189] A. Tschiche, B. N. Thota, F. Neumann, A. Schafer, N. Ma, R. Haag, *Macromol. Biosci.* **2016**, *16*, 811-823.
- [190] M. Balakirev, G. Schoehn, J. Chroboczek, *Chem. Biol.* **2000**, *7*, 813-819.
- [191] J. B. Lepecq, C. Paoletti, *Journal of Molecular Biology* **1967**, *27*, 87-+.
- [192] J. Olmsted, 3rd, D. R. Kearns, *Biochemistry* **1977**, *16*, 3647-3654.
- [193] D. Cilloni, G. Saglio, *Clin. Cancer Res.* **2012**, *18*, 930-937.
- [194] H. Shinohara, M. Kumazaki, Y. Minami, Y. Ito, N. Sugito, Y. Kuranaga, K. Taniguchi, N. Yamada, Y. Otsuki, T. Naoe, Y. Akao, *Cancer Lett.* **2016**, *371*, 1-11.
- [195] M. Hussein Kamareddine, Y. Ghosn, A. Tawk, C. Elia, W. Alam, J. Makdessi, S. Farhat, *Technol. Cancer Res. Treat.* **2019**, *18*, 1533033819879902.
- [196] G. Lin, H. Zhang, L. Huang, *Mol. Pharm.* **2015**, *12*, 314-321.
- [197] K. C. Remant, B. Thapa, J. Valencia-Serna, S. S. Domun, C. Dimitroff, X. Jiang, H. Uludag, *J. Biomed. Mater. Res. A* **2020**, *108*, 565-580.
- [198] J. Valencia-Serna, H. Gul-Uludag, P. Mahdipoor, X. Jiang, H. Uludag, *J. Control. Release* **2013**, *172*, 495-503.
- [199] J. Valencia-Serna, H. M. Aliabadi, A. Manfrin, M. Mohseni, X. Jiang, H. Uludag, *Eur. J. Pharm. Biopharm.* **2018**, *130*, 66-70.
- [200] M. R. Lorenz, V. Holzapfel, A. Musyanovych, K. Nothelfer, P. Walther, H. Frank, K. Landfester, H. Schrezenmeier, V. Mailander, *Biomaterials* **2006**, *27*, 2820-2828.
- [201] A. Zielińska, F. Carreiró, A. M. Oliveira, A. Neves, B. Pires, D. N. Venkatesh, A. Durazzo, M. Lucarini, P. Eder, A. M. Silva, A. Santini, E. B. Souto, *Molecules (Basel, Switzerland)* **2020**, *25*, 3731.
- [202] P. G. Silva-Flores, L. A. Pérez-López, V. M. Rivas-Galindo, D. Paniagua-Vega, S. A. Galindo-Rodríguez, R. Álvarez-Román, *J. Anal. Methods Chem.* **2019**, *2019*, 2837406.
- [203] B. N. V. Hari, N. Narayanan, K. Dhevendaran, D. Ramyadevi, *Mater. Sci. Eng. C Mater. Biol. Appl.* **2016**, *67*, 522-532.
- [204] C. Moorthi, C. S. Kumar, S. Mohan, K. Krishnan, K. Kathiresan, *J. Pharm. Res.* **2013**, *7*, 224-229.
- [205] J. Tang, N. Xu, H. Ji, H. Liu, Z. Wang, L. Wu, *Int. J. Nanomedicine* **2011**, *6*, 2429-2435.
- [206] R. Jain, P. Dandekar, B. Loretz, M. Koch, C.-M. Lehr, *Med. Chem. Comm.* **2015**, *6*, 691-701.
- [207] A. Basarkar, J. Singh, *Pharm. Res.* **2009**, *26*, 72-81.
- [208] Y. Wang, J. Xu, Y. Zhang, H. Yan, K. Liu, *Macromol. Biosci.* **2011**, *11*, 1499-1504.
- [209] J. S. Suk, Q. Xu, N. Kim, J. Hanes, L. M. Ensign, *Adv. Drug. Deliv. Rev.* **2016**, *99*, 28-51.
- [210] K. Knop, R. Hoogenboom, D. Fischer, U. S. Schubert, *Angew. Chem. Int. Ed.* **2010**, *49*, 6288-6308.
- [211] R. Tenchov, R. Bird, A. E. Curtze, Q. Zhou, *ACS Nano* **2021**, *15*, 16982-17015.
- [212] Y. Fang, J. Xue, S. Gao, A. Lu, D. Yang, H. Jiang, Y. He, K. Shi, *Drug Deliv.* **2017**, *24*, 22-32.
- [213] S. Mishra, P. Webster, M. E. Davis, *Eur. J. Cell Biol.* **2004**, *83*, 97-111.
- [214] B. Li, Z. Yuan, H. C. Hung, J. Ma, P. Jain, C. Tsao, J. Xie, P. Zhang, X. Lin, K. Wu, S. Jiang, *Angew. Chem. Int. Ed. Engl.* **2018**, *57*, 13873-13876.
- [215] D. J. Peeler, D. L. Sellers, S. H. Pun, *Bioconjug. Chem.* **2019**, *30*, 350-365.
- [216] Q. Yang, T. M. Jacobs, J. D. McCallen, D. T. Moore, J. T. Huckaby, J. N. Edelstein, S. K. Lai, *Anal. Chem.* **2016**, *88*, 11804-11812.

## REFERENCES

---

- [217] T. T. Hoang Thi, E. H. Pilkington, D. H. Nguyen, J. S. Lee, K. D. Park, N. P. Truong, *Polymers* **2020**, *12*, 298.
- [218] P. Zhang, F. Sun, S. Liu, S. Jiang, *J. Control. Release* **2016**, *244*, 184-193.
- [219] P. H. Kierstead, H. Okochi, V. J. Venditto, T. C. Chuong, S. Kivimae, J. M. J. Frechet, F. C. Szoka, *J. Control. Release* **2015**, *213*, 1-9.
- [220] T. Ishihara, T. Maeda, H. Sakamoto, N. Takasaki, M. Shigyo, T. Ishida, H. Kiwada, Y. Mizushima, T. Mizushima, *Biomacromolecules* **2010**, *11*, 2700-2706.
- [221] J. Cai, Y. Yue, D. Rui, Y. Zhang, S. Liu, C. Wu, *Macromolecules* **2011**, *44*, 2050-2057.
- [222] S. El-Andaloussi, H. Johansson, A. Magnúsdóttir, P. Jarver, P. Lundberg, U. Langel, *J. Control. Release* **2005**, *110*, 189-201.
- [223] K. Kilk, S. El-Andaloussi, P. Jarver, A. Meikas, A. Valkna, T. Bartfai, P. Kogerman, M. Metsis, U. Langel, *J. Control. Release* **2005**, *103*, 511-523.
- [224] J. Song, M. Kai, W. Zhang, J. Zhang, L. Liu, B. Zhang, X. Liu, R. Wang, *Peptides* **2011**, *32*, 1934-1941.
- [225] I. Dewald, J. Gensel, E. Betthausen, O. V. Borisov, A. H. Muller, F. H. Schacher, A. Fery, *ACS Nano* **2016**, *10*, 5180-5188.
- [226] A. C. Rinkenauer, A. Schallon, U. Gunther, M. Wagner, E. Betthausen, U. S. Schubert, F. H. Schacher, *ACS Nano* **2013**, *7*, 9621-9631.
- [227] C. V. Synatschke, T. Nomoto, H. Cabral, M. Fortsch, K. Toh, Y. Matsumoto, K. Miyazaki, A. Hanisch, F. H. Schacher, A. Kishimura, N. Nishiyama, A. H. Muller, K. Kataoka, *ACS Nano* **2014**, *8*, 1161-1172.
- [228] D. V. Pergushov, A. H. Muller, F. H. Schacher, *Chem. Soc. Rev.* **2012**, *41*, 6888-6901.
- [229] V. Vergaro, F. Scarlino, C. Bellomo, R. Rinaldi, D. Vergara, M. Maffia, F. Baldassarre, G. Giannelli, X. Zhang, Y. M. Lvov, S. Leporatti, *Adv. Drug. Deliv. Rev.* **2011**, *63*, 847-864.
- [230] D. Finsinger, J. S. Remy, P. Erbacher, C. Koch, C. Plank, *Gene Ther.* **2000**, *7*, 1183-1192.
- [231] V. A. Sethuraman, K. Na, Y. H. Bae, *Biomacromolecules* **2006**, *7*, 64-70.
- [232] J. Schindelin, I. Arganda-Carreras, E. Frise, V. Kaynig, M. Longair, T. Pietzsch, S. Preibisch, C. Rueden, S. Saalfeld, B. Schmid, J. Y. Tinevez, D. J. White, V. Hartenstein, K. Eliceiri, P. Tomancak, A. Cardona, *Nat. Methods.* **2012**, *9*, 676-682.

## List of abbreviations

AmOx	2-(4-aminobutyl)-2-oxazoline
BMA-mic	micellar assembly of P(DMAEMA- <i>b</i> - <i>n</i> BMA)
BMP	bis(monoacryloyl glycerol)phosphate
CC <sub>50</sub>	(polymer) concentration where 50 % of the cells are viable/dead
CLSM	confocal laser scanning microscopy
CML	chronic myeloid leukemia
CPP	cell penetrating peptide
CROP	cationic ring-opening polymerization
cryo-TEM	cryo transmission electron microscopy
DCC	N,N'-dicyclohexylcarbodiimide
DLS	dynamic light scattering
DMAc	dimethylacetamide
DMAP	4-dimethylaminopyridine
DP	degree of polymerization
EBA	ethidium bromide quenching assay
EGFP	enhanced green fluorescent protein
ELS	electrophoretic light scattering
EMA	European Medicines Agency
EtOx	2-ethyl-2-oxazoline
FDA	Food and Drug Administration
FSC	forward scatter
HAC-mic	micellar assembly of P( <i>n</i> BA- <i>b</i> -AA- <i>b</i> -DMAEAm)
HBG	HEPES-buffered glucose
HC(-mic)	micellar assembly of P( <i>n</i> BA- <i>b</i> -DMAEAm)
HC <sub>50</sub>	heparin concentration required to release 50 % of pDNA
HCA	HC-mic layered with PAA (A)
HCAS	HC-mic layered with P(NAM- <i>b</i> -AA) (AS)
HCS	HC-mic layered with PNAM (S)
HEPES	4-(2-hydroxyethyl)-1-piperazineethanesulfonic acid
<sup>1</sup> H NMR	proton nuclear magnetic resonance
HRA	heparin release assay
ILEV	intra late endosomal vesicle
IPA	iso-propanol
LAMA	lipoic acid methacrylate, 2-(methacryloyloxy)ethyl 5-(1,2-dithiolan-3-yl)pentanoate
LAMA-mic	micellar assembly of P(DMAEMA- <i>b</i> -[ <i>n</i> BMA- <i>co</i> -LAMA])
LDH	lactate dehydrogenase
LPEI	linear polyethyleneimine
MeOH	methanol
MFI	mean fluorescence intensity
MMA	methyl methacrylate
N*/P ratio	ratio of active amines (polymer) to phosphates (pDNA)
<i>n</i> BA	<i>n</i> -butyl acrylate
<i>n</i> BMA	<i>n</i> -butyl methacrylate
A	

## LIST OF ABBREVIATIONS

---

NEt <sub>3</sub>	triethylamine
NonOx	2-nonyl-2-oxazoline
OEGA	oligo (ethylene glycol) methyl ether acrylate
P/N ratio	ratio of lipid-phosphate to polymer-amine
P2VP	poly(2-vinylpyridine)
PAA	poly(acrylic acid)
PAAm	poly(amino acrylamide)
PAEAm	poly(aminoethyl acrylamide)
PBMD	poly(DMAEMA- <i>co</i> - <i>n</i> BMA- <i>co</i> -MMA)
PC	phosphatidyl choline
PDI	polydispersity index
PDMAEAm	poly(dimethylaminoethyl acrylamide)
PDMAEMA	poly(2-(dimethylamino)ethyl methacrylate)
PDMAPAm	poly(dimethylaminopropyl acrylamide)
pDNA	plasmid DNA
PE	phosphatidyl ethanolamine
PEG	poly(ethylene glycol)
PGPAm	poly(guanidinopropyl acrylamide)
PIC	polyion complex
PMMA	poly(methyl methacrylate)
PNAEP	poly(N-acryloyl-N'-ethylpiperazine)
PNA <i>i</i> PP	poly(N-acryloyl- N'- <i>iso</i> -propylpiperazine)
PNAM	poly(N-acryloyl- N'-morpholine)
PNAMP	poly(N-acryloyl- N'-methylpiperazine)
PNAP	poly(N-acryloyl piperazines)
PNA <i>t</i> BP	poly(N-acryloyl- N'- <i>tert</i> -butylpiperazine)
POEGMA	poly(oligo(ethylene glycol) methyl ether methacrylate)
POx	poly(oxazoline)
PS	polystyrol
RAFT	reversible addition–fragmentation chain transfer
RDRP	reversible deactivation radical polymerization
rFI	relative fluorescence intensity
rMFI	relative mean fluorescence intensity
SD	standard deviation
SEC	size exclusion chromatography
SSC	sideward scatter
TE	transfection efficiency
TFA	trifluoroacetic acid
THF	tetrahydrofuran
TP10	Transportan 10

## Description of unpublished methods

### For Figure 3.4A: Calcein release by PAAMs via CLSM

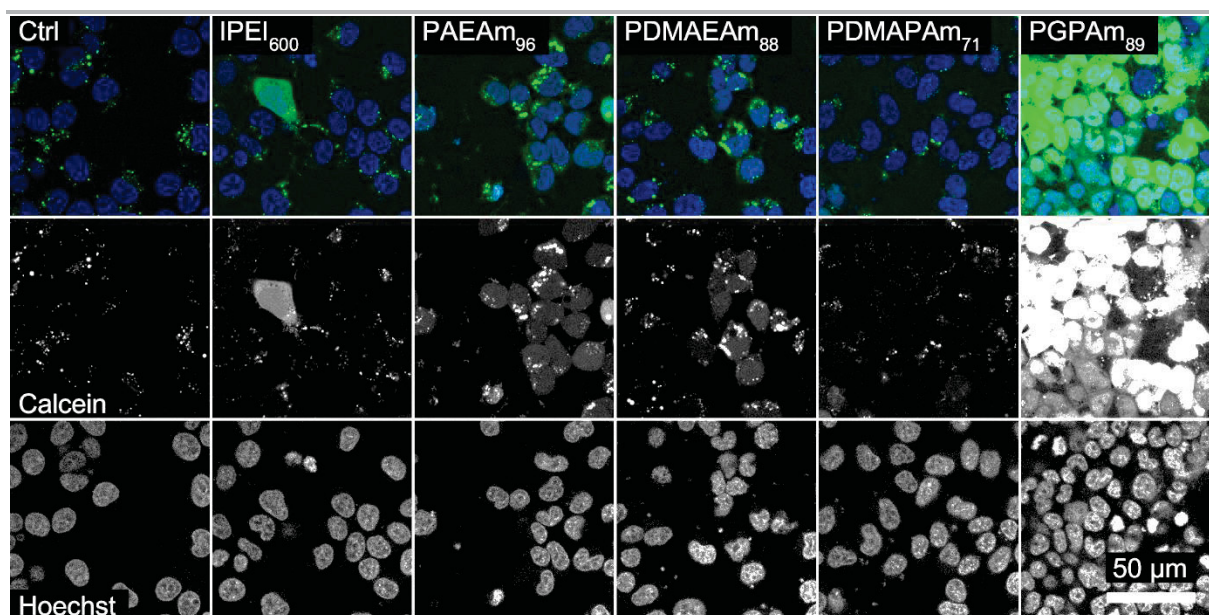


**Figure 8.1.** Additional images for Figure 3.4 acquired according to the method described below.

To determine the calcein release by the PAAM polymers, HEK293T cells were seeded at a density of  $10^5$  cells per well in 4-well glass bottom dishes and cultured for 24 h in growth medium (DMEM + 10% FCS + 10 mM HEPES). They were treated with polyplexes as described for transfection studies in **Pub2**. One hour prior to treatment with polyplexes, the medium was replaced by 450  $\mu$ L serum reduced Opti-MEM. Polyplexes were prepared with isolated pEGFP-N1 pDNA (labeled with BOBO-3, images not shown) and added to the cells diluting the polyplexes 1:10 in the cell culture medium. Just before the addition of polyplexes, the non-cell-permeable dye calcein was added to the cells to give a final concentration of 25  $\mu$ g  $\text{mL}^{-1}$ . Following incubation for 4 h, cells were carefully washed twice with cold PBS followed by addition of 500  $\mu$ L FC-buffer (Hanks' Balanced Salt Solution, supplemented with 2% FCS and 20 mM HEPES) and 8  $\mu$ M Hoechst 33342 for 10 min.

To image the intracellular distribution pattern of calcein in living cells, live cell imaging was performed using a LSM880, Elyra PS.1 system (Zeiss, Germany) applying the argon laser for excitation at 488 nm (1%) and diode lasers for excitation at 405 nm (0.5%) and 561 nm (2%), respectively. Emission filters for 410-469 nm (Hoechst), 490-544 nm (Calcein) and 608-719 (BOBO-3) with gains of 800, 800 and 650, respectively and a pinhole of 27  $\mu$ m were utilized. To avoid cross talk between the different channels, calcein was imaged simultaneously in a different track than the Hoechst 33342 and BOBO-3. For fast imaging, the tracks were switched



in every line of the image. For magnification, a  $40 \times 1.4$  NA plan apochromat oil objective was applied. Images were acquired using the ZEN software, version 2.3 SP1 (Zeiss, Germany). The images were processed regarding their blue (Hoechst 33342) and green (calcein) channels in batch mode using ImageJ, version 1.52<sup>[232]</sup> as follows: First, the background of both channels was corrected using the rolling ball background subtraction tool applying a sliding paraboloid without previous image smoothing. The contrast of both channels was enhanced automatically with a normalization of 0.01% saturation. For the overlay image, both channels were merged.

### For Table 4.2: Characterization data for polymers and micelles of the LAMA library

The size (hydrodynamic diameter) of the polyplexes was measured following poly-/micelleplex preparation at N\*/P 30 in 100  $\mu$ L HBG buffer as described in the manuscript. For PDMAEMA I and LAMA-mic I, each sample was measured in quintuplicates with three runs of 30 s at 25 °C after an equilibration time of 30 s. For PDMAEMA II, each sample was measured in triplicates with three runs of 30 s at 25 °C after an equilibration time of 30 s. Data are expressed as mean of at least three replicates.

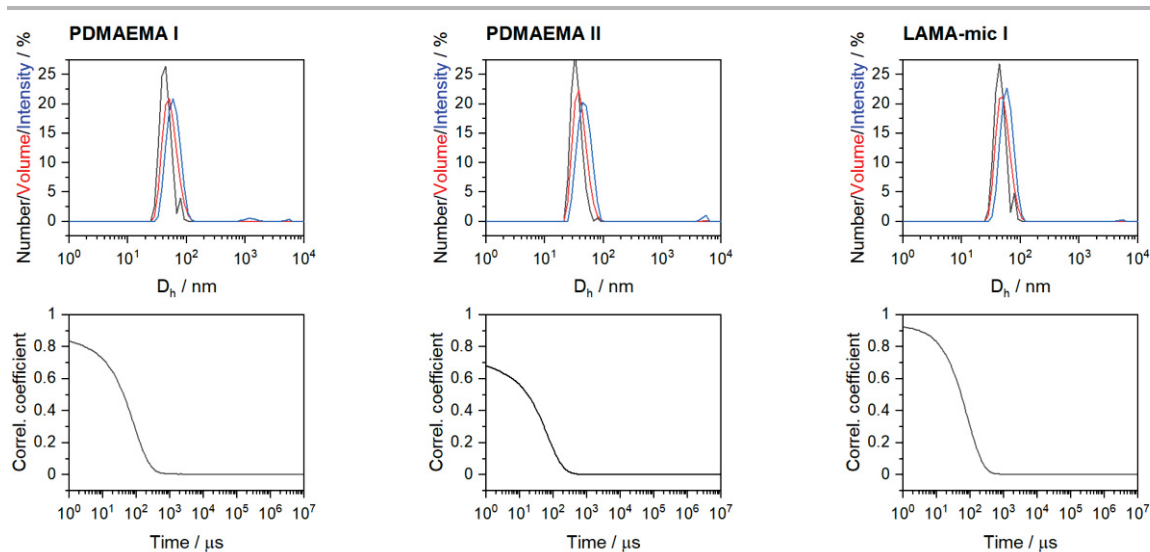


**Figure 8.2.** Representative DLS curves for unpublished data in **Table 4.2** obtained according to the method described above.

## **Curriculum vitae**

## Publication List

### Peer-reviewed publications

C. Chen, **F. Richter**, J. Zhang, C. Guerrero-Sanchez, A. Traeger, U. S. Schubert, A. Feng, S. H. Thang, Synthesis of functional miktoarm star polymers in an automated parallel synthesizer, *Eur. Polym. J.* **2021**, *160*, 110777.

**F. Richter**, K. Leer, L. Martin, P. Mapfumo, J. I. Solomun, M. T. Kuchenbrod, S. Hoepfener, J. C. Brendel, A. Traeger, The impact of anionic polymers on gene delivery: how composition and assembly help evading the toxicity-efficiency dilemma, *J. Nanobiotechnology* **2021**, *19*, 292.

F. Hausig, F. H. Sobotta, **F. Richter**, D. O. Harz, A. Traeger, J. C. Brendel, Correlation between Protonation of Tailor-Made Polypiperazines and Endosomal Escape for Cytosolic Protein Delivery, *ACS Appl. Mater. Interfaces* **2021**, *13*, 35233-35247.

**F. Richter**, P. Mapfumo, L. Martin, J. I. Solomun, F. Hausig, J. J. Frietsch, T. Ernst, S. Hoepfener, J. C. Brendel, A. Traeger, Improved gene delivery to K-562 leukemia cells by lipoic acid modified block copolymer micelles, *J. Nanobiotechnology* **2021**, *19*, 70.

J. I. Solomun, G. Cinar, P. Mapfumo, **F. Richter**, E. Moek, F. Hausig, L. Martin, S. Hoepfener, I. Nischang, A. Traeger, Solely aqueous formulation of hydrophobic cationic polymers for efficient gene delivery, *Int. J. Pharm.* **2021**, *593*, 120080.

**F. Richter**, L. Martin, K. Leer, E. Moek, F. Hausig, J. C. Brendel, A. Traeger, Tuning of endosomal escape and gene expression by functional groups, molecular weight and transfection medium: a structure-activity relationship study, *J. Mater. Chem. B* **2020**, *8*, 5026-5041.

C. Chen, **F. Richter**, C. Guerrero-Sanchez, A. Traeger, U. S. Schubert, A. Feng, S. H. Thang, Cell-Penetrating, Peptide-Based RAFT Agent for Constructing Penetration Enhancers, *ACS Macro Lett.* **2020**, *9*, 260-265.

N. A. Hoang, **F. Richter**, M. Schubert, S. Lorkowski, L. O. Klotz, H. Steinbrenner, Differential capability of metabolic substrates to promote hepatocellular lipid accumulation, *European journal of nutrition* **2019**, *58*, 3023-3034.

M. N. Leiske, F. H. Sobotta, **F. Richter**, S. Hoepfener, J. C. Brendel, A. Traeger, U. S. Schubert, How To Tune the Gene Delivery and Biocompatibility of Poly(2-(4-aminobutyl)-2-oxazoline) by Self- and Coassembly, *Biomacromolecules* **2018**, *19*, 748-760.

### Manuscripts in submission

F. Hausig, **F. Richter**, M. Hoernke, J. C. Brendel, A. Traeger, Tracing the endosomal escape: A closer look at calcein and related reporters, *J. Mat. Chem. B* **2022**, submitted.

F. Hausig, G. Dekevic, F. H. Sobotta, J. I. Solomun, **F. Richter**, D. Salzig, A. Traeger, J. C. Brendel, Optimizing charge density of polypiperazines for effective gene delivery and evaluation of transfection mechanism, *J. Mat. Chem. B* **2022**, submitted.

P. Klemm, J. I. Solomun, M. Rodewald, M. T. Kuchenbrod, V. G. Hänsch, **F. Richter**, J. Popp, C. Hertweck, S. Hoepfener, C. Bonduelle, S. Lecommandoux, A. Traeger, S. Schubert, Gene delivery by tailored amphiphilic polypeptides: The impact of polyplex “surfing” and membrane interactions, *J. Nanobiotechnology* **2022**, submitted.

### **Poster presentations**

**F. Richter**, K. Leer, P. Mapfumo, J. I. Solomun, F. Hausig, M. T. Kuchenbrod, S. Hoepfener, J. C. Brendel, A. Traeger, Optimizing polymeric micelles for non-viral pDNA delivery, *European Society for Gene and Cell Therapy (ESGCT) Collaborative Virtual Congress*, **2021**, online.

**F. Richter**, K. Leer, P. Mapfumo, J. I. Solomun, M. T. Kuchenbrod, S. Hoepfener, J. C. Brendel, A. Traeger, The impact of anionic polymers on gene delivery, *Biennial Meeting of the GDCh Division of Macromolecular Chemistry*, **2021**, online.

**F. Richter**, L. Martin, K. Leer, F. Hausig, E. Moek, J. C. Brendel, A. Traeger, A Structure-Activity Relationship Study on Polyacrylamides for Non-Viral Gene Delivery, *Controlled Release Society Virtual Annual Meeting*, **2020**, online.

**F. Richter**, L. Martin, K. Leer, E. Moek, A. Traeger, Polyacrylamide als nicht-virale Nanotransporter für genetisches Material in Zellen, *1. Doktoranden- und PostDoc-Konferenz der BMBF-Fördermaßnahme ProMatLeben*, **2019**, Berlin, Germany.

**F. Richter**, L. Martin, E. Moek, A. Traeger, Polymer Vectors for Gene Delivery: Influence of Amine Moieties, *26<sup>th</sup> European Society for Animal Cell Technology (ESACT) Meeting*, **2019**, Copenhagen, Denmark.

**F. Richter**, D. Schnoor, L. Martin, F. Hausig, J. C. Brendel, A. Traeger, NanoMatFutur – PolyBioMik – Entwicklung von effizienten Polymer-basierten Nano-transportern durch Einbinden von biologischen Konzepten, *BMBF-Konferenz Materialinnovationen* **2018**, München, Germany.

L. Martin, **F. Richter**, E. Moek, A. Traeger, Ampholytic pH-Responsive Micelles for Non-Viral DNA Delivery, *Bordeaux Polymer Conference (BPC)* **2018**, Bordeaux, France.

### **Oral presentations**

**F. Richter**, L. Martin, K. Leer, F. Hausig, E. Moek, J. C. Brendel, A. Traeger, A Structure-Activity Relationship Study on Polyacrylamides for Non-Viral Gene Delivery, *Young Macromolecular Researcher Webinar (University of Warwick)*, **2020**, online.

## **Acknowledgement/Danksagung**



## **Declaration of authorship/Selbstständigkeitserklärung**

Ich erkläre, dass ich die vorliegende Arbeit selbständig und unter Verwendung der angegebenen Hilfsmittel, persönlichen Mitteilungen und Quellen angefertigt habe

Jena, \_\_\_\_\_

Ort, Datum

\_\_\_\_\_

Friederike Richter

## Publications Pub1 to Pub8

**Pub1** F. Hausig,<sup>‡</sup> F. Richter,<sup>‡</sup> M. Hoernke, J. C. Brendel, A. Traeger, Tracking the endosomal escape: A closer look at calcein and related reporters, *J. Mater. Chem. B* **2022**, submitted.

**Pub2** F. Richter, L. Martin, K. Leer, E. Moek, F. Hausig, J. C. Brendel, A. Traeger, Tuning of endosomal escape and gene expression by functional groups, molecular weight and transfection medium: A structure–activity relationship study, *J. Mater. Chem. B* **2020**, 8, 5026-5041.

**Pub3** F. Hausig, F. H. Sobotta, D. O. Harz, F. Richter, A. Traeger, J. C. Brendel, Correlation between protonation of tailor-made polypiperazines and endosomal escape for cytosolic protein delivery, *ACS App. Mater. Inter.* **2021**, 13, 35233-35247.

**Pub4** F. Richter,<sup>‡</sup> K. Leer,<sup>‡</sup> L. Martin, P. Mapfumo, J. I. Solomun, Maren T. Kuchenbrod, S. Hoepfener, J. C. Brendel, A. Traeger, The impact of anionic polymers on gene delivery: How composition and assembly help evading the toxicity-efficiency dilemma, *J. Nanobiotechnol.* **2021**, 19, 292.

**Pub5** F. Richter,<sup>‡</sup> P. Mapfumo,<sup>‡</sup> L. Martin, J. I. Solomun, F. Hausig, J. J. Frietsch, T. Ernst, S. Hoepfener, J. C. Brendel, A. Traeger, Improved gene delivery to K-562 leukemia cells by lipoic acid modified block copolymer micelles, *J. Nanobiotechnol.* **2021**, 19, 70.

**Pub6** J. I. Solomun, G. Cinar, P. Mapfumo, F. Richter, E. Moek, F. Hausig, L. Martin, S. Hoepfener, I. Nischang, A. Traeger, Solely aqueous formulation of hydrophobic cationic polymers for efficient gene delivery, *Int. J. Pharm.* **2021**, 593, 120080.

**Pub7** M. N. Leiske, F. H. Sobotta, F. Richter, S. Hoepfener, J. C. Brendel, A. Traeger, U. S. Schubert, How to tune the gene delivery and biocompatibility of poly(2-(4aminobutyl)-2-oxazoline) by self- and coassembly, *Biomacromolecules* **2018**, 19, 748-760.

**Pub8** C. Chen, F. Richter, C. Guerrero-Sanchez, A. Traeger, U. S. Schubert, A. Feng, S. H. Thang, A cell penetrating peptide based RAFT agent for constructing penetration enhancers, *ACS Macro Lett* **2020**, 9, 260-265.

<sup>‡</sup> Authors contributed equally to this work.

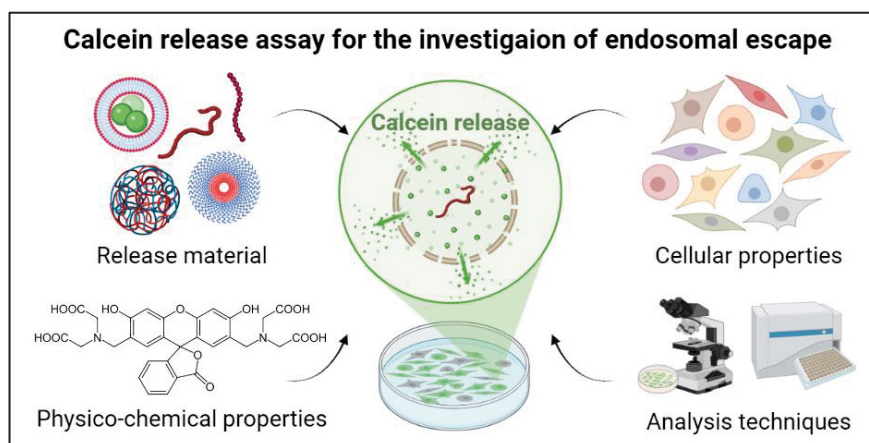


## Publication Pub1

### Tracking the endosomal escape: A closer look at calcein and related reporters

F. Hausig,<sup>‡</sup> F. Richter,<sup>‡</sup> M. Hoernke, J. C. Brendel, A. Traeger

*J. Mater. Chem. B* 2022, submitted.



1 Tracking the Endosomal Escape: A Closer Look at  
2 Calcein and Related Reporters.

3 *Franziska Hausig,<sup>a,b,†</sup> Friederike Richter,<sup>a,b,†</sup> Maria Hoernke,<sup>c</sup> Johannes C. Brendel,<sup>\*a,b</sup> Anja*  
4 *Traeger<sup>\*a,b</sup>*

5 <sup>a</sup>Laboratory of Organic and Macromolecular Chemistry (IOMC), Friedrich Schiller University  
6 Jena, Humboldtstrasse 10, 07743 Jena, Germany.

7 <sup>b</sup>Jena Center for Soft Matter (JCSM), Friedrich Schiller University Jena, Philosophenweg 7,  
8 07743 Jena, Germany.

9 <sup>c</sup>Chemistry and Pharmacy, Albert-Ludwigs-Universität Freiburg, Hermann-Herder-Str. 9, 79104  
10 Freiburg i.Br., Germany

11  
12 †Authors contributed equally

13 \*Correspondence to A. Traeger ([anja.traeger@uni-jena.de](mailto:anja.traeger@uni-jena.de))  
14 and J. C. Brendel ([johannes.brendel@uni-jena.de](mailto:johannes.brendel@uni-jena.de))

15

16 KEYWORDS

17 Endosomal escape, calcein release, leakage, pore formation, polymer-membrane interactions,  
18 method comparison

19 ABSTRACT (242/250 words)

20 Crossing the cellular membrane and delivery of active pharmaceuticals or biologicals into the  
21 cytosol of cells is an essential step in the development of new nanomedicines, which recently  
22 became particularly emphasized in the rapid evolving of vaccines during the SARS-CoV-2  
23 pandemic. One of the most important intracellular processes regarding the required cellular uptake  
24 of biologicals is the endolysosomal pathway. Sophisticated release materials have been developed  
25 to escape endosomal entrapment and deliver their cargoes to the required site of action. Various in  
26 vitro assays have been established, to study the release materials and their performance at this  
27 obstacle. Among these, the release of the small, membrane-impermeable dye calcein from vesicles  
28 or within cells has become a very popular and straightforward method as it is accessible for most  
29 labs worldwide, allows for rapid and simple conclusions about the release potential, and enables  
30 the study of release mechanisms. This review is intended to provide an overview and guidance for  
31 scientist applying the calcein release assay, beginning with indications on the chemistry and history  
32 of the molecule. It further provides an overview of its use in the study of endosomal escape,  
33 considerations of potential pitfalls, challenges and limitations of the assay, and a brief summary of  
34 complementary methods. Based on this review, we hope to encourage further research groups to  
35 take advantage of the calcein release assay for their own purposes and thus help to create a database  
36 for a more efficient cross-correlations between release materials.

37	1. Introduction .....	4
38	2. Chemical background of calcein .....	8
39	3. Calcein leakage from artificial model vesicles .....	13
40	4. Calcein release studied within cells .....	21
41	4.1. Release of encapsulated calcein within cells .....	22
42	4.2. Simultaneous and sequential addition of release material and calcein as sensor.....	25
43	4.3. Analytical Methods .....	31
44	5. Potential pitfalls of the calcein release assay <i>in cells</i> .....	34
45	5.1. Physicochemical factors relevant for the calcein solution .....	35
46	5.2. Biological factors relevant for the incubation time.....	36
47	5.3. Factors influencing the accuracy of the measurement .....	40
48	6. Complementary methods .....	42
49	7. Conclusion & perspectives .....	47
50	8. Declarations .....	51
51	8.1. Competing interests.....	51
52	8.2. Acknowledgements.....	51
53	9. References .....	52
54		
55		

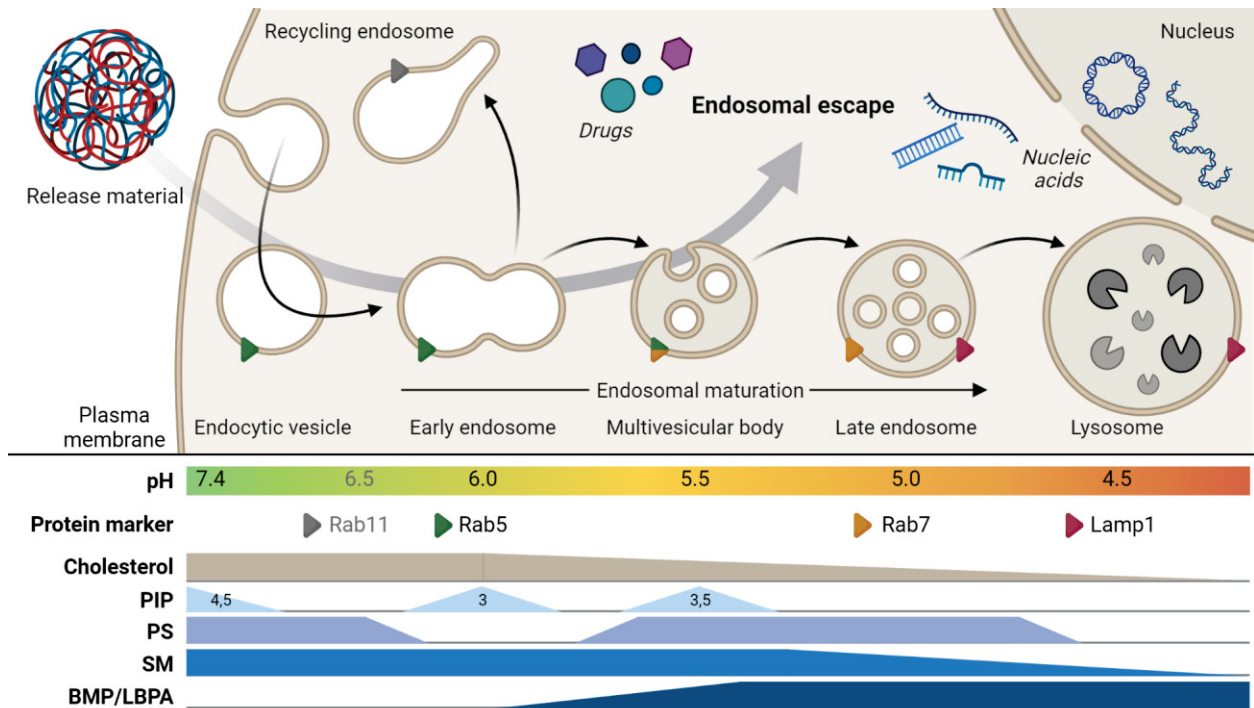
## 56 1. INTRODUCTION

57 The field of non-viral nanocarriers for the delivery of nucleic acids into cells has made great  
58 progress in the last decades. In particular the nucleic acid-based systems such as the SARS-CoV-  
59 2 vaccines or novel cancer therapies underline the enormous potential of this technology. Despite  
60 the current success of lipid-based gene carriers, the number of papers on polymer-based gene  
61 carriers is also constantly increasing due to their impressive versatility and stability. For the  
62 successful delivery of nucleic acids, several challenges need to be addressed, including  
63 nanoparticle formulation, targeting, intracellular release, and transport to its destination.  
64 Especially, the intracellular processes represent a key aspect, which surprisingly is still not well  
65 understood. Therefore, no consistent theory can be applied to the various nanocarrier systems, but  
66 two aspects predominate among the cellular barriers, cellular uptake and endosomal release.  
67 Further hurdles may also play a role such as the transfer of genetic material into the cell nucleus,  
68 which can be neglected in mRNA/siRNA applications, because their site of action is inside the  
69 cytosol. Cellular uptake is obviously fundamental and depends on the physicochemical parameters  
70 of the nanocarrier or the introduction of active target components, which is well reviewed  
71 elsewhere.<sup>1-4</sup> However, successful uptake into cells does not necessarily correlate with efficient  
72 gene expression. Therefore, escape from the endo-lysosomal compartment is considered as a  
73 critical cellular step for the successful carrier-dependent delivery of sensitive cargos such as  
74 genetic material or proteins.<sup>5</sup> The main reasons are, on the one hand, the risk of enzymatic  
75 degradation and, on the other hand, the fact that genetic material can only exert its effect outside  
76 the endosomes. Unfortunately, several nanocarriers fail in this regard, as they are either excreted  
77 (exocytosis) or degraded (lysosome), which means that endosomal release can be considered an  
78 important lever for improving cellular gene delivery.<sup>6-8</sup> The lack of knowledge on underlying  
79 processes emphasizes the importance of studying endosomal release, not only to better understand  
80 the mode of action of different nanocarriers or release materials, respectively, but also to develop

81 new, more efficient systems. In this review, we refer to the general term release material instead  
82 of nanocarrier, since not all mentioned materials may contain a cargo as it is implied for carriers.  
83 The term comprises all compounds that promote endosomal release and include lipid-based  
84 materials (liposomes, lipid nanoparticles), polymer-based materials (linear or branched polymers,  
85 polymersomes, micelles, nanoparticles and peptides), as well as peptide-based materials.

86 In order to optimize the design of release materials, the biological processes must be considered  
87 in more detail, because they determine the conditions the release materials have to deal with.  
88 Particles as well as liquids, solutes, macromolecules, or plasma membrane components are taken  
89 up by the cell through endocytosis, in which the plasma membrane is first invaginated and then  
90 segregated, allowing for the formation of intracellular vesicles.<sup>4, 9</sup> Besides their role in nutrient  
91 uptake, endosomes are involved in the regulation and fine-tuning of numerous signaling pathways  
92 in the cell, *e.g.*, the recycling of receptors. After vesicle formation, they fuse to form early  
93 endosomes and become linked to the microtubule network.<sup>10</sup> In this way, the vesicles and their  
94 cargos are able to move alongside the microtubules toward the perinuclear region and gradually  
95 transform into late endosomes, where hydrolases and membrane components of the secretory  
96 pathway are recruited. Subsequently, they enlarge in size, form more intraluminal vesicles and  
97 finally fuse with the lysosome to form the endolysosomes.<sup>9</sup> During endosomal maturation, the size  
98 of endocytic vesicles increases from  $\approx 100$  nm (early endosome) to  $\approx 1000$   $\mu$ m (lysosome).<sup>9, 11-13</sup>  
99 Inside the endolysosomes a variety of digestive processes take place, which degrade most  
100 compounds of biological origin and, thus, represent a dead end for the release materials which  
101 should be avoided. During endosomal maturation, not only the size and structure of the organelles  
102 change, but more importantly the intravesicular pH value and the composition of the membrane,  
103 both, in terms of proteins and lipids (see Figure 1).<sup>9, 14</sup> In early endosomes, the membrane consists  
104 mainly of neutral lipids (including sphingolipids, sterols), similar to the cytoplasmic membrane.  
105 Along with the acidification of the vesicles (from 7.4 to 4.5), the proportion of sterols decreases

106 leading to an increase in membrane fluidity. Furthermore, the proportion of anionic lipids (*e.g.*,  
 107 lysobisphosphatidic acid (LBPA), also termed bis(monoacylglycerol)phosphate (BMP))  
 108 increases.<sup>15-18</sup>



109  
 110 **Figure 1. Endosome maturation.** Following endocytosis, the endocytic vesicle delivers the  
 111 internalized cargo to the early endosome, where it is either recycled through the recycling  
 112 endosome or evolves further along the endolysosomal pathway to be degraded. Beside the fusion  
 113 of different vesicles and membrane invagination, this is accompanied by changes in the  
 114 intravesicular pH value, membrane lipid composition and important protein markers. To avoid the  
 115 enzymatic degradation within the lysosome, the release material (representative for polymers,  
 116 liposomes, nanoparticles) delivering drugs or nucleic acids, thus, must escape this process at an  
 117 earlier stage. PIP – phosphoinositides (numbers indicate phosphate positions on the inositol ring),  
 118 PS – phosphatidylserine, SM – sphingomyelin, BMP/LBPA – bis(monoacylglycerol)phosphate/  
 119 lysobisphosphatidic acid. Adapted from <sup>16</sup>.

120 This complex process is exploited by viruses, which can thus enter the cell in an optimized way  
 121 and reprogram it without destroying it. Viruses cross the endosomal membrane by a pH-dependent  
 122 change of conformation or hydrophobicity of their surface peptides leading to penetration of the  
 123 vesicular membrane. This inspired material designers to mimic the efficiency of viral systems and  
 124 optimize them with a lower risk potential, *e.g.*, in the form of cell-penetrating peptides (CPPs),

125 liposomes, synthetic polymers, and nanoparticles.<sup>19, 20</sup> To circumvent lysosomal digestion, pH-  
126 dependent cationic amines were commonly included in polymers or lipids. Along the endosomal  
127 pathway, the amines become increasingly protonated and enable electrostatic interactions with  
128 anionic lipids or facilitate hydrogen bonding between the amino groups of the nanocarrier and the  
129 phosphate groups of the lipids. Hence, the release materials can interact locally with the membrane  
130 destabilizing it and, thereby, promoting the escape of the release materials and their cargoes into  
131 the cytoplasm.<sup>21</sup> Furthermore, the "proton-sponge" hypothesis remains an accepted explanation for  
132 the endosomal release of some polymers. The buffering capacity of polycations is considered to  
133 cause a change in vesicular pH and an influx of ions, which increases the osmotic pressure and  
134 eventually causes a rupture of the lipid membrane.<sup>22</sup> However, this hypothesis is under debate in  
135 the community.<sup>23</sup>

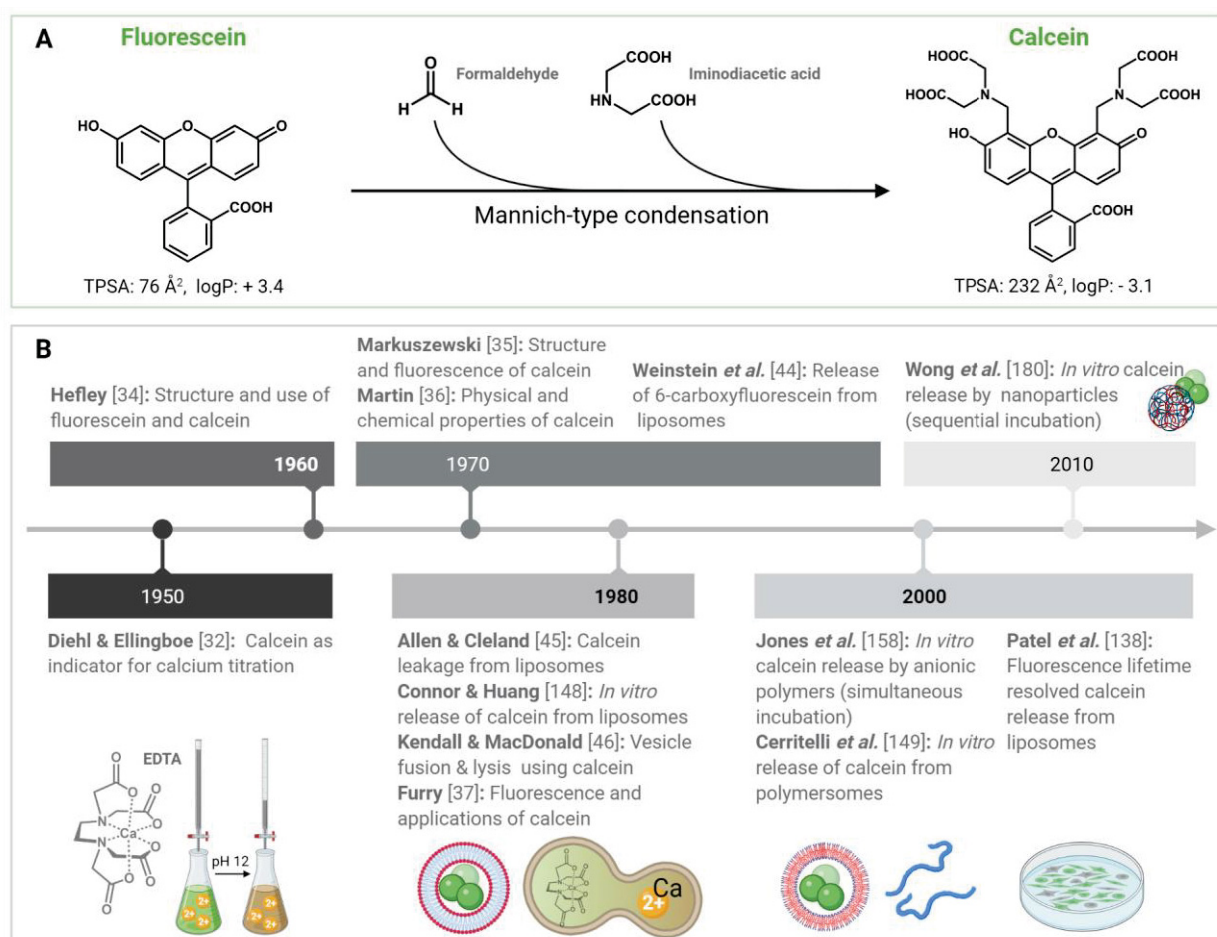
136 For the detailed investigation of the cellular fate of nanoparticles and in particular the endosomal  
137 release, different techniques can be applied. Predominantly, the integrity of the endosomal  
138 membrane is evaluated for endosomal escape. Related experiments can be performed in cells,  
139 isolated cell organelles and artificial or model vesicles. The latter represents a more controlled and  
140 reproducible environment since endosomes can be modeled by liposomes with membranes of  
141 known phospholipid composition. The variety of applied methods can be found elsewhere.<sup>24, 25</sup>  
142 However, the potency and limitations of each approach should be kept in mind. In the case of gene  
143 delivery, the expression or functionality of the genetic material (*e.g.*, expression or knock down)  
144 is one possible test, representing a global read-out and functionality. Fluorescent dyes/proteins or  
145 reporter systems can be used additionally to study endosomal release in more detail.<sup>5, 26-31</sup> The  
146 most popular sensor molecule is calcein, which is straightforward to apply, affordable and easily  
147 accessible. Therefore, it is used to study a variety of different release materials.

148 However, different experimental settings, conditions and analytical methods are used for this  
149 purpose, which makes it difficult to evaluate/compare different materials. In this review, we



150 elucidate the key application of calcein as a powerful yet simple tool to investigate the endosomal  
 151 escape. Various conditions have been reported, which reflects the complexity of the calcein release  
 152 assay and sometimes might even cause contradictive outcomes. In the following sections, calcein  
 153 is first introduced regarding its basic chemistry and historical development, followed by overviews  
 154 of the different applied methods in models or cells, and a section reflecting on pitfalls, challenges,  
 155 and limitations of the calcein release assay within the cellular environment. A few complementary  
 156 methods are described in the last section, which certainly does not represent a comprehensive  
 157 overview, but provides some guidance to alternatives overcoming the previously mentioned issues.

## 158 2. CHEMICAL BACKGROUND OF CALCEIN



159  
 160 **Figure 2. Synthesis and utilization of calcein.** (A) The synthesis route of calcein starting from  
 161 fluorescein with indicated polarity (TPSA: topological polar surface area) and hydrophobicity

162 measures for both molecules. (B) Historical overview on the development of calcein as a  
163 fluorescent molecule and its utilization to investigate endosomal escape.

164 Calcein, also known as bis[*N,N*-bis(carboxymethyl)aminomethyl] fluorescein, fluorescein  
165 complexone and fluorexon, was first described by Diehl and Ellingboe in 1956 as an indicator for  
166 the complexometric titration of calcium<sup>32, 33</sup> followed by several PhD theses at the Iowa State  
167 University with detailed descriptions regarding its synthesis, characterization and applications  
168 (Figure 2).<sup>34-37</sup> It is synthesized *via* a Mannich-type condensation of fluorescein, formaldehyde,  
169 and iminodiacetic acid and can, thus, be considered as a derivative of fluorescein belonging to the  
170 substance class of xanthenes.<sup>32, 35, 38</sup> Due to the condensation reaction, calcein combines two  
171 features within one molecule: the fluorescence of fluorescein and the chelation property of  
172 iminodiacetic acid, which is also part of the well-known chelator ethylenediaminetetraacetic acid  
173 (EDTA).<sup>35</sup> Comparable to fluorescein, calcein absorbs light in the cyan spectrum range and  
174 fluoresces in the green range with absorption and emission maxima at  $\lambda_{\text{Ex/Em}} = 495/515 \text{ nm}$ .<sup>34, 39</sup>  
175 The self-quenching of fluorescein at high concentrations, known since 1888,<sup>40-42</sup> also characterizes  
176 calcein and other derivatives, such as 6-carboxyfluorescein (Figure 3A, 1). This property has been  
177 exploited since the late 1970s to investigate the stability of liposomes encapsulating 6-  
178 carboxyfluorescein<sup>43, 44</sup> or calcein<sup>45, 46</sup>, as a damage of the liposomal membrane would result in  
179 dilution of the dye and an increase in its fluorescence intensity. Regarding calcein, a self-quenching  
180 concentration of 70 mM is often utilized,<sup>47, 48</sup> but there are also studies showing different values  
181 which could be attributed to different buffer systems and fluorescence measurement methods  
182 (Table 1).

183

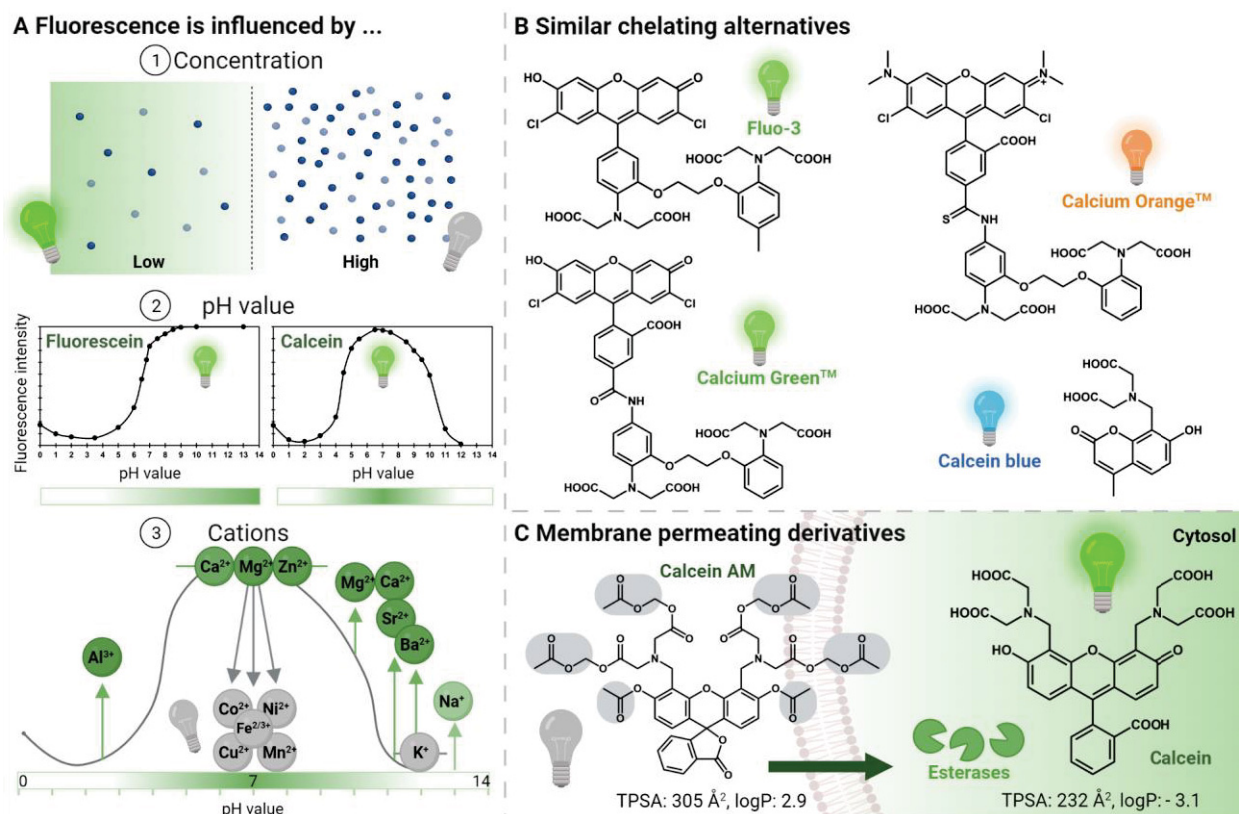
184

185 **Table 1.** Overview of quenching concentrations (conc.) and pH values in different studies.

Ref.	Buffer (mM)	pH value	conc. at FImax mM	conc. at 50 % FImax mM	conc. at 10 % FImax mM
Hamann 2002 <sup>49</sup>	119 Na <sup>+</sup> , 5 K <sup>+</sup> , <b>0.8 Mg<sup>2+</sup></b> , <b>1.8 Ca<sup>2+</sup></b> , 114 Cl <sup>-</sup> , 0.8 SO <sub>4</sub> <sup>2-</sup> , 25 HEPES, 5.6 glucose, 44 mannitol	7.4	4.000	8.400 <sup>[b]</sup>	> <b>30.00</b> <sup>[b]</sup>
Roberts 2003 <sup>50</sup>	PBS (350 mOsmol L <sup>-1</sup> )	7.4	0.019	0.055	<b>0.20</b> <sup>[b]</sup>
Andersson 2007 <sup>51</sup>	50 PBS + POPC	7.0	0.032 <sup>[b]</sup>	0.100 <sup>[b]</sup>	> <b>0.10</b> <sup>[b]</sup>
Imamura 2017 <sup>52</sup>	PBS	7.4	2.000	9.000 <sup>[b]</sup>	<b>25.00</b> <sup>[b]</sup>
Dorrington 2018 <sup>53</sup>	0.1 EDTA, 10 Tris, 100 NaCl	7.8	0.970	N/A	> <b>6.40</b> <sup>[b]</sup>
Brkovic 2020 <sup>54</sup>	0.2 Na <sub>2</sub> HPO <sub>4</sub> -NaH <sub>2</sub> PO <sub>4</sub>	7.5	0.002 <sup>[b]</sup>	0.005 <sup>[b]</sup>	<b>0.01</b> <sup>[b]</sup>
Bae 2021 <sup>55</sup>	50 HEPES, 100 Na <sup>+</sup> , 100 Cl <sup>-</sup> , 5 % glycerol	7.4	0.001	0.002 <sup>[b]</sup>	> <b>0.20</b> <sup>[b]</sup>
own data <sup>[a]</sup>	20 HEPES, 5 % glucose	5, 6, 7	0.080	1.120	> <b>3.20</b>

[a] not published.  
[b] Values were read from the graph.

186  
187 Another factor influencing the fluorescence of calcein is the pH value (Figure 3A, 2). However,  
188 with the six carboxy groups available for protonation, the fluorescence of calcein is less pH  
189 dependent than that of fluorescein and exhibits high intensities between pH 4.5 and 10.<sup>34, 37, 56</sup>  
190 Therefore, it remains fluorescent within the biologically relevant pH range including  
191 endolysosomal pH values important for the analysis of endosomal escape. Additionally, the  
192 carboxy moieties lead to a higher polarity and increased hydrophilicity of calcein compared to  
193 fluorescein (for TPSA and logP values refer to Figure 2A) and, thus, make it less membrane  
194 permeable at low pH values.<sup>44, 57, 58</sup> The pH value also affects the solubility in water of calcein  
195 with higher pH values leading to a better solubility.<sup>37</sup>



196

197 **Figure 3. Physico-chemical properties and derivatives of calcein.** (A) Factors influencing the  
 198 fluorescence intensity of calcein: Concentration, pH value and different cations. Arrows in 3  
 199 indicate an increase or decrease in fluorescence intensity through the respective cation. (B) Further  
 200 cation chelating molecules with structures similar to calcein. (C) Principle for the identification of  
 201 viable cells using calcein AM.

202 In addition, the calcein fluorescence is influenced by various di- or multivalent metal ions, more  
 203 precisely by their chelation which has been used for the determination of the cations in various  
 204 tissues and fluids (Figure 3A, 3). The complexation of the cations has two different effects, which  
 205 in turn are pH and concentration dependent.<sup>39</sup> Under the tested conditions, the ions of the alkaline  
 206 earth metals magnesium, calcium, barium, and strontium enhance the calcein fluorescence at  
 207 alkaline pH values when calcein would otherwise be quenched.<sup>36, 37, 56</sup> At neutral pH values and  
 208 metal:calcein ratios of 4 or 10:1, however, these ions only influence the absorption spectrum in the  
 209 UV range but not the fluorescence of the brightly emitting calcein.<sup>56</sup> By contrast, ions of the  
 210 transition metals manganese, cobalt, nickel, copper,<sup>36, 56, 59, 60</sup> and iron<sup>37, 61-63</sup> have been shown to  
 211 quench the fluorescence in liposomes at neutral pH values. Furthermore, ions with higher valencies

212 are able to increase the fluorescence intensity of calcein, such as aluminum ions at low pH  
213 values.<sup>36, 56, 64</sup> On the other side, the addition of sodium can enhance fluorescence at high pH  
214 values. Interestingly, potassium or lithium ions, however, do not affect the fluorescence, favoring  
215 KOH solutions over NaOH solutions to dissolve the calcein.<sup>39, 65</sup> Besides calcein, there are also  
216 other combinations of the iminodiacetic acid and various dyes that can be used to chelate cations  
217 (Figure 3B). Calcein blue (umbellikomplexon), *e.g.*, belongs to the coumarins and has similar  
218 properties like calcein.<sup>66-70</sup> Furthermore, Calcium Green<sup>TM</sup>, Calcium Orange<sup>TM</sup> and Fluo-3 are able  
219 to indicate calcium even at neutral pH and have thus been applied as fluorescent intracellular Ca<sup>2+</sup>  
220 sensors.<sup>71-73</sup>

221 Besides the determination of cations, calcein or more precisely its acetoxymethyl ester (calcein  
222 AM) is also used to identify viable cells. In contrast to calcein, the hydrophobic and non-  
223 fluorescent calcein AM is membrane permeable (Figure 3C). Upon entering the cells, the esters of  
224 calcein AM are hydrolyzed by non-specific intracellular esterases resulting in the fluorescent  
225 calcein that cannot easily permeate the cellular membrane and is retained within the cells. Since  
226 only living cells are able to convert the calcein AM, this method can be utilized to identify viable  
227 cells.<sup>74-77</sup> The mechanism has been known already for fluorescein and its diacetate ester (FDA),<sup>78,</sup>  
228 <sup>79</sup> but due to its above-mentioned advantages calcein prevailed.<sup>80</sup> Apart from general cell viability,  
229 this method is also used to determine the membrane integrity of cells by pre-loading the cells with  
230 calcein AM/calcein and measuring the release of calcein upon membrane destruction by various  
231 substances.<sup>81-83</sup> In general, the method allows tracking of different cells<sup>84, 85</sup> and even extracellular  
232 vesicles (microvesicles, exosomes)<sup>86</sup> for various purposes, *e.g.*, the formation of gap junctions.<sup>87</sup>

### 233 3. CALCEIN LEAKAGE FROM ARTIFICIAL MODEL VESICLES

234 Early experiments to investigate interactions of potential release materials with lipid membranes  
235 include release studies with artificial liposomes, also called lipid vesicles. The strong self-  
236 quenching properties of calcein and the related 6-carboxyfluorescein at high concentrations had  
237 already been exploited in these experiments, *i.e.*, for the investigation of endosomal escape. These  
238 dyes still represent prominent reporters to monitor the release from lipid vesicles by different  
239 release materials or vectors. As liposomes have been used as artificial cell models since the 1970s,  
240 numerous reviews and protocols are available, which we like to refer to, *e.g.*,<sup>88-92</sup>. In the present  
241 review, we focus on studies directly related to endosomal escape to illustrate the liposomal features  
242 that can be exploited for the investigation of the specific characteristics of endosomal escape.  
243 (Table 2).

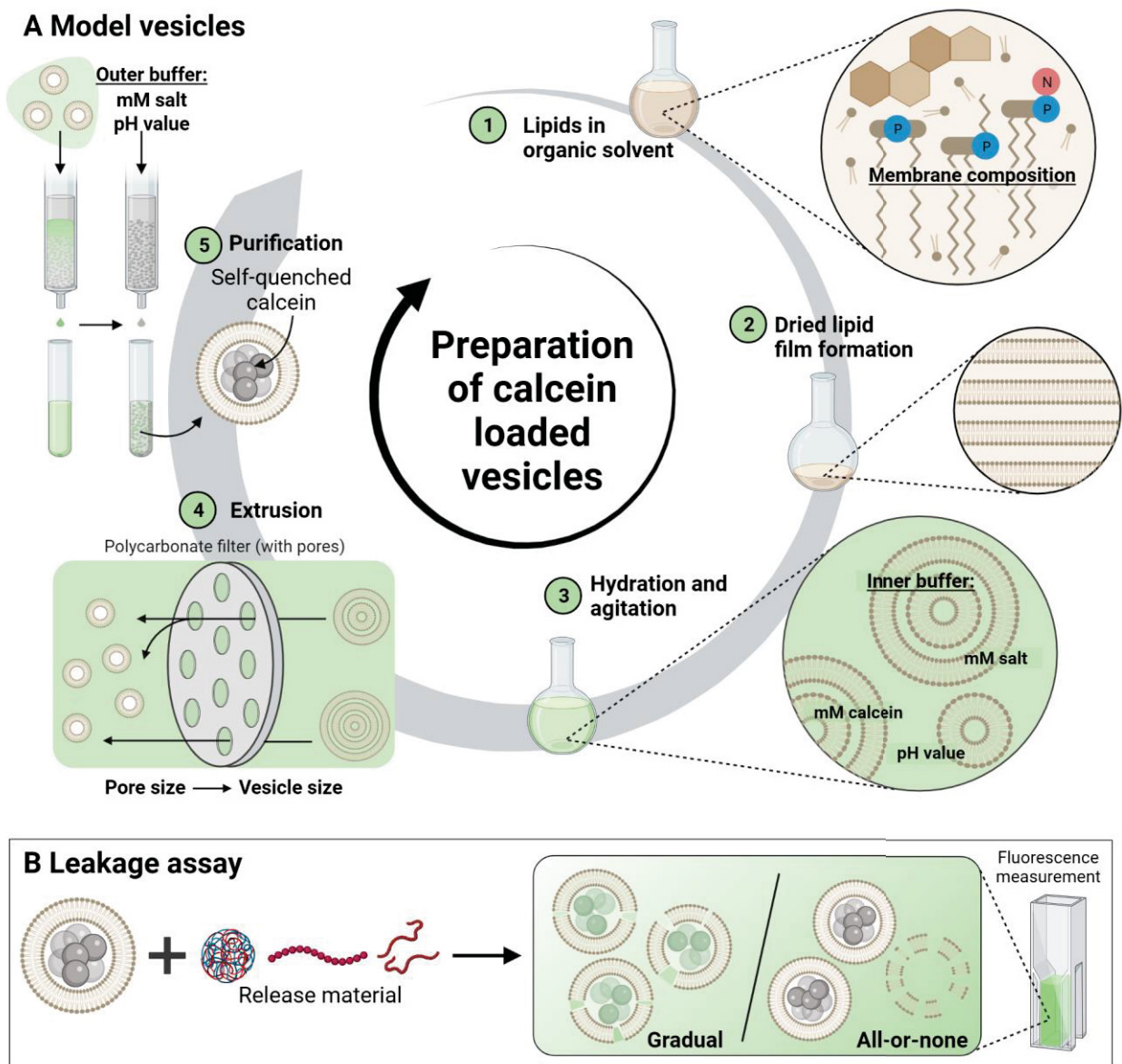
244 In general, typical leakage experiments involve the addition of the investigated release material  
245 to a dispersion of vesicles with encapsulated calcein (Figure 4). Upon permeabilization of the lipid  
246 bilayer, the released calcein is diluted in the outer buffer. In the case of a gradual leakage, also  
247 calcein that remains entrapped is diluted. Thereby, self-quenching is reduced, and the fluorescence  
248 increases. This effect can be monitored *via* the fluorescence intensity and normalized to the  
249 maximal fluorescence reached by lysis of the remaining liposomes. Alternatively, the fluorescence  
250 lifetime and amount of free and entrapped dye can be determined. Typically, leakage is examined  
251 after 1 h incubation time. However, studying the time course of leakage over several hours can  
252 indicate certain leakage mechanisms.<sup>93, 94</sup>

253 **Table 2.** Investigation of calcein release from model vesicles.

Release material	Vesicle type <sup>[a]</sup>	Lipids <sup>[b]</sup>	c(calcein)		Incubation conditions	Ref.
				mM		
Polymer	SUV	DHP, PC, Chol	40		● 10 mM phosphate, pH 7.4, 25 °C or 65 °C, 20 min	95
	LUV	PC, PG	80		● 10 mM HEPES + glucose, pH 5.8-7.6, up to 60 min	96
		PC	200		● 10 mM Tris-HCl, 100 mM NaCl, pH 10, 25 °C, up to 60 min	97
Peptide	LUV	PC, PE, BMP, Chol	60		● <b>in:</b> 10 mM NaH <sub>2</sub> PO <sub>4</sub> , 100 mM NaCl, pH 7.4 ● <b>out:</b> 10 mM NaH <sub>2</sub> PO <sub>4</sub> , 100 mM NaCl, pH 5.5, (or pH 7.4) RT, 60 min	98-100
			60		● 5 mM NaH <sub>2</sub> PO <sub>4</sub> , 100 mM KCl, pH 7.4, RT, 60 min	101
		PC, PE, BMP, PG	70		● 10 mM phosphate, 100 mM NaCl, pH 7.4, RT, up to 20 min, 60 min	102
		PC, PE, BMP, Chol, PA, PG	60		● 10 mM NaH <sub>2</sub> PO <sub>4</sub> , 100 mM NaCl, pH 5.5, RT, 60 min	103
		70		● PBS, pH 7.4, up to 30 min	104	
		100		● <b>in:</b> 375 mM NaOH, 50 mM NaCl, pH 7.4 ● <b>out:</b> 200 mM NaCl, 20 mM citrate, pH 7.4/5, up to 60 min	105	
		GUV	PC, PE, BMP, PG	70		● 10 mM phosphate, 100 mM NaCl, pH 7.4, RT, up to 20 min, 60 min
		PC, PG, Chol	50		● <b>in:</b> 130 mM NaCl, 20 mM Na <sub>3</sub> PO <sub>4</sub> ● <b>out:</b> 130 mM KCl, 20 mM K <sub>3</sub> PO <sub>4</sub> , pH 7, 4 h	106
Peptide/Polymer	LUV	PC	40		● 10 mM NaH <sub>2</sub> PO <sub>4</sub> , pH 7.4, 5 min	107
		PC, Chol	90		● <b>in:</b> 137 mM HEPES, pH 7.4 ● <b>out:</b> 137 mM HEPES, pH 7.4 or 137 mM sodium citrate buffer, pH 5.0; 37 °C, 60 min	108
Peptide/Liposome	LUV	PC, Chol	90		● 5 mM HEPES, 150 mM NaCl, pH 7.4, RT, 60 min	109
		PC, PS, Chol	40		● <b>in:</b> 1 mM EDTA, ● <b>out:</b> PBS or citrate/phosphate, pH 7.4/5.5, 37 °C 30 min	110, 111

[a] SUV -small unilamellar vesicle (30 nm - 100 nm), LUV – large unilamellar vesicle (100 nm -1 μm), GUV – giant unilamellar vesicle (1 μm - 200 μm)

[b] in different ratios. Only types of phospholipids are distinguished, fatty acids can vary. DHP – dihexadecyl phosphate, PC – phosphatidylcholine, Chol – cholesterol, PE – phosphatidylethanolamine, BMP - bis(monoacylglycero)phosphate, PG – phosphatidylglycerol, PA – phosphatidic acid, PI – phosphatidylinositol, PS – phosphatidylserine.



255  
 256 **Figure 4. Preparation and calcein leakage from model vesicles.** (A) The model liposomes  
 257 (LUVs) can be modified at different steps to mimic different properties of the endolysosomal  
 258 pathway. (B) Upon mixing of the liposomes with different release materials, the release of calcein  
 259 can be determined and characterized regarding the release mechanism (for example, gradual or all-  
 260 or-none, transient or continuous). Adapted from “Liposome Preparation *via* Thin Film Hydration”  
 261 (2022) by BioRender.com. Retrieved from <https://app.biorender.com/biorender-templates>.

262 The model vesicles can roughly be classified according to their size into small unilamellar  
 263 vesicles (SUV, 0.02-0.1  $\mu\text{m}$ ), large unilamellar vesicles (LUV, 0.1-1  $\mu\text{m}$ ) and giant unilamellar  
 264 vesicles (GUV, 1-200  $\mu\text{m}$ ).<sup>112</sup> However, the size of the lipid vesicles only matters for comparison  
 265 purposes. In the surveyed studies, mostly LUVs and GUVs have been investigated, which have



266 too small membrane curvature to result in packing defects. More importantly, identical leakage  
267 mechanisms can appear different in vesicles of different sizes.<sup>113</sup> LUVs are commonly prepared  
268 by solvent-free self-assembly (Figure 4). For this, thin lipid films are obtained from organic  
269 solutions containing all lipid components. The films are rehydrated with an aqueous calcein buffer,  
270 followed by multiple freeze-thaw cycles,<sup>96, 99, 102, 104</sup> and repeated extrusion through polycarbonate  
271 membranes with pore sizes of 100 nm,<sup>95, 96, 98-100, 102, 103, 107</sup> or larger.<sup>104, 110</sup> The outer buffer with  
272 free dye is exchanged *via* size exclusion chromatography (SEC) or centrifugation protocols.<sup>109</sup>  
273 GUVs can be obtained by swelling of the dried lipid film in the desired buffer<sup>114, 115</sup>, sometimes  
274 involving a polymer gel.<sup>102</sup> Electroformation can also be utilized, but GUVs obtained this way  
275 might suffer from artefacts when using charged lipids and calcein might also interfere.<sup>116, 117</sup>

276 Not only the size, but more importantly the membrane composition is known to change during  
277 endolysosomal maturation (see as well 1. Introduction).<sup>9</sup> These changes in composition inspired  
278 investigations of different lipid compositions containing BMP. It was found that liposomal leakage  
279 by different variants of the CPP TAT occurred only in presence of BMP, but not if other anionic  
280 phospholipids such as phosphatidylglycerol (PG) or phosphatidic acid (PA) were incorporated.<sup>98-</sup>  
281 <sup>100, 102, 103</sup> The influence of the changing cholesterol content on the leakage of further peptides was  
282 studied similarly,<sup>105</sup> demonstrating the potential of experiments with model liposomes to address  
283 specific questions more precisely.

284 Another aspect relevant for the design of leakage experiments in LUVs is the endolysosomal  
285 acidification process that can be mimicked by the appropriate pH value of the buffers. Changes in  
286 pH can lead to a change in the degree of charge not only of the tested release material but also of  
287 the anionic phospholipids, which can be exploited to design pH-responsive release materials and  
288 lipidic drug delivery systems. To correctly reflect the role of the endolysosomal acidification, the  
289 appropriate, isosmotic buffers and salts have to be used for vesicle preparation, purification, and  
290 incubation. In most cases, phosphate buffers are employed, although concentrations and the type

291 of added salt can vary significantly. For instance, Pellois and coworkers used an intra-liposomal  
292 pH of 7.4 to mimic the cytosol and an extra-liposomal pH of 5.5 to mimic the endolysosomal  
293 lumen.<sup>98-100, 103</sup> By contrast, Sarkar *et al.* used HEPES buffer (4-(2-hydroxyethyl)-1-  
294 piperazineethanesulfonic acid) to investigate calcein leakage of triblock copolymer micelles by  
295 varying the pH range from 5.8 to 7.6 outside the liposomes.<sup>96</sup> Furthermore, glucose was added to  
296 balance the different osmotic pressures inside and outside the liposomes, whereas other studies  
297 mostly used NaCl or KCl for compensation. If very high calcein concentrations (> 70 mM) are  
298 required, also the weak solubility of calcein at low pH values has to be considered which requires  
299 the use of basic buffers (*e.g.*, Tris-HCl pH 10)<sup>97</sup> for the hydration of the lipid film. Additionally,  
300 also a Na<sup>+</sup>/K<sup>+</sup> gradient can be applied to liposomes to mimic conditions present in nascent  
301 endosomes,<sup>118</sup> as Rangasamy *et al.* have shown with LUVs composed of PC, PG and Chol with a  
302 sodium inside-buffer and a potassium outside-buffer mimicking high intra-liposomal Na<sup>+</sup>-  
303 concentrations and high cytosolic K<sup>+</sup>-concentrations, respectively.<sup>106</sup>

304 Despite the large variations in the experimental procedures limiting comparability of results, the  
305 calcein release from model vesicles represents a straightforward method to mimic selected aspects  
306 of endosomal escape in a controlled environment independent of the complex cellular processes.  
307 Nevertheless, membrane models, other conditions and procedures as well as theoretical concepts  
308 are still being advanced to further optimize the transferability of the results to experiments in  
309 cells.<sup>48, 119</sup> For example, some studies chose an incubation temperature of 37 °C instead of room  
310 temperature.<sup>110, 111</sup> This corresponds to the cellular environment and, together with the choice of  
311 fatty acid chains, may have an impact on the membrane fluidity of liposomes.<sup>112, 120</sup> Furthermore,  
312 mimicking the exact membrane composition of endolysosomal organelles including different fatty  
313 acids and associated proteins is very complex and can only gradually be approached. To increase  
314 the similarity to natural lipid compositions, also naturally derived vesicles can be utilized. They  
315 can be obtained either *via* chemically induced cell blebbing followed by harvesting of the resulting

316 GUVs, or by the rehydration of total lipid extracts from different cells/tissues.<sup>121</sup> The advantages  
317 and relevance of natural lipid compositions are limited by the uncertainty of their lipid  
318 composition, which is rather similar to the plasma membrane, or by missing asymmetry in the lipid  
319 distribution over the membrane. Nevertheless, these improvements are invaluable in filling the gap  
320 between mechanistic conclusions from simplified model studies to the biological behavior in cells.

321 To investigate vesicle compositions more comparable to endolysosomes, exosomes can be  
322 isolated from the cell culture supernatant since they originate from the multivesicular endosome  
323 (see also Figure 9) and also comprise the characteristics of different cell types.<sup>122, 123</sup> While they  
324 are difficult to load with hydrophilic molecules such as calcein directly,<sup>124</sup> the non-fluorescent  
325 derivative calcein AM can be used instead. Calcein AM can diffuse into the exosomes and is  
326 subsequently converted to calcein by the esterases contained therein.<sup>86</sup> One minor limitation is that  
327 the high calcein concentrations required for the full information range encoded in self-quenching  
328 behavior cannot be reached. A similar approach is also utilized to examine the leakage of calcein  
329 AM from red blood cells upon perturbation of their plasma membrane by different release  
330 materials.<sup>75, 125, 126</sup> Another aspect which has rarely been considered so far, is that release materials  
331 in cellular endolysosomal organelles escape from the inside to the outside of the organelles,  
332 whereas they have to take the opposite way in assays using model vesicles. This could have an  
333 impact on the apparent leakage since the concentration gradient of the entrapped release material  
334 is reversed and the asymmetric membrane composition is not reproduced correctly. Furthermore,  
335 osmotic swelling as hypothesized for the proton-sponge mechanism cannot be modelled.

336 Strikingly, the calcein-based methods can be slightly modified in various ways, to not only  
337 examine the occurrence of calcein release from these model vesicles, but also the mechanism of  
338 the release. Here, we will only summarize assays using calcein, even though they might be based  
339 on calcein-free variants and there are calcein-free alternatives mentioned elsewhere.<sup>92</sup>

340 There are many postulated release mechanisms that can be classified in different aspects. One  
341 way is to distinguish transient leakage from continuous leakage.<sup>127</sup> Transient leakage occurs fast  
342 upon interaction of the release material and the membrane and stops thereafter. Most commonly,  
343 this behavior is explained by the asymmetry stress mechanism,<sup>128-130</sup> or an involvement of  
344 membrane fusion in leakage (see below).<sup>102, 131</sup> Continuous leakage, on the other hand, will happen  
345 through stochastically re-occurring leakage events or pores, thus slowly continues and affects the  
346 sample over several hours.<sup>93, 127, 132</sup> These types of pore formation kinetics can be distinguished for  
347 example by visualizing GUVs by confocal microscopy and acquiring time-resolved images, which  
348 allows for a direct optical monitoring of the leakage process in individual vesicles.<sup>102, 106, 133-135</sup>  
349 The large number of LUVs in a sample cuvette can also be exploited, when leakage is monitored  
350 over time. This allows for the same distinction of transient or re-occurring leakage.<sup>93, 136</sup>

351 Release mechanisms can also be classified according to the number of pores or other leakage  
352 events affecting a given vesicle.<sup>113, 137</sup> In all-or-none leakage, rare leakage events are distributed  
353 heterogeneously over the vesicle population. While the entire dye has been released through these  
354 strong events from some vesicles, others are not affected at all. In contrast, many weak pores or  
355 defects need to occur much more often in an individual vesicle to cause detectable leakage. These  
356 events are distributed homogeneously over all vesicles and cause gradual or graded leakage. It can  
357 be distinguished by measuring the concentration of entrapped dye, for example. For this, the  
358 relation of the calcein concentration to the extent of its self-quenching and hence the fluorescence-  
359 lifetime can be exploited.<sup>47, 113, 138, 139</sup>

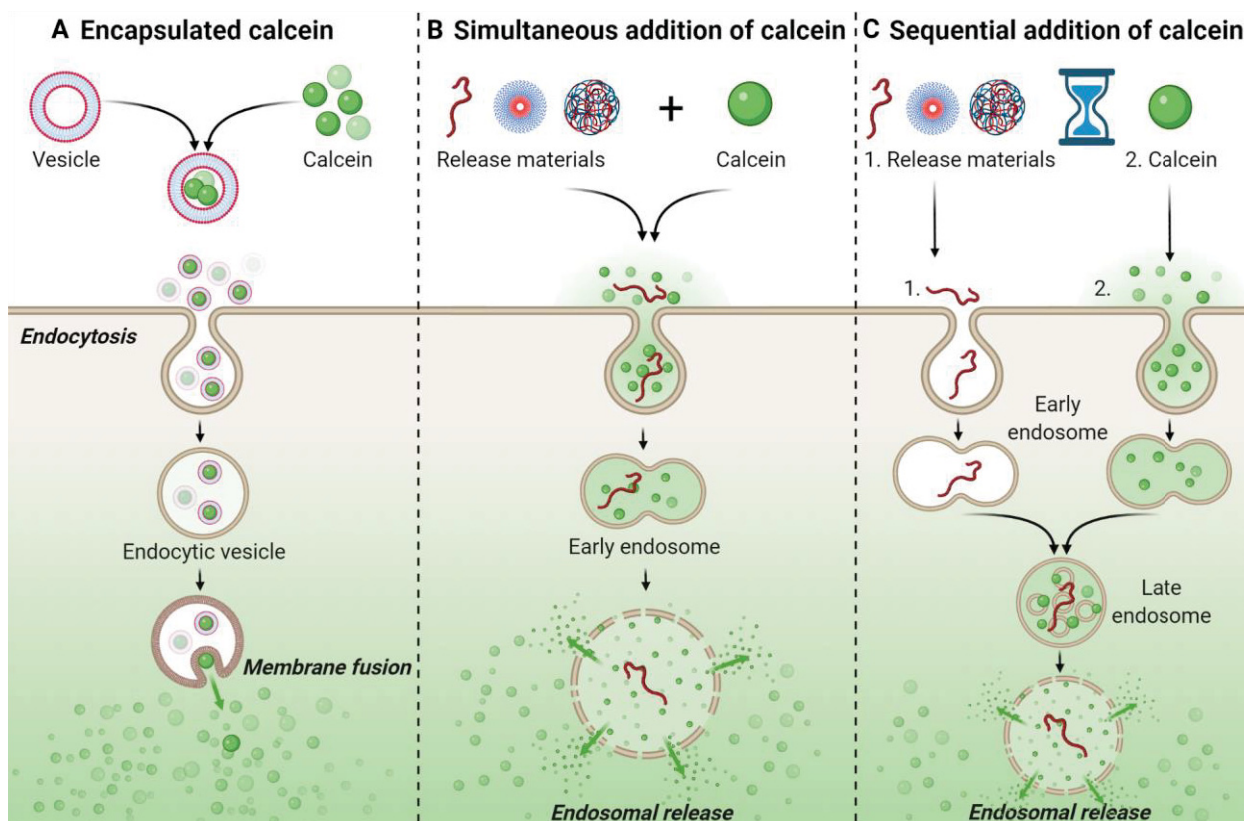
360 Furthermore, release mechanisms might involve additional effects such as membrane fusion of  
361 vesicles in models or intra-endosomal vesicles in cells. For example, an interesting approach relies  
362 on the chelation property of calcein with divalent cations such as  $\text{Co}^{2+}$  or  $\text{Cu}^{2+}$ , which allows to  
363 investigate if calcein release occurs *via* the fusion of vesicles. Different vesicles are combined,  
364 some being loaded with EDTA (or divalent ions) and the others loaded with a mix of calcein and

365 divalent ions (or calcein alone). Upon fusion of these vesicles, the fluorescence intensity increases  
366 (or decreases) due to the fluorescence (de)quenching.<sup>95, 109, 140</sup> If transferred to endolysosomal  
367 vesicles, these methods could provide valuable information on the endosomal escape mechanism.  
368

#### 369 4. CALCEIN RELEASE STUDIED WITHIN CELLS

370 The central focus of this review is the study of calcein release in cells. In the following chapter,  
371 we revise calcein as a marker for studying endosomal escape. As a general procedure of all  
372 considered experiments, the dye (encapsulated or not) is first taken up by cells *via* endocytotic  
373 pathways. In this stage, a dotted pattern is often found in fluorescence microscopy since the  
374 fluorescence of the dye is often only partially quenched at the given concentrations. If appropriate  
375 experimental conditions are chosen with respect to calcein concentration, self-quenching in  
376 combination with acidic pH is sufficient to reduce the fluorescence intensity of calcein in  
377 endosomes. In the next stage, *i.e.*, with occurrence of an endosomal leakage event, calcein rapidly  
378 diffuses and dilutes into the neutral cytosol, which microscopically causes not only a more diffuse  
379 fluorescent signal, but may also lead to a significant increase in intensity, if appropriate conditions  
380 are chosen initially.<sup>141</sup>

381 In this way, calcein has been used to evaluate the endosomal escape efficiency of various release  
382 materials. Thereby, the escape has been investigated in a range of different cell lines, with  
383 experimental settings varying in terms of media composition, calcein concentration, incubation  
384 time, type of calcein addition as well as cell analyses. The type of calcein addition can be  
385 categorized into encapsulated and non-encapsulated or simultaneous and sequential addition and  
386 is described in detail in the following section (Figure 5).



387

388 **Figure 5. Types of calcein addition.** The type of calcein addition is primarily determined by the  
 389 type of release material (peptides/polymers, dendrimers, or nanoparticles). In the case of  
 390 simultaneous addition, calcein can either be (A) encapsulated in the nanostructure (often using  
 391 self-quenching concentrations) or (B) added to the cell culture medium at the same time as the  
 392 agents. (C) Sequential addition is also possible. In most cases, the cells are pre-incubated with the  
 393 release material and calcein is added afterwards.

#### 394 4.1. Release of encapsulated calcein within cells

395 In this approach, the investigated release materials are able to encapsulate calcein at self-  
 396 quenching concentrations within their hydrophilic interior. These nanostructures often consist of  
 397 amphiphilic lipids forming liposomes similar to the model vesicles described above (Table 3). To  
 398 facilitate drug delivery *via* endosomal release, modified lipids or lipids with advantageous  
 399 properties are included, *e.g.*, phosphatidylethanolamine (PE), cholesteryl hemisuccinate  
 400 (CHEMS), or 1,2-dioleoyl-3-trimethylammonium propane (DOTAP).<sup>142-148</sup> Furthermore,  
 401 synthetic variants of liposomes, polymersomes, formed by amphiphilic block copolymers have  
 402 been investigated regarding their endosomal escape.<sup>149-151</sup> Combinations of lipids and

403 polymers,<sup>152-154</sup> peptides and liposomes<sup>155</sup> or completely different nanostructures such as hollow  
404 capsules<sup>54</sup> have also been studied.

405 In general, the incubation times varied within a wide range, from ten minutes to four days which  
406 could be related to different endocytosis kinetics of the different release materials. Long incubation  
407 times, *e.g.*, could be related to the incorporation of molecules such as PEG-chains that shield the  
408 surface of the release material and may interfere with a fast and efficient endosomal escape.<sup>124, 156</sup>

409 The applied calcein concentrations in the nanostructures exhibited greater variation than those  
410 reported for the model liposomes, which may be attributed to the different preparation methods.  
411 Most of the polymer- and/or lipid-containing structures were assembled *via* the already mentioned  
412 thin film hydration<sup>142-153, 155</sup> usually resulting in high encapsulation efficiencies.<sup>88</sup> Thus, the calcein  
413 concentration within the polymersomes/liposomes is assumed to be similar to that used to  
414 rehydrate the thin film. However, some vesicles were prepared by more complex procedures and  
415 the actual amount of calcein within the nanocapsules was determined afterwards.<sup>54, 124, 156</sup>  
416 Nevertheless, endosomal escape can still be detected with low (non-quenching) calcein  
417 concentrations as a change from a punctate fluorescence pattern to diffuse cytosolic fluorescence.  
418 Illes and coworkers described another interesting approach using metal-organic frameworks  
419 (MOF) to encapsulate calcein first in nanoparticles and then coating these with exosomal  
420 membranes derived from HeLa cells. This resulted in a strong shielding from the immune system  
421 and high calcein release from both, the exosome coated MOF and the endosome following four  
422 days of incubation in HeLa cells.<sup>124</sup>

423



424 **Table 3.** Investigation of calcein release from vesicles inside cells.

Release material	Polymers/Lipids <sup>[a]</sup>	Lipid composition mol%	c(calcein) <sup>[b]</sup> mM	Cells <sup>[c]</sup>	Incubation time	Analysis <sup>[d]</sup>	Ref.
Liposome	PE:PHC, PC	8:2	60 (0.3)	L929 in PBS + 16 mM D-glucose	1.5 + 2 h	quant.	148
	CHEMS:PE/PC	4:6	50	RAW264.7 in D10	1 h	qual., stabil.	142
	CHEMS:PE:PEG-PE:Chol	21:43:6:30	40	Hs578t in D10, HG	15 min	qual., stabil., FC	143
	PEG-PE:PC:Chol	6:47:47				qual., stabil., FC	
	CHEMS:PE (:PEG-PE/ PC)	4:6 (:0.06)	80	differentiated THP-1 in R10	4 h	qual., stabil., FC	144
	CHEMS:PE (:PEG-PE/PC/PS/PG)	4:6 (:0.3/6/4/4)				qual., FC	
	CHEMS:PE:PEG-PE/PEG- Hz-CHEMS:PC:Chol	2:4:0.5:2:2	80	Mia-Paca 2	1, 2 h	qual.	146
	DOTAP:PEG-PE:PC:Chol	1:0.25:4.8:2.3	60	HeLa in D10, HG	4 h	qual., stabil.	147
DOTAP:PEG-PE:PC:Chol: PE	1:1.3:1.9:9.6:1.8	qual., stabil.					
Polymer- some	PEG-SS-PPS	-	100	J7774A in D10	10, 60, 120 min	qual.	149
	PEG- <i>b</i> -PPS		200	mouse dendritic cells in D	6, 12, 24 h	qual.	150
	PEG- <i>b</i> -PPS		30	RAW264.7 in D	2 h	qual., stabil.	151
Polymer/ Lipid	Suc-poly(glycidol) + PC	-	200	CV-1 in D10	3 h	qual.	152
	PEtOx-CHMC + Chol, PC	-	60	HeLa in D10	1, 4 h	qual., stabil., FC, LC	153
	DOX-PLGA + DMAB + PC	-	0.008*	MCF-7, HL-60 in R	15, 60, 240 min	qual., FC	154
Peptide/ Liposome	(GALA-)His-ZHER2-BNC + PC, Chol, PG	-	105	SKBR3 in R10	1 + 5-47 h	qual.	155
Other	gold NP + PSS, PAH	-	4.8**	MCF-7 in D10, HG	over night	quant., LC	54
	exosome coated MOF-NP	-	1**	HeLa in D	2, 3, 4 d	quant. stabil., LC	124
	MSN-PVP-PEG	-	1**	HeLa or KB in D10- F12	18 h	qual., LC	156

[a] Types of phospholipids by headgroup are mentioned. Fatty acids can be different, for PC and PE they were mostly dioleoyl or distearoyl.

**BNC** – bio-nanocapsule, **CHEMS** – cholesteryl hemisuccinate, **CHMC** – cholesteryl methyl carbonate, **Chol** – cholesterol, **DMAB** – dimethyldidodecylammonium bromide, **DOTAP** – 1,2-dioleoyl-3-trimethylammonium propane, **DOX** – doxorubicin, **Hz** – hydrazone, **MOF** – metal-organic framework, **MSN** – mesoporous silica nanoparticles, **NP** – nanoparticle, **PAH** – poly(allylamine), **PC** – phosphatidylcholine, **PE** – phosphatidylethanolamine, **PEG** – poly(ethylene glycol), **PEtOx** – poly(2-ethyl-oxazoline), **PG** – phosphatidylglycerol, **PHC** – palmitoyl homocysteine, **PLGA** – poly(lactic-co-glycolic acid) **PPS** – poly(propylene sulfide), **PS** – phosphatidylserine, **PSS** – poly(styrenesulfonate), **PVP** – poly(2-vinylpyridine), **Suc** – succinylated.

[b] Gray shade indicates capsule preparation other than thin film rehydration or reverse phase evaporation. \* – converted based on information from the original publications. \*\* – concentration of capsule loading solution

[c] **D** – DMEM, **D10** – DMEM + 10% FCS, **F12** – Ham's F12 medium, **HG** – high glucose (4.5 g L<sup>-1</sup>), **R** – RPMI, **R10** – RPMI + 10% FCS

[d] **FC** – flow cytometry, **LC** – loading capacity/encapsulation efficiency, **qual.** – qualitative microscopy, **quant.** – quantitative image analyses, **stabil.** – stability against changes in environment,

425

426 Moreover, high (quenching) calcein concentrations inside the release material can be used to

427 determine the stability of the release material similar to the method for the calcein release from

428 artificial liposomes, by changing the ambient conditions, such as temperature,<sup>142, 143, 147</sup> serum  
429 content,<sup>142, 147</sup> or pH-value.<sup>124, 143, 144, 153</sup> In case of low calcein concentrations, also a calcein  
430 diffusion method (Franz cell diffusion) was used. The released calcein diffuses into a buffer  
431 without the release material which is separated by a dialysis membrane allowing for the  
432 discrimination between fluorescence originating from inside the release material and from released  
433 calcein in the solution.<sup>88, 124</sup> Therefore, encapsulating release materials allow for both, a general  
434 investigation within the natural environment (cells), and a detailed investigation of one specific  
435 feature of the endosomal escape within only one approach (stability of the release material).

#### 436 **4.2. Simultaneous and sequential addition of release material and calcein as** 437 **sensor**

438 The calcein assay is influenced by the nature of the release materials and how it is performed,  
439 particularly with respect to the simultaneous presence and concentrations of the two substances  
440 (calcein and material) in the endosome. Calcein, as a small molecule, is rapidly taken up by cells,  
441 while release materials may take longer to accumulate in the endosome, depending on their size  
442 and charge. Often, the release material and calcein are added simultaneously to the cells (Table 4),  
443 without mixing the two components beforehand.

444

445 **Table 4.** Investigation of calcein release with simultaneous addition of vector and calcein *in*  
 446 *vitro*.

Type of material <sup>[a]</sup>	Material <sup>[b]</sup>	Delivery of <sup>[c]</sup>	Cell line	c(Calcein) μM	Incubation conditions	Analysis <sup>[d]</sup>	Ref.
Oligomers	oligo(ethanamino) amides	pDNA	DU145	803	growth medium + 10% serum, 3.5 h	quant.	157
	poly(2-alkylacrylic acid)s	pDNA	U937 (Jurkat)	3214	growth medium + 5% serum, 30 min	quant. + FC	158
Linear Polymers	poly( <i>N</i> -isopropylacrylamide)	siRNA	Hela, MG-63	161	growth medium + 10% serum, 4 h	quant.	159
	poly(aminoethyl-methacrylate)s	pDNA	HEK	25	Opti-MEM, 4 h or 4 h + 20 h	quant.	160
	PDMAEMA	-	U937, (Jurkat)	3214	growth medium + 5% serum, 30 min, 48 h	quant.	161
	polyacrylamides, l-PEI	pDNA	HEK 293T	40	growth medium + 10% serum + HEPES, Opti-MEM, 4 h	FC	162
	polypiperazines, l-PEI	dextran, BSA, RNase A, EGFP	HEK 293T	40	Opti-MEM, 16 h	Quant. + kinetics, FC	163
	(crosslinked) PEI	pDNA	KB	241	Opti-MEM, 2 h	quant.	164
Dendritic Polymers	poly(amidoamine)	pDNA	DU145	25	Opti-MEM, 4 h	quant.	165
Micelles	PDMAEMA-containing shell, PEI	pDNA	HEK 293T, K562	40	growth medium + 10% serum + HEPES, 1, 4, 24 h	FC	166
	PDMAEMA-containing shell, l-PEI	pDNA	HEK 293T	40	growth medium + 10% serum + HEPES, 1, 4, 24 h	quant.	167
Nano-particles	core: PDEAMA, shell: poly(aminomethyl-methacrylate)	proteins	dendritic cells	241	growth medium + 10% serum, 1 h	quant.	168
	PLGA/PDMAEMA-co-PAA-BMA blend particles	- dextrans	DC2.4	321	growth medium + 10% serum + HEPES, 4 h	fixated, qual.	169
	Polyaminoester particles with lipid shell	mRNA	DC2.4	240	Growth medium + 10% serum + HEPES, 1 h	qual., FC	171
	graft of poly(lauryl methacrylate- <i>co</i> -methacrylic acid) on acetylated dextran	-	CT-26	321	growth medium (+ 10% serum), 1 + 3 h	LTR, qual.	172
	Org./inorg. Nanoparticles with poly(phenol tannic acid) and metal ions	-	MDA-MB-231	241	growth medium + 10% serum, 4 h	bafi, qual.	173
CPPs	arginine-rich TAT with residues of cecropin-A and melittin	EGFP-TAT fusion protein, dextrans, pDNA	Hela, CHO-K1, HUVEC	250	according to cell manufacturer's instructions, 30 min	quant. + kinetics, FC with threshold	174
	poly(acrylamide- <i>co</i> -methacrylic acid) nanogels with peptides	NPs	SW-48	161	growth medium + 2% serum, 4 h	qual.	175

[a] CPPs – cell-penetrating peptides

[b] BMA – butylmethacrylate, PAA – 2-propylacrylic acid, PDEAEMA – poly[2-(diethylamino)ethyl methacrylate), PDMAEMA – poly(2-(dimethylamino)-ethylmethacrylate, PEI – poly(ethylenimine), PLGA – poly(lactic-*co*-glycolic acid), RNase A – ribo-nuclease A, TAT – trans-activator of transcription

[c] BSA – bovine serum albumin, EGFP – enhanced green fluorescent protein, mRNA – messenger RNA, NPs – nanoparticles, pDNA – plasmid DNA, siRNA – small interfering RNA, TAT – trans-activator of transcription

[d] bafi – bafilomycin-A1, FC – flow cytometry, LTR – LysoTracker Red, qual. – qualitative microscopy, quant. – quantitative image analyses

447 Cationic polymers are often considered as synthetic gene transporters and release materials to  
448 facilitate endosomal escape. The most studied polymeric gene transporters include PEI and  
449 PDMAEMA, whose endosomal release has also been investigated in several studies with calcein.  
450 PEI represents the commercial gold standard and is particularly interesting for the study of calcein  
451 release not only because of the controversial proton-sponge hypothesis. Bonner *et al.* tested  
452 different PEI architectures (crosslinked, linear, branched) and found endosomal escape in 75 % of  
453 cells using the calcein assay if a crosslinked PEI variant was applied, which showed no toxic effects  
454 at this concentration and incubation time.<sup>164</sup> Vermeulen *et al.* investigated the endosomal escape  
455 mechanism of linear PEI (JetPEI) and performed the calcein release assay in cell lines differing in  
456 endosomal size. They conclude that endosomal release can be promoted by smaller endosomes  
457 and an undisturbed buildup of osmotic potential. (Table 5).<sup>11</sup> Another well-known polymer is  
458 PDMAEMA as it is easily applied for a variety of release materials and enables endosomal release  
459 of calcein.<sup>160, 166</sup> This was demonstrated in fibroblasts and dendritic cells with different  
460 nanoparticle compositions, where calcein was added sequentially (after treatment with the  
461 polymer) or simultaneously with the polymer.<sup>169, 176-179</sup> By inhibiting endosomal escape with  
462 bafilomycin A1, Wong *et al.* showed that acidification of the endosomes is crucial for release of  
463 calcein.<sup>179</sup> However, the large number of studies on vinyl polymers such as PDMAEMA do not  
464 yield clear correlations, which can also be attributed to the different investigation methods.  
465 Therefore, no final conclusion can be drawn about the release mechanism.  
466

467 **Table 5.** Investigation of calcein release with subsequent calcein addition *in vitro*.

Type of material	Material <sup>[a]</sup>	Delivery of <sup>[b]</sup>	Cell line	c(Calcein) μM	Incubation conditions	Analysis <sup>[c]</sup>	Ref.
Linear Polymers	JetPEI	pDNA	Hela, ARPE-19, A549, H1299	3000	growth medium + 10% serum, 15 min + 15 min	quant. + FC	11
	PDMAEMA- <i>b</i> -PEG	-	3T3 MEFs WT	161	growth medium + 10% serum, 2 + 2 h	quant.	179
Nano-particles	PEG- <i>b</i> -PDEAEMA	Ovalbumin	NIH/3T3	161	growth medium + 10% serum, 2 h + 2 h	quant.	176, 177
	crosslinked PLGA/PEI particles	BSA, SOD	NIH-3T3	50 μg/dish	growth medium + 10% serum, 2 h + 30 min	qual.	180
Peptides	cytotransmab, TAT	-	Hela	150	serum-free medium, 4 h + 2 h	inhibitors, fixated, quant.	181
	Polymer/cyclic peptide conjugate	-	HEK 293	146	growth medium + 10% serum, 16 h + 30 min	quant.	107

[a] **PDEAEMA** – poly[2-(diethylamino)ethyl methacrylate], **PDMAEMA** – poly(2-(dimethylamino)- ethylmethacrylate), **PEG** – poly(ethylenglycol), **PEI** – poly(ethylenimine), **PLGA** – poly(lactic-*co*-glycolic acid), **TAT** – trans-activator of transcription  
[b] **BSA** – bovine serum albumin, **pDNA** – plasmid DNA, **SOD** – superoxide dismutase  
[c] **qual.** – qualitative microscopy, **quant.** – quantitative image analyses

468

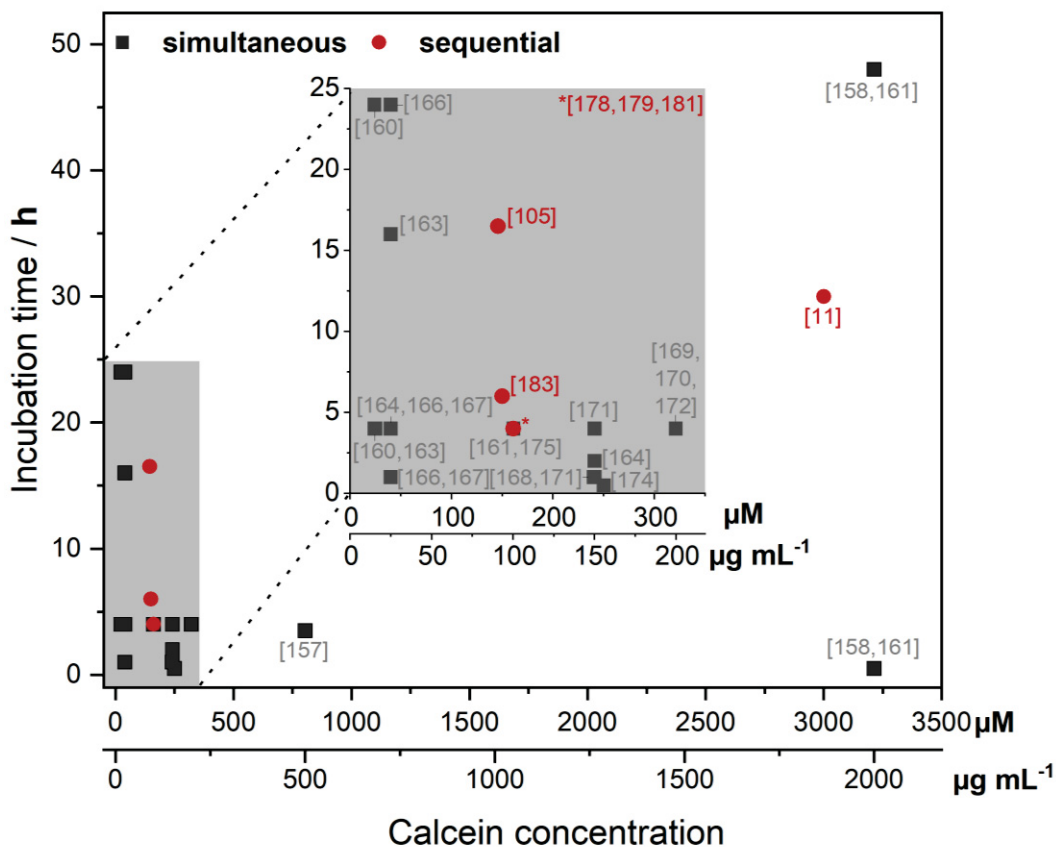
469 Due to its wide application and good availability, it is not surprising that different calcein

470 concentrations and incubation times were used to study the endosomal escape of release materials

471 (Figure 6). Concentrations from 10 μM to 3.21 mM were reported to study systems co-delivering

472 calcein,<sup>158, 161, 182</sup> with the majority of studies applying concentrations between

473 161 and 322 μM.<sup>159, 164, 168-177, 181, 183</sup>



474

475 **Figure 6. Concentrations and incubation times in experimental setups of calcein release.**

476 Different research groups have applied a range of different calcein concentrations and incubation  
 477 times, whereas the assay has also differed in the type of calcein addition (simultaneous or  
 478 sequential) as well as the release materials and cell lines used.

479 Using a calcein concentration of 161  $\mu\text{M}$ , Deshpande *et al.* have shown that poly(N-  
 480 isopropylacrylamide nanogels with poly- $\epsilon$ -lysine can release calcein in cervical cancer cells.<sup>159</sup>

481 Similar concentrations were used to study nanoparticles with hydrophobic components. Su and  
 482 coworkers showed that pH-responsive polyaminoester nanoparticles with lipid shells induce  
 483 highly efficient endosomal escape in dendritic cells at a calcein concentration of 240  $\mu\text{M}$ .<sup>171</sup>

484 Wannasarit and colleagues were able to induce a poly(lauryl methacrylate-*co*- methacrylic acid)-  
 485 mediated calcein release in three different colorectal adenocarcinoma cell lines using a calcein  
 486 concentration of 322  $\mu\text{M}$ .<sup>172</sup> Calcein concentrations in a similar range have also been shown to be

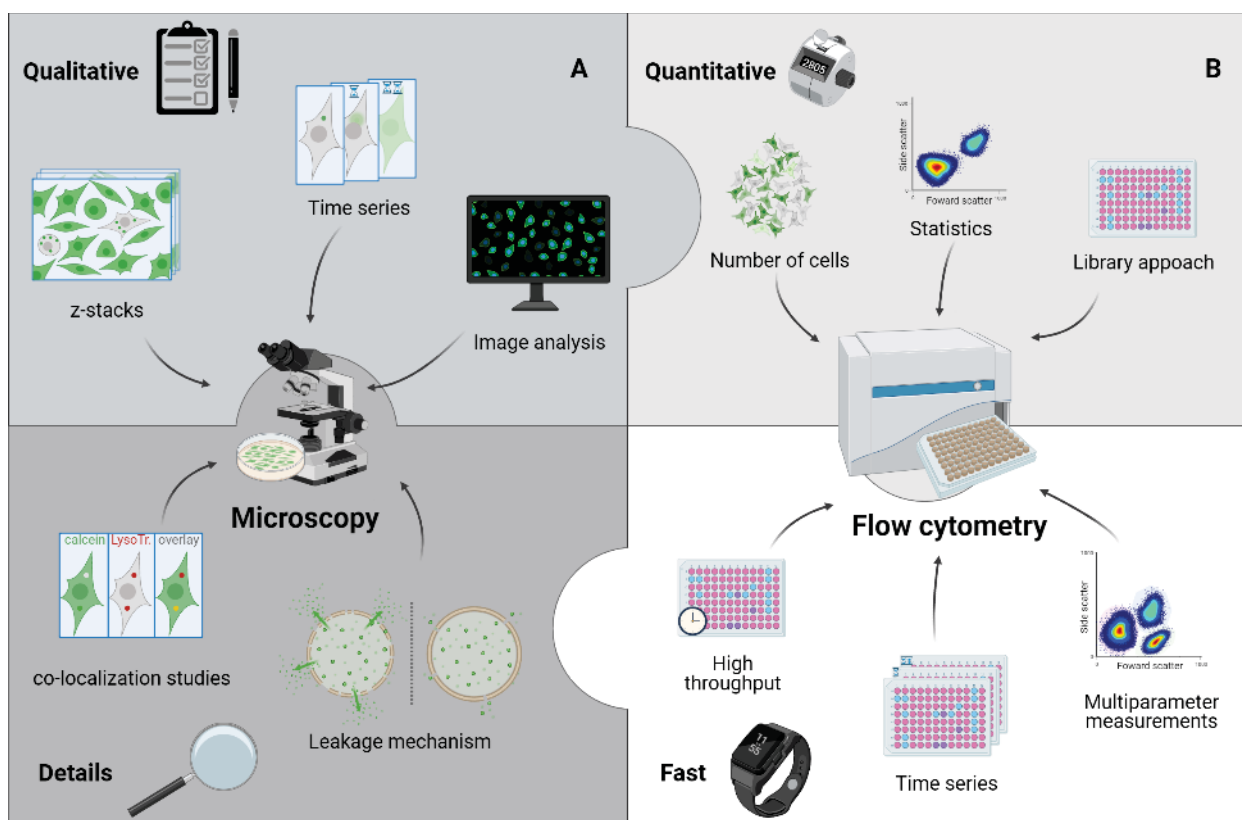
487 useful for studying CPPs.<sup>175</sup> As an example, Salomone and colleagues showed that a fusion peptide

488 from the arginine-rich TAT motif with additional residues of cecropin-A and melittin can  
489 efficiently release calcein within 30 min with a calcein concentration of 250  $\mu\text{M}$ .<sup>174</sup> However,  
490 endosomal escape could also be detected with significantly lower calcein doses of 40  $\mu\text{M}$  or less.  
491 In HEK cells, calcein release was detectable with concentrations  $\leq 40 \mu\text{M}$  applying differently  
492 structured polyvinyl polymers and culture conditions.<sup>160, 162, 166, 167</sup> Calcein concentrations in this  
493 lower range were also successfully used in leukemia cells and human prostate cancer cells to show  
494 escape induced by polyamidoamides and a PDMAEMA-containing micelle.<sup>165, 166</sup> Jones *et al.*  
495 showed that PAA (poly(2-alkylacrylic acid)) can deliver calcein to the cytosol by disrupting  
496 endosomes.<sup>158</sup> For this purpose, they co-incubated human myelomonocytic cells in complete  
497 medium with the polymers and calcein concentration of 3.21 mM for 30 min. In contrast to this,  
498 Ren *et al.* investigated receptor-mediated endosomal escape in human lymphoblastic leukemia  
499 cells in serum-containing medium by incubating the cells with 25  $\mu\text{M}$  calcein for 6 h.<sup>184</sup> As can be  
500 seen from the experimental set-up in these two studies, the calcein concentration and incubation  
501 time for efficient release detection are mutually dependent. The two studies also differed in the  
502 type of microscopy conducted (confocal or non-confocal) and their analyses (qualitative or  
503 quantitative image analyses).

504 Overall, a successful endosomal escape can be detected with different assay parameters  
505 optimized for each investigated carrier material, medium, and cell type (Figure 6). The broad  
506 varieties in these settings hardly allow to derive any specific trends from the yet given set of  
507 experiments found in literature. Indeed, our screening of literature reported data further raised the  
508 question, whether significantly different experimental procedures to studying endosomal release  
509 efficiency may even lead to different conclusions for similar systems. In this regard, we also like  
510 to refer to Chapter 5 and our final conclusions at this point.

511 **4.3. Analytical Methods**

512 The analysis of the calcein release assay can be performed in a variety of ways, depending on  
513 the problem to be addressed. The requirements for the analysis of the assay vary from attention to  
514 detail (accurate spatial and/or temporal resolution of the intracellular signal) to statistical  
515 significance of the data. To address the diverse requirements, the different analytical methods and  
516 their applications and limitations are discussed in the following (Figure 7).



517 **Figure 7. Analysis techniques of the calcein release assay.** The predominant analytical technique  
518 for the calcein release assay is microscopy, as it provides spatial (and in the case of live cell  
519 microscopy, temporal) resolution of the fluorescence signal. The primarily qualitative conclusions  
520 can also be supplemented by statistically more robust conclusions through the use of image  
521 analysis techniques. For rapid quantitative measurements, flow cytometry can also be used to  
522 increase the statistical power of the data.

524 In most studies, confocal microscopy has been shown to be a very powerful tool, even more  
525 useful than epifluorescence microscopy as the subcellular distribution of calcein can be  
526 elucidated.<sup>160</sup> For this purpose, also z-stacks can be prepared.<sup>159, 169, 170</sup> Primarily, live cell



527 microscopy is used, also allowing kinetic studies.<sup>163, 174</sup> Less commonly, cells are studied after  
528 fixation.<sup>169, 181</sup> Besides, the subcellular distribution and fluorescence intensity of the calcein signal  
529 have been analyzed quantitatively.<sup>54, 124, 148, 159, 164, 165, 168, 179</sup> It is possible to count the cells with  
530 punctate and diffused calcein signal manually,<sup>176, 177</sup> but a more effective approach relies on the  
531 use of various image analysis software, where regions of interest and/or thresholds are defined for  
532 an automated analysis.<sup>157, 160, 161</sup> The acquisition of many cells, *e.g.*, with the help of montages, is  
533 also desirable for statistical significance. Colocalization studies with acidic compartments can  
534 further be conducted (mainly Mander's coefficient)<sup>172</sup> and may provide further information about  
535 the efficacy of calcein release, with lower colocalization indicating more efficient escape.<sup>170</sup>  
536 Another very interesting approach was shown by Connor and Huang already in 1985 who  
537 established a calibration curve of calcein using a microscope photometer so that the cytosolic  
538 concentration of calcein within L929 cells was quantified.<sup>148</sup>

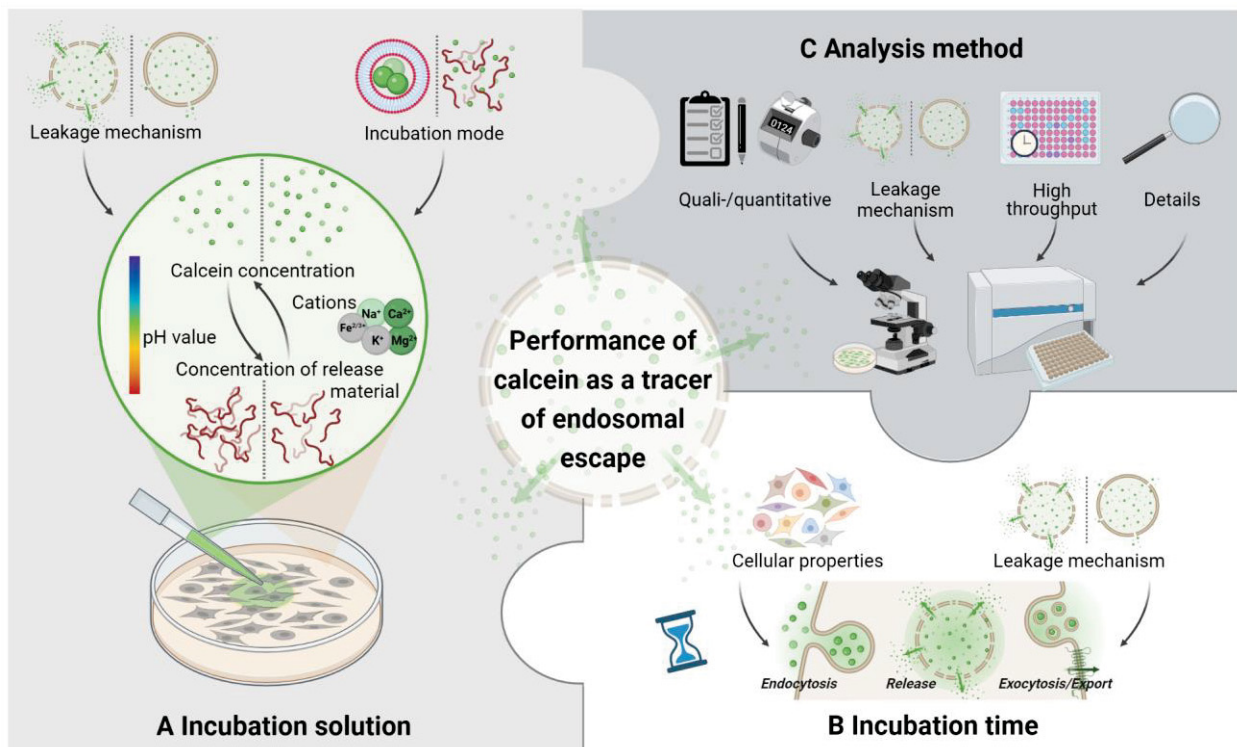
539 Furthermore, high-throughput methods based on flow cytometry are also used to quantify the  
540 calcein release, with higher cellular fluorescence intensities generally indicating released calcein  
541 compared to control cells with punctuate fluorescence.<sup>11, 143-145, 153, 154, 162, 166, 174</sup> Again, appropriate  
542 thresholds must be defined for the fluorescence intensity of escape-positive cells. Microscopic and  
543 flow cytometric methods can also be combined, which more robust insights about endosomal  
544 escape.<sup>158, 174</sup> Because microscopic studies allow spatial (and in the case of live cell microscopy,  
545 temporal) resolution of the calcein signal, release events can be measured unambiguously, with  
546 varying degrees of attention to detail. Microscopy is still the most commonly used technique but  
547 is comparatively time consuming and can only provide statistical information if a large number of  
548 cells are analyzed. For statistically robust results, flow cytometry is a faster complementary  
549 method, but it cannot spatially resolve the calcein signal within a cell. For fast statistically robust  
550 results, flow cytometry is a complementary method, but it cannot spatially resolve the calcein  
551 signal within a cell. In the best case, both methods are used in a complementary manner to provide

552 a detailed picture of any potential escape. Although, both analytical techniques ideally coincide in  
553 the number of escape-positive cells in order to provide reliable results, deviations nevertheless  
554 might occur for example due to the applied thresholding.<sup>163</sup>

555

556 5. POTENTIAL PITFALLS OF THE CALCEIN RELEASE ASSAY *IN CELLS*

557 Calcein has been extensively used to investigate endosomal escape of various types of release  
558 materials within cells. However, the performed methods show differences in several aspects which  
559 demonstrates the complexity as well as the robustness of the assay. In general, it can be concluded  
560 that the performance of calcein as an indicator for endosomal escape depends on three main  
561 parameters which should be considered when planning a calcein release assay and will be  
562 discussed in this section: i) incubation solution, ii) incubation time, and iii) the analysis method  
563 (Figure 8). Regarding the calcein leakage assay with model vesicles, experimental parameters  
564 affecting liposomal leakiness have recently been reviewed elsewhere, *e.g.*,<sup>88, 112</sup>, and are therefore  
565 not considered further.



566  
567 **Figure 8.** Factors determining the performance of the calcein release assay within cells. When  
568 planning the parameters of the assay, *i.e.*, incubation solution, incubation time and analysis  
569 method, the influence of different factors needs to be considered, *e.g.*, the leakage mechanism of  
570 the release material, the incubation mode, cellular properties, and the requirements of the desired  
571 readout.

## 572        **5.1. Physicochemical factors relevant for the calcein solution**

573        As described before, three main factors influence the calcein fluorescence and should therefore  
574        be considered when thinking about the composition of the calcein solution: pH value, calcein  
575        concentration and the presence of cations (Figure 8A). However, the pH value is only of interest  
576        for the preparation of the calcein stock solution due to the pH dependent solubility of calcein.

577        Since the calcein release assay is based on the change in the fluorescence pattern upon  
578        endosomal escape (punctate endolysosomal to diffuse cytosolic) which also leads to an increase in  
579        the fluorescence intensity within the cytosol, the calcein concentration is of major importance. A  
580        wide range of calcein concentrations has been applied by different research groups, demonstrating  
581        the robustness of the calcein release assay. The applied concentrations can roughly be related to  
582        the incubation mode of calcein, either encapsulated (self-quenching concentrations) or in  
583        simultaneous or sequential incubation with the release material (< 3.5 mM calcein). Higher (self-  
584        quenching) concentrations could lead to an increase in the fluorescence intensity difference  
585        between endolysosome and cytosol and, hence, an easier detection of endosomal escape.  
586        Nevertheless, higher concentrations could also be problematic for the cells due to osmotic stress,  
587        chelation of calcium ions or other negative side effects. To increase the difference in the  
588        fluorescence intensity between endolysosomes and cytosol, also other factors can be adjusted such  
589        as the incubation time of calcein (shorter, subsequent to the release material) or the measurement  
590        settings in microscopy (optimal for the bright cytosolic fluorescence). So far, only in one case,  
591        non-fluorescent endosomes (indicative of quenched calcein fluorescence) have been observed in a  
592        study applying 146  $\mu$ M calcein pointing towards further mechanisms influencing the calcein  
593        fluorescence.<sup>107</sup>

594        When choosing calcein concentrations for *in vitro* investigations, also the release mechanism of  
595        the release material is of importance, which again can be influenced by the concentration of the  
596        release material. As an example, the combination of a release material gradually releasing calcein

597 with too low concentrations of calcein could lead to the observation of no calcein leakage, which  
598 would be different at higher calcein concentrations. Therefore, a concentration-dependent calcein  
599 release could enable the investigation of gradual calcein release and may provide insights into the  
600 endosomal escape mechanism.

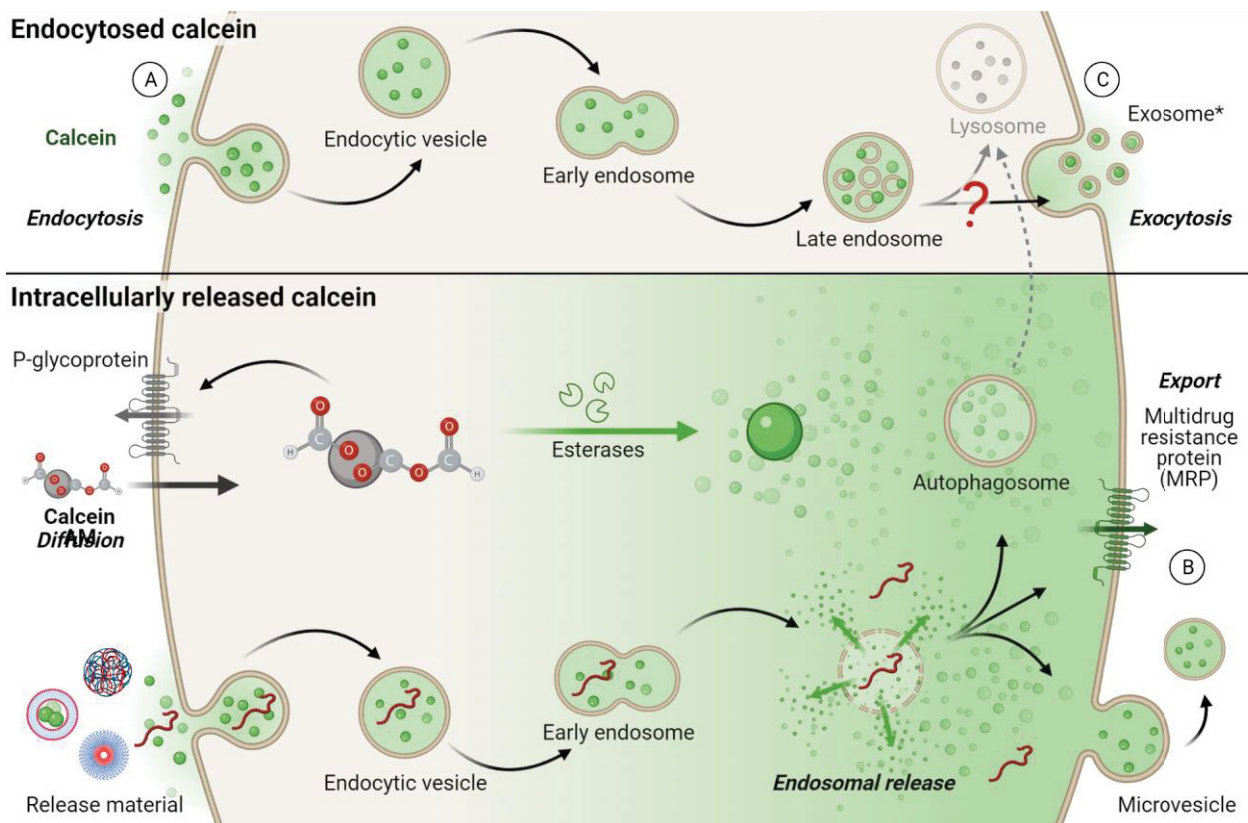
601 Regarding the presence of cations, it should be considered that these may interact differently  
602 with calcein at various pH values and concentrations, very well illustrating the mutual dependence  
603 of these factors. Although the influence of different ions on the calcein fluorescence was already  
604 the topic of the earliest calcein studies, the conditions present in the calcein release assay to study  
605 endosomal escape inside cells can be more complex making it difficult to draw conclusions. A  
606 calibration curve of calcein in the respective buffer composition and/or cell culture medium as well  
607 as the inclusion of a corresponding control without the release material can help in visualizing the  
608 influence of ions in the applied buffers or cell culture media. Since release materials for gene  
609 delivery are often cationic, they could interact with the calcein also electrostatically and influence  
610 its fluorescence intensity. This fact should further be considered for the design of the experiments,  
611 in particular regarding either a premixing of release material and calcein or their sequential  
612 addition. However, studies on potential interactions are seldom reported and the different addition  
613 modes of calcein and release material are rarely compared within a publication.

## 614 **5.2. Biological factors relevant for the incubation time**

615 Consideration of various parameters is particularly relevant when choosing the incubation time  
616 (Figure 8B). On the one hand, the uptake of the release material into the cell matters. On the other  
617 hand, the intracellular fate of the applied calcein should also be regarded, in particular if longer  
618 incubation times are studied. To visualize endosomal escape, calcein and the release material have  
619 to be present in the same compartment. Hu et al. examined this factor in their study and were able  
620 to verify the importance of the simultaneous presence of calcein and the delivering core-shell  
621 particles within the endolysosome for the investigated system. When calcein and the core-shell

622 particles were added simultaneously, endosomal escape was successfully reported by calcein  
623 release. However, when the cells were first treated with calcein and then, after a washing step, the  
624 release particles were added, no endosomal escape was observed, but might have occurred  
625 unnoticed,<sup>178</sup> suggesting a rapid transport of calcein into, through, and out of the cell.

626 Since there is no evidence that calcein is metabolized within cells, conclusions about the  
627 intracellular fate of calcein might be drawn based on the fluorescence and its temporal and spatial  
628 changes. Thus, a punctate fluorescence pattern within cells incubated with calcein alone indicates  
629 an endocytotic uptake mechanism (Figure 9A). With regard to the calcein release assay, it should  
630 be considered that different cell types can exhibit different endocytosis rates for different  
631 (macro)molecules,<sup>185, 186</sup> and might therefore require different incubation times to take up similar  
632 amounts of calcein or the release material. Although the details of endocytosis in different cell  
633 lines were not investigated for calcein so far, they have been shown for different release  
634 materials.<sup>11, 166, 187, 188</sup> Considering more quantitative measurements (flow cytometry), the  
635 normalization of the calcein release induced by any release material to a control sample (cells  
636 treated with calcein only) can be used to attenuate cell type dependent endocytosis rates of  
637 calcein.<sup>11, 162, 163, 166</sup> In addition to the different endocytosis rates of the release material, the release  
638 material itself can have an impact on the endocytosis rate of calcein which is however not as easy  
639 to determine and therefore difficult to take into account. Nevertheless, one way to compensate for  
640 at least different endocytosis rates of the various release materials is to report the calcein release  
641 in relation to the uptake of the release material.<sup>144, 145, 163, 167</sup>



642

643 **Figure 9. Intracellular pathways of calcein.** (A) Punctate fluorescence patterns within cells point  
 644 towards an endocytotic uptake mechanism of calcein. (B) Cytosolic/released calcein can be  
 645 exported *via* the multidrug resistance protein or within microvesicles as shown in studies of cells  
 646 loaded with calcein AM. (C) Regarding the excretion of endocytosed calcein, exocytosis is a  
 647 hypothesis for calcein not released from endolysosomes.

648 Interestingly, a decrease of the overall calcein fluorescence intensity in the cytosol was observed  
 649 upon increasing incubation times with different polymers and cell lines.<sup>160, 166</sup> Such observations  
 650 hint towards a calcein excretion mechanism from the cytosol (Figure 9B). Since calcein AM is  
 651 intracellularly converted into calcein upon esterase activity in viable cells, conclusions can be  
 652 drawn from studies with multidrug resistant (MDR) cells and calcein AM. In these studies, calcein  
 653 has been shown to be ATP-dependently exported from the cytosol *via* the multidrug resistance  
 654 protein (MRP) belonging to the ATP binding cassette transport proteins,<sup>189, 190</sup> whereas the calcein  
 655 AM itself has been shown to be exported *via* the multidrug transporter 1 (MDR1) encoded P-

656 glycoprotein.<sup>191, 192</sup> Furthermore, cytosolic calcein can be exported within microvesicles or *via* gap  
657 junctions to other cells, which can be derived from studies utilizing calcein AM as a tracking label,  
658 *e.g.*, for extracellular vesicles derived from calcein AM loaded cells.<sup>193-195</sup> Regarding the calcein  
659 efflux *via* gap junctions, a cell type dependency was observed when measuring the inward  
660 diffusion of calcein within spheroids of different cell lines which were preloaded with calcein  
661 AM.<sup>196</sup> The influence of the cell type on calcein efflux was further demonstrated using different  
662 prostate cancer cells and bone marrow endothelial cells. The results revealed a halving of  
663 intracellular calcein fluorescence already 6 h after calcein AM loading of the cells.<sup>197</sup>

664 Additionally, the calcein which is not released from endolysosomes can be expected to either  
665 end up in the lysosome, where it's fluorescence might for example be quenched due to the  
666 decreased pH value, or to be exported *via* secretion in extracellular vesicles, since cells are known  
667 to dispose redundant, non-digestible molecules (Figure 9C).<sup>122</sup> Over time, this can also lead to a  
668 decreased intracellular calcein concentration ready to be released from endosomes which in turn  
669 can vary between different cell types. However, the accuracy of this assumption remains an open  
670 question, since the intracellular pathway of calcein, more importantly its kinetics and cell line  
671 dependencies, have not been investigated in detail so far. Nevertheless, this information could  
672 provide more insights into the calcein release assay including hints on how the assay should be  
673 planned and should therefore be thoroughly investigated.

674 A delayed addition of calcein (sequential incubation) might circumvent potential interferences  
675 of excretion mechanisms with release materials requiring longer incubation times due to low  
676 endocytosis rates,<sup>107</sup> which could possibly result in misleading conclusions. If calcein is initially  
677 encapsulated within the release material (*e.g.*, in liposomes), at least the degradation and/or  
678 exocytosis of calcein seem to be of limited importance, as the release material might disturb the  
679 endolysosomal maturation process and might protect the encapsulated calcein. Hence, the  
680 incubation time mainly depends on the time required for the release material to escape the



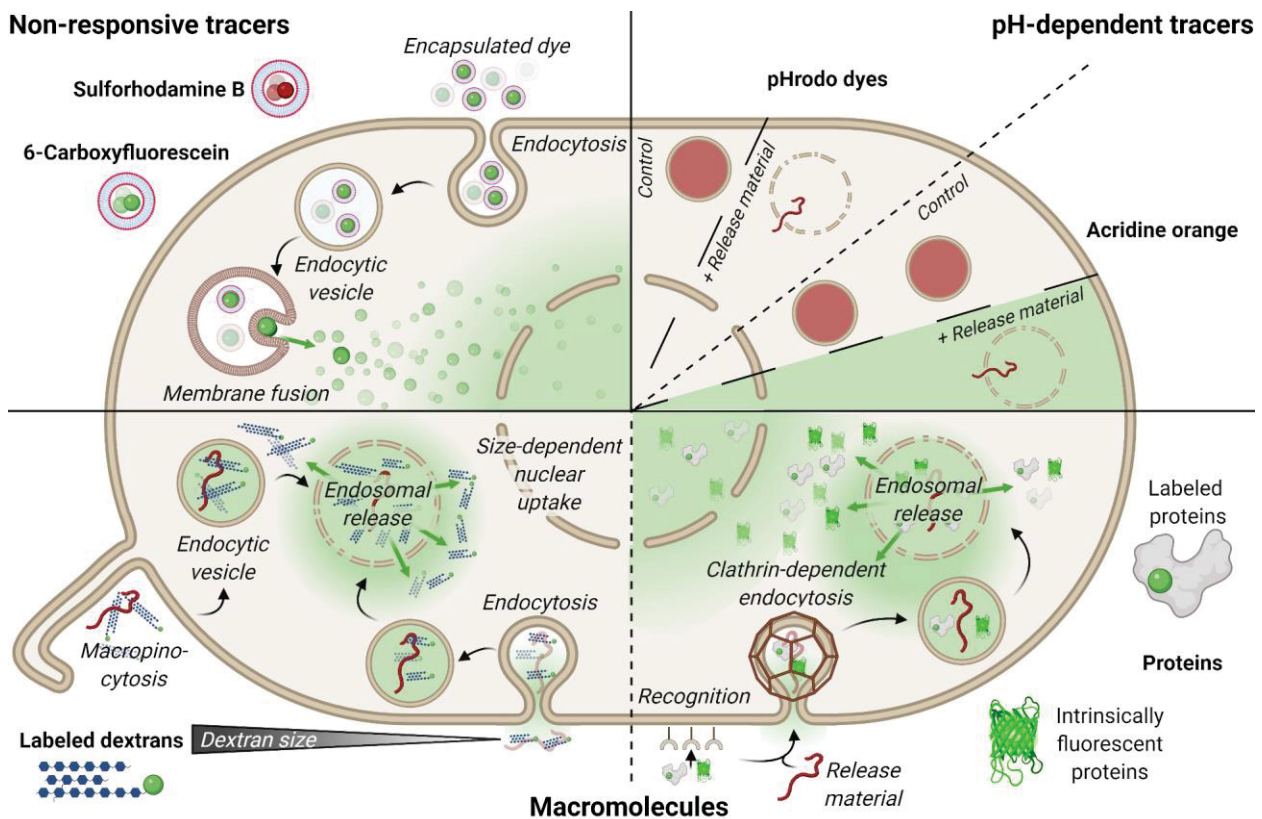
681 endolysosome. In some studies, calcein release was observed following four days of incubation,<sup>124</sup>  
682 or even following incubation with the release material encapsulating calcein for 1 h and medium  
683 for further 47 h.<sup>155</sup> This points towards slow uptake or endosomal escape kinetics.

684 All in all, the incubation time should be chosen long enough to allow i) a sufficient amount of  
685 calcein and release material inside the endolysosomes and ii) intracellular fusion of the organelles  
686 along the endolysosomal pathway, in case calcein and the release material were taken up by  
687 different organelles. In case of release materials encapsulating calcein, the incubation time only  
688 has to be adapted to the former one. For comparison purposes, not only the uptake and excretion  
689 rates of calcein and the release material should be considered, but also the differences between cell  
690 types.

### 691 **5.3. Factors influencing the accuracy of the measurement**

692 As described in the preceding section, different analytical methods have been utilized to  
693 characterize the calcein release within cells qualitatively or even quantitatively with different  
694 degrees of detail. When deciding which method to perform, (confocal) microscopy is preferred,  
695 due to a straightforward (and more reliable) discrimination of endocytosed and released calcein.  
696 Continuous advancement in technology allows images to also be quantified and processed using  
697 high-throughput analysis. Moreover, kinetic investigations can be performed, which can lead to  
698 conclusions regarding the escape mechanism (see Chapter 0). Nevertheless, flow cytometry is the  
699 method of choice if more reliable statistics (fast analysis of >10 000 cells possible) are required,  
700 which would still be very tedious using confocal microscopy even if advanced image analysis  
701 software is used. However, there are certain pitfalls to be aware of and, in some cases, it should be  
702 considered more as a screening method that requires verification by microscopy. The latter  
703 becomes particularly important if the release material might alter the endocytosis rate of the cells  
704 leading to variations in fluorescence intensity within the endosomes, but not the cytosol. As only  
705 the overall fluorescence intensity per cell is detected in flow cytometry, this analysis alone would

706 result in a false positive outcome compared to a control without the release material. On the  
707 contrary, a release material which induces only limited calcein release from endosomes can also  
708 hardly be detected but could suffice for transfection in the actual application. Therefore, it would  
709 lead to a false negative result due to the limited overall increase of fluorescence intensity within  
710 the cytosol which is overlaid by that of the endosomes. This issue has to be kept in mind in  
711 microscopy as well. In particular, acquisition settings which are optimized for the rather bright  
712 endosomes might not allow an identification of a graded or weak release. In general, it is advisable  
713 to combine several methods for determining calcein release, to enable quantitative as well as  
714 qualitative analysis.



716  
 717 **Figure 10. Complementary methods to the calcein release assay.** In addition to calcein, other  
 718 tracers such as sulforhodamine B or 6-carboxyfluorescein can be encapsulated in vesicles to  
 719 determine their release capabilities in cells. pH-dependent tracers such as pHrodo or acridine  
 720 orange can also be of interest, as they indicate the pH in their environment through changes in  
 721 fluorescence. Besides small molecules, macromolecules such as dextrans or proteins are intriguing,  
 722 as their size and complexity provide additional information about the escape.

723 Besides calcein, other dyes are frequently used for dequenching assays in artificial vesicles, such  
 724 as 6-carboxyfluorescein and sulforhodamine B. The recent review by Nasr and colleagues provides  
 725 information on the use of these fluorophores for the study of liposomal membrane integrity.<sup>88</sup>  
 726 These dyes are also inexpensive and easily accessible but have drawbacks as well. For example,  
 727 the fluorescence of 6-carboxyfluorescein is strongly pH-dependent in the physiologically  
 728 interesting pH range from the extracellular space to early endosome, whereas calcein is less  
 729 sensitive in this regard.<sup>45, 88, 198</sup> Although the fluorescence intensity of sulforhodamine B is entirely

730 pH-independent in the physiological relevant pH range,<sup>199</sup> its higher self-quenching concentration  
731 is rather disadvantageous.

732 The review by Martens *et al.* provides more information on other methods for studying  
733 endosomal escape in cells, as well as an overview of escape mechanisms.<sup>24, 92</sup> This present review  
734 focuses on methods that can be used complementary and provides comparisons to the calcein  
735 release assay. Sulforhodamine B can also be used inside cells as calcein analog to study endosomal  
736 escape.<sup>199</sup> However, it has been suggested that sulforhodamine B distributes less rapidly within the  
737 cell than calcein,<sup>54</sup> which may delay accurate timing of the endosomal escape event and could be  
738 disadvantageous in live cell microscopy.

739 In addition to the above mentioned chromophores, more specific indicators can be used which  
740 change their fluorescence in dependence of pH and, thus, provide further insight into the  
741 endosomal escape process.<sup>5</sup> Both, dyes that are quenched in a pH-dependent manner and those that  
742 shift in their excitation/emission wavelength are of interest. An interesting example are the  
743 commercially available, pH-sensitive pHrodo dyes (rhodamine derivatives), which show little to  
744 no fluorescent signal at neutral pH but are highly fluorescent in acidic environments.<sup>200, 201</sup> These  
745 properties render the uncharged, membrane-permeable dyes ideal candidates for use as pH  
746 indicators in endosomal escape investigations when covalently bound to an endocytosed  
747 macromolecule. Consequently, a limited or impeded acidification of endosomes can be monitored  
748 by the absence of fluorescence in comparison to a control experiment, which allows to evaluate  
749 for example the pore formation in treatment with a release material by microscopy or cytometry.<sup>107</sup>  
750 Another interesting alternative is the membrane-penetrating, acidotropic and metachromatic dye  
751 acridine orange. When cells are treated with acridine orange, the dye penetrates the membrane and  
752 distributes within the cell entering also any present endolysosomes. In the acidic endosomal milieu,  
753 acridine orange becomes protonated and is then no longer able to penetrate the cell membranes,  
754 which eventually leads to an accumulation in lysosomes. At the resulting higher concentrations in

755 the lysosomes, acridine orange forms red fluorescent dimers, trimers and oligomers,<sup>202</sup> which can  
756 be observed as red fluorescence if the endo/lysosomes remain intact. Release of protonated  
757 acridine orange, *e.g.*, by permeabilization of endosomes in the presence of any release material,  
758 results in deprotonation of the dye in the cytosol and thus in strong green cytosolic fluorescence  
759 of the homogenously distributed monomer, which can be analyzed microscopically or by flow  
760 cytometry.<sup>158, 203</sup> The strong concentration-dependent difference in the spectra of the dye,  
761 therefore, allows a clear distinction between cytosolic and endosomal fluorescence, *i.e.*,  
762 differentiation between uptake and endosomal escape. To remove diffusing acridine orange, cells  
763 must be washed thoroughly both immediately after addition of acridine orange as well as before  
764 each analysis. It represents an elegant method in addition to investigations with calcein.

765 All complementary methods for calcein release discussed so far provide information on the  
766 occurrence of small pores, because of the size of the marker dye. However, in the evaluation of  
767 release materials for biomedical applications, it is also of interest if larger compounds or  
768 macromolecules can be released. Thus, other methods can be combined with the release of the  
769 small molecule calcein to evaluate the escape mechanism and delivery efficiency of a drug  
770 regarding biomedical applications. Calcein release is frequently studied in the context of nucleic  
771 acid transfection with cationic polymers. Often, calcein escape efficiency is correlated with pDNA  
772 transfection, independent of the used release material.<sup>157, 160, 162, 164-166</sup> However, this correlation  
773 does not hold true in all cases. For example, Vermeulen and coworkers investigated the endosomal  
774 escape mechanism of JetPEI polyplexes, a linear PEI derivate,<sup>11</sup> and tried to correlate the release  
775 of calcein or labeled oligonucleotide according to a previously published procedure with the  
776 transfection efficiency.<sup>6</sup> Interestingly, a calcein release was observed in far more cells than the  
777 transfection and therefore does not correlate well, but the oligonucleotide release appeared to be a  
778 more reliable indicator for efficient transfection. The authors conclude that endosomal leakiness  
779 for small molecules can be induced by membrane destabilization due to the interaction with

780 cationic polyplexes, hindering an effective buildup of osmotic pressure due to ion flux across this  
781 disturbed membrane and thus preventing the endosomal burst and escape of any macromolecules.  
782 Thus, investigations of calcein release may provide further indications about the mechanism of  
783 endosomal escape in addition to its efficacy.

784 If calcein release is studied in comparison to the escape of macromolecules of different sizes, a  
785 conclusion can be drawn about the size of the membrane defect that has occurred. For such studies,  
786 polysaccharides can be used such as dextrans, which have a rather rapid diffusion rate through the  
787 cytosol despite their different sizes. This favors a temporal determination of the escape event.<sup>54</sup>  
788 Ogris and colleagues used a FITC-labeled dextran (10 kDa), which allowed them to study the  
789 release of melittin-modified PEI polyplexes. In this case, the fluorescence of the FITC is enhanced  
790 upon release due to the increase in pH.<sup>204</sup> In another example, Zhan and colleagues<sup>170</sup> measured  
791 the release of various dextrans by blend particles featuring a PDMAEMA domain in comparison  
792 to calcein. They incubated dendritic DC2.4 cells simultaneously with calcein and dextrans of  
793 different sizes (4 - 2000 kDa), respectively.<sup>170</sup> Their study showed that endosomal release of  
794 compounds was not depending on the composition of the blend but on the size of the sensor  
795 molecule, whereas the smaller ones are released more easily. In addition to calcein release,  
796 Salomone *et al.* also investigated the release of different sized dextrans (3 - 40 kDa) by CPPs and  
797 found endosomal release.<sup>174</sup>

798 In addition to polysaccharides, peptides and proteins can also be used as markers to study  
799 endosomal escape and place even greater demands on the release material due to their 3D  
800 structure.<sup>163</sup> Fluorescent proteins such as R-phycoerythrin (R-PE, 240 kDa) or EGFP (27 kDa) can  
801 also be used to study endosomal release. Although the endosomal uptake of these proteins without  
802 additional treatment with an uptake-inducing material is low, the mechanism of endosomal escape  
803 of the same material can be studied in more detail with fluorescent proteins. Since these proteins  
804 undergo a loss of fluorescence along the endolysosomal pathway due to denaturation, a release of

805 the fluorescent signal clearly indicates an escape from the early endosome. Kopp and colleagues  
806 delivered R-PE into four different cell lines using calcium phosphate nanoparticles as delivery  
807 materials.<sup>205</sup> Labelled proteins can also be used to investigate endosomal escape, but unlike  
808 intrinsically fluorescent proteins, the timing of the endosomal escape event cannot be investigated  
809 with labelled proteins since denaturation of the protein has no influence on the fluorescence  
810 intensity of the dye. Also, a positive signal does not necessarily indicate a complete release of the  
811 entire protein with its intact 3D structure. Here, too, a combination with other methods is  
812 meaningful. Nevertheless, labelled bovine serum albumin (BSA) is a suitable and easily available  
813 candidate, since it is efficiently taken up *via* endocytosis and can be detected more quickly than  
814 other complex proteins after the escape event due to its moderate diffusion speed. Diffusion in the  
815 cytosol is slower than for a small molecule like calcein, because the higher molar mass and the  
816 more complex structure of the protein result in comparatively slower diffusion.<sup>54, 163</sup>

817 Actual transfection, *i.e.*, the delivery of genetic material to its site of action, can also serve as  
818 evidence of endosomal release. Depending on the type of genetic cargo, different read-outs are  
819 used. In the case of pDNA transfection, protein expression provides very clear evidence that  
820 endosomal release of the plasmid must have been successful. However, the intensity of protein  
821 expression does not necessarily correlate with the rate of release. Rather, protein expression in this  
822 case indicates a successful overcoming of the nuclear barrier in addition to various other aspects.  
823 In the case of successful delivery of RNAs, either protein expression (mRNA) or silencing (*e.g.*,  
824 siRNA) may indicate successful delivery, depending on the cargo. In either case, successful  
825 delivery (measurable as expression or knockdown) represents a global read-out that demonstrates  
826 the functionality of the genetic cargo.

## 827 7. CONCLUSION & PERSPECTIVES

828 Initially being developed for the detection of multivalent ions, calcein has without doubt become  
829 a working horse in the analysis of lipid membrane leakage in cells as well as in artificial liposomes.  
830 In particular, the detection of escape events from endo-/lysosomal compartments after cellular  
831 uptake renders this simple molecule a powerful tool in the investigation of diverse release materials  
832 such as cell entry vectors or membrane destabilization agents. Its unique set of properties (*i.e.*, a  
833 high charge density due to the multiple carboxylic acid groups, a low toxicity, a high extinction  
834 coefficient and quantum yield, the self-quenching at increased concentrations, and a low sensitivity  
835 towards changes in pH) hinders undesired membrane penetrations, allows its detection in even low  
836 concentrations, enables a broad applicability in relevant physiological environments, and most  
837 importantly facilitates the detection of release events, respectively. On top, calcein is affordable  
838 for most researchers worldwide, since the straightforward synthetic access keeps costs low  
839 compared to many other complex sensor dyes used in biology or pharmacy. Its application further  
840 appears straightforward, since no additional chemical modifications are required, and simple co-  
841 incubation is sufficient to monitor intracellular release events.

842 Nevertheless, various aspects should be kept in mind when planning experiments with calcein  
843 as reporter, since several pitfalls might deteriorate sensitivity, affect outcomes, or entirely lead to  
844 false interpretations of the data. The presence of multivalent ions or unintended interactions with  
845 release materials (*e.g.*, cationic polymers) can, among other factors, impact fluorescence intensities  
846 and have to be assessed prior to the experiments. Further down the road, additional difficulties  
847 may arise from the incubation conditions, the incubation time, or most of all the analysis of a  
848 potential escape. In particular, individual methods, such as microscopy or flow cytometry  
849 measurements, may underestimate or overrate escape events, respectively, if not carefully analyzed  
850 and compared to suitable controls. It is overall advisable to combine several methods to investigate  
851 the calcein release assay, in order to facilitate not only a qualitative but also a quantitative analysis.



852 For example, a combination of fluorescence-activated cell sorting and downstream microscopy or  
853 fluorescence correlation spectroscopy could be interesting to confirm the correlation between the  
854 different fluorescence intensities of the cells and the subcellular distribution of the fluorescent dye  
855 but has not yet been reported for calcein.

856 Besides this individual optimization of experiments, a more global challenge resides in the  
857 comparability of datasets across various studies and particularly across different research groups.  
858 Of course, each release material or vector might require a specific set of conditions to effectively  
859 induce endosomal escape, which is further related to different analysis methods or assay  
860 parameters optimized for the respective system. Differences arise from the employed cell lines,  
861 the applied medium, or the potency and toxicity of the release material. The application of  
862 significantly different conditions might ultimately lead to different conclusions for similar or even  
863 the same release materials. Fundamental understanding of key factors influencing endosomal  
864 escape however require that experimental setups allow a certain degree of comparison between  
865 results obtained in different laboratories worldwide. A minimum step towards a better  
866 comparability is in our opinion a comprehensive and detailed description of the experimental  
867 conditions including the initial preparation of the calcein solution, the incubation times with  
868 calcein and/or the applied release material, the incubation conditions and media, as well as the  
869 analytical methods. Ideally, any future study on this matter should maintain reasonable ranges of  
870 concentration for calcein,<sup>5</sup> which avoids the appearance of artifacts in the measurements, and  
871 include control experiments with established and commercial release materials for  
872 comparability.<sup>206</sup> We are convinced that all research groups would benefit from such measures.

873 In a long-term perspective, certainly more advanced sensors will gain growing interest and  
874 complement the calcein release assay. Interesting candidates include among others pH-sensitive  
875 dyes, which allow for an additional readout of the increasing acidification during endosome  
876 maturation. Dye modified macromolecules or proteins of various sizes further allow more detailed

877 conclusions on the release process, since far larger pores or a burst of the compartments are  
878 required to release these molecules. The application of specific proteins or attached ligands might  
879 even facilitate to select specific uptake routes and gain information on the influence of different  
880 entry pathways. In addition, the application of fluorescent proteins represents a promising  
881 approach to verify a release prior to any degradation processes along the endo-/lysosomal pathway,  
882 which is crucial if the delivery of active enzymes is for example considered. Dyes that react in the  
883 presence of certain enzymes may also be of interest.<sup>207</sup> Combined with knowledge of the processes  
884 along the uptake pathway, a timing of release could become accessible.

885 The calcein assay nonetheless remains a basic, but potent method, which represents a  
886 straightforward entry into the analysis of potential release events, and it might not yet have  
887 revealed its full potential. If the nanocarrier is investigated with different calcein concentrations  
888 and at different incubation times, conclusions could be drawn about the release mechanism. For  
889 instance, distinguishing continuous release over time from more concerted, transient release, or  
890 distinguishing the individual release events as gradual or all-or-none. Furthermore, the excretion  
891 of released calcein from the cytosol might be detected. However, for such detailed conclusions, a  
892 more thorough understanding of the intracellular processing/trafficking/transport (rate) of calcein  
893 (in different cell lines) are required. Also, the combination with complementary sensor molecules  
894 or dyes promises to reveal a deeper understanding of the responsible processes for release or a  
895 more quantitative evaluation of efficacies. The continuous developments in fluorescence imaging,  
896 might provide additional insight into the cellular release mechanism (graded leakage vs. all-or-  
897 none leakage mechanism) based on the increasing knowledge derived from artificial liposomes.  
898 Furthermore, the model liposomes allow for the detailed investigation of the release material's  
899 performance in response to a specific feature of endosome maturation (change in pH or membrane  
900 composition), which certainly does not reflect the complex cellular environment but can give at  
901 least a hint on the release mechanism.

902 Overall, we are convinced that the calcein assay will remain an essential tool in the  
903 characterization of release from lipid compartments in cells and a key towards a more fundamental  
904 understanding of the mode of action of many release materials. The presented review hopefully  
905 inspires further groups to apply this assay and provides a sufficient database for efficient cross-  
906 correlations, which holds the potential to reveal key features relevant for the design of future  
907 release materials.

908 8. DECLARATIONS

909 **8.1. Competing interests.**

910 The authors declare that they have no competing interests.

911 **8.2. Acknowledgements.**

912 The authors gratefully acknowledge the Bundesministerium für Bildung und Forschung (BMBF,  
913 Germany, #13XP5034A PolyBioMik); the German Research Foundation (DFG) for generous  
914 funding within the Emmy-Noether Programme (Projekt ID: 358263073); German Research  
915 Foundation (DFG, ID: 415894560); and the support by the DFG-funded Collaborative Research  
916 Centre PolyTarget (SFB 1278, project A05, B01, Z01, project ID: 316213987). The figures were  
917 created with BioRender.com, which was also provided by the SFB 1278.

918

## 919 9. REFERENCES

- 920 1. M. J. Mitchell, M. M. Billingsley, R. M. Haley, M. E. Wechsler, N. A. Peppas and R.  
921 Langer, *Nat. Rev. Drug Discov.*, 2021, **20**, 101-124.
- 922 2. V. Sanna and M. Sechi, *ACS Med. Chem. Lett.*, 2020, **11**, 1069-1073.
- 923 3. P. Foroozandeh and A. A. Aziz, *Nanoscale Res. Lett.*, 2018, **13**, 339.
- 924 4. S. Behzadi, V. Serpooshan, W. Tao, M. A. Hamaly, M. Y. Alkawareek, E. C. Dreaden, D.  
925 Brown, A. M. Alkilany, O. C. Farokhzad and M. Mahmoudi, *Chem. Soc. Rev.*, 2017, **46**,  
926 4218-4244.
- 927 5. K. Deprey, L. Becker, J. Kritzer and A. Pluckthun, *Bioconjug. Chem.*, 2019, **30**, 1006-  
928 1027.
- 929 6. Z. ur Rehman, D. Hoekstra and I. S. Zuhorn, *ACS Nano*, 2013, **7**, 3767-3777.
- 930 7. A. T. Dinh, C. Pangarkar, T. Theofanous and S. Mitragotri, *Biophys. J.*, 2007, **92**, 831-846.
- 931 8. T. Merdan, K. Kunath, D. Fischer, J. Kopecek and T. Kissel, *Pharm. Res.*, 2002, **19**, 140-  
932 146.
- 933 9. J. Huotari and A. Helenius, *EMBO J.*, 2011, **30**, 3481-3500.
- 934 10. S. R. Pfeffer, *Nat. Cell Biol.*, 1999, **1**, E145-147.
- 935 11. L. M. P. Vermeulen, T. Brans, S. K. Samal, P. Dubruel, J. Demeester, S. C. De Smedt, K.  
936 Remaut and K. Braeckmans, *ACS Nano*, 2018, **12**, 2332-2345.
- 937 12. M. E. G. de Araujo, G. Liebscher, M. W. Hess and L. A. Huber, *Traffic*, 2020, **21**, 60-75.
- 938 13. A. El-Sayed and H. Harashima, *Mol. Ther.*, 2013, **21**, 1118-1130.
- 939 14. H. D. Gallala, B. Breiden and K. Sandhoff, *J. Neurochem.*, 2011, **116**, 702-707.
- 940 15. J. Gruenberg, *Traffic*, 2020, **21**, 76-93.
- 941 16. F. Hullin-Matsuda, T. Taguchi, P. Greimel and T. Kobayashi, *Semin. Cell. Dev. Biol.*, 2014,  
942 **31**, 48-56.
- 943 17. T. Kobayashi, M. H. Beuchat, J. Chevallier, A. Makino, N. Mayran, J. M. Escola, C.  
944 Lebrand, P. Cosson, T. Kobayashi and J. Gruenberg, *J. Biol. Chem.*, 2002, **277**, 32157-  
945 32164.
- 946 18. H. Schulze and K. Sandhoff, *Cold Spring Harb. Perspect. Biol.*, 2011, **3**, a004804.
- 947 19. M. P. Stewart, A. Lorenz, J. Dahlman and G. Sahay, *Wiley Interdiscip. Rev. Nanomed.*  
948 *Nanobiotechnol.*, 2016, **8**, 465-478.
- 949 20. A. Ahmad, J. M. Khan and S. Haque, *Biochimie*, 2019, **160**, 61-75.
- 950 21. T. Bus, A. Traeger and U. S. Schubert, *J. Mater. Chem. B*, 2018, **6**, 6904-6918.
- 951 22. O. Boussif, F. Lezoualc'h, M. A. Zanta, M. D. Mergny, D. Scherman, B. Demeneix and J.  
952 P. Behr, *Proc. Natl. Acad. Sci. U. S. A.*, 1995, **92**, 7297-7301.
- 953 23. R. V. Benjaminsen, M. A. Matthebjerg, J. R. Henriksen, S. M. Moghimi and T. L. Andresen,  
954 *Mol. Ther.*, 2013, **21**, 149-157.
- 955 24. T. F. Martens, K. Remaut, J. Demeester, S. C. De Smedt and K. Braeckmans, *Nano Today*,  
956 2014, **9**, 344-364.
- 957 25. E. Xu, W. M. Saltzman and A. S. Piotrowski-Daspit, *J. Control. Release*, 2021, **335**, 465-  
958 480.
- 959 26. S. L. Y. Teo, J. J. Rennick, D. Yuen, H. Al-Wassiti, A. P. R. Johnston and C. W. Pouton,  
960 *Nat. Commun.*, 2021, **12**, 3721.
- 961 27. N. I. Zahaf, A. E. Lang, L. Kaiser, C. D. Fichter, S. Lassmann, A. McCluskey, A.  
962 Augspach, K. Aktories and G. Schmidt, *Sci. Rep.*, 2017, **7**, 41252.
- 963 28. S. Schmidt, M. J. Adjobo-Hermans, R. Wallbrecher, W. P. Verdurmen, P. H. Bovee-  
964 Geurts, J. van Oostrum, F. Milletti, T. Enderle and R. Brock, *Angew. Chem. Int. Ed. Engl.*,  
965 2015, **54**, 15105-15108.
- 966 29. N. Milech, B. A. Longville, P. T. Cunningham, M. N. Scobie, H. M. Bogdawa, S. Winslow,  
967 M. Anastasas, T. Connor, F. Ong, S. R. Stone, M. Kerfoot, T. Heinrich, K. M. Kroeger, Y.

- 968 F. Tan, K. Hoffmann, W. R. Thomas, P. M. Watt and R. M. Hopkins, *Sci. Rep.*, 2015, **5**,  
969 18329.
- 970 30. B. C. Evans, R. B. Fletcher, K. V. Kilchrist, E. A. Dailing, A. J. Mukalel, J. M. Colazo, M.  
971 Oliver, J. Cheung-Flynn, C. M. Brophy, J. W. Tierney, J. S. Isenberg, K. D. Hankenson,  
972 K. Ghimire, C. Lander, C. A. Gersbach and C. L. Duvall, *Nat. Commun.*, 2019, **10**, 5012.
- 973 31. H. Du Rietz, H. Hedlund, S. Wilhelmson, P. Nordenfelt and A. Wittrup, *Nat. Commun.*,  
974 2020, **11**, 1809.
- 975 32. H. Diehl and J. L. Ellingboe, *Anal. Chem.*, 1956, **28**, 882-884.
- 976 33. H. Diehl, *Anal. Chem.*, 1967, **39**, A30-+.
- 977 34. A. J. Hefley, Doctor of Philosophy, Iowa State University, 1967.
- 978 35. Richard Markuszewski, Doctor of Philosophy, Iowa State University, 1976.
- 979 36. D. B. Martin, Doctor of Philosophy, Iowa State University, 1977.
- 980 37. J. W. Furry, Doctor of Philosophy, Iowa State University, 1985.
- 981 38. R. W. Sabnis, in *Handbook of Biological Dyes and Stains*, John Wiley & Sons, Inc. ,  
982 Hoboken, New Jersey, 2010, DOI: 10.1002/9780470586242.ch3, pp. 71-122.
- 983 39. H. Diehl, G. Frederick Smith Chemical Company, 1964.
- 984 40. B. Walter, *Annalen der Physik*, 1888, **270**, 316-326.
- 985 41. B. Walter, *Annalen der Physik*, 1889, **272**, 502-518.
- 986 42. B. Walter, *Annalen der Physik*, 1889, **272**, 518-532.
- 987 43. R. F. Chen and J. R. Knutson, *Anal. Biochem.*, 1988, **172**, 61-77.
- 988 44. J. N. Weinstein, S. Yoshikami, P. Henkart, R. Blumenthal and W. A. Hagins, *Science*,  
989 1977, **195**, 489-492.
- 990 45. T. M. Allen and L. G. Cleland, *Biochim. Biophys. Acta*, 1980, **597**, 418-426.
- 991 46. D. A. Kendall and R. C. MacDonald, *Anal. Biochem.*, 1983, **134**, 26-33.
- 992 47. H. Patel, C. Tscheka, K. Edwards, G. Karlsson and H. Heerklotz, *Biochim. Biophys. Acta*,  
993 2011, **1808**, 2000-2008.
- 994 48. S. Salassi, F. Simonelli, A. Bartocci and G. Rossi, *J. Phys. D: Appl. Phys*, 2018, **51**,  
995 384002.
- 996 49. S. Hamann, J. F. Kiilgaard, T. Litman, F. J. Alvarez-Leefmans, B. R. Winther and T.  
997 Zeuthen, *J Fluoresc*, 2002, **12**, 139-145.
- 998 50. K. E. Roberts, A. K. O'Keeffe, C. J. Lloyd and D. J. Clarke, *J. Fluoresc.*, 2003, **13**, 513-  
999 517.
- 1000 51. A. Andersson, J. Danielsson, A. Graslund and L. Maler, *Eur. Biophys. J.*, 2007, **36**, 621-  
1001 635.
- 1002 52. R. Imamura, N. Murata, T. Shimanouchi, K. Yamashita, M. Fukuzawa and M. Noda,  
1003 *Sensors (Basel)*, 2017, **17**, 1630.
- 1004 53. G. Dorrington, N. P. Chmel, S. R. Norton, A. M. Wemyss, K. Lloyd, D. Praveen  
1005 Amarasinghe and A. Rodger, *Biophys. Rev.*, 2018, **10**, 1385-1399.
- 1006 54. N. Brkovic, L. Zhang, J. N. Peters, S. Kleine-Doepke, W. J. Parak and D. Zhu, *Small*, 2020,  
1007 **16**, e2003639.
- 1008 55. W. Bae, T. Y. Yoon and C. Jeong, *PLoS One*, 2021, **16**, e0247326.
- 1009 56. D. F. H. Wallach and T. L. Steck, *Anal. Chem.*, 2002, **35**, 1035-1044.
- 1010 57. R. M. Straubinger, K. Hong, D. S. Friend and D. Papahadjopoulos, *Cell*, 1983, **32**, 1069-  
1011 1079.
- 1012 58. F. C. Szoka, K. Jacobson and D. Papahadjopoulos, *Biochim. Biophys. Acta*, 1979, **551**,  
1013 295-303.
- 1014 59. C. B. Billesbolle, C. M. Azumaya, R. C. Kretsch, A. S. Powers, S. Gonen, S. Schneider, T.  
1015 Arvedson, R. O. Dror, Y. Cheng and A. Manglik, *Nature*, 2020, **586**, 807-811.
- 1016 60. N. Oku, D. A. Kendall and R. C. Macdonald, *Biochim. Biophys. Acta*, 1982, **691**, 332-340.
- 1017 61. A. Ali, Q. Zhang, J. Dai and X. Huang, *Biometals*, 2003, **16**, 285-293.

- 1018 62. B. B. Hasinoff, *J. Inorg. Biochem.*, 2003, **95**, 157-164.
- 1019 63. F. Thomas, G. Serratrice, C. Beguin, E. S. Aman, J. L. Pierre, M. Fontecave and J. P.  
1020 Laulhere, *J. Biol. Chem.*, 1999, **274**, 13375-13383.
- 1021 64. H. B. Li and F. Chen, *Fresenius J. Anal. Chem.*, 2000, **368**, 501-504.
- 1022 65. J. Körbl, F. Vydra and R. Přibil, *Talanta*, 1958, **1**, 281-282.
- 1023 66. J. H. Eggers, *Talanta*, 1960, **4**, 38-43.
- 1024 67. A. M. Escarilla, *Talanta*, 1966, **13**, 363-370.
- 1025 68. G. M. Huitink and H. Diehl, *Talanta*, 1974, **21**, 1193-1202.
- 1026 69. G. M. Huitink, D. P. Poe and H. Diehl, *Talanta*, 1974, **21**, 1221-1229.
- 1027 70. D. H. Wilkins, *Talanta*, 1960, **4**, 182-184.
- 1028 71. I. D. Johnson, in *Molecular Probes Handbook: A Guide to Fluorescent Probes and*  
1029 *Labeling Technologies*, ed. I. D. Johnson, Life Technologies Corporation, 11 edn., 2010,  
1030 pp. 833-882.
- 1031 72. D. Thomas, S. C. Tovey, T. J. Collins, M. D. Bootman, M. J. Berridge and P. Lipp, *Cell*  
1032 *Calcium*, 2000, **28**, 213-223.
- 1033 73. A. B. Harkins, N. Kurebayashi and S. M. Baylor, *Biophys. J.*, 1993, **65**, 865-881.
- 1034 74. E. S. Kaneshiro, M. A. Wyder, Y. P. Wu and M. T. Cushion, *J. Microbiol. Methods*, 1993,  
1035 **17**, 1-16.
- 1036 75. D. Bratosin, L. Mitrofan, C. Palii, J. Estaquier and J. Montreuil, *Cytometry A*, 2005, **66**,  
1037 78-84.
- 1038 76. K. I. McConnell, S. Shamsudeen, I. M. Meraz, T. S. Mahadevan, A. Ziemys, P. Rees, H.  
1039 D. Summers and R. E. Serda, *J. Biomed. Nanotechnol.*, 2016, **12**, 154-164.
- 1040 77. S. Neri, E. Mariani, A. Meneghetti, L. Cattini and A. Facchini, *Clin. Diagn. Lab. Immunol.*,  
1041 2001, **8**, 1131-1135.
- 1042 78. E. L. Medzon and M. L. Brady, *J. Bacteriol.*, 1969, **97**, 402-415.
- 1043 79. M. Mitz and G. Blanchard, *BIOCHEMICAL DETECTION METHODS FOR BACTERIA*  
1044 *AND VIRUSES*, MELPAR FALLS CHURCH VA, 1963.
- 1045 80. R. P. Haugland, I. C. MacCoubrey and P. L. Moore, *Journal*, 1994.
- 1046 81. G. Drin, S. Cottin, E. Blanc, A. R. Rees and J. Temsamani, *J. Biol. Chem.*, 2003, **278**,  
1047 31192-31201.
- 1048 82. R. Lichtenfels, W. E. Biddison, H. Schulz, A. B. Vogt and R. Martin, *J. Immunol. Methods*,  
1049 1994, **172**, 227-239.
- 1050 83. A. Nitsch, L. Haralambiev, R. Eickenel, D. O. Muzzio, M. T. Zygmunt, A. Ekkernkamp,  
1051 M. Burchardt and M. B. Stope, *In Vivo*, 2019, **33**, 1767-1771.
- 1052 84. J. K. Stoltenborg, P. W. Tsao, H. J. George, P. J. Bouchard, E. J. Wexler and E. A. Hausner,  
1053 *J. Immunol. Methods*, 1994, **175**, 59-68.
- 1054 85. S. A. Weston and C. R. Parish, *J. Immunol. Methods*, 1990, **133**, 87-97.
- 1055 86. W. D. Gray, A. J. Mitchell and C. D. Searles, *MethodsX*, 2015, **2**, 360-367.
- 1056 87. J. Czyz, U. Irmer, G. Schulz, A. Mindermann and D. F. Hulser, *Exp. Cell. Res.*, 2000, **255**,  
1057 40-46.
- 1058 88. G. Nasr, H. Greige-Gerges, A. Elaissari and N. Khreich, *Int. J. Pharm.*, 2020, **580**, 119198.
- 1059 89. A. Akbarzadeh, R. Rezaei-Sadabady, S. Davaran, S. W. Joo, N. Zarghami, Y. Hanifehpour,  
1060 M. Samiei, M. Kouhi and K. Nejati-Koshki, *Nanoscale Res. Lett.*, 2013, **8**, 102.
- 1061 90. S. Chatterjee and D. K. Banerjee, in *Liposome Methods and Protocols*, eds. S. C. Basu and  
1062 M. Basu, Humana Press, Totowa, NJ, 2002, DOI: 10.1385/1-59259-175-2:03, pp. 3-16.
- 1063 91. S. Dutta, B. G. Watson, S. Mattoo and J. C. Rochet, *Bio. Protoc.*, 2020, **10**, e3690.
- 1064 92. S. Guha, J. Ghimire, E. Wu and W. C. Wimley, *Chem. Rev.*, 2019, **119**, 6040-6085.
- 1065 93. A. Stulz, A. Vogt, J. S. Saar, L. Akil, K. Lienkamp and M. Hoernke, *Langmuir*, 2019, **35**,  
1066 16366-16376.
- 1067 94. W. C. Wimley and K. Hristova, *Aust. J. Chem.*, 2019, **73**, 96-103.

- 1068 95. I. Tsogas, D. Tsiourvas, G. Nounesis and C. M. Paleos, *Langmuir*, 2006, **22**, 11322-11328.
- 1069 96. Y. Sarkar, S. Roy, R. Majumder, S. Das, D. V. Bhalani, A. Ray, S. K. Jewrajka and P. P.
- 1070 Parui, *Soft Matter*, 2020, **16**, 798-809.
- 1071 97. J. L. Thomas, H. You and D. A. Tirrell, *J. Am. Chem. Soc.*, 1995, **117**, 2949-2950.
- 1072 98. J. Allen, K. Najjar, A. Erazo-Oliveras, H. M. Kondow-McConaghy, D. J. Brock, K.
- 1073 Graham, E. C. Hager, A. L. J. Marschall, S. Dubel, R. L. Juliano and J. P. Pellois, *ACS*
- 1074 *Chem. Biol.*, 2019, **14**, 2641-2651.
- 1075 99. D. J. Brock, L. Kustigian, M. Jiang, K. Graham, T. Y. Wang, A. Erazo-Oliveras, K. Najjar,
- 1076 J. Zhang, H. Rye and J. P. Pellois, *Traffic*, 2018, **19**, 421-435.
- 1077 100. K. Najjar, A. Erazo-Oliveras, D. J. Brock, T. Y. Wang and J. P. Pellois, *J. Biol. Chem.*,
- 1078 2017, **292**, 847-861.
- 1079 101. K. Sudo, K. Niikura, K. Iwaki, S. Kohyama, K. Fujiwara and N. Doi, *J. Control. Release*,
- 1080 2017, **255**, 1-11.
- 1081 102. D. J. Brock, H. Kondow-McConaghy, J. Allen, Z. Brkljaca, L. Kustigian, M. Jiang, J.
- 1082 Zhang, H. Rye, M. Vazdar and J. P. Pellois, *Cell Chem. Biol.*, 2020, **27**, 1296-1307 e1295.
- 1083 103. A. Erazo-Oliveras, K. Najjar, D. Truong, T. Y. Wang, D. J. Brock, A. R. Prater and J. P.
- 1084 Pellois, *Cell. Chem. Biol.*, 2016, **23**, 598-607.
- 1085 104. Z. Qian, A. Martyna, R. L. Hard, J. Wang, G. Appiah-Kubi, C. Coss, M. A. Phelps, J. S.
- 1086 Rossman and D. Pei, *Biochemistry*, 2016, **55**, 2601-2612.
- 1087 105. S. M. Van Rossenberg, K. M. Sliedregt-Bol, N. J. Meeuwenoord, T. J. Van Berkel, J. H.
- 1088 Van Boom, G. A. Van Der Marel and E. A. Biessen, *J. Biol. Chem.*, 2002, **277**, 45803-
- 1089 45810.
- 1090 106. L. Rangasamy, V. Chelvam, A. K. Kanduluru, M. Srinivasarao, N. A. Bandara, F. You, E.
- 1091 A. Orellana, A. L. Kasinski and P. S. Low, *Bioconjug. Chem.*, 2018, **29**, 1047-1059.
- 1092 107. J. C. Brendel, J. Sanchis, S. Catrouillet, E. Czuba, M. Z. Chen, B. M. Long, C. Nowell, A.
- 1093 Johnston, K. A. Jolliffe and S. Perrier, *Angew. Chem. Int. Ed. Engl.*, 2018, **57**, 16678-
- 1094 16682.
- 1095 108. A. M. Funhoff, C. F. van Nostrum, M. C. Lok, J. A. Kruijtzter, D. J. Crommelin and W. E.
- 1096 Hennink, *J. Control. Release*, 2005, **101**, 233-246.
- 1097 109. E. Mastrobattista, G. A. Koning, L. van Bloois, A. C. Filipe, W. Jiskoot and G. Storm, *J.*
- 1098 *Biol. Chem.*, 2002, **277**, 27135-27143.
- 1099 110. A. El-Sayed, I. A. Khalil, K. Kogure, S. Futaki and H. Harashima, *J. Biol. Chem.*, 2008,
- 1100 **283**, 23450-23461.
- 1101 111. A. El-Sayed, T. Masuda, I. Khalil, H. Akita and H. Harashima, *J. Control. Release*, 2009,
- 1102 **138**, 160-167.
- 1103 112. E. Rideau, R. Dimova, P. Schwille, F. R. Wurm and K. Landfester, *Chem. Soc. Rev.*, 2018,
- 1104 **47**, 8572-8610.
- 1105 113. S. Braun, S. Pokorna, R. Sachl, M. Hof, H. Heerklotz and M. Hoernke, *ACS Nano*, 2018,
- 1106 **12**, 813-819.
- 1107 114. A. Jesorka and O. Orwar, *Annu. Rev. Anal. Chem. (Palo Alto Calif)*, 2008, **1**, 801-832.
- 1108 115. P. Walde, K. Cosentino, H. Engel and P. Stano, *ChemBioChem*, 2010, **11**, 848-865.
- 1109 116. H. Stein, S. Spindler, N. Bonakdar, C. Wang and V. Sandoghdar, *Front. Physiol.*, 2017, **8**,
- 1110 63.
- 1111 117. J. Steinkuhler, P. De Tillieux, R. L. Knorr, R. Lipowsky and R. Dimova, *Sci. Rep.*, 2018,
- 1112 **8**, 11838.
- 1113 118. C. C. Scott and J. Gruenberg, *Bioessays*, 2011, **33**, 103-110.
- 1114 119. T. Shimanouchi, H. Ishii, N. Yoshimoto, H. Umakoshi and R. Kuboi, *Colloids Surf. B*
- 1115 *Biointerfaces*, 2009, **73**, 156-160.
- 1116 120. N. Wang, M. Chen and T. Wang, *J. Control. Release*, 2019, **303**, 130-150.



- 1117 121. L. Wang, N. Hartel, K. Ren, N. A. Graham and N. Malmstadt, *Environ. Sci. Nano*, 2020,  
1118 7, 963-974.
- 1119 122. G. Raposo and W. Stoorvogel, *J. Cell Biol.*, 2013, **200**, 373-383.
- 1120 123. C. Zivko, G. Fuhrmann and P. Luciani, *Biochim. Biophys. Acta Gen. Subj.*, 2021, **1865**,  
1121 129559.
- 1122 124. B. Illes, P. Hirschle, S. Barnert, V. Cauda, S. Wuttke and H. Engelke, *Chem. Mater.*, 2017,  
1123 **29**, 8042-8046.
- 1124 125. I. Sovadinova, E. F. Palermo, R. Huang, L. M. Thoma and K. Kuroda, *Biomacromolecules*,  
1125 2011, **12**, 260-268.
- 1126 126. S. K. Zhang, L. Gong, X. Zhang, Z. M. Yun, S. B. Li, H. W. Gao, C. J. Dai, J. J. Yuan, J.  
1127 M. Chen, F. Gong, Y. X. Tan and S. P. Ji, *J. Gene Med.*, 2020, **22**, e3259.
- 1128 127. W. C. Wimley and K. Hristova, *Aust. J. Chem.*, 2020, **73**, 96-103.
- 1129 128. S. Esteban-Martin, H. J. Risselada, J. Salgado and S. J. Marrink, *J. Am. Chem. Soc.*, 2009,  
1130 **131**, 15194-15202.
- 1131 129. H. Heerklotz, *Biophys. J.*, 2001, **81**, 184-195.
- 1132 130. S. Shi, A. M. Markl, Z. Lu, R. Liu and M. Hoernke, *Langmuir*, 2022, **38**, 2379-2391.
- 1133 131. S. T. Yang, E. Zaitseva, L. V. Chernomordik and K. Melikov, *Biophys. J.*, 2010, **99**, 2525-  
1134 2533.
- 1135 132. C. Mazzuca, B. Orioni, M. Coletta, F. Formaggio, C. Toniolo, G. Maulucci, M. De Spirito,  
1136 B. Pispisa, M. Venanzi and L. Stella, *Biophys. J.*, 2010, **99**, 1791-1800.
- 1137 133. I. Plaza-Ga, V. Manzaneda-Gonzalez, M. Kisovec, V. Almendro-Vedia, M. Munoz-Ubeda,  
1138 G. Anderluh, A. Guerrero-Martinez, P. Natale and I. Lopez Montero, *J.*  
1139 *Nanobiotechnology*, 2019, **17**, 108.
- 1140 134. Y. Tamba and M. Yamazaki, *Biochemistry*, 2005, **44**, 15823-15833.
- 1141 135. G. Fuertes, A. J. Garcia-Saez, S. Esteban-Martin, D. Gimenez, O. L. Sanchez-Munoz, P.  
1142 Schwille and J. Salgado, *Biophys. J.*, 2010, **99**, 2917-2925.
- 1143 136. S. G. Hovakeemian, R. Liu, S. H. Gellman and H. Heerklotz, *Soft Matter*, 2015, **11**, 6840-  
1144 6851.
- 1145 137. A. S. Ladokhin, W. C. Wimley and S. H. White, *Biophys. J.*, 1995, **69**, 1964-1971.
- 1146 138. H. Patel, C. Tscheka and H. Heerklotz, *Soft Matter*, 2009, **5**, 2849-2851.
- 1147 139. B. Apellaniz, J. L. Nieva, P. Schwille and A. J. Garcia-Saez, *Biophys. J.*, 2010, **99**, 3619-  
1148 3628.
- 1149 140. D. A. Kendall and R. C. MacDonald, *J. Biol. Chem.*, 1982, **257**, 13892-13895.
- 1150 141. D. F. Wallach and T. L. Steck, *Anal. Biochem.*, 1963, **6**, 176-180.
- 1151 142. C. J. Chu, J. Dijkstra, M. Z. Lai, K. Hong and F. C. Szoka, *Pharm. Res.*, 1990, **7**, 824-834.
- 1152 143. E. Ducat, J. Deprez, A. Gillet, A. Noel, B. Evrard, O. Peulen and G. Piel, *Int. J. Pharm.*,  
1153 2011, **420**, 319-332.
- 1154 144. V. A. Slepishkin, S. Simoes, P. Dazin, M. S. Newman, L. S. Guo, M. C. Pedroso de Lima  
1155 and N. Duzgunes, *J. Biol. Chem.*, 1997, **272**, 2382-2388.
- 1156 145. S. Simoes, V. Slepishkin, N. Duzgunes and M. C. P. de Lima, *Biochim. Biophys. Acta*  
1157 *Biomembr.*, 2001, **1515**, 23-37.
- 1158 146. M. Kanamala, B. D. Palmer, H. Ghandehari, W. R. Wilson and Z. Wu, *Pharm. Res.*, 2018,  
1159 **35**, 154.
- 1160 147. P. Enzian, C. Schell, A. Link, C. Malich, R. Pries, B. Wollenberg and R. Rahmanzadeh,  
1161 *Mol. Pharm.*, 2020, **17**, 2779-2788.
- 1162 148. J. Connor and L. Huang, *J. Cell Biol.*, 1985, **101**, 582-589.
- 1163 149. S. Cerritelli, D. Velluto and J. A. Hubbell, *Biomacromolecules*, 2007, **8**, 1966-1972.
- 1164 150. E. A. Scott, A. Stano, M. Gillard, A. C. Maio-Liu, M. A. Swartz and J. A. Hubbell,  
1165 *Biomaterials*, 2012, **33**, 6211-6219.

- 1166 151. A. E. Vasdekis, E. A. Scott, C. P. O'Neil, D. Psaltis and J. A. Hubbell, *ACS Nano*, 2012, **6**,  
1167 7850-7857.
- 1168 152. K. Kono, T. Igawa and T. Takagishi, *Biochim. Biophys. Acta*, 1997, **1325**, 143-154.
- 1169 153. H. Xu, W. Zhang, Y. Li, F. F. Ye, P. P. Yin, X. Yu, M. N. Hu, Y. S. Fu, C. Wang and J.  
1170 Shang de, *Pharm. Res.*, 2014, **31**, 3038-3050.
- 1171 154. Z. Li, B. Li, M. Wang, M. Xie, H. Shen, S. Shen, X. Wang, X. Guo, M. Yao and Y. Jin, *J.*  
1172 *Mater. Chem. B*, 2013, **1**, 1466-1474.
- 1173 155. Y. Nishimura, K. Takeda, R. Ezawa, J. Ishii, C. Ogino and A. Kondo, *J.*  
1174 *Nanobiotechnology*, 2014, **12**, 11.
- 1175 156. S. Niedermayer, V. Weiss, A. Herrmann, A. Schmidt, S. Datz, K. Muller, E. Wagner, T.  
1176 Bein and C. Brauchle, *Nanoscale*, 2015, **7**, 7953-7964.
- 1177 157. U. Lachelt, P. Kos, F. M. Mickler, A. Herrmann, E. E. Salcher, W. Rodl, N. Badgular, C.  
1178 Brauchle and E. Wagner, *Nanomedicine*, 2014, **10**, 35-44.
- 1179 158. R. A. Jones, C. Y. Cheung, F. E. Black, J. K. Zia, P. S. Stayton, A. S. Hoffman and M. R.  
1180 Wilson, *Biochem. J.*, 2003, **372**, 65-75.
- 1181 159. S. Deshpande, S. Patil and N. Singh, *ACS Omega*, 2018, **3**, 8042-8049.
- 1182 160. A. K. Trutzschler, T. Bus, M. Reifarth, J. C. Brendel, S. Hoepfener, A. Traeger and U. S.  
1183 Schubert, *Bioconjug. Chem.*, 2018, **29**, 2181-2194.
- 1184 161. R. A. Jones, M. H. Poniris and M. R. Wilson, *J. Control. Release*, 2004, **96**, 379-391.
- 1185 162. F. Richter, L. Martin, K. Leer, E. Moek, F. Hausig, J. C. Brendel and A. Traeger, *J. Mater.*  
1186 *Chem. B*, 2020, **8**, 5026-5041.
- 1187 163. F. Hausig, F. H. Sobotta, F. Richter, D. O. Harz, A. Traeger and J. C. Brendel, *ACS Appl.*  
1188 *Mater. Interfaces*, 2021, **13**, 35233-35247.
- 1189 164. D. K. Bonner, X. Zhao, H. Buss, R. Langer and P. T. Hammond, *J. Control. Release*, 2013,  
1190 **167**, 101-107.
- 1191 165. D. K. Bonner, C. Leung, J. Chen-Liang, L. Chingozha, R. Langer and P. T. Hammond,  
1192 *Bioconjug. Chem.*, 2011, **22**, 1519-1525.
- 1193 166. F. Richter, P. Mapfumo, L. Martin, J. I. Solomun, F. Hausig, J. J. Frietsch, T. Ernst, S.  
1194 Hoepfener, J. C. Brendel and A. Traeger, *J. Nanobiotechnology*, 2021, **19**, 70.
- 1195 167. F. Richter, K. Leer, L. Martin, P. Mapfumo, J. I. Solomun, M. T. Kuchenbrod, S.  
1196 Hoepfener, J. C. Brendel and A. Traeger, *J. Nanobiotechnology*, 2021, **19**, 292.
- 1197 168. Y. Hu, T. Litwin, A. R. Nagaraja, B. Kwong, J. Katz, N. Watson and D. J. Irvine, *Nano*  
1198 *Lett.*, 2007, **7**, 3056-3064.
- 1199 169. K. K. Tran, X. Zhan and H. Shen, *Adv. Healthc. Mater.*, 2014, **3**, 690-702.
- 1200 170. X. Zhan, K. K. Tran, L. Wang and H. Shen, *Pharm. Res.*, 2015, **32**, 2280-2291.
- 1201 171. X. Su, J. Fricke, D. G. Kavanagh and D. J. Irvine, *Mol. Pharm.*, 2011, **8**, 774-787.
- 1202 172. S. Wannasarit, S. Q. Wang, P. Figueiredo, C. Trujillo, F. Eburnea, L. Simon-Gracia, A.  
1203 Correia, Y. P. Ding, T. Teesalu, D. F. Liu, R. Wiwattanapatapee, H. A. Santos and W. Li,  
1204 *Adv. Funct. Mater.*, 2019, **29**, 1905352.
- 1205 173. J. Chen, J. Li, J. Zhou, Z. Lin, F. Cavalieri, E. Czuba-Wojnilowicz, Y. Hu, A. Glab, Y. Ju,  
1206 J. J. Richardson and F. Caruso, *ACS Nano*, 2019, **13**, 11653-11664.
- 1207 174. F. Salomone, F. Cardarelli, M. Di Luca, C. Boccardi, R. Nifosi, G. Bardi, L. Di Bari, M.  
1208 Serresi and F. Beltram, *J. Control. Release*, 2012, **163**, 293-303.
- 1209 175. J. R. Clegg, J. A. Sun, J. Gu, A. K. Venkataraman and N. A. Peppas, *J. Control. Release*,  
1210 2021, **329**, 1162-1171.
- 1211 176. N. Kongkatigumjorn, S. A. Smith, M. Chen, K. T. Fang, S. L. Yang, E. R. Gillies, A. P. R.  
1212 Johnston and G. K. Such, *Acs Appl Nano Mater*, 2018, **1**, 3164-3173.
- 1213 177. N. Kongkatigumjorn, C. Cortez-Jugo, E. Czuba, A. S. Wong, R. Y. Hodgetts, A. P.  
1214 Johnston and G. K. Such, *Macromol. Biosci.*, 2017, **17**, 1600248.

- 1215 178. Y. Hu, P. U. Atukorale, J. J. Lu, J. J. Moon, S. H. Um, E. C. Cho, Y. Wang, J. Chen and  
1216 D. J. Irvine, *Biomacromolecules*, 2009, **10**, 756-765.
- 1217 179. A. S. Wong, S. K. Mann, E. Czuba, A. Sahut, H. Liu, T. C. Suekama, T. Bickerton, A. P.  
1218 Johnston and G. K. Such, *Soft Matter*, 2015, **11**, 2993-3002.
- 1219 180. M. Galliani, C. Tremolanti and G. Signore, *Nanomaterials (Basel)*, 2019, **9**, 652.
- 1220 181. J. S. Kim, D. K. Choi, J. Y. Shin, S. M. Shin, S. W. Park, H. S. Cho and Y. S. Kim, *J.*  
1221 *Control. Release*, 2016, **235**, 165-175.
- 1222 182. G. Rong, C. Wang, L. Chen, Y. Yan and Y. Cheng, *Sci. Adv.*, 2020, **6**, eaaz1774.
- 1223 183. D. Adams, A. Gonzalez-Duarte, W. D. O'Riordan, C. C. Yang, M. Ueda, A. V. Kristen, I.  
1224 Tournev, H. H. Schmidt, T. Coelho, J. L. Berk, K. P. Lin, G. Vita, S. Attarian, V. Plante-  
1225 Bordeneuve, M. M. Mezei, J. M. Campistol, J. Buades, T. H. Brannagan, 3rd, B. J. Kim, J.  
1226 Oh, Y. Parman, Y. Sekijima, P. N. Hawkins, S. D. Solomon, M. Polydefkis, P. J. Dyck, P.  
1227 J. Gandhi, S. Goyal, J. Chen, A. L. Strahs, S. V. Nochur, M. T. Sweetser, P. P. Garg, A. K.  
1228 Vaishnav, J. A. Gollob and O. B. Suhr, *N. Engl. J. Med.*, 2018, **379**, 11-21.
- 1229 184. K. Ren, Y. Liu, J. Wu, Y. Zhang, J. Zhu, M. Yang and H. Ju, *Nat. Commun.*, 2016, **7**,  
1230 13580.
- 1231 185. B. Alberts, A. Johnson, J. Lewis, P. Walter, M. Raff and K. Roberts, *Molecular Biology of*  
1232 *the Cell 4th Edition: International Student Edition*, Routledge, 2002.
- 1233 186. S. Kumari, S. Mg and S. Mayor, *Cell. Res.*, 2010, **20**, 256-275.
- 1234 187. Q. Xia, J. Huang, Q. Feng, X. Chen, X. Liu, X. Li, T. Zhang, S. Xiao, H. Li, Z. Zhong and  
1235 K. Xiao, *Int. J. Nanomedicine*, 2019, **14**, 6957-6970.
- 1236 188. H. Shin, M. Kwak, T. G. Lee and J. Y. Lee, *Nanoscale*, 2020, **12**, 15743-15751.
- 1237 189. M. Essodaigui, H. J. Broxterman and A. Garnier-Suillerot, *Biochemistry*, 1998, **37**, 2243-  
1238 2250.
- 1239 190. N. Feller, H. J. Broxterman, D. C. R. Wahrer and H. M. Pinedo, *FEBS Letters*, 1995, **368**,  
1240 385-388.
- 1241 191. L. Homolya, Z. Hollo, U. A. Germann, I. Pastan, M. M. Gottesman and B. Sarkadi, *J. Biol.*  
1242 *Chem.*, 1993, **268**, 21493-21496.
- 1243 192. Z. Hollo, L. Homolya, C. W. Davis and B. Sarkadi, *Biochim. Biophys. Acta Biomembr.*,  
1244 1994, **1191**, 384-388.
- 1245 193. V. B. Cismasiu and L. M. Popescu, *J. Cell. Mol. Med.*, 2015, **19**, 351-358.
- 1246 194. K. A. Sinclair, S. T. Yerkovich, P. M. Hopkins and D. C. Chambers, *Stem Cell Res. Ther.*,  
1247 2016, **7**, 91.
- 1248 195. S. Strassburg, N. W. Hodson, P. I. Hill, S. M. Richardson and J. A. Hoyland, *PLoS One*,  
1249 2012, **7**, e33739.
- 1250 196. T. M. Achilli, S. McCalla, J. Meyer, A. Tripathi and J. R. Morgan, *Mol. Pharm.*, 2014, **11**,  
1251 2071-2081.
- 1252 197. F. L. Miles, J. E. Lynch and R. A. Sikes, *J. Biol. Methods*, 2015, **2**, e29.
- 1253 198. S. A. Smith, L. I. Selby, A. P. R. Johnston and G. K. Such, *Bioconjug. Chem.*, 2019, **30**,  
1254 263-272.
- 1255 199. W. Viricel, A. Mbarek and J. Leblond, *Angew. Chem. Int. Ed. Engl.*, 2015, **54**, 12743-  
1256 12747.
- 1257 200. N. J. Dolman, J. A. Kilgore and M. W. Davidson, *Curr. Protoc. Cytom.*, 2013, **Chapter**  
1258 **12**, Unit 12 30.
- 1259 201. M. Ogawa, N. Kosaka, C. A. Regino, M. Mitsunaga, P. L. Choyke and H. Kobayashi, *Mol.*  
1260 *Biosyst.*, 2010, **6**, 888-893.
- 1261 202. M. G. Palmgren, *Anal. Biochem.*, 1991, **192**, 316-321.
- 1262 203. R. Kandil, Y. Xie, R. Heermann, L. Isert, K. Jung, A. Mehta and O. M. Merkel, *Adv. Ther.*  
1263 *(Weinh.)*, 2019, **2**, 1900047.

- 1264 204. M. Ogris, R. C. Carlisle, T. Bettinger and L. W. Seymour, *J. Biol. Chem.*, 2001, **276**, 47550-  
1265 47555.
- 1266 205. M. Kopp, O. Rotan, C. Papadopoulos, N. Schulze, H. Meyer and M. Epple, *PLoS One*,  
1267 2017, **12**, e0178260.
- 1268 206. N. Bono, F. Ponti, D. Mantovani and G. Candiani, *Pharmaceutics*, 2020, **12**, 183.
- 1269 207. C. R. Drake, D. C. Miller and E. F. Jones, *Curr. Org. Synth.*, 2011, **8**, 498-520.

1270

## Publication Pub2

### Tuning of endosomal escape and gene expression by functional groups, molecular weight and transfection medium: A structure–activity relationship study

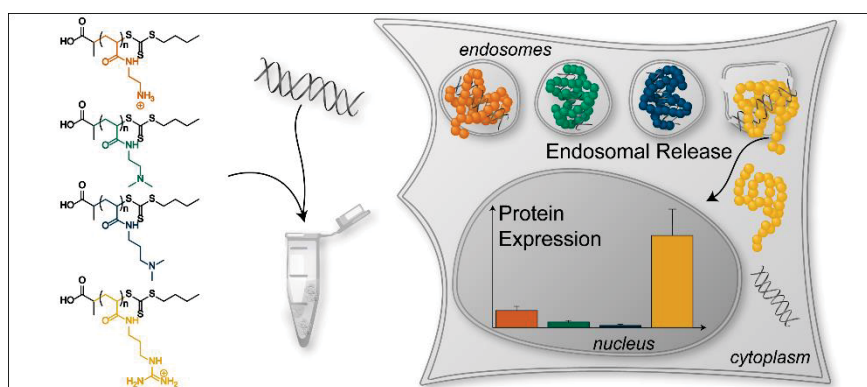
F. Richter, L. Martin, K. Leer, E. Moek, F. Hausig, J. C. Brendel, A. Traeger

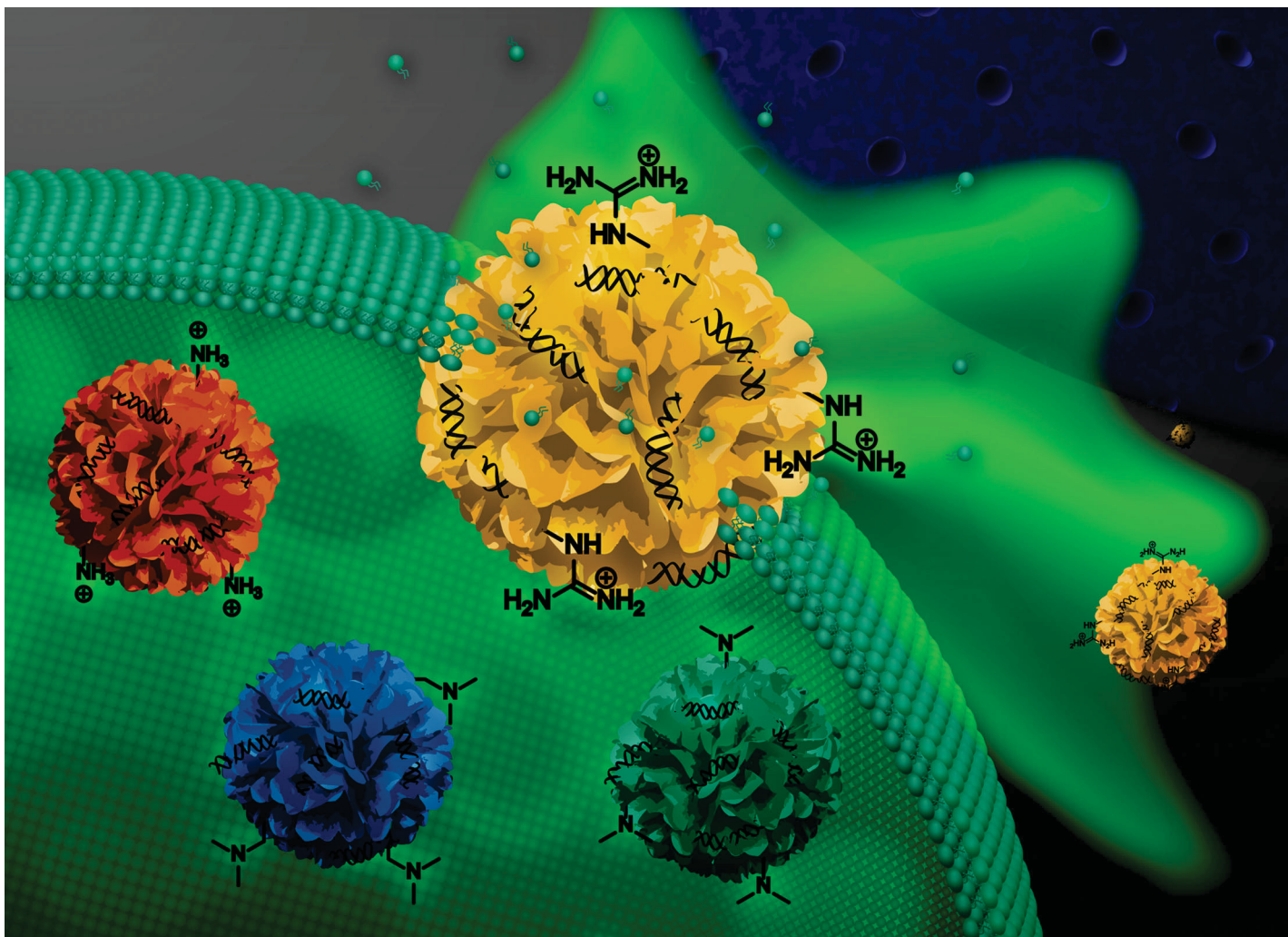
*J. Mater. Chem. B* **2020**, 8, 5026-5041

Reprinted with permission of The Royal Society of Chemistry. Copyright © 2020.

The article and the supporting information are available online:

[doi.org/10.1039/D0TB00340A](https://doi.org/10.1039/D0TB00340A)



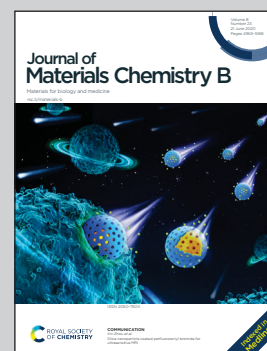


A study on polyacrylamides with different amine moieties for gene delivery by F. Richter and Dr A. Traeger at Friedrich Schiller University Jena

Tuning of endosomal escape and gene expression by functional groups, molecular weight and transfection medium: a structure–activity relationship study

Guanidinium-containing homopolymers showed superior endosomal escape and transfection efficiency, although the degree of protonation does not change during the transfection process.


As featured in:



See Anja Traeger *et al.*,  
*J. Mater. Chem. B*, 2020, **8**, 5026.

Cite this: *J. Mater. Chem. B*, 2020,  
8, 5026

## Tuning of endosomal escape and gene expression by functional groups, molecular weight and transfection medium: a structure–activity relationship study†

Friederike Richter,<sup>a</sup> Liam Martin,<sup>a</sup> Katharina Leer,<sup>a</sup> Elisabeth Moek,<sup>a</sup>  
Franziska Hausig,<sup>a</sup> Johannes C. Brendel <sup>ab</sup> and Anja Traeger <sup>\*ab</sup>

The use of genetic material by non-viral transfer systems is still in its initial stages, but there are high expectations for the development of targeted therapies. However, nucleic acids cannot enter cells without help, they must be well protected to prevent degradation and overcome a variety of biological barriers, the endosomal barrier being one of the greatest cellular challenges. Herein, the structure–property–relationship was investigated in detail, using well-defined polymers. Polyacrylamides were synthesized via RAFT polymerization resulting in a polymer library of (i) different cationic groups as aminoethyl acrylamide (AEAm), dimethylaminoethyl acrylamide (DMAEAm), dimethylaminopropyl acrylamide (DMAPAm) and guanidinopropyl acrylamide (GPAm); (ii) different degree of polymerization; and investigated (iii) in different cell culture settings. The influence of molar mass and cationic moiety on complex formation with pDNA, cytotoxicity and transfection efficiency of the polymers were investigated. The systematic approach identified a pH-independent guanidinium-containing homopolymer (PGPAm<sub>89</sub>) as the polymer with the highest transfection efficiency and superior endosomal release under optimal conditions. Since PGPAm<sub>89</sub> is not further protonated inside endosomes, common escape theories appear unsuitable. Therefore, the interaction with bis(monoacryloylglycerol)phosphate, a lipid specific for endosomal vesicles, was investigated. Our research suggests that the interactions between amines and lipids may be more relevant than anticipated.

Received 7th February 2020,  
Accepted 6th April 2020

DOI: 10.1039/d0tb00340a

rsc.li/materials-b

## Introduction

Gene therapy is a powerful approach towards treating genetic disorders, cancer and other diseases. Due to an instability against nucleases and reduced uptake ability of naked genetic material, carriers are needed for effective protection and transportation.<sup>1</sup> Carriers designed by nature are known as viruses, some of which have already been approved by different agencies.<sup>2</sup> However, viruses pose a high risk due to unexpected side-effects, show limitations in modification as well as in the amount of delivered genetic material, and are not amenable to scale-up. Polymers are thus an extremely appealing alternative.<sup>3,4</sup> To protect their genetic cargo, the polymers form

stable complexes with the negatively charged phosphate groups of the genetic material and are, as such, typically positively charged.<sup>5</sup> Moreover, the cationic charge aids in overcoming gene delivery barriers like the cellular membrane and lysosomal entrapment. Especially the endosomal escape is important to prevent recycling or enzymatic degradation and to transport the genetic material closer to its site of action.<sup>6–8</sup> A well-known cationic polymer is linear poly(ethylene imine) (LPEI) which shows high transfection efficiency, but also low biocompatibility, promoting the development of less toxic alternatives.<sup>9–11</sup>

Beyond PEI, various cationic polymers with a range of backbone chemistries have been studied as non-viral gene delivery vectors. Polymers based on vinyl backbones are of particular interest, since they can possess a broad range of functional pendant groups, and may be readily synthesized by various polymerization techniques, including radical polymerization. For example, poly(2-(dimethylamino)ethyl methacrylate) (PDMAEMA) shows a propensity for gene delivery and is extensively studied. PDMAEMA possesses tertiary amine pendant groups and a p*K*<sub>a</sub> which renders it pH-responsive within a physiologically useful pH window (≈ 7.4).<sup>12,13</sup> While there are many other examples of

<sup>a</sup> Laboratory of Organic and Macromolecular Chemistry (IOMC),  
Friedrich Schiller University Jena, Humboldtstrasse 10, 07743 Jena, Germany.  
E-mail: anja.traeger@uni-jena.de

<sup>b</sup> Jena Center for Soft Matter (JCSM), Friedrich Schiller University Jena,  
Philosophenweg 7, 07743 Jena, Germany

† Electronic supplementary information (ESI) available: Material, additional methods and results, Fig. S1–S18, supplementary Tables S1–S8. See DOI: 10.1039/d0tb00340a

vinyl cationic polymers in polymer-based gene delivery, such as polybutylamino vinyl ethers (PBAVE),<sup>14,15</sup> work has mostly been limited to polymethacrylates or polymethacrylamides. The polyacrylamides (PAMs) represent an interesting alternative since they are hydrolytically stable (unlike many polymethacrylates) and are considered to possess more hydrophilic polymeric backbones than their acrylate, methacrylate and methacrylamide counterparts. Therefore, they are more stable to store and less likely to be modified in the body. Regarding their polymerization, acrylamide monomers possess a comparatively high rate constant of propagation ( $k_p$ ) and are typically less prone to side reactions of transfer during radical polymerization, which makes them well suited for reversible deactivation radical polymerization (RDRP) techniques such as reversible addition–fragmentation chain transfer (RAFT) polymerization.<sup>16–19</sup> Concerning gene delivery, Nakayama and co-workers developed cationic star polymers based on poly(*N,N*-dimethylaminopropyl acrylamide) (PDMAPAm) and showed higher transfection efficiency than PEI in COS-1 cells.<sup>20–23</sup> The group of Young studied linear PAMs bearing primary amine pendant groups with varying spacer length and also reported promising transfection efficiency with primary amine/imidazole functional polymers, with or without the presence of the stealth polymer poly(ethylene glycol) (PEG).<sup>24–26</sup> However, to the best of our knowledge, no further systematic studies have been performed with polyacrylamides as cationic homopolymers of linear architecture for gene delivery. In addition to the polymer backbone chemistry, there are a number of other properties which influence gene delivery potential. The molar mass of a given cationic polymer has been demonstrated in several cases to play an important role. Increasing molar masses typically correspond to increased transfection efficiency, but also increased cytotoxicity.<sup>27–31</sup>

Moreover, the nature of the cationic moiety is of crucial importance, since it is a vital feature for DNA binding, cellular uptake, endosomal escape and DNA release. There are only few systematic studies focusing on the investigation of the correlation between the nature of the cationic moiety and the transfection mechanism; and they were not conducted with polyacrylamides. Reineke and coworkers investigated methacrylamide-based RAFT copolymers bearing primary, secondary, tertiary or ternary amine and carbohydrate pendant groups in different copolymer compositions (block *vs.* statistical copolymer, monomer ratio).<sup>32,33</sup> More recently, a library of methacrylate-based homo- and co-polymers (bearing primary, secondary and/or tertiary amines) identified primary amine-based polymers to possess high potential.<sup>34</sup> However, the spacing between the cationic moiety and the polymer backbone also had an effect on the physicochemical properties.<sup>12,29,35</sup>

Most studies focused on pH-responsive polymers that were (partially) protonated at physiological pH values.<sup>12,34,36</sup> pH-independent polymers with quaternized amines, for example, have rarely been investigated so far. They showed the efficiency-effectiveness dilemma: less toxicity but also less efficiency compared to their pH-dependent analogs. The assumed reasons are an inefficient DNA release and/or a lower endosomal release.<sup>13,33,37,38</sup> Another interesting cationic moiety is

the guanidinium group, that is not pH-dependent in a physiological context ( $pK_a > 12$ ). Guanidine occurs in many different biomolecules and contributes to protein denaturation, DNA-synthesis inhibition or in the amino acid arginine in active sites of enzymes.<sup>39</sup> Many cell penetrating peptides, such as the TAT peptide, are rich in arginine residues.<sup>40</sup> However, while their proficiency for intracellular trafficking is well known, their mechanism of cellular entry, *i.e.* *via* transduction or endocytosis, remains a topic for debate.<sup>41–46</sup> Assuming endocytosis, the mechanism of endosomal escape for guanidinium containing cell penetrating peptides (CPP) has to be considered. In studies with membrane lipids of the endolysosomal pathway, arginine containing CPPs were shown to bind bis(monoacryloyl glycerol)phosphate (BMP), a lipid present at the inner side of the membrane of intra late endosomal vesicles (ILEV) and to disrupt BMP-containing liposomes, indicating a possible pathway for the endosomal escape.<sup>47,48</sup> Since this feature is of great importance in applications such as drug or gene delivery, the guanidinium group is frequently exploited for the development of synthetic vectors.<sup>46,49–53</sup> Regarding examples possessing vinyl polymeric backbones, Funhoff *et al.* reported promising transfection and uptake in COS-7 cells for poly(3-guanidinopropyl methacrylate) (PGPMA) homopolymers prepared *via* free radical polymerization.<sup>38</sup> However, well-defined homopolymers of guanidinium-functional PAMs have not been systematically studied as gene delivery vectors, nor compared with other cationic moieties. Still, they are of vital importance for the potential utilization of nature-inspired specific cation–lipid-interactions.

In this work, we synthesized a library of well-defined cationic PAM homopolymers of varying molar mass bearing either primary amine, tertiary amine or guanidinium pendant groups *via* RAFT polymerization in order to assess their potential for gene delivery. The influence of the different properties on the transfection efficiency of the polymers was investigated and they were further characterized regarding the media influence, their pDNA binding capability, uptake and different types of toxicity. Due to the outstanding performance of the guanidinium functionalized polymer, the underlying endosomal escape mechanism was investigated in more detail using calcein release and lipid–polymer binding assays.

## Material and methods

Materials, instruments, further methods and calculations can be found in the ESI.†

### RAFT polymerization

**Typical synthesis of P(GPAm<sup>diBoc</sup>) *via* RAFT polymerization.** A 5.0 wt% solution of 2-(Butylthiocarbonothioylthio) propanoic acid (PABTC) in DMAc (89.6 mg, 4.48 mg PABTC,  $1.88 \times 10^{-2}$  mmol), GPAm<sup>diBoc</sup> (700.6 mg, 1.89 mmol), a 1.0 wt% solution of V65B in 1,4-dioxane (301.1 mg, 3.01 mg V65B,  $1.17 \times 10^{-2}$  mmol), DMAc (316.4 mg), 1,4-dioxane (731.3 mg) and 1,3,5-trioxane (external NMR standard, 8.4 mg) were introduced to a 4 mL microwave vial



equipped with a magnetic stirring bar. The vial was sealed, and the solution deoxygenated by bubbling argon through it for *ca.* 10 min. The vial was placed in an oil bath set at 45 °C and allowed to stir for 5 h. The polymer was precipitated three times (from THF) into cold hexane, and then dried under vacuum to give a yellow solid.

**Typical synthesis of P(AEAmBoc) via RAFT polymerization.** PABTC (27.0 mg, 0.113 mmol), AEAm<sup>Boc</sup> (602.4 mg, 2.81 mmol), a 1.0 wt% solution of V65B in 1,4-dioxane (290.0 mg, 2.90 mg V65B,  $1.12 \times 10^{-2}$  mmol), DMAc (394.4 mg), 1,4-dioxane (695.4 mg) and 1,3,5-trioxane (external NMR standard, 9.2 mg) were introduced to a 4 mL microwave vial equipped with a magnetic stirring bar. The vial was sealed, and the solution deoxygenated by bubbling argon through it for *ca.* 10 min. The vial was placed in an oil bath set at 50 °C and allowed to stir for 5 h. The polymer was precipitated three times from THF into cold hexane, and then dried under vacuum to give a yellow solid.

**Typical synthesis of P(DMAPAm) via RAFT polymerization.** PABTC (19.9 mg,  $8.35 \times 10^{-2}$  mmol), DMAPAm (383.3 mg, 2.95 mmol), a 1.5 wt% solution of V65B in 1,4-dioxane (140.7 mg, 2.11 mg V65B,  $8.17 \times 10^{-3}$  mmol), DMAc (193.0 mg), 1,4-dioxane (70.6 mg) and 1,3,5-trioxane (external NMR standard, 3.3 mg) were introduced to a 2 mL vial equipped with a magnetic stirring bar. The vial was sealed, and the solution deoxygenated by bubbling argon through it for *ca.* 10 min. The vial was placed in an oil bath set at 60 °C and allowed to stir for 4 h. The polymer was precipitated three times from THF into cold hexane, and then dried under vacuum to give a yellow solid. The polymer was then dissolved in distilled H<sub>2</sub>O and dried by lyophilization.

**Typical synthesis of P(DMAEAm) via RAFT polymerization.** PABTC (25.1 mg, 0.105 mmol), DMAEAm (371.8 mg, 2.62 mmol), a 1.5 wt% solution of V65B in 1,4-dioxane (203.5 mg, 3.05 mg V65B,  $1.18 \times 10^{-2}$  mmol), DMAc (218.8 mg), 1,4-dioxane (36.1 mg) and 1,3,5-trioxane (external NMR standard, 5.9 mg) were introduced to a 2 mL vial equipped with a magnetic stirring bar. The vial was sealed, and the solution deoxygenated by bubbling argon through it for *ca.* 10 min. The vial was placed in an oil bath set at 60 °C and allowed to stir for 4 h. The polymer was precipitated three times from THF into cold hexane, and then dried under vacuum to give a yellow solid. The polymer was then dissolved in distilled H<sub>2</sub>O and dried by lyophilization.

**Deprotection of P(diBocGPAm) and P(BocAEAm).** Polymers were dissolved at 50 mg mL<sup>-1</sup> in TFA/H<sub>2</sub>O (97/3 v/v) and allowed to stir for 4 h. The TFA was then blown off using compressed air, the polymers were precipitated three times into diethyl ether from methanol and dried under reduced pressure to give a yellow solid.

Experimental details of all polymerizations are provided in the Tables S1 and S2 (ESI<sup>†</sup>).

### Polypeptide preparation

For the preparation of polyplexes, plasmid DNA (pDNA) and different amounts of polymer dissolved in water were mixed in HBG buffer (20 mM 4-(2-hydroxyethyl)piperazine-1-ethanesulfonic acid (HEPES) and 5% (w/v) glucose, pH 7.2) to give a final pDNA concentration of 15 µg mL<sup>-1</sup>, with varying N\*/P ratios

(molar ratio of protonatable nitrogen atoms to phosphates of pDNA, see ESI<sup>†</sup>). Immediately after combination, the mixtures were vortexed for 10 s at maximum speed (3200 rpm) and incubated at room temperature for 15 min to ensure complex formation.

### Ethidium bromide quenching (EBA) and heparin dissociation assays (HRA)

The formation of polyplexes with pDNA was identified *via* quenching of ethidium bromide (EtBr) fluorescence by polymers interacting with pDNA. Briefly, 15 µg mL<sup>-1</sup> pCMV-GFP pDNA in a total volume of 100 µL HBG buffer were incubated with EtBr (1 µg mL<sup>-1</sup>) at room temperature for 10 min. Subsequently, polyplexes with different quantities of polymer stock solutions (various N\*/P ratios) were prepared in black 96-well plates (Nunc, Thermo Fisher, Germany) and incubated at 37 °C for 15 min before measuring the fluorescence intensity at  $\lambda_{\text{EX}} = 525$  nm/ $\lambda_{\text{EM}} = 605$  nm. A sample containing only pDNA and EtBr was defined as maximum fluorescence (100%).

For the heparin dissociation assay, heparin was added to the formed polyplex–EtBr mixtures using the dispenser of the microplate reader to obtain the indicated concentrations (Table S4, ESI<sup>†</sup>). After each addition, the plate was shaken, incubated at 37 °C for 10 min and fluorescence intensity was measured.

The percentage of EtBr displaced upon polyplex formation or re-intercalating following pDNA release by heparin was calculated using eqn (1):

$$\text{rFI}/\% = \frac{F_{\text{Sample}}}{F_{\text{pDNA}}} \times 100 \quad (1)$$

where rFI is the relative fluorescence intensity and  $F_{\text{Sample}}$ , and  $F_{\text{pDNA}}$  are the fluorescence intensities of a given sample and the EtBr intercalated into pDNA alone (in the case of the HRA with heparin), respectively. Data are expressed as mean  $\pm$  SD of three independent determinations.

For a summarized depiction of the EBA results, the % of bound pDNA was calculated as 100% – rFI%. The heparin concentration needed to release the maximum of pDNA was calculated with OriginPro, Version 2018b (OriginLab Corporation, US) which can be found in the ESI<sup>†</sup>.

### Determination of cytotoxicity

Cytotoxicity studies were performed with the mouse fibroblast cell line L929 (CLS, Germany), as recommended by ISO10993-5. For cytotoxicity of the polymers in HEK293T cells, refer to ESI<sup>††</sup>. The L929 cells were cultured in low glucose Dulbecco's modified eagle's medium (DMEM) supplemented with 10% fetal calf serum (FCS, Capricorn), 100 U mL<sup>-1</sup> penicillin and 100 µg mL<sup>-1</sup> streptomycin at 37 °C in a humidified 5% (v/v) CO<sub>2</sub> atmosphere. In detail, cells were seeded at 10<sup>4</sup> cells per well in a 96-well plate without using the outer wells and incubated in medium containing 10 mM HEPES for 24 h. 1 h after medium change, cells were treated in sextuplicates with polymers at different concentrations, ranging from 5 µg mL<sup>-1</sup> to 500 µg mL<sup>-1</sup>, and incubated for additional 24 h. The medium was replaced

by a 10% (v/v) alamarBlue solution in fresh culture medium, prepared according to the manufacturer's instructions. Following an incubation for 4 h at 37 °C, the fluorescence was measured at  $\lambda_{\text{Ex}} = 570/\lambda_{\text{Em}} = 610$  nm. Non-treated control cells on the same plate were referred to as 100% viability. Values below 70% were regarded as cytotoxicity. Data are expressed as mean  $\pm$  SD of at least three independent determinations or as  $CC_{50}$  values  $\pm$  95% confidence interval (CI). Information regarding  $CC_{50}$  calculations can be found in the ESI.††

### Transfection of adherent cells

Transfection studies were performed with the human embryonic kidney cell line HEK293T (CLS, Germany). The cells were routinely cultured in DMEM medium (1 g L<sup>-1</sup> glucose) supplemented with 10% FCS, 100  $\mu\text{g mL}^{-1}$  streptomycin and 100 U mL<sup>-1</sup> penicillin at 37 °C in a humidified 5% (v/v) CO<sub>2</sub> atmosphere.

For transfection studies, HEK293T cells were seeded at a density of 10<sup>5</sup> cells per well in 24-well plates and incubated at 37 °C (5% CO<sub>2</sub>) for 24 h. One hour prior to transfection, the medium was replaced by 450  $\mu\text{L}$  serum reduced Opti-MEM™ or fresh growth medium (DMEM + 10% FCS + 10 mM HEPES) to reduce pH variance during the experiments. Polyplexes were prepared as described above with isolated pEGFP-N1 pDNA and added to the cells diluting the polyplexes 1:10 in the cell culture medium. If incubated in Opti-MEM™, the supernatant was replaced by fresh growth medium after 4 h and incubated for further 20 h. When transfections were performed in growth medium, the cells were incubated with polyplexes for 24 h. For analysis *via* flow cytometry, cells were harvested by trypsinization and resuspension in Hanks' Balanced Salt Solution, supplemented with 2% FCS and 20 mM HEPES (FC-buffer). For determination of transfection efficiency, cells were analyzed as described in the instrumentation section (see ESI†). Viable cells showing EGFP signal higher than the control cells incubated with pDNA only were gated as % of cells expressing EGFP and the relative mean fluorescence intensity (rMFI) of all viable cells was calculated in relation to the control. The experiments were performed at least three times and data are expressed as mean  $\pm$  SD.

### Polyplex uptake

To study the uptake of polymers over time, cells were seeded at a density of 10<sup>5</sup> cells per well in 24-well plates and cultured for 24 h in growth medium. One hour prior to the addition of the polyplexes, the medium was changed to serum reduced Opti-MEM™ or fresh growth medium. Polyplexes were prepared as described above after labelling 1  $\mu\text{g}$  pCMV-GFP pDNA with 0.027 nmol YOYO-1 iodide. Subsequently, the polymer-pDNA-solutions were added to the cells, diluting the polyplexes 1:10 in cell culture medium. Following incubation for 4 h, cells were harvested by trypsinization and resuspension in FC-buffer. Trypan blue solution (0.4%) was added to a final concentration of 0.04% to quench fluorescence of polyplexes outside the cells. Cells were analyzed *via* flow cytometry as described in the instrumentation section (see ESI†). Viable cells showing YOYO-1 signal higher than the control cells, which were

incubated with YOYO-1-pDNA only, were gated as % of cells that have taken up pDNA and the relative mean fluorescence intensity (rMFI) of all viable cells was calculated in relation to the control cells. The experiments were performed at least three times.

### Hemolysis assay

The interaction of polymers with cellular membranes was examined by analyzing the release of hemoglobin from erythrocytes as published before.<sup>36,54</sup> Blood from human donors, collected in tubes with citrate, was obtained from the Department of Transfusion Medicine of the University Hospital, Jena. The blood was centrifuged at 4500  $\times g$  for 5 min, and the pellet was washed three times with cold phosphate buffered saline (PBS, pH 7.4). Following a 10 times dilution with PBS (either pH 7.4 or pH 6.0), 500  $\mu\text{L}$  aliquots of erythrocyte suspension were mixed 1:1 with the polymer solutions, which were prepared with PBS pH 7.4 or pH 6.0, and incubated at 37 °C for 60 min. After centrifugation at 2400  $\times g$  for 5 min, the supernatant was transferred to a clear flat bottomed 96-well plate (VWR, Germany) and the hemoglobin release was determined as the hemoglobin absorption at  $\lambda = 544$  nm. Absorption at  $\lambda = 630$  nm was used as reference. Complete hemolysis (100%) was achieved using 1% Triton X-100 as positive control. Pure PBS was used as negative control (0% hemolysis). The hemolytic activity of the polyplexes was calculated as follows (2):

$$\text{Hemolysis}/\% = \frac{(A_{\text{Sample}} - A_{\text{Negative control}})}{(A_{\text{Positive control}} - A_{\text{Negative control}})} \times 100 \quad (2)$$

where  $A_{\text{Sample}}$ ,  $A_{\text{Negative control}}$  and  $A_{\text{Positive control}}$  are the absorption values of a given sample, the PBS treatment and the Triton X-100 treatment, respectively. A value less than 2% hemolysis rate was classified as non-hemolytic, 2 to 5% as slightly hemolytic and values >5% as hemolytic. Experiments were run in technical duplicates and were performed with three different blood donors.

### Erythrocyte aggregation

Erythrocytes were isolated as described above. For determining the aggregation, 100  $\mu\text{L}$  of the erythrocyte-polymer suspension were transferred to a clear flat bottomed 96-well plate (VWR, Germany). The cells were incubated at 37 °C for 2 h, and the absorbance was measured at  $\lambda = 645$  nm. Cells treated with PBS served as negative control and cells treated with 50  $\mu\text{g mL}^{-1}$  10 kDa BPEI were used as positive control. Aggregation potential of the polymers was calculated as follows (3):

$$\text{Aggregation} = \frac{A_{\text{Negative control}}}{A_{\text{Sample}}} \quad (3)$$

where  $A_{\text{Sample}}$  and  $A_{\text{Negative control}}$  are the absorption values of a given sample and the PBS treatment, respectively. Experiments were run in technical duplicates and were performed with blood from three different blood donors.

### Calcein release assay

To determine the endosomal escape efficiency of the polymers, a calcein release assay was performed. HEK293T cells were

seeded at a density of  $10^5$  cells per well in 24-well plates and cultured for 24 h in growth medium. They were treated with polyplexes as described for transfection studies. Just before the addition of polyplexes, the non-cell-permeable dye calcein was added to the cells to give a final concentration of  $25 \mu\text{g mL}^{-1}$ . Following incubation for 4 h, cells were carefully washed twice with cold PBS and harvested by trypsinization and resuspension in FC-buffer. *Via* flow cytometry, cells were analyzed as described in the instrumentation section (ESI†). Viable cells showing a calcein signal higher than the control cells incubated with calcein only were gated as % of cells that show strong calcein signal and the relative mean fluorescence intensity (rMFI) of all viable cells was calculated in relation to the control cells. The experiments were performed three times.

### Lipid–polymer binding assay

To investigate the polymer–membrane-interaction in more detail, the binding of the polymers to several lipids specific for different membrane stages along the endolysosomal pathway was determined using a lipid–polymer binding assay which was modified according to Erazo-Olivereas *et al.* 2016.<sup>47</sup> The lipids were dissolved in hexane and the DY635-labeled polymers (see ESI†) were diluted in acetate buffer (0.1 M, pH 5.7) at equal amine concentrations ( $\approx$  N\*/P 30, 1.2–1.4 mM). The lipid and polymer solutions were vigorously mixed at a ratio of 1 : 1 in 200  $\mu\text{L}$  for one minute. Following incubation at  $-20^\circ\text{C}$  for 10 min, all samples were centrifuged in a microcentrifuge at 6000 rpm (Carl Roth, Germany) to allow phase separation. To determine the amount of polymer binding to the lipids, 50  $\mu\text{L}$  of the aqueous phase were diluted 1 : 2 with acetate buffer, transferred to a black 96-well plate (Nunc, Thermo Fisher, Germany) and fluorescence intensity of DY635 was measured at  $\lambda_{\text{Ex}} = 633/\lambda_{\text{Em}} = 680 \text{ nm}$  in a plate reader. The mixture of pure hexane and the respective labeled polymer in the aqueous phase was used as the negative control (0% lipid binding). The polymer–lipid interaction was calculated as follows (4):

$$\text{rFI} = \frac{F_{\text{Sample}} - F_0}{F_{\text{Negative control}} - F_0} \quad (4)$$

where  $F_{\text{Sample}}$ ,  $F_{\text{Negative control}}$  and  $F_0$  represent the fluorescence intensity of the aqueous phase following lipid incubation, the fluorescence intensity of the aqueous phase following pure hexane incubation and the fluorescence intensity of pure buffer, respectively.

### Statistics

To determine the statistical significance, analysis of variance (ANOVA) was performed. If the ANOVA revealed significant differences ( $p < 0.05$ ), *post hoc* analyses with a Bonferroni correction were applied. All statistical analyses with data of  $n \geq 3$  and the determination of the Pearson's correlation coefficient were performed with Origin, Version 2018b (OriginLab Corporation, US). Further details can be found in the ESI.†

## Results and discussion

### Monomer synthesis and characterization

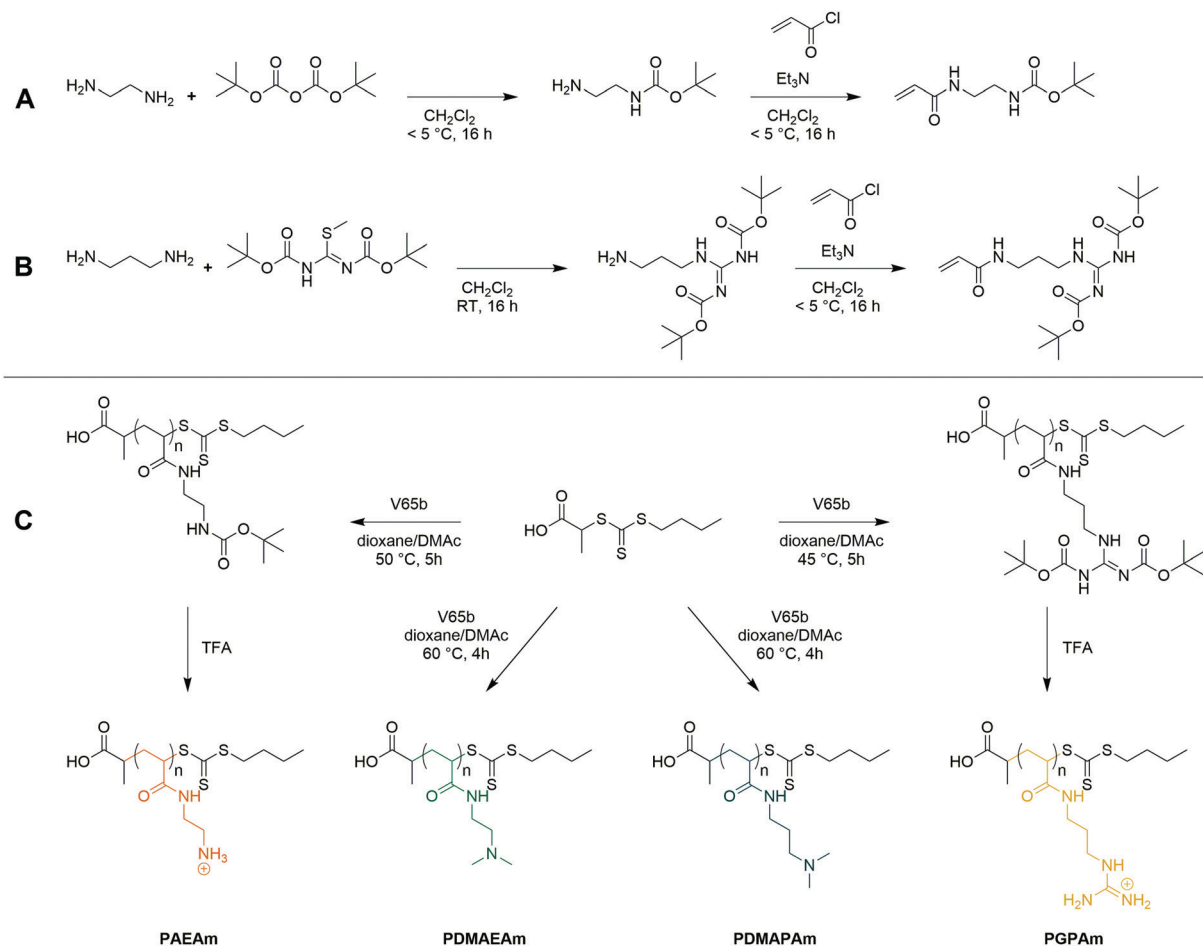
Four acrylamide-based monomers were selected to prepare the cationic polymer library. Dimethylamino ethyl acrylamide (DMAEAm) is the acrylamide analogue of widely studied DMAEMA, while dimethylamino propyl acrylamide (DMPAm) is a pertinent addition since PDMPAm is a promising instance of cationic polyacrylamides used in gene delivery.<sup>20–23</sup> While both monomers bear the same cationic moiety, the different length of the alkyl chain should influence the hydrophobicity and the  $\text{p}K_{\text{a}}$  of the resulting polymers, which in turn influences their interactions with DNA and cells, and ultimately their propensity for transfection.<sup>12</sup> Boc-protected forms of the primary amine- and guanidinium-functional monomers were used in this work since it permits the use of typical RAFT polymerization conditions, circumventing the need to conduct polymerizations in aqueous buffer. The Boc-protected primary amine-functional monomer, Boc-aminoethyl acrylamide (AEAm<sup>Boc</sup>), was synthesized according to literature (A),<sup>55</sup> while a newly reported di-Boc-protected guanidinium-functional monomer, di-Boc-Guanidine propyl acrylamide (GPAm<sup>Boc</sup>), was synthesized in a two-step synthesis adapted from literature (Scheme 1B).<sup>56</sup> Characterization of the monomers may be found in the ESI.†

### Polymer synthesis and characterization

For each monomer, homopolymers with average degrees of polymerization (DP) ranging from 10 to 100 were targeted, in order to assess the influence of the polymer molar mass on biological activity. The library of cationic polymers was synthesized by RAFT polymerization using PABTC or its NHS activated ester derivative NHS-PABTC as CTA, with 1,4-dioxane/DMAc as a solvent system and V65B as azoinitiator (Scheme 1C). PABTC has been extensively used for the controlled polymerization of acrylamide and acrylate monomers.<sup>17,19</sup> Moreover, the COOH R-group may be used to functionalize the polymers at the  $\alpha$ -chain end. The solvent system was found to be suitable for the polymerization of all four monomers, while V65B (10 h half-life temperature of  $51^\circ\text{C}$  in toluene) offers a reasonable rate of radical generation across the range of polymerization temperatures employed ( $45\text{--}60^\circ\text{C}$ ) in this solvent system.

Polymerizations of DMAPAm were stopped at monomer conversions of 70–80% in order to reduce the occurrence of side reactions, while for the other monomers, polymerizations were able to reach higher conversions (typically 85–95% as determined *via*  $^1\text{H NMR}$ ). SEC analysis of the polymers revealed monomodal populations with narrow molar mass distributions ( $D \leq 1.3$ ) in most cases (Table 1, Fig. 1E–H and Table S2, ESI†). The experimental molar masses ( $M_{\text{n,SEC}}$ ) were slightly different to the theoretically determined values in most cases, which may be attributed to differences in the hydrodynamic radii of the polymers and the standards used to calibrate the respective SEC systems (PMMA for DMAc-SEC and P2VP for Aq-SEC).

Deprotection of the PGPAm<sup>diBoc</sup> and PAEAm<sup>Boc</sup> polymers to give well-defined guanidinium and primary amine polymers, respectively, was performed using TFA. Quantitative removal of



Scheme 1 Synthesis of the AEAmBoc (A) and GPAmBoc (B) monomers used in this work and synthetic route towards cationic polyacrylamide library (C).

the Boc-protecting groups was confirmed using  $^1\text{H}$  NMR (Fig. 1A and D), while Aq-SEC of the resulting polymers revealed monomodal populations with narrow molar mass distributions in all cases ( $D \leq 1.3$ ) (Fig. 1E and H).

To better understand the behavior of these cationic homopolymers at different pH values, the  $\text{p}K_a$  values of the highest and lowest molar mass polymers from each set were determined. Acidified solutions ( $\sim\text{pH}$  2) of the polymers in 125 mM NaCl were titrated with  $0.1 \text{ mol L}^{-1}$  NaOH ( $0.5 \text{ mol L}^{-1}$  in the case of PGPAm polymers) and  $\text{p}K_a$  values were determined using the Henderson-Hasselbalch equation ((S5) and Fig. S4–S6, ESI $^\dagger$ ). Fig. S8 (ESI $^\dagger$ ) shows the calculated degree of protonation of the polymers at different pH values. All measured polymers possessed a  $\text{p}K_a$  of 7.8 or above, while for the PGPAm polymers the  $\text{p}K_a$  could not be determined with the available system (assumed to be 12 or above, Fig. S7, ESI $^\dagger$ ). All polymers are mainly positively charged under physiological conditions (pH 7.4) promoting the complexation with nucleic acids. A small molar mass dependence on  $\text{p}K_a$  value was observed for each cationic polymer type, with the lowest molar mass polymer possessing the higher  $\text{p}K_a$  in each case. This trend is consistent with simulations conducted by Nová and co-workers, where the difference in  $\text{p}K_a$  showed little variation after a DP of  $\sim 50$ .<sup>57</sup>

However, it was also observed that the titration curves become increasingly non-ideal with increasing polymer length (again up to a DP of  $\sim 50$ ), due to local effects of the neighboring monomers. There is a clear trend in the  $\text{p}K_a$  of the different cationic moieties, with PDMAEAm (7.8–8.0) < PAEAm (8.3–8.5) < PDMAPAm (8.7–8.9) < PGPAm (assumed  $\approx 12$ ). The values for PDMAEAm and PDMAPAm are comparable to those obtained for methacrylamide-based systems.<sup>12,58</sup> The significant difference between PDMAEAm and PDMAPAm can likely be attributed to the distance between protonatable groups, where increasing distance would reduce electrostatic repulsion between charged groups, leading to higher  $\text{p}K_a$  values.<sup>59</sup>

#### Transfection efficiency and cytotoxicity

Since all polymers contain positively charged amines suitable for gene delivery, the polymer library was investigated regarding their potential for protein expression (Fig. 2A). HEK293T cells were incubated with polyplexes at N\*/P 30 of pDNA encoding the EGFP protein using different transfection protocols: (i) adding polyplex to growth medium for 24 h or (ii) adding polyplex to serum-reduced Opti-MEM<sup>™</sup> for 4 h and further incubation in growth medium for 20 h. For the different types of cationic polymer an increased EGFP-expression was observed with

**Table 1** Summary of cationic homopolymers prepared via RAFT polymerization

Polymer	DP <sup>a</sup>	$M_{n,th}^b$	$M_{n,th}^c$	$M_{n,SEC}^d$	$D^d$
		(kg mol <sup>-1</sup> )			
PGPAm <sub>8</sub>	8	2.0	1.7	1.8	1.12
PGPAm <sub>22</sub>	22	4.8	4.0	3.4	1.12
PGPAm <sub>43</sub>	43	9.1	7.6	5.0	1.18
PGPAm <sub>94</sub>	94	19.6	16.3	8.5	1.27
PAEAm <sub>9</sub>	9	2.3	1.3	2.6	1.09
PAEAm <sub>24</sub>	24	5.7	3.0	4.5	1.08
PAEAm <sub>45</sub>	45	7.0	5.4	7.0	1.15
PAEAm <sub>96</sub>	96	14.6	11.3	10.0	1.17
PDMAEAm <sub>8</sub>	8	1.4	—	3.3	1.13
PDMAEAm <sub>22</sub>	22	3.4	—	4.2	1.13
PDMAEAm <sub>45</sub>	45	6.6	—	5.6	1.50
PDMAEAm <sub>88</sub>	88	12.7	—	10.0	1.48
PDMAPAm <sub>11</sub>	11	2.0	—	3.5	1.19
PDMAPAm <sub>24</sub>	24	4.0	—	5.1	1.13
PDMAPAm <sub>38</sub>	38	6.2	—	6.2	1.41
PDMAPAm <sub>71</sub>	71	11.3	—	9.7	1.26

<sup>a</sup> Determined via <sup>1</sup>H NMR. <sup>b</sup> Determined using eqn (6), ESI. <sup>c</sup> Excluding mass of counter-ion. <sup>d</sup> Determined via Aq.-SEC with P2VP standards.

increasing molar mass, but to different extents for each type of cationic polymer. The transfection efficiency in Opti-MEM™ was increased compared to growth medium for LPEI (28% vs. 12% EGFP-positive cells) and PGPAm (30% vs. 3% EGFP-positive cells) with the highest increase of about ten-fold by PGPAm<sub>89</sub> ( $p < 0.001$ ). The highest transfection efficiency was achieved with the PGPAm<sub>89</sub>-based polyplex using Opti-MEM™ (30% EGFP-positive cells), which showed no significant difference to the positive control LPEI ( $p = 1.000$ ). Taking the different DP of these polymers into account (89 for PGPAm vs. 600 for LPEI) the observed transfection efficiency showed the potential of the PGPAm polymers. All other polymers in the PAm library revealed less transfection efficiency compared to commercial LPEI ( $p < 0.05$ ). Moderate transfection efficiency of PAEAm<sub>96</sub> (7% EGFP-positive cells) was observed in serum-reduced medium. In growth medium, PAEAm<sub>96</sub> showed the highest transfection efficiency among the PAm polymers (7% EGFP-positive cells,  $p = 1.000$  compared to LPEI). Enhanced transfection efficiency in Opti-MEM™ is well-known and was also found for other polymer-based transfection agents.<sup>34,36,60</sup> The lower transfection efficiency in growth medium could indicate interaction with serum proteins.

Polymers for gene delivery, in particular homopolymers, are known to reduce the viability of cells due to their cationic charges affecting the integrity of the cellular membrane.<sup>29</sup> Therefore, the alamarBlue assay was performed in L929 cells according to ISO10993-5 (Fig. S9 and S10, ESI†) and of the interesting polymers with longer DP values in HEK293T cells (B). All tested acrylamide-based cationic polymers were found to be less toxic than the commercial gold standard LPEI ( $CC_{50} = 26 \mu\text{g mL}^{-1}$ ; see ESI†) and showed a reduced viability with increasing molar mass and concentration. The type of the cationic group influenced the viability and the following trend

of cytotoxicity was observed: PDMAEAm < PDMAEAm < PAEAm = PGPAm, indicating the polymers with tertiary amines as least cytotoxic. The length of the side chain (propyl vs. ethyl) appeared to have a slight influence on the cytotoxic profile of the dimethylamino functional polymers. However, the concentrations used for further biological investigations ( $N^*/P$  30; 19–24  $\mu\text{g mL}^{-1}$ ) showed high viability ( $\geq 90\%$ ) for all polymers (Table S6, ESI†). Regarding the cytotoxicity of  $N^*/P$  30 polyplexes in HEK293T cells, a similar trend was observed but with slightly less viability of PAEAm and PGPAm polymers (65–85%; Fig. 2B).

To the best of our knowledge, this is the first systematic study of PAm homopolymers of different molar mass, cationic moiety and hydrophobicity for gene delivery. However, some structure–property–relationships were already described in literature. The molar mass dependency of transfection efficiency and cytotoxicity has been shown for a variety of polymers such as PEI, PDMAEMA or lysine-functionalized methacrylamides.<sup>28,29,31,61–66</sup> This dependency on molar mass could be attributed to the charge distribution in relation to the cell membrane by the polymers: in high molar mass polymers the positive charge is present in one large coiled molecule focusing the charge at one spot of the cellular membrane which could lead to its disruption. In low molar mass polymers, the same amount of charges is distributed within several small molecules and therefore spread over a larger membrane area. Regarding different cationic moieties, an increased toxicity for polymers with primary amines compared to the tertiary analogs was also shown for poly(2-oxazolines).<sup>67</sup> In our study, the polymers with tertiary amines showed slight differences in toxicity and in protein expression with the ethyl spacer polymers performing slightly better than polymers with propyl spacer. This was also observed in studies of other vinyl polymers and could be due to increased interactions between propyl spacer polymers and DNA leading to a slow release of the genetic material inside the cytosol.<sup>12,24</sup>

Guanidinium-containing polymers are inspired by nature, more precisely by the amino acid arginine, which is abundant in well-known CPPs such as TAT or R8.<sup>68,69</sup> However, the known polymer backbones differ to the polymers investigated herein and the guanidinium group is often used in combination with other functional moieties. Relatively low molar mass guanidinium-bearing poly(methacrylamides) (DP of 20) offered transfection efficiency of about 50% of that of jetPEI in HEK293T cells in serum free medium and 48 h post transfection.<sup>70</sup> On the other hand, a guanidinium-bearing polymethacrylate with an approximately twofold higher number average molar mass (25 kg mol<sup>-1</sup>) compared to PGPAm<sub>89</sub> and a 42.4 kDa poly-arginine exhibited lower transfection efficiency than PDMAEMA in COS-7 cells and serum-free medium.<sup>38</sup> In another study a similar poly-arginine showed transfection efficiency comparable to lipofectamine in mixed cortical cells.<sup>71</sup> The observed toxicity was also described with comparable guanidinium functional polymers of different backbone chemistry and spacer length.<sup>38,56,72</sup>

In the case of PGPAm polymers with low molecular weight, comparisons are only possible with oligo-arginines. Oligo-arginines ranging from 5 to 11 residues in length showed

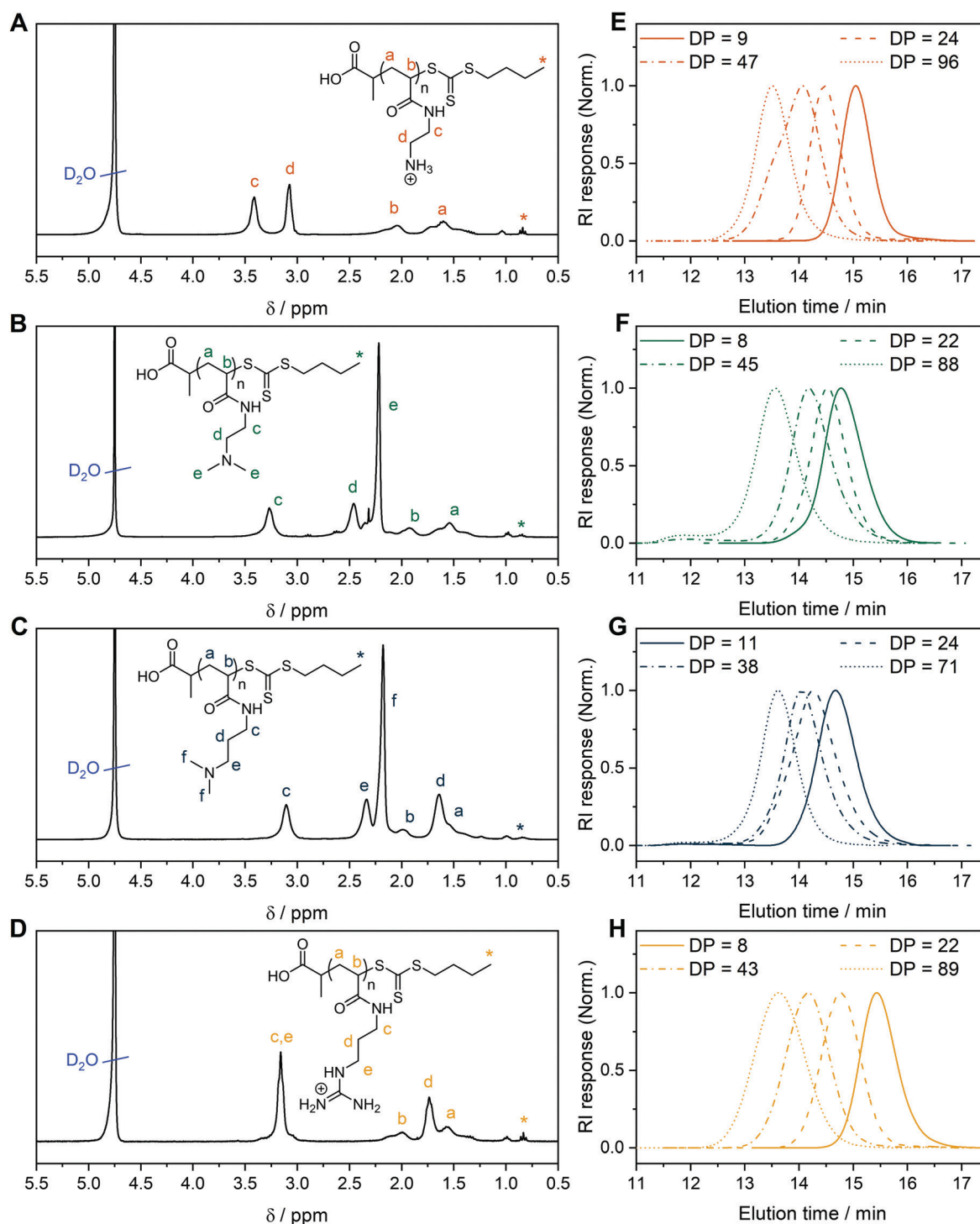
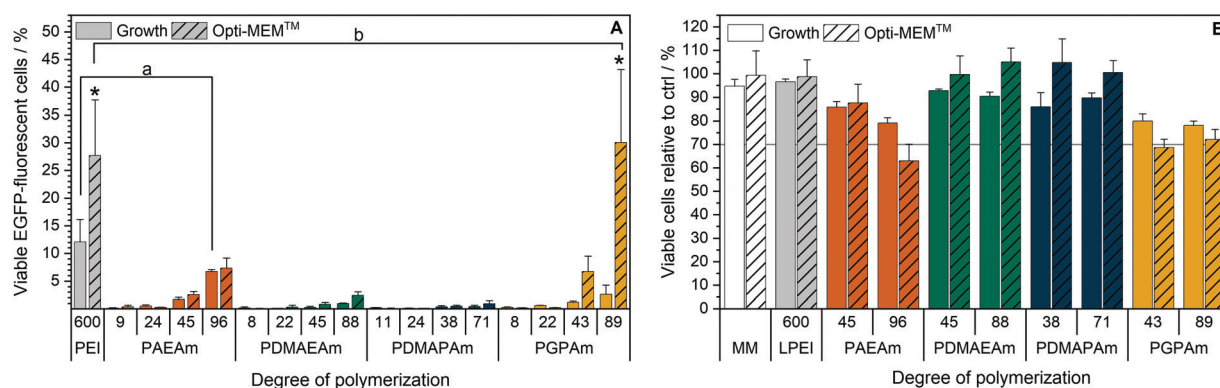


Fig. 1 <sup>1</sup>H NMR of (A) PAEAm<sub>24</sub>, (B) PDMAEAm<sub>22</sub>, (C) PDMAPAm<sub>24</sub>, (D) PGPAm<sub>22</sub> in D<sub>2</sub>O. Aqueous (0.1% TFA + 0.1 mol L<sup>-1</sup> NaCl) SEC traces of (E) PAEAm, (F) PDMAEAm, (G) PDMAPAm, (H) PGPAm polymers synthesized via RAFT polymerization.

transfection of about 50% of that of BPEI (25 kDa) in A549 cells in serum free medium.<sup>73</sup>

All in all, the high molar mass guanidinium functional polyacrylamide PGPAm<sub>89</sub> led to promising transfection results, comparable to commercial LPEI, which nicely demonstrates the potential of the controlled synthesis of this polymer class. However, the mechanism for the pDNA delivery of PGPAm<sub>89</sub>

remains to be investigated, as the guanidinium functionality was used to support gene delivery in random studies before, but successful protein expression was not shown with a homopolymer. The common design of polymers for gene delivery is based on the pH-sensitive character of the polymers, which changes the protonation and thus partly also the hydrophilicity in the endosome.<sup>74,75</sup> However, the influence of the buffer



**Fig. 2** Transfection efficiency and toxicity of PAm homopolymers in HEK293T cells. (A) Transfection efficiency: cells were incubated with polyplexes of pEGFP-N1 pDNA and polymers at N\*/P 30 (Table S6, ESI†). EGFP expression of viable cells was analyzed via flow cytometry. Two different transfection protocols were applied; either 24 h in growth medium (DMEM + 10% FCS + 10 mM HEPES) or 4 h in serum-reduced Opti-MEM™ followed by medium change to growth medium and further incubation for 20 h. Values represent mean  $\pm$  SD ( $n \geq 3$ ). a: no significant difference ( $p > 0.05$ ) to LPEI in growth medium, b: no significant difference ( $p > 0.05$ ) to LPEI in Opti-MEM™, \*: significant difference ( $p < 0.001$ ) to same polymer in growth medium. (B) Cytotoxicity of PAm homopolymers in HEK293T cells. Metabolic activity was measured in HEK293T cells using the alamarBlue assay following incubation with indicated polymers at equal amine concentrations ( $\approx$  N\*/P 30) for 4 h. Values represent mean  $\pm$  SD ( $n = 3$ ).

capacity of the polymer was also discussed contrarily.<sup>76</sup> Since the protonation of PGPAm<sub>89</sub> does not change at endosomal pH (Fig. S8, ESI†), more detailed investigations of the transfection mechanism can help to design more efficient polymers.

### Polyplex formation and characterization

To investigate the transfection mechanism, different bottle necks were investigated, starting at the formation of polyplexes. Therefore, the interaction between polymer and pDNA was investigated using the ethidium bromide quenching assay (EBA, Fig. 3A). The formation of polyplexes is indicated by displacement of intercalated ethidium bromide from the pDNA due to hydrophobic and electrostatic interactions of pDNA with the polymer, resulting in a decrease of ethidium bromide fluorescence. Various N\*/P ratios were analyzed to determine

the optimal conditions for sufficient pDNA binding (Fig. S11A, ESI†). In the EBA, all polymers reduced the fluorescence intensity of the pDNA-ethidium bromide solution with increasing N\*/P ratios, plateauing at values of N\*/P 5 or above. However, while the molar mass of the polymer within each cation set had no impact on the value of the plateaus, the nature of the cationic group showed an influence. At N\*/P 30, PDMAEAm polymers led to a binding of about 75% of the pDNA, whereas all other polymer groups, including LPEI, bound about 85–90% of the pDNA.

Subsequently, the HRA and pH dependent EBA were used to further investigate the influence of cationic moiety, side chain length and DP on polyplex properties. In the case of the HRA, the formed polyplexes were incubated with heparin, a competing polyanion disrupting the electrostatic interaction between pDNA and polymer, which leads to re-intercalation of ethidium

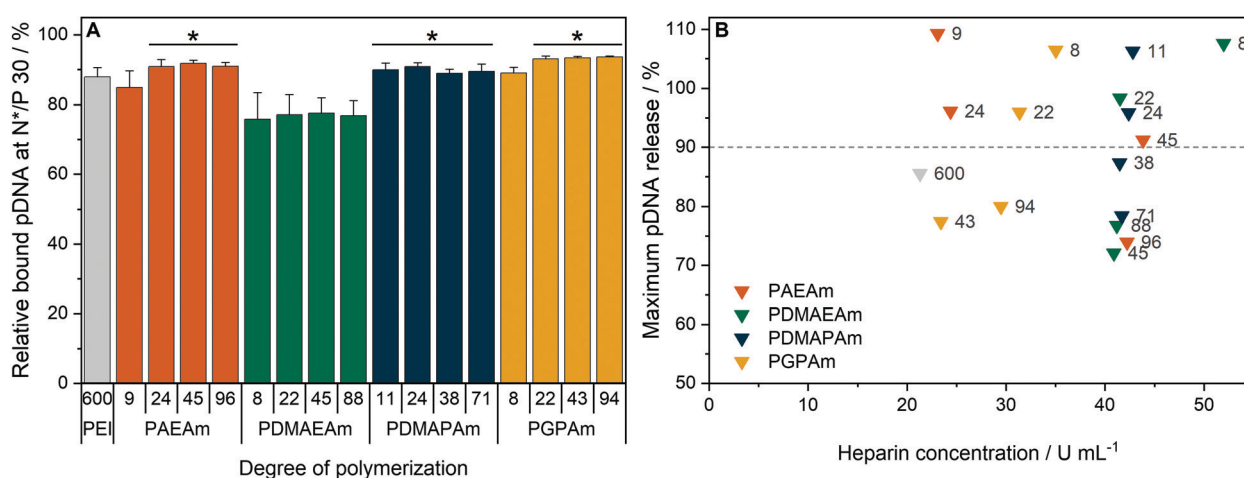


**Fig. 3** Polyplex formation and stability tests with pDNA and PAm homopolymers. (A) EBA of all polymers at N\*/P 30 in HBG buffer. Values represent mean  $\pm$  SD ( $n \geq 3$ ). \*: significant difference to all PDMAEAm polymers ( $p < 0.05$ ). (B) HRA of polymers at N\*/P 30. Values were calculated as the heparin concentration needed to release the maximum amount of pDNA (defined as the beginning of the plateau, see Fig. S1 and S11B, ESI†) following fitting of a piecewise equation to the respective data ( $n = 3$ ) for each polymer. Numbers in plot represent the degree of polymerization.

bromide and therefore increased rFI. The release of genetic material was observed with all investigated polymers, albeit with different release profiles and plateaus. At N\*/P 30, only the polymers with lower molar mass ( $DP < 50$ ) were able to release the pDNA completely, as indicated by an increase of the rFI above 90% (B). Interestingly at  $DP < 25$ , the PAEAm and PGPAm polymers required less heparin ( $20\text{--}35\text{ U mL}^{-1}$ ) to release the same amount of pDNA than PDMAEAm and PDMA-PAm polymers with tertiary amines ( $40\text{--}50\text{ U mL}^{-1}$ ). Regarding the higher molar mass polymers with  $DP > 50$ , only PGPAm<sub>94</sub> ( $30\text{ U mL}^{-1}$ ) released the pDNA at low heparin concentrations comparable to LPEI ( $21\text{ U mL}^{-1}$ ). This molar mass dependency was not observed for PDMAEAm and PDMAPAm polymers. In contrast to the EBA, these results showed a dependency on the polymer length for PAEAm and PGPAm and on the property of the side chain (Fig. S11B, ESI†). Furthermore, the results identify the polyplexes with PGPAm<sub>43</sub> and PGPAm<sub>94</sub> to be promising polymers, showing strong binding but no full release of pDNA by electrostatic competitors.

Additionally, a pH-dependent EBA (pH value 5 to 9) was performed and differences between PGPAm and the other PAm were observed (Fig. S12, ESI†). The PGPAm polyplexes showed a strong and pH-independent polyplex formation, whereas the other polymers showed less pDNA binding at higher pH values.

The investigation of polyplex formation and stability indicated that PAEAm and PGPAm polymers bind pDNA very well (Fig. 3A), complexing pDNA to a slightly greater extent than LPEI and releasing it at moderate heparin concentrations (B). The good binding of PGPAm polymers could be attributed to the nature of the bidentate binding of guanidinium to the phosphate of the pDNA displacing EtBr more efficiently than the other polymers.<sup>77</sup> On the other hand, the low heparin concentration needed to partially release the PGPAm could indicate a high affinity of guanidinium for the sulphate groups of heparin compared to the phosphate groups of the pDNA.<sup>78,79</sup> In the case of the longer PGPAm, the inefficient release of pDNA by heparin may also be due to further, non-electrostatic interactions of the polymers with the DNA. In contrast, pDNA binding with PDMAEAm appeared to be weaker despite higher concentration of heparin being required for release of the genetic material (Fig. 3). The other tertiary amine-based system, PDMAPAm, showed the same strong pDNA-polymer interaction once the polyplex was formed. This difference in pDNA binding affinity between primary and tertiary amine moieties has been observed previously with polymers comprising methacrylate backbones.<sup>34</sup> The higher pDNA complexation by PDMAPAm polymers compared to PDMAEAm could be due to the increased hydrophobicity conferred by the propyl spacer of the side chain.<sup>80,81</sup> Moreover, Van de Wetering *et al.* explained this reduced affinity for the phosphates of the pDNA with the reduced steric availability of the tertiary amines of ethyl spacer polymers.<sup>12</sup> In the end, the complexation of less pDNA by PDMAEAm compared to the other PAm polymers could also be explained by the partial protonation of the PDMAEAm polymers, which possess the lowest  $pK_a$  of this library, at pH 7.4 leading to a decrease in protonated amines available for pDNA binding (see Fig. S8 and S12, ESI†).

To further characterize the formed polyplexes, their size (hydrodynamic diameter) was investigated (Table S7 and Fig. S13, S14, ESI†). Indeed, several studies have reported that polyplex sizes below 100 nm offer increased transfection efficiency.<sup>74,82</sup> The size of polyplexes formed at N\*/P 30 was assessed *via* dynamic light scattering (DLS). The Z-average diameter of all polyplexes ranged from 32 to 69 nm with only PAEAm<sub>9</sub> and PDMAEAm<sub>22</sub> showing polyplex sizes of 127 and 115 nm, respectively. Therefore, the main size-population was in the favored size range for all polyplexes.

In summary, no significant influence of hydrophobicity or type of cationic moiety on the polyplex size was found. The molar mass of the polymers showed only a slight influence on the size of the polyplexes. These results correspond very well to conclusions of other research groups using various cationic polymeric materials.<sup>12,29,62,83</sup> So far, the only difference that corresponds to high transfection efficiency is the low heparin concentration required to release a high amount of the pDNA. Hydrophobic interactions might be a reason for the incomplete release by heparin. They were also promoted for other gene carrier systems.<sup>84</sup>

#### Cellular internalization of PAm homopolymers

To further investigate the difference in transfection efficiency between the PAm polymers, pDNA uptake properties were studied using flow cytometry or confocal laser scanning microscopy (CLSM) with HEK293T cells following incubation of the cells with polyplexes of YOYO-1 iodide labeled pDNA and polymers at N\*/P 30 for 4 h. This method was used to assess the influence of temperature, media and molar mass of the polymers.

To visualize the uptake, HEK293T cells were incubated with YOYO-1-labeled polyplexes containing the highest molar mass polymers or LPEI at N\*/P 30 in Opti-MEM™ for 4 h and imaged with CLSM (Fig. 4A). Hoechst 33342 was added 10 min before imaging to stain the nuclei and trypan blue was used to quench the fluorescence of YOYO-1-labeled pDNA outside the cells. All tested polymers led to a punctate pattern of green fluorescence within the cells, whereas the control with YOYO-1 labeled pDNA and no polymer did not show green fluorescence. These results indicate an efficient uptake of YOYO-1-labeled pDNA by the PAm polymers or LPEI.

The uptake was investigated in more detail by flow cytometry (Fig. 4B). First, the common method of incubating cells at low temperature was used to find out whether the polyplexes were taken up *via* energy-dependent processes like clathrin-mediated endocytosis, often proposed for nanoparticles below 200 nm, or by translocation across the membrane.<sup>82</sup> Therefore, HEK293T cells were incubated with the polyplexes in growth medium at 4 °C for 4 h, to inhibit all energy-dependent processes. All tested polymers showed a significant decrease of pDNA uptake compared to that observed in growth medium at 37 °C ( $p < 0.001$ ). Furthermore, no difference in pDNA uptake was observed between the different polyplexes at 4 °C ( $p = 0.937$ ).

Subsequently, the influence of the used transfection media on cellular uptake was studied. All polymers showed increased rMFI in both media. When incubated in Opti-MEM™, the quantity of internalized pDNA was slightly increased compared



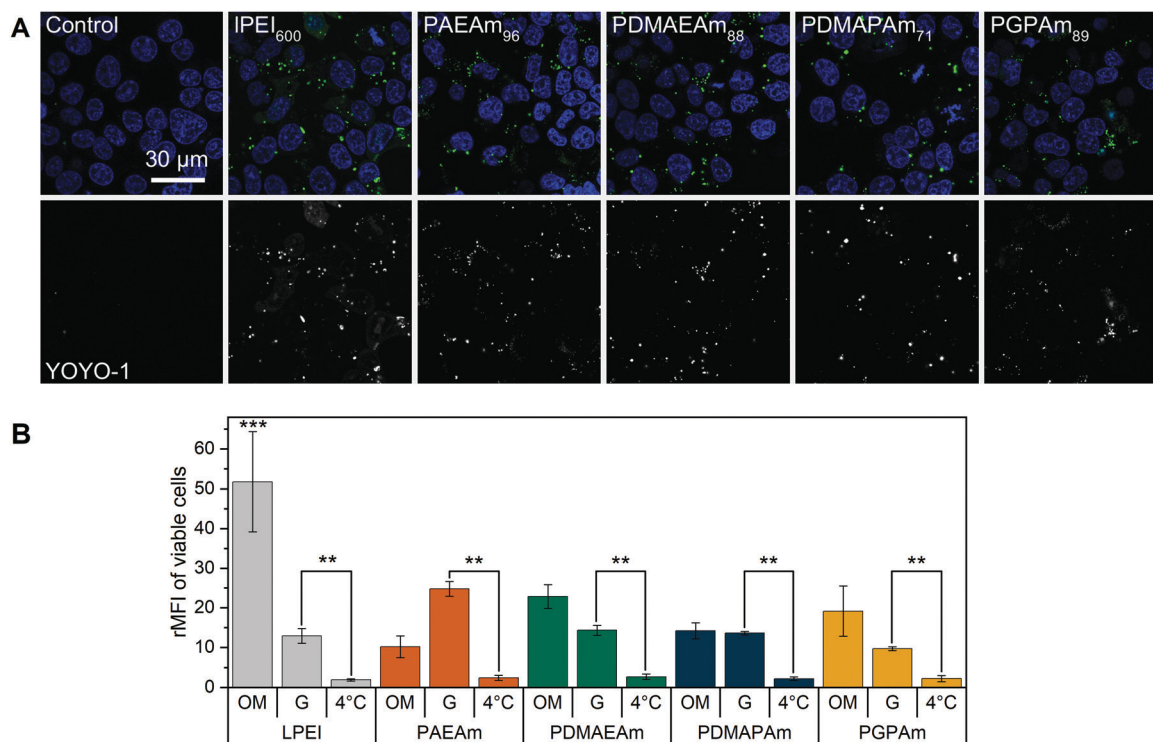


Fig. 4 Polyplex uptake with PAM polymers (A) CLSM: HEK293T cells were incubated with polyplexes of YOYO-1-labeled pDNA and polymers at N\*/P 30 (Table S6, ESI†) in Opti-MEM™ for 4 h. Nuclei were stained with Hoechst33342 and YOYO-1 fluorescence was quenched with trypan blue. (B) Flow cytometry: HEK293T cells were incubated with polyplexes of YOYO-1-labeled pDNA and LPEI, PAEAm<sub>96</sub>, PDMAEAm<sub>88</sub>, PDMAPAm<sub>71</sub> or PGPAm<sub>89</sub> at N\*/P 30. Incubation was in growth medium at 37 °C for 4 h (G), in serum-reduced Opti-MEM™ at 37 °C for 4 h (OM) or in growth medium at 4 °C for 4 h (4 °C). Cells incubated with labeled pDNA served as control (rMFI = 1). Values represent mean ± SD (n ≥ 3). \*\*: significant difference to indicated sample (p < 0.001). \*\*\*: significant difference to all other samples (p < 0.001).

to growth medium, but only for LPEI significance (p < 0.001) was found. The highest increase in uptake of pDNA in Opti-MEM™ was observed for all PDMAEAm polymers and LPEI with rMFI of up to 25 and 51.8, respectively. However, LPEI-polyplexes showed a threefold higher pDNA uptake compared to all PAM homopolymers (p < 0.001). In growth medium, the highest increase in rMFI was observed for PAEAm<sub>96</sub>, indicating a possible explanation for the higher transfection efficiency of the polymer in the presence of serum. Interestingly, molar mass dependence was only observed for the PAEAm polymers in growth medium (Fig. S15, ESI†).

The temperature dependent uptake and a punctuate uptake pattern in CLSM studies, demonstrate that polyplexes (pDNA) were taken up *via* an energy-dependent mechanism. Although this was not previously investigated for PAM homopolymers, it is known for other cationic polymers used for gene delivery.<sup>34,36,85</sup> Regarding the guanidinium functional polymers, previous studies of other research groups showed contradictory results of temperature-independent and temperature-dependent uptake, respectively.<sup>38,70</sup> This inconsistency is also known for guanidinium-containing peptides,<sup>86</sup> indicating that there are other factors additional to the type of functional group determining the way of internalization and should therefore be considered for novel polymers.

A reduced uptake of pDNA in the presence of growth medium was also observed by other groups.<sup>87,88</sup> In the presence

of serum, the cationic charged polyplexes tend to interact with negatively charged proteins, leading to aggregation and therefore reduced uptake.<sup>6,89,90</sup> It could also be assumed that the interaction with extracellular matrix components such as heparan sulfate proteoglycans is less pronounced due to competition with serum proteins, so that less pDNA can be uptaken.<sup>91–94</sup> However, in our study, the uptake of pDNA did not correlate well to the observed EGFP expression, where PGPAm<sub>96</sub> showed the best performance in Opti-MEM™ whereas the other PAM polymers exhibited only slight EGFP expression. This was also observed in previous studies using methacrylate-based polymers.<sup>34</sup> Therefore, further mechanistic assays were performed to find out, why PDMAEAm delivered as much pDNA into the cells as PGPAm, but showed nearly no transfection efficiency.

#### Interaction of polymers with cellular membranes

To further investigate the structure–property relationship of polymers for efficient gene delivery, the interaction with membranes, representing the main biological barriers, was analyzed. The influence of the polymers on the membrane integrity was tested *via* hemolysis and aggregation assays using human erythrocytes, which are well known for studies regarding membrane–polymer-interaction. The cells were washed with PBS and incubated with the polymers at equal amine concentrations

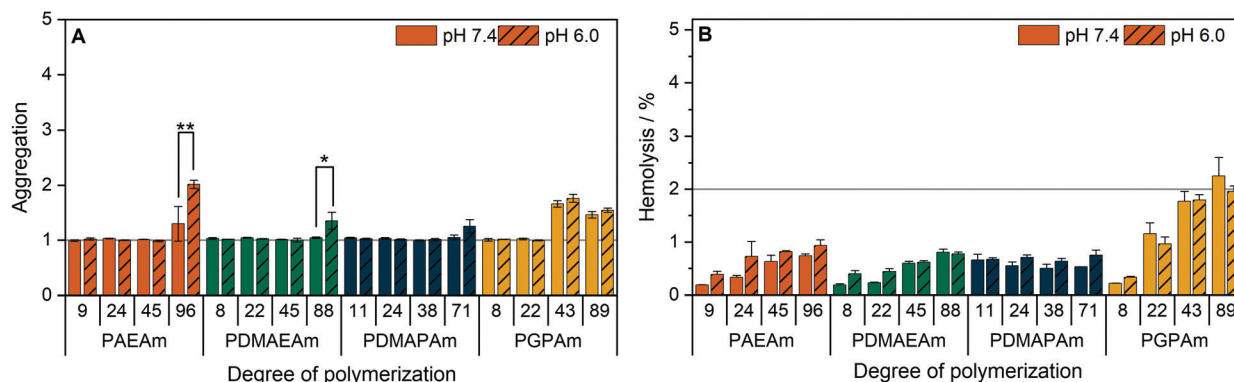


Fig. 5 Interaction of PAMs with erythrocyte membranes. Human erythrocytes were washed and incubated with polymers at equal amine concentrations ( $\approx N^*/P$  30, Table S6, ESI<sup>†</sup>) in PBS of different pH values present in blood/cytoplasm (pH 7.4) or endosomal compartments (pH 6). (A) Aggregation of indicated polymers measured as light absorption by erythrocytes. Values are calculated as the negative control (PBS value) relative to the sample value and represent mean  $\pm$  SD ( $n = 3$ ). \*: significant difference ( $p < 0.05$ ), \*\*: significant difference to indicated sample ( $p < 0.001$ ). (B) Hemolysis as the amount of released hemoglobin calculated relative to 1% Triton X-100 as positive control (100% hemolysis). Values represent mean  $\pm$  SD ( $n = 3$ ) and are classified as slightly hemolytic between 2% and 5%, as non- or hemolytic if lower or higher than 2% or 5%, respectively.

( $\approx N^*/P$  30) before either the release of hemoglobin from the cells as indicator for cell lysis or the absorption of light by the cells as indicator for cell aggregation was measured.

The low molar mass polymers can be considered as non-aggregating at the tested conditions (Fig. 5A). Meanwhile, the highest molar mass polymers (additionally PGPAm<sub>43</sub>) exhibited a potential for aggregation of erythrocytes ( $p < 0.001$ ). The influence of the pH value was dependent on the type of cationic polymer, whereby only PAEAm<sub>96</sub> ( $p < 0.001$ ) and PDMAEAm<sub>88</sub> ( $p = 0.02$ ) showed significant dependence.

Beside the aggregation of erythrocytes, the potential of the polymers to induce membrane leakage was tested (Fig. 5B). It was found that all polymers were non-hemolytic (values below 2%). Moreover, the pH value had no significant influence on the hemolytic activity.

The increased aggregation of the red blood cells by the high DP polymers does not necessarily relate to membrane destruction but rather to membrane interaction *via* the high positive charge density of cationic polymers.<sup>95</sup> The findings of this study indicate that, at concentrations equal to  $N^*/P$  30, no severe lysis of the erythrocyte membrane occurred in the presence of any of the polymers and also the pH values showed no influence on the membrane leakage potential of the polymers.

Since the membrane composition of erythrocytes differs from that of the cells used for transfection, the influence of polyplexes on membranes of HEK293T cells was studied (Fig. S16, ESI<sup>†</sup>).<sup>96,97</sup> Therefore, a LDH assay was performed following incubation of the cells with polyplexes of the highest DP polymers at  $N^*/P$  30 in growth medium or in Opti-MEM<sup>™</sup> for 4 h. If the polyplex or polymer decreases the integrity of the cellular membrane, the enzyme LDH will be released to the medium, which can be measured indirectly *via* the conversion of its substrates into fluorescent molecules. All polymers showed higher LDH release profiles in Opti-MEM<sup>™</sup> compared to growth medium with only PAEAm<sub>96</sub> and PGPAm<sub>89</sub> showing significant differences ( $p < 0.001$ ). The tertiary amine polymers and LPEI caused minor increases in both media (up to 5% relative to Triton X-100),

whereas PAEAm<sub>96</sub> and PGPAm<sub>89</sub> in Opti-MEM<sup>™</sup> showed an increase of about 26 and 31%, respectively ( $p < 0.001$ ), indicating membrane-lytic activity. In growth medium, the LDH release by PGPAm<sub>89</sub> was comparable to that of the tertiary amine polymers (2% relative to Triton X-100), whereas PAEAm<sub>96</sub> exhibited the highest LDH-release of 14% ( $p = 1.000$ ). This correlates well with the results for transfection efficiency and could again point out a medium dependency of PGPAm.

#### Endosomal release of polymers

To elucidate the mechanism of transfection for the polymer library, in particular for PGPAm, further investigations were required. The PGPAm polymers showed high transfection and only slight membrane destruction, while being pH unresponsive. The common hypotheses for endosomal release “proton sponge” as well as the “membrane permeability and pore formation” are based on the concept of pH-dependent increased protonation of the polymers during endosomal maturation.<sup>74</sup> These hypotheses do not fit for polymers such as PGPAm exhibiting very high  $pK_a$  values ( $\approx 12$ ). To study the endosomal release of the polymer library, a calcein release assay was performed. Calcein is a non-cell-permeable, fluorescent dye taken up *via* endocytic pathways resulting in the formation of a punctuated pattern inside the cytoplasm. If polymers are able to destabilize the endosomal membrane, calcein is released into the cytoplasm giving a diffused fluorescence pattern.<sup>98,99</sup> This effect can be detected by flow cytometry as an increase in fluorescence intensity as well as in an altered histogram (see Fig. S18, ESI<sup>†</sup>). Based on the previous results, only the polymers with the highest molar masses were screened using HEK293T cells following incubation with the polyplexes at  $N^*/P$  30 and calcein (25  $\mu\text{g mL}^{-1}$ ) for 4 h (Fig. 6A).

A significant increase in calcein fluorescence was observed following incubation with PGPAm<sub>89</sub>-containing polyplexes ( $p < 0.001$ ). All other tested polyplexes caused only a slight increase in rMFI. Interestingly, the endosomal release of PGPAm<sub>89</sub>-polyplexes was again influenced by the medium. The calcein fluorescence in growth medium was about 80% lower than in Opti-MEM<sup>™</sup>

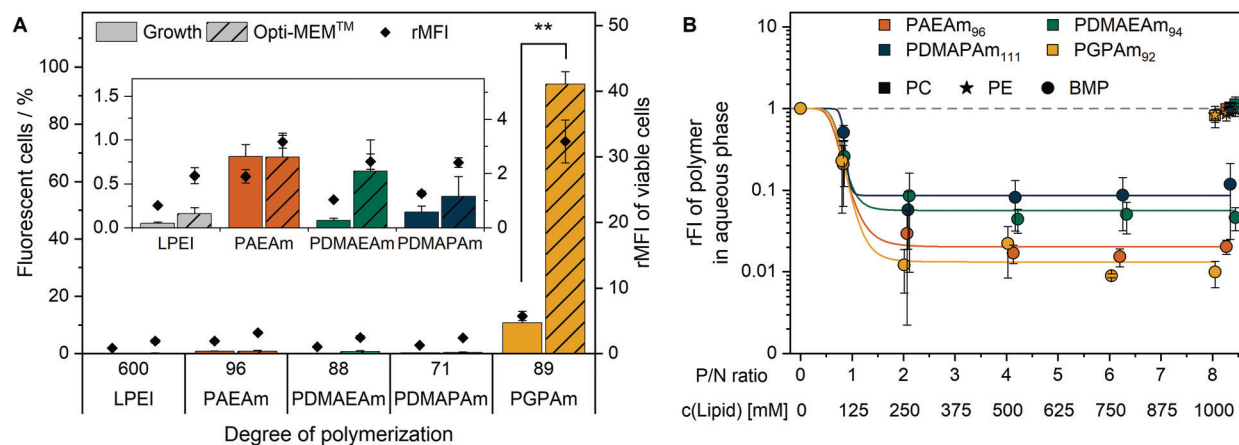


**Fig. 6** Endosomal escape of PAm homopolymers. (A) Calcein release assay: HEK293T cells were incubated with indicated polymers at N\*/P 30 (Table S6, ESI†) for 4 h at 37 °C and the mean fluorescence intensity relative to the calcein control as well as the number of viable cells with higher fluorescence than the calcein control (%) were analyzed *via* flow cytometry. Values represent mean  $\pm$  SD ( $n = 3$ ). \*\*: significant difference to indicated sample ( $p < 0.001$ ). (B) Lipid binding assay: DY635-labeled PAm polymers in acetate buffer (pH 5.7) were incubated with different lipids in hexane at indicated concentrations and P/N ratios (lipid-phosphate to polymer-amine). Following phase separation, FI of the aqueous phase was measured and rFI calculated relative to the control with no lipids in the hexane phase. A decrease in rFI indicated partitioning of the DY635-labeled polymer into the hexane phase. Dots represent mean  $\pm$  SD ( $n = 3$ ). Lines represent a logistic equation fitted to the values of each replicate.

and only 10.7% of cells showed higher fluorescence than the calcein control ( $p < 0.001$ ).

The results of the calcein release assay demonstrate the potential of PGPAm<sub>89</sub>-polyplexes to escape the endosome. In serum-reduced and growth medium, the endosomal release of polyplexes with PGPAm<sub>89</sub> outperformed all other tested polyplexes including those with LPEI. The difference between transfection and calcein release of LPEI-polyplexes could be explained with the higher pDNA uptake with LPEI compared to all other polymers, so that few calcein release from a higher number of endosomes was sufficient to yield a high transfection efficiency. The endosomal release potential for PDMAEMA, the methacrylate analog to PDMAEAm and PDMAPAm, was also found to be low.<sup>100</sup> However, for guanidinium-containing CPPs an efficient endosomal release is known.<sup>41</sup> To our knowledge, the high level of calcein release achieved with polyplexes of PGPAm<sub>89</sub> homopolymers in this study was not shown for guanidinium functional polymers before. The results indicate an efficient and pH-independent endosomal release for PGPAm<sub>89</sub>.

Since the PGPAm polymers were not pH-sensitive but able to escape the endosome, the endosomal escape mechanism of those polymers was investigated in more detail. For guanidinium-containing CPPs, the endosomal release was proposed to occur *via* binding to BMP, a lipid present in the membranes of ILEV, but not in the limiting membrane of late endosomes or lysosomes.<sup>47,101,102</sup> Therefore, the lipid-polymer binding assay was conducted to investigate the interaction of the PAm homopolymers with this lipid (Fig. 6B). DY635-labeled PAm polymers were diluted in acetate buffer (pH 5.7) to equal amine concentrations and mixed thoroughly with different concentrations of BMP in hexane. For comparison to other phosphate-containing but neutral lipids, PC and PE were used in the hexane phase. Following phase separation and isolation of the aqueous phase, the fluorescence of the aqueous phase was measured.

A decrease in fluorescence intensity indicated the removal of the polymer from the aqueous phase and therefore lipid binding.

The incubation of the polymers with PC or PE in the hexane phase caused a negligible decrease in relative fluorescence intensity (rFI) by all tested polymers. When incubated with BMP, all tested polymers showed a decrease in fluorescence intensity with increasing P/N ratio (lipid-phosphate to polymer-amine). PGPAm exhibited the highest decrease in rFI indicating a slightly stronger binding than PAEAm and the tertiary amine analogues. The results are comparable to those for dTAT of Erazo-Oliveras *et al.*, who propose BMP-binding as the mechanism for endosomal escape of this peptide.<sup>47</sup> In our study however, the non-calcein-releasing polymers also showed BMP-binding properties, albeit not as strong as PGPAm. This might be due to the higher density of cationic moieties in the PAm homopolymers compared to the density in dTAT. The investigations indicate a multifactorial endosomal escape of PGPAm.

## Conclusions

In this study, a library of cationic PAm homopolymers was synthesized and investigated for their transfection efficiency. RAFT polymerization was used to yield a series of well-defined polymers with narrow dispersity and narrow molar mass distributions. The polymers differ in their properties regarding (i) molar mass (DP10-100), (ii) cationic moiety (primary, tertiary, guanidinium) and (iii) length of alkyl spacer in the side chain (ethyl, propyl). The primary and tertiary amine functional polymers possessed  $pK_a$  values slightly above physiological pH, whereas for PGPAm the  $pK_a$  value could not be determined. Therefore, all PAm polymers in principle possess a high degree of protonation ( $\geq 70\%$ ) at physiological

pH values and exhibited good pDNA binding ( $\geq 80\%$ ) as determined *via* EBA.

Toxicity and efficiency are the main characteristics of transfection polymers. Therefore, the polymer library was investigated to identify interesting candidates. All PAM homopolymers were found to be less cytotoxic than LPEI in L929 cells, but only the highest molar mass guanidinium polymer, PGPAm<sub>94</sub>, was able to achieve a transfection efficiency as high as LPEI. The primary amine functional PAEm<sub>96</sub> polymers also resulted in notable transfection efficiency. For a better understanding of the transfection mechanism of the polymers, further investigations were performed, in detail: polyplex uptake, membrane interaction and endosomal release. The results showed beneficial effects of increasing molar mass and the presence of guanidinium- as well as primary amine-functional groups on transfection relevant aspects.

There was evidence for an endocytic uptake with a punctuate pattern of YOYO-1-labeled pDNA in CLSM studies and no uptake of all PAM polymers at 4 °C (inhibition of ATP-dependent uptake). Furthermore, there was a strong correlation with increased lysis of cytoplasmic membranes (erythrocyte, HEK293T) and efficient endosomal release (Fig. 7).

Interestingly, PGPAm<sub>89</sub> exhibited superior endosomal release properties, although it is not pH responsive. Therefore, we postulate a strong interaction of the polymer with the endolysosomal membrane as a mechanism for endosomal escape. However, the lipid-polymer binding assay investigating the binding of the PAMs to BMP revealed that all tested polymers were able to bind BMP, albeit PGPAM was the most efficient. A possible explanation could be the difference to the composition of natural ILEV consisting of more than just one lipid or a more effective mechanism of guanidinium polymers to leave the endolysosome once the polymers escaped the ILEV. Further aspects should also be considered. The pDNA release could be a further crucial step in the delivery process, since the results showed a strong correlation between the amount of

heparin needed to achieve an incomplete pDNA release and transfection efficiency (Fig. 7).

Finally, with a transfection efficiency as high as that of LPEI and superior calcein release properties, the guanidinium functional PAM polymers present a promising class of polymers for gene delivery.

## Conflicts of interest

The authors declare that the research was conducted in the absence of any commercial or financial relationships that could be construed as a potential conflict of interest.

## Acknowledgements

The authors gratefully acknowledge the Bundesministerium für Bildung und Forschung (BMBF, Germany, #13XP5034A PolyBioMik), the German Research Foundation (DFG) for generous funding within the Emmy-Noether Programme (Projekt ID: 358263073), and the support by the DFG-funded Collaborative Research Centre PolyTarget (SFB 1278, project B06, project ID: 316213987). The authors thankfully acknowledge Karina Rost for performing toxicity assays and Prof. U. S. Schubert for providing excellent facilities. Furthermore, the authors acknowledge Bärbel Beringer-Siemers, Carolin Kellner, Elisabeth Preußger and Jana Solomun for their excellent technical assistance and discussions.

## References

- 1 D. Lechardeur, K. Sohn, M. Haardt, P. Joshi, M. Monck, R. Graham, B. Beatty, J. Squire, H. O'brodovich and G. Lukacs, *Gene Ther.*, 1999, **6**, 482.
- 2 K. Lundstrom, *Diseases*, 2018, **6**, 42.
- 3 R. Gardlik, R. Palfy, J. Hodossy, J. Lukacs, J. Turna and P. Celec, *Med. Sci. Monit.*, 2005, **11**, Ra110–Ra121.
- 4 B. Kealy, A. Liew, J. M. McMahon, T. Ritter, A. O'Doherty, M. Hoare, U. Greiser, E. E. Vaughan, M. Maenz and C. O'Shea, *Tissue Eng., Part C*, 2009, **15**, 223–231.
- 5 D. He and E. Wagner, *Macromol. Biosci.*, 2015, **15**, 600–612.
- 6 R. J. Christie, N. Nishiyama and K. Kataoka, *Endocrinology*, 2010, **151**, 466–473.
- 7 U. Lächelt and E. Wagner, *Chem. Rev.*, 2015, **115**, 11043–11078.
- 8 Z. Zhou, X. Liu, D. Zhu, Y. Wang, Z. Zhang, X. Zhou, N. Qiu, X. Chen and Y. Shen, *Adv. Drug Delivery Rev.*, 2017, **115**, 115–154.
- 9 D. Fischer, Y. Li, B. Ahlemeyer, J. Krieglstein and T. Kissel, *Biomaterials*, 2003, **24**, 1121–1131.
- 10 H. K. de Wolf, J. Lutén, C. J. Snel, G. Storm and W. E. Hennink, *Mol. Pharmaceutics*, 2008, **5**, 349–357.
- 11 M. Neu, D. Fischer and T. Kissel, *J. Gene Med.*, 2005, **7**, 992–1009.
- 12 P. van de Wetering, E. E. Moret, N. M. E. Schuurmans-Nieuwenbroek, M. J. van Steenberg and W. E. Hennink, *Bioconjugate Chem.*, 1999, **10**, 589–597.

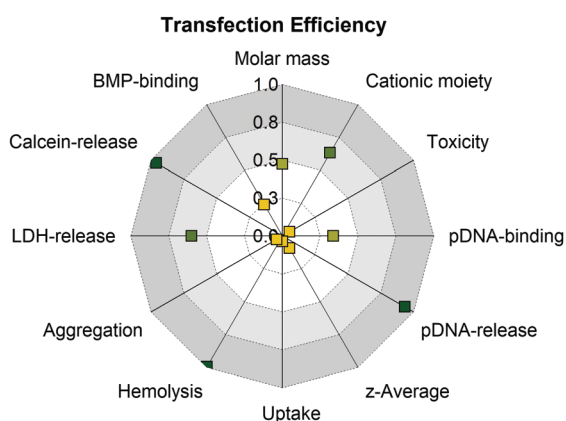


Fig. 7 Analysis of structure–property–correlations for PAMs using the squared Pearson's correlation coefficient ( $R^2$ ) to determine linearity of the correlation. Values around 1.0 indicate strong positive (green) and values around 0 indicate no correlation (yellow). For a detailed overview which data were used for correlation see Table S8 (ESI†).

- 13 S. Agarwal, Y. Zhang, S. Maji and A. Greiner, *Mater. Today*, 2012, **15**, 388–393.
- 14 D. B. Rozema, D. L. Lewis, D. H. Wakefield, S. C. Wong, J. J. Klein, P. L. Roesch, S. L. Bertin, T. W. Reppen, Q. Chu, A. V. Blokhin, J. E. Hagstrom and J. A. Wolff, *Proc. Natl. Acad. Sci. U. S. A.*, 2007, **104**, 12982–12987.
- 15 D. H. Wakefield, J. J. Klein, J. A. Wolff and D. B. Rozema, *Bioconjugate Chem.*, 2005, **16**, 1204–1208.
- 16 J. Schrooten, I. Lacík, M. Stach, P. Hesse and M. Buback, *Macromol. Chem. Phys.*, 2013, **214**, 2283–2294.
- 17 G. Gody, T. Maschmeyer, P. B. Zetterlund and S. Perrier, *Nat. Commun.*, 2013, **4**, 2505.
- 18 G. Gody, T. Maschmeyer, P. B. Zetterlund and S. Perrier, *Macromolecules*, 2014, **47**, 639–649.
- 19 L. Martin, G. Gody and S. Perrier, *Polym. Chem.*, 2015, **6**, 4875–4886.
- 20 I. Mizoguchi, Y. Ooe, S. Hoshino, M. Shimura, T. Kasahara, S. Kano, T. Ohta, F. Takaku, Y. Nakayama and Y. Ishizaka, *Biochem. Biophys. Res. Commun.*, 2005, **338**, 1499–1506.
- 21 Y. Nakayama, C. Kakei, A. Ishikawa, Y.-M. Zhou, Y. Nemoto and K. Uchida, *Bioconjugate Chem.*, 2007, **18**, 2037–2044.
- 22 Y. Nemoto, A. Borovkov, Y.-M. Zhou, Y. Takewa, E. Tatsumi and Y. Nakayama, *Bioconjugate Chem.*, 2009, **20**, 2293–2299.
- 23 N. Yasuhide, M. Takeshi, N. Makoto, H. Michiko, O. Moto and H.-S. Mariko, *Curr. Drug Delivery*, 2005, **2**, 53–57.
- 24 J.-H. Ke, M.-F. Wei, M.-J. Shieh and T.-H. Young, *J. Biomater. Sci., Polym. Ed.*, 2011, **22**, 1215–1236.
- 25 J.-H. Ke, M.-F. Wei, M.-J. Shieh and T.-H. Young, *J. Biomater. Sci., Polym. Ed.*, 2011, **22**, 1753–1775.
- 26 J.-H. Ke and T.-H. Young, *Biomaterials*, 2010, **31**, 9366–9372.
- 27 A. Aied, U. Greiser, A. Pandit and W. Wang, *Drug Discovery Today*, 2013, **18**, 1090–1098.
- 28 J. Cai, Y. Yue, D. Rui, Y. Zhang, S. Liu and C. Wu, *Macromolecules*, 2011, **44**, 2050–2057.
- 29 A. C. Rinkenauer, S. Schubert, A. Traeger and U. S. Schubert, *J. Mater. Chem. B*, 2015, **3**, 7477–7493.
- 30 M. Wagner, A. C. Rinkenauer, A. Schallon and U. S. Schubert, *RSC Adv.*, 2013, **3**, 12774–12785.
- 31 C. V. Synatschke, A. Schallon, V. Jérôme, R. Freitag and A. H. E. Müller, *Biomacromolecules*, 2011, **12**, 4247–4255.
- 32 D. Sprouse and T. M. Reineke, *Biomacromolecules*, 2014, **15**, 2616–2628.
- 33 H. Li, M. A. Cortez, H. R. Phillips, Y. Wu and T. M. Reineke, *ACS Macro Lett.*, 2013, **2**, 230–235.
- 34 A. K. Trutzschler, T. Bus, M. Reifarh, J. C. Brendel, S. Hoepfener, A. Traeger and U. S. Schubert, *Bioconjugate Chem.*, 2018, **29**, 2181–2194.
- 35 C. Zhu, S. Jung, G. Si, R. Cheng, F. Meng, X. Zhu, T. G. Park and Z. Zhong, *J. Polym. Sci., Part A: Polym. Chem.*, 2010, **48**, 2869–2877.
- 36 T. Bus, C. Englert, M. Reifarh, P. Borchers, M. Hartlieb, A. Vollrath, S. Hoepfener, A. Traeger and U. S. Schubert, *J. Mater. Chem. B*, 2017, **5**, 1258–1274.
- 37 C. Arigita, N. J. Zuidam, D. J. A. Crommelin and W. E. Hennink, *Pharm. Res.*, 1999, **16**, 1534–1541.
- 38 A. M. Funhoff, C. F. van Nostrum, M. C. Lok, M. M. Fretz, D. J. A. Crommelin and W. E. Hennink, *Bioconjugate Chem.*, 2004, **15**, 1212–1220.
- 39 E. D. Raczyńska, M. K. Cyrański, M. Gutowski, J. Rak, J. F. Gal, P. C. Maria, M. Darowska and K. Duczmal, *J. Phys. Org. Chem.*, 2003, **16**, 91–106.
- 40 C. Bechara and S. Sagan, *FEBS Lett.*, 2013, **587**, 1693–1702.
- 41 J. K. Allen, D. J. Brock, H. M. Kondow-McConaghy and J.-P. Pellois, *Biomolecules*, 2018, **8**, 50.
- 42 F. Madani, S. Lindberg, Ü. Langel, S. Futaki and A. Gräslund, *J. Biophys.*, 2011, 414729.
- 43 A. Pantos, I. Tsogas and C. M. Paleos, *Biochim. Biophys. Acta, Biomembr.*, 2008, **1778**, 811–823.
- 44 M. Silhol, M. Tyagi, M. Giacca, B. Lebleu and E. Vivès, *Eur. J. Biochem.*, 2002, **269**, 494–501.
- 45 S. Futaki and I. Nakase, *Acc. Chem. Res.*, 2017, **50**, 2449–2456.
- 46 J. D. Ramsey and N. H. Flynn, *Pharmacol. Ther.*, 2015, **154**, 78–86.
- 47 A. Erazo-Oliveras, K. Najjar, D. Truong, T. Y. Wang, D. J. Brock, A. R. Prater and J. P. Pellois, *Cell Chem. Biol.*, 2016, **23**, 598–607.
- 48 S.-T. Yang, E. Zaitseva, L. V. Chernomordik and K. Melikov, *Biophys. J.*, 2010, **99**, 2525–2533.
- 49 Y. Kim, S. Binauld and M. H. Stenzel, *Biomacromolecules*, 2012, **13**, 3418–3426.
- 50 N. Schmidt, A. Mishra, G. H. Lai and G. C. Wong, *FEBS Lett.*, 2010, **584**, 1806–1813.
- 51 M. Ahmed, *Biomater. Sci.*, 2017, **5**, 2188–2211.
- 52 K. J. Abd Karim, R. H. Utama, H. Lu and M. H. Stenzel, *Polym. Chem.*, 2014, **5**, 6600–6610.
- 53 C. Cokca, L. Zartner, I. Tabujew, D. Fischer and K. Peneva, *Macromol. Rapid Commun.*, 2020, **41**, 1900668.
- 54 M. Bauer, C. Lautenschlaeger, K. Kempe, L. Tauhardt, U. S. Schubert and D. Fischer, *Macromol. Biosci.*, 2012, **12**, 986–998.
- 55 A. Kuroki, P. Sangwan, Y. Qu, R. Peltier, C. Sanchez-Cano, J. Moat, C. G. Dowson, E. G. L. Williams, K. E. S. Locock, M. Hartlieb and S. Perrier, *ACS Appl. Mater. Interfaces*, 2017, **9**, 40117–40126.
- 56 L. Martin, R. Peltier, A. Kuroki, J. S. Town and S. Perrier, *Biomacromolecules*, 2018, **19**, 3190–3200.
- 57 L. Nová, F. Uhlík and P. Košovan, *Phys. Chem. Chem. Phys.*, 2017, **19**, 14376–14387.
- 58 A. Kuroki, P. Sangwan, Y. Qu, R. Peltier, C. Sanchez-Cano, J. Moat, C. G. Dowson, E. G. L. Williams, K. E. S. Locock, M. Hartlieb and S. Perrier, *ACS Appl. Mater. Interfaces*, 2017, **9**, 40117–40126.
- 59 M. Ullner, B. Jönsson, B. Söderberg and C. Peterson, *J. Chem. Phys.*, 1996, **104**, 3048–3057.
- 60 D. M. Drake, R. K. Keswani and D. W. Pack, *Pharm. Res.*, 2010, **27**, 2457–2465.
- 61 J. M. Layman, S. M. Ramirez, M. D. Green and T. E. Long, *Biomacromolecules*, 2009, **10**, 1244–1252.
- 62 A. C. Rinkenauer, A. Vollrath, A. Schallon, L. Tauhardt, K. Kempe, S. Schubert, D. Fischer and U. S. Schubert, *ACS Comb. Sci.*, 2013, **15**, 475–482.

- 63 W. T. Godbey, K. K. Wu and A. G. Mikos, *J. Biomed. Mater. Res.*, 1999, **45**, 268–275.
- 64 R. N. Johnson, D. S. H. Chu, J. Shi, J. G. Schellinger, P. M. Carlson and S. H. Pun, *J. Controlled Release*, 2011, **155**, 303–311.
- 65 B. D. Monnery, M. Wright, R. Cavill, R. Hoogenboom, S. Shaunak, J. H. G. Steinke and M. Thanou, *Int. J. Pharm.*, 2017, **521**, 249–258.
- 66 C. J. Bishop, K. L. Kozielski and J. J. Green, *J. Controlled Release*, 2015, **219**, 488–499.
- 67 A. C. Rinkenauer, L. Tauhardt, F. Wendler, K. Kempe, M. Gottschaldt, A. Traeger and U. S. Schubert, *Macromol. Biosci.*, 2015, **15**, 414–425.
- 68 D. M. Copolovici, K. Langel, E. Eriste and U. Langel, *ACS Nano*, 2014, **8**, 1972–1994.
- 69 S. Deshayes, M. C. Morris, G. Divita and F. Heitz, *Cell. Mol. Life Sci.*, 2005, **62**, 1839–1849.
- 70 Z. Tan, Y. K. Dhande and T. M. Reineke, *Bioconjugate Chem.*, 2017, **28**, 2985–2997.
- 71 J.-B. Kim, J. S. Choi, K. Nam, M. Lee, J.-S. Park and J.-K. Lee, *J. Controlled Release*, 2006, **114**, 110–117.
- 72 A. Kuroki, A. Kengmo Tchoupa, M. Hartlieb, R. Peltier, K. E. S. Locock, M. Unnikrishnan and S. Perrier, *Biomaterials*, 2019, **217**, 119249.
- 73 N. A. Alhakamy and C. J. Berkland, *Mol. Pharmaceutics*, 2013, **10**, 1940–1948.
- 74 T. Bus, A. Traeger and U. S. Schubert, *J. Mater. Chem. B*, 2018, **6**, 6904–6918.
- 75 D. W. Pack, A. S. Hoffman, S. Pun and P. S. Stayton, *Nat. Rev. Drug Discovery*, 2005, **4**, 581–593.
- 76 A. M. Funhoff, C. F. van Nostrum, G. A. Koning, N. M. E. Schuurmans-Nieuwenbroek, D. J. A. Crommelin and W. E. Hennink, *Biomacromolecules*, 2004, **5**, 32–39.
- 77 D. M. Perreault, L. A. Cabell and E. V. Anslyn, *Bioorg. Med. Chem.*, 1997, **5**, 1209–1220.
- 78 P. Juhasz and K. Biemann, *Proc. Natl. Acad. Sci. U. S. A.*, 1994, **91**, 4333–4337.
- 79 K. A. Schug and W. Lindner, *Chem. Rev.*, 2005, **105**, 67–114.
- 80 Z. Liu, Z. Zhang, C. Zhou and Y. Jiao, *Prog. Polym. Sci.*, 2010, **35**, 1144–1162.
- 81 A. Alshamsan, A. Haddadi, V. Incani, J. Samuel, A. Lavasanifar and H. Uludag, *Mol. Pharming*, 2009, **6**, 121–133.
- 82 S. Prabha, G. Arya, R. Chandra, B. Ahmed and S. Nimesh, *Artif. Cells, Nanomed., Biotechnol.*, 2016, **44**, 83–91.
- 83 I. Tabujew, C. Cokca, L. Zartner, U. S. Schubert, I. Nischang, D. Fischer and K. Peneva, *J. Mater. Chem. B*, 2019, **7**, 5920–5929.
- 84 E. Mastrobattista and W. E. Hennink, *Nat. Mater.*, 2012, **11**, 10–12.
- 85 T. Lühmann, M. Rimann, A. G. Bittermann and H. Hall, *Bioconjugate Chem.*, 2008, **19**, 1907–1916.
- 86 E. Wexselblatt, J. D. Esko and Y. Tor, *J. Org. Chem.*, 2014, **79**, 6766–6774.
- 87 A. K. Trutzschler, T. Bus, M. Sahn, A. Traeger, C. Weber and U. S. Schubert, *Biomacromolecules*, 2018, **19**, 2759–2771.
- 88 S. Pan, D. Cao, R. Fang, W. Yi, H. Huang, S. Tian and M. Feng, *J. Mater. Chem. B*, 2013, **1**, 5114–5127.
- 89 R. Kircheis, S. Schüller, S. Brunner, M. Ogris, K. H. Heider, W. Zauner and E. Wagner, *J. Gene Med.*, 1999, **1**, 111–120.
- 90 M. Ogris, P. Steinlein, M. Kursa, K. Mechtler, R. Kircheis and E. Wagner, *Gene Ther.*, 1998, **5**, 1425–1433.
- 91 I. Kopatz, J.-S. Remy and J.-P. Behr, *J. Gene Med.*, 2004, **6**, 769–776.
- 92 K. A. Mislick and J. D. Baldeschwieler, *Proc. Natl. Acad. Sci. U. S. A.*, 1996, **93**, 12349–12354.
- 93 P. C. Billings and M. Pacifici, *Connect. Tissue Res.*, 2015, **56**, 272–280.
- 94 G. W. Doorley and C. K. Payne, *Chem. Commun.*, 2011, **47**, 466–468.
- 95 E. Moreau, M. Domurado, P. Chapon, M. Vert and D. Domurado, *J. Drug Targeting*, 2002, **10**, 161–173.
- 96 A. A. Spector and M. A. Yorek, *J. Lipid Res.*, 1985, **26**, 1015–1035.
- 97 T. Harayama and H. Riezman, *Nat. Rev. Mol. Cell Biol.*, 2018, **19**, 281–296.
- 98 S. A. Smith, L. I. Selby, A. P. R. Johnston and G. K. Such, *Bioconjugate Chem.*, 2019, **30**, 263–272.
- 99 Y. Hu, T. Litwin, A. R. Nagaraja, B. Kwong, J. Katz, N. Watson and D. J. Irvine, *Nano Lett.*, 2007, **7**, 3056–3064.
- 100 R. A. Jones, M. H. Poniris and M. R. Wilson, *J. Controlled Release*, 2004, **96**, 379–391.
- 101 T. Kobayashi, M.-H. Beuchat, J. Chevallier, A. Makino, N. Mayran, J.-M. Escola, C. Lebrand, P. Cosson, T. Kobayashi and J. Gruenberg, *J. Biol. Chem.*, 2002, **277**, 32157–32164.
- 102 W. Mobius, E. van Donselaar, Y. Ohno-Iwashita, Y. Shimada, H. F. Heijnen, J. W. Slot and H. J. Geuze, *Traffic*, 2003, **4**, 222–231.

*Supporting Information:*

Tuning of Endosomal Escape and Gene Expression  
by Functional Groups, Molecular Weight and  
Transfection Medium: A Structure-Activity  
Relationship Study

*Friederike Richter<sup>a</sup>, Liam Martin<sup>a</sup>, Katharina Leer<sup>a</sup>, Elisabeth Moek<sup>a</sup>, Franziska Hausig<sup>a</sup>,  
Johannes C. Brendel<sup>a,b</sup>, Anja Traeger<sup>\*a,b</sup>*

<sup>a</sup>Laboratory of Organic and Macromolecular Chemistry (IOMC), Friedrich Schiller University  
Jena, Humboldtstrasse 10, 07743 Jena, Germany.

<sup>b</sup>Jena Center for Soft Matter (JCSM), Friedrich Schiller University Jena, Philosophenweg 7,  
07743 Jena, Germany.

\*Correspondence to A. Traeger (anja.traeger@uni-jena.de)

## List of Tables.

<b>Table S1.</b> Amount of different substances used for polymerization of PGPAMs and PAEAMs. 10	
<b>Table S2.</b> Amount of different substances used for polymerization of PDMAEAMs and PDMAPAMs. .... 11	
<b>Table S3.</b> Amount of different substances used for attachment to DY-635 amine to PAMs ..... 12	
<b>Table S4.</b> Kinetic cycle protocol for automated heparin addition by the microplate reader ..... 13	
<b>Table S5.</b> Summary of (protected) cationic homopolymers prepared <i>via</i> RAFT polymerization. .... 20	
<b>Table S6.</b> Toxicity and concentration at N*/P 30 and CC <sub>50</sub> values calculated <i>via</i> non-linear fit. 25	
<b>Table S7.</b> Size determination of formed polyplexes <i>via</i> DLS. .... 27	
<b>Table S8.</b> Data used for determination of the squared Pearson's correlation coefficient (R <sup>2</sup> )..... 31	

## List of Figures.

<b>Figure S1.</b> Equations used by OriginPro, Version 2018b to provide the piecewise linear fit functions for the polymers. Screenshots taken from the software. .... 14	
<b>Figure S2.</b> NMR spectra of GPAM <sup>diBoc</sup> . .... 18	
<b>Figure S3.</b> NMR spectra of AEAM <sup>Boc</sup> . .... 19	
<b>Figure S4.</b> Titration curves and equivalence point recognition criterion for titrations of PAEAM polymers..... 21	
<b>Figure S5.</b> Titration curves and equivalence point recognition criterion for titrations of PDMAEAM polymers..... 21	
<b>Figure S6.</b> Titration curves and equivalence point recognition criterion for titrations of PDMAPAM polymers..... 22	
<b>Figure S7.</b> Titration curves and equivalence point recognition criterion for titrations of PGPAM polymers..... 22	
<b>Figure S8.</b> Theoretical determination of the degree of protonation..... 23	
<b>Figure S9.</b> Cytotoxicity of PAM homopolymers in L929 cells..... 24	
<b>Figure S10.</b> Cytotoxicity of PAM homopolymers. Metabolic activity was measured in L929 cells after 24 h incubation with PAM polymers at indicated concentrations (Figure S8) using the alamarBlue™ assay. Values represent CC <sub>50</sub> values calculated after fitting the resulting toxicity values to a logistic function ± 95% CI (n = 3). Upwards pointing arrows and striped columns indicate CC <sub>50</sub> values above 500 μg mL <sup>-1</sup> ..... 25	
<b>Figure S11.</b> Polyplex formation and stability tests with pCMV-GFP pDNA and PAM homopolymers..... 26	
<b>Figure S12.</b> Polyplex formation with pCMV-GFP pDNA and polyacrylamide-homopolymers at different pH values..... 26	
<b>Figure S13.</b> Size determination of formed polyplexes <i>via</i> DLS. .... 27	
<b>Figure S14.</b> DLS traces of polyplexes formed with PAM polymers and 15 μg mL <sup>-1</sup> DNA at N*/P 30 in HBG buffer. .... 28	
<b>Figure S15.</b> Influence of degree of polymerization on polyplex uptake in HEK293T cells..... 29	



<b>Figure S16.</b> LDH release assay with PAm polyplexes in HEK293T cells. ....	29
<b>Figure S17.</b> LDH release assay with HEK293T cells. ....	30
<b>Figure S18.</b> Flow Cytometry Analysis of Calcein Release Assay. ....	30

## ADDITIONAL METHODS

### Materials.

All chemicals were used as received unless stated otherwise. BocAEAm was prepared according to a previously described procedure.<sup>1,2</sup> The chain transfer agents 2-(Butylthiocarbonothioylthio)propanoic acid (PABTC) and 2-(Butylthiocarbonothioylthio)propanoic acid-*N*-hydroxysuccinimide (NHS-PABTC) were prepared following previously reported procedures.<sup>3</sup> Dimethylamino propyl acrylamide (DMPAm) was obtained from ABCR (Germany). Dimethylamino ethyl acrylamide (DMAEAm) was obtained from ABCR and purified by column chromatography (silica, ethyl acetate). Sodium hydrogen carbonate (NaHCO<sub>3</sub>) and sodium chloride (NaCl) was obtained from Fisher (Germany). Acryloyl chloride (97%), 1,3-bis-(*tert*-butoxycarbonyl)-2-methyl-2-thiopseudourea (98%), ethylene diamine and 1,3-diaminopropane (≥99%) were obtained from Sigma (Germany). Trimethylamine (≥99.5%) was obtained from Carl Roth (Germany). Di-*tert*-butyl dicarbonate and trifluoroacetic acid (TFA) were obtained from TCI (Germany). 2,2'-Azobis(2,4-dimethylvaleronitrile) (V65B) was obtained from FUJIFILM Wako Chemicals (Germany). HPLC grade dimethylformamide (DMF) (HiPerSolv CHROMANORM) was obtained from VWR (Germany). Anhydrous *N,N*-dimethylacetamide (99.8%, DMAc) was obtained from Sigma. 1,4-dioxane (>99.5%) was obtained from Carl Roth and purified over inhibitor remover beads (for hydroquinone and monomethyl ether hydroquinone) at 4 °C. Dichloromethane (DCM) was obtained from a solvent purification system (SPS) on site, tetrahydrofuran (THF), methanol, hexane and ethyl acetate were distilled on site. DY-635 amine and DY-635 NHS ester were obtained from Dyomics (Germany). 2-(1H-Benzotriazol-1-yl)-1,1,3,3-tetramethyluronium hexafluorophosphate (HBTU) was obtained from Iris Biotech (Germany). 4-methylmorpholine (99%) was obtained from Alfa Aesar (Germany). For biological studies, following substances were ordered from suppliers in brackets: cell culture media and

supplements (Biochrom, Merck Millipore, Germany), Opti-MEM™ reduced serum medium (Gibco, Thermo Fisher, Germany), fetal calf serum (FCS, Capricorn Scientific, Germany), alamarBlue™ solution, YOYO™-1 iodide (Life Technologies, Thermo Fisher, Germany), trypsin-EDTA-solution, Triton X-100, 0.4% trypan blue solution and Hanks' balanced salt solution, calcein, L- $\alpha$ -phosphatidylcholine (PC), L- $\alpha$ -phosphatidylethanolamine, dioleoyl (PE, Sigma-Aldrich), Bis(monomyristoyl-glycero)phosphate (BMP, Avanti Polar Lipids, US), 1% ethidium bromide solution (EtBr, Carl Roth), heparin sodium salt from porcine intestinal mucosa (Alfa Aesar) and linear poly(ethyleneimine) (LPEI,  $M_w = 25 \text{ kg mol}^{-1}$ ) and branched PEI (BPEI,  $M_w = 10 \text{ kg mol}^{-1}$ , Polysciences, Germany). Plasmid DNA (pDNA) encoding the enhanced green fluorescent protein (EGFP) for transfection studies was isolated with the Giga Plasmid Kit (Qiagen, Germany) from *E. coli* containing pEGFP-N1 (4.7 kb, Clontech, USA). For all other studies, like pDNA binding or uptake, the ready-to-use plasmid pCMV-GFP (PlasmidFactory, Germany) was used.

### **Instruments.**

*Nuclear magnetic resonance (NMR) spectroscopy.*  $^1\text{H}$  NMR (300 MHz) and DEPT  $^{13}\text{C}$  (75 MHz) spectra were recorded on a Bruker AC 300 MHz spectrometer at 300 K. The delay time (d1) was set at 1 s for  $^1\text{H}$  NMR and 2 s for DEPT  $^{13}\text{C}$ . Chemical shifts ( $\delta$ ) are reported in ppm.

*Size exclusion chromatography (SEC).* SEC was conducted on one of two instruments. Dimethylacetamide (DMAc)-SEC was conducted using an Agilent 1200 series instrument equipped with differential refractive index (DRI) and UV/vis (DAD) detector. The liquid chromatography system used 1  $\times$  PSS GRAM 30 Å column (300  $\times$  0.8 mm, 10  $\mu\text{m}$  particle size) and 1  $\times$  PSS GRAM 1000 Å column (300  $\times$  0.8 mm, 10  $\mu\text{m}$  particle size). The DMAc eluent contained 0.21 wt.% LiCl as additive. Samples were run at 1 mL  $\text{min}^{-1}$  at 40 °C. Analyte samples

were filtered through a polytetrafluoroethylene (PTFE) membrane with 0.45  $\mu\text{m}$  pore size prior to injection. Poly(methyl methacrylate) (PMMA) narrow standards (PSS) were used to calibrate the SEC system. Aq.-SEC was conducted using a Jasco instrument equipped with DRI and UV (DAD) detector. The liquid chromatography system used 2  $\times$  PSS NOVEMA-MAX column (300  $\times$  0.8 mm, 10  $\mu\text{m}$  particle size). The aqueous eluent contained 0.1% TFA + 0.1 mol L<sup>-1</sup> NaCl as additive. Samples were run at 1 mL min<sup>-1</sup> at 30 °C. Analyte samples were filtered through a nylon membrane with 0.45  $\mu\text{m}$  pore size prior to injection. Poly(2-vinylpyridine) (P2VP) narrow standards (Polymer Source Inc. Dorval, Quebec, Canada) were used to calibrate the SEC system. Experimental  $M_{n,SEC}$  and  $\mathcal{D}$  ( $M_w/M_n$ ) values of synthesized polymers were determined using PSS WinGPC UniChrom GPC software.

*Titration.* Titration of the polymers was conducted using a Metrohm OMNIS integrated titration system. For a typical measurement, the polymer was dissolved in 125 mM NaCl (in ultrapure water) (1.0 mg mL<sup>-1</sup>), which was acidified with addition of 1 M hydrochloric acid (pH  $\sim$  2). The polymers were titrated (with dynamic flow rate adjustment) against 0.1 M NaOH solution up to a pH value of 12. The PGPAm polymers were titrated against 0.5 M NaOH. The  $pK_a$  values were estimated using the Henderson-Hasselbalch equation (5) from equivalence points determined by the OMNIS titration software.

$$\text{pH} = \text{p}K_a + \log \frac{[\text{A}^-]}{[\text{HA}]} \quad (5)$$

*Flow cytometry.* Flow cytometry was conducted on either the Cytomics FC 500 or the CytoFlex S by Beckman Coulter. With both instruments 10<sup>4</sup> cells were analyzed regarding their forward and sideward scattering (FSC, SSC) and their fluorescence at  $\lambda_{\text{Ex}} = 488$  with a 525 nm bandpass filter, since all employed stains (YOYO-1, EGFP, calcein) were green fluorescent.

*Microplate reader.* Fluorescence intensity measurements for EBA, HRA, alamarBlue™, LDH and BMP assays as well as absorption measurements for hemolysis and aggregation assays were performed on the Infinite M200 PRO microplate reader (Tecan, Germany) with  $\lambda_{\text{Ex}} / \lambda_{\text{Em}}$  used as indicated in the respective method sections and gain set to optimal.

### **Monomer Synthesis.**

*Synthesis of 1,3-Di-Boc-guanidinopropyl acrylamide, GPAm<sup>diBoc</sup>.* 1,3-Bis(*tert*-butoxycarbonyl)-2-methyl-2-thiopseudourea (10.34 g,  $3.56 \times 10^{-2}$  moles) in dry DCM (85 mL) was added dropwise *via* a pressure-equalizing dropping funnel to a solution of 1,3-diaminopropane (7.99 g, 9.0 mL,  $1.08 \times 10^{-1}$  moles) in DCM (85 mL) in a 250 mL round-bottomed flask equipped with a magnetic stirring bar. Following complete addition, the reaction was left to stir at room temperature overnight. A white precipitate formed. Dry DCM (40 mL) was added, and the solution was filtered to remove the precipitate. The solution was washed with deionized H<sub>2</sub>O (3 × 200 mL) and brine (2 × 200 mL), the organic layer was dried over MgSO<sub>4</sub> and the DCM was removed under vacuum to yield crude 2-[1,3- Bis(*tert*-butoxycarbonyl)guanidine]ethylamine as a colourless, slightly turbid oil (12.40 g,  $3.92 \times 10^{-2}$  moles). The crude product was dissolved in dry DCM (200 mL) and transferred to a 500 mL two-necked round-bottomed-flask equipped with a magnetic stirring bar. Et<sub>3</sub>N (6.6 mL,  $4.74 \times 10^{-2}$  moles) was added, the flask was fitted with a pressure-equalising dropping funnel, sealed, purged with argon, and cooled in an ice bath. Acryloyl chloride (2.84 g, 3.20 mL,  $3.94 \times 10^{-2}$  moles) in dry DCM (40 mL) was added dropwise and the reaction was left to stir at room temperature overnight, to give a clear pale-yellow solution. Dry DCM (100 mL) was added, then saturated NaHCO<sub>3</sub> (400 mL) was added and the aqueous layer was extracted with DCM (3 × 3400 mL). The organic layers were dried over MgSO<sub>4</sub> and the solvent was removed under vacuum to give a viscous yellow oil, which was subjected to flash column chromatography

(silica, hexane/ethyl acetate) to afford 2-[1,3-Bis(*tert*-butoxycarbonyl)guanidine]propyl acrylamide as a white solid.  $^1\text{H}$  NMR (300 MHz, 300 K,  $\text{CDCl}_3$ ,  $\delta$ ): 11.44 (s, 1 H,  $-\text{NH}(-\text{N}=\text{C})-\text{NH}-$ ), 8.47 (t, 6.1 Hz, 1 H,  $-\text{CH}_2-\text{NH}-(\text{C}=\text{N}-)\text{NH}-$ ), 7.91 (t, 1 H,  $-\text{CH}_2-\text{NH}-(\text{C}=\text{O})-$ ), 6.30 (1 H,  $-(\text{C}=\text{O})-\text{CH}=\text{CH}_2$ ), 6.28 (d, 1 H,  $-(\text{C}=\text{O})-\text{CH}=\text{CH}_2$ ), 5.55 – 5.59 (dd, 1 H,  $-(\text{C}=\text{O})\text{CH}=\text{CH}_2$ ), 3.46 – 3.52 (m, 2 H,  $-\text{CH}_2-\text{NH}-(\text{C}=\text{N}-)\text{NH}-$ ), 3.30 – 3.36 (m, 2 H,  $-\text{CH}_2-\text{NH}-(\text{C}=\text{O})-$ ), 1.69 (m, 2 H,  $-\text{CH}_2-\text{CH}_2-\text{CH}_2-$ ), 1.49 (2  $\times$  s, 18 H,  $-\text{O}-\text{C}((\text{CH}_3)_3)$ ).  $^{13}\text{C}$  NMR (75 MHz, 300 K,  $\text{CDCl}_3$ ,  $\delta$ ): 131.8 ( $\text{CH}_2=\text{CH}-(\text{C}=\text{O})-$ ), 125.4 ( $\text{CH}_2=\text{C}-$ ), 37.1 ( $-\text{CH}_2-\text{NH}-(\text{C}=\text{O})-$ ), 34.8 ( $-\text{CH}_2-\text{NH}-(\text{C}=\text{N}-)\text{NH}-$ ), 29.7 ( $-\text{CH}_2-\text{CH}_2-\text{CH}_2-$ ), 28.3 ( $-\text{O}-\text{C}((\text{CH}_3)_3)$ ), 28.0 ( $-\text{O}-\text{C}((\text{CH}_3)_3)$ ). MS:  $[\text{M} + \text{H}]^+$  371.22 (calculated), 371.23 (found).

*Synthesis of N-tert-butoxycarbonyl-N'-acryloyl-1,2-diaminoethane (AEAm<sup>Boc</sup>)*. Ethylene diamine (30.02 g,  $5.00 \times 10^{-1}$  moles) was dissolved in dry DCM (280 mL) in a 500 mL round-bottomed-flask equipped with a magnetic stirring bar. The flask was fitted with a pressure-equalising dropping funnel, sealed, purged with argon, and cooled in an ice bath. Di-*tert*-butyl dicarbonate (27.6 g,  $1.25 \times 10^{-1}$  moles) in dry DCM (120 mL) added dropwise with stirring over 1 h. The reaction was allowed to reach room temperature and left to stir overnight. The resulting solution was filtered to remove precipitate, and concentrated under vacuum. Deionized  $\text{H}_2\text{O}$  (350 mL) added, and the solution was filtered to remove the resulting precipitate (*N,N'*-(bis-*tert*-butoxycarbonyl)-1,2-diaminoethane). The aqueous solution was saturated with NaCl, and extracted with EtOAc (3  $\times$  300 mL), the organic layers combined, dried over  $\text{MgSO}_4$  and concentrated under vacuum to yield *N-tert*-butoxycarbonyl-1,2-diaminoethane as a clear oil (14.39 g,  $8.985 \times 10^{-2}$  moles), which was dissolved in dry DCM (300 mL) and transferred to a 500 mL two-necked round-bottomed-flask equipped with a magnetic stirring bar.  $\text{Et}_3\text{N}$  (15.0 mL,  $1.08 \times 10^{-1}$  moles) was added, the flask was fitted with a pressure-equalizing dropping funnel, sealed,

purged with argon, and cooled in an ice bath. Acryloyl chloride (7.30 mL,  $8.96 \times 10^{-2}$  moles) in dry DCM (100 mL) was added dropwise and the reaction was left to stir at room temperature overnight. The solution was concentrated under vacuum, dissolved in deionized H<sub>2</sub>O (300 mL), and extracted with CHCl<sub>3</sub> (3 × 300 mL). The organic layers were combined, dried over MgSO<sub>4</sub> and concentrated under vacuum to give a white solid, which was subjected to flash column chromatography (silica, hexane/ethyl acetate) to afford *N-tert*-butoxycarbonyl-*N'*-acryloyl-1,2- as a white solid. <sup>1</sup>H NMR (300 MHz, 300 K, CDCl<sub>3</sub>, δ): 6.65 (br, 1 H, -NH-(C=O)CH=CH<sub>2</sub>), 6.22 – 6.28 (dd, 17.1 Hz, 1.4 Hz, 1 H, -NH-(C=O)CH=CH<sub>2</sub>), 6.05 – 6.14 (dd, 17.1 Hz, 10.1 Hz, 1 H, -NH-(C=O)CH=CH<sub>2</sub>), 5.60 – 6.64 (dd, 10.1 Hz, 1.6 Hz, 1 H, -NH-(C=O)CH=CH<sub>2</sub>), 5.11 (br, 1 H, -NH-(C=O)O-), 3.40 – 3.45 (m, 2 H, -CH<sub>2</sub>-NH-(C=O)CH=CH<sub>2</sub>), 3.27 – 3.32 (m, 2 H, -CH<sub>2</sub>-NH-(C=O)O-), 1.42 (s, 9 H, -O-C((CH<sub>3</sub>)<sub>3</sub>)). <sup>13</sup>C NMR (75 MHz, 300 K, CDCl<sub>3</sub>, δ): 130.9 (CH<sub>2</sub>=CH-(C=O)-), 126.3 (CH<sub>2</sub>=C-), 41.0 (-CH<sub>2</sub>-NH-(C=O)CH=CH<sub>2</sub>), 40.1 (-CH<sub>2</sub>-NH-(C=O)O-), 28.3 (-O-C((CH<sub>3</sub>)<sub>3</sub>)). MS: [M + H]<sup>+</sup> 237.13 (calculated), 237.12 (found).

### Calculations for RAFT Polymerization.

Monomer conversion (*p*) was calculated from <sup>1</sup>H NMR data by comparing the integrals of vinyl peaks (5.5-6.3 ppm) against an external reference (1,3,5-trioxane, 5.14 ppm) before (*t*=0) and after (*t*=final) polymerization. The theoretical number-average molar mass (*M*<sub>n,th</sub>) was then calculated using equation (6):

$$M_{n,th} = \frac{[M]_0 p M_M}{[CTA]_0} + M_{CTA} \quad (6)$$

Where [M]<sub>0</sub> and [M]<sub>0</sub> are the initial concentrations of monomer and chain transfer agent (CTA), respectively, *M*<sub>M</sub> and *M*<sub>CTA</sub> are the molecular weight of the monomer and CTA, respectively, and *p* is the monomer conversion.

**Table S1.** Amount of different substances used for polymerization of PGPAms and PAEAms.

Monomer	PGPAm <sub>8</sub>	PGPAm <sub>22</sub>	PGPAm <sub>43</sub>	PGPAm <sub>89</sub>	PGPAm <sub>94</sub>	PAEAms <sub>9</sub>	PAEAms <sub>24</sub>	PAEAms <sub>45</sub>	PAEAms <sub>96</sub>
$DP_{n,target}$	10	25	50	100	100	BocAEAm	BocAEAm	BocAEAm	BocAEAm
$n_{CTA}$ added (mg)	38.2	15.41	4.13*[a]	4.48	3.25[a]	68.4	27.0	6.12[a]	5.44[a]
$n_{CTA}$ added (moles)	$1.60 \times 10^{-4}$	$6.46 \times 10^{-5}$	$1.24 \times 10^{-5}$	$1.88 \times 10^{-5}$	$9.74 \times 10^{-6}$	$2.87 \times 10^{-4}$	$1.13 \times 10^{-4}$	$1.83 \times 10^{-5}$	$1.63 \times 10^{-5}$
$n_{monomer}$ added (mg)	597.7	599.9	230.7	700.6	362.7	600.2	602.4	194.2	348.6
$n_{monomer}$ added (moles)	$1.61 \times 10^{-3}$	$1.61 \times 10^{-3}$	$6.20 \times 10^{-4}$	$1.89 \times 10^{-3}$	$9.74 \times 10^{-4}$	$2.80 \times 10^{-3}$	$2.81 \times 10^{-3}$	$9.07 \times 10^{-4}$	$1.63 \times 10^{-3}$
$n_{V65b}$ added (mg)	3.18	3.23	0.65	3.01	0.515	5.40	2.90	0.63	0.42
$n_{V65b}$ added (moles)	$1.23 \times 10^{-5}$	$1.25 \times 10^{-5}$	$2.51 \times 10^{-6}$	$1.17 \times 10^{-5}$	$1.99 \times 10^{-6}$	$2.09 \times 10^{-5}$	$1.12 \times 10^{-5}$	$2.43 \times 10^{-6}$	$1.63 \times 10^{-6}$
Dioxane added (uL)	835.6	841.9	185.5	1029.4	540.9	949.9	951.1	283.4	563.7
DMAc added (uL)	375.9	365.8	430.6	428.5	222.3	420.8	369.6	297.8	269.8
PABTC/V65b	13.0	5.2	4.9	1.6	4.9	13.7	10.1	7.6	10.0
T (°C)	45	45	50	45	45	50	50	50	60
Time (min)	540	540	360	300	300	300	300	360	240



**Table S2.** Amount of different substances used for polymerization of PDMAEAm<sub>s</sub> and PDMAPEAm<sub>s</sub>.

Monomer	PDMAEAm <sub>8</sub>	PDMAEAm <sub>22</sub>	PDMAEAm <sub>45</sub>	PDMAEAm <sub>88</sub>	PDMAPEAm <sub>11</sub>	PDMAPEAm <sub>24</sub>	PDMAPEAm <sub>38</sub>	PDMAPEAm <sub>71</sub>
	DMAEAm	DMAEAm	DMAEAm <sup>[a]</sup>	DMAEAm <sup>[a]</sup>	DMAPEAm <sup>[a]</sup>	DMAPEAm <sup>[a]</sup>	DMAPEAm <sup>[a]</sup>	DMAPEAm <sup>[a]</sup>
DP <sub>n,target</sub>	10	25	49	99	14	30	50	99
m <sub>CTA</sub> added (mg)	67.1	25.1	8.25 <sup>[b]</sup>	5.97 <sup>[b]</sup>	50.3	19.9	7.49 <sup>[b]</sup>	5.33 <sup>[b]</sup>
n <sub>CTA</sub> added (moles)	$2.81 \times 10^{-4}$	$1.05 \times 10^{-4}$	$2.47 \times 10^{-5}$	$1.79 \times 10^{-5}$	$2.11 \times 10^{-4}$	$8.35 \times 10^{-5}$	$2.24 \times 10^{-5}$	$1.60 \times 10^{-5}$
m <sub>monomer</sub> added (mg)	400.7	371.8	174.0	252.2	461.0	383.3	175.5	248.9
n <sub>monomer</sub> added (moles)	$2.82 \times 10^{-3}$	$2.62 \times 10^{-3}$	$1.22 \times 10^{-3}$	$1.77 \times 10^{-3}$	$2.95 \times 10^{-3}$	$2.46 \times 10^{-3}$	$1.12 \times 10^{-3}$	$1.59 \times 10^{-3}$
m <sub>V65b</sub> added (mg)	5.77	3.05	1.21	0.93	5.07	2.11	1.16	0.85
n <sub>V65b</sub> added (moles)	$2.23 \times 10^{-5}$	$1.18 \times 10^{-5}$	$4.67 \times 10^{-6}$	$3.60 \times 10^{-6}$	$1.96 \times 10^{-5}$	$8.17 \times 10^{-6}$	$4.49 \times 10^{-6}$	$3.27 \times 10^{-6}$
Dioxane added (uL)	461.4	229.0	514.4	574.1	242.3	202.5	483.5	577.0
DMAc added (uL)	209.6	233.5	141.9	140.9	249.7	206.0	136.8	34.5
PABTC/V65b	12.6	8.9	5.3	5.0	10.8	10.2	5.0	4.9
T (°C)	60	60	50	60	60	60	50	60
Time (min)	240	240	420	240	240	240	420	240

[a] Monomer was not purified

[a] Polymerization using PBTC-NHS

### Typical Attachment of DY-635 to PAm Polymers.

New batches of polymers were used in each instance (Aq.-SEC, P2VP standards): PAEAm<sub>96</sub>,  $M_{n,SEC} = 12.8 \text{ kg mol}^{-1}$ ,  $\bar{D} = 1.16$ ; PGPAm<sub>94</sub>,  $M_{n,SEC} = 9.2 \text{ kg mol}^{-1}$ ,  $\bar{D} = 1.25$ ; PDMAEAm<sub>94</sub>,  $M_{n,SEC} = 10.3 \text{ kg mol}^{-1}$ ,  $\bar{D} = 1.26$ ; PDMAPAm<sub>111</sub>,  $M_{n,SEC} = 11.9 \text{ kg mol}^{-1}$ ,  $\bar{D} = 1.51$ . The respective polymer, a 2 mg mL<sup>-1</sup> solution of DY-635 amine in HPLC grade DMF, a 2 mg mL<sup>-1</sup> solution of HBTU in HPLC grade DMF and a 2 mg mL<sup>-1</sup> solution of NMM in HPLC grade DMF were added to a screw-cap vial equipped with a magnetic stirring bar (Table S3). The reaction was left to stir in the dark for 24 h. The solution was diluted in ultrapure water and dialyzed against first H<sub>2</sub>O/MeOH (4/1) for 2 days and then against H<sub>2</sub>O for 3 days. The polymer was obtained as a blue solid following lyophilization. For PDMAEAm<sub>94</sub>, a 5 mg mL<sup>-1</sup> solution of DY-635 amine and a 1 mg mL<sup>-1</sup> solution of NMM were used. Regarding dye attachment to PAEAm<sub>96</sub>, the DY-635 NHS-ester was used.

**Table S3.** Amount of different substances used for attachment to DY-635 amine to PAmS

Substance	Mass mg	Amount of substance mol
<b>PGPAm<sub>94</sub></b>	39.6	$1.35 \times 10^{-6}$
DY-635-Amine	0.99	$1.39 \times 10^{-6}$
HBTU	0.84	$2.02 \times 10^{-6}$
NMM	0.41	$4.04 \times 10^{-6}$
<b>PAEAm<sub>96</sub></b>	29.0	$1.31 \times 10^{-6}$
DY-635-NHS	0.99	$1.35 \times 10^{-6}$
NMM	0.40	$3.93 \times 10^{-6}$
<b>PDMAEAm<sub>94</sub></b>	21.3	$1.57 \times 10^{-6}$
DY-635-Amine	1.16	$1.57 \times 10^{-6}$
HBTU	0.97	$2.35 \times 10^{-6}$
NMM	0.48	$4.7 \times 10^{-6}$
<b>PDMAPAm<sub>111</sub></b>	22.7	$1.34 \times 10^{-6}$
DY-635-Amine	0.99	$1.34 \times 10^{-6}$
HBTU	0.83	$2.02 \times 10^{-6}$
NMM	0.41	$4.03 \times 10^{-6}$

### N\*/P Ratio Calculations.

The N\*/P ratio was defined as the ratio of the total amount of protonatable amines in polymer solution in relation to the total amount of phosphates in the pDNA solution.

The volume of polymer needed to prepare polyplexes with 15  $\mu\text{g mL}^{-1}$  pDNA at different N\*/P ratios was calculated as described by the following equations:

$$V_{\text{total}} \cdot P = V_{\text{poly}} \cdot N_{\text{poly}}$$

$$V_{\text{poly}} = \frac{V_{\text{total}} \cdot P}{N_{\text{poly}}}$$

$$V_{\text{poly}} = V_{\text{total}} \cdot \frac{n_{\text{pDNA}} \cdot P}{n_{\text{poly}} \cdot N}$$

$$V_{\text{poly}} = V_{\text{total}} \cdot \frac{m_{\text{pDNA}} \cdot P \cdot M_{\text{poly}}}{m_{\text{poly}} \cdot N \cdot M_{\text{pDNA}}}$$

Where  $V_{\text{total}}$ ,  $P$ ,  $V_{\text{poly}}$  and  $N_{\text{poly}}$  are the total required volume, the total number of phosphates of the pDNA, the required volume of polymer and the total number of active amines of the polymer, respectively.

### Heparin dissociation assay.

**Table S4.** Kinetic cycle protocol for automated heparin addition by the microplate reader

Kinetic cycle	Repetitions	Addition of heparin		Orbital shake	Incubation	Measurement
		V / $\mu\text{L}$	Stock Solution / $\text{U mL}^{-1}$			
1	2	5	100	10 s	10 min, 37°C	$\lambda_{\text{Ex}} = 525 \text{ nm} / \lambda_{\text{Em}} = 605 \text{ nm}$
2	1	15	100	10 s	10 min, 37°C	$\lambda_{\text{Ex}} = 525 \text{ nm} / \lambda_{\text{Em}} = 605 \text{ nm}$
3	3	5	500	10 s	10 min, 37°C	$\lambda_{\text{Ex}} = 525 \text{ nm} / \lambda_{\text{Em}} = 605 \text{ nm}$
4	1	10	500	10 s	10 min, 37°C	$\lambda_{\text{Ex}} = 525 \text{ nm} / \lambda_{\text{Em}} = 605 \text{ nm}$

The heparin concentration needed to release the maximum of pDNA was calculated with OriginPro, Version 2018b (OriginLab Corporation, US) using a piecewise linear function with three segments fitted to the respective data ( $n \geq 3$ ) of each polymer, keeping the value of the first and third slopes constant at 0 (Figure S1). The values for the heparin concentration ( $x_{i2}$ ) required to release maximum pDNA ( $a_3$ ) were read off the equation.

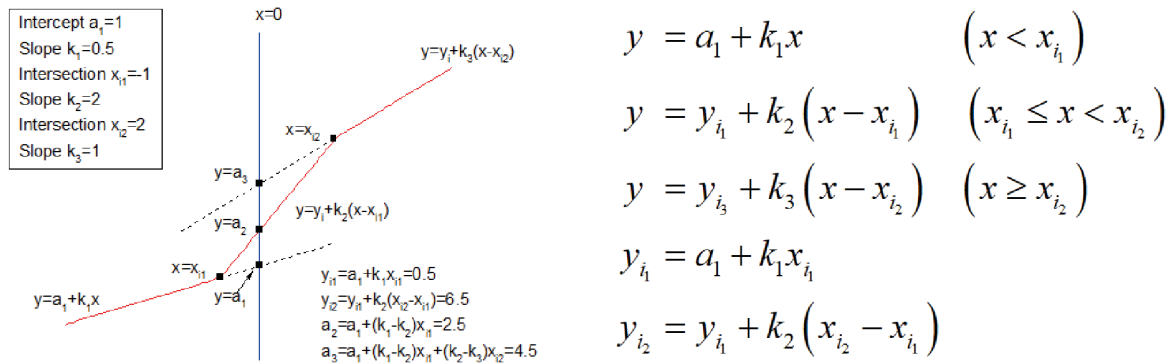


**Figure S1.** Equations used by OriginPro, Version 2018b to provide the piecewise linear fit functions for the polymers. Screenshots taken from the software.

### Dynamic Light Scattering.

The size (diameter) of the polyplexes was investigated by dynamic light scattering (DLS). The polyplexes were prepared at N\*/P 30 in 100  $\mu$ L HBG buffer as described above. Measurements were conducted on a Zetasizer Nano ZS (Malvern Instruments, Germany) with a He–Ne laser operating at a wavelength of 633 nm. Each sample was measured in quintuplicates with three runs of 30 s at 25  $^{\circ}$ C after an equilibration time of 30 s. The counts were detected at an angle of 173 $^{\circ}$ . The mean particle size was approximated as the effective (z-average) diameter and the width of the distribution as the polydispersity index of the particles (PDI) obtained by the cumulants method assuming a spherical shape. Data are expressed as mean  $\pm$  SD of two independent determinations.

### Determination of Cytotoxicity in HEK293T Cells.

The HEK293T cells were seeded at  $10^5$  cells per well in a 24-well plate and incubated in medium containing 10 mM HEPES for 24 h. 1 h after medium change, cells were treated with polymers at concentrations equal to N\*/P 30 and incubated for additional 4 h. Cells on the same plate incubated with 10% (v/v) in growth medium served as non-treated controls. The medium was replaced by a 10% (v/v) alamarBlue<sup>TM</sup> solution in fresh culture medium, prepared according to the manufacturer's instructions. Following an incubation for 4 h at 37  $^{\circ}$ C, the fluorescence was

measured at  $\lambda_{\text{Ex}} = 570$  /  $\lambda_{\text{Em}} = 610$  nm. The non-treated control cells were referred to as 100 % viability. Values below 70 % were regarded as cytotoxic. Data are expressed as mean  $\pm$  SD of at least three independent determinations.

### **Determination of CC<sub>50</sub> and Cell Viability at N\*/P 30.**

With OriginPro, version 2018b a logistic function was fitted to the data of each polymer with the following equation (7):

$$y = \frac{A_1 - A_2}{1 + (x/x_0)^p} + A_2 \quad (7)$$

Where  $A_1$  and  $A_2$  are the initial and the final values, respectively,  $x_0$  is the center and  $p$  is the power of the curve. For polymers reaching  $\geq 50\%$  toxicity,  $A_1$  and  $A_2$  were kept constant at 1 and 0, respectively. For polymers not reaching 50% toxicity,  $A_2$  and  $p$  were kept constant at 0 and 1.5, respectively. With the obtained equations, the “polymer concentration needed to kill 50% of the cells” (CC<sub>50</sub>) or the “cell viability at N\*/P 30” were calculated by substituting  $y$  with 50 or  $x$  with the concentration of the respective polymer at N\*/P 30, respectively.

### **Polyplex Uptake with CLSM and Image Processing.**

For uptake studies *via* confocal laser scanning microscopy (CLSM), HEK293T cells were seeded and cultured as described above in glass-bottomed dishes (CellView cell culture dishes with four compartments, Greiner Bio-One) and analyzed following incubation with polyplexes containing YOYO-1 labeled pDNA (0.31 nmol per 1  $\mu$ g pDNA) and indicated polymers for 4 h. To image intracellular distribution in living cells, Hoechst 33342 was added for 10 min to stain cell nuclei. Prior to imaging, trypan blue was added to a final concentration of 0.04% to quench fluorescence of YOYO-1 outside the cells. Live cell imaging was performed using a LSM880, Elyra PS.1 system (Zeiss, Germany) applying the argon laser for excitation at 488 nm (0.2%) and 405 nm

(0.5%), emission filters for 410-479 nm (Hoechst) and 508-553 nm (YOYO-1) with gains of 750 and 800, respectively. For magnification, a  $40 \times 1.4$  NA plan apochromat oil objective was applied. Images were acquired using the ZEN software, version 2.3 SP1 (Zeiss, Germany). The experiments were performed at least twice. All images were processed in batch mode using ImageJ, version 1.52.<sup>4</sup> They were resized with a scaling factor of 2 in x- and y-dimension and bicubic interpolation. Regarding the Hoechst-channel, the images were processed as follows: The background was corrected using the rolling ball background subtraction tool applying a sliding paraboloid with a radius of 23.5 pixels without previous image smoothing. The contrast was enhanced automatically with a normalization of 0.01% saturation. For YOYO-1 fluorescence, only the background was corrected applying a sliding paraboloid with a radius of 7 pixels following image smoothing. For the overlay image, both channels were merged.

#### **Lactate Dehydrogenase Release (LDH) Assay.**

To analyze membrane interactions of the polymers with HEK293T cells, the LDH release assay was performed using the CytoTox-ONE™ assay (Promega, Germany) according to the manufacturer's instructions. Briefly, cells were seeded at a density of  $10^5$  cells per well in 24-well plates and treated with polyplexes as described for uptake studies (including YOYO-1 for pDNA staining, having no influence on the performed assay, see Figure S16). Following incubation for 4 h, while cells were used to analyze uptake efficiency *via* flow cytometry, the supernatant was transferred to a new 96-well plate as a triplicate and allowed to cool down to room temperature. Subsequently, the substrate mixture including assay buffer was added and incubated at room temperature for 10 min. After the addition of the stop solution fluorescence intensity was measured at  $\lambda_{\text{Ex}} = 560 \text{ nm}$  /  $\lambda_{\text{Em}} = 590 \text{ nm}$ . For the positive control (100 % LDH release), cells were incubated with 0.2% Triton X-100 for 30 min prior to analysis. Cells incubated with only pDNA

and YOYO-1 were used as negative control (0% LDH release). The LDH release of the polymers was calculated as follows (8):

$$\text{LDH release} / \% = \frac{F_{\text{Sample}} - F_0}{F_{\text{Positive control}} - F_0} \cdot 100 \quad (8)$$

Where  $F_{\text{sample}}$ ,  $F_0$ , and  $F_{\text{Positive control}}$  represent the fluorescence intensity of a given sample, medium without cells, and of the Triton X-100 treated cells, respectively.

## FURTHER RESULTS

### Characterization of Polymers.

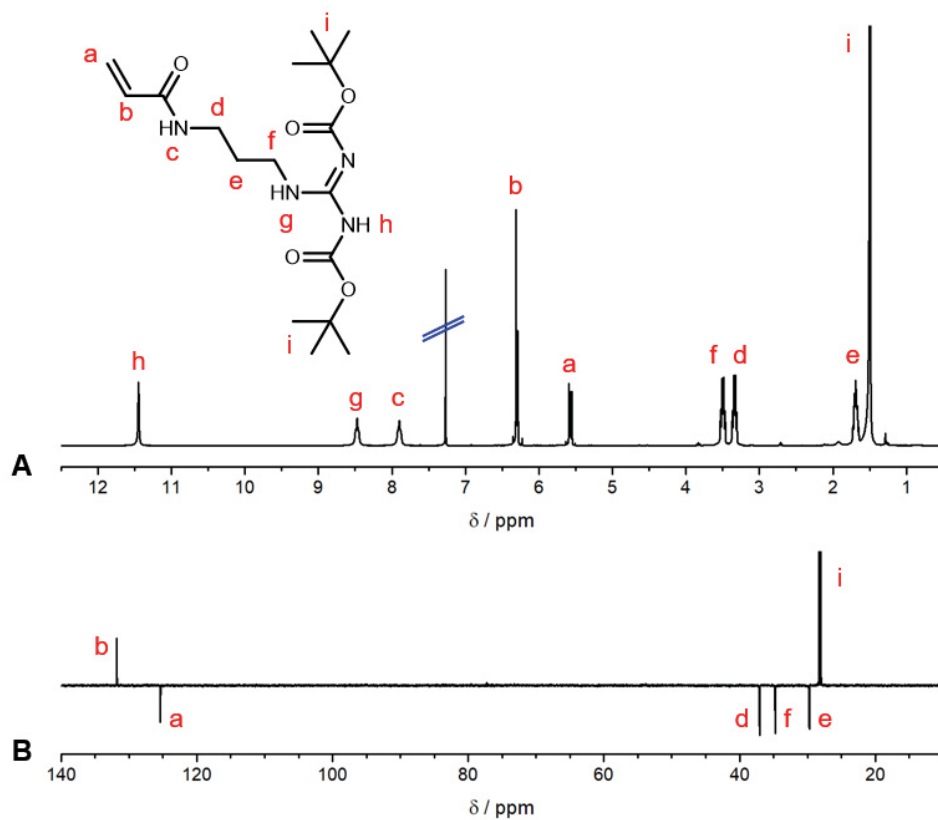


**Figure S2.** NMR spectra of GPAm<sup>diBoc</sup>.

<sup>1</sup>H (A) and DEPT <sup>13</sup>C (B) NMR spectra of GPAm<sup>diBoc</sup> in CDCl<sub>3</sub>.



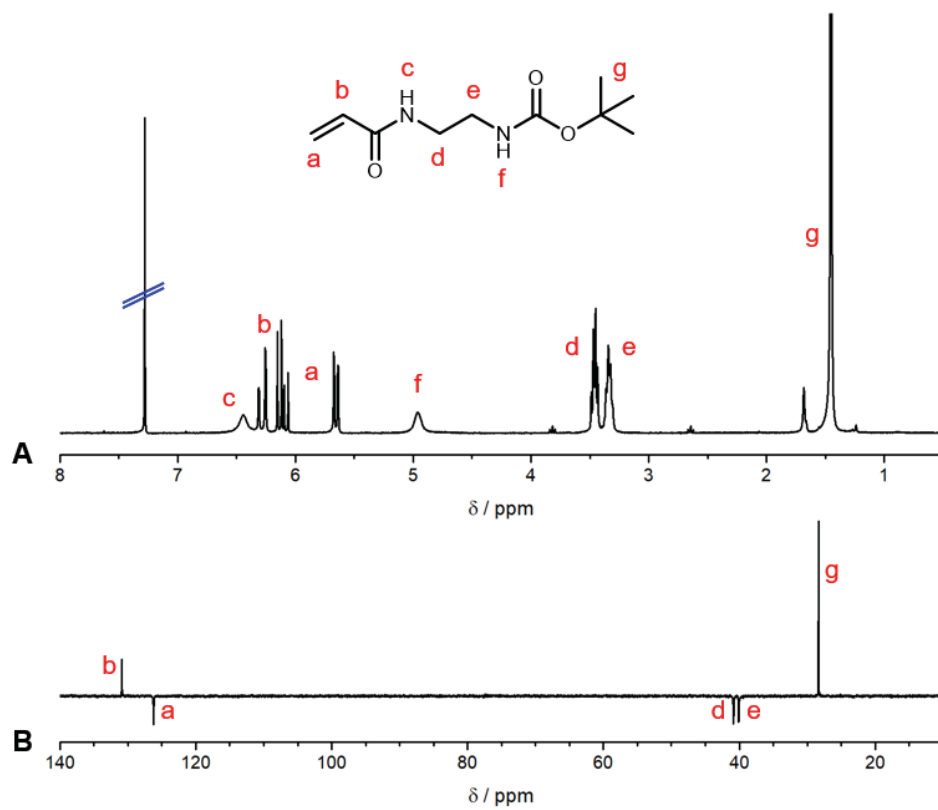


**Figure S3.** NMR spectra of AEAm<sup>Boc</sup>.

<sup>1</sup>H (A) and DEPT <sup>13</sup>C (B) NMR spectra of AEAm<sup>Boc</sup> in CDCl<sub>3</sub>.

**Table S5.** Summary of (protected) cationic homopolymers prepared *via* RAFT polymerization.

Polymer	DP <sub>n</sub> [a]	Protected polymers		
		M <sub>n,th</sub> [b]	M <sub>n,SEC</sub> [c]	Đ [c]
(kg mol <sup>-1</sup> )				
PGPAm <sub>8</sub>	8	3.3	5.1	1.11
PGPAm <sub>22</sub>	22	8.4	9.9	1.11
PGPAm <sub>43</sub>	43	16.2	14.7	1.22
PGPAm <sub>94</sub>	94	35.0	27.4	1.31
PAEAm <sub>9</sub>	9	2.2	4.3	1.11
PAEAm <sub>24</sub>	24	5.4	8.3	1.11
PAEAm <sub>45</sub>	45	9.9	16.1	1.09
PAEAm <sub>96</sub>	96	20.8	26.3	1.15
PDMAEAm <sub>8</sub>	8	-	-	-
PDMAEAm <sub>22</sub>	22	-	-	-
PDMAEAm <sub>45</sub>	45	-	-	-
PDMAEAm <sub>88</sub>	88	-	-	-
PDMAPAm <sub>11</sub>	11	-	-	-
PDMAPAm <sub>24</sub>	24	-	-	-
PDMAPAm <sub>38</sub>	38	-	-	-
PDMAPAm <sub>71</sub>	71	-	-	-

[a] Determined *via* <sup>1</sup>H NMR.  
[b] Determined using equation 6.  
[c] Determined *via* DMAc-SEC with PMMA standards.

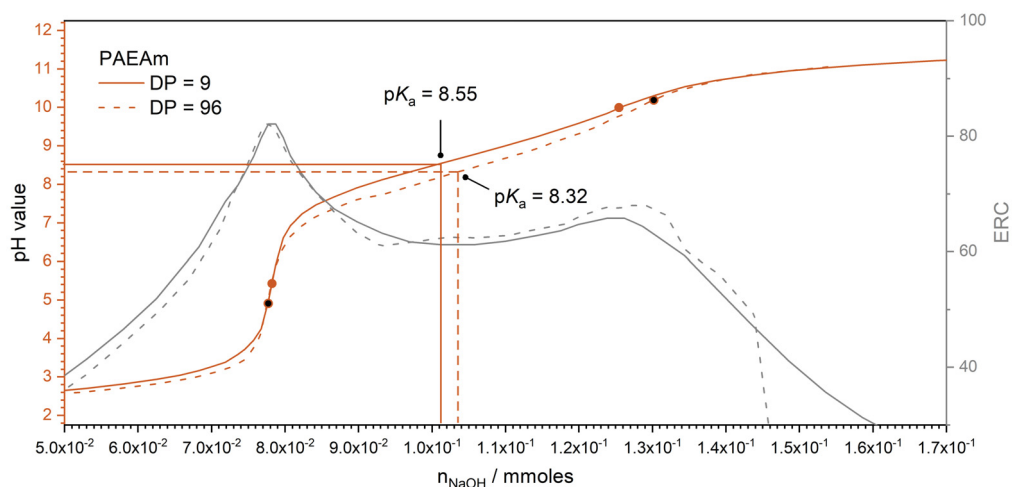


**Figure S4.** Titration curves and equivalence point recognition criterion for titrations of PAEAm polymers.

Polymers were dissolved at  $1 \text{ mg mL}^{-1}$  in  $125 \text{ mM NaCl}$  and titrated against  $0.1 \text{ M NaOH}$  up to pH 11. A new batch of PAEAm (PAEAm<sub>96</sub>, Aq.-SEC, P2VP standards:  $M_{n,SEC} = 12.8 \text{ kg mol}^{-1}$ ,  $\bar{D} = 1.16$ ) was used in this case.

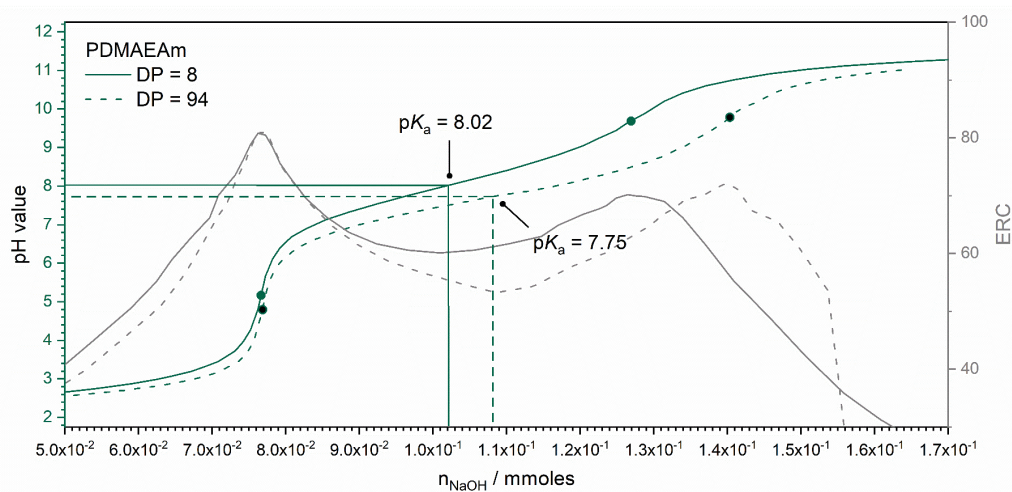


**Figure S5.** Titration curves and equivalence point recognition criterion for titrations of PDMAEAm polymers.

Polymers were dissolved at  $1 \text{ mg mL}^{-1}$  in  $125 \text{ mM NaCl}$  and titrated against  $0.1 \text{ M NaOH}$  up to pH 11. A new batch of PDMAEAm (PDMAEAm<sub>94</sub>, Aq.-SEC, P2VP standards:  $M_{n,SEC} = 10.3 \text{ kg mol}^{-1}$ ,  $\bar{D} = 1.26$ ) was used in this case.

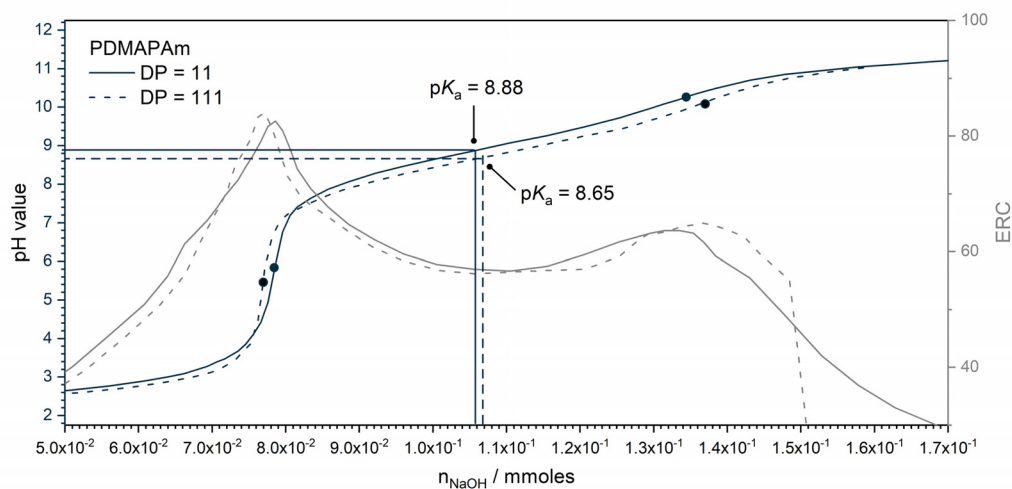


**Figure S6.** Titration curves and equivalence point recognition criterion for titrations of PDMAPAm polymers.

Polymers were dissolved at  $1 \text{ mg mL}^{-1}$  in  $125 \text{ mM NaCl}$  and titrated against  $0.1 \text{ M NaOH}$  up to pH 11. A new batch of PDMAPAm (PDMAPAm<sub>111</sub>, Aq.-SEC, P2VP standards:  $M_{n,SEC} = 11.9 \text{ kg mol}^{-1}$ ,  $D = 1.51$ ) was used in this case.

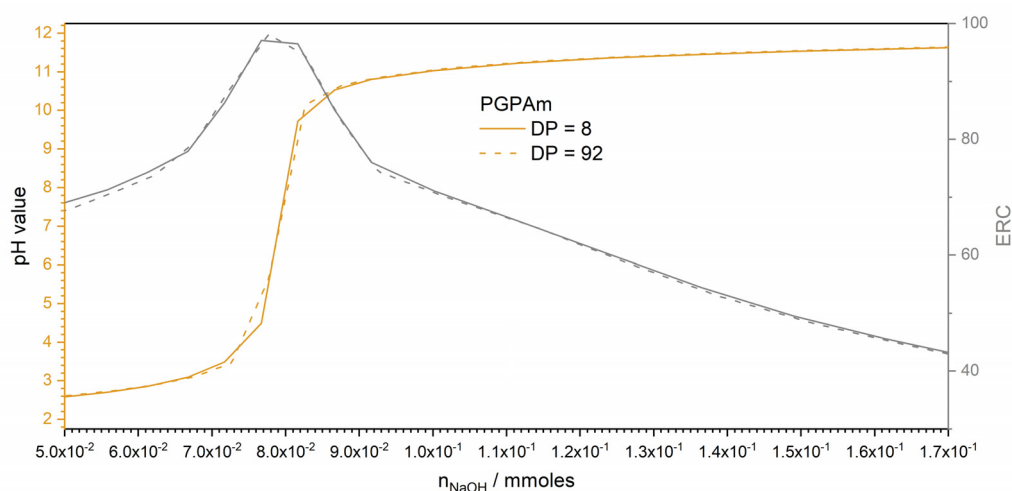


**Figure S7.** Titration curves and equivalence point recognition criterion for titrations of PGPAm polymers.

Polymers were dissolved at  $1 \text{ mg mL}^{-1}$  in  $125 \text{ mM NaCl}$  and titrated against  $0.5 \text{ M NaOH}$  up to pH 12. A new batch of PGPAm (PGPAm<sub>92</sub>, Aq.-SEC, P2VP standards:  $M_{n,SEC} = 10.6 \text{ kg mol}^{-1}$ ,  $D = 1.24$ ) was used in this case.

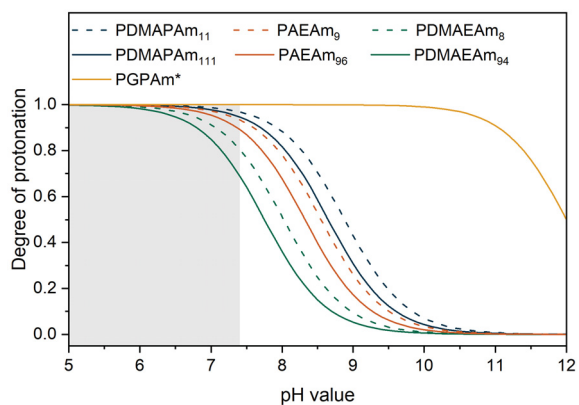


**Figure S8.** Theoretical determination of the degree of protonation.

The pH for the cationic polymer library based on their  $pK_a$  values calculated using the Henderson–Hasselbalch equation (1). Since the  $pK_a$  of PGPAm could not be determined the curve is generated assuming a  $pK_a$  of 12. The grey region designates the physiologically relevant pH window.

## Biological Results.

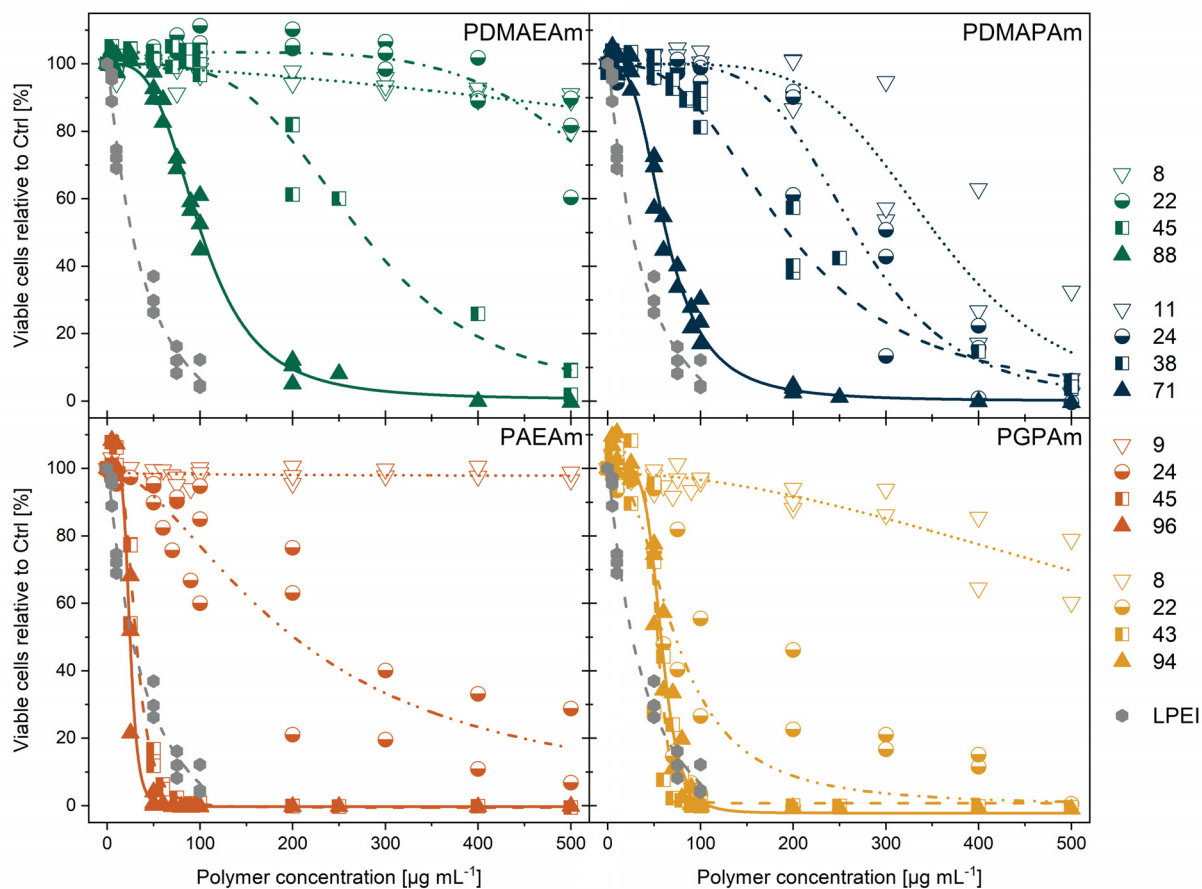


**Figure S9.** Cytotoxicity of PAM homopolymers in L929 cells.

Metabolic activity was measured in L929 cells using the alamarBlue™ assay following incubation with (A) PDMAEAm, (B) PDMAPAm, (C) PAEAm, (D) PGPAm polymers at indicated concentrations for 24 h. Dots represent values of single repetitions and lines represent logistic fit functions calculated via OriginPro ( $n = 3$ ).

**Table S6.** Toxicity and concentration at N\*/P 30 and CC<sub>50</sub> values calculated *via* non-linear fit.

ID	DP	Viability at N*/P 30 / % (c in $\mu\text{g mL}^{-1}$ )	CC <sub>50</sub> / $\mu\text{g mL}^{-1}$
PAEAm	9	99 (19)	> 500
	24	99 (17)	201.27
	45	93 (16)	30.92
	96	95 (16)	24.59
PDMAEAm	8	99 (23)	> 500
	22	105 (21)	> 500
	45	100 (20)	274.26
	88	100 (20)	101.22
PDMAPAm	11	100 (24)	353.24
	24	100 (22)	267.26
	38	100 (22)	194.31
	71	96 (22)	62.80
PGPAm	8	99 (27)	> 500
	22	92 (25)	72.93
	43	100 (24)	53.72
	94	99 (24)	57.41
PEI	600	88 (6)	22.73

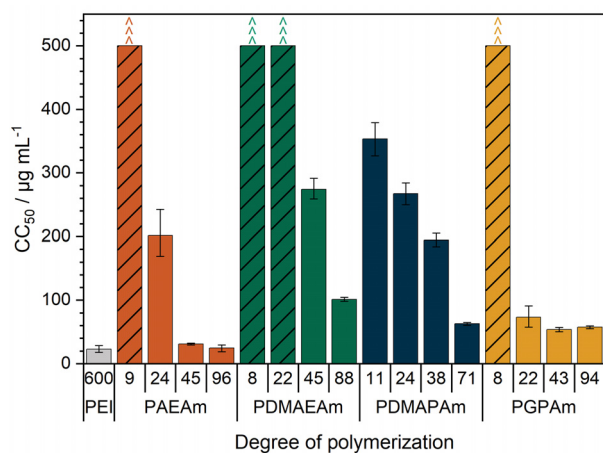


**Figure S10.** Cytotoxicity of PAm homopolymers of different DP and amino group. Metabolic activity was measured in L929 cells after 24 h incubation with PAm polymers at indicated concentrations (Figure S8) using the alamarBlue™ assay. Values represent CC<sub>50</sub> values calculated after fitting the resulting toxicity values to a logistic function  $\pm$  95% CI (n = 3). Upwards pointing arrows and striped columns indicate CC<sub>50</sub> values above 500  $\mu\text{g mL}^{-1}$ .

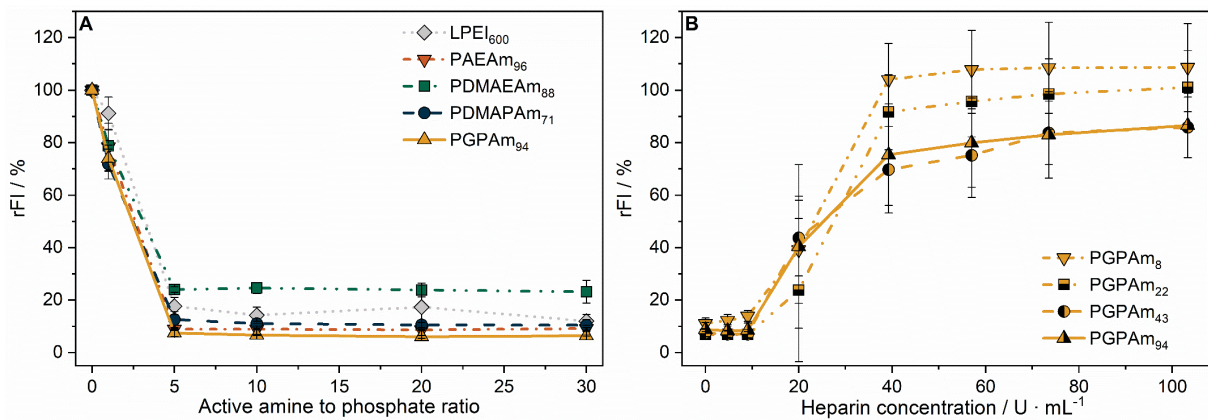


**Figure S11.** Polyplex formation and stability tests with pCMV-GFP pDNA and PAM homopolymers.

(A) EBA of polymers with highest DP at different N\*/P ratios in HBG buffer showing strong pDNA binding of all polymers. Values represent mean  $\pm$  SD ( $n \geq 3$ ). (B) HRA of polyplexes formed with P(GPAm) polymers at N\*/P 30 using heparin as a competing polyanion showing the reversible binding of the polyplex. Values represent mean  $\pm$  SD ( $n \geq 3$ ).

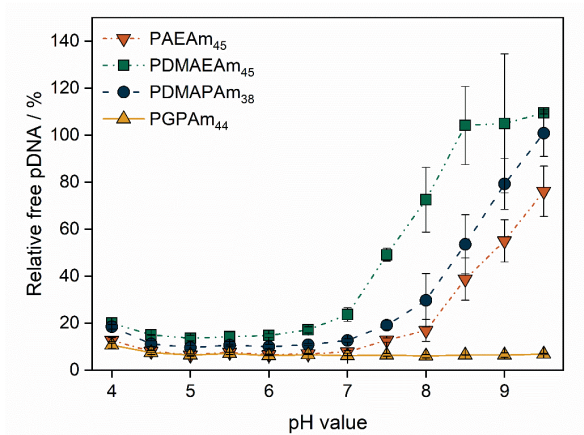


**Figure S12.** Polyplex formation with pCMV-GFP pDNA and polyacrylamide-homopolymers at different pH values.

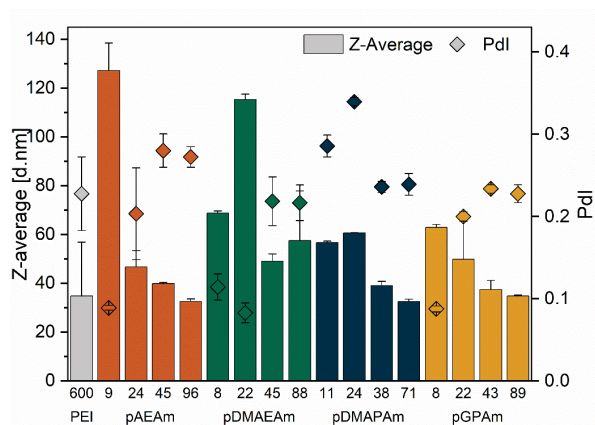
EBA of polymers with second highest DP at N\*/P 30 in HBG buffer of different pH showing a good pDNA binding of all polymers from pH 4 to pH 7 but differences between the polymers at pH > 7. Values represent mean  $\pm$  SD ( $n \geq 2$ ).



**Table S7.** Size determination of formed polyplexes via DLS.

Polyplexes were formed using  $15 \mu\text{g mL}^{-1}$  DNA at N\*/P ratio of 30 in HBG buffer.

Polymer	DP	Z-Average (d / nm)	PdI	Main peak (d / nm)	Intensity-weighted % of main peak
PAEAm	9	$127 \pm 11$	$0.09 \pm 0.00$	$135 \pm 13$	$100 \pm 0$
	24	$47 \pm 7$	$0.20 \pm 0.06$	$54 \pm 6$	$98 \pm 2$
	45	$40 \pm 0$	$0.28 \pm 0.02$	$43 \pm 1$	$92 \pm 3$
	96	$33 \pm 1$	$0.27 \pm 0.01$	$44 \pm 1$	$92 \pm 8$
PDMAEAm	8	$69 \pm 1$	$0.11 \pm 0.02$	$73 \pm 2$	$100 \pm 0$
	22	$115 \pm 2$	$0.08 \pm 0.01$	$123 \pm 5$	$100 \pm 0$
	45	$49 \pm 3$	$0.22 \pm 0.03$	$58 \pm 3$	$100 \pm 0$
	88	$58 \pm 20$	$0.22 \pm 0.02$	$66 \pm 23$	$96 \pm 3$
PDMAPAm	11	$57 \pm 1$	$0.29 \pm 0.01$	$61 \pm 2$	$89 \pm 4$
	24	$61 \pm 0$	$0.34 \pm 0.01$	$71 \pm 7$	$54 \pm 3$
	38	$39 \pm 2$	$0.24 \pm 0.01$	$51 \pm 0$	$87 \pm 1$
	71	$32 \pm 1$	$0.24 \pm 0.01$	$39 \pm 1$	$87 \pm 1$
PGPAm	8	$63 \pm 1$	$0.09 \pm 0.00$	$68 \pm 2$	$100 \pm 0$
	22	$50 \pm 18$	$0.20 \pm 0.01$	$58 \pm 19$	$100 \pm 0$
	43	$37 \pm 4$	$0.23 \pm 0.01$	$46 \pm 6$	$100 \pm 0$
	89	$35 \pm 0$	$0.23 \pm 0.01$	$42 \pm 1$	$99 \pm 1$
PEI	600	$59 \pm 22$	$0.25 \pm 0.04$	$60 \pm 11$	$82 \pm 1$

**Figure S13.** Size determination of formed polyplexes of PAm library of different DP *via* DLS.

Polyplexes were formed using  $15 \mu\text{g mL}^{-1}$  DNA at N\*/P ratio of 30 in HBG buffer.

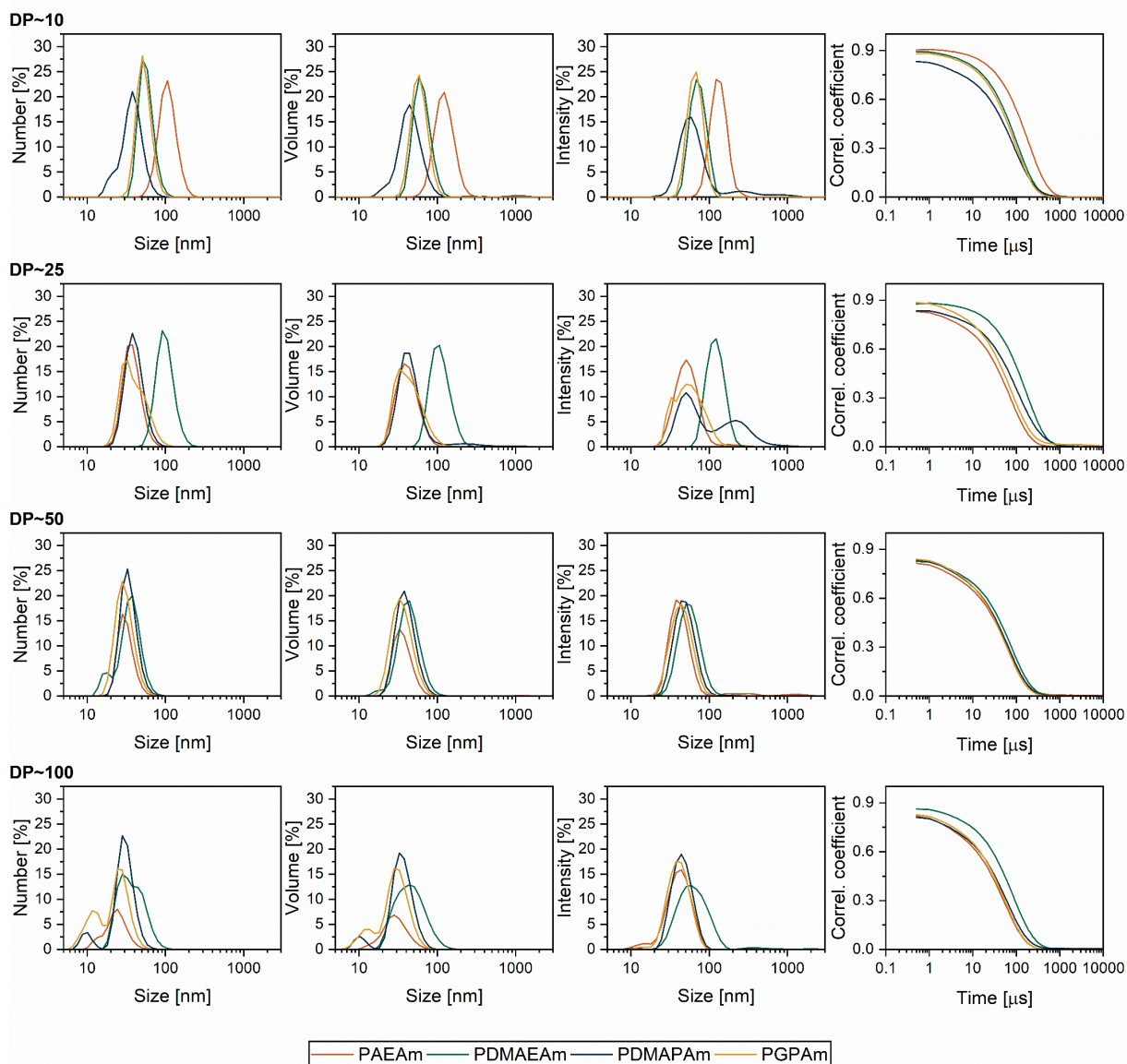


**Figure S14.** DLS traces of polyplexes formed with PAM polymers and  $15 \mu\text{g mL}^{-1}$  DNA at N\*/P 30 in HBG buffer.

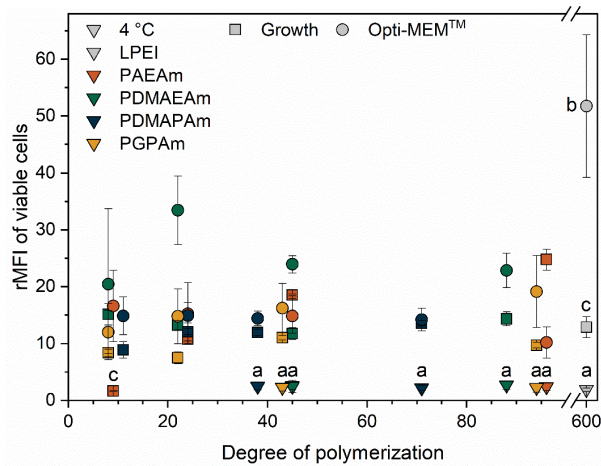


**Figure S15.** Influence of degree of polymerization on polyplex uptake in HEK293T cells.

Flow cytometry following incubation with polyplexes of YOYO-1-labeled pDNA and polymers at N\*/P 30. Incubation was in growth medium at 37°C for 4 h (G), in serum-reduced Opti-MEM™ at 37 °C for 4 h (OM) or in growth medium at 4 °C for 4 h (4 °C). Cells incubated with labeled pDNA served as control (rMFI = 1). Values represent mean ± SD (n ≥ 3). a: significant difference to the same polymer in G, b: significant difference to all polymers in OM, c: significant difference to same polymer in OM ( $p < 0.001$ )

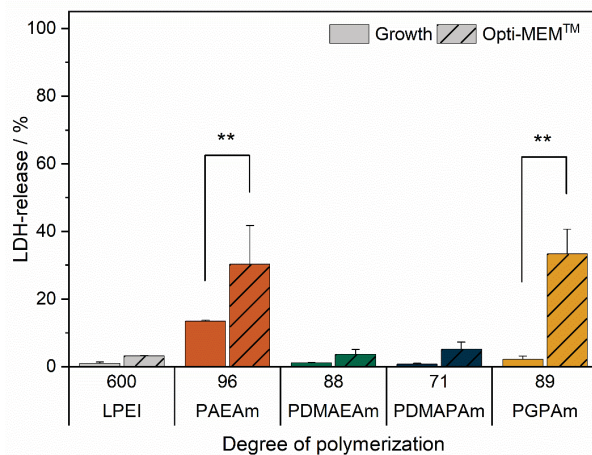


**Figure S16.** LDH release assay with PAm polyplexes in HEK293T cells.

Cells were incubated with YOYO-1 labeled polyplexes at N\*/P 30 in growth medium or Opti-MEM™ for 4 h. Values represent mean ± SD (n ≥ 1). \*\*: significant difference ( $p < 0.001$ ).

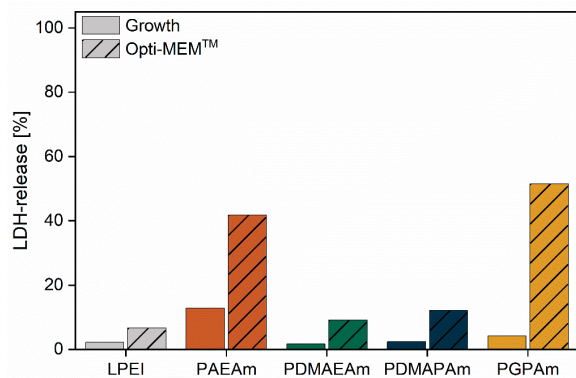


**Figure S17.** LDH release assay with HEK293T cells.

Cells were incubated with polyplexes (not labeled) at N\*/P 30 in growth medium or Opti-MEM™ for 4 h and showed no difference to the results with YOYO-1 labeled polyplexes. Determination was performed once.

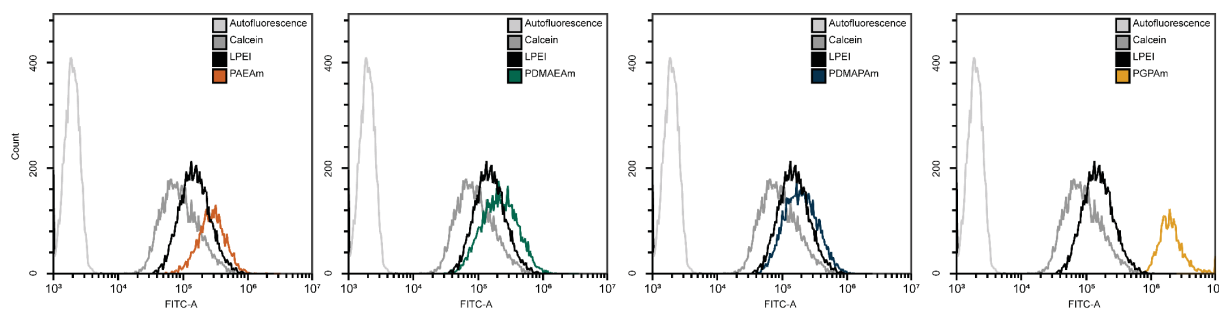


**Figure S18.** Flow cytometry analysis of calcein release assay.

Representative plots of the calcein channel following flow cytometry of HEK293T cells incubated with the respective polymers at equal amine concentrations ( $\cong$  N\*/P 30) in Opti-MEM™ for 4 h.

**Table S8.** Data used for determination of the squared Pearson's correlation coefficient ( $R^2$ ).

Title of factor in correlation graph	Data
Transfection	Viable EGFP-fluorescent HEK293T cells in Opti-MEM in %
Molar mass <sup>a</sup>	Theoretical molar mass without counter ion in g mol <sup>-1</sup>
Cationic moiety <sup>b</sup>	C/N ratio of the different amine moieties (3 for tertiary amines, 1 for primary amines, 0.6 for guanidinium)
Toxicity <sup>b</sup>	CC <sub>50</sub> values in µg mL <sup>-1</sup> polymer following 24 h incubation in L929 cells
pDNA-binding <sup>b</sup>	Results of EBA as rFI at N*/P 30
pDNA-release <sup>b</sup>	Heparin concentration needed to release maximum amount of DNA at N*/P 30 in U/mL
Uptake <sup>b</sup>	rMFI values of viable HEK293T cells following 4 h incubation in Opti-MEM
Hemolysis <sup>b</sup>	Hemolysis in % of positive control Triton X-100 at pH 6
Aggregation <sup>b</sup>	Negative control PBS relative to respective polymer at pH 6
LDH release <sup>b</sup>	Mean of LDH release in Opti-MEM in % of positive control Triton X-100
Calcein-release <sup>b</sup>	Viable calcein-fluorescent HEK293T cells in Opti-MEM in %
pDNA-binding <sup>b</sup>	Results of EBA as rFI at N*/P 30
BMP-binding <sup>b</sup>	rFI values of lipid-polymer-binding assay at BMP-concentration of 1 mM

[a] Data of all PAm polymers were considered

[b] Only data of longest PAm polymers were considered.

## REFERENCES

1. L. J. Hobson and W. J. Feast, *Polymer*, 1999, **40**, 1279-1297.
2. A. Kuroki, P. Sangwan, Y. Qu, R. Peltier, C. Sanchez-Cano, J. Moat, C. G. Dowson, E. G. L. Williams, K. E. S. Locock, M. Hartlieb and S. Perrier, *ACS Appl. Mater. Interfaces*, 2017, **9**, 40117-40126.
3. S. C. Larnaudie, J. C. Brendel, K. A. Jolliffe and S. Perrier, *J. Polym. Sci., Part A: Polym. Chem.*, 2016, **54**, 1003-1011.
4. J. Schindelin, I. Arganda-Carreras, E. Frise, V. Kaynig, M. Longair, T. Pietzsch, S. Preibisch, C. Rueden, S. Saalfeld, B. Schmid, J.-Y. Tinevez, D. J. White, V. Hartenstein, K. Eliceiri, P. Tomancak and A. Cardona, *Nat. Methods*, 2012, **9**, 676.



### Publication Pub3

## Correlation between protonation of tailor-made polypiperazines and endosomal escape for cytosolic protein delivery

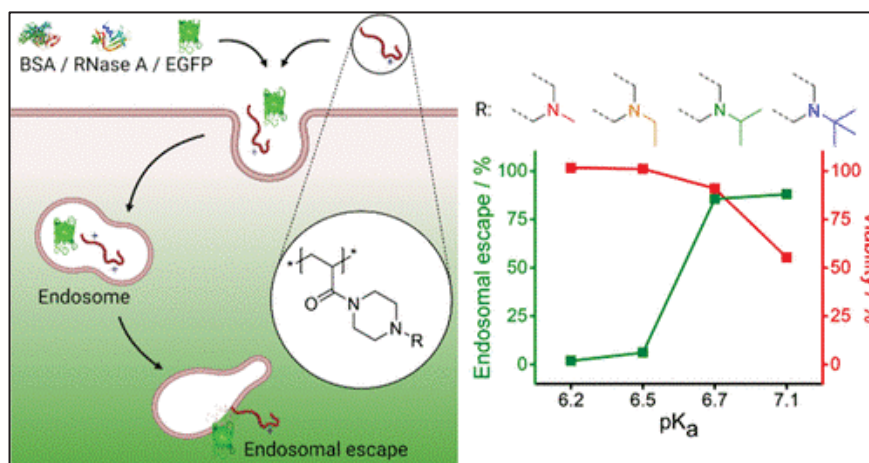
F. Hausig, F. H. Sobotta, D. O. Harz, F. Richter, A. Traeger, J. C. Brendel

*ACS App. Mater. Inter.* **2021**, 13, 35233-35247

Reproduced with permission of The American Chemical Society. Copyright © 2021.

The article and the supporting information are available online:

[doi.org/10.1021/acsami.1c00829](https://doi.org/10.1021/acsami.1c00829)



# Correlation between Protonation of Tailor-Made Polypiperazines and Endosomal Escape for Cytosolic Protein Delivery

Franziska Hausig, Fabian H. Sobotta, Friederike Richter, Dominic O. Harz, Anja Traeger, and Johannes C. Brendel\*



Cite This: *ACS Appl. Mater. Interfaces* 2021, 13, 35233–35247



Read Online

ACCESS |



Metrics & More



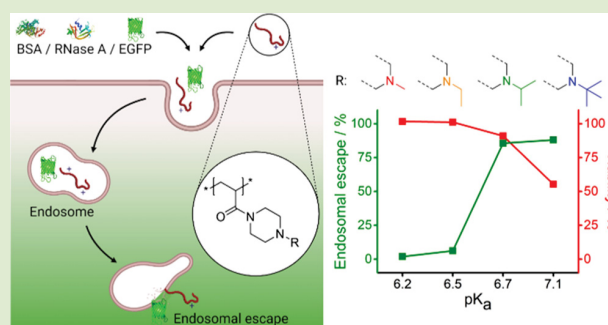
Article Recommendations



Supporting Information

**ABSTRACT:** Responsive polymers, which become protonated at decreasing pH, are considered a milestone in the development of synthetic cell entry vectors. Exact correlations between their properties and their ability to escape the endosome, however, often remain elusive due to hydrophobic interactions or limitations in the design of water-soluble materials with suitable basicity. Here, we present a series of well-defined, hydrophilic polypiperazines, where systematic variation of the amino moiety facilitates an unprecedented fine-tuning of the basicity or  $pK_a$  value within the physiologically relevant range (pH 6–7.4). Coincubation of HEK 293T cells with various probes, including small fluorophores or functioning proteins, revealed a rapid increase of endosomal release for polymers with  $pK_a$  values above 6.5 or 7 in serum-free or serum-containing media, respectively. Similarly, cytotoxic effects became severe at increased  $pK_a$  values ( $>7$ ). Although the window for effective transport appears narrow, the discovered correlations offer a principal guideline for the design of effective polymers for endosomal escape.

**KEYWORDS:** membrane leakage, calcein release, endosomolytic polymers, pH-responsive polymers, basicity



## INTRODUCTION

Despite continuous improvements in delivery systems, the development of materials for efficient and safe delivery of biologicals remains challenging for therapeutic treatments such as protein or gene therapy. On a cellular level, the cell membrane and endosomal entrapment represent the most challenging barriers.<sup>1–3</sup> Crossing the areas of biology to materials science and chemistry, scientists have, therefore, developed a large variety of strategies based on nano-scaled virus capsids,<sup>4,5</sup> liposomes,<sup>6,7</sup> peptides,<sup>8,9</sup> or polymers<sup>10,11</sup> to overcome these barriers. Because nanocarriers are mainly taken up by endocytotic processes, release from the endosome is essential to bring the therapeutic agents to their site of action and to avoid degradation in the lysosome. Membrane-permeabilizing or cell-penetrating peptides, for example, were often derived from virus proteins and inspired the design of cell-penetrating polymers.<sup>12–18</sup> Another concept relies on the use of smart polymers, which are able to react to changes in their environment. In particular, the inherent decrease in pH during the internalization process from the bloodstream (pH 7.4) via the early (pH 5.9–6.5) and late endosome (pH 5.9–4.9) to the lysosome (pH 4.9–4.0) attracted considerable attention in the design of such polymers.<sup>19–22</sup> In comparison to biological carrier systems (e.g., viruses), polymers offer the advantage of scalable synthesis, limited immunogenicity, and

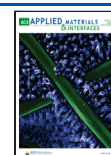
tunable chemistry. Nevertheless, most of these materials face an efficacy–toxicity dilemma, that is, cationic pH-responsive delivery agents can facilitate efficient endosomal escape of therapeutics, but often cause severe cytotoxic side effects.<sup>23,24</sup> Despite its toxicity, poly(ethylene imine) (PEI) is still considered the “gold standard” for polymer-based nucleic acid delivery, and different theories have been investigated to enlighten the endosomal escape mechanism of this cationic polymer.<sup>25</sup> The proton sponge theory has been postulated with the first applications of PEI,<sup>26</sup> but it remains heavily debated in the literature.<sup>27</sup> Other reports describe an endosomal escape concept based on the destabilization of the endosomal membrane due to the interaction with increasingly cationic polymers.<sup>11,28,29</sup>

Independent of the endosomal escape mechanism, the effects of all these different materials rely on their reaction to the change of the pH value or the influx of protons into the endosome. Despite the knowledge on this dependency and its

Received: January 13, 2021

Accepted: July 9, 2021

Published: July 20, 2021





influence on the endosomal escape, clear structure–property relationships for the purposeful design of polymers are hard to derive from the reported studies and materials. First, most of the reported polymers were designed for gene delivery and have to fulfill several tasks including the complexation of genetic materials. In this context, several studies identified correlations between the pH response of the polymers, often referred to as buffer capacity, in the interesting range (pH 5–7.4) and their efficacy in gene delivery. For example, the type of amine (primary, secondary, or tertiary) was found to have a crucial influence on plasmid DNA delivery.<sup>17,30–32</sup> An interesting study was reported by Du et al.,<sup>33</sup> which focused on the impact of the acid dissociation constant ( $pK_a$ ), a measure of the basicity of a material correlating with the buffer range, of various copolymers on the efficacy of siRNA delivery. While  $pK_a$  values between 5.8 and 6.2 were identified as the most effective, the reported polymers also undergo a phase transition with the change of the pH value, which is related to their inherent hydrophobic structure. Indeed, most pH-responsive polymers with  $pK_a$  values in the interesting range of 6–7 are hydrophobic in their neutral state, which certainly impacts their membrane interaction and complicates the evaluation of independent factors.<sup>34,35</sup> Pure hydrophilic polymers with  $pK_a$  values close to 6 are based on imidazole units, as also present in histidine.<sup>36</sup> While no clear conclusion on structure–property correlations can be drawn from the reported materials, the incorporation of imidazole or histidine moieties clearly enhanced the efficacy of the delivery systems, which was attributed to the beneficial  $pK_a$  value.<sup>37–39</sup> Moreover, the second protonation of diamino ethylene moieties (a subunit of PEI) was also found to occur around pH 6 and is crucial for efficient gene delivery,<sup>40</sup> while similar units with a slightly lower second  $pK_a$  ( $\approx 5.5$ ) previously resulted in no enhancement.<sup>41</sup> Therefore, we consider it crucial to investigate the fundamental impact of the  $pK_a$  or buffer capacity, respectively, in the decisive range (pH 5–7.4) for endosomal escape independently of the delivery of biologicals.<sup>42</sup> The key challenge remains to find suitable materials, which enable a fine-tuning of the  $pK_a$  without major structural changes and good solubility in aqueous media over a broad pH range.

Inspired by the chemical structure of commonly used biological buffers (e.g., HEPES buffer), we envisaged polypiperazines as an interesting class of pH-responsive materials, which have so far not been considered for any biomedical applications. Nevertheless, previous reports indicate favorable  $pK_a$  values, which can be tuned by the respective substituents.<sup>43,44</sup> Moreover, the monomers are accessible with a simple reaction step and the acrylamide structure allows controlled polymerization via the reversible addition–fragmentation chain transfer (RAFT) process. Small but systematic variations of the substituents on the amino group should influence the resulting  $pK_a$  value of the polymers by an enhanced inductive effect from methyl (Me) to ethyl (Et), *iso*-propyl (*i*Pr), and finally *tert*-butyl (*t*Bu) groups. The resulting homopolymers of various sizes were tested for cytotoxicity and the ability to induce an endosomal escape in HEK 293T cells. The latter was first investigated by a fluorescence-based assay, which evaluates the release of either the dye calcein, a tetramethylrhodamine (TRITC)-labeled dextran (70 kDa), or the model protein bovine serum albumin [BSA, 66.4 kDa, isoelectric point (pI): 4.7].<sup>45</sup> In addition, the escape of intact proteins was tested using a pH-sensitivity-

enhanced green fluorescent protein (EGFP, 33 kDa, pI: 6.2),<sup>46</sup> and RNase A (14 kDa, pI: 8.6),<sup>45</sup> which induces apoptosis if released into the cytosol. Cytotoxicity and biocompatibility were evaluated by cell viability assays (metabolic rate and integrity of plasma membranes) using HEK 293T cells. In addition, erythrocyte aggregation and hemolysis assays at different pH values were conducted.

## MATERIALS AND METHODS

**General Procedure for the Homopolymerization of Piperazine Monomers.** A typical procedure for the homopolymerization of piperazine monomers was as follows: NAI<sub>2</sub>PP (0.5 g, 2.74 mmol, 500 equiv) was dissolved in ultrapure water (2.19 mL) and the pH-value was adjusted to 3–5 by the addition of aqueous hydrochloric acid solution. The mixture was transferred into a microwave vial, 2-(((butylthio)carbonothioyl)thio)propanoic acid (PABTC, 1.0  $\mu$ L of a 0.5 M solution in 1,4-dioxane, 5.49  $\mu$ mol, 1 equiv), VA-044 solution (9.1  $\mu$ L of a 2 wt % aqueous solution, 0.549  $\mu$ mol, 0.1 equiv), 1,4-dioxane (547  $\mu$ L), and 1,3,5-trioxane (20 mg) as an internal standard were added. To the red-labeled polymer P(NAI<sub>2</sub>PP<sub>499-co</sub>-SR101<sub>1</sub>) 3C<sup>''</sup>, a sulforhodamine monomer (907.9  $\mu$ L of a 6 mM solution in dimethylformamide, 5.49  $\mu$ mol, 1 equiv) was added additionally. After sealing with a rubber septum, the mixture was deoxygenated by a stream of bubbled nitrogen for 20 min. To start the polymerization, the vial was placed in a preheated oil bath at 50 °C, samples (100  $\mu$ L) were successively taken, and the monomer conversion was monitored by <sup>1</sup>H NMR (D<sub>2</sub>O). When no monomer could be detected, the mixture was cooled to room temperature and opened to air. For subsequent neutralization, the solution was diluted by ultrapure water (20 mL) and stirred over an excess of basic Amberlyst A21 resin for 24 h. After filtration, the neutralized polymer was obtained after lyophilization and characterized by <sup>1</sup>H NMR and size-exclusion chromatography (SEC). SEC (eluent: DMAc + 0.21% LiCl, PS-standard):  $M_n$ : 65 000 g mol<sup>-1</sup>,  $M_w$ : 79 900 g mol<sup>-1</sup>,  $\bar{D}$  = 1.23.

**Size-Exclusion Chromatography.** SEC of the polymers was performed on a Shimadzu system equipped with a SCL-10A system controller, a LC-10AD pump, a RID-10A refractive index (RI) detector, and a PSS SDV column with *N,N*-dimethylacetamide (DMAc) + 0.21% LiCl as the eluent.

DMAc–SEC was conducted using an Agilent 1200 series instrument (Shimadzu, Japan) equipped with a SCL-10A system controller, a LC-10AD pump, a RID-10A differential RI, and an UV/vis detector (diode array detector). The liquid chromatography system used a 1  $\times$  GRAM 30 Å column (300  $\times$  0.8 mm, 10  $\mu$ m particle size, PSS, Mainz, Germany) and a 1  $\times$  PSS GRAM 1000 Å column (300  $\times$  0.8 mm, 10  $\mu$ m particle size, PSS). The DMAc eluent contained 0.21% (w/w) LiCl as the additive. The column oven was set to 50 °C. Samples were run at 1 mL min<sup>-1</sup> at 40 °C. Analyte samples were filtered through a polytetrafluoroethylene membrane with a 0.45  $\mu$ m pore size prior to injection. Polystyrene (PS) narrow standards (PSS) were used to calibrate the SEC system.

**Potentiometric Titration.** The  $pK_a^{app}$  values were determined by potentiometric titrations of acidified solutions of the polymers using sodium hydroxide. Approximately 10 mL of solution at 1 mg mL<sup>-1</sup> was used for each potentiometric titration experiment. Potentiometric titration was performed at room temperature using automated titration (Metrohm, Herisau, Switzerland). The addition of the titrant (NaOH at 0.1 mol L<sup>-1</sup>) occurred dynamically at a flow rate of 0.05 mL min<sup>-1</sup>. The pH of the solution as a function of the volume of the titrant was derived from the raw titration data. From these data, the  $pK_a^{app}$  of the polymers was determined as the corresponding pH of the mean value of the volume of the titrant at the two maxima of the first derivative of this function according to the Henderson–Hasselbalch eq 1

$$\text{pH} = \text{p}K_a + \log \frac{[A^-]}{[HA]} \quad (1)$$

The degree of charge was calculated and plotted as a function of pH. The data were treated according to the published procedures with some minor modifications to fit for poly(base)s instead of poly(acid)s.<sup>47</sup> The buffer capacity was calculated as reported<sup>27,32,48</sup> according to eq 2

$$\beta = \frac{\Delta n(\text{OH}^-)}{\Delta \text{pH}} \quad (2)$$

**Cell Culture.** HEK 293T cells (ACC 635, DSMZ) were routinely cultured in Dulbecco's modified eagle's medium (DMEM) with 2 mM L-glutamine (Biochrom, Berlin, Germany) supplemented with 10% fetal calf serum (FCS, Capricorn Scientific, Ebersdorfergrund, Germany), 100 U mL<sup>-1</sup> penicillin, and 100  $\mu\text{g mL}^{-1}$  streptomycin (Biochrom) at 37 °C under a humidified 5% (v/v) CO<sub>2</sub> atmosphere.

**Cellular Uptake Studies.** To investigate the uptake of the polypiperazines into cells, the homopolymers with the highest degrees of polymerization (DP) (DP: 500) were labeled with Oregon Green postpolymerization. HEK 293T cells were seeded with 10<sup>5</sup> cells mL<sup>-1</sup> in 24-well plates (VWR, Radnor, US) and cultured for 32 h. The medium was changed to a fresh cell culture medium 1 h prior to treatment. The cells were incubated with Oregon Green-labeled polypiperazines in PBS (Biochrom) at 37 °C under a humidified 5% (v/v) CO<sub>2</sub> atmosphere. The control cells were incubated with fresh culture medium containing the same amount of PBS as the treated cells. The cells were harvested by trypsin treatment and diluted in Hank's buffered salt solution (HBSS, Sigma-Aldrich, St. Louis, US) supplemented with 2% FCS and 20 mM 4-(2-hydroxyethyl)-1-piperazineethanesulfonic acid (HEPES, Biochrom) after 16 h. To quench the outer fluorescence of the cells, a 0.4% trypan blue solution (Sigma-Aldrich, filtered through a cellulose-mixed ester membrane with a 0.22  $\mu\text{m}$  pore size) was added to obtain a final concentration of 0.04%. To determine the relative uptake of the labeled homopolymers, 10,000 events were measured via flow cytometry (Cytoflex S, Beckman Coulter, Brea, US) using gates of forward and side scatters to exclude the debris and cell aggregates.

**Calcein and Labeled BSA Release Assays.** The cell membrane-impermeable dye calcein and the labeled protein BSA were used to determine the endosomal escape properties of the homopolymers. Calcein (Sigma-Aldrich) was dissolved in 1 M NaOH at a concentration of 50 mg mL<sup>-1</sup> to create a stock solution, which was diluted with water to generate solutions of desired concentrations for the experiments. BSA, Alexa Fluor 488 conjugate (Thermo Fisher, Waltham, US, catalogue number A13100), was dissolved in PBS at 2 mg mL<sup>-1</sup>. Investigations were carried out at dimmed light. HEK 293T cells were seeded with 2  $\times$  10<sup>5</sup> cells mL<sup>-1</sup> in cell culture dishes with a glass bottom (Cellview, Greiner Bio-One, Kremsmünster, Austria) or with 10<sup>5</sup> cells mL<sup>-1</sup> in 24-well plates and cultured for 32 h. The medium was changed to fresh cell culture medium 1 h prior to treatment. The incubation solutions were prepared in PBS and diluted 1:10 into the medium. The cells were incubated at 100  $\mu\text{g mL}^{-1}$  of the respective polymer solutions in PBS and 25  $\mu\text{g mL}^{-1}$  calcein or 5  $\mu\text{g mL}^{-1}$  labeled BSA at 37 °C under a humidified 5% (v/v) CO<sub>2</sub> atmosphere for 16 h. The control cells were incubated with fresh culture medium containing the same concentration of calcein or labeled BSA as well as the same amount of PBS as the treated cells. Endosomal escape was evaluated either via confocal laser scanning microscopy (CLSM) or flow cytometry.

For microscopic investigations, cells were either treated with sulforhodamine 101-labeled or nonlabeled homopolymers. In any case, cells were washed twice with PBS. To image the intracellular distribution in living cells, Hoechst 33342 (Thermo Fisher) was added at a final concentration of 10  $\mu\text{g mL}^{-1}$  for 10 min to stain cell nuclei. For microscopic evaluation of endosomal escape, cells were imaged in HBSS supplemented with 2% FCS and 20 mM HEPES. Confocal live cell imaging was performed using a LSM880, Elyra PS.1 system (Zeiss, Oberkochen, Germany) applying an argon laser for excitation at 405 nm (1%) and 488 nm (5%) as well as emission filters for Hoechst (410–450 nm) and green fluorescence (490–570 nm) with gains of 800 and 700, respectively. In the case of imaging

sulforhodamine 101-labeled polymers, a laser for excitation at 561 nm (3%) and an emission filter for sulforhodamine 101 (610–700 nm) with a gain of 800 were utilized. For three-dimensional (3D) investigations, confocal live cell imaging was conducted acquiring z-stack images. HEK 293T cells in Opti-MEM were treated with the same concentrations of the compounds as described before, but were incubated for 24 h before washing. For measurements, the aforementioned LSM880, Elyra PS.1 system was used applying an argon laser for excitation at 405 nm (0.2%) and 488 nm (0.5%) as well as emission filters for Hoechst (410–450 nm) and calcein fluorescence (500–570 nm) with gains of 700 and 800, respectively. The step width for the z-steps was set to optimal (0.31  $\mu\text{m}$ ) with adapted pin holes. For the time series investigations of the calcein release, HEK 293T cells were seeded and treated with calcein and 100  $\mu\text{g mL}^{-1}$  P(NAiPP)<sub>500</sub> 3C'' as described above. The LSM880, Elyra PS.1 system was used to apply an argon laser for excitation at 488 nm (0.5%) and 561 nm (2%) as well as emission filters for calcein (499–570 nm) and SR101 fluorescence (571–710 nm) with gains of 800 for both channels. Cells were incubated at 37 °C under a 5% (v/v) CO<sub>2</sub> atmosphere within the microscope, while measurements were conducted every 15 min. For magnification, a 40  $\times$  1.4 NA plan apochromatic oil objective was applied for all the microscopy conducted. All images of all experiments were acquired (ZEN, black edition, version 2.3 SP1, Zeiss) and processed (ImageJ, Java 8) consistently across polymer-treated cells with cells serving as control.

For high-throughput analysis, cells grown in 24-well plates were harvested by trypsin treatment and resuspended in HBSS supplemented with 2% FCS and 20 mM HEPES following the washing step. 10,000 events were measured via flow cytometry using gates of forward and side scatters to exclude the debris and cell aggregates. The sides of viable cells showing a higher Alexa Fluor 488 signal than the control cells treated with the labeled BSA solely were gated.

**Cytosolic RNase A Delivery.** RNase A (Merck, Darmstadt, Germany, catalogue number 10109169001) was suspended in sterile ultrapure water at 10 mg mL<sup>-1</sup>. RNase A delivery studies were performed using HEK 293T cells that were either treated with RNase A only or coincubated with the same RNase A concentration and various concentrations of the polypiperazines. The incubation solutions were prepared in PBS and diluted 1:10 into the medium. In order to assess the efficiency of the RNase A delivery, the alamarBlue assay was conducted. In detail, HEK 293T cells were seeded at 10<sup>3</sup> cells mL<sup>-1</sup> (10<sup>4</sup> cells per well) in a 96-well plate (VWR) and incubated for 32 h. No cells were seeded in the outer wells. The medium was changed to fresh cell culture medium 1 h prior to treatment. The cells were incubated with (i) the solvent PBS only, and they serve as control cells, (ii) RNase A at a final concentration of 500  $\mu\text{g mL}^{-1}$ , (iii) the polymer solutions in PBS at the indicated concentrations (from 5 to 100  $\mu\text{g mL}^{-1}$ ), or (iv) both RNase A and the polymers. The control cells were incubated with fresh culture medium containing the same amount of PBS as the treated cells. After 16 h of incubation, the medium was changed to DMEM containing 10% FCS and cells were incubated for an additional 24 h. Subsequently, the medium was replaced by a mixture of fresh culture medium and the resazurin-based solution alamarBlue (Thermo Fisher). The relative cell viability relative to untreated cells (i) was analyzed as described in the Methods section for the determination of cytotoxicity (see Supporting Information).

**EGFP Release Assay.** Lyophilized EGFP (BioVision Inc., Milpitas, US) was reconstituted to 1 mg mL<sup>-1</sup> with sterile PBS according to the manufacturer's instructions. HEK 293T cells were seeded with 10<sup>5</sup> cells mL<sup>-1</sup> in cell culture dishes with glass bottom and treated analogously to calcein and BSA release assays, but employing 50  $\mu\text{g mL}^{-1}$  EGFP and P(NAiPP)<sub>499-co-SR101</sub> 3C''. CLSM studies were conducted as described for the calcein and BSA release assays, but applying an argon laser for excitation at 405 nm (1%), 488 nm (5%), and 561 nm (3%) as well as emission filters for Hoechst (410–450 nm), EGFP (490–570 nm), and sulforhodamine 101 fluorescence (610–700 nm) with gains of 800, 850, and 800. Flow cytometry analysis was conducted immediately following CLSM

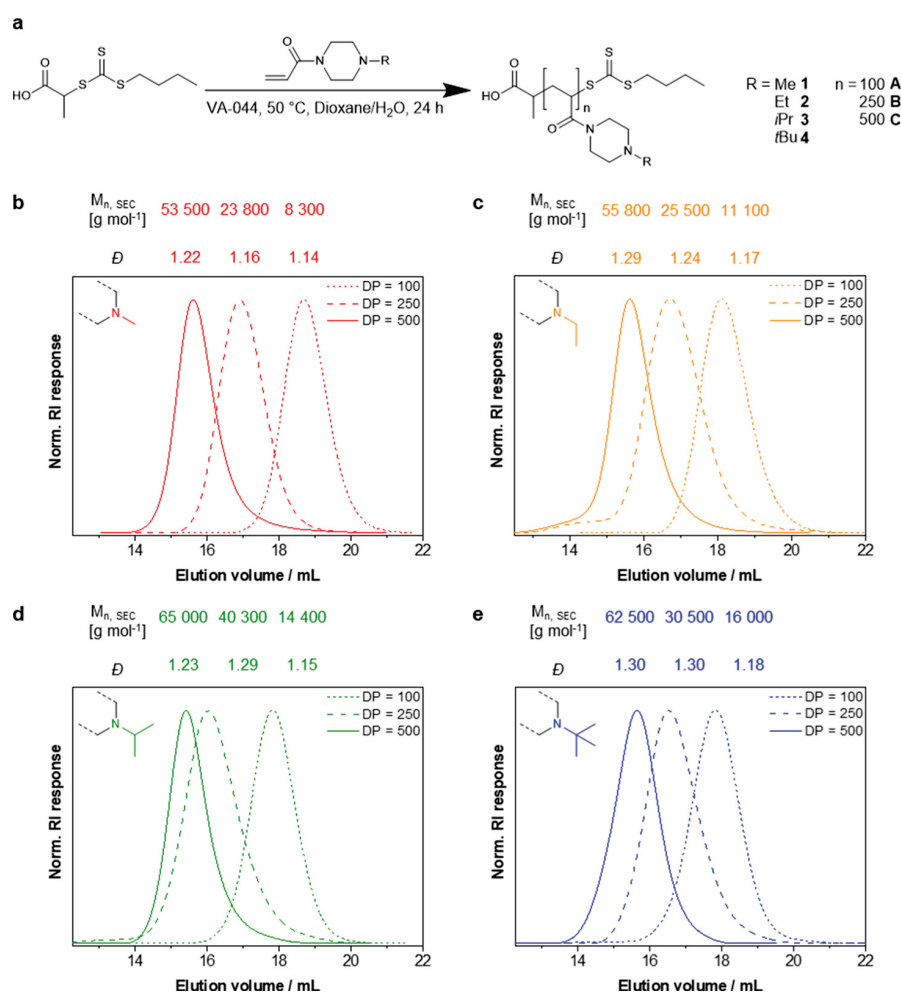


**Figure 1.** Synthesis and SEC traces of polypiperazines. (a) Piperazine-based vinyl monomers were polymerized via RAFT polymerization. (b–e) SEC traces of P(NAMP)<sub>n</sub> (b), P(NAEP)<sub>n</sub> (c), P(NAiPP)<sub>n</sub> (d), and P(NAtBP)<sub>n</sub> (e). SEC: DMAc + 0.21 wt % LiCl, RI detection, and PS calibration.

studies. Therefore, cells were washed with prewarmed PBS once and harvested by trypsin treatment in HBSS supplemented with 2% FCS and 20 mM HEPES. 10,000 events were measured via flow cytometry using gates of forward and side scatters to exclude the debris and cell aggregates.

**Statistical Analysis.** Statistical analysis was performed using SPSS Statistics (IBM, Armonk, US) version 26. Homogeneity of variances was assessed with Levene's test. In the case of homogeneity of variances, the one-way analysis of variance (ANOVA) was used, followed by Dunnett's multiple comparison test. In the case of heterogeneity of variances, Welch-ANOVA, followed by Dunnett's T3 test was conducted. For comparisons between two means (Figure 7b), the unpaired two-tailed Student's *t*-test was applied. Differences with  $P > 0.05$  were considered statistically significant. The results are presented as the mean value  $\pm$  standard deviation (mean  $\pm$  SD) of at least three independent determinations.

## RESULTS

**Synthesis of pH-Responsive Polypiperazines.** The initial monomers were prepared from acryloylchloride and the respective monofunctionalized (Me, Et, *i*Pr, or *t*Bu) piperazine (Figure S2). Straightforward reaction and purification by distillation enable reasonable yields and access to sufficient quantities (>20 g). In accordance with our experience on similar acrylamides,<sup>49</sup> the chosen RAFT

polymerization facilitates access to well-defined polymers with variable DP. The polymerization can conveniently be conducted in deionized water, which was slightly acidified to prevent hydrolysis of the trithiocarbonate chain transfer agent (CTA). Typical for the radical polymerization of acrylamide monomers in water, the polymerization rate was very high, and therefore quantitative conversions (>99%) were reached within a few hours. Consequently, a library of different homopolymers poly(*N*-acryloyl-*N'*-methylpiperazine) (P(NAMP)<sub>n</sub>), poly(*N*-acryloyl-*N'*-ethylpiperazine) (P(NAEP)<sub>n</sub>), poly(*N*-acryloyl-*N'*-*iso*-propylpiperazine) (P(NAiPP)<sub>n</sub>), and poly(*N*-acryloyl-*N'*-*tert*-butylpiperazine) (P(NAtBP)<sub>n</sub>) with DPs ranging from 100 to high values of 500 were prepared (Figures 1a and S3) while retaining good to moderate dispersities ( $\bar{D} \leq 1.3$ ) as determined by size exclusion chromatography (SEC, Figure 1b–e). Although no purification of the residual monomer was required, the polymers were neutralized and deionized to remove the present chloride ions prior to further investigations.

All resulting polymers (Figure 2a) were fully water-soluble even in their neutralized state and at temperatures of up to 50 °C (data not shown), which is crucial for the following studies. In contrast to the lower critical solution temperatures

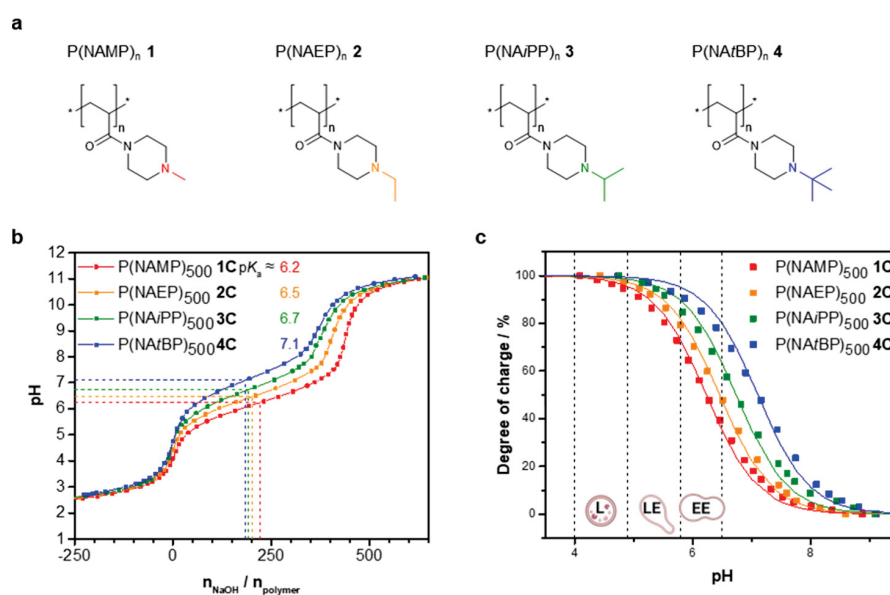


**Figure 2.** pH-responsiveness of polypiperazines depending on substituents. (a) Polypiperazines of the investigated library differ in their DP and pendant group. (b) Titration curves of the polypiperazines were obtained from potentiometric titrations of acidified polymer solutions against sodium hydroxide in water with 150 mM sodium chloride. The red, orange, green, and blue squares represent  $P(\text{NAMP})_{500}$ ,  $P(\text{NAEP})_{500}$ ,  $P(\text{NAiPP})_{500}$ , and  $P(\text{NAiBP})_{500}$ , respectively. The  $pK_a$  is indicated for each material. (c) Degree of charge at different pH values was calculated from the titration data (symbols) and according to the Henderson–Hasselbalch eq 1 (lines) for  $P(\text{NAMP})_{500}$  (red),  $P(\text{NAEP})_{500}$  (orange),  $P(\text{NAiPP})_{500}$  (green), and  $P(\text{NAiBP})_{500}$  (blue). The pH ranges within the compartments of the endolysosomal pathway, early endosomes, late endosomes, and lysosomes, are indicated according to Maxfield and Yamashiro<sup>19</sup> and Huotari and Helenius.<sup>51</sup> EE: Early endosome; LE: late endosome; and L: lysosome.

for previously reported poly(*N*-acryloyl-*N'*-propylpiperazine) (*n*Pr substituent),<sup>43</sup> the compact structure of our *t*Pr and *t*Bu renders the respective polymers more hydrophilic. To determine the  $pK_a$  values of the materials, acidified polymer solutions (excess of HCl) in water were titrated potentiometrically using sodium hydroxide solution. In contrast to previous titrations,<sup>44</sup> we added 150 mM sodium chloride to resemble physiological salt concentrations. As clearly visible in the titration profile (Figure 2b), the tested polypiperazines exhibit a broad buffer range in the desired pH range. Moreover, the systematic modifications of the pendant group resulted in a gradual shift of this buffer capacity toward higher pH values with increasing size of the substituent and in accordance with our initial hypothesis (Figure S4). To the same extent, our calculations revealed a stepwise increase of the respective  $pK_a^{\text{app}}$  values ranging from 6.2 to 7.1 (Figure 2b). A comparable titration of commercial l-PEI of 25 kDa gave a  $pK_a^{\text{app}}$  of 8.2 (Figure S5a), with a steeper increase of the pH value in the buffer region spanning a wide range of pH values (6–10, Figure S5b). This is considered a key factor for the efficacy of PEI and related to the close proximity of the reactive amino groups in PEI.<sup>27,50</sup>

From the titration data, a degree of charge (ratio between the amounts of protonated units to the total amount of units) can be estimated for each pH value (Figure 2c). At the physiological pH value of blood and within the extracellular space, all polymers are partially cationic, whereas  $P(\text{NAMP})_{500}$  1C is approximately 9%,  $P(\text{NAEP})_{500}$  2C 13%,  $P(\text{NAiPP})_{500}$  3C 22%, and  $P(\text{NAiBP})_{500}$  4C 36% protonated. Along the endolysosomal pathway, all the materials become completely protonated and thus fully charged, considering the respective pH values as indicated in the Introduction section. Interestingly, the steepest increase in the degree of charge

for all materials can be expected during the transition from the extracellular space to the early endosome (Figure 2c). Within the late endosome (pH 4.9–6.0),<sup>51</sup> the different materials become highly charged (70–90% depending on the substituent).

#### Cytotoxicity and Cellular Uptake of Polypiperazines.

Following the determination of basicity, the degree of charge, and buffer capacity of the polymers, we focused on their fundamental in vitro properties. Therefore, all materials were analyzed concerning their concentration-dependent cytotoxicity (tested according to ISO 10993-5) using the resazurin-based alamarBlue cell viability reagent. Despite the present cationic charges at pH 7.4, no indication of cytotoxicity was observed for  $P(\text{NAMP})_n$  1A–C,  $P(\text{NAEP})_n$  2A–C, and  $P(\text{NAiPP})_n$  3A, and B (A: DP 100, B: DP 250, and C: 500) up to a final concentration of 1 mg mL<sup>-1</sup> (Figure S6).  $P(\text{NAiPP})_{500}$  3C with a high DP of 500 showed slight toxicity at concentrations above 100 μg mL<sup>-1</sup> (cell viability of 70.0 ± 5.4% at 200 μg mL<sup>-1</sup>). In contrast to the polymers 1–3,  $P(\text{NAiBP})_n$  4 induced cytotoxic effects at concentrations above 50 μg mL<sup>-1</sup> independent of the DP (Figure S6). This result indicates a rather sharp transition from nontoxic to harmful materials with only minor changes in terms of  $pK_a$  or charge density on the linear polymers.

For further evaluation of the cell interaction of these materials, their uptake was studied. Therefore, the polymers with highest DP were functionalized with Oregon Green (see Supporting Information for details, Figure S1a). The uptake of the labeled polymers (1C', 2C', 3C', and 4C') in HEK 293T cells was investigated via flow cytometry using different cell culture media. The obtained mean fluorescence intensities (MFI) were corrected with the respective degree of labeling. Concentration-dependent uptake studies revealed a negligible

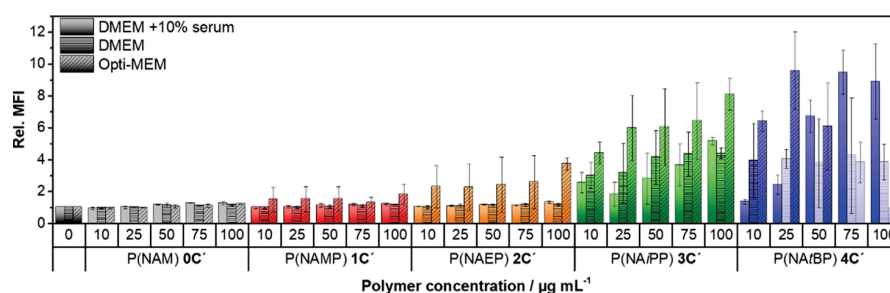


**Figure 3.** Cellular uptake of Oregon Green-labeled polypiperazines investigated by flow cytometry. The cellular uptake of Oregon Green-labeled polymers (DP: 500) at different concentrations was assessed by flow cytometry after 16 h. The obtained MFI values were corrected by the labeling efficiency of the polymers and are given in relation to the untreated control (see Figure S7 for the raw data and their correction). Mean  $\pm$  SD of three independent experiments is shown. Transparency of bars indicates reduced viability of the samples.

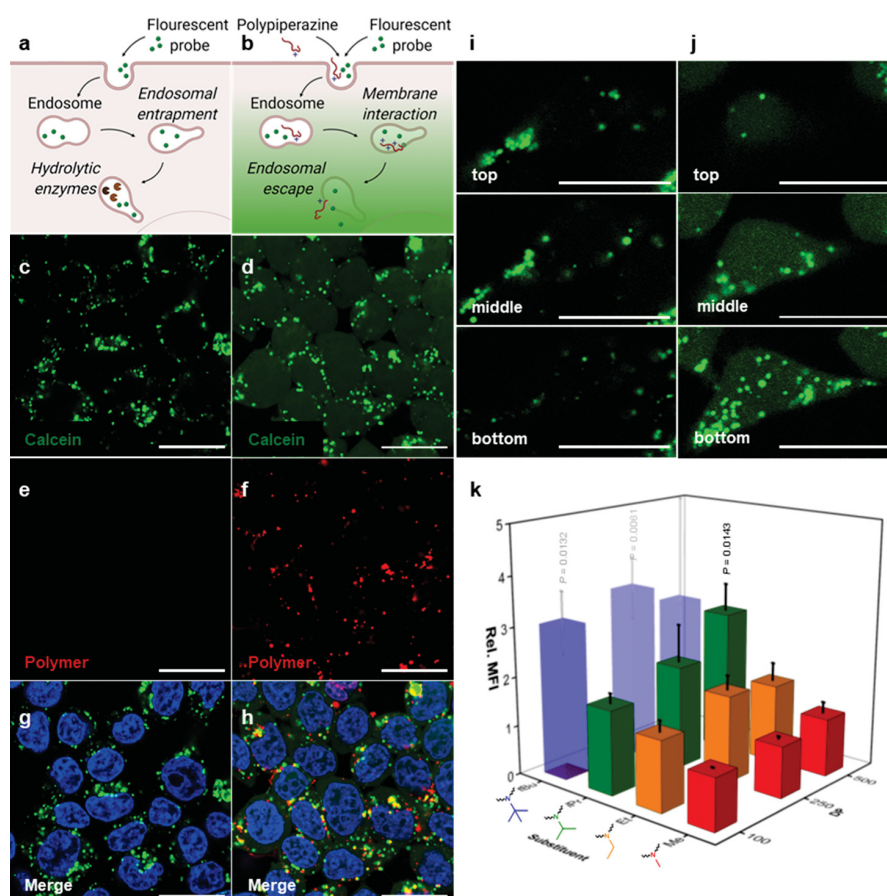


**Figure 4.** Endosomal escape of calcein. (a) Schematic presentation of the endocytosis and endosomal entrapment of fluorescent probes in cells not treated with endosomolytic polymers and (b) of the cytosolic and nuclear delivery of fluorescent probes facilitated by the polypiperazines. (c,e,g) Confocal images of HEK 293T cells in Opti-MEM treated with the nonmembrane permeable dye calcein as control. (d,f,h) Cellular uptake and endosomal release of calcein were imaged using HEK 293T cells that were treated with the same concentration of calcein as the control cells and additional  $100 \mu\text{g mL}^{-1}$  labeled P(NAiPP)<sub>500</sub> 3C'' for 16 h. The calcein channel (c,d) and the corresponding image of the red channel (polymer, e,f) as well as the merge of the calcein, polymer, and Hoechst channel (g,h) are shown. (i,j) Example images of a z-stack acquisition from the lower, middle, and upper parts of a cell treated either with calcein alone as control (i) or with P(NAiPP)<sub>500</sub> 3C'' and calcein (j, also see S12 for images showing a co-staining with Hoechst). (c–j) Scale bar  $20 \mu\text{m}$ . All corresponding images comparing the calcein control with the polymer-treated samples were acquired and processed with the same settings. (k) High-throughput analysis of fluorescence intensities of HEK 293T cells in Opti-MEM treated with calcein and  $100 \mu\text{g mL}^{-1}$  polypiperazines. The means  $\pm$  SD of three independent experiments relative to control cells treated with calcein only (rel. MFI = 1) are shown. For comparison, an analogous treatment with  $25 \mu\text{g mL}^{-1}$  l-PEI resulted in a rel. MFI of  $2.7 \pm 0.3$  (mean  $\pm$  SD of three independent experiments), although only 62% of the cells were considered viable in this case. Significant differences between the means were calculated with Dunnett's T3 test. Transparency of bars indicates gated cell populations below 70% (slight transparency) or 50% (distinct transparency) according to reduced viability of the samples. (a,b) Created with [biorender.com](http://biorender.com). rel. MFI—relative mean fluorescence intensity.

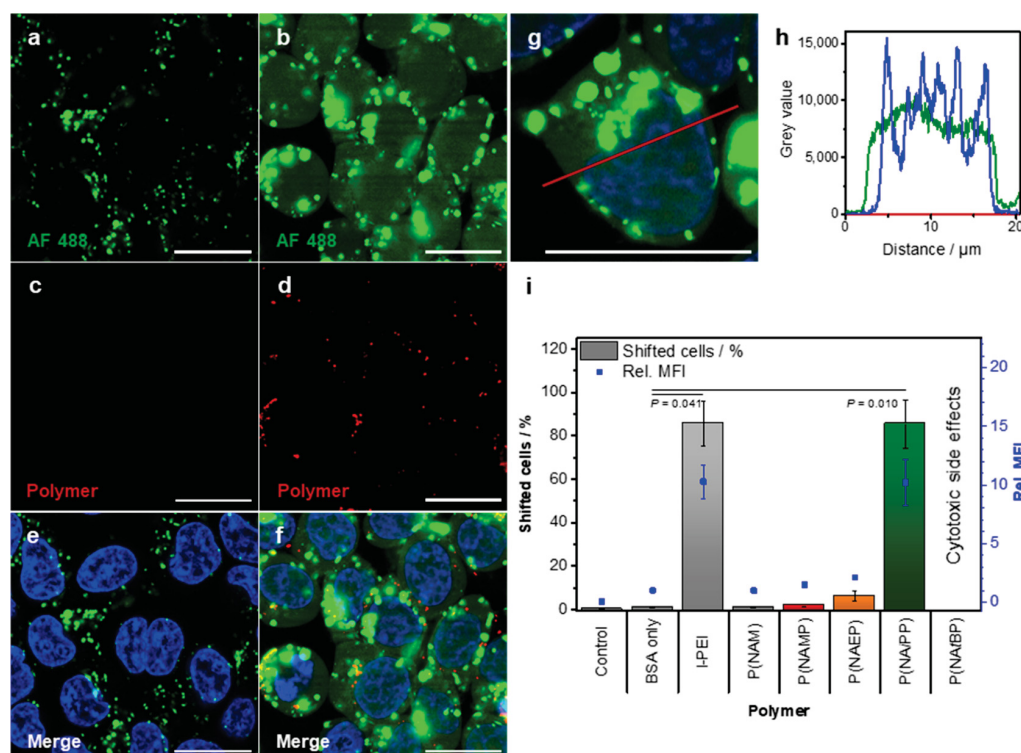


**Figure 5.** Endosomal escape of labeled BSA. (a) Confocal images of HEK 293T cells in Opti-MEM show cellular uptake and endosomal entrapment of AF 488-labeled BSA. (b) Diffuse fluorescence signals in the cytosol and nuclei were observed in HEK 293T cells treated with the same concentration of AF 488-labeled BSA as control cells but with additional  $100 \mu\text{g mL}^{-1}$  labeled P(NAiPP)<sub>500</sub> 3C'' for 16 h. (a,b) AF 488 channel (BSA) and (c,d) corresponding images of the polymer channel as well as (e,f) merged images with the Hoechst channel are shown. (a–f) All images comparing control and treated sample were acquired and processed with the same settings. (g) A merged image of the Hoechst and the BSA channel of a HEK 293T cell treated as described for (b), and (h) the corresponding plot profile of the AF 488 signal in comparison to the Hoechst signal are shown (refer to S14 for the corresponding image of the control). (a–g) Scale bar  $20 \mu\text{m}$ . (i) Endosomal escape was quantified via flow cytometry in HEK 293T cells treated with labeled BSA and polymers at comparable reactive amine contents. Means  $\pm$  SD of three independent experiments are shown. Significant differences between the means of the percentages of shifted cells were calculated with Dunnett's T3 test. AF 488—Alexa Fluor 488, and rel. MFI—relative mean fluorescence intensity.

cellular uptake of labeled P(NAMP)<sub>500</sub> 1C' and P(NAEP)<sub>500</sub> 2C' into HEK 293T cells in DMEM with 10% or without serum (Figure 3). P(NAiPP)<sub>500</sub> 3C' and P(NAtBP)<sub>500</sub> 4C', the more cationic polymers, are taken up to a greater extent, with the increase for P(NAtBP)<sub>500</sub> 4C' being superior. In Opti-MEM, a modified DMEM with reconciled ingredients including buffers, polypiperazine uptake is generally increased compared to DMEM with or without serum. However, a similar trend was found for the basicity of the material (Figure S7). Differences observed for P(NAtBP)<sub>500</sub> 4C' in nonserum media may probably be due to increased membrane interaction and cytotoxic side effects. All in all, the uptake of polymers seems to be rather low, particularly for P(NAMP)<sub>500</sub> 1C' and P(NAEP)<sub>500</sub> 2C' according to the flow cytometry data, which is surprising for cationic polymers. A reduced uptake could be explained with the polymers' moderate degree of charge at pH 7.4 and their high structural similarities to P(NAM), which is considered to suppress unspecific interactions similar to polyethylene oxide (PEO) or polyoxazolines.<sup>52–55</sup>

**Hemocompatibility and Interaction with Plasma Membranes.** To assess the biocompatibility of the materials, their influence on human red blood cells was investigated. At the physiological pH of blood, no hemoglobin release above 2% was found (Figure S8c) classifying all the materials as nonhemolytic up to a concentration of  $100 \mu\text{g mL}^{-1}$ . An

aggregation of erythrocytes at pH 7.4 was only observed for P(NAtBP)<sub>500</sub> 4C that induced severe aggregation (Figure S8a). From this, we conclude that there are no noteworthy interactions between the polymers [except P(NAtBP)<sub>500</sub> 4C] and the plasma membrane of human erythrocytes, indicating high biocompatibility of the materials. In addition, similar tests were performed at pH 6 to obtain an insight into the interaction of the polymer with cellular membranes at endosomal pH. Interestingly, the behavior of some of the polymers differs considerably from their behavior at pH 7.4. Proportionally to the  $pK_3^{\text{PP}}$  and to a smaller extent to the DP of the polymers, the aggregation of erythrocytes increases considerably (Figure S8b). However, no hemolytic activity was observed at pH 6, thus indicating that the interactions between the polypiperazines and the plasma membrane are insufficient to induce leakage of hemoglobin (Figure S8d).

To investigate the interactions between the materials and plasma membranes of HEK 293T cells, the CytoTox-ONE homogenous membrane integrity assay was employed. Here, the release of the cytosolic enzyme lactate dehydrogenase (LDH) from cells with damaged plasma membranes is measured in relation to cells lysed with Triton X-100. Besides the polypiperazines 1C, 2C, 3C, and 4C with the highest DP, the commercial l-PEI (25 kDa, equal to DP  $\approx$  580) was included in this study (Figure S9). To ensure similar

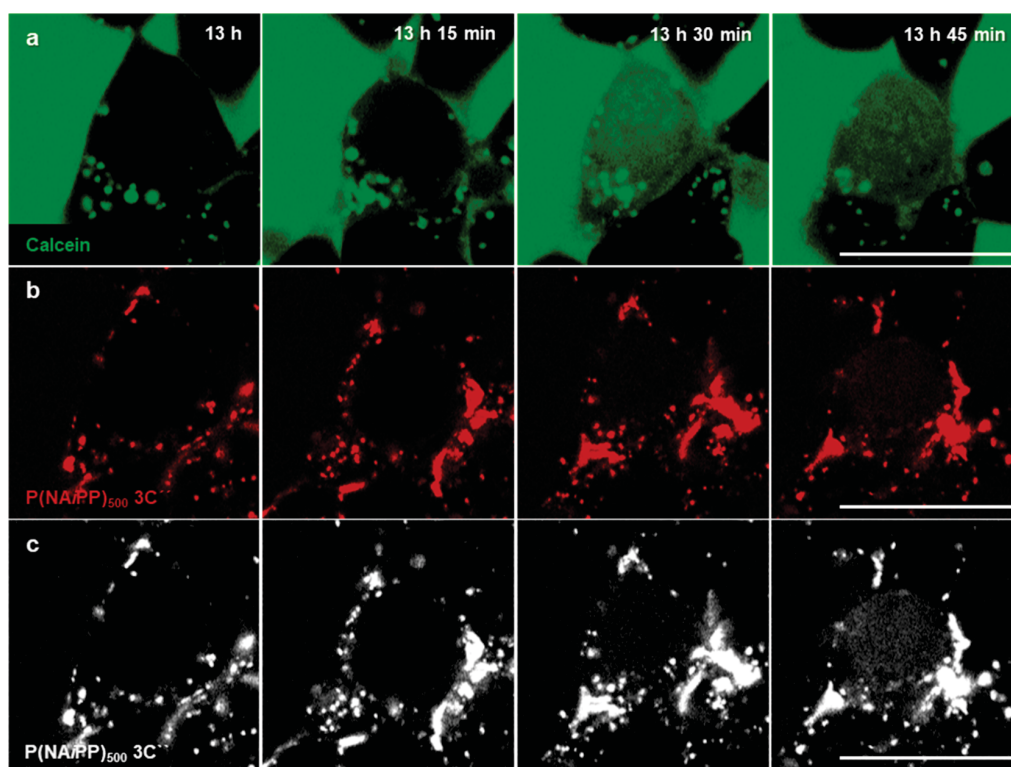


**Figure 6.** Timescale of endosomal calcein release by P(NAiPP)<sub>500</sub> 3C''. The endosomal escape of calcein in HEK 293T cells in Opti-MEM treated with 25  $\mu\text{g mL}^{-1}$  calcein and 100  $\mu\text{g mL}^{-1}$  P(NAiPP)<sub>500</sub> 3C'' was monitored over time. (a) Calcein channel and (b) polymer channel are shown. (c) Latter channel was added in the enhanced grayscale to improve the visibility of the faint signal in the cytosol.

concentrations of reactive amino groups, the concentrations were set to 100  $\mu\text{g mL}^{-1}$  for the polypiperazines and 25  $\mu\text{g mL}^{-1}$  for l-PEI. No significant LDH release was detected except for P(NAiBP)<sub>500</sub> 4C and l-PEI, both of which caused a slight LDH release of  $4.3 \pm 3.7$  and  $6.1 \pm 0.7\%$ , respectively. In Opti-MEM, on the other hand, LDH release increases considerably and correlates with the increasing activity and basicity previously observed for the materials.

**Endosomal Escape Efficiency Depending on Basicity, Molar Mass, and Biocompatibility.** Although the experiments conducted so far are essential investigations and have already revealed interesting trends in terms of cytotoxicity as well as membrane interaction, a key element of this study is to identify correlations between the basicity/ $\text{pK}_a$  of the materials and their capability to facilitate endosomal escape. Therefore, different fluorescent model probes, ranging from the small molecule calcein to the biomacromolecule dextran (70 kDa) or the protein BSA (66.4 kDa), were coinubated with the respective polymers to enable monitoring of a size-dependent endosomal escape. In preliminary tests, calcein, dextran, and BSA were not found to form any complexes with the tested polymers (Figure S10). Besides, the concentrations of the various compounds, polymers and buffers were kept within the isotonic range to ensure that no osmotic stress for the cells is to be expected. The pure probes were also tested as control. Initially, the subcellular distribution of the model probes and the fate of the polymers were imaged using a confocal laser scanning microscope. A punctate fluorescence pattern was observed for probes entrapped in organelles (Figure 4a,c), while more diffuse fluorescence signals indicated a cytosolic localization (Figure 4b,d).<sup>11,42,56</sup> P(NAiPP)<sub>500</sub> 3C was

investigated first due to its pH response in the physiologically relevant pH range, sufficient uptake, and membrane activity at endosomal pH values, while it displays good biocompatibility and cell viability under physiological conditions. In order to simultaneously localize the polymer and the probe, a red fluorescent version (3C'') was synthesized (see Supporting Information for details, Figure S1b). Figure 4c–d displays HEK 293T cells treated with either calcein (control) or calcein and 3C''. The control reflects a punctated pattern, while a diffuse green fluorescence within the cytoplasm can be observed for 3C'' indicating the release of calcein from the endosome (also see Figure S19e for a lower magnification image showing a larger number of cells). The red fluorescence is visible within closed compartments, which indicates that the polymer remains mostly within the endolysosomes (Figure 4e,f). To further assess the subcellular distribution of the released calcein, confocal live cell imaging in z-stacks was conducted to image the cells in 3D. A uniform calcein signal through the entire cell interior including the nucleus was observed (Figures 4i–j and S12).

Interestingly, a similar effect was also monitored for the larger BSA (66.4 kDa, Figure 5b,f, also see Figure S13). Confocal measurements confirmed the cytosolic and nuclear localization of the AF 488 signal (Figure 5g–h, also see Figure S22e for a lower magnification image), which is surprising considering the large size of BSA in comparison to the nuclear pore size. In some cases, even small quantities of the polymer were observed in the nuclei of cells (see Figure S16b), which may be an indication that the polymer is further able to assist a nuclear entry of BSA. Due to the extended incubation time of 16 h, it is also possible that BSA could be distributed

throughout the cell during mitosis when the nuclear envelope disintegrates. During a few measurements (data not shown), the AF 488 signal appeared diminished in the nucleus compared to the cytosol, which may hint at such a mechanism, but clearly further studies are required to prove the underlying process, which was beyond the scope of this work. In both cases, calcein and BSA, the rate of endosomal escape facilitated by the labeled P(NAiPP)<sub>500</sub> 3C'' is moderate because a strong punctate fluorescence signal is still detectable within enclosed compartments. It is worth mentioning that coinubation of TRITC-labeled dextran (70 kDa) and P(NAiPP)<sub>500</sub> 3C revealed cytosolic, but no nuclear distribution of the fluorescence signal in contrast to calcein and BSA (Figure S15). The latter difference might be attributed to a different uptake pathway of the dextran requiring an extended time frame for a possible nuclear entry in the course of mitosis, which, however, was not further pursued here. In contrast to BSA, the used dextran might further not pass the nuclear membrane due to its more random conformation and thus larger hydrodynamic size.<sup>57</sup>

In an attempt to investigate the time dependency of this process, confocal microscopy images of the treated cells were recorded every 15 min over a period of 14 h. Interestingly, P(NAiPP)<sub>500</sub> 3C'' showed a very clear accumulation at the plasma membrane immediately after the addition of the polymer (see Figure S16a). In our studies, the cells began to take up this polymer within the first 30 min. Cytosolic release of calcein was first observed in just over 13 h (see exemplarily chosen cell in Figure 6a). In contrast to the occurrence of a clear calcein signal throughout the cell, the amount of released polymer in the cytosol remained low, although still a very faint signal could be observed in the examined cell (see Figure 6b and gray scale image in Figure 6c for a more visible contrast, third and fourth images at 13 h 30 min and 13 h 45 min, respectively). In accordance with previous studies on PEI, only a small amount of polymer may be released, which quickly dilutes in the cytosol.<sup>58</sup> Considering the strong affinity of the polymers with the cell membrane, a further attachment to the remaining endolysosomal membrane is feasible, which is in accordance with the mostly punctual concentration of the SR101 signal (see Figure 6b). Following calcein release, we also could in part detect a fluorescence signal of the polymer in the nuclei (see Figure S16b, third image). However, the nuclear signal was low compared to the intensities of the remaining endolysosomes. The rather slow delivery is likely owing to the coincidence that calcein and polymer have to be present in one endosome in sufficient amounts, as they do not form any complex (see Figure S10b).

In order to investigate the endosomal escape of the polymer library, flow cytometry was used because it provides a rapid high-throughput quantification of fluorescence intensities of cells. The applied method is based on the difference of the fluorescence intensities of cells with entrapped fluorescent probes (lower relative fluorescence signal) compared to cells, where the labeled probe is released from the endolysosome (higher relative fluorescence signal).<sup>59</sup> When examining all polymers with regard to their endosomal escape in Opti-MEM using calcein as the probe, two accumulative trends were observed (Figure 4k, see Figure S17 for the serum-containing medium). Both DP and basicity correlate with the MFI indicating more efficient endosomal escape of the respective polymers. Similar to the uptake studies (Figure 3), the trend collapses with increasing cytotoxicity of the materials.

Cytotoxic effects, identified prior to flow cytometry by changes in the cell morphology (data not shown, also see Figure S18), occurred in particular for P(NAtBP)<sub>n</sub> 4 (Figure 4k) and the data should, therefore, be considered with care. In the case of the nontoxic materials, the best calcein release was observed for P(NAiPP)<sub>500</sub> 3C showing a significant increase in MFI compared to cells treated with calcein only (Figure S18h rel. MFI,  $P = 0.014$ ). An evaluation of the ratio of positive cells was not attempted in this case due to a rather broad scattering of the data resulting in a limited accuracy in gating the appropriate cells (Figure S18d–f). As an alternative approach to determine the number of affected cells in Opti-MEM, the release was exemplarily quantified for P(NAiPP)<sub>500</sub> 3C'' analyzing large area microscopy images (see example in Figure S19), which should further verify that this increase is due to the additional cytosolic fluorescence. For this purpose, binary images of the Hoechst and the calcein channels were generated based on a minimal threshold, which was determined in the control experiment. All cells with a significant overlap of the calcein signal and nucleus were counted as positive for a successful endosomal escape (see Supporting Information for further details). An average value of  $87.7 \pm 16.5\%$  positive cells is obtained for P(NAiPP)<sub>500</sub> 3C'' (three images compared to two control images with  $0.3 \pm 0.4\%$  positive cells), which is in good agreement with the increased MFI from the flow cytometry measurements.

Because the basicity and  $pK_a$  of the polymers had a higher influence on the endosomal escape efficiency than the DP, only the polypiperazines with the highest DP were considered in following experiments and further compared to commercial l-PEI. In contrast to calcein, a more distinct pattern was observed for the release of labeled BSA (Figure S21), which facilitated a more accurate gating into positive cells compared to the control. In particular, coinubation with P(NAiPP)<sub>500</sub> 3C resulted in a drastic increase of fluorescence intensities and the number of positive cells ( $86 \pm 11\%$ ,  $P = 0.010$ ), while all other polypiperazines only led to insignificant release (Figure S1). This result, however, might be because of an increased uptake of BSA in the presence of the polymers, which is why larger microscopy images as described for the calcein release were again analyzed (five different areas were evaluated, see exemplarily shown images in Figure S22). A value of  $89.4 \pm 9.6\%$  positive cells was determined, which is in excellent agreement with the data from flow cytometry. In contrast to the calcein study, this drastic increase cannot only be related to the enhanced uptake (Figure 3) of P(NAiPP)<sub>500</sub> 3C compared to the less-basic polymers. Despite its very different basicity and buffer capacity, this efficiency is only comparable to l-PEI 25 kDa ( $86 \pm 10\%$ ,  $P = 0.041$ ). P(NAtBP)<sub>500</sub> 4C was not investigated as cytotoxic effects in Opti-MEM were observed, although its  $pK_a$  and degree of protonation are lower compared to those of l-PEI under the same conditions (see Figure S20 for the serum-containing medium). Of course, the different concentrations ( $100 \mu\text{g mL}^{-1}$  for P(NAtBP)<sub>500</sub> vs  $25 \mu\text{g mL}^{-1}$  for l-PEI) have to be considered in this comparison, but this adjustment results in a similar amount of protonatable amino groups.

Due to the promising results, the influence of cell culture medium and polymer concentration was examined in more detail for the most promising candidates P(NAiPP)<sub>500</sub> 3C and P(NAtBP)<sub>500</sub> 4C as well as for the commercial l-PEI. Costaining of endolysosomes using LysoTracker Red first of all confirmed the localization of P(NAiPP)<sub>500</sub> 3C' and P-



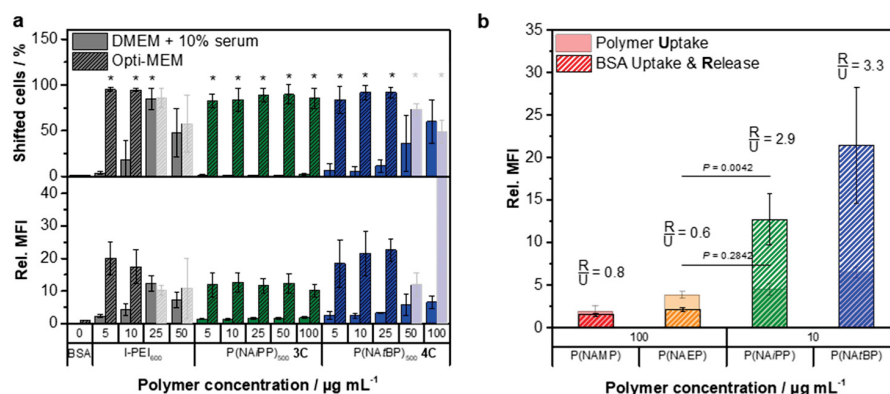


**Figure 7.** Polymer concentration-dependent endosomal escape of labeled BSA by novel polypiperazines. (a) Endosomal escape in HEK 293T cells treated with  $5 \mu\text{g mL}^{-1}$  Alexa Fluor 488-labeled BSA, and the respective polymer concentration was quantified via flow cytometry. Means  $\pm$  SD of three independent experiments are shown. Significant differences between the means were calculated with Dunnett's T3 test ( $*P < 0.001$  vs BSA). (b) Cellular uptake of Oregon Green-labeled polymers (DP: 500) as well as the endosomal escape of labeled BSA in HEK 293T cells in Opti-MEM was assessed by flow cytometry after 16 h. For the uptake studies, the obtained MFI values were corrected by the labeling efficiency of the polymers and are given in relation to the untreated control. Regarding the endosomal escape studies, the relative MFI values are given in relation to cells treated without polymers. Mean  $\pm$  SD of three independent experiments is shown. The ratio of BSA release to polymer uptake ( $R/U$ ) is given for the respective polymers at the concentration shown. Significant differences between the means of rel. MFI were calculated with unpaired two-tailed student's  $t$ -test. rel. MFI—relative mean fluorescence intensity.

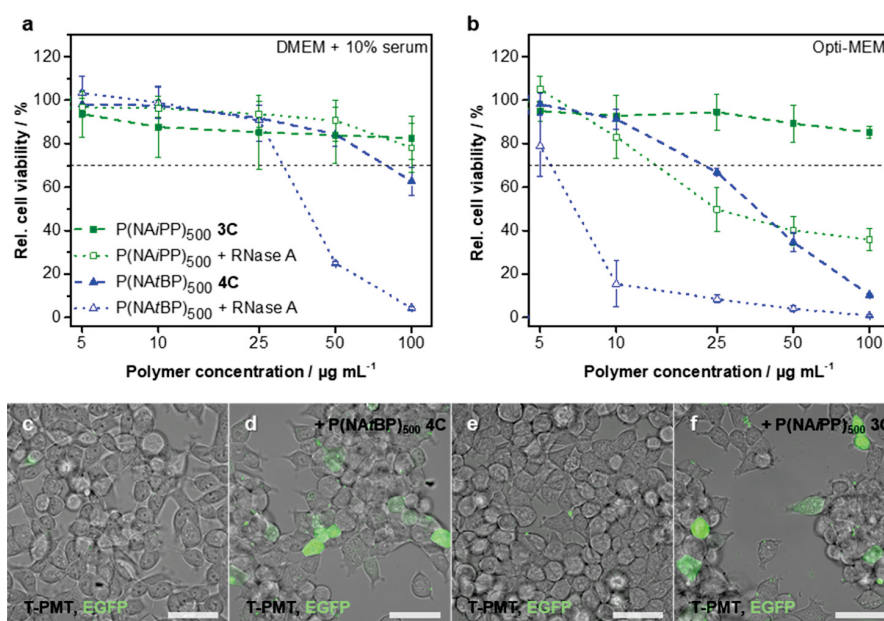


**Figure 8.** Cytosolic and nuclear delivery of functioning proteins. (a) Relative viability of HEK 293T cells in the presence of serum treated with indicated concentrations of the polymers  $\text{P}(\text{NAiPP})_{500}$  3C (green, solid squares) and  $\text{P}(\text{NAiBP})_{500}$  4C (blue, solid triangles) or with additional  $500 \mu\text{g mL}^{-1}$  RNase A (respective color, open symbols) measured via the alamarBlue assay. (b) Relative viability of HEK 293T cells in Opti-MEM treated with different concentrations of  $\text{P}(\text{NAiPP})_{500}$  3C (green, solid squares),  $\text{P}(\text{NAiBP})_{500}$  4C (blue, solid triangles), or with additional  $500 \mu\text{g mL}^{-1}$  RNase A (respective color, open symbols) measured via the alamarBlue assay. (a,b) Means  $\pm$  SD of three independent experiments are shown. (c) HEK 293T cells in the serum-containing medium were treated with EGFP for 16 h and analyzed via CLSM as a control. The overlay of the T-PMT and EGFP channel is shown. (d) HEK 293T cells in the serum-containing medium were treated with the same concentration of EGFP as control cells but with additional  $50 \mu\text{g mL}^{-1}$   $\text{P}(\text{NAiBP})_{500}$  4C at the same time and analyzed as described in (c). (e) HEK 293T cells in Opti-MEM were treated with EGFP for 16 h and analyzed as described in (c). (f) HEK 293T cells in Opti-MEM were treated with the same concentration of EGFP as control cells but with additional  $50 \mu\text{g mL}^{-1}$   $\text{P}(\text{NAiPP})_{500}$  3C at the same time and analyzed as described in (c). Scale bar  $25 \mu\text{m}$ . EGFP—enhanced green fluorescent protein and T-PMT—transmitted light detector.

$(\text{NAiBP})_{500}$  4C' in endolysosomes (Figure S23). The most pronounced difference is caused by the type of medium (Figure 7a). In accordance with the results above, superior endosomal escape of BSA was found for these polymers in Opti-MEM. The endosomal escape efficiency regarding the

number of positive cells in Opti-MEM appears to be largely independent of the concentration for  $\text{P}(\text{NAiPP})_{500}$  3C and  $\text{P}(\text{NAiBP})_{500}$  4C. A further evaluation of the impact of uptake rates on the release efficiency was made based on the data obtained for different applied concentrations of the polymers

(Figure 7b). Comparing the uptake rates of P(NAMP)<sub>500</sub> 1C and P(NAEP)<sub>500</sub> 2C at the highest tested concentration (100 μg mL<sup>-1</sup>) with P(NAiPP)<sub>500</sub> 3C and P(NAfBP)<sub>500</sub> 4C at low concentrations of 10 μg mL<sup>-1</sup>, similar amounts of taken up polymer are found in particular for the samples P(NAEP)<sub>500</sub> 2C and P(NAiPP)<sub>500</sub> 3C,  $P = 0.2842$ ). However, significantly more BSA is released into the cytosol for the latter ( $P = 0.0042$ , see Figure 7b). To further correlate the amount of taken up polymer with the release, we also calculated the ratio of BSA release to polymer uptake (R/U) for the above-mentioned samples. A considerable increase in this ratio is observed from P(NAEP)<sub>500</sub> 2C to P(NAiPP)<sub>500</sub> 3C. Overall, the relative MFI values for P(NAiPP)<sub>500</sub> 3C remained below the ones for P(NAfBP)<sub>500</sub> 4C or I-PEI, implying that the overall amount of released BSA from the endosome may be lower in the first case. The coincubation of HEK 293T cells with labeled BSA and various concentrations of P(NAiPP)<sub>500</sub> 3C in growth medium revealed no significant increase of the fluorescent signal and the number of affected cells compared to the control. Only P(NAfBP)<sub>500</sub> 4C and I-PEI resulted in a polymer concentration-dependent increase of the fluorescence signal and number of shifted cells.

**Transport of Functioning Proteins.** A crucial factor for the efficient delivery of any biological therapeutic is the preservation of its structure during this process. Commonly, the decrease of pH and the presence of hydrolases following the endolysosomal pathway trigger a degradation of biological material such as proteins. Therefore, an escape from the early endosome is the key to bypass this degradation and ensure an intact delivery of proteins, antibodies, or genetic material. Following previous reports,<sup>60</sup> RNase A was coincubated with our most promising polymers P(NAiPP)<sub>500</sub> 3C and P(NAfBP)<sub>500</sub> 4C in different media to investigate their capability for intact release of this protein. Also in this case, no aggregation of polymer and protein was detected (Figure S10a) and no osmotic stress is to be expected at the chosen experimentation settings. Although the pure enzyme displays no toxic activity on the cells (Figure S24), a release into the cytosol induces cell death due to the degradation of cytosolic RNA, which can be monitored by a concentration-dependent cell viability assay (Figure 8a–b). In accordance with previous experiments, a distinct difference for Opti-MEM and the serum-containing medium was observed. In the presence of serum proteins, P(NAiPP)<sub>500</sub> 3C induced no effect for concentrations up to 100 μg mL<sup>-1</sup>. In contrast, P(NAfBP)<sub>500</sub> 4C was found to efficiently induce endosomal escape at 50 μg mL<sup>-1</sup> as the viability was reduced to  $25.0 \pm 0.7\%$  in the presence of RNase A compared to the pure polymer causing no cytotoxic effects. The further increase of the polymer content enhanced the effect indicating a concentration-dependent release by P(NAfBP)<sub>500</sub> 4C, although an increased cytotoxicity of the polymer at these concentrations has to be considered. In Opti-MEM, coincubation of RNase A with both P(NAiPP)<sub>500</sub> 3C as well as P(NAfBP)<sub>500</sub> 4C affected the cell viability in a concentration-dependent manner. In particular, the coincubation of RNase A and P(NAiPP)<sub>500</sub> 3C, which itself caused no adverse effects on cell viability, resulted in declining cell viabilities by  $50.2 \pm 0.7\%$  starting at a polymer concentration of 25 μg mL<sup>-1</sup>. However, the most significant decrease (by  $84.5 \pm 10.5\%$ ) was found for P(NAfBP)<sub>500</sub> 4C at a concentration of 10 μg mL<sup>-1</sup>. While the pure polymer displayed no adverse effect in this case, the cell viability was reduced to approx. 10% relative to the untreated controls by

coincubation of P(NAfBP)<sub>500</sub> 4C and RNase A. A further increase in the polymer concentration affected cytotoxicity more than it increased endosomal escape efficiency.

In order to visually confirm the previous results, P(NAiPP)<sub>500</sub> 3C and P(NAfBP)<sub>500</sub> 4C were further tested for the delivery of EGFP monitored by CLSM. It has to be mentioned, however, that HEK 293T cells in general display a limited EGFP uptake (Figure 8c,e), which reduces the probability of concurrent presence with the polymer in the same compartments. Interestingly, coincubation with 50 μg mL<sup>-1</sup> P(NAfBP)<sub>500</sub> 4C in the presence of serum caused a more distinct punctate fluorescence pattern and several cells showed a diffuse EGFP fluorescence signal throughout the cytosol with varying intensities (Figure 8d). A similar result was found in the case of P(NAiPP)<sub>500</sub> 3C in Opti-MEM (Figure 8f). In both cases, the numbers of affected cells investigated by flow cytometry appear small compared to the results from BSA delivery (Figure S25), which again might be a result of the limited uptake of this protein.

## DISCUSSION

Endosomal escape is crucial for the delivery of many therapeutics and can be facilitated by pH-responsive cationic polymeric vectors. Thereby, the  $pK_a$  or basicity of the polymers is considered as an important factor. Previous studies on correlations between  $pK_a$  and escape, however, often focused on the delivery of genetic materials, where complexation is an additional key factor,<sup>17,32</sup> or comprise transitions from hydrophilic to hydrophobic at the  $pK_a$  of the materials, which alter their solubility and interactions with membranes.<sup>33</sup> A limiting factor is certainly the scarce number of hydrophilic polymers with  $pK_a$  values and buffer capacities between 5 and 7.4. The described polypiperazines, therefore, represent an exciting new set of materials, where protonation occurs exactly in this range and the basicity of the amino group can gradually be increased with subtle modifications on the substituent without notably affecting its solubility. This fine-tuning of buffer capacity and  $pK_a$  in this region is to our knowledge unprecedented and renders these materials ideal for investigating the impact of basicity on endosomal release and cytotoxicity. As a controlled polymerization (RAFT process) appeared feasible, we were able to create a library of different polypiperazines with DPs ranging from 100 up to 500 and  $pK_a$  values of 6.2, 6.5, 6.7, or 7.1, respectively, covering the most interesting pH region from the extracellular environment to early and late endosomes.<sup>19,51</sup> The necessity of such a fine-tuning becomes already apparent from the biocompatibility tests, where significant cytotoxic effects were only observed for the most basic P(NAfBP)<sub>n</sub> and elevated concentrations of P(NAiPP)<sub>n</sub> with the highest DP, while all other polymers revealed no toxicity. The results corroborate a previous study about the impact of charge density and molar mass of poly(cation)s on cytotoxicity and even allow a more distinct differentiation.<sup>61</sup> Interestingly, our release studies on various compounds ranging from small dyes (calcein) to macromolecules (proteins or dextran) depict similar correlations. A closer look, however, reveals a greater impact of the molar mass of the polymers, as only the highest DPs caused a significant release in the case of calcein. A similar trend was observed for other types of cationic polymers before,<sup>17,62–64</sup> and considering the minor impact on cytotoxicity in the case of the highly charged polymers such as P(NAfBP)<sub>n</sub>, the tuning of the polymer size might represent an interesting step to

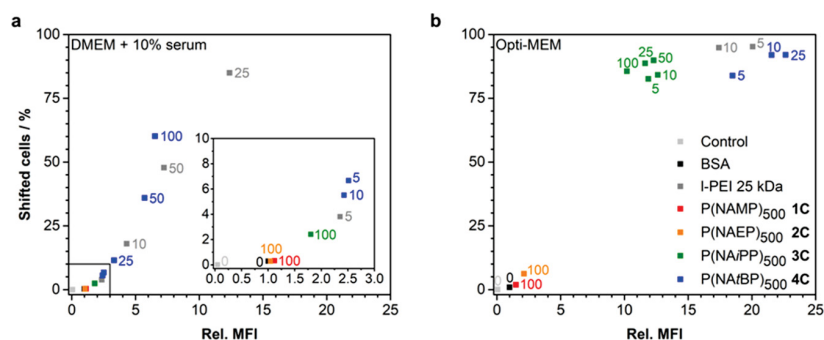


**Figure 9.** Influence of the cell culture medium, basicity, and concentration of the polypiperazines on endosomal escape. Exemplarily, the endosomal escape facilitated by the polypiperazines in comparison to commercial I-PEI 25 kDa is plotted to show correlations between the polymers' basicity and concentration depending on the media composition. Endosomal escape of labeled BSA in HEK 293T cells was quantified via flow cytometry in (a) serum-containing medium and (b) Opti-MEM (see Figure 5). The polymer concentration is given near the corresponding data point, including the highest investigated concentration only in the case of P(NAiPP)<sub>500</sub> 3C in the serum-containing medium to support clarity. Means of three independent experiments are shown. rel. MFI - relative mean fluorescence intensity.

optimize release with insignificant loss of viability. Differences in the release of BSA are on first sight accounted for an increased uptake rate for the more basic polymers. Nevertheless, a direct comparison of P(NAEP)<sub>n</sub> and P(NAiPP)<sub>n</sub> at concentrations, where a similar uptake is given (Figure 7b), revealed that an important factor for efficient release of larger molecules seems to be the  $pK_a$  of the polymers. More significantly, the most basic polymers P(NAiBP)<sub>n</sub> and P(NAiPP)<sub>n</sub> appeared to be effective at any tested concentration (Figure 9), which was as low as 5  $\mu\text{g mL}^{-1}$ , which corroborates our assumption that a key factor is the basicity of the polymers. However, a clear distinction has to be made between the applied conditions. Although P(NAiPP)<sub>n</sub> can cause a considerable release in Opti-MEM without signs of toxicity in the tested range, almost no effect is found in the serum-containing medium (DMEM). On the contrary, the more alkaline P(NAiBP)<sub>n</sub> suffers from increased toxicity in the first case but facilitates a concentration-dependent escape despite the presence of serum, which is comparable to the commercial I-PEI. Despite the lack of an interaction with BSA according to DLS measurements, we assume that the polypiperazines interact with other proteins or components of the serum-containing medium, resulting in a partial shielding of the charges. This aspect is also reflected in the influence of the medium on plasma membrane integrity in the presence of these polymers (Figure S9). The release efficiency in the serum-containing medium is consequently only enhanced at higher  $pK_a$  values compensating for the shielding effect of the charges by serum components, while they also mitigate toxic effects. These findings emphasize the peculiarities of media such as Opti-MEM, and demonstrate potential difficulties induced by serum proteins narrowing the window for efficient release without causing severe toxicity. Despite these challenges in the delivery itself, our final tests on RNase A and EGFP confirm that an intact transport of sensitive biological molecules can be achieved with these polymers and the activity of the proteins in the cytosol is preserved. As mentioned for the potential release mechanisms of PEI in the introduction, either a proton sponge effect or a membrane destabilization can be responsible for the release. In both cases, the protonation of the polypiperazines during the pH decrease along the endosomal maturation is crucial. The rather fast nature of the release as well as the effectivity in delivering molecules of different sizes indicate a proton sponge

effect, although similar effects would be expected for a severer destabilization of the endosomal membrane and the formation of large pores. Further detailed studies are certainly required to unequivocally determine the nature of the endosomal escape mechanism. In addition, investigations on other cell types are certainly of interest to evaluate the potential of these polypiperazines because the present study was performed exclusively using HEK 293T cells, which are considered easy-to-transfect and not very sensitive to high transfection efficiencies. However, still the presented results support that  $pK_a$  values and thus maximum buffer capacities need to be close to 7 for efficient endosomal escape, which is in good agreement with the research on ionizable lipids, where a substantial increase in delivery efficiency was identified at a  $pK_a$  value of 6.8, while  $pK_a$  values of 6.8–7 were described as the most effective.<sup>65–68</sup> Consequently, the often considered range of 5–7.4<sup>21,69,70</sup> for polymeric vectors should be narrowed down, which might explain previously observed discrepancies concerning the importance of buffer capacities in this range.<sup>40,41</sup>

## CONCLUSIONS

In summary, our study reveals a fine balance between efficiency and cytotoxicity of cationic polymers for endosomal escape and further highlights the influence by the media used. As we initially hypothesized, the fine-tuning of basicity and  $pK_a$  is pivotal for pH-responsive polymers and a clear correlation between the proportion of cationic moieties at endosomal pH and the endosomal escape efficiency was observed. The most significant response is observed if the greatest change in the degree of protonation or the maximum buffer capacity occurs in a narrow window between 7.4 and around 6.5. Further aspects can certainly be addressed in future studies, but we are convinced that the presented findings further inspire the design of tailor-made pH-responsive polymers for enhanced endosomal release. The newly discovered polypiperazines may also play a key role in this development and further studies are already ongoing in our group.

## ASSOCIATED CONTENT

### Supporting Information

The Supporting Information is available free of charge at <https://pubs.acs.org/doi/10.1021/acsami.1c00829>.

Polymer labeling strategies; <sup>1</sup>H NMR traces; potentiometric titration data; biocompatibility studies; polymer uptake data; investigations of possible polymer–protein interactions; microscopic investigations of endosomal escape of calcein, dextran, BSA, and EGFP; and image analyses and flow cytometry gating strategies (PDF)

## AUTHOR INFORMATION

### Corresponding Author

Johannes C. Brendel – Laboratory of Organic and Macromolecular Chemistry (IOMC), Friedrich Schiller University Jena, 07743 Jena, Germany; Jena Center for Soft Matter (JCSM), Friedrich Schiller University Jena, 07743 Jena, Germany; [orcid.org/0000-0002-1206-1375](https://orcid.org/0000-0002-1206-1375); Email: [johannes.brendel@uni-jena.de](mailto:johannes.brendel@uni-jena.de)

### Authors

Franziska Hausig – Laboratory of Organic and Macromolecular Chemistry (IOMC), Friedrich Schiller University Jena, 07743 Jena, Germany

Fabian H. Sobotta – Laboratory of Organic and Macromolecular Chemistry (IOMC), Friedrich Schiller University Jena, 07743 Jena, Germany

Friederike Richter – Laboratory of Organic and Macromolecular Chemistry (IOMC), Friedrich Schiller University Jena, 07743 Jena, Germany

Dominic O. Harz – Laboratory of Organic and Macromolecular Chemistry (IOMC), Friedrich Schiller University Jena, 07743 Jena, Germany

Anja Traeger – Laboratory of Organic and Macromolecular Chemistry (IOMC), Friedrich Schiller University Jena, 07743 Jena, Germany; Jena Center for Soft Matter (JCSM), Friedrich Schiller University Jena, 07743 Jena, Germany; [orcid.org/0000-0001-7734-2293](https://orcid.org/0000-0001-7734-2293)

Complete contact information is available at: <https://pubs.acs.org/10.1021/acsami.1c00829>

### Author Contributions

This manuscript was written through contributions of all authors. All authors have given approval to the final version of the manuscript. J.C.B. and F.H. conceived the study. F.S. and D.O.H. synthesized the polymers. F.S., D.O.H., and F.H. characterized the polymers. F.H. and J.C.B. planned the biological experiments in consultation with A.T. and F.R. F.H. conducted the biological characterization and analyzed the data. A.T. and J.C.B. contributed to the interpretation of the results. F.H. and J.C.B. took the lead in writing the manuscript. All authors provided critical feedback and helped shape the research, analysis, and manuscript.

### Notes

The authors declare no competing financial interest.

## ACKNOWLEDGMENTS

This work was supported by the German Science Foundation (DFG) within the Emmy-Noether Program (project-ID: 358263073), the Collaborative Research Center PolyTarget, project A05 and B01 (project-ID: 316213987—SFB 1278), the Federal Ministry of Education and Research (BMBF, #13XP5034A PolyBioMik), and the Fonds der Chemischen Industrie (FCI). The authors thankfully acknowledge Bärbel Beringer-Siemers, Dr. Grit Festag, Lena Jesse, Carolin Kellner, Elisabeth Preußner, and Karina Rost for technical assistance as

well as Elisabeth Moek, Dr. David Pretzel, and Jana Solomun for discussions. The LSM880 ELYRA PS.1 was funded with a grant from the DFG. Furthermore, Prof. U. S. Schubert is acknowledged for his continuous support and providing access to excellent research facilities. Finally, the authors acknowledge the reviewers for their expert opinions and the resulting improvement of this work.

## ABBREVIATIONS

AF 488, Alexa Fluor 488  
ANOVA, analysis of variance  
BSA, bovine serum albumin  
CLSM, confocal laser scanning microscopy  
CTA, chain transfer agent  
DAD, diode array detector  
DMac, *N,N*-dimethylacetamide  
DMEM, Dulbecco's modified Eagle's medium  
DRI, differential refractive index  
EE, early endosome  
EGFP, enhanced green fluorescent protein  
FCS, fetal calf serum  
L, lysosome  
LE, late endosome  
LCST, lower critical solution temperature  
LDH, lactate dehydrogenase  
MFI, mean fluorescence intensity  
PABTC, 2-(((butylthio)carbonothioyl)thio)propanoic acid  
PEI, poly(ethylenimine)  
pI, isoelectric point  
 $pK_a$ , acid dissociation constant  
 $pK_a^{app}$ , apparent acid dissociation constant  
P(NAEP), poly(*N*-acryloyl-*N'*-ethylpiperazine)  
P(NAiPP), poly(*N*-acryloyl-*N'*-iso-propylpiperazine)  
P(NAM), poly(*N*-acryloyl-*N'*-morpholine)  
P(NAMP), poly(*N*-acryloyl-*N'*-methylpiperazine)  
P(NAfBP), poly(*N*-acryloyl-*N'*-*tert*-butylpiperazine)  
PS, polystyrene  
PTFE, polytetrafluoroethylene  
RAFT, reversible addition–fragmentation chain transfer  
rel. MFI, relative mean fluorescence intensity  
SEC, size exclusion chromatography  
SR 101, sulforhodamine 101  
T-PMT, transmitted light detector

## REFERENCES

- (1) Blanco, E.; Shen, H.; Ferrari, M. Principles of Nanoparticle Design for Overcoming Biological Barriers to Drug Delivery. *Nat. Biotechnol.* **2015**, *33*, 941.
- (2) Zhao, J.; Stenzel, M. H. Entry of Nanoparticles into Cells: The Importance of Nanoparticle Properties. *Polym. Chem.* **2018**, *9*, 259–272.
- (3) Pei, D.; Buyanova, M. Overcoming Endosomal Entrapment in Drug Delivery. *Bioconjugate Chem.* **2019**, *30*, 273–283.
- (4) Chailertvanitkul, V. A.; Pouton, C. W. Adenovirus: A Blueprint for Non-Viral Gene Delivery. *Curr. Opin. Biotechnol.* **2010**, *21*, 627–632.
- (5) Suwan, K.; Yata, T.; Waramit, S.; Przystal, J. M.; Stoneham, C. A.; Bentayebi, K.; Asavarut, P.; Chongchai, A.; Pothachareon, P.; Lee, K.-Y.; Topanurak, S.; Smith, T. L.; Gelovani, J. G.; Sidman, R. L.; Pasqualini, R.; Arap, W.; Hajitou, A. Next-Generation of Targeted Aavp Vectors for Systemic Transgene Delivery against Cancer. *Proc. Natl. Acad. Sci. U.S.A.* **2019**, *116*, 18571–18577.
- (6) Zhen, S.; Li, X. Liposomal Delivery of Caspr/Cas9. *Cancer Gene Ther.* **2020**, *27*, 515–527.

- (7) Ichimizu, S.; Watanabe, H.; Maeda, H.; Hamasaki, K.; Ikegami, K.; Chuang, V. T. G.; Kinoshita, R.; Nishida, K.; Shimizu, T.; Ishima, Y.; Ishida, T.; Seki, T.; Katsuki, H.; Futaki, S.; Otagiri, M.; Maruyama, T. Cell-Penetrating Mechanism of Intracellular Targeting Albumin: Contribution of Macropinocytosis Induction and Endosomal Escape. *J. Controlled Release* **2019**, *304*, 156–163.
- (8) LeCher, J. C.; Nowak, S. J.; McMurry, J. L. Breaking in and Busting Out: Cell-Penetrating Peptides and the Endosomal Escape Problem. *Biomol. Concepts* **2017**, *8*, 131–141.
- (9) Allen, J.; Brock, D.; Kondow-McConaghy, H.; Pellois, J.-P. Efficient Delivery of Macromolecules into Human Cells by Improving the Endosomal Escape Activity of Cell-Penetrating Peptides: Lessons Learned from Dftat and Its Analogs. *Biomolecules* **2018**, *8*, 50.
- (10) Evans, B. C.; Fletcher, R. B.; Kilchrist, K. V.; Dailing, E. A.; Mukalel, A. J.; Colazo, J. M.; Oliver, M.; Cheung-Flynn, J.; Brophy, C. M.; Tierney, J. W.; Isenberg, J. S.; Hankenson, K. D.; Ghimire, K.; Lander, C.; Gersbach, C. A.; Duvall, C. L. An Anionic, Endosome-Escaping Polymer to Potentiate Intracellular Delivery of Cationic Peptides, Biomacromolecules, and Nanoparticles. *Nat. Commun.* **2019**, *10*, 5012.
- (11) Smith, S. A.; Selby, L. I.; Johnston, A. P. R.; Such, G. K. The Endosomal Escape of Nanoparticles: Toward More Efficient Cellular Delivery. *Bioconjugate Chem.* **2019**, *30*, 263–272.
- (12) Prchla, E.; Plank, C.; Wagner, E.; Blaas, D.; Fuchs, R. Virus-Mediated Release of Endosomal Content in Vitro: Different Behavior of Adenovirus and Rhinovirus Serotype 2. *J. Cell Biol.* **1995**, *131*, 111–123.
- (13) Li, W.; Nicol, F.; Szoka, F. C. Gala: A Designed Synthetic Ph-Responsive Amphipathic Peptide with Applications in Drug and Gene Delivery. *Adv. Drug Delivery Rev.* **2004**, *56*, 967–985.
- (14) Stewart, M. P.; Langer, R.; Jensen, K. F. Intracellular Delivery by Membrane Disruption: Mechanisms, Strategies, and Concepts. *Chem. Rev.* **2018**, *118*, 7409.
- (15) Erazo-Oliveras, A.; Najjar, K.; Dayani, L.; Wang, T.-Y.; Johnson, G. A.; Pellois, J.-P. Protein Delivery into Live Cells by Incubation with an Endosomolytic Agent. *Nat. Methods* **2014**, *11*, 861.
- (16) Tabujew, I.; Freidel, C.; Krieg, B.; Helm, M.; Koynov, K.; Müllen, K.; Peneva, K. The Guanidinium Group as a Key Part of Water-Soluble Polymer Carriers for SiRNA Complexation and Protection against Degradation. *Macromol. Rapid Commun.* **2014**, *35*, 1191–1197.
- (17) Richter, F.; Martin, L.; Leer, K.; Moek, E.; Hausig, F.; Brendel, J. C.; Traeger, A. Tuning of Endosomal Escape and Gene Expression by Functional Groups, Molecular Weight and Transfection Medium: A Structure-Activity Relationship Study. *J. Mater. Chem. B* **2020**, *8*, 5026–5041.
- (18) Cokca, C.; Zartner, L.; Tabujew, I.; Fischer, D.; Peneva, K. Incorporation of Indole Significantly Improves the Transfection Efficiency of Guanidinium-Containing Poly(Methacrylamide)s. *Macromol. Rapid Commun.* **2020**, *41*, 1900668.
- (19) Maxfield, F. R.; Yamashiro, D. J. Endosome Acidification and the Pathways of Receptor-Mediated Endocytosis. In *Immunobiology of Proteins and Peptides IV: T-Cell Recognition and Antigen Presentation*; Atassi, M. Z., Ed.; Springer US: Boston, MA, 1987; pp 189–198.
- (20) Wagner, E. Polymers for Nucleic Acid Transfer—an Overview. In *Advances in Genetics*; Huang, L.; Liu, D.; Wagner, E., Eds.; Academic Press, 2014; Vol. 88, Chapter 8, pp 231–261.
- (21) Lächelt, U.; Wagner, E. Nucleic Acid Therapeutics Using Polyplexes: A Journey of 50 Years (and Beyond). *Chem. Rev.* **2015**, *115*, 11043–11078.
- (22) Peng, L.; Wagner, E. Polymeric Carriers for Nucleic Acid Delivery: Current Designs and Future Directions. *Biomacromolecules* **2019**, *20*, 3613–3626.
- (23) Lv, H.; Zhang, S.; Wang, B.; Cui, S.; Yan, J. Toxicity of Cationic Lipids and Cationic Polymers in Gene Delivery. *J. Controlled Release* **2006**, *114*, 100–109.
- (24) Kargaard, A.; Sluijter, J. P. G.; Klumperman, B. Polymeric SiRNA Gene Delivery – Transfection Efficiency Versus Cytotoxicity. *J. Controlled Release* **2019**, *316*, 263–291.
- (25) Lungwitz, U.; Breunig, M.; Blunk, T.; Göpferich, A. Polyethylenimine-Based Non-Viral Gene Delivery Systems. *Eur. J. Pharm. Biopharm.* **2005**, *60*, 247–266.
- (26) Boussif, O.; Lezoualc'h, F.; Zanta, M. A.; Mergny, M. D.; Scherman, D.; Demeneix, B.; Behr, J. P. A Versatile Vector for Gene and Oligonucleotide Transfer into Cells in Culture and in Vivo: Polyethylenimine. *Proc. Natl. Acad. Sci. U.S.A.* **1995**, *92*, 7297–7301.
- (27) Benjaminsen, R. V.; Matthebjerg, M. A.; Henriksen, J. R.; Moghimi, S. M.; Andresen, T. L. The Possible “Proton Sponge” Effect of Polyethylenimine (Pei) Does Not Include Change in Lysosomal Ph. *Mol. Ther.* **2013**, *21*, 149–157.
- (28) Vaidyanathan, S.; Orr, B. G.; Banaszak Holl, M. M. Role of Cell Membrane–Vector Interactions in Successful Gene Delivery. *Acc. Chem. Res.* **2016**, *49*, 1486–1493.
- (29) Bus, T.; Traeger, A.; Schubert, U. S. The Great Escape: How Cationic Polyplexes Overcome the Endosomal Barrier. *J. Mater. Chem. B* **2018**, *6*, 6904–6918.
- (30) Li, H.; Cortez, M. A.; Phillips, H. R.; Wu, Y.; Reineke, T. M. Poly(2-Deoxy-2-Methacrylamido Glucopyranose)-B-Poly(Methacrylate Amine)s: Optimization of Diblock Glycopolycations for Nucleic Acid Delivery. *ACS Macro Lett.* **2013**, *2*, 230–235.
- (31) Sprouse, D.; Reineke, T. M. Investigating the Effects of Block Versus Statistical Glycopolycations Containing Primary and Tertiary Amines for Plasmid DNA Delivery. *Biomacromolecules* **2014**, *15*, 2616–2628.
- (32) Trützschler, A.-K.; Bus, T.; Reifarth, M.; Brendel, J. C.; Hoepfener, S.; Traeger, A.; Schubert, U. S. Beyond Gene Transfection with Methacrylate-Based Polyplexes—the Influence of the Amino Substitution Pattern. *Bioconjugate Chem.* **2018**, *29*, 2181–2194.
- (33) Du, L.; Wang, C.; Meng, L.; Cheng, Q.; Zhou, J.; Wang, X.; Zhao, D.; Zhang, J.; Deng, L.; Liang, Z.; Dong, A.; Cao, H. The Study of Relationships between Pka Value and SiRNA Delivery Efficiency Based on Tri-Block Copolymers. *Biomaterials* **2018**, *176*, 84–93.
- (34) Kocak, G.; Tuncer, C.; Bütüin, V. Ph-Responsive Polymers. *Polym. Chem.* **2017**, *8*, 144–176.
- (35) Thavanesan, T.; Herbert, C.; Plamper, F. A. Insight in the Phase Separation Peculiarities of Poly(Dialkylaminoethyl Methacrylate)s. *Langmuir* **2014**, *30*, 5609–5619.
- (36) Velasco, D.; Réthoré, G.; Newland, B.; Parra, J.; Elvira, C.; Pandit, A.; Rojo, L.; Román, J. S. Low Polydispersity (N-Ethyl Pyrrolidine Methacrylamide-Co-1-Vinylimidazole) Linear Oligomers for Gene Therapy Applications. *Eur. J. Pharm. Biopharm.* **2012**, *82*, 465–474.
- (37) Truong, N. P.; Gu, W.; Prasad, I.; Jia, Z.; Crawford, R.; Xiao, Y.; Monteiro, M. J. An Influenza Virus-Inspired Polymer System for the Timed Release of SiRNA. *Nat. Commun.* **2013**, *4*, 1902.
- (38) Lächelt, U.; Kos, P.; Mickler, F. M.; Herrmann, A.; Salcher, E. E.; Rödl, W.; Badgajar, N.; Bräuchle, C.; Wagner, E. Fine-Tuning of Proton Sponges by Precise Diaminoethanes and Histidines in Pdna Polyplexes. *Nanomedicine* **2014**, *10*, 35–44.
- (39) Gallon, E.; Matini, T.; Sasso, L.; Mantovani, G.; Armiñan de Benito, A.; Sanchis, J.; Caliceti, P.; Alexander, C.; Vicent, M. J.; Salmaso, S. Triblock Copolymer Nanovesicles for Ph-Responsive Targeted Delivery and Controlled Release of SiRNA to Cancer Cells. *Biomacromolecules* **2015**, *16*, 1924–1937.
- (40) Kanayama, N.; Fukushima, S.; Nishiyama, N.; Itaka, K.; Jang, W.-D.; Miyata, K.; Yamasaki, Y.; Chung, U.-i.; Kataoka, K. A Peg-Based Biocompatible Block Cationomer with High Buffering Capacity for the Construction of Polyplex Micelles Showing Efficient Gene Transfer toward Primary Cells. *ChemMedChem* **2006**, *1*, 439–444.
- (41) Funhoff, A. M.; van Nostrum, C. F.; Koning, G. A.; Schuurmans-Nieuwenbroek, N. M. E.; Crommelin, D. J. A.; Hennink, W. E. Endosomal Escape of Polymeric Gene Delivery Complexes Is Not Always Enhanced by Polymers Buffering at Low Ph. *Biomacromolecules* **2004**, *5*, 32–39.

- (42) Selby, L. I.; Cortez-Jugo, C. M.; Such, G. K.; Johnston, A. P. R. Nanoescapology: Progress toward Understanding the Endosomal Escape of Polymeric Nanoparticles. *WIREs Nanomed. Nanobi.* **2017**, *9*, No. e1452.
- (43) Gan, L. H.; Gan, Y. Y.; Deen, G. R. Poly(N-Acryloyl-N'-Propylpiperazine): A New Stimuli-Responsive Polymer. *Macromolecules* **2000**, *33*, 7893–7897.
- (44) Roshan Deen, G.; Gan, L. H. Influence of Amino Group Pka on the Properties of Stimuli-Responsive Piperazine-Based Polymers and Hydrogels. *J. Appl. Polym. Sci.* **2008**, *107*, 1449–1458.
- (45) Liu, C.; Wan, T.; Wang, H.; Zhang, S.; Ping, Y.; Cheng, Y. A Boronic Acid-Rich Dendrimer with Robust and Unprecedented Efficiency for Cytosolic Protein Delivery and Crispr-Cas9 Gene Editing. *Sci. Adv.* **2019**, *5*, No. eaaw8922.
- (46) Gurunathan, S.; Woong Han, J.; Kim, E.; Kwon, D.-N.; Park, J.-K.; Kim, J.-H. Enhanced Green Fluorescent Protein-Mediated Synthesis of Biocompatible Graphene. *J. Nanobiotechnol.* **2014**, *12*, 41.
- (47) Colombani, O.; Lejeune, E.; Charbonneau, C.; Chassenieux, C.; Nicolai, T. Ionization of Amphiphilic Acidic Block Copolymers. *J. Phys. Chem. B* **2012**, *116*, 7560–7565.
- (48) Chiriac, V.; Balea, G. Buffer Index and Buffer Capacity for a Simple Buffer Solution. *J. Chem. Educ.* **1997**, *74*, 937.
- (49) Sobotta, F. H.; Kuchenbrod, M. T.; Grune, C.; Fischer, D.; Hoepfener, S.; Brendel, J. C. Elucidating Preparation-Structure Relationships for the Morphology Evolution During the Raft Dispersion Polymerization of N-Acryloyl Thiomorpholine. *Polym. Chem.* **2021**, *12*, 1668–1680.
- (50) Ziebarth, J. D.; Wang, Y. Understanding the Protonation Behavior of Linear Polyethylenimine in Solutions through Monte Carlo Simulations. *Biomacromolecules* **2010**, *11*, 29–38.
- (51) Huotari, J.; Helenius, A. Endosome Maturation. *EMBO J.* **2011**, *30*, 3481–3500.
- (52) Knop, K.; Hoogenboom, R.; Fischer, D.; Schubert, U. S. Poly(Ethylene Glycol) in Drug Delivery: Pros and Cons as Well as Potential Alternatives. *Angew. Chem., Int. Ed.* **2010**, *49*, 6288–6308.
- (53) Mochizuki, A.; Kimura, M.; Ina, A.; Tomono, Y.; Tanaka, M. Study on the Water Structure and Blood Compatibility of Poly(Acryloylmorpholine-R-Butyl Methacrylate). *J. Biomater. Sci. Polym. Ed.* **2010**, *21*, 1895–1910.
- (54) Gorman, M.; Chim, Y. H.; Hart, A.; Riehle, M. O.; Urquhart, A. J. Poly(N-Acryloylmorpholine): A Simple Hydrogel System for Temporal and Spatial Control over Cell Adhesion. *J. Biomed. Mater. Res.* **2014**, *102*, 1809–1815.
- (55) Gardey, E.; Sobotta, F. H.; Hoepfener, S.; Bruns, T.; Stallmach, A.; Brendel, J. C. Influence of Core Cross-Linking and Shell Composition of Polymeric Micelles on Immune Response and Their Interaction with Human Monocytes. *Biomacromolecules* **2020**, *21*, 1393–1406.
- (56) Martens, T. F.; Remaut, K.; Demeester, J.; De Smedt, S. C.; Braeckmans, K. Intracellular Delivery of Nanomaterials: How to Catch Endosomal Escape in the Act. *Nano Today* **2014**, *9*, 344–364.
- (57) Ribbeck, K.; Görlich, D. Kinetic Analysis of Translocation through Nuclear Pore Complexes. *EMBO J.* **2001**, *20*, 1320–1330.
- (58) Rehman, Z. u.; Hoekstra, D.; Zuhorn, I. S. Mechanism of Polyplex- and Lipoplex-Mediated Delivery of Nucleic Acids: Real-Time Visualization of Transient Membrane Destabilization without Endosomal Lysis. *ACS Nano* **2013**, *7*, 3767–3777.
- (59) Salomone, F.; Cardarelli, F.; Di Luca, M.; Boccardi, C.; Nifosi, R.; Bardi, G.; Di Bari, L.; Serresi, M.; Beltram, F. A Novel Chimeric Cell-Penetrating Peptide with Membrane-Disruptive Properties for Efficient Endosomal Escape. *J. Controlled Release* **2012**, *163*, 293–303.
- (60) Dubois, J. L. N.; Lavignac, N. Cationic Poly(Amidoamine) Promotes Cytosolic Delivery of Bovine Rnase a in Melanoma Cells, While Maintaining Its Cellular Toxicity. *J. Mater. Chem. B* **2015**, *3*, 6501–6508.
- (61) Fischer, D.; Li, Y.; Ahlemeyer, B.; Kriegelstein, J.; Kissel, T. In vitro cytotoxicity testing of polycations: influence of polymer structure on cell viability and hemolysis. *Biomaterials* **2003**, *24*, 1121–1131.
- (62) Kunath, K.; von Harpe, A.; Fischer, D.; Petersen, H.; Bickel, U.; Voigt, K.; Kissel, T. Low-Molecular-Weight Polyethylenimine as a Non-Viral Vector for DNA Delivery: Comparison of Physicochemical Properties, Transfection Efficiency and in Vivo Distribution with High-Molecular-Weight Polyethylenimine. *J. Controlled Release* **2003**, *89*, 113–125.
- (63) Ahn, C.-H.; Chae, S. Y.; Bae, Y. H.; Kim, S. W. Biodegradable Poly(Ethylenimine) for Plasmid DNA Delivery. *J. Controlled Release* **2002**, *80*, 273–282.
- (64) Breunig, M.; Lungwitz, U.; Liebl, R.; Goepferich, A. Breaking up the Correlation between Efficacy and Toxicity for Nonviral Gene Delivery. *Proc. Natl. Acad. Sci. U.S.A.* **2007**, *104*, 14454–14459.
- (65) Semple, S. C.; Akin, A.; Chen, J.; Sandhu, A. P.; Mui, B. L.; Cho, C. K.; Sah, D. W. Y.; Stebbing, D.; Crosley, E. J.; Yaworski, E.; Hafez, I. M.; Dorkin, J. R.; Qin, J.; Lam, K.; Rajeev, K. G.; Wong, K. F.; Jeffs, L. B.; Nechev, L.; Eisenhardt, M. L.; Jayaraman, M.; Kazem, M.; Maier, M. A.; Srinivasulu, M.; Weinstein, M. J.; Chen, Q.; Alvarez, R.; Barros, S. A.; De, S.; Klimuk, S. K.; Borland, T.; Kosovrasti, V.; Cantley, W. L.; Tam, Y. K.; Manoharan, M.; Ciufolini, M. A.; Tracy, M. A.; de Fougères, A.; MacLachlan, L.; Cullis, P. R.; Madden, T. D.; Hope, M. J. Rational Design of Cationic Lipids for siRNA Delivery. *Nat. Biotechnol.* **2010**, *28*, 172–176.
- (66) Alabi, C. A.; Love, K. T.; Sahay, G.; Yin, H.; Luly, K. M.; Langer, R.; Anderson, D. G. Multiparametric Approach for the Evaluation of Lipid Nanoparticles for siRNA Delivery. *Proc. Natl. Acad. Sci. U.S.A.* **2013**, *110*, 12881–12886.
- (67) Jayaraman, M.; Ansell, S. M.; Mui, B. L.; Tam, Y. K.; Chen, J.; Du, X.; Butler, D.; Eltepu, L.; Matsuda, S.; Narayanannair, J. K.; Rajeev, K. G.; Hafez, I. M.; Akin, A.; Maier, M. A.; Tracy, M. A.; Cullis, P. R.; Madden, T. D.; Manoharan, M.; Hope, M. J. Maximizing the Potency of siRNA Lipid Nanoparticles for Hepatic Gene Silencing in Vivo. *Angew. Chem., Int. Ed.* **2012**, *51*, 8529–8533.
- (68) Whitehead, K. A.; Dorkin, J. R.; Vegas, A. J.; Chang, P. H.; Veisheh, O.; Matthews, J.; Fenton, O. S.; Zhang, Y.; Olejnik, K. T.; Yesilyurt, V.; Chen, D.; Barros, S.; Klebanov, B.; Novobrantseva, T.; Langer, R.; Anderson, D. G. Degradable Lipid Nanoparticles with Predictable in Vivo siRNA Delivery Activity. *Nat. Commun.* **2014**, *5*, 4277.
- (69) Varkouhi, A. K.; Scholte, M.; Storm, G.; Haisma, H. J. Endosomal Escape Pathways for Delivery of Biologicals. *J. Controlled Release* **2011**, *151*, 220–228.
- (70) Behr, J.-P. The Proton Sponge: A Trick to Enter Cells the Viruses Did Not Exploit. *Chimia* **1997**, *51*, 34–36.

# Supporting Information

## Correlation between Protonation of Tailor-Made Polypiperazines and Endosomal Escape for Cytosolic Protein Delivery

*Franziska Hausig<sup>1</sup>, Fabian H. Sobotta<sup>1</sup>, Friederike Richter<sup>1</sup>, Dominic O. Harz<sup>1</sup>, Anja Traeger<sup>1,2</sup>,  
Johannes C. Brendel<sup>1,2\*</sup>*

<sup>1</sup>Laboratory of Organic and Macromolecular Chemistry (IOMC), Friedrich Schiller University  
Jena, Jena, Germany

<sup>2</sup>Jena Center for Soft Matter (JCSM), Friedrich Schiller University Jena, Jena, Germany

(\*) corresponding author (johannes.brendel@uni-jena.de)

## Tables

Table S1 Summary of polypiperazines used in this study. ....	13
--	----

## Figures

Figure S1 Polymer labeling strategies.....	10
Figure S2 <sup>1</sup> H NMR traces of piperazine-based monomers. ....	11
Figure S3 <sup>1</sup> H NMR traces of polypiperazines. ....	12
Figure S4 Relative buffer capacity of polypiperazines at different pH values. ....	14
Figure S5 Potentiometric titration of commercial l-PEI. ....	14
Figure S6 Cytotoxicity of polypiperazines.....	15
Figure S7 Evaluation of polymer uptake by flow cytometry and data correction .....	16
Figure S8 Hemolysis and erythrocyte aggregation at different pH values. ....	17
Figure S9 Interaction of polypiperazines with the plasma membrane of HEK 293T cells.....	18
Figure S10 Investigations of possible interactions between polymer and tested model compounds. .....	19
Figure S11 T-PMT images visualizing endosomal escape of calcein.....	20
Figure S12 3D-Images of calcein release.....	20
Figure S13 T-PMT images visualizing endosomal escape of BSA. ....	21
Figure S14 Plot profile of BSA treated control cell. ....	21
Figure S15 Endosomal escape of labeled dextran investigated by CLSM. ....	22
Figure S16 Polymer and calcein localization at different time points. ....	23
Figure S17 Quantification of endosomal escape of calcein by flow cytometry.....	24
Figure S18 Evaluation of endosomal escape of calcein via flow cytometry.....	23
Figure S19 Quantification of nuclear calcein delivery (image analysis). ....	26
Figure S20 Quantification of endosomal escape of labeled BSA by flow cytometry.....	27
Figure S21 Evaluation of endosomal escape of labeled BSA via flow cytometry. ....	28
Figure S22 Quantification of nuclear BSA delivery (image analysis). ....	29
Figure S23 Colocalisation of polypiperazines and endolysosomes in HEK 293T cells. ....	30
Figure S24 Cytotoxicity studies of RNase A without polymer addition.....	31
Figure S25 Evaluation of endosomal escape of EGFP via flow cytometry. ....	32



## Further methods

### Chemicals

All chemicals and solvents were purchased from Sigma-Aldrich, Carl Roth, Acros Organics, ThermoFisher Scientific, and Iris Biotech and used without further purification, if not stated otherwise. 2-(Butylthiocarbonothioylthio)propanoic acid (PABTC) was prepared as previously reported[1]. 1,4-dioxane was treated with inhibitor remover resin for 24 h prior to use.

### General procedure for the synthesis of piperazine monomers

A typical procedure for the synthesis of piperazine monomers was as follows: 1-*Iso*-propylpiperazine (10 g, 77.97 mmol, 1 eq.) was dissolved in distilled dichloromethane (40 mL) and 4-methoxyphenol (20 mg) was added as inhibitor. Subsequently, the solution was placed in an ice-bath and a solution of acryloylchloride (9.5 mL, 116.96 mmol, 1.5 eq.) in 10 mL distilled dichloromethane was added dropwise under stirring. As the addition was finished, the mixture was allowed to warm to room temperature and stirred overnight. The color of the solution changed from yellowish to brown-red during the reaction. Afterward, 25 mL saturated NaOH solution was added, the organic phase separated and the aqueous phase washed with dichloromethane (3 × 20 mL). Next, the combined organic phase were washed with saturated NaHCO<sub>3</sub> solution, dried over Na<sub>2</sub>SO<sub>4</sub>, and filtrated. Subsequent to evaporation of the solvent, the crude product was purified by vacuum distillation (130 °C, 6 mbar) to obtain the pure product as colorless oil.

NAMP:

Yield: 45%. <sup>1</sup>H NMR (MeOH-d<sub>4</sub>, 300 MHz): δ = 2.30-2.38 (s, 3H, -CH<sub>3</sub>), 2.40-2.56 (m, 4H, -CH<sub>2</sub>-N-), 3.62-3.78 (m, 4H, -CO-N-CH<sub>2</sub>-), 3.56-3.80 (m, 4H, -CO-N-CH<sub>2</sub>-), 5.73-5.79 (d, 1H, 3J = 9.0, -CH=CH<sub>2</sub>), 6.19-6.25 (d, 1H, 3J = 18.0, -CH=CH<sub>2</sub>), 6.73-6.82 (dd, 1H, 3J = 9.0, 3J = 18.0, -CH=CH<sub>2</sub>).

NAEP:

Yield: 57%. <sup>1</sup>H NMR (MeOH-d<sub>4</sub>, 300 MHz): δ = 1.12-1.16 (t, 3H, 3J = 6.0, -CH<sub>3</sub>), 2.40-2.65 (m, 6H, -CH<sub>2</sub>-N-, -N-CH<sub>2</sub>-), 3.69 (m, 4H, -CO-N-CH<sub>2</sub>-), 5.74-5.78 (d, 1H, 3J = 9.0, -CH=CH<sub>2</sub>), 6.19-6.25 (d, 1H, 3J = 18.0, -CH=CH<sub>2</sub>), 6.73-6.82 (dd, 1H, 3J = 9.0, 3J = 18.0, -CH=CH<sub>2</sub>).

NA*i*PP:

Yield: 76%. <sup>1</sup>H NMR (MeOH-d<sub>4</sub>, 300 MHz): δ = 1.09-1.11 (d, 6H, 3J = 6.0, -CH<sub>3</sub>), 2.58 (m, 4H, -CH<sub>2</sub>-N-), 2.68-2.81 (sept, 1H, 3J = 6.0, -CH-), 3.67 (m, 4H, -CO-N-CH<sub>2</sub>-), 5.74-5.78 (d, 1H, 3J = 9.0, -CH=CH<sub>2</sub>), 6.18-6.25 (d, 1H, 3J = 18.0, -CH=CH<sub>2</sub>), 6.73-6.82 (dd, 1H, 3J = 9.0, 3J = 18.0, -CH=CH<sub>2</sub>).

NA*t*BP:

Yield: 79%. <sup>1</sup>H NMR (CDCl<sub>3</sub>, 300 MHz): δ = 1.06 (s, 9H, -(CH<sub>3</sub>)<sub>3</sub>), 2.54-2.57 (t, 4H, 3J = 6.0, -CH<sub>2</sub>-N-), 3.54-3.67 (m, 4H, -CO-N-CH<sub>2</sub>-), 5.65-5.69 (d, 1H, 3J = 9.0, -CH=CH<sub>2</sub>), 6.24-6.30 (d, 1H, 3J = 18.0, -CH=CH<sub>2</sub>), 6.52-6.61 (dd, 1H, 3J = 9.0, 3J = 18.0, -CH=CH<sub>2</sub>).

### Fluorescence labeling of piperazine polymers

The fluorescence labeling of piperazine polymers was proceeded as follows: PNA*i*PP<sub>500</sub> (150 mg, 1.64 μmol, 1 eq.) was dissolved in anhydrous dimethylformamide (DMF, 2 mL). Afterwards, triethylamine (0.455 μL, 3.28 μmol, 2 eq.), Oregon Green cadaverine isomer 5 (164 μL of a 5 mM solution in DMF, 0.821 μmol, 0.5 eq.) and PyBOP (1.23 mg, 3.28 μmol, 2 eq.) were added under stirring. The mixture was stirred for 7 days at room temperature and a labeling efficiency of 78% was monitored by SEC (eluent: DMAc + 0.21% LiCl, UV/Vis: 480-513 nm). Afterward, the polymers were purified from free dye by dialysis of DMF solutions against deionized water for several days (MWCO: 10-12 kDa) until no more free dye could be detected.

### Nuclear magnetic resonance (NMR)

<sup>1</sup>H NMR were performed at room temperature on a AC 300 MHz spectrometer (Bruker, US). Chemical shifts (δ) are reported in ppm.

### **Determination of cytotoxicity**

Cytotoxicity studies were performed using the mouse fibroblast cell line L929 (400620, CLS), as recommended by ISO10993-5. In detail, cells were seeded at  $10^3$  cells  $\text{mL}^{-1}$  ( $10^4$  cells per well) in a 96-well plate (VWR, Germany) and incubated for 24 h. No cells were seeded in the outer wells. The medium was changed to the fresh cell culture medium 1 h prior to treatment. Afterward, the polymer solutions in phosphate buffered saline (PBS) were added to the cells at the indicated concentrations (from 5 to 1000  $\mu\text{g mL}^{-1}$ ), and the plates were incubated for an additional 24 h. The control cells were incubated with fresh culture medium containing the same amount of PBS as the treated cells. Subsequently, the medium was replaced by a mixture of a fresh culture medium and the resazurin-based solution alamarBlue (Thermo Fisher, Germany, prepared according to the manufacturer's instructions). After further incubation for 4 h at 37 °C under a humidified 5% (V/V) CO<sub>2</sub> atmosphere, the fluorescence was measured at  $\lambda_{\text{ex}} = 570 \text{ nm}/\lambda_{\text{em}} = 610 \text{ nm}$ , with untreated cells on the same well plate serving as negative controls. The negative control was standardized as 0% of metabolism inhibition and referred to as 100% viability. Cell viability below 70% was considered to be indicative of cytotoxicity. Experiments were conducted in five technical replicates. All experiments were conducted including Blanks, negative controls and cells treated with l-PEI (25 kDa) serving as positive control.

### **Lactate dehydrogenase (LDH) release assay**

To investigate the polymers influence on the integrity of the cell membrane of HEK 293T cells the leakage of LDH from the cytosol to the surrounding cell culture medium was investigated utilizing the CytoTox-ONE™ Homogeneous Membrane Integrity Assay (Promega, Germany) according to the manufacturer's instructions. Briefly, cells were seeded, incubated and treated as described for uptake studies. Following incubation for 16 h the supernatant was transferred into a 96 well plate in triplicates and allowed to equilibrate to room temperature. Subsequently, the assay buffer including the resaruzin-based substrate was added to the supernatant 1:1 and incubated at room temperature for 10 min. After the addition of a stop solution included in the kit the fluorescence intensity was measured at  $\lambda_{\text{EX}}=560 \text{ nm}/\lambda_{\text{EM}}=590 \text{ nm}$ . Cells treated with 0.9% (w/V) Triton X-100 30 min prior to harvest of the supernatant served as positive control (100 % LDH release). Cells

incubated solely with the same amount of PBS were used as negative control (0% LDH release). The LDH release of the polymers was calculated as follows (3):

$$\text{LDH-release} / \% = \frac{\text{FI}(\text{sample}) - \text{FI}(\text{Blank})}{\text{FI}(\text{Triton X-100}) - \text{FI}(\text{Blank})} \cdot 100 \quad (\text{S1})$$

Where FI(sample), FI(Blank), and FI(Triton X-100) represent the fluorescence intensity of a given sample, respective cell culture medium without cells, and Triton X-100 treated cells, respectively.

### **Hemolysis assay**

The membrane damaging properties of the polymers were quantified by analyzing the release of hemoglobin from erythrocytes. Human blood was provided by the Department of Transfusion Medicine, Jena University Hospital. Briefly, human blood was centrifuged at 4 500g for 5 min. The pellet was washed three times with PBS (pH 7.4) by centrifugation at 4 500g for 5 min. Human erythrocytes were suspended in PBS at pH 7.4 to resemble physiological conditions in blood/cytoplasm or in PBS at pH 6 to mimic the slightly acidic environment in the early endosome. Polymer suspensions of different concentrations, also prepared in the respective PBS buffer, were mixed 1:1 with erythrocyte suspensions and were incubated at 37°C for 1 h. Erythrocyte suspensions were centrifuged at 2 400g for 5 min. The release of hemoglobin in the supernatant was determined at 544 nm. The absorbance was measured using a plate reader (Tecan, Germany). Concurrently, determinations were conducted with washed erythrocytes either lysed with 1% Triton X-100 or suspended in PBS at the respective pH as a reference. The hemolytic activity of the homopolymers was calculated as follows (4):

$$\text{Hemolysis} / \% = \frac{\text{A}(\text{sample}) - \text{A}(\text{PBS})}{\text{A}(\text{Triton X-100})} \quad (\text{S2})$$

Here, A(sample), A(PBS), and A(Triton X-100) are the absorbance of erythrocytes incubated with a respective sample, suspended in PBS, and erythrocytes lysed with Triton X-100, respectively. The analysis was repeated with blood from three different donors.

### **Erythrocyte aggregation**

To investigate the behaviour of the pH-sensitive homopolymers towards cellular membranes at different pH values, human erythrocytes were treated with homopolymers under physiological

conditions in human blood (pH 7.4) and in slightly acidic environment representing the pH of the early endosome (pH 6). Erythrocyte suspensions in PBS at different pH values were prepared as described above and mixed 1:1 with polymer solutions leading to final concentrations of  $100 \mu\text{g mL}^{-1}$ . After incubation at  $37 \text{ }^\circ\text{C}$  for 2 h, erythrocyte aggregation was measured at 645 nm (Tecan, Switzerland). In addition, erythrocyte aggregation was evaluated by microscopic evaluation (100x magnification). As positive and negative assay controls erythrocytes were treated with  $50 \mu\text{g mL}^{-1}$  25 kDa branched poly(ethylene imine) (bPEI) solution (Polysciences Inc., Warrington, US) or PBS buffer at respective pH. The aggregation activity of the homopolymers is given as an aggregation rate calculated as follows (5):

$$\text{Aggregation rate} = \frac{1}{A(\text{sample})} \quad (\text{S3})$$

Here,  $A(\text{sample})$  is the mean absorbance of a given sample.

### **Dynamic light scattering (DLS)**

Hydrodynamic diameter of polypiperazines with and without addition of BSA (Sigma, catalogue number 05470) or RNase A (Merck, catalogue number 10109169001) were determined by using dynamic light scattering (DLS, Zetasizer Nano-ZS, Malvern Instruments, U.K.). The polymers and BSA were diluted in PBS (pH 7.4) for size determinations. RNase A was suspended in water at a concentration of  $10 \text{ mg mL}^{-1}$ . The instrument was operated with a 633 nm He-Ne Laser and intensity fluctuations at a backscattering angle of  $173^\circ$  at a temperature of  $25 \text{ }^\circ\text{C}$  were measured in three runs (each an average of  $3 \times 30 \text{ s}$ ). A cumulants fit was used to calculate the Z-average. The derived hydrodynamic radii are presented as mean  $\pm$  SD.

### **Agarose gel electrophoresis**

Potential interactions between the polymers and calcein were investigated by agarose gel electrophoresis. Polymers (DP: 500, final concentration of  $1 \text{ mg mL}^{-1}$ ) mixed with calcein (final concentration of  $250 \mu\text{g mL}^{-1}$ ) in PBS as well as Oregon Green-labeled polymers ( $10 \text{ mg mL}^{-1}$ ) were diluted 1:6 with green gel loading buffer (Jena Biosciences, Jena, Germany) and applied to an agarose gel (1% in TBE buffer). Electrophoresis was run in TBE buffer at 80 V for 60 min

followed by analysis with a gel documentation system (RED, Alpha Innotech, Germany, UV excitation).

### **Aqueous size exclusion chromatography (SEC)**

Aqueous SEC was conducted using a Jasco instrument equipped with DRI and UV detector. The liquid chromatography system used PSS NOVEMA-MAX columns (guard/30/1 000/1 000 Å, 5 µm particle size). The aqueous eluent contained 0.3% (v/v) trifluoroacetic acid + 0.1 mol L<sup>-1</sup> NaCl as additive. Samples were run at 1 mL min<sup>-1</sup> at 30 °C. Aqueous SEC was measured for a 1+1 mixture of P(NA<sub>i</sub>PP)<sub>500</sub> **3C** (concentration: 2.1 mg mL<sup>-1</sup>) and TRITC-Dex ((Tetramethylrhodamine-labeled dextran, 70 kDa, 20 mg mL<sup>-1</sup>) as well as both solutions individually, using 100 µL injection volume each.

### **Dextran release assay**

A tetramethylrhodamine functionalized dextran (70 kDa, Thermo Fisher, catalogue number D1818) was dissolved in sterile PBS at 20 mg mL<sup>-1</sup>. HEK 293T cells were seeded and treated analogous to the calcein and BSA release assays but with a final concentration of 1 mg mL<sup>-1</sup> labeled dextran. CLSM analysis was conducted analogously to calcein and BSA release assays, but applying an argon laser for excitation at 405 nm (1%) and 561 nm (2%) as well as emission filters for Hoechst (410-450 nm) and TRITC fluorescence (610-670 nm) with gains of 700 and 800.

### **Polymer uptake with endolysosomal co-staining.**

To study the uptake and fate of the polypiperazines in cells, the homopolymers with the highest DP (DP: 500) were labeled with Oregon Green after polymerization. The labeling efficiency was determined spectrometrically. To obtain equal labeling efficiencies for the microscopic studies, the labeled polymers were adjusted with unlabeled ones. HEK 293T cells (ACC 635, DSMZ) were seeded at 2 x 10<sup>5</sup> cells mL<sup>-1</sup> in glass-bottomed cell culture dishes (Cellview, Greiner Bio-One, Austria) and allowed to grow for 32 h. The medium was replaced with fresh Opti-MEM 1 h before treatment. Cells were incubated with 100 µg mL<sup>-1</sup> of the respective polymer solutions at 37 °C

under a humidified 5% (v/v) CO<sub>2</sub> atmosphere for 16 h. To image intracellular distribution in live cells, Hoechst 33342 (Thermo Fisher, USA) was added at a final concentration of 5 µg mL<sup>-1</sup> for 10 min to stain cell nuclei. Five minutes before imaging, 50 nM LysoTracker Red DND-99 was added to the cells. Live cell imaging was performed with an LSM880, Elyra PS.1 system (Zeiss, Germany) using an argon laser for excitation at 405 nm (1%), 488 nm (1.2%), and 561 nm (2%), and emission filters for Hoechst (410-451 nm), Oregon green (508-544 nm), and LysoTracker Red (644-722 nm) with gains of 700, 850, and 800, respectively. An apochromatic 40 × 1.4 NA plan oil immersion objective was used for magnification. All images of all experiments were acquired (ZEN, black edition, version 2.3 SP1, Zeiss, Germany) and processed (ImageJ, Java 8[2]) consistently for polymer-treated cells and cells that served as controls. The colocalization image was created with the Image Calculator following background subtraction showing all pixels with green and red signal.

### **Image analysis for the quantification of endosomal escape**

To check for a correlation between the microscopic data and the flow cytometry studies, endosomal release was quantified in the microscopic images. HEK 293T cells were treated as described in the main section. For this purpose, control and polymer images were acquired and processed (ImageJ, Java 8[2]) in the same way. To obtain binary images of the Hoechst and respective green channels (calcein or AF 488 for BSA), the Auto Threshold function of ImageJ was used with Huang's method. Using the Analysis Particles function, the cell nuclei were counted (corresponding to 100% of the cells). To count all nuclei with a green signal, an image was generated using the Image Calculator, showing all nuclei with a green signal. Lastly, these were also counted and related to the total number of nuclei.

## Polymer synthesis

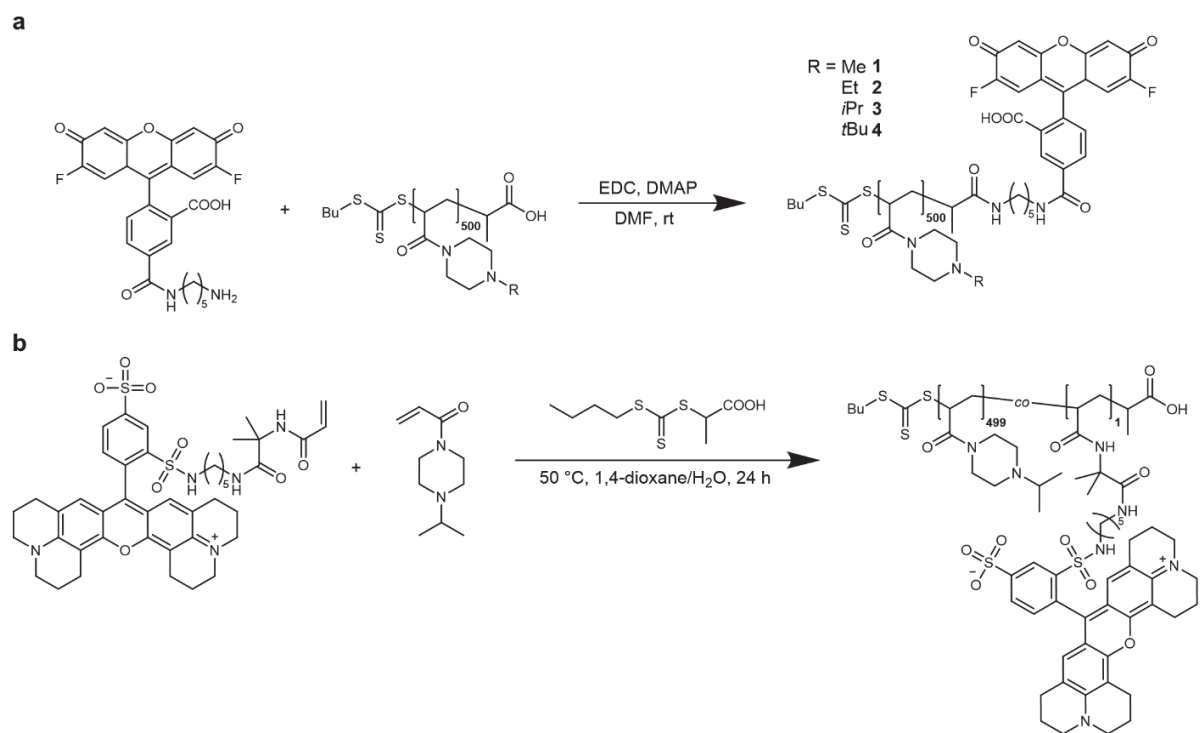


**Figure S1 Polymer labeling strategies.** **a** The materials with DP 500 were labeled with Oregon Green following a post-polymerization strategy. **b** NAIiPP was co-polymerized with a monomer which comprised the fluorescent dye sulforhodamine 101 to obtain a labeled version of the polymer (**3C''**) complementary to the dyes used in the study.



## Polymer characterization

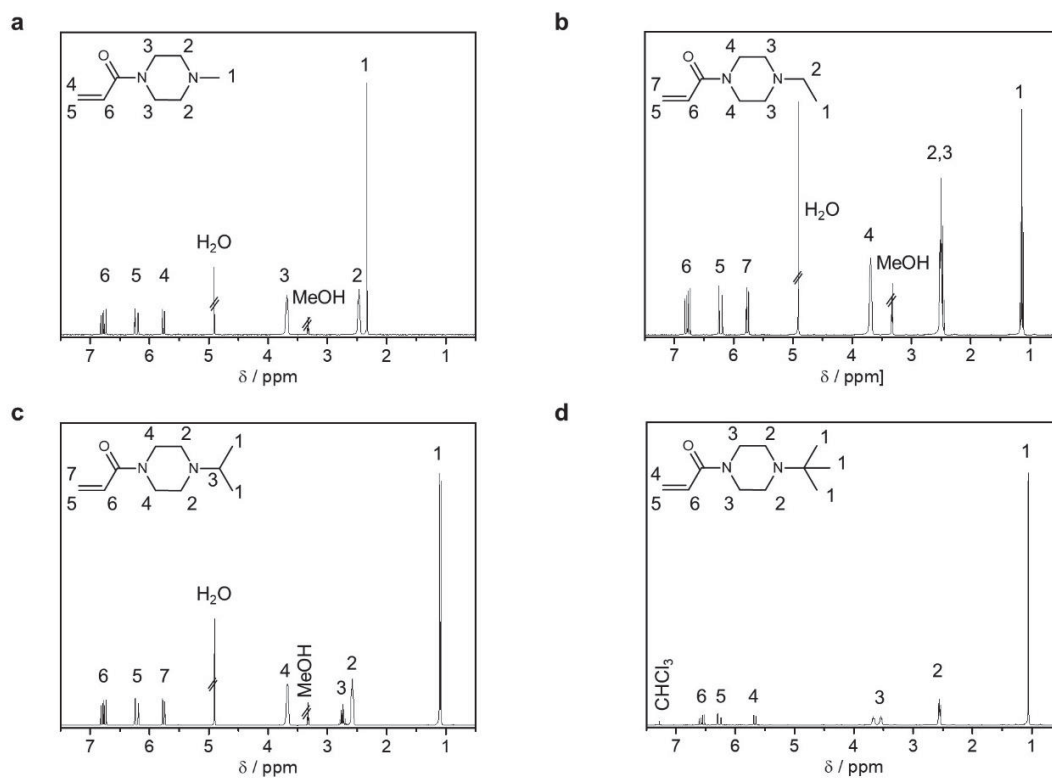


**Figure S2**  $^1\text{H}$  NMR traces of piperazine-based monomers.  $^1\text{H}$  NMR traces of **a** NAMP, **b** NAEP, **c** NAiPP and **d** NAiBP.

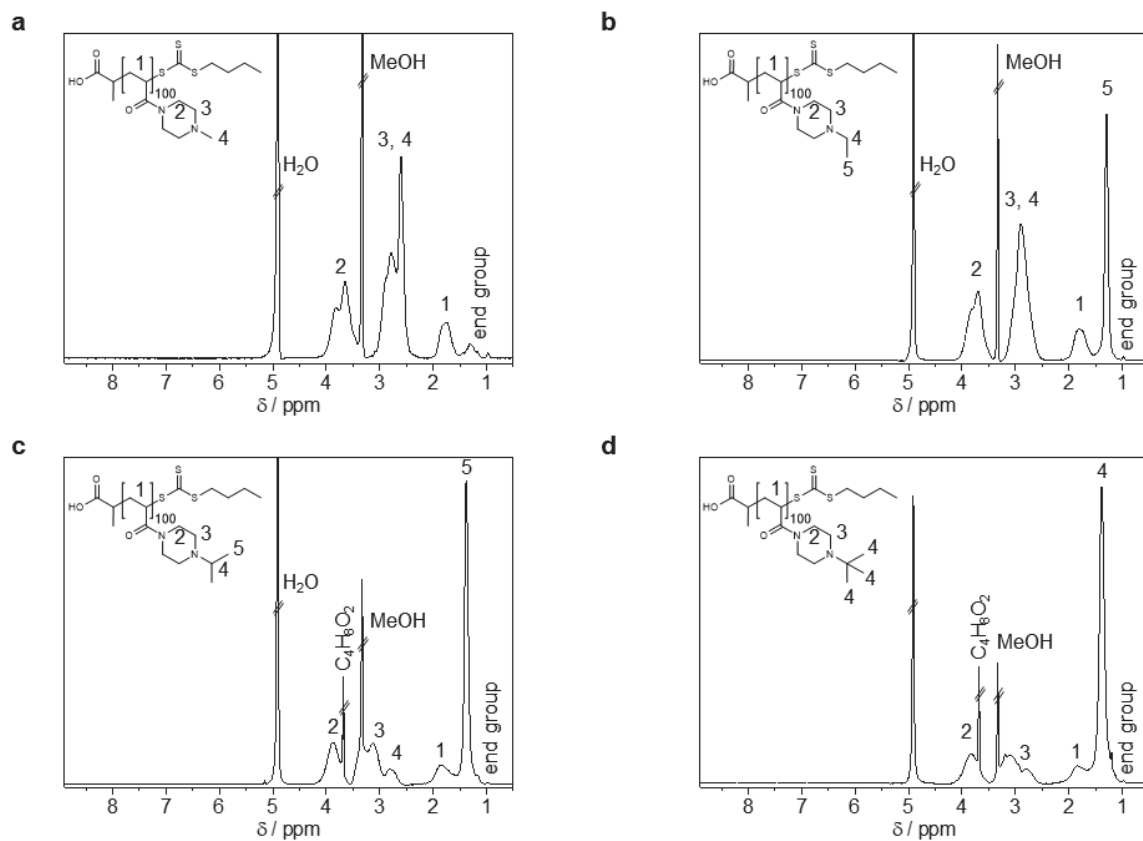


**Figure S3**  $^1\text{H}$  NMR traces of polypiperazines.  $^1\text{H}$  NMR traces of **a** P(NAMP) $_{100}$ , **b** P(NAEP) $_{100}$ , **c** P(NAiPP) $_{100}$  and **d** P(NAiBP) $_{100}$ .

**Table S1 Summary of polypiperazines used in this study.**

Polymer ID	Polymer abbreviation	$M_{n, th}^a / \text{g mol}^{-1}$	$M_{n, SEC}^b / \text{g mol}^{-1}$	$D^b$
0A	P(NAM) <sub>100</sub>	14 400	13 100	1.06
0B	P(NAM) <sub>250</sub>	35 500	24 800	1.20
0C	P(NAM) <sub>500</sub>	70 800	47 200	1.30
0C'	P(NAM) <sub>500</sub> -OG	71 300	52 600	1.32
1A	P(NAMP) <sub>100</sub>	15 700	8 300	1.14
1B	P(NAMP) <sub>250</sub>	38 800	23 800	1.16
1C	P(NAMP) <sub>500</sub>	77 300	53 500	1.22
1C'	P(NAMP) <sub>500</sub> -OG	77 800	62 000	1.31
2A	P(NAEP) <sub>100</sub>	17 100	11 100	1.17
2B	P(NAEP) <sub>250</sub>	42 300	25 500	1.24
2C	P(NAEP) <sub>500</sub>	84 400	55 800	1.29
2C'	P(NAEP) <sub>500</sub> -OG	84 900	68 200	1.45
3A	P(NA <i>i</i> PP) <sub>100</sub>	18 500	14 400	1.15
3B	P(NA <i>i</i> PP) <sub>250</sub>	45 800	40 300	1.29
3C	P(NA <i>i</i> PP) <sub>500</sub>	91 400	65 000	1.23
3C'	P(NA <i>i</i> PP) <sub>500</sub> -OG	91 900	67 600	1.30
3C''	P(NA <i>i</i> PP <sub>499-co</sub> -SR101 <sub>1</sub> )	92 000	52 900	1.29
4A	P(NA <i>t</i> BP) <sub>100</sub>	19 900	16 000	1.18
4B	P(NA <i>t</i> BP) <sub>250</sub>	49 300	30 500	1.30
4C	P(NA <i>t</i> BP) <sub>500</sub>	98 400	62 500	1.30
4C'	P(NA <i>t</i> BP) <sub>500</sub> -OG	98 900	59 000	1.33

a Calculated based on  $[M]_0/[CTA]_0 \times \text{monomer conversion}$ . b Determined by SEC (Eluent: DMAc + 0.21 wt% LiCl, polystyrene calibration). OG: Oregon green cadavarine 5-isomer, SR101: Sulforhodamine 101 cadavarine.

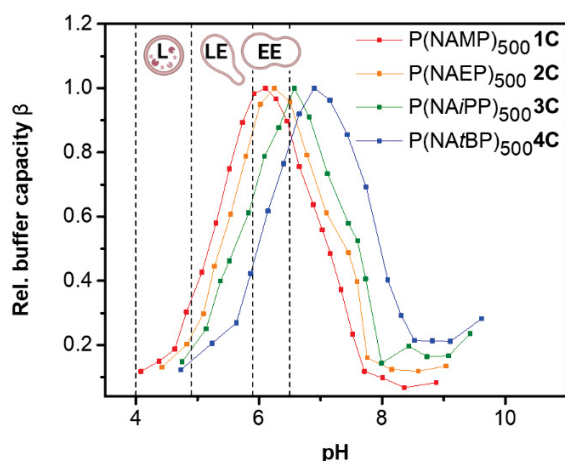


**Figure S4 Relative buffer capacity of polypiperazines at different pH values.** The relative buffer capacity  $\beta$  was calculated from the titration data according to equation (2) (see methods section) for P(NAMP)<sub>500</sub> (red), P(NAEP)<sub>500</sub> (orange), P(NAiPP)<sub>500</sub> (green) and P(NAfBP)<sub>500</sub> (blue). According to Maxfield & Yamashiro et al.[3] the pH ranges within the compartments of the end-lysosomal pathway, early endosomes, late endosomes and lysosomes are indicated. EE - early endosome, LE - late endosome, L - lysosome.

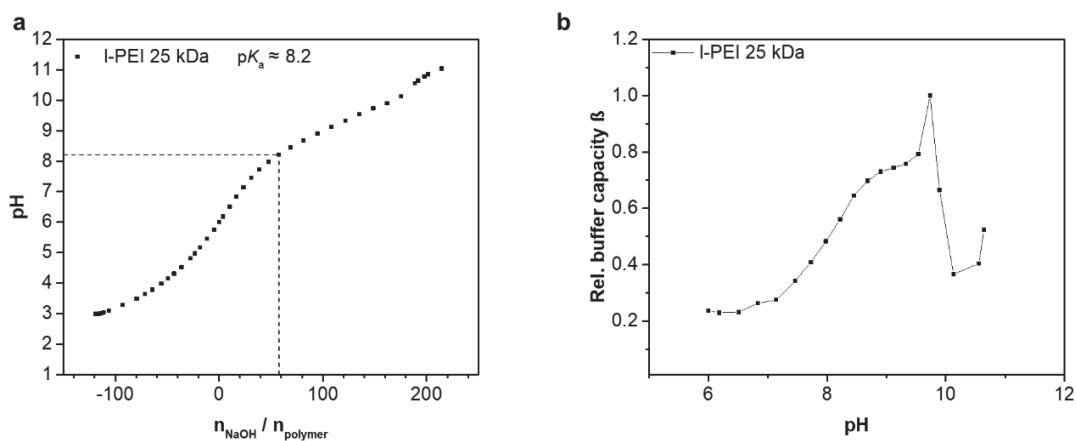


**Figure S5 Potentiometric titration of commercial l-PEI.** **a** The titration curve of commercial l-PEI (25 kDa) was obtained from potentiometric titration of the acidified polymer solution against sodium hydroxide in water with 150 mM sodium chloride. The  $pK_a$  is indicated. **b** The relative buffer capacity  $\beta$  was calculated from the titration data according to equation (2).

## Biological studies

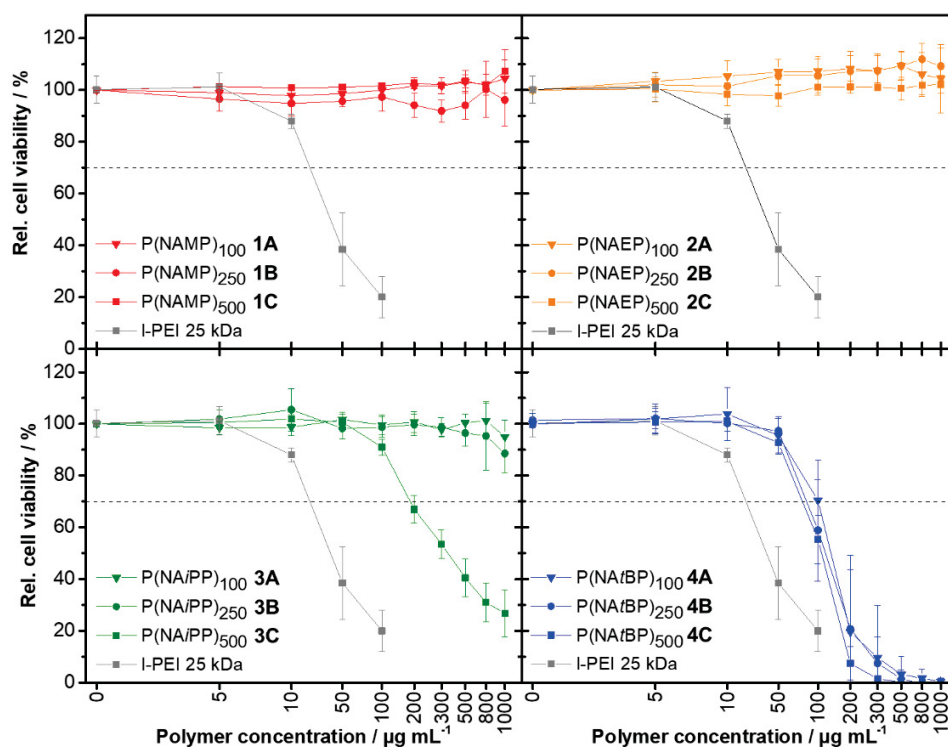


**Figure S6 Cytotoxicity of polypiperazines.** Polymer concentration-dependent viability of murine fibroblasts L929 was assed according to ISO10993-5 for P(NAMP)<sub>n</sub> (red), P(NAEP)<sub>n</sub> (orange), P(NAiPP)<sub>n</sub> (green) and P(NAiBP)<sub>n</sub> (blue) with DP: 100 (triangle), DP: 250 (circle) and DP: 500 (square). Mean  $\pm$  SD of at least three independent experiments is shown. The viability of L929 cells treated with commercial I-PEI (25 kDa, grey squares) is given for comparison. Connecting lines do not represent actual data points; for visual support.

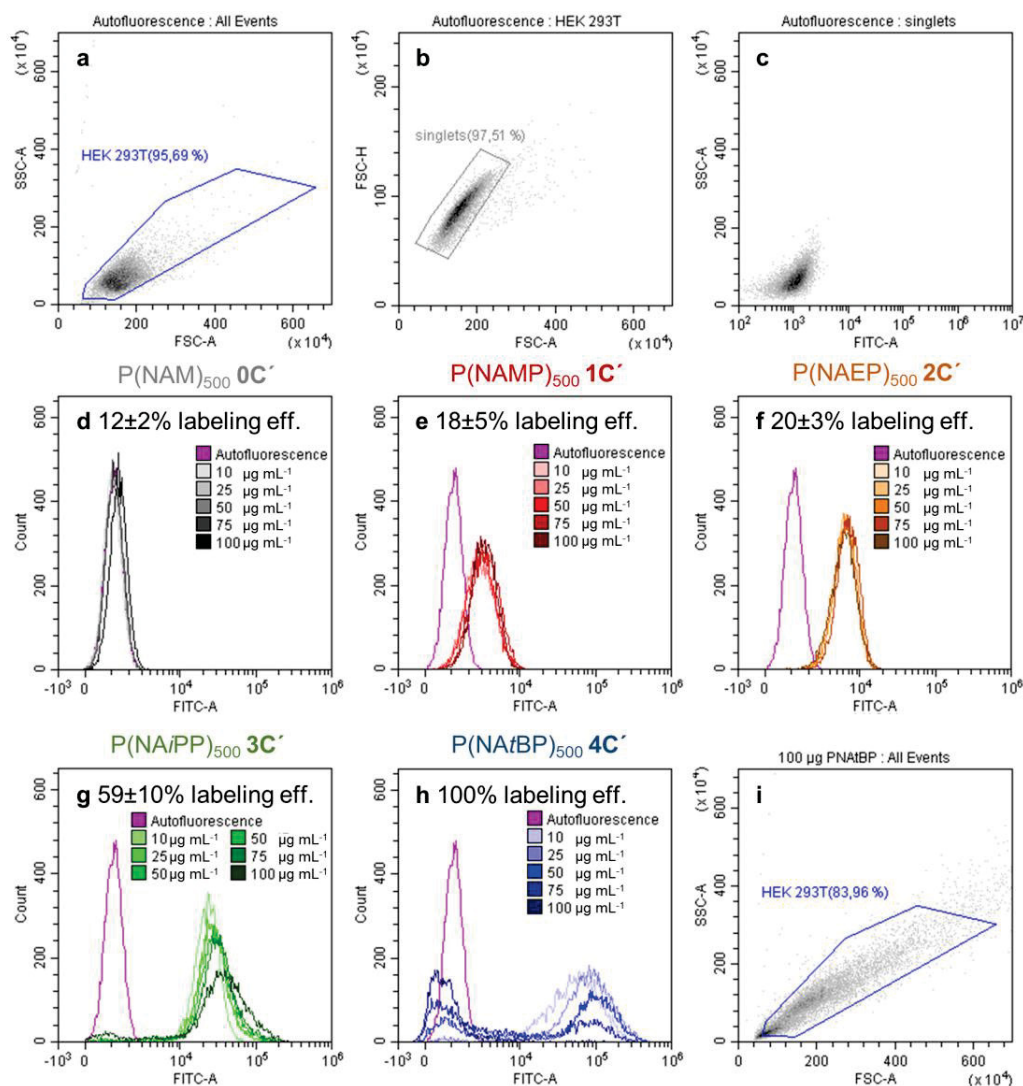


**Figure S7 Evaluation of polymer uptake by flow cytometry and data correction.** The cellular uptake of Oregon Green-labeled polymers (DP: 500) was assessed by flow cytometry after 16 h. Here, the gating strategy of flow cytometry analysis including forward/sideward scatter (**a**) to exclude debris, doublet discrimination (**b**) and the sideward scatter/Oregon Green signal (**c**) are shown. Histograms of HEK 293T cells in Opti-MEM incubated with  $100 \mu\text{g mL}^{-1}$  of the respective polypiperazines (**e-h**) or  $\text{P(NAM)}_{500} \mathbf{0C}'$  (**d**) are displayed. The corresponding labeling efficiency of the polymer in relation to  $\text{P(NA}t\text{BP)}_{500} \mathbf{4C}'$  is given with each histogram. For further data analyses, a correction factor was applied to the obtained data to account for the different labeling efficiencies. **i** It should be noted that the viability of the  $\text{P(NA}t\text{BP)}_{500} \mathbf{4C}'$  treated cells was reduced.

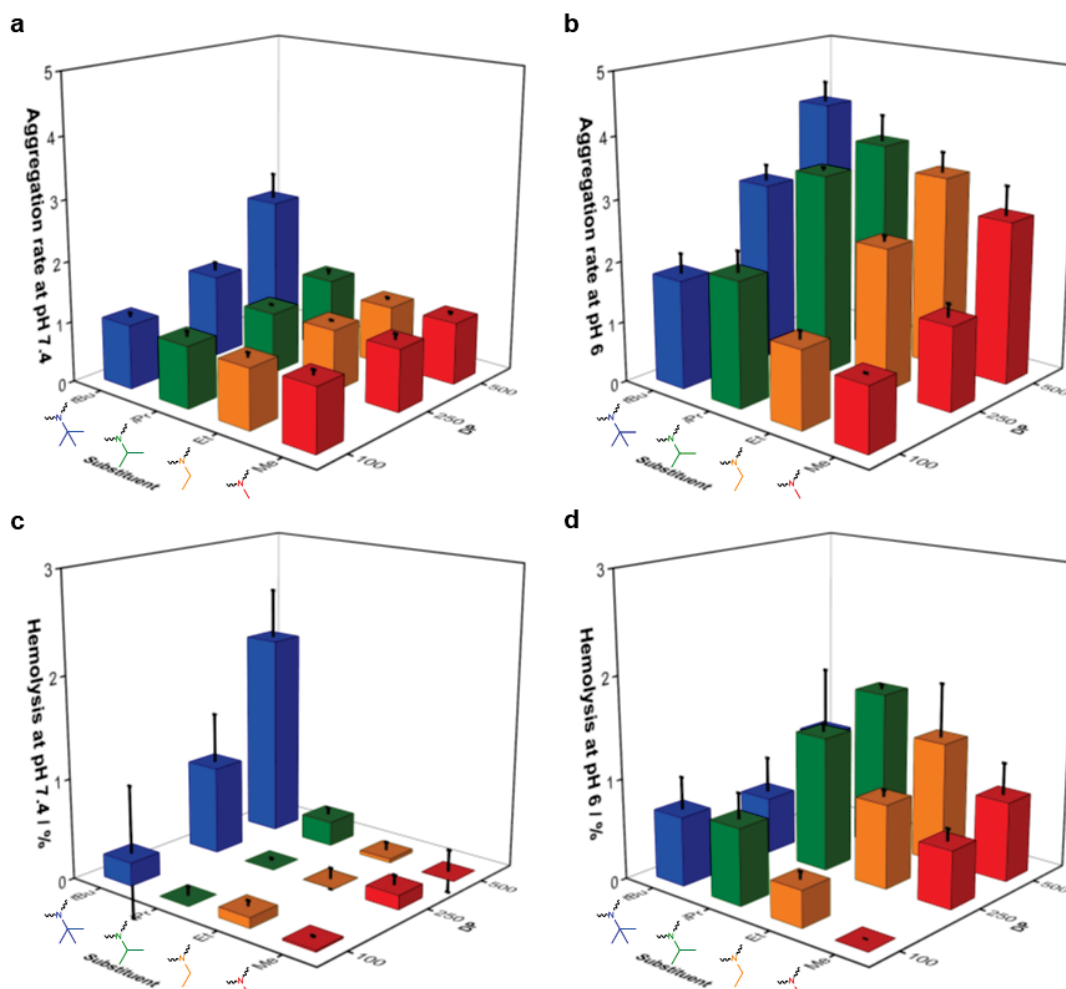


**Figure S8 Hemolysis and erythrocyte aggregation at different pH values.** Human blood was collected from three different donors. The containing erythrocytes were washed separately and re-suspended in PBS buffers with pH 7.4 (**a**, **c**) and pH 6 (**b**, **d**), respectively. Red blood cells **a** in PBS (pH 7.4) or **b** in PBS (pH 6) were incubated with the respective polymers at a polymer concentration of  $100 \mu\text{g mL}^{-1}$  at  $37^\circ\text{C}$  for 1 h. The absorbance was measured via a microplate reader (Tecan) and the aggregation rate was calculated according to equation (S3). The erythrocyte aggregation was also evaluated microscopically (data not shown.) Erythrocytes **c** in PBS (pH 7.4) and **d** in PBS (pH 6) were incubated with the polymers at a concentration of  $100 \mu\text{g mL}^{-1}$  at  $37^\circ\text{C}$  for 2 h and centrifuged. The absorbance of the supernatant was determined using a microplate reader (Tecan). Hemolysis was calculated in relation to Triton-X according to equation (S3). **a - d** A hemoglobin release below 2% classifies the polymers as non-hemolytic according to the ASTM standard F756-00. Mean  $\pm$  SD of experiments with blood from three different donors is given.

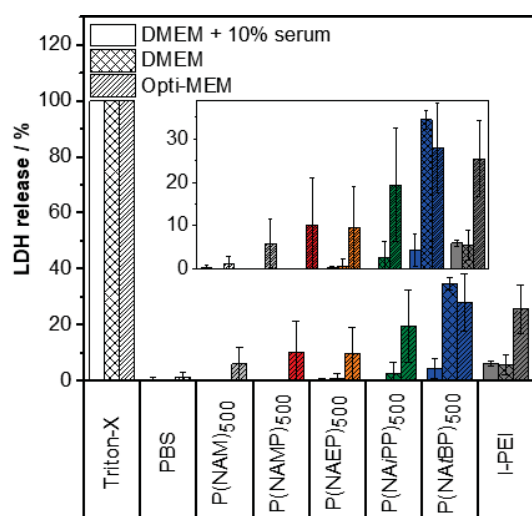


**Figure S9 Interaction of polypiperazines with the plasma membrane of HEK 293T cells.** The amount of released lactate dehydrogenase (LDH) in the supernatant of HEK 293T cells incubated with Oregon Green-labeled polypiperazines was measured (CytoTox-ONETM Homogeneous Membrane Integrity Assay, Promega, Germany). Cells lysed with Triton X-100 and treated with the buffer PBS only served as assay-internal positive and negative controls, respectively. Labeled P(NAM)<sub>500</sub> (light grey) served as a non-pH-responsive control. Commercial l-PEI (25 kDa, dark grey) was included for comparison. Mean  $\pm$  SD of three independent experiments is shown.



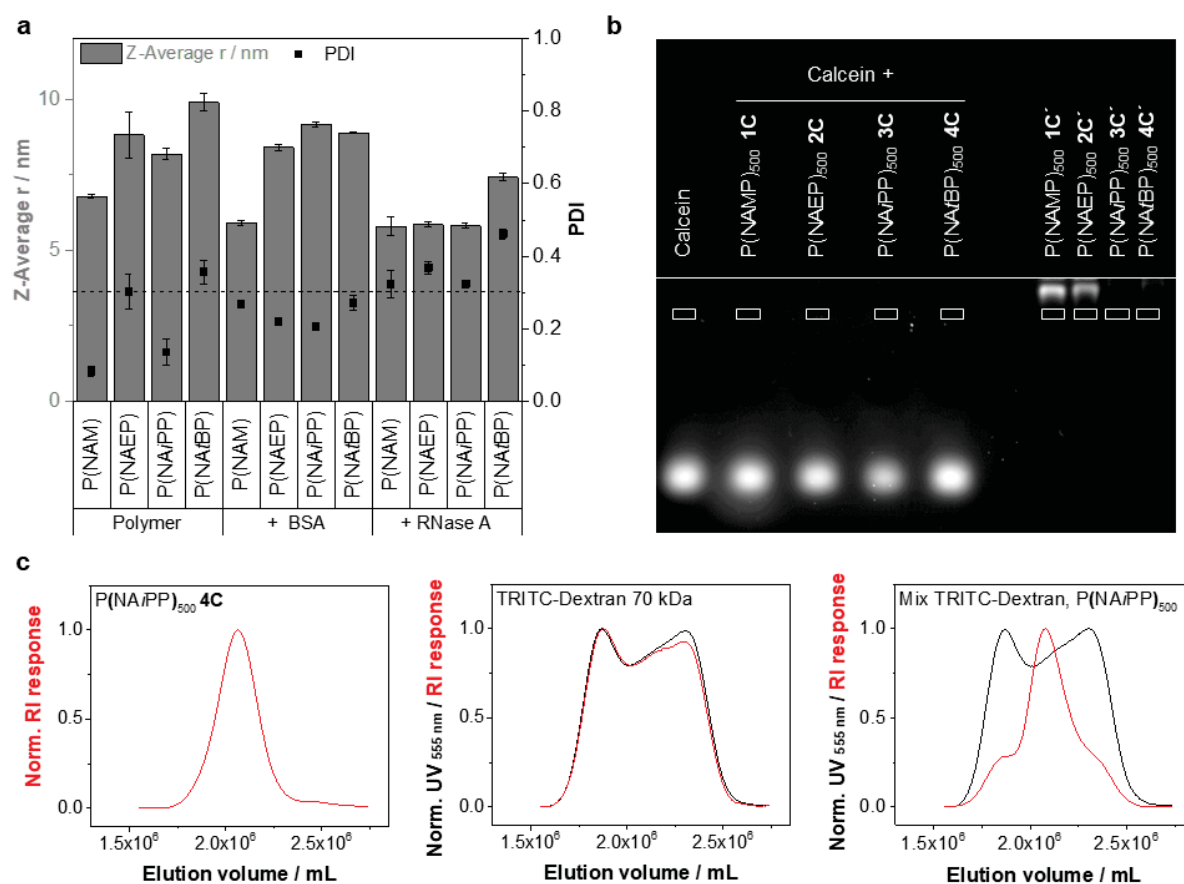


**Figure S10 Investigations of possible interactions between polymer and tested model compounds.** **a** Pure polymers (DP: 500) or polymers mixed with proteins were suspended in PBS at a final concentration of  $5 \text{ mg mL}^{-1}$  and investigated via DLS ( $\circ 173$ ), mean  $\pm$  SD of three runs is shown. **b** Unlabeled polymers (left, DP: 500,  $1 \text{ mg mL}^{-1}$ ) mixed with calcein ( $250 \mu\text{g mL}^{-1}$ ) in PBS or labeled polymers (right,  $10 \text{ mg mL}^{-1}$ ) were applied to an agarose gel (1% in TBE buffer) and run in the TBE buffer at 80 V for 60 min followed by analysis with a gel documentation system (RED, Alpha Innotech, UV excitation). Pockets of agarose gel are marked with white boxes. **c** Pure PNAiPP<sub>500</sub> 3C, pure TRITC-Dex (Tetramethylrhodamine-labeled dextran, 70 kDa) or a 1+1 mixture of both were measured by SEC (Jasco, Eluent: 0.3% (v/v) trifluoroacetic acid + 0.1 M NaCl in water) at  $1 \text{ mL min}^{-1}$  at  $30 \text{ }^\circ\text{C}$  (Columns: PSS NOVEMA-MAX 30/1000/1000 Å) equipped with UV (555 nm) and RI detection.

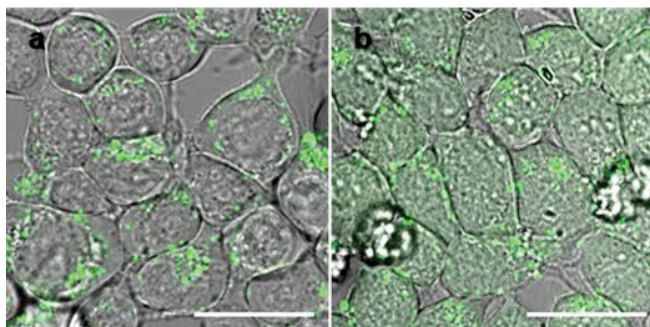


**Figure S11 T-PMT images visualizing endosomal escape of calcein.** The merge of the calcein channel and T-PMT of HEK 293T in Opti-MEM treated **a** with  $25 \mu\text{g mL}^{-1}$  calcein or **b** with additional  $100 \mu\text{g mL}^{-1}$  P(NAiPP) **3C''** for 16 h are shown. See Figure 3 for further channels. **a-b** Scale bar  $20 \mu\text{m}$ . T-PMT - transmitted light detector.

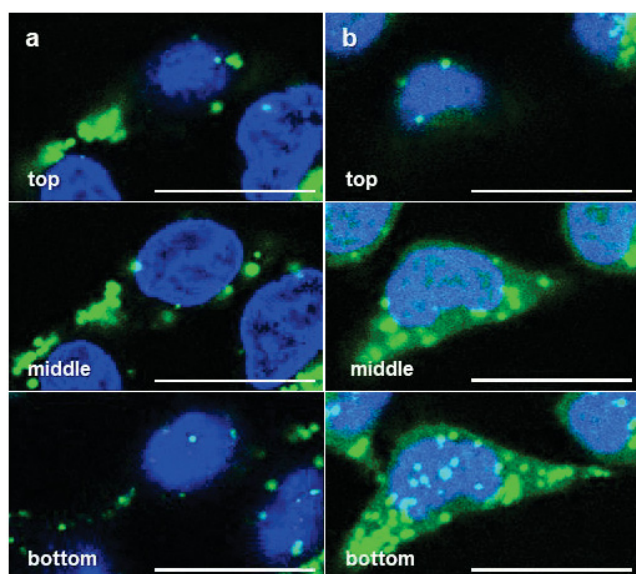


**Figure S12 3D-Images of calcein release.** **a** Example images from a z-stack acquisition from the lower, middle and upper part of a cell treated with calcein are given as a merge with the Hoechst channel visualizing the nuclei. **b** Corresponding images from the z-stack of a cell additionally treated with P(NAiPP)<sub>500</sub> **3C''** reveal endosomal release and cytosolic as well as nuclear delivery of calcein (also see Figure 3j for images showing the calcein channel only). **a-b** Scale bar  $20 \mu\text{m}$ .

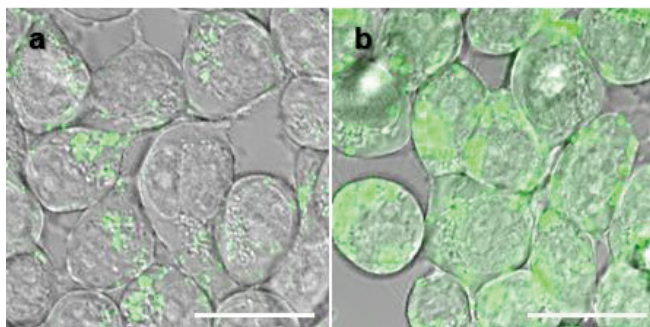


**Figure S13 T-PMT images visualizing endosomal escape of BSA.** The merged image of the AF488 channel (BSA) and T-PMT of HEK 293T in Opti-MEM treated **a** with  $5 \mu\text{g mL}^{-1}$  labeled BSA or **b** with additional  $100 \mu\text{g mL}^{-1}$  P(NAiPP) 3C'' for 16 h are shown. See Figure 4b, d and f in the main manuscript for further channels. **a-b** Scale bar  $20 \mu\text{m}$ . T-PMT - transmitted light detector.

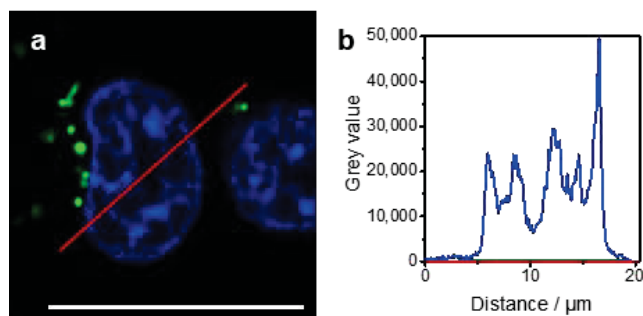


**Figure S14 Plot profile of BSA treated control cell.** **a** The merged image of the Hoechst and the BSA channel of a HEK 293T cell treated with  $5 \mu\text{g mL}^{-1}$  labeled BSA as a control and **b** the corresponding plot profile is shown, indicating no AF488 signal within the cytosol and nucleus for cells that were not treated with endosomolytic polymers. See Figure 4g-h for the polymer treated cell. **a** Scale bar  $20 \mu\text{m}$ .

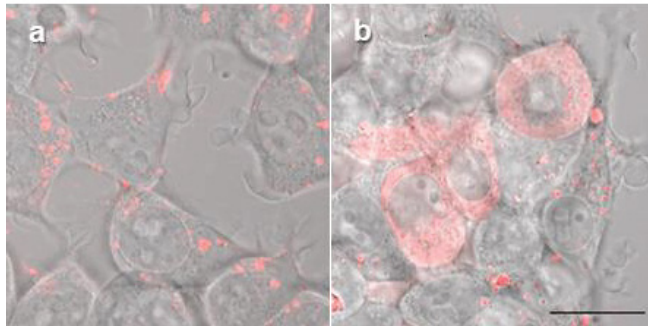


**Figure S15 Endosomal escape of labeled dextran investigated by CLSM.** **a** HEK 293T cells were treated with  $1 \text{ mg mL}^{-1}$  TRITC-labeled dextran (70 kDa) or **b** with additional  $100 \text{ } \mu\text{g mL}^{-1}$  P(NAiPP)<sub>500</sub> **3C**, washed twice and imaged via CLSM. In contrast to the other microscopic studies, unlabeled polymer was used in this experiment because SR 101 and TRITC would not have been indistinguishable due to their similar spectra. Scale bar  $20 \text{ } \mu\text{m}$ . SR 101 – sulforhodamine 101, TRITC – tetramethylrhodamine.

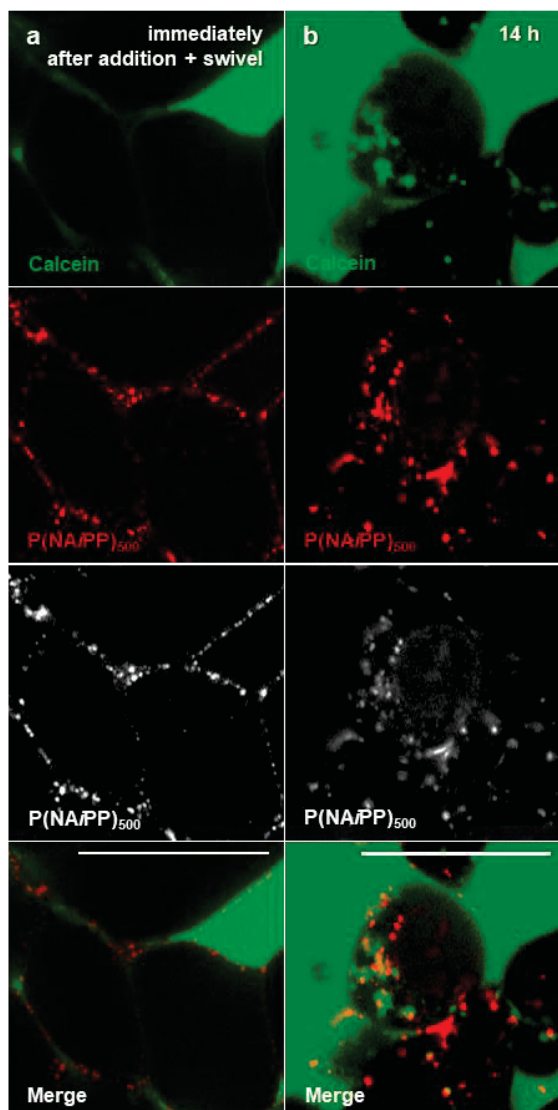


**Figure S16 Polymer and calcein localization at different time points.** **a** P(NAiPP)<sub>500</sub> **3C''** interacts with the plasma membrane immediately after polymer and calcein addition and a short swivel. **b** After the calcein release (see Figure 6), partial localization of P(NAiPP)<sub>500</sub> **3C''** within the nucleus was observed in some HEK 293T cells. **a-b** The calcein channel (first row) and the corresponding image of the red channel in red or gray scale (polymer, second or third rows) as well as the merge of the calcein and polymer channel (fourth row) are shown. Scale bar 20  $\mu$ m.

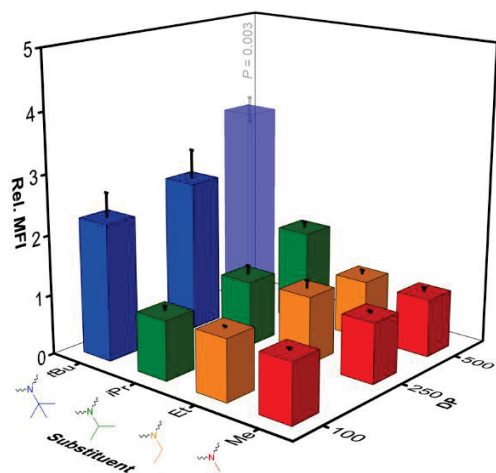


**Figure S17 Quantification of endosomal escape of calcein by flow cytometry.** HEK 293T cells in DMEM + 10% serum were treated with calcein and  $100 \mu\text{g mL}^{-1}$  polypiperazines, washed twice, trypsinized and analyzed via flow cytometry. The means  $\pm$  SD of three independent experiments relative to control cells treated with calcein only (rel. MFI = 1) are shown. Statistical differences between the means were calculated with Dunnett's T3 test. The slight transparency of a bar indicates gated cell populations below 70%. rel. MFI, relative mean fluorescence intensity.

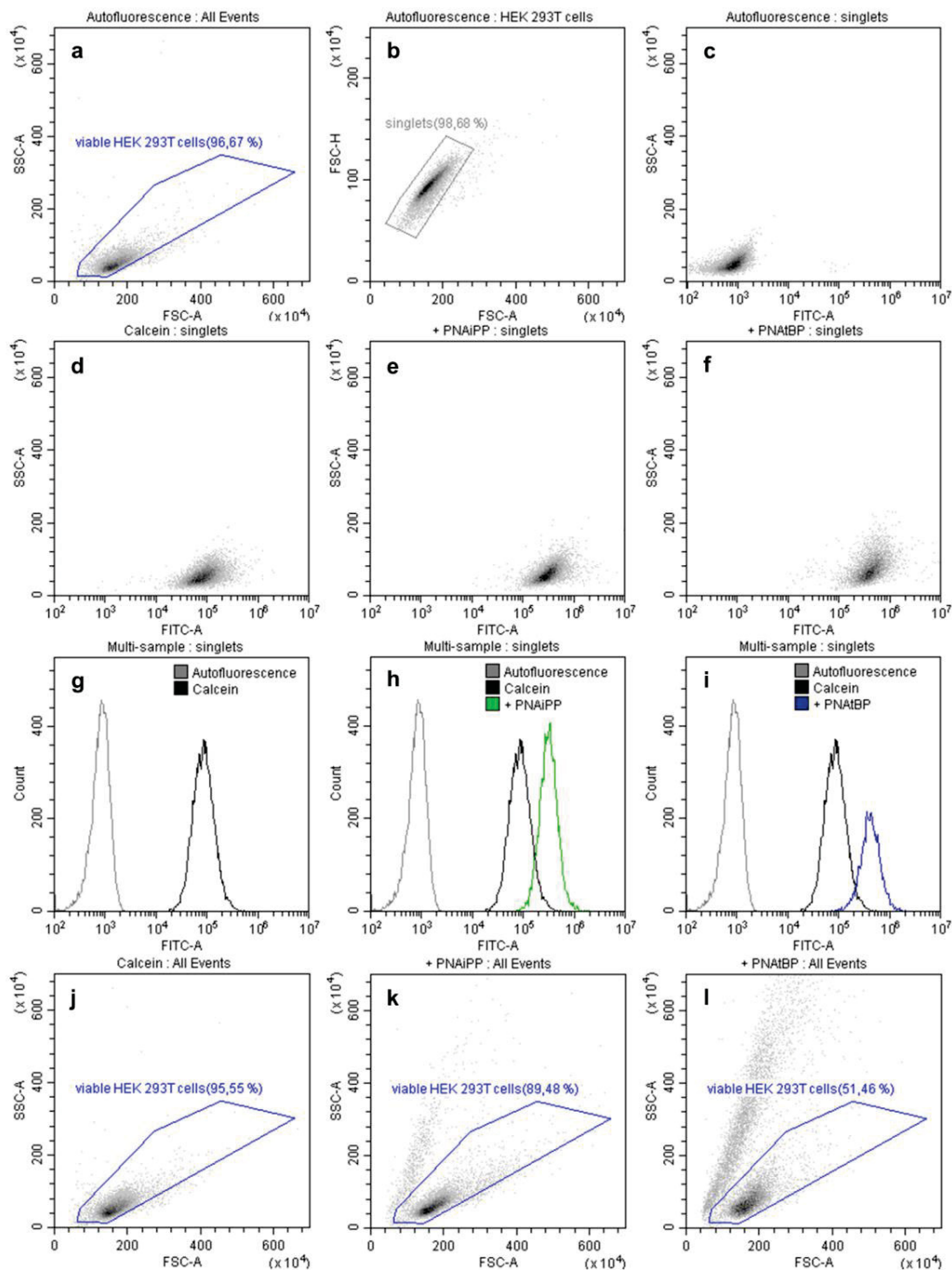


**Figure S18 Evaluation of endosomal escape of calcein via flow cytometry.** The gating strategy of flow cytometry analysis including forward/sideward scatter (a) to exclude debris, doublet discrimination (b) and the calcein/sideward scatter plot (c) are shown. Scatter plots and histograms of HEK 293T cells in Opti-MEM incubated with  $25 \mu\text{g mL}^{-1}$  calcein only (d, g, j), with additional  $100 \mu\text{g mL}^{-1}$  P(NAiPP)<sub>500</sub> 3C (e, h, k) and with additional  $100 \mu\text{g mL}^{-1}$  P(NAiBP)<sub>500</sub> 4C (f, i, l) are shown., indicating changes in the forward/sideward scatter for P(NAtBP)500 4C.

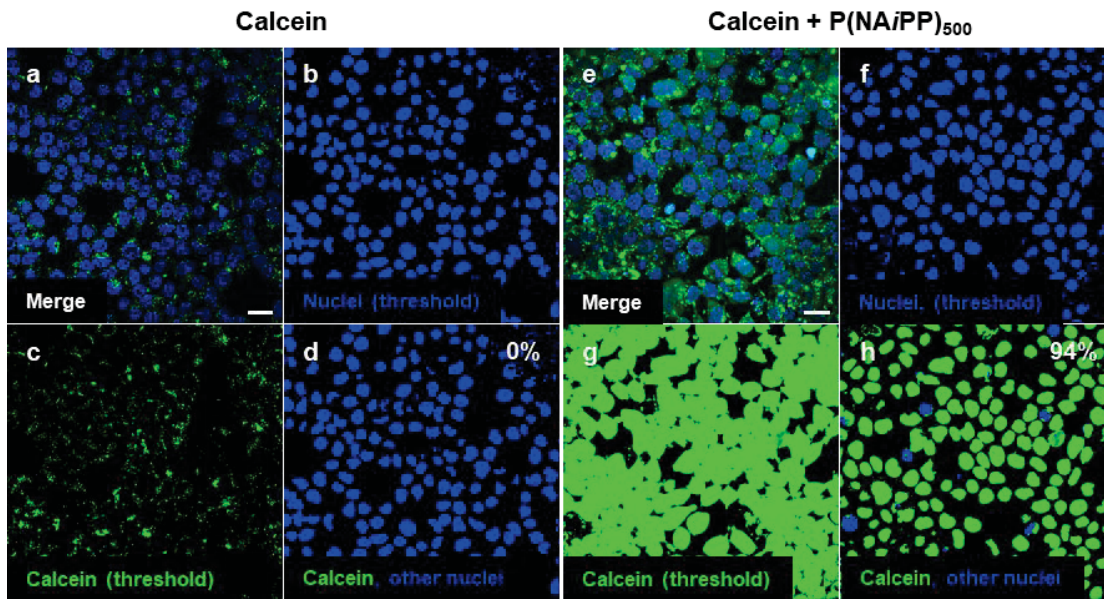


**Figure S19 Quantification of nuclear calcein delivery (image analysis).** **a-d** Live-cell confocal microscopy was conducted with HEK 293T cells in Opti-MEM either treated with  $25 \mu\text{g mL}^{-1}$  calcein or **e-h** additional  $100 \mu\text{g mL}^{-1}$  P(NAiPP)<sub>500</sub> for 16 h. Cells were washed and nuclei stained with Hoechst 33342. **b, f** A binary image of the nuclei was obtained from the Hoechst channel image using thresholding to determine the number of nuclei. **c, g** A binary image of the calcein channel was also obtained using thresholding. **d, h** From the image showing the number of nuclei (**b, f**) and the threshold image of the calcein channel (**c, g**), an image was calculated that outputs all pixels that are simultaneously blue in the nuclei image and green in the calcein image (given in green). These nuclei were counted and specified as a percentage in relation to the number of all nuclei to provide a percentage of cells that show nuclear calcein delivery for this image. For better understanding, the blue nuclei without calcein signal are also indicated (green + blue nuclei correspond to 100%). All images were acquired and processed with the same settings. All image analyses were carried out with ImageJ.[2] Scale bar  $20 \mu\text{m}$ .



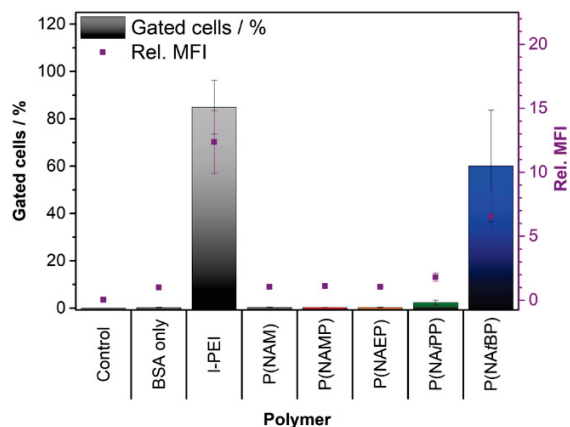


**Figure S20 Quantification of endosomal escape of labeled BSA by flow cytometry.** HEK 293T cells in DMEM with 10% serum were treated with  $5 \mu\text{g mL}^{-1}$  labeled BSA and polymers at comparable reactive amine contents, washed twice, trypsinized and analyzed via flow cytometry. Means  $\pm$  SD of three independent experiments are shown. The statistical differences between the means are not significant ( $P < 0.05$ ) according to Dunnett's T3 test. rel. MFI relative mean fluorescence intensity.

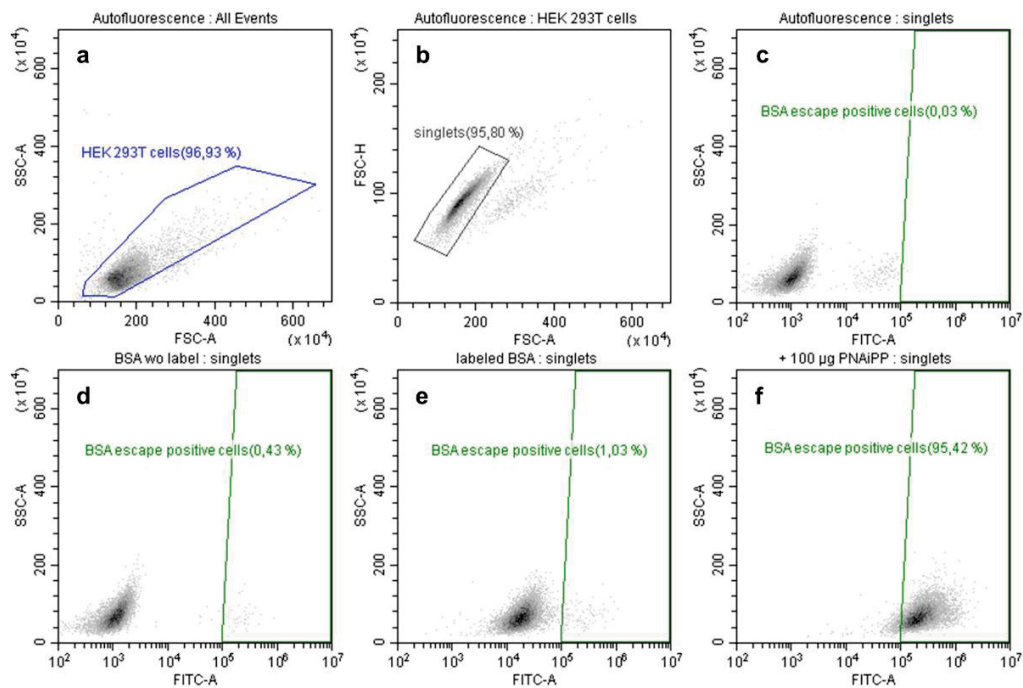


**Figure S21 Evaluation of endosomal escape of labeled BSA via flow cytometry.** The gating strategy of flow cytometry analysis including forward/sideward scatter (**a**) to exclude debris, doublet discrimination (**b**) and the gate for BSA escape positive cells (**c**) are shown. Scatter plots of HEK 293T cells in Opti-MEM incubated with  $5 \mu\text{g mL}^{-1}$  BSA without the Alexa Fluor 488 label only (**d**), with  $5 \mu\text{g mL}^{-1}$  BSA bearing the Alexa Fluor 488 tag (**e**) and with  $5 \mu\text{g mL}^{-1}$  labeled BSA and additional  $100 \mu\text{g mL}^{-1}$  P(NAiPP)<sub>500</sub> **3C** (**f**) are shown.

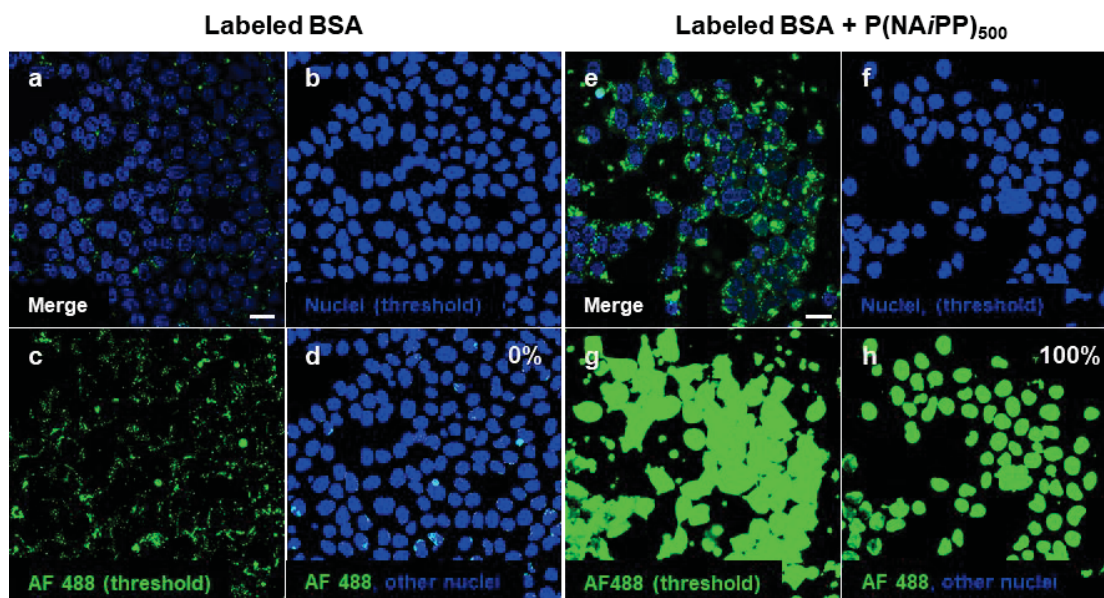


**Figure S22 Quantification of nuclear BSA delivery (image analysis).** **a-d** Live-cell confocal microscopy was conducted with HEK 293T cells in Opti-MEM either treated with  $5 \mu\text{g mL}^{-1}$  AF 488-functionalized BSA or **e-h** additional  $100 \mu\text{g mL}^{-1}$  P(NAiPP)<sub>500</sub> for 16 h. Cells were washed and nuclei stained with Hoechst 33342. **b, f** A binary image of the nuclei was obtained from the Hoechst channel image using thresholding to determine the number of nuclei. **c, g** A binary image of the AF 488 channel was also obtained using thresholding. **d, h** From the image showing the number of nuclei (**b, f**) and the threshold image of the AF 488 channel (**c, g**), an image was calculated that outputs all pixels that are simultaneously blue in the nuclei image and green in the calcein image (given in green). These nuclei were counted and specified as a percentage in relation to the number of all nuclei to provide a percentage of cells that show nuclear AF 488 delivery for this image. In case of this image all nuclei show AF 488 signal next to the Hoechst signal. All images were acquired and processed with the same settings. All image analyses were carried out with ImageJ.[2] Scale bar 20  $\mu\text{m}$ .

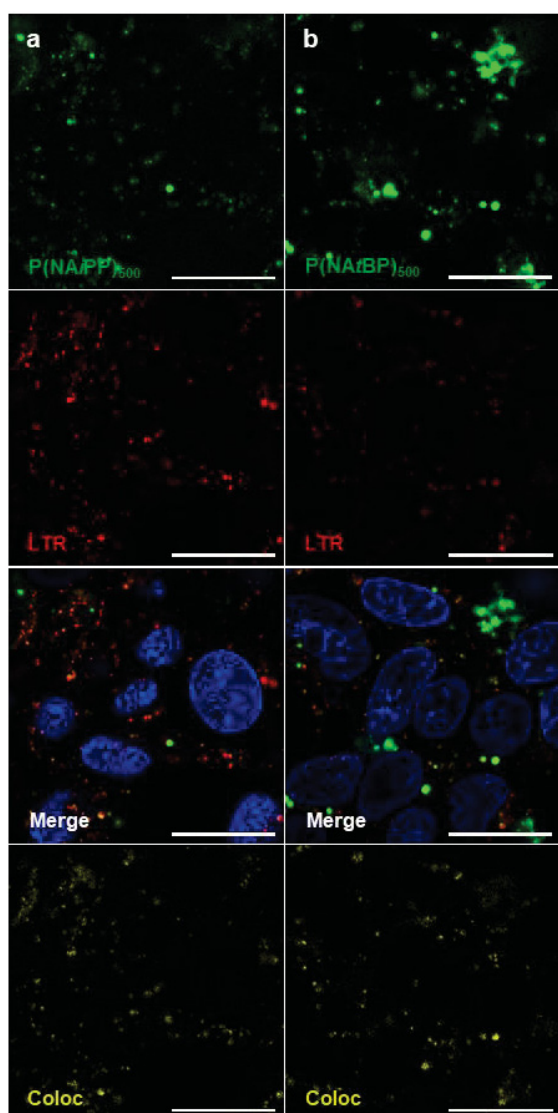


**Figure S23 Colocalisation of polypiperazines and endolysosomes in HEK 293T cells.** HEK 293T cells in Opti-MEM were treated with  $100 \text{ ug mL}^{-1}$  Oregon Green-labeled polypiperazines (**a** P(NAiPP)<sub>500</sub> **3C'**, **b** P(NAiBP)<sub>500</sub> **4C'**) for 16 h. Cells were stained with Hoechst 33342 and LysoTracker Red. The colocalization image was created with the Image Calculator showing all pixels with green and red signal.[2] Scale bar 20  $\mu\text{m}$ . Coloc – colocalization, LTR – LysoTracker Red.

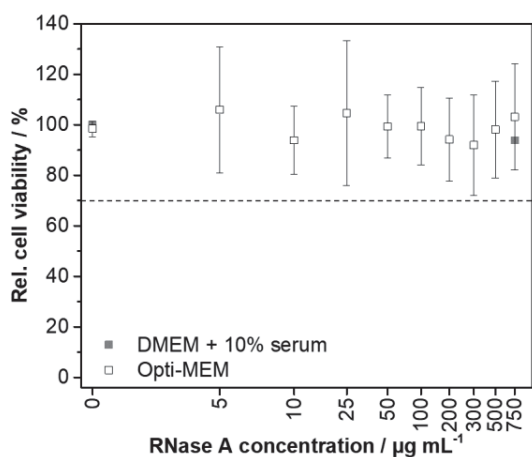


**Figure S24 Cytotoxicity studies of RNase A without polymer addition.** HEK 293T cells were incubated with RNase A (Roche) at the indicated concentrations (0 – 750  $\mu\text{g mL}^{-1}$ ) for 24 h, the culture medium was changed to DMEM + 10% serum and the cell viability was determined via the alamarBlue assay (Thermo Fisher). The activity of RNase A was investigated in DMEM + 10% serum (grey solid squares, mean  $\pm$  minimum/maximum of two independent experiments is shown) and Opti-MEM (black void squares, mean  $\pm$  SD of four independent experiments is shown).

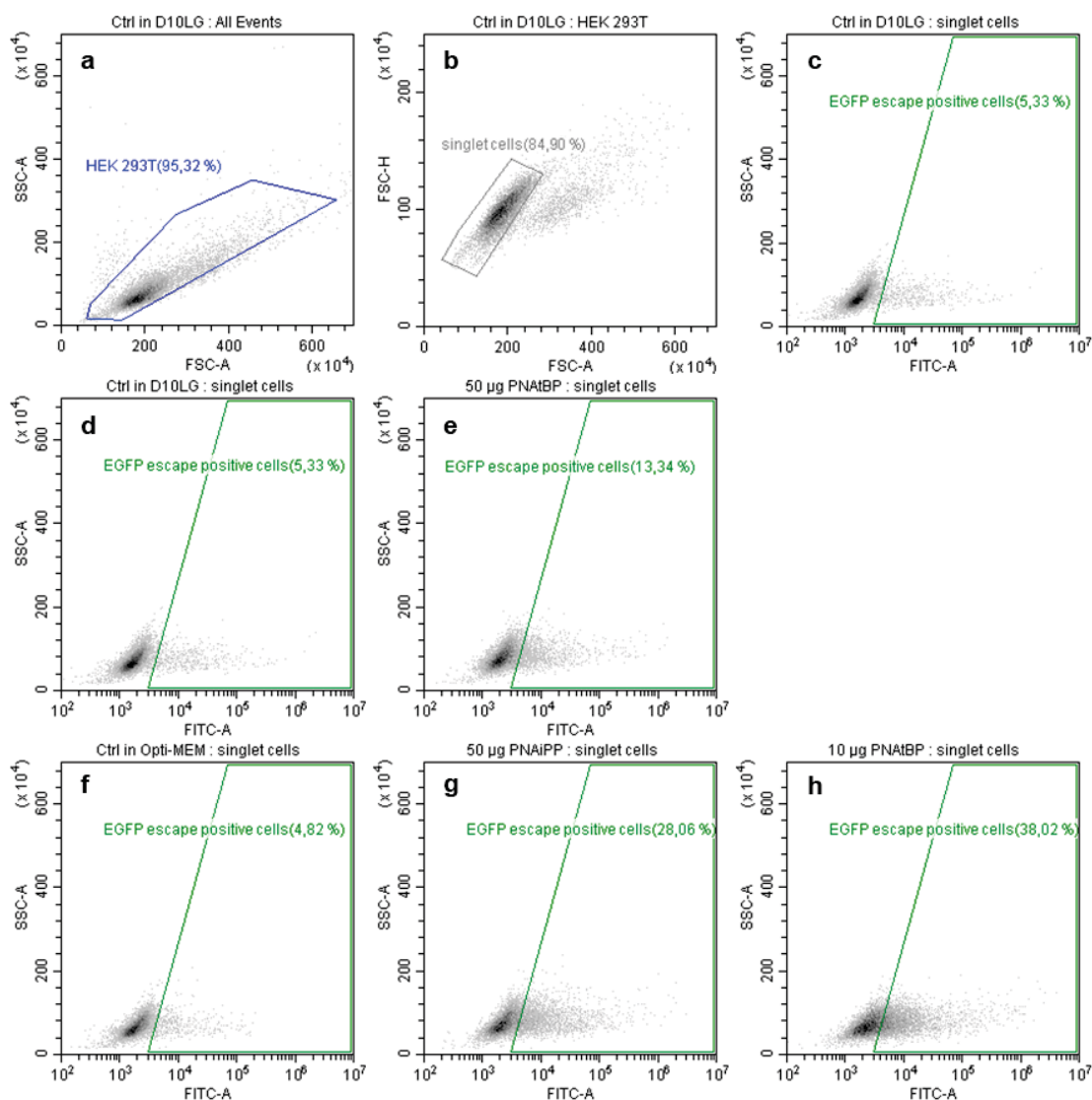


**Figure S25 Evaluation of endosomal escape of EGFP via flow cytometry.** a, b, c The gating strategy of flow cytometry analysis including forward/sideward scatter (a) to exclude debris, doublet discrimination (b) and the gate for EGFP escape positive cells (c) is shown. Scatter plots of HEK 293T cells in DMEM + 10% serum incubated with 50 µg mL<sup>-1</sup> EGFP only (d) and with additional 50 µg mL<sup>-1</sup> P(NA*t*BP)<sub>500</sub> 4C (e) are shown. Scatter plots of HEK 293T cells in Opti-MEM incubated with 50 µg mL<sup>-1</sup> EGFP only (f), with additional 50 µg mL<sup>-1</sup> P(NA*i*PP)<sub>500</sub> 3C''(g) and with additional 10 µg mL<sup>-1</sup> P(NA*t*BP)<sub>500</sub> 4C (h) are shown.

## References

- [1] Larnaudie, S. C., Brendel, J. C., Jolliffe, K. A., Perrier, S. Cyclic Peptide–Polymer Conjugates: Grafting-to Vs Grafting-From. *J. Polym. Sci., Part A: Polym. Chem.* 54, 1003-1011 (2016).
- [2] J. Schindelin, I. Arganda-Carreras, E. Frise, V. Kaynig, M. Longair, T. Pietzsch, S. Preibisch, C. Rueden, S. Saalfeld, B. Schmid, J.-Y. Tinevez, D.J. White, V. Hartenstein, K. Eliceiri, P. Tomancak, A. Cardona, Fiji: an open-source platform for biological-image analysis, *Nature Methods* 9(7) (2012) 676-682. 10.1038/nmeth.2019.
- [3] Maxfield, F. R., Yamashiro, D. J. Endosome Acidification and the Pathways of Receptor-Mediated Endocytosis. In: *Immunobiology of Proteins and Peptides Iv: T-Cell Recognition and Antigen Presentation* (ed Atassi, M. Z.). Springer US (1987).





## Publication Pub4

---

### The impact of anionic polymers on gene delivery: How composition and assembly help evading the toxicity-efficiency dilemma

F. Richter,<sup>‡</sup> K. Leer,<sup>‡</sup> L. Martin, P. Mapfumo, J. I. Solomun, Maren T. Kuchenbrod, S. Hoepfener, J. C. Brendel, A. Traeger

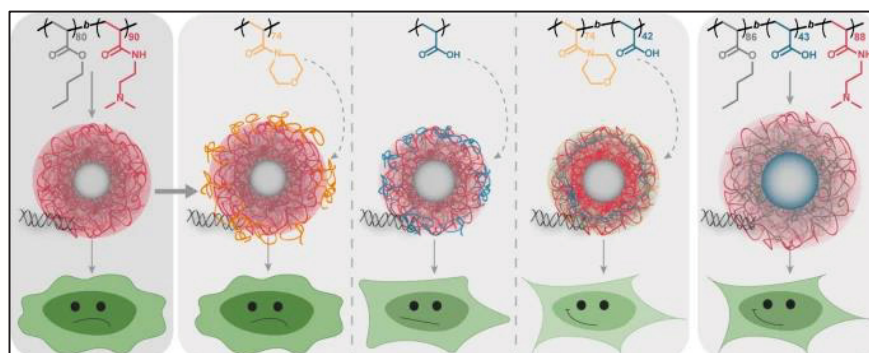
*J. Nanobiotechnol.* **2021**, 19, 292

---

Reproduced with permission of Springer Nature. Copyright © 2021.

The article and the supporting information are available online:

[doi.org/10.1186/s12951-021-00994-2](https://doi.org/10.1186/s12951-021-00994-2)



RESEARCH

Open Access



# The impact of anionic polymers on gene delivery: how composition and assembly help evading the toxicity-efficiency dilemma

Friederike Richter<sup>1†</sup>, Katharina Leer<sup>1†</sup> , Liam Martin<sup>1</sup>, Prosper Mapfumo<sup>1</sup>, Jana I. Solomun<sup>1</sup> , Maren T. Kuchenbrod<sup>1</sup>, Stephanie Hoepfner<sup>1,2</sup>, Johannes C. Brendel<sup>1,2</sup> and Anja Traeger<sup>1,2\*</sup>

## Abstract

Cationic polymers have been widely studied for non-viral gene delivery due to their ability to bind genetic material and to interact with cellular membranes. However, their charged nature carries the risk of increased cytotoxicity and interaction with serum proteins, limiting their potential in vivo application. Therefore, hydrophilic or anionic shielding polymers are applied to counteract these effects. Herein, a series of micelle-forming and micelle-shielding polymers were synthesized via RAFT polymerization. The copolymer poly[(*n*-butyl acrylate)-*b*-(2-(dimethyl amino)ethyl acrylamide)] (P(*n*BA-*b*-DMAEAm)) was assembled into cationic micelles and different shielding polymers were applied, i.e., poly(acrylic acid) (PAA), poly(4-acryloyl morpholine) (PNAM) or P(NAM-*b*-AA) block copolymer. These systems were compared to a triblock terpolymer micelle comprising PAA as the middle block. The assemblies were investigated regarding their morphology, interaction with pDNA, cytotoxicity, transfection efficiency, polyplex uptake and endosomal escape. The naked cationic micelle exhibited superior transfection efficiency, but increased cytotoxicity. The addition of shielding polymers led to reduced toxicity. In particular, the triblock terpolymer micelle convinced with high cell viability and no significant loss in efficiency. The highest shielding effect was achieved by layering micelles with P(NAM-*b*-AA) supporting the colloidal stability at neutral zeta potential and completely restoring cell viability while maintaining moderate transfection efficiencies. The high potential of this micelle-layer-combination for gene delivery was illustrated for the first time.

**Keywords:** Gene delivery, Cationic polymer, Micelle, Transfection, Anionic polymer, Shielding

## Introduction

In the last decades, the development of non-viral nanocarriers for the (targeted) delivery of genetic material has seen great progress [1, 2], not least because of the urgent need for effective vaccines [3–5]. Optimal gene delivery vectors should be non-toxic, form stable complexes with the genetic material, exhibit low interaction with serum proteins, transfer their cargo to the desired cells, enable

endosomal escape and finally ensure its activity inside the cells. Among the different non-viral gene delivery methods, cationic polymers have been investigated due to their (pH-dependent) positive charges interacting with the polyanionic genetic material and cellular membranes [6, 7]. One major advantage of using polymers is their variety due to the possibility to combine different functionalized monomers, and thus characteristics, in one polymer chain or in one assembly. Cationic polymers with vinylic backbones such as poly(meth)acrylates or poly(meth)acrylamides offer a great versatility with many monomers being commercially available, while the development of reversible deactivation radical

\*Correspondence: anja.traeger@uni-jena.de

<sup>†</sup>Friederike Richter and Katharina Leer contributed equally to this work

<sup>1</sup>Laboratory of Organic and Macromolecular Chemistry (IOMC), Friedrich Schiller University Jena, Humboldtstrasse 10, 07743 Jena, Germany  
Full list of author information is available at the end of the article



© The Author(s) 2021. **Open Access** This article is licensed under a Creative Commons Attribution 4.0 International License, which permits use, sharing, adaptation, distribution and reproduction in any medium or format, as long as you give appropriate credit to the original author(s) and the source, provide a link to the Creative Commons licence, and indicate if changes were made. The images or other third party material in this article are included in the article's Creative Commons licence, unless indicated otherwise in a credit line to the material. If material is not included in the article's Creative Commons licence and your intended use is not permitted by statutory regulation or exceeds the permitted use, you will need to obtain permission directly from the copyright holder. To view a copy of this licence, visit <http://creativecommons.org/licenses/by/4.0/>. The Creative Commons Public Domain Dedication waiver (<http://creativecommons.org/publicdomain/zero/1.0/>) applies to the data made available in this article, unless otherwise stated in a credit line to the data.

polymerization methods (RDRP) facilitates straightforward access to various polymer architectures [8–10]. In particular, the reversible-addition fragmentation chain transfer (RAFT) polymerization is proven to be tolerant towards many functional groups under relatively simple reaction conditions, which is advantageous for the design of polymeric gene delivery vectors [11–13]. Considering nanomedicine in general, functional amphiphilic block copolymers have gained increasing attention due to their ability to self-assemble into higher ordered structures such as micelles or vesicles in aqueous solutions [14–18]. Different compositions of these polymeric micelles have been investigated for gene delivery, utilizing a cationic polymer block within their shell to form complexes with genetic material (polyplexes) [19, 20], whereas another approach uses cationic-hydrophilic block copolymers to incorporate the genetic material inside a polyion complex (PIC) with a neutral shell [14, 21]. Compared to polyplexes of cationic homopolymers, micelles have been demonstrated to increase the stability of polyplexes and the delivery efficiency [22–25], which is, among others, related to an increased interaction of the hydrophobic block with cellular membranes [26].

It is well known, that the positive charges of the cationic polymers also pose a high risk of cytotoxic side effects on cells [27–30]. This can be alleviated by designing the structure of the nanocarrier more similar to that of the plasma membrane, e.g., by the addition of hydrophilic polymers creating a steric hydration barrier around the micelle to shield the cationic charges and to decrease the interaction with serum proteins, thus prolonging circulation times within the blood [31, 32]. The most prominent example of these so-called stealth polymers is poly(ethylene glycol) (PEG), which has been incorporated into various nanocarriers for the transport of different cargos [6, 20, 31]. Nevertheless, it also has disadvantages such as the dilemma of decreasing delivery with increasing shielding efficiency [33, 34], and an accelerated blood clearance upon re-administration being linked to the occurrence of allergic reactions [35–37]. This leads to an interest in alternative stealth polymers such as poly(*N*-2-hydroxypropyl methacrylamide), poly(4-acryloylmorpholine) (PNAM) or poly(oxazoline) [31, 38, 39]. Another route towards increased cell viability is the introduction of anionic polymers, such as poly(acrylic acid) (PAA), which can reduce the positive charge density by electrostatic interaction with the cationic polymers [40]. For example, poly(methacrylic acid) (PMAA) has been incorporated into multicompartiment micelles (degree of polymerization > 1000) which exhibited superior transfection efficiency while maintaining high viability [41–43]. The interaction of polyanions and polycations was also described in terms of intra- and

interpolyelectrolyte complexes [44] and a layer-by-layer assembly [45]. A third possibility is the combination of both above described strategies in copolymers comprising anionic and hydrophilic blocks [46, 47], but this has not been investigated with cationic micelles so far. In general, the different shielding strategies were mostly investigated using PIC micelles or micelles/liposomes for drug delivery [48–50]. However, the opportunity of an addition of anionic polymers to cationic micelles complexed with genetic material in order to reduce toxicity while maintaining high transfection efficiency, has not been exploited so far.

Therefore, a diblock copolymer micelle with a hydrophobic core (H) of *n*-butyl acrylate (*n*BA), and a pH-responsive cationic block (C) of 2-(dimethyl amino) ethyl acrylamide) (DMAEAm) is presented in this study and used to investigate the influence of different shielding polymers on the pDNA delivery efficiency of this system. While *n*BA is well studied as a micellar core and biocompatible [51, 52], PDMAEAm has not been studied in micelles for gene delivery so far. Its low transfection efficiency as a homopolymer has certainly limited applications, but the moderate cytotoxicity make it an optimal candidate for optimization in a micellar assembly [24, 53, 54]. Different shielding polymers were added following micelle formulation (and polyplex formation) and comprised the anionic polymer poly(acrylic acid) (PAA, HC<sup>A</sup>), the hydrophilic stealth polymer poly(4-acryloylmorpholine) (PNAM, HC<sup>S</sup>), and a combination of both within a diblock copolymer P(NAM-*b*-AA) (HC<sup>AS</sup>). Furthermore, the performance of the layered micellar assemblies was compared to the HAC-micelle from the triblock terpolymer P(*n*BA-*b*-AA-*b*-DMAEAm), where PAA is integrated between the hydrophobic core and the cationic shell of the micelle. The physicochemical and biological properties of the assemblies were investigated using dynamic light scattering (DLS), pDNA binding and cytotoxicity assays, flow cytometry for the investigation of EGFP expression and polyplex uptake, as well as confocal laser scanning microscopy (CLSM) to investigate endosomal escape. This work aims at demonstrating the impact of the precise molecular arrangement of polymer blocks on transfection efficiency and toxicity and presents strategies for an efficient design of polymeric micelles for gene delivery.

## Main methods

Materials, instruments, detailed polymer syntheses as well as deprotection are described in the Additional file 1. Further methods such as dynamic and electrophoretic light scattering (DLS, ELS), cryo transmission electron microscopy (cryo-TEM), ethidium bromide quenching assay (EBA) and heparin dissociation assay (HRA),

cytotoxicity assays, polyplex uptake and calculations are also described in the Additional file 1, since they have been performed similar as published before [23, 53].

## Synthesis and characterization

### General procedure

All polymers investigated in this work were synthesized via RAFT polymerization. While the homopolymers PDMAEAm [53], PNAM [55] were synthesized as described previously, the synthesis of P*n*BA can be found in the Additional file 1. The block copolymers were synthesized with P*n*BA or PNAM, respectively, as macroCTAs. Briefly, the respective macroCTA, the next monomer in the block copolymer (DMAEAm or *tert*-butyl acrylate [*t*BA]), 1,4-dioxane, V-65B and 1,3,5-trioxane as an internal standard for determination of conversion by NMR were introduced to a vial equipped with a magnetic stirring bar which was sealed with a cap. The mixture was deoxygenated by bubbling argon through the solution. The vial was transferred to an oil bath set at the desired temperature. Following polymerization, the flask was cooled to room temperature (RT) and exposed to air. 2–3 droplets of the polymerization mixture were used for <sup>1</sup>H NMR and SEC analysis. Afterward, the crude polymer was precipitated and dried under vacuum. Subsequently, the *t*BA containing polymers were deprotected with TFA. For exact details of each polymer, refer to the Additional file 1.

### Assembly procedure for micelle formation

#### Typical assembly procedure

A sample of P(*n*BA<sub>80</sub>-*b*-DMAEAm<sub>90</sub>) was dissolved in distilled water to reach a concentration of 75 mg mL<sup>-1</sup> and treated with 0.5 equivalents of a 1 M HCl solution, followed by lyophilization. A sample of protonated P(*n*BA<sub>80</sub>-*b*-DMAEAm<sub>90</sub>) or P(*n*BA<sub>86</sub>-*b*-AA<sub>43</sub>-*b*-DMAEAm<sub>88</sub>) was dissolved in a mixture of THF/MeOH (80/20). Then, the same volume of a 150 mM NaCl solution in ultrapure water was added over 40 min with a syringe pump. The polymer solution was dialyzed against a 50 mM sodium acetate buffer solution (pH 5) (MWCO = 3.5–5.0 kDa). The polymer concentration was determined by lyophilization and the micelles were characterized regarding their hydrodynamic diameter and morphology by dynamic light scattering (DLS) and cryo-TEM, respectively. Experimental details for each analysis are provided in the Additional file 1. During the investigation process, different batches of micelle assemblies from the very same diblock or triblock copolymer were used for preliminary experiments. While all the results in this manuscript were performed with one batch, comparisons of the different batches can be found in the Additional file 1: Figures S6, S9, S15, Table S4)

### Preparation of (layered) polyplexes

The polyplexes were prepared similarly to literature procedures [53] in HBG buffer (20 mM 4-(2-hydroxyethyl) piperazine-1-ethanesulfonic acid (HEPES) and 5% (w/v) glucose, pH 7.4), but 1.3-fold concentrated. Briefly, a 40 µg mL<sup>-1</sup> solution of pDNA was mixed 1 + 1 with polymer solutions or micelle suspensions containing different quantities of polymer to vary the ratio of protonatable nitrogen atoms to phosphates of pDNA (N\*/P ratio). If not stated otherwise, the pDNA concentration within the polyplex solution was 15 µg mL<sup>-1</sup>. Immediately after combination, the mixtures were vortexed for 10 s at maximum speed (3200 rpm) and incubated at RT for 15 min to ensure complex formation. Meanwhile, a four-fold concentrated shielding solution was prepared to give a PNAM/P*n*BA molar ratio of 1.0 or a carboxy to amine group ratio (COOH/NH-ratio) of 0.5 in the final micelle-shielding-mix. Subsequently, the polyplex solution was slowly pipetted directly into the shielding solution, giving an assembly of 75% (v/v) polyplex and 25% (v/v) layer. Where no shielding was desired, the volume was replaced by HBG buffer.

### Cell culture

The mouse fibroblast cell line L-929 and the human embryonic kidney cell line HEK293T were obtained from CLS (Germany). They were maintained as recommended by the supplier and cultured in D10 (low glucose Dulbecco's modified eagle's medium (DMEM) supplemented with 10% (v/v) fetal calf serum (FCS), 100 U mL<sup>-1</sup> penicillin and 100 µg mL<sup>-1</sup> streptomycin) at 37 °C in a humidified 5% (v/v) CO<sub>2</sub> atmosphere.

### Transfection efficiency

To determine the influence of the polymers on the expression of EGFP, the HEK293T cells were seeded at 0.2 × 10<sup>6</sup> cells mL<sup>-1</sup> in growth medium (D10) containing 10 mM HEPES (D10H) in 24-well plates, followed by incubation at 37 °C in a humidified 5% (v/v) CO<sub>2</sub> atmosphere for 24 h and a medium change to fresh D10H 1 h prior to treatment. The cells were treated with polyplexes with or without shielding at N\*/P 30 and a final pDNA concentration of 1.5 µg mL<sup>-1</sup> in the well. The polyplexes were prepared as described above with isolated mEGFP-N1 pDNA and added to the cells diluting the polyplexes 1:10 in the cell culture medium for an incubation period of 24 h or 48 h. For analysis via flow cytometry, HEK293T cells were harvested by transferring the supernatant to a 24-well plate, trypsinizing the cells and resuspending them in the respective supernatant again. Half of the suspension was transferred to a 96-well plate for

measurement, while the remaining cell suspension was diluted 1:2 with D20 (D10 + 10% FCS) and incubated for further 24 h.

For determination of transfection efficiency, cells were analyzed as described in the instrumentation section (Additional file 1). Viable cells showing EGFP signal higher than the mock control cells incubated with polyplexes of the respective polymer and pKMyC pDNA were gated as percentage of cells expressing EGFP (Additional file 1: Figure S18) and the relative mean fluorescence intensity (rMFI) of all viable cells was calculated in relation to the respective mock control. MFI values of the controls can be found in the Additional file 1: Table S8. The experiments were performed three times and data are expressed as mean  $\pm$  SD.

#### Calcein release assay

To determine the endosomal escape efficiency of the polymers, a calcein release assay was performed with HEK293T cells seeded at  $0.2 \times 10^6$  cells  $\text{mL}^{-1}$  in D10H in 4-well glass bottom dishes. Following incubation at 37 °C in a humidified 5% (v/v) CO<sub>2</sub> atmosphere for 24 h, the cells were treated with polyplexes at N\*/P 30 with or without shielding. Just before the addition of polyplexes, the non-cell-permeable dye calcein was added to the cells to give a final concentration of 25  $\mu\text{g mL}^{-1}$ . Following incubation for 1 h, the cells were washed twice with warm FC-buffer (Hanks' Balanced Salt Solution, supplemented with 2% FCS and 20 mM HEPES) followed by addition of fresh warm D20 and incubation with 8  $\mu\text{M}$  Hoechst 33342 for 10 min. Cells were analyzed via confocal laser scanning microscopy (CLSM) and the images were processed using ImageJ, version 1.52 [56]. A detailed description can be found in the Additional file 1. The amount of cells with calcein release was quantified by determining and counting nuclei showing green calcein fluorescence in a high-throughput analysis (<170 cells/repetition) via ImageJ:

$$\text{Cells with calcein release/\%} = \frac{\text{Number of nuclei with coincident calcein staining}}{\text{Number of nuclei}} \cdot 100 \quad (1)$$

Subsequently, the escape efficiency was calculated relative to the number of YOYO-1 positive cells at the same time point (2):

$$\text{Escape efficiency} : \frac{\text{Cells with calcein release (1 h)}}{\text{YOYO - 1 positive cells (1 h)}} \cdot 100 \quad (2)$$

#### Statistics

To determine the statistical significance, repeated measures analysis of variance (RM-ANOVA) was performed.

If the RM-ANOVA revealed significant differences ( $p < 0.05$ ), post-hoc analyses with a Bonferroni correction were applied. If not stated otherwise, statistically significant differences were indicated with \* for  $p < 0.05$  \*\* for  $p < 0.01$  and with \*\*\* for  $p < 0.001$ . All statistical analyses were performed with data of  $n \geq 3$  in Origin, Version 2020b (OriginLab Corporation, US).

## Results and discussion

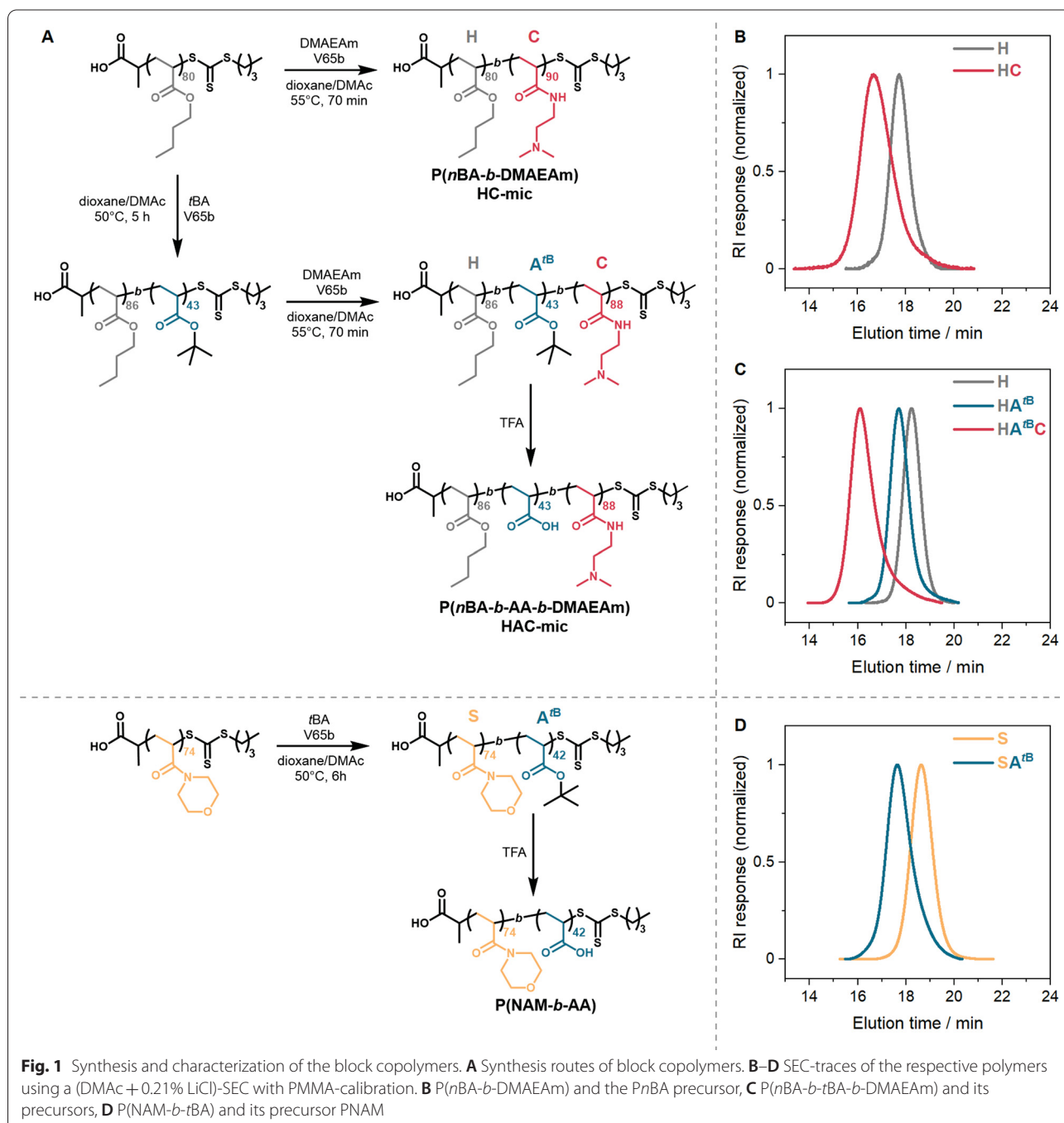
### Polymer synthesis and characterization

The diblock and triblock copolymers were synthesized via sequential RAFT polymerizations with purification after each block synthesis step (Fig. 1A). (Propanoic acid) yl butyl trithiocarbonate (PABTC) was used as the chain transfer agent (CTA), since it is suitable to control the polymerization of acrylates and acrylamides [57]. The core-forming hydrophobic block was synthesized by polymerization of *n*-butyl acrylate (*n*BA) and was used as a macroCTA for the subsequent RAFT polymerizations. This block was chain extended (i) with the amine-functional cationic monomer dimethylaminoethyl acrylamide (DMAEAm) yielding the diblock copolymer P(*n*BA-*b*-DMAEAm), or (ii) with the carboxyl-functional anionic monomer *tert*-butyl acrylate (*t*BA), followed by chain extension with DMAEAm to give the triblock terpolymer P(*n*BA-*b*-*t*BA-*b*-DMAEAm).

A PDMAEAm homopolymer was synthesized as a control polymer as described previously [53]. Three different shielding polymers were used: (i) 2 kDa poly(acrylic acid) (PAA) which is commercially available, while (ii) poly(*N*-acryloylmorpholine) (PNAM) and (iii) a diblock copolymer comprising NAM and acrylic acid, P(NAM-*b*-AA), were synthesized by RAFT polymerization, starting with the hydrophilic PNAM followed by chain extension with *t*BA to obtain the diblock copolymer.

The size exclusion chromatography (SEC) curves in Fig. 1 display monomodal populations with relatively narrow molar mass distributions. The experimental

number-average molar masses differ from the theoretical values, since the hydrodynamic radii of the applied polymers and standards utilized for calibration of the SEC systems were different (Table 1). Following characterization, P(NAM-*b*-*t*BA) and P(*n*BA-*b*-*t*BA-*b*-DMAEAm) were deprotected with TFA to expose the anionic carboxyl-group of *t*BA, obtaining the anionic PAA block, as confirmed by <sup>1</sup>H NMR spectroscopy (Additional file 1: Figures S3, S4). The molar mass distribution of P(NAM-*b*-AA) after deprotection obtained by aqueous SEC can be found in Additional file 1: Figure S4. It was not



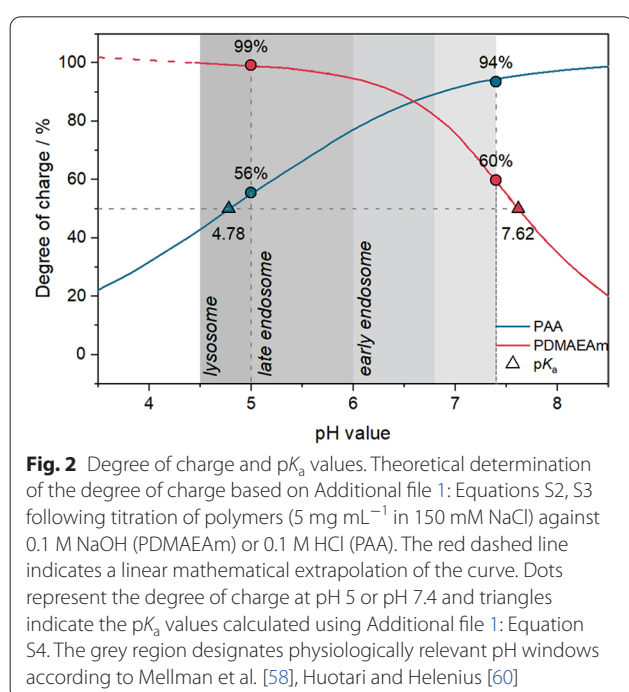
possible to measure the molar mass distribution by aqueous SEC for the diblock copolymer  $P(nBA-b-DMAEAm)$  and triblock terpolymer  $P(nBA-b-AA-b-DMAEAm)$  due to their amphiphilic characters.

To investigate the influence of different pH-values present in the biological system (e.g., pH 7.4 extracellularly and pH 5.5 in endolysosomes) [58] on the behavior and interactions of PAA and PDMAEAm, both polymers

were titrated against HCl or NaOH, respectively, and the proportion of protonated amine groups (degree of charge) was calculated using Additional file 1: Equations S2, S3 (Fig. 2) [59]. At pH 7.4, PDMAEAm shows a moderate degree of charge (60%), whereas PAA is nearly completely negatively charged (94%). By contrast, the degrees of charge are reversed at pH 5.0 (PDMAEAm: 99%, PAA: 56%). These results indicate on the one hand

**Table 1** Summary of polymer characterization

Polymer-ID <sup>a</sup>	Assembly code	$M_{n,th}$ <sup>b</sup> (kg mol <sup>-1</sup> )	$M_{n,SEC}$ <sup>c</sup> (kg mol <sup>-1</sup> )	$\bar{D}$ <sup>c</sup> (kg mol <sup>-1</sup> )
P( <i>n</i> BA <sub>80</sub> - <i>b</i> -DMAEAm <sub>90</sub> )	HC	23.3	28.4	1.37
P( <i>n</i> BA <sub>86</sub> - <i>b</i> - <i>t</i> BA <sub>43</sub> - <i>b</i> -DMAEAm <sub>88</sub> )	HAC	29.3	34.6	1.26
PNAM <sub>72</sub>	HC <sup>S</sup>	10.4	8.8	1.12
P(NAM <sub>74</sub> - <i>b</i> - <i>t</i> BA <sub>42</sub> )	HC <sup>AS</sup>	16.0	15.2	1.20
PAA	HC <sup>A</sup>	2.0 <sup>d</sup>	1.0 <sup>e</sup>	1.27 <sup>e</sup>

<sup>a</sup> DP was determined via <sup>1</sup>H NMR<sup>b</sup> Determined using Additional file 1: Equation S1<sup>c</sup> Determined via DMAC-SEC with PMMA standards<sup>d</sup> According to the distributor<sup>e</sup> Determined via aqueous SEC with PEG-standards

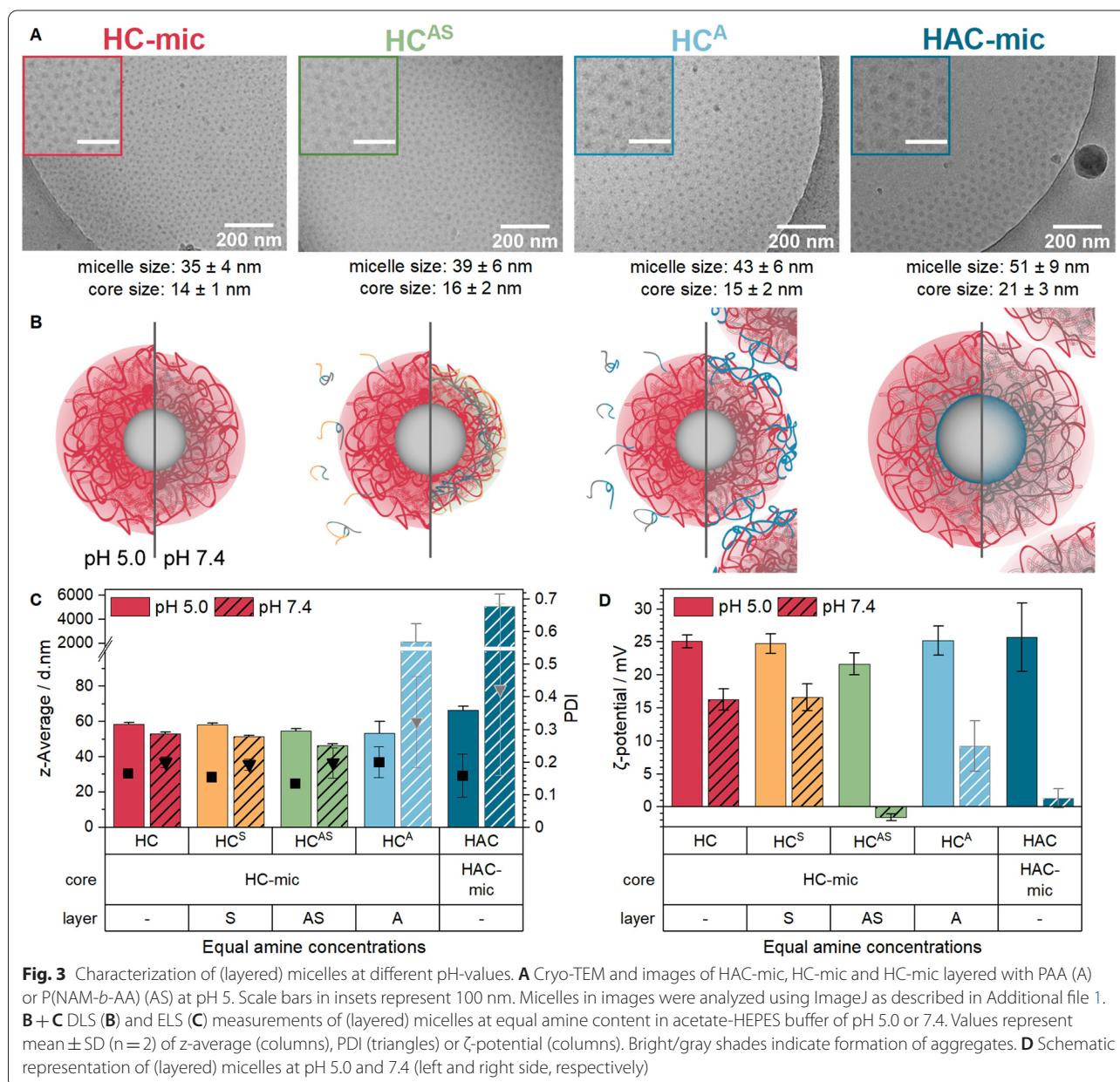
that PAA would neutralize a majority of the remaining positive charges of PDMAEAm at pH 7.4 in the extracellular environment, which could lead to reduced cytotoxicity. On the other hand, when the pH is decreasing in the endolysosomal pathway, the reducing amount of negative charge would unleash further positive charges which is beneficial for endosomal escape.

### Micelle formation and pH dependence

Micelles of P(*n*BA-*b*-DMAEAm) and P(*n*BA-*b*-AA-*b*-DMAEAm) were prepared by gradually adding 150 mM NaCl solution as selective solvent to the polymer dissolved in the good solvent THF/MeOH (80/20 v/v). During this process, the block copolymers eventually

underwent microphase separation, where P*n*BA formed the core (H—hydrophobic), and PAA (A—anionic) and/or PDMAEAm (C—cationic) the corona, resulting in the assembly of HC- and HAC-micelles, respectively. The polymer solutions were dialyzed against 50 mM sodium acetate buffer solution (pH 5.0) to replace the solvent mixture and to enhance the stability of the micelles by avoiding neutralization of the cationic charges by PAA at higher pH-values. The formation of micelles was verified first by DLS measurements (Additional file 1: Figure S6). In addition, the reproducible formulation and stability at RT for at least 1 year indicate high application potential (Additional file 1: Figures S9, S14).

The effect of a post-assembly addition of shielding to the HC-mic was investigated by mixing the HC-mic solution with shielding polymer solutions 3 + 1 (v/v) resulting in carboxy to amine (COOH/NH) ratios of 0.5 for the HC<sup>A</sup> and HC<sup>AS</sup> assemblies, which was similar to the HAC-mic. The assembly of HC-mic and PNAM (S—stealth, HC<sup>S</sup>) was prepared with a PNAM/P*n*BA molar ratio of 1.0. To investigate the behavior of the (layered) micelles at pH-values relevant for biological studies, the different assemblies were tested in 100 mM acetate-HEPES buffer of pH 5.0 or pH 7.4. At pH 5, cryo-TEM, DLS and ELS measurements showed no considerable differences regarding the size, morphology or the surface charge of the assemblies compared to the naked HC-mic (Fig. 3). Due to the measurement of the hydrodynamic diameter by DLS, the assemblies appeared to be slightly larger (55–66 nm) than in the cryo-TEM images (35–51 nm) but both methods provided comparable tendencies: The HAC micelles were slightly larger than the HC micelles, which can be attributed to the presence of the additional third PAA block. This partially uncharged anionic PAA block in the HAC-mic at pH 5.0 might form intramicellar interpolyelectrolyte complexes (im-IPECs) with protonated PDMAEMA or collapse to the micelle core [61], leading to a slightly increased size



of the micelle core (21 ± 3 nm) in the cryo-TEM images compared to the HC-mic (14 ± 1 nm). With ζ-potentials in the order of 24 mV, all assemblies showed strong positive surface charges.

However, when DLS measurements were performed at pH 7.4, the hydrodynamic diameter decreased by about 7 ± 2 nm for HC-mic, HC<sup>S</sup> and HC<sup>AS</sup>. By contrast, HAC-mic and HC<sup>A</sup> formed large aggregates and turbid suspensions, which could be due to neutralization of PDMAEAm by PAA (Fig. 2). Moreover, the ζ-potential of all assemblies was decreased when measured in 100 mM acetate-HEPES buffer of pH 7.4, with the

greatest difference being observed for the anionic polymer-containing assemblies HAC-mic, HC<sup>A</sup> and HC<sup>AS</sup>. Interestingly, HC<sup>AS</sup> exhibited a ζ-potential close to zero and comparable to the HAC-mic, but still formed stable and defined nanostructures instead of aggregates at pH 7.4. This indicates a beneficial contribution of the additional hydrophilic PNAM block to the micelle stability, in particular at neutral pH-values.

#### Polyplex formation and characterization

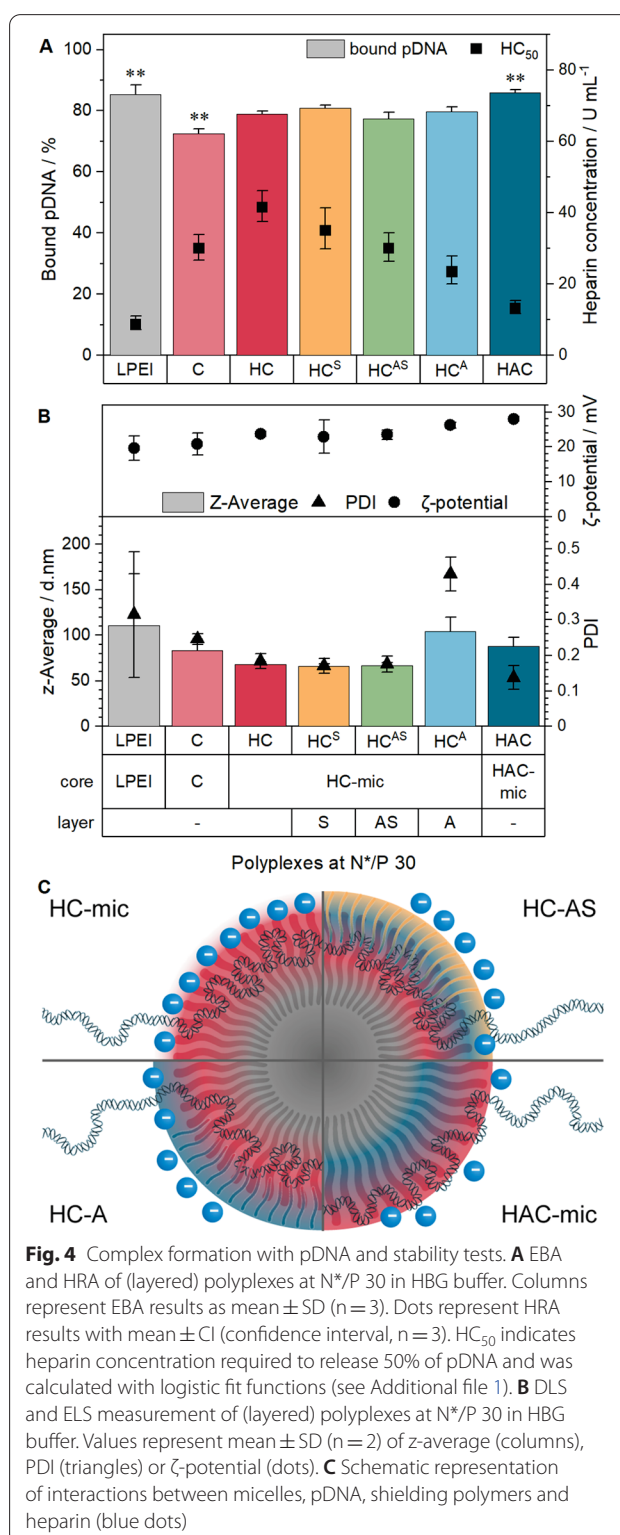
Since the micelles were designed for the purpose of transporting genetic material into cells, their interaction



with genetic material was investigated with the combined ethidium bromide binding and heparin release assay (EBA, HRA) as described previously [53]. The assay uses the increase in the relative fluorescence intensity (rFI) of ethidium bromide (EtBr) upon (re)intercalation into the pDNA as a fluorescence indicator for unbound pDNA. A decreasing rFI relates to displacement of EtBr from the pDNA due to the binding of polymers. The polysaccharide heparin was used to investigate the stability of the polymer–pDNA complexes (polyplexes) against polyanions outside the cells, since it competes with the pDNA for the binding to the polymers. As a starting point, an N\*/P ratio (active amines of the polymer to phosphates of the pDNA) of 30 was chosen. To investigate the influence of shielding on the obtained polyplexes, the respective shielding polymers were added post-polyplex formation at an COOH/NH-ratio of 0.5 (HC<sup>A</sup>, HC<sup>AS</sup>) or at a PNAM/PnBA molar ratio of 1.0 (HC<sup>S</sup>). To increase biocompatibility and avoid aggregation of HAC-mic and HC<sup>A</sup> but still enable micelle-shielding interaction, a less strong buffer system was used for this and all further assays involving complexes of pDNA and polymer (polyplexes). The buffer contained 20 mM HEPES and 5% (w/v) glucose at pH 7.4 (HBG-buffer), resulting in pH-values of the polyplex solutions of pH 6.3 (HAC-mic) and 7.2 (remaining assemblies), which will be adjusted to pH 7.4 upon 1:10 dilution of the polyplexes with growth medium of pH 7.4 for cell treatment.

The results showed a high proportion of bound pDNA for all assemblies from 73 ± 2% (PDMAEAm, C) to 86 ± 1% (HAC-mic) being comparable to the commercial control linear poly(ethylene imine) (LPEI, 85 ± 3%, Fig. 4A). While slight increases were observed for the introduction of a hydrophobic core to the cationic PDMAEAm homopolymer (HC-mic: 79 ± 1%) and for the addition of the anionic block (HAC-mic), the addition of the shielding polymers did not change the proportion of bound pDNA compared to the naked micelle (HC-mic). Regarding the polyplex stability, the HC-mic required the highest concentration of heparin to release 50% of the pDNA, (HC<sub>50</sub>: 41.6 U mL<sup>-1</sup>) indicating a strong polymer–pDNA-interaction. The addition of the shielding polymers led to decreased HC<sub>50</sub>-values for the layered micelle assemblies compared to the naked micelle (HC-mic) with the HC<sup>A</sup> showing the lowest values (23.5 U mL<sup>-1</sup>). However, they were still higher than the HAC-mic (13.2 U mL<sup>-1</sup>), which was comparable to LPEI (8.7 U mL<sup>-1</sup>), and therefore represents a good candidate for transfection efficiency assays.

The decreased polyplex stability of the HAC-mic can be caused by the covalent connection of the anionic PAA with the cationic PDMAEAm blocks, effectively reducing the amount of excess positively charged amines available



after polyplex formation (N\*/P ratio). Therefore, a lower amount of heparin can be trapped by excess cationic charges (see also Fig. 4C). By contrast, the polyplex in the

HC<sup>A</sup> assembly was formed in absence of PAA, which can therefore interact only with the remaining, free positively charged amines not occupied by the phosphate groups of the pDNA. Since the negatively charged heparin is repelled by the negatively charged PAA, increased concentrations of heparin were required to release the same amount of pDNA as the HAC-mic.

To further investigate the polyplex properties, DLS and ELS measurements were performed with (layered) polyplexes at N\*/P 30 to determine the hydrodynamic diameter of the assemblies. Compared to the assemblies without pDNA in HBG buffer (Additional file 1: Figure S10), the formation of polyplexes led to slightly increased sizes (Fig. 4B), as observed in other studies before [23, 24, 62]. All polyplexes were slightly below 100 nm in diameter being optimal for endocytotic uptake [63]. The HC-mic and the HC<sup>S</sup> and HC<sup>AS</sup> assemblies exhibited the smallest polyplexes ( $\approx 70$  nm), whereas the other assemblies showed sizes of 90 to 100 nm. Regarding the HC<sup>A</sup> assembly, two distinct peaks were observed in the intensity plot (Additional file 1: Figure S8). Together with the increased PDI values, this could indicate the aggregation of several micelles due to the strong attraction between the positively charged shell of the HC-mic and the negatively charged shielding polymer PAA. Regarding the electrical potential, all assemblies containing micelles exhibited similar  $\zeta$ -potentials of about 25 mV, which was slightly higher compared to the homopolymer polyplexes (C,  $21 \pm 3$  mV) and could be explained with an increased charge density in the micellar corona [24].

### Cytotoxicity

As polycations are known for their interaction with cell membranes, different cytotoxicity assays were performed: (i) the PrestoBlue assay determining the metabolic activity, (ii) the LDH release assay determining the membrane integrity and (iii) flow cytometry determining the cell viability due to their appearance in the FSC/SSC plot. For all assays, the cells were incubated with the above described (layered) polyplexes.

The evaluation of the metabolic activity revealed differences between the assemblies. Polyplexes of the HC-mic and the HC<sup>S</sup> assembly caused the highest reduction in cell viability ( $\approx 50\%$ ), whereas cells incubated with the PDMAEAM polyplexes (C) showed no cytotoxicity (Fig. 5A). This indicates that the hydrophobic block and the micellar structure of the HC-mic contributed to cytotoxic effects, which have been also observed with other hydrophobic-cationic micelle systems and can be explained by a high local concentration of cationic moieties [23]. The addition of anionic polymer, either post-polyplex formation (HC<sup>A</sup>) or within the micelle (HAC-mic), showed medium to low toxicity, while the combination with the stealth polymer PNAM (HC<sup>AS</sup>) eliminated the cytotoxic effect. Layering with only PNAM in the HC<sup>S</sup> assembly did not reduce cytotoxicity, since this assembly lacks an anionic counterpart for ionic interaction with the micelle. Furthermore, the HAC-mic also showed toxicity alleviating effects compared to the HC-mic in concentration dependent studies without pDNA in L-929 cells (Additional file 1: Figure S12A),

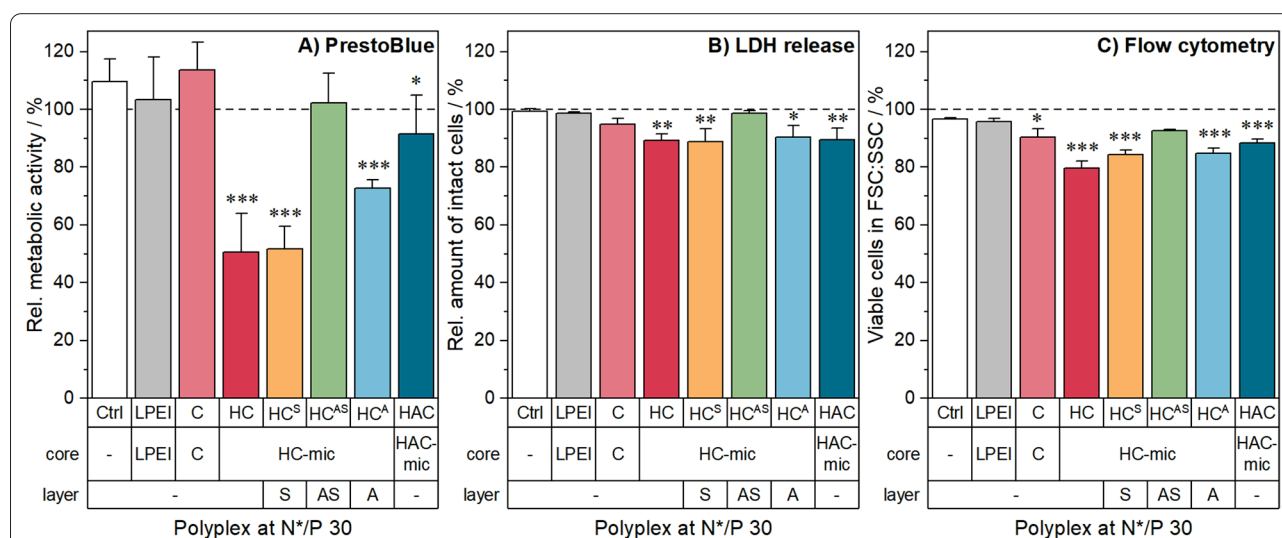


**Fig. 5** Toxicity of polyplexes in HEK293T cells. The cells were treated with (layered) polyplexes at N\*/P 30 for 24 h. Incubation with pDNA only was used as control. Subsequently, the viability of the cells was investigated using **A** the PrestoBlue assay for metabolic activity, **B** the LDH release assay, or **C** flow cytometry with gating for viable cells in the FSC/SSC plot. Cells treated with pDNA only served as control. Values represent mean  $\pm$  SD ( $n = 3$ ). \*/\*\*/\*\* Significant differences to control ( $p < 0.05/0.01/0.001$ )

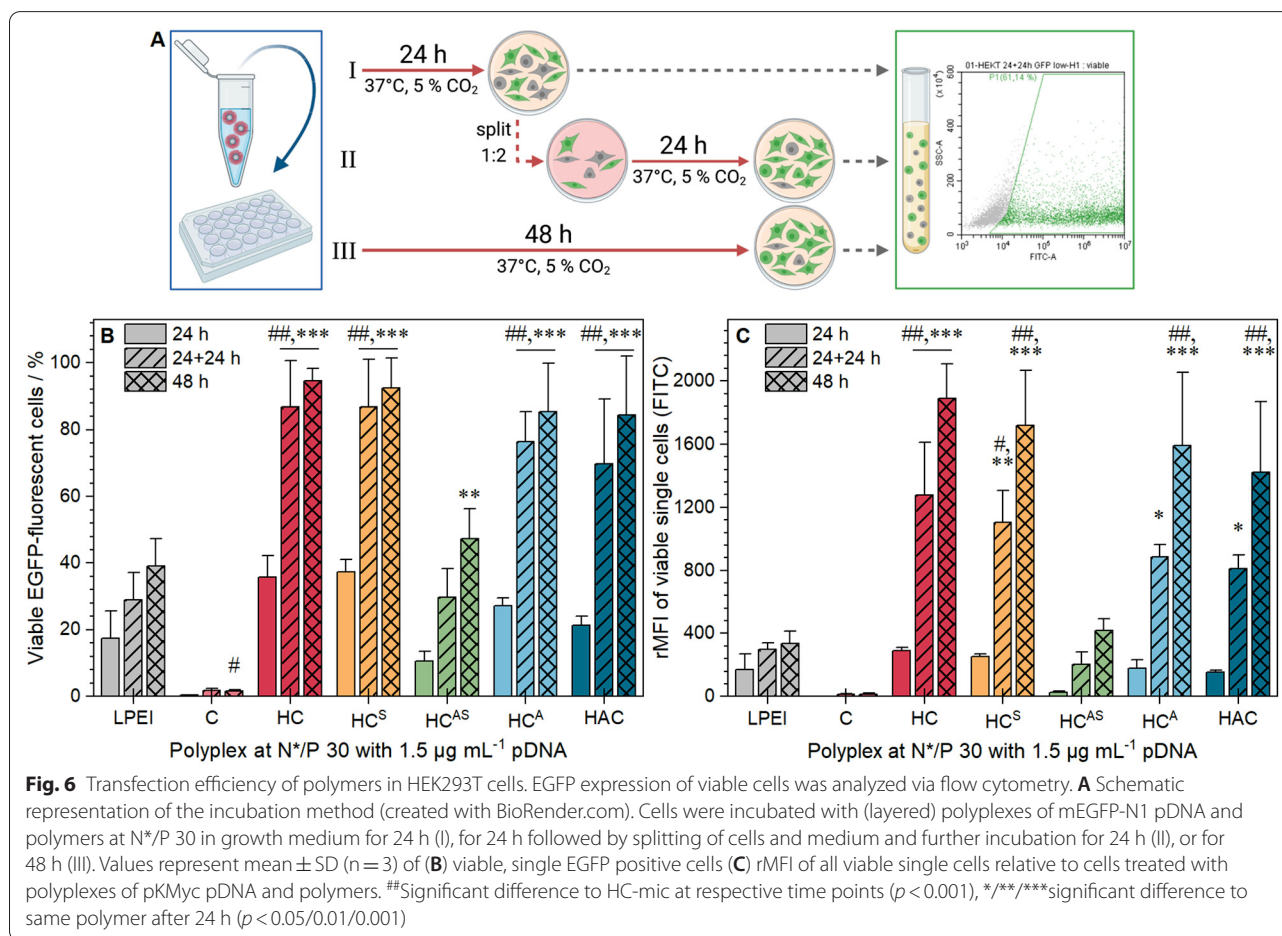
which might be due to the decreased degree of positive charges in the HAC-mic.

In contrast to the PrestoBlue assay, there were only slight differences between the different polyplex assemblies in the LDH-release and flow cytometry assays. All assemblies led to viabilities above 80% (Fig. 5B, C). This indicates only slight or no influence of the polymers on the cell membrane and morphology, which is supported by hemolysis and aggregation assays with human erythrocytes and in microscopic investigations of HEK293T cells (Additional file 1: Figures S12C, D, S13). However, cells incubated with the HC<sup>AS</sup> assembly or the HAC-mic exhibited the highest viabilities and, therefore, represent promising candidates for further studies.

### EGFP expression with (layered) micelles

Since all polymers exhibited high interaction with pDNA and led to low to moderate cytotoxicity, their transfection efficiency (amount of EGFP expressing cells) was investigated. For a better understanding of possible shielding effects, different incubation periods were examined. Therefore, HEK293T cells were incubated with the

(layered) polyplexes at N\*/P 30 for 24 h, 48 h or for 24 h followed by 1:2 splitting of the cells with fresh medium and an additional 24 h observation period (Fig. 6A). Subsequently, flow cytometry was used to determine the amount and relative mean fluorescence intensity (rMFI) of EGFP expressing cells. The results showed different EGFP expression for all assemblies in serum-containing media with slightly higher efficiencies than LPEI and mostly consistent within different assembly batches (Fig. 6, Additional file 1: Figure S16). A fourfold increase in transfection efficiency was observed when the incubation time (48 h) or the observation time (24+24 h) were extended, leading to transfection efficiencies of up to 95% viable EGFP positive cells with no changes in cytotoxicity (Additional file 1: Figure S12B). After 48 h, the homopolymer PDMAEAm resulted in nearly no transfected cells, whereas the HC-mic showed the highest transfection efficiency (95 ± 4% viable EGFP positive cells). The layering with PNAM alone (HC<sup>S</sup>) did not influence the effect of the HC-mic, but in combination with the anionic block (HC<sup>AS</sup>) the transfection efficiency was significantly reduced (47 ± 9%), but was still comparable



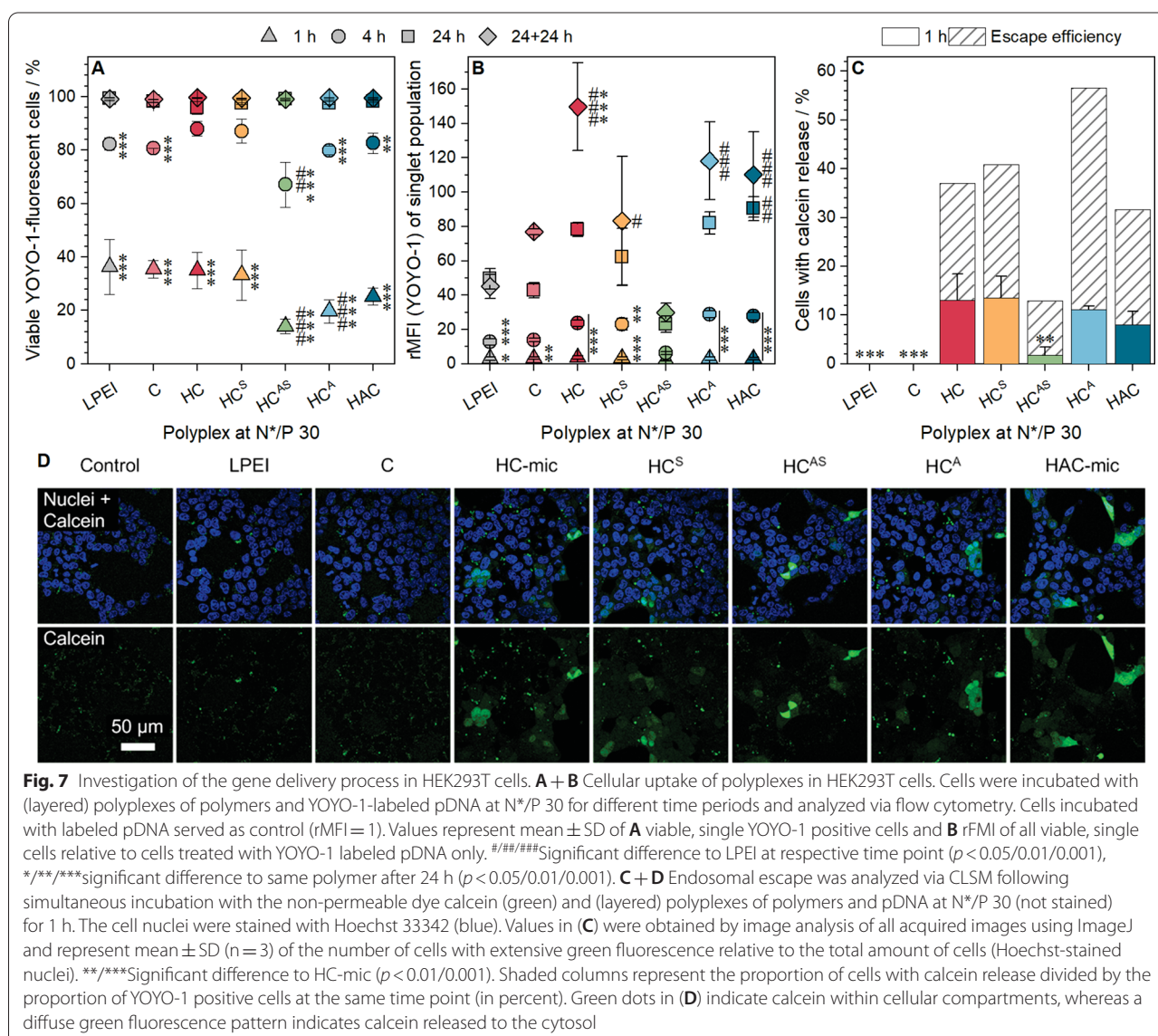
with the commercial control LPEI. The two PAA containing assemblies without PNAM (HAC-mic and HC<sup>A</sup>) were comparable to the HC-mic ( $85 \pm 14$  and  $85 \pm 18\%$ , respectively).

Furthermore, LPEI could only reach these values when the pDNA concentration was increased to  $3.0 \mu\text{g mL}^{-1}$  and the polymer concentration remained the same (Additional file 1: Figure S16), whereas the transfection efficiencies of the assemblies did not change. This indicates a higher efficacy of these systems, requiring only half of the pDNA to achieve similar transfection rates as LPEI. The reason might be seen in the differences between polyplexes of micelles and pDNA compared to those of homopolymers with pDNA, leading to increased stability and the preservation of the pDNA structure as shown by Tan and coworkers [24]. Although the HC-mic showed higher efficiency than the HAC-mic under these conditions, it is worth noticing, that HAC-mic outperformed the HC-mic at higher polymer concentrations due to cytotoxicity issues (Additional file 1: Figure S17).

#### Transfection mechanism of (layered) micelles

To gain an in-depth look into the transfection mechanism, the (layered) polyplexes were investigated regarding their performance at two crucial steps of the transfection process: (i) polyplex uptake and (ii) endosomal escape. For the polyplex uptake, the HEK293T cells were incubated with (layered) polyplexes of YOYO-1 labeled pDNA and polymers at N\*/P 30 in serum-containing media for different time periods, before they were measured and analyzed via flow cytometry regarding the amount of YOYO-1 positive cells and the relative MFI (rMFI) of viable single cells (Fig. 7A, B). All assemblies exhibited a time-dependent increase of the uptake in nearly all cells after 24 h. Following 1 h of incubation, 14 to 36% of the cells were YOYO-1 positive with comparable rMFI values. Although, all cells showed polyplex uptake after 24 h, the anionic polymer containing assemblies led to slightly increased rMFI values compared to the pure cationic assemblies (HAC/HC<sup>A</sup>:  $86$  vs. HC/HC<sup>S</sup>:  $70$ ,  $p = 1.000$ ). The HC<sup>AS</sup> assembly exhibited the lowest proportion of YOYO-1 positive cells and rMFI values. This could be due to the “stealth-dilemma” or due to a decreased aggregation number of micelles within one polyplex as it was shown for PEG-*b*-PDMAEMA-*b*-P*n*-BMA micelles [62]. Interestingly, the rMFI values for the successful assemblies (HC, HC<sup>A</sup>, HC<sup>S</sup>, HAC) increased although the cells and medium were split after 24 h and the observation time was increased (24 + 24 h, Fig. 6AII). This could point towards an interaction between these polymers and either cells or the culture vessel which is not disturbed by trypsinization.

The uptake of polyplexes following incubation of 1 h was further confirmed by CLSM (Additional file 1: Figure S20) showing a similar trend for the number of polyplexes per cell as observed via flow cytometry. By staining the plasma membrane and membrane originating organelles with CellMask Deep Red Plasma membrane stain, a colocalization analysis of polyplexes could be performed, which revealed the presence of about 10% free polyplexes for all treatments. Therefore, the second crucial cellular hurdle for transfection efficiency, the endosomal escape, was investigated using calcein as a non-permeable fluorescence dye leading to (i) a dotted pattern inside the cells following uptake via endocytosis or (ii) a diffuse fluorescence pattern upon its release into the cytosol if the endosomal membrane was disrupted, e.g., by a polymer. The HEK293T cells were incubated as described above with (layered) polyplexes at N\*/P 30 and calcein. Following washing of the cells and staining of nuclei with Hoechst 33342, images were acquired by CLSM (Fig. 7D). The quantification of the number of cells showing calcein release was performed with ImageJ (see Additional file 1: Methods), and revealed that only the micellar assemblies displayed remarkable calcein release (Fig. 7C). The absence of calcein release by LPEI and PDMAEMA could point towards different endosomal escape mechanisms for linear polymers and micellar systems. As an example, different types of calcein leakage from vesicles (graded, all-or-none) have already been reported for detergents [64]. Moreover, differences were also observed for the fluorescence pattern of the polyplexes in the CLSM uptake study (Additional file 1: Figure S21, weak fluorescence of linear polymers vs. bright, large spots for micellar systems), which could be an indication of different amounts of YOYO-1 labeled pDNA. However, the exact mechanism and quantification of the endosomal escape remain to be elucidated. All in all, the values of the micelles correlated well with those observed for transfection efficiency, with HC-mic and HC<sup>S</sup> leading to the highest ( $13 \pm 5$  and  $14 \pm 4\%$  cells, respectively) and HC<sup>AS</sup> exhibiting the lowest calcein release ( $1.8 \pm 1.6\%$  cells). Calculating the escape efficiency [proportion of cells positive for calcein release (Fig. 7C) normalized to the proportion of YOYO-1 positive cells (Fig. 7A, 1 h)] demonstrated a superior escape efficiency for the HC<sup>A</sup> assembly. This could be due to an enhanced surface-accessibility of the PAA outside the micelle compared to the HAC-mic leading to a pH-dependent unmasking of cationic charges, and to an increased concentration of molecules which could also be beneficial for endosomal escape.

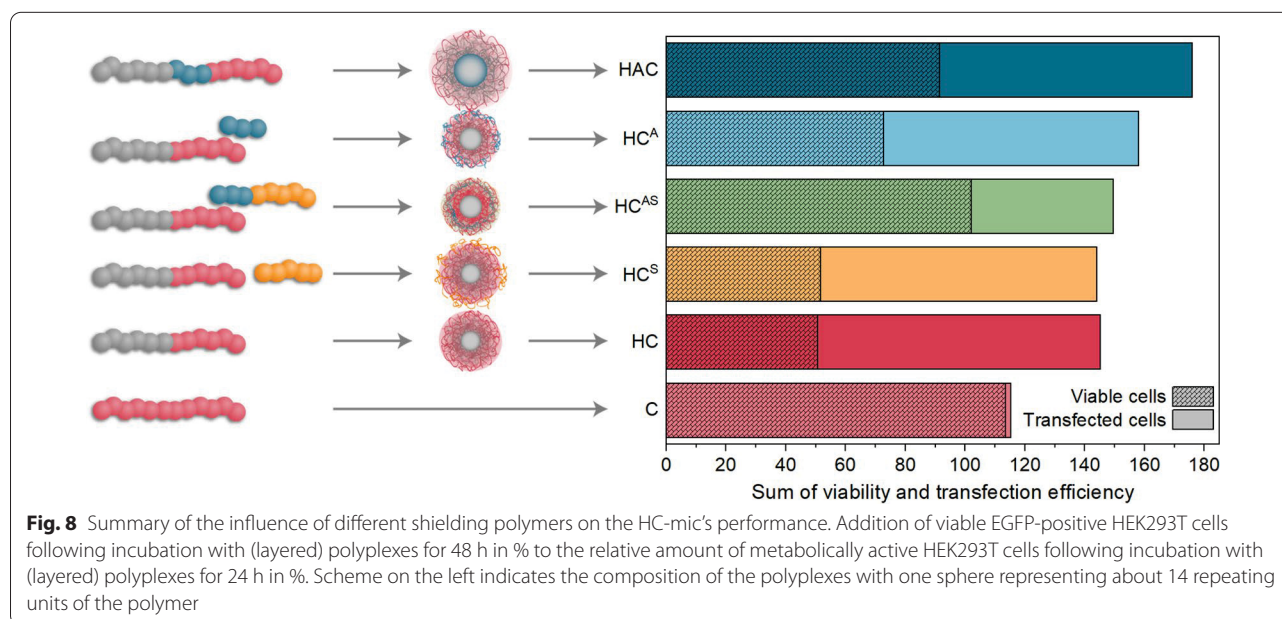


## Conclusion

Since cationic polymers for non-viral gene delivery are known to be cytotoxic and immune active, shielding polymers with anionic or hydrophilic moieties are being investigated, either covalently bound within block copolymers forming micelles or as a post-formulation addition to nanoparticles and homopolymer polyplexes. In this study, the post-formulation addition of three different shielding polymers, PAA, PNAM and P(NAM-*b*-AA), to a cationic micelle of P(*n*BA-*b*-DMAEAm) (HC-mic) was compared to a triblock terpolymer micelle containing the anionic PAA as the middle block (HAC-mic). With the exception of the commercial PAA, the polymers were synthesized via RAFT polymerization, resulting in well-defined

homo- and block copolymers. The assembled micelles were small (around 50 nm) with narrow size distributions, favored for biological investigations. Layered micelles were obtained by mixing the shielding polymers with the HC-mic.

The assemblies were characterized regarding their performance at crucial key steps for gene delivery, such as interaction with pDNA, cytotoxicity, transfection efficiency, polyplex uptake, and endosomal escape. The naked HC-mic formed the most stable complexes with pDNA and exhibited increased transfection efficiency (95% transfected cells following prolonged incubation) that was even twice as efficient as the commercial control LPEI. However, only moderate cell viabilities were observed. Among the different shielding polymers, the



anionic PAA could alleviate the cytotoxic effects with nearly no loss in transfection efficiency, irrespective of whether it was part of the parent micelle (HAC-mic) or applied as a shielding polymer (HC<sup>A</sup>). Nevertheless, there were slight differences between both assemblies with the HAC-mic showing slightly less stable polyplex formation and less efficient endosomal escape compared to HC<sup>A</sup>. This indicates a stronger influence of PAA on the HC-mic's performance when covalently incorporated inside the micelle than when electrostatically interacting with the micelle corona. Still, the HAC-mic convinced with the best ratio of viability to transfection efficiency (Fig. 8).

The highest shielding effect was observed for the combination of anionic and hydrophilic polymer (HC<sup>AS</sup>). It formed moderately stable polyplexes with pDNA and preserved the micellar structure even at neutral  $\zeta$ -potentials but reached only 50% of the HC-mic's transfection efficiency, which still resulted in 40% transfected cells. Remarkably, HC<sup>AS</sup> was able to completely eliminate cytotoxic effects which can be attributed to a decreased membrane interaction, which was also indicated by a severely reduced uptake into the cells. In combination with suitable ligands, this shielding block copolymer could therefore be applied for targeted gene delivery *in vivo* additionally offering the benefits of simple synthesis and flexible combination with different core micelles. Both, the HAC-mic and the HC<sup>AS</sup> system led to the highest cell viability with still good transfection efficiency and will be investigated in further studies. Moreover, these findings illustrate the dependence of the system's performance on the precise molecular arrangement of the

polymer blocks. Even the incorporation of anionic polymer blocks alone greatly improved the performance of the HC-mic by reducing the cytotoxic effect of the naked cationic micelles without mitigating their efficiency. The addition of stealth polymers further improved their toxicity profile. Therefore, layered micelles represent an efficient design principle for gene transfer due to the synthesis of diblock copolymers being less challenging than multiblock copolymers, and the possibility to vary micelle and layer in a modular fashion allowing adjustments for further applications. The toxicity and side effects of transfection can thus be efficiently and elegantly circumvented.

### Supplementary Information

The online version contains supplementary material available at <https://doi.org/10.1186/s12951-021-00994-2>.

**Additional file 1.** Materials, additional methods and supplementary figures.

### Acknowledgements

The authors gratefully acknowledge C. Kellner and B. Beringer-Siemers for taking splendid care of the cell lines and performing toxicity and pDNA binding assays. Furthermore, the authors gratefully acknowledge E. Moek for assistance in transfection assays, and her as well as F. Hausig, E. Preußger, C. Kellner and B. Beringer-Siemers for fruitful discussions. The authors gratefully acknowledge Dr. G. Festag for maintaining the SEC facilities. Furthermore, the authors thankfully acknowledge Prof. U. S. Schubert for providing excellent facilities.

### Authors' contributions

FR: conceptualization, investigation, methodology, writing—preparation of the manuscript, visualization; KL: conceptualization, investigation, writing—preparation of the manuscript; LM: methodology, writing—correction of the manuscript; PM: synthesis, writing—correction of the manuscript, JIS:

methodology, writing—correction of the manuscript; MTK: investigation, writing—correction of the manuscript; SH: cryo-TEM investigations, writing—correction of the manuscript; JCB: writing—correction of the manuscript, consulting; AT: conceptualization, supervision, writing—editing of the manuscript, project administration, funding acquisition. All authors read and approved the final manuscript.

### Funding

Open Access funding enabled and organized by Projekt DEAL. This work was supported by the Bundesministerium für Bildung und Forschung (BMBF, Germany, #13XP5034A PolyBioMik); the German Research Foundation (DFG, Emmy-Noether Programme, Projekt ID: 358263073); and by the DFG-funded Collaborative Research Centre PolyTarget (SFB 1278, Project B01, Z01, Project ID: 316213987). Cryo-TEM investigations were performed at the Electron Microscopy facilities of the Jena Center for Soft Matter (JCSM), which were established with Grants from the Deutsche Forschungsgemeinschaft (DFG) and the European Fund for Regional Development (EFRE). The LSM880 DLYRA PS.1 and the Cytoflex LX were further funded with Grants from the DFG and the Thüringer Aufbaubank (TAB), respectively.

### Declarations

#### Ethics approval and consent to participate

Not applicable.

#### Consent for publication

Not applicable.

#### Availability of data and materials

The datasets used and/or analyzed during the current study are available from the corresponding author on reasonable request. Additional information available: Material, additional methods and results, Additional Figures S1–S22, Additional Tables S1–S8 (PDF).

#### Competing interests

The authors declare that they have no competing interests.

#### Author details

<sup>1</sup>Laboratory of Organic and Macromolecular Chemistry (IOMC), Friedrich Schiller University Jena, Humboldtstrasse 10, 07743 Jena, Germany. <sup>2</sup>Jena Center for Soft Matter (JCSM), Friedrich Schiller University Jena, Philosophenweg 7, 07743 Jena, Germany.

Received: 8 June 2021 Accepted: 10 August 2021

Published online: 27 September 2021

### References

- Zhang P, Wagner E. History of polymeric gene delivery systems. *Top Curr Chem (Cham)*. 2017;375:26. <https://doi.org/10.1007/s41061-017-0112-0>.
- Wahane A, Waghmode A, Kapphahn A, Dhuri K, Gupta A, Bahal R. Role of lipid-based and polymer-based non-viral vectors in nucleic acid delivery for next-generation gene therapy. *Molecules*. 2020;25:2866. <https://doi.org/10.3390/molecules25122866>.
- Campos EVR, Pereira AES, de Oliveira JL, Carvalho LB, Guilger-Casagrande M, de Lima R, Fraceto LF. How can nanotechnology help to combat COVID-19? Opportunities and urgent need. *J Nanobiotechnol*. 2020;18:125. <https://doi.org/10.1186/s12951-020-00685-4>.
- Tang Z, Zhang X, Shu Y, Guo M, Zhang H, Tao W. Insights from nanotechnology in COVID-19 treatment. *Nano Today*. 2021;36: 101019. <https://doi.org/10.1016/j.nantod.2020.101019>.
- Tang Z, Kong N, Zhang X, Liu Y, Hu P, Mou S, Liljestrom P, Shi J, Tan W, Kim JS, et al. A materials-science perspective on tackling COVID-19. *Nat Rev Mater*. 2020;5:1–14. <https://doi.org/10.1038/s41578-020-00247-y>.
- Jhaveri AM, Torchilin VP. Multifunctional polymeric micelles for delivery of drugs and siRNA. *Front Pharmacol*. 2014;5:77. <https://doi.org/10.3389/fphar.2014.00077>.
- Durymanov M, Reineke J. Non-viral delivery of nucleic acids: insight into mechanisms of overcoming intracellular barriers. *Front Pharmacol*. 2018;9:971. <https://doi.org/10.3389/fphar.2018.00971>.
- Gregory A, Stenzel MH. Complex polymer architectures via RAFT polymerization: from fundamental process to extending the scope using click chemistry and nature's building blocks. *Prog Polym Sci*. 2012;37:38–105. <https://doi.org/10.1016/j.progpolymsci.2011.08.004>.
- Matyjaszewski K. Atom transfer radical polymerization (ATRP): current status and future perspectives. *Macromolecules*. 2012;45:4015–39. <https://doi.org/10.1021/ma3001719>.
- Sieglwart DJ, Oh JK, Matyjaszewski K. ATRP in the design of functional materials for biomedical applications. *Prog Polym Sci*. 2012;37:18–37. <https://doi.org/10.1016/j.progpolymsci.2011.08.001>.
- Moad G. RAFT polymerization to form stimuli-responsive polymers. *Polym Chem*. 2017;8:177–219. <https://doi.org/10.1039/c6py01849a>.
- Moad CL, Moad G. Fundamentals of reversible addition–fragmentation chain transfer (RAFT). *Chem Teach Int*. 2021;3:3–17. <https://doi.org/10.1515/cti-2020-0026>.
- Ahmed M, Narain R. Progress of RAFT based polymers in gene delivery. *Prog Polym Sci*. 2013;38:767–90. <https://doi.org/10.1016/j.progpolymsci.2012.09.008>.
- Cabral H, Miyata K, Osada K, Kataoka K. Block copolymer micelles in nanomedicine applications. *Chem Rev*. 2018;118:6844–92. <https://doi.org/10.1021/acs.chemrev.8b00199>.
- Oerlemans C, Bult W, Bos M, Storm G, Nijssen JF, Hennink WE. Polymeric micelles in anticancer therapy: targeting, imaging and triggered release. *Pharm Res*. 2010;27:2569–89. <https://doi.org/10.1007/s11095-010-0233-4>.
- Letchford K, Burt H. A review of the formation and classification of amphiphilic block copolymer nanoparticulate structures: micelles, nanospheres, nanocapsules and polymersomes. *Eur J Pharm Biopharm*. 2007;65:259–69. <https://doi.org/10.1016/j.ejpb.2006.11.009>.
- Mane SR, Sathyan A, Shunmugam R. Biomedical applications of pH-responsive amphiphilic polymer nanoassemblies. *ACS Appl Nano Mater*. 2020;3:2104–17. <https://doi.org/10.1021/acsnano.0c00410>.
- Gao D, Guo X, Zhang X, Chen S, Wang Y, Chen T, Huang G, Gao Y, Tian Z, Yang Z. Multifunctional phototheranostic nanomedicine for cancer imaging and treatment. *Mater Today Bio*. 2020;5:100035. <https://doi.org/10.1016/j.mtbio.2019.100035>.
- Wang H, Ding S, Zhang Z, Wang L, You Y. Cationic micelle: a promising nanocarrier for gene delivery with high transfection efficiency. *J Gene Med*. 2019;21:e3101. <https://doi.org/10.1002/jgm.3101>.
- Navarro G, Pan J, Torchilin VP. Micelle-like nanoparticles as carriers for DNA and siRNA. *Mol Pharm*. 2015;12:301–13. <https://doi.org/10.1021/mp5007213>.
- Uchida S, Kataoka K. Design concepts of polyplex micelles for in vivo therapeutic delivery of plasmid DNA and messenger RNA. *J Biomed Mater Res A*. 2019;107:978–90. <https://doi.org/10.1002/jbm.a.36614>.
- Yousefpour Marzbali M, Yari Khosroushahi A. Polymeric micelles as mighty nanocarriers for cancer gene therapy: a review. *Cancer Chemother Pharmacol*. 2017;79:637–49. <https://doi.org/10.1007/s00280-017-3273-1>.
- Richter F, Mapfumo P, Martin L, Solomon JI, Hausig F, Frietsch JJ, Ernst T, Hoepfener S, Brendel JC, Traeger A. Improved gene delivery to K-562 leukemia cells by lipoic acid modified block copolymer micelles. *J Nanobiotechnol*. 2021;19:70. <https://doi.org/10.1186/s12951-021-00801-y>.
- Tan Z, Jiang Y, Zhang W, Karls L, Lodge TP, Reineke TM. Polycation architecture and assembly direct successful gene delivery: micelleplexes outperform polyplexes via optimal DNA packaging. *J Am Chem Soc*. 2019;141:15804–17. <https://doi.org/10.1021/jacs.9b06218>.
- Convertine AJ, Benoit DS, Duvall CL, Hoffman AS, Stayton PS. Development of a novel endosomolytic diblock copolymer for siRNA delivery. *J Control Release*. 2009;133:221–9. <https://doi.org/10.1016/j.jconrel.2008.10.004>.
- Liu ZH, Zhang ZY, Zhou CR, Jiao YP. Hydrophobic modifications of cationic polymers for gene delivery. *Prog Polym Sci*. 2010;35:1144–62. <https://doi.org/10.1016/j.progpolymsci.2010.04.007>.
- Monnery BD, Wright M, Cavill R, Hoogenboom R, Shaunak S, Steinke JHG, Thanou M. Cytotoxicity of polycations: relationship of molecular weight and the hydrolytic theory of the mechanism of toxicity. *Int J Pharm*. 2017;521:249–58. <https://doi.org/10.1016/j.ijpharm.2017.02.048>.
- van de Wetering P, Cherng J-Y, Talsma H, Hennink WE. Relation between transfection efficiency and cytotoxicity of poly(2-(dimethylamino)ethyl

- methacrylate)/plasmid complexes. *J Control Release*. 1997;49:59–69. [https://doi.org/10.1016/s0168-3659\(97\)00059-x](https://doi.org/10.1016/s0168-3659(97)00059-x).
29. Lv H, Zhang S, Wang B, Cui S, Yan J. Toxicity of cationic lipids and cationic polymers in gene delivery. *J Control Release*. 2006;114:100–9. <https://doi.org/10.1016/j.jconrel.2006.04.014>.
  30. Pack DW, Hoffman AS, Pun S, Stayton PS. Design and development of polymers for gene delivery. *Nat Rev Drug Discov*. 2005;4:581–93. <https://doi.org/10.1038/nrd1775>.
  31. Hu CM, Fang RH, Luk BT, Zhang L. Polymeric nanotherapeutics: clinical development and advances in stealth functionalization strategies. *Nanoscale*. 2014;6:65–75. <https://doi.org/10.1039/c3nr05444f>.
  32. Yang JL, Zhang XC, Liu C, Wang Z, Deng LF, Feng C, Tao W, Xu XY, Cui WG. Biologically modified nanoparticles as theranostic bionanomaterials. *Prog Mater Sci*. 2021;118:100768. <https://doi.org/10.1016/j.pmatsci.2020.100768>.
  33. Fang Y, Xue J, Gao S, Lu A, Yang D, Jiang H, He Y, Shi K. Cleavable PEGylation: a strategy for overcoming the “PEG dilemma” in efficient drug delivery. *Drug Deliv*. 2017;24:22–32. <https://doi.org/10.1080/10717544.2017.1388451>.
  34. Mishra S, Webster P, Davis ME. PEGylation significantly affects cellular uptake and intracellular trafficking of non-viral gene delivery particles. *Eur J Cell Biol*. 2004;83:97–111. <https://doi.org/10.1078/0171-9335-00363>.
  35. Li B, Yuan Z, Hung HC, Ma J, Jain P, Tsao C, Xie J, Zhang P, Lin X, Wu K, Jiang S. Revealing the immunogenic risk of polymers. *Angew Chem Int Ed Engl*. 2018;57:13873–6. <https://doi.org/10.1002/anie.201808615>.
  36. Peeler DJ, Sellers DL, Pun SH. pH-sensitive polymers as dynamic mediators of barriers to nucleic acid delivery. *Bioconjug Chem*. 2019;30:350–65. <https://doi.org/10.1021/acs.bioconjchem.8b00695>.
  37. Yang Q, Jacobs TM, McCallen JD, Moore DT, Huckaby JT, Edelstein JN, Lai SK. Analysis of pre-existing IgG and IgM antibodies against polyethylene glycol (PEG) in the general population. *Anal Chem*. 2016;88:11804–12. <https://doi.org/10.1021/acs.analchem.6b03437>.
  38. Kierstead PH, Okochi H, Venditto VJ, Chuong TC, Kivimae S, Frechet JMJ, Szoka FC. The effect of polymer backbone chemistry on the induction of the accelerated blood clearance in polymer modified liposomes. *J Control Release*. 2015;213:1–9. <https://doi.org/10.1016/j.jconrel.2015.06.023>.
  39. Ishihara T, Maeda T, Sakamoto H, Takasaki N, Shigyo M, Ishida T, Kiwada H, Mizushima Y, Mizushima T. Evasion of the accelerated blood clearance phenomenon by coating of nanoparticles with various hydrophilic polymers. *Biomacromol*. 2010;11:2700–6. <https://doi.org/10.1021/bm100754e>.
  40. Felber AE, Dufresne MH, Leroux JC. pH-sensitive vesicles, polymeric micelles, and nanospheres prepared with polycarboxylates. *Adv Drug Deliv Rev*. 2012;64:979–92. <https://doi.org/10.1016/j.addr.2011.09.006>.
  41. Dewald I, Gensel J, Betthausen E, Borisov OV, Muller AH, Schacher FH, Fery A. Splitting of surface-immobilized multicompartment micelles into clusters upon charge inversion. *ACS Nano*. 2016;10:5180–8. <https://doi.org/10.1021/acsnano.6b00670>.
  42. Rinkebauer AC, Schallon A, Gunther U, Wagner M, Betthausen E, Schubert US, Schacher FH. A paradigm change: efficient transfection of human leukemia cells by stimuli-responsive multicompartment micelles. *ACS Nano*. 2013;7:9621–31. <https://doi.org/10.1021/nn402072d>.
  43. Synatschke CV, Nomoto T, Cabral H, Fortsch M, Toh K, Matsumoto Y, Miyazaki K, Hanisch A, Schacher FH, Kishimura A, et al. Multicompartment micelles with adjustable poly(ethylene glycol) shell for efficient in vivo photodynamic therapy. *ACS Nano*. 2014;8:1161–72. <https://doi.org/10.1021/nn4028294>.
  44. Pergushov DV, Muller AH, Schacher FH. Micellar interpolyelectrolyte complexes. *Chem Soc Rev*. 2012;41:6888–901. <https://doi.org/10.1039/c2cs35135h>.
  45. Vergaro V, Scarlino F, Bellomo C, Rinaldi R, Vergara D, Maffia M, Baldassarre F, Giannelli G, Zhang X, Lvov YM, Leporatti S. Drug-loaded polyelectrolyte microcapsules for sustained targeting of cancer cells. *Adv Drug Deliv Rev*. 2011;63:847–64. <https://doi.org/10.1016/j.addr.2011.05.007>.
  46. Finsinger D, Remy JS, Erbacher P, Koch C, Plank C. Protective copolymers for nonviral gene vectors: synthesis, vector characterization and application in gene delivery. *Gene Ther*. 2000;7:1183–92. <https://doi.org/10.1038/sj.gt.3301227>.
  47. Sethuraman VA, Na K, Bae YH. pH-responsive sulfonamide/PEI system for tumor specific gene delivery: an in vitro study. *Biomacromol*. 2006;7:64–70. <https://doi.org/10.1021/bm0503571>.
  48. Nakamura N, Mochida Y, Toh K, Fukushima S, Cabral H, Anraku Y. Effect of mixing ratio of oppositely charged block copolymers on polyion complex micelles for in vivo application. *Polymers*. 2021;13:5. <https://doi.org/10.3390/polym13010005>.
  49. Sanati S, Taghavi S, Abnous K, Taghdisi SM, Babaei M, Ramezani M, Alibolandi M. Fabrication of anionic dextran-coated micelles for aptamer targeted delivery of camptothecin and survivin-shRNA to colon adenocarcinoma. *Gene Ther*. 2021. <https://doi.org/10.1038/s41434-021-00234-0>.
  50. Yu L, Lin C, Zheng Z, Li Z, Wang X. Self-assembly of pH-responsive biodegradable mixed micelles based on anionic and cationic polycarbonates for doxorubicin delivery. *Colloids Surf B Biointerfaces*. 2016;145:392–400. <https://doi.org/10.1016/j.colsurfb.2016.05.029>.
  51. Colombani O, Ruppel M, Burkhardt M, Drechsler M, Schumacher M, Gradzielski M, Schweins R, Muller AHE. Structure of micelles of poly(n-butyl acrylate)-block-poly(acrylic acid) diblock copolymers in aqueous solution. *Macromolecules*. 2007;40:4351–62. <https://doi.org/10.1021/ma0609580>.
  52. Gardey E, Sobotta FH, Hoepfner S, Bruns T, Stallmach A, Brendel JC. Influence of core cross-linking and shell composition of polymeric micelles on immune response and their interaction with human monocytes. *Biomacromol*. 2020;21:1393–406. <https://doi.org/10.1021/acs.biomac.9b01656>.
  53. Richter F, Martin L, Leer K, Moek E, Hausig F, Brendel JC, Traeger A. Tuning of endosomal escape and gene expression by functional groups, molecular weight and transfection medium: a structure-activity relationship study. *J Mater Chem B*. 2020;8:5026–41. <https://doi.org/10.1039/d0tb00340a>.
  54. van de Wetering P, Moret EE, Schuurmans-Nieuwenbroek NM, van Steenberg MJ, Hennink WE. Structure-activity relationships of water-soluble cationic methacrylate/methacrylamide polymers for nonviral gene delivery. *Bioconjug Chem*. 1999;10:589–97. <https://doi.org/10.1021/bc980148w>.
  55. Martin L, Gody G, Perrier S. Preparation of complex multiblock copolymers via aqueous RAFT polymerization at room temperature. *Polym Chem*. 2015;6:4875–86. <https://doi.org/10.1039/c5py00478k>.
  56. Schindelin J, Arganda-Carreras I, Frise E, Kaynig V, Longair M, Pietzsch T, Preibisch S, Rueden C, Saalfeld S, Schmid B, et al. Fiji: an open-source platform for biological-image analysis. *Nat Methods*. 2012;9:676–82. <https://doi.org/10.1038/nmeth.2019>.
  57. Gody G, Maschmeyer T, Zetterlund PB, Perrier S. Exploitation of the degenerative transfer mechanism in RAFT polymerization for synthesis of polymer of high livingness at full monomer conversion. *Macromolecules*. 2014;47:639–49. <https://doi.org/10.1021/ma402286e>.
  58. Mellman I, Fuchs R, Helenius A. Acidification of the endocytic and exocytic pathways. *Annu Rev Biochem*. 1986;55:663–700. <https://doi.org/10.1146/annurev.bi.55.070186.003311>.
  59. Catrouillet S, Brendel JC, Larnaudie S, Barlow T, Jolliffe KA, Perrier S. Tunable length of cyclic peptide-polymer conjugate self-assemblies in water. *ACS Macro Lett*. 2016;5:1119–23. <https://doi.org/10.1021/acsmacrolett.6b00586>.
  60. Huotari J, Helenius A. Endosome maturation. *EMBO J*. 2011;30:3481–500. <https://doi.org/10.1038/emboj.2011.286>.
  61. Betthausen E, Drechsler M, Fortsch M, Schacher FH, Muller AHE. Dual stimuli-responsive multicompartment micelles from triblock terpolymers with tunable hydrophilicity. *Soft Matter*. 2011;7:8880–91. <https://doi.org/10.1039/c1sm05822c>.
  62. Jiang Y, Lodge TP, Reineke TM. Packaging pDNA by polymeric ABC micelles simultaneously achieves colloidal stability and structural control. *J Am Chem Soc*. 2018;140:11101–11. <https://doi.org/10.1021/jacs.8b06309>.
  63. Bus T, Traeger A, Schubert US. The great escape: how cationic polyplexes overcome the endosomal barrier. *J Mater Chem B*. 2018;6:6904–18. <https://doi.org/10.1039/c8tb00967h>.
  64. Braun S, Pokorna S, Sachl R, Hof M, Heerklotz H, Hoernke M. Biomembrane permeabilization: statistics of individual leakage events harmonize the interpretation of vesicle leakage. *ACS Nano*. 2018;12:813–9. <https://doi.org/10.1021/acsnano.7b08184>.

## Publisher's Note

Springer Nature remains neutral with regard to jurisdictional claims in published maps and institutional affiliations.



## Additional file 1

# The Impact of Anionic Polymers on Gene Delivery: How Composition and Assembly Help Evading the Toxicity-Efficiency Dilemma

*Friederike Richter,<sup>a,‡</sup> Katharina Leer,<sup>a,‡</sup> Liam Martin,<sup>a</sup> Prosper Mapfumo,<sup>a</sup> Jana I. Solomun,<sup>a</sup>  
Maren T. Kuchenbrod,<sup>a</sup> Stephanie Hoepfener,<sup>a,b</sup> Johannes C. Brendel,<sup>a,b</sup> Anja Traeger<sup>\*a,b</sup>*

<sup>a</sup>Laboratory of Organic and Macromolecular Chemistry (IOMC), Friedrich Schiller University  
Jena, Humboldtstrasse 10, 07743 Jena, Germany.

<sup>b</sup>Jena Center for Soft Matter (JCSM), Friedrich Schiller University Jena, Philosophenweg 7,  
07743 Jena, Germany.

<sup>‡</sup>Authors contributed equally

\*Correspondence to A. Traeger (anja.traeger@uni-jena.de)

List of Tables. ....	3
List of Figures. ....	3
ADDITIONAL METHODS .....	4
Materials. ....	4
Instruments.....	5
Detailed Polymer Synthesis and Characterization. ....	6
Calculations for RAFT Polymerization. ....	10
Dynamic and Electrophoretic Light Scattering (DLS & ELS). ....	12
Cryo Transmission Electron Microscopy (cryo-TEM).....	13
Titration.....	14
N*/P Ratio Calculations.....	15
Ethidium Bromide Quenching Assay (EBA) and Heparin Dissociation Assay (HRA). ....	16
Determination of Cytotoxicity. ....	17
Erythrocyte Aggregation and Hemolysis.....	19
Polyplex Uptake <i>via</i> Flow Cytometry.....	20
Polyplex Uptake <i>via</i> CLSM. ....	21
Image Acquisition and Processing for the Calcein Release Assay <i>via</i> CLSM. ....	24
FURTHER RESULTS .....	26
Characterization of Polymers.....	26
Original Cryo-TEM images .....	30
DLS Measurements.....	32
pDNA Binding Assays.....	38
Cytotoxicity Assays. ....	39
Microscopic Images of Treated HEK293T Cells.....	40
Transfection Efficiency.....	41
Polyplex Uptake.....	45
Calcein Release. ....	48

## List of Tables.

<b>Table S1.</b> Amount of different substances used for polymerization of block copolymers. ....	11
<b>Table S2.</b> Amount of different substances used for polymerization of (shielding) polymers. ....	11
<b>Table S3.</b> Kinetic cycle protocol for automated heparin addition by the microplate reader.....	17
<b>Table S4.</b> Overview of the different assembly batches of HC- and HAC-mic. ....	31
<b>Table S5.</b> Polymer concentrations in different assays.....	31
<b>Table S6.</b> Summary of micelle characterization at different pH-values, high concentrations. ....	32
<b>Table S7.</b> Summary of micelle characterization at different pH values, low concentrations. ....	32
<b>Table S8.</b> MFI values of different controls in flow cytometry.....	43

## List of Figures.

<b>Figure S1.</b> Characterization of PDMAEAm <sub>82</sub> .....	26
<b>Figure S2.</b> NMR results of the HC-mic in CDCl <sub>3</sub> .....	27
<b>Figure S3.</b> NMR results of the HAC-mic. ....	28
<b>Figure S4.</b> Characterization of the layer diblock copolymer. ....	29
<b>Figure S5.</b> Original cryo-TEM images of micelles.....	30
<b>Figure S6.</b> DLS measurements of micelle stock solutions directly after formulation. ....	33
<b>Figure S7.</b> DLS measurements of (layered) micelles at different pH values.....	34
<b>Figure S8.</b> DLS measurements of (layered) polyplexes in HBG buffer. ....	35
<b>Figure S9.</b> DLS measurements of different batches of (layered) micelles. ....	36
<b>Figure S10.</b> DLS/ELS measurements of different batches of (layered) polyplexes. ....	37
<b>Figure S11.</b> Additional EBA&HRA results. ....	38
<b>Figure S12.</b> Additional cytotoxicity assays.....	39
<b>Figure S13.</b> Influence of (layered) polyplexes on cell morphology. ....	40
<b>Figure S14.</b> Influence of storage time on transfection efficiency. ....	41
<b>Figure S15.</b> Influence of different assembly batches on transfection efficiency. ....	41
<b>Figure S16.</b> Transfection efficiency with increased pDNA concentration in HEK293T cells. ...	42
<b>Figure S17.</b> Influence of concentration on transfection efficiency. ....	42
<b>Figure S18.</b> Gating strategy for pDNA transfection using examples of 24 h incubation. ....	44
<b>Figure S19.</b> Gating strategy for polyplex uptake using examples of 1 and 24 h incubation. ....	45
<b>Figure S20.</b> Quantitative analysis of polyplex uptake by CLSM. ....	46
<b>Figure S21.</b> CLSM images of polyplex uptake by HEK293T cells.....	47
<b>Figure S22.</b> Brightfield (BF) and gray images of HEK293T cells for calcein CLSM study.....	48

## ADDITIONAL METHODS

### Materials.

All chemicals were used as received unless stated otherwise. The chain transfer agent 2-(Butylthiocarbonothioylthio) propanoic acid (PABTC) was prepared following a previously reported procedure.[1] Dimethylamino ethyl acrylamide (DMAEAm) was obtained from ABCR (Germany) and purified by column chromatography (silica, ethyl acetate). Sodium sulfate ( $\text{Na}_2\text{SO}_4$ ) was obtained from Grüssing GmbH (Germany). Trifluoroacetic acid (TFA) was obtained from TCI (Japan). Acetic acid glacial (HOAc), sodium hydrogen carbonate ( $\text{NaHCO}_3$ ), sodium hydroxide (NaOH) and sodium chloride (NaCl) were obtained from Fisher Scientific (U.S.). 2,2'-Azobis(2,4-dimethylvaleronitrile) (V65B) was obtained from FUJIFILM Wako Chemicals (Germany). Sodium acetate trihydrate ( $\text{NaOAc}\times 3\text{H}_2\text{O}$ ), 4-Acryloylmorpholine (NAM), 1,3,5-trioxane and anhydrous *N,N*-dimethylacetamide (99.8%, DMAc) were obtained from Sigma Aldrich (U.S.). 1,4-Dioxane (>99.5%) was obtained from Carl Roth (Germany). *n*-Butyl acrylate (*n*BA), hydrogen chloride (HCl) and dimethylformamide (DMF) were obtained from Alfa Aesar (U.S.). NAM, *n*BA and 1,4-dioxane were stored over inhibitor remover beads (for hydroquinone and monomethyl ether hydroquinone) and stored at 4 °C. Tetrahydrofuran (THF), *n*-hexane, methanol and chloroform were distilled on site.

For biological studies, Dulbecco's modified eagle medium (DMEM), 4-(2-hydroxyethyl)-1-piperazineethanesulfonic acid) (HEPES) buffer and phosphate buffered saline (PBS) were obtained from Biowest SAS (France). Fetal calf serum (FCS) was obtained from Capricorn Scientific (Germany). PrestoBlue™ solution, YOYO-1 iodide, CellMask™ Deep Red Plasma membrane (CMDR-PM) and Penicillin-Streptomycin were obtained from Thermo Fisher Scientific (U.S.). Trypsin-EDTA-solution, Triton X-100, 0.4% trypan blue solution, Hanks'

balanced salt solution (HBSS) and calcein were obtained from Sigma Aldrich (U.S.). 1% ethidium bromide solution (EtBr) was obtained from Carl Roth (Germany). Heparin sodium salt from porcine intestinal mucosa was obtained from Alfa Aesar (U. S.). Poly(acrylic acid) (PAA, MW 2000), linear poly(ethyleneimine) (LPEI,  $M_w = 25 \text{ kg mol}^{-1}$ ) and branched PEI (BPEI,  $M_w = 10 \text{ kg mol}^{-1}$ ) were obtained from Polysciences (U.S.), CytoTox-ONE™ Homogeneous Membrane Integrity Assay was obtained from Promega (U.S.). Plasmid DNA (pDNA) encoding mEGFP-N1 and pKMyc were gifts from Michael Davidson (Addgene plasmid #54767; <http://n2t.net/addgene:54767>; RRID: Addgene\_54767) and Ian Macara (Addgene plasmid #19400; <http://n2t.net/addgene:19400>; RRID: Addgene\_19400), respectively, and were isolated from E. Coli using a Giga plasmid kit (Quiagen, Germany).

### **Instruments.**

*Nuclear magnetic resonance (NMR) spectroscopy.*  $^1\text{H}$  NMR (300 MHz) and DEPT  $^{13}\text{C}$  (75 MHz) spectra were recorded on a Bruker AC 300 MHz spectrometer at 300 K. The delay time (d1) was set at 1 s for  $^1\text{H}$  NMR and 2 s for DEPT  $^{13}\text{C}$ . Chemical shifts ( $\delta$ ) are reported in ppm.

*Size exclusion chromatography (SEC).* SEC was conducted on one of two instruments. Dimethylacetamide (DMAc)-SEC was conducted using an Agilent 1200 series instrument equipped with differential refractive index (DRI) and UV/vis (DAD) detector. The liquid chromatography system used 1  $\times$  PSS GRAM 30 Å column (300  $\times$  0.8 mm, 10  $\mu\text{m}$  particle size) and 1  $\times$  PSS GRAM 1000 Å column (300  $\times$  0.8 mm, 10  $\mu\text{m}$  particle size). The DMAc eluent contained 0.21 wt.% LiCl as additive. Samples were run at 1 mL  $\text{min}^{-1}$  at 40 °C. Analyte samples were filtered through a polytetrafluoroethylene (PTFE) membrane with 0.45  $\mu\text{m}$  pore size prior to injection. Poly(methyl methacrylate) (PMMA) narrow standards were used to calibrate the SEC system. The measurements in aqueous solution for P(NAM-*b*-AA) were carried out on a Jasco

system equipped with a AS-2051 Plus autosampler, a DG-2080-53 degasser, a PU-980 pump, a RI-2031 Plus RI detector, a Jasco oven and a PSS SUPREMA guard/1000/30 Å (10 µm particle size). A mixture of 0.08 M Na<sub>2</sub>HPO<sub>4</sub>/0.05% NaN<sub>3</sub> (pH 9) was used as an eluent at a flow rate of 1 mL min<sup>-1</sup> and an oven temperature of 30 °C. PEG standards (400-800,000 g mol<sup>-1</sup>) were used to calibrate the system. Experimental  $M_{n,SEC}$  and  $D (M_w/M_n)$  values of synthesized polymers were determined using PSS WinGPC UniChrom GPC software.

*Flow cytometry.* Flow cytometry was conducted on the CytoFlex S by Beckman Coulter GmbH, Germany. For each experiment,  $\geq 10^4$  cells per sample were analyzed regarding their viability, single cells and fluorescence at  $\lambda_{Ex} = 488$  with a 525 nm bandpass filter (all employed stains, YOYO-1 & EGFP, were green fluorescent) in forward/sideward scatter (FSC, SSC), in FSC-Area /FSC-Height, and in FITC/SSC scatter plots, respectively.

*Microplate reader.* Fluorescence intensity measurements for PrestoBlue, LDH assays and absorption measurements for hemolysis and aggregation assays were performed on the Infinite M200 PRO microplate reader (Tecan, Germany) with  $\lambda_{Ex} / \lambda_{Em}$  used as indicated in the respective method sections and gain set to optimal. The combined EBA&HRA assay was conducted on the Cytation 5 multi-mode reader by BioTek, U.S.

### **Detailed Polymer Synthesis and Characterization.**

*Synthesis of P(DMAEAm)<sub>82</sub>* was performed as described before.[2] PABTC (11.9 mg,  $5.0 \times 10^{-5}$  mol), DMAEAm (682.3 mg,  $64.8 \times 10^{-3}$  mol), 1,4-dioxane (428.5 mg, 416.0 µL), DMAc (247.8 mg, 263.6 µL), V-65B (213.1 mg of a 1 wt.% solution in 1,4-dioxane, 2.1 mg,  $8.2 \times 10^{-6}$  mol) and 1,3,5-trioxane (16.3 mg) as an external NMR reference were introduced to a vial equipped with a magnetic stirring bar which was sealed with a cap. The mixture was deoxygenated

by bubbling argon through the solution for 10 min. The vial was then transferred to a thermostated oil bath set at 60 °C. After a polymerization time of 4 h, the flask was cooled to room temperature (RT) and exposed to air. 2-3 droplets of the polymerization mixture were used for <sup>1</sup>H NMR and SEC analysis. Afterward, the crude polymer was precipitated three times from THF into -80 °C cold *n*-hexane. The polymer was dried under vacuum. Then, the polymer was dissolved in distilled water and lyophilized.

*Synthesis of P(nBA)*. PABTC (230.40 mg,  $9.7 \times 10^{-4}$  mol), *n*BA (12389.6 mg,  $9.7 \times 10^{-2}$  mol), 1,4-dioxane (4164.2 mg, 4042.9 μL), V-65B (1497.0 mg of a 0.5 wt.% solution in 1,4-dioxane, 7.5 mg,  $2.9 \times 10^{-5}$  mol) and 1,3,5-trioxane (33.0 mg) as an external NMR reference were introduced to a vial equipped with a magnetic stirring bar which was sealed with a cap. The mixture was deoxygenated by bubbling argon through the solution for 20 min. The vial was then transferred to a thermostated oil bath set at 50 °C. After a polymerization time of 4 h, the flask was cooled to RT and exposed to air. 2-3 droplets of the polymerization mixture were used for <sup>1</sup>H NMR and SEC analysis. Afterward, the solvent was removed and the crude polymer was precipitated three times from THF into cold MeOH/ H<sub>2</sub>O (75/25). Finally, the polymer was dried under vacuum.

*Synthesis of P(nBA<sub>80</sub>-b-DMAEAm<sub>90</sub>)*. P(*n*BA)<sub>80</sub> (631.7 mg,  $6.0 \times 10^{-5}$  mol), DMAEAm (1226.2 mg,  $8.6 \times 10^{-3}$  mol), 1,4-dioxane (842.1 mg, 817.6 μL), V-65B (553.6 mg of a 0.5 wt.% solution in 1,4-dioxane, 2.8 mg,  $1.0 \times 10^{-5}$  mol) and 1,3,5-trioxane (8.7 mg) as an external NMR reference were introduced to a vial equipped with a magnetic stirring bar which was sealed with a cap. The mixture was deoxygenated by bubbling argon through the solution for 20 min. The vial was then transferred to a thermostated oil bath set at 55 °C. After a polymerization time of 70 min, the flask was cooled to RT and exposed to air. 2-3 droplets of the polymerization mixture were used

for  $^1\text{H}$  NMR and SEC analysis. Afterward, the crude polymer was precipitated three times from THF into  $-80\text{ }^\circ\text{C}$  cold *n*-hexane. Finally, the polymer was dried under vacuum.

*Synthesis of P(nBA<sub>86</sub>-b-tBA<sub>43</sub>).* P(nBA)<sub>86</sub> (1521.3 mg,  $1.4 \times 10^{-4}$  mol), tBA (868.9 mg,  $6.8 \times 10^{-3}$  mol), 1,4-dioxane (2491.1 mg, 2418.5  $\mu\text{L}$ ), V-65B (394.5 mg of a 1.0 wt.% solution in 1,4-dioxane, 4.0 mg,  $1.5 \times 10^{-5}$  mol) and 1,3,5-trioxane (14.3 mg) as an external NMR reference were introduced to a vial equipped with a magnetic stirring bar which was sealed with a cap. The mixture was deoxygenated by bubbling argon through the solution for 15 min. The vial was then transferred to a thermostated oil bath set at  $50\text{ }^\circ\text{C}$ . After a polymerization time of 5 h, the flask was cooled to RT and exposed to air. 2-3 droplets of the polymerization mixture were used for  $^1\text{H}$  NMR and SEC analysis. Afterward, the crude polymer was precipitated twice from THF into cold MeOH/ H<sub>2</sub>O (90/10). Finally, the polymer was dried under vacuum.

*Synthesis of P(nBA<sub>86</sub>-b-tBA<sub>43</sub>-b-DMAEAm<sub>88</sub>).* P(nBA<sub>86</sub>-b-tBA<sub>43</sub>) (504.7 mg,  $3.0 \times 10^{-5}$  mol), DMAEAm (604.0 mg,  $4.3 \times 10^{-3}$  mol), 1,4-dioxane (1220 mg, 1184.5  $\mu\text{L}$ ), V-65B (101.9 mg of a 2.0 wt.% solution in 1,4-dioxane, 2.0 mg,  $7.9 \times 10^{-6}$  mol) and 1,3,5-trioxane (7.3 mg) as an external NMR reference were introduced to a vial equipped with a magnetic stirring bar which was sealed with a cap. The mixture was deoxygenated by bubbling argon through the solution for 15 min. The vial was then transferred to a thermostated oil bath set at  $55\text{ }^\circ\text{C}$ . After a polymerization time of 70 min, the flask was cooled to RT and exposed to air. 2-3 droplets of the polymerization mixture were used for  $^1\text{H}$  NMR and SEC analysis. Afterward, the crude polymer was precipitated three times from THF into  $-80\text{ }^\circ\text{C}$  cold *n*-hexane. The polymer was dried under vacuum.

*Synthesis of P(NAM).* PABTC (105.0 mg,  $4.4 \times 10^{-5}$  mol), NAM (4660.0 mg,  $3.3 \times 10^{-2}$  mol), 1,4-dioxane (8800.0 mg, 8518.9  $\mu\text{L}$ ), V-65B (318.6 mg of a 1.0 wt.% solution in 1,4-dioxane, 3.19 mg,



$1.2 \times 10^{-5}$  mol) and 1,3,5-trioxane (75.0 mg) as an external NMR reference were introduced to a vial equipped with a magnetic stirring bar which was sealed with a cap. The mixture was deoxygenated by bubbling argon through the solution for 10 min. The vial was then transferred to a thermostated oil bath set at 50 °C. After a polymerization time of 21 h, the flask was cooled to RT and exposed to air. 2-3 droplets of the polymerization mixture were used for  $^1\text{H}$  NMR and SEC analysis. Afterward, the crude polymer was precipitated three times from THF into -80 °C cold *n*-hexane. The polymer was dried under vacuum.

*Synthesis of P(NAM<sub>74</sub>-b-tBA<sub>42</sub>).* P(NAM<sub>74</sub>) (850.0 mg,  $7.98 \times 10^{-5}$  mol), *t*BA (511.7 mg,  $3.99 \times 10^{-3}$  mol), 1,4-dioxane (1800.0 mg, 1747.6  $\mu\text{L}$ ), V-65B (134.0 mg of a 1.0 wt.% solution in 1,4-dioxane, 1.34 mg,  $5.18 \times 10^{-6}$  mol) and 1,3,5-trioxane (28.0 mg) as an external NMR reference were introduced to a vial equipped with a magnetic stirring bar which was sealed with a cap. The mixture was deoxygenated by bubbling argon through the solution for 10 min. The vial was then transferred to a thermostated oil bath set at 50 °C. After a polymerization time of 6 h, the flask was cooled to RT and exposed to air. 2-3 droplets of the polymerization mixture were used for  $^1\text{H}$  NMR and SEC analysis. Afterward, the crude polymer was precipitated three times from chloroform into cold *n*-hexane. Finally, the polymer was dried under vacuum.

*Boc-deprotection of P(nBA<sub>86</sub>-b-tBA<sub>43</sub>-b-DMAEAm<sub>88</sub>).* A sample of Boc-protected polymer was introduced to a 25 mL round-bottom flask equipped with a magnetic stirring bar and TFA/deionized water (97/3, v/v) was added to reach a concentration of 147 mg mL<sup>-1</sup>. A small amount of THF was added to aid the solubility. The solution was stirred for 3 h at RT and the TFA was blown off overnight using compressed air. Subsequently, the crude deprotected polymer was precipitated three times from THF into -80 °C cold hexane. Finally, the deprotected polymer was dried under vacuum.

*Boc-deprotection of P(NAM<sub>74</sub>-b-tBA<sub>42</sub>).* A sample of Boc-protected polymer was introduced to a 25 mL round-bottom flask equipped with a magnetic stirring bar and TFA/DMF (34/66, v/v) were added. The solution was stirred overnight at RT and quenched with sat. NaHCO<sub>3</sub> to reach pH 7. Then, the solution was dialyzed in water over 2 d with changing solution every 2 h for the first 8 h, and twice the following 2 d. After dialysis, the solution was concentrated under vacuum and lyophilized to yield the product.

### **Calculations for RAFT Polymerization.**

The monomer conversion ( $p$ ) was calculated from <sup>1</sup>H NMR data by comparing the integrals of vinyl peaks (5.5-5.75 ppm) against the external reference 1,3,5-trioxane (5.10 ppm) before and after polymerization. The theoretical number-average molar mass ( $M_{n,th}$ ) was calculated with Equation S1:

$$M_{n,th} = \frac{[M]_0 p M_M}{[CTA]_0} + M_{CTA} \quad (S1)$$

$[M]_0$  and  $[CTA]_0$  are the initial concentrations of monomer and chain transfer agent (CTA), respectively.  $M_M$  and  $M_{CTA}$  are the molecular masses of the monomer and CTA, respectively.

**Table S1.** Amount of different substances used for polymerization of block copolymers.

Assembly code	-	HC	-	-	HAC
Composition	P( <i>n</i> BA) <sub>80</sub>	P( <i>n</i> BA <sub>80</sub> - <i>b</i> -DMAEAm <sub>90</sub> )	P( <i>n</i> BA) <sub>86</sub>	P( <i>n</i> BA <sub>86</sub> - <i>b</i> - <i>t</i> BA <sub>43</sub> )	P( <i>n</i> BA <sub>86</sub> - <i>b</i> - <i>t</i> BA <sub>43</sub> - <i>b</i> -DMAEAm <sub>88</sub> )
Monomer	<i>n</i> BA	DMAEAm	<i>n</i> BA	<i>t</i> BA	DMAEAm
DP <sub><i>n</i>,target</sub>	100	145	100	50	140
m <sub>CTA</sub> added (mg)	230.4	631.7	185.9	1521.3	504.7
n <sub>CTA</sub> added (mol)	9.66 × 10 <sup>-4</sup>	5.97 × 10 <sup>-5</sup>	7.80 × 10 <sup>-4</sup>	1.36 × 10 <sup>-4</sup>	3.02 × 10 <sup>-5</sup>
m <sub>monomer</sub> added (mg)	12389.6	1226.2	9996.2	868.9	604.0
n <sub>monomer</sub> added (mol)	9.67 × 10 <sup>-2</sup>	8.63 × 10 <sup>-3</sup>	7.80 × 10 <sup>-2</sup>	6.78 × 10 <sup>-3</sup>	4.25 × 10 <sup>-3</sup>
m <sub>V-65B</sub> added (mg)	7.49	2.77	8.63	3.95	2.04
n <sub>V-65B</sub> added (mol)	2.90 × 10 <sup>-5</sup>	1.07 × 10 <sup>-5</sup>	3.34 × 10 <sup>-5</sup>	1.53 × 10 <sup>-5</sup>	7.89 × 10 <sup>-6</sup>
Dioxane added (g)	4164.2	842.1	6216.4	2491.1	1220.0
CTA/V-65B	33.3	5.6	23.3	9.0	3.9
T (°C)	50	55	50	50	55
Time (min)	240	70	300	300	65

**Table S2.** Amount of different substances used for polymerization of (shielding) polymers.

Assembly code	C	S	-	SA
Composition	P(DMAEAm) <sub>82</sub>	P(NAM) <sub>72</sub>	P(NAM) <sub>74</sub>	P(NAM <sub>74</sub> - <i>b</i> - <i>t</i> BA <sub>42</sub> )
Monomer	DMAEAm	NAM	NAM	<i>t</i> BA
DP <sub><i>n</i>,target</sub>	96	75	75	50
m <sub>CTA</sub> added (mg)	11.9	105.0	105.0	850.0
n <sub>CTA</sub> added (mol)	4.99 × 10 <sup>-5</sup>	4.40 × 10 <sup>-5</sup>	4.40 × 10 <sup>-5</sup>	7.98 × 10 <sup>-5</sup>
m <sub>monomer</sub> added (mg)	682.3	4660.0	4660.0	511.7
n <sub>monomer</sub> added (mol)	4.80 × 10 <sup>-3</sup>	3.30 × 10 <sup>-2</sup>	3.30 × 10 <sup>-2</sup>	3.99 × 10 <sup>-3</sup>
m <sub>V-65B</sub> added (mg)	2.13	3.19	3.19	1.34
n <sub>V-65B</sub> added (mol)	8.25 × 10 <sup>-6</sup>	1.23 × 10 <sup>-5</sup>	1.23 × 10 <sup>-5</sup>	5.18 × 10 <sup>-6</sup>
Dioxane added (g)	428.5	8800.0	8800.0	1800.0
DMAc added (g)	247.8	-	-	-
CTA/V-65B	6.2	3.6	3.6	15.4
T (°C)	60	50	50	50
Time (min)	240	1260	1260	360

### **Dynamic and Electrophoretic Light Scattering (DLS & ELS).**

The hydrodynamic diameters and  $\zeta$ -potential of the nano assemblies were monitored for three different sample preparations similar to as described before[3] by DLS or ELS using a Zetasizer Nano ZS (Malvern Instruments, Germany) with a He–Ne laser operating at a wavelength of 633 nm. The sample preparations were i) pure micelle solutions as obtained after dialysis, ii) micelle solutions mixed 3+1 with shielding polymer solution or buffer at different pH values, and iii) polyplexes of micelles mixed 3+1 with shielding polymer solution or buffer as control. Regarding the pure micelle suspensions, no further sample preparation was necessary. Each sample was measured in triplicates at 25 °C with measurement duration of five times 60 s after an equilibration time of 60 s. The counts were detected at an angle of 173°. The mean particle size was approximated as the effective (z-average) diameter and the width of the distribution as the polydispersity index of the particles (PDI) obtained by the cumulants method assuming a spherical shape. The curves and data are presented in Figure S6 and Figure S9, respectively.

For the measurement of the second sample preparation, layered micelles, the samples were prepared similar to the polyplex and layering protocol, but without pDNA and at higher polymer concentrations keeping the amount of amine moieties constant within all samples. The micelle solutions were prepared by dilution with 50 mM acetate buffer, pH 5. For measurements at pH 7.4, 1 M NaOH was added to a final concentration of 20 mM. The shielding polymer solutions were prepared fourfold concentrated by diluting the polymer stock solutions in 100 mM acetate-HEPES buffer of the respective pH value (50 mM acetate + 50 mM HEPES, pH 5.0 or pH 7.4). Subsequently, the micelle suspension was slowly added to the shielding polymer solution (3+1 volume ratio) and carefully resuspended, obtaining either a molar PNAM/PnBA ratio of 1.0 or a carboxy to amine group (COOH/NH) ratio of 0.5. Where no layering was required, the shielding

polymer solution was replaced by acetate-HEPES buffer of the respective pH value. The samples were incubated at RT for 15 min and measured as described above but with measurement duration of three times 30 s after an equilibration time of 30 s. The samples were measured again after dilution of 1:3 with ultrapure water. Subsequently,  $\zeta$ -potential of the diluted samples was measured in triplicates at 25 °C and 40 mV with measurement duration set to automatic (10-20 runs) after an equilibration time of 30 s and with a delay of 30 s between each measurement. Data are expressed as mean  $\pm$  SD of two by three measurements (n = 2).

The third class of samples, the polyplexes, was measured following polyplex preparation at N\*/P 30 in 75  $\mu$ L HBG buffer and mixing with 25  $\mu$ L shielding polymer solution or HBG buffer as described in the polyplex preparation section. The hydrodynamic diameter and  $\zeta$ -potential of the samples were measured as described in the paragraph above, but this time the samples were diluted 1:8. Data are expressed as mean  $\pm$  SD of two by three measurements (n = 2).

### **Cryo Transmission Electron Microscopy (cryo-TEM).**

The samples for cryo-TEM were prepared as described for the second preparation for DLS and ELS measurements, but only in acetate-HEPES buffer of pH 5.0. For the pure HC and HAC assemblies, the stock solutions of the micelles in 50 mM acetate buffer were used. Cryo-TEM images were acquired with a 120 kV FEI Tecnai G2 20 equipped with a 4k  $\times$  4k Eagle HS CCD and an Olympus MegaView camera (1379  $\times$  1024 pixels) for overview images. Sample preparation was performed by plunge-freezing the samples with a Vitrobot Mark IV system. 8.5  $\mu$ L of the aqueous solutions were blotted (blot force -2; blotting time 1 s) on Quantifoil grids (R2/2, Quantifoil, Jena, Germany) and were vitrified in liquid ethane. The grids were rendered hydrophilic by Ar-plasma cleaning for 30 s (Diener Electronics, Germany). Prior to sample preparation, samples were stored in liquid nitrogen until transfer to the cryo holder (Gatan 626).

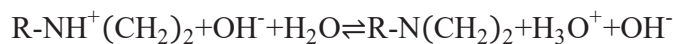
Transfer to the microscope was performed with a Gatan cryo stage and the temperature was maintained below -172 °C at all times after vitrification.

The size of the micelles was determined using ImageJ, version 1.52.[4] Briefly, hexagonal arrangements of seven micelles each were identified and the distance between the core of the center micelle and the core of each micelle in a corner was measured. For the estimation of the size of the micellar core, the diameter of a circle drawn around the micellar core was measured. The results are presented as mean  $\pm$  SD of all measurements of the respective sample.

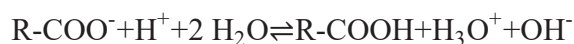
### **Titration.**

Titration of the polymers was conducted using a Metrohm OMNIS integrated titration system. For a typical measurement, the polymers were dissolved at 5 mg mL<sup>-1</sup> in 150 mM NaCl (in ultrapure water). In case of PDMAEAm<sub>82</sub>, the solution was acidified with addition of 1 M HCl (pH  $\sim$  2), the PAA solution was alkalized with addition of 1 M NaOH solution (pH  $\sim$  11). The polymers were titrated (with dynamic flow rate adjustment) against 0.1 M NaOH solution up to a pH value of 12 or against 0.1 M HCl up to a pH value of 2, respectively.

The degree of charge (DOC) at different pH values was calculated as the amount of negatively or positively charged units per total amount of carboxy or amine groups, respectively (Equations S2-3)[5]:



$$\text{DOC (PDMAEAm)} = \frac{[\text{R-NH}^+(\text{CH}_2)_2]}{[\text{R-N}(\text{CH}_2)_2]_{\text{tot}}} \cdot 100 \quad (\text{S2})$$



$$\text{DOC(PAA)} = \frac{[\text{R-COO}^-]}{[\text{R-COOH}]_{\text{tot}}} \cdot 100 \quad (\text{S3})$$

Subsequently, a logistic curve was fitted to the obtained DOC values using Origin Pro, Version 2020b (OriginLab Corporation, US). The  $pK_a$  values were calculated as the pH value where the DOC was 50% ( $y = 50$ ) by substitution into the respective functions of the logistic curves (Equation S4).

$$y = \frac{A_1 - A_2}{1 + (x/x_0)^p} + A_2 \quad (\text{S4})$$

Where  $A_1$ ,  $A_2$ ,  $x_0$  and  $p$  are the initial value, the final value, the center and the power of the curve, respectively.

#### **N\*/P Ratio Calculations.**

The N\*/P ratio was defined as the ratio of the total amount of protonatable amines in polymer solution in relation to the total amount of phosphates in the pDNA solution.

The volume of polymer needed to prepare polyplexes with  $15 \mu\text{g mL}^{-1}$  pDNA at different N\*/P ratios was calculated as described by the following equations:

$$V_{\text{total}} \cdot P = V_{\text{poly}} \cdot N_{\text{poly}}$$

$$V_{\text{poly}} = \frac{V_{\text{total}} \cdot P}{N_{\text{poly}}}$$

$$V_{\text{poly}} = V_{\text{total}} \cdot \frac{n_{\text{pDNA}} \cdot P}{n_{\text{poly}} \cdot N}$$

$$V_{\text{poly}} = V_{\text{total}} \cdot \frac{m_{\text{pDNA}} \cdot P \cdot M_{\text{poly}}}{m_{\text{poly}} \cdot N \cdot M_{\text{pDNA}}}$$

Where  $V_{\text{total}}$ ,  $P$ ,  $V_{\text{poly}}$  and  $N_{\text{poly}}$  are the total required volume, the total number of phosphates of the pDNA, the required volume of polymer and the total number of active amines of the polymer, respectively.

### **Ethidium Bromide Quenching Assay (EBA) and Heparin Dissociation Assay (HRA).**

The formation of polyplexes with pDNA was identified *via* quenching of ethidium bromide (EtBr) fluorescence by polymers interacting with pDNA as described before.[2] Briefly,  $40 \mu\text{g mL}^{-1}$  pKMyC pDNA in HBG buffer (pH 7.4) were incubated with EtBr ( $1 \mu\text{g mL}^{-1}$ ) at RT for 10 min. The polymer solutions were prepared by dilution with HBG buffer (pH 7.4) to give an N\*/P ratio of 30. Subsequently, the pDNA-EtBr solution was mixed 1+1 with the different polymer solutions in black 96-well plates (Nunc, Thermo Fisher, Germany) and incubated at  $37 \text{ }^\circ\text{C}$  for 15 min. Meanwhile, four times concentrated shielding polymer solutions were prepared to yield a molar PNAM/PnBA ratio of 1.0 or a carboxy to amine ratio of 0.5, respectively. They were added to the polyplex solutions in a ratio of 1+3, followed by careful resuspension and further 5 min incubation at  $37 \text{ }^\circ\text{C}$  before measuring the fluorescence intensity at  $\lambda_{\text{Ex}} = 525 \text{ nm}$  /  $\lambda_{\text{Em}} = 605 \text{ nm}$ . Where no layering was desired, the same amount of HBG buffer was added instead of the shielding polymer solution. A sample containing only pDNA and EtBr was defined as maximum fluorescence (100%).

For the heparin dissociation assay, heparin was added to the formed polyplex-EtBr mixtures using the dispenser of the microplate reader to obtain the indicated concentrations (Table S3). After each addition, the plate was shaken, incubated at  $37 \text{ }^\circ\text{C}$  for 10 min and fluorescence intensity was measured.



**Table S3.** Kinetic cycle protocol for automated heparin addition by the microplate reader

Kinetic cycle	Repetitions	Addition of heparin		Orbital shake	Incubation	Measurement
		V / $\mu\text{L}$	Stock Solution / $\text{U mL}^{-1}$			
1	2	5	100	10 s	10 min, 37 °C	$\lambda_{\text{Ex}} = 525 \text{ nm} / \lambda_{\text{Em}} = 605 \text{ nm}$
2	1	15	100	10 s	10 min, 37 °C	$\lambda_{\text{Ex}} = 525 \text{ nm} / \lambda_{\text{Em}} = 605 \text{ nm}$
3	3	5	500	10 s	10 min, 37 °C	$\lambda_{\text{Ex}} = 525 \text{ nm} / \lambda_{\text{Em}} = 605 \text{ nm}$
4	1	10	500	10 s	10 min, 37 °C	$\lambda_{\text{Ex}} = 525 \text{ nm} / \lambda_{\text{Em}} = 605 \text{ nm}$

The percentage of EtBr displaced upon polyplex formation or re-intercalating following pDNA release by heparin was calculated using Equation S5:

$$\text{rFI} / \% = \frac{F_{\text{Sample}}}{F_{\text{pDNA}}} \cdot 100 \quad (\text{S5})$$

Where rFI is the relative fluorescence intensity and  $F_{\text{Sample}}$ , and  $F_{\text{pDNA}}$  are the fluorescence intensities of a given sample and the EtBr intercalated into pDNA alone (in the case of the HRA with heparin), respectively. Data are expressed as mean  $\pm$  SD of three independent determinations. The heparin concentration needed to release 50% of pDNA was calculated with OriginPro, Version 2020b (OriginLab Corporation, US) using a logistic function fitted to the respective single measurement points ( $n = 3$ ) of each polymer (S4). The  $\text{HC}_{50}$ -values ( $y = 50$ ) were calculated by substitution of the respective values into the equation.

#### Determination of Cytotoxicity.

For determination of cytotoxicity of the polymers, the PrestoBlue<sup>TM</sup> assay was performed with the L-929 cells based on ISO10993-5. In detail, cells were seeded at  $0.1 \times 10^6$  cells  $\text{mL}^{-1}$  in growth medium (D10) containing 10 mM HEPES (D10H) in a 96-well plate without using the outer wells. Following incubation, the medium was changed to fresh D10H 1 h prior to treatment. The cells were treated in sextuplicates with polymers at different concentrations, ranging from  $5 \mu\text{g mL}^{-1}$  to  $130 \mu\text{g mL}^{-1}$  for 24 h. The medium was replaced by a 10% (v/v) PrestoBlue<sup>TM</sup> solution in fresh culture medium, prepared according to the manufacturer's instructions. Following an incubation

at 37 °C for 45 min, the fluorescence was measured at  $\lambda_{\text{Ex}} = 570$  /  $\lambda_{\text{Em}} = 610$  nm. Non-treated control cells on the same plate were referred to as 100% viability. Values above 70% were regarded as non-toxic. To assess the toxicity of polyplexes used for transfection, HEK293T cells were seeded at  $0.2 \times 10^6$  cells mL<sup>-1</sup> in D10H in a 24-well plate and incubated at 37 °C in a humidified 5% (v/v) CO<sub>2</sub> atmosphere for 24 h. 1 h prior to treatment the medium was changed to fresh D10H and the cells were treated with the polyplexes with or without layering at N\*/P 30 and a final pDNA concentration of 1.5  $\mu\text{g mL}^{-1}$  for 24 h prior to the PrestoBlue™ assay. The (layered) polyplexes were prepared as described in the main article with isolated pKMyc pDNA and added to the cells diluting the polyplexes 1:10 in the cell culture medium. Data are expressed as mean  $\pm$  SD of at least three independent determinations

For determination of the release of lactate dehydrogenase (LDH) due to membrane disruption, the CytoTox-ONE™ assay (LDH-assay) was performed according to the manufacturer's instructions following incubation of the HEK293T cells with polyplexes with or without layering as described above in a 24-well plate for 24 h. The supernatant was transferred to a new 96-well plate as a triplicate and allowed to cool down to RT for 30 min. Subsequently, the substrate mixture including assay buffer was added and incubated at RT for 10 min. The fluorescence intensity was measured at  $\lambda_{\text{Ex}} = 560$  nm /  $\lambda_{\text{Em}} = 590$  nm following the addition of the stop solution. For the positive control (100% LDH release), cells were incubated with 0.2% Triton X-100 for 30 min prior to analysis. Cells incubated with only pDNA were used as negative control (0% LDH-release). The relative number of viable cells with intact membranes was calculated as follows (Equation S6):

$$\text{Viability} / \% = 100 - \frac{F_{\text{Sample}} - F_0}{F_{\text{Positive control}} - F_0} \cdot 100 \quad (\text{S6})$$

Where  $F_{\text{sample}}$ ,  $F_0$ , and  $F_{\text{Positive control}}$  represent the fluorescence intensity of a given sample, medium without cells, and of the Triton X-100 treated cells, respectively.

### **Erythrocyte Aggregation and Hemolysis.**

The interaction of polymers with cellular membranes was examined by analyzing the release of hemoglobin from erythrocytes as published before.[2, 6] Blood from human donors, collected in tubes with citrate, was obtained from the Department of Transfusion Medicine of the University Hospital, Jena. The blood was centrifuged without pooling at  $4,500 \times g$  for 5 min, and the pellet was washed three times with cold phosphate buffered saline (PBS, pH 7.4). Following a 10-fold dilution with PBS (either pH 7.4 or pH 6.0), 500  $\mu\text{L}$  aliquots of erythrocyte suspension were mixed 1+1 with the (layered) polymer solutions. These were prepared as described in the main article and diluted 1:5 with PBS pH 7.4 or pH 6.0. The erythrocyte-polymer suspensions were incubated at 37 °C for 60 min. After centrifugation at  $2,400 \times g$  for 5 min, the supernatant was transferred to a clear flat bottomed 96-well plate (VWR, Germany) and the hemoglobin release was determined as the hemoglobin absorption at  $\lambda = 544 \text{ nm}$ . Absorption at  $\lambda = 630 \text{ nm}$  was used as reference. Complete hemolysis (100%) was achieved using 1% Triton X-100 as positive control. Pure PBS was used as negative control (0% hemolysis). The hemolytic activity of the polycations was calculated as follows (Equation S7):

$$\text{Hemolysis} / \% = \frac{(A_{\text{Sample}} - A_{\text{Negative control}})}{(A_{\text{Positive control}} - A_{\text{Negative control}})} \cdot 100 \quad (\text{S7})$$

Where  $A_{\text{Sample}}$ ,  $A_{\text{Negative control}}$  and  $A_{\text{Positive control}}$  are the absorption values of a given sample, the PBS treatment and the Triton X-100 treatment, respectively. A value less than 2% hemolysis rate was classified as non-hemolytic, 2 to 5% as slightly hemolytic and values  $> 5\%$  as hemolytic.

To determine the cell aggregation, erythrocytes were isolated as described above. Subsequently, 100  $\mu\text{L}$  of the erythrocyte-polymer suspension were transferred to a clear flat bottomed 96-well plate (VWR, Germany). The cells were incubated at 37  $^{\circ}\text{C}$  for 2 h, and the absorbance was measured at  $\lambda = 645$  nm. Cells treated with PBS served as negative control and cells treated with 50  $\mu\text{g mL}^{-1}$  10 kDa BPEI were used as positive control. Aggregation potential of the polymers was calculated as follows (Equation S8):

$$\text{Aggregation} = \frac{A_{\text{Negative control}}}{A_{\text{Sample}}} \quad (\text{S8})$$

Where  $A_{\text{Sample}}$  and  $A_{\text{Negative control}}$  are the absorption values of a given sample and the PBS treatment, respectively. Experiments were run in technical triplicates and were performed with blood from three different blood donors.

#### **Polyplex Uptake via Flow Cytometry.**

To study the uptake of polymers over time in HEK293T cells, the cells were seeded at  $0.2 \times 10^6$  cells  $\text{mL}^{-1}$  in D10H in 24-well plates, followed by incubation at 37  $^{\circ}\text{C}$  in a humidified 5% (v/v)  $\text{CO}_2$  atmosphere for 24 h and medium change to fresh D10H 1 h prior to treatment. The cells were treated with polyplexes with or without layering at N\*/P 30 and a final pDNA concentration of 1.5  $\mu\text{g mL}^{-1}$  for indicated time periods. The polyplexes were prepared as described above after labelling 1  $\mu\text{g}$  pKMyc pDNA with 0.027 nmol YOYO-1 iodide. Subsequently, the polymer-pDNA-solutions were added to the cells, diluting the polyplexes 1:10 in cell culture medium. Following incubation, the HEK293T cells were harvested by collecting the supernatant in a separate 24-well plate, trypsinization and resuspension in the respective supernatant again. Trypan blue solution (0.4%) was added to half of the cell suspension to a final concentration of 0.04% to quench fluorescence of polyplexes outside the cells. The remaining cell suspension was diluted

1:2 with D20 and further incubated as described in the transfection section. Cells were analyzed *via* flow cytometry as described in the instrumentation section. Viable cells showing YOYO-1 signal higher than the control cells, which were incubated with YOYO-1-pDNA only, were gated as % of cells that have taken up pDNA and the rMFI of all viable cells was calculated in relation to the control cells (Figure S19). MFI values of control cells can be found in Table S8. The experiments were performed at least three times and data are expressed as mean  $\pm$  SD.

### **Polyplex Uptake *via* CLSM.**

To study the uptake of polymers *via* CLSM, HEK293T cells were seeded at  $0.2 \times 10^6$  cells mL<sup>-1</sup> in D10H in 8-well slides (ibidi, Germany), followed by incubation at 37 °C in a humidified 5% (v/v) CO<sub>2</sub> atmosphere for 24 h and medium change to FC-buffer (Hanks' Balanced Salt Solution, supplemented with 2% FCS and 20 mM HEPES) containing 5  $\mu\text{g mL}^{-1}$  CellMask™ Deep Red Plasma membrane (CMDR-PM) stain. Following incubation for 8 min, the medium was again changed to fresh D10H and incubated for 15 min prior to treatment. The cells were treated with (layered) polyplexes with or without layering at N\*/P 30 and a final pDNA concentration of 1.5  $\mu\text{g mL}^{-1}$ . The polyplexes were prepared as described above after labelling 1  $\mu\text{g}$  pKMyC pDNA with 0.027 nmol YOYO-1 iodide. Subsequently, the polymer-pDNA-solutions were added to the cells, diluting the polyplexes 1:10 in cell culture medium. Following incubation for 1 h, the cells were incubated with 8  $\mu\text{M}$  Hoechst 33342 and 5  $\mu\text{g mL}^{-1}$  CMDR-PM for 10 min. Subsequently, the medium was changed to fresh warm D20. Just before imaging of each well, trypan blue solution (0.4%) was added to a final concentration of 0.04% to quench YOYO-1 fluorescence outside the cells.

To image the intracellular distribution pattern of the polyplexes in living cells, live cell imaging was performed using a LSM880, Elyra PS.1 system (Zeiss, Germany) applying the argon laser for

excitation at 488 nm (2%), 405 nm (0.2%) and 633 nm (2%), emission filters for 410-468 nm (Hoechst), 508-553 nm (YOYO-1) and 666-755 nm (CMDR-PM) with a gain of 800, 550 and 650, respectively, and a pinhole of 68  $\mu\text{m}$ . To avoid cross talk between the different channels, Hoechst 33342, YOYO-1 and CMDR-PM were imaged simultaneously in different tracks. For fast imaging, the tracks were switched in every line of the image. For magnification, a  $63 \times 1.4$  NA plan apochromat oil objective was applied. Images were acquired using the ZEN software, version 2.3 SP1 (Zeiss, Germany). The experiments were performed three times acquiring at least 5 images per sample each time. These images consisted of three images as a z-stack with 1-2  $\mu\text{m}$  between the slices. All images were processed in batch mode using the image analysis wizard of the ZEN software, version 3.1 (Zeiss, Germany) to quantify the number of polyplexes per cell nucleus and the amount of free polyplexes (YOYO-1 signal not colocalized with CMDR-PM). For the depiction of polyplex uptake, representative images of all samples were processed using ImageJ, version 1.52[4] as follows: First, the three slices of the z-stack images were combined using the maximum intensity projection method. Subsequently, the background of the Hoechst 33342 channel was corrected using the rolling ball background subtraction tool applying a sliding paraboloid with a radius of 215 pixels without previous image smoothing. The background of the YOYO-1 channel was corrected by subtraction of a mean fluorescence measured previously in spots without cells (value: 2500). The contrast of all channels was enhanced automatically with a normalization of 0.2% (YOYO-1) or 0.3% (Hoechst, CMDR-PM) saturation. For the overlay images, either all three or the YOYO-1 and the CMDR-PM channels were merged.

Regarding the quantification of polyplexes out/inside organelles, the following settings were used to extract three different feature classes, nuclei, polyplexes and organelles (with the subclass: colocalized polyplexes). Regarding the nuclei, the Hoechst channel images were smoothed (size =

3) followed by segmentation using global thresholding (10,000-65,535) with a tolerance of 3% and watershed separation (count = 25). Objects larger than 20,000,000  $\mu\text{m}^2$  were counted as nuclei. For the polyplexes, the YOYO-1 channel images were smoothed (size = 3) followed by background subtraction (radius of rolling ball = 30  $\mu\text{m}$ ), segmentation using global thresholding (5,500-65,535) with a tolerance of 3% and watershed separation (count = 3). Objects larger than 250  $\mu\text{m}^2$  were counted as polyplexes. Regarding the organelles, the CMDR-PM channel images were smoothed (size = 3) followed by segmentation using global thresholding (4,000-65,535) with a tolerance of 3% and dilation (count = 3). The number of polyplexes within organelles was determined as a subclass within objects designated as organelles previously using the same settings as for the polyplexes class. All steps were repeated with the same settings for all images of all samples in batch mode. The relative amount of free polyplexes was calculated using Equation S9:

$$\text{Free polyplexes} / \% = \frac{(N_{\text{Polyplexes}} - N_{\text{Colocalized polyplexes}})}{(N_{\text{Polyplexes}})} \cdot 100 \quad (\text{S9})$$

Where  $N_{\text{Polyplexes}}$ , and  $N_{\text{Colocalized polyplexes}}$  are the total counts of the respective feature classes of one repetition.

The number of polyplexes per cell was calculated as follows (Equation S10):

$$\text{Polyplexes per cell} = \frac{(N_{\text{Polyplexes}})}{(N_{\text{Nuclei}})} \quad (\text{S10})$$

Where  $N_{\text{Polyplexes}}$ , and  $N_{\text{Nuclei}}$  are the total counts of the respective feature classes of one repetition. In case of the nuclei, the values were divided by three due to the acquisition of z-stack images with three slices.

### **Image Acquisition and Processing for the Calcein Release Assay *via* CLSM.**

To image the intracellular distribution pattern of calcein in living cells, live cell imaging was performed using a LSM880, Elyra PS.1 system (Zeiss, Germany) applying the argon laser for excitation at 488 nm (1%) and 405 nm (0.5%), emission filters for 410-469 nm (Hoechst) and 490-544 nm (Calcein) with a gain of 800 and a pinhole of 27  $\mu\text{m}$ , respectively. To avoid cross talk between the different channels, Hoechst 33342 and calcein were imaged simultaneously in different tracks. For fast imaging, the tracks were switched in every line of the image. For magnification, a  $40 \times 1.4$  NA plan apochromat oil objective was applied. Images were acquired using the ZEN software, version 2.3 SP1 (Zeiss, Germany). The experiments were performed three times acquiring at least three images per sample each time. All images were processed in batch mode using ImageJ, version 1.52[4] with different macros for depiction and quantification of calcein release, respectively. For the depiction of calcein release, representative images of all samples were processed as follows: First, the background of the Hoechst 33342 channel was corrected using the rolling ball background subtraction tool applying a sliding paraboloid with a radius of 297 pixels without previous image smoothing. The contrast of both channels was enhanced automatically with a normalization of 0.01% saturation. For the overlay image, both channels were merged.

Regarding the quantification of calcein release, the images of the respective channels first had to be optimized regarding specific features (Hoechst – nuclei, calcein – extensive intracellular fluorescence). Therefore, the single channel images were made binary following special processing with the rolling ball background subtraction tool, automatic contrast enhancement and the setting of an automatic threshold. In case of the calcein channel, the “minimum” convolution filter was applied additionally before the contrast enhancement. The binary images were modified



to eliminate small holes inside the feature areas. Subsequently, the processed images of both channels were combined using the “AND” combination mode, leaving only the nuclei with coincident calcein staining, representing cells with calcein release. These were then counted *via* “Analyze Particles” setting the threshold for the size to 30 square pixels/unit. The same step was repeated with the Hoechst channel images to determine the number of nuclei per image. All steps were repeated with the same settings for all images of all samples in batch mode. A minimum of 170 cells were analyzed per sample and repetition. Finally, the proportion of cells showing calcein release was calculated as described in the main article.

## FURTHER RESULTS

### Characterization of Polymers.

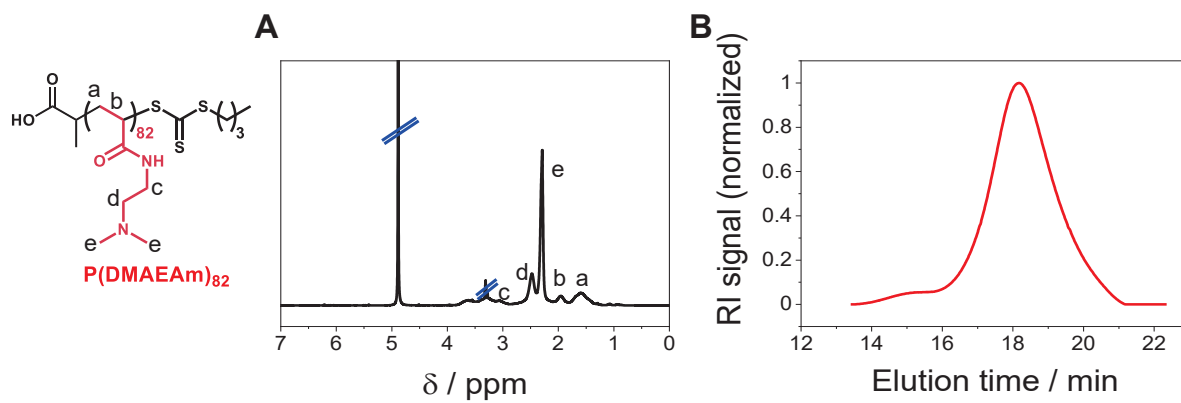


**Figure S1.** Characterization of PDMAEAm<sub>82</sub>.

(A) <sup>1</sup>H NMR spectrum in CD<sub>3</sub>OD; (B) (DMAc + 0.21wt.% LiCl) SEC trace – PMMA calibration;

$M_{n,SEC} = 14300 \text{ g mol}^{-1}$ ,  $D = 1.67$ .

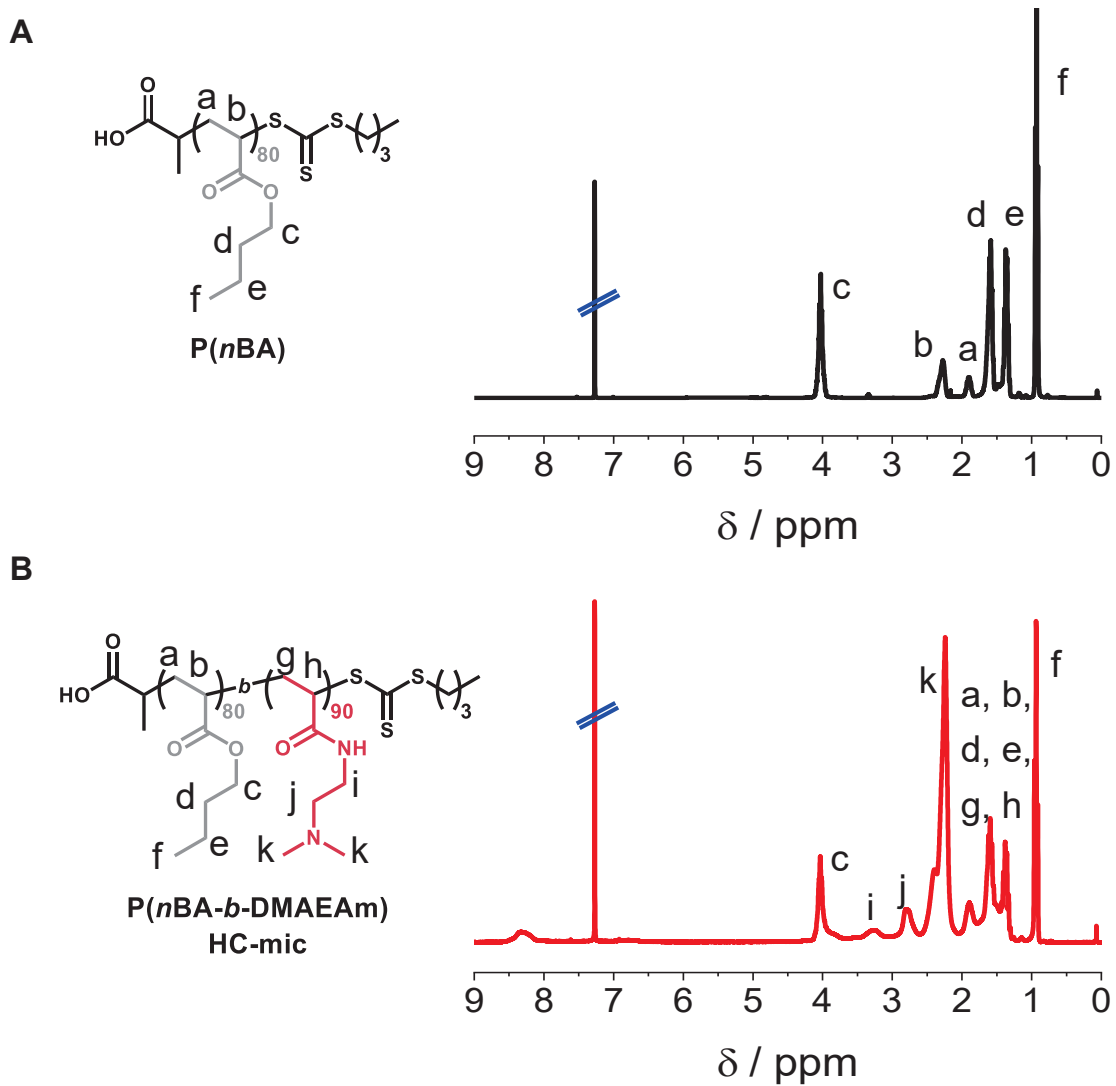


**Figure S2.** NMR results of the HC-mic in  $\text{CDCl}_3$ .

**(A)**  $\text{P}(n\text{BA}_{80})$  and **(B)**  $\text{P}(n\text{BA}_{80}\text{-}b\text{-DMAEAm}_{90})$ .

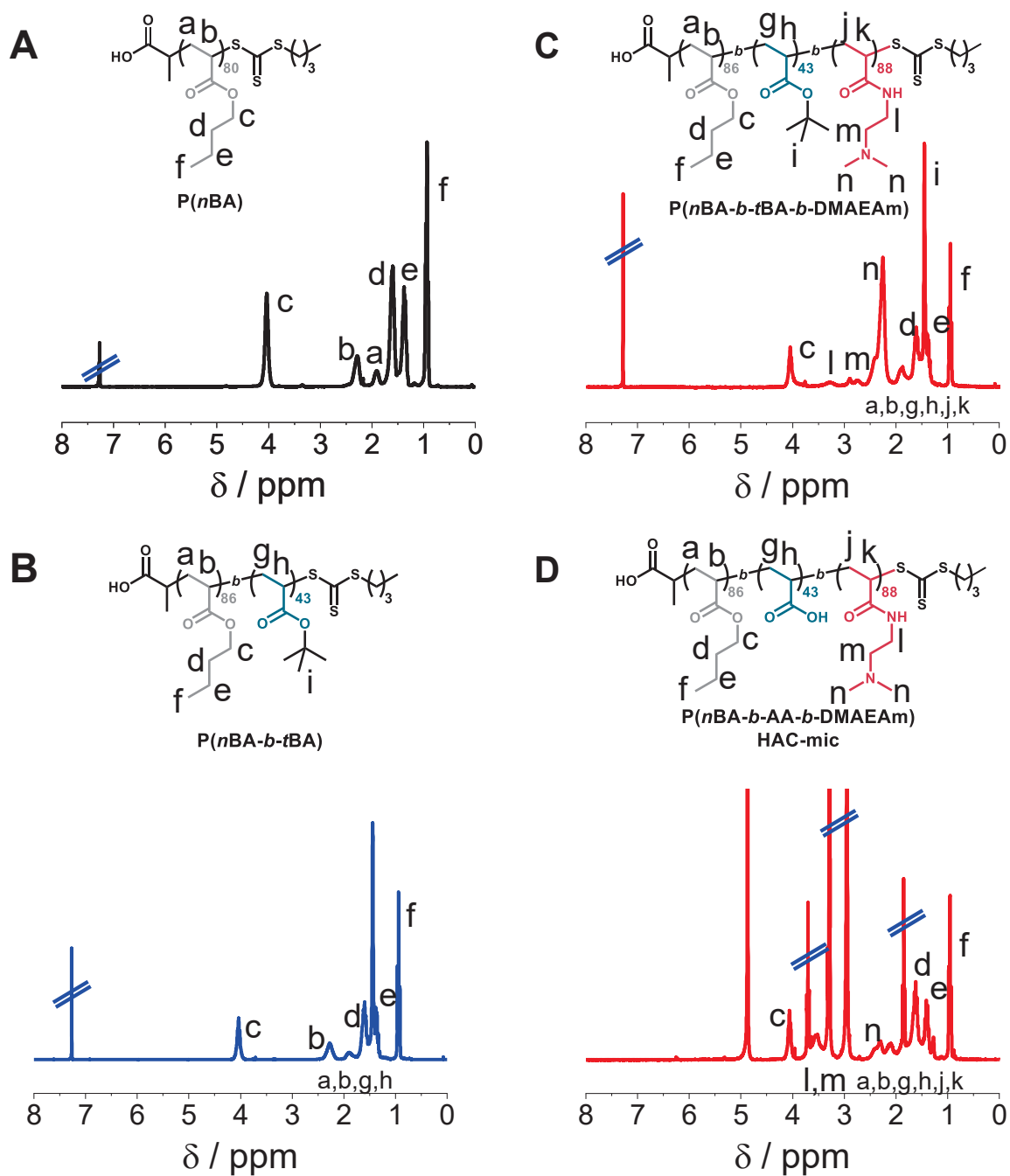


**Figure S3.** NMR results of the HAC-mic.

(A)  $P(nBA_{86})$ , (B)  $P(nBA_{86}-b-tBA_{43})$ , (C)  $P(nBA_{86}-b-tBA_{43}-b-DMAEAm_{88})$  in  $CDCl_3$  and (D)  $P(nBA_{86}-b-AA_{43}-b-DMAEAm_{88})$  in  $CD_3OD$ .

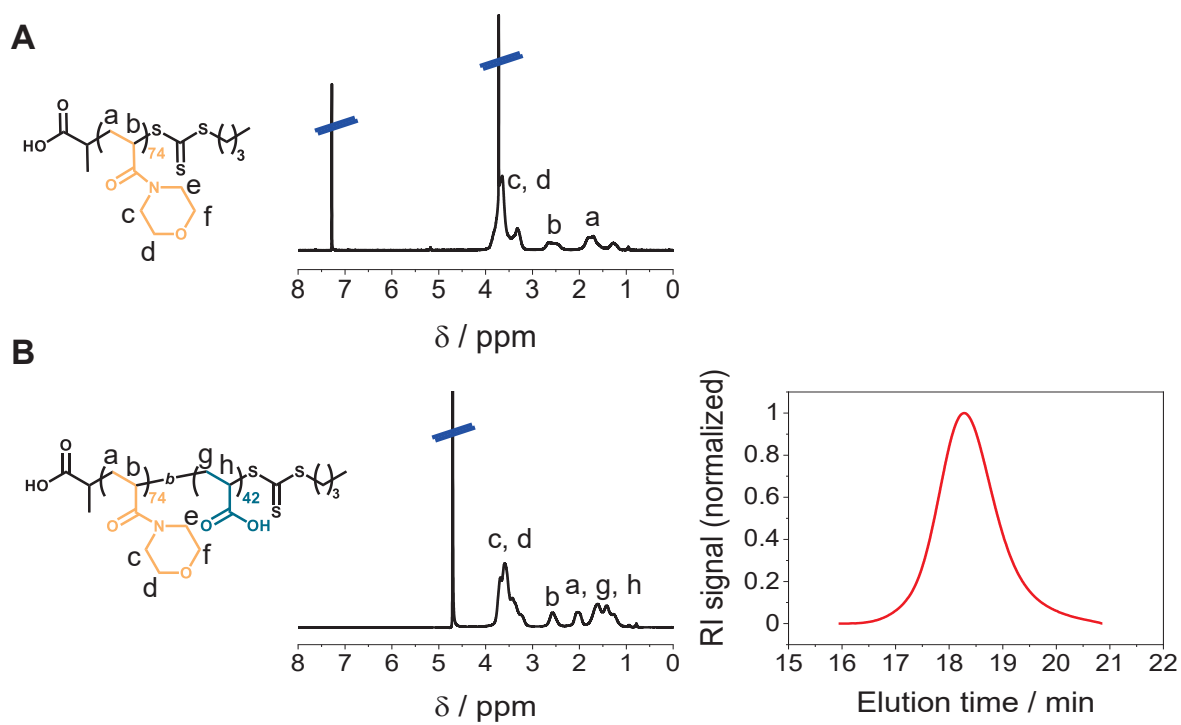


**Figure S4.** Characterization of the layer diblock copolymer.

(A)  $^1\text{H}$  NMR of P(NAM<sub>74</sub>) in  $\text{CDCl}_3$ , (B)  $^1\text{H}$  NMR in  $\text{D}_2\text{O}$  and aqueous (0.08 M  $\text{Na}_2\text{HPO}_4$  + 0.05%  $\text{NaN}_3$ ) SEC trace – PEG calibration;  $M_{n,\text{SEC}} = 17700 \text{ g mol}^{-1}$ ,  $D = 1.26$  of P(NAM<sub>74</sub>-*b*-AA<sub>42</sub>).

## Original Cryo-TEM images

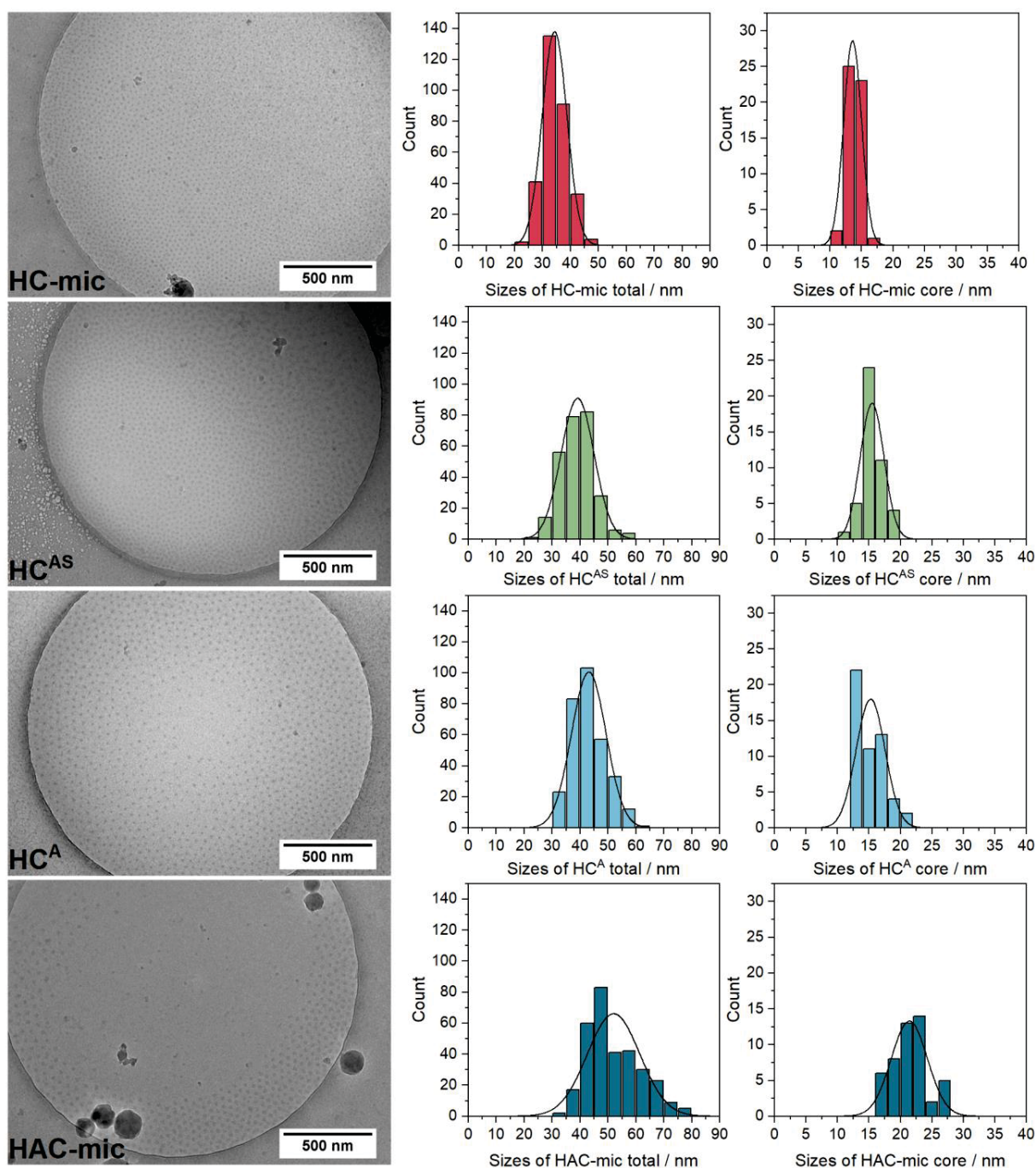


**Figure S5.** Original cryo-TEM images of micelles.

The samples of HC<sup>A</sup> and HC<sup>AS</sup> were prepared in acetate-HEPES buffer of pH 5.0 at a COOH/NH ratio of 0.5 with a final concentration of 2.7 mg mL<sup>-1</sup> for the HC-mic. For the naked HC and HAC assemblies, the stock solutions of the micelles in 50 mM acetate buffer, pH 5 were used with

concentrations of 1.9 and 1.3 mg mL<sup>-1</sup>, respectively. The histograms depict the size distributions of the total micelles or the micelle core within all analyzed images using ImageJ as described above. On an average, 50 micelles (*i.e.*, 300 lines, 50 circles) were measured per sample in different images.

**Table S4.** Overview of the different assembly batches of HC- and HAC-mic.

Polymer	Assembly	Dissolved in	Dialyzed against	Final concentration
				μg mL <sup>-1</sup>
HC	1 <sup>[a]</sup>	THF	Acetate, pH 5.9	1860
	2	THF/MeOH	Acetate, pH 5.9	1620
	3	THF/MeOH	Acetate, pH 5.0	3580
HAC	1	THF/MeOH	Acetate, pH 5.0	1740
	2	THF/MeOH	Acetate, pH 5.0	943
	3	THF/MeOH	Acetate, pH 5.0	1130
	3.2	THF/MeOH	Acetate, pH 5.0	1330

[a] Block copolymer was not treated with 0.5 eq. HCl.

**Table S5.** Polymer concentrations in different assays.

	DLS, pH	ELS, pH	EBA/HRA, DLS pDNA	Cell-based assays, ELS pDNA
	μg mL <sup>-1</sup>	μg mL <sup>-1</sup>	μg mL <sup>-1</sup>	μg mL <sup>-1</sup>
	-	-	N*/P 30	N*/P 30
pDNA	-	-	15	1.5
LPEI	-	-	59	5.9
PDMAEAm	-	-	229	22.9
HC-mic	845.4	281.8	357.1	35.7
HC <sup>S</sup>	+ 377.7	+ 125.9	+ 159.5	+ 16.0
HC <sup>AS</sup>	+ 533.4	+ 177.8	+ 225.3	+ 22.5
HC <sup>A</sup>	+ 116.7	+ 38.9	+ 49.3	+ 4.93
HAC-mic	997.5	332.5	421.4	42.1

## DLS Measurements.

**Table S6.** Summary of micelle characterization at different pH-values, high concentrations.

Code	Concentration	pH-Value	z-Average [a]	PDI [a]	Main peak [a]	Area of main peak [a]
	$\mu\text{g mL}^{-1}$		nm		nm	%
ABC-mic	998	5.0	$66.4 \pm 2.3$	$0.16 \pm 0.07$	$66.4 \pm 2.2$	$98 \pm 5$
	998	7.4	$\gg 1000$	$0.42 \pm 0.26$	$\gg 1000$	$100 \pm 0$
AC-mic	845	5.0	$58.4 \pm 0.9$	$0.17 \pm 0.01$	$65.1 \pm 5.4$	$98 \pm 3$
	845	7.4	$53.0 \pm 1.0$	$0.20 \pm 0.02$	$51.9 \pm 3.3$	$89 \pm 6$
N-AC	+378	5.0	$58.1 \pm 1.1$	$0.15 \pm 0.01$	$64.4 \pm 5.2$	$100 \pm 0$
	+378	7.4	$51.5 \pm 0.4$	$0.19 \pm 0.02$	$52.9 \pm 1.7$	$96 \pm 4$
NB-AC	+534	5.0	$54.7 \pm 1.2$	$0.13 \pm 0.01$	$59.0 \pm 3.3$	$99 \pm 2$
	+534	7.4	$46.2 \pm 1.2$	$0.20 \pm 0.05$	$48.5 \pm 2.3$	$94 \pm 4$
B-AC	+117	5.0	$53.4 \pm 6.5$	$0.20 \pm 0.05$	$52.5 \pm 6.6$	$93 \pm 8$
	+117	7.4	$\gg 1000$	$0.42 \pm 0.26$	$\gg 1000$	$100 \pm 0$

[a] Determined *via* DLS (concentrations see Table S5).

[b] Determined *via* ELS.

**Table S7.** Summary of micelle characterization at different pH values, low concentrations.

Code	Concentration	pH-Value	z-Average [a]	PDI [a]	Main peak [a]	Area of main peak [a]	Zeta potential [b]	
	$\mu\text{g mL}^{-1}$		nm		nm	%	mV	
HAC-mic	333	5.0	$70.3 \pm 0.5$	$0.10 \pm 0.02$	$77.8 \pm 1.4$	$100 \pm 0$	$26 \pm 5$	
HC-mic	219	5.0	$63.3 \pm 0.7$	$0.20 \pm 0.01$	$68.5 \pm 1.6$	$97 \pm 1$	$25 \pm 1$	
	HC <sup>S</sup>	+126	5.0	$63.6 \pm 0.9$	$0.20 \pm 0.01$	$72.2 \pm 3.7$	$98 \pm 1$	$25 \pm 2$
	HC <sup>AS</sup>	+178	5.0	$57.8 \pm 0.3$	$0.15 \pm 0.03$	$65.2 \pm 1.5$	$99 \pm 1$	$22 \pm 2$
	HC <sup>A</sup>	+39	5.0	$57.2 \pm 2.4$	$0.21 \pm 0.03$	$64.4 \pm 2.6$	$97 \pm 2$	$25 \pm 2$
HAC-mic	333	7.4	$\gg 1000$	$0.79 \pm 0.28$	$323 \pm 505$	$33 \pm 52$	$1 \pm 1$	
HC-mic	219	7.4	$55.8 \pm 1.7$	$0.22 \pm 0.03$	$61.4 \pm 3.5$	$95 \pm 2$	$16 \pm 2$	
	HC <sup>S</sup>	+126	7.4	$56.3 \pm 3.5$	$0.22 \pm 0.06$	$63.1 \pm 3.7$	$96 \pm 3$	$17 \pm 2$
	HC <sup>AS</sup>	+178	7.4	$47.8 \pm 1.4$	$0.26 \pm 0.02$	$50.5 \pm 1.2$	$92 \pm 3$	$-2 \pm 0$
	HC <sup>A</sup>	+39	7.4	$\gg 1000$	$0.56 \pm 0.34$	$63.1 \pm 96.8$	$27 \pm 41$	$9 \pm 4$

[a] Determined *via* DLS (concentrations see Table S5).

[b] Determined *via* ELS.



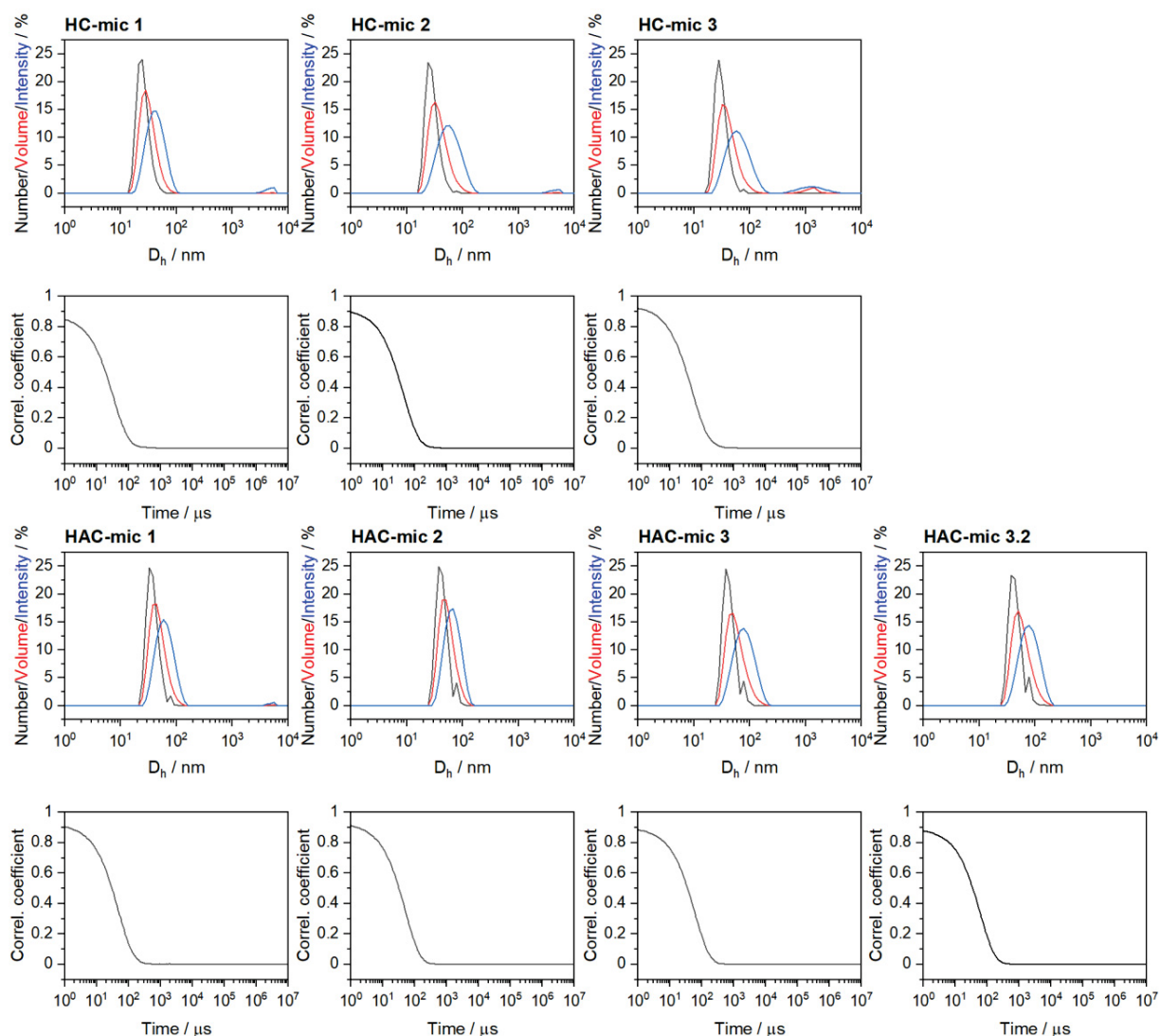


**Figure S6.** DLS measurements of micelle stock solutions directly after formulation.

Depiction of exemplary intensity, number, and volume weighted plots and exponential decay correlation coefficients of single measurements. Numbers indicate different formulation batches. Concentrations of the solutions were as indicated in Table S4.

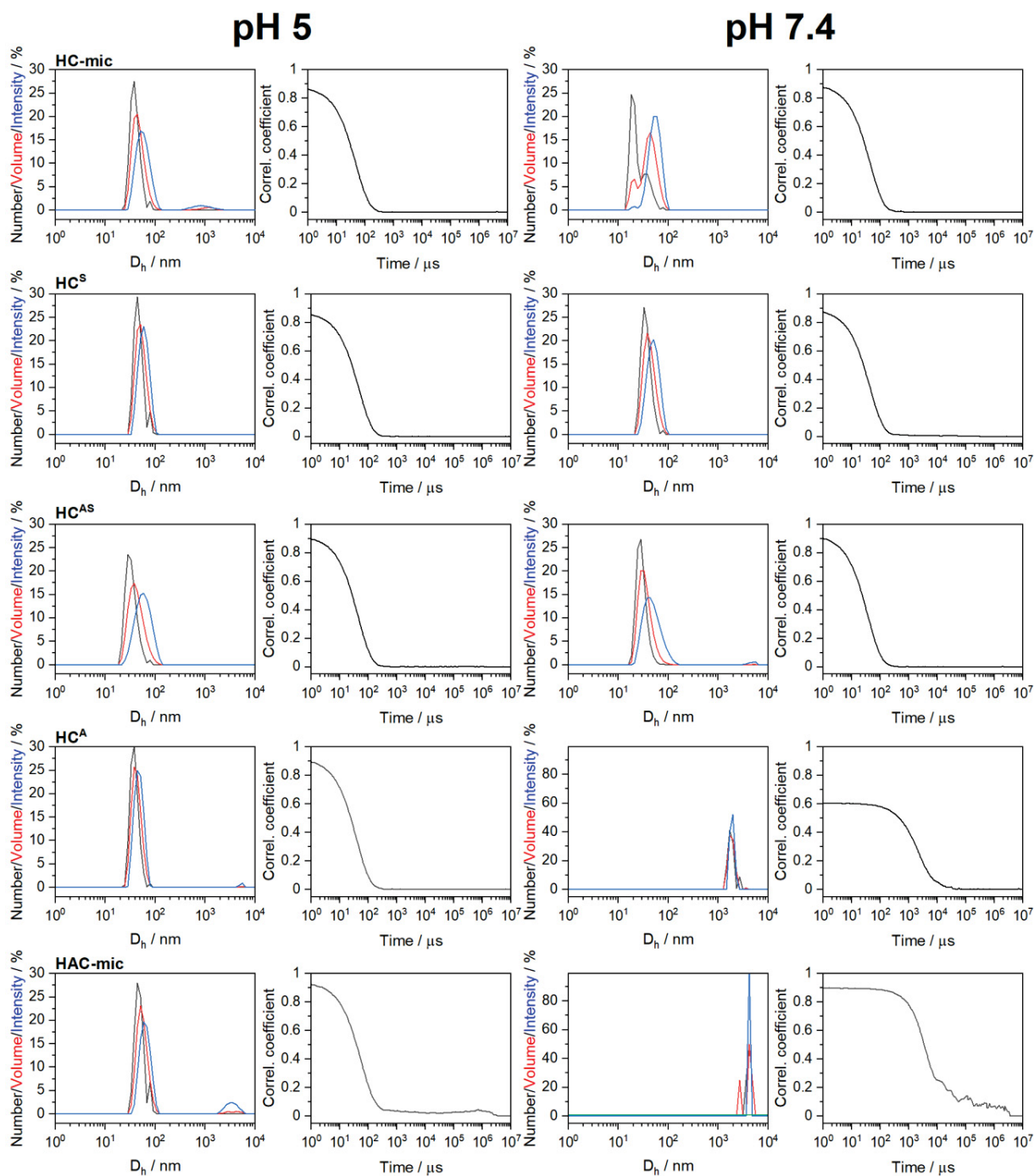


**Figure S7.** DLS measurements of (layered) micelles at different pH values.

Depiction of exemplary intensity, number, and volume weighted plots and exponential decay correlation coefficients of single measurements. Concentrations of the solutions were as indicated in Table S6.

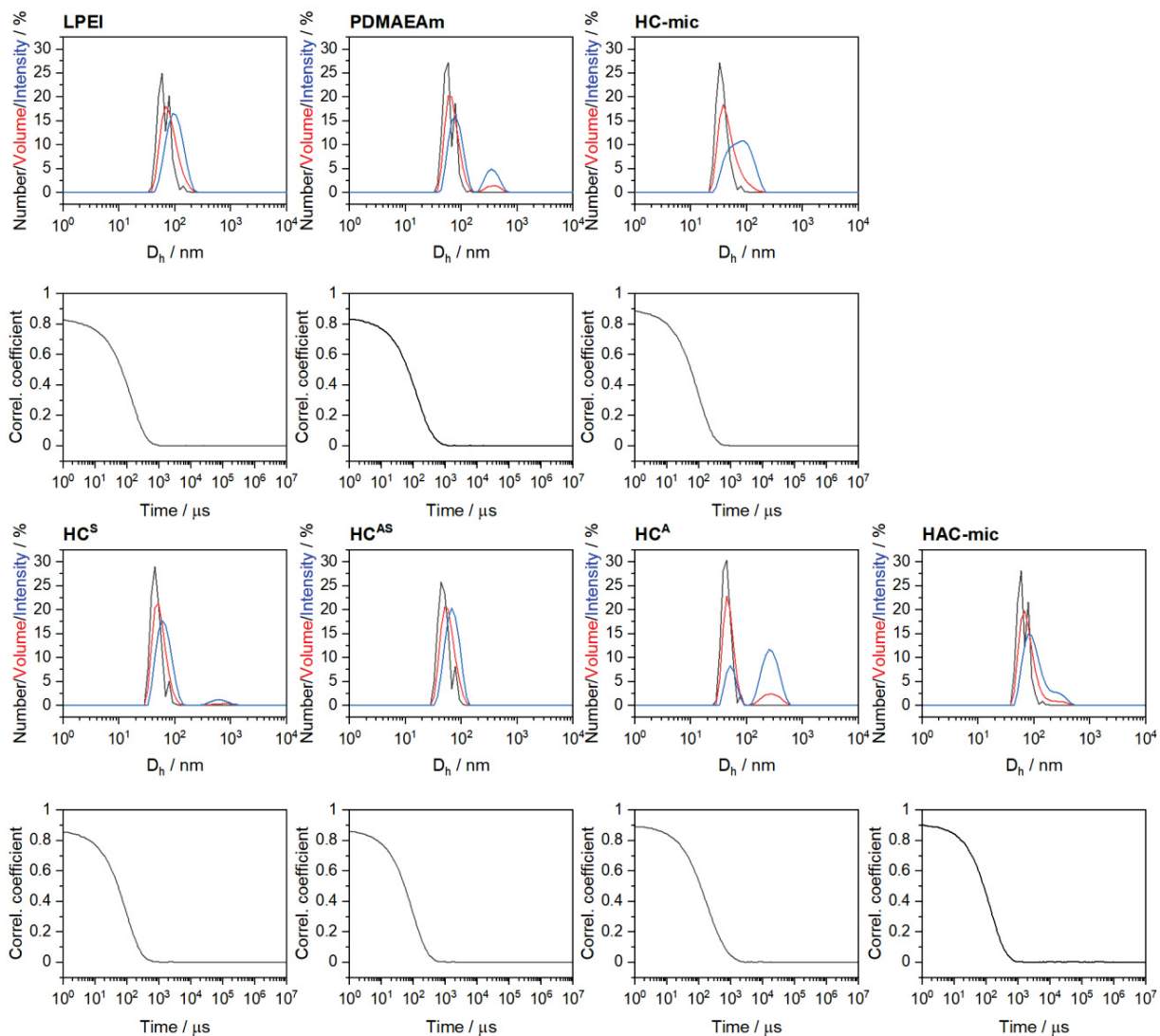


**Figure S8.** DLS measurements of (layered) polyplexes in HBG buffer.

Depiction of exemplary intensity, number, and volume weighted plots and exponential decay correlation coefficients of single measurements. Concentrations of the solutions were as indicated in Table S5.

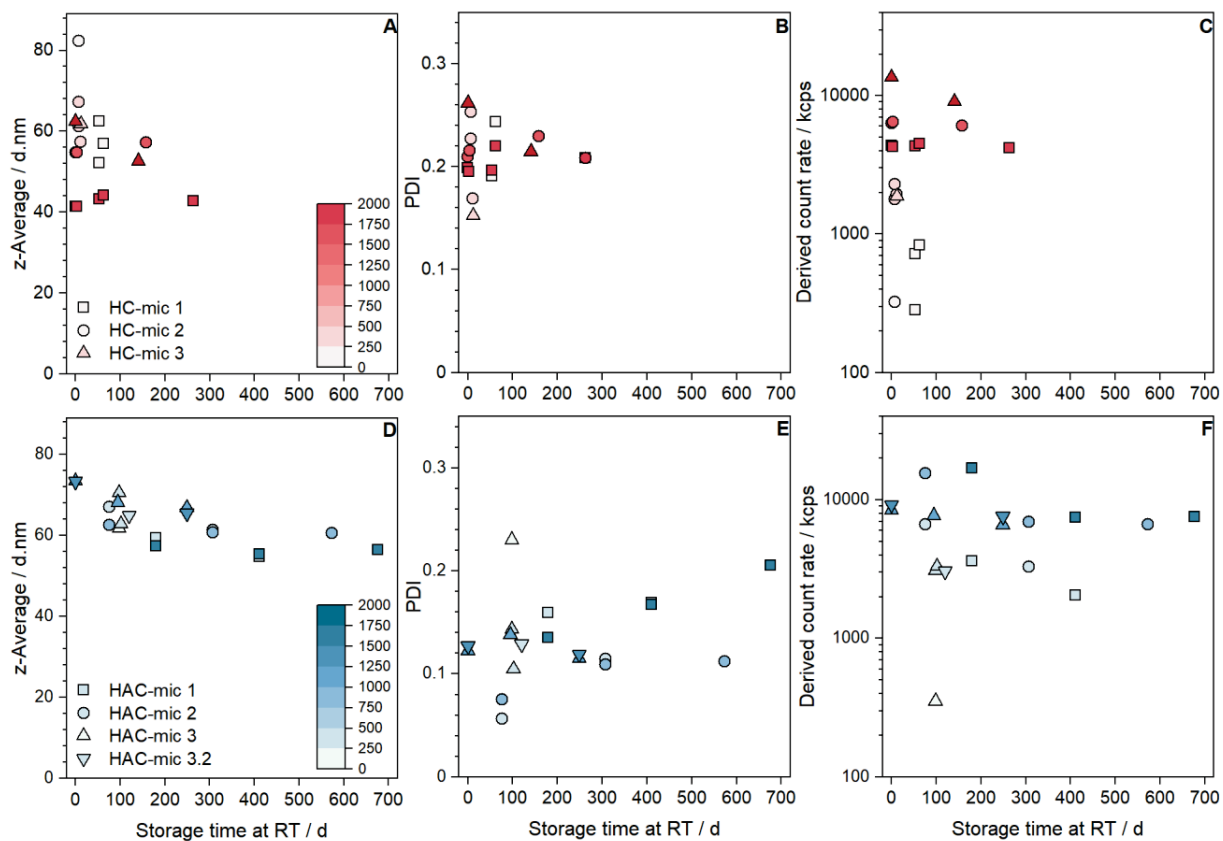


**Figure S9.** DLS measurements of different batches of (layered) micelles.

HC- (A-C) or HAC-micelles (D-F) were measured at different concentrations following different storage times. Different symbols represent different assembly batches (Table S4) of the respective polymer. Color code indicates polymer concentration in  $\mu\text{g mL}^{-1}$ .

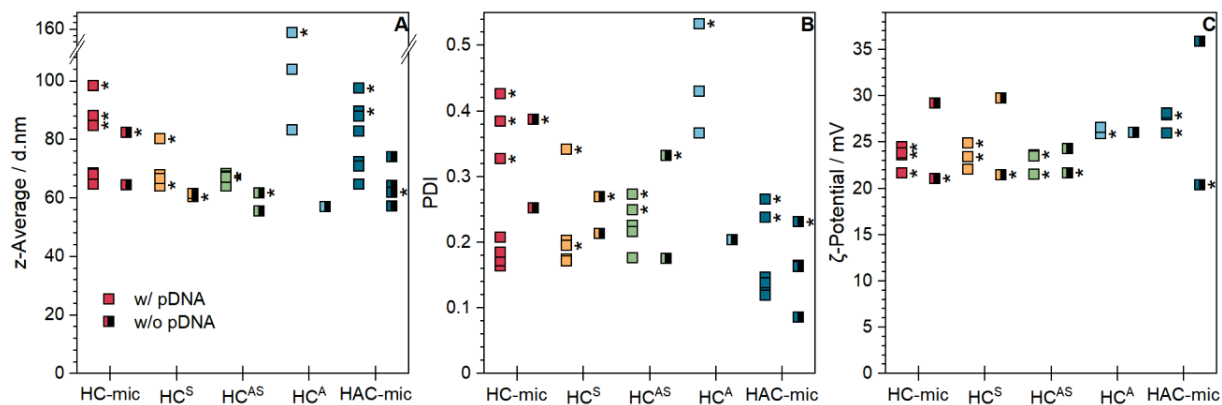


**Figure S10.** DLS/ELS measurements of different batches of (layered) polyplexes.

DLS/ELS measurements of (layered) polyplexes vs. (layered) micelles. Polyplexes were formed with  $15 \mu\text{g mL}^{-1}$  pDNA at N\*/P 30 (Table S5). Dots of the same color represent different assembly batches of the respective polymer (Table S4). Stars next to dots indicate dilution of polyplexes in HBG or water to concentrations below  $100 \mu\text{g mL}^{-1}$ .

## pDNA Binding Assays.

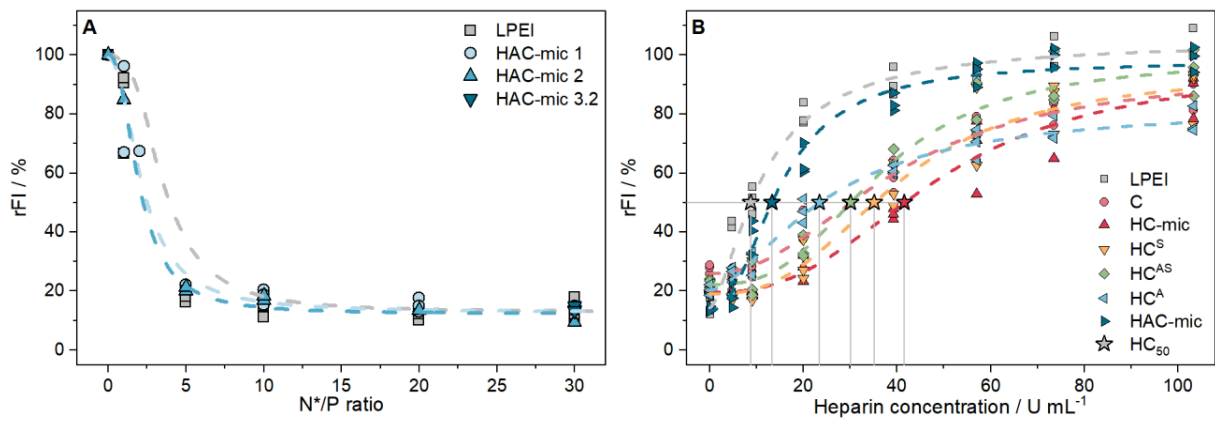


**Figure S11.** Additional EBA&HRA results.

(A) EBA of polyplexes of pDNA and different batches of HAC-mic (Table S4) at different N\*/P ratios in HBG buffer ( $n \geq 2$ ). (B) HRA of (layered) polyplexes at N\*/P 30 ( $n = 3$ ). Stars indicate heparin concentration needed to release 50% of pDNA (HC<sub>50</sub>) as presented in the main article.

## Cytotoxicity Assays.

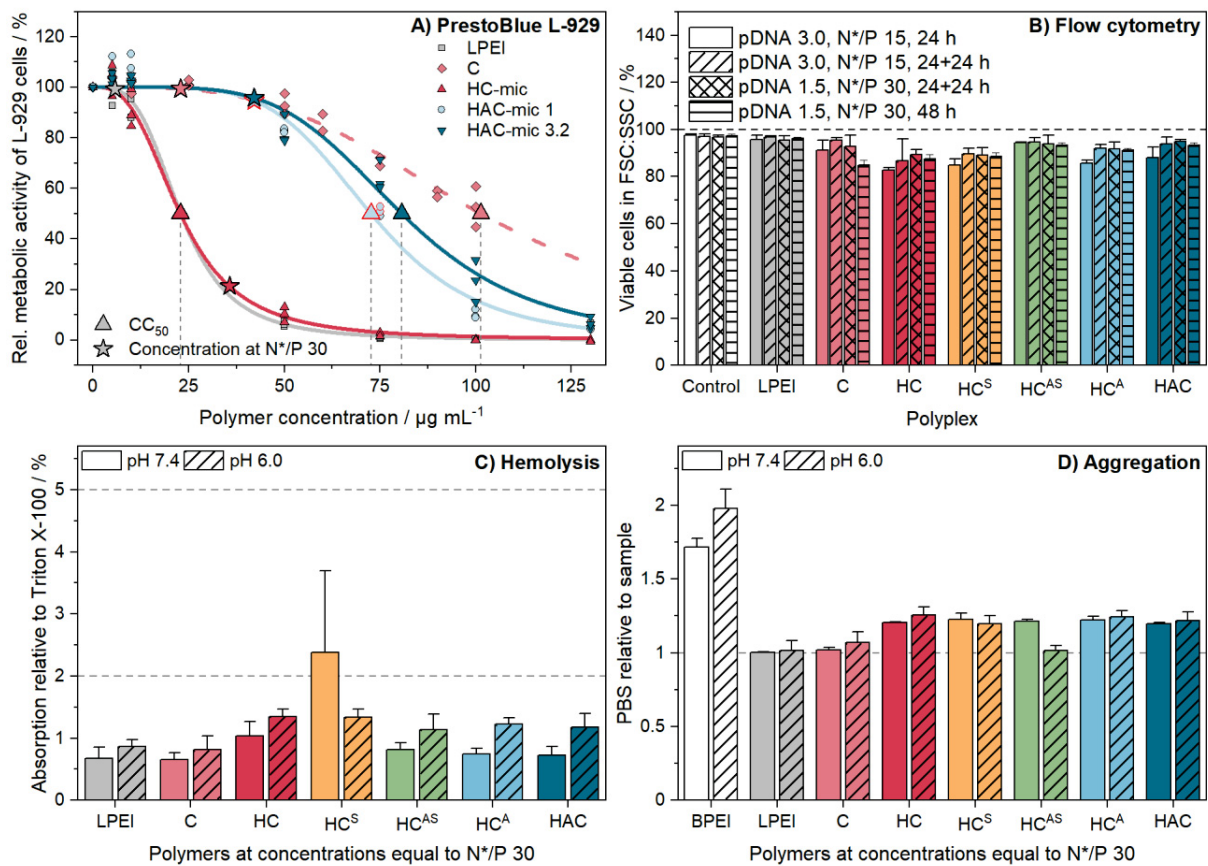


**Figure S12.** Additional cytotoxicity assays.

(A) Metabolic activity using the PrestoBlue™ assay following incubation of cells with polymers at indicated concentrations for 24 h. Dots represent values of single repetitions and lines represent logistic functions fitted to the single measurements ( $n = 3$ ). Stars indicate concentration and viability of N\*/P 30, and triangles indicate the critical concentration corresponding to 50% viable cells ( $\text{CC}_{50}$ ). The curve of C was also shown in the SI of Richter *et al.* 2020.[2] (B) Hemolysis as the amount of released hemoglobin calculated relative to 1% Triton X-100 as positive control (100% hemolysis). Human erythrocytes were washed and incubated with polymers at indicated concentrations in PBS of different pH values without FCS. Values represent mean  $\pm$  SD ( $n = 3$ ). and are classified as slightly hemolytic between 2% and 5%, and as non- or hemolytic if lower or higher than 2% or 5%, respectively. (C) Aggregation of indicated polymers was measured as light absorption by erythrocytes. Erythrocytes were washed and incubated as described in (B). 10 kDa

BPEI was used as positive control. Values are calculated as the negative control (PBS value) relative to the sample value and represent mean  $\pm$  SD (n = 3).

#### Microscopic Images of Treated HEK293T Cells.

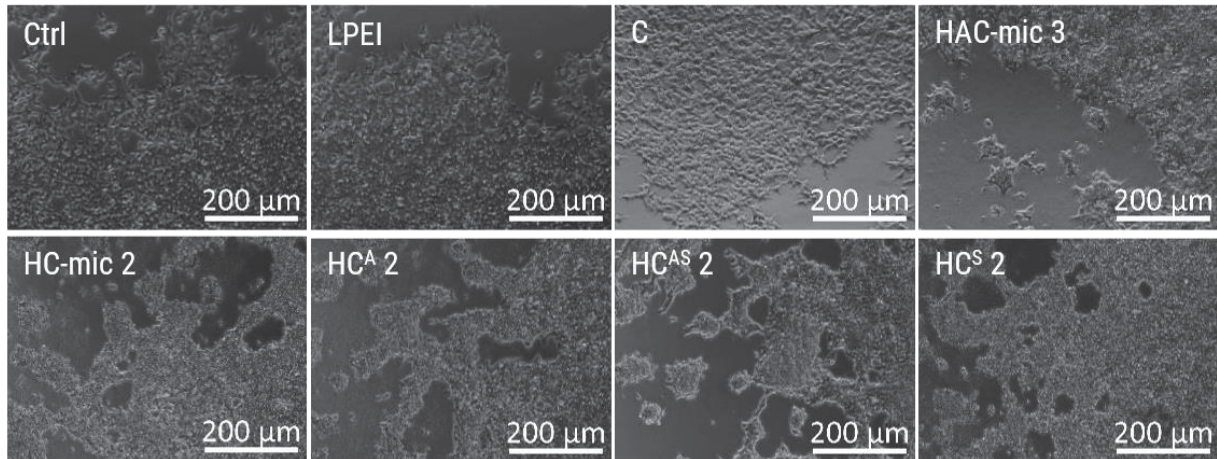


**Figure S13.** Influence of (layered) polyplexes on cell morphology.

Cells were incubated with (layered) polyplexes of polymers and pDNA at N\*/P 30 for 24 h. Images were acquired *via* light microscopy.



## Transfection Efficiency.

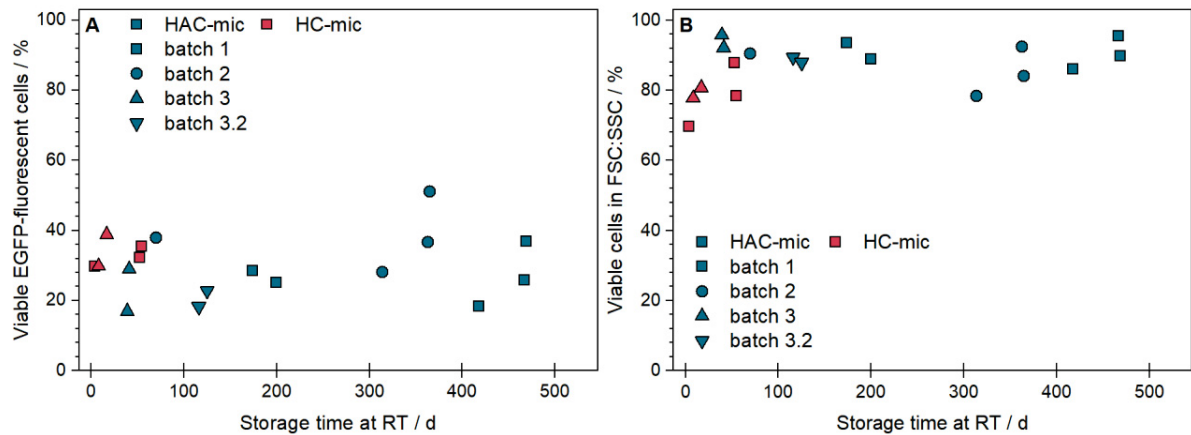


**Figure S14.** Influence of storage time on transfection efficiency.

Storage time dependent transfection efficiency in HEK293T cells following incubation with polyplexes of  $1.5 \mu\text{g mL}^{-1}$  pDNA and micelles at N\*/P 30 for 24 h. The micelle assemblies were stored at RT for indicated time periods. Values represent (A) viable EGFP fluorescent cells or (B) viable cells in FSC/SSC scatter plot of single measurements.

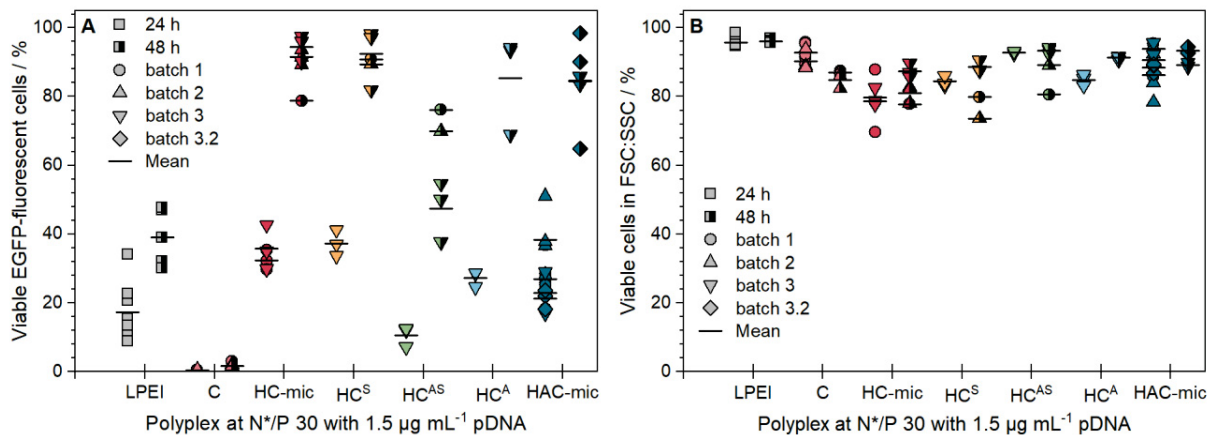


**Figure S15.** Influence of different assembly batches on transfection efficiency.

Batch dependent transfection efficiency in HEK293T cells following incubation with (layered) polyplexes of  $1.5 \mu\text{g mL}^{-1}$  pDNA and polymers at N\*/P 30 for 24 or 48 h. Values represent (A) viable EGFP fluorescent cells or (B) viable cells in FSC/SSC scatter plot of single measurements. Lines indicate the mean of one batch.

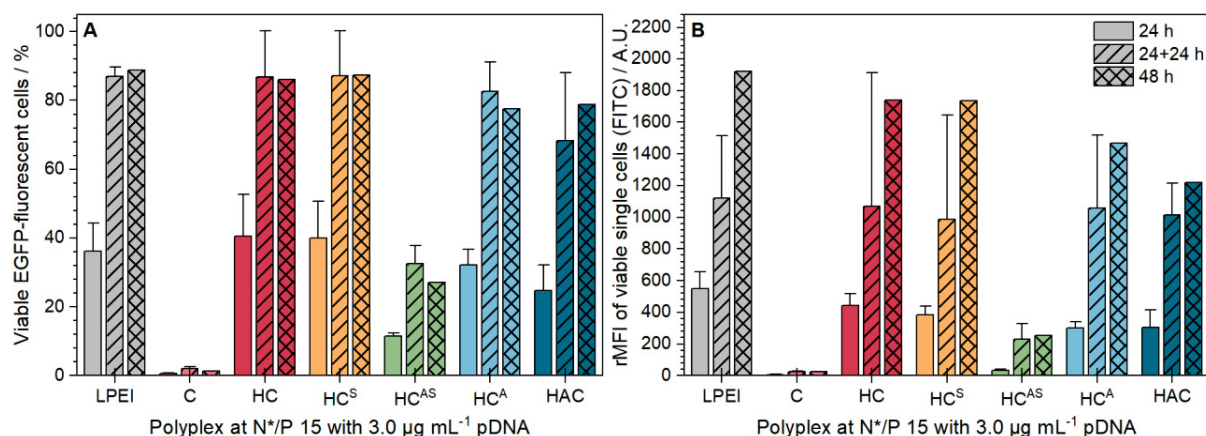


**Figure S16.** Transfection efficiency with increased pDNA concentration in HEK293T cells. EGFP expression of viable cells was analyzed *via* flow cytometry following incubation of cells with (layered) polyplexes of mEGFP-N1 pDNA ( $3.0 \mu\text{g mL}^{-1}$ ) and polymers at N\*/P 15 in growth medium for 24 h, for 24 h followed by splitting of cells and medium and further incubation for 24 h, or for 48 h. Values represent mean  $\pm$  SD of (A) viable, single EGFP positive cells (B) rMFI of all viable single cells ( $n = 1-3$ ).

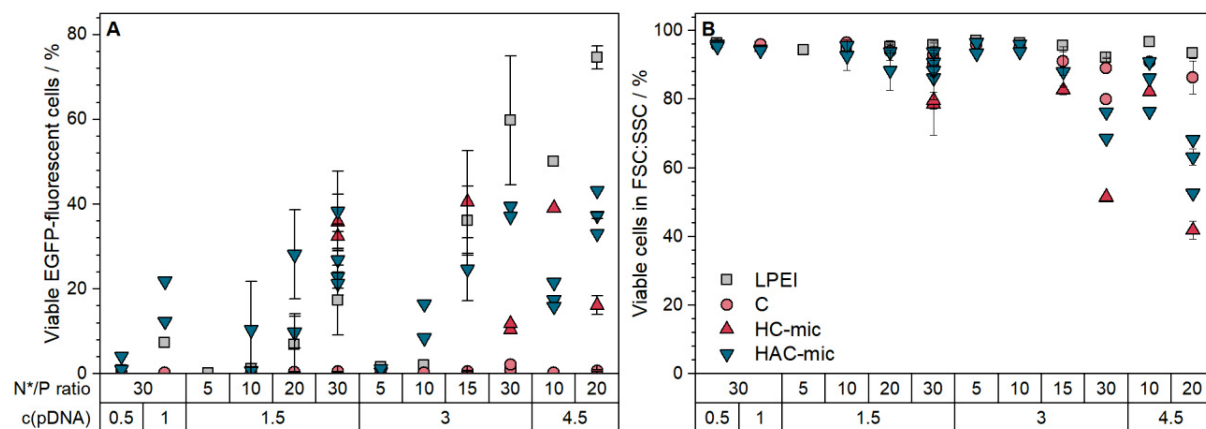


**Figure S17.** Influence of concentration on transfection efficiency. Concentration dependent transfection efficiency in HEK293T cells following incubation with polyplexes of mEGFP-N1 pDNA and polymers in D10H for 24 h. Values represent mean  $\pm$  SD of (A) viable EGFP fluorescent cells or (B) viable cells in FSC/SSC scatter plot ( $n \geq 1$ ). Dots of the same color represent different batches of the respective polymer. c(pDNA) in  $\mu\text{g mL}^{-1}$ .

**Table S8.** MFI values of different controls in flow cytometry.

Assay	Conditions	MFI of all viable single cells		
		Only buffer	Only mEGFP pDNA/ YOYO-1 labeled pDNA	pKMyc pDNA + polymers <sup>[a]</sup>
Transfection efficiency	1.5 $\mu\text{g mL}^{-1}$ pDNA, N*/P 30, 24 h	1693 $\pm$ 209	1719 $\pm$ 82	2164 $\pm$ 483
	1.5 $\mu\text{g mL}^{-1}$ pDNA, N*/P 30, 24+24 h	1753 $\pm$ 106	1634 $\pm$ 29	2314 $\pm$ 517
	1.5 $\mu\text{g mL}^{-1}$ pDNA, N*/P 30, 48 h	1623 $\pm$ 200	1415 $\pm$ 66	1991 $\pm$ 468
Polyplex uptake	1.5 $\mu\text{g mL}^{-1}$ pDNA, N*/P 30, 1 h		2276 $\pm$ 280	
	1.5 $\mu\text{g mL}^{-1}$ pDNA, N*/P 30, 4 h		2741 $\pm$ 199	
	1.5 $\mu\text{g mL}^{-1}$ pDNA, N*/P 30, 24 h		2433 $\pm$ 383	
	1.5 $\mu\text{g mL}^{-1}$ pDNA, N*/P 30, 24+24 h		2461 $\pm$ 78	

[a] Mean of all pKMyc pDNA-polymer polyplexes.

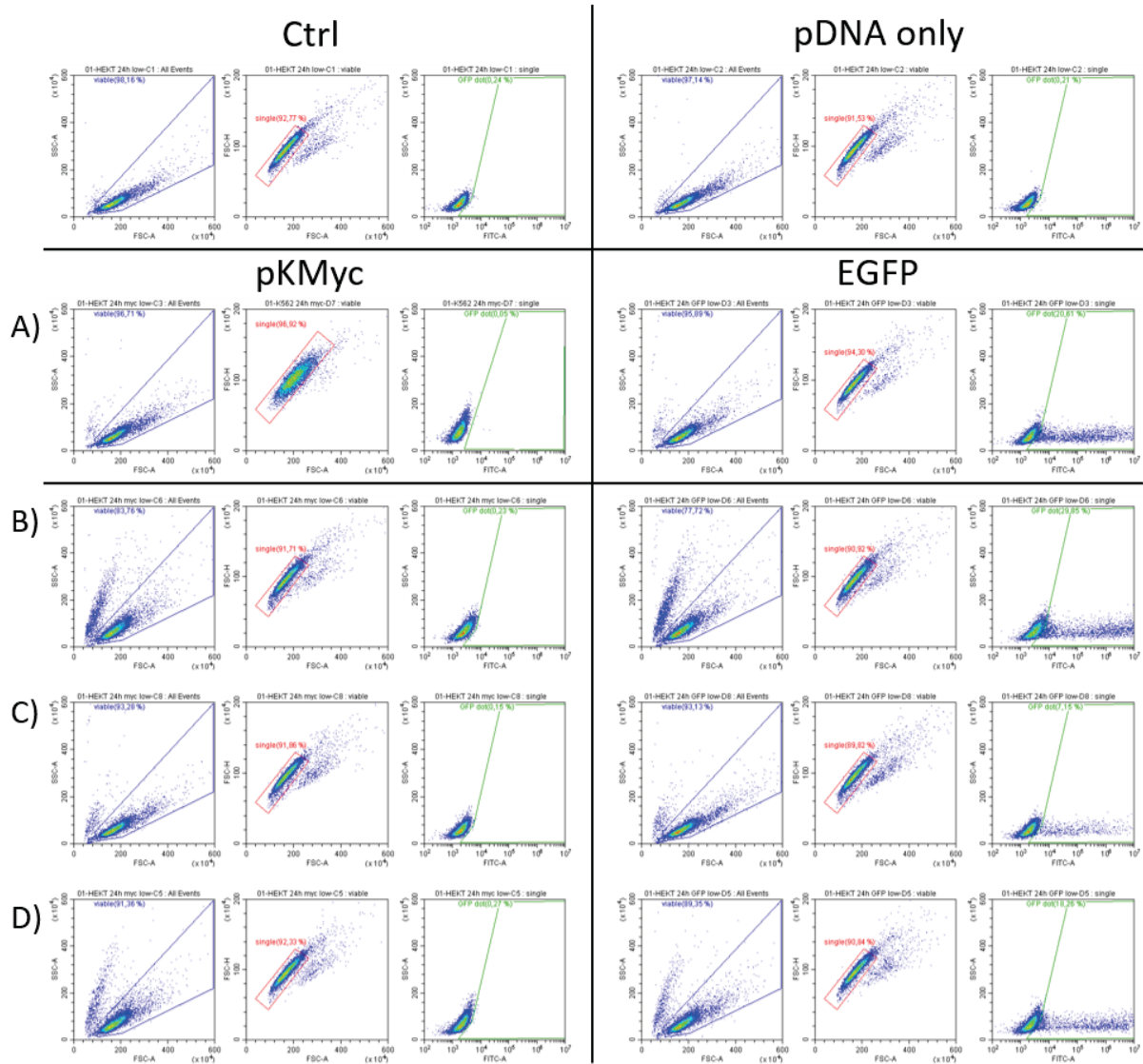


**Figure S18.** Gating strategy for pDNA transfection using examples of 24 h incubation.

Viable single cells were gated in FSC/SSC and FSC-A/FSC-H dot plots (blue and red gates). Subsequently cells with EGFP fluorescence were discriminated by gating to the respective pKMyc control (green gates). Plots of HEK293T cells incubated with (layered) polyplexes of  $1.5 \mu\text{g mL}^{-1}$  pDNA and (A) LPEI, (B) HC-mic, (C) HC<sup>AS</sup>, (D) HAC-mic at N\*/P 30 are shown.

## Polyplex Uptake.

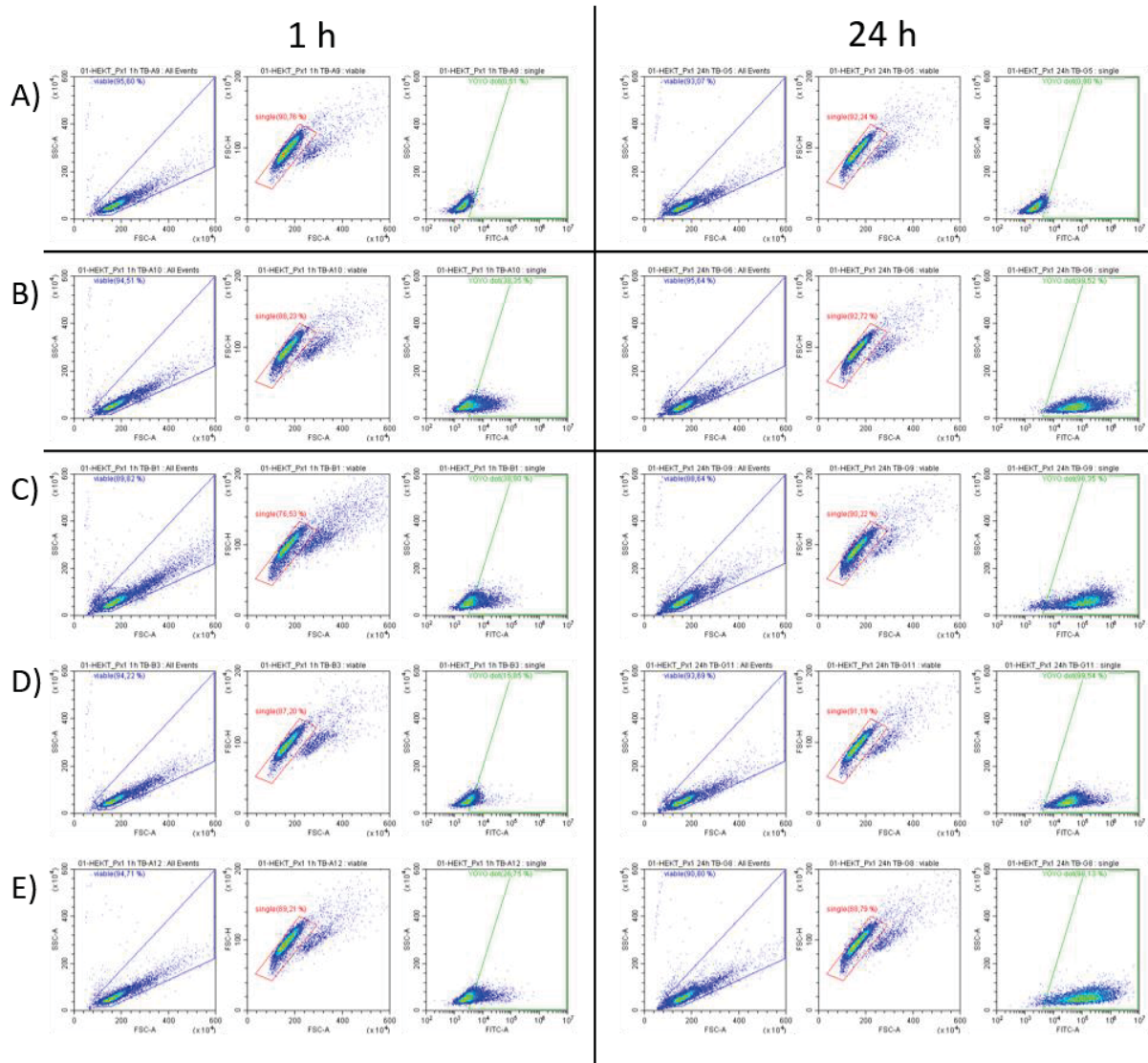


**Figure S19.** Gating strategy for polyplex uptake using examples of 1 and 24 h incubation.

Viable single cells were gated in FSC/SSC and FSC-A/FSC-H dot plots (blue and red gates). Subsequently cells with YOYO-1 fluorescence were discriminated by gating to the pDNA-YOYO-1 control of the respective incubation time (A, green gates). Plots of HEK293T cells incubated with (layered) polyplexes of  $1.5 \mu\text{g mL}^{-1}$  YOYO-1 labeled pDNA and (B) LPEI, (C) HC-mic, (D) HC<sup>AS</sup>, (E) HAC-mic at N\*/P 30 are shown.

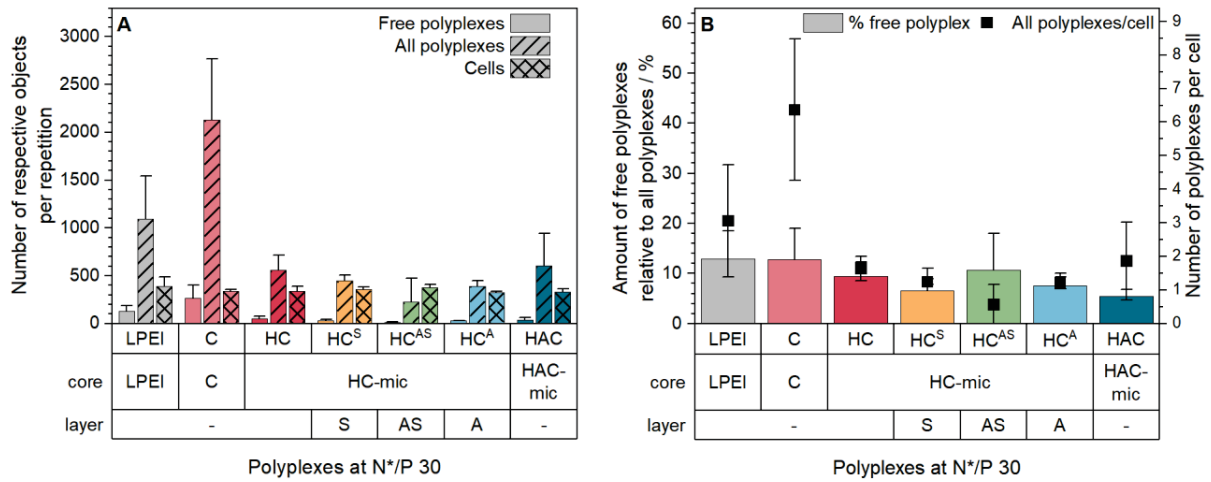


**Figure S20.** Quantitative analysis of polyplex uptake by CLSM.

HEK293T cells were stained for plasma membrane and membrane-associated organelles with CMDR-PM followed by incubation with (layered) polyplexes of YOYO-1-labeled pDNA and polymers at N\*/P 30 in D10H for 1 h. Live cell imaging was performed following further staining of the cells with Hoechst 33342 for the nuclei and again with CMDR-PM. YOYO-1 fluorescence outside the cells was quenched by addition of trypan blue to a final concentration of 0.04% just before imaging. Values were obtained by image analysis of all acquired images (Figure S21) using the analysis wizard of ZEN 3.1 (Zeiss, Germany) and represent mean  $\pm$  SD ( $n = 3$ ) of (A) the raw counts of the respective segmented features, and (B) the respective relative calculations (see additional methods section).

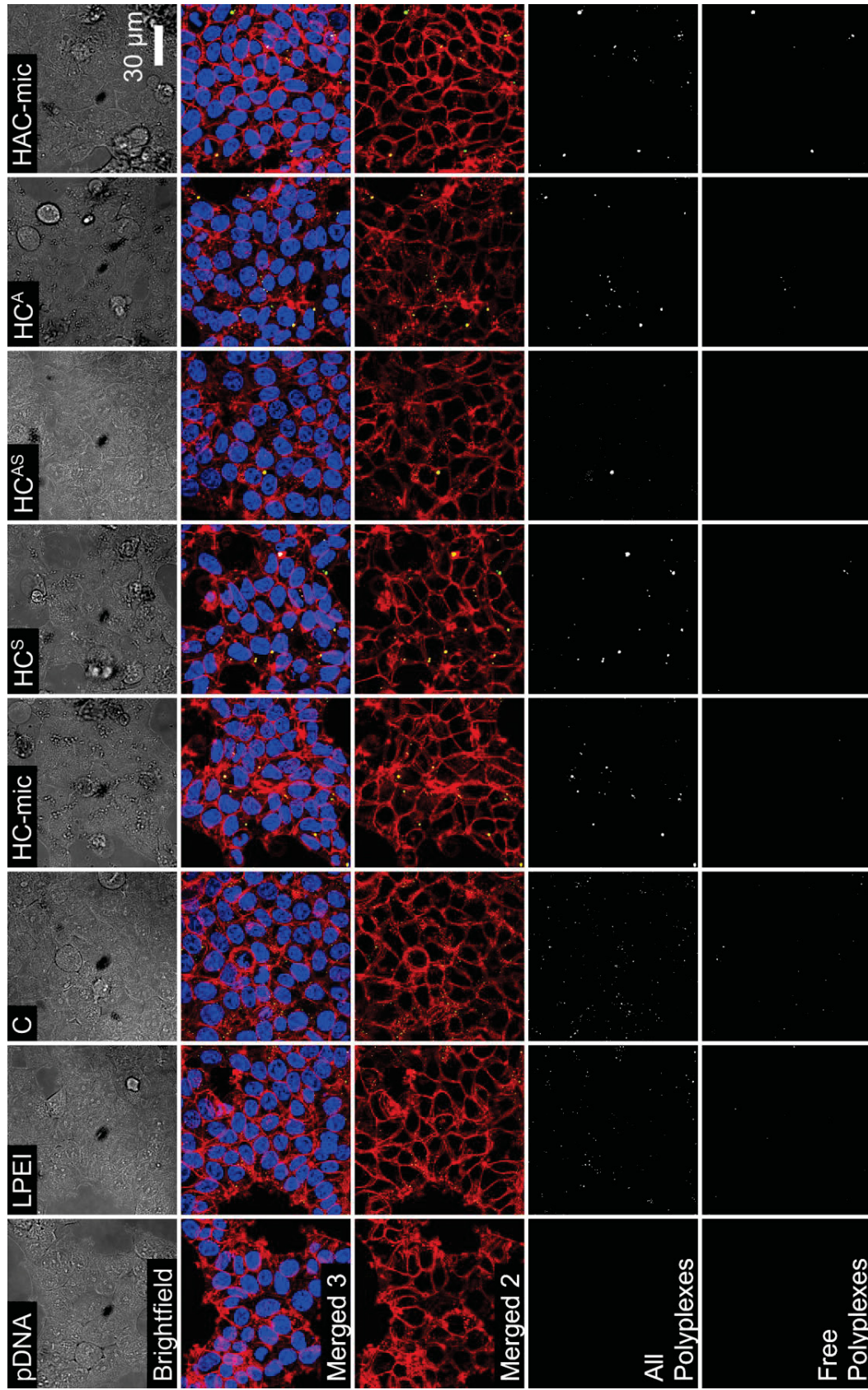


**Figure S21.** CLSM images of polyplex uptake by HEK293T cells.

Representative images of HEK293T cells stained for plasma membrane and membrane-associated organelles (red) with CMDR-PM followed by incubation with (layered) polyplexes (green) of YOYO-1-labeled pDNA and polymers at N\*/P 30 in D10H for 1 h. Live cell imaging was performed following further staining of the cells with Hoechst 33342 for the nuclei (blue) and again with CMDR-PM. Yellow dots indicate colocalization of CMDR-PM and YOYO-1. The images of the free polyplexes were generated by subtraction of the respective binary colocalization image from the binary polyplex image obtained during image analysis.

### Calcein Release.

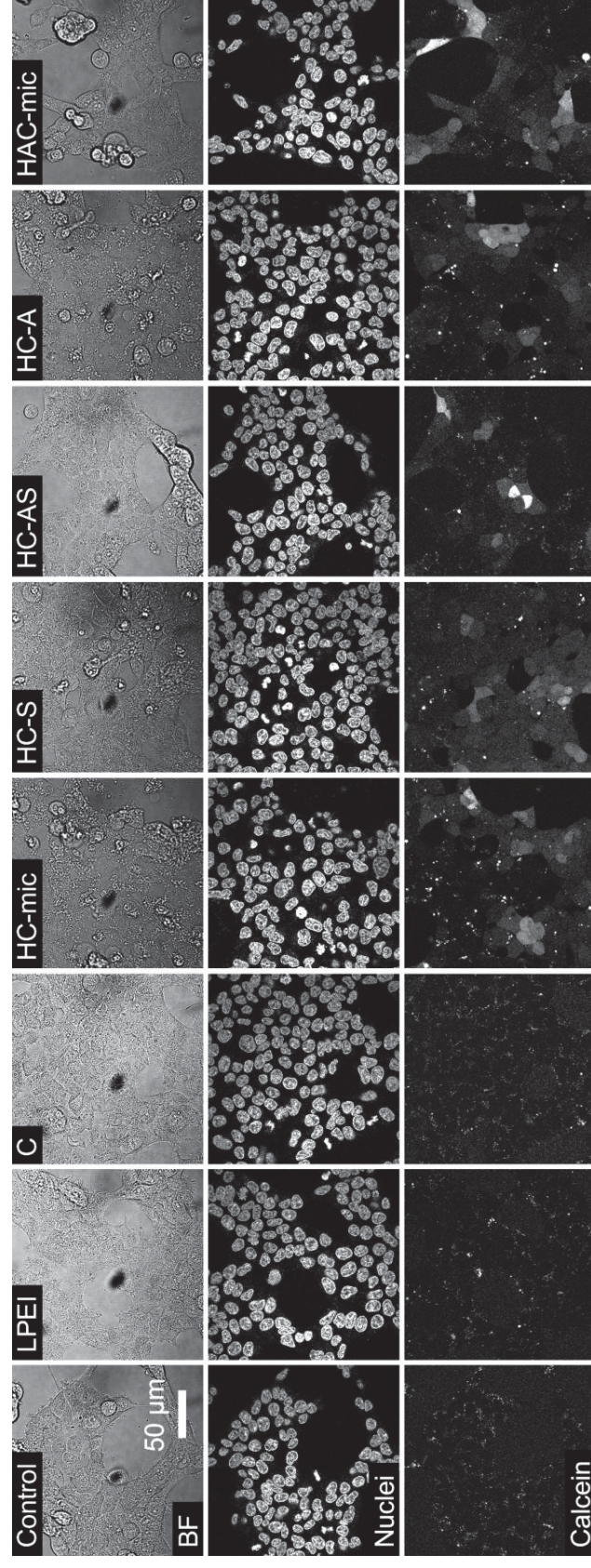


**Figure S22.** Brightfield (BF) and gray images of HEK293T cells for calcein CLSM study. HEK293T cells were incubated with (layered) polyplexes of pDNA and polymers at N\*/P 30 in D10H for 1 h. Just before the addition of polyplexes, calcein was added to a final concentration of  $25 \mu\text{g mL}^{-1}$ . Cells were washed twice with warm FC-buffer before the



addition of fresh warm D20 and staining of nuclei with Hoechst 33342. Images of the T-PMT channel are shown. Colored images of the calcein and the Hoechst 33342 channels can be found in the main article.

## REFERENCES

1. Larnaudie SC, Brendel JC, Jolliffe KA, Perrier S: **Cyclic peptide–polymer conjugates: Grafting-to vs grafting-from.** *J Polym Sci, Part A: Polym Chem* 2016, **54**:1003-1011.
2. Richter F, Martin L, Leer K, Moek E, Hausig F, Brendel JC, Traeger A: **Tuning of endosomal escape and gene expression by functional groups, molecular weight and transfection medium: a structure-activity relationship study.** *J Mater Chem B* 2020, **8**:5026-5041.
3. Richter F, Mapfumo P, Martin L, Solomun JI, Hausig F, Frietsch JJ, Ernst T, Hoepfener S, Brendel JC, Traeger A: **Improved gene delivery to K-562 leukemia cells by lipoic acid modified block copolymer micelles.** *Journal of Nanobiotechnology* 2021, **19**:70.
4. Schindelin J, Arganda-Carreras I, Frise E, Kaynig V, Longair M, Pietzsch T, Preibisch S, Rueden C, Saalfeld S, Schmid B, et al: **Fiji: an open-source platform for biological-image analysis.** *Nat Methods* 2012, **9**:676.
5. Catrouillet S, Brendel JC, Larnaudie S, Barlow T, Jolliffe KA, Perrier S: **Tunable Length of Cyclic Peptide–Polymer Conjugate Self-Assemblies in Water.** *ACS Macro Lett* 2016, **5**:1119-1123.
6. Bauer M, Lautenschlaeger C, Kempe K, Tauhardt L, Schubert US, Fischer D: **Poly(2-ethyl-2-oxazoline) as Alternative for the Stealth Polymer Poly(ethylene glycol): Comparison of in vitro Cytotoxicity and Hemocompatibility.** *Macromol Biosci* 2012, **12**:986-998.

## Publication Pub5

### Improved gene delivery to K-562 leukemia cells by lipoic acid modified block copolymer micelles

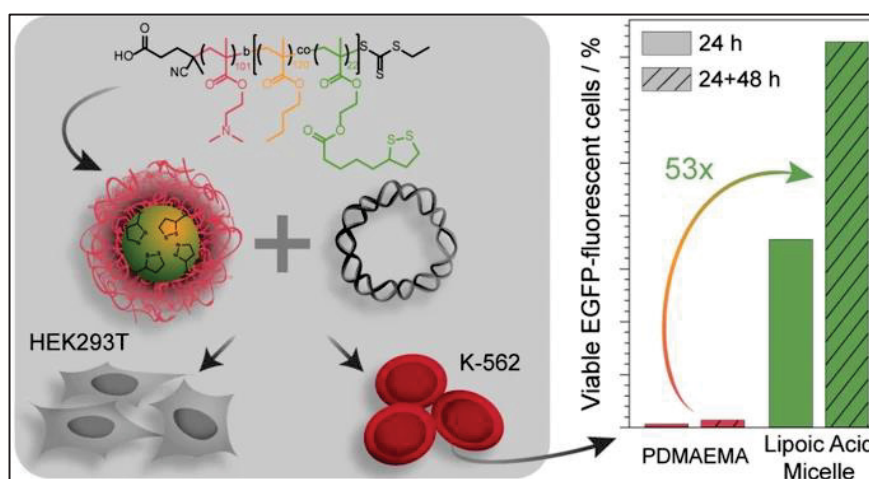
F. Richter,<sup>‡</sup> P. Mapfumo,<sup>‡</sup> L. Martin, J. I. Solomun, F. Hausig, J. J. Frietsch, T. Ernst, S. Hoepfener, J. C. Brendel, A. Traeger

*J. Nanobiotechnol.* **2021**, 19, 70

Reproduced with permission of Springer Nature. Copyright © 2021.

The article and the supporting information are available online:

[doi.org/10.1186/s12951-021-00801-y](https://doi.org/10.1186/s12951-021-00801-y)



RESEARCH

Open Access



# Improved gene delivery to K-562 leukemia cells by lipoic acid modified block copolymer micelles

Friederike Richter<sup>1†</sup>, Prosper Mapfumo<sup>1†</sup>, Liam Martin<sup>1</sup>, Jana I. Solomun<sup>1</sup>, Franziska Hausig<sup>1</sup>, Jochen J. Frietsch<sup>2</sup> , Thomas Ernst<sup>2</sup>, Stephanie Hoepfener<sup>1,3</sup>, Johannes C. Brendel<sup>1,3</sup> and Anja Traeger<sup>1,3\*</sup>

## Abstract

Although there has been substantial progress in the research field of gene delivery, there are some challenges remaining, e.g. there are still cell types such as primary cells and suspension cells (immune cells) known to be difficult to transfect. Cationic polymers have gained increasing attention due to their ability to bind, condense and mask genetic material, being amenable to scale up and highly variable in their composition. In addition, they can be combined with further monomers exhibiting desired biological and chemical properties, such as antioxidative, pH- and redox-responsive or biocompatible features. By introduction of hydrophobic monomers, in particular as block copolymers, cationic micelles can be formed possessing an improved chance of transfection in otherwise challenging cells. In this study, the antioxidant biomolecule lipoic acid, which can also be used as crosslinker, was incorporated into the hydrophobic block of a diblock copolymer, poly{[2-(dimethylamino)ethyl methacrylate]<sub>101</sub>-*b*-[*n*-(butyl methacrylate)<sub>124</sub>-*co*-(lipoic acid methacrylate)<sub>22</sub>]} (P(DMAEMA<sub>101</sub>-*b*-[*n*BMA<sub>124</sub>-*co*-LAMA<sub>22</sub>])), synthesized by RAFT polymerization and assembled into micelles (LAMA-mic). These micelles were investigated regarding their pDNA binding, cytotoxicity mechanisms and transfection efficiency in K-562 and HEK293T cells, the former representing a difficult to transfect, suspension leukemia cell line. The LAMA-mic exhibited low cytotoxicity at applied concentrations but demonstrated superior transfection efficiency in HEK293T and especially K-562 cells. In-depth studies on the transfection mechanism revealed that transfection efficiency in K-562 cells does not depend on the specific oncogenic fusion gene *BCR-ABL* alone. It is independent of the cellular uptake of polymer-pDNA complexes but correlates with the endosomal escape of the LAMA-mic. A comparison of the transfection efficiency of the LAMA-mic with structurally comparable micelles without lipoic acid showed that lipoic acid is not solely responsible for the superior transfection efficiency of the LAMA-mic. More likely, a synergistic effect of the antioxidative lipoic acid and the micellar architecture was identified. Therefore, the incorporation of lipoic acid into the core of hydrophobic-cationic micelles represents a promising tailor-made transfer strategy, which can potentially be beneficial for other difficult to transfect cell types.

**Keywords:** Gene delivery, Cationic polymer, Lipoic acid, Micelle, K-562 cells, Transfection

## Introduction

Non-viral gene therapy has become an important research field, with the aim of finding new methods for the treatment of diseases like cancer or genetic disorders or for the development of vaccines [1, 2]. Cationic polymers are of interest due to their ability to form complexes with the genetic material (polyplexes) through

\*Correspondence: anja.traeger@uni-jena.de

<sup>†</sup>Friederike Richter, Prosper Mapfumo contributed equally to this work

<sup>3</sup>Jena Center for Soft Matter (JCSM), Friedrich Schiller University Jena, Philosophenweg 7, 07743 Jena, Germany

Full list of author information is available at the end of the article



electrostatic interaction, thereby protecting it from degradation, facilitating its cellular uptake, enabling escape from the endolysosomal pathway, and finally releasing it inside the cytosol [3]. Furthermore, polymers are easy and cost-effective to produce on a large scale, show low immunogenicity and can transport high molecular weight genetic materials, such as plasmid DNA (pDNA) [4, 5].

Despite remarkable progress, there are still many challenges encountered for these applications, e.g. not all cell types can be genetically modified (transfected) easily, including primary cells and suspension cells (immune cells) [6–8]. To date, viral infection, electroporation or nucleofection have been successfully applied for these cells. However, this is not suitable for all applications [4, 9, 10]. Alternatively, cationic polymers can be applied to transfect cells. The ability to genetically modify suspension cells is of great interest, not only for vaccinations, inflammation-related diseases or cancer in general, but also for leukemia patients where the immune cells are directly affected. For example, chronic myeloid leukemia (CML) can still only be clinically healed but not cured, with 40% of patients free of treatment after therapy [11–13]. Polymeric nanocarriers could be a promising strategy to interact more efficiently with immune cells and enhance the intracellular concentration of active agents to counteract mechanisms such as drug resistance or poor response to treatment [14, 15]. In this regard, the group of E. Wagner could already show successful transfection of pDNA with poly(ethylene imine) (PEI) only in combination with transferrin [16–18]. Another promising strategy was demonstrated by H. Uludağ and coworkers who statistically incorporated hydrophobic moieties into polymeric nanocarriers that were beneficial for the transfection of siRNA and subsequent knockdown of the BCR-ABL fusion protein in the CML cell line K-562 [19–21].

One key advantage of polymeric gene carriers is their versatility in composition, allowing the introduction of different additional features such as temperature-, pH- or redox-responsiveness, thereby generating nanocarriers tailored for a specific site of action [5, 22]. The advancement of living or controlled polymerization methods resulted in preparation of polymers with various compositions and complex architectures such as, gradient, block, star and comb copolymers [23]. Among reversible deactivation radical polymerization (RDRP) methods, reversible addition fragmentation chain transfer (RAFT) polymerization, a process based on an equilibrium between active and dormant chains achieved by a degenerative transfer system, is promising due to the relative insensitivity towards functional groups of the monomers and can therefore be

applied for a wide range of suitable monomers. However, disulfide bonds are a potential exception since they are susceptible to radicals [23, 24]. Additionally, RAFT polymerization is compatible with a wide range of unprotected monomer functionalities, such as quaternary amino, carboxylic acid, epoxy, hydroxyl (e.g. in hydroxyethyl methacrylate (HEMA)) and tertiary amino (e.g. in 2-dimethylaminoethyl methacrylate (DMAEMA)) groups. This makes the production of polymers with the desired functionalities easier compared to, e.g. the post-modification strategy of polymers to obtain defined polymer architectures [25].

Polymeric micelles with various compositions have already been investigated for gene delivery [26–29]. Due to the amphiphilic nature of the block copolymers, microphase separation occurs during self-assembly, resulting in micellar formation of diverse morphologies [30]. A commonly applied method for polymer assemblies is dispersion of polymers, which involves solvent evaporation, salting-out, dialysis, supercritical fluid technology and nanoprecipitation [31].

In general, polymeric micelles for gene delivery contain a hydrophilic cationic segment, responsible for condensing the genetic material and protecting it from degradation, e.g. PDMAEMA with a  $pK_a$  ( $\approx 7.5$ ) within a physiologically relevant pH range [32, 33]. Besides, micelles also contain a hydrophobic segment responsible for its stability and potentially contributing to efficient transfection as they can facilitate interaction with the lipophilic cell membranes promoting cellular uptake and release from the endosomes [34–36]. Among others, *n*-butyl methacrylate (*n*BMA) has been shown to form a stable hydrophobic core and, as such, been included for hydrophobic modifications of polymers and formation of micelles [36–38].

To stabilize the micelle architecture, crosslinkers such as disulfide linkage have been applied. Disulfide linkages are stable under oxidizing conditions and break down under reductive conditions, which are found inside cells [39]. A stable micelle can therefore be prepared by incorporating sulfur containing moieties, e.g. the antioxidant biomolecule lipoic acid, which is an essential fatty acid, a potential therapeutic [40, 41], and capable of forming disulfide linkages in the micellar core [42]. For drug delivery systems, Zhong and coworkers demonstrated that different lipoic acid conjugated materials possessed superior stability in the extracellular environment and underwent rapid de-crosslinking and disassembly under reductive conditions [39, 43–45]. Moreover, lipoic acid was beneficial for transfection of siRNA or pDNA in different adherent cell lines when incorporated into nanogels [46], as hydrophobic modification of linear poly(ethylene imine) (LPEI) [47], or as amphiphiles

[48, 49]. However, the contribution of liponic acid within micelles to gene transfer into immune cells is not known.

In the present study, liponic acid derived micelles were investigated as a potent nanocarrier for genetic material into the CML cell line K-562. The micelles were formulated from a block copolymer synthesized via RAFT polymerization, the first block comprising PDMAEMA and the second liponic acid methacrylate (LAMA) and *n*BMA. Whereas PDMAEMA forms the shell and contributes to pDNA binding and endosomal escape, *n*BMA forms the micellar core into which liponic acid-containing monomers were introduced to establish antioxidant and crosslinking potential. Following physicochemical characterization, the pDNA binding properties, cytotoxicity, and transfection efficiency (expression of enhanced green fluorescent protein (EGFP)) in the erythroleukemic suspension cell line K-562 were investigated. The results were compared to the human embryonic kidney cell line HEK293T. The contribution of liponic acid to the superior transfection efficiency in K-562 cells was investigated in detail by further testing of other leukemia cell lines as well as pDNA uptake and endosomal escape properties. Additionally, the influence of structure and composition was investigated by comparing the potential of the LAMA-micelles with liponic acid-free precursor micelles.

## Main methods

Materials, instruments, further methods and calculations can be found in the Additional file 1.

### Synthesis and characterization, general procedure

(4-cyano pentanoic acid) ethyl trithiocarbonate (CPAETC) (24.9 mg,  $9.47 \times 10^{-5}$  moles), 2-(dimethylamino)ethyl methacrylate (DMAEMA) (2.25 g,  $1.43 \times 10^{-2}$  moles), 1,4-dioxane (3.0 g), a 1 wt.% solution of 4,4'-azobis(4-cyanovaleric acid) (ACVA) in 1,4-dioxane (318.4 mg, 3.18 mg ACVA,  $1.1 \times 10^{-5}$  moles) and 1,3,5-trioxane (external NMR standard, 25 mg) were introduced to a 8 mL microwave vial equipped with a magnetic stirring bar. The vial was sealed, and the solution deoxygenated by bubbling argon through it for 10 min. The vial was placed in an oil bath at 70 °C and allowed to stir for 7 h. The polymer was precipitated three times from tetrahydrofuran (THF) into cold hexane and dried under reduced pressure to give a yellow solid. A portion of the precursor, macro-chain transfer agent (macro-CTA) of poly[2-(dimethylamino)ethyl methacrylate] (PDMAEMA) (347.0 mg,  $2.29 \times 10^{-5}$  moles), butyl methacrylate (*n*BMA) (557.0 mg,  $3.92 \times 10^{-3}$  moles), liponic acid methacrylate (LAMA) (220.0 mg,  $6.88 \times 10^{-4}$  moles), THF (4.1 g), a 0.5 wt.% solution of ACVA in THF (250 mg,  $4.46 \times 10^{-6}$  moles) and 1,3,5-trioxane (external NMR standard, 20.0 mg) were introduced

to a 8 mL microwave vial equipped with a magnetic stirring bar. The vial was sealed, and the solution deoxygenated by bubbling argon through it for 10 min. The vial was placed in an oil bath at 70 °C and allowed to stir for 7 h. The polymer was precipitated three times from THF into cold hexane and dried under reduced pressure to give a yellow solid. For further experimental details of all polymerizations refer to Additional file 1.

### Assembly procedure for micelle formation

*Typical assembly procedure.* 30 mg of polymer was dissolved in THF (3 mL) and added to a 20 mL vial. Water (6 mL) was added to this solution through a syringe using a syringe pump (rate:  $0.2 \text{ mL min}^{-1}$ ). Afterwards, (A) the polymer solution was added to a dialysis bag (Standard RC Tubing MWCO: 6–8 kDa) and dialyzed against water over three days, changing the bulk water twice a day or, (B), the polymer solution was left for two days at room temperature until THF was completely evaporated. The final concentration was determined by measuring the mass difference of three freeze dried samples of known volume. The micelles were characterized regarding their critical micelle concentration (CMC), hydrodynamic diameter and morphology using Nile Red as a fluorescent probe, dynamic light scattering (DLS) and cryo transmission electron microscopy, respectively. Experimental details for each analysis are provided in Additional file 1.

### Cryo transmission electron microscopy (cryo-TEM)

Cryo-TEM images were acquired with a 200 kV FEI Tecnai G2 20 transmission electron microscope equipped with a  $4k \times 4k$  Eagle HS CCD and an Olympus MegaView camera ( $1379 \times 1024$  pixels) for overview images. Sample preparation was performed by plunge-freezing the samples with a Vitrobot Mark IV system. 8.5  $\mu\text{L}$  of the aqueous solutions were blotted (blot force –2; blotting time 1 s) on Quantifoil grids (R2/2, Quantifoil, Jena, Germany) and were vitrified in liquid ethane. The grids were rendered hydrophilic by Ar-plasma cleaning for 30 s (Diener Electronics, Germany). Samples were stored in liquid nitrogen until transfer to the cryo holder (Gatan 626). Transfer to the microscope was performed with a Gatan cryo stage and the temperature was maintained below  $-172 \text{ }^\circ\text{C}$  at all times after vitrification.

### Polyplex preparation

The polyplexes were prepared in HBG buffer (20 mM 4(2hydroxethyl) piperazine-1-ethanesulfonic acid (HEPES) and 5% (w/v) glucose, pH 7.4). A 30  $\mu\text{g mL}^{-1}$  solution of pDNA was mixed 1:2 with different quantities of dissolved polymer to give a final pDNA concentration of 15  $\mu\text{g mL}^{-1}$ , with varying N\*/P ratios (molar ratio of protonatable nitrogen atoms to phosphates of pDNA,

see Additional file 1). Immediately after combination, the mixtures were vortexed for 10 s at maximum speed (3200 rpm) and incubated at room temperature for 15 min to ensure complex formation.

#### Ethidium bromide quenching assay (EBA) and heparin release assay (HRA)

The formation of polyplexes with pDNA was identified via quenching of ethidium bromide (EtBr) fluorescence by polymers interacting with pDNA as described before. [50] Briefly, 30  $\mu\text{g mL}^{-1}$  pKMyC pDNA in HBG buffer (pH 7.4) were incubated with EtBr (1  $\mu\text{g mL}^{-1}$ ) at room temperature for 10 min. Different polymer stock solutions were prepared by dilution with HBG buffer (pH 7.4) to give different N\*/P ratios. Subsequently, the pDNA-EtBr solution was mixed 1:2 with the different polymer stock solutions in black 96-well plates (Nunc, Thermo Fisher, Germany) and incubated at 37 °C for 15 min before measuring the fluorescence intensity at  $\lambda_{\text{Ex}} = 525 \text{ nm}$  /  $\lambda_{\text{Em}} = 605 \text{ nm}$ . A sample containing only pDNA and EtBr was defined as maximum fluorescence (100%).

For the HRA, heparin was added to the formed polyplex-EtBr mixtures using the dispenser of the microplate reader to obtain the indicated concentrations (Additional file 1: Table S2). After each addition, the plate was shaken, incubated at 37 °C for 10 min and fluorescence intensity was measured.

The percentage of EtBr displaced upon polyplex formation or re-intercalating following pDNA release by heparin was calculated using Eq. (1):

$$\text{rFI}/\% = \frac{F_{\text{Sample}}}{F_{\text{pDNA}}} \cdot 100 \quad (1)$$

Where rFI is the relative fluorescence intensity and  $F_{\text{Sample}}$ , and  $F_{\text{pDNA}}$  are the fluorescence intensities of a given sample and the EtBr intercalated into pDNA alone (in the case of the HRA with heparin), respectively. Data are expressed as mean  $\pm$  SD of three independent determinations.

The heparin concentration needed to release 70% of pDNA was calculated with OriginPro, Version 2018b (OriginLab Corporation, US) and can be found in the Additional file 1.

#### Cell culture

The mouse fibroblast cell line L-929 and the human embryonic kidney cell line HEK293T were obtained from CLS (Germany). They were maintained as recommended by the supplier and cultured in D10 (low glucose Dulbecco's modified eagle's medium (DMEM) supplemented with 10% (v/v) fetal calf serum (FCS), 100 U  $\text{mL}^{-1}$

penicillin and 100  $\mu\text{g mL}^{-1}$  streptomycin) at 37 °C in a humidified 5% (v/v)  $\text{CO}_2$  atmosphere. The chronic myeloid leukemia (CML) cell line K-562 was obtained from DSMZ (Germany) and cultured in R10 (Roswell Park Memorial Institute (RPMI) 1640 medium supplemented with 10% (v/v) FCS, 100 U  $\text{mL}^{-1}$  penicillin and 100  $\mu\text{g mL}^{-1}$  streptomycin) at 37 °C in a humidified 5% (v/v)  $\text{CO}_2$  atmosphere. For comparison to other leukemia cell lines and determining the influence of BCR-ABL, the transformed acute myeloid leukemia (AML) cell line M07p210 [51] and the CML blast crisis cell lines LAMA-84 and KCL-22 were analyzed. All cell lines, except for M07p210, were obtained from DSMZ. The cells were cultured as described for the K-562 cells.

For experiments, L-929 and HEK293T cells were seeded at 0.1 or  $0.2 \times 10^6$  cells  $\text{mL}^{-1}$ , respectively, in growth medium (D10) containing 10 mM HEPES for stability of the pH value and incubated at 37 °C in a humidified 5% (v/v)  $\text{CO}_2$  atmosphere for 24 h. One hour prior to transfection, the medium was changed to fresh growth medium with HEPES. Unless stated otherwise, the K-562 and other leukemia cell lines were seeded at  $0.3 \times 10^6$  cells  $\text{mL}^{-1}$  in growth medium (R10) containing 10 mM HEPES and incubated at 37 °C in a humidified 5% (v/v)  $\text{CO}_2$  atmosphere for about 3 h before transfection.

#### Determination of cytotoxicity

For determination of cytotoxicity of the polymers, two different methods were used: The PrestoBlue™ assay for metabolic activity and the CytoTox-ONE™ assay for membrane integrity of the cells. The PrestoBlue™ assay was performed with the L-929 cells based on ISO10993-5. In detail, cells (concentration as indicated above) were seeded in 100  $\mu\text{L}$  per well in a 96-well plate without using the outer wells and treated in sextuplicates with polymers at different concentrations, ranging from 5  $\mu\text{g mL}^{-1}$  to 200  $\mu\text{g mL}^{-1}$  for 24 h. The medium was replaced by a 10% (v/v) PrestoBlue™ solution in fresh culture medium, prepared according to the manufacturer's instructions. Following an incubation at 37 °C for 45 min, the fluorescence was measured at  $\lambda_{\text{Ex}} = 570 \text{ nm}$  /  $\lambda_{\text{Em}} = 610 \text{ nm}$ . Non-treated control cells on the same plate were referred to as 100% viability. Values above 70% were regarded as non-toxic. To assess the toxicity of polyplexes used for transfection, K-562 and HEK293T cells were seeded in 500  $\mu\text{L}$  per well in a 24-well plate and treated with the polyplexes at N\*/P 30 for 24 h prior to the PrestoBlue™ assay. The polyplexes were prepared as described above with isolated pKMyC pDNA and added to the cells diluting the polyplexes 1:10 in the cell culture medium. Data are expressed as mean  $\pm$  SD of at least three independent determinations.

For determination of the release of lactate dehydrogenase (LDH) due to membrane disruption, the CytoTox-ONE™ assay (LDH-assay) was performed according to the manufacturer's instructions following incubation of the cells with polyplexes as described above in 500  $\mu\text{L}$  per well of a 24-well plate for 24 h. The supernatant was transferred to a new 96-well plate as a triplicate and allowed to cool down to room temperature for 30 min. Subsequently, the substrate mixture including assay buffer was added and incubated at room temperature for 10 min. The fluorescence intensity was measured at  $\lambda_{\text{Ex}}=560\text{ nm}$  /  $\lambda_{\text{Em}}=590\text{ nm}$  following the addition of the stop solution. For the positive control (100% LDH release), cells were incubated with 0.2% Triton X-100 for 30 min prior to analysis. Cells incubated with only pDNA were used as negative control (0% LDH-release). The relative number of viable cells with intact membranes was calculated as follows (2):

$$\text{Viability}/\% = 100 - \frac{F_{\text{Sample}} - F_0}{F_{\text{Positive control}} - F_0} \cdot 100 \quad (2)$$

Where  $F_{\text{Sample}}$ ,  $F_0$ , and  $F_{\text{Positive control}}$  represent the fluorescence intensity of a given sample, medium without cells, and of the Triton X-100 treated cells, respectively.

### Transfection efficiency

Transfection studies were performed in HEK293T, K-562 and further leukemia cells. The cells were seeded in 500  $\mu\text{L}$  per well in 24-well plates and treated with polyplexes at N\*/P 30. The polyplexes were prepared as described above with isolated mEGFP-N1 pDNA and added to the cells diluting the polyplexes 1:10 in the cell culture medium for an incubation period of 24 h. For analysis via flow cytometry, HEK293T cells were harvested by transferring the supernatant to a 24-well plate, trypsinizing the cells and resuspending them in the respective supernatant again. Subsequently, fresh D10 was added, diluting the cell suspension 1:2. Half of the suspension was transferred to a 96-well plate for measurement, while the remaining cells were incubated for another 48 h. K-562 cells were harvested by resuspension and subsequent transfer of half of the cell suspension to a 96-well plate for measurement. For long-term transfection (72 h), the remaining cell suspension was split 1:2 by adding the same amount of fresh R10 and incubated for further 48 h.

For determination of transfection efficiency, cells were analyzed as described in the instrumentation section (Additional file 1). Viable cells showing EGFP signal higher than the mock control cells incubated with polyplexes of the respective polymer and pKMyC pDNA were gated as percentage of cells expressing EGFP and the

relative mean fluorescence intensity (rMFI) of all viable cells was calculated in relation to the respective mock control. The experiments were performed at least three times and data are expressed as mean  $\pm$  SD.

### Polyplex uptake

To study the uptake of polymers over time in HEK293T and K-562 cells, the cells were seeded in 500  $\mu\text{L}$  per well in 24-well plates and treated with polyplexes at N\*/P 30 for indicated time periods. The polyplexes were prepared as described above after labelling 1  $\mu\text{g}$  pKMyC pDNA with 0.027 nmol YOYO-1 iodide. Subsequently, the polymer-pDNA-solutions were added to the cells, diluting the polyplexes 1:10 in cell culture medium. Following incubation, the HEK293T cells were harvested by trypsinization and resuspension in FC-buffer (Hanks' Balanced Salt Solution, supplemented with 2% FCS and 20 mM HEPES), while the K-562 cells were only resuspended. Trypan blue solution (0.4%) was added to a final concentration of 0.04% to quench fluorescence of polyplexes outside the cells. Cells were analyzed via flow cytometry or confocal laser scanning microscopy (CLSM) as described in the instrumentation section (Additional file 1). Viable cells showing YOYO-1 signal higher than the control cells, which were incubated with YOYO-1-pDNA only, were gated as percentage of cells that have taken up pDNA and the rMFI of all viable cells was calculated in relation to the control cells. The experiments were performed at least three times and data are expressed as mean  $\pm$  SD.

### Calcein release assay

To determine the endosomal escape efficiency of the polymers, a calcein release assay was performed with HEK293T and K-562 cells. The cells were seeded in 500  $\mu\text{L}$  per well in 24-well plates and treated with polyplexes at N\*/P 30. Just before the addition of polyplexes, the non-cell-permeable dye calcein was added to the cells to give a final concentration of 25  $\mu\text{g mL}^{-1}$ . Following incubation for different time periods, the cells were washed via centrifugation at 250  $\times g$  for 5 min. Prior to the washing step, the HEK293T cells were harvested by trypsinization and resuspension in FC-buffer, whereas the K-562 cells were only resuspended. Via flow cytometry, cells were analyzed as described in the instrumentation section (Additional file 1). Viable cells showing a calcein signal higher than the control cells incubated with calcein only were gated as percentage of cells that show strong calcein signal and the rMFI of all viable cells was calculated in relation to the control cells. The experiments were performed three times.



## Statistics

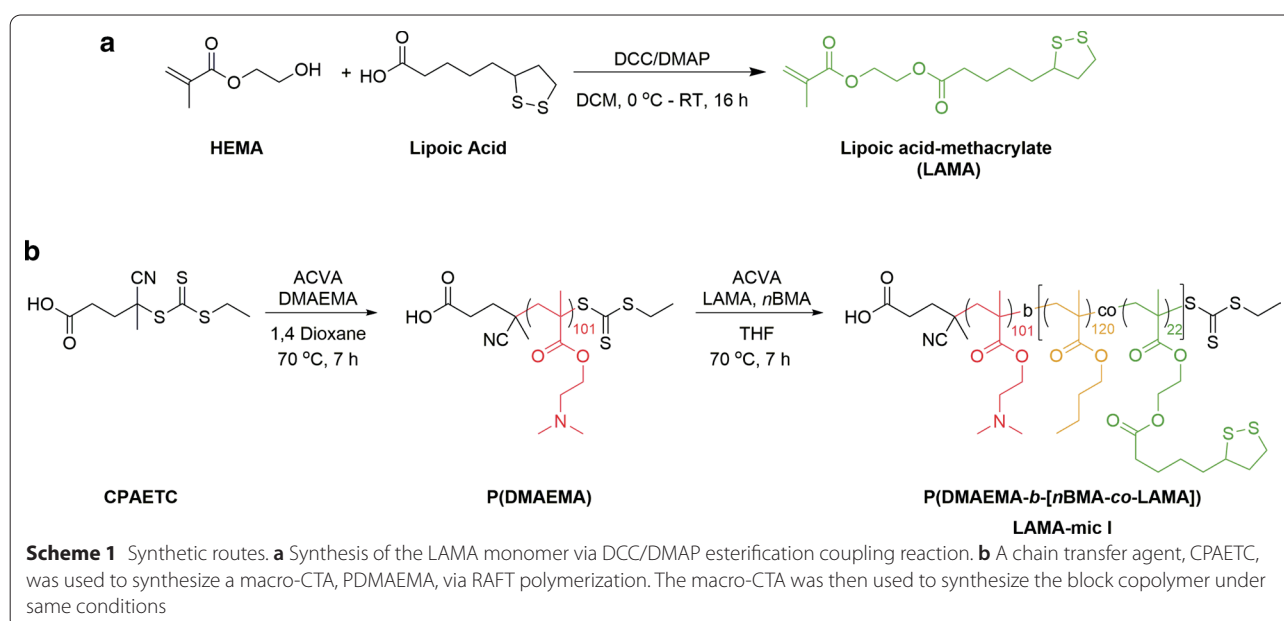
To determine the statistical significance, repeated measures analysis of variance (RM-ANOVA) was performed. If the RM-ANOVA revealed significant differences ( $p < 0.05$ ), post-hoc analyses with a Bonferroni correction were applied. If not stated otherwise, statistically significant differences to the control were indicated with \* for  $p < 0.05$ , \*\* for  $p < 0.01$ , and with \*\*\* for  $p < 0.001$ . All statistical analyses were performed with data of  $n \geq 3$  in Origin, Version 2018b (OriginLab Corporation, US). Further details can be found in the Additional file 1.

## Results and discussion

### Polymer synthesis and micelle formation

Lipoic acid has antioxidant potential and has been studied for treatment of different diseases. In addition, studies have shown that lipoic acid exhibits redox properties, thus, they can be used as a crosslinking agent when incorporated in micelles or nanoparticles [52]. Two approaches for incorporating functional groups into polymers include (i) coupling them to a monomer and (ii) post-modification of a polymer. In this study, we opted for the first method due to the advantages for quantification and analysis that are provided by this method. Lipoic acid-methacrylate (2-(methacryloyloxy)ethyl 5-(1,2-dithiolan-3-yl)pentanoate, LAMA), was synthesized by a *N,N'*-dicyclohexylcarbodiimide (DCC)/4-(dimethylamino)pyridine (DMAP) coupling reaction (Scheme 1a), which is a well-established method for esterification reactions [53].

The polymers were synthesized by RAFT polymerization with (4-cyano pentanoic acid)yl ethyl trithiocarbonate (CPAETC) as a chain transfer agent (CTA) and 4,4'-azobis(4-cyanovaleric acid) (ACVA) as the initiator. Firstly, a PDMAEMA homopolymer was synthesized to serve as a macro-CTA for block copolymer synthesis as well as a control polymer for biological studies (Scheme 1b). Previous research had demonstrated that homopolymers of DMAEMA as well as the acrylamide analogue dimethylamino ethyl acrylamide (DMAEAm) were less toxic than LPEI but exhibited decreasing viability of cells with increasing molar mass [50, 54]. For this reason, a target degree of polymerization (DP) of 100 was chosen for the cationic homopolymer and more importantly, to achieve desired spherical micelles of sizes less than 100 nm. The macro-CTA was subsequently chain-extended with LAMA and *n*BMA to form a block copolymer P(DMAEMA-*b*-[*n*BMA-*co*-LAMA]). *n*BMA was chosen because of its biological benefits, i.e. for the interaction with cell membranes [55]. While PDMAEMA was incorporated as the hydrophilic and pH-responsive segment, the LAMA monomer was statistically integrated into the hydrophobic block of *n*BMA. The overall composition (hydrophobic to hydrophilic) was optimized to facilitate the formation of spherical micelles. All polymerizations were carried out at 70 °C and stopped after 7 h to avoid high polydispersity due to dead chain formation. Monomer conversions were typically in the range of 65 to 70% for the homopolymers and 40 to 80% of the subsequently extended block (determined via <sup>1</sup>H NMR, Additional file 1: Table S3, Fig. S2). SEC analysis of the



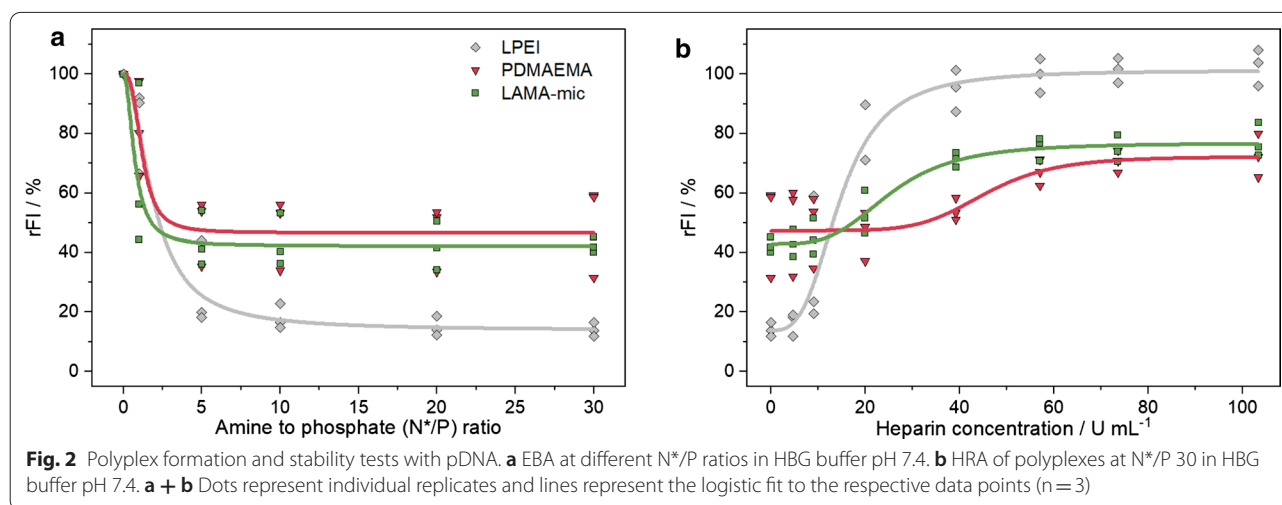
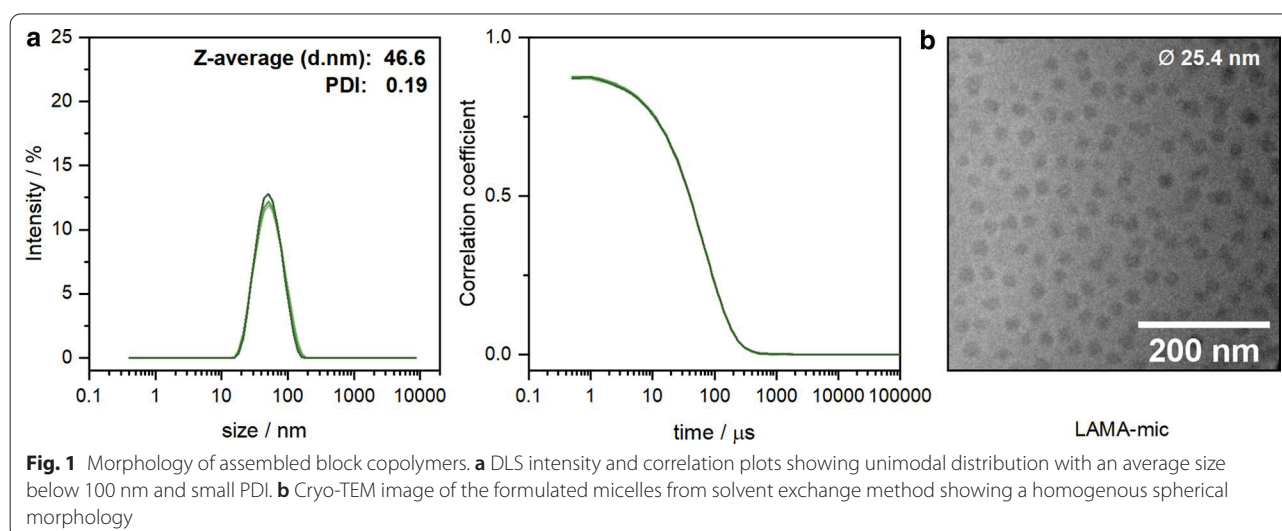
polymers showed narrow molar mass distributions ( $\mathcal{D} = 1.17$  for PDMAEMA and  $\mathcal{D} = 1.19$  for P(DMAEMA-*b*-[*n*BMA-*co*-LAMA]), Additional file 1: Fig. S1, S3).

Micelles of the diblock copolymers P(DMAEMA<sub>101</sub>-*b*-[*n*BMA<sub>120</sub>-*co*-LAMA<sub>22</sub>]) (LAMA-mic), were formed by solvent-exchange followed by dialysis in water. DLS measurements were conducted to determine the hydrodynamic size of the formulated micelles (Fig. 1a, Additional file 1: Table S4). The results showed a monomodal distribution with an average hydrodynamic radius of 47 nm and a polydispersity index of 0.19. It is worth noting that the size below 100 nm is favorable for endocytic uptake [56]. Additionally, cryo-TEM measurements were conducted to investigate the morphology of the particles (Fig. 1b). The images showed micelles featuring a spherical morphology with rather homogeneous particle size distributions ( $\varnothing 25.4 \pm 2.9$  nm). The slightly smaller

size measured by cryo-TEM compared to DLS is common due to the micellar shell and the hydrodynamic interactions measured by cryo-TEM showing little or no contrast.

### Polyplex formation and characterization

To investigate whether the targeted micelle, LAMA-mic, is able to bind genetic material such as pDNA, fluorescence-based assays as EBA and HRA were performed (Fig. 2). The EBA was conducted at different N\*/P ratios (molar ratio of amines of the polymer to phosphates of the genetic material) with a constant amount of pDNA. A decrease in the fluorescence signal of the pDNA-EtBr solution upon addition of the polymers indicated a successful formation of polyplexes due to the displacement of the EtBr from the pDNA. To investigate the stability



of the polyplex, the polyanionic polysaccharide heparin was added to polyplexes of N\*/P 30. Due to its negative charge, heparin can bind to the cationic moiety, replace the pDNA and EtBr can thus intercalate again into the pDNA, resulting in an increasing fluorescence intensity (FI). All tested polymers were shown to decrease the relative FI (rFI) in the EBA but to a different extent. The binding efficiency of the LAMA-mic ( $42 \pm 3\%$  rFI) was comparable to that of the PDMAEMA homopolymer ( $50 \pm 16\%$  rFI) demonstrating that the architecture has no influence here. However, the EtBr displacement with the LAMA-mic was not as strong as with LPEI ( $14 \pm 2\%$  rFI). A gel retardation assay (GRA) indicated a complete retention of the pDNA in polyplexes at  $N^*/P \geq 10$  for all polymers in contrast to the migration of pure pDNA (Additional file 1: Fig. S6). Since the increase in EtBr fluorescence intensity is based on an intercalation between the hydrophobic base pairs of the double helix, [57, 58] the EtBr displacement in case of the LAMA-mic and PDMAEMA may be distorted by the presence of more hydrophobic monomers (for logP values refer to Additional file 1: Table S6) and uncharged cationic moieties at pH 7.4, respectively.

Regarding polyplex stability, the influence of the micellar composition is more pronounced. While LPEI required only  $18 \text{ U mL}^{-1}$  heparin to release 70% of the pDNA, the LAMA-mic required double and PDMAEMA

nearly four times the amount of heparin, indicating an increased stability of the latter against anionic antagonists, which was also shown for other micellar systems [55]. The PDMAEMA-based systems reached plateaus around 70% rFI. This could be caused by hydrophobic interactions with the pDNA, e.g. by the hydrophobic monomers or uncharged DMAEMA moieties at pH 7.4, which are less influenced by an anionic reagent like heparin. Overall, the LAMA-mic exhibits strong pDNA binding properties required for efficient gene carriers.

### Cytotoxicity

Since the presence of cationic charges and hydrophobic side chains in polymers might be problematic for cells, [36, 59] the LAMA-mic was investigated regarding its cytotoxic effects in different cell lines. To assess the metabolic activity of the cells, the PrestoBlue™ assay was performed based on ISO10993-5 with L-929 cells (Fig. 3a). The cells incubated with LAMA-mic and the PDMAEMA homopolymer showed less cytotoxicity at higher concentrations than the commercial LPEI which served as control. At concentrations equal to N\*/P 30, which was later used to investigate the transfection efficiency, incubation with polymers resulted in cell viability above 70% in all cases, indicating good viabilities. The metabolic activity was further investigated in HEK293T and K-562 cells applying polyplexes at N\*/P

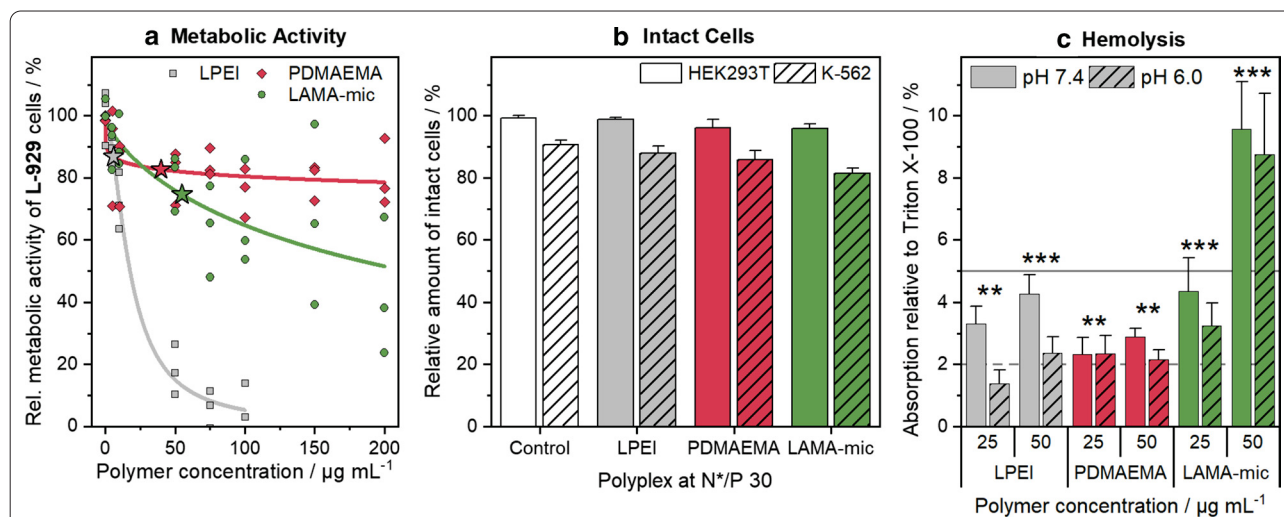


**Fig. 3** Toxicity of LAMA-mic in different cell lines. **a** PrestoBlue™ assay in L-929 cells following incubation with respective polymers at indicated concentrations for 24 h. Dots represent values of single repetitions and lines represent logistic fit functions ( $n = 3$ ). Stars indicate polymer concentrations used for N\*/P 30 in transfection assays. **b** LDH-assay in HEK293T and K-562 cells following incubation with polyplexes of respective polymers and pDNA at N\*/P 30 for 24 h. Values were calculated relative to the positive control Triton X-100 (100% LDH release  $\hat{=}$  0% viability) and represent mean  $\pm$  SD ( $n = 3$ ). **c** Hemolysis as the amount of released hemoglobin calculated relative to 1% Triton X-100 as positive control (100% hemolysis). Human erythrocytes were washed and incubated with polymers at indicated concentrations in PBS of different pH values without serum. Values represent mean  $\pm$  SD ( $n = 3$ ) and are classified as slightly hemolytic between 2% and 5%, and as non- or hemolytic if lower or higher than 2% or 5%, respectively. Regarding significant differences, the main effects of the treatment were determined since there was no significant interaction of pH value and treatment

30 (Additional file 1: Fig. S7A). Especially in HEK293T cells, the LAMA-mic exhibited lower metabolic activity ( $57 \pm 8\%$  viable cells), although the cells did not appear to be dead when observed by light microscopy (Additional file 1: Fig. S8). Upon treatment with the LAMA-mic, HEK293T cells exhibited a rounded shape, formed spheroids, and started to detach. This phenomenon was observed for other polymers as well, [60] but more detailed investigations are required to understand the principle mechanism for this material, which was not the focus of this study.

To ensure that the decreased metabolic activity was not caused by a removal of viable yet detached cells during the washing steps or by the assay reagent not reaching the center of the HEK293T spheroids, other assays employing different cytotoxicity mechanisms were performed. The influence of the polyplexes on the membrane integrity was investigated using the LDH-assay and propidium iodide staining in combination with flow cytometry (Fig. 3b, Additional file 1: Fig. S7B, C). In both assays, an entering of the reagent into the cells is not necessary and the supernatant is measured either pure (LDH-assay) or together with the single cell suspension by re-addition after trypsinization (flow cytometry). The LDH-assay is based on resazurin, measuring the activity of the enzyme LDH after its release into the medium if the membrane integrity of the cells was destroyed. In flow cytometry, on the other hand, dead cells can be identified due to their changes in shape and granularity in the FSC/SSC plot. Propidium iodide staining was used as a further identification of dead cells to adjust the analysis parameters. HEK293T cells treated with the LAMA-mic exhibited viabilities above 90% with both methods, LDH-release and FSC/SSC, whereas K-562 cells showed nearly the same viability as observed in the PrestoBlue™ assay (70 to 80% viable cells). These results indicate that the LAMA-mic is not or only slightly influencing the membrane integrity of HEK293T and K-562 cells, respectively, and that the spheroid formation of the HEK293T cells could be a result of the LAMA-mic's influence on the interaction between HEK293T cells and the surface of the cultivation vessel rather than of toxic effects.

The impact of the polymers on membranes was investigated using human erythrocytes in hemolysis (Fig. 3c) and aggregation assays (Additional file 1: Fig. S9). Following serum removal, the cells were resuspended in PBS of pH values present in blood/cytoplasm (pH 7.4) or endosomal compartments (pH 6) and incubated with the polymers for 1 h, followed by centrifugation and absorption measurement of the released hemoglobin in the supernatant. Whereas LPEI and PDMAEMA were only slightly hemolytic ( $\leq 4.4\%$  hemoglobin release), the LAMA-mic showed doubled hemolytic activity at  $50 \mu\text{g}$

$\text{mL}^{-1}$ , indicating a contribution of the micellar hydrophobic core or the locally increased amount of cationic charges due to micellar architecture to membrane interaction. With the exception of LPEI, there was no significant influence of pH value on hemolysis ( $p = 0.06$ ).

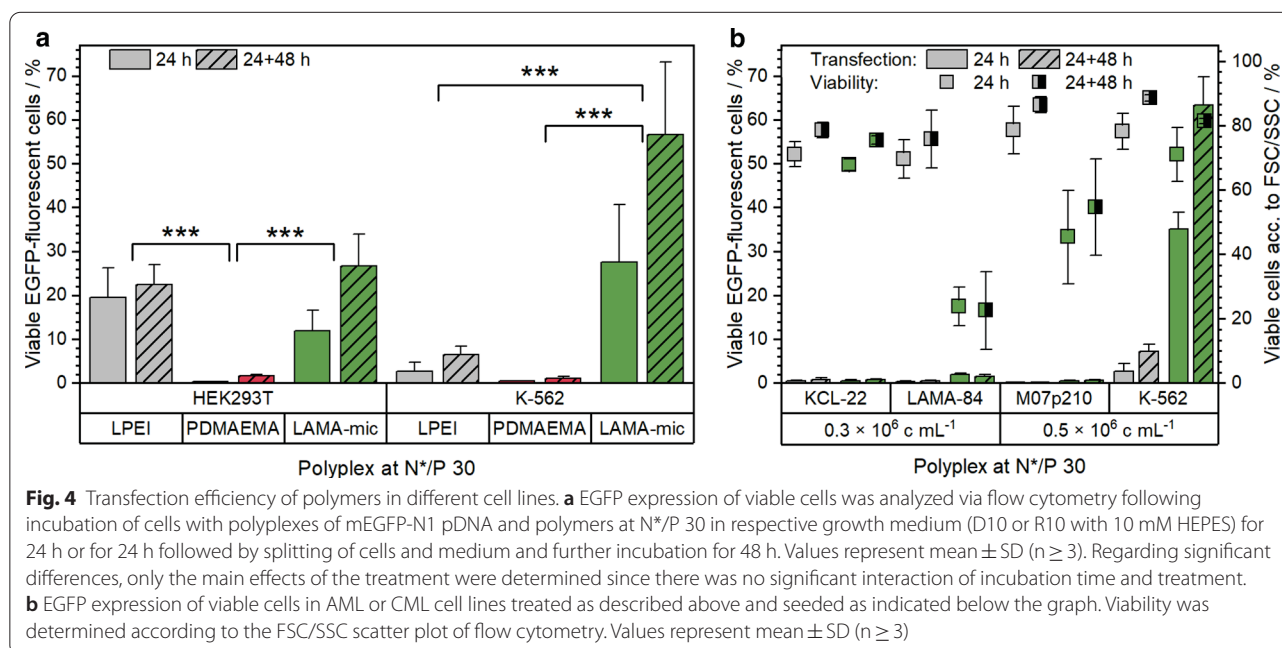
The observed low toxicity for PDMAEMA is consistent with results of previous studies [54, 61]. However, the increased membrane interactions of the LAMA-mic are not too surprising as the integration of hydrophobic moieties (e.g. *n*BMA) is known for this effect [62, 63].

### Transfection efficiency

The gene delivery to suspension cells is for unresolved reasons less efficient in comparison to adherent cells [8]. Therefore, the transfection efficiency of the polymers was investigated by treating HEK293T and K-562 cells with polyplexes of polymers and pDNA encoding for EGFP at the optimal N\*/P ratio 30. Following incubation (24 h or 24 h with additional 48 h in growth media), cells were analyzed via flow cytometry regarding the amount of viable and EGFP-positive cells (Fig. 4a) and the relative mean fluorescence intensity (rMFI) of all viable single cells (Additional file 1: Fig. S10).

In both cell lines, the LAMA-mic showed an increased number of EGFP-positive cells but with peculiar differences. Whereas in HEK293T cells the transfection efficiency of LAMA-mic and LPEI were comparable after 24 h, the LAMA-mic outperformed LPEI by more than seven times in K-562 cells ( $29 \pm 12\%$  vs.  $2 \pm 2\%$  viable EGFP-positive cells,  $p < 0.001$ ). Interestingly, the transfection efficiency of the LAMA-mic increased almost twofold in both cell lines following incubation in growth media for further 48 h, although being only significant in K-562 cells ( $p(\text{HEK293T}) = 0.15$ ,  $p(\text{K-562}) = 0.03$ ). This could indicate a slower, continuous transfection mechanism (i.e. polyplex uptake and endosomal escape) for the LAMA-mic, whereas LPEI could reach its maximum already after 24 h. In contrast, the homopolymer PDMAEMA showed nearly no transfected cells in both cell lines ( $< 2\%$  EGFP-positive cells). This is in accordance to previous studies of PDMAEMA [54, 61, 64]. Successful transfections with PDMAEMA could only be observed at higher molecular weight and/or higher pDNA concentration [65, 66].

Since the LAMA-mic results in a remarkably efficient gene expression in K-562 cells, even without the addition of transferrin and although these cells are considered to be difficult to transfect, the following sections will discuss, which parameter can be responsible for this. One reason could be the altered metabolism of these cells due to the generation of the *BCR-ABL* oncogene encoding for the BCR-ABL fusion protein [67, 68]. Hence,



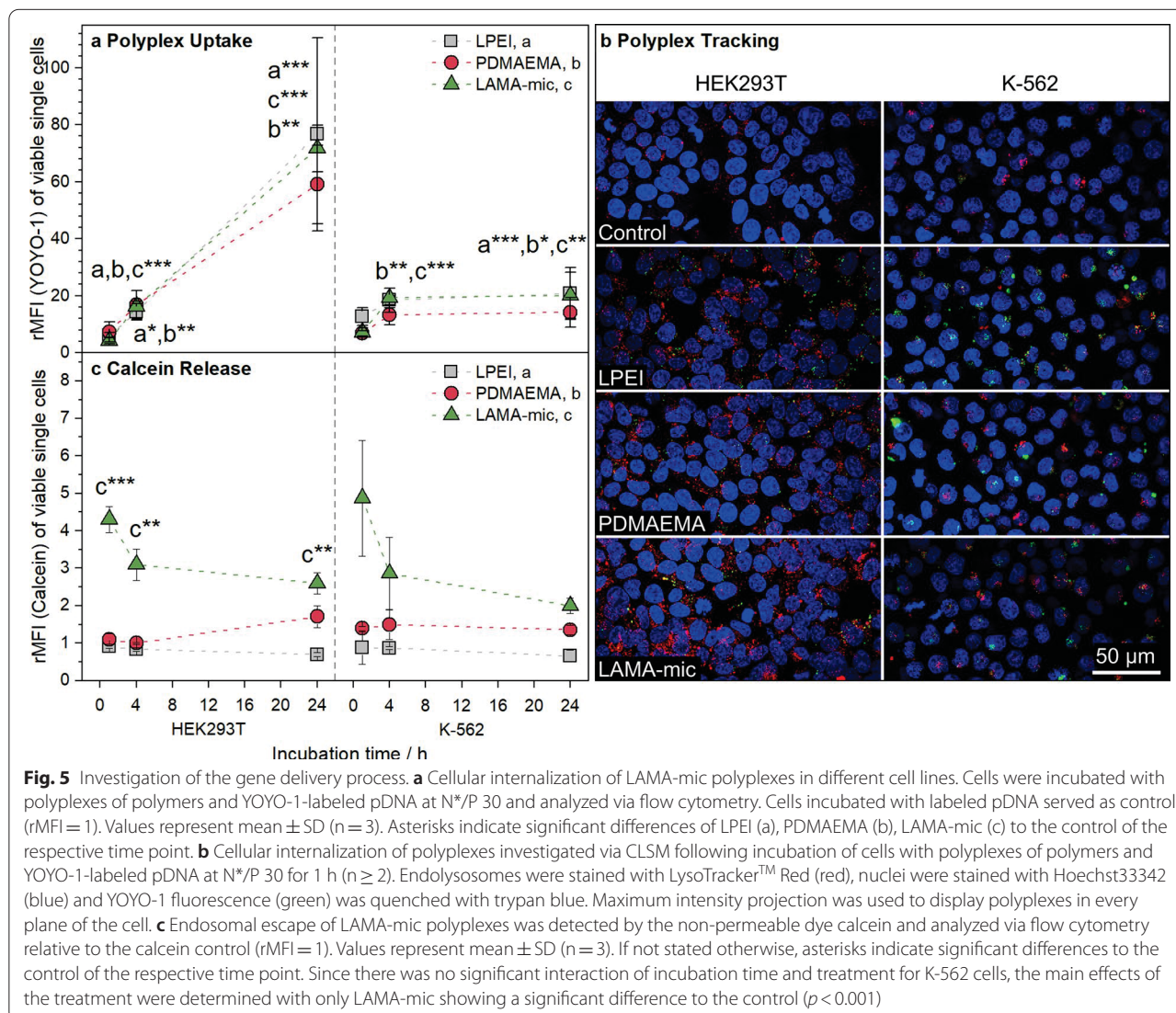
the transfection efficiency of the LAMA-mic was investigated in the additional BCR-ABL positive CML cell lines LAMA-84 and KCL-22, and in the AML cell line M07p210 expressing the fusion protein as well. As shown in Fig. 4b, none of the cell lines could be transfected with the same conditions which were successful in K-562 cells. On the contrary, the LAMA-84 and M07p210 cells showed severe toxicity following incubation with the LAMA-mic implying that BCR-ABL is not the crucial point for the transfection efficiency of the LAMA-mic, and that there must be other/additional parameters whose determination will need more profound investigations, e.g. regarding the influence of differences in signaling and metabolism of the cell lines [69] on the transfection efficiency.

#### Transfection mechanism of LAMA-mic

For elucidation of the LAMA-mic's high transfection efficiency in the suspension cell line K-562, two crucial cellular issues of gene delivery, namely, the cellular uptake and the endosomal release, were studied in more detail. To assess the polyplex uptake, K-562 and HEK293T cells were incubated with YOYO-1 labelled polyplexes at N\*/P 30 for different time periods and analyzed via flow cytometry regarding the amount of YOYO-1 positive cells (Additional file 1: Fig. S12A) and rMFI of all viable single cells or via CLSM regarding the intracellular distribution of the polyplexes (Fig. 5a, b and S15-16). For CLSM studies, the cells were additionally labeled with LysoTracker<sup>TM</sup> Red for endolysosomes and Hoechst 33342 for nuclei. Both cell lines show YOYO-1

positive cells after 1 h already with some of the polyplexes located in acidic compartments. It is remarkable that no significant differences between the polymers were observed regarding the rMFI in flow cytometry. To the contrary, the uptake patterns of the cell lines were found to be different. Only PDMAEMA showed slightly lower rMFI values in both cell lines. In HEK293T cells, a time-dependent uptake was found for all polyplexes, whereas in K-562 cells the uptake reached a constant level after 4 h. After 1 h and consistent with the CLSM images, the uptake in K-562 cells was slightly higher than in HEK293T cells, whereas after 24 h, the uptake in HEK293T was almost four times as high as in K-562 cells. A low endocytosis rate by suspension cells was also observed in other studies [20, 70]. This may also be associated with increased exocytosis, where the uptaken polyplexes are removed at a rate comparable to the rate they are taken up. As these results do not correlate to the observed transfection efficiencies, the observed differences of cellular uptake are not a critical aspect for the LAMA-mic in K562 cells.

Moreover, the endosomal escape was investigated using the calcein release assay. Calcein is a non-membrane-permeable dye taken up by endosomes. If a polymer is able to escape the endosome by attacking the endosomal membrane, calcein can be released into the cytoplasm, causing a diffuse fluorescence pattern, which can be detected via flow cytometry, e.g. in an alteration in the pattern of the FITC channel (Additional file 1: Fig. S14). Therefore, the cells were incubated with calcein and polyplexes at N\*/P 30 for different periods of time and



were analyzed via flow cytometry (Additional file 1: Fig. S12B and Fig. 5b). In contrast to the pDNA uptake, the endosomal release showed almost no dependence on the cell line but on the polymer used. In both cell lines the LAMA-mic exhibited a significantly better release of calcein ( $p < 0.01$ ), in particular during the first hours (1–4 h), indicating the potential of block copolymers for endosomal release also in difficult to transfect cell lines.

#### Influence of lipolic acid on stability and transfection efficiency

To investigate the role of lipolic acid for the improved transfection efficiency of the LAMA-mic in detail, an additional set of polymers was prepared comprising two polymers without lipolic acid, P(DMAEMA<sub>89</sub>-*b*-*n*BMA<sub>68</sub>) and P(DMAEMA<sub>89</sub>-*b*-[*n*BMA<sub>92</sub>-*co*-HEMA<sub>17</sub>]) (see Additional file 1: Table S3). The first resembled an amphiphilic

block copolymer, which lacks the LAMA moiety, while the second was synthesized to mimic a hydrolyzed and cleaved lipolic acid from the original LAMA copolymer. Another version of the LAMA-mic (P(DMAEMA<sub>89</sub>-*b*-[*n*BMA<sub>101</sub>-*co*-LAMA<sub>19</sub>]) copolymer, LAMA-mic II) was synthesized for the comparison of all polymers with the same macro-CTA. The polymeric micelles (BMA-mic, HEMA-mic and LAMA-mic II) were spherical, unimodal and similar in size (Additional file 1: Table S4, Fig. S4, S5).

To investigate the influence of lipolic acid on the micelle stability, the critical micelle concentration (CMC) was determined using Nile Red encapsulation as a fluorescence probe (Additional file 1: Fig. S18) [71]. The results showed comparable CMC values for all micelles below the concentrations used for cell experiments (LAMA-mic II: 29, HEMA-mic: 30, BMA-mic: 26  $\mu\text{g mL}^{-1}$ ) indicating the presence of mainly micelles with comparable

physicochemical properties during transfection (Additional file 1: Table S5). Additionally, the polyplex stability was investigated by DLS following dilution of the respective polyplexes to concentrations used for transfection (Additional file 1: Fig. S17, Table S4). Although the sizes of the micelles hardly changed, the correlation coefficient of lipoic acid free HEMA- and BMA-mic decreased, whereas it remained constant in the case of LAMA-mic

II polyplexes, indicating a synergistic stabilizing effect of lipoic acid and the hydrophobic monomers.

With suitable polymers available, HEK293T and K-562 cells were incubated and analyzed as described before with the corresponding polyplexes at N\*/P 15 and 30 (Fig. 6a, b). When comparing the different micelles, the micelles without lipoic acid were also able to transfect HEK293T cells, although to a slightly lesser extent. In K-562 cells, the transfection efficiency of the LAMA-mic

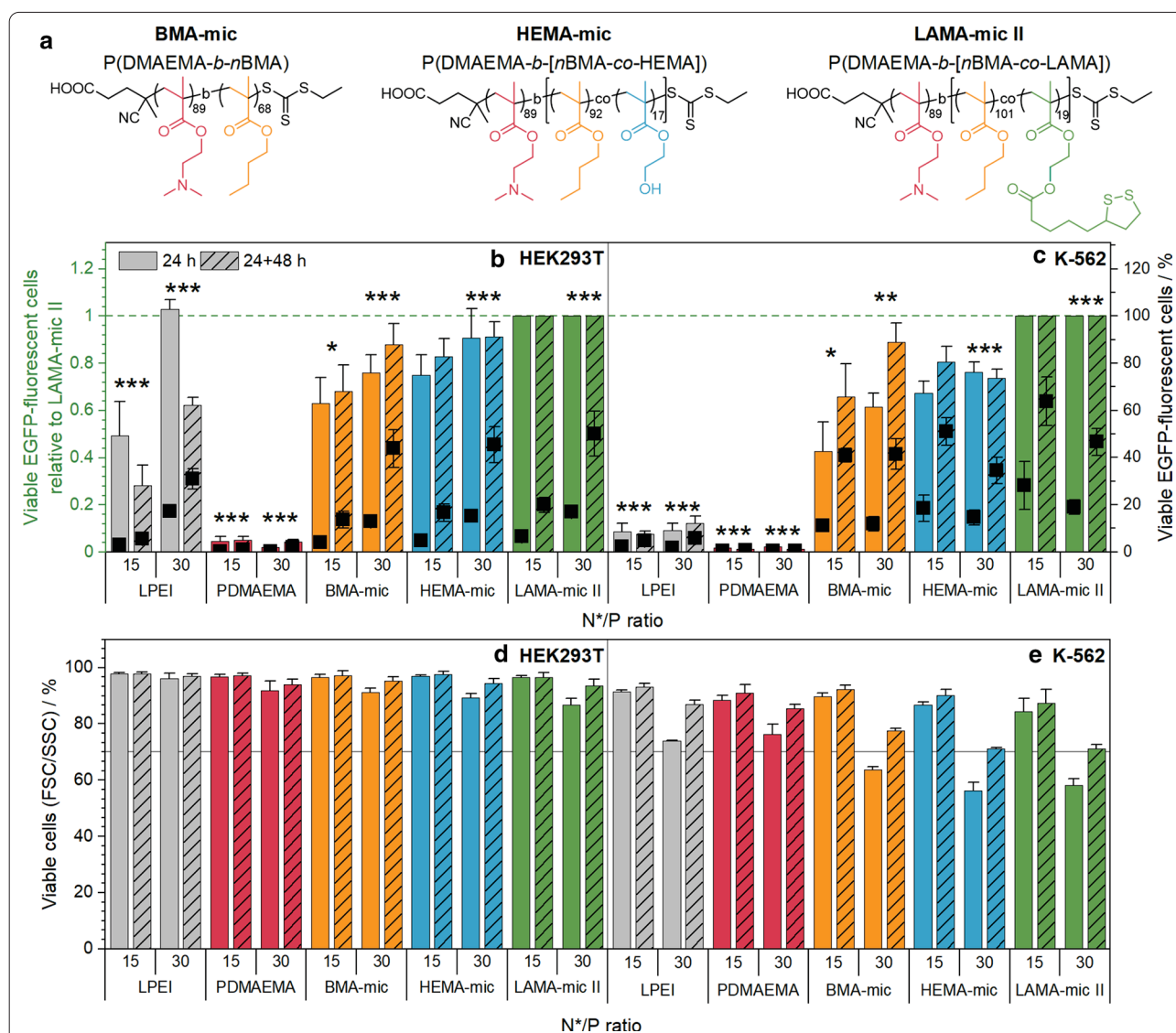


**Fig. 6** Transfection efficiency and toxicity of LAMA-mic compared to control micelles. **a** Overview of the structures of the additional polymer set. **b + c** EGFP expression of viable cells was analyzed via flow cytometry following incubation of cells with polyplexes of mEGFP-N1 pDNA and polymers at N\*/P 30, in respective growth medium (D10 or R10 with 10 mM HEPES) either for 24 h or for 24 h followed by splitting of cells and medium and further incubation for 48 h. Values represent mean  $\pm$  SD (n = 3) of EGFP-positive cells relative (columns) and not relative (squares) to the respective LAMA-mic treatment. **d + e** Viability was determined according to the FSC/SSC scatter plot of flow cytometry. Values represent mean  $\pm$  SD (n = 3). **b + d** HEK293T cells. **c + e** K-562 cells. Regarding significant differences, the main effects of the treatment were determined since there was no significant interaction of incubation time and treatment. \*: significant difference to LAMA-mic II, N\*/P 15 ( $p < 0.05$ ). \*\*: significant difference to LAMA-mic II, N\*/P 15 ( $p < 0.01$ ). \*\*\*: significant difference to LAMA-mic II, N\*/P 15 ( $p < 0.001$ )

II polyplexes at N\*/P 15 was significantly higher than the polyplexes of the other micelles at N\*/P 30 (HEMA-mic:  $22 \pm 11\%$  points, ppt;  $p < 0.001$ ; BMA-mic:  $19 \pm 4$  ppt,  $p = 0.002$ ) indicating an increase in efficiency by the incorporation of lipoic acid into micelles. The FSC/SSC plot of the flow cytometer was used to investigate the cytotoxicity of the polyplexes at the applied concentrations (Fig. 6c, d). Whereas the HEK293T cells showed no viabilities less than 89% in all cases, the K-562 cells exhibited decreased viability, in particular at N\*/P 30 after 24 h (BMA-mic:  $64 \pm 1\%$ , HEMA-mic:  $56 \pm 3\%$ , LAMA-mic II:  $58 \pm 2\%$  viable cells). Nevertheless, the K-562 cells could recover as indicated by an increase in viability to more than 70% viable cells following splitting and incubation for further 48 h, which is linked to higher transfection efficiency at N\*/P 15, especially for LAMA-mic II (black squares in Fig. 6a, b). For HEK293T cells, however, the increase in efficiency was less pronounced compared to the K-562 cells.

In summary, all three micelle systems represent promising candidates for efficient gene delivery to K-562 cells with the higher transfection efficiency of the LAMA-mic II indicating a synergistic effect for the lipoic acid and the architecture.

## Conclusions

Since the cells of our immune system and blood are known to be hard to transfect or modulate, diseases like CML still suffer problems like drug resistance or poor treatment response. Polymeric nanocarriers could be a solution to enhance interaction with blood cells and to increase the intracellular concentration of active agents. Therefore, a well-defined lipoic acid containing diblock copolymer, P(DMAEMA<sub>101</sub>-*b*-[*n*BMA<sub>124</sub>-*co*-LAMA<sub>22</sub>]), was synthesized *via* RAFT polymerization and formulated into defined spherical micelles (LAMA-mic) to investigate its transfection efficiency of pDNA in different cell lines, including the CML cell line K-562. The LAMA-mic is able to bind and release the genetic cargo, caused low toxicity at used concentrations and exhibited transfection efficiencies comparable to that of the commercial control LPEI in HEK293T cells. Remarkably, whereas LPEI showed almost no transfection in K-562 suspension cells, the LAMA-mic exhibited an increase in EGFP-positive cells by more than sevenfold. Compared to the homopolymer PDMAEMA, the 54-fold increase in transfection efficiency was even more impressive and demonstrated the impact of the polymer design and/or architecture. This transfection efficiency does not seem to depend on the BCR-ABL fusion protein as a crucial point, since no other tested CML or AML cell line with this fusion protein could be transfected. Further mechanistic studies were performed regarding endosomal

escape and polyplex uptake kinetics, which however could not be correlated to the performance of the polymers. In contrast to LPEI, the LAMA-mic showed good endosomal escape in both cell lines, pointing to potentially different escape mechanisms. The polymers did not show any effect on cellular uptake, although the cell line itself made a difference.

To investigate the effect of the lipoic acid functionality on transfection efficiency, two precursor polymers without the LAMA monomer, BMA-mic and HEMA-mic, were synthesized and formulated into micelles of comparable sizes and CMCs. It was found that the incorporation of lipoic acid into the core of a hydrophobic-cationic micelle enhances its gene delivery efficacy, especially in the difficult-to-transfect K-562 suspension cells. However, the influence of the architecture in general was more pronounced, as all micelles showed good efficiencies. Therefore, the LAMA-mic represents a promising nanocarrier system for gene delivery in hard-to-transfect blood cells.

## Supplementary Information

The online version contains supplementary material available at <https://doi.org/10.1186/s12951-021-00801-y>.

**Additional file 1.** Description of further methods and results.

## Acknowledgements

The authors gratefully acknowledge Carolin Kellner and Bärbel Beringer-Siemers for taking splendid care of the different cell lines and performing toxicity assays. Furthermore, the authors gratefully acknowledge Elisabeth Moek for assistance in transfection assays, and her as well as Elisabeth Preußner, Carolin Kellner and Bärbel Beringer-Siemers for fruitful discussions. The authors gratefully acknowledge Dr. Turgay Yildirim and Daniel Schnoor for preliminary studies. Furthermore, the authors thankfully acknowledge Prof. U. S. Schubert for providing excellent facilities.

## Authors' contributions

FR: Conceptualization, Investigation, Methodology, Writing—Preparation of the manuscript, Visualization; PM: Conceptualization, Investigation, Writing—Preparation of the manuscript; LM: Methodology, Writing—Correction of the manuscript; JS: Methodology, Writing—Correction of the manuscript; FH: Methodology, Writing—Correction of the manuscript; JJF: Writing—Correction of the manuscript, Consulting; TE: Writing—Correction of the manuscript; SH: cryo-TEM investigations, Writing—Correction of the manuscript; JCB: Writing—Correction of the manuscript, Funding acquisition; AT: Conceptualization, Supervision, Writing—Editing of the Manuscript, Project administration, Funding acquisition. All authors read and approved the final manuscript.

## Funding

Open Access funding enabled and organized by Projekt DEAL. This work was supported by the Bundesministerium für Bildung und Forschung (BMBF, Germany, #13XP5034A PolyBioMik); the German Research Foundation (DFG, Emmy-Noether Programme, Projekt ID: 358263073); and by the DFG-funded Collaborative Research Centre PolyTarget (SFB 1278, project B01, Z01, project ID: 316213987). Cryo-TEM investigations were performed at the Electron Microscopy facilities of the Jena Center for Soft Matter (JCSM), which was established with grants from the DFG and the European Fund for Regional Development (EFRE). The LSM880 ELYRA PS.1 was further funded with a grant from the DFG.



**Availability of data and materials**

The datasets used and/or analyzed during the current study are available from the corresponding author on reasonable request. Supporting information available: Material, additional methods and results, Additional file 1: Fig. S1–S18, Tables S1–S6.

**Ethics approval and consent to participate**

Not applicable.

**Consent for publication**

Not applicable.

**Competing interests**

The authors declare that they have no competing interests.

**Author details**

<sup>1</sup> Laboratory of Organic and Macromolecular Chemistry (IOMC), Friedrich Schiller University Jena, Humboldtstrasse 10, 07743 Jena, Germany. <sup>2</sup> Klinik für Innere Medizin II, Abteilung Hämatologie und Internistische Onkologie, Universitätsklinikum Jena, Am Klinikum 1, 07747 Jena, Germany. <sup>3</sup> Jena Center for Soft Matter (JCSM), Friedrich Schiller University Jena, Philosophenweg 7, 07743 Jena, Germany.

Received: 6 October 2020 Accepted: 9 February 2021

Published online: 06 March 2021

**References**

- Zhang P, Wagner E. History of polymeric gene delivery systems. *Top Curr Chem (Cham)*. 2017;375:26.
- Shim G, Kim D, Le QV, Park GT, Kwon T, Oh YK. Nonviral delivery systems for cancer gene therapy: strategies and challenges. *Curr Gene Ther*. 2018;18:3–20.
- Durymanov M, Reineke J. Non-viral delivery of nucleic acids: insight into mechanisms of overcoming intracellular barriers. *Front Pharmacol*. 2018;9:971.
- Bono N, Ponti F, Mantovani D, Candiani G. Non-viral in vitro gene delivery: it is now time to set the bar! *Pharmaceutics*. 2020;12:183.
- Helal NA, Osami A, Helmy A, McDonald T, Shaaban LA, Nounou MI. Non-viral gene delivery systems: hurdles for bench-to-bedside transformation. *Pharmazie*. 2017;72:627–93.
- Olden BR, Cheng Y, Yu JL, Pun SH. Cationic polymers for non-viral gene delivery to human T cells. *J Control Release*. 2018;282:140–7.
- Gresch O, Engel FB, Nestic D, Tran TT, England HM, Hickman ES, Korner I, Gan L, Chen S, Castro-Obregon S, et al. New non-viral method for gene transfer into primary cells. *Methods*. 2004;33:151–63.
- Basiouni S, Fuhrmann H, Schumann J. High-efficiency transfection of suspension cell lines. *Biotechniques*. 2012;53:1–4.
- Mellott AJ, Forrest ML, Detamore MS. Physical non-viral gene delivery methods for tissue engineering. *Ann Biomed Eng*. 2013;41:446–68.
- Riedl SAB, Kaiser P, Raup A, Synatschke CV, Jerome V, Freitag R. Non-viral transfection of human T lymphocytes. *Processes*. 2018;6:1–17.
- Ross DM, Branford S, Seymour JF, Schwarzer AP, Arthur C, Yeung DT, Dang P, Goynes JM, Slader C, Filshie RJ, et al. Safety and efficacy of imatinib cessation for CML patients with stable undetectable minimal residual disease: results from the TWISTER study. *Blood*. 2013;122:515–22.
- Hochhaus A, Bacarani M, Silver RT, Schiffer C, Apperley JF, Cervantes F, Clark RE, Cortes JE, Deininger MW, Guilhot F, et al. European LeukemiaNet 2020 recommendations for treating chronic myeloid leukemia. *Leukemia*. 2020;34:966–84.
- Mahon FX. Treatment-free remission in CML: who, how, and why? *Hematology Am Soc Hematol Educ Program*. 2017;2017:102–9.
- Hussein Kamareddine M, Ghosn Y, Tawk A, Elia C, Alam W, Makdessi J, Farhat S. Organic nanoparticles as drug delivery systems and their potential role in the treatment of chronic myeloid leukemia. *Technol Cancer Res Treat*. 2019;18:1533033819879902.
- Lin G, Zhang H, Huang L. Smart polymeric nanoparticles for cancer gene delivery. *Mol Pharm*. 2015;12:314–21.
- Kursa M, Walker GF, Roessler V, Ogris M, Roedel W, Kircheis R, Wagner E. Novel shielded transferrin—polyethylene glycol—polyethylenimine/DNA complexes for systemic tumor-targeted gene transfer. *Bioconj Chem*. 2003;14:222–31.
- Ogris M, Steinlein P, Kursa M, Mechtler K, Kircheis R, Wagner E. The size of DNA/transferrin-PEI complexes is an important factor for gene expression in cultured cells. *Gene Ther*. 1998;5:1425–33.
- Ogris M, Steinlein P, Carotta S, Brunner S, Wagner E. DNA/polyethylenimine transfection particles: influence of ligands, polymer size, and PEGylation on internalization and gene expression. *AAPS PharmSci*. 2001;3:E21–1.
- Remant KC, Thapa B, Valencia-Serna J, Domun SS, Dimitroff C, Jiang X, Uludag H. Cholesterol grafted cationic lipopolymers: potential siRNA carriers for selective chronic myeloid leukemia therapy. *J Biomed Mater Res A*. 2020;108:565–80.
- Valencia-Serna J, Gul-Uludag H, Mahdipoor P, Jiang X, Uludag H. Investigating siRNA delivery to chronic myeloid leukemia K562 cells with lipophilic polymers for therapeutic BCR-ABL down-regulation. *J Control Release*. 2013;172:495–503.
- Valencia-Serna J, Aliabadi HM, Manfrin A, Mohseni M, Jiang X, Uludag H. siRNA/lipopolymer nanoparticles to arrest growth of chronic myeloid leukemia cells in vitro and in vivo. *Eur J Pharm Biopharm*. 2018;130:66–70.
- Muhammad K, Zhao J, Gao B, Feng Y. Polymeric nano-carriers for on-demand delivery of genes via specific responses to stimuli. *J Mater Chem B*. 2020;8:9621–41.
- Quinn JF, Davis TP, Barner L, Barner-Kowollik C. The application of ionizing radiation in reversible addition–fragmentation chain transfer (RAFT) polymerization: renaissance of a key synthetic and kinetic tool. *Polymer*. 2007;48:6467–80.
- Sohn CH, Gao J, Thomas DA, Kim TY, Goddard III WA, Beauchamp JL. Mechanisms and energetics of free radical initiated disulfide bond cleavage in model peptides and insulin by mass spectrometry. *Chem Sci*. 2015;6:4550–60.
- Moad G, Rizzardo E, Thang SH. CHAPTER 6. Fundamentals of RAFT polymerization. In: *Fundamentals of controlled/living radical polymerization*. The Royal Society of Chemistry; 2013, pp 205–249. *Polymer Chemistry Series*.
- Wang H, Ding S, Zhang Z, Wang L, You Y. Cationic micelle: a promising nanocarrier for gene delivery with high transfection efficiency. *J Gene Med*. 2019;21:e3101.
- Uchida S, Kataoka K. Design concepts of polyplex micelles for in vivo therapeutic delivery of plasmid DNA and messenger RNA. *J Biomed Mater Res A*. 2019;107:978–90.
- Yousefpour Marzbali M, Yari Khosroushahi A. Polymeric micelles as mighty nanocarriers for cancer gene therapy: a review. *Cancer Chemother Pharmacol*. 2017;79:637–49.
- Cabral H, Miyata K, Osada K, Kataoka K. Block copolymer micelles in nanomedicine applications. *Chem Rev*. 2018;118:6844–92.
- Mai Y, Eisenberg A. Self-assembly of block copolymers. *Chem Soc Rev*. 2012;41:5969–85.
- Rao JP, Geckeler KE. Polymer nanoparticles: preparation techniques and size-control parameters. *Prog Polym Sci*. 2011;36:887–913.
- van de Wetering P, Moret EE, Schuurmans-Nieuwenbroek NM, van Steenberg M, Hennink WE. Structure–activity relationships of water-soluble cationic methacrylate/methacrylamide polymers for nonviral gene delivery. *Bioconj Chem*. 1999;10:589–97.
- Agarwal S, Zhang Y, Maji S, Greiner A. PDMAEMA based gene delivery materials. *Mater Today*. 2012;15:388–93.
- Wakefield DH, Klein JJ, Wolff JA, Rozema DB. Membrane activity and transfection ability of amphiphatic polycations as a function of alkyl group size. *Bioconj Chem*. 2005;16:1204–8.
- Convertine AJ, Benoit DS, Duvall CL, Hoffman AS, Stayton PS. Development of a novel endosomolytic diblock copolymer for siRNA delivery. *J Control Release*. 2009;133:221–9.
- Liu ZH, Zhang ZY, Zhou CR, Jiao YP. Hydrophobic modifications of cationic polymers for gene delivery. *Prog Polym Sci*. 2010;35:1144–62.
- Incani V, Lavasanifar A, Uludag H. Lipid and hydrophobic modification of cationic carriers on route to superior gene vectors. *Soft Matter*. 2010;6:2124–38.
- Sprouse D, Jiang Y, Laaser JE, Lodge TP, Reineke TM. Tuning cationic block copolymer micelle size by pH and ionic strength. *Biomacromol*. 2016;17:2849–59.

39. Li YL, Zhu L, Liu Z, Cheng R, Meng F, Cui JH, Ji SJ, Zhong Z. Reversibly stabilized multifunctional dextran nanoparticles efficiently deliver doxorubicin into the nuclei of cancer cells. *Angew Chem Int Ed Engl*. 2009;48:9914–8.
40. Bast A, Haenen GRMM. The toxicity of antioxidants and their metabolites. *Environ Toxicol Phar*. 2002;11:251–8.
41. Gomes MB, Negrato CA. Alpha-lipoic acid as a pleiotropic compound with potential therapeutic use in diabetes and other chronic diseases. *Diabetol Metab Syndr*. 2014;6:80.
42. Talelli M, Barz M, Rijcken CJ, Kiessling F, Hennink WE, Lammers T. Core-crosslinked polymeric micelles: principles, preparation, biomedical applications and clinical translation. *Nano Today*. 2015;10:93–117.
43. Wei R, Cheng L, Zheng M, Cheng R, Meng F, Deng C, Zhong Z. Reduction-responsive disassemblable core-cross-linked micelles based on poly(ethylene glycol)-b-poly(N-2-hydroxypropyl methacrylamide)-lipoic acid conjugates for triggered intracellular anticancer drug release. *Biomacromol*. 2012;13:2429–38.
44. Wu L, Zou Y, Deng C, Cheng R, Meng F, Zhong Z. Intracellular release of doxorubicin from core-crosslinked polypeptide micelles triggered by both pH and reduction conditions. *Biomaterials*. 2013;34:5262–72.
45. Xu Y, Meng F, Cheng R, Zhong Z. Reduction-sensitive reversibly crosslinked biodegradable micelles for triggered release of doxorubicin. *Macromol Biosci*. 2009;9:1254–61.
46. Li RQ, Wu W, Song HQ, Ren Y, Yang M, Li J, Xu FJ. Well-defined reducible cationic nanogels based on functionalized low-molecular-weight PGMA for effective pDNA and siRNA delivery. *Acta Biomater*. 2016;41:282–92.
47. Zheng M, Zhong Y, Meng F, Peng R, Zhong Z. Lipoic acid modified low molecular weight polyethylenimine mediates nontoxic and highly potent in vitro gene transfection. *Mol Pharm*. 2011;8:2434–43.
48. Tschiche A, Thota BN, Neumann F, Schafer A, Ma N, Haag R. Crosslinked Redox-Responsive Micelles Based on Lipoic Acid-Derived Amphiphiles for Enhanced siRNA Delivery. *Macromol Biosci*. 2016;16:811–23.
49. Balakirev M, Schoehn G, Chroboczek J. Lipoic acid-derived amphiphiles for redox-controlled DNA delivery. *Chem Biol*. 2000;7:813–9.
50. Richter F, Martin L, Leer K, Moek E, Hausig F, Brendel JC, Traeger A. Tuning of endosomal escape and gene expression by functional groups, molecular weight and transfection medium: a structure-activity relationship study. *J Mater Chem B*. 2020;8:5026–41.
51. Matsuguchi T, Salgia R, Hallek M, Eder M, Druker B, Ernst TJ, Griffin JD. Shc phosphorylation in myeloid cells is regulated by granulocyte macrophage colony-stimulating factor, interleukin-3, and steel factor and is constitutively increased by p210BCR/ABL. *J Biol Chem*. 1994;269:5016–21.
52. Cheng R, Feng F, Meng F, Deng C, Feijen J, Zhong Z. Glutathione-responsive nano-vehicles as a promising platform for targeted intracellular drug and gene delivery. *J Control Release*. 2011;152:2–12.
53. Neises B, Steglich W. Simple method for the esterification of carboxylic acids. *Angewandte Chemie International Edition in English*. 1978;17:522–4.
54. Synatschke CV, Schallon A, Jerome V, Freitag R, Muller AH. Influence of polymer architecture and molecular weight of poly(2-(dimethylamino)ethyl methacrylate) polycations on transfection efficiency and cell viability in gene delivery. *Biomacromol*. 2011;12:4247–55.
55. Rinkenauer AC, Schallon A, Gunther U, Wagner M, Betthausen E, Schubert US, Schacher FH. A paradigm change: efficient transfection of human leukemia cells by stimuli-responsive multicompartement micelles. *ACS Nano*. 2013;7:9621–31.
56. Tan Z, Jiang Y, Zhang W, Karls L, Lodge TP, Reineke TM. Polycation architecture and assembly direct successful gene delivery: micelleplexes outperform polyplexes via optimal DNA packaging. *J Am Chem Soc*. 2019;141:15804–17.
57. Lepecq JB, Paoletti C. A fluorescent complex between ethidium bromide and nucleic acids—physical-chemical characterization. *J Mol Biol*. 1967;27:87.
58. Olmsted J, Kearns DR. Mechanism of ethidium bromide fluorescence enhancement on binding to nucleic acids. *Biochemistry*. 1977;16:3647–54.
59. Monnery BD, Wright M, Cavill R, Hoogenboom R, Shaunak S, Steinke JHG, Thanou M. Cytotoxicity of polycations: Relationship of molecular weight and the hydrolytic theory of the mechanism of toxicity. *Int J Pharm*. 2017;521:249–58.
60. Cui X, Hartanto Y, Zhang H. Advances in multicellular spheroids formation. *J R Soc Interface*. 2017;14:20160877.
61. Schallon A, Jerome V, Walther A, Synatschke CV, Muller AHE, Freitag R. Performance of three PDMAEMA-based polycation architectures as gene delivery agents in comparison to linear and branched PEI. *React Funct Polym*. 2010;70:1–10.
62. Kuroda K, Caputo GA, DeGrado WF. The role of hydrophobicity in the antimicrobial and hemolytic activities of polymethacrylate derivatives. *Chemistry*. 2009;15:1123–33.
63. Manganiello MJ, Cheng C, Convertine AJ, Bryers JD, Stayton PS. Diblock copolymers with tunable pH transitions for gene delivery. *Biomaterials*. 2012;33:2301–9.
64. Trutzschler AK, Bus T, Reifarth M, Brendel JC, Hoepfner S, Traeger A, Schubert US. Beyond Gene Transfection with Methacrylate-Based Polyplexes-The Influence of the Amino Substitution Pattern. *Bioconj Chem*. 2018;29:2181–94.
65. Cheng JY, van de Wetering P, Talsma H, Crommelin DJ, Hennink WE. Effect of size and serum proteins on transfection efficiency of poly(2-(dimethylamino)ethyl methacrylate)-plasmid nanoparticles. *Pharm Res*. 1996;13:1038–42.
66. Layman JM, Ramirez SM, Green MD, Long TE. Influence of polycation molecular weight on poly(2-dimethylaminoethyl methacrylate)-mediated DNA delivery in vitro. *Biomacromol*. 2009;10:1244–52.
67. Cillonì D, Saglio G. Molecular pathways: BCR-ABL. *Clin Cancer Res*. 2012;18:930–7.
68. Shinohara H, Kumazaki M, Minami Y, Ito Y, Sugito N, Kuranaga Y, Taniguchi K, Yamada N, Otsuki Y, Naoe T, Akao Y. Perturbation of energy metabolism by fatty-acid derivative AIC-47 and imatinib in BCR-ABL-harboring leukemic cells. *Cancer Lett*. 2016;371:1–11.
69. Fontana S, Alessandro R, Barraza M, Giordano M, Corrado C, Zanella-Cleon I, Becchi M, Kohn EC, De Leo G. Comparative proteome profiling and functional analysis of chronic myelogenous leukemia cell lines. *J Proteome Res*. 2007;6:4330–42.
70. Lorenz MR, Holzapfel V, Musyanovych A, Nothelfer K, Walther P, Frank H, Landfester K, Schrezenmeier H, Mailander V. Uptake of functionalized, fluorescent-labeled polymeric particles in different cell lines and stem cells. *Biomaterials*. 2006;27:2820–8.
71. Knop K, Pretzel D, Urbanek A, Rudolph T, Scharf DH, Schallon A, Wagner M, Schubert S, Kiehnopf M, Brakhage AA, et al. Star-shaped drug carriers for doxorubicin with PEOGMA and POEtOxMA brush-like shells: a structural, physical, and biological comparison. *Biomacromol*. 2013;14:2536–48.

## Publisher's note

Springer Nature remains neutral with regard to jurisdictional claims in published maps and institutional affiliations.

### Ready to submit your research? Choose BMC and benefit from:

- fast, convenient online submission
- thorough peer review by experienced researchers in your field
- rapid publication on acceptance
- support for research data, including large and complex data types
- gold Open Access which fosters wider collaboration and increased citations
- maximum visibility for your research: over 100M website views per year

At BMC, research is always in progress.

Learn more [biomedcentral.com/submissions](https://biomedcentral.com/submissions)



## *Supporting Information:*

# Improved gene delivery to K-562 leukemia cells by lipoic acid modified block copolymer micelles

*Friederike Richter,<sup>a,†</sup> Prosper Mapfumo,<sup>a,†</sup> Liam Martin,<sup>a</sup> Jana I. Solomun,<sup>a</sup> Franziska Hausig,<sup>a</sup>  
Jochen J. Frietsch,<sup>b</sup> Thomas Ernst,<sup>b</sup> Stephanie Hoepfener,<sup>a,c</sup> Johannes C. Brendel,<sup>a,c</sup> Anja  
Traeger<sup>\*a,c</sup>*

<sup>a</sup>Laboratory of Organic and Macromolecular Chemistry (IOMC), Friedrich Schiller University  
Jena, Humboldtstrasse 10, 07743 Jena, Germany.

<sup>b</sup>Klinik für Innere Medizin II, Abteilung Hämatologie und Internistische Onkologie,  
Universitätsklinikum Jena, Am Klinikum 1, 07747 Jena, Germany.

<sup>c</sup>Jena Center for Soft Matter (JCSM), Friedrich Schiller University Jena, Philosophenweg 7,  
07743 Jena, Germany.

<sup>†</sup>Authors contributed equally

\*Correspondence to A. Traeger (anja.traeger@uni-jena.de)

## List of Tables.

<b>Table S1.</b> Amount of different substances used for polymerization of polymers.....	8
<b>Table S2.</b> Kinetic cycle protocol for automated heparin addition by the microplate reader.....	10
<b>Table S3.</b> Summary of polymer characterization.....	17
<b>Table S4.</b> Summary of micelle characterization. ....	17
<b>Table S5.</b> Polymer concentrations in different assays.....	20
<b>Table S6.</b> Computational analysis of monomer hydrophobicity by Molinspiration. ....	21

## List of Figures.

<b>Figure S1.</b> Characterization of PDMAEMA <sub>101</sub> and PDMAEMA <sub>89</sub> .....	14
<b>Figure S2.</b> NMR results. ....	15
<b>Figure S3.</b> Kinetic results.....	16
<b>Figure S4.</b> DLS measurements of the micelles. ....	18
<b>Figure S5.</b> Original cryo-TEM images of micelles.....	19
<b>Figure S6.</b> Gel retardation assay. ....	20
<b>Figure S7.</b> Cytotoxicity of polymers in HEK293T and K-562 cells.....	21
<b>Figure S8.</b> Spheroid formation in different cell lines.....	22
<b>Figure S9.</b> Interaction of polymers with erythrocyte membranes.....	22
<b>Figure S10.</b> Transfection efficiency of LAMA-mic in different cell lines. ....	23
<b>Figure S11.</b> Gating strategy for pDNA transfection using the example of 24 h incubation. ....	24
<b>Figure S12.</b> Investigation of the gene delivery process. ....	25
<b>Figure S13.</b> Gating strategy for polyplex uptake using the example of 4 h incubation.....	26
<b>Figure S14.</b> Gating strategy for calcein release using the example of the 4 h incubation. ....	27
<b>Figure S15.</b> CLSM study of polyplex uptake in K-562 cells.....	27
<b>Figure S16.</b> CLSM study of polyplex uptake in HEK293T cells.....	28
<b>Figure S17.</b> DLS measurement of the micelles at different concentrations.....	29
<b>Figure S18.</b> CMC determination.....	30

## ADDITIONAL METHODS

### Materials.

2-(Dimethylamino)ethyl methacrylate (DMAEMA) (98%), 2-Hydroxyethyl methacrylate (HEMA) (99%), *n*-Butyl methacrylate (*n*BMA) (99%), N,N'-Dicyclohexylcarbodiimide (DCC) (99%), 4-(Dimethylamino)pyridine (DMAP) (99%) and Nile Red (98%) were obtained from Sigma-Aldrich (Germany) and used as received.  $\alpha,\alpha'$ -Azobisisobutyronitrile (AIBN) was obtained from Sigma-Aldrich and recrystallized from methanol. (4-cyano pentanoic acid)yl ethyl trithiocarbonate (CPAETC) and 2-(methacryloyloxy)ethyl 5-(1,2-dithiolan-3-yl)pentanoate (LAMA) were synthesized according to previous literature.[1, 2]

For biological studies, following substances were ordered from suppliers in brackets: cell culture media and supplements (Biowest, France), fetal calf serum (FCS, Capricorn Scientific, Germany), PrestoBlue™ solution, YOYO™-1 iodide (Life Technologies, Thermo Fisher, Germany), trypsin-EDTA-solution, Triton X-100, 0.4% trypan blue solution and Hanks' balanced salt solution, calcein (Sigma-Aldrich), 1% ethidium bromide solution (EtBr, Carl Roth, Germany), heparin sodium salt from porcine intestinal mucosa (Alfa Aesar), linear poly(ethyleneimine) (LPEI,  $M_w = 25 \text{ kg mol}^{-1}$ ) and branched PEI (BPEI,  $M_w = 10 \text{ kg mol}^{-1}$ , Polysciences, Germany), Green Gel Loading Buffer and High Range DNA Ladder (Jena Bioscience, Germany). mEGFP-N1 was a gift from Michael Davidson (Addgene plasmid #54767; <http://n2t.net/addgene:54767>; RRID: Addgene\_54767). pKMyC was a gift from Ian Macara (Addgene plasmid #19400; <http://n2t.net/addgene:19400>; RRID: Addgene\_19400).

## **Instruments.**

*Nuclear magnetic resonance (NMR) spectroscopy.*  $^1\text{H}$  NMR (300 MHz) and DEPT  $^{13}\text{C}$  (75 MHz) spectra were recorded on a Bruker AC 300 MHz spectrometer at 300 K. The delay time (d1) was set at 1 s for  $^1\text{H}$  NMR and 2 s for DEPT  $^{13}\text{C}$ . Chemical shifts ( $\delta$ ) are reported in ppm.

*Size exclusion chromatography (SEC).* SEC was conducted on one of two instruments. Dimethylacetamide (DMAc)-SEC was conducted using an Agilent 1200 series instrument equipped with differential refractive index (DRI) and UV/VIS (DAD) detector. The liquid chromatography system used 1  $\times$  PSS GRAM 30 Å column (300  $\times$  0.8 mm, 10  $\mu\text{m}$  particle size) and 1  $\times$  PSS GRAM 1000 Å column (300  $\times$  0.8 mm, 10  $\mu\text{m}$  particle size). The DMAc eluent contained 0.21 wt.% LiCl as additive. Samples were run at 1 mL min $^{-1}$  at 40 °C. Analyte samples were filtered through a polytetrafluoroethylene (PTFE) membrane with 0.45  $\mu\text{m}$  pore size prior to injection. Poly(methyl methacrylate) (PMMA) narrow standards (PSS) were used to calibrate the SEC system. The measurements in chloroform were carried out on a Shimadzu system (Shimadzu Corp., Kyoto, Japan) equipped with a SCL-10A VP system controller, a SIL-10AD VP auto sampler, a LC-10AD VP pump, a RID-10A RI detector, a CTO-10A VP oven and a PSS SDVguard/lin S column (5 mm particle size). A mixture of chloroform/iso-propanol/triethylamine (94/2/4 vol%) was used as an eluent at a flow rate of 1 mL min $^{-1}$  and an oven temperature of 40 °C. PMMA standards (400-100,000 gmol $^{-1}$ ) were used to calibrate the system. Experimental  $M_{n,SEC}$  and  $D$  ( $M_w/M_n$ ) values of synthesized polymers were determined using PSS WinGPC UniChrom GPC software.

*Flow cytometry.* Flow cytometry was conducted on the CytoFlex S by Beckman Coulter GmbH, Germany. For each experiment, 10 $^4$  cells per sample were analyzed regarding their viability in the

forward and sideward scatter (FSC/SSC) plot and their fluorescence at  $\lambda_{\text{Ex}} = 488$  with a 525 nm bandpass filter, since all employed stains (YOYO-1, EGFP, calcein) were green fluorescent.

*Microplate reader.* Fluorescence intensity measurements for EBA, HRA, PrestoBlue™ and LDH assays as well as absorption measurements for hemolysis and aggregation assays were performed on the Infinite M200 PRO microplate reader (Tecan, Germany) with  $\lambda_{\text{Ex}} / \lambda_{\text{Em}}$  used as indicated in the respective method sections and gain set to optimal.

### **Detailed Monomer/Polymer Synthesis and Characterization.**

*Synthesis of lipoic acid methacrylate (2-(Methacryloyloxy)ethyl 5-(1,2-dithiolan-3-yl)pentanoate, LAMA).* Lipoic acid (2.77 g,  $1.34 \times 10^{-2}$  moles), 2-Hydroxyethyl methacrylate (HEMA) (1.66 g,  $1.27 \times 10^{-2}$  moles) and 4-(Dimethylamino)pyridine (DMAP) (1.02 g,  $8.37 \times 10^{-3}$  moles) were dissolved in Dichloromethane (22 mL) in a round bottom flask and cooled under stirring over ice for approx. 10 min. N,N'-Dicyclohexylcarbodiimide (DCC) (3.36 g,  $1.62 \times 10^{-2}$  moles) dissolved in Dichloromethane (22 mL) was added dropwise to the mixture. The reaction mixture was cooled with ice for 30 min and then left at room temperature overnight. The crude mixture was dried under reduced pressure and then a flash column chromatography was performed to purify the product (hexane 60: ethyl acetate 40).  $^1\text{H}$  NMR (300 MHz, Chloroform-*d*)  $\delta$  6.14 (s, 1H), 5.61 (s, 1H), 4.35 (s, 4H), 3.64 – 3.47 (m, 1H), 3.26 – 3.05 (m, 2H), 2.55 – 2.41 (m, 1H), 2.36 (t,  $J = 7.4$  Hz, 2H), 1.98 – 1.83 (m, 4H), 1.78 – 1.58 (m, 4H), 1.56 – 1.41 (m, 2H).  $^{13}\text{C}$  NMR (75 MHz, Chloroform-*d*)  $\delta$  173.16, 167.06, 135.93, 126.00, 62.41, 61.98, 56.28, 40.19, 38.47, 34.57, 33.86, 28.67, 24.60, 18.25.

*Typical synthesis of P(DMAEMA) via RAFT polymerization.* CPAETC (24.9 mg,  $9.47 \times 10^{-5}$  moles), DMAEMA (2.25 g,  $1.43 \times 10^{-2}$  moles), 1,4-dioxane (3.0 g), a 1% (w/w) ACVA in 1,4-dioxane (318,4 mg,  $1.1 \times 10^{-5}$  moles) and 1,3,5-trioxane (external NMR standard, 25 mg) were

introduced to a 8 mL microwave vial equipped with a magnetic stirring bar. The vial was sealed, and the solution deoxygenated by bubbling argon through it for 10 min. The vial was placed in an oil bath at 70 °C and allowed to stir for 7 h. The polymer was precipitated three times from THF into cold hexane and dried under reduced pressure to give a yellow solid.

*Typical synthesis of P(DMAEMA-*b*-[*n*BMA-*st*-LAMA]) via RAFT polymerization.* A portion of the precursor P(DMAEMA) macro-CTA (347.0 mg,  $2.29 \times 10^{-5}$  moles), *n*BMA (557.0 mg,  $3.92 \times 10^{-3}$  moles), LAMA (220.0 mg,  $6.88 \times 10^{-4}$  moles), THF (4.1 g), a 0.5% (w/w) solution of ACVA in THF (250 mg,  $4.46 \times 10^{-6}$  moles) and 1,3,5-trioxane (external NMR standard, 20.0 mg) were introduced to a 8 mL microwave vial equipped with a magnetic stirring bar. The vial was sealed, and the solution deoxygenated by bubbling argon through it for 10 min. The vial was placed in an oil bath at 70 °C and allowed to stir for 7 h. The polymer was precipitated three times from THF into cold hexane and dried under reduced pressure to give a yellow solid.

*Synthesis of P(DMAEMA-*b*-[*n*BMA-*st*-HEMA]) via RAFT polymerization.* A portion of the precursor P(DMAEMA) macro-CTA (200.0 mg,  $1.41 \times 10^{-5}$  moles), *n*BMA (339.9 mg,  $2.39 \times 10^{-3}$  moles), HEMA (54.9 mg,  $4.22 \times 10^{-4}$  moles), THF (3.68 g), a 1.0% (w/w) solution of ACVA in THF (105.0 mg,  $3.75 \times 10^{-6}$  moles) and 1,3,5-trioxane (external NMR standard, 31.0 mg) were introduced to a 8 mL microwave vial equipped with a magnetic stirring bar. The vial was sealed, and the solution deoxygenated by bubbling argon through it for 10 min. The vial was placed in an oil bath set at 70 °C and allowed to stir for 7 h. The polymer was precipitated three times from THF into cold hexane and dried under reduced pressure to give a pale yellow solid.

*Synthesis of P(DMAEMA-*b*-*n*BMA) via RAFT polymerization.* A portion of the precursor P(DMAEMA) macro-CTA (200.0 mg,  $1.41 \times 10^{-5}$  moles), *n*BMA (339.8 mg,  $2.39 \times 10^{-3}$  moles),



THF (3.52 g), a 1.0% (w/w) solution of ACVA in THF (94.0 mg,  $3.35 \times 10^{-6}$  moles) and 1,3,5-trioxane (external NMR standard, 28.0 mg) were introduced to a 8 mL microwave vial equipped with a magnetic stirring bar. The vial was sealed, and the solution deoxygenated by bubbling argon through it for 10 min. The vial was placed in an oil bath set at 70 °C and allowed to stir for 7 h. The polymer was precipitated three times from THF into cold hexane and dried under reduced pressure to give a pale yellow solid.

### Calculations for RAFT Polymerization.

Monomer conversion ( $p$ ) was calculated from  $^1\text{H}$  NMR data by comparing the integrals of vinyl peaks (5.5-6.3 ppm) against an external reference (1,3,5-trioxane, 5.14 ppm) before ( $t = 0$ ) and after ( $t = \text{final}$ ) polymerization. The theoretical number-average molar mass ( $M_{n,\text{th}}$ ) was then calculated using equation 3a and b for PDMAEMA and P(DMAEMA-*b*-[*n*BMA-*st*-LAMA]) respectively:

$$M_{n,\text{th}} \left( \frac{\text{g}}{\text{mol}} \right) = (Mw_{\text{DMAEMA}} * DP * p) + Mw_{\text{CTA}} \dots\dots (3a)$$

$$M_{n,\text{th}} \left( \frac{\text{g}}{\text{mol}} \right) = (Mw_{\text{LAMA}} * DP * p) + (Mw_{n\text{BMA}} * DP * p) + Mw_{\text{macroCTA}} \dots\dots (3b)$$

Where DP is the target degree of polymerization of each monomer and,  $Mw_{\text{DMAEMA}}$ ,  $Mw_{n\text{BMA}}$ ,  $Mw_{\text{MMA}}$ ,  $Mw_{\text{CTA}}$  and  $Mw_{\text{macroCTA}}$  are the molecular weight of the monomers, CTA and macro-CTA (PDMAEMA), respectively, and  $p$  is the monomer conversion of each monomer. Note: same formula was used for control polymers by substituting variables.

**Table S1.** Amount of different substances used for polymerization of polymers.

	PDMAEMA	P(DMAEMA- <i>b</i> -[ <i>n</i> BMA- <i>st</i> -LAMA])	PDMAEMA	P(DMAEMA- <i>b</i> - <i>n</i> BMA)	P(DMAEMA- <i>b</i> -[ <i>n</i> BMA- <i>st</i> -LAMA])	P(DMAEMA- <i>b</i> -[ <i>n</i> BMA- <i>st</i> -HEMA])
Monomer	DMAEMA	LAMA, <i>n</i> BMA	DMAEMA	<i>n</i> BMA	LAMA, <i>n</i> BMA	HEMA, <i>n</i> BMA
DP <sub><i>n</i>,target</sub>	150	200	150	170	200	200
m <sub>CTA</sub> added (mg)	50	250.0	50	200	200	200
n <sub>CTA</sub> added (moles)	1.90 × 10 <sup>-4</sup>	1.65 × 10 <sup>-5</sup>	1.9 × 10 <sup>-4</sup>	1.44 × 10 <sup>-5</sup>	1.14 × 10 <sup>-5</sup>	1.14 × 10 <sup>-5</sup>
m <sub>monomer</sub> added (mg)	4483	557.7	4483	340	474.2	394.8
n <sub>monomer</sub> added (moles)	2.85 × 10 <sup>-2</sup>	3.31 × 10 <sup>-3</sup>	2.85 × 10 <sup>-2</sup>	2.39 × 10 <sup>-3</sup>	2.81 × 10 <sup>-3</sup>	2.81 × 10 <sup>-3</sup>
m <sub>ACVA</sub> added (mg)	4.26	1.24	4.26	0.89	1.05	1.05
n <sub>ACVA</sub> added (moles)	1.5 × 10 <sup>-5</sup>	4.4 × 10 <sup>-6</sup>	1.5 × 10 <sup>-5</sup>	3.19 × 10 <sup>-6</sup>	1.41 × 10 <sup>-6</sup>	3.75 × 10 <sup>-6</sup>
Dioxane added (μL)	2361	4583	2470	3500	4060	4140
CPAETC/ACVA	12.5	3.8	12.5	4.41	3.75	13.7
T (°C)	70	70	70	70	70	70
Time (min)	420	420	420	420	420	420

From left to right, each PDMAEMA was a precursor of the subsequent block copolymer/s.

### Critical Micelle Concentration.

Critical micelle concentrations (CMC) were determined by fluorescence measurements at 25 °C with a Tecan Infinite M200 PRO microplate reader, using Nile Red as the fluorescence dye. A bulk solution of each polymer with concentrations ranging from 3.8-4.6 mg mL<sup>-1</sup> were prepared and a solution of Nile Red in THF, 3.14 × 10<sup>-4</sup> M (0.01 mg mL<sup>-1</sup>). Sample concentrations ranging from 1.0 mg mL<sup>-1</sup> to 0.001 mg mL<sup>-1</sup> of polymer were prepared in a vial by diluting the stock solutions, followed by a solution of Nile Red (0.01 mg mL<sup>-1</sup>) and incubated for 4 h at room temperature under reduced pressure. Then 100 μL of each sample was transferred to a 96-well plate and equilibrated at each temperature for 30 min. The fluorescence was measured in 96-well plates using an excitation wavelength of 535 nm. The fluorescence emission spectra were measured from 400 to 600 nm in 2 nm steps. For CMC determination the maximum of each fluorescence emission spectra was plotted versus the micelle concentration for each sample,

respectively. The CMC was determined as the intersection point in the plot of the maximum fluorescence emission versus the micelle concentration.

### **Dynamic Light Scattering (DLS) Measurements.**

The hydrodynamic diameters of the nanoassemblies were monitored by DLS using a Zetasizer Nano ZS (Malvern Instruments, Germany) with a He–Ne laser operating at a wavelength of 633 nm. Each sample was measured in triplicates at 25 °C with measurement duration set to automatic (about 10 min) after an equilibration time of 120 s. The counts were detected at an angle of 173°. The mean particle size was approximated as the effective (*z*-average) diameter and the width of the distribution as the polydispersity index of the particles (PDI) obtained by the cumulants method assuming a spherical shape. Data are expressed as mean  $\pm$  SD of three technical repetitions. Each micelle suspension was measured after filtration (0.20  $\mu$ m polytetrafluoroethylene (PTFE) membrane) except for P(DMAEMA<sub>101</sub>-*b*-[*n*BMA<sub>124</sub>-*st*-LAMA<sub>22</sub>]). Filtered bulk polymer solutions were stored at room temperature (RT).

The size (hydrodynamic diameter) of the polyplexes was measured following polyplex preparation at N\*/P 30 in 100  $\mu$ L HBG buffer as described in the manuscript. Each sample was measured in triplicates with three runs of 30 s at 25 °C after an equilibration time of 30 s. Data are expressed as mean of three technical replicates.

### **N\*/P Ratio Calculations.**

The N\*/P ratio was defined as the ratio of the total amount of protonatable amines in polymer solution in relation to the total amount of phosphates in the pDNA solution.

The volume of polymer needed to prepare polyplexes with 15  $\mu$ g mL<sup>-1</sup> pDNA at different N\*/P ratios was calculated as described by the following equations:

$$V_{\text{total}} \cdot P = V_{\text{poly}} \cdot N_{\text{poly}}$$

$$V_{\text{poly}} = \frac{V_{\text{total}} \cdot P}{N_{\text{poly}}}$$

$$V_{\text{poly}} = V_{\text{total}} \cdot \frac{n_{\text{pDNA}} \cdot P}{n_{\text{poly}} \cdot N}$$

$$V_{\text{poly}} = V_{\text{total}} \cdot \frac{m_{\text{pDNA}} \cdot P \cdot M_{\text{poly}}}{m_{\text{poly}} \cdot N \cdot M_{\text{pDNA}}}$$

Where  $V_{\text{total}}$ ,  $P$ ,  $V_{\text{poly}}$  and  $N_{\text{poly}}$  are the total required volume, the total number of phosphates of the pDNA, the required volume of polymer and the total number of active amines of the polymer, respectively.

### Heparin dissociation assay.

**Table S2.** Kinetic cycle protocol for automated heparin addition by the microplate reader

Kinetic cycle	Repetitions	Addition of heparin		Orbital shake	Incubation	Measurement
		V / $\mu\text{L}$	Stock Solution / $\text{U mL}^{-1}$			
1	2	5	100	10 s	10 min, 37°C	$\lambda_{\text{Ex}} = 525 \text{ nm} / \lambda_{\text{Em}} = 605 \text{ nm}$
2	1	15	100	10 s	10 min, 37°C	$\lambda_{\text{Ex}} = 525 \text{ nm} / \lambda_{\text{Em}} = 605 \text{ nm}$
3	3	5	500	10 s	10 min, 37°C	$\lambda_{\text{Ex}} = 525 \text{ nm} / \lambda_{\text{Em}} = 605 \text{ nm}$
4	1	10	500	10 s	10 min, 37°C	$\lambda_{\text{Ex}} = 525 \text{ nm} / \lambda_{\text{Em}} = 605 \text{ nm}$

The heparin concentration needed to release 70% of pDNA was calculated with OriginPro, Version 2018b (OriginLab Corporation, US) using a logistic function fitted to the respective single measurement points ( $n = 3$ ) of each polymer (4).

$$y = \frac{A_1 - A_2}{1 + (x/x_0)^p} + A_2 \quad (4)$$

Where  $A_1$ ,  $A_2$ ,  $x_0$  and  $p$  are the initial value, the final value, the center and the power of the curve, respectively. The  $\text{HC}_{70}$ -values ( $y = 70$ ) were calculated by substitution of the respective values into the equation.

### **Gel Retardation Assay (GRA).**

The complex formation of the polymers with pDNA was further investigated with the GRA. Briefly, polyplexes were formed at varying N\*/P ratios as described in the respective section. Following the 15 min incubation, the samples were diluted 1:6 with Green Gel Loading Buffer and run on a 1% (w/v) agarose gel containing 0.1  $\mu\text{g mL}^{-1}$  ethidium bromide (EtBr) at 80 V for 1 h. The gel was imaged using the Red™ Imaging System (Alpha Innotech, Kasendorf, Germany).

### **Erythrocyte Aggregation and Hemolysis.**

The interaction of polymers with cellular membranes was examined by analyzing the release of hemoglobin from erythrocytes as published before.[3, 4] Blood from human donors, collected in tubes with citrate, was obtained from the Department of Transfusion Medicine of the University Hospital, Jena. The blood was centrifuged without pooling at  $4,500 \times g$  for 5 min, and the pellet was washed three times with cold phosphate buffered saline (PBS, pH 7.4). Following a 10 times dilution with PBS (either pH 7.4 or pH 6.0), 500  $\mu\text{L}$  aliquots of erythrocyte suspension were mixed 1:1 with the polymer solutions, which were prepared with PBS pH 7.4 or pH 6.0, and incubated at 37 °C for 60 min. After centrifugation at  $2,400 \times g$  for 5 min, the supernatant was transferred to a clear flat bottomed 96-well plate (VWR, Germany) and the hemoglobin release was determined as the hemoglobin absorption at  $\lambda = 544 \text{ nm}$ . Absorption at  $\lambda = 630 \text{ nm}$  was used as reference. Complete hemolysis (100 %) was achieved using 1 % Triton X-100 as positive control. Pure PBS was used as negative control (0 % hemolysis). The hemolytic activity of the polycations was calculated as follows (5):

$$\text{Hemolysis} / \% = \frac{(A_{\text{Sample}} - A_{\text{Negative control}})}{(A_{\text{Positive control}} - A_{\text{Negative control}})} \cdot 100 \quad (5)$$

Where  $A_{\text{Sample}}$ ,  $A_{\text{Negative control}}$  and  $A_{\text{Positive control}}$  are the absorption values of a given sample, the PBS treatment and the Triton X-100 treatment, respectively. A value less than 2% hemolysis rate was classified as non-hemolytic, 2 to 5% as slightly hemolytic and values  $> 5\%$  as hemolytic.

To determine the cell aggregation, erythrocytes were isolated as described above. Subsequently, 100  $\mu\text{L}$  of the erythrocyte-polymer suspension were transferred to a clear flat bottomed 96-well plate (VWR, Germany). The cells were incubated at 37 °C for 2 h, and the absorbance was measured at  $\lambda = 645 \text{ nm}$ . Cells treated with PBS served as negative control and cells treated with 50  $\mu\text{g mL}^{-1}$  10 kDa bPEI were used as positive control. Aggregation potential of the polymers was calculated as follows (6):

$$\text{Aggregation} = \frac{A_{\text{Negative control}}}{A_{\text{Sample}}} \quad (6)$$

Where  $A_{\text{Sample}}$  and  $A_{\text{Negative control}}$  are the absorption values of a given sample and the PBS treatment, respectively. Experiments were run in technical triplicates and were performed with blood from three different blood donors.

### **Polyplex Uptake with CLSM and Image Processing.**

For uptake studies *via* confocal laser scanning microscopy (CLSM), cells were seeded and treated as described for flow cytometry analysis, but in glass-bottomed dishes (CellView cell culture dishes with four compartments, Greiner Bio-One) and analyzed following incubation with polyplexes containing YOYO-1 labeled pDNA (0.027 nmol per 1  $\mu\text{g}$  pDNA) and indicated polymers for 1 h. To image intracellular distribution in living cells, Hoechst 33342 was added for 5 min to stain cell nuclei. To stain acidic compartments inside the cells, 50 nM LysoTracker™ Red (LTR) were added for 5 min. Prior to imaging, trypan blue was added to a final concentration of 0.04% to quench fluorescence of YOYO-1 outside the cells. Live cell imaging was performed

using a LSM880, Elyra PS.1 system (Zeiss, Germany) applying the argon laser for excitation at 488 nm (2%) and 405 nm (0.5%), emission filters for 410-479 nm (Hoechst) and 508-553 nm (YOYO-1) with a gain of 700, respectively. LTR was excited at 561 nm and detected with an emission filter for 589-690 nm and a gain of 650. To avoid cross talk between the different channels, Hoechst and LTR were imaged simultaneously in one track and YOYO-1 in a second track. For fast imaging, the tracks were switched in every line of the image. The images were acquired as z-stacks of 6 slices around the center of the cells (in total 7  $\mu\text{m}$  for HEK293T and 15  $\mu\text{m}$  for K-562 cells) to image also polyplexes not present in the center of the cells. For magnification, a  $40 \times 1.4$  NA plan apochromat oil objective was applied. Images were acquired using the ZEN software, version 2.3 SP1 (Zeiss, Germany). The experiments were performed at least twice. All images were processed in batch mode using ImageJ, version 1.52.<sup>4</sup> At first, the 3D data of the images were turned into 2D images *via* maximum intensity projection of all 6 slices. Subsequently, the lower and upper limits of the grey values were adjusted for each channel to enhance the contrast of the images. Same values were applied to all images within one cell line.

## FURTHER RESULTS

### Characterization of Polymers.

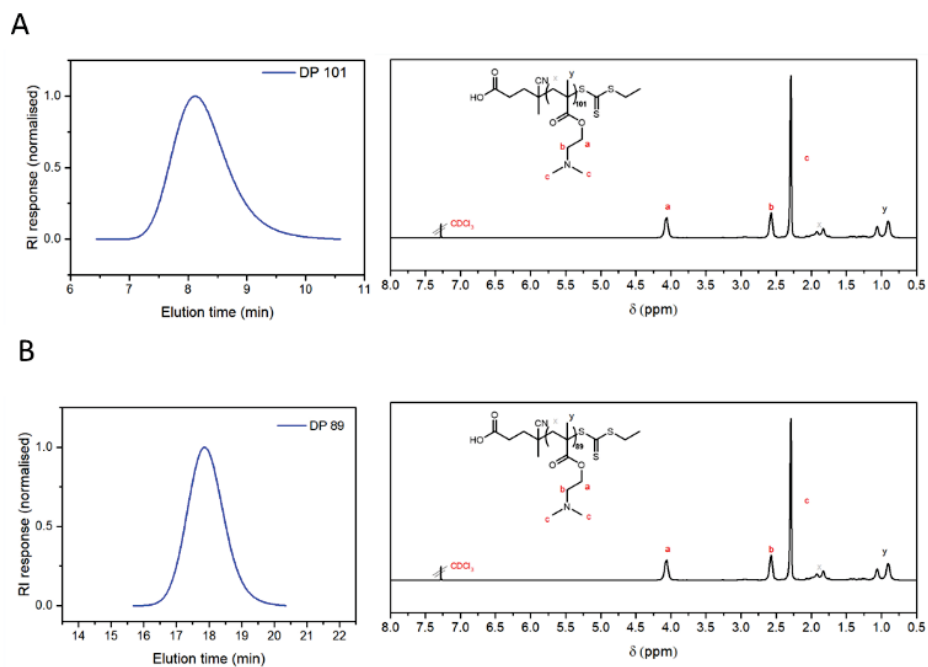


**Figure S1.** Characterization of PDMAEMA<sub>101</sub> and PDMAEMA<sub>89</sub>.

Conversion from <sup>1</sup>H NMR, molar masses determined by (A) (CHCl<sub>3</sub>/IPA/NEt<sub>3</sub>) SEC traces–PMMA calibration and (B) (DMAc + 0.21 % LiCl) SEC traces–PMMA calibration.



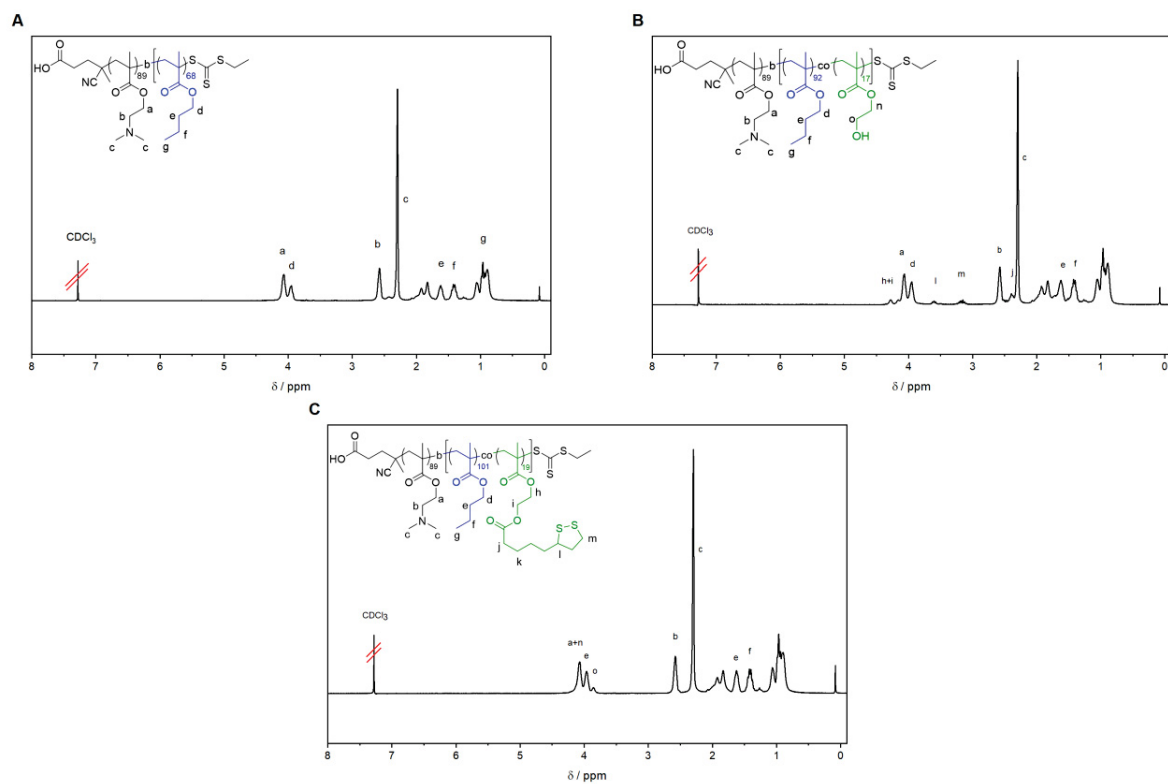


**Figure S2.** NMR results.

**(A)** P(DMAEMA<sub>89</sub>-*b*-nBMA<sub>68</sub>), **(B)** P(DMAEMA<sub>89</sub>-*b*-[nBMA<sub>92</sub>-*st*-HEMA<sub>17</sub>]), **(C)** P(DMAEMA<sub>89</sub>-*b*-[nBMA<sub>101</sub>-*st*-LAMA<sub>19</sub>]).

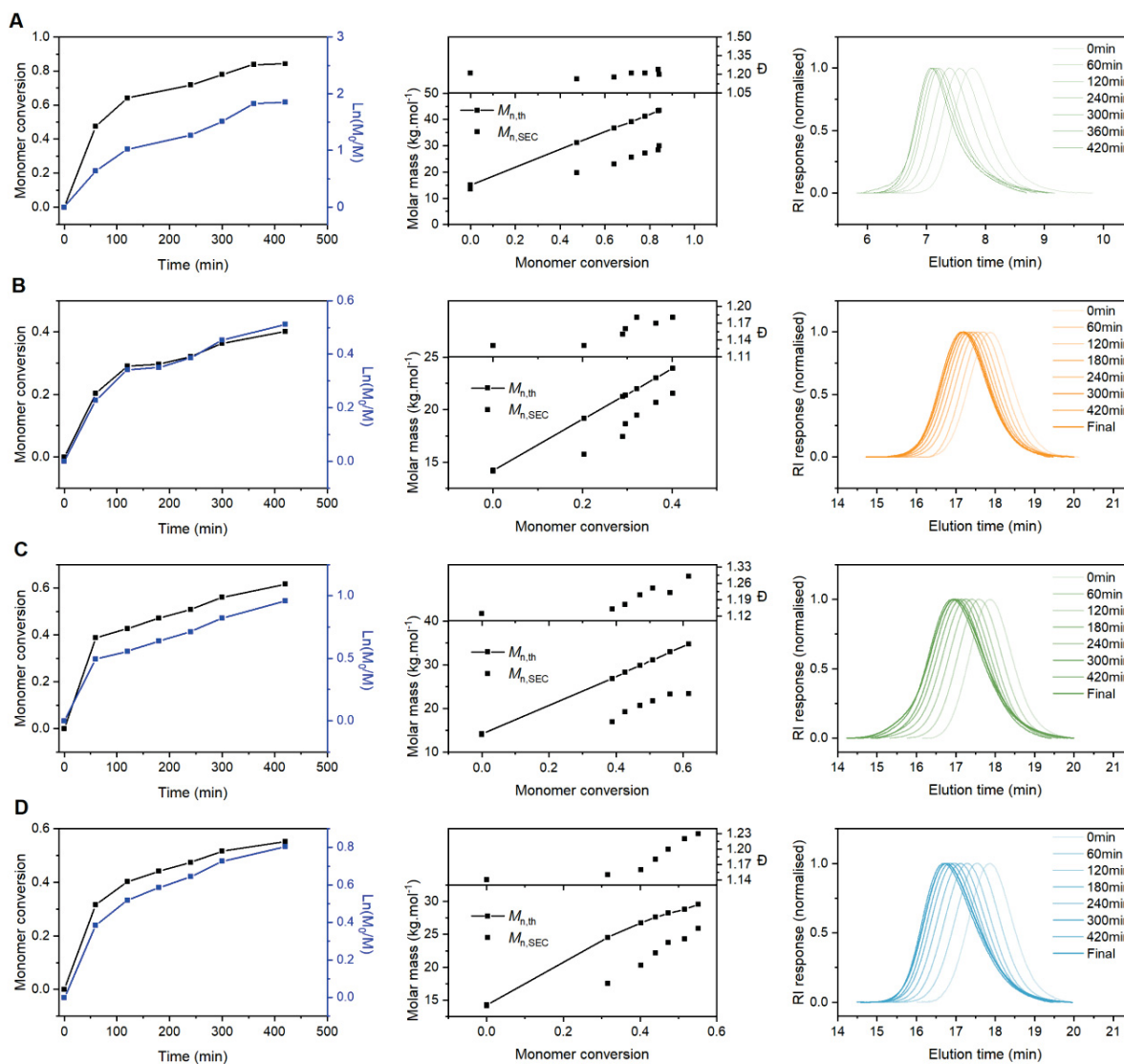


**Figure S3.** Kinetic results.

(A) P(DMAEMA<sub>101</sub>-*b*-[*n*BMA<sub>120</sub>-*st*-LAMA<sub>22</sub>]), (B) P(DMAEMA<sub>89</sub>-*b*-*n*BMA<sub>68</sub>) (C) P(DMAEMA<sub>89</sub>-*b*-[*n*BMA<sub>101</sub>-*st*-LAMA<sub>19</sub>]), (D) P(DMAEMA<sub>89</sub>-*b*-[*n*BMA<sub>92</sub>-*st*-HEMA<sub>17</sub>]). Conversion from <sup>1</sup>H NMR, molar masses determined by (CHCl<sub>3</sub>/IPA/NEt<sub>3</sub>) SEC traces-PMMA calibration (A) and SEC-9: DMAc + 0.21 % LiCl – PMMA calibration (B-D).

**Table S3.** Summary of polymer characterization.

Polymer-ID [a]	$M_{n,th}$ [b]	$M_{n,SEC}$ [c]	$\bar{D}$ [c]
	kg mol <sup>-1</sup>		
PDMAEMA <sub>101</sub>	16.1	13.8	1.17
P(DMAEMA <sub>101</sub> - <i>b</i> -[ <i>n</i> BMA <sub>120</sub> - <i>co</i> -LAMA <sub>22</sub> ])	39.2	30.0	1.19
PDMAEMA <sub>89</sub>	14.2	14.0	1.15
P(DMAEMA <sub>89</sub> - <i>b</i> - <i>n</i> BMA <sub>68</sub> )	23.9	21.0	1.18
P(DMAEMA <sub>89</sub> - <i>b</i> -[ <i>n</i> BMA <sub>92</sub> - <i>co</i> -HEMA <sub>17</sub> ])	29.6	24.7	1.26
P(DMAEMA <sub>89</sub> - <i>b</i> -[ <i>n</i> BMA <sub>101</sub> - <i>co</i> -LAMA <sub>19</sub> ])	34.7	23.1	1.32

[a] Degree of Polymerization was determined *via* <sup>1</sup>H NMR.  
[b] Determined using equation 6 of the ESL.  
[c] Determined *via* CHCl<sub>3</sub>-SEC and DMAc-SEC with PMMA standards.

**Table S4.** Summary of micelle characterization.

Code	Stock-solution		Micelle			Polyplex			
	Size [a]	PDI [b]	370-540 μg mL <sup>-1</sup>		CMC [c]	370-540 μg mL <sup>-1</sup>		37-54 μg mL <sup>-1</sup>	
			Size [a]	PDI [b]		Size [a]	PDI [b]	Size [a]	PDI [b]
	nm		nm		μg mL <sup>-1</sup>	nm		nm	
LAMA-mic	46.6	0.19	53.4	0.15	-	-	-	-	-
BMA-mic	19.5	0.25	46.6	0.10	26	56.8	0.21	73.4	0.38
HEMA-mic	21.7	0.19	51.3	0.08	30	54.1	0.10	63.3	0.26
LAMA-mic II	24.2	0.23	54.2	0.12	29	61.1	0.14	62.4	0.26

[a] Determination of the size as the hydrodynamic diameter *via* DLS (concentrations see Table S3).  
[b] Determined *via* DLS (concentrations see Table S3).  
[c] Determined using Nile Red encapsulation as fluorescence probe.

## DLS Measurement of Micelles.

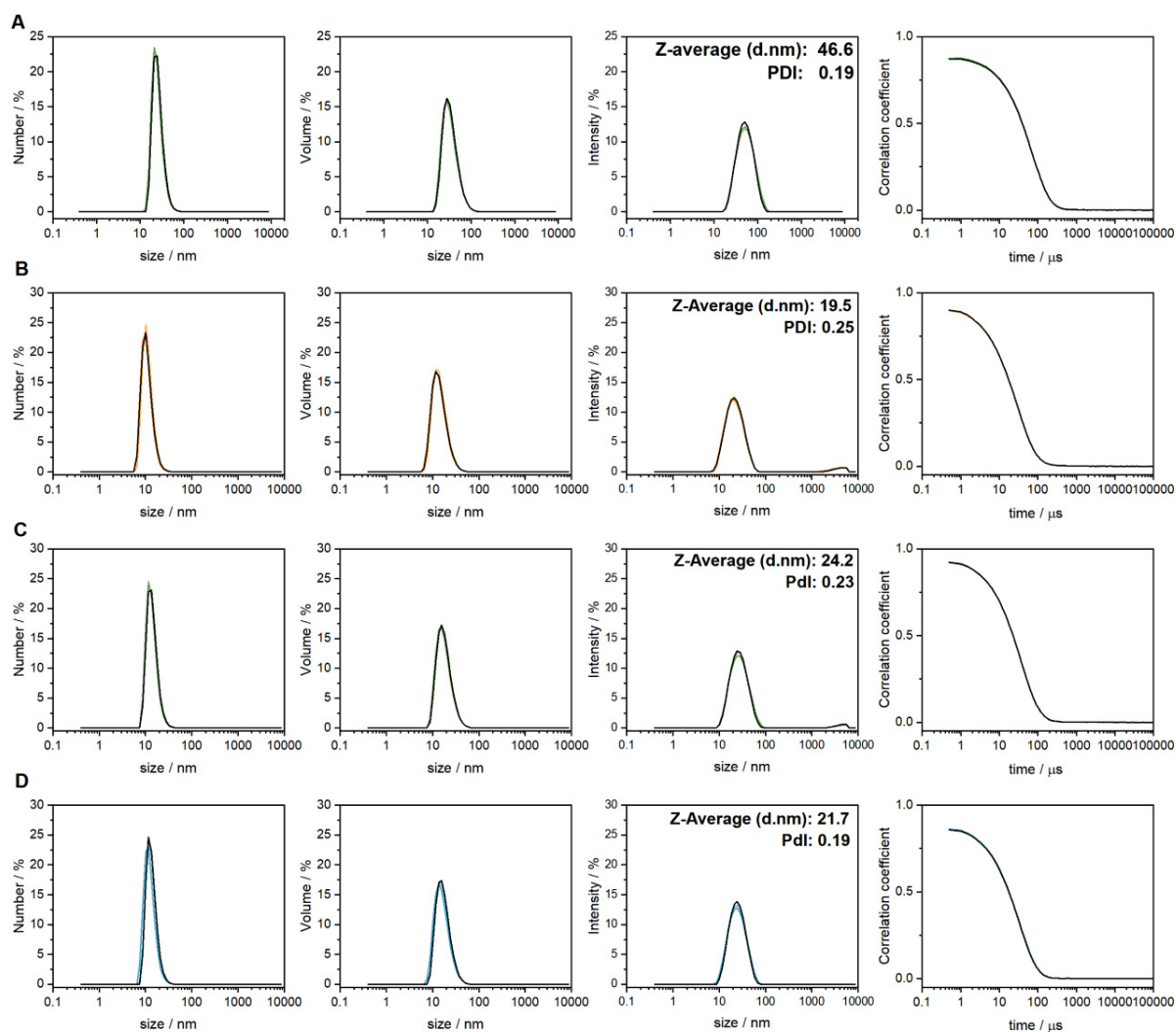


**Figure S4.** DLS measurements of the micelles.

(A) LAMA-mic, (B) BMA-mic, (C) LAMA-mic II and (D) HEMA-mic; stock solutions.

### Original Cryo-TEM images

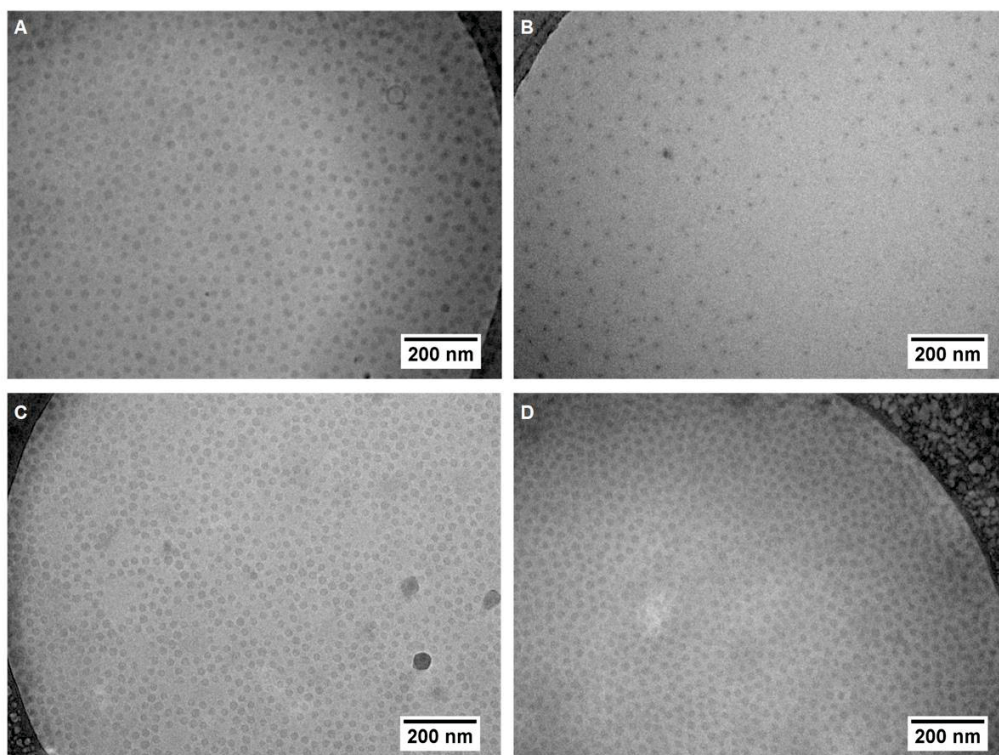


**Figure S5.** Original cryo-TEM images of micelles.

(A) LAMA-mic, (B) BMA-mic, (C) LAMA-mic II, (D) HEMA-mic.

## Further Biological Results.

**Table S5.** Polymer concentrations in different assays.

	Stock solutions	EBA/HRA, DLS		Cell—based assays		Amount of lipoic acid on cells	
	$\mu\text{g mL}^{-1}$	$\mu\text{g mL}^{-1}$		$\mu\text{g mL}^{-1}$		$\mu\text{M}$	
	-	N*/P 15	N*/P 30	N*/P 15	N*/P 30	N*/P 15	N*/P 30
pDNA	-	15	15	1.5	1.5	-	-
LPEI	1000	30	59	3.0	5.9	-	-
PDMAEMA	10000	111	221	11.1	22.1	-	-
LAMA-mic	2100	275	549	27.5	54.9	14.8	29.5
PDMAEMA II	10000	111	221	11.1	22.1	-	-
BMA-mic	4940	189	371	18.9	37.1	-	-
HEMA-mic	4600	228	455	22.8	45.5	-	-
LAMA-mic II	4580	269	538	26.9	53.8	14.8	29.5

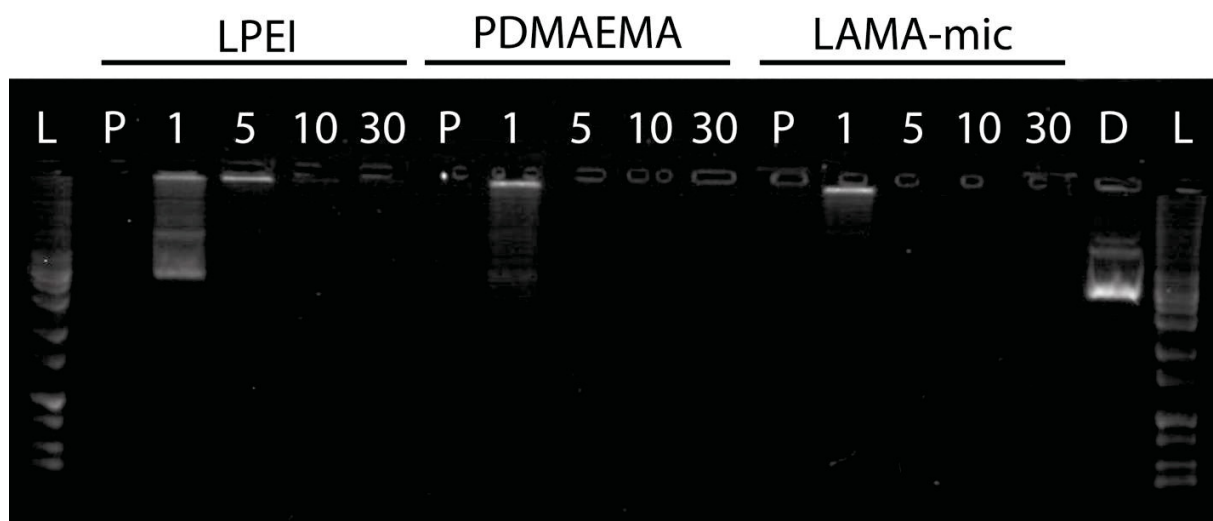


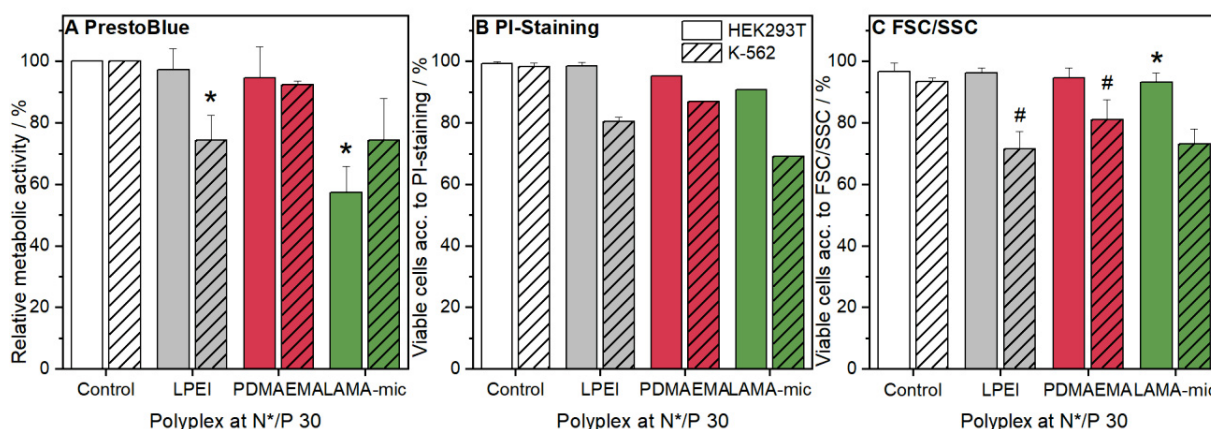
**Figure S6.** Gel retardation assay.

The agarose gel was loaded with polyplexes prepared as described before. L: High Range DNA Ladder, P: only Polymer at concentrations equal to N\*/P 30, numbers indicate the respective N\*/P ratios, D: pDNA in HBG buffer at the same concentration used for polyplexes.

**Table S6.** Computational analysis of monomer hydrophobicity by Molinspiration.

	EI	DMAEMA	nBMA	LAMA
Structure				
MW	45.09	157.21	142.20	318.46
logP <sup>1</sup>	0.1	1.4	2.81	3.43

<sup>1</sup>The logP values were calculated using the Molinspiration Property Calculation Service of the Molinspiration Cheminformatics website (<https://www.molinspiration.com/cgi-bin/properties>).

**Figure S7.** Cytotoxicity of polymers in HEK293T and K-562 cells.

(A) Metabolic activity using the PrestoBlue<sup>TM</sup> assay following incubation of cells with polyplexes of indicated polymers and pDNA at N\*/P 30 for 24 h. Values represent mean  $\pm$  SD of  $n = 3$ . (B) Membrane integrity using propidium iodide (PI) staining and flow cytometry following incubation of cells with polyplexes of indicated polymers and pDNA at N\*/P 30 for 24 h. Viability was calculated as the difference of 100 and the percentage of PI positive cells gated in the ECD-channel. Values represent mean  $\pm$  SD of  $n > 1$ . (C) Viable cells according to appearance of cells in FSC/SSC plot of flow cytometry. Values represent mean  $\pm$  SD of  $n > 1$ .

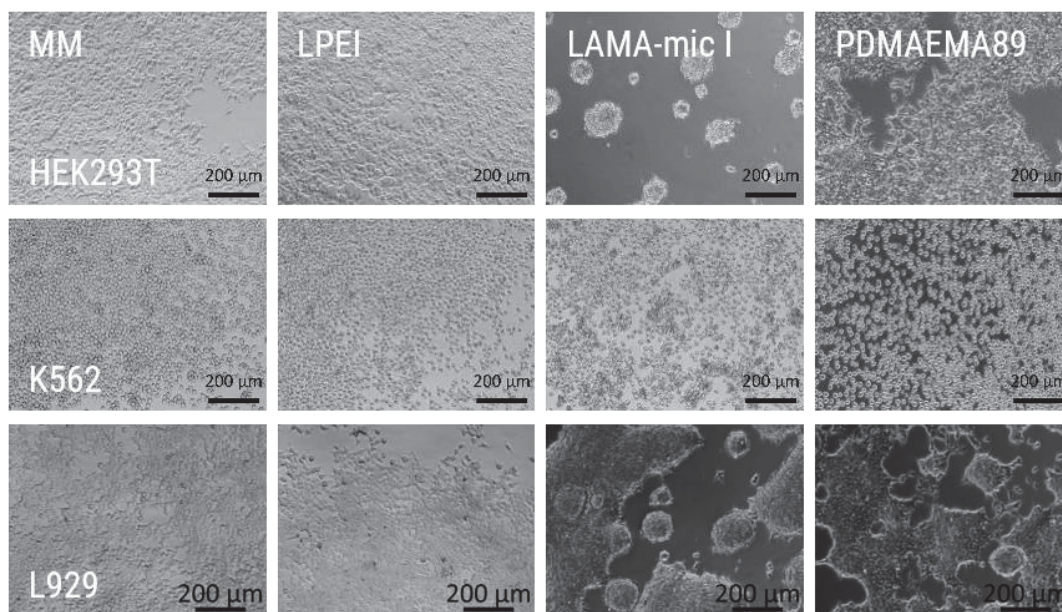


**Figure S8.** Spheroid formation in different cell lines.

Cells were incubated with polyplexes and pDNA at N\*/P 30 for 24 h. Images were acquired *via* light microscopy.

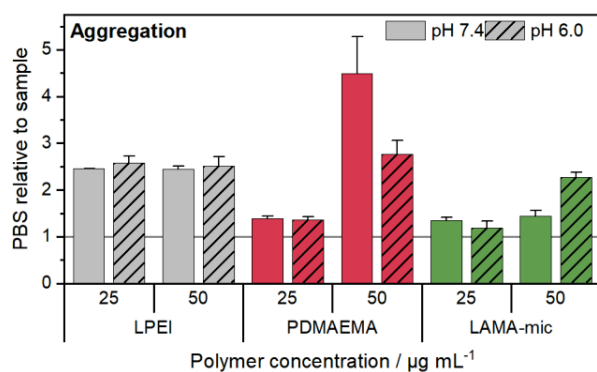


**Figure S9.** Interaction of polymers with erythrocyte membranes.

Human erythrocytes were washed and incubated with polymers at different concentrations in PBS of different pH values present in blood/cytoplasm (pH 7.4) or endosomal compartments (pH 6). Aggregation of indicated polymers was measured as light absorption by erythrocytes. Values are calculated as the negative control (PBS value) relative to the sample value and represent mean  $\pm$  SD (n = 3).



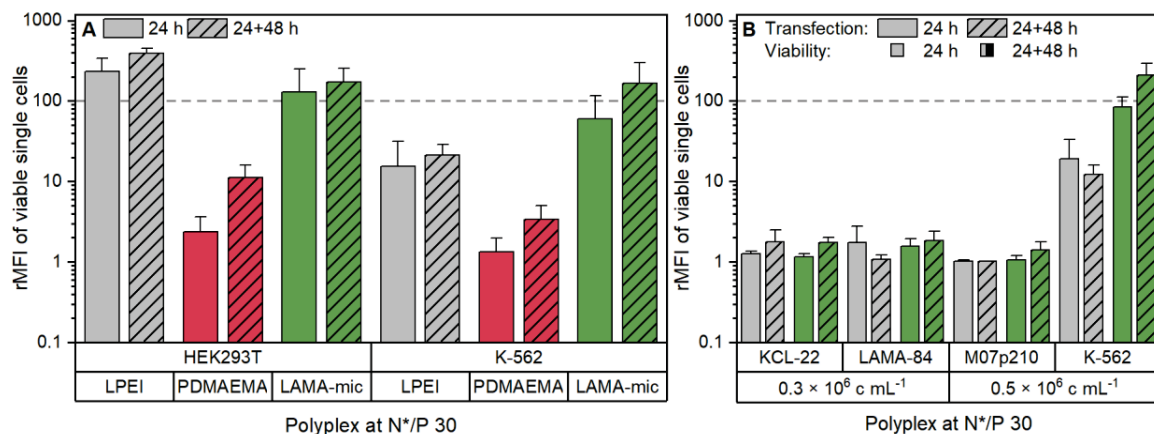


**Figure S10.** Transfection efficiency of LAMA-mic in different cell lines.

EGFP expression of viable cells was analyzed *via* flow cytometry following incubation of cells with polyplexes of mEGFP-N1 pDNA and polymers at N\*/P 30 in respective growth medium (D10 or R10 with 10 mM HEPES) either for 24 h or for 24 h, splitting the cell suspension 1:2 and further incubation for 48 h. Values represent mean  $\pm$  SD of rMFI values of viable, single cells ( $n \geq 3$ ).

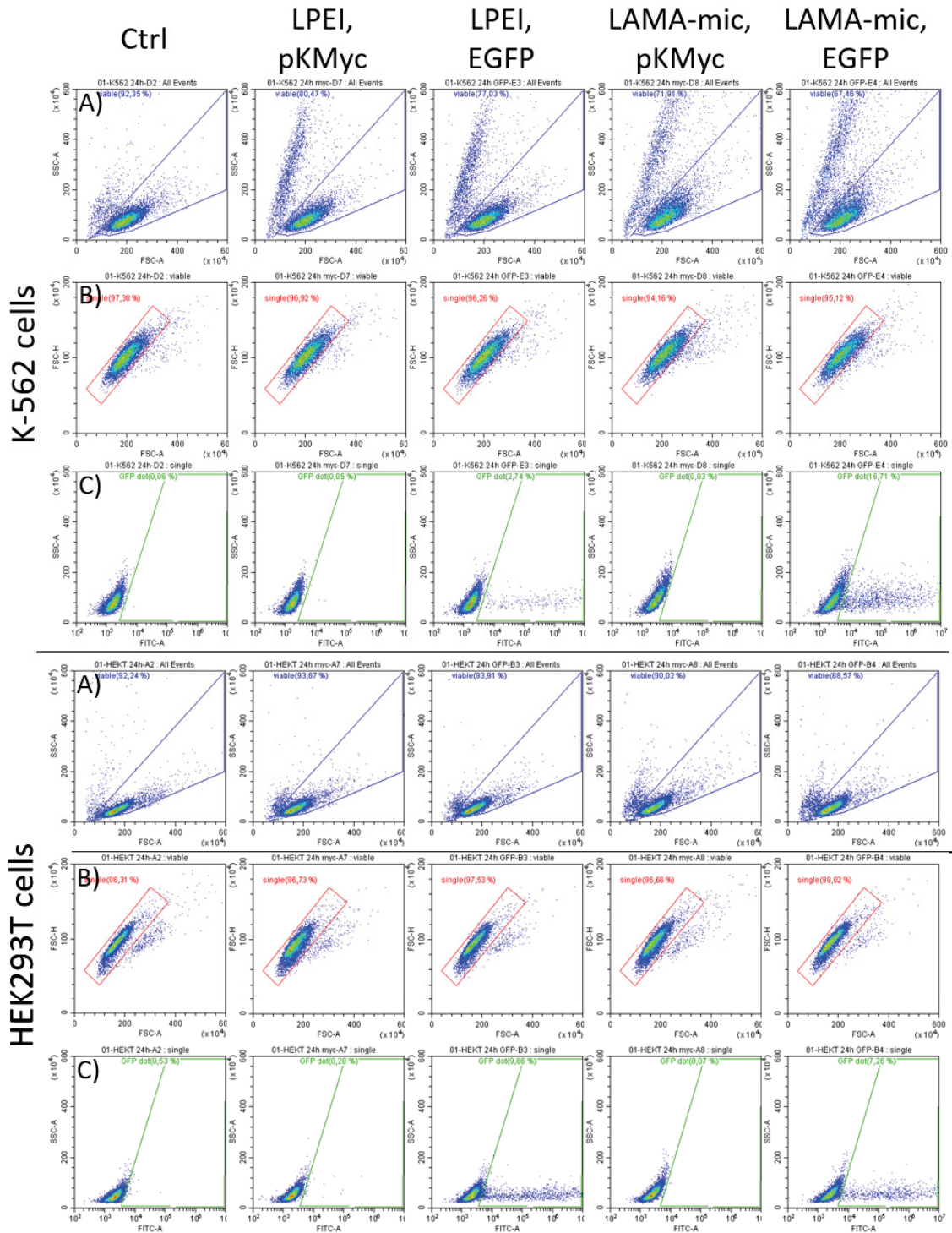


**Figure S11.** Gating strategy for pDNA transfection using the example of 24 h incubation. Viable single cells were gated in FSC/SSC and FSC-A/FSC-H dot plots (A,B). Subsequently cells with EGFP fluorescence were discriminated by gating to the respective pKMyc control.

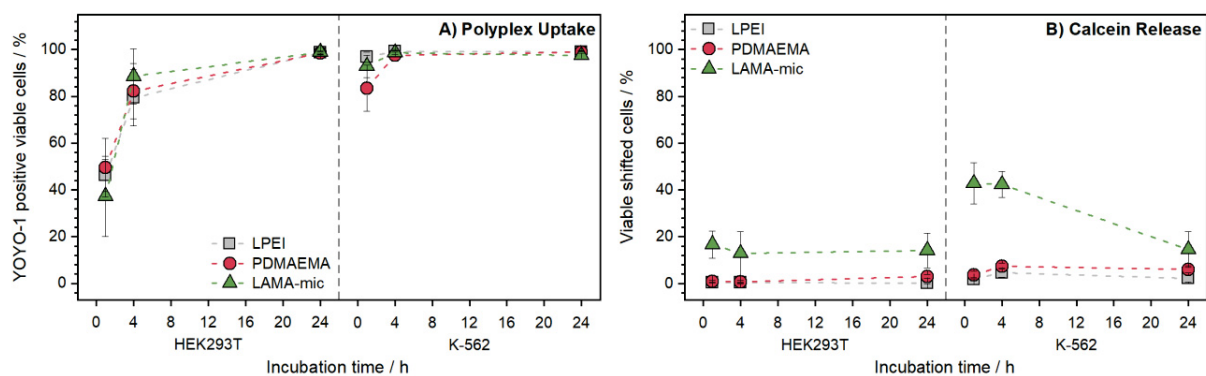


**Figure S12.** Investigation of the gene delivery process.

(A) Cellular internalization of LAMA-mic polyplexes in different cell lines. Cells were incubated with polyplexes of polymers and YOYO-1-labeled pDNA at N\*/P 30 and analyzed *via* flow cytometry. Cells incubated with labeled pDNA served as control. Values represent mean  $\pm$  SD of % cells showing YOYO-1 fluorescence higher than the control (n = 3). (B) Endosomal escape of LAMA-mic polyplexes detected by the non-permeable dye calcein and analyzed *via* flow cytometry. Values represent mean  $\pm$  SD of % cells showing higher fluorescence intensity than the calcein control (n = 3).

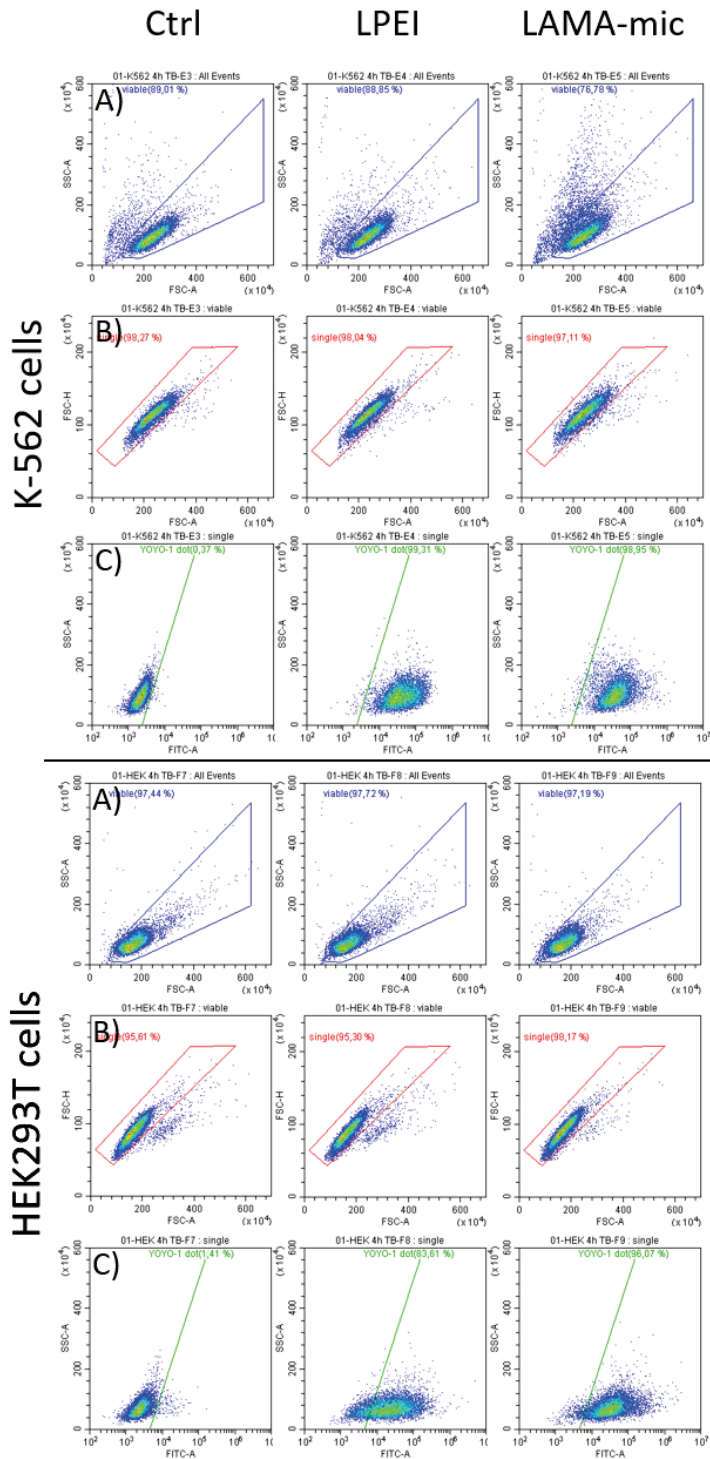


**Figure S13.** Gating strategy for polyplex uptake using the example of 4 h incubation.

Viable single cells were gated in FSC/SSC and FSC-A/FSC-H dot plots (A,B). Subsequently cells with YOYO-1 fluorescence were discriminated by gating to the pDNA-YOYO-1 control of the respective incubation time.

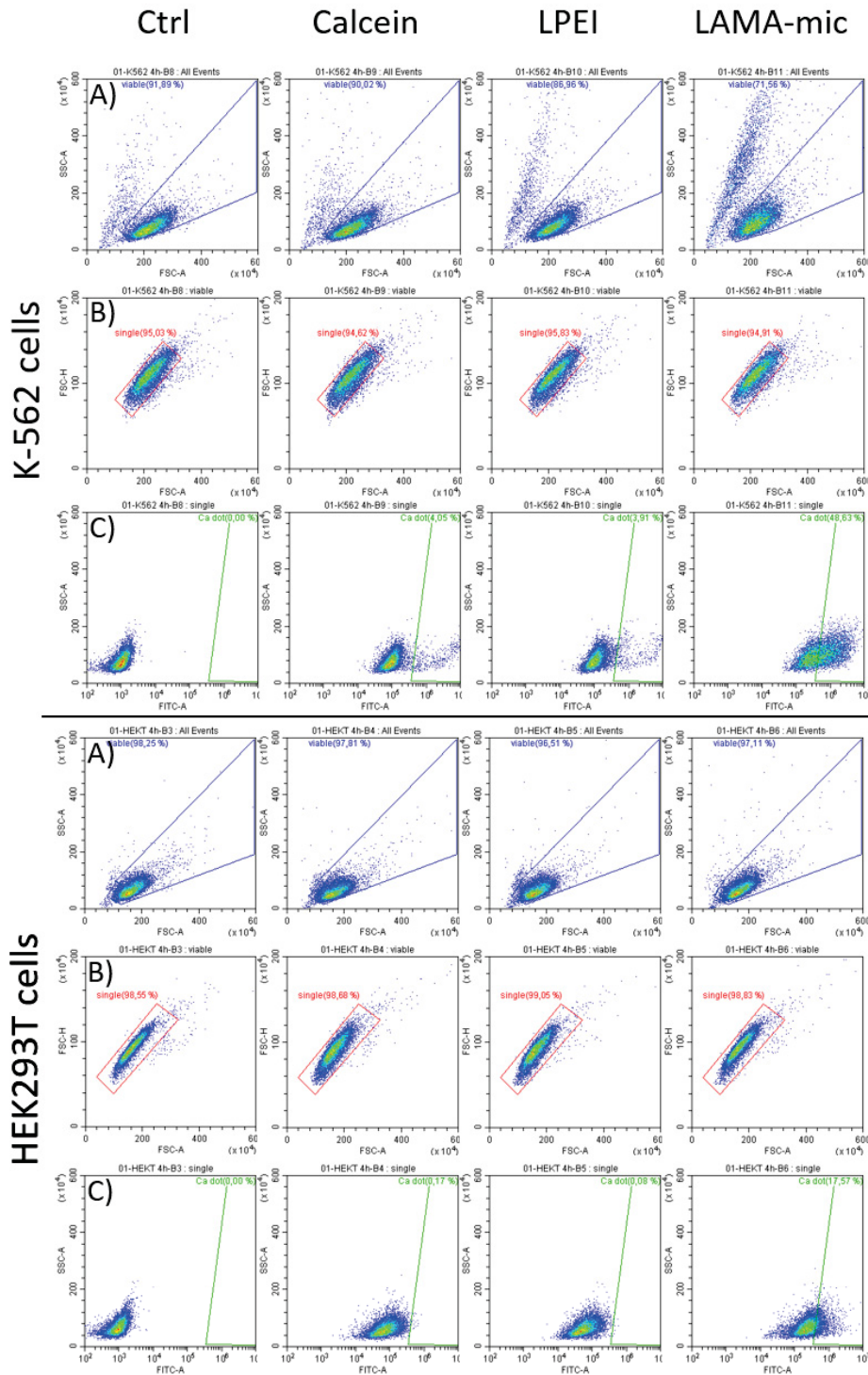


**Figure S14.** Gating strategy for calcein release using the example of the 4 h incubation.

Viable single cells were gated in FSC/SSC and FSC-A/FSC-H dot plots (A,B). Subsequently cells with calcein fluorescence higher than the control were discriminated by gating to the calcein control of the respective incubation time.

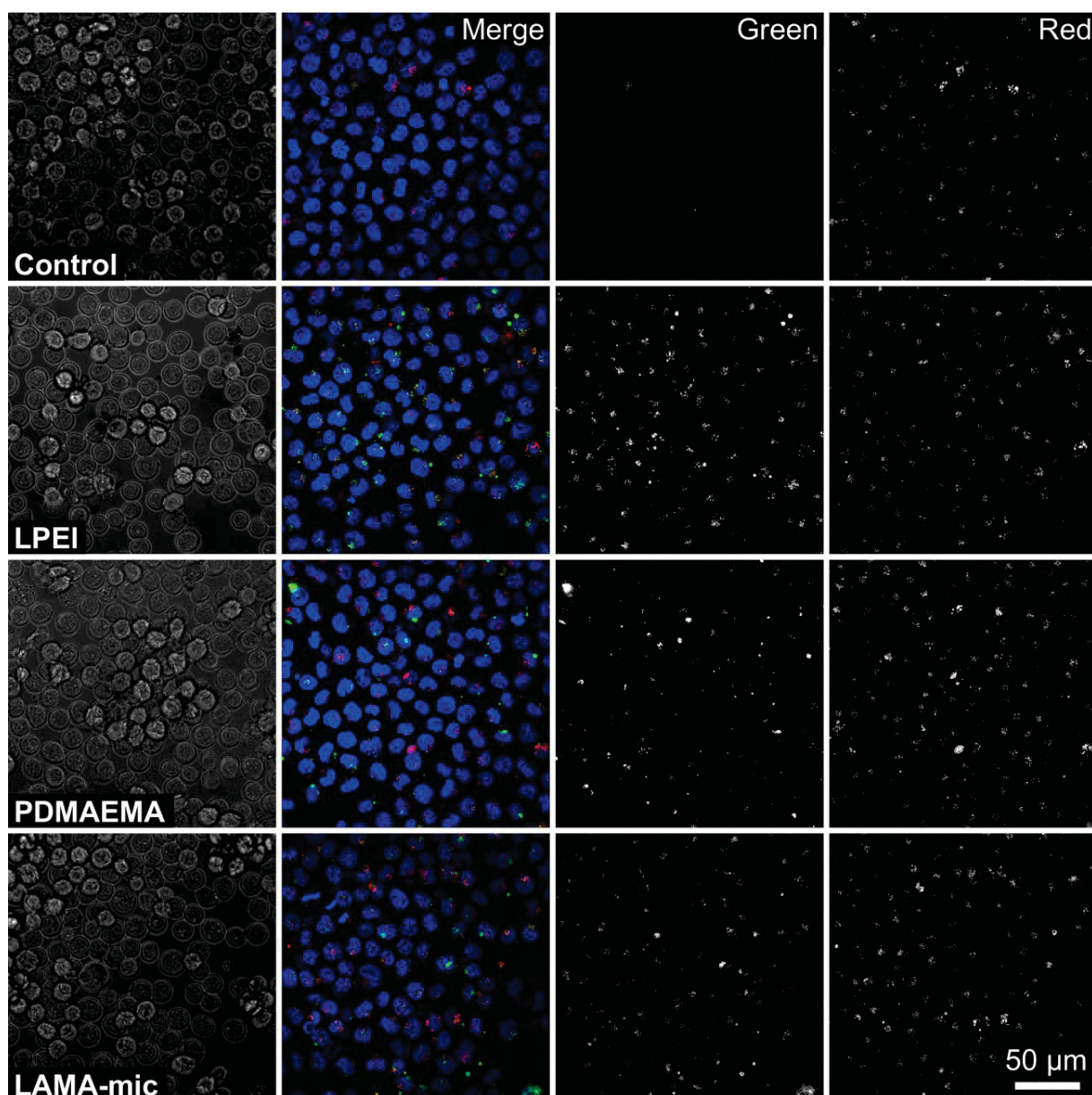


**Figure S15.** CLSM study of polyplex uptake in K-562 cells.

K-562 cells were incubated with polyplexes of YOYO-1-labeled pDNA and polymers at N\*/P 30 in growth medium (R10 with 10 mM HEPES) for 1 h. Endolysosomes were stained with LysoTracker<sup>TM</sup> Red (red), Nuclei were stained with Hoechst 33342 (blue) and YOYO-1 fluorescence (green) was quenched with trypan blue.

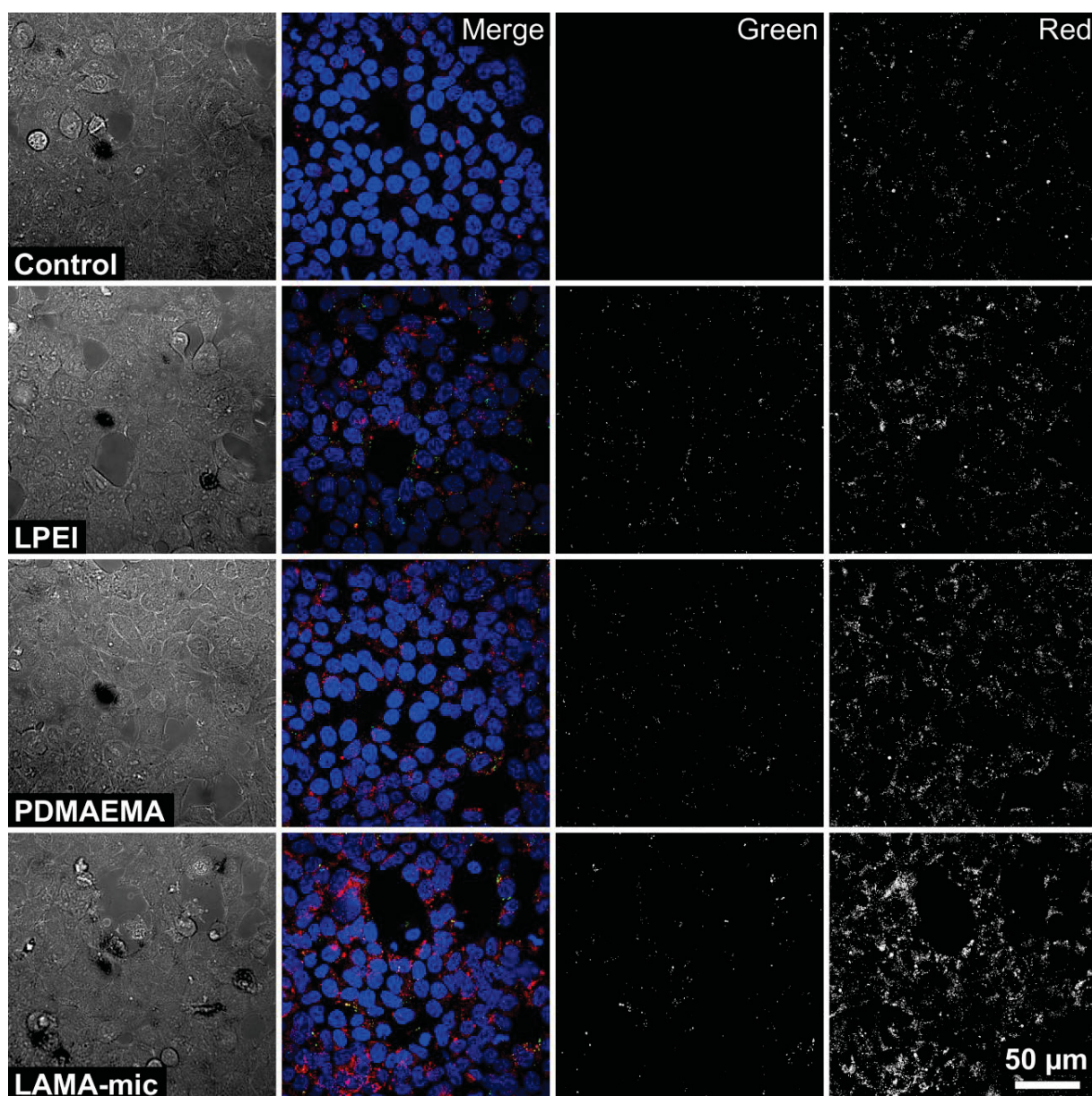


**Figure S16.** CLSM study of polyplex uptake in HEK293T cells.

HEK293T cells were incubated with polyplexes of YOYO-1-labeled pDNA and polymers at N\*/P 30 in growth medium (D10 with 10 mM HEPES) for 1 h. Endolysosomes were stained with LysoTracker™ Red (red), nuclei were stained with Hoechst 33342 (blue) and YOYO-1 fluorescence (green) was quenched with trypan blue.

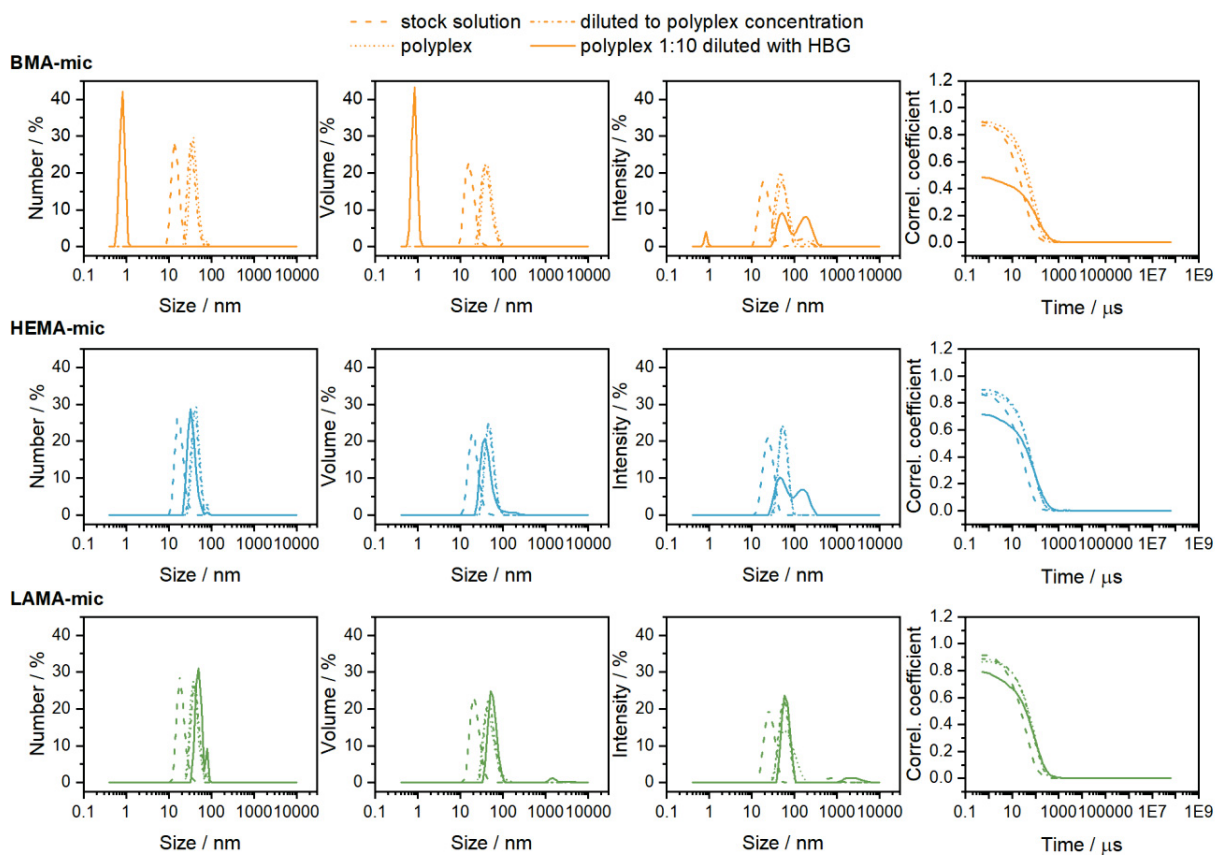
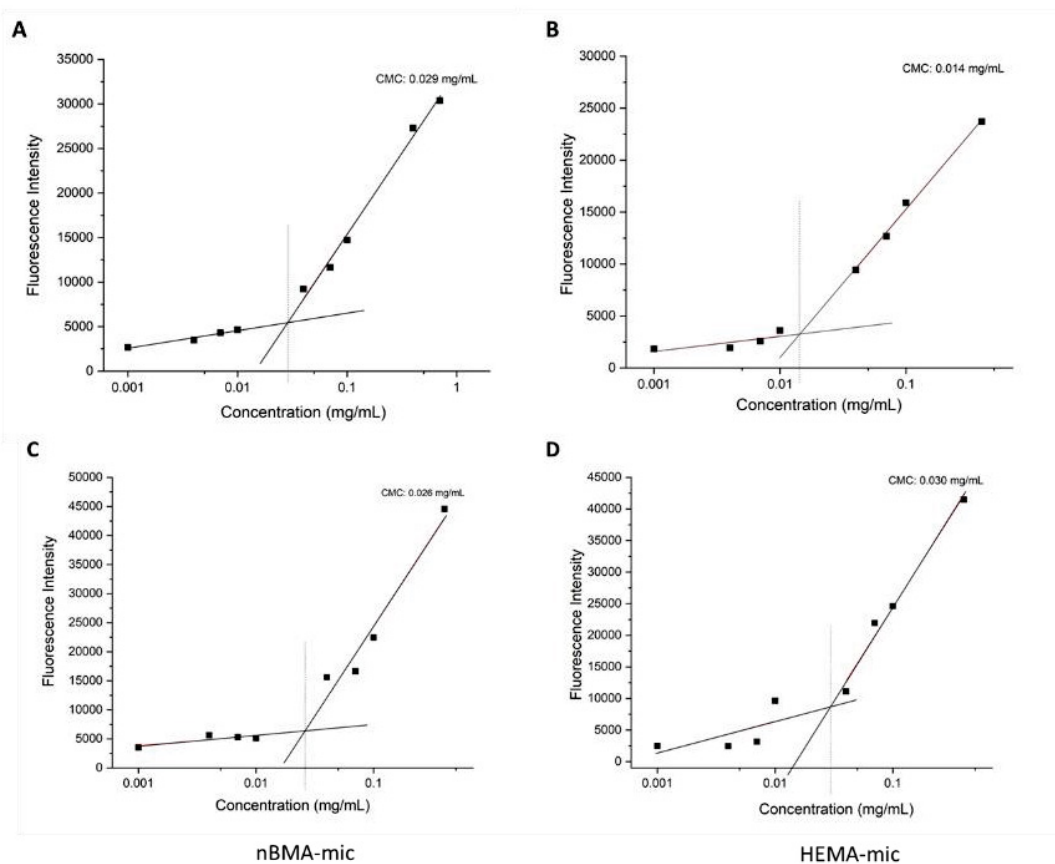


Figure S17. DLS measurement of the micelles at different concentrations.





**Figure S18.** CMC determination.

Maximum of each fluorescence emission spectra was plotted versus the micelle concentration for each sample respectively at 25 °C with a Tecan Infinite M200 PRO microplate reader, using Nile Red as the fluorescence dye as a probe. A) LAMA-mic II, B) LAMA-mic I, C) nBMA-mic, D) HEMA-mic.

## REFERENCES

1. McRae Page S, Martorella M, Parelkar S, Kosif I, Emrick T: **Disulfide cross-linked phosphorylcholine micelles for triggered release of camptothecin.** *Molecular pharmaceutics* 2013, **10**:2684-2692.
2. Larnaudie S: **Supramolecular cyclic peptide-polymer nanotubes as drug delivery vectors.** University of Warwick, 2017.
3. Bauer M, Lautenschlaeger C, Kempe K, Tauhardt L, Schubert US, Fischer D: **Poly(2-ethyl-2-oxazoline) as Alternative for the Stealth Polymer Poly(ethylene glycol): Comparison of in vitro Cytotoxicity and Hemocompatibility.** *Macromol Biosci* 2012, **12**:986-998.
4. Richter F, Martin L, Leer K, Moek E, Hausig F, Brendel JC, Traeger A: **Tuning of endosomal escape and gene expression by functional groups, molecular weight and transfection medium: a structure-activity relationship study.** *J Mater Chem B* 2020, **8**:5026-5041.

## Publication Pub6

### Solely aqueous formulation of hydrophobic cationic polymers for efficient gene delivery

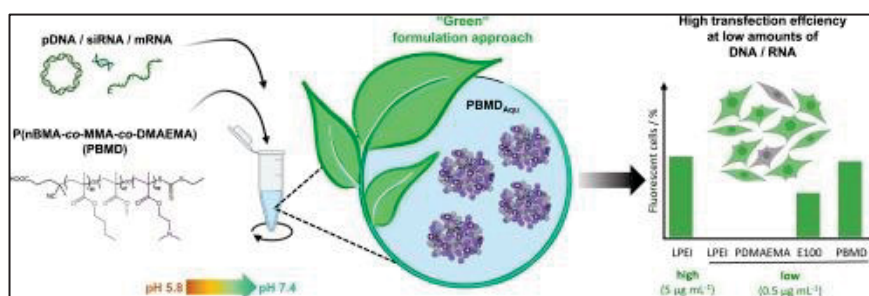
J. I. Solomun, G. Cinar, P. Mapfumo, F. Richter, E. Moek, F. Hausig, L. Martin, S. Hoepfener, I. Nischang, A. Traeger

*Int. J. Pharm.* **2021**, 593, 120080

Reproduced with permission of Elsevier. Copyright © 2021.

The article and the supporting information are available online:

[doi.org/10.1016/j.ijpharm.2020.120080](https://doi.org/10.1016/j.ijpharm.2020.120080)





Contents lists available at ScienceDirect

## International Journal of Pharmaceutics

journal homepage: [www.elsevier.com/locate/ijpharm](http://www.elsevier.com/locate/ijpharm)

## Solely aqueous formulation of hydrophobic cationic polymers for efficient gene delivery

Jana I. Solomun<sup>a</sup>, Gizem Cinar<sup>a</sup>, Prosper Mapfumo<sup>a</sup>, Friederike Richter<sup>a</sup>, Elisabeth Moek<sup>a</sup>, Franziska Hausig<sup>a</sup>, Liam Martin<sup>a</sup>, Stephanie Hoepfener<sup>a,b</sup>, Ivo Nischang<sup>a,b</sup>, Anja Traeger<sup>a,b,\*</sup><sup>a</sup> Laboratory of Organic Chemistry and Macromolecular Chemistry (IOMC), Friedrich Schiller University Jena, Humboldtstrasse 10, 07743 Jena, Germany<sup>b</sup> Jena Center for Soft Matter (JCSM), Friedrich Schiller University Jena, Philosophenweg 7, 07743 Jena, Germany

## ARTICLE INFO

## Keywords:

Aqueous formulation  
Cationic polymer  
Hydrophobicity  
mRNA delivery  
RAFT polymerization  
siRNA delivery

## ABSTRACT

Cationic polymers are promising gene delivery vectors due to their ability to bind and protect genetic material. The introduction of hydrophobic moieties into cationic polymers can further improve the vector efficiency, but common formulations of hydrophobic polymers involve harsh conditions such as organic solvents, impairing intactness and loading efficiency of the genetic material. In this study, a mild, aqueous formulation method for the encapsulation of high amounts of genetic material is presented. A well-defined pH-responsive hydrophobic copolymer, *i.e.* poly(*n*-butylmethacrylate)-*co*-(methylmethacrylate)-*co*-(2-(dimethylamino) ethylmethacrylate)), (PBMD) was synthesized by reversible addition fragmentation chain transfer (RAFT) polymerization. Exploiting the pH-dependent solubility behavior of the polymer, stable pDNA loaded nanoparticles were prepared and characterized using analytical ultracentrifugation (AUC), cryo-transmission electron microscopy (cryo-TEM) and dynamic light scattering (DLS). This novel formulation approach showed high transfection efficiencies in HEK293T cells, while requiring 5- to 10-fold less pDNA compared to linear polyethylenimine (LPEI), in particular at short incubation times and in serum-containing media. Furthermore, the formulation was successfully adopted for siRNA and mRNA encapsulation and the commercially approved polymer Eudragit® E(PO/100). Overall, the aqueous formulation approach, accompanied by a tailor-made hydrophobic polymer and detailed physico-chemical and application studies, led to improved gene delivery vectors with high potential for further applications.

## 1. Introduction

In the past years, it has been shown that several human diseases have a genetic origin and result in symptoms caused by a malfunction in the protein expression. Such malfunctions may be mitigated by the introduction of genetic material into affected cells (Dunbar et al., 2018; Pack et al., 2005). Furthermore, the introduction of nucleic acids such as pDNA and mRNA encoding for antigens is a promising approach for vaccination against infectious diseases and in tumor immunotherapies (Ginn et al., 2018; Hobernik and Bros, 2018; Lopes et al., 2019). Nucleic acids are easily degraded by ubiquitously present nucleases, and their negative net charge also hampers their ability to cross cellular membranes. Therefore, a suitable delivery system is required (Abdelhady et al., 2003; Yin et al., 2014). To date, mostly viral vectors have entered clinical trials for evaluation due to their natural ability to infect cells and

their high delivery efficiency. However, viral vectors are potentially immunogenic and pathogenic, encapsulate only a limited quantity of genetic material per vector, and can be costly to produce (Lundstrom, 2018; Shirley et al., 2020).

Polymer-based, synthetic systems represent a promising area of research to bypass the above-mentioned obstacles. The versatility in architecture, design, and functionalization of cationic polymers offers numerous possibilities to tune the interaction with genetic material, ultimately controlling the size, charge distribution, and stability of the polymer-DNA complexes under physiological conditions (Wong et al., 2007). Additionally, polymers possess the ability to protect negatively charged genetic material from degradation and can facilitate cellular uptake (Bloomfield, 1997). The cationic moieties further contribute to passing intracellular barriers such as the endosomal membrane to avoid lysosomal degradation and to release the intact genetic material at its

\* Corresponding author at: Laboratory of Organic and Macromolecular Chemistry (IOMC), Friedrich Schiller University Jena, Humboldtstrasse 10, 07743 Jena, Germany.

E-mail address: [anja.traeger@uni-jena.de](mailto:anja.traeger@uni-jena.de) (A. Traeger).

<https://doi.org/10.1016/j.ijpharm.2020.120080>

Received 26 August 2020; Received in revised form 5 November 2020; Accepted 8 November 2020

Available online 25 November 2020

0378-5173/© 2020 Elsevier B.V. All rights reserved.

desired site of action (Laechelt and Wagner, 2015; Pack et al., 2005). The introduction of hydrophobic moieties into cationic polymers has been found to be beneficial for delivery systems *in vitro* and *in vivo* as this facilitates association and interaction with the lipophilic cell membrane surfaces, thus, promoting cellular uptake and subsequent release from the endosomes (Adolph et al., 2014; Convertine et al., 2009; Incani et al., 2010; Liu et al., 2010; Wakefield et al., 2005). Furthermore, hydrophobicity can induce assembly of polymers in polar environments, improving the complex stability through hydrophobic interactions, particularly under physiological conditions in the presence of proteins and salts (Adolph et al., 2014; Eltoukhy et al., 2013; Rinkenauer et al., 2015a). Optimization of these effects can be facilitated through controlling the hydrophilic-hydrophobic balance within the polymer over the entire physiologically relevant pH range by fine-tuning the combination of cationic pH-responsive and hydrophobic groups (Convertine et al., 2009). The hydrophobic character of the polymers can be introduced in a number of ways, such as functionalization of the cationic polymer with lipophilic moieties such as acetyl groups, lipids, and cholesterol, (Forrest et al., 2004; Han et al., 2001; Schroeder et al., 2012) by the choice of the polymer backbone chemistry, (e.g., norbornenes, methacrylates, acrylates), (Breitenkamp and Emrick, 2008; Rinkenauer et al., 2015b; Smith et al., 2007; van de Wetering et al., 1999) or by introducing monomers in the polymer architecture with hydrophobic side chains such as alkanes, fluorinated, synthetic, or natural aromatic systems (Adolph et al., 2014; Buerkli et al., 2014; Cokca et al., 2020; Eltoukhy et al., 2013; Nelson et al., 2013; Shen et al., 2020; Tan et al., 2018; Wakefield et al., 2005). It was shown that hydrophobic modifications of e.g., poly(2-(dimethylamino)ethyl methacrylate) (PDMAEMA) led to enhancing effects on the gene delivery efficiency (Cheng et al., 2012; Convertine et al., 2009; Manganiello et al., 2012; Nelson et al., 2013). However, most studies were conducted with water-soluble polymers enabling complexation of genetic material in aqueous media. In this case, solubility was maintained by limiting the number of the hydrophobic groups incorporated into the polymer or by designing amphiphilic block copolymers that self-assemble into larger structures in solution (e.g., micelles). However, by a further increase in hydrophobicity, not only water solubility of the polymers is reduced, but also the encapsulation of the genetic material becomes more challenging due to the hydrophilic character of the nucleic acids. Therefore, the formulation method should be carefully designed to ensure sufficient complexation or encapsulation of the genetic material.

Common methods applied for formulation of nanoparticles from water-insoluble, hydrophobic polymers are the emulsion/solvent evaporation and the nanoprecipitation techniques. These methods are applicable to a wide variety of polymers and cargos, and allow to tune nanoparticle size and dispersity (Perevyazko et al., 2012; Yildirim et al., 2015). Genetic material can be encapsulated via different approaches: (i) pre-complexation with cationic polymers followed by encapsulation via emulsion techniques (Press et al., 2014); (ii) addition of the genetic material during the formulation (Cohen et al., 2000; Niu et al., 2009), (iii) complexation to the surface of preformulated cationic particles by electrostatic interactions (Bivas-Benita et al., 2004; Jain et al., 2015), or (iv) complexation of genetic material to the surface of particles coated with cationic surfactants or polymers (Fay et al., 2010). The emulsion method requires the application of ultrasonication or high-speed homogenization, exposing the genetic material to harsh conditions during the formulation process, potentially impairing its integrity and, therefore, its functionality (Lengsfeld and Anchordoquy, 2002). Subsequent addition of genetic material to preformulated nanoparticles is a possibility to avoid exposure to such harsh conditions. However, limitation of pDNA complexation to the nanoparticle surface potentially leads to reduced encapsulation/binding efficiencies compared to encapsulation within the nanoparticle. In comparison to the emulsion technique, nanoprecipitation is a relatively simple and mild method, which does not expose genetic material to high shear forces or temperatures during formulation. It also allows the encapsulation of genetic material during

the formulation process. However, the typical use of organic solvents, which potentially induce cytotoxicity and other adverse effects in biological systems, requires extensive post-formulation purification procedures (evaporation or dialysis) before they can be used as a therapeutic agent (Brayton, 1986; Jamalzadeh et al., 2016).

A well-known example for a hydrophobic cationic polymer used for nanoparticle formulation by the emulsion or nanoprecipitation technique is the commercial polymer Eudragit® E(PO/100) composed of a pH-responsive cationic 2-(dimethylamino)ethyl methacrylate (DMAEMA) unit copolymerized with *n*-butyl methacrylate (*n*BMA) and methyl methacrylate (MMA) as hydrophobic moieties in a typical mass ratio of 2:1:1. This copolymer was approved by the Food and Drug Administration (FDA) and European Medicines Agency (EMA) as a coating material for orally administered drugs and has been used for nanoparticulate encapsulation and binding of several drugs (e.g., curcumin, genistein, efavirenz) (Hari et al., 2016; Moorthi et al., 2013; Tang et al., 2011) including genetic material. In a study by Lehr and colleagues, Eudragit® E(PO/100) nanoparticles formulated by the emulsion technique were used to bind siRNA and were shown to induce knock-down of the Bfl1/A1 gene in macrophages (Jain et al., 2015). Another approach by Singh and coworkers used nanoparticles composed of Eudragit® E(PO/100) and PLGA coated with the cationic surfactant cetyltrimethylammonium bromide (CTAB) to transport IL-10 encoding pDNA *in vivo* (Basarkar and Singh, 2009). Both studies demonstrated the potential of the Eudragit® E(PO/100) polymer for efficient gene delivery, but were limited to organic solvent-based formulation methods or surface binding of the genetic material.

The aim of this study was to fully exploit the potential of cationic hydrophobic polymers and to develop a new “green” and organic solvent-free formulation technique that allows the encapsulation of genetic material without the associated cytotoxic effects potentially imposed by the use of organic solvents. Reversible addition fragmentation chain transfer (RAFT) polymerization was used to synthesize a well-defined statistical copolymer P(*n*BMA-*co*-MMA-*co*-DMAEMA) (PBMD) with a monomer composition comparable to the Eudragit® E(PO/100) polymer. Firstly, the PBMD polymer was tested for pDNA binding and release capability in the physiologically relevant pH range (lysosomal to blood pH, pH 5 to pH 7.4). Subsequently, the PBMD polymer was used for encapsulation of pDNA by applying an organic solvent-free, pH-driven formulation technique. The formulated pDNA-polymer complexes (PBMD<sub>Aqu</sub>(pDNA)) were then characterized by dynamic light scattering (DLS), cryo-transmission electron microscopy (cryo-TEM), and analytical ultracentrifugation (AUC). The transfection efficiency was compared to nanoparticles manufactured by the common nanoprecipitation method with surface-bound pDNA. The PBMD<sub>Aqu</sub>(pDNA) complexes were further optimized for transfection efficiency in HEK293T cells. The optimized formulation and transfection conditions were then also applied to the commercially available polymer Eudragit® E(PO/100), and compared to other commercially-available and polymer-based transfection agents such as LPEI and Viromer® RED. Furthermore, the new formulation technique was successfully implemented for the complexation and transfection of siRNA and mRNA, thus demonstrating the broad application potential of the polymer and formulation method developed here.

## 2. Materials and methods

Materials and further methods can be found in the [supporting information](#) (SI).

### 2.1. Synthesis of P(*n*BMA-*co*-MMA-*co*-DMAEMA) (PBMD) via RAFT polymerization

(4-cyanopentanoic acid)ylethyl trithiocarbonate (CPAETC) (130.7 mg,  $4.96 \times 10^{-4}$  mol), *n*BMA (3.5 g,  $2.48 \times 10^{-2}$  mol), MMA (2.5 g,  $2.52 \times 10^{-2}$  mol), DMAEMA (7.8 g,  $4.97 \times 10^{-2}$  mol), 1,4-dioxane (6.2

g), a 1.0% (w/w) solution of 4,4-azobis(4-cyanovaleic acid) (ACVA) in 1,4-dioxane (1.4 g, 14.4 mg ACVA,  $5.12 \times 10^{-5}$  mol) and 1,3,5-trioxane (external NMR standard, 23.7 mg) were introduced to a 20 mL micro-wave vial equipped with a magnetic stirring bar. The vial was sealed, and the solution deoxygenated by bubbling argon through it for approx. 10 min. The vial was placed in an oil bath set at 70 °C and allowed to stir for 21 h, with samples taken for  $^1\text{H}$  NMR and size exclusion chromatography in DMAc (DMAc-SEC) at designated times. The polymer was precipitated three times from THF into cold hexane and dried under reduced pressure to give a yellow solid. DMAc-SEC:  $M_{n,SEC} = 25.1$  kg  $\text{mol}^{-1}$ ,  $D = 1.13$ .

## 2.2. Acid-base titration

Titration of the polymers was conducted using a Metrohm OMNIS integrated titration system (Metrohm, Herisau, Switzerland). For a typical measurement, the polymer was dissolved in 150 mM NaCl (in 0.02 M HCl) at 5 mg  $\text{mL}^{-1}$ . 9 mL of this solution was taken, and 1 M HCl (50  $\mu\text{L}$ ) was added to give an acidic solution (pH < 2). The polymers were titrated against 0.1 M NaOH solution to a pH value of  $\approx 12$ . The  $pK_a$  values were estimated from equivalence points determined by the OMNIS titration software, using the Henderson-Hasselbalch equation (1), where [HA] is the concentration of acid and  $[A^-]$  the concentration of the corresponding base:

$$pH = pK_a + \log \frac{[A^-]}{[HA]} \quad (1)$$

## 2.3. Gel retardation assay (GRA)

pDNA binding ability of LPEI, PDMAEMA, and the PBMD polymer at varying nitrogen to phosphate (N/P) ratios were determined by agarose gel electrophoresis. PDMAEMA and PBMD polymer were dissolved in 0.2 M sodium acetate buffer (pH 5.8) at a concentration of 2 mg  $\text{mL}^{-1}$ . LPEI was dissolved in water acidified with HCl at a concentration of 1 mg  $\text{mL}^{-1}$ . Subsequently, the polymers and the pKMyC pDNA stock solution in water were diluted in HBG buffer (5% (w/v) glucose, 20 mM (4-(2-hydroxyethyl)-1-piperazineethanesulfonic acid) (HEPES), pH 7.4) to the respective concentrations needed for various N/P ratios, mixed 1:2 by vortexing and incubated for 15 min. The samples were diluted 6:1 with green gel loading buffer (Jena Biosciences, Jena, Germany) and were run on a 1% (w/v) agarose gel stained with ethidium bromide (EtBr, 0.1  $\mu\text{g mL}^{-1}$ ) at 80 V for 1.5 h. The gels were subsequently imaged by using a gel imager (Red™ Imaging System, Alpha Innotech, Kasendorf, Germany).

## 2.4. Ethidium bromide binding assay (EBA) and heparin release assay (HRA)

pDNA complexation and complex stability were further investigated by using an EtBr quenching and heparin release assay as described elsewhere (Richter et al., 2020). Briefly, pKMyC-pDNA at a concentration of 15  $\mu\text{g mL}^{-1}$  was incubated with EtBr in HBG buffer (pH 7.4) for 10 min. The polymer stock solutions (prepared as described above) were diluted with HBG buffer (pH 7.4) in a black 96-well plate (Nunc, Thermo Fisher, Waltham, MA, U.S.) to reach N/P ratios ranging from 1 to 50. Subsequently, pDNA was added and the complexes were incubated at 37 °C for 15 min. EtBr fluorescence intensity was measured at  $\lambda_{\text{Ex}} = 525$  nm /  $\lambda_{\text{Em}} = 605$  nm. pDNA without polymer was defined as 100% free pDNA. The release of complexed pDNA was studied by stepwise addition of heparin and measurement of the resulting changes in EtBr fluorescence intensity. Influence of the pH value on pDNA binding and release was studied by performing the assay at varying pH values in the respective buffers (0.2 M acetate buffer pH 5; 5.8 and HBG buffer pH 6.5; 7; 7.4). The obtained measurement points were fitted using Origin Pro Software (Version 2018b, Origin Lab Corporation, Northampton, MA, U.

S.) using either logistic or exponential functions to represent the apparent experimental results as a guide to the eye.

## 2.5. Aqueous formulation approach for pDNA encapsulation (PBMD<sub>Aqu</sub>(pDNA))

A stock solution of the PBMD polymer was prepared by dissolution in 0.2 M sodium acetate buffer (pH 5.8). pDNA (pCMV-GFP, mEGFP-N1 or pKMyC) was dissolved in ultrapure water. The solutions were stored at 4 °C prior to use. To prepare PBMD<sub>Aqu</sub>(pDNA) complexes the PBMD polymer and the pDNA were, accordingly to the GRA and EBA, diluted in HBG buffer (pH 7.4; for DLS and transfection experiments) or 20 mM HEPES buffer (for cryo-TEM and AUC measurements) to reach the respective N/P ratios and mixed in a ratio of 1:2. The mixtures were vortexed immediately for 10 s and incubated for at least 15 min at room temperature (RT) before usage.

## 2.6. Organic solvent-based formulation of nanoparticles (PBMD<sub>Org</sub>(out, pDNA), PBMD<sub>Org</sub>(in,pDNA))

For nanoparticle formulation, the polymer was dissolved in 2.5 mL acetone (2 mg  $\text{mL}^{-1}$ ). The polymer solution was dropped manually into 5 mL ultrapure water and the resulting nanoparticle suspension was stirred at 800 rpm overnight to allow the organic solvent to evaporate. Then, the suspensions were stored at 4 °C until usage. To determine the concentration after solvent evaporation, a known volume of the nanoparticle suspension was lyophilized, and the dry residues were weighed afterwards. To reach the respective N/P ratios, pDNA (pCMV-GFP) at varying concentrations was either added during the formulation process to the polymer dissolved in acetone (prior to precipitation in water, PBMD<sub>Org</sub>(in,pDNA)) or after nanoprecipitation to the final aqueous particle suspension (PBMD<sub>Org</sub>(out,pDNA)).

## 2.7. Dynamic light scattering (DLS)

Hydrodynamic diameter and zeta potential of PBMD<sub>Org</sub>(out,pDNA), PBMD<sub>Org</sub>(in,pDNA), and PBMD<sub>Aqu</sub>(pDNA) complexes formulated with pCMV-GFP pDNA at varying N/P ratios were determined by using dynamic and electrophoretic light scattering (DLS/ELS, Zetasizer Nano-ZS, Malvern Instruments, Worcestershire, U.K.). The nanoparticles were diluted in ultrapure water for size and zeta potential determinations. PBMD<sub>Aqu</sub>(pDNA) complexes were prepared at a pDNA concentration of 15  $\mu\text{g mL}^{-1}$  in 50  $\mu\text{L}$  HBG buffer for size measurements and were further diluted to 800  $\mu\text{L}$  with ultrapure water for zeta potential determination. The instrument was operated with a 633 nm He-Ne Laser and intensity fluctuations at a backscattering angle of 173° at a temperature of 25 °C were measured. At least three batches were measured per sample. The derived hydrodynamic diameters are presented as mean  $\pm$  SD. Large aggregates ( $\geq 1000$  nm) were considered as a fixed value (1000 nm) when calculating the mean and standard deviation. Original data, exemplary decay functions, and derived hydrodynamic diameter distributions are shown in the SI (Table S1 to S4, Fig. S2, S3).

## 2.8. Cryo-transmission electron microscopy (cryo-TEM) and scanning electron microscopy (SEM) measurements

PBMD<sub>Aqu</sub>(pDNA) at N/P 20 using mEGFP-N1 pDNA in 20 mM HEPES buffer and PBMD<sub>Org</sub>(in,pDNA) nanoparticles using pCMV-GFP pDNA were prepared as described above. Electron microscopy imaging was performed with a Sigma VP Field Emission Scanning Electron Microscope (Carl-Zeiss, Jena, Germany) using an InLens detector with an acceleration voltage of 6 kV. The samples were coated with a thin layer of platinum (4 nm) via sputter coating (CCU-010 HV, Safematic, Zizers, Switzerland). Cryo-TEM investigations were performed on a FEI Tecnai G<sup>2</sup> 20 transmission electron microscope at an acceleration voltage of 200 kV. Samples were blotted onto a Quantifoil grid (R 2/2, Quantifoil,

8.5  $\mu\text{L}$  of solutions with a concentration of  $250 \mu\text{g mL}^{-1}$  utilizing a VitroBot Mark IV preparation unit (blotting time 1 s, offset  $-6 \text{ mm}$ ). Samples were vitrified utilizing liquid ethane as a cryogen. After blotting, the sample temperature was maintained at a temperature below  $-165 \text{ }^\circ\text{C}$  at all times. The grids were loaded into the cryo-holder (Gatan 626) using the Gatan cryo transfer stage. Images were acquired with a CCD camera (MegaView, Olympus Soft Imaging Solutions, Muenster, Germany). Contrast adjustments and image analysis was performed by ImageJ (Version 1.52a, National Institutes of Health, Bethesda, MD, U.S.).

## 2.9. Sedimentation velocity experiments via analytical ultracentrifugation (AUC)

The PBMD<sub>Aqu</sub>(pDNA) complexes and PDMAEMA polyplexes at N/P 20 were prepared in 20 mM HEPES buffer using td-tomato-N1 pDNA to obtain concentrations up to  $1 \text{ mg mL}^{-1}$ . The complexes were investigated via sedimentation velocity AUC experiments at different concentrations ( $0.1\text{--}1 \text{ mg mL}^{-1}$ ) using the universal refractive index (RI) detection in terms of interference fringes and the absorbance detection in terms of optical density (OD). A rotor speed of 7,500 rpm was used for 24 h, followed by spinning the rotor at a speed of 42,000 rpm for a further 24 h in order to investigate potentially present smaller species. All AUC experiments were performed using an Optima AUC (Beckman Coulter Instruments, Brea, CA, U.S.) with an An-50 Ti eight-hole rotor. The ultracentrifuge cells contained double sector epon centerpieces with a 12 mm optical solution path length. The cells were assembled with sapphire windows. The corresponding sectors were filled with approx.  $440 \mu\text{L}$  pure solvent in the reference sector and approx.  $420 \mu\text{L}$  of diluted sample solution in the sample sector. Rotor position eight was used as the counterbalance and for the optical module calibration. Scans were acquired in six-minute intervals. All experiments were performed at  $20 \text{ }^\circ\text{C}$ . The RI detection as well as absorbance detection in terms of OD at the wavelength of the RAFT-agent containing polymer, *i.e.* at  $\lambda = 310 \text{ nm}$ , and that of the DNA, *i.e.* at  $\lambda = 260 \text{ nm}$ , were utilized for the observation of sedimentation boundaries in respect to time in the AUC cells. The recorded sedimentation velocity data were numerically analyzed with SEDFIT and the  $ls - g^*(s)$  model considering non-diffusing species (Schuck and Rossmanith, 2000).

## 2.10. Transfection of HEK293T cells with mEGFP-N1 pDNA

The HEK293T cell line was cultured in Dulbecco's modified eagle medium (DMEM,  $1 \text{ g L}^{-1}$  glucose, 10% (v/v), fetal bovine serum (FBS),  $100 \text{ U mL}^{-1}$  penicillin and  $100 \mu\text{g mL}^{-1}$  streptomycin) (growth medium) at  $37 \text{ }^\circ\text{C}$  in a humidified 5% (v/v)  $\text{CO}_2$  atmosphere. For transfection experiments,  $0.2 \times 10^6$  cells  $\text{mL}^{-1}$  were seeded into a 24-well plate in  $500 \mu\text{L}$  growth medium supplemented with 10 mM HEPES and allowed to recover for 24 h. 1 h prior to treatment, medium was changed to  $450 \mu\text{L}$  fresh growth medium (with 10 mM HEPES). PBMD<sub>Aqu</sub>(pDNA) complexes and LPEI and PDMAEMA polyplexes were freshly prepared as described above using mEGFP-N1 pDNA and pMyc pDNA (not encoding for green fluorescent protein as negative control). Cells were treated with  $50 \mu\text{L}$  sample solution of the indicated N/P ratio and pDNA concentration or HBG buffer as control and incubated for 1 or 4 h. Subsequently, the supernatant was removed, replaced by fresh growth medium (with 10 mM HEPES) and the cells were further incubated up to 24 h. After incubation, the cells were detached by trypsin-EDTA, resuspended in Hank's Balanced Salt Solution (HBSS) (2% (v/v) FBS, 20 mM HEPES) and measured by flow cytometry (CytoFlex S, Beckman Coulter, Brea, CA, U.S.). A quantity of  $10^4$  cells was analyzed by their forward and sideward scatter (FSC/SSC) to determine the viable single cells. The EGFP expression of the viable single cells was analyzed at  $\lambda_{\text{Ex}} = 488 \text{ nm}$  combined with a  $525/40 \text{ nm}$  bandpass filter (FITC channel). Fluorescent cells were identified by gating to the negative control not encoding for EGFP (pMyc-polymer complex). A detailed gating

strategy is shown in the supporting information (SI, Fig. S5). Further, the cells were imaged by using a Cytation5 Cell Imaging Multi-Mode Reader (BioTek Instruments, Inc., Winooski, VT, USA) equipped with a 4x objective using brightfield imaging and the FITC channel ( $\lambda_{\text{Ex}} = 469/35 \text{ nm}$ ,  $\lambda_{\text{Em}} = 525/39 \text{ nm}$ ). Images were processed using ImageJ software

## 2.11. Knock-down of GFP in HEK-GFP cells using anti-GFP-siRNA

The HEK-GFP cell line was cultivated in growth medium at  $37 \text{ }^\circ\text{C}$  in a humidified 5% (v/v)  $\text{CO}_2$  atmosphere. 24 h prior to transfection experiments,  $0.1 \times 10^6$  cells  $\text{mL}^{-1}$  were placed in a 24-well plate in  $500 \mu\text{L}$  growth medium supplemented with 10 mM HEPES and allowed to grow. The growth medium was replaced by  $450 \mu\text{L}$  fresh growth medium (with 10 mM HEPES) 1 h prior to treatment. PBMD<sub>Aqu</sub>(siRNA) complexes were freshly prepared as described for pDNA-complexes using anti-GFP siRNA (sense: GCAAGCUGACCCUGAAGUUCAU, antisense: GAACUUCAGGGU-CAGCUUGCCG and neg. control siRNA (sense: UUCUCCGAACGUGU-CAGUdTdT, antisense: ACGUGACACGUUCGGAGAAdTdT). The cells were treated with  $50 \mu\text{L}$  of the freshly prepared complexes. Complexes with negative control siRNA and HBG buffer were used as negative controls. Lipofectamine was used as a commercial positive control prepared according to the manufacturers protocol using the same siRNA concentration as for the PBMD<sub>Aqu</sub>(siRNA) complexes. 24 h after treatment, the samples were removed, replaced by fresh growth medium (with 10 mM HEPES), and incubated up to 72 h. The cells were detached with trypsin-EDTA. After resuspension in HBSS, the cells were analyzed by flow cytometry at an excitation wavelength of 488 nm and a  $525/40 \text{ nm}$  bandpass filter (OD1; FITC-OD1 channel). The gating strategy is shown in the SI (Fig. S6).

## 2.12. Transfection of HEK293T cells with GFP-mRNA

The HEK293T cell line was cultivated and seeded into 24-well plates prior to experiments as described above. The medium was replaced by  $450 \mu\text{L}$  fresh growth medium (10 mM HEPES) 1 h prior to treatment. PBMD<sub>Aqu</sub>(mRNA) complexes with GFP-mRNA were freshly prepared as described for pDNA complexes. Complexes with Viromer® RED were prepared as described by the manufacturers protocol and subsequently diluted to the respective mRNA concentration.  $50 \mu\text{L}$  of the samples was added to the cells and incubated for 4 h. Subsequently, the samples were replaced by fresh growth medium and the cells were incubated for another 20 h. After incubation, the cells were detached by trypsin-EDTA and resuspended in HBSS for analysis by flow cytometry. The fluorescence of the viable single cells was analyzed at  $\lambda_{\text{Ex}} = 488 \text{ nm}$  using the FITC channel (gating strategy: Fig. S7).

## 2.13. PrestoBlue™ assay for determination of cytotoxicity in HEK293T and L-929 cells

For cytotoxicity assays, HEK293T cells were seeded into 24-well plates at a density of  $0.2 \times 10^6$  cells  $\text{mL}^{-1}$  in  $500 \mu\text{L}$  growth medium (with 10 mM HEPES) and incubated for 24 h to allow cell recovery. After a media change to  $450 \mu\text{L}$  fresh growth medium 1 h prior to treatment,  $50 \mu\text{L}$  of PBMD<sub>Aqu</sub>(pDNA) complex was added to test a concentration range of  $0.25\text{--}1.5 \mu\text{g mL}^{-1}$  pDNA. The cells were incubated with the samples for 1, 4 or 24 h. Subsequently, the supernatant was removed and replaced with  $500 \mu\text{L}$  fresh growth medium (with 10 mM HEPES). 24 h after treatment, the medium was replaced by a 10% (v/v) solution of PrestoBlue™ diluted with growth medium. The cells were incubated for 45 min and the supernatant was transferred to a 96-well plate ( $100 \mu\text{L}$  per well) to measure fluorescence intensity ( $\lambda_{\text{Ex}} = 560 \text{ nm}$ ,  $\lambda_{\text{Em}} = 590 \text{ nm}$ ). Cells treated with HBG buffer were used as a control, and the viability was calculated relative to the buffer control after subtracting the blank (PrestoBlue™ diluted in medium 1:10 without cells). Data were fitted in OriginPro2018b (OriginLab Corporation, Northampton, MA, U.S) with a logistic function. The  $\text{IC}_{50}$  was calculated as the value

where the samples show 50% viability relative to the control.

For toxicity tests in L-929 cells, the cells were seeded in a 96-well plate format at a density of  $0.1 \times 10^6$  cells  $\text{mL}^{-1}$  and incubated with the dissolved polymers without addition of pDNA for 1, 4 or 24 h. Cell viability was analyzed as described for the HEK293T cells.

### 2.14. Statistical analysis

Data analysis was conducted using OriginPro2018b software. Multiple groups were analyzed by one-way analysis of variance (one-way ANOVA) followed by Bonferroni's post-hoc test. Normality and homogeneity of variances were assumed. Sample pairs were analyzed by the unpaired t-Test and the Welch-correction was applied when homogeneity of variances was not given. Statistical significance is denoted as follows: \* $P < 0.05$ , \*\* $P < 0.01$ , and \*\*\* $P < 0.001$ .

## 3. Results and discussion

### 3.1. Polymer synthesis and characterization

The terpolymer P(*n*BMA-co-MMA-co-DMAEMA) (PBMD) was prepared via RAFT polymerization in 1,4-dioxane at 70 °C using (4-cyanopentanoic acid)ylethyl trithiocarbonate (CPAETC) as the chain transfer agent (CTA) and 4,4'-azobis(4-cyanovaleric acid) (ACVA) as the azoinitiator (Fig. 1a). An overall degree of polymerization ( $DP_n$ ) of 200 was targeted with a 2:1:1 molar ratio of DMAEMA, *n*BMA, and MMA, respectively, at a combined monomer concentration of 62% (w/w) and a [CPAETC]<sub>0</sub>/[ACVA]<sub>0</sub> ratio of 10. The polymerization kinetics were followed using <sup>1</sup>H NMR spectroscopy and SEC (Fig. 1b). The Ln([M]<sub>0</sub>/

[M]) plot revealed a pseudo first-order polymerization kinetics for all three monomers, each reaching a final conversion of approximately 90% after 21 h. Furthermore, the rate of polymerization for each monomer was found to be very similar, indicating a statistical distribution of moieties throughout the terpolymer backbone and a consistent composition of different molar ratios. The linear evolution of molar mass values with monomer conversion (Fig. 1b) and narrow molar mass distributions ( $D = 1.14$ ) indicate that the RAFT polymerization proceeded in a controlled fashion. The purified polymer possessed a theoretical molar mass ( $M_{n,th}$ ) of 25.4 kg  $\text{mol}^{-1}$  and a molar fraction of 0.51, 0.25, and 0.24 for DMAEMA, *n*BMA, and MMA, respectively, as calculated from <sup>1</sup>H NMR (Fig. 1c). A PDMAEMA homopolymer ( $DP_n = 101$ ), containing a similar number of DMAEMA monomers per chain as the PBMD polymer, served as a control polymer (SI, Fig. S1).

To assess the solubility behavior and pH responsiveness of the PBMD polymer at physiological conditions, titration experiments were conducted (Fig. 1d). The PBMD polymer was dissolved under acidic conditions in 150 mM NaCl and titrated against 0.1 M NaOH. It should be noted that precipitation of the PBMD polymer was observed at higher pH values. Using the Henderson-Hasselbalch equation, the  $pK_a$  from the resulting titration curve gives a value of  $pK_a \sim 6.9$ , noticeably lower than the  $pK_a$  value reported for PDMAEMA ( $pK_a$  7.4) (van de Wetering et al., 1999). This decreased  $pK_a$  value may be attributed to the PBMD polymer chains precipitating out of solution at lower degrees of DMAEMA protonation, due to the incorporation of hydrophobic comonomers. Therefore, the calculated value for the PBMD polymer was only designated as apparent  $pK_a$  of the polymer. Above all, the polymer exhibited a pH-dependent behavior as well as pH-dependent solubility, within the physiological pH range.

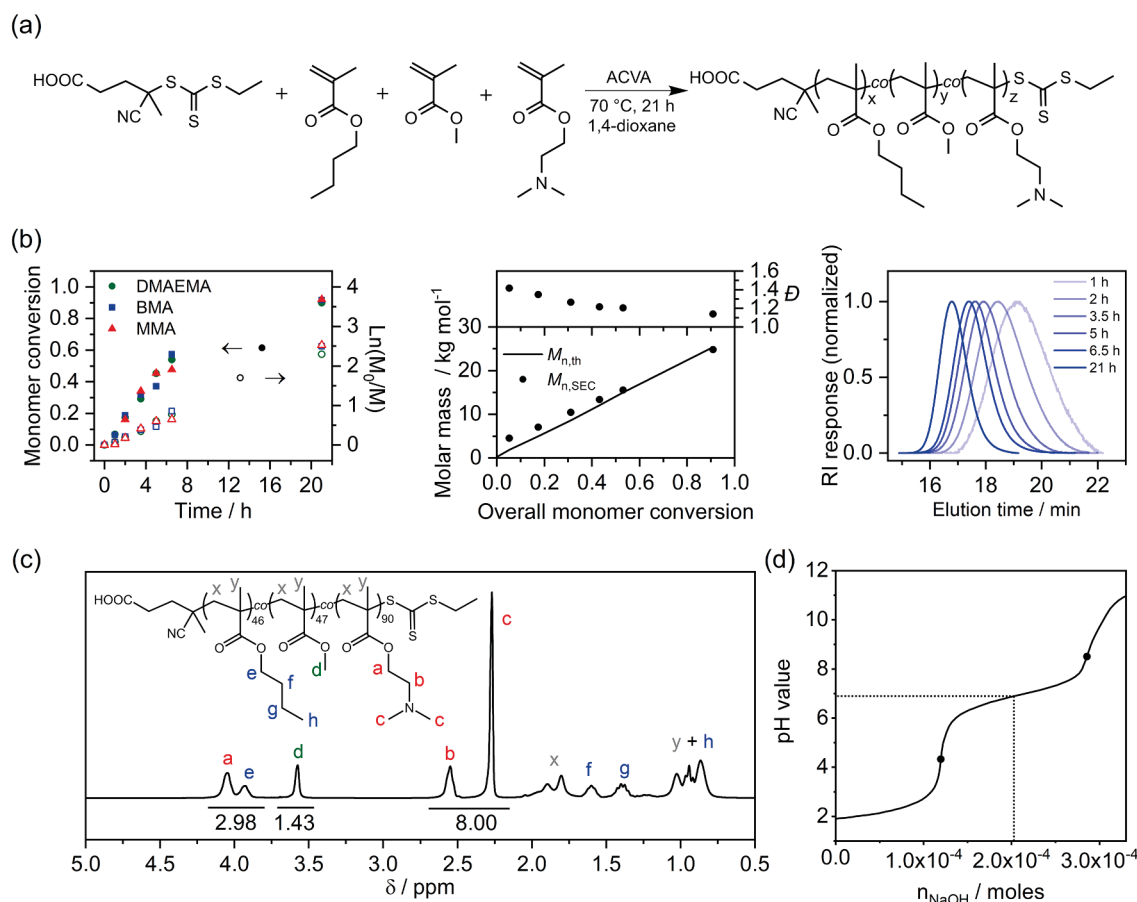


**Fig. 1.** Synthesis and characterization of P(*n*BMA-co-MMA-co-DMAEMA) (PBMD). (a) Polymerization synthesis scheme of P(*n*BMA-co-MMA-co-DMAEMA) (PBMD) via statistical RAFT polymerization. (b) Polymerization kinetics of the RAFT polymerization of PBMD as determined by <sup>1</sup>H NMR and SEC. (c) <sup>1</sup>H NMR of purified PBMD, and (d) titration curve of PBMD in 150 mM NaCl.



### 3.2. pDNA binding and release behavior

An efficient binding of pDNA is the first crucial step in the gene delivery process and required for protection and transport of genetic material. To assess the pDNA binding ability of the PBMD polymer under aqueous conditions, agarose gel electrophoresis was performed for different nitrogen (of the polymer) to phosphate (of the pDNA) ratios (N/P ratios), by dissolving the PBMD polymer in acidic sodium acetate buffer. LPEI and a PDMAEMA homopolymer were investigated as controls, the latter composed of the same number of cationic groups as the PBMD polymer. In the so-called gel retardation assay (GRA), non-

complexed pDNA typically appears with multiple bands representing various plasmid conformations, while complex formation with polymers prevents pDNA migration (Meyers et al., 1976). For all polymers, free pDNA was detectable at N/P 1, but at N/P ratios of 5 and higher, PBMD and the other polymers showed efficient complexation (Fig. 2a). To investigate the pDNA-polymer-interaction in more detail, the binding was further characterized by the ethidium bromide binding assay (EBA). The fluorescence of ethidium bromide (EtBr) is reduced in the presence of water, while it is increased by intercalation into the hydrophobic region between DNA base pairs (LePecq and Paoletti, 1967; Olmsted and Kearns, 1977). EtBr can be displaced by complex formation of pDNA

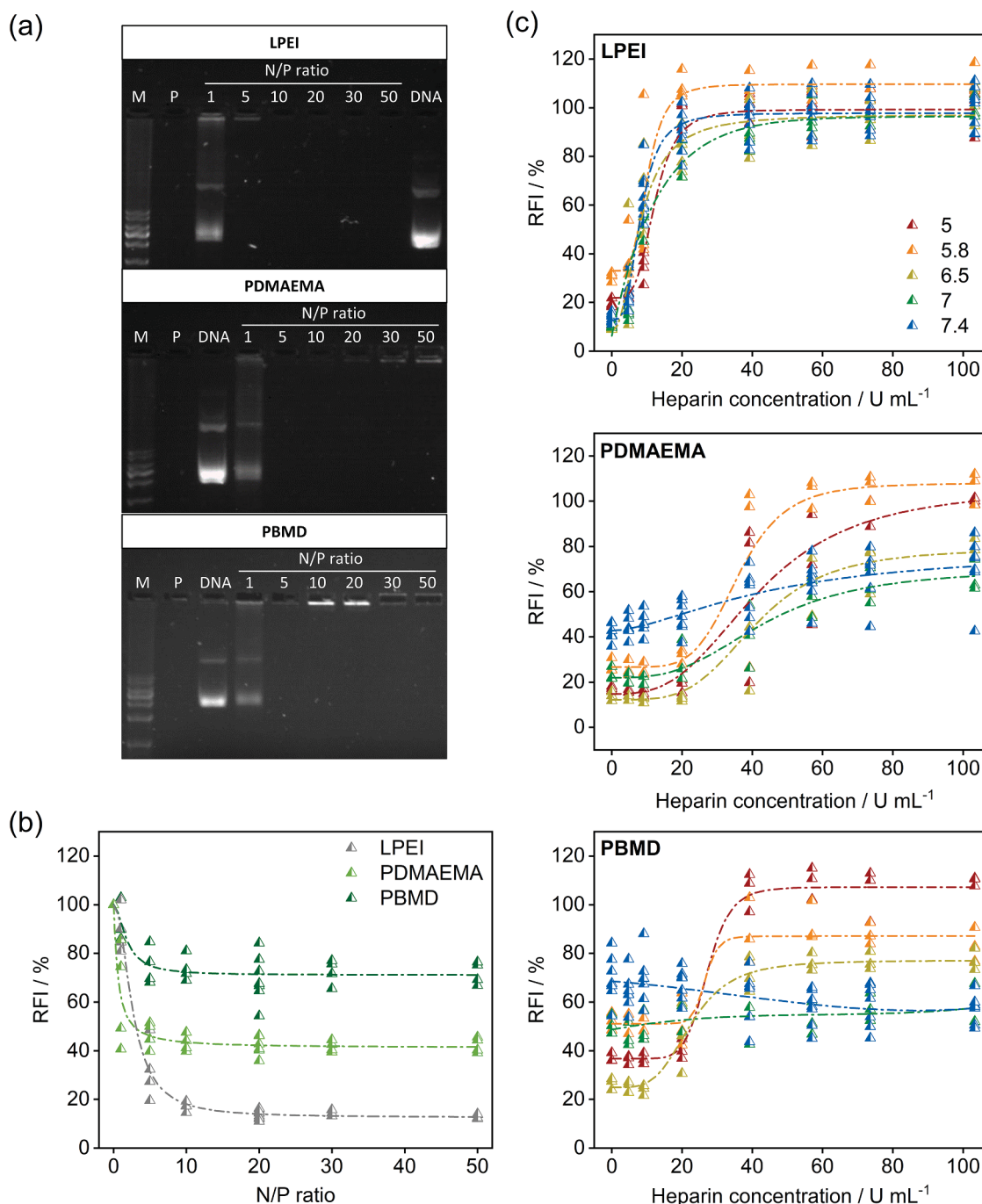


**Fig. 2.** DNA binding and release behavior of the PBMD polymer, PDMAEMA, and LPEI. pDNA binding ability of the polymers was studied by (a) agarose gel electrophoresis (M: marker; DNA: pDNA; P: polymer without pDNA) and (b) EBA in HBG buffer at pH 7.4 at different N/P ratios (1–50). (c) To investigate the pH dependent stability, DNA binding and release was studied by performing EBA and HRA with complexes formed at N/P 20 in a pH range from 5 to 7.4, representing the physiologically relevant pH range during transfection experiments.

with cationic polymers, which leads to a reduction in fluorescence intensity, used to study polymer interaction (Geall and Blagbrough, 2000; Trutzschler et al., 2018). The EBA was performed with increasing N/P ratios to assess the influence of increasing polymer amount on complex formation. At pH 7.4, all polymers showed a N/P ratio-dependent decrease in relative fluorescence intensity (RFI) reaching a plateau at N/P 10, indicating stable complex formation (Fig. 2b). Interestingly, the binding behavior of the polymers differed considerably, with LPEI showing strong EtBr exclusion (13% free pDNA), followed by PDMAEMA (42% free pDNA) and PBMD (72% free pDNA). The complete complexation of pDNA (GRA) and the different plateaus reached for each polymer indicated differences in the polymer-pDNA interactions. It can be assumed that the low charge density and pronounced hydrophobicity of PBMD causes a lower pDNA condensation compared to PDMAEMA or LPEI, the latter being known for a high charge density. Further, a larger proportion of hydrophobic interactions and therefore a more hydrophobic environment within the complex can be responsible for a reduced displacement of EtBr or even reduced quenching of EtBr by exclusion of water as fluorescence quencher from the complex (LePecq and Paoletti, 1967).

To investigate the stability of pDNA complexation and demonstrate its dynamic release behavior in the relevant physiological pH range, the dissociation of the complexes was studied by incubation with the competing polyanion heparin at pH values ranging from 5 (lysosomal/endosomal pH) to 7.4 (blood/cytosolic pH) (Bertschinger et al., 2006). The resulting release of pDNA from the complex enables the reintercalation of EtBr and increased RFI values.

Interestingly, the observed pDNA release behavior of the investigated polymers differed substantially (Fig. 2c). While 20 U mL<sup>-1</sup> heparin was sufficient to release pDNA from LPEI complexes irrespective of the pH, the influence of the pH value increased from PDMAEMA to PBMD (Fig. 2c). The total release of pDNA from PDMAEMA complexes at more acidic pH values required elevated heparin concentrations (~60 to 100 U mL<sup>-1</sup>), while at higher pH values no complete release could be observed. The PBMD polymer showed an even more pronounced pH-dependent behavior with complete pDNA release only observed at pH 5, whereas with increasing pH values, the RFI values were rather reduced at higher heparin concentrations (>40 U mL<sup>-1</sup>).

Variation of the pH value is affecting the balance between positive charge and hydrophobicity of the polymers, noticeably more pronounced in the case of the PBMD polymer due to the additional hydrophobic side chains (nBMA and MMA). It can be assumed that the PBMD-complexes are more stable at neutral pH values, since the increasing hydrophobic interactions at neutral pH values seem to prevent interaction with competing polyanions such as glycoproteins or negatively charged amino acids of serum proteins. This stabilizing effect

was shown for water-soluble polymers where hydrophobic modifications increased complex stability and, thus, transfection efficiency (Eltoukhy et al., 2013; Nelson et al., 2013; Wang et al., 2018). Since high stability in the presence of polyanions and the prevention of premature dissociation at neutral pH values are advantageous, the PBMD polymer revealed high potential as gene delivery vector.

### 3.3. Encapsulation of pDNA

Since the PBMD polymer showed a promising pH-dependent solubility and a promising DNA binding capability, it was used for the development of a nanoparticle formulation aiming for efficient loading of pDNA while maintaining particle sizes below 200 nm with a narrow size distribution. Such size allows controlled cellular uptake by endocytosis (Rejman et al., 2004). However, encapsulation of pDNA by hydrophobic polymers remains challenging due to its large size, charged character, and sensitivity to harsh formulation conditions. To produce stable pDNA-loaded nanoparticles using the PBMD polymer, three formulation strategies were investigated within this study: Two variants of conventional nanoprecipitation (Fig. 3a) were compared with a newly introduced, “green”, aqueous complexation and formulation method (PBMD<sub>Aqu</sub>(pDNA), Fig. 3b). The former differed in the point of pDNA addition, after the formation of nanoparticles (PBMD<sub>Org</sub>(out,pDNA)) or during the precipitation process (PBMD<sub>Org</sub>(in,pDNA)). The aqueous formulation exploited the solubility of the PBMD polymer in aqueous acidic buffer with a pH-driven nanoprecipitation approach at increased pH values.

First, the PBMD polymer was investigated for particle formation by nanoprecipitation from organic solvents without genetic material (PBMD<sub>Org</sub>), resulting in nanoparticles with a hydrodynamic diameter (z-average, determined by DLS) of approximately 130 nm and an overall positive zeta potential (+51 mV) (Fig. 4). As the positively charged nanoparticles should facilitate the binding and complexation of negatively charged pDNA without the need for an additional cationic surface coating, pDNA was added in different amounts to the preformed nanoparticles (PBMD<sub>Org</sub>(out,pDNA)). The addition of pDNA led to an increased size and polydispersity (PDI) (Fig. 4a and b, SI Fig. S2), resulting in nanoparticles that are unsuitable for the desired application. Nanoparticles meeting the specifications (sizes below 200 nm and PDI values below 0.250) could only be obtained at very low and high N/P ratios of 5 and 100. Using the coprecipitation of pDNA and polymer from acetone (PBMD<sub>Org</sub>(in,pDNA)), suitable nanoparticles were formed at high N/P ratios (100), whereas at lower N/P ratios (<N/P 30) only larger nanoparticle populations could be observed by DLS measurements. In addition, an increasing number of particles with larger diameters was observed by scanning electron microscopy (SEM),

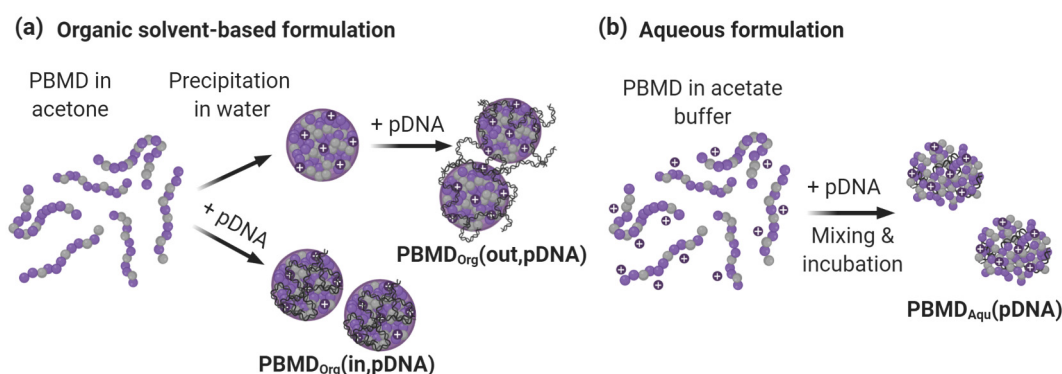


**Fig. 3.** Schematic overview of applied formulation methods for encapsulation, binding, and complexation of pDNA with the PBMD polymer. (a) Nanoprecipitation using solvent-evaporation techniques was combined with pDNA added at different stages of formulation. pDNA was either added subsequently to nanoprecipitation to the nanoparticle suspension (after-process addition; PBMD<sub>Org</sub>(out,pDNA)) or to the organic acetone phase during formulation (in-process addition; PBMD<sub>Org</sub>(in,pDNA)). (b) For the organic solvent-free pH-driven formulation, the PBMD polymer was dissolved under acidic conditions and directly mixed with pDNA for encapsulation (in-process addition; PBMD<sub>Aqu</sub>(pDNA)). This figure was created with Biorender.com.

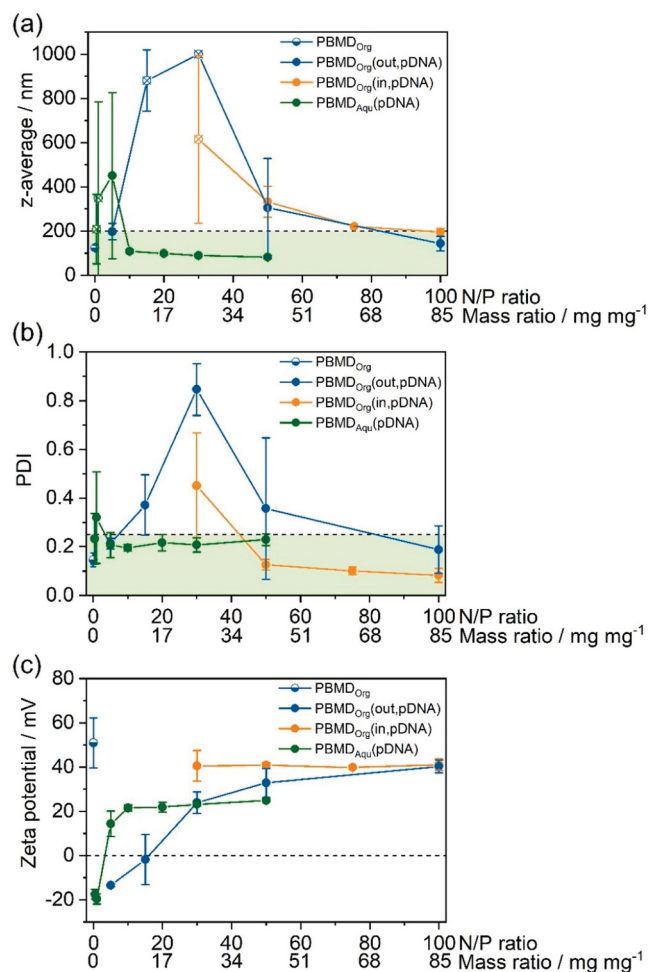


**Fig. 4.** Comparison of different formulation methods for pDNA-loaded nanoparticles. Formulations were characterized in terms of (a) diameter (z-average) and (b) polydispersity (PDI) by DLS. Empty symbols in panel (a) mark the occurrence of large aggregates ( $\geq 1000$  nm) that were taken into account as 1000 nm during calculation of the mean. The green areas indicate the desired size ( $\leq 200$  nm) and PDI range ( $\leq 0.250$ ), respectively. (c) The formulations were further characterized in terms of surface charge before (PBMD<sub>Org</sub>) and after pDNA addition. The measured values are plotted against N/P ratio and mass ratio of polymer to pDNA ( $\text{mg mg}^{-1}$ ) (mean of  $n \geq 3 \pm \text{SD}$ ). (For interpretation of the references to colour in this figure legend, the reader is referred to the web version of this article.)

confirming the increasing size observed by DLS (see SI, Fig. S4). Interestingly, the way in which genetic material was added also had an influence on the apparent surface charge of the nanoparticles. As expected, the positive zeta potential of PBMD<sub>Org</sub> nanoparticles decreased with increasing amount of pDNA (lower N/P ratios) to the point where an inversion of the zeta potential to negative values occurred (approx. N/P 20, Fig. 4c). In comparison, the zeta potential remained in the positive range when pDNA was added during nanoprecipitation (PBMD<sub>Org</sub>(in,pDNA)), mainly due to the inability of successful formulation at low N/P ratios (below 30) as this was leading to large visible aggregates during the formulation process. Based on these experiments it can be concluded that the conventional formulation of stable, highly pDNA-loaded nanoparticles cannot be successfully applied for the PBMD polymer by these methods.

Thus, to increase the amount of pDNA encapsulated in stable and defined nanoparticles, a new formulation approach based on the pH-dependent binding and release behavior of the PBMD polymer was developed (Fig. 3b). For this purpose, the pH-dependent solubility of PBMD under acidic conditions ( $\text{pH} < 6$ , Fig. 1d) was exploited by

dissolving the polymer in sodium acetate buffer ( $\text{pH} 5.8$ ) for nanoparticle formulation without the use of organic solvents. Thereafter, the aqueous polymer solution was mixed 1:2 with pDNA diluted in HBG buffer ( $\text{pH} 7.4$ ) to shift the pH to neutral values during complexation. This formulation approach was tested at N/P ratios ranging from 0.5 to 50, obtaining nanoparticles in the range of 100 nm and low PDI values (around 0.2) at N/P ratios above 5. As the N/P ratio decreased, the positive surface charge changed from  $+25$  mV (N/P 50) to  $-18$  mV (N/P 0.5), while being neutral between N/P 1 and 5. This occurred at lower N/P ratios (higher amounts of pDNA) compared to organic-solvent based pre-formulated nanoparticles (PBMD<sub>Org</sub>(out,pDNA), with a zeta potential of 0 at  $\sim$ N/P 20).

Overall, the pH-dependent PBMD<sub>Aqu</sub>(pDNA) formulation was successfully applied to form stable nanoparticles in a suitable size range ( $< 200$  nm) with low PDI values at low N/P ratios, which can likely be explained by a high number of charged groups within the polymer dissolved in acetate buffer, interacting with negatively charged pDNA moieties. The use of HBG buffer at  $\text{pH} 7.4$  within the formulation process leads to neutralization of the solution and further stabilization of the complex through hydrophobic interactions as already indicated by the EBA/HRA assay (Fig. 2).

There are only a few approaches in the literature reporting water-insoluble cationic polymers such as Eudragit® E(PO/100) for pDNA delivery; all using organic solvents for the formulations. (Basarkar and Singh, 2009; Kanthamneni et al., 2016) The sufficient removal of organic solvents is necessary prior to biological applications and is often a costly and time-consuming additional step. Further, in comparison to the aqueous formulation, during the nanoprecipitation formulation, the cationic hydrophobic polymer can be considered uncharged when dissolved in acetone only, which leads to a reduced electrostatic interaction with genetic material and, in the case of preformed nanoparticles (e.g., PBMD<sub>Org</sub>(out,pDNA)) to less exposed positively charged moieties on the particle surface. Consequently, this also limits the amount of pDNA that can be bound. On that account, additives such as cationic surfactants (CTAB) or cationic polymers (LPEI) are typically used in both formulation approaches to improve nanoparticle surface charge and thus pDNA binding.

However, the use of organic solvents and additives can be avoided by applying the aqueous, pH-driven nanoprecipitation technique (PBMD<sub>Aqu</sub>(pDNA)). Moreover, high amounts of pDNA were complexed by the pH-responsive hydrophobic cationic polymer within stable nanoparticles, which turns the method into a simple, straightforward approach for the encapsulation of genetic material.

#### 3.4. Characterization of PBMD<sub>Aqu</sub>(pDNA) complexes by cryo-TEM and AUC

As the PBMD<sub>Aqu</sub>(pDNA) complexes obtained by a fully aqueous approach possessed excellent potential for biological applications such as gene delivery, they were further characterized by cryo-TEM and AUC in order to examine particle shape and morphology. Further, the presence of free pDNA and/or polymer chains, and detailed information regarding particle size distributions in dependence of the concentration were evaluated. The PBMD<sub>Aqu</sub>(pDNA) complexes were studied at N/P 10 and 20, as this led to well-defined particle distributions as evaluated by DLS. Cryo-TEM measurements revealed nanostructures with diameters of approx. 50 nm, clearly smaller than the intensity-weighted hydrodynamic diameters as measured by DLS but closer to the number-weighted distributions (Fig. 5a, Fig. 4a, Fig. S3). Additionally, a few larger structures, although not exceeding the overall 100 nm size range, being favored for biological applications, were observed.

Further, the PBMD<sub>Aqu</sub>(pDNA) complexes were investigated via sedimentation velocity AUC experiments over a suitable concentration range ( $0.1\text{--}1\text{ mg mL}^{-1}$ ) using RI and absorbance multidetection. The experiments were conducted at a rotor speed of 7,500 rpm for 24 h, followed by spinning the rotor at a speed of 42,000 rpm for further 24 h

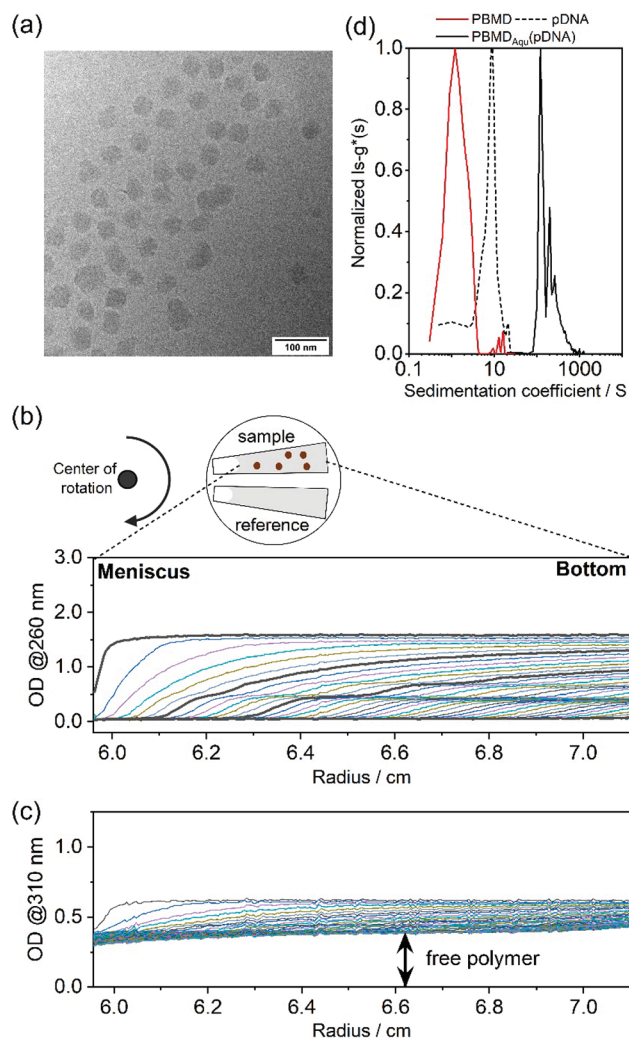


**Fig. 5.** Characterization of PBMD<sub>Aqu</sub>(pDNA) complexes at N/P 20 by cryo-TEM and AUC. (a) Cryo-TEM measurements of PBMD<sub>Aqu</sub>(pDNA) complexes at N/P 20. (b) Sketch of *in situ* sedimentation velocity AUC measurements leading to radially-resolved sedimentation velocity profile scans of the PBMD<sub>Aqu</sub>(pDNA) complexes at N/P 20, a concentration of 1 mg mL<sup>-1</sup>, and a rotor speed of 7,500 rpm monitored at  $\lambda = 260$  nm. (c) Same as in (b) but monitored at  $\lambda = 310$  nm. (d) Normalized differential distributions of sedimentation coefficients of free RAFT-group containing polymer monitored at  $\lambda = 310$  nm by acceleration of the rotor speed to 42,000 rpm after the measurement at 7,500 rpm, free DNA at  $\lambda = 260$  nm measured separately at a rotor speed of 42,000 rpm, and the PBMD-complexes at N/P 10 at  $\lambda = 260$  nm at a rotor speed of 7,500 rpm.

to investigate potentially smaller species present (Cinar et al., 2020). Strikingly, the radially-resolved sedimentation velocity profiles recorded at  $\lambda = 260$  nm in terms of optical density (OD) contained several discernable steps (Fig. 6b). However, when the run was finished at 7,500 rpm, a plateau at nearly zero OD was observed. This suggests practically no absorbance at  $\lambda = 260$  nm in the supernatant, showing no detectable free pDNA, thereby supporting the results of the GRA (Fig. 2a). When monitoring sedimentation velocity at  $\lambda = 310$  nm, a clearly discernable residual OD was observed in the supernatant (Fig. 5c). This could indicate the presence of free polymer in the sample, that is in excess to that bound to the monitored PBMD<sub>Aqu</sub>(pDNA) complexes. The apparently free polymer, which absorbs at  $\lambda = 310$  nm due to the trithiocarbonate RAFT end-group, is too small to efficiently sediment at a rotor speed of 7,500 rpm, and largely remained in the supernatant. Additionally, polymer that is an integral component of the complex apparently sedimented, because it is associated to the pDNA (Fig. 5c).

This situation is also pointed out when comparing the normalized

differential distributions of sedimentation coefficients of the PBMD<sub>Aqu</sub>(pDNA) complex, free polymer, and free DNA separately (Fig. 5d). The overlap at  $\lambda = 260$  nm and  $\lambda = 310$  nm and the RI, proved the simultaneous sedimentation of species, respectively the close association of the RAFT group-containing polymer and the pDNA in the form of a complex (Fig. 6a).

By increasing the sample concentration, a third peak in the differential distributions of sedimentation coefficients could be discerned more clearly (dotted line in Fig. 6b). At higher concentrations, the complexes showed a more pronounced tendency to aggregate and/or form larger species, observed by the presence of larger sedimentation coefficients with a discernable peak. In contrast to this observation, the lower sample concentrations featured two major discernable populations (solid black line in Fig. 6b). The differential distributions of sedimentation coefficients (Fig. 6a-c) were also representative for the discernable steps in the sedimentation velocity profiles displayed in, e.g., Fig. 5b. Here, the partial resolution of several species of an increased hydrodynamic size indicated by partly resolved peaks, was more pronounced at higher concentrations.

After sedimentation of all such larger species after 24 h, observation of sedimentation processes in the remaining supernatant revealed sedimentation of the remaining free polymer at a wavelength of  $\lambda = 310$  nm (Fig. 5d and Fig. S8). This was also nicely shown by differential distributions of sedimentation coefficients in Fig. 6d. An increase of sample concentrations showed an approximately linear increase of signal intensity of the sedimenting RAFT agent-containing polymer at higher rotor speeds as well (Fig. 6d and 6e). This further represented an increased concentration of free polymer. No free RAFT agent or loss of the RAFT-containing chain-ends of the polymers was observable, indicated by the absence of a remaining plateau of the recorded sedimentation profiles in Fig. S8.

Differences in the N/P ratio of the PBMD<sub>Aqu</sub>(pDNA) complex were investigated at the lowest sample concentration (0.1 mg mL<sup>-1</sup>) as this is more close to the experimental implementations in transfection experiments (Fig. 6c). A decrease of the N/P ratio to 10 resulted in the loss of the distinct third population in the differential distributions of sedimentation coefficients, barely indicated at N/P 20 at lower concentrations. Polyplexes formed with the PDMAEMA homopolymer at different N/P ratios were studied in the same manner (Fig. S9). It can be seen in Fig. 6c that N/P 20 revealed a prominent distribution of (lowest) sedimentation coefficients with an apparent shoulder (toward higher sedimentation coefficients). Besides, the differential distribution of sedimentation coefficients at N/P 10 exhibited a clearly discernable further population. Also, an increased amount of free polymer, as already observed for increasing sample concentrations (Fig. 6d) was also observed for higher N/P ratios (Fig. 6f).

When comparing the two N/P ratios, both showed nearly similar distributions in the DLS, with an even slightly larger size and broader distribution for N/P 10 (Fig. 4, Fig. S3). The difference in populations present in the two samples could only be observed by AUC measurements, revealing the importance of detailed characterization of such delivery systems by various techniques. Furthermore, AUC measurements confirmed full pDNA binding within the PBMD complex, which is consistent with results obtained by GRA (Fig. 2a).

### 3.5. Influence of the formulation approach on transfection of HEK293T cells

After the formation of controlled and stable PBMD<sub>Aqu</sub>(pDNA) complexes, their transfection performance was investigated, with the PBMD<sub>Org</sub>(out,pDNA) formulation serving as a control, while the PBMD<sub>Org</sub>(in,pDNA) formulation was not further investigated since pDNA loaded nanoparticles could only be obtained at high N/P ratios which was not suitable for the intended investigation. For transfection experiments, pDNA encoding for enhanced green fluorescent protein (EGFP) was delivered into HEK293T cells and EGFP expression was

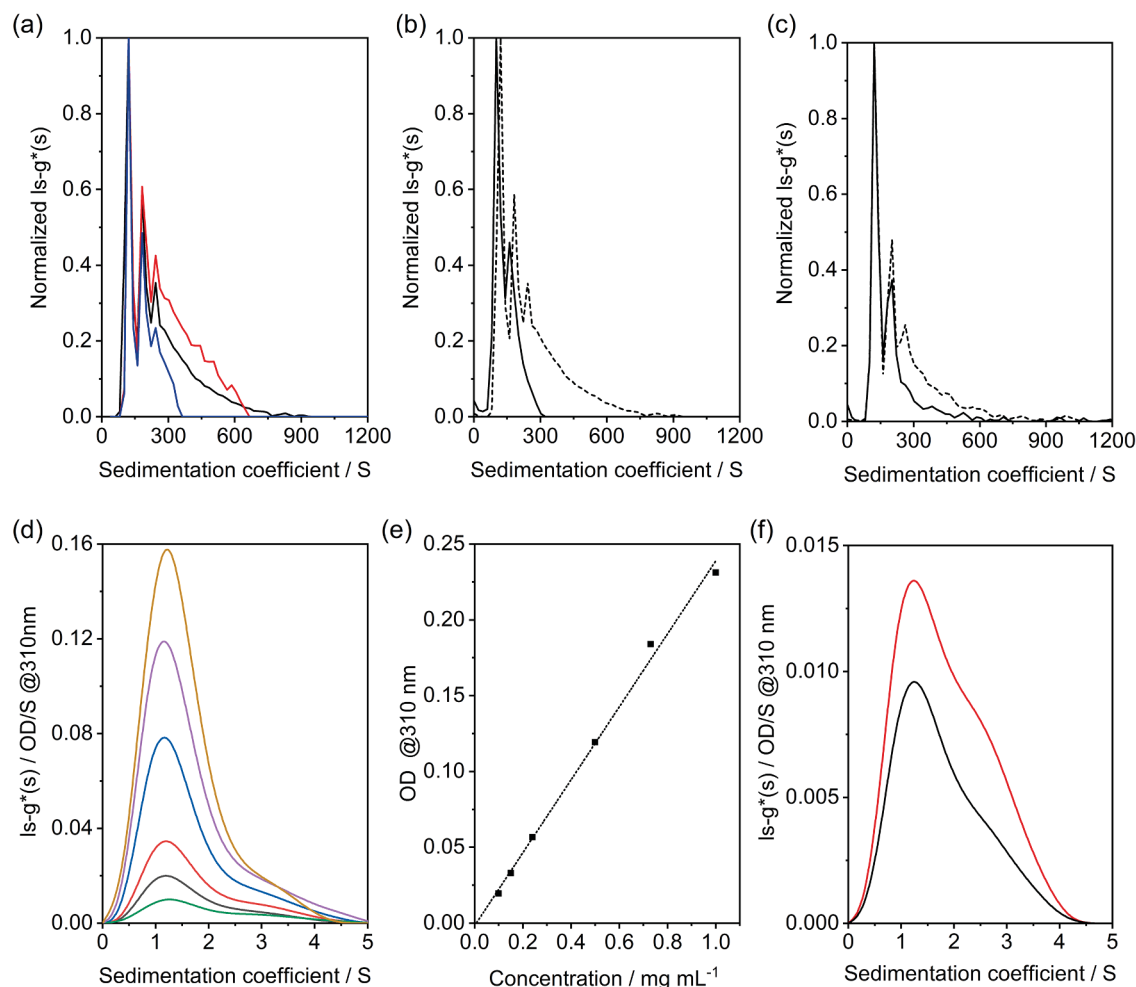


**Fig. 6.** Normalized differential distributions of sedimentation coefficients of complexes formed with PBMD polymer (PBMD<sub>Aqu</sub>(pDNA)) at a N/P 20 obtained at a rotor speed of 7,500 rpm. (a) The concentration utilized was 1 mg mL<sup>-1</sup> by using RI detection (blue solid line) and the absorbance detection in terms of OD, representative of the DNA at  $\lambda = 260$  nm (red solid line) as well as at  $\lambda = 310$  nm, being representative of the RAFT agent-containing polymer (black solid line). (b) Same concentration as in (a) using absorbance detection at  $\lambda = 260$  nm in terms of OD (black dashed line) and 0.1 mg mL<sup>-1</sup> (black solid line), (c) with the PBMD polymer at N/P 10 (black dashed line) and N/P 20 (black solid line). (d) Differential distributions of sedimentation coefficients monitored from data at a subsequent rotor speed of 42,000 rpm and at increasing overall sample concentrations (from bottom to top) at  $\lambda = 310$  nm with (e) the obtained linear correlation of integrated ODs of such differential distributions in respect to the overall sample concentration and (f) increased existence of free polymer by comparing (PBMD<sub>Aqu</sub>(pDNA)) samples at a N/P 10 (black solid line) and at a N/P 20 (red solid line). (For interpretation of the references to colour in this figure legend, the reader is referred to the web version of this article.)

analyzed by flow cytometry and fluorescence microscopy. The transfection efficiency (percentage of viable fluorescent cells) of the formulations were assessed under various conditions by evaluation of (i) two N/P ratios in the lower range (10 and 20), (ii) two media (under serum-free conditions and in the presence of 10% serum), and (iii) varying incubation times (1 and 4 h) followed by analysis at 24 h post transfection. In general, both formulations enabled EGFP expression in HEK293T cells under all tested conditions, with higher expression levels observed under serum-free conditions (Opti-MEM<sup>TM</sup>) and longer incubation times (Fig. 7). In addition, higher amounts of cationic polymer (higher N/P ratios) further increased expression levels. The PBMD<sub>Aqu</sub>(pDNA) complex showed significantly higher EGFP expression levels at N/P 20 when compared to the PBMD<sub>Org</sub>(out,pDNA) formulation, particularly at short incubation times (1 h), in serum-free environment ( $61 \pm 9\%$  vs.  $27 \pm 15\%$ ) and even in the presence of serum ( $32 \pm 8\%$  vs.  $17 \pm 8\%$ ).

Overall, an EGFP expression of both formulation approaches is in accordance to the literature, reporting the ability of cationic hydrophobic polymers to successfully transfect eukaryotic cells (Basarkar and Singh, 2009; Kanthamneni et al., 2016). The difference in transfection

efficiency could potentially be attributed to the assumed difference in pDNA distribution within the formulation approaches. In one case, the pDNA was present solely on the exterior of the nanoparticles (PBMD<sub>Org</sub>(out,pDNA)) as opposed to the PBMD<sub>Aqu</sub>(pDNA) complex where the DNA is expected to be distributed throughout the particle, potentially also affecting pDNA stability. Further, differences in nanoparticle size, PDI, and surface charge might affect cellular uptake, but also endosomal escape ability and, therefore, overall transfection efficiency.

### 3.6. Optimization of transfection efficiency in HEK293T cells

As the PBMD<sub>Aqu</sub>(pDNA) complexes resulted in promising efficiencies in the first transfection experiments, and characterization by AUC proved that the pDNA is completely bound to, respectively complexed into the polymer, the transfection protocol was optimized for increasing transfection efficiency while maintaining high cell viability. Therefore, the influence of the polymer itself without the addition of genetic material on the viability of L-929 cells, a standard cell line for cytotoxicity testing recommended by the ISO 10993-5 guideline, was evaluated at

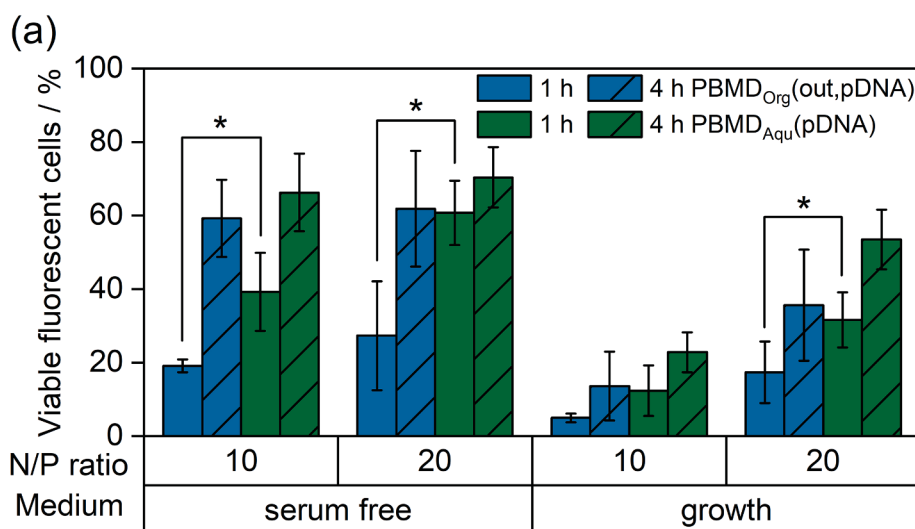
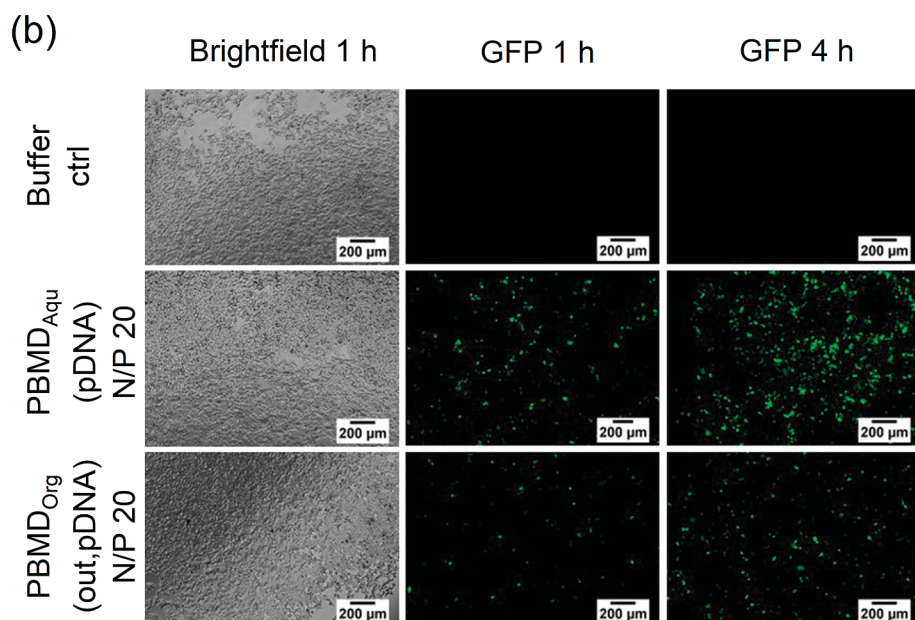


**Fig. 7.** Influence of the formulation method on the transfection efficiency (percentage of viable fluorescent cells) in HEK293T cells. The pH-dependent formulation (PBMD<sub>Aqu</sub>(pDNA)) and the nanoprecipitation/after-process addition of pDNA (PBMD<sub>Org</sub>(out,pDNA)) were tested in growth medium (10% FBS) and under serum free conditions (Opti-MEM™) at varying incubation times. pDNA is encoding for EGFP. Transfection efficiency was investigated by measuring EGFP expression by (a) flow cytometry (mean of  $n \geq 3 \pm SD$ ) and (b) fluorescence microscopy. Statistical significance is denoted as follows: \* $P < 0.05$ , \*\* $P < 0.01$ , and \*\*\* $P < 0.001$ .



varying incubation times (Fig. 8a).

The PBMD polymer showed time and concentration dependent cytotoxicity, whereas shorter incubation times and lower concentrations resulted in higher cell viability, and the  $IC_{50}$  values increased from  $7.6 \mu\text{g mL}^{-1}$  (after 24 h) to  $12.2 \mu\text{g mL}^{-1}$  (after 4 h) to  $15.6 \mu\text{g mL}^{-1}$  (after 1 h). Therefore, low polymer concentrations and short incubation times were favored for the optimization of the transfection conditions. To evaluate cell viability at transfection conditions, the cytotoxicity of the PBMD<sub>Aqu</sub>(pDNA) formulation in HEK293T cells was evaluated additionally (Fig. 8b), revealing a similar concentration dependent trend. Cell viability above 70% was obtained at pDNA concentrations below  $0.5 \mu\text{g mL}^{-1}$ , while an increase in pDNA concentration and N/P ratio reduced cell viability. To optimize transfection conditions, different pDNA concentrations were tested, while keeping the N/P ratio constant at 20 (Fig. 8b). Overall, PBMD<sub>Aqu</sub>(pDNA) complexes showed high transfection efficiencies already at low pDNA concentrations and short treatment times (Fig. 8b), while longer treatment (4 h) resulted in even higher expression levels over the whole concentration range. The ideal pDNA concentration at N/P 20 was identified as  $0.5 \text{ mg mL}^{-1}$  resulting in  $41 \pm 3\%$  viable EGFP fluorescent cells after 4 h of incubation, while maintaining above 70% viability. Therefore, the N/P ratio was

subsequently optimized by keeping the pDNA concentration at  $0.5 \mu\text{g mL}^{-1}$ . Overall, changes in the N/P ratio did not substantially improved transfection efficiency, but rather resulted in decreased cell viability, and, therefore, a pDNA concentration of  $0.5 \mu\text{g mL}^{-1}$  with N/P 20 and 4 h treatment were chosen as ideal conditions for pDNA transfection with the PBMD<sub>Aqu</sub>(pDNA) complex. The results were compared with LPEI polyplexes as a well-known polymer for pDNA transfection and revealed, that very low amounts of pDNA were required to reach high transfection efficiencies with PBMD<sub>Aqu</sub>(pDNA) complexes at short incubation times ( $\leq 4\text{h}$ ). To obtain similar expression levels with LPEI, either the pDNA concentration needed to be increased by 5- to 10-fold ( $2.5\text{--}5 \mu\text{g mL}^{-1}$ ) or treatment durations up to 24 h were required (Fig. 8c).

Various studies reported the application of the commercial polymer Eudragit® E(PO/100) with a comparable composition like PBMD for gene or drug delivery. The reported toxicity was typically lower than that observed in this study (Hari et al., 2016; Jain et al., 2015). This could be due to the slightly higher DMAEMA content within the PBMD polymer when compared to Eudragit® E(PO/100). However, the increase of the molar content of DMAEMA is only 10%, which is relatively low to explain these effects. In both previous studies, the nanoparticles

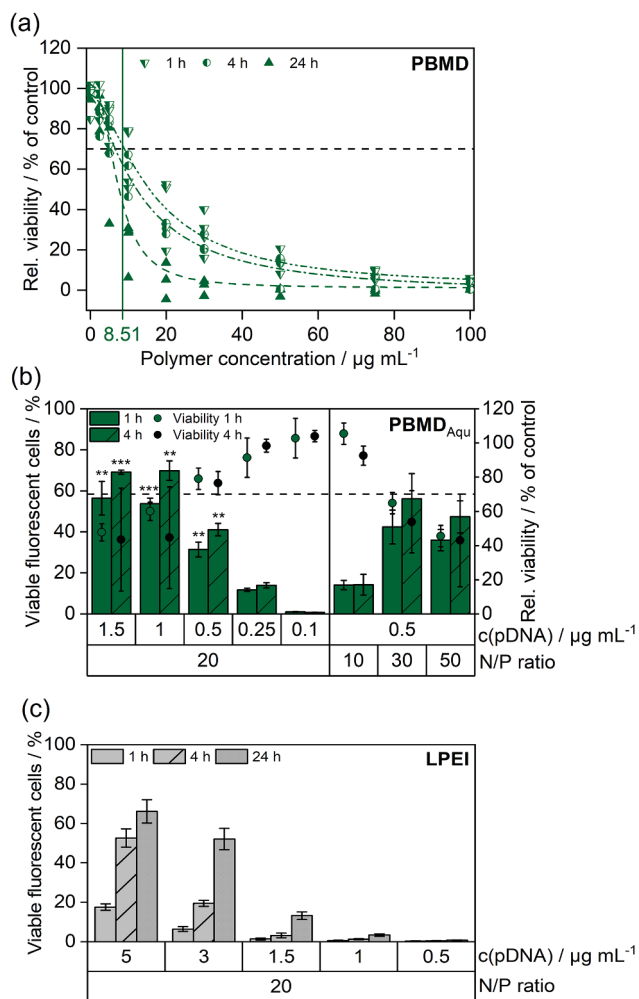


**Fig. 8.** Optimization of transfection conditions of PBMD<sub>Aqu</sub>(pDNA) formulated with the pH-dependent method in HEK293T cells. (a) Evaluation of the cytotoxicity of the PBMD polymer dissolved in acetate buffer in L-929 cells. Cells were treated with the polymer for 1, 4 and 24 h and cytotoxicity was determined by the PrestoBlue™ assay after 24 h. The dashed line indicates 70% cell viability and the concentration of PBMD polymer under optimized transfection conditions is indicated by the green line. (b) N/P ratio and pDNA concentrations were optimized to achieve high efficiencies (high number of viable fluorescent cells) while maintaining low cytotoxicity. The expression of EGFP in HEK293T cells after transfection (columns) was measured via flow cytometry (mean of  $n = 3 \pm \text{SD}$ ). Cytotoxicity of the PBMD<sub>Aqu</sub>(pDNA) complexes (dots) was determined under conditions used for transfection by the PrestoBlue™ assay (mean of  $n = 3 \pm \text{SD}$ ). (c) Transfection efficiency of LPEI-pDNA complexes at varying pDNA concentrations and incubation times was investigated by measuring EGFP expression in HEK293T cells by flow cytometry (mean of  $n = 3 \pm \text{SD}$ ). Statistical significance in comparison to LPEI at the respective pDNA concentration and N/P ratio is denoted as follows: \* $P < 0.05$ , \*\* $P < 0.01$ , and \*\*\* $P < 0.001$ . (For interpretation of the references to colour in this figure legend, the reader is referred to the web version of this article.)

were manufactured with the help of surfactants (PVA, Pluronic F-68). Eudragit® E(PO/100) is known for its amphipathic and membrane-destabilizing properties when interacting with lipoproteins, liposomes, and eukaryotic cell membranes. (Alasino et al., 2005, 2012) This is a potential mechanism for cytotoxicity but, on the other hand, if well dosed, useful for application in gene delivery to facilitate cellular uptake, endosomal release, and therefore high transfection efficiencies. Within the PBMD<sub>Aqu</sub>(pDNA) formulation, no surfactants were present. This could result in stronger interaction with cellular membranes, explaining the high EGFP expression levels already at low complex

concentrations compared to LPEI polyplexes, while maintaining cell viability.

### 3.7. PBMD vs. commercial controls and for the delivery of siRNA and mRNA

Since the PBMD<sub>Aqu</sub>(pDNA) complexes showed improved transfection at low pDNA concentrations, the formulation method was applied to the commercial polymer Eudragit® E(PO/100) and tested under optimized transfection conditions (N/P 20, 0.5  $\mu\text{g mL}^{-1}$  pDNA, 4 h incubation). EGFP expression levels under these conditions were further compared with the PDMAEMA homopolymer and the commercial polymer-based transfection reagent Viromer® RED, which was optimized for pDNA and mRNA transfection (Fig. 9a). Viromer® RED is known for its superior endosomal release mechanism, rendering it a very efficient commercial control (Rao et al., 2015). The pH-dependent formulation applied to the commercial polymer Eudragit® E(PO/100) showed comparable EGFP expression to the PBMD<sub>Aqu</sub>(pDNA) complexes. Both polymers, PBMD and Eudragit® E(PO/100), were at a comparable level or even outperformed the commercial transfection agents Viromer® RED and LPEI under these optimized conditions. At 4 h incubation time PBMD showed 50  $\pm$  10% and Eudragit® E(PO/100) 30  $\pm$  2% fluorescent cells, while Viromer® RED and LPEI resulted in 31  $\pm$  21% and 0.35  $\pm$  0.12%, respectively. As expected, the PDMAEMA homopolymer, composed of the same number of cationic groups as the PBMD polymer, showed, similarly to LPEI, no transfection under these conditions (0.48  $\pm$  0.22%). It is known, that the efficiency of PDMAEMA is lower under these conditions, in particular if low molar masses are applied (Layman et al., 2009; Samsonova et al., 2011; Van de Wetering et al., 1998). The high efficiency of the PBMD polymer as well as the commercial control Eudragit® E(PO/100) showed the potential of the novel formulation, which is not only fast and based on a fully aqueous approach, but also increases the transfection efficiency compared to other formulations.

In order to exploit the full potential of the PBMD polymer, the formulation method was applied for complexation and transfection of various genetic materials and was further tested in comparison to commercially available controls more suitable for the respective genetic material than LPEI. siRNA and mRNA are promising candidates for gene delivery offering several advantages over pDNA. Both siRNA and mRNA do not pose the risks accompanied by integration into the genome, since their site of action is within the cytosol. Thus, they avoid the passage of the nuclear membrane, and, importantly, they offer various therapeutic applications such as protein displacement or inhibition of protein expression (Dunbar et al., 2018; Hajj and Whitehead, 2017).

As Eudragit® E(PO/100) has been evaluated for siRNA delivery to macrophages using PVA coated nanoparticles showing significantly reduced protein expression levels, (Jain et al., 2015) PBMD<sub>Aqu</sub>(siRNA) complexes were tested for knock-down efficiency in HEK-GFP cells, stably expressing GFP. The knock-down efficiency after 72 h incubation was compared to Lipofectamine, which is commonly used for siRNA transfections in the literature, loaded with the same amount of siRNA. A reduction in the percentage of GFP positive cells was observed with Lipofectamine and the PBMD<sub>Aqu</sub>(siRNA) complexes when compared to the control. PBMD<sub>Aqu</sub>(siRNA) complexes resulted in 45  $\pm$  13% GFP negative cells whereas for Lipofectamine 54  $\pm$  5% GFP negative cells were observed. Thus, the PBMD<sub>Aqu</sub>(siRNA) complexes showed knock-down efficiencies comparable to Lipofectamine, revealing the high potential for the introduction of siRNA into cells by the PBMD polymer. Furthermore, the transfection efficiency of PBMD<sub>Aqu</sub>(mRNA) complexes was evaluated by delivering GFP-mRNA into HEK293T cells. The GFP expression was measured after 24 h. The transfection efficiency of the PBMD<sub>Aqu</sub>(mRNA) formulation was compared with the commercially available Viromer® RED. PBMD<sub>Aqu</sub>(mRNA) complexes resulted in GFP expression in 73  $\pm$  12% of cells, while Viromer® RED transfected 87  $\pm$  1% of cells. Although the percentages of transfected cells were comparable, the polymers exhibited different transfection patterns (SI, Fig. S7),

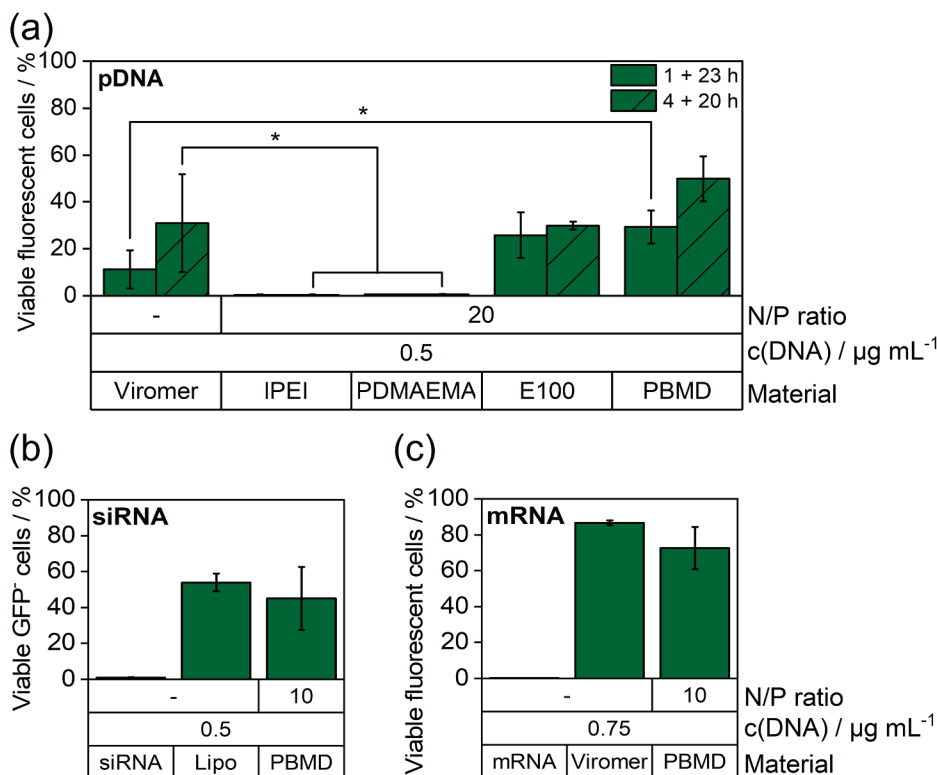


**Fig. 9.** Transfection efficiency of the aqueous pH-driven formulation (PBMD<sub>Aqu</sub>(pDNA)) in comparison to commercial transfection agents and its application to siRNA and mRNA encapsulation. (a) Formulation and transfection conditions optimized for the PBMD polymer (N/P ratio 20, 0.5 μg mL<sup>-1</sup> pDNA) were applied to Eudragit® E(PO/100) and compared to the PDMAEMA homopolymer in terms of the percentage of viable fluorescent cells. Viomer® RED was used with 0.5 μg mL<sup>-1</sup> pDNA for comparison. EGFP expression in HEK293T cells was measured by flow cytometry (mean of n ≥ 3 ± SD). The formulation method was further applied for encapsulation of siRNA and mRNA. (b) Knock-down efficiency of anti-GFP siRNA complexed with PBMD (PBMD<sub>Aqu</sub>(siRNA)) was investigated in HEK-GFP cells at an N/P ratio of 10 (mean of n ≥ 3 ± SD). (c) Transfection efficiency of PBMD<sub>Aqu</sub>(mRNA) complexes was investigated by introducing GFP-mRNA into HEK293T cells. GFP expression was measured by flow cytometry (mean of n ≥ 3 ± SD). Statistical significance in comparison to the respective commercial controls (Viomer® RED, Lipofectamine) is denoted as follows: \*P < 0.05, \*\*P < 0.01, and \*\*\*P < 0.001. (For interpretation of the references to colour in this figure legend, the reader is referred to the web version of this article.)

which remain to be investigated in further studies. Nevertheless, the PBMD<sub>Aqu</sub>(mRNA) complex displayed excellent potential for mRNA delivery as the complex is transfecting a high number of cells.

**4. Conclusions**

In this study, a new, fast, and straightforward formulation strategy for the encapsulation of pDNA without the need of organic solvents into cationic polymer nanoparticles was established. The key requirement for successful encapsulation was the insolubility of the polymer in water under neutral pH conditions. For the development of the utilized pH-dependent formulation method, a well-defined PBMD polymer was synthesized using RAFT polymerization. The PBMD polymer exhibited the desired pH-dependent solubility and pDNA binding behavior under physiological solution conditions, which can be exploited for the assembly of pDNA-polymer complexes, in a fully aqueous scenario. By dissolution of the PBMD polymer in acidic buffer, pDNA binding was facilitated, while shifting the pH to neutral values during the formulation process increased hydrophobic interactions stabilizing the formed nanoparticles. The utilized aqueous pH-driven formulation of cationic hydrophobic polymers showed high pDNA encapsulation efficiencies and desired stability under physiological conditions. In-depth characterization by AUC, cryo-TEM, and DLS/ELS proved a full complexation of the genetic material. The novel formulation resulted in enhanced transfection efficiency at reduced pDNA concentrations compared to commercial controls such as LPEI or Viomer® RED and was successfully applied to the commercially approved Eudragit® E(PO/100) and various types of genetic material, such as siRNA and mRNA. The formulation approach showed a readily high versatility and promising potential to further be optimized and applied to other classes of hydrophobic cationic copolymers for a general delivery vehicle design concerning genetic material.

**CRediT authorship contribution statement**

**Jana I. Solomun:** Conceptualization, Investigation, Methodology, Visualization, Writing - original draft. **Gizem Cinar:** Investigation, Methodology, Visualization, Writing - review & editing. **Prosper Mapfumo:** Investigation, Methodology, Writing - review & editing. **Friederike Richter:** Writing - review & editing, Methodology. **Elisabeth Moek:** Investigation, Writing - review & editing. **Franziska Hausig:** Writing - review & editing, Methodology. **Liam Martin:** Investigation, Methodology, Visualization, Writing - review & editing. **Stephanie Hoepfener:** Investigation, Writing - review & editing. **Ivo Nischang:** Methodology, Supervision, Writing - review & editing, Funding acquisition. **Anja Traeger:** Conceptualization, Supervision, Writing - review & editing, Project administration, Funding acquisition.

**Declaration of Competing Interest**

The authors declare the following financial interests/personal relationships which may be considered as potential competing interests: The Friedrich Schiller University of Jena has applied for a patent based on some data presented here, in which A. Traeger and J. I. Solomun are named as inventors.

**Acknowledgements**

This work was financially supported by the Collaborative Research Center PolyTarget (SFB 1278 - projects B01/06 and Z01, project ID 316213987) funded by the German Research Foundation (DFG). Further, the authors thank the Bundesministerium für Bildung und Forschung (BMBF, Germany, #13XP5034A PolyBioMik) and the DFG for generous funding within the Emmy-Noether Programme (Projekt ID: 358263073). The authors further acknowledge the support from the Free State of Thuringia and the European Social Fund (2019SD0129). This work was as well supported by the “Thüringer Aufbaubank (TAB)” and the “Europäischer Fonds für regionale Entwicklung (EFRE)”



(2018FGI0025) through funding analytical ultracentrifugation facilities at the Jena Center for Soft Matter (JCSM). The SEM/TEM facilities of the JCSM were established with a grant from the DFG and the EFRE. Further, the authors thank Prof. U. S. Schubert for his continuous support and providing excellent facilities. The authors thankfully acknowledge Carolin Kellner, Bärbel Beringer-Siemers, Elisabeth Preußger, Steffi Stumpf, Maria Strumpf, and Franziska Stanzel for their excellent technical support and helpful discussions.

## Appendix A. Supplementary material

Additional methods, materials, synthesis and characterization of PDMAEMA, DLS data of the different formulation methods, DLS measurements with different plasmids, SEM measurements, gating strategy for transfection experiments, AUC measurements of PDMAEMA and additional AUC data for the PBMD polymer and complex solutions can be found in the SI. Supplementary data to this article can be found online at <https://doi.org/10.1016/j.ijpharm.2020.120080>.

## References

- Abdelhady, H.G., Allen, S., Davies, M.C., Roberts, C.J., Tendler, S.J., Williams, P.M., 2003. Direct real-time molecular scale visualisation of the degradation of condensed DNA complexes exposed to DNase I. *Nucleic Acids Res.* 31, 4001–4005. <https://doi.org/10.1093/nar/gkg462>.
- Adolph, E.J., Nelson, C.E., Werfel, T.A., Guo, R., Davidson, J.M., Guelcher, S.A., Duvall, C.L., 2014. Enhanced Performance of Plasmid DNA Polyplexes Stabilized by a Combination of Core Hydrophobicity and Surface PEGylation. *J. Mater. Chem. B* 2, 8154–8164. <https://doi.org/10.1039/C4TB00352G>.
- Alasino, R.V., Ausar, S.F., Bianco, I.D., Castagna, L.F., Contigiani, M., Beltramo, D.M., 2005. Amphipathic and membrane-destabilizing properties of the cationic acrylate polymer Eudragit E100. *Macromol. Biosci.* 5, 207–213. <https://doi.org/10.1002/mabi.200400168>.
- Alasino, R.V., Leonhard, V., Bianco, I.D., Beltramo, D.M., 2012. Eudragit E100 surface activity and lipid interactions. *Colloids Surf. B Biointerfaces* 91, 84–89. <https://doi.org/10.1016/j.colsurfb.2011.10.041>.
- Basarkar, A., Singh, J., 2009. Poly (lactide-co-glycolide)-polymethacrylate nanoparticles for intramuscular delivery of plasmid encoding interleukin-10 to prevent autoimmune diabetes in mice. *Pharm. Res.* 26, 72–81. <https://doi.org/10.1007/s11095-008-9710-4>.
- Bertschinger, M., Backliwal, G., Schertenleib, A., Jordan, M., Hacker, D.L., Wurm, F.M., 2006. Disassembly of polyethylenimine-DNA particles in vitro: implications for polyethylenimine-mediated DNA delivery. *J. Control. Release* 116, 96–104. <https://doi.org/10.1016/j.jconrel.2006.09.006>.
- Bivas-Benita, M., Romeijn, S., Junginger, H.E., Borchard, G., 2004. PLGA-PEI nanoparticles for gene delivery to pulmonary epithelium. *Eur. J. Pharm. Biopharm.* 58, 1–6.
- Bloomfield, V.A., 1997. DNA condensation by multivalent cations. *Biopolym.: Original Res. Biomol.* 44, 269–282. <https://doi.org/10.1016/j.ejpb.2004.03.008>.
- Brayton, C.F., 1986. Dimethyl sulfoxide (DMSO): a review. *Cornell Veterinarian* 76, 61–90.
- Breitenkamp, R.B., Emrick, T., 2008. Pentalysine-grafted ROMP polymers for DNA complexation and delivery. *Biomacromolecules* 9, 2495–2500. <https://doi.org/10.1021/bm800511p>.
- Buerkli, C., Lee, S.H., Moroz, E., Stuparu, M.C., Leroux, J.C., Khan, A., 2014. Amphipathic homopolymers for siRNA delivery: probing impact of bifunctional polymer composition on transfection. *Biomacromolecules* 15, 1707–1715. <https://doi.org/10.1021/bm5001197>.
- Cheng, C., Convertine, A.J., Stayton, P.S., Bryers, J.D., 2012. Multifunctional triblock copolymers for intracellular messenger RNA delivery. *Biomaterials* 33, 6868–6876. <https://doi.org/10.1016/j.biomaterials.2012.06.020>.
- Cinar, G., Englert, C., Lehmann, M., Nischang, I., 2020. In situ, quantitative assessment of multifunctional nanoscale drug delivery systems in human serum. *Anal. Chem.* 92 (11), 7932–7939. <https://doi.org/10.1021/acs.analchem.0c01323>.
- Cohen, H., Levy, R., Gao, J., Fishbein, I., Kousaev, V., Sosnowski, S., Slomkowski, S., Golomb, G., 2000. Sustained delivery and expression of DNA encapsulated in polymeric nanoparticles. *Gene Ther.* 7, 1896–1905. <https://doi.org/10.1038/sj.gt.3301318>.
- Cocka, C., Zartner, L., Tabujew, I., Fischer, D., Peneva, K., 2020. Incorporation of Indole Significantly Improves the Transfection Efficiency of Guanidinium-Containing Poly (Methacrylamide) s. *Macromol. Rapid Commun.* 41, 1900668. <https://doi.org/10.1002/marc.201900668>.
- Convertine, A.J., Benoit, D.S., Duvall, C.L., Hoffman, A.S., Stayton, P.S., 2009. Development of a novel endosomal diblock copolymer for siRNA delivery. *J. Control Release* 133, 221–229. <https://doi.org/10.1016/j.jconrel.2008.10.004>.
- Dunbar, C.E., High, K.A., Joung, J.K., Kohn, D.B., Ozawa, K., Sadelain, M., 2018. Gene therapy comes of age. *Science* 359, eaan4672. <https://doi.org/10.1126/science.aan4672>.
- Eltoukhy, A.A., Chen, D., Alabi, C.A., Langer, R., Anderson, D.G., 2013. Degradable terpolymers with alkyl side chains demonstrate enhanced gene delivery potency and nanoparticle stability. *Adv. Mater.* 25, 1487–1493. <https://doi.org/10.1002/adma.201204346>.
- Fay, F., Quinn, D.J., Gilmore, B.F., McCarron, P.A., Scott, C.J., 2010. Gene delivery using dimethylidodecylammonium bromide-coated PLGA nanoparticles. *Biomaterials* 31, 4214–4222.
- Forrest, M.L., Meister, G.E., Koerber, J.T., Pack, D.W., 2004. Partial acetylation of polyethylenimine enhances in vitro gene delivery. *Pharm. Res.* 21, 365–371. <https://doi.org/10.1016/j.biomaterials.2010.01.143>.
- Geall, A.J., Blagbrough, I.S., 2000. Rapid and sensitive ethidium bromide fluorescence quenching assay of polyamine conjugate-DNA interactions for the analysis of lipoplex formation in gene therapy. *J. Pharm. Biomed. Anal.* 22, 849–859. [https://doi.org/10.1016/S0731-7085\(00\)00250-8](https://doi.org/10.1016/S0731-7085(00)00250-8).
- Ginn, S.L., Amaya, A.K., Alexander, I.E., Edelstein, M., Abedi, M.R., 2018. Gene therapy clinical trials worldwide to 2017: An update. *J. Gene Med.* 20, e3015. <https://doi.org/10.1002/jgm.3015>.
- Hajj, K.A., Whitehead, K.A., 2017. Tools for translation: non-viral materials for therapeutic mRNA delivery. *Nat. Rev. Mater.* 2, 1–17. <https://doi.org/10.1038/natrevmats.2017.56>.
- Han, S.-O., Mahato, R.I., Kim, S.W., 2001. Water-soluble lipopolymer for gene delivery. *Bioconjug. Chem.* 12, 337–345. <https://doi.org/10.1021/bc000120w>.
- Hari, B.N.V., Narayanan, N., Dhevendaran, K., Ramyadevi, D., 2016. Engineered nanoparticles of Efavirenz using methacrylate co-polymer (Eudragit-E100) and its biological effects in-vivo. *Mater. Sci. Eng. C Mater. Biol. Appl.* 67, 522–532. <https://doi.org/10.1016/j.msec.2016.05.064>.
- Hobernik, D., Bros, M., 2018. DNA vaccines—how far from clinical use? *Int. J. Mol. Sci.* 19, 3605. <https://doi.org/10.3390/ijms19113605>.
- Incani, V., Lavasanifar, A., Uludağ, H., 2010. Lipid and hydrophobic modification of cationic carriers on route to superior gene vectors. *Soft Matter* 6, 2124–2138. <https://doi.org/10.1039/B916362J>.
- Jain, R., Dandekar, P., Loretz, B., Koch, M., Lehr, C.-M., 2015. Dimethylaminoethyl methacrylate copolymer-siRNA nanoparticles for silencing a therapeutically relevant gene in macrophages. *MedChemComm* 6, 691–701. <https://doi.org/10.1039/C4MD00490F>.
- Jamalzadeh, L., Ghafouri, H., Sariri, R., Rabuti, H., Nasirzade, J., Hasani, H., Aghamaali, M.R., 2016. Cytotoxic effects of some common organic solvents on MCF-7, RAW-264.7 and human umbilical vein endothelial cells. *Avicenna J. Med. Biochem.* 4, 10–33453. <https://doi.org/10.17795/ajmb-33453>.
- Kanthamneni, N., Yung, B., Lee, R.J., 2016. Effect of Eudragit on In Vitro Transfection Efficiency of PEI-DNA Complexes. *Anticancer Res.* 36, 81–85.
- Laechelt, U., Wagner, E., 2015. Nucleic Acid Therapeutics Using Polyplexes: A Journey of 50 Years (and Beyond). *Chem. Rev.* 115, 11043–11078. <https://doi.org/10.1021/cr5006793>.
- Layman, J.M., Ramirez, S.M., Green, M.D., Long, T.E., 2009. Influence of polycation molecular weight on poly (2-dimethylaminoethyl methacrylate)-mediated DNA delivery in vitro. *Biomacromolecules* 10, 1244–1252. <https://doi.org/10.1021/bm9000124>.
- Lengsfeld, C., Anchordouy, T., 2002. Shear-induced degradation of plasmid DNA. *J. Pharm. Sci.* 91, 1581–1589. <https://doi.org/10.1002/jps.10140>.
- LePecq, J.-B., Paoletti, C., 1967. A fluorescent complex between ethidium bromide and nucleic acids: physical—chemical characterization. *J. Mol. Biol.* 27, 87–106. [https://doi.org/10.1016/0022-2836\(67\)90353-1](https://doi.org/10.1016/0022-2836(67)90353-1).
- Liu, Z., Zhang, Z., Zhou, C., Jiao, Y., 2010. Hydrophobic modifications of cationic polymers for gene delivery. *Prog. Polym. Sci.* 35, 1144–1162. <https://doi.org/10.1016/j.progpolymsci.2010.04.007>.
- Lopes, A., Vandermeulen, G., Pr at, V., 2019. Cancer DNA vaccines: current preclinical and clinical developments and future perspectives. *J. Exp. Clin. Cancer Res.* 38, 146.
- Lundstrom, K., 2018. Viral vectors in gene therapy. *Diseases* 6, 42. <https://doi.org/10.1186/s13046-019-1154-7>.
- Manganiello, M.J., Cheng, C., Convertine, A.J., Bryers, J.D., Stayton, P.S., 2012. Diblock copolymers with tunable pH transitions for gene delivery. *Biomaterials* 33, 2301–2309. <https://doi.org/10.1016/j.biomaterials.2011.11.019>.
- Meyers, J.A., Sanchez, D., Elwell, L.P., Falkow, S., 1976. Simple agarose gel electrophoretic method for the identification and characterization of plasmid deoxyribonucleic acid. *J. Bacteriol.* 127, 1529–1537.
- Moorthi, C., Kumar, C.S., Mohan, S., Krishnan, K., Kathiresan, K., 2013. Application of validated RP-HPLC-PDA method for the simultaneous estimation of curcumin and piperine in Eudragit E 100 nanoparticles. *J. Pharm. Res.* 7, 224–229. <https://doi.org/10.1016/j.jopr.2013.03.006>.
- Nelson, C.E., Kintzing, J.R., Hanna, A., Shannon, J.M., Gupta, M.K., Duvall, C.L., 2013. Balancing cationic and hydrophobic content of PEGylated siRNA polyplexes enhances endosome escape, stability, blood circulation time, and bioactivity in vivo. *ACS Nano* 7, 8870–8880. <https://doi.org/10.1021/nn403325f>.
- Niu, X., Zou, W., Liu, C., Zhang, N., Fu, C., 2009. Modified nanoprecipitation method to fabricate DNA-loaded PLGA nanoparticles. *Drug Dev. Ind. Pharm.* 35, 1375–1383.
- Olmsted, J., Kearns, D.R., 1977. Mechanism of ethidium bromide fluorescence enhancement on binding to nucleic acids. *Biochemistry* 16, 3647–3654. <https://doi.org/10.3109/03639040902939221>.
- Pack, D.W., Hoffman, A.S., Pun, S., Stayton, P.S., 2005. Design and development of polymers for gene delivery. *Nat. Rev. Drug Discovery* 4, 581–593. <https://doi.org/10.1038/nrd1775>.
- Perevyazko, I.Y., Vollrath, A., Pietsch, C., Schubert, S., Pavlov, G.M., Schubert, U.S., 2012. Nanoprecipitation of poly (methyl methacrylate)-based nanoparticles: Effect of the molar mass and polymer behavior. *J. Polym. Sci., Part A: Polym. Chem.* 50, 2906–2913. <https://doi.org/10.1002/pola.26071>.
- Press, A.T., Traeger, A., Pietsch, C., Mosig, A., Wagner, M., Clemens, M.G., Jbeily, N., Koch, N., Gottschaldt, M., Beziere, N., Ermolayev, V., Ntziachristos, V., Popp, J.,

- Kessels, M.M., Qualmann, B., Schubert, U.S., Bauer, M., 2014. Cell type-specific delivery of short interfering RNAs by dye-functionalised theranostic nanoparticles. *Nat. Commun.* 5, 5565. <https://doi.org/10.1038/ncomms5565>.
- Rao, S., Morales, A.A., Pearse, D.D., 2015. The comparative utility of viromer RED and lipofectamine for transient gene introduction into glial cells. *Biomed. Res. Int.* 2015 <https://doi.org/10.1155/2015/458624>.
- Rejman, J., Oberle, V., Zuhorn, I.S., Hoekstra, D., 2004. Size-dependent internalization of particles via the pathways of clathrin- and caveolae-mediated endocytosis. *Biochem. J.* 377, 159–169. <https://doi.org/10.1042/bj20031253>.
- Richter, F., Martin, L., Leer, K., Moek, E., Hausig, F., Brendel, J.C., Traeger, A., 2020. Tuning of Endosomal Escape and Gene Expression by Functional Groups, Molecular Weight and Transfection Medium: A Structure-Activity Relationship Study. *J. Mater. Chem. B* 8, 5026–5041. <https://doi.org/10.1039/D0TB00340A>.
- Rinkenauer, A.C., Press, A.T., Raasch, M., Pietsch, C., Schweizer, S., Schworer, S., Rudolph, K.L., Mosig, A., Bauer, M., Traeger, A., Schubert, U.S., 2015a. Comparison of the uptake of methacrylate-based nanoparticles in static and dynamic in vitro systems as well as in vivo. *J. Control Release* 216, 158–168. <https://doi.org/10.1016/j.jconrel.2015.08.008>.
- Rinkenauer, A.C., Tauhardt, L., Wendler, F., Kempe, K., Gottschaldt, M., Traeger, A., Schubert, U.S., 2015b. A Cationic Poly (2-oxazoline) with High In Vitro Transfection Efficiency Identified by a Library Approach. *Macromol. Biosci.* 15, 414–425. <https://doi.org/10.1002/mabi.201400334>.
- Samsonova, O., Pfeiffer, C., Hellmund, M., Merkel, O.M., Kissel, T., 2011. Low molecular weight pDMAEMA-block-pHEMA block-copolymers synthesized via RAFT-polymerization: potential non-viral gene delivery agents? *Polymers* 3, 693–718. <https://doi.org/10.3390/polym3020693>.
- Schroeder, A., Dahlman, J.E., Sahay, G., Love, K.T., Jiang, S., Eltoukhy, A.A., Levins, C. G., Wang, Y., Anderson, D.G., 2012. Alkane-modified short polyethyleneimine for siRNA delivery. *J. Control Release* 160, 172–176. <https://doi.org/10.1016/j.jconrel.2011.11.030>.
- Schuck, P., Rossmanith, P., 2000. Determination of the sedimentation coefficient distribution by least-squares boundary modeling. *Biopolym.: Original Res. Biomol.* 54, 328–341. [https://doi.org/10.1002/1097-0282\(20001015\)54:5<328::AID-BIP40>3.0.CO;2-P](https://doi.org/10.1002/1097-0282(20001015)54:5<328::AID-BIP40>3.0.CO;2-P).
- Shen, W., Wang, R., Fan, Q., Gao, X., Wang, H., Shen, Y., Li, Y., Cheng, Y., 2020. Natural Polyphenol Inspired Polycatechols for Efficient siRNA Delivery. *CCS Chem.* 146–157. <https://doi.org/10.31635/ccschem.020.201900084>.
- Shirley, J.L., de Jong, Y.P., Terhorst, C., Herzog, R.W., 2020. Immune Responses to Viral Gene Therapy Vectors. *Mol. Ther.* 28 (3), 709–722. <https://doi.org/10.1016/j.ymthe.2020.01.001>.
- Smith, D., Pentzer, E.B., Nguyen, S.T., 2007. Bioactive and therapeutic ROMP polymers. *J. Macromol. Sci., Part C: Polym. Rev.* 47, 419–459. <https://doi.org/10.1080/15583720701455186>.
- Tan, E., Lv, J., Hu, J., Shen, W., Wang, H., Cheng, Y., 2018. Statistical versus block fluoropolymers in gene delivery. *J. Mater. Chem. B* 6, 7230–7238. <https://doi.org/10.1039/C8TB01470A>.
- Tang, J., Xu, N., Ji, H., Liu, H., Wang, Z., Wu, L., 2011. Eudragit nanoparticles containing genistein: formulation, development, and bioavailability assessment. *Int. J. Nanomed.* 6, 2429–2435. <https://doi.org/10.2147/IJN.S24185>.
- Trutzschler, A.K., Bus, T., Reifarth, M., Brendel, J.C., Hoepfner, S., Traeger, A., Schubert, U.S., 2018. Beyond Gene Transfection with Methacrylate-Based Polyplexes-The Influence of the Amino Substitution Pattern. *Bioconjug. Chem.* 29, 2181–2194. <https://doi.org/10.1021/acs.bioconjchem.8b00074>.
- Van de Wetering, P., Cherg, J.-Y., Talsma, H., Crommelin, D., Hennink, W., 1998. 2-(Dimethylamino) ethyl methacrylate based (co) polymers as gene transfer agents. *J. Control. Release* 53, 145–153. [https://doi.org/10.1016/S0168-3659\(97\)00248-4](https://doi.org/10.1016/S0168-3659(97)00248-4).
- Van de Wetering, P., Moret, E.E., Schuurmans-Nieuwenbroek, N.M., van Steenberg, M. J., Hennink, W.E., 1999. Structure– activity relationships of water-soluble cationic methacrylate/methacrylamide polymers for nonviral gene delivery. *Bioconjug. Chem.* 10, 589–597. <https://doi.org/10.1021/bc980148w>.
- Wakefield, D.H., Klein, J.J., Wolff, J.A., Rozema, D.B., 2005. Membrane activity and transfection ability of amphipathic polycations as a function of alkyl group size. *Bioconjug. Chem.* 16, 1204–1208.
- Wang, Y., Ye, M., Xie, R., Gong, S., 2018. Enhancing the in vitro and in vivo stabilities of polymeric nucleic acid delivery nanosystems. *Bioconjug. Chem.* 30, 325–337. <https://doi.org/10.1021/bc050067h>.
- Wong, S.Y., Pelet, J.M., Putnam, D., 2007. Polymer systems for gene delivery—past, present, and future. *Prog. Polym. Sci.* 32, 799–837. <https://doi.org/10.1016/j.progpolymsci.2007.05.007>.
- Yildirim, T., Rinkenauer, A.C., Weber, C., Traeger, A., Schubert, S., Schubert, U.S., 2015. RAFT made methacrylate copolymers for reversible pH-responsive nanoparticles. *J. Polym. Sci., Part A: Polym. Chem.* 53, 2711–2721. <https://doi.org/10.1002/pola.27734>.
- Yin, H., Kanasty, R.L., Eltoukhy, A.A., Vegas, A.J., Dorkin, J.R., Anderson, D.G., 2014. Non-viral vectors for gene-based therapy. *Nat. Rev. Genet.* 15, 541–555. <https://doi.org/10.1038/nrg3763>.

## Supporting information

# Solely aqueous formulation of hydrophobic cationic polymers for efficient gene delivery

*Jana I. Solomun,<sup>a</sup> Gizem Cinar,<sup>a</sup> Prosper Mapfumo,<sup>a</sup> Friederike Richter,<sup>a</sup> Elisabeth Moek,<sup>a</sup>*

*Franziska Hausig,<sup>a</sup> Liam Martin,<sup>a</sup> Stephanie Hoepfener,<sup>a,b</sup> Ivo Nischang,<sup>a,b</sup>*

*Anja Traeger\*<sup>a,b</sup>*

<sup>a</sup>Laboratory of Organic and Macromolecular Chemistry (IOMC), Friedrich Schiller University  
Jena, Humboldtstrasse 10, 07743 Jena, Germany.

<sup>b</sup>Jena Center for Soft Matter (JCSM), Friedrich Schiller University Jena, Philosophenweg 7,  
07743 Jena, Germany.

\*Correspondence to A. Traeger (anja.traeger@uni-jena.de)

## List of Tables

<b>Table S1.</b> DLS/ELS measurements of the PBMD <sub>Org</sub> (out,pDNA) formulation. ....	7
<b>Table S2.</b> DLS/ELS measurements of the PBMD <sub>Org</sub> (in,pDNA) formulation. ....	7
<b>Table S3.</b> DLS/ELS measurements of the PBMD <sub>Aqu</sub> (pDNA) formulation. ....	8
<b>Table S4.</b> DLS measurements of PBMD <sub>Aqu</sub> (pDNA) formed with different plasmids used within the study. ....	10
<b>Table S5.</b> DLS measurements of PBMD <sub>Aqu</sub> (siRNA) and of PBMD <sub>Aqu</sub> (mRNA) at N/P 10. ...	17

## List of Figures

<b>Fig. S1.</b> Synthesis and characterization of PDMAEMA.....	6
<b>Fig. S2.</b> DLS hydrodynamic diameter distributions and example exponential decays from samples of the different formulation methods at N/P 50.....	9
<b>Fig. S3.</b> DLS hydrodynamic diameter distributions and example exponential decays of PBMD <sub>Aqu</sub> (pDNA) complexes at N/P 10 and 20.....	10
<b>Fig. S4.</b> Scanning electron microscopy measurements (SEM) of PBMD <sub>Org</sub> (in,pDNA) and PBMD <sub>Org</sub> . ....	11
<b>Fig. S5.</b> Gating strategy for pDNA transfection experiments.....	12
<b>Fig. S6.</b> Gating strategy for siRNA transfection experiments. ....	13
<b>Fig. S7.</b> Gating strategy for mRNA transfection experiments.....	14
<b>Fig.S8.</b> Sedimentation velocity profiles of free RAFT agent-containing polymer.....	15
<b>Fig. S9.</b> AUC measurements of PDMAEMA-polyplexes. ....	15
<b>Fig. S10.</b> AUC measurements at increasing sample concentrations.....	16
<b>Fig. S11.</b> Comparison of AUC measurements of PBMD <sub>Aqu</sub> (pDNA) and PDMAEMA-polyplexes.....	17

# 1. Additional methods and materials

## 1.1 Materials

2-(Dimethylamino)ethyl methacrylate (DMAEMA) (98%) was obtained from Sigma-Aldrich (now Merck KGaA, St. Louis, MO, U.S.) and used as received. Butyl methacrylate (*n*BMA) (99%) and methyl methacrylate (MMA) (99%) were obtained from TCI (Tokyo, Japan) and used as received. Bis(ethylsulfanyl thiocarbonyl)disulfide was synthesized according to the literature.[1]  $\alpha,\alpha'$ -Azobisisobutyronitrile (AIBN) was obtained from Sigma-Aldrich (now Merck KGaA, St. Louis, MO, U.S.) and recrystallized from methanol. Organic solvents for synthesis were obtained from Sigma-Aldrich (now Merck KGaA, St. Louis, MO, U.S.) and re-distilled on-site. All the following materials were ordered from the suppliers stated in brackets: HEK293T cells (DSMZ, Braunschweig, Germany), L-929 cells (CLS Cell Lines Service, Eppelheim, Germany), HEK293-GFP cells (Amsbio LLC, Abington, U.K.), TC treated cell culture flasks (Greiner Bio-One International GmbH, Kremsmünster, Austria), TC treated multiwell cell culture plates (VWR International GmbH, Darmstadt, Germany), Dulbecco's modified eagle medium (DMEM) and 4-(2-hydroxyethyl)-1-piperazineethanesulfonic acid (HEPES) buffer (Biowest SAS, Nuaille, France), fetal bovine serum (FBS, Capricorn Scientific, Ebsdorfergrund, Germany), Opti-MEM™ reduced serum medium, Penicillin-Streptomycin, PrestoBlue™ cell viability reagent (Thermo Fisher Scientific, Waltham, MA, U.S.), trypsin-EDTA, Hanks' balanced salt solution (HBSS) (Sigma-Aldrich, St. Louis, MO, U.S.), ethidiumbromide solution, agarose-HR PLUS (Carl Roth, Karlsruhe, Germany), heparin sodium salt (Alfa Aesar, Haverhill, MA, U.S.), Eudragit® E(PO/E100) (Evonik Industries, Essen, Germany), linear poly(ethylenimine) (25 kDa, Polysciences, Warrington, PA, U.S.), Viomer® RED (Lipocalyx, now BioNTech, Mainz, Germany). Plasmid DNA encoding for enhanced green fluorescent protein (mEGFP-N1, 4.7 kb), td-tomato (td-tomato-N1, 5.4 kb) or Myc (pKMyc, 4.7 kb) was isolated from E. Coli using a Giga plasmid kit (Quiagen, Hilden, Germany). mEGFP-N1 was a gift from Michael Davidson (Addgene plasmid #54767;

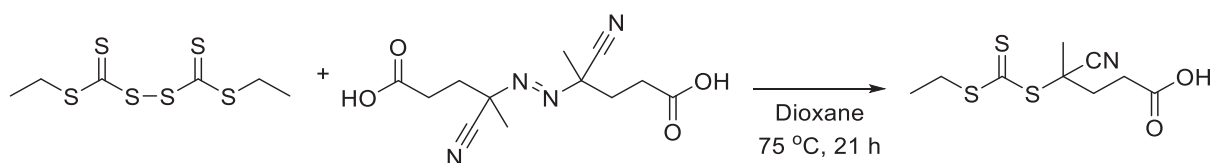
[http://n2t.net/addgene:54767;RRID: Addgene\\_54767](http://n2t.net/addgene:54767;RRID:Addgene_54767)), tdTomato-N1 was a gift from Michael Davidson & Nathan Shaner & Roger Tsien (Addgene plasmid #54642; [http://n2t.net/addgene: 54642; RRID: Addgene\\_54642](http://n2t.net/addgene:54642;RRID:Addgene_54642)) and pKMyC was a gift from Ian Macara (Addgene plasmid #19400; [http://n2t.net/addgene: 19400;RRID: Addgene\\_19400](http://n2t.net/addgene:19400;RRID:Addgene_19400)). pCMV-GFP plasmid was ordered from Plasmid Factory (Bielefeld, Germany, 3.5 kb). GFP-22 siRNA targeting green fluorescent protein (GFP) and negative control siRNA were ordered from Qiagen (Hilden, Germany). mRNA encoding for GFP was obtained from Oz Biosciences (Marseille, France).

## 1.2 Synthesis of (4-cyanopentanoic acid)ylethyl trithiocarbonate (CPAETC)

To a solution of bis-(ethylsulfanylthiocarbonyl) disulfide (2.5 g, 9.1 mmol) in 1,4-dioxane (62 mL), 4,4'-azobis(4-cyanovaleric acid) (5.4 g, 2.1 eq., 19.13 mmol) was added and the mixture was stirred for 21 hours at 75 °C. After removal of the solvent under reduced pressure, the crude product was subjected to column chromatography (silica, hexane: ethyl acetate, with a content of ethyl acetate varying from 60 to 30%). The product fractions were collected and dried under vacuum; an orange powder was obtained (81% yield).

<sup>1</sup>H NMR (300 MHz, CDCl<sub>3</sub>-d) δ [ppm] = 3.36 (q, *J* = 7.4 Hz, 2H, S-CH<sub>2</sub>-CH<sub>3</sub>), 2.76 – 2.61 (m, 2H, C(O)-CH<sub>2</sub>-CH<sub>2</sub>-), 2.65 – 2.33 (m, 2H, C(O)-CH<sub>2</sub>-CH<sub>2</sub>-), 1.90 (s, 3H, C(CN)(CH<sub>3</sub>)), 1.37 (t, *J* = 7.4 Hz, 4H, CH<sub>2</sub>-CH<sub>3</sub>).

<sup>13</sup>C-NMR (75 MHz, CDCl<sub>3</sub>) δ [ppm] = 216.66, 177.24, 118.88, 46.37, 77.41, 76.63, 33.47, 31.40, 29.52, 24.84, 12.74.



### 1.3 Reversible addition fragmentation chain-transfer (RAFT) polymerization

Conversion ( $p$ ) of each monomer was calculated from  $^1\text{H-NMR}$  data by comparing the integrals between vinyl peaks (5.5 - 6.3 ppm) and polymer peaks against an external reference (1,3,5-trioxane, 5.14 ppm) before ( $t=0$ ) and at designated time points throughout the polymerization. The theoretical number-average molar mass ( $M_{n,\text{th}}$ ) was then calculated using equation (1):

$$M_{n,\text{th}} = \frac{[\text{DMAEMA}]_0 p_{\text{DMAEMA}} M_{\text{DMAEMA}} + [\text{BMA}]_0 p_{\text{BMA}} M_{\text{BMA}} + [\text{MMA}]_0 p_{\text{MMA}} M_{\text{MMA}}}{[\text{CTA}]_0} + M_{\text{CTA}} \quad (1)$$

Where  $[\text{DMAEMA}]_0$ ,  $[\text{BMA}]_0$ ,  $[\text{MMA}]_0$  and  $[\text{CTA}]_0$  are the initial concentrations of the monomers and the chain transfer agent (CTA), respectively,  $M_{\text{DMAEMA}}$ ,  $M_{\text{BMA}}$ ,  $M_{\text{MMA}}$ , and  $M_{\text{CTA}}$  are the molar mass of the monomer and CTA, respectively, and  $p$  is the monomer conversion of each monomer.

### 1.4 Synthesis of P(DMAEMA) *via* RAFT polymerization

CPAETC (50.0 mg,  $1.9 \times 10^{-4}$  moles), DMAEMA (4.5 g,  $2.9 \times 10^{-2}$  moles), 1,4-dioxane (2.5 g), 1% (w/w) ACVA in 1,4-dioxane (426.0 mg,  $1.5 \times 10^{-5}$  moles) and 1,3,5-trioxane (external NMR standard, 21 mg) were introduced to a 20 mL microwave vial equipped with a magnetic stirring bar. The vial was sealed, and the solution deoxygenated by bubbling argon through it for approx. 10 min. The vial was placed in an oil bath set at 70 °C and allowed to stir for 7 h, with samples taken for  $^1\text{H-NMR}$  and  $\text{CHCl}_3\text{-SEC}$  analysis at designated times. The polymer was precipitated three times from THF into cold hexane and dried under reduced pressure to give a yellow solid.  $\text{CHCl}_3\text{-SEC}$ :  $M_{n,\text{SEC}} = 14.2 \text{ kg mol}^{-1}$ ,  $D = 1.19$ .

## 2. Further Results

### 2.1 Characterization of PDMAEMA

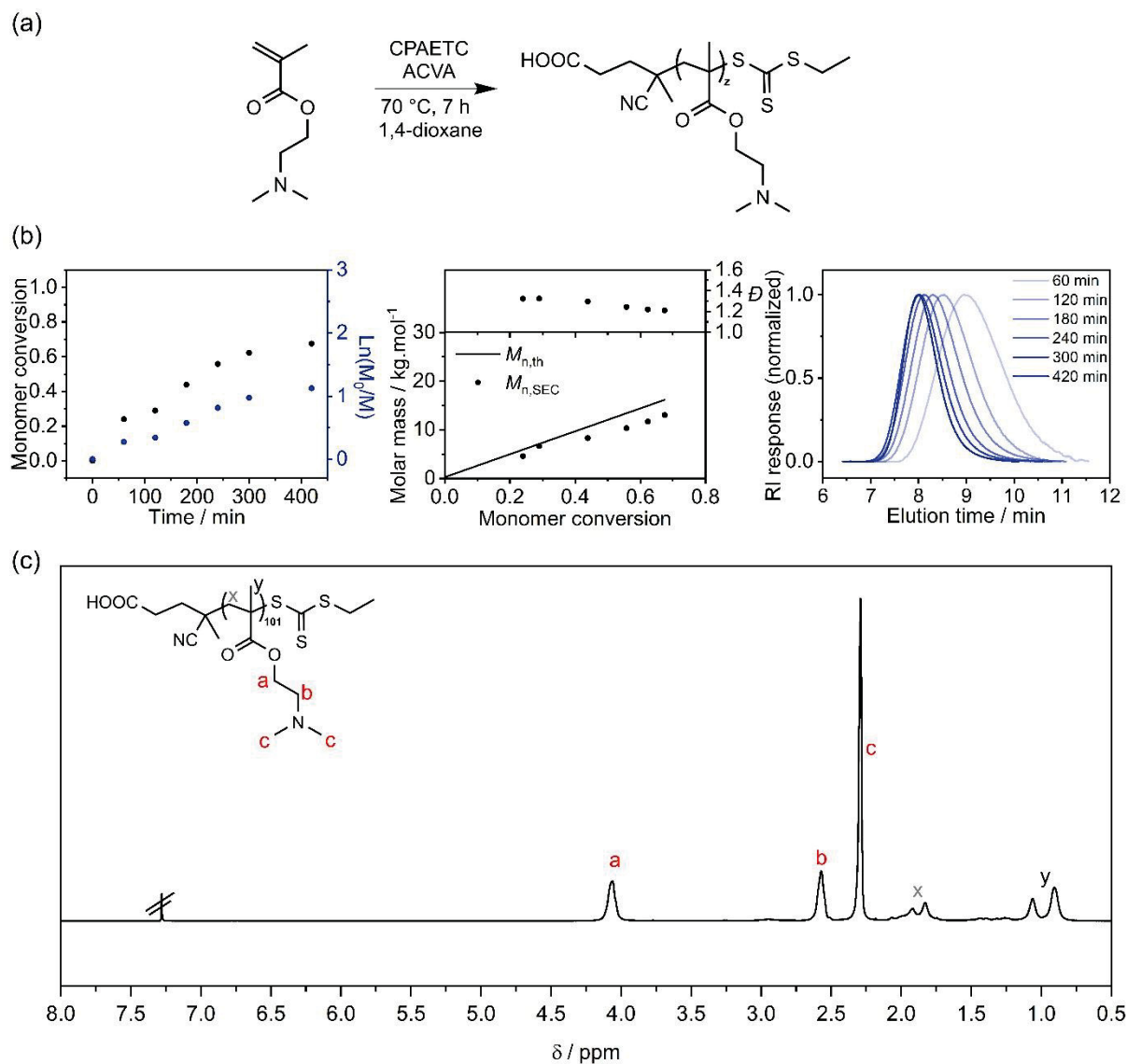


**Fig. S1.** Synthesis and characterization of PDMAEMA.

(a) Schematic representation of the RAFT polymerization to obtain PDMAEMA. (b) Kinetics of PDMAEMA formation was measured by  $^1\text{H-NMR}$  and SEC. (c)  $^1\text{H-NMR}$  was measured after precipitation.



## 2.2 DLS measurements

**Table S1.** DLS/ELS measurements of the PBMD<sub>Org</sub>(out,pDNA) formulation.

Size and zeta potential measured by DLS/ELS. Each measurement is displayed as a single value.

Formulation	N/P ratio	z-average / nm	PDI	Zeta potential / mV
PBMD <sub>Org</sub> (out,pDNA)	0	118.4	0.186	67.1
		144.7	0.141	50.1
		111.9	0.131	44.4
		123.4	0.125	42.1
	5	165.6	0.221	-14.0
		193.6	0.209	-12.9
		248.7	0.237	-14.0
		182.8	0.184	-12.9
	15	764.4	0.376	-7.2
		757.8	0.324	-8.0
		7824.8	0.247	15.4
		1104.3	0.539	-7.3
	30	1168.2	0.699	18.4
		1160.8	0.842	21.6
		7789.0	0.902	29.3
		2673.4	0.943	26.4
	50	608.8	0.489	25.9
		338.7	0.704	32.1
		127.2	0.111	41.6
		148.7	0.123	31.8
100	188.0	0.329	39.1	
	146.0	0.179	42.3	
	113.3	0.131	42.9	
	126.9	0.111	36.8	

**Table S2.** DLS/ELS measurements of the PBMD<sub>Org</sub>(in,pDNA) formulation.

Size and zeta potential measured by DLS/ELS. Each measurement is displayed as a single value.

Formulation	N/P ratio	z-average / nm	PDI	Zeta potential / mV
PBMD <sub>Org</sub> (in,pDNA)	30	1139.8	0.686	45.6
		241.0	0.260	32.6
		605.4	0.405	43.3
	50	4111.0	0.143	42.2
		276.7	0.134	40.3
		311.2	0.102	39.8
	75	214.5	0.117	39.6
		225.5	0.086	40.4
		223.4	0.100	39.6
	100	183.8	0.071	41.9
		188.4	0.115	43.1
		215.4	0.061	38.1

**Table S3.** DLS/ELS measurements of the PBMD<sub>Aqu</sub>(pDNA) formulation.

Size and zeta potential measured by DLS/ELS. Each measurement is displayed as a single value.

Formulation	N/P ratio	z-average / nm	PDI	Zeta potential / mV
PBMD <sub>Aqu</sub> (pDNA)	0.5	113.4	0.236	-19.5
		147.6	0.161	-15.2
		442.8	0.377	-17.7
		129.7	0.155	
	1	2104.0	0.324	-22.3
		73.1	0.582	-18.2
		163.7	0.159	-18.3
		159.7	0.214	
	5	120.4	0.161	8.1
		188.3	0.176	
		101.0	0.150	15.5
		1503.5	0.218	
		535.1	0.269	19.5
	10	759.4	0.264	
		110.1	0.205	23.2
		109.8	0.173	
		98.7	0.190	20.6
		120.5	0.208	20.8
	20	102.1	0.200	
		96.2	0.189	21.9
		98.4	0.179	
		92.7	0.231	24.2
		107.2	0.219	19.7
	30	100.0	0.263	
		89.9	0.176	23.6
		94.4	0.187	
		79.9	0.204	23.4
		93.0	0.221	22.3
50	90.6	0.252		
	72.2	0.220	24.6	
	85.3	0.202		
	75.2	0.238	24.6	
	92.7	0.220	25.5	
	83.6	0.264		

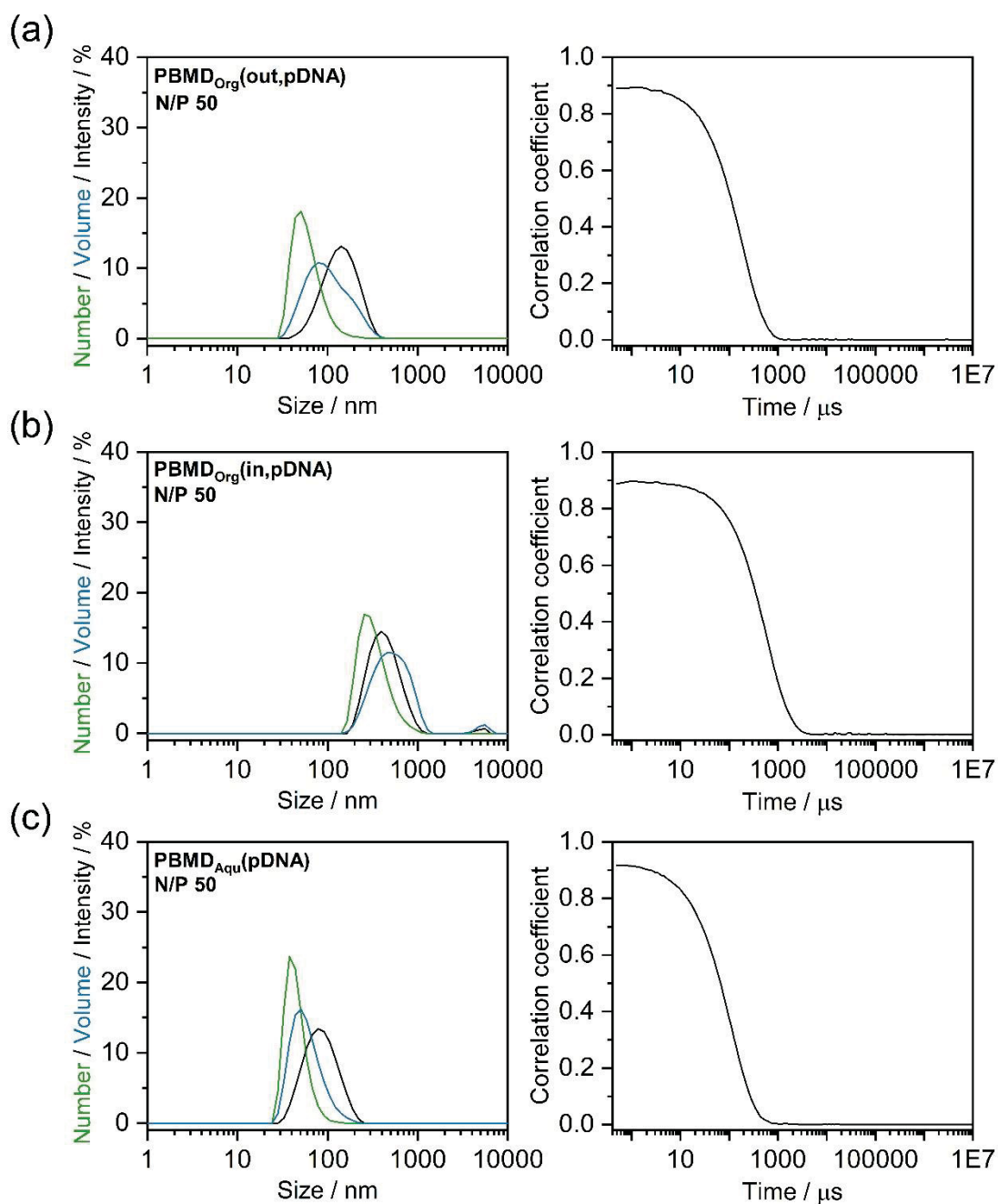


**Fig. S2.** DLS hydrodynamic diameter distributions and example exponential decays from samples of the different formulation methods at N/P 50.

pDNA-loaded NPs or complexes obtained by different formulation methods at N/P 50 and  $15 \mu\text{g mL}^{-1}$  pCMV-GFP plasmid. Exemplary intensity, number, and volume weighted plots and exponential decay correlation coefficients of single measurements are displayed for (a) PBMD<sub>Org</sub>(out,pDNA), (b) PBMD<sub>Org</sub>(in,pDNA) and (c) PBMD<sub>Aqu</sub>(pDNA) formulations.

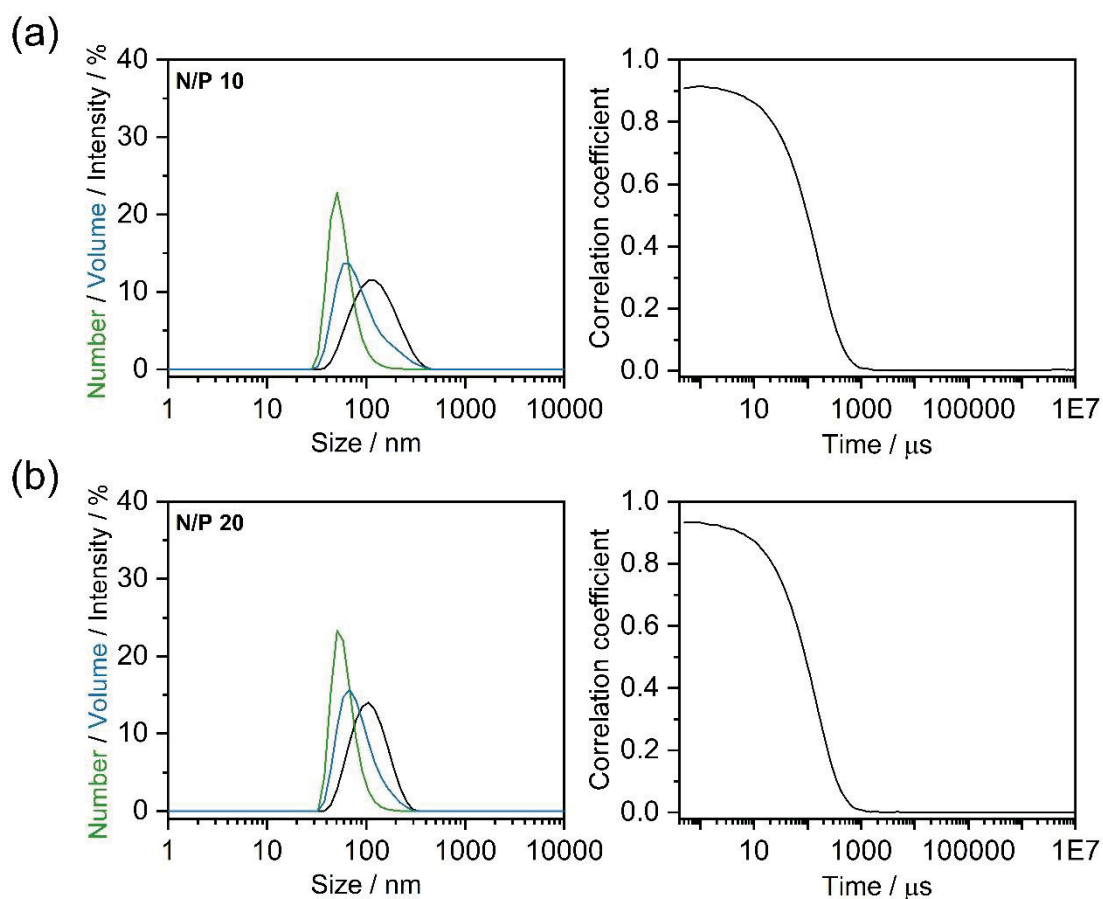


**Fig. S3.** DLS hydrodynamic diameter distributions and example exponential decays of  $\text{PBMD}_{\text{Aqui}}(\text{pDNA})$  complexes at N/P 10 and 20.

Complexes at (a) N/P 10 and (b) N/P 20 formed using  $15 \mu\text{g mL}^{-1}$  pCMV-GFP plasmid.

**Table S4.** DLS measurements of  $\text{PBMD}_{\text{Aqui}}(\text{pDNA})$  formed with different plasmids used within the study.

Size was measured by DLS (mean of  $n=3 \pm \text{SD}$ ).

pDNA	z-average / nm	PDI
pCMV-GFP	$90.9 \pm 1.5$	$0.182 \pm 0.015$
mEGFP-N1	$97.3 \pm 2.2$	$0.175 \pm 0.002$
pKmyc	$94.6 \pm 1.0$	$0.180 \pm 0.009$
td-tomato-N1	$87.2 \pm 1.7$	$0.164 \pm 0.024$

## 2.3 Scanning electron microscopy measurements (SEM)

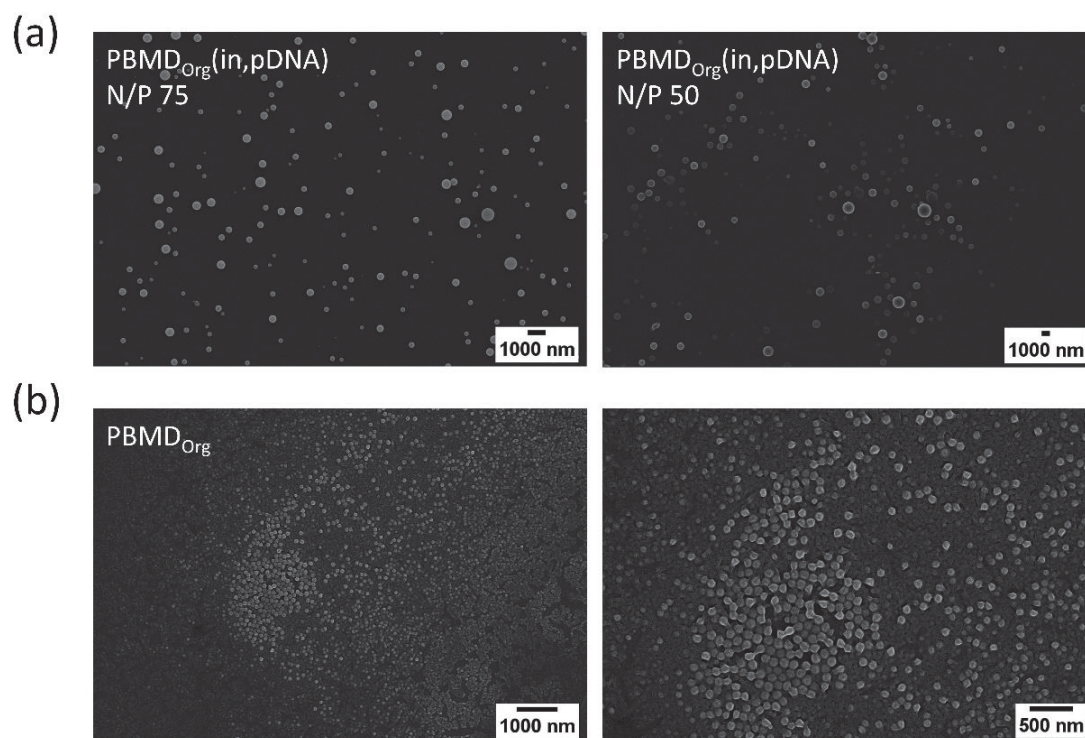


**Fig. S4.** Scanning electron microscopy measurements (SEM) of PBMD<sub>Org</sub>(in,pDNA) and PBMD<sub>Org</sub>. (a) nanoparticles obtained by the PBMD<sub>Org</sub>(in,pDNA) formulation at N/P ratios of 75 and 50 and (b) nanoparticles formulated by nanoprecipitation in acetone prior to addition of pDNA (PBMD<sub>Org</sub>).

## 2.4 Gating strategy for transfection experiments

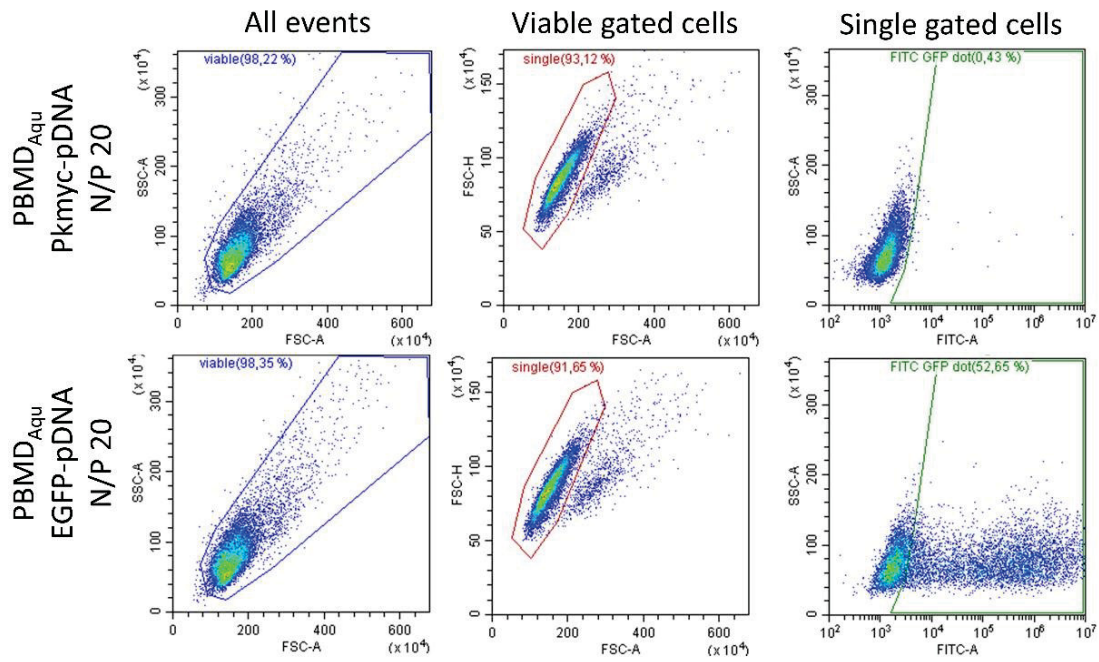


**Fig. S5.** Gating strategy for pDNA transfection experiments.

Viable cells were gated according to the FSC/SSC pattern. Subsequently the single cells were discriminated from doublets in the sample using the area of FSC signal plotted against the FSC height.

GFP positive cells were identified by gating the single cells to the unstained control (PBMD<sub>Aqu</sub>(pDNA) complex with pKMyC plasmid).

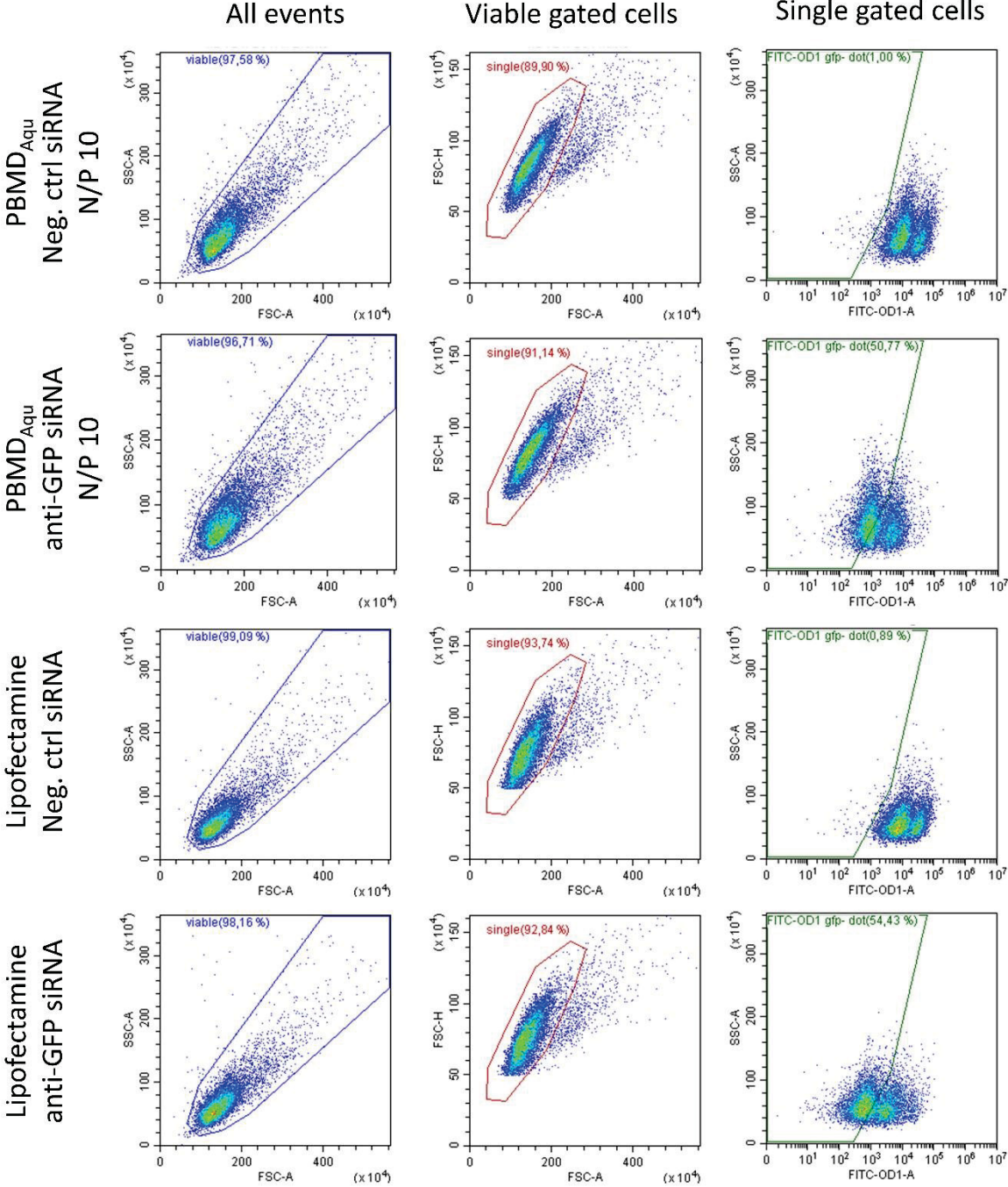


**Fig. S6.** Gating strategy for siRNA transfection experiments.

Viable single cells were gated as described for pDNA transfection. Subsequently, cells with reduced GFP fluorescence were discriminated by gating to the control (PBMD<sub>Aqu</sub>(siRNA) complex with neg. ctrl GFP siRNA).

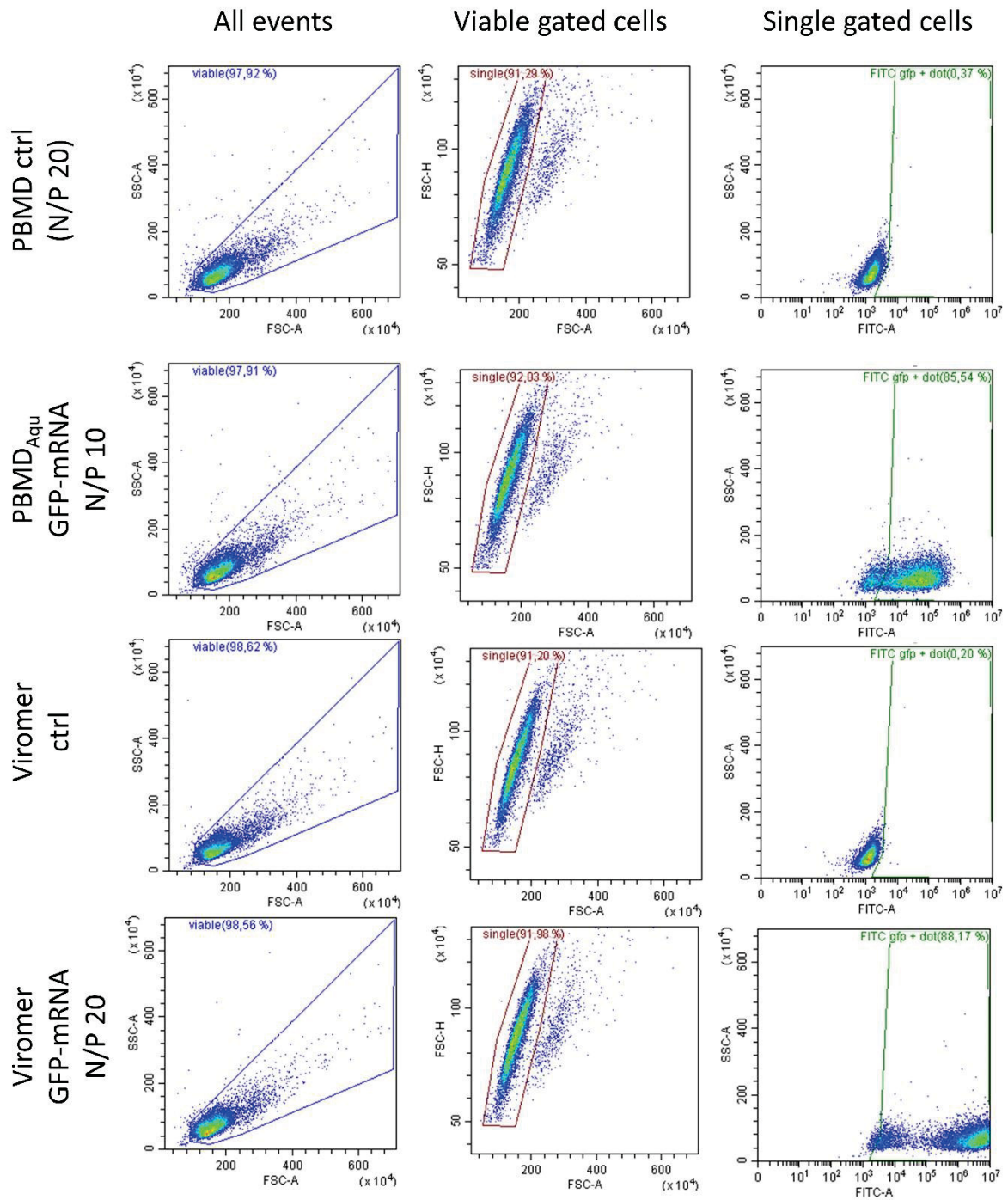


**Fig. S7.** Gating strategy for mRNA transfection experiments.

Viable single cells were gated as described. Cells expressing GFP were identified by gating to the control (polymer without mRNA).



## 2.5 Analytical ultracentrifugation (AUC) measurements

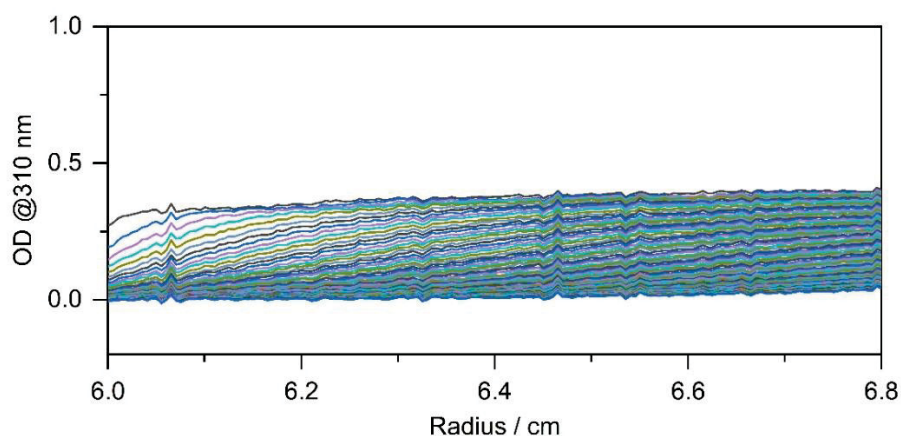


**Fig.S8.** Sedimentation velocity profiles of free RAFT agent-containing polymer.

Radially resolved sedimentation velocity profiles of free RAFT agent-containing polymer of the PBMD<sub>Aqu</sub>(pDNA) complex at an N/P ratio of 20 (in terms of OD) at a concentration of  $c = 1 \text{ mg mL}^{-1}$  monitored at a wavelength of  $\lambda = 310 \text{ nm}$  in terms of OD at a subsequent a rotor speed at 42,000 rpm.

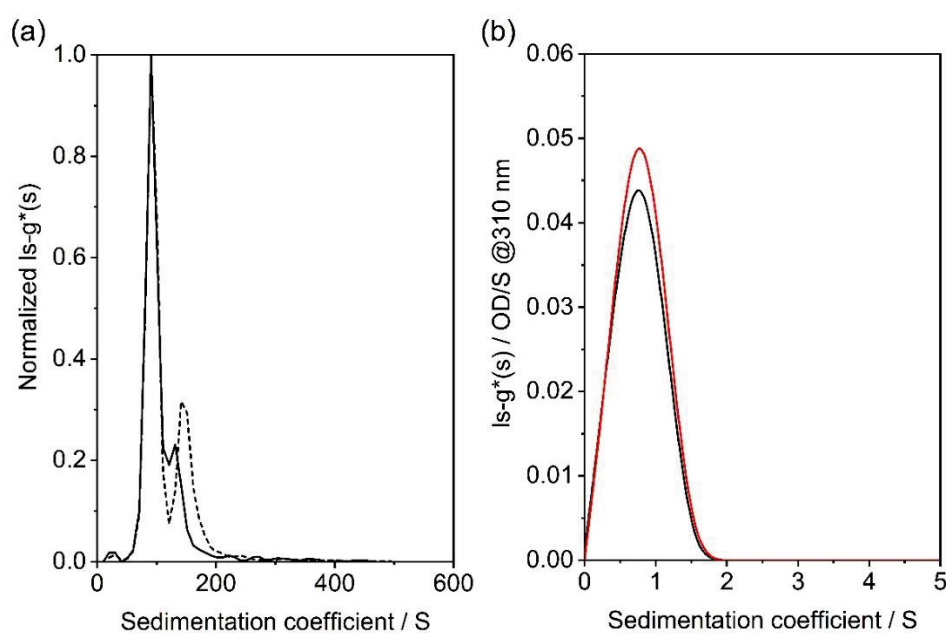


**Fig. S9.** AUC measurements of PDMAEMA-polyplexes.

(a) Normalized differential distributions of sedimentation coefficients of PDMAEMA complexes at a rotor speed of 7,500 rpm and at  $\lambda = 260 \text{ nm}$  in terms of OD formed at N/P 10 (black dashed line) and N/P 20 (black solid line). (b) Differential distributions of sedimentation coefficients at a subsequent

rotor speed of 42,000 rpm and at  $\lambda = 310$  nm in terms of OD of the free polymer. Complex formed with PDMAEMA at N/P 10 (black solid line) and N/P 20 (red solid line).

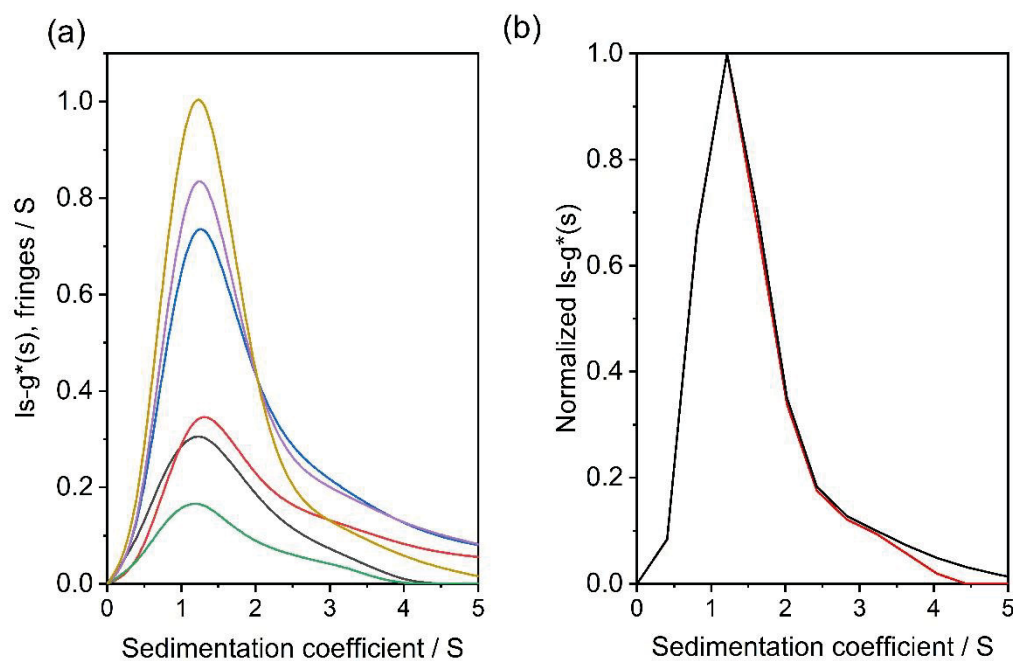


**Fig. S10.** AUC measurements at increasing sample concentrations.

(a) Differential distributions of sedimentation coefficients obtained at a subsequent rotor speed of 42,000 rpm and at increasing sample concentrations of the PBMD<sub>Aqu</sub>(pDNA) formulation at N/P 20 (from bottom to top) via RI detection, and (b) overlay of normalized differential distributions of sedimentation coefficients at  $\lambda = 310$  nm (red solid line) and RI detection (black solid line) at a rotor speed at 42,000 rpm.

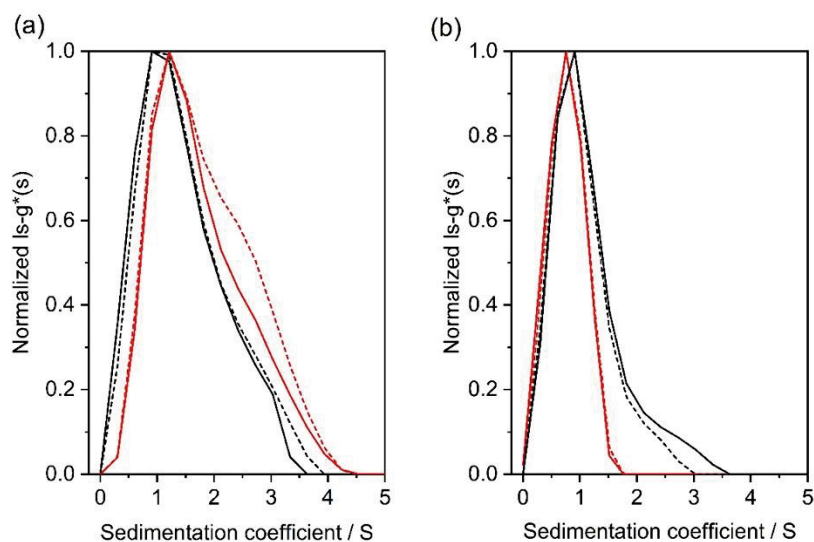


**Fig. S11.** Comparison of AUC measurements of PBMD<sub>Aqu</sub>(pDNA) and PDMAEMA-polyplexes.

Normalized differential distributions of sedimentation coefficients at a rotor speed of 42,000 rpm and at  $\lambda = 310$  nm of the free polymer. (a) PBMD<sub>Aqu</sub>(pDNA) complex at an N/P ratio of 10 (solid lines) and N/P20 (dashed lines) at a wavelength of  $\lambda = 310$  nm (red lines) and RI detection (black lines). (b) Polyplexes formed with PDMAEMA at an N/P ratio of 10 (solid lines) and N/P 20 (dashed lines) at a wavelength of  $\lambda = 310$  nm (red lines) and RI detection (black lines).

**Table S5.** DLS measurements of PBMD<sub>Aqu</sub>(siRNA) and of PBMD<sub>Aqu</sub>(mRNA) at N/P 10.

Size measured by DLS at a RNA concentration of  $15 \mu\text{g mL}^{-1}$  ( $n = 1$ , mean  $\pm$  SD of three sub-runs).

Formulation	z-average / nm	PDI
PBMD <sub>Aqu</sub> (siRNA) N/P10	$165.7 \pm 4.1$	$0.229 \pm 0.022$
PBMD <sub>Aqu</sub> (mRNA) N/P 10	$139.7 \pm 2.0$	$0.174 \pm 0.021$

## References

[1] K. Ishitake, K. Satoh, M. Kamigaito, Y. Okamoto, Stereogradient polymers formed by controlled/living radical polymerization of bulky methacrylate monomers, *Angewandte Chemie*, 121 (2009) 2025-2028.



## Publication Pub7

---

### How To Tune the Gene Delivery and Biocompatibility of Poly(2-(4aminobutyl)-2-oxazoline) by Self- and Coassembly

M. N. Leiske, F. H. Sobotta, F. Richter, S. Hoepfner, J. C. Brendel, A. Traeger, U. S. Schubert

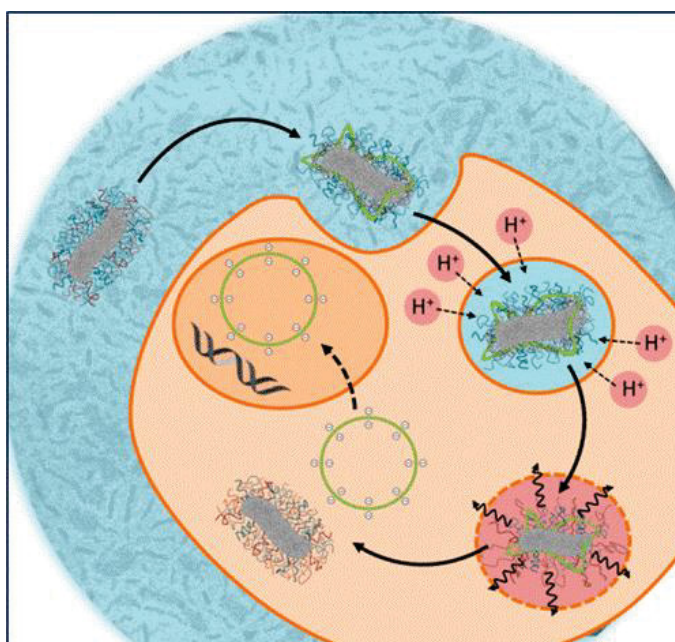
*Biomacromolecules* **2018**, 19, 748-760

---


Reproduced with permission of The American Chemical Society. Copyright © 2018.

The article and the supporting information are available online:

[doi.org/10.1021/acs.biomac.7b01535](https://doi.org/10.1021/acs.biomac.7b01535)



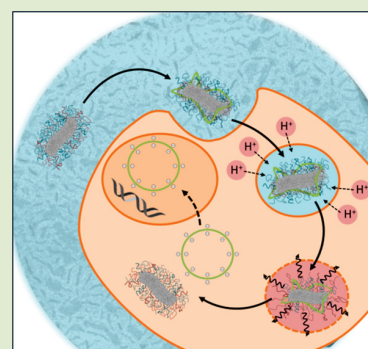
# How To Tune the Gene Delivery and Biocompatibility of Poly(2-(4-aminobutyl)-2-oxazoline) by Self- and Coassembly

Meike N. Leiske,<sup>†,‡</sup> Fabian H. Sobotta,<sup>†,‡</sup> Friederike Richter,<sup>†,‡</sup> Stephanie Hoepfner,<sup>†,‡</sup> Johannes C. Brendel,<sup>†,‡</sup> Anja Traeger,<sup>\*,†,‡</sup> and Ulrich S. Schubert<sup>\*,†,‡</sup> 

<sup>†</sup>Laboratory of Organic and Macromolecular Chemistry (IOMC) and <sup>‡</sup>Jena Center for Soft Matter (JCSM), Friedrich Schiller University Jena, Humboldtstrasse 10, 07743 Jena, Germany

## Supporting Information

**ABSTRACT:** Despite their promising potential in gene transfection, the toxicity and limited efficiency of cationic polymers as nonviral vectors are major obstacles for their broader application. The large amount of cationic charges, for example, in poly(ethylene imine) (PEI) is known to be advantageous in terms of their transfection efficiency but goes hand-in-hand with a high toxicity. Consequently, an efficient shielding of the charges is required to minimize toxic effects. In this study, we use a simple mixed-micelle approach to optimize the required charge density for efficient DNA complex formation and to minimize toxicity by using a biocompatible polymer. In detail, we coassembled mixed poly(2-oxazoline) nanostructures ( $d \approx 100$  nm) consisting of a hydrophobic-cationic block copolymer (P(NonOx<sub>52</sub>-*b*-AmOx<sub>184</sub>)) and a hydrophobic–hydrophilic stealth block copolymer (P(EtOx<sub>155</sub>-*b*-NonOx<sub>76</sub>)) in ratios of 0, 20, 40, 60, 80, and 100 wt % P(NonOx<sub>52</sub>-*b*-AmOx<sub>184</sub>). All micelles with cationic polymers exhibited a very good DNA binding efficiency and dissociation ability, while the bio- and hemocompatibility improved with increasing EtOx content. Analytics via confocal laser scanning microscopy and flow cytometry showed an enhanced cellular uptake, transfection ability, and biocompatibility of all prepared micelleplexes compared to AmOx homopolymers. Micelleplexes with 80 or 100 wt % revealed a similar transfection efficiency as PEI, while the cell viability was significantly higher (80 to 90% compared to 60% for PEI).



## ■ INTRODUCTION

Modern gene therapy uses two different types of gene carriers, namely viral and nonviral systems. Because of their high transfection efficiency and approval in clinical trials, virus-based systems are more common in recent gene therapy approaches.<sup>1</sup> Although viruses are predestinated for gene delivery, caused by their evolutionary optimization, there are some disadvantages, which hamper the use of viruses in gene therapy. One major drawback of viral vectors is the occurring immunogenicity, which may cause an activation of inflammatory cells leading to the degeneration of treated tissue. Moreover, toxin production and insertional mutagenesis were observed in some cases. Because of their size, viral vectors are limited by the transgenic capacity; furthermore, the upscaling of these systems is challenging.<sup>2</sup>

Thus, even if the efficiency of nonviral systems is lower compared to viral systems, there are significant advantages, which constitute nonviral systems as relevant alternatives in the area of gene delivery. In general, nonviral vectors show relatively low host immunogenicity; moreover, they allow an almost unlimited transgene size and provide the ability of repeated application.<sup>3</sup> Additionally, compared to viruses, nonviral systems benefit from low-cost production and their ability for an easy upscaling. Most commonly, cationic polymers are used for gene delivery since they are capable of forming polyplexes with the negatively charged phosphate backbone of

nucleic acids. Because of the positive charges of the polymer, the polyplex can interact with the negatively charged cell membrane and is consequently internalized via endocytosis. Subsequently, the complexes need to undergo endosomal escape into the cytoplasm, resulting in the release of the polyplexes.<sup>4</sup> P. Stayton et al. demonstrated that pH-dependent amphiphilic nanocarriers are capable to trigger an enhanced endosomal release by interaction with the endosomal membrane.<sup>5</sup> Thus, changes in the pH value and protein interactions trigger the dissociation of the polyplex, and thus, the genetic material can enter the nucleus to transfect the cells. Poly(ethylene imine) (PEI) is one of the most commonly used materials for gene delivery applications and for a long time it was claimed to be the gold standard for the transfection of genetic material.<sup>6</sup> Its high charge density leads to the formation of physiological stable PEI–DNA polyplexes. In general, the high efficiency of PEI is based on the ability of the amine groups to buffer the pH value over a wide range, causing an efficient endosomal escape (proton sponge effect).<sup>7</sup> Disadvantages of PEI-based systems are their high *in vitro* and *in vivo* toxicity and their resistance against biodegradation, leading to the accumulation of the polymer in the cells or tissue, which

**Received:** October 26, 2017

**Revised:** December 11, 2017

**Published:** December 20, 2017

can elicit further toxicity effects.<sup>8</sup> Furthermore, the cytotoxicity has been shown to be dependent on the molar mass of the polymers<sup>9</sup> but can be improved by the introduction of stealth units, that is, EtOx, into the polymer chain.<sup>10,11</sup> These drawbacks lead to a necessity to search for alternative polymer systems for gene delivery applications, which reveal high transfection efficiencies while expressing a low cytotoxicity. K. Miyata et al. introduced primary and secondary amines into the side chains of poly(aspartamide) to induce pH-sensitive membrane destabilization at an endosomal pH value of 5, resulting in enhanced cytocompatibility at physiological pH values of 7.<sup>12</sup> Another possibility to fulfill this aim was shown to be the introduction of hydrophobic units, such as cholesterol<sup>13</sup> or stearic acid,<sup>14</sup> to the cationic polymer chains. The hydrophobic units could be shown to increase the cellular uptake as well as the transfection efficiency, however, not the cytotoxicity.

The aim of this study was the development of a micellar polymeric gene delivery system with low cytotoxicity combined with enhanced cellular uptake and transfection efficiency by adjusting the ratio of stealth and cationic units. Poly(2-oxazoline)s (P(Ox)s) are a class of polymers that were intensively studied during the past years in the context of several potential applications.<sup>15–17</sup> In the field of nanomedicine, the combination of enhanced biocompatibility and structure variability has been shown to be an essential benefit of this polymer class.<sup>17–19</sup> The synthesis of P(Ox)s by the living cationic ring-opening polymerization (CROP) provides even access to sophisticated polymer architectures such as block copolymers<sup>20</sup> and star-shaped,<sup>21,22</sup> hyperbranched,<sup>23</sup> and cross-linked networks.<sup>24,25</sup> The combination of monomer units bearing side-chains with different hydrophilicities leads to amphiphilic copolymers, which can self-assemble into different nanostructures.<sup>25</sup> Block copolymers of two or more chemically different polymer chains,<sup>26</sup> which potentially phase separate in bulk or selective solvents, provide access to several defined self-assembled structures. Furthermore, cationic P(Ox)s have already shown their potential in gene delivery applications.<sup>27,28</sup>

For these reasons, we synthesized two different amphiphilic block copolymers. The first copolymer consisted of NonOx for the formation of a hydrophobic core and the amino-functionalized AmOx to facilitate polyplex formation with the genetic material. The second copolymer consisted of the same hydrophobic unit; however, EtOx served as the hydrophilic block since it is known for its stealth properties.<sup>29</sup> Finally, mixed nanostructures with different weight ratios of these two block copolymers were prepared and characterized regarding the micelle size, PDI value, pH-responsiveness, CMC, toxicity, polyplex formation, and dissociation as well as their cellular uptake and transfection efficiency.

## MATERIALS AND METHODS

**Materials and Instrumentation.** Triethylamine (TEA, Sigma-Aldrich), butyronitrile (VWR), 2-ethyl-2-oxazoline (EtOx, Sigma-Aldrich), 2-nonyl-2-oxazoline (NonOx, Henkel), and methyl tosylate (MeTos, Sigma-Aldrich) were distilled to dryness over calcium hydride (VWR) under argon atmosphere prior to usage. Ethyl acetate (EtOAc) and acetone, hydrochloric acid, *N,N*-dimethylformamide (DMF), and tetrahydrofuran (THF) were purchased from VWR Chemicals. Acetonitrile was obtained from a solvent purification system (MB-SPS-800 by MBraun) and stored under argon. All other solvents used were obtained from standard suppliers. Ethidium bromide solution (1%, 10 mg mL<sup>-1</sup>) was purchased from Carl Roth (Karlsruhe, Germany). AlamarBlue YOYO-1 iodide and Hoechst

33342 trihydrochloride as well as all other indicated CLSM dyes were obtained from Life Technologies (Thermo Fisher Scientific, Germany). If not stated otherwise, cell culture media and solutions (L-glutamine, antibiotics) were obtained from Biochrom (Berlin, Germany). Plasmid eGFP (pEGFP-N1, 4.7 kb, Clontech, USA) enhanced green fluorescent protein (eGFP) was isolated with the Giga Plasmid Kit provided by Qiagen (Hilden, Germany). Plasmid pCMV-GFP was obtained from PlasmidFactory (Bielefeld, Germany).

The synthesis of 2-(4-((*tert*-butoxycarbonyl)amino)butyl)-2-oxazoline (BocOx) was described previously in our research group.<sup>24</sup>

Cryo transmission electron microscopy (cryoTEM) investigations were conducted with a FEI Tecnai G<sup>2</sup> 20 at 200 kV acceleration voltage. Specimens were vitrified by a Vitrobot Mark V system on Quantifoil grids (R2/2). The blotting time was 1 s with an amount of solution of 8.5 μL. Samples were plunge frozen in liquid ethane and stored under liquid nitrogen until transfer to the Gatan cryo-holder and brought into the microscope. Images were acquired with an Olympus Mega View camera (Olympus Soft Imaging Solutions; 1376 × 1032 pixels) or an Eagle 4 × 4 k CCD camera system.

Proton NMR spectroscopy (<sup>1</sup>H NMR) was performed at room temperature using a Bruker Avance I 300 MHz spectrometer, utilizing either CDCl<sub>3</sub>, CD<sub>3</sub>OD, or D<sub>2</sub>O as solvent. The chemical shifts were given in ppm relative to the signal from the residual nondeuterated solvent.

Size exclusion chromatography (SEC) of the copolymers was performed on an Agilent 1200 series system, equipped with a PSS degasser, G1329A pump, a PSS GRAM guard/30/1000 Å with 10 μm particle size, and a G1362 refractive index (RI) detector. DMAc containing 0.21% LiCl served as eluent. The column oven was set to 40 °C at a flow rate of 1 mL min<sup>-1</sup> and polystyrene (PS, 400–1 000 000 g mol<sup>-1</sup>) served as the calibration.

SEC of the Boc-protected P(EtOx<sub>3</sub>-*b*-BocOx<sub>157</sub>) was performed on a Shimadzu system equipped with a CBM-20A controller, GDU-14A degasser and a LC-10AD VP pump, a PSS SDV guard/linear S column with 5 μm particle size, and a RID-10A RI detector. CHCl<sub>3</sub>-*iso*-propanol (*i*-PrOH)-NEt<sub>3</sub> (94:2:4) served as eluent. The column oven was set to 40 °C using a flow rate of 1 mL min<sup>-1</sup>. PS (400–100 000 g mol<sup>-1</sup>) served as the calibration.

SEC of the P(EtOx<sub>3</sub>-*b*-AmOx<sub>157</sub>) was conducted using a Jasco system equipped with a DG-980–50 degasser and a PU-980 pump, PSS SUPREMA-MAX guard/300 Å column with 10 μm particle size, and a RI-930 RI detector. 0.3% (v/v) TFA containing 0.1 M NaCl served as aqueous eluent. The column oven was set to 30 °C utilizing a flow rate of 1 mL min<sup>-1</sup>. Poly(2-vinylpyridine) (P2VP, 1 300–81 000 g mol<sup>-1</sup>) served as the calibration.

Lyophilization of the nanostructure suspensions was conducted using an Alpha 1–2 LDplus freeze-dryer from Martin Christ Gefrier Trocknungsanlagen GmbH (Germany). Absorbance and fluorescence measurements of the bioassays were performed at RT using a TECAN Infinite M200 PRO.

Confocal laser scanning microscopy (CLSM) was performed with an LSM880 ELYRA PS.1 system (Zeiss, Oberkochen, Germany) applying a 63 × 1.4 NA plan apochromat oil objective.

Batch dynamic light scattering (DLS) was performed on a Zetasizer Nano ZS (Malvern Instruments, Herrenberg, Germany). All measurements were performed in standard polypropylene semi micro cuvettes, Malvern Instruments, Herrenberg, Germany). After an equilibration time of 180 s, 3 × 300 s runs were carried out at 25 °C (λ = 633 nm). Scattered light was detected at an angle of 173°. Each measurement was performed in triplicates (three measurements consisting of three runs each per sample). Apparent hydrodynamic radii, *R<sub>h</sub>*, were calculated according to the Stokes–Einstein eq 1:

$$R_h = \frac{kT}{6\pi\eta D} \quad (1)$$

**Synthesis of P(Ox)s.** All polymerization solutions were prepared within a glovebox under nitrogen atmosphere.

Polymerization reactions of 2-oxazolines were performed under microwave irradiation using an Initiator Sixty single-mode microwave

synthesizer from Biotage, equipped with a noninvasive IR sensor (accuracy: 2%). Microwave vials were heated overnight at 100 °C under vacuum and allowed to cool to room temperature under argon before usage. Polymerizations were performed under temperature control. According to the polymer characteristics, SEC of the polymers was performed on different systems and noted in the respective part. The synthesis of P(Ox)<sub>s</sub> was described previously.<sup>30</sup>

**P(EtOx<sub>3</sub>-*b*-BocOx<sub>157</sub>).** In a microwave vial, MeTos (1.9 mg, 0.01 mmol), EtOx (3.0 mg, 0.03 mmol), and acetonitrile (392.6 mg) were mixed under inert conditions and heated in the microwave to 140 °C for 63.5 min. Subsequently the vial was opened under an inert atmosphere, and BocOx (477.4 mg, 1.97 mmol) was added. The reaction mixture was heated in the microwave at 140 °C for additional 18.0 min. The resulting polymer diluted with chloroform and precipitated in ice-cold diethyl ether. The precipitate was filtered off and redissolved in chloroform. The solvent was evaporated under reduced pressure to obtain the product as a white solid (391 mg, 82%).

**Deprotection of P(EtOx<sub>3</sub>-*b*-BocOx<sub>157</sub>) Yielding P(EtOx<sub>3</sub>-*b*-AmOx<sub>157</sub>).** P(EtOx<sub>3</sub>-*b*-BocOx<sub>157</sub>) (390 mg, 10.2 mmol) was dissolved in 10 mL of MeOH, and 2 mL of concentrated hydrochloric acid was added. The reaction mixture was stirred at room temperature for 24 h. Subsequently, the solvent was evaporated under reduced pressure, and the crude product was redissolved in 10 mL of MeOH and precipitated in ice cold diethyl ether. Then the precipitate was filtered off and redissolved in 100 mL of MeOH. Amberlyst A21 was added and the mixture was stirred slowly (100 rpm) overnight at room temperature. Then the Amberlyst A21 was filtered off and the organic solvent was evaporated under reduced pressure. The polymer was redissolved in 10 mL of deionized water and lyophilized to obtain the product as a white powder (186 mg, 81%).

**P(EtOx<sub>155</sub>-*b*-NonOx<sub>76</sub>).** In a microwave vial, MeTos (24.8 mg, 0.13 mmol), EtOx (1.98 g, 20.0 mmol), and butyronitrile (13.0 g) were mixed under inert conditions and heated in the microwave to 140 °C for 130 min. Subsequently, the vial was opened under an inert atmosphere, a sample of 100 μL was taken, and NonOx (1.58 g, 8.0 mmol) was added. The reaction mixture was heated in the microwave at 140 °C for another 120 min. The resulting polymer was precipitated in ice-cold diethyl ether and centrifuged at 11 000 rpm for 5 min. The supernatant was discarded, and the solid was redissolved in CH<sub>2</sub>Cl<sub>2</sub>. The solvent was evaporated under reduced pressure to obtain the product as a white solid (1.7 g, 86%).

**P(NonOx<sub>52</sub>-*b*-BocOx<sub>184</sub>).** In a microwave vial, MeTos (7.8 mg, 0.04 mmol), NonOx (493 mg, 2.5 mmol), and butyronitrile (6.1 g) were mixed under inert conditions and heated in the microwave to 140 °C for 120 min. Subsequently, the vial was opened under an inert atmosphere, a sample of 100 μL was taken, and BocOx (1.75 g, 7.2 mmol) was added. The reaction mixture was heated in the microwave at 140 °C for another 90 min. The resulting polymer was precipitated in ice-cold diethyl ether, and the solid was resuspended in deionized water and centrifuged at 11 000 rpm for 5 min. The supernatant was discarded, and the solid was suspended in deionized water. The solvent was lyophilized under reduced pressure to obtain the product as a white powder (740 mg, 33%).

**Deprotection of P(NonOx<sub>52</sub>-*b*-BocOx<sub>184</sub>) Yielding P(NonOx<sub>52</sub>-*b*-AmOx<sub>184</sub>).** P(NonOx<sub>52</sub>-*b*-BocOx<sub>184</sub>) (700 mg, 12.8 mmol) was dissolved in 5 mL of TFA and stirred at room temperature overnight. Subsequently, 5 mL of MeOH was added, and the polymer was precipitated in ice-cold diethyl ether. The precipitate was redissolved in MeOH, Amberlyst A21 was added, and the solution was stirred slowly at room temperature for 72 h. Afterward, Amberlyst A21 was filtered off, and the solvent was evaporated under reduced pressure. The polymer was resuspended in deionized water, and the solvent was lyophilized under reduced pressure to obtain the product as a white powder (457 mg, 98%).

**Self-Assembly.** Fifty milligrams of polymer was dissolved in 10 mL of DMAc by vortexing and ultrasonification. Subsequently, 10 mL of ultrapure water was added slowly using a syringe pump (5 mL h<sup>-1</sup>) under continuous stirring (1000 rpm). After that, the resulting solution was transferred to a dialysis tube (cellulose, MWCO 3.5 kDa) and dialyzed against distilled water for 4 days by daily water exchange. Subsequently, it was diluted using a 1.8 wt % aqueous NaCl solution to adjust the salt concentration to 0.9 wt % (pH = 6). The resulting nanostructures were filtered using a 0.2 μm syringe filter and characterized by DLS measurements.

The concentration of the polymer in the resulting solution was determined gravimetrically (*n* = 3) after lyophilization of the samples. For this reason, also a 0.9 wt % aq. NaCl solution was lyophilized (*n* = 3). The mean of the mass of the NaCl samples was subtracted from each polymer containing sample to obtain the absolute polymer mass.

The average molar mass of the micelles was calculated by using eq 2:

$$M = \frac{M_n \times Wt \% (P(\text{NonOx}_{52} - b - \text{AmOx}_{184})) + M_n \times Wt \% (P(\text{EtOx}_{155} - b - \text{NonOx}_{76}))}{100} \quad (2)$$

**pH Responsive Behavior.** The pH-responsiveness of the nanostructures was determined by mixing 1 mL of a 1.0 mg mL<sup>-1</sup> solution with 1 mL of the following buffers (Table S1).

The solutions were incubated at room temperature overnight at 200 rpm (BioShake iQ, Quantifoil Instruments GmbH, Jena, Germany). Afterward the pH value was checked and the Z-average and PDI were determined by DLS measurements.

**Determination of Critical Micelle Concentration (CMC).** The determination of the CMC via pyrene method was described previously.<sup>31</sup> Fluorescence was recorded with a Jasco FP 6500. A serial dilution of the nanostructure suspension in 0.9 wt % aq. NaCl was prepared.

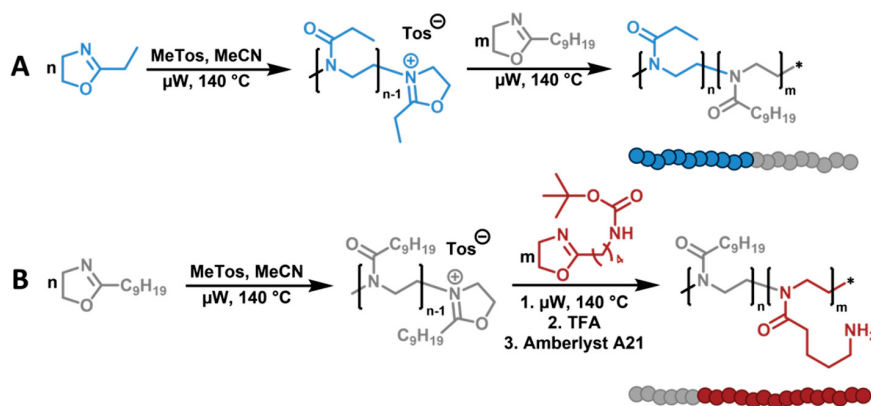
A saturated pyrene solution in 0.9 wt % aq. NaCl was prepared as follows. Pyrene was dissolved in acetone (1 mg mL<sup>-1</sup>) and added dropwise to a solution of 0.9 wt % in ultrapure water until a slight precipitation (visible turbidity) occurred. The solution was stirred for 48 h at room temperature (1000 rpm) to evaporate the acetone. Then the solution was filtered using a pleated filter to remove any precipitate. Subsequently, the same volume of the saturated solution of pyrene in 0.9 wt % aq. NaCl was added to each dilution of the micelles to obtain a total volume of 2 mL. The mixtures were incubated overnight at room temperature at 200 rpm (BioShake iQ, Quantifoil Instruments GmbH, Jena, Germany). Excitation spectra were collected

at λ<sub>Em</sub> = 390 nm and λ<sub>Ex</sub> = 300–380 nm. The pyrene stock solution served as the calibration sample and was subtracted from all spectra prior to calculations to remove any fluorescence artifacts. For calculation of the CMC, the resulting spectra were used. The fluorescence intensity at λ<sub>Em</sub> = 390.0 nm while exciting at λ<sub>Ex2</sub> = 338.0 nm was divided by the fluorescence intensity at λ<sub>Em</sub> = 390.0 nm while exciting at λ<sub>Ex2</sub> = 332.5 nm and plotted against the log of the polymer concentration. A nonlinear Boltzmann fitting and a subsequent linear fitting were conducted using OriginPro 2015G. Hereby, the Boltzmann fitting was used to visualize visible areas, while the linear fit was utilized to obtain the cross-point of two different linear areas, which corresponds to the CMC of the nanostructures.

**Cell Culture.** HEK-293 cells (CRL-1573) were cultured in DMEM medium with L-glutamine (Biochrom, Berlin, Germany) supplemented with 1 g L<sup>-1</sup> glucose, 10% fetal calf serum (FCS, v/v), 100 μg mL<sup>-1</sup> streptomycin and 100 IU mL<sup>-1</sup> penicillin at 37 °C in a humidified 5% CO<sub>2</sub> atmosphere.

**Cytotoxicity.** The cytotoxicity was tested with L929 cells, as this cell line is recommended by ISO10993-5. In detail, cells were seeded at 10<sup>4</sup> cells per well in a 96-well plate and incubated for 24 h. No cells were seeded in the outer wells. After exchanging the media with fresh one and 30 min incubation, polymers at the indicated end concentrations were added, and the cells were incubated at 37 °C



Scheme 1. Schematic Representation of Block Copolymerization of 2-Oxazolines via CROP<sup>a</sup>

<sup>a</sup>(A) P(EtOx<sub>155</sub>-*b*-NonOx<sub>72</sub>) was synthesized using the sequential monomer addition of EtOx and NonOx. (B) P(NonOx<sub>52</sub>-*b*-AmOx<sub>184</sub>) was synthesized via the sequential monomer addition of NonOx and BocOx. The resulting block copolymers were deprotected using TFA and neutralized with Amberlyst A21. Blue: EtOx. Grey: NonOx. Red: BocOx/AmOx.

for additional 24 h. Subsequently, the medium was replaced by fresh media and AlamarBlue (Life Technologies, Darmstadt, Germany) as recommended by the supplier. After incubation for 4 h, the fluorescence was measured at  $\lambda_{\text{Ex}} = 570$  nm,  $\lambda_{\text{Em}} = 610$  nm, with untreated cells on the same well plate serving as controls. The experiments were performed independently three times on three different well-plates.

**Hemolysis Assay and Erythrocyte Aggregation.** All animal husbandry is performed in compliance with the relevant European and German laws, institutional guidelines, and to state the institutional animal committee. The sheep blood was taken for general veterinary management of the animal health.

To assess the hemolytic activity of the polymer solutions, blood from sheep, collected in heparinized-tubes (Institut für Versuchstierkunde und Tierschutz/Laboratory of Animal Science and Animal Welfare, Friedrich Schiller University Jena), was centrifuged at  $4500 \times g$  for 5 min, and the pellet was washed three times with cold  $1.5 \text{ mmol L}^{-1}$  phosphate buffered saline (PBS, pH = 7.4). After dilution with PBS in a ratio of 1:7, aliquots of erythrocyte suspension were mixed 1:1 with the polymer solution and incubated in a water bath at  $37^\circ\text{C}$  for 60 min. After centrifugation at  $2400 \times g$  for 5 min, the hemoglobin release into the supernatant was determined spectrophotometrically using a microplate reader at  $\lambda_{\text{Ex}} = 544$  nm wavelength. Complete hemolysis (100%) was achieved using 1% Triton X-100 serving as positive control. Thereby, PBS served as negative control (0%). A value less than 2% hemolysis rate was taken as nonhemolytic. Experiments were run in triplicates and were performed with three different blood donors. The hemolytic activity of the polycations was calculated by eq 3:

$$\% \text{ Hemolysis} = 100 \times \frac{(A_{\text{sample}} - A_{\text{negative control}})}{A_{\text{positive control}}} \quad (3)$$

For the examination of the erythrocyte aggregation, erythrocytes were isolated as described above. An erythrocytes suspension was mixed with the same volume of polymeric micelle solution in a clear flat bottomed 96-well plate. The cells were incubated at  $37^\circ\text{C}$  for 2 h, and the absorbance was measured at  $\lambda_{\text{Ex}} = 645$  nm in a microplate reader. *b*-PEI (25 kDa,  $50 \mu\text{g mL}^{-1}$ ) was used as positive control and PBS-treated cells served as the negative control. Absorbance values of the test solutions lower than the negative control were regarded as aggregation. Experiments are the result of triplicates and were performed with three different donor blood batches.

**Polyplex Formation.** Polyplexes of pDNA and polymeric micelles were prepared by mixing stock solutions of  $1.5 \mu\text{L}$  pDNA ( $1 \text{ mg mL}^{-1}$ ) and different amounts of polymeric micelle solutions ( $1 \text{ mg mL}^{-1}$ ) to obtain various N\*/P ratios (amines of polymer to phosphate

of pDNA)  $150 \text{ mM aq. NaCl}$  solution.  $150 \text{ mM aq. NaCl}$  was used to equalize the volumina of the different solutions. The solutions were vortexed for 10 s at maximal speed ( $2700 \text{ min}^{-1}$ ) and incubated at room temperature for 20 min to ensure complex formation.

**Ethidium Bromide Quenching Assay (EBA).** Briefly, a master mix containing  $69 \mu\text{g mL}^{-1}$  pDNA and  $4.6 \mu\text{g mL}^{-1}$  ethidium bromide was prepared in  $150 \text{ mM NaCl}$  and incubated in the dark for 10 min at room temperature. Subsequently, polyplexes were prepared in black 96-well plates (Nunc Thermo Fisher) by adding different amounts of polymeric micelles (various N\*/P ratios) to  $20 \mu\text{L}$  of master mix per well. The differences in the final volume of polymer were equalized by filling up with  $150 \text{ mM NaCl}$  to  $230 \mu\text{L}$  per well (for exact amounts, see also Table S2; for final polymer concentrations, see Table S3).

The samples were incubated in the dark at room temperature for 5 min. The fluorescence of the samples was measured at  $\lambda_{\text{Ex}} = 525$  nm and  $\lambda_{\text{Em}} = 605$  nm using a microplate reader. A sample containing the same amount of pDNA and ethidium bromide diluted using  $150 \text{ mM NaCl}$  was used as a reference for 100% fluorescence to calculate the percentage of dye displaced upon polyplex formation (eq 4):

$$\text{RFU} [\%] = \frac{F_{\text{sample}}}{F_{\text{pDNA}}} \times 100 \quad (4)$$

Here, RFU is the relative fluorescence, and  $F_{\text{sample}}$  and  $F_{\text{pDNA}}$  are the fluorescence intensities of a given sample and the ethidium bromide intercalated into pDNA alone.

**Heparin Dissociation Assay.** To investigate the release of pDNA from polyplexes, the heparin dissociation assay was performed. Polyplexes with an N\*/P ratio of 50 were prepared as described above in a total volume of  $115 \mu\text{L}$  of  $150 \text{ mM NaCl}$  containing ethidium bromide ( $0.4 \mu\text{g mL}^{-1}$ ) (for exact amounts, see also Table S2). After incubation in the dark at room temperature for 10 min, the master mix was transferred into  $1.5 \text{ mL}$  reaction tubes (one per polymer) and polymers were added. Subsequently, the polyplexes were transferred into a black 96-well plate, and heparin of indicated concentrations was added. The solution was mixed and incubated for further 15 min at  $37^\circ\text{C}$  in the dark.

**Flow Cytometry.** For transfection and uptake studies, HEK-293 cells were used. In detail,  $5 \times 10^4$  cells were seeded in each well of a 24-well plate and cultured for 24 h. One hour prior to the addition of the polyplexes, the medium was changed to  $0.5 \text{ mL}$  of fresh culture media. For kinetic studies, pDNA was labeled with YOYO-1 iodide (YOYO-1) prior to the polyplex preparation. For labeling of  $1 \mu\text{g}$  of pDNA,  $0.026 \mu\text{L}$  of  $1 \text{ M YOYO-1}$  solution was mixed with pDNA and incubated for 20 min at  $4^\circ\text{C}$  protected from light. The polyplexes were prepared as described above, and at least  $50 \mu\text{L}$  was added to the cells (dependent on the N\*/P ratio of the polymers, for the exact

Table 1. Key Properties of Synthesized Polymers

ID	SEC <sup>a</sup>			<sup>1</sup> H NMR <sup>b</sup>					
	<i>M<sub>n</sub></i> [kDa]	<i>M<sub>w</sub></i> [kDa]	<i>Đ</i>	DP hydrophilic block	DP NonOx block	mol % hydrophilic block	mol % NonOx block	wt % hydrophilic block	wt % NonOx block
P(EtOx) <sub>155</sub>	22.6 7.6 <sup>d</sup>	25.0 9.4 <sup>d</sup>	1.11 1.24 <sup>d</sup>	155	n.a. <sup>f</sup>	100	n.a.	100	n.a.
P(EtOx <sub>155</sub> - <i>b</i> -NonOx <sub>76</sub> )	38.3 17.2 <sup>d</sup>	43.6 18.4 <sup>d</sup>	1.14 1.07 <sup>d</sup>	155	76	67	33	45	55
P(NonOx) <sub>52</sub>	12.4 9.0 <sup>d</sup>	13.0 9.7 <sup>d</sup>	1.04 1.08 <sup>d</sup>	n.a.	52	n.a.	100	n.a.	100
P(NonOx <sub>52</sub> - <i>b</i> -BocOx <sub>184</sub> )	32.2 22.1 <sup>d</sup>	38.3 22.9 <sup>d</sup>	1.19 1.29 <sup>d</sup>	184	52	78	22	81	19
P(NonOx <sub>52</sub> - <i>b</i> -AmOx <sub>184</sub> )	24.3	30.5	1.26	184 <sup>c</sup>	52 <sup>c</sup>	78 <sup>c</sup>	22 <sup>c</sup>	72 <sup>c</sup>	28 <sup>c</sup>
P(EtOx <sub>3</sub> - <i>b</i> -BocOx <sub>157</sub> )	15.3 <sup>d</sup>	16.8 <sup>d</sup>	1.10 <sup>d</sup>	160	0	100	0	100	0
P(EtOx <sub>3</sub> - <i>b</i> -AmOx <sub>157</sub> )	13.5 <sup>e</sup>	21.0 <sup>e</sup>	1.56 <sup>e</sup>	160 <sup>c</sup>	0 <sup>c</sup>	100 <sup>c</sup>	0 <sup>c</sup>	100 <sup>c</sup>	0 <sup>c</sup>

<sup>a</sup>SEC (eluent: DMAc, 0.21% LiCl; PS-standard). <sup>b</sup><sup>1</sup>H NMR (300 MHz). <sup>c</sup>Calculated from Boc-protected precursor polymer. <sup>d</sup>SEC (eluent: CHCl<sub>3</sub>-*i*-PrOH-NEt<sub>3</sub>, 94:2:4; PS-standard). <sup>e</sup>SEC (eluent: 0.1 M NaCl(aq) + 0.3% TFA; P2VP-standard). <sup>f</sup>n.a., not available.

amounts see also Table S4). The amount of pDNA added to the cells was kept constant (0.75 μg pDNA). The plates were incubated for the indicated time point at 37 °C, 5% CO<sub>2</sub>. Afterward, the cells were harvested by trypsinization and were resuspended in PBS supplemented with 1% FCS. To determine the transfection efficiency or polyplex uptake of the polyplexes, 10 000 cells were measured by flow cytometry using a Cytomics FC 500 (Beckman Coulter). The amount of viable cells showing YOYO-1 or eGFP signals were gated and the mean fluorescence intensity (MFI) of all viable cells were compared. To quench the outer fluorescence of YOYO-1 labeled polyplexes, 10% trypan blue was added prior to the measurement. Dead cells were identified via shift in the side and forward scatter of cells.<sup>32</sup> The experiments were performed at least three times.

**Confocal Microscopy.** For CLSM studies, 5 × 10<sup>4</sup> cells were seeded on glass-bottomed dishes (CellView cell culture dishes with four compartments, Greiner bio-one) and cultivated for 24 h. One hour prior to the polymer addition, the medium was changed to 0.5 mL of fresh growth media. The polyplexes were formed using YOYO-labeled pDNA as described above, added to the cells, and incubated for additional 4 h. Subsequently, medium was replaced by fresh culture medium supplemented with Hoechst 33342 for nucleus staining, LysoTracker Red DND-99 (all from Thermo Fisher Scientific) for lysosome staining respecting the instructions given by the Supplier. Prior to imaging, 10% trypan blue was added to quench the outer fluorescence of YOYO-1 labeled pDNA.

Live-cell imaging was performed on an LSM880, Elyra PS.1 system (Zeiss, Oberkochen, Germany). Three color channels were recorded: blue (nucleus, Hoechst 33342, λ<sub>Ex</sub> = 405 nm), green (pDNA, YOYO-1 Iodide, λ<sub>Ex</sub> = 488 nm), and red (lysosome, LysoTracker Red DND-99, λ<sub>Ex</sub> = 561 nm). To avoid possible cellular motions in the time frame of the experiment, a quick measurement was warranted by the simultaneous acquisition of all three color channels.

## RESULTS AND DISCUSSION

**Polymer Synthesis.** The aim of this study was to obtain mixed polymeric micelles, with a cationic and a stealth polymer within the shell for efficient cellular uptake, transfection, and reduced cyto- and hemotoxicity. For this purpose, two different block copolymers were synthesized via the sequential monomer addition method (Scheme 1). By using this preparation method, the order of the block sequence is of significance importance for the dispersity of the resulting block copolymers. Utilizing the less reactive monomer first might lead to slower initiation speeds during the polymerization of the second block, and, consequently a loss of the living/controlled character of

the polymerization. For this reason, the nonionic copolymer was polymerized with EtOx representing the first and NonOx as the second block (Scheme 1A). For a successful preparation of the cationic block copolymer, on the other hand, it was necessary to use NonOx as the first block since the polymerization of Boc-protected primary amine functionalized 2-oxazolines with common initiators leads to side-reactions during polymerization.<sup>33</sup>

NonOx served as the hydrophobic block in both copolymers, while the hydrophilic block either contained AmOx, to obtain good DNA binding capabilities, or EtOx to enhance the biocompatibility of the micelles due to its stealth properties. The polymers were analyzed using <sup>1</sup>H NMR and SEC measurements (Table 1, Figures S1–S5). In both polymers, the degree of polymerization (DP) of the NonOx block was kept similar, resulting in different weight ratios of the hydrophobic and the hydrophilic blocks, namely 55% to 45% in case of P(EtOx<sub>155</sub>-*b*-NonOx<sub>76</sub>) and 28% to 72% in case of P(NonOx<sub>52</sub>-*b*-AmOx<sub>184</sub>), respectively. The DP of the AmOx block was adjusted higher than the EtOx block to facilitate the endosomal release of the micelle–DNA complexes (micelle-plexes) and, consequently, of the genetic material by stretching of the cationic blocks within the endolysosome (fusion of an endosome and a lysosome) caused by a decrease of the pH value from 7.4 to 5. Preliminary polymerizations in acetonitrile (data not shown) lead to the precipitation of NonOx containing polymers. For this reason, butyronitrile was chosen as a suitable solvent for block copolymerization, even though the obtained dispersity of polymers is in general increased compared to polymers synthesized in acetonitrile. Nevertheless, both block copolymers also showed a comparable total DP as well as a narrow dispersity (*Đ* < 1.2) regarding SEC measurements in DMAc (Figure S4). In addition to that, an entirely hydrophilic polymer, mainly consisting of AmOx (P(EtOx<sub>3</sub>-*b*-AmOx<sub>157</sub>)), was synthesized using an oligo(EtOx) initiator and characterized for comparison. Since the controllability of the polymer dispersity was determined to be enhanced by using acetonitrile as the solvent for polymerization compared to butyronitrile, this polymer was prepared in acetonitrile. Because of its high AmOx content, it is entitled as AmOx homopolymer in the following discussion.

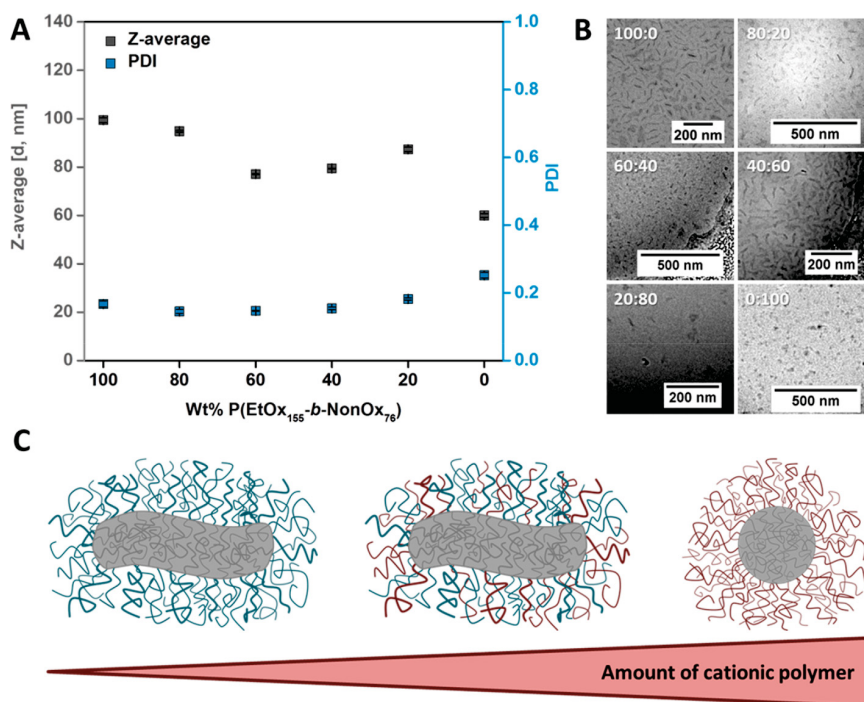


**Figure 1.** (A) Z-average and PDI values of the prepared nanostructures in 0.9 wt % aq. NaCl determined by DLS. (B) Zoom-in cryoTEM images of the prepared nanostructures in 0.9 wt % aq. NaCl. Ratios describe the mass ratios of P(EtOx<sub>155</sub>-b-NonOx<sub>76</sub>) to P(NonOx<sub>52</sub>-b-AmOx<sub>184</sub>) being used during nanostructure preparation. Full pictures can be found in the [Supporting Information](#). (C) Schematic representation of the obtained shapes of the nanostructures dependent on the used block copolymers in different ratios. Blue represents EtOx, gray represents NonOx, and red represents the cationic AmOx block.

**Self-Assembly.** For self-assembly, the polymers were mixed in different weight ratios and dissolved in DMAc serving as the nonselective solvent. Subsequently, an equal amount of ultrapure water serving as the selective solvent was added very slowly ( $1 \text{ mL h}^{-1}$ ) to induce micelle formation. Subsequently, the solution was dialyzed against deionized water to allow a slow increase of the total water content while the organic solvent diffuses out. The stability of the nanostructures in physiological media, for example, NaCl solution, represents an important criterion for further *in vivo* applications. For this reason, the nanostructures were mixed with aq. NaCl to obtain a total NaCl amount of 0.9 wt % in solution. All micelles were characterized regarding their size and PDI value by DLS measurements (Figure 1A and S6, Tables S5 and S6). All nanostructures containing P(EtOx<sub>155</sub>-b-NonOx<sub>76</sub>) formed nanostructures with an average diameter of about 80 to 100 nm, while the self-assembly of P(NonOx<sub>52</sub>-b-AmOx<sub>184</sub>) resulted in significantly smaller structures with a diameter of 60 nm. Furthermore, all micelles with P(EtOx<sub>155</sub>-b-NonOx<sub>76</sub>) exhibited a PDI below 0.2 while micelles, which consist only of P(NonOx<sub>52</sub>-b-AmOx<sub>184</sub>), showed a PDI of 0.25.

The size differences of the self-assembled micelles of either P(EtOx<sub>155</sub>-b-NonOx<sub>76</sub>) or P(NonOx<sub>52</sub>-b-AmOx<sub>184</sub>) are distinct and all measured DLS curves were monomodal in terms of intensity, volume, and number PSD (Figures 1A and S6, Table S2).

After size determination via DLS, cryoTEM measurements were used to obtain further information about the shape and uniformity of the nanostructures (Figure 1B, Figure S8). Micelles consisting of only of P(EtOx<sub>155</sub>-b-NonOx<sub>76</sub>) formed rod-like structures, while those prepared from pure

P(NonOx<sub>52</sub>-b-AmOx<sub>184</sub>) were predominantly spherical. Next to the rod-like structures formed exclusively by P(EtOx<sub>155</sub>-b-NonOx<sub>76</sub>) also sheet-like structures were observable. Darker rods are presumably sheets with a parallel orientation with respect to the electron beam. More interestingly, by mixing the two polymers P(EtOx<sub>155</sub>-b-NonOx<sub>76</sub>) and P(NonOx<sub>52</sub>-b-AmOx<sub>184</sub>) using ratios of 20, 40, 60, or even 80% of P(NonOx<sub>52</sub>-b-AmOx<sub>184</sub>), the micelles were still rod-like with respect to the cryoTEM measurements. Furthermore, in cryoTEM, all samples feature the same mixture of similar structures that indicates the formation of mixed micelles rather than the formation of two species consisting of the two polymer components. Moreover, already the 100:0 sample featured the coexistence of rod-like structures and sheet-like aggregates. Recently, S. Jaksch et al. reported on the formation of worm-like micelles using triblock (ABA) copolymers with NonOx as the hydrophobic block (B) and MeOx as the hydrophilic blocks (A).<sup>34</sup> Hereby, it was also possible to observe changes in the nanostructure by the encapsulation of hydrophobic drugs such as paclitaxel.

After characterization of the micelles via DLS and cryoTEM, the critical micelle concentration (CMC) in physiological sodium chloride solution was determined by the pyrene method. After incubation overnight, excitation measurements at  $\lambda_{\text{Em}} = 390.0 \text{ nm}$  were conducted. The peak intensities at  $\lambda_{\text{Ex1}} = 332.5 \text{ nm}$  and  $\lambda_{\text{Ex2}} = 338.0 \text{ nm}$  were compared to calculate the CMC (Table 2, Figure S9). The nanostructures consisting of 100, 80, and 60 wt % P(EtOx<sub>155</sub>-b-NonOx<sub>76</sub>) exhibited a CMC of around  $2 \times 10^{-7} \text{ M}$ , those with 40, 20, and 0 wt % P(EtOx<sub>155</sub>-b-NonOx<sub>76</sub>) showed a CMC of about  $1 \times 10^{-6} \text{ M}$ . These values are expected since nanostructures from P(MeOx<sub>n</sub>-

**Table 2.** CMC of Nanostructures in 0.9 wt % aq. NaCl by the Pyrene Method<sup>a</sup>

wt % P(EtOx <sub>155</sub> - <i>b</i> -NonOx <sub>76</sub> )	wt % P(NonOx <sub>52</sub> - <i>b</i> -AmOx <sub>184</sub> )	<i>M</i> <sup>b</sup> [kg mol <sup>-1</sup> ]	CMC [μg mL <sup>-1</sup> ]	CMC [mol L <sup>-1</sup> ]
100	0	30.3	8.3	2.7 × 10 <sup>-7</sup>
80	20	31.5	7.3	2.3 × 10 <sup>-7</sup>
60	40	32.7	6.8	2.2 × 10 <sup>-7</sup>
40	60	34.0	36.6	1.1 × 10 <sup>-6</sup>
20	80	35.2	45.2	1.3 × 10 <sup>-6</sup>
0	100	36.4	35.5	9.8 × 10 <sup>-7</sup>

<sup>a</sup>For calculation of the CMC, the fluorescence intensity at  $\lambda_{Em} = 390.0$  nm while exciting at  $\lambda_{Ex2} = 338.0$  nm was divided by the fluorescence intensity at  $\lambda_{Em} = 390.0$  nm while exciting at  $\lambda_{Ex2} = 332.5$  nm and is plotted against the log of the polymer concentration. <sup>b</sup>Molar mass was calculated by using eq 2 (see Figure S8 for original plots).

*b*-NonOx<sub>m</sub>) are reported to have a CMC between 10<sup>-6</sup> and 10<sup>-5</sup> M.<sup>35–37</sup>

**pH Responsiveness.** The transport of the genetic material is presumably realized by endosomal pathways. Hereby, the decrease in the pH values inside the endolysosomes leads to an endosomal burst and the subsequent release of the polyplex. Cationic charges are known to force this membrane disruption.<sup>38</sup> This side effect should be reduced outside the cell but be active inside the endolysosomes. Consequently, a pH-dependent shielding of the cationic charges is a favorable

polymer design strategy.<sup>39</sup> By the preparation of mixed micelles, we aim to obtain a system that is composed of the pH dependent AmOx shell that expands upon reduction of the surrounding pH value, mixed with EtOx units, which should provide stealth properties and do not show pH-responsiveness (Figure 2A).

To prove our assumption, we diluted the nanostructures in aqueous buffers of different pH values (pH = 4.10, 5.04, 6.17, 7.04, 7.58, 8.00, Table S1) and determined the changes in Z-average and PDI value by DLS measurements (Figure S9). Control measurements, diluting the nanostructures with an equal volume of 0.9 wt % NaCl did not reveal any significant changes regarding size or PDI (Table S7). Furthermore, the PDI values of the nanostructures at different pH values remained constant, verifying the stability of the nanostructures. Furthermore, with regard cryoTEM measurements, no morphological changes could be observed by increasing the pH value to 8 (Figure S11). Figure 2B and C show a dependence of the pH responsiveness on the amount of P(NonOx<sub>52</sub>-*b*-AmOx<sub>184</sub>). While nanostructures with 100 wt % P(EtOx<sub>155</sub>-*b*-NonOx<sub>76</sub>) maintained a similar size at any tested pH value, nanostructures of 100 wt % P(NonOx<sub>52</sub>-*b*-AmOx<sub>184</sub>) increased in size up to 130% when changing the pH value from 7 to 5. This increased size at acidic conditions is related to an increased charge density on the AmOx block, which causes the stretching of the polymer chains in the shell. The increased charge density might help to force an enhanced endosomal

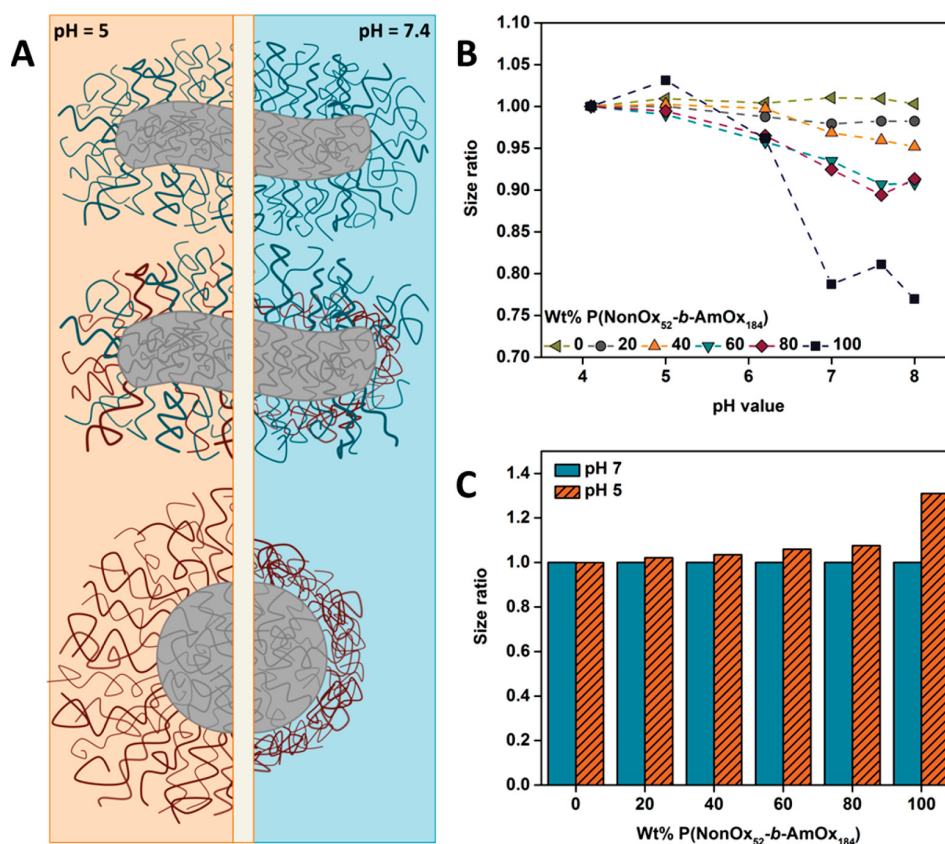


**Figure 2.** (A) Schematic representation of the changes in size of the mixed micelles induced by changes in the pH value. Gray represents NonOx, blue represents EtOx, and red represents the cationic AmOx block. (B) Size ratios of the nanostructure dependency on the pH value (calculated by division of the Z-average at distinct pH values by the Z-average at a pH value of 4). (C) Size ratios of the nanostructures at pH values of 5 and 7 (calculated by division of the Z-average at distinct pH values by the Z-average at a pH value of 7). For values, see Figure S10.

release, one major bottleneck during the transfection process. By reducing the content of the AmOx polymer, the change in size with decreasing pH value becomes less pronounced, which correlates well with the assumption of mixed micelles, as only the responsive AmOx in the shell will react on the change in pH value and become more stretched at low pH values, but not the EtOx polymer. For this reason, the measurability of the changes in size of the mixed nanostructures might be difficult since the hydrodynamic radius is influenced by both blocks in the shell, EtOx or AmOx. This might explain the rather low changes of nanostructures containing 60 or 80% AmOx. Additionally, all intensity weighted size distributions revealed a monomodal distribution, further proving the assumption of mixed micelles instead of two species.

**Cytotoxicity, Hemolysis, and Erythrocyte Aggregation.** Enhanced cyto- and hemocompatibility of polymeric gene carriers represents an important criterion for *in vivo* investigations. Unfortunately, PEI, the gold standard in terms of transfection abilities, is very cytotoxic and leads to high hemoglobin release and erythrocyte aggregation,<sup>40,41</sup> which might cause severe side-effects.

For this reason, subsequently to the characterization of the physical properties of the prepared micelles, they were also investigated regarding their cytotoxicity, hemolysis, and erythrocyte aggregation (Figure 3). The cytotoxicity measurements (AlamarBlue assay) demonstrated that the micelles are not toxic up to a concentration of  $50 \mu\text{g mL}^{-1}$  (rel. cell viability  $\geq 80\%$ ). As expected, an increase of the cytotoxicity with the AmOx content in the micelle shell was observed (Figure 3A), that is, all micelles with EtOx in the shell, are nontoxic at  $100 \mu\text{g mL}^{-1}$ . These data support our assumption that the toxicity can be reduced by introduction of a neutral, biocompatible polymer such as EtOx into the micellar shell. These results comply with previous studies conducted on copolymers of P(EtOx) and PEI.<sup>10,11</sup> By preparing statistically distributed copolymers, the cytotoxicity could be decreased significantly at concentrations of  $5 \text{ mg mL}^{-1}$  when reducing the PEI content from 100 to 59% (24 h incubation).<sup>11</sup> Block copolymers of P(EtOx) and PEI also reduced the cytotoxicity;<sup>10</sup> however, the cell viability was lower (40 to 60% in HeLa cells) compared to the statistic copolymers (80% in 3T3 fibroblasts) with a similar PEI amount ( $\sim 60\%$ ). These differences might be caused by the charge density within the polymers. Presumably, the shielding of the cytotoxic cationic charges is enhanced by a random distribution of the stealth units compared to the block structures, when assuming the polymers to coil in aqueous solution. Within the current study, the cationic blocks consisted of more repeating units than the stealth block to enhance the endosomal release of the polyplexes caused by a possible stretching of the cationic arms. This circumstance might also explain the lack in terms of cytocompatibility and could be further evaluated by preparing nanostructures with longer stealth blocks. However, this was not part of the current study. Interestingly, the P(AmOx) homopolymers revealed a reduced viability to approximately 50% even at concentrations of  $50 \mu\text{g mL}^{-1}$ , whereas our group previously showed that *l*-PEI<sub>575</sub> reveals a similar effect on different cell lines after treatment with a  $3.5 \mu\text{g mL}^{-1}$  solution.<sup>41</sup> B. D. Monnery et al. recently published results on the dependency of the cytotoxicity of polycations on their molar mass.<sup>9</sup> Even though both polymers have a similar molar mass ( $M_n \approx 24 \text{ kDa}$ ), their cytotoxicity differs significantly. Consequently, we attribute these differences to the amount of cationic charges, respectively the charge

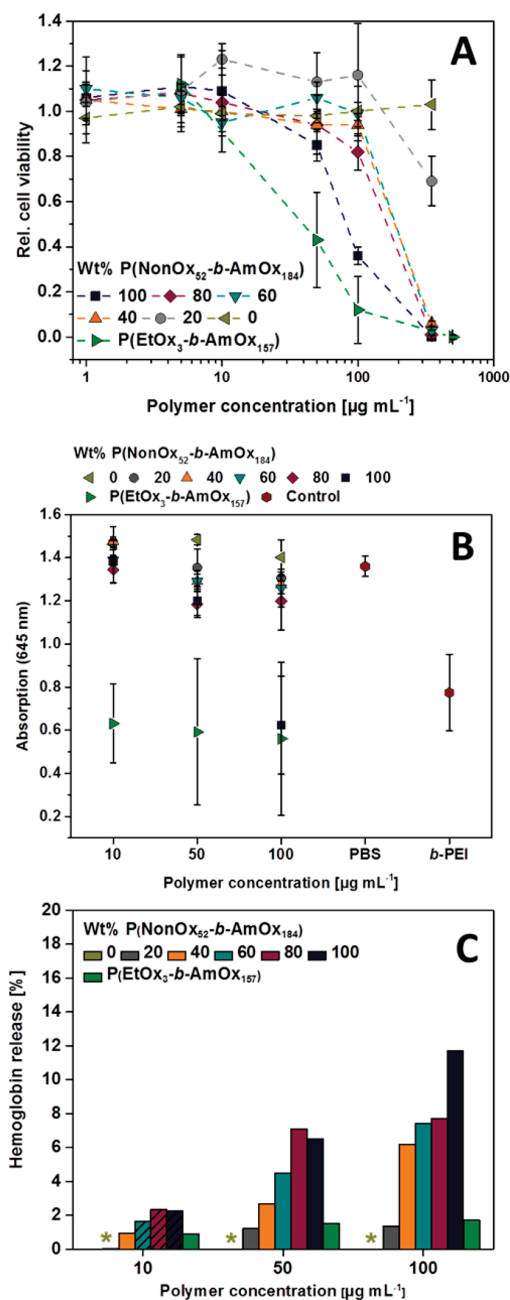


**Figure 3.** Concentration dependent cyto- and hemocompatibility of nanostructures. (A) Cytotoxicity assay of indicated polymers using AlamarBlue. Nontreated cells served as 100% relative viability. L929 cells were treated 24 h with the indicated concentrations of the polymer micelle solutions. Values represent the mean  $\pm$  SD ( $n = 3$ ). (B) Concentration dependent erythrocyte aggregation of nanostructures. *b*-PEI represents the positive control (p.c.) and PBS the negative control (n.c.). Values represent the mean  $\pm$  SD ( $n = 3$ ). For microscopy images, see Figure S12. (C) Hemolysis assay of erythrocytes after incubation with nanostructures at indicated concentrations. A value of less than 2% hemoglobin release is classified as nonhemolytic and more than 5% as hemolytic. Stars depict the position of nonhemolytic samples. Triton X was used as the p.c. (100%) and PBS served as the n.c. and was subtracted from the values. Values represent the mean ( $n = 3$ ). Striped columns are below the CMC of the nanostructures.

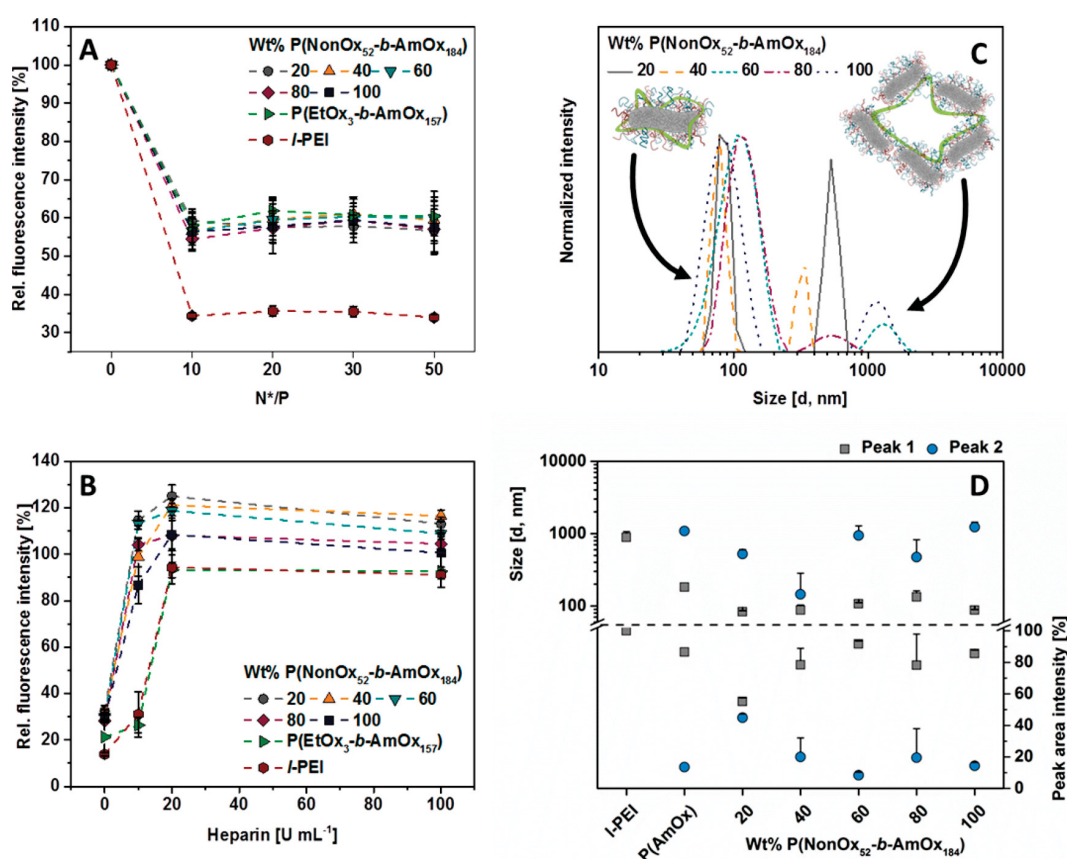


**Figure 4.** Micelleplex formation with pDNA and stability test using the polymer P(EtOx<sub>3</sub>-b-AmOx<sub>157</sub>) and micelles with 20 to 100 wt % P(NonOx<sub>52</sub>-b-AmOx<sub>184</sub>). (A) EBA of all polymers at the indicated N\*/P (amino groups in the polymers per phosphate groups in the DNA) ratios utilizing a pCMV-GFP plasmid for polyplex formation in HBG buffer. Values represent the mean  $\pm$  SD ( $n = 3$ ). (B) Heparin dissociation assay of polyplexes formed at N\*/P 50 using heparin as polyanion. Values represent the mean  $\pm$  SD ( $n = 3$ ). (C, D) DLS determination of size (diameter) and size distribution of polyplexes (N\*/P = 50) formed with pCMV-GFP plasmid and homopolymers as well as polyplex forming micelles. Values represent the mean and SD ( $n = 3$ ). (C) One representative DLS curve and possible micelleplex structures are shown. (D) As two populations were found, the intensity as well as the size of the two populations was plotted.

density within the different polymers, which is 3.5-times higher in the utilized l-PEI.

In addition to the AlamarBlue cytotoxicity assay, the hemolysis of the nanostructures at varying polymer concentrations was measured (Figure 3C). Using these measurements, a hemoglobin release below 2% is considered to be not hemolytic, while 2 to 5% is slightly hemolytic and a rate above 5% is hemolytic. At low polymer concentration of 10  $\mu\text{g mL}^{-1}$ , none of the tested nanostructures was hemolytic; however, it should be mentioned that this concentration was already below the CMC of nanostructures with 60, 80, and 100 wt % P(NonOx<sub>52</sub>-b-AmOx<sub>184</sub>), which were hemolytic at concentrations of 50  $\mu\text{g mL}^{-1}$ . In contrast to that, micelles with 0 or 20 wt % P(NonOx<sub>52</sub>-b-AmOx<sub>184</sub>) as well as the homopolymers were not hemolytic even at polymer concentrations of 100  $\mu\text{g mL}^{-1}$ , while those with 40 wt % P(NonOx<sub>52</sub>-b-AmOx<sub>184</sub>) were not hemolytic up to 50  $\mu\text{g mL}^{-1}$ . l-PEI was only slightly hemolytic at concentrations of 100  $\mu\text{g mL}^{-1}$ .<sup>40</sup> By comparing these results, it is obvious that the hemolytic activity of the polymeric micelles depends on the amount of AmOx within the shell and that the micellar structure enhances the membrane disruption. It should be mentioned that the hemolytic activity was tested in PBS as buffer system without any proteins to further protect the cells, meaning that the critical concen-

trations might be different in *in vivo* or even *in vitro* situations. However, the erythrocyte aggregation represents also a method to measure the membrane interactions of polymers (Figure 3B).<sup>42,43</sup> Again, the aggregation rate of cells was clearly dependent on the ratio of cationic to stealth units within the micellar shell. In particular, the homopolymers of AmOx showed membrane aggregation comparable to the ISO-standard b-PEI even at the lowest concentration, whereas the micelles revealed no erythrocyte aggregation except the 100 wt % P(NonOx<sub>52</sub>-b-AmOx<sub>184</sub>) at 100  $\mu\text{g mL}^{-1}$ . Interestingly, P(EtOx<sub>3</sub>-b-AmOx<sub>157</sub>) did not show hemolytic activity but a high membrane aggregation potential. Micelles, on the other hand, were more hemolytic, however, had a lower membrane aggregation potential. This indicates that the micelles forces a membrane hole formation in contrast to the homopolymers, which is beneficial for the endosomal release of these nanostructures.

**DNA Binding and Dissociation Capabilities.** As the prepared nanostructures are supposed to act as transfection vectors, investigations on the DNA binding and dissociation capabilities of nanostructures with 20 to 100 wt % P(NonOx<sub>52</sub>-b-AmOx<sub>184</sub>) were conducted. The DNA binding ability was determined by the ethidium bromide assay (EBA) and was evaluated with respect to the nitrogen atoms bearing the

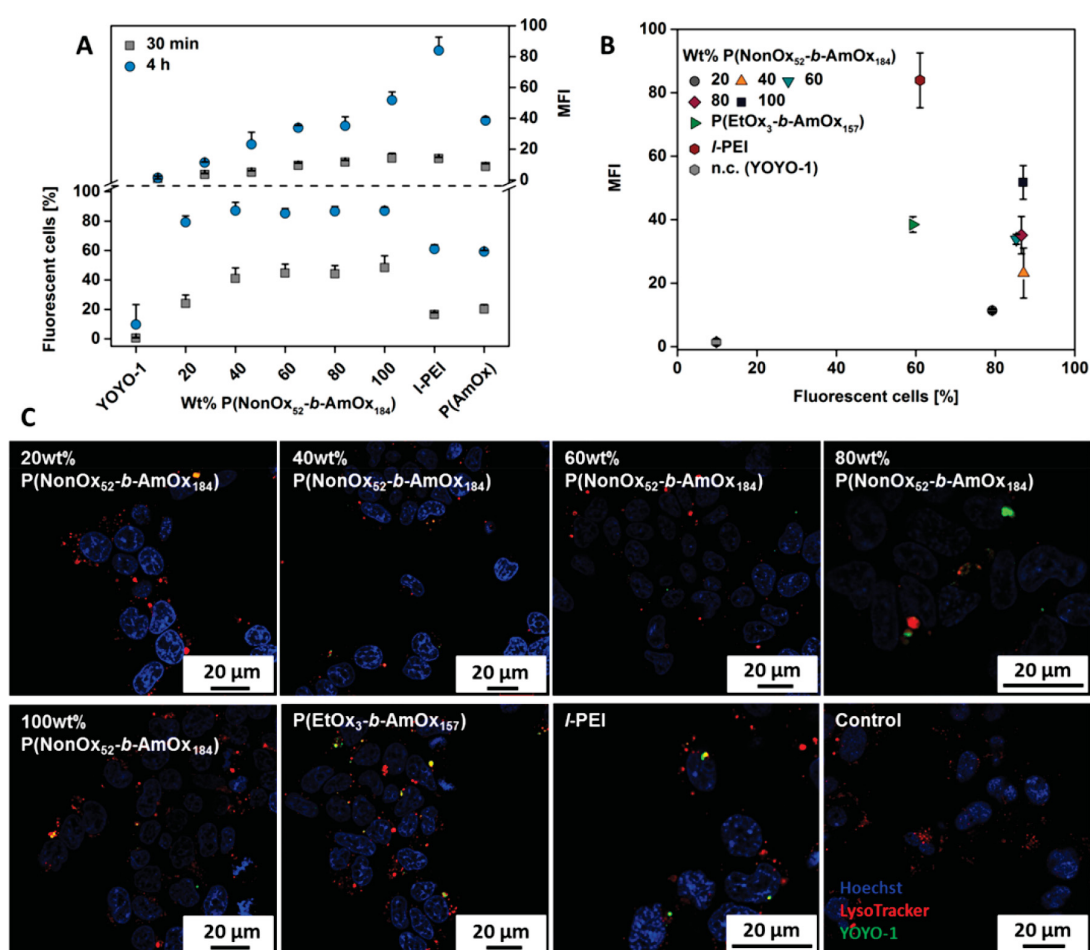


**Figure 5.** Cellular uptake study of different polyplexes (N\*/P 50) using YOYO-1 labeled pDNA. (A) HEK-293 cells were treated with micelleplexes for 30 min and 4 h in growth media and uptake was analyzed via flow cytometry (MFI, mean fluorescence intensity). Values represent the mean and SD ( $n = 3$ ). (B) MFI of the cells in dependence on the amount of fluorescent cells after 4 h of incubation. (C) CLSM images of micelleplexes (N\*/P 50) after 4 h of incubation. The cell nucleus is stained with Hoechst (blue), endosomes are stained with LysoTracker (red), and pDNA with YOYO-1 (green). Yellow dots indicate a colocalization of green and red fluorescence. Dead cells and outer fluorescence of noninternalized micelleplexes were quenched by the addition of trypan blue.

potential for DNA binding (amino group in the polymer side chain) (N\*/P, Figure 4A).

By comparing the nanostructures of different AmOx content in the micelle shell with respect to the DNA complexation, the N\*/P ratios are similar for all nanostructures. Interestingly, the same plateau at approximately 60% fluorescence intensity was reached, even if only 20% of the shell contains DNA binding amines. It leads to the conclusion that all nanostructures are of the same quality for polyplex formation and the EtOx units do not interfere with the DNA interaction, demonstrating the potential of the block copolymers. Subsequently, the DNA dissociation of the polyplexes was investigated by the heparin assay (Figure 4B). A release of the DNA from micelles and homopolymers was possible using 20 U mg<sup>-1</sup> heparin, a representative polyanion commonly used for DNA release.<sup>44,45</sup> In the case of the micelles, a release was even observed at 10 U mL<sup>-1</sup> heparin. This result supported the assumption that the self-assembly has an influence on the critical gene carrier parameters, for example, caused by sterically phenomena of the charging density. A release of the genetic material is desired to enable transfer to the nucleus or transcription. Polyplexes were further evaluated via DLS measurements, showing a main peak

distribution with a diameter of 100 nm and some larger aggregates (Figure 4C,D). Even though a quantification and discussion of the DLS results are difficult, the micelleplexes containing 60 to 100 wt % of P(NonOx<sub>52</sub>-b-AmOx<sub>184</sub>) seem to form less aggregates than micelleplexes with 20 or 40 wt % P(NonOx<sub>52</sub>-b-AmOx<sub>184</sub>), possibly due to higher local charge densities. For this reason, it is likely that micelles with more cationic charges tend to bind one molecule of pDNA per micelle, while micelles with less density of cationic charges might be bound to the pDNA in groups (Figure 4C). Since the polyplexes are prepared by aiming an N\*/P ratio of 50, we observe an excess of polymeric micelles in all cases; however, the amount of polymers increases with a decreasing amount of P(NonOx<sub>52</sub>-b-AmOx<sub>184</sub>), which makes the formation of such larger micelleplexes quite likely.

**Cellular Uptake.** To prove whether the micelles are able to transport the genetic material into cells, the pDNA was stained with the intercalating dye YOYO-1 that is also not released by the cationic polymers. Different amounts of micelleplex solution were added to the cells according to their N\*/P ratio. The amount of pDNA added was kept constant. After 30 min and 4 h of incubation, the cells were analyzed via flow

cytometry using trypan blue to quench fluorescent polyplexes outside the cells. All polymers revealed a time-dependent uptake in the mean fluorescence intensity (MFI) as well as the amount of cells, which internalized the micelleplexes (Figure 5A).

The transport of the genetic material of the micelles was enhanced with increasing AmOx amount in the shell and the micelle with 100% AmOx in the shell showed an enhanced transfer capacity compared to the AmOx homopolymer. If these structures are compared with the gold standard PEI it is obvious that more cells take up polyplexes; in particular the amount of cells is increased for all tested micelles. However, the MFI of PEI exceeded the micelles after 4 h of incubation, showing the better transport potential of PEI, although less cells take up the polyplexes. This can be also observed by CLSM investigations, where the green signal (YOYO-1) was more intensive for the homopolymers compared to the micelles (Figure 5C). For a better comparison of the polymers and to obtain insight into a structure–property-relationship, the MFI was plotted against the amount of cells (Figure 5B). Here, two trends are visible. (i) The MFI increased with increasing amount of AmOx in the micellar shell. The amount of cells was constant throughout the different compositions except for the micelles with the lowest AmOx content (20 wt % P(NonOx<sub>52</sub>-*b*-AmOx<sub>184</sub>)), which showed a slightly reduced percentage. These facts indicate an uptake independent of the cationic charge density in the micellar shell. In particular, the micelles with lower AmOx content can therefore be considered as a potential gene carrier with high bio- and hemocompatibility, which still can transfect a high percentage of the desired cells. (ii) The micellar structure enhances the performance of AmOx in terms of MFI and the amount of cells taking up the genetic material. These results underline the favorable uptake and transport capabilities of micellar structures compared to homopolymers.

**Transfection Efficiency.** Finally, the transfection efficiencies of the polymers were investigated using an eGFP expressing plasmid and the analysis via flow cytometry. Again, the amount of cells expressing eGFP as well as the MFI of all viable cells was detected. Moreover, the viability of each measurement was analyzed and plotted against the transfection efficiency (Figure 6). The polymers can be categorized into two classes, where the first showed only marginal transfection efficiency, namely P(EtOx<sub>3</sub>-*b*-AmOx<sub>157</sub>), and the nanostructures that are composed of 20 or 40 wt % P(NonOx<sub>52</sub>-*b*-AmOx<sub>184</sub>), respectively. The second class revealed acceptable to high transfection efficiencies in the following order: 60 wt % P(NonOx<sub>52</sub>-*b*-AmOx<sub>184</sub>) < 80 wt % P(NonOx<sub>52</sub>-*b*-AmOx<sub>184</sub>) < 100 wt % P(NonOx<sub>52</sub>-*b*-AmOx<sub>184</sub>) < *l*-PEI. In parallel to the uptake efficiency of the polymers, the performance of the micelles increased with increasing P(NonOx<sub>52</sub>-*b*-AmOx<sub>184</sub>) content from 40 to 100 wt %. Micelles with 100 and 80 wt % P(NonOx<sub>52</sub>-*b*-AmOx<sub>184</sub>) showed transfection efficiencies similar to PEI with a distinct reduction in cytotoxicity (micelles >80% viability, PEI 60% viability). It is noteworthy that architecture or the assembly of the materials, respectively, has a tremendous influence on the transfection efficiency. Although P(EtOx<sub>3</sub>-*b*-AmOx<sub>157</sub>) revealed the smallest transfection efficiency, the micelle of 100 wt % P(NonOx<sub>52</sub>-*b*-AmOx<sub>184</sub>) showed a performance similar to PEI, although applying the same N\*/P ratio (same amount of protonable nitrogen atoms). This result demonstrates the potential of the micellar structure

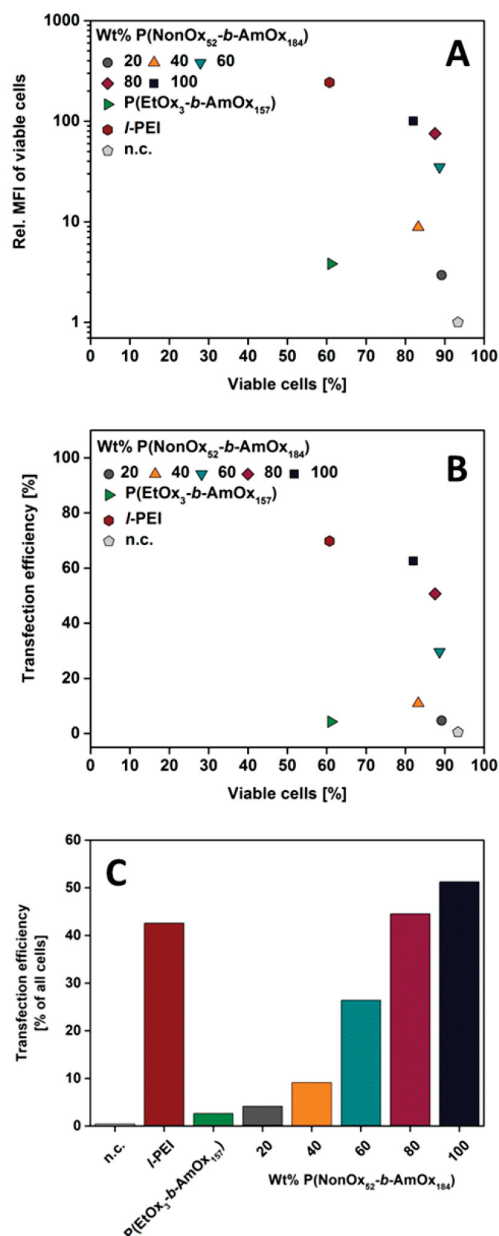


**Figure 6.** Transfection efficiency of different polyplexes for adherent HEK-293 cells in growth media at N\*/P = 50 after 4 d analyzed via flow cytometry. Values represent the mean. ( $n = 3$ ). (A) Relative MFI of all viable cells normalized by the negative control (n.c.). (B) Transfection efficiency of all viable cells. (C) Transfection efficiency of all cells. For values, see Table S8.

for the development of more efficient polymeric materials for transfection.

## CONCLUSIONS

In the current study, we synthesized two different amphiphilic block copolymers, namely P(NonOx<sub>52</sub>-*b*-AmOx<sub>184</sub>), to induce cationic charges and P(EtOx<sub>155</sub>-*b*-NonOx<sub>75</sub>) for the introduction of stealth units. The two (Ox)s were coassembled in aqueous physiological NaCl solution and subsequently characterized via DLS and cryoTEM. All nanostructures that contained at least a maximum P(NonOx<sub>52</sub>-*b*-AmOx<sub>184</sub>) content



of 80 wt % resulted in rod-like micelles with an apparent average diameter of 100 nm (assuming spheres by DLS measurements), whereas pure P(NonOx<sub>52</sub>-*b*-AmOx<sub>184</sub>) micelles were spherical. DLS measurements of the nanostructures in buffers of distinct pH values resulted in a pH-dependent alteration of the size with respect to the pH value and the amount of P(NonOx<sub>52</sub>-*b*-AmOx<sub>184</sub>). A reversible polyplex formation was possible with all amino group containing nanostructures. We observed that the cytotoxicity, erythrocyte aggregation, and hemolytic activity were dependent on the polymer composition within the nanostructures. The high charge density of the micelles led to an enhanced hemoglobin release compared to the P(AmOx) homopolymer. Examinations on the cellular uptake showed that the number of fluorescent cells is similar for all nanostructures (~80%), while the MFI increases applying micelles with more cationic charges. In comparison, we observed 60% fluorescent cells using *l*-PEI or AmOx homopolymers and the MFI of P(AmOx) was considerably lower than for *l*-PEI. Flow cytometry analysis of the transfection efficiency revealed an enhanced viability of the cells when treated with micelleplexes (80–90%) compared to polyplexes of P(AmOx) or *l*-PEI (60%). The transfection efficiency was strongly dependent on the amount of cationic polymer within the micelles and ranged from less than 5% (20 wt % P(NonOx<sub>52</sub>-*b*-AmOx<sub>184</sub>)) to more than 60% (100 wt % P(NonOx<sub>52</sub>-*b*-AmOx<sub>184</sub>)). Micelleplexes with 80 or 100 wt % P(NonOx<sub>52</sub>-*b*-AmOx<sub>184</sub>) showed a better overall performance in terms of transfection efficiency than *l*-PEI, while P(AmOx) was worse than the micelleplexes with 20 wt % P(NonOx<sub>52</sub>-*b*-AmOx<sub>184</sub>). We attribute these advantages to the architecture of the micelles and the following accumulation of cationic charges on their surface due to the cationic blocks. On the basis of these findings, we were able to improve the performance of a toxic, poorly transfecting polymer by appropriate self- and coassembly process to obtain nanostructures with a decreased cytotoxicity and improved transfection efficiency compared to *l*-PEI and the AmOx homopolymer.

Further studies might concentrate on the utilization of cationic block copolymers with different lengths to obtain nanostructures, which have an optimum balance between shielding by the EtOx blocks and efficient endosomal release by the stretching of the cationic blocks within the endolysosomes. These experiments might help to find biocompatible and efficient gene carrier systems.

## ■ ASSOCIATED CONTENT

### 5 Supporting Information

The Supporting Information is available free of charge on the ACS Publications website at DOI: 10.1021/acs.biomac.7b01535.

NMR spectra, SEC traces, DLS curves, magnified cryoTEM images, CMC determination graphs, erythrocyte aggregation microscopy images, raw values of DLS measurements (PDF)

## ■ AUTHOR INFORMATION

### Corresponding Authors

\*E-mail: [anja.traeger@uni-jena.de](mailto:anja.traeger@uni-jena.de).

\*E-mail: [ulrich.schubert@uni-jena.de](mailto:ulrich.schubert@uni-jena.de).

### ORCID

Ulrich S. Schubert: 0000-0003-4978-4670

## Author Contributions

The manuscript was written through contributions of all authors. All authors have given approval to the final version of the manuscript.

## Notes

The authors declare no competing financial interest.

## ■ ACKNOWLEDGMENTS

The authors gratefully acknowledge the Bundesministerium für Bildung und Forschung (BMBF, Germany, No. 13N13416 smart-dye-livery) and the Thüringer Ministerium für Wirtschaft, Wissenschaft und Digitale Gesellschaft (ProExzellenzII, NanoPolar). Furthermore, funding of the collaborative research center PolyTarget (SFB 1278) by the Deutsche Forschungsgemeinschaft (DFG) is highly acknowledged. A.T. acknowledges the Carl Zeiss Foundation and the BMBF (No. 13XP5034A PolyBioMik) for funding. J.C.B. further thanks the DFG for support (Emmy-Noether Program, BR 4905/3-1). The authors thankfully acknowledge Carolin Kellner and Elisabeth Moek for the conduction of AlamarBlue, hemolysis, and aggregation assays as well as Dr. Grit Festag for SEC measurements on an aqueous system. CryoTEM investigations were performed at the Electron Microscopy facilities of the Jena Center for Soft Matter (JCSM), which was established with grants from the Deutsche Forschungsgemeinschaft (DFG) and the European Fund for Regional Development (EFRE). The LSM880 ELYRA PS.1 was further funded with a grant from the DFG.

## ■ REFERENCES

- (1) Huang, Y.; Liu, X.; Dong, L.; Liu, Z.; He, X.; Liu, W. Development of viral vectors for gene therapy for chronic pain. *Pain Res. Treat.* **2011**, *2011*, 968218.
- (2) Schatzlein, A. G. Non-viral vectors in cancer gene therapy: Principles and progress. *Anti-Cancer Drugs* **2001**, *12* (4), 275–304.
- (3) Gardlik, R.; Palfy, R.; Hodossy, J.; Lukacs, J.; Turna, J.; Celec, P. Vectors and delivery systems in gene therapy. *Med. Sci. Monit.* **2005**, *11* (4), Ra110–21.
- (4) Zhang, S.; Zhao, B.; Jiang, H.; Wang, B.; Ma, B. Cationic lipids and polymers mediated vectors for delivery of siRNA. *J. Controlled Release* **2007**, *123* (1), 1–10.
- (5) Bulmus, V.; Woodward, M.; Lin, L.; Murthy, N.; Stayton, P.; Hoffman, A. A new pH-responsive and glutathione-reactive, endosomal membrane-disruptive polymeric carrier for intracellular delivery of biomolecular drugs. *J. Controlled Release* **2003**, *93* (2), 105–120.
- (6) Godbey, W. T.; Barry, M. A.; Saggau, P.; Wu, K. K.; Mikos, A. G. Poly(ethylenimine)-mediated transfection: A new paradigm for gene delivery. *J. Biomed. Mater. Res.* **2000**, *51* (3), 321–8.
- (7) Behr, J.-P. The proton sponge: A trick to enter cells the viruses did not exploit. *Chimia* **1997**, *51* (1–2), 34–36.
- (8) Ahn, C. H.; Chae, S. Y.; Bae, Y. H.; Kim, S. W. Biodegradable poly(ethylenimine) for plasmid DNA delivery. *J. Controlled Release* **2002**, *80* (1–3), 273–82.
- (9) Monnery, B. D.; Wright, M.; Cavill, R.; Hoogenboom, R.; Shaunak, S.; Steinke, J. H. G.; Thanou, M. Cytotoxicity of polycations: Relationship of molecular weight and the hydrolytic theory of the mechanism of toxicity. *Int. J. Pharm.* **2017**, *521* (1), 249–258.
- (10) Hsiue, G. H.; Chiang, H. Z.; Wang, C. H.; Juang, T. M. Nonviral gene carriers based on diblock copolymers of poly(2-ethyl-2-oxazoline) and linear polyethylenimine. *Bioconjugate Chem.* **2006**, *17* (3), 781–6.
- (11) Shah, R.; Kronekova, Z.; Zahoranová, A.; Roller, L.; Saha, N.; Saha, P.; Kronek, J. *in vitro* study of partially hydrolyzed poly(2-ethyl-2-oxazolines) as materials for biomedical applications. *J. Mater. Sci.: Mater. Med.* **2015**, *26* (4), 157.
- (12) Miyata, K.; Oba, M.; Nakanishi, M.; Fukushima, S.; Yamasaki, Y.; Koyama, H.; Nishiyama, N.; Kataoka, K. Polyplexes from

- poly(aspartamide) bearing 1,2-diaminoethane side chains induce ph-selective, endosomal membrane destabilization with amplified transfection and negligible cytotoxicity. *J. Am. Chem. Soc.* **2008**, *130* (48), 16287–16294.
- (13) Oba, M.; Miyata, K.; Osada, K.; Christie, R. J.; Sanjoh, M.; Li, W.; Fukushima, S.; Ishii, T.; Kano, M. R.; Nishiyama, N.; Koyama, H.; Kataoka, K. Polyplex micelles prepared from  $\omega$ -cholesteryl peg-polycation block copolymers for systemic gene delivery. *Biomaterials* **2011**, *32* (2), 652–663.
- (14) Kim, H. J.; Ishii, A.; Miyata, K.; Lee, Y.; Wu, S.; Oba, M.; Nishiyama, N.; Kataoka, K. Introduction of stearyl moieties into a biocompatible cationic polyaspartamide derivative, pasp(det), with endosomal escaping function for enhanced siRNA-mediated gene knockdown. *J. Controlled Release* **2010**, *145* (2), 141–148.
- (15) Barz, M.; Luxenhofer, R.; Zentel, R.; Vicent, M. J. Overcoming the peg-addiction: Well-defined alternatives to peg, from structure-property relationships to better defined therapeutics. *Polym. Chem.* **2011**, *2* (9), 1900–1918.
- (16) Hoogenboom, R. Poly(2-oxazoline)s: A polymer class with numerous potential applications. *Angew. Chem., Int. Ed.* **2009**, *48* (43), 7978–94.
- (17) Luxenhofer, R.; Han, Y.; Schulz, A.; Tong, J.; He, Z.; Kabanov, A. V.; Jordan, R. Poly(2-oxazoline)s as polymer therapeutics. *Macromol. Rapid Commun.* **2012**, *33* (19), 1613–1631.
- (18) Gaertner, F. C.; Luxenhofer, R.; Blechert, B.; Jordan, R.; Essler, M. Synthesis, biodistribution and excretion of radiolabeled poly(2-alkyl-2-oxazoline)s. *J. Controlled Release* **2007**, *119* (3), 291–300.
- (19) Salzinger, S.; Huber, S.; Jaksch, S.; Busch, P.; Jordan, R.; Papadakis, C. M. Aggregation behavior of thermo-responsive poly(2-oxazoline)s at the cloud point investigated by fcs and sans. *Colloid Polym. Sci.* **2012**, *290* (5), 385–400.
- (20) Cai, G.; Litt, M. H. Preparation and characterization of phenyl and undecyl oxazoline block copolymers. *J. Polym. Sci., Part A: Polym. Chem.* **1989**, *27* (11), 3603–3618.
- (21) McAlvin, J. E.; Fraser, C. L. Metal-centered star block copolymers: Amphiphilic iron tris(bipyridine)-centered polyoxazolines and their chemical fragmentation to bipyridine-centered triblock copolymers. *Macromolecules* **1999**, *32* (5), 1341–1347.
- (22) Jin, R.-H. Water soluble star block poly(oxazoline) with porphyrin label: A unique emulsion and its shape direction. *J. Mater. Chem.* **2004**, *14* (3), 320–327.
- (23) Lach, C.; Hanselmann, R.; Frey, H.; Mühlaupt, R. Hyperbranched carbosilane oxazoline-macromonomers: Polymerization and coupling to a trimesic acid core. *Macromol. Rapid Commun.* **1998**, *19* (9), 461–465.
- (24) Hartlieb, M.; Pretzel, D.; Kempe, K.; Fritzsche, C.; Paulus, R. M.; Gottschaldt, M.; Schubert, U. S. Cationic poly(2-oxazoline) hydrogels for reversible DNA binding. *Soft Matter* **2013**, *9* (18), 4693–4704.
- (25) Christova, D.; Velichkova, R.; Goethals, E. J.; Du Prez, F. E. Amphiphilic segmented polymer networks based on poly(2-alkyl-2-oxazoline) and poly(methyl methacrylate). *Polymer* **2002**, *43* (17), 4585–4590.
- (26) Hadjichristidis, N.; Pispas, S.; Floudas, G. A. *Block Copolymers: Synthetic Strategies, Physical Properties, and Applications*; Wiley: Weinheim, 2003.
- (27) He, Z.; Miao, L.; Jordan, R.; S-Manickam, D.; Luxenhofer, R.; Kabanov, A. V. A low protein binding cationic poly(2-oxazoline) as non-viral vector. *Macromol. Biosci.* **2015**, *15* (7), 1004–1020.
- (28) Rinkenauer, A. C.; Tauhardt, L.; Wendler, F.; Kempe, K.; Gottschaldt, M.; Traeger, A.; Schubert, U. S. A cationic poly(2-oxazoline) with high in vitro transfection efficiency identified by a library approach. *Macromol. Biosci.* **2015**, *15* (3), 414–425.
- (29) Bauer, M.; Lautenschlaeger, C.; Kempe, K.; Tauhardt, L.; Schubert, U. S.; Fischer, D. Poly(2-ethyl-2-oxazoline) as alternative for the stealth polymer poly(ethylene glycol): Comparison of in vitro cytotoxicity and hemocompatibility. *Macromol. Biosci.* **2012**, *12* (7), 986–998.
- (30) Wiesbrock, F.; Hoogenboom, R.; Abeln, C. H.; Schubert, U. S. Single-mode microwave ovens as new reaction devices: Accelerating the living polymerization of 2-ethyl-2-oxazoline. *Macromol. Rapid Commun.* **2004**, *25* (22), 1895–1899.
- (31) Wilhelm, M.; Zhao, C. L.; Wang, Y.; Xu, R.; Winnik, M. A.; Mura, J. L.; Riess, G.; Croucher, M. D. Poly(styrene-ethylene oxide) block copolymer micelle formation in water: A fluorescence probe study. *Macromolecules* **1991**, *24* (5), 1033–1040.
- (32) Vollrath, A.; Schallon, A.; Pietsch, C.; Schubert, S.; Nomoto, T.; Matsumoto, Y.; Kataoka, K.; Schubert, U. S. A toolbox of differently sized and labeled pmma nanoparticles for cellular uptake investigations. *Soft Matter* **2013**, *9* (1), 99–108.
- (33) Cesana, S.; Auernheimer, J.; Jordan, R.; Kessler, H.; Nuyken, O. First poly(2-oxazoline)s with pendant amino groups. *Macromol. Chem. Phys.* **2006**, *207* (2), 183–192.
- (34) Jaksch, S.; Schulz, A.; Di, Z.; Luxenhofer, R.; Jordan, R.; Papadakis, C. M. Amphiphilic triblock copolymers from poly(2-oxazoline) with different hydrophobic blocks: Changes of the micellar structures upon addition of a strongly hydrophobic cancer drug. *Macromol. Chem. Phys.* **2016**, *217* (13), 1448–1456.
- (35) Bonné, T. B.; Papadakis, C. M.; Lüdtke, K.; Jordan, R. Role of the tracer in characterizing the aggregation behavior of aqueous block copolymer solutions using fluorescence correlation spectroscopy. *Colloid Polym. Sci.* **2007**, *285* (5), 491–497.
- (36) Bonné, T. B.; Lüdtke, K.; Jordan, R.; Štěpánek, P.; Papadakis, C. M. Aggregation behavior of amphiphilic poly(2-alkyl-2-oxazoline) diblock copolymers in aqueous solution studied by fluorescence correlation spectroscopy. *Colloid Polym. Sci.* **2004**, *282* (8), 833–843.
- (37) Ivanova, R.; Komenda, T.; Bonné, T. B.; Lüdtke, K.; Mortensen, K.; Pranzas, P. K.; Jordan, R.; Papadakis, C. M. Micellar structures of hydrophilic/lipophilic and hydrophilic/fluorophilic poly(2-oxazoline) diblock copolymers in water. *Macromol. Chem. Phys.* **2008**, *209* (21), 2248–2258.
- (38) Jain, K.; Kesharwani, P.; Gupta, U.; Jain, N. K. Dendrimer toxicity: Let's meet the challenge. *Int. J. Pharm.* **2010**, *394* (1), 122–142.
- (39) Betthausen, E.; Drechsler, M.; Fortsch, M.; Schacher, F. H.; Müller, A. H. E. Dual stimuli-responsive multicompartment micelles from triblock terpolymers with tunable hydrophilicity. *Soft Matter* **2011**, *7* (19), 8880–8891.
- (40) Bus, T.; Englert, C.; Reifarth, M.; Borchers, P.; Hartlieb, M.; Vollrath, A.; Hoepfner, S.; Traeger, A.; Schubert, U. S., 3rd generation poly(ethylene imine)s for gene delivery. *J. Mater. Chem. B* **2017**, *5* (6), 1258–1274.
- (41) Englert, C.; Pröhl, M.; Czaplewska, J. A.; Fritzsche, C.; Preußner, E.; Schubert, U. S.; Traeger, A.; Gottschaldt, M. D-fructose-decorated poly(ethylene imine) for human breast cancer cell targeting. *Macromol. Biosci.* **2017**, *17* (8), 1600502.
- (42) Lee, Y.; Miyata, K.; Oba, M.; Ishii, T.; Fukushima, S.; Han, M.; Koyama, H.; Nishiyama, N.; Kataoka, K. Charge-conversion ternary polyplex with endosome disruption moiety: A technique for efficient and safe gene delivery. *Angew. Chem.* **2008**, *120* (28), 5241–5244.
- (43) Rinkenauer, A. C.; Schallon, A.; Günther, U.; Wagner, M.; Betthausen, E.; Schubert, U. S.; Schacher, F. H. A paradigm change: Efficient transfection of human leukemia cells by stimuli-responsive multicompartment micelles. *ACS Nano* **2013**, *7* (11), 9621–9631.
- (44) Mislick, K. A.; Baldeschwieler, J. D. Evidence for the role of proteoglycans in cation-mediated gene transfer. *Proc. Natl. Acad. Sci. U. S. A.* **1996**, *93* (22), 12349–12354.
- (45) Xu, Y.; Szoka, F. C. Mechanism of DNA release from cationic liposome/DNA complexes used in cell transfection. *Biochemistry* **1996**, *35* (18), 5616–5623.

# Supporting Information

## *How to tune the gene delivery and biocompatibility of poly(2-(4-aminobutyl)-2-oxazoline) by self- and co-assembly*

*Meike N. Leiske,<sup>a,b</sup> Fabian H. Sobotta,<sup>a,b</sup> Friederike Richter,<sup>†,‡</sup> Stephanie Hoepfener,<sup>a,b</sup> Johannes  
C. Brendel,<sup>a,b</sup> Anja Traeger,<sup>a,b,\*</sup> Ulrich S. Schubert<sup>a,b,\*</sup>*

<sup>a</sup>Laboratory of Organic and Macromolecular Chemistry (IOMC), Friedrich Schiller University  
Jena, Humboldtstrasse 10, 07743 Jena, Germany.

<sup>b</sup>Jena Center for Soft Matter (JCSM), Friedrich Schiller University Jena, Philosophenweg 7,  
07743 Jena, Germany.

\*Correspondence to A. Traeger ([anja.traeger@uni-jena.de](mailto:anja.traeger@uni-jena.de)) and U. S. Schubert  
([ulrich.schubert@uni-jena.de](mailto:ulrich.schubert@uni-jena.de))

## Results

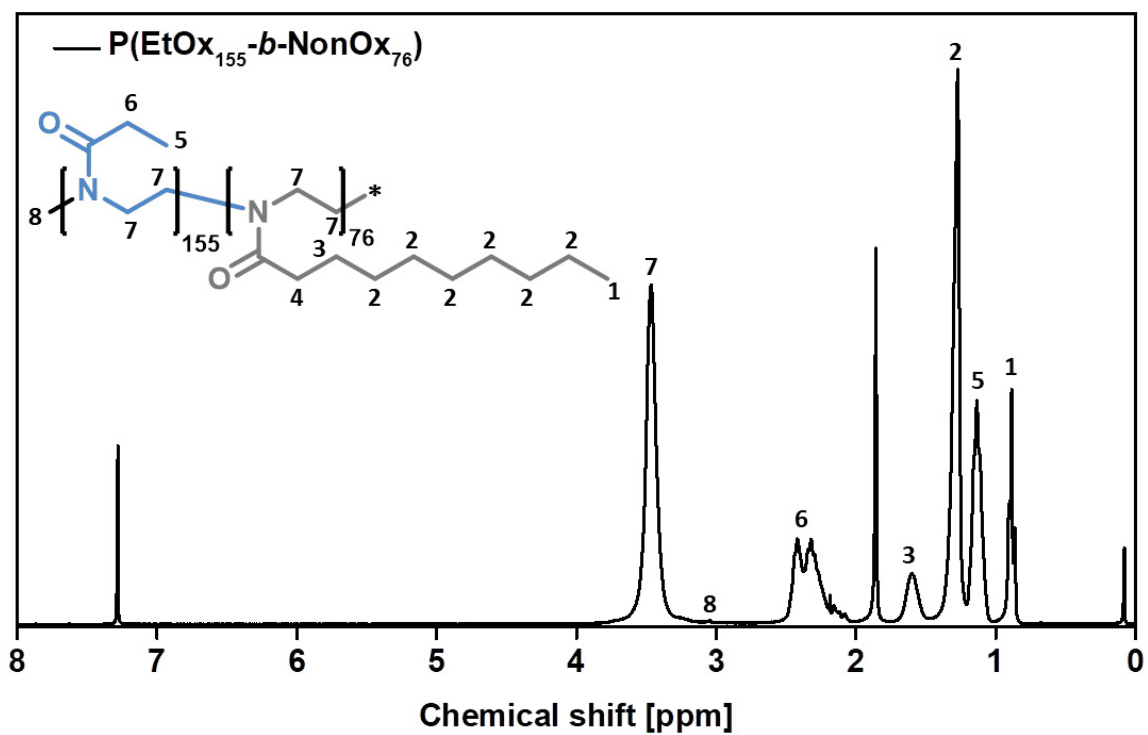


Figure S1. <sup>1</sup>H-NMR (300 MHz, CDCl<sub>3</sub>) of P(EtOx<sub>155</sub>-*b*-NonOx<sub>76</sub>).

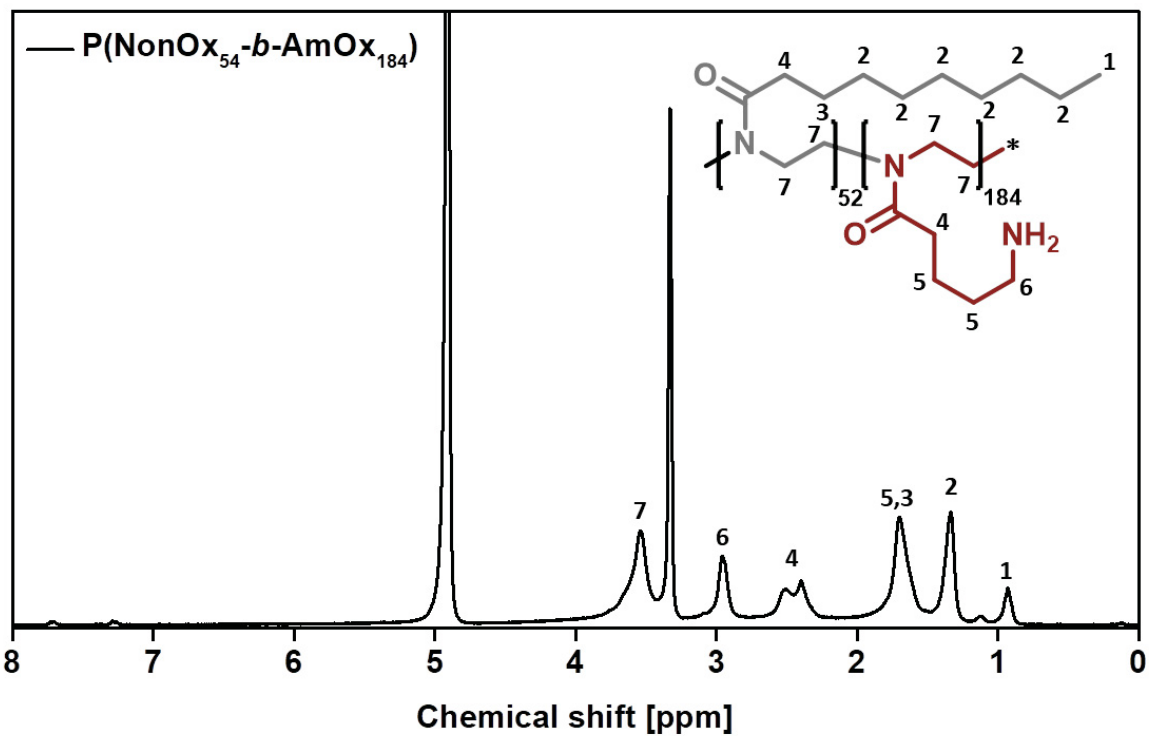


Figure S2.  $^1\text{H-NMR}$  (300 MHz, MeOD) of P(NonOx<sub>52</sub>-*b*-AmOx<sub>184</sub>).

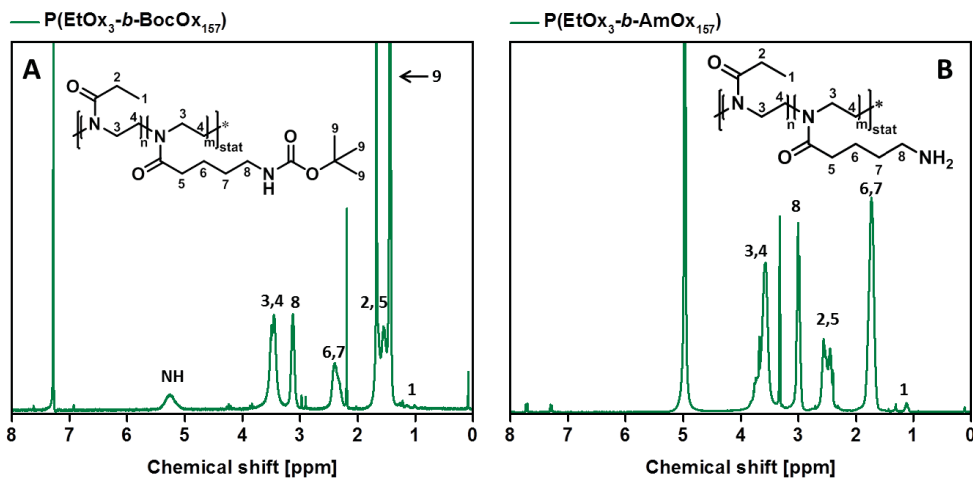
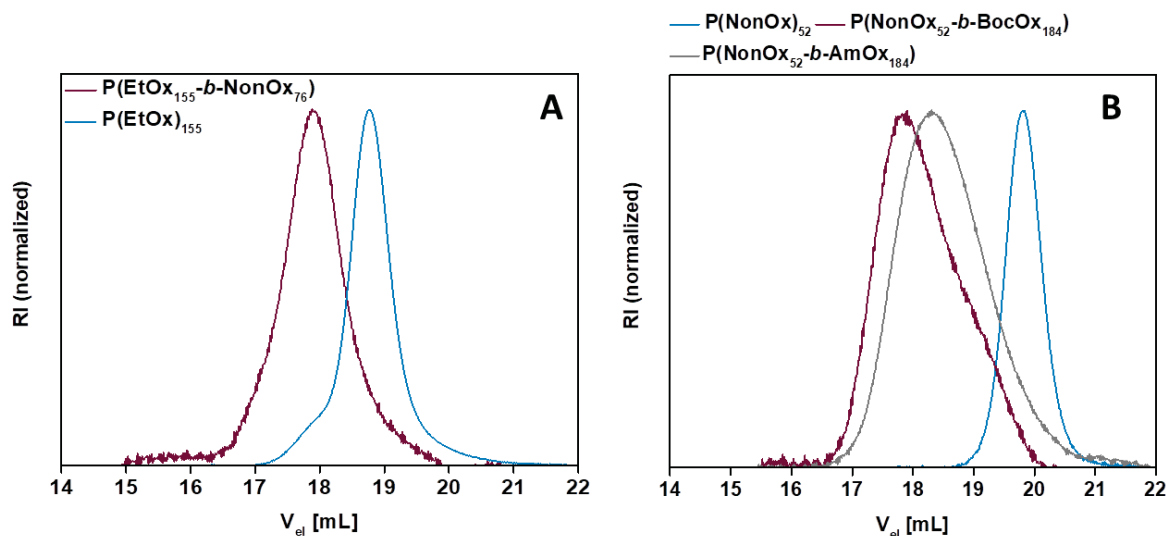
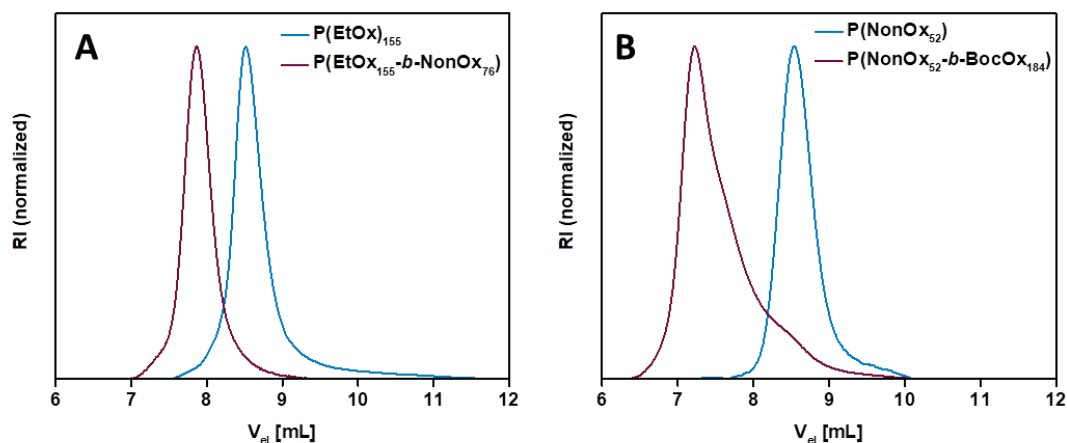


Figure S3.  $^1\text{H-NMR}$  (300 MHz) of A) P(EtOx<sub>3</sub>-*b*-BocOx<sub>157</sub>) in CDCl<sub>3</sub> and B) P(EtOx<sub>3</sub>-*b*-AmOx<sub>157</sub>) in D<sub>2</sub>O.



**Figure S4.** SEC overlays (DMAc + 0.21% LiCl, PS calibration) of the block copolymers. A) P(EtOx)<sub>155</sub> and P(EtOx)<sub>155</sub>-*b*-NonOx<sub>76</sub>; B) P(NonOx)<sub>52</sub>, P(NonOx)<sub>52</sub>-*b*-BocOx<sub>184</sub> and P(NonOx)<sub>52</sub>-*b*-AmOx<sub>184</sub>.



**Figure S5.** SEC overlays (CHCl<sub>3</sub>-*i*-PrOH-NEt<sub>3</sub> (94:2:4), PS calibration) of the block copolymers. A) P(EtOx)<sub>155</sub> and P(EtOx)<sub>155</sub>-*b*-NonOx<sub>76</sub>; B) P(NonOx)<sub>52</sub> and P(NonOx)<sub>52</sub>-*b*-BocOx<sub>184</sub>.

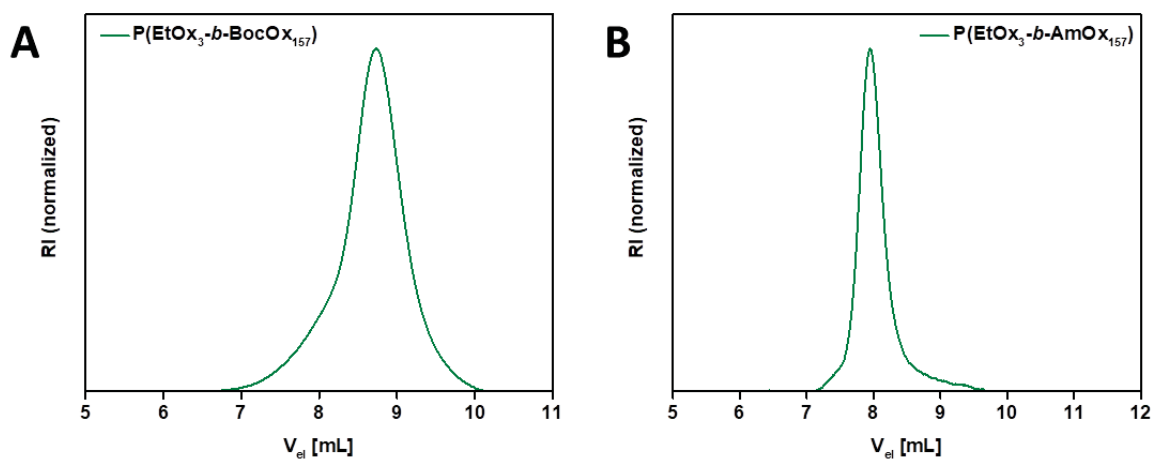


**Figure S6.** SEC traces of A) P(EtOx<sub>3</sub>-b-EtOx<sub>157</sub>) (CHCl<sub>3</sub>-*i*-PrOH-NEt<sub>3</sub> (94:2:4), PS calibration) and B) P(EtOx<sub>3</sub>-b-AmOx<sub>157</sub>) (0.3% TFA in 0.1 M NaCl, P2VP calibration).

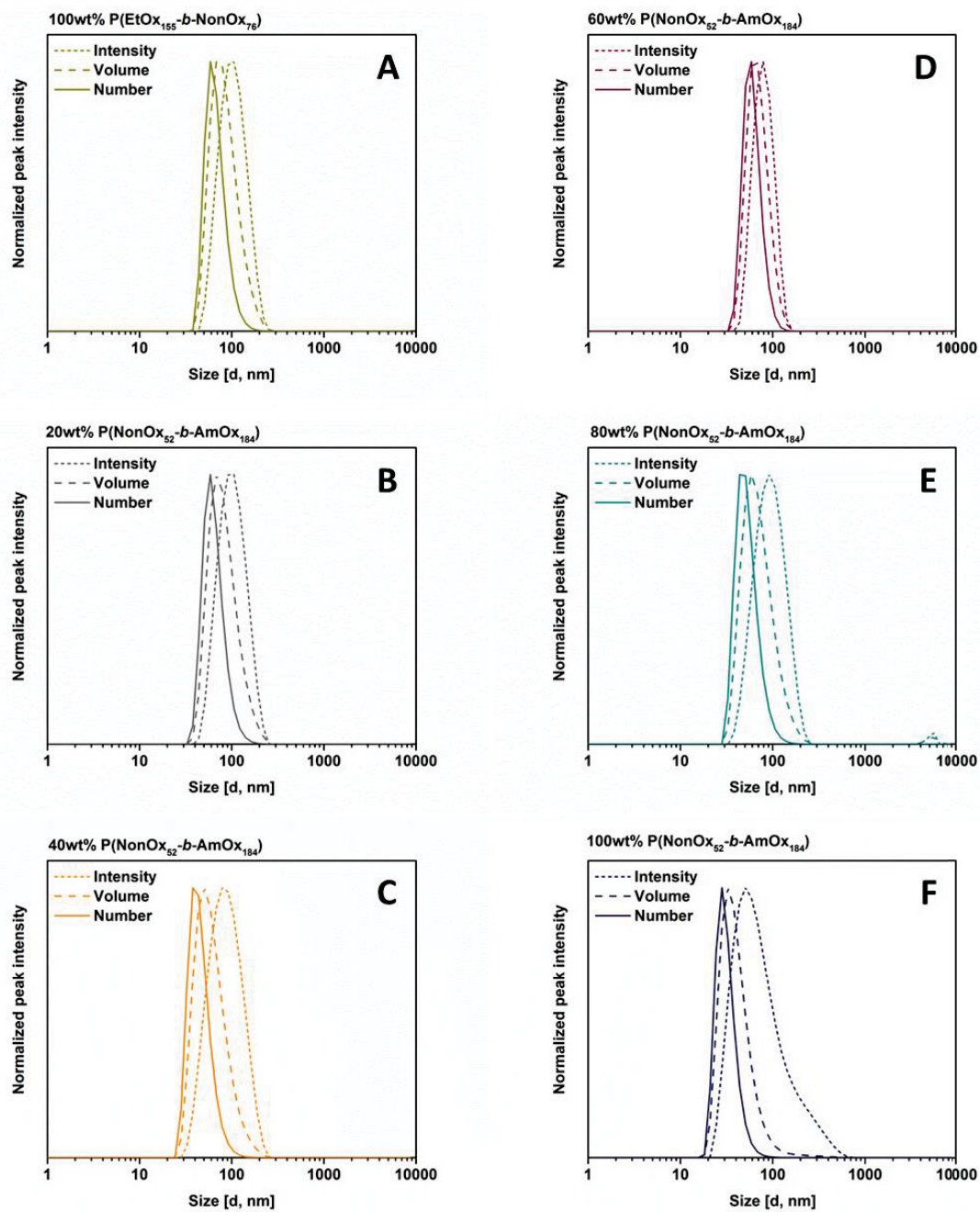


**Figure S7.** Representative curves of number, volume and intensity distributions of the prepared nanostructures with different polymer ratios determined by DLS measurements.



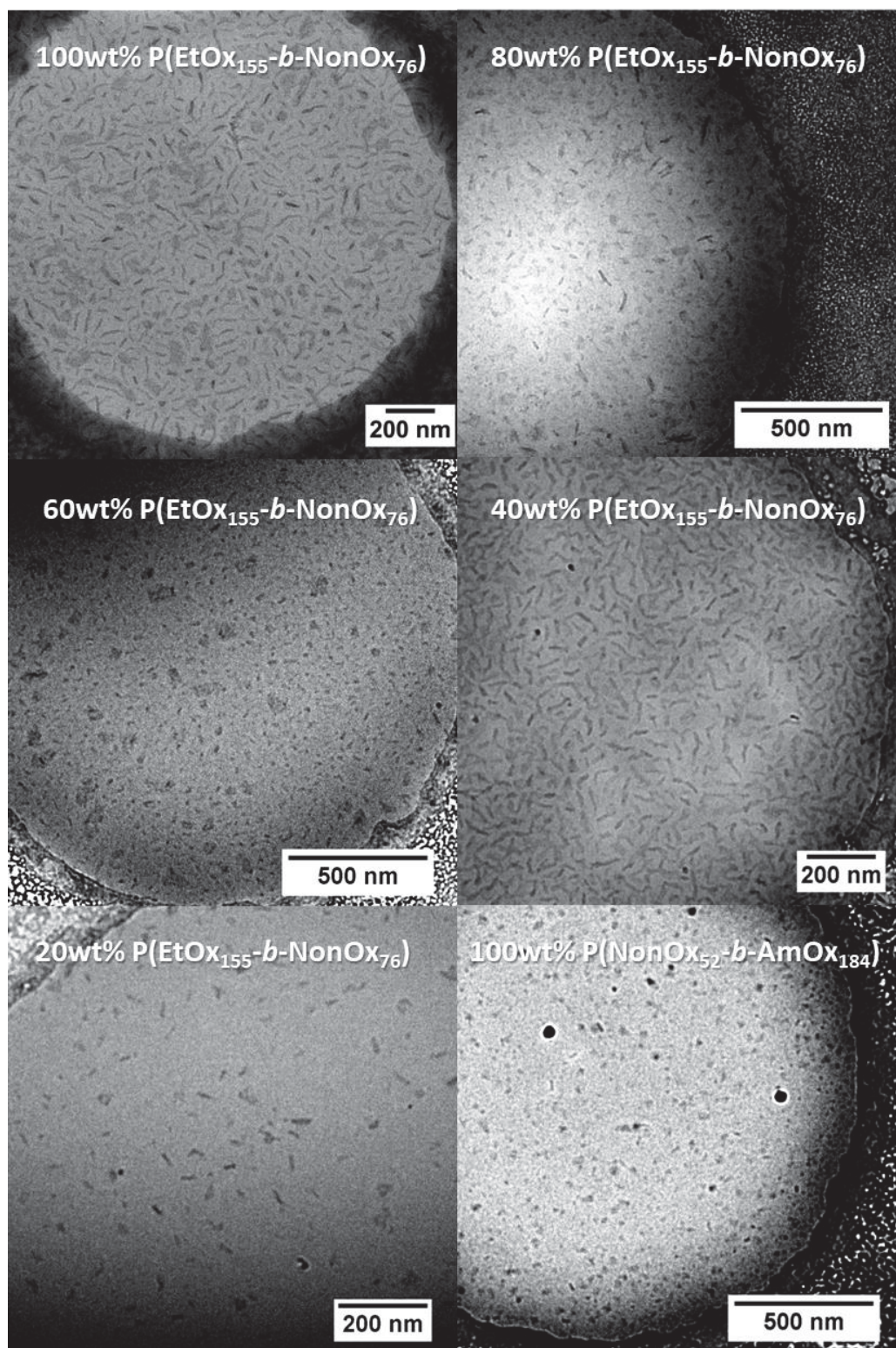


**Figure S8.** CryoTEM images of the prepared nanostructures in 0.9wt% aq. NaCl.

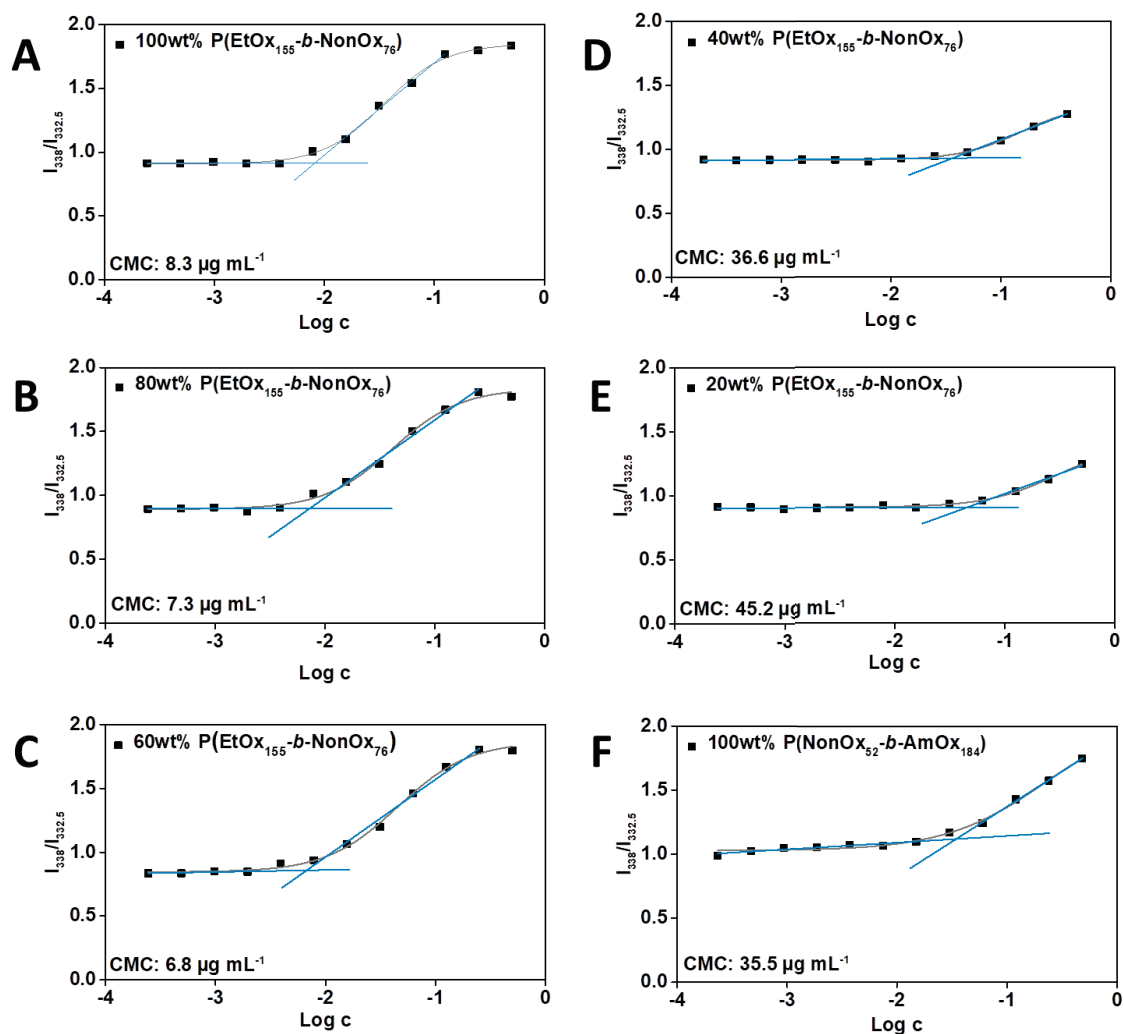


**Figure S9.** CMC of the nanostructures determined by the pyrene method. For calculation of the CMC, the fluorescence intensity at,  $\lambda_{\text{Em}} = 390.0 \text{ nm}$  while exciting at  $\lambda_{\text{Ex2}} = 338.0 \text{ nm}$  was divided by the fluorescence intensity at,  $\lambda_{\text{Em}} = 390.0 \text{ nm}$  while exciting at  $\lambda_{\text{Ex2}} = 332.5 \text{ nm}$  and plotted against the log of the polymer concentration. Intersection of blue lines indicates CMC.

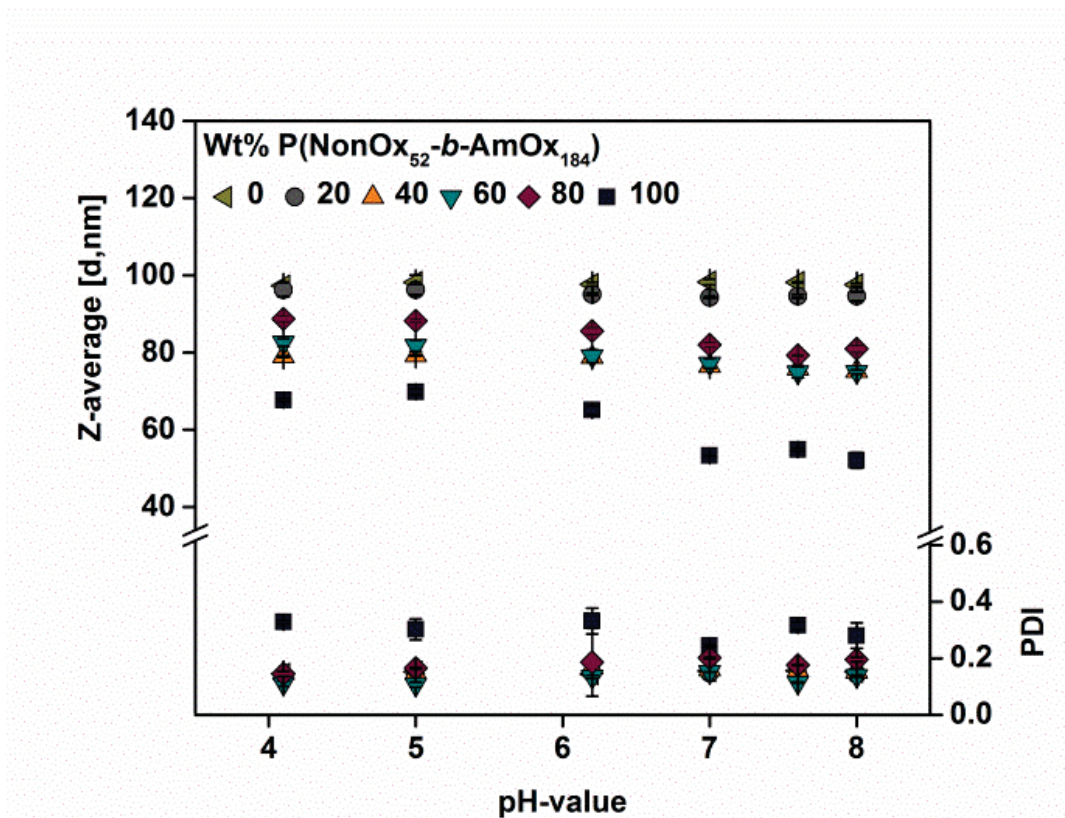


**Figure S10.** Z-average and PDI of the nanostructures in dependency of the pH value determined by DLS (3 measurements, 15 min each).

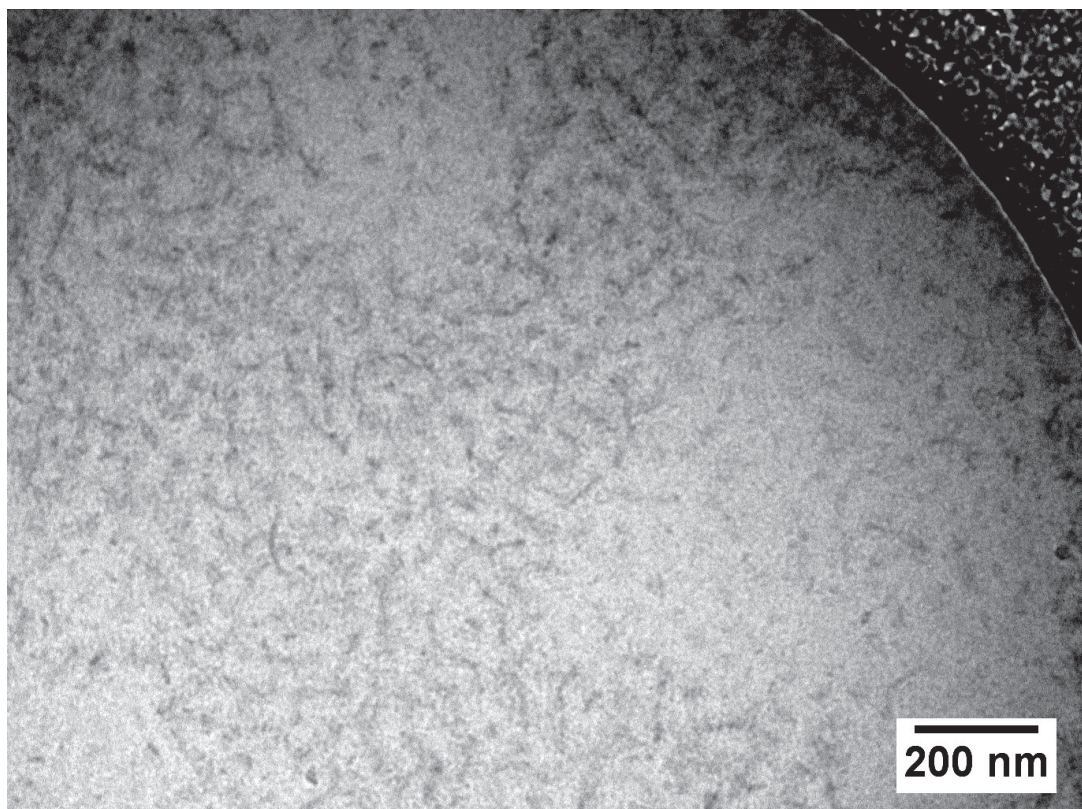


**Figure S11.** CryoTEM image of the nanostructures consisting of 80wt% P(NonO<sub>x52</sub>-*b*-AmO<sub>x184</sub>) measured at a pH value of 8.0.

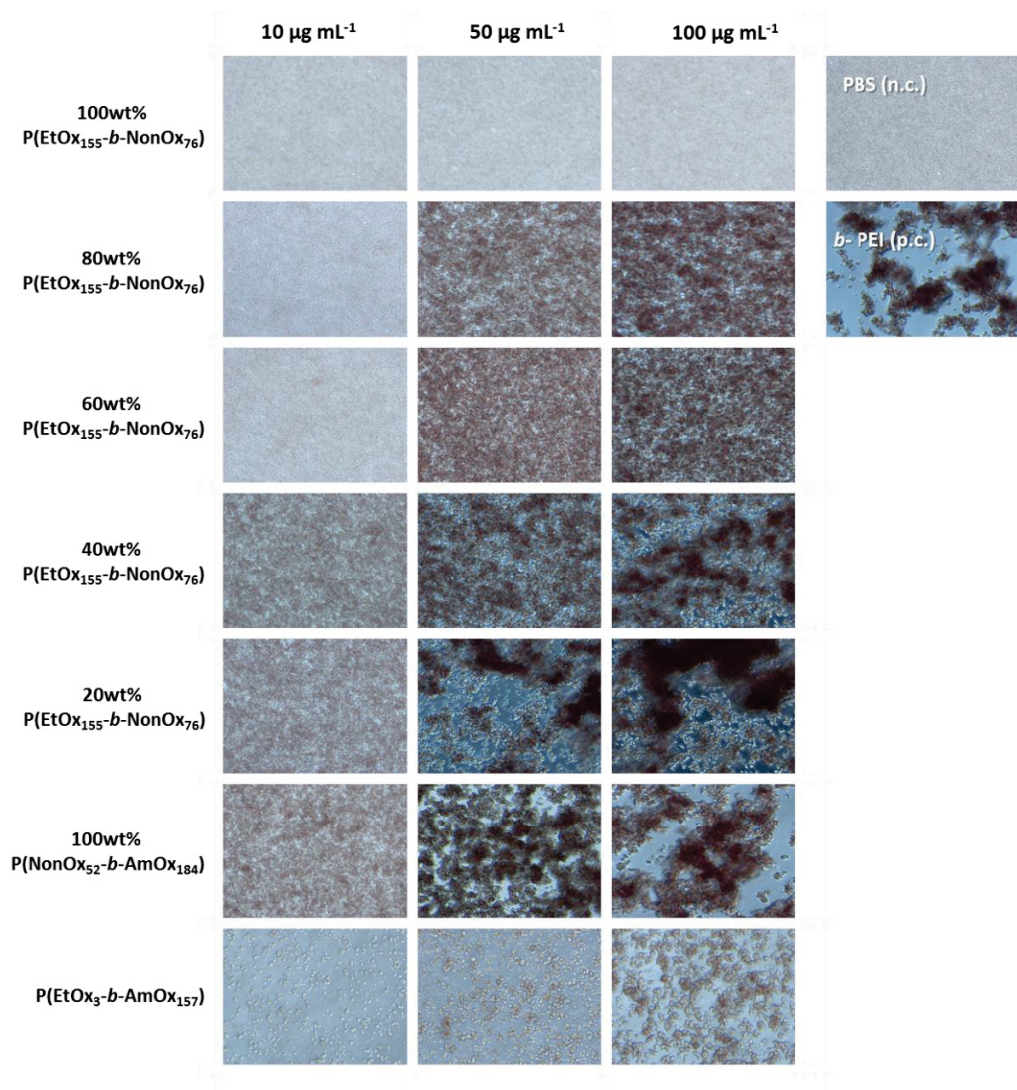


**Figure S12.** Erythrocyte aggregation. An erythrocytes suspension was mixed with the same volume of polymer solution in a clear flat bottomed 96-well plate. The cells were incubated at 37 °C for 2 h, and the absorbance was measured at  $\lambda_{\text{EX}} = 645$ . 25 kDa *b*-PEI (50  $\mu\text{g mL}^{-1}$ ) was used as positive control and PBS treated cells served as the negative control. Absorbance values of the test solutions lower than negative control were regarded as aggregation. Experiments are the result of triplicates and were performed with three different donor blood batches.

**Table S1.** Concentration and pH value of various buffers used for pH responsiveness measurements of prepared nanostructures.

Buffer	Concentration [mol L <sup>-1</sup> ]	pH value
Acetate buffer	0.1	4.10
Acetate buffer	0.1	5.04
Phosphate buffer	0.1	6.17
Phosphate buffer	0.1	7.04
Phosphate buffer	0.1	7.58
Phosphate buffer	0.1	8.00

**Table S2.** Utilized volumina for polyplex formation (master mix, polymer solutions and 150 mM aq. NaCl) used for EBA. Heparin dissociation assay was performed with half of all mentioned volumina at N\*/P = 50. Polymer concentrations are 1 mg mL<sup>-1</sup> in all cases. Concentrations of pDNA and EtBr stock solutions are 1 mg mL<sup>-1</sup>.

Wt% P(NonOx <sub>52</sub> - <i>b</i> - AmOx <sub>184</sub> ) in micelle	Master mix	N*/P = 10		N*/P = 20		N*/P = 30		N*/P = 50	
		V <sub>Polymer</sub> [μL]	V <sub>NaCl</sub> [μL]	V <sub>Polymer</sub> [μL]	V <sub>NaCl</sub> [μL]	V <sub>Polymer</sub> [μL]	V <sub>NaCl</sub> [μL]	V <sub>Polymer</sub> [μL]	V <sub>NaCl</sub> [μL]
20		41.6	168.4	83.2	126.8	124.7	85.3	208.0	2.0
40	1.5 μL	20.8	189.2	41.6	168.4	62.4	147.6	104.0	106.0
60	pDNA	13.9	196.1	27.7	183.3	41.6	168.4	69.4	140.6
80	0.1 μL EtBr	10.4	199.6	20.8	189.2	31.2	178.8	52.0	158.0
100	18.4 μL	8.3	201.7	16.6	193.4	24.9	185.1	41.6	168.4
P(EtOx <sub>3</sub> - <i>b</i> - AmOx <sub>157</sub> )	150 mM NaCl	6.1	203.9	12.1	197.9	18.2	191.8	30.2	179.8
<i>l</i> -PEI		1.8	208.2	3.6	206.4	5.4	204.6	9.0	201.0

**Table S3.** Final polymer concentrations ( $\mu\text{g mL}^{-1}$ ) used in the EBA and heparin dissociation assay.

Wt% P(NonOx <sub>52</sub> - <i>b</i> - AmOx <sub>184</sub> ) in micelle	N*/P = 10	N*/P = 20	N*/P = 30	N*/P = 50
20	180	362	542	904
40	90	180	271	452
60	60	120	180	302
80	45	90	136	226
100	36	72	108	180
P(EtOx <sub>3</sub> - <i>b</i> - AmOx <sub>157</sub> )	27	53	79	131
<i>l</i> -PEI	8	16	23	39

**Table S4.** Utilized volumina for polyplex formation (master mix and polymer solutions) used for uptake and transfection determination experiments. Polymer concentrations are  $1 \text{ mg mL}^{-1}$  in all cases. Concentrations of pDNA and YOYO-1 stock solutions are  $1 \text{ mg mL}^{-1}$ .

Wt% P(NonOx <sub>52</sub> - <i>b</i> - AmOx <sub>184</sub> ) in micelle	Master mix	V <sub>Polymer</sub> [ $\mu\text{L}$ ]	c <sub>pDNA</sub> [ $\mu\text{g mL}^{-1}$ ]	V added to cell culture [ $\mu\text{L}$ ]	c <sub>Polymer</sub> in cell culture [ $\mu\text{g mL}^{-1}$ ]
20	1.5 $\mu\text{L}$	208.0	4.9	153.9	
40	pDNA	104.0	7.3	102.0	
60	0.04 $\mu\text{L}$ YOYO-1	69.4	8.9	84.6	
80	98.46 $\mu\text{L}$	52.0	10.0	76.0	
100	150 mM NaCl	41.6	10.6	70.8	
P(EtOx <sub>3</sub> - <i>b</i> - AmOx <sub>157</sub> )		30.2	11.3	65.1	
<i>l</i> -PEI		9.0	13.8	54.5	

**Table S5.** Characteristics of the prepared nanostructures in 0.9wt% aq. NaCl determined by DLS (n=3). The polymer concentration was determined gravimetrically after lyophilization (n=3).

Wt%	Wt%	Z-average	PDI	Concentration
P(EtOx <sub>155</sub> - <i>b</i> -NonOx <sub>76</sub> )	P(NonOx <sub>52</sub> - <i>b</i> -AmOx <sub>184</sub> )	[d, nm]		[mg mL <sup>-1</sup> ]
100	0	99 ± 1	0.167 ± 0.009	1.0
80	20	95 ± 0	0.145 ± 0.006	1.0
60	40	77 ± 0	0.147 ± 0.001	1.0
40	60	79 ± 0	0.154 ± 0.004	1.0
20	80	87 ± 1	0.182 ± 0.003	1.0
0	100	60 ± 1	0.252 ± 0.008	1.0

**Table S6.** Intensity and number mean of the prepared nanostructures in 0.9wt% aq. NaCl determined by DLS (n=3).

Wt%	Wt%	Intensity mean	Number mean
P(EtOx <sub>155</sub> - <i>b</i> -NonOx <sub>76</sub> )	P(NonOx <sub>52</sub> - <i>b</i> -AmOx <sub>184</sub> )	[d, nm]	[d, nm]
100	0	107 ± 2	68 ± 10
80	20	110 ± 4	56 ± 8
60	40	88 ± 5	47 ± 15
40	60	77 ± 8	62 ± 2
20	80	154 ± 7	45 ± 12
0	100	101 ± 13	27 ± 12



**Table S7.** Characteristics of the prepared nanostructures in 0.9wt% aq. NaCl prior and after dilution (1:1) with 0.9wt% NaCl determined by DLS (n=3).

Polymer composition		Prior dilution		After dilution	
Wt% P(EtOx <sub>155</sub> - <i>b</i> - NonOx <sub>76</sub> )	Wt% P(NonOx <sub>52</sub> - <i>b</i> -AmOx <sub>184</sub> )	Z-average [d, nm]	PDI	Z-average [d, nm]	PDI
100	0	99 ± 1	0.167 ± 0.009	100 ± 1	0.163 ± 0.004
80	20	95 ± 0	0.145 ± 0.006	96 ± 2	0.170 ± 0.040
60	40	77 ± 0	0.147 ± 0.001	78 ± 1	0.162 ± 0.004
40	60	79 ± 0	0.154 ± 0.004	79 ± 0	0.124 ± 0.010
20	80	87 ± 1	0.182 ± 0.003	86 ± 0	0.168 ± 0.002
0	100	60 ± 1	0.252 ± 0.008	64 ± 1	0.328 ± 0.011

**Table S8.** Transfection efficiency of different polyplexes for adherent HEK-293 cells in growth media at N\*/P = 50 after 4 d analyzed *via* flow cytometry. Values represent the mean. (n = 3). Relative MFI of all viable cells normalized by the negative control (n.c.). Transfection efficiency of all viable cells.

Wt%	Wt%	Viability	TE	MFI
P(EtOx <sub>155</sub> - <i>b</i> -NonOx <sub>76</sub> )	P(NonOx <sub>52</sub> - <i>b</i> -AmOx <sub>184</sub> )	[%]	[%]	
80	20	89.2 ± 10.5	4.7 ± 1.4	3.0 ± 1.4
60	40	83.3 ± 20.0	11.0 ± 6.2	8.9 ± 6.3
40	60	88.7 ± 11.6	30.0 ± 16.8	35.1 ± 11.3
20	80	87.5 ± 10.0	50.6 ± 18.7	75.5 ± 30.2
0	100	82.9 ± 18.0	62.5 ± 16.0	100.5 ± 28.4
P(EtOx <sub>3</sub> - <i>b</i> -AmOx <sub>157</sub> )		61.1 ± 19.0	4.3 ± 2.6	3.8 ± 1.9
<i>l</i> -PEI		60.7 ± 15.0	69.8 ± 36.1	242.8 ± 197.9
n.c.		93.3 ± 5.0	0.5 ± 0.2	1.0 ± 0.0

## Publication Pub8

### A Cell Penetrating Peptide Based RAFT Agent for Constructing Penetration Enhancers

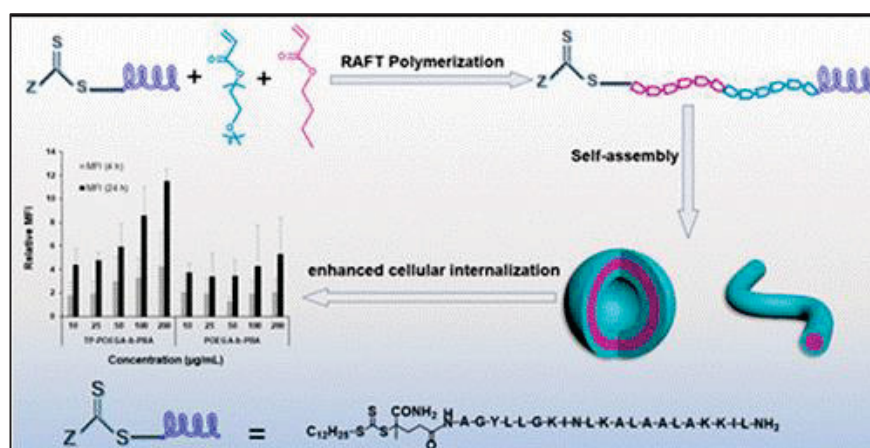
C. Chen, F. Richter, C. Guerrero-Sanchez, A. Traeger, U. S. Schubert, A. Feng, S. H. Thang

*ACS Macro Lett* **2020**, *9*, 260-265

Reproduced with permission of The American Chemical Society. Copyright © 2020.

The article and the supporting information are available online:

[doi.org/10.1021/acsmacrolett.9b00647](https://doi.org/10.1021/acsmacrolett.9b00647)





has been established as a versatile process because of the tolerance against many functional groups, the absence of metal catalysts, and mild reaction conditions.

To obtain CPP-modified polymers with high conjugation efficiency and well-defined properties, a TP 10-based RAFT agent (TP-CTA) was designed and synthesized. TP-CTA was prepared in an automated peptide synthesizer via a solid phase peptide synthesis method. Thereafter, RAFT polymerization allowed direct access to well-defined peptide–polymer conjugates, including block copolymer architectures. To the best of our knowledge, this is the first report on TP 10 peptide-modified polymers via RAFT polymerization.

The TP 10 peptide was prepared via a solid phase peptide synthesis method. Thereafter, the RAFT agent 4-cyano-4-[(dodecylsulfanylthiocarbonyl) sulfanyl] pentanoic acid (CDTPA) was directly linked to the terminal amino group of TP 10 peptide. A high purity product (97%, Figure S1) was obtained by semipreparative high performance liquid chromatography (HPLC). The chemical structure of TP-CTA is shown in Figure 1A. Mass spectrometry (MS) data (see Figure 1B)

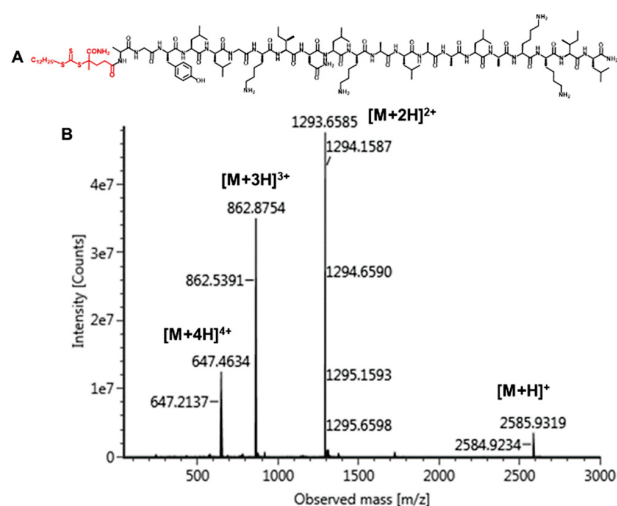


**Figure 1.** (A) Schematic representation of the chemical structure and (B) MS data of TP-CTA.

revealed consistency of the observed mass, with the calculated molar mass demonstrating the successful synthesis of TP-CTA. Though the nitrile (CN) group was hydrolyzed to carboxamide (CONH<sub>2</sub>), a kinetic investigation showed a “living” behavior of the corresponding RAFT polymerization. This kind of reaction was also reported in our previous contribution.<sup>27</sup> Nuclear magnetic resonance (NMR) was also utilized to further determine the structure of TP-CTA (Figures S2 and S3). The <sup>13</sup>C NMR data shown in Figures S3 and S4 indicated that the amino groups of TP-CTA were in the form of trifluoroacetate salts. It is well-known that the RAFT agent could be aminolyzed by primary amines. However, owing to the trifluoroacetate groups, TP-CTA avoids aminolysis during RAFT polymerization.<sup>31–33</sup> Furthermore, the absence of the F peak (ca. –76 ppm) in <sup>19</sup>F NMR investigation demonstrated that trifluoroacetate was easily removed from the obtained polymers by dialysis against sodium chloride solution (Figure S5).

The secondary structure of peptides/proteins is a crucial factor for their biological activity. CD spectra (Figure 2A) of TP-CTA revealed one positive signal (ca. 192 nm) and two negative

signals (ca. 208 and 222 nm), which correspond to a typical  $\alpha$ -helix structure. This is consistent with previous reported results for the TP 10 peptide<sup>22</sup> and also indicates that the CTA modification process does not break the secondary structure of TP 10. During a thermal cycling process, heating from 30 to 80 °C and cooling again back to 30 °C, the ultraviolet–visible (UV–vis; Figure 2B) and CD (Figure 2A) curves at 30 °C almost overlap, demonstrating a high thermostability of TP-CTA in aqueous solution.

To demonstrate the chain transfer ability and effectiveness of the TP-CTA, two distinctive types of polymers (hydrophilic and hydrophobic) were synthesized using oligo(ethylene glycol) methyl ether acrylate (OEGA) and *n*-butyl acrylate (BA) as monomers, respectively. The thermal initiator at low decomposition temperature, 2,2′-azobis[2-(2-imidazolin-2-yl) propane] dihydrochloride, was used, and the polymerization was carried out in *N,N*-dimethylformamide (DMF) at 40 °C. Size exclusion chromatography (SEC) traces of these polymers are shown in Figures S6 and S7. As displayed in Figure 2D,F, the number average molar mass ( $M_n$ ) linearly increased with monomer conversion throughout the course of the polymerization for both monomers. In addition, the corresponding semilogarithmic kinetic plots revealed a linear pseudo-first-order kinetic behavior for both investigated polymerizations (Figures 2C and 3E). Furthermore, all the synthesized polymers showed low dispersity ( $\bar{D}$ ; i.e., <1.25). All these results prove that RAFT polymerizations were efficiently controlled by the TP-CTA RAFT agent.

Rhodamine B acrylate monomer (Figure S8, top) was copolymerized with OEGA to prepare fluorescent polymers for further cell uptake studies. Purified TP-POEGA was obtained by precipitation in *n*-hexane and vacuum drying. Thereafter, a block copolymer TP-POEGA-*b*-PBA was synthesized using TP-POEGA as macroCTA. As shown in Table S1 and Figures S8 (bottom) and S9, pure block copolymers of low  $\bar{D}$  were obtained. SEC traces of the obtained block copolymers are shown in Figure S10. Even though trifluoroacetate eliminates aminolysis of TP-CTA, trifluoroacetate may lead to cytotoxicity. Therefore, the TP-POEGA-*b*-PBA was treated with saturated sodium chloride solution to obtain trifluoroacetate-free copolymers. It is worth noting that the block copolymers maintained a  $\alpha$ -helix structure (Figure 3A). Dynamic light scattering (DLS) results (Figure S11) revealed that TP-POEGA-*b*-PBA self-assembled into nanosized structures in aqueous solution. TEM was used for further investigating the obtained morphologies. As shown in Figure 3B, the block copolymers formed rod-(diameter ~ 60 nm) and vesicle-like (diameter ~ 200 nm) nanostructures. Hinde et al.<sup>34</sup> investigated the effect of polymeric nanoparticle shapes on the efficiency of cell uptake. Their results showed that rods and worms, but not micelles and vesicles, entered the nucleus by passive diffusion. The adequate size (<200 nm), shape, and biosegment of these nanostructures make TP-POEGA-*b*-PBA a good candidate to be developed as a potential drug delivery platform.

In order to evaluate the cytotoxicity of the synthesized block copolymers, HEK293T cells were incubated with these materials for 24 h at different concentrations. Afterward, the AlamarBlue assay was performed (Figure S12). The results showed no obvious cytotoxicity and only at the highest tested concentration of 200  $\mu$ g/mL, a slight increase in cytotoxicity of the polymer with TP 10 was observed. However, these results are over the critical value of 75%, confirming no significant impact of the TP.

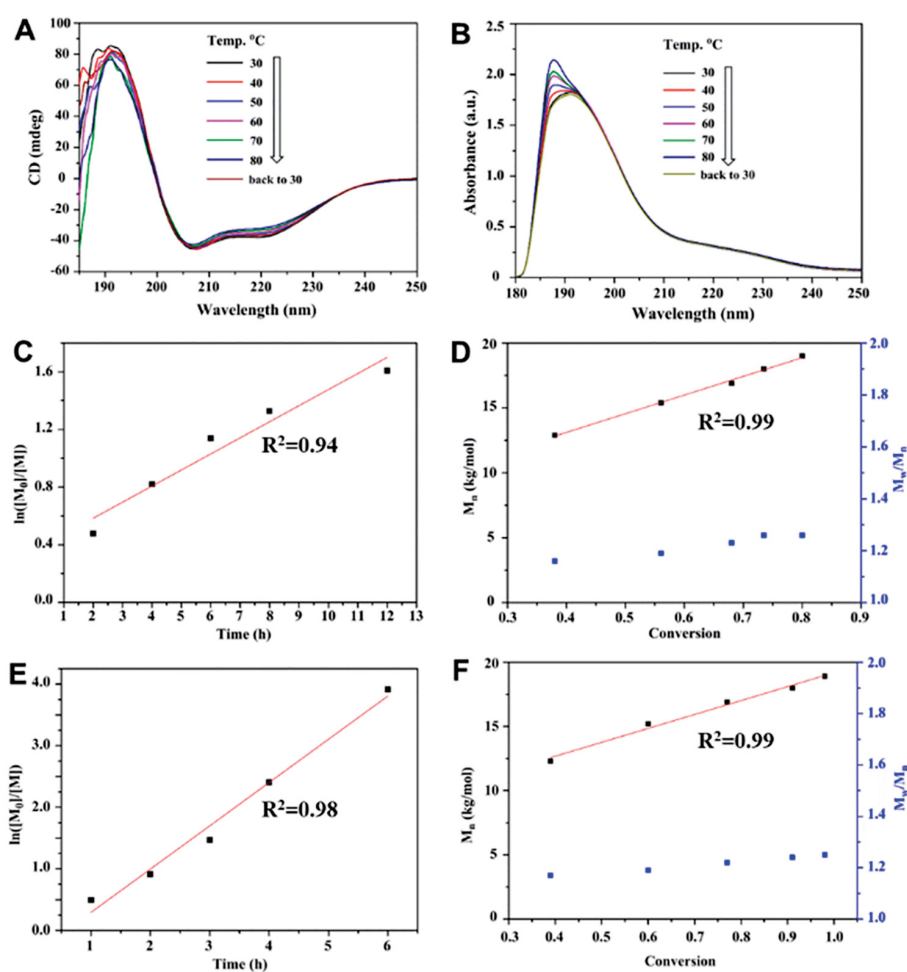


**Figure 2.** (A) CD spectra and (B) UV-vis spectra of TP 10 at different temperatures. Pseudo-first-order kinetics plots for the RAFT polymerization of BA (C) and OEGA (E), and the corresponding  $M_n$  vs the monomer conversion plots of BA (D) and OEGA (F).

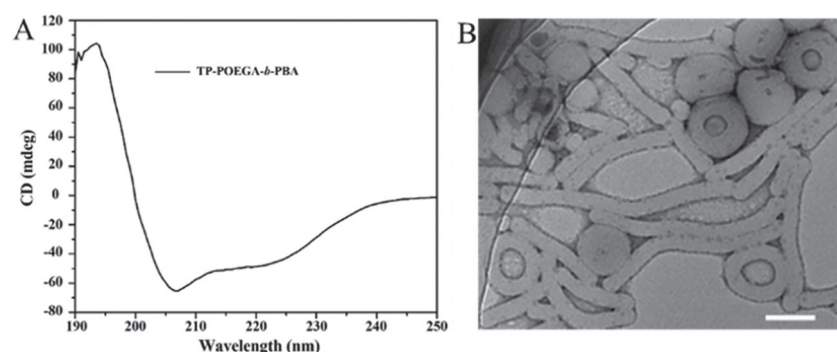


**Figure 3.** (A) CD spectrum of TP-POEGA-*b*-PBA and (B) TEM image for the assemblies of block copolymer. Scale bar: 200 nm.

For quantitative evaluation of cellular uptake, block copolymers were labeled with a rhodamine B fluorescent probe. By detecting the fluorescence intensity of a series of rhodamine B monomer solutions with known concentrations, a standard curve was generated, correlating the fluorescence intensity of rhodamine B with concentration (Figure S13). The equation of the standard curve is  $y = 158678x - 204.87$ , with a correlation coefficient  $>0.99$ . The fluorescence intensities of the block copolymers were detected at the same concentrations (50

mg/mL) using the method described above. Finally, the content of rhodamine B in the block copolymers was calculated using the equation mentioned above. The calculated amounts of rhodamine B in both investigated block copolymers were almost the same (TP-POEGA-*b*-PBA: 0.745  $\mu\text{g}/\text{mg}$  of polymer; POEGA-*b*-PBA: 0.750  $\mu\text{g}/\text{mg}$  of polymer).

Successful cell uptake is known to be a prerequisite for effective drug or gene delivery. For the confirmation of enhanced cellular internalization of the TP 10 functionalized block

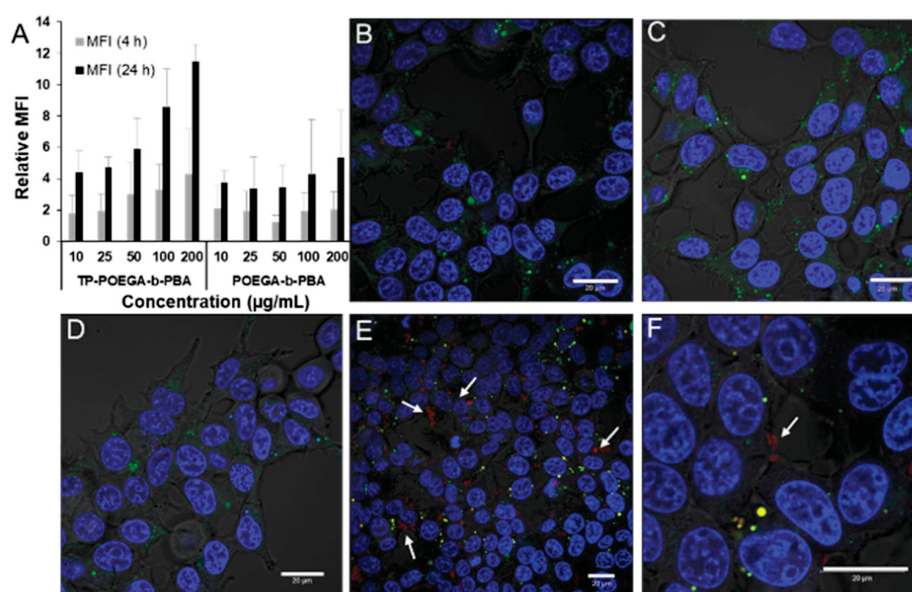


**Figure 4.** Cellular uptake of block copolymers in HEK293T cells. (A) Results of flow cytometry; columns represent mean  $\pm$  SD of  $n = 3$ . (B–F) CLSM images for POEGA-*b*-PBA (B, C), TP-POEGA-*b*-PBA (E, F), and untreated cells (D). Blue: Hoechst-stained nuclei; green: LysoTracker Green stained endolysosomes; red: rhodamine B-labeled polymers. The scale bar is 20  $\mu\text{m}$ . Arrows indicate polymers inside the cells.

copolymers, quantitative cell uptake was investigated via flow cytometry of HEK293T cells, which were incubated with different concentrations of the rhodamine B-labeled polymers for 4 or 24 h. As shown in Figures 4A and S14, the cellular uptake of TP-POEGA-*b*-PBA is higher than that of POEGA-*b*-PBA, which show nearly no uptake. At a high concentration, TP-POEGA-*b*-PBA revealed more than a 3-fold increase in cellular internalization compared to the block copolymer without TP 10. POEGA-*b*-PBA also showed a time and concentration independent uptake behavior. On the contrary, the cellular uptake of TP-POEGA-*b*-PBA strongly depended on the incubation time and polymer concentration. These results demonstrate that the presence of TP 10 highly enhances the cellular uptake of the investigated polymers. The internalization of block copolymers into cells can also be studied by monitoring their fluorescence intensity with the confocal microscopy imaging technique. Therefore, HEK293T cells were incubated with block copolymers for 4 h and stained with Hoechst for nuclei and LysoTracker Green for endolysosomes just before imaging. As shown in Figure 4E, there is more rhodamine B fluorescence in cells treated with TP-POEGA-*b*-PBA than that of the POEGA-*b*-PBA case. A colocalization of polymers in the endolysosomes is demonstrated by an increased yellow fluorescence. This is caused by the overlaying of the green fluorescence of acid organelles as lysosomes and the red fluorescence of labeled polymers. Both polymers showed colocalization with lysoendosomes, although this is stronger in TP-coupled polymers. However, only the incubation with TP-POEGA-*b*-PBA led to exclusively red fluorescing dots (Figure 4, arrows), indicating free polymer inside the cell and, therefore, the direct internalization and enhanced endosomal escape ability of TP-POEGA-*b*-PBA.<sup>35</sup>

In conclusion, a cell penetrating peptide-based RAFT agent, TP-CTA has been successfully synthesized. Linear pseudo-first-order kinetics were observed using TP-CTA as a RAFT agent. Furthermore, well-defined block copolymers TP-POEGA-*b*-PBA and POEGA-*b*-PBA were prepared via RAFT polymer-

ization. Additionally, rod-like and vesicle morphologies were obtained, while TP-POEGA-*b*-PBA self-assembled in an aqueous media. By evaluating the cytotoxicity on HEK293T cells, the prepared block copolymers were proven to be biocompatible. The semiquantitative cell uptake assay via flow cytometry demonstrated enhanced cellular internalization of TP-POEGA-*b*-PBA. Moreover, the block copolymer has been endowed with endosomal escape ability by TP 10 modification. This novel peptide-based RAFT agent might have vast potential for peptide-polymer conjugation and construction of drug/gene delivery systems.

## ■ ASSOCIATED CONTENT

### SI Supporting Information

The Supporting Information is available free of charge at <https://pubs.acs.org/doi/10.1021/acsmacrolett.9b00647>.

Experimental details and additional characterization data, including Table S1 and Figures S1–S14 (PDF)

## ■ AUTHOR INFORMATION

### Corresponding Authors

**Ulrich S. Schubert** – Laboratory of Organic and Macromolecular Chemistry (IOMC) and Jena Center for Soft Matter (JCSM), Friedrich Schiller University Jena, 07743 Jena, Germany; [orcid.org/0000-0003-4978-4670](https://orcid.org/0000-0003-4978-4670); Email: [ulrich.schubert@uni-jena.de](mailto:ulrich.schubert@uni-jena.de)

**Anchao Feng** – Beijing Advanced Innovation Center for Soft Matter Science and Engineering; College of Materials Science and Engineering, Beijing University of Chemical Technology, Beijing 100029, China; [orcid.org/0000-0002-8755-4772](https://orcid.org/0000-0002-8755-4772); Email: [fengac@mail.buct.edu.cn](mailto:fengac@mail.buct.edu.cn)

**San H. Thang** – School of Chemistry, Monash University, Victoria 3800, Australia; [orcid.org/0000-0003-2629-3895](https://orcid.org/0000-0003-2629-3895); Email: [san.thang@monash.edu](mailto:san.thang@monash.edu)

## Authors

**Chao Chen** – Beijing Advanced Innovation Center for Soft Matter Science and Engineering; College of Materials Science and Engineering, Beijing University of Chemical Technology, Beijing 100029, China; [orcid.org/0000-0002-0413-2604](https://orcid.org/0000-0002-0413-2604)

**Friederike Richter** – Laboratory of Organic and Macromolecular Chemistry (IOMC) and Jena Center for Soft Matter (JCSM), Friedrich Schiller University Jena, 07743 Jena, Germany

**Carlos Guerrero-Sanchez** – Laboratory of Organic and Macromolecular Chemistry (IOMC) and Jena Center for Soft Matter (JCSM), Friedrich Schiller University Jena, 07743 Jena, Germany; [orcid.org/0000-0001-6772-4765](https://orcid.org/0000-0001-6772-4765)

**Anja Traeger** – Laboratory of Organic and Macromolecular Chemistry (IOMC) and Jena Center for Soft Matter (JCSM), Friedrich Schiller University Jena, 07743 Jena, Germany; [orcid.org/0000-0001-7734-2293](https://orcid.org/0000-0001-7734-2293)

Complete contact information is available at:

<https://pubs.acs.org/10.1021/acsmacrolett.9b00647>

## Notes

The authors declare no competing financial interest.

## ACKNOWLEDGMENTS

This work was supported by the National Natural Science Foundation of China (21704001), the Fundamental Research Funds for the Central Universities (buctrc201724), and the Beijing Advanced Innovation Center for Soft Matter Science and Engineering. Furthermore, the authors gratefully acknowledge the Bundesministerium für Bildung und Forschung (BMBF, Germany, #13XP5034A PolyBioMik) and the support of the Deutsche Forschungsgemeinschaft (DFG-funded, Germany) through the Collaborative Research Centre Poly-Target (Project No. 316213987, SFB 1278, Projects A04, B01, B02, and Z01).

## REFERENCES

- (1) Stewart, M. P.; Langer, R.; Jensen, K. F. Intracellular Delivery by Membrane Disruption: Mechanisms, Strategies, and Concepts. *Chem. Rev.* **2018**, *118*, 7409–7531.
- (2) Barber, M. A. A Technic for the Inoculation of Bacteria and Other Substances into Living Cells. *J. Infect. Dis.* **1911**, *8*, 348–360.
- (3) Guo, M.; Ehrlicher, A. J.; Jensen, M. H.; Renz, M.; Moore, J. R.; Goldman, R. D.; Lippincott-Schwartz, J.; Mackintosh, F. C.; Weitz, D. A. Probing the Stochastic, Motor-Driven Properties of the Cytoplasm Using Force Spectrum Microscopy. *Cell* **2014**, *158*, 822–832.
- (4) Neumann, E.; Schaefferridder, M.; Wang, Y.; Hofschneider, P. H. Gene Transfer into Mouse Lyoma Cells by Electroporation in High Electric-Fields. *EMBO J.* **1982**, *1*, 841–845.
- (5) Potter, H.; Heller, R. Transfection by electroporation. *Curr. Protoc. Mol. Biol.* **2018**, *121*, 9.3.1–9.3.13.
- (6) Kotterman, M. A.; Chalberg, T. W.; Schaffer, D. V. Viral vectors for gene therapy: translational and clinical outlook. *Annu. Rev. Biomed. Eng.* **2015**, *17*, 63–89.
- (7) Pooga, M.; Hällbrink, M.; Zorko, M.; Langel, Ü. Cell penetration by transportan. *FASEB J.* **1998**, *12*, 67–77.
- (8) Yu, Z.; Yu, B.; Kaye, J. B.; Tang, C.; Chen, S.; Dong, C.; Shen, B. Perspectives and Challenges of Cell-Penetrating Peptides in Effective siRNA Delivery. *Nano LIFE* **2014**, *04*, 1441016–1–1441016–10.
- (9) Copolovici, D. M.; Langel, K.; Eriste, E.; Langel, Ü. Cell-Penetrating Peptides: Design, Synthesis, and Applications. *ACS Nano* **2014**, *8*, 1972–1994.
- (10) Stewart, K. M.; Horton, K. L.; Kelley, S. O. Cell-penetrating peptides as delivery vehicles for biology and medicine. *Org. Biomol. Chem.* **2008**, *6*, 2242–2255.
- (11) Fonseca, S. B.; Pereira, M. P.; Kelley, S. O. Recent advances in the use of cell-penetrating peptides for medical and biological applications. *Adv. Drug Delivery Rev.* **2009**, *61*, 953–964.
- (12) Vives, E.; Schmidt, J.; Pelegrin, A. Cell-penetrating and cell-targeting peptides in drug delivery. *Biochim. Biophys. Acta, Rev. Cancer* **2008**, *1786*, 126–138.
- (13) Green, M.; Loewenstein, P. M. Autonomous functional domains of chemically synthesized human immunodeficiency virus tat trans-activator protein. *Cell* **1988**, *55*, 1179–1188.
- (14) Frankel, A. D.; Pabo, C. O. Cellular uptake of the tat protein from human immunodeficiency virus. *Cell* **1988**, *55*, 1189–1193.
- (15) Deshayes, S.; Morris, M. C.; Divita, G.; Heitz, F. Cell-penetrating peptides: tools for intracellular delivery of therapeutics. *Cell. Mol. Life Sci.* **2005**, *62*, 1839–1849.
- (16) Kurrikoff, K.; Gestin, M.; Langel, Ü. Recent in vivo advances in cell-penetrating peptide-assisted drug delivery. *Expert Opin. Drug Delivery* **2016**, *13*, 373–387.
- (17) Wang, F.; Wang, Y.; Zhang, X.; Zhang, W.; Guo, S.; Jin, F. Recent progress of cell-penetrating peptides as new carriers for intracellular cargo delivery. *J. Controlled Release* **2014**, *174*, 126–136.
- (18) Soomets, U.; Lindgren, M.; Gallet, X.; Hällbrink, M.; Elmquist, A.; Balaspiri, L.; Zorko, M.; Pooga, M.; Brasseur, R.; Langel, Ü. Deletion analogues of transportan. *Biochim. Biophys. Acta, Biomembr.* **2000**, *1467*, 165–176.
- (19) Yandek, L. E.; Pokorny, A.; Florén, A.; Knoelke, K.; Langel, Ü.; Almeida, P. F. Mechanism of the cell-penetrating peptide transportan 10 permeation of lipid bilayers. *Biophys. J.* **2007**, *92*, 2434–2444.
- (20) Islam, M. Z.; Ariyama, H.; Alam, J. M.; Yamazaki, M. Entry of cell-penetrating peptide transportan 10 into a single vesicle by translocating across lipid membrane and its induced pores. *Biochemistry* **2014**, *53*, 386–396.
- (21) Song, J.; Kai, M.; Zhang, W.; Zhang, J.; Liu, L.; Zhang, B.; Liu, X.; Wang, R. Cellular uptake of transportan 10 and its analogs in live cells: selectivity and structure–activity relationship studies. *Peptides* **2011**, *32*, 1934–1941.
- (22) Eiriksdottir, E.; Konate, K.; Langel, Ü.; Divita, G.; Deshayes, S. Secondary structure of cell-penetrating peptides controls membrane interaction and insertion. *Biochim. Biophys. Acta, Biomembr.* **2010**, *1798*, 1119–1128.
- (23) Kilk, K.; EL-Andaloussi, S.; Jarver, P.; Meikas, A.; Valkna, A.; Bartfai, T.; Kogerman, P.; Metsis, M.; Langel, U. Evaluation of transportan 10 in PEI mediated plasmid delivery assay. *J. Controlled Release* **2005**, *103*, 511–523.
- (24) El-Andaloussi, S.; Johansson, H.; Magnusdottir, A.; Järver, P.; Lundberg, P.; Langel, Ü. TP10, a delivery vector for decoy oligonucleotides targeting the Myc protein. *J. Controlled Release* **2005**, *110*, 189–201.
- (25) Jones, S. W.; Christison, R.; Bundell, K.; Voyce, C. J.; Brockbank, S. M.; Newham, P.; Lindsay, M. A. Characterisation of cell-penetrating peptide-mediated peptide delivery. *Br. J. Pharmacol.* **2005**, *145*, 1093–10102.
- (26) Layek, B.; Singh, J. Cell penetrating peptide conjugated polymeric micelles as a high performance versatile nonviral gene carrier. *Biomacromolecules* **2013**, *14*, 4071–4081.
- (27) Chen, C.; Kong, F.; Wei, X.; Thang, S. H. Syntheses and effectiveness of functional peptide-based RAFT agents. *Chem. Commun.* **2017**, *53*, 10776–10779.
- (28) Hentschel, J.; Bleek, K.; Ernst, O.; Lutz, J. F.; Börner, H. G. Easy access to bioactive peptide-polymer conjugates via RAFT. *Macromolecules* **2008**, *41*, 1073–1075.
- (29) Ten Cate, M. G.; Rettig, H.; Bernhardt, K.; Börner, H. G. Sequence-Defined Polypeptide-Polymer Conjugates Utilizing Reversible Addition Fragmentation Transfer Radical Polymerization. *Macromolecules* **2005**, *38*, 10643–10649.
- (30) Klumperman, B. *Encyclopedia of Polymer Science & Technology*; John Wiley & Sons Inc., 2015, DOI: [DOI: 10.1002/0471440264.pst453](https://doi.org/10.1002/0471440264.pst453).
- (31) Alidedeoglu, A. H.; York, A. W.; McCormick, C. L.; Morgan, S. E. Aqueous RAFT polymerization of 2-aminoethyl methacrylate to



produce well-defined, primary amine functional homo- and copolymers. *J. Polym. Sci., Part A: Polym. Chem.* **2009**, *47*, 5405–5415.

(32) He, L.; Read, E. S.; Armes, S. P.; Adams, D. J. Direct synthesis of controlled-structure primary amine-based methacrylic polymers by living radical polymerization. *Macromolecules* **2007**, *40*, 4429–4438.

(33) Liu, G.; Shi, H.; Cui, Y.; Tong, J.; Zhao, Y.; Wang, D.; Cai, Y. Toward rapid aqueous RAFT polymerization of primary amine functional monomer under visible light irradiation at 25° C. *Polym. Chem.* **2013**, *4*, 1176–1182.

(34) Hinde, E.; Thammasiraphop, K.; Duong, H. T.; Yeow, J.; Karagoz, B.; Boyer, C.; Gooding, J. J.; Gaus, K. Pair correlation microscopy reveals the role of nanoparticle shape in intracellular transport and site of drug release. *Nat. Nanotechnol.* **2017**, *12*, 81–89.

(35) Mager, I.; Eiriksdottir, E.; Langel, K.; El Andaloussi, S.; Langel, U. Assessing the uptake kinetics and internalization mechanisms of cell-penetrating peptides using a quenched fluorescence assay. *Biochim. Biophys. Acta, Biomembr.* **2010**, *1798*, 338–343.

## Supporting Information

### A Cell Penetrating Peptide Based RAFT Agent for Constructing Penetration Enhancers

Chao Chen,<sup>a</sup> Friederike Richter,<sup>b,c</sup> Carlos Guerrero-Sanchez,<sup>b,c</sup> Anja Traeger,<sup>b,c</sup> Ulrich S. Schubert,<sup>\*,b,c</sup> Anchao Feng <sup>\*,a</sup> and San H. Thang <sup>\*,d</sup>

<sup>a</sup>Beijing Advanced Innovation Center for Soft Matter Science and Engineering; College of Materials Science and Engineering, Beijing University of Chemical Technology, Beijing 100029 China.

<sup>b</sup>Laboratory of Organic and Macromolecular Chemistry (IOMC), Friedrich -Schiller -University Jena, Humboldtstrasse 10, 07743 Jena, Germany

<sup>c</sup>Jena Center for Soft Matter (JCSM), Friedrich -Schiller -University Jena, Philosophenweg 7, 7743 Jena, Germany

<sup>d</sup>School of Chemistry, Monash University, Clayton Campus, VIC 3800 Australia.

## Experimental Section

### Table of Contents

1. Materials
2. Instrumentation
3. Synthetic Procedures

#### 1. Materials

4-Cyano-4-[(dodecylsulfanylthiocarbonyl)sulfanyl]pentanoic acid (CDTPA) was prepared as previously reported.<sup>1</sup> Acryloxyethyl thiocarbamoyl Rhodamine B (ARhB) was purchased from Polysciences. Oligo(ethylene glycol) methyl ether acrylate (OEGA,  $M_n \sim 480 \text{ g mol}^{-1}$ ; purchased from Sigma-Aldrich) and *n*-butyl acrylate (BA; purchased from Sigma-Aldrich) were purified by stirring in the presence of inhibitor-remover. 2,2'-Azobis[2-(2-imidazolin-2-yl) propane] dihydrochloride (VA-044, AIBI), trifluoroacetic acid (TFA), *N,N*-diisopropylethylamine (DIEA) and triisopropylsilane (TIPS) were purchased from J&K Chemical and used as received. Fmoc-amino acid

derivatives Fmoc-Gly-OH, Fmoc-Ala-OH, Fmoc-Leu-OH, Fmoc-Ile-OH, Fmoc-Tyr(tbu)-OH, Fmoc-Lys(Boc)-OH, Fmoc-Asn(trt)-OH, 2-(1H-benzotriazole-1-yl)-1,1,3,3-tetramethyluronium hexafluorophosphate (HBTU), 2-(7-Aza-1H-benzotriazole-1-yl)-1,1,3,3-tetramethyluronium hexafluorophosphate (HATU, 1-hydroxy-7-azabenzotriazole (HOAt) and Rink amide AM resin (loading: 0.89 mmol/g) were purchased from CS Bio Co. and used as received. All solvents used were obtained from J&K Chemical.

## 2. Instrumentation

NMR spectra were recorded on a Bruker Avance 300 or 400 MHz spectrometer at room temperature.

Purification of products was performed on a preparative Shimadzu HPLC system (LC 20 AR, SIL, SPD) using a Dr. Maisch column (Reprosil-Pur Basic-C18, 250 × 10 mm, 5 μm) with a flow rate of 4 mL/min and a UV-detection at 254 nm (eluent: A: 0.1% TFA in water and B: 0.1% TFA in acetonitrile).

Mass spectrometry was performed on ADC Bioscientific ESI-TOF system. Analysis of the molar mass of the polymer samples were determined by a Shimadzu SEC system (using low dispersity PS as standards) equipped with a SIL-20A auto sampler, a 20 A refractive index detector, three Shodex KF-805L columns (8 × 300 mm, 10 μm, 5000 Å) and one Shodex KF-801 column (8 × 300 mm, 6 μm, 50 Å) using *N,N*-dimethylacetamide (containing 2.1 g/L Lithium Chloride) as eluent at 80 °C with a flow rate of 1 mL min<sup>-1</sup>.

The hydrodynamic sizes of synthesized polymers were determined using dynamic light scattering (DLS) utilizing a Zetasizer Nano ZS (Malvern). The visualized images of the assemblies were obtained from a Hitachi HT7700 microscope with an accelerating voltage of 120 kV.

The fluorescence spectra were recorded on a Hitachi F4600. Circular dichroism (CD) and UV-vis absorption spectra were recorded using a JASCO J-810 spectropolarimeter.

The Peptide was synthesized using a peptide automatic synthesizer (136 XT, purchased from CS Bio Co.).

### 3. Synthetic Procedures

#### 3.1 Synthesis of TP10 peptide functionalized RAFT agents (TP-CTA)

TP10 oligopeptide was synthesized via standard fluorenylmethoxycarbonyl (Fmoc) solid-phase peptide synthesis method on Rink amide AM resin (0.45 mmol). The *N*-terminal Fmoc-protecting group was removed by using 20% piperidine in DMF. For the coupling of Fmoc-protected amino acids, four equivalents of amino acid, 3.8 equivalents of HBTU, and 8 equivalents of DIEA were used. After all the amino acids were linked to the resin, CDTPA was conjugated to the terminal of the oligopeptide using HATU/HOAt/DIEA for activation. Then the conjugates were cleaved by 2 h treatment with a cleavage cocktail of TFA/TIPS/water (95: 2.5: 2.5). The crude TP-CTA could be separated by three times of precipitation in cold diethyl ether. The purification of crude peptide was performed by reverse-phase HPLC using a 20-100% buffer B gradient over 40 min. Analysis of product was performed on the same HPLC system with a Shimadzu column (5 $\mu$ m, 4.6  $\times$  250 mm), employing a 10-90 % buffer B gradient at a flow rate of 1 mL/min.

<sup>1</sup>H NMR (MeOD),  $\delta$  in ppm: 1.25–1.38 (18H, –S–C(=S) S–CH<sub>2</sub>–CH<sub>2</sub>–(CH<sub>2</sub>)<sub>9</sub>–CH<sub>3</sub>; 8H, –CH<sub>2</sub>–(CH<sub>2</sub>)<sub>2</sub>–NH<sub>2</sub>), 1.76 (3H, –CH<sub>3</sub>), 7.12 (2H, *o*-ArH), 6.77 (2H, *m*-ArH). (**Figure S2**)

<sup>13</sup>C NMR (DMSO-*d*<sub>6</sub>),  $\delta$  in ppm: 128 (ArC), 130 (*o*-ArC), 115 (*m*-ArC), 156 (*p*-ArC), 221 (C=S). (**Figure S3**)

#### 3.2 RAFT polymerization of OEGA and BA using TP-CTA as CTA

In a typical procedure, 0.52 mmol (250 mg) of the monomer OEGA, 5  $\mu$ mol (0.62 mg) of AIBI, 0.01 mmol (25 mg) of TP-CTA and DMF (250  $\mu$ L) were added into a Schlenk tube, followed by degassed with three freeze-pump-thaw cycles. Then the sealed tube was placed into a preheated oil bath at 40 °C for a specified time. Finally, the polymerization was quenched using liquid nitrogen. An aliquot of the solution was collected for SEC and <sup>1</sup>H NMR analysis. The PBA was synthesized using the same procedure as POEGA.

#### 3.3 Synthesis of block copolymers using POEGA and BA

A typical block copolymerization procedure is described as follows: 100 mg POEGA macroCTA (POEGA was copolymerized with 1 wt.% ARhB, 8.5  $\mu\text{mol}$ ), BA (200 mg, 1.56 mmol), AIBI (0.55 mg, 1.7  $\mu\text{mol}$ ) and DMF (300 mg) were added to a Schlenk tube. Then the solution was degassed by three freeze-pump-thaw cycles and the sealed tube was placed into a preheated oil bath at 40 °C. After a predetermined time, the polymerization was quenched using liquid nitrogen. The block copolymer was dried under vacuum at room temperature after precipitation in cold *n*-hexane.

#### 3.4 Procedure of polymer self-assembly

Typically, nanoprecipitation method was used to prepare the polymer aqueous solution: 25 mg of the block copolymer were firstly dissolved in 1 mL THF, a good solvent to all blocks. Then 9 mL deionized water was injected at a slow rate (0.9 mL/h) to yield a translucent colloidal solution and the organic phase was finally removed by dialysis against water.

### 4. Biological Studies

#### 4.1 Cell lines and culture conditions

HEK293T cells were routinely cultivated in Dulbecco's minimal essential medium (DMEM, with stable glutamine, Biochrom, Berlin) containing 10 % fetal calf serum (FCS), 100 U/mL penicillin and 100  $\mu\text{g/mL}$  streptomycin. They were maintained at 37 °C in a humidified 5 %  $\text{CO}_2$  atmosphere.

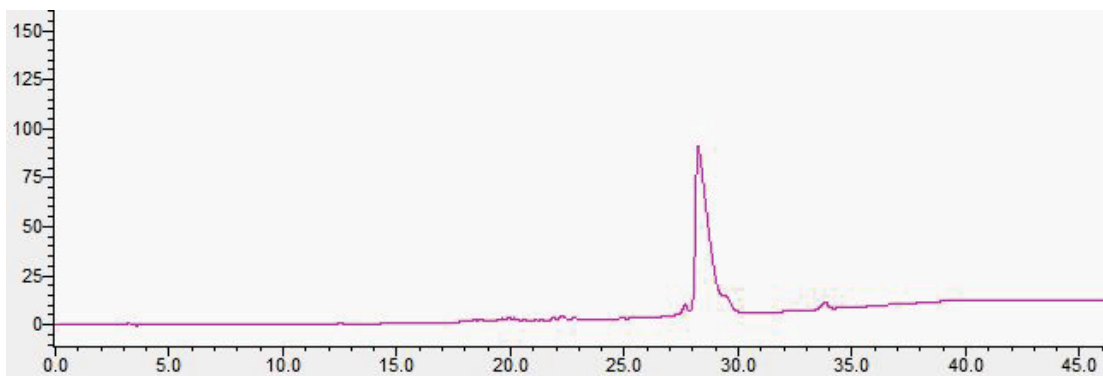
#### 4.2 Determination of cytotoxicity

HEK293T cells were seeded at a density of  $10^5$  cells/mL into a 96-well plate and incubated for 24 h. No cells were seeded in the outer wells. Afterwards, the medium was changed to fresh medium. After one hour, polymer solutions of the indicated concentrations were added and incubated at 37 °C for further 24 h. Control cells were incubated with fresh culture medium or the same amount of DMSO as present in the respective polymer solutions. Subsequently, the medium was replaced by a mixture of fresh culture medium and 10 % alamarBlue™ solution and incubated at 37 °C for another 4 h. Finally, fluorescence was measured at Ex 570/Em 610 nm, with the untreated cells on the same plate serving as negative control. The negative control was standardized as 0 % of metabolism inhibition and referred to as 100 % viability. Cell

viability below 70 % was considered as cytotoxicity. Data are expressed as mean  $\pm$  SD of three independent determinations.

### 4.3 Determination of particle uptake

For uptake studies, HEK293T cells were used. In detail,  $10^5$  cells / mL were seeded in each well of a 24-well plate and cultured for 24 h in growth media. One hour prior to the addition of the polyplexes, the medium was changed to 0.5 mL fresh culture media. Polymers were added to the indicated concentrations and incubated at 37 °C and 5 % CO<sub>2</sub> for 4 and 24 h, respectively. For flow cytometry experiments, the cells were harvested by trypsinization and were resuspended in Phosphate buffered saline (PBS, Biochrom) supplemented with FCS and 10% trypan blue solution to quench outer fluorescence. Viable cells, determined by FSC/SSC gating, were analyzed regarding the mean fluorescence intensity (MFI). The experiments were performed at least three times. For confocal imaging experiments cells were seeded on glass-bottomed dishes (CellView cell culture dishes with four compartments, Greiner bio-one) and were analyzed following 4 h of incubation. To determine intracellular distribution, LysoTracker Green and Hoechst 33342 were added for 10 min to stain the endolysosomes and cell nuclei, respectively. Prior to imaging, 10 % trypan blue was added to quench outer fluorescence of polymers. Live-cell imaging was performed on an LSM880, Elyra PS.1 system. Three color channels were recorded: blue (nucleus, Hoechst 33342,  $\lambda_{\text{Ex}}$  = 405 nm), green (Lysoendosomes, LysoTracker Green,  $\lambda_{\text{Ex}}$  = 488 nm) and red (Polymers,  $\lambda_{\text{Ex}}$  = 561 nm).



### Solid-phase peptide synthesis Procedures

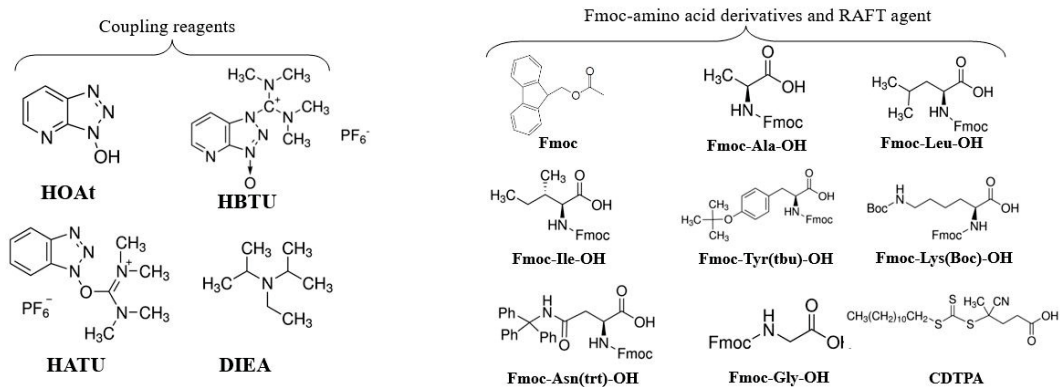
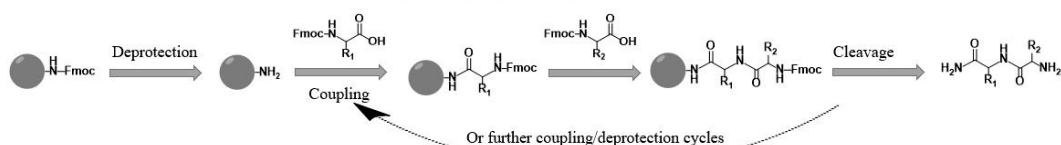


**Figure S1.** HPLC spectrum of TP-CTA (top) and solid phase peptide synthesis procedures and chemicals for the synthesis of TP-CTA (bottom).

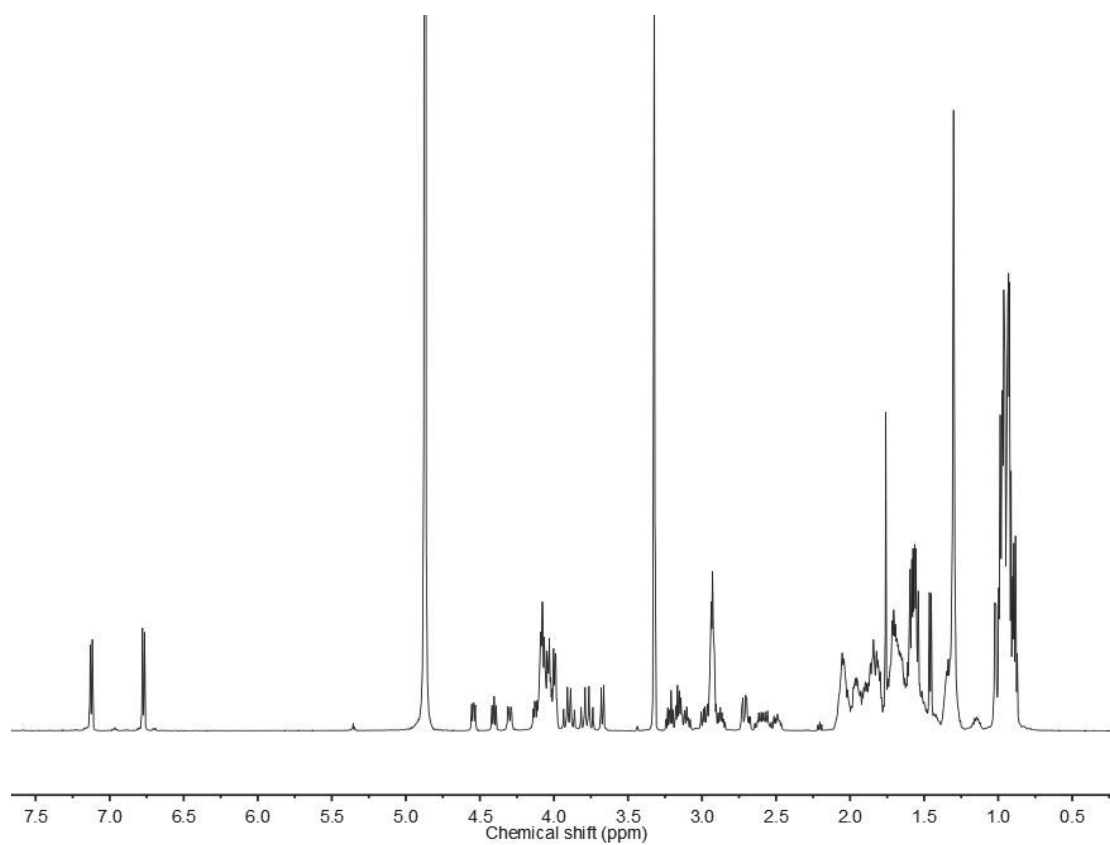


**Figure S2.**  $^1\text{H}$  NMR spectrum of TP-CTA ( $\text{CD}_3\text{OD}$ ).

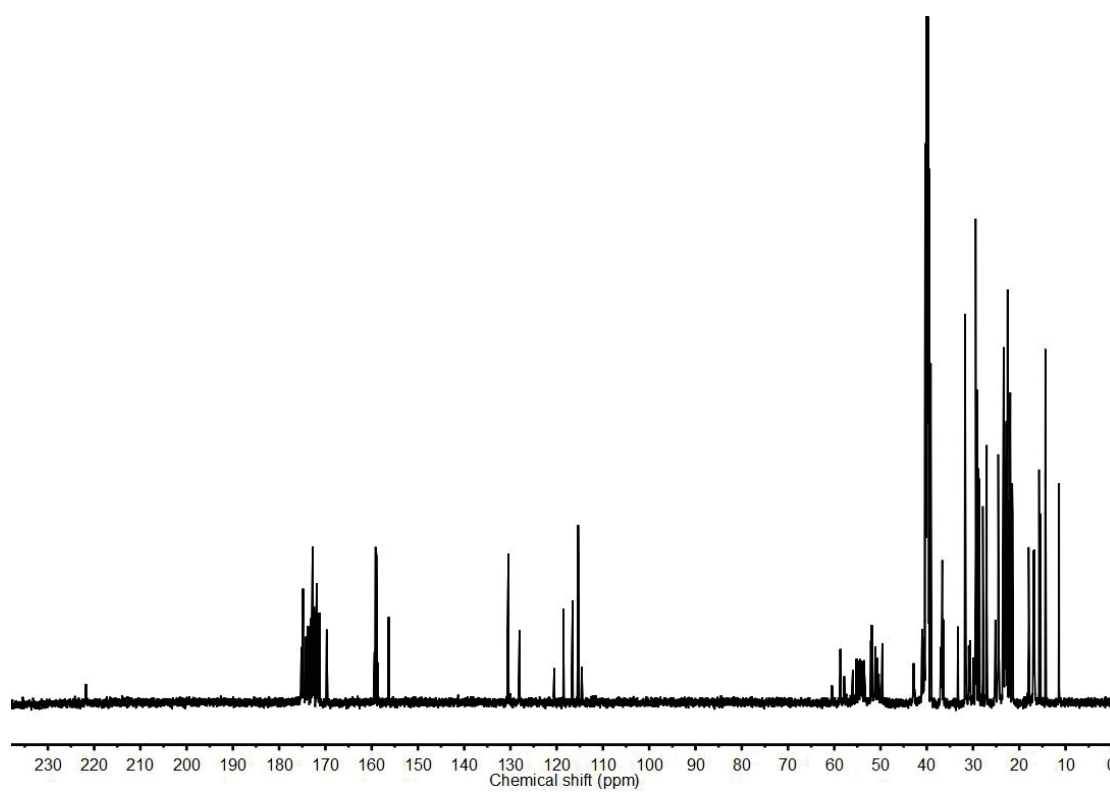


**Figure S3.**  $^{13}\text{C}$  NMR spectra of TP-CTA ( $\text{DMSO}-d_6$ ).



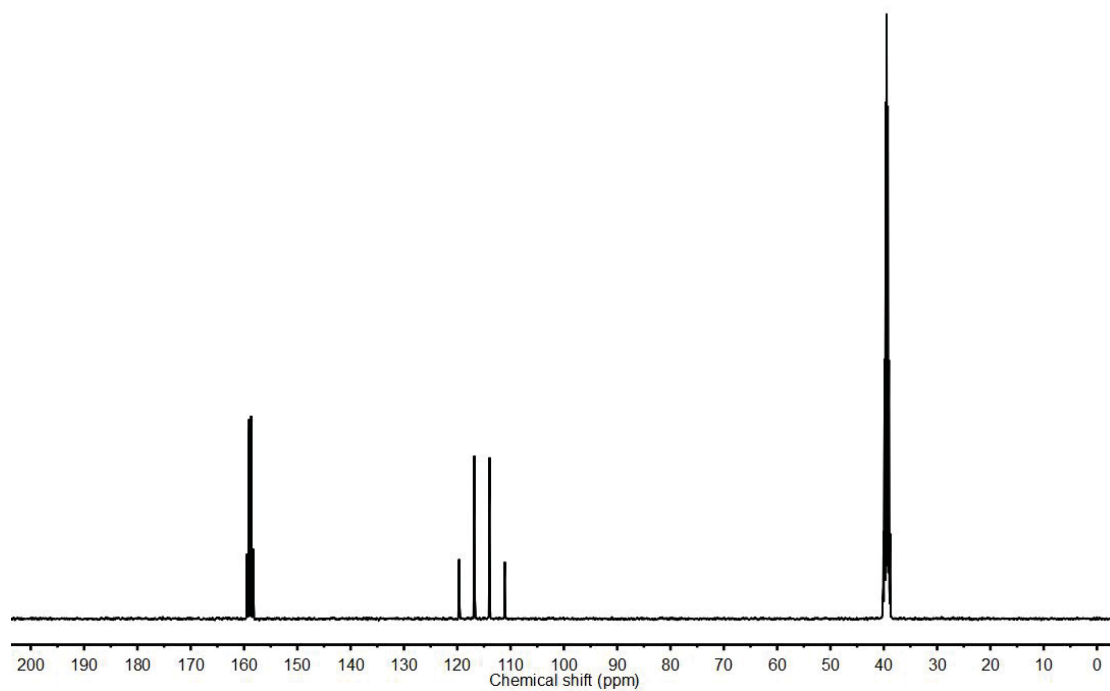


**Figure S4.**  $^{13}\text{C}$  NMR spectrum of TFA ( $\text{DMSO-}d_6$ ).

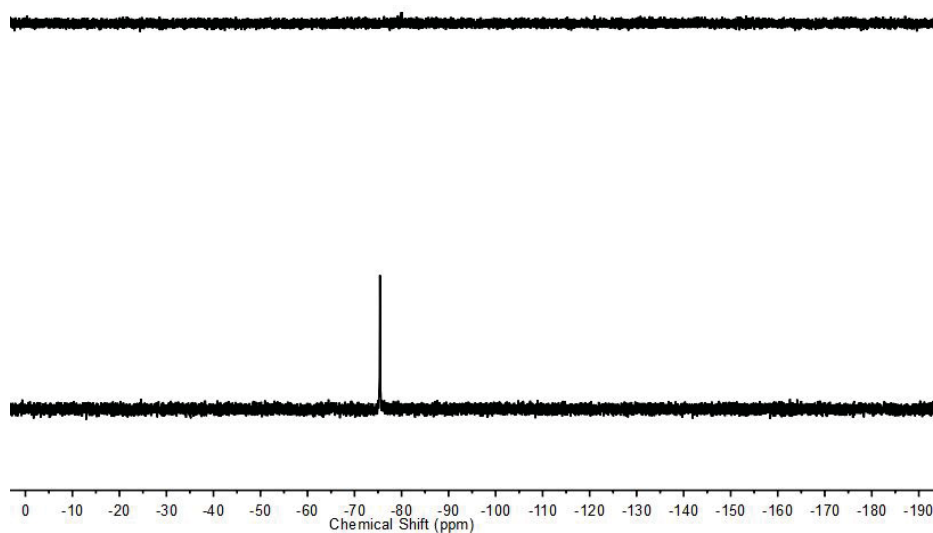


**Figure S5.**  $^{19}\text{F}$  NMR spectrum of pure TP-POEGA-*b*-PBA (bottom) and TP-POEGA-*b*-PBA treated with sodium chloride solution (top).

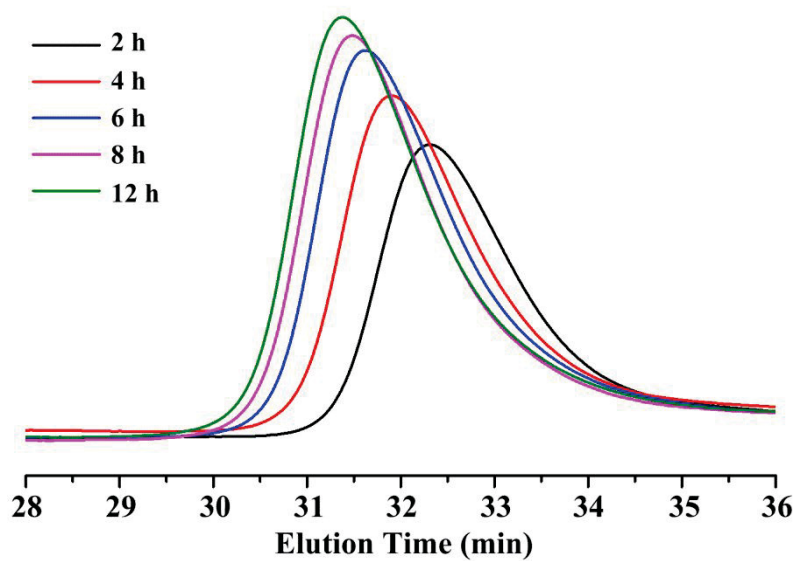


**Figure S6.** SEC traces for the synthesis of PBA using TP-CTA as RAFT agent.

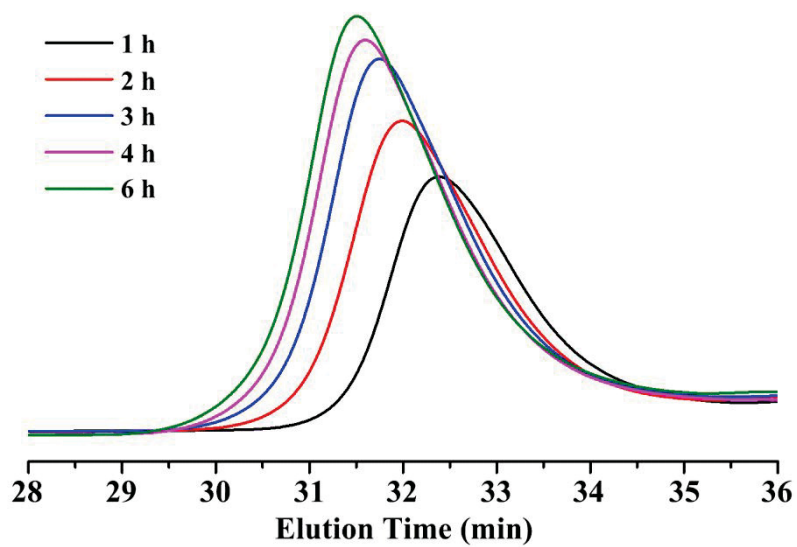


**Figure S7.** SEC traces for the synthesis of POEGA using TP-CTA as RAFT agent.

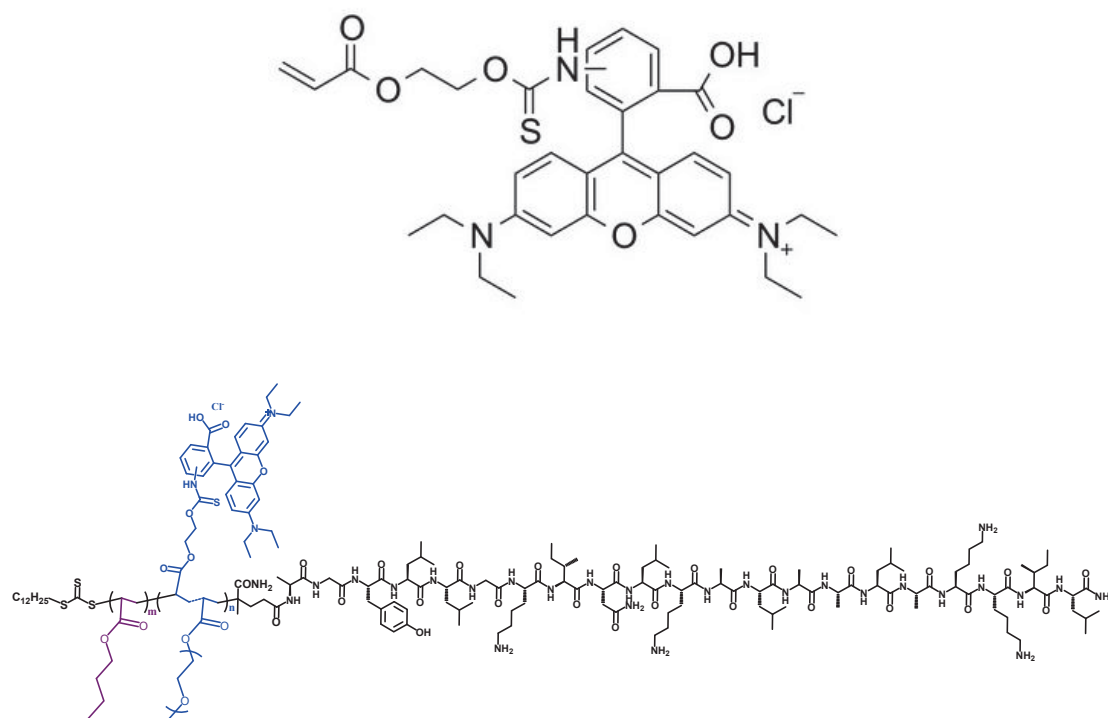


**Figure S8.** The structure of Rhodamine B acrylate (top) and Rhodamine B labeled TP-POEGA-*b*-PBA (bottom).

**Table S1.** Selected characterization data for the block copolymers.

Polymer	$M_n$ (kDa)	$\bar{D}$
TP-POEGA	11.7	1.18
TP-POEGA- <i>b</i> -PBA	36.7	1.27
POEGA	11.2	1.18
POEGA- <i>b</i> -PBA	31.8	1.22

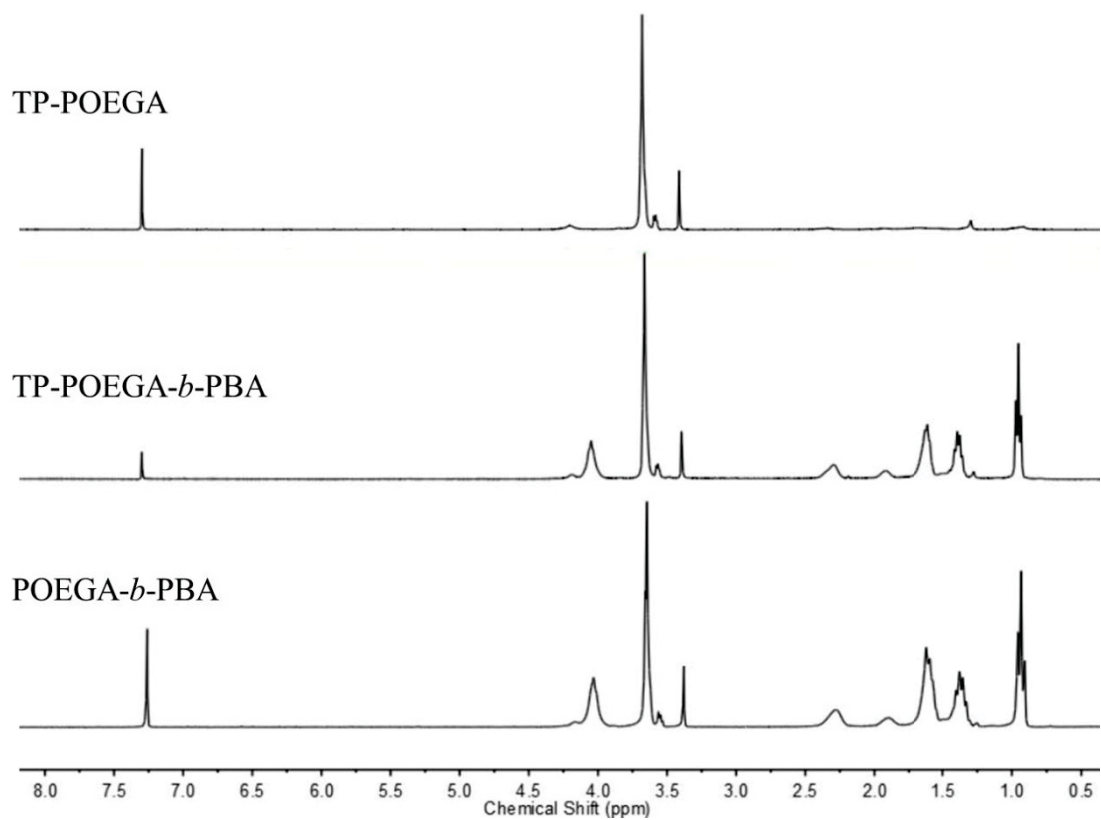


**Figure S9.**  $^1\text{H}$  NMR spectra of TP-POEGA, POEGA-*b*-PBA copolymers with and without TP10 peptides ( $\text{CDCl}_3$ ).

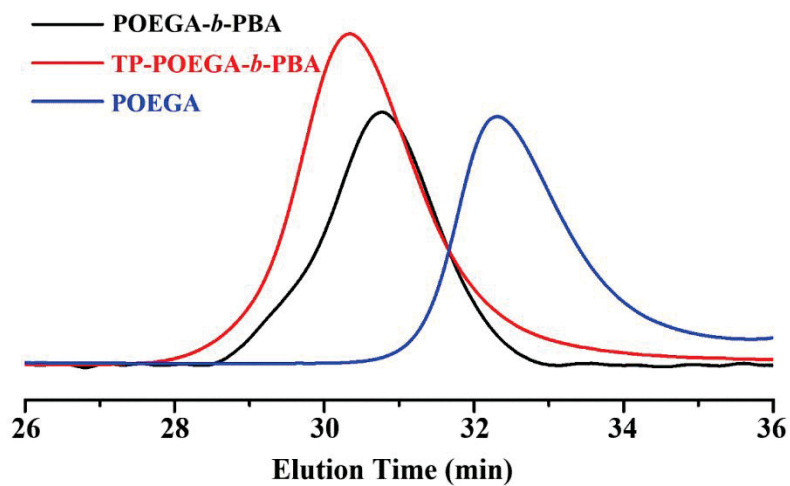


**Figure S10.** SEC traces of POEGA, POEGA-PBA block copolymers with and without TP10.

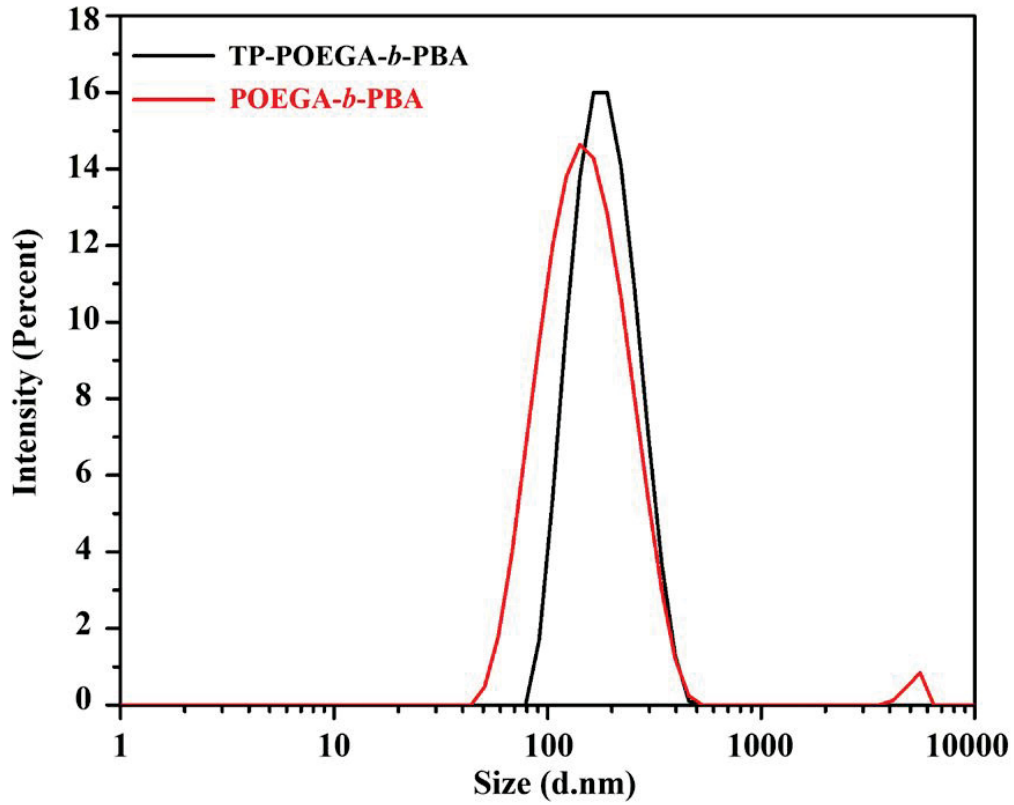


Figure S11. DLS results for block copolymers of TP-POEGA-*b*-PBA and POEGA-*b*-PBA.

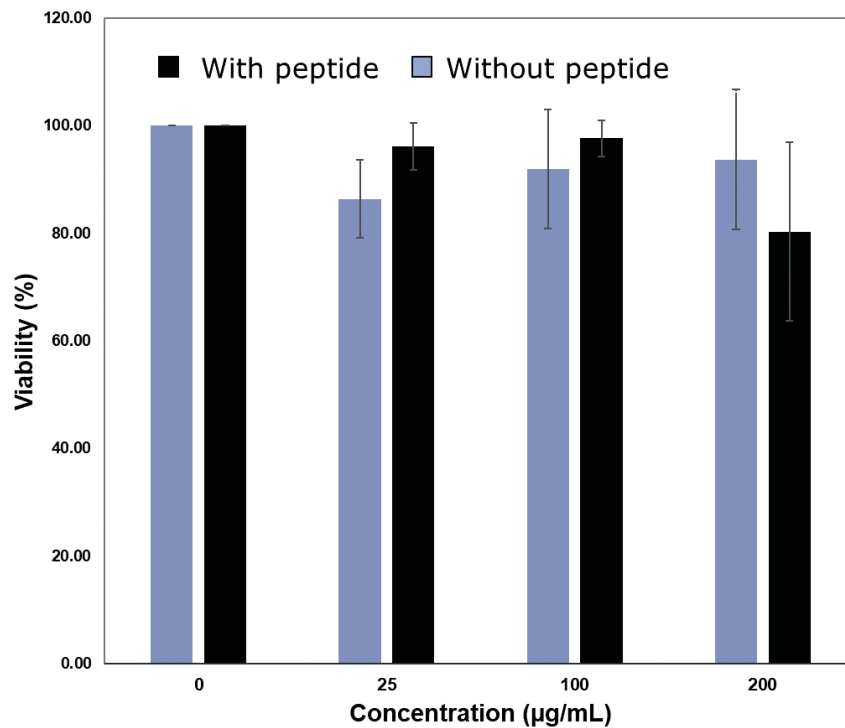
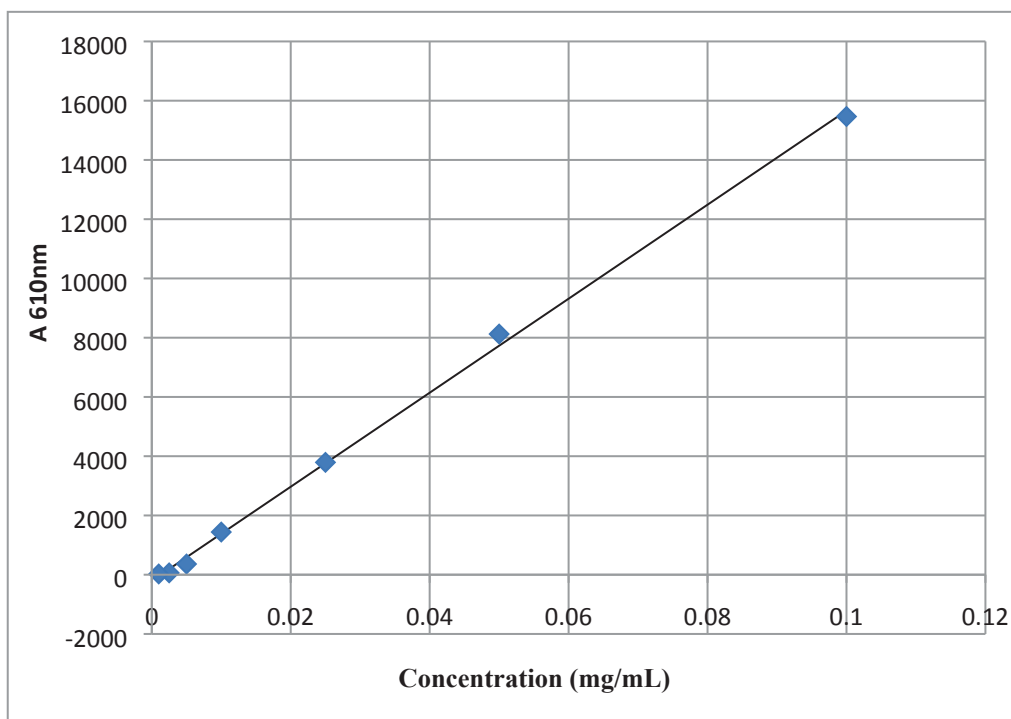
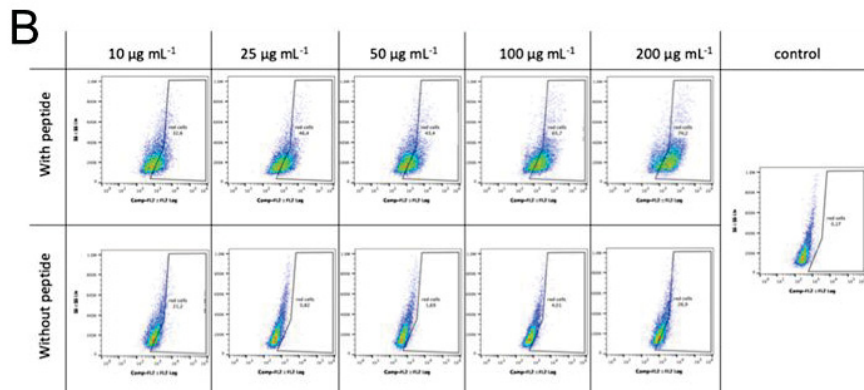
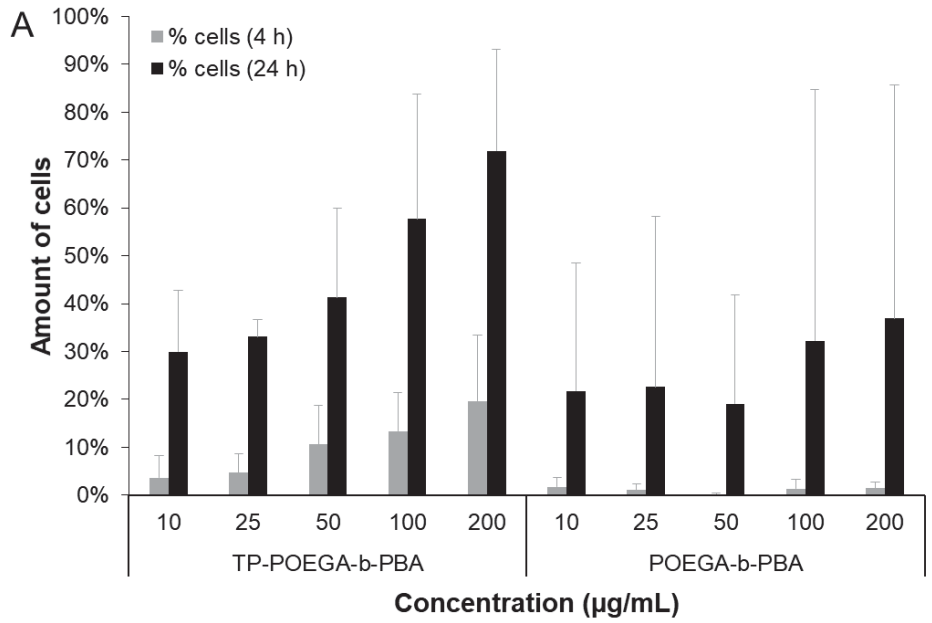


Figure S12. Toxicity of block copolymers in HEK293T cells, measured *via* AlamarBlue assay. Columns represent mean  $\pm$  SD of  $n = 3$ .



**Figure S13.** Standard fluorescence intensity curve of rhodamine B monomer. Data for known concentrations of rhodamine B monomer are used to make the standard curve.

The equation of the standard curve is  $y=158678x-204.87$  with a correlation coefficient  $> 0.99$ .



**Figure S14.** Cellular uptake of block copolymers in HEK293T cells analyzed by flow cytometry. (A) Amount (%) of viable cells taken up respective polymers in a time and concentration dependent manner; mean  $\pm$  SD of  $n = 3$ . (B) Dot blot (SSC vs. Fluorescence) of the time and concentration dependent increase in cells taken up fluorescent polymers.

## Publication Pub1

---

### Tracking the endosomal escape: A closer look at calcein and related reporters

F. Hausig-Punke,<sup>‡</sup> F. Richter,<sup>‡</sup> M. Hoernke, J. C. Brendel, A. Traeger

*Macromol. Biosci.* **2022**, *22*, 2200167.

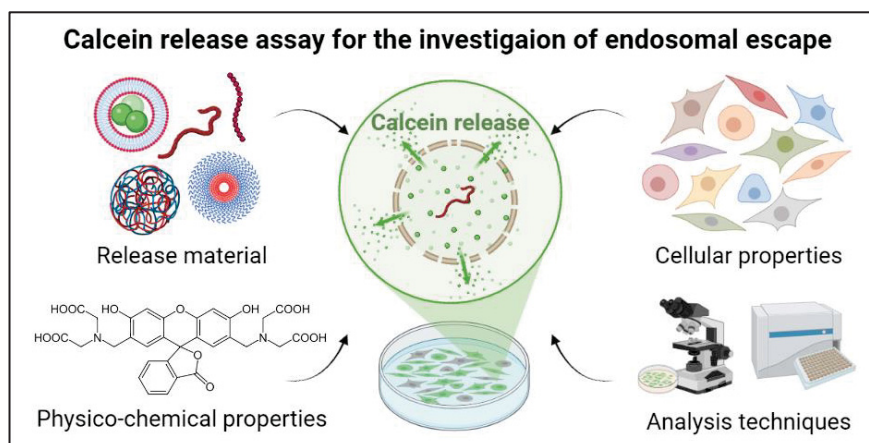
---

Reproduced with permission of John Wiley and Sons (Wiley-VCH GmbH).

Copyright © 2022. The article and the supporting information are available online:

[doi.org/10.1002/mabi.202200167](https://doi.org/10.1002/mabi.202200167)

Note: This paper was declared “as submitted” when this thesis was submitted on the 14.04.2022 and has been published in the meantime.





# Tracking the Endosomal Escape: A Closer Look at Calcein and Related Reporters

Franziska Hausig-Punke, Friederike Richter, Maria Hoernke, Johannes C. Brendel,\* and Anja Traeger\*

Crossing the cellular membrane and delivering active pharmaceuticals or biologicals into the cytosol of cells is an essential step in the development of nanomedicines. One of the most important intracellular processes regarding the cellular uptake of biologicals is the endolysosomal pathway. Sophisticated nanocarriers are developed to overcome a major hurdle, the endosomal entrapment, and delivering their cargo to the required site of action. In parallel, *in vitro* assays are established analyzing the performance of these nanocarriers. Among them, the release of the membrane-impermeable dye calcein has become a popular and straightforward method. It is accessible for most researchers worldwide, allows for rapid conclusions about the release potential, and enables the study of release mechanisms. This review is intended to provide an overview and guidance for scientists applying the calcein release assay. It comprises a survey of several applications in the study of endosomal escape, considerations of potential pitfalls, challenges, and limitations of the assay, and a brief summary of complementary methods. Based on this review, it is hoped to encourage further research groups to take advantage of the calcein release assay for their own purposes and help to create a database for more efficient cross-correlations between nanocarriers.

In particular the nucleic acid-based systems, such as the SARS-CoV-2 vaccines or novel cancer therapies underline the enormous potential of this technology. Despite the current success of lipid-based gene carriers, the number of papers on polymer-based gene carriers is also constantly increasing due to their impressive versatility and stability. For the successful delivery of nucleic acids, several challenges need to be addressed, including nanoparticle formulation, targeting, intracellular release, and transport to its destination. Especially, the intracellular processes represent a key aspect, which surprisingly are still not well understood. Therefore, no consistent theory can be applied to the various nanocarrier systems, but two aspects predominate among the cellular barriers, cellular uptake, and endosomal release. Further hurdles may also play a role such as the transfer of genetic material into the cell nucleus, which can be neglected in mRNA/siRNA applications, because their site of action is inside


## 1. Introduction

The field of nonviral nanocarriers for the delivery of nucleic acids into cells has made great progress in the last decades.

F. Hausig-Punke, F. Richter, J. C. Brendel, A. Traeger  
 Laboratory of Organic and Macromolecular Chemistry (IOMC)  
 Friedrich Schiller University Jena  
 Humboldtstrasse 10, 07743 Jena, Germany  
 E-mail: johannes.brendel@uni-jena.de; anja.traeger@uni-jena.de

F. Hausig-Punke, F. Richter, J. C. Brendel, A. Traeger  
 Jena Center for Soft Matter (JCSM)  
 Friedrich Schiller University Jena  
 Philosophenweg 7, 07743 Jena, Germany

M. Hoernke  
 Chemistry and Pharmacy  
 Albert-Ludwigs-Universität Freiburg  
 Hermann-Herder-Str. 9, 79104 Freiburg i.Br., Germany

 The ORCID identification number(s) for the author(s) of this article can be found under <https://doi.org/10.1002/mabi.202200167>

© 2022 The Authors. Macromolecular Bioscience published by Wiley-VCH GmbH. This is an open access article under the terms of the Creative Commons Attribution-NonCommercial License, which permits use, distribution and reproduction in any medium, provided the original work is properly cited and is not used for commercial purposes.

DOI: 10.1002/mabi.202200167

the cytosol. Cellular uptake is obviously fundamental and depends on the physicochemical parameters of the nanocarrier or the introduction of active target components, which is well reviewed elsewhere.<sup>[1–4]</sup> However, successful uptake into cells does not necessarily correlate with efficient gene expression. Therefore, escape from the endo-lysosomal compartment is considered as a critical cellular step for the successful carrier-dependent delivery of sensitive cargos, such as genetic material or proteins.<sup>[5]</sup> The main reasons are, on the one hand, the risk of enzymatic degradation and, on the other hand, the fact that genetic material can only exert its effect outside the endosomes. Unfortunately, several nanocarriers fail in this regard, as they are either excreted (exocytosis) or degraded (lysosome), which means that endosomal release can be considered an important lever for improving cellular gene delivery.<sup>[6–8]</sup> In this review, we refer to the general term nanocarrier, although not all mentioned materials may contain a cargo as it is implied for carriers. The term comprises all compounds that promote endosomal release and include lipid-based materials (liposomes, lipid nanoparticles), polymer-based materials (linear or branched polymers, polymersomes, micelles, nanoparticles and peptides), as well as peptide-based materials.

In order to optimize the design of nanocarriers, the biological processes must be considered in more detail, because they determine the conditions the nanocarriers have to deal with.

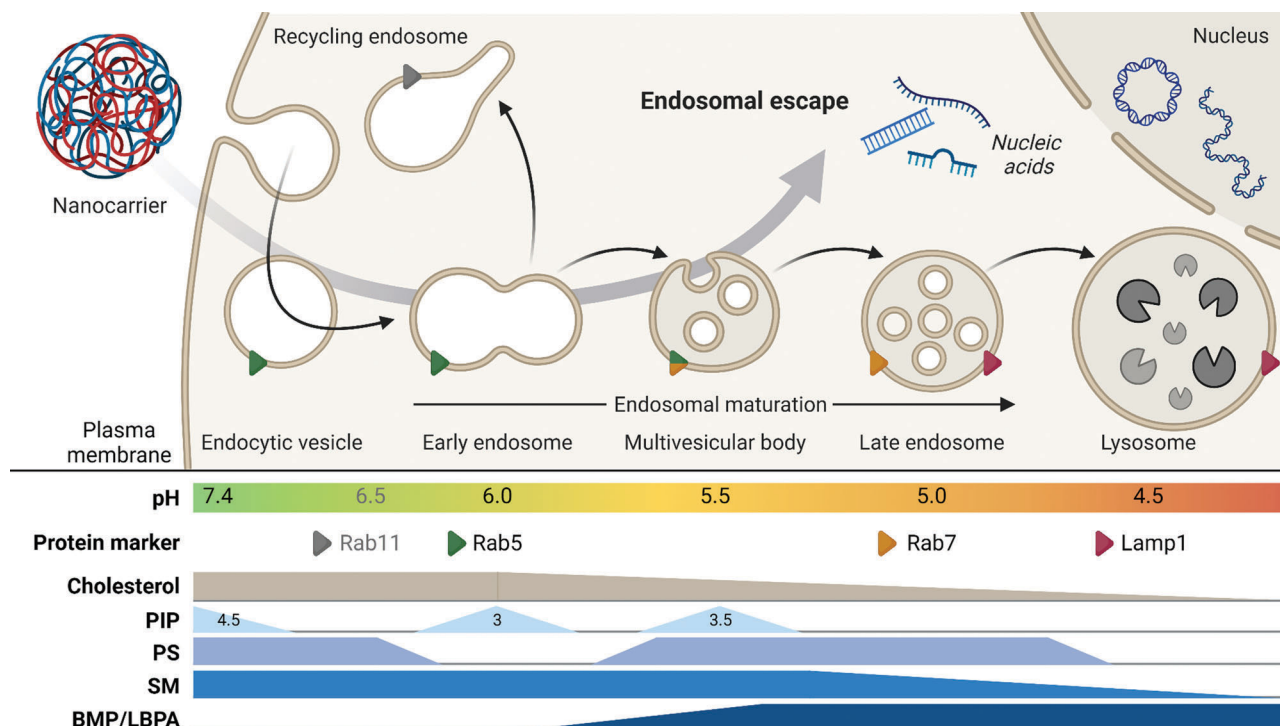


**Figure 1.** Endosome maturation. Following endocytosis, the endocytic vesicle delivers the internalized cargo to the early endosome, where it is either recycled through the recycling endosome or evolves further along the endolysosomal pathway to be degraded. Beside the fusion of different vesicles and membrane invagination, this is accompanied by changes in the intravesicular pH value, membrane lipid composition, and important protein markers. To avoid the enzymatic degradation within the lysosome, the nanocarrier (representative for polymers, liposomes, nanoparticles) delivering drugs or nucleic acids, thus, must escape this process at an earlier stage. PIP—phosphoinositides (numbers indicate phosphate positions on the inositol ring), PS—phosphatidylserine, SM—sphingomyelin, BMP/LBPA—bis(monoacylglycerol)phosphate/lysobisphosphatidic acid. Adapted with permission.<sup>[16]</sup> Copyright 2014, Elsevier.

Particles as well as liquids, solutes, macromolecules, or plasma membrane components are taken up by the cell through endocytosis, in which the plasma membrane is first invaginated and then segregated, allowing for the formation of intracellular vesicles.<sup>[4,9]</sup> Besides their role in nutrient uptake, endosomes are involved in the regulation and fine-tuning of numerous signaling pathways in the cell, e.g., the recycling of receptors. After vesicle formation, they fuse to form early endosomes and become linked to the microtubule network.<sup>[10]</sup> In this way, the vesicles and their cargos are able to move alongside the microtubules toward the perinuclear region and gradually transform into late endosomes, where hydrolases and membrane components of the secretory pathway are recruited. Subsequently, they enlarge in size, form more intraluminal vesicles and finally fuse with the lysosome to form the endolysosomes.<sup>[9]</sup> During endosomal maturation, the size of endocytic vesicles increases from  $\approx 100$  nm (early endosome) to  $\approx 1000$  nm (lysosome).<sup>[9,11–13]</sup> Inside the endolysosomes a variety of digestive processes take place, which degrade most compounds of biological origin and, thus, represent a dead end for the nanocarriers which should be avoided. During endosomal maturation, not only the size and structure of the organelles change, but more importantly the intravesicular pH value and the composition of the membrane, both, in terms of proteins and lipids (see **Figure 1**).<sup>[9,14]</sup> In early endosomes, the membrane consists mainly of neutral lipids (including sphingolipids, sterols), similar to the cytoplasmic

membrane. Along with the acidification of the vesicles (from 7.4 to 4.5), the proportion of sterols decreases leading to an increase in membrane fluidity. Furthermore, the proportion of anionic lipids (e.g., lysobisphosphatidic acid (LBPA), also termed bis(monoacylglycerol)phosphate (BMP)) increases.<sup>[15–18]</sup> This increase in LBPA during endosomal maturation was identified as critical for the mode of endosomal escape.<sup>[19,20]</sup>

This complex process is exploited by viruses, which can thus enter the cell in an optimized way and reprogram it without destroying it. Viruses cross the endosomal membrane by a pH-dependent change of conformation or hydrophobicity of their surface peptides leading to penetration of the vesicular membrane. This inspired material designers to mimic the efficiency of viral systems and optimize them with a lower risk potential, e.g., in the form of cell-penetrating peptides (CPPs), liposomes, synthetic polymers, and nanoparticles.<sup>[21,22]</sup> To circumvent lysosomal digestion, pH-dependent cationic amines were commonly included in polymers or lipids. Along the endosomal pathway, the amines become increasingly protonated and enable electrostatic interactions with anionic lipids or facilitate hydrogen bonding between the amino groups of the nanocarrier and the phosphate groups of the lipids. Hence, the nanocarriers can interact locally with the membrane destabilizing it and, thereby, promoting the escape of the nanocarriers and their cargos into the cytoplasm.<sup>[23]</sup> Furthermore, the “proton-sponge” hypothesis remains an accepted explanation for the endosomal

release of some polymers. The buffering capacity of polycations is considered to cause a change in vesicular pH and an influx of ions, which increases the osmotic pressure and eventually causes a rupture of the lipid membrane.<sup>[24]</sup> However, this hypothesis is under debate in the community.<sup>[25]</sup> Comparison of polymers with different buffer capacities revealed that a reduction in buffer capacity toward the early endosomal pH range was often associated with higher transfection efficiencies,<sup>[26–28]</sup> although high buffer capacities at low pH values along the endolysosomal pathway were identified as not beneficial.<sup>[29]</sup> However, it should be noted that any modifications to the polymers may have affected the performance of the carrier at the level of intracellular barriers upstream or downstream of the endosomal exit (vector packing and unpacking, endocytosis rates, changes in hydrophobicity). In addition, the read-out of the transfection may not be the best approach to evaluate the proton sponge effect. Others have questioned the validity of the proton sponge hypothesis by considering endosomal acidification. While some studies have demonstrated the necessity of acidification for the escape of poly(ethylenimine) (PEI) polyplexes,<sup>[8,26,30–32]</sup> other researchers investigated the effect of buffer polymers on the actual pH in endosomes. Several reports showed that endosomal acidification was slowed down after administration of buffer polymers, while the pH of endosomes containing a nonbuffering polymer decreased more rapidly.<sup>[28,30]</sup> However, these observations have been questioned by other authors because buffering polymers are not able to increase endolysosomal pH, which could refute the proton sponge effect.<sup>[25,33]</sup> In addition, there is a debate about the lack of colocalization with LysoTracker in microscopy images, as the buffering effect of the polymer inhibits staining with acidotropic dyes such as LysoTracker,<sup>[34,35]</sup> because even if the polymers have a buffering effect in endosomes, this is no guarantee that the pH of the vesicle will remain elevated.<sup>[25,36]</sup>

For the detailed investigation of the cellular fate of nanoparticles and in particular the endosomal release, different techniques can be applied. Predominantly, the integrity of the endosomal membrane is evaluated for endosomal escape. Related experiments can be performed in cells, isolated cell organelles and artificial or model vesicles. The latter represents a more controlled and reproducible environment since endosomes can be modeled by liposomes with membranes of known phospholipid composition. The variety of applied methods can be found elsewhere.<sup>[37,38]</sup> However, the potency and limitations of each approach should be kept in mind. In the case of gene delivery, the expression or functionality of the genetic material (e.g., expression or knock down) is one possible test, representing a global read-out and functionality. Fluorescent dyes/proteins or reporter systems can be used additionally to study endosomal release in more detail.<sup>[5,39–44]</sup> Although they might not exactly match the intended cargos of the investigated nanocarrier with regard to size, charge or hydrophilicity and, hence, might not reflect its real cargo delivery potential, they can be used as well-available and less expensive model molecules for the investigation of the release mechanism. The most popular sensor molecule is calcein, which is straightforward to apply, affordable, and easily accessible. Therefore, it is used to study a variety of different nanocarriers.

However, different experimental settings, conditions, and analytical methods are used for this purpose, which makes it difficult to evaluate/compare different materials. In this review, we eluci-

date the key application of calcein as a powerful yet simple tool to investigate the endosomal escape. Various conditions have been reported, which reflects the complexity of the calcein release assay and sometimes might even cause contradictory outcomes. In Sections 2–5, calcein is first introduced regarding its basic chemistry and historical development, followed by overviews of the different applied methods in models or cells, and a section reflecting on pitfalls, challenges, and limitations of the calcein release assay within the cellular environment. A few complementary methods are described in Section 6, which certainly does not represent a comprehensive overview, but provides some guidance to alternatives overcoming the previously mentioned issues.

## 2. Chemical Background of Calcein

Calcein, also known as bis[*N,N*-bis(carboxymethyl)aminomethyl] fluorescein, fluorescein complexone, and fluorexon, was first described by Diehl and Ellingboe in 1956 as an indicator for the complexometric titration of calcium<sup>[45,46]</sup> followed by several Ph.D. theses at the Iowa State University with detailed descriptions regarding its synthesis, characterization and applications (Figure 2).<sup>[47–50]</sup> It is synthesized via a Mannich-type condensation of fluorescein, formaldehyde, and iminodiacetic acid and can, thus, be considered as a derivative of fluorescein belonging to the substance class of xanthenes.<sup>[45,48,51]</sup> Due to the condensation reaction, calcein combines two features within one molecule: the fluorescence of fluorescein and the chelation property of iminodiacetic acid, which is also part of the well-known chelator ethylenediaminetetraacetic acid (EDTA).<sup>[48]</sup> Comparable to fluorescein, calcein absorbs light in the cyan spectrum range and fluoresces in the green range with absorption and emission maxima at  $\lambda_{\text{Ex/Em}} = 495/515 \text{ nm}$ .<sup>[47,52]</sup> The self-quenching of fluorescein at high concentrations, known since 1888,<sup>[53–55]</sup> also characterizes calcein and other derivatives, such as 6-carboxyfluorescein (Figure 3A, 1). This property has been exploited since the late 1970s to investigate the stability of liposomes encapsulating 6-carboxyfluorescein<sup>[56,57]</sup> or calcein,<sup>[58,59]</sup> as a damage of the liposomal membrane would result in dilution of the dye and an increase in its fluorescence intensity. Regarding calcein, a self-quenching concentration of 70  $\mu\text{M}$  is often utilized,<sup>[60,61]</sup> but there are also studies showing different values which could be attributed to different buffer systems and fluorescence measurement methods (Table 1).

Another factor influencing the fluorescence of calcein is the pH value (Figure 3A, 2). However, with the six carboxy groups available for protonation, the fluorescence of calcein is less pH dependent than that of fluorescein and exhibits high intensities between pH 4.5 and 10.<sup>[47,50,69]</sup> Therefore, it remains fluorescent within the biologically relevant pH range including endolysosomal pH values important for the analysis of endosomal escape. Additionally, the carboxy moieties lead to a higher polarity and increased hydrophilicity of calcein compared to fluorescein (for TPSA and logP values refer to Figure 2A) and, thus, make it less membrane permeable at low pH values.<sup>[57,70,71]</sup> The pH value also affects the solubility in water of calcein with higher pH values leading to a better solubility.<sup>[50]</sup>

In addition, the calcein fluorescence is influenced by various di- or multivalent metal ions, more precisely by their chelation which has been used for the determination of the cations in

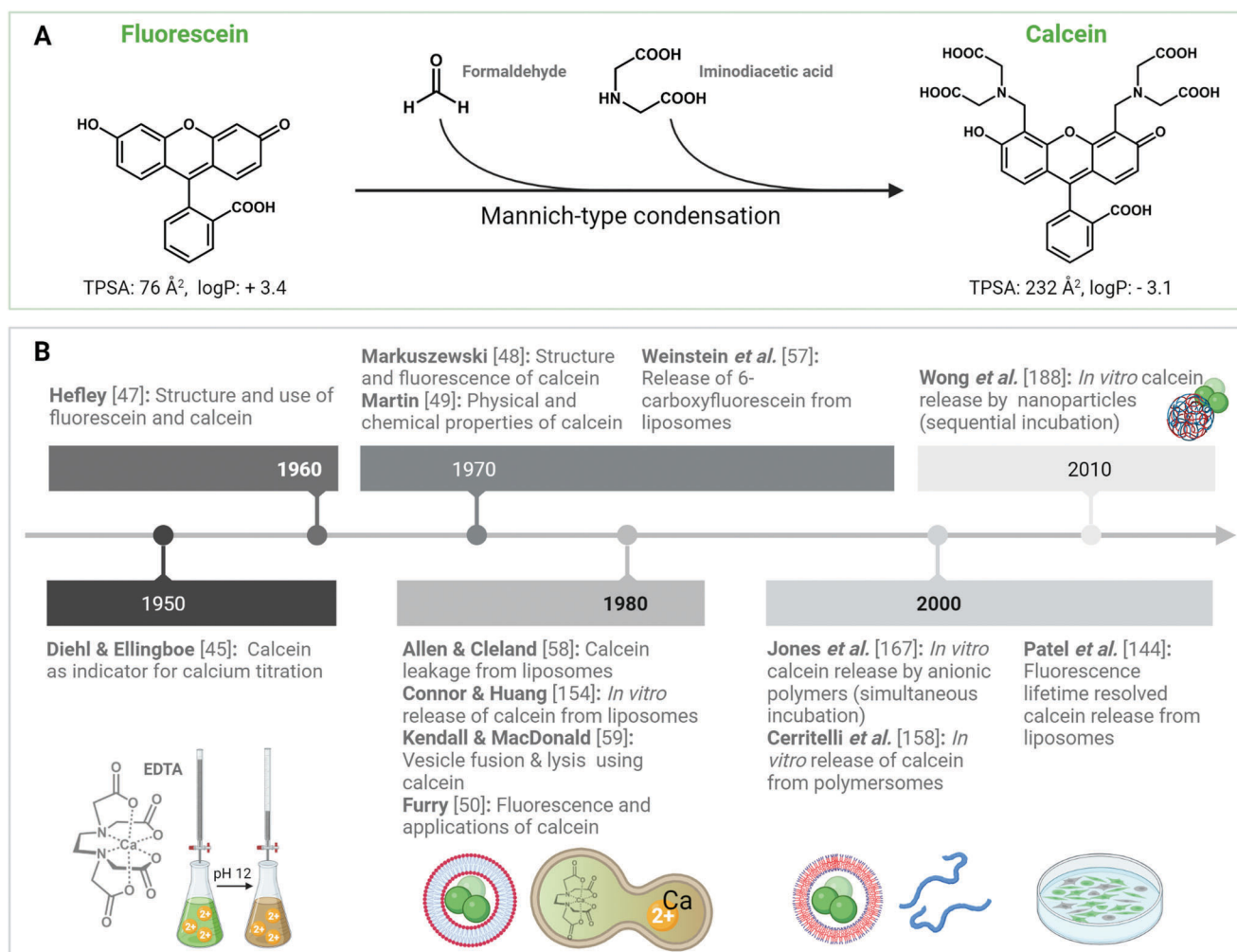


**Figure 2.** Synthesis and utilization of calcein. A) The synthesis route of calcein starting from fluorescein with indicated polarity (TPSA: topological polar surface area) and hydrophobicity measures for both molecules. B) Historical overview on the development of calcein as a fluorescent molecule and its utilization to investigate endosomal escape.

various tissues and fluids (Figure 3A, 3). The complexation of the cations has two different effects, which in turn are pH and concentration dependent.<sup>[52]</sup> Under the tested conditions, the ions of the alkaline earth metals magnesium, calcium, barium, and strontium enhance the calcein fluorescence at alkaline pH values when calcein would otherwise be quenched.<sup>[49,50,69]</sup> At neutral pH values and metal:calcein ratios of 4 or 10:1, however, these ions only influence the absorption spectrum in the UV range but not the fluorescence of the brightly emitting calcein.<sup>[69]</sup> By contrast, ions of the transition metals manganese, cobalt, nickel, copper,<sup>[49,69,72,73]</sup> and iron<sup>[50,74–76]</sup> have been shown to quench the fluorescence in liposomes at neutral pH values. Furthermore, ions with higher valencies are able to increase the fluorescence intensity of calcein, such as aluminum ions at low pH values.<sup>[49,69,77]</sup> On the other side, the addition of sodium can enhance fluorescence at high pH values. Interestingly, potassium or lithium ions, however, do not affect the fluorescence, favoring KOH solutions over NaOH solutions to dissolve the calcein.<sup>[52,78]</sup> Besides calcein, there are also other combinations of the iminodiacetic acid and various dyes that can be used to

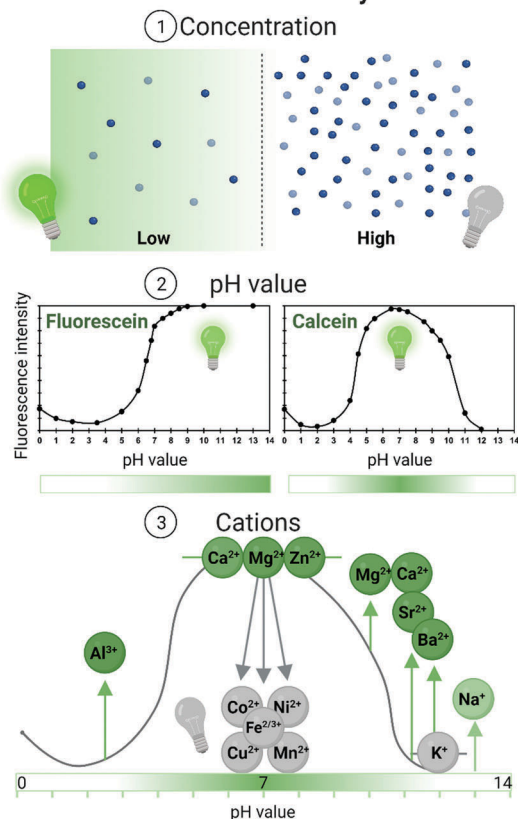
chelate cations, such as calcein blue (umbellikomplexon),<sup>[79–83]</sup> or Calcium Green, Calcium Orange, and Fluo-3 (Figure 3B).<sup>[84–86]</sup>

Besides the determination of cations, calcein, or more precisely its acetoxymethyl ester (calcein AM) is also used to identify viable cells. In contrast to calcein, the hydrophobic and nonfluorescent calcein AM is membrane permeable (Figure 3C). Upon entering the cells, the esters of calcein AM are hydrolyzed by non-specific intracellular esterases active only in living cells resulting in the fluorescent calcein that cannot easily permeate the cellular membrane and is retained within the cells.<sup>[87–90]</sup> Similarly, this method is also used to determine the membrane integrity of cells by preloading the cells with calcein AM/calcein and measuring the release of calcein upon membrane destruction by various substances.<sup>[91–93]</sup>

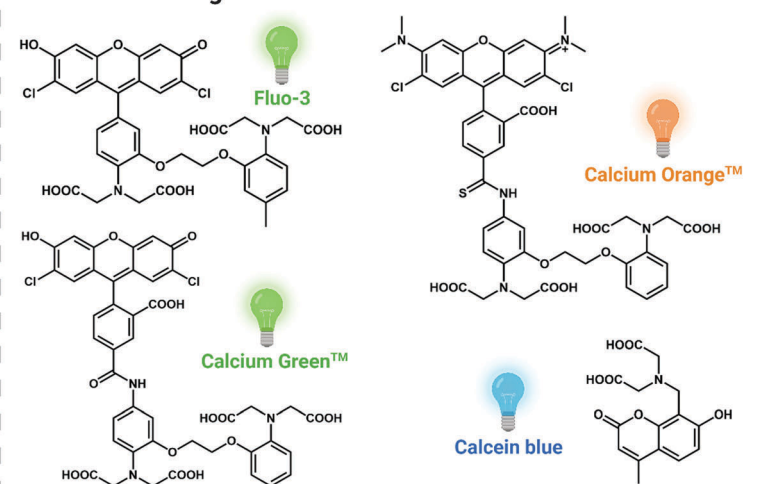
### 3. Calcein Leakage from Artificial Model Vesicles

Early experiments to investigate interactions of potential nanocarriers with lipid membranes include release studies with artificial liposomes, also called lipid vesicles. The

### A Fluorescence is influenced by ...



### B Similar chelating alternatives



### C Membrane permeating derivatives

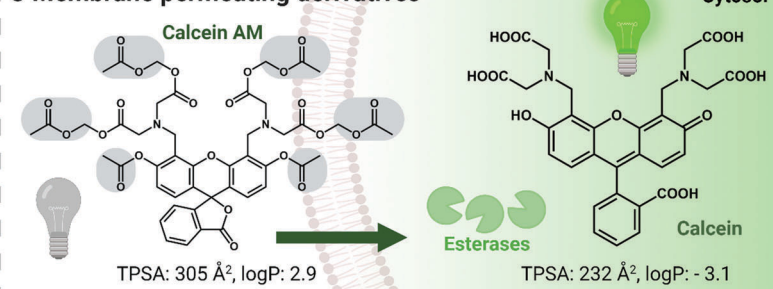


**Figure 3.** Physico-chemical properties and derivatives of calcein. A) Factors influencing the fluorescence intensity of calcein: Concentration, pH value and different cations. Arrows in 3 indicate an increase or decrease in fluorescence intensity through the respective cation. B) Further cation chelating molecules with structures similar to calcein. C) Principle for the identification of viable cells using calcein AM.

**Table 1.** Overview of quenching concentrations (conc.) and pH values in different studies.

Ref.	Buffer [mM]	pH value	Conc. at Flmax [mM]	Conc. at 50% Flmax [mM]	Conc. at 10% Flmax [mM]
Hamann 2002 <sup>[62]</sup>	119 Na <sup>+</sup> , 5 K <sup>+</sup> , 0.8 Mg <sup>2+</sup> , 1.8 Ca <sup>2+</sup> , 114 Cl <sup>-</sup> , 0.8 SO <sub>4</sub> <sup>2-</sup> , 25 HEPES, 5.6 glucose, 44 mannitol	7.4	4.000	8.400 <sup>a)</sup>	> 30.00 <sup>a)</sup>
Roberts 2003 <sup>[63]</sup>	PBS (350 mOs mol L <sup>-1</sup> )	7.4	0.019	0.055	0.20 <sup>a)</sup>
Andersson 2007 <sup>[64]</sup>	50 PBS + POPC	7.0	0.032 <sup>a)</sup>	0.100 <sup>a)</sup>	> 0.10 <sup>a)</sup>
Imamura 2017 <sup>[65]</sup>	PBS	7.4	2.000	9.000 <sup>a)</sup>	25.00 <sup>a)</sup>
Dorrington 2018 <sup>[66]</sup>	0.1 EDTA, 10 Tris, 100 NaCl	7.8	0.970	N/A	> 6.40 <sup>a)</sup>
Brkovic 2020 <sup>[67]</sup>	0.2 Na <sub>2</sub> HPO <sub>4</sub> -NaH <sub>2</sub> PO <sub>4</sub>	7.5	0.002 <sup>a)</sup>	0.005 <sup>a)</sup>	0.01 <sup>a)</sup>
Bae 2021 <sup>[68]</sup>	50 HEPES, 100 Na <sup>+</sup> , 100 Cl <sup>-</sup> , 5 % glycerol	7.4	0.001	0.002 <sup>a)</sup>	> 0.20 <sup>a)</sup>
Own data <sup>b)</sup>	20 HEPES, 5% glucose	5, 6, 7	0.080	1.120	> 3.20 <sup>a)</sup>

<sup>a)</sup> Values were read from the graph. <sup>b)</sup> Not published.

strong self-quenching properties of calcein and the related 6-carboxyfluorescein at high concentrations had already been exploited in these experiments, i.e., for the investigation of endosomal escape. These dyes still represent prominent reporters to monitor the release from lipid vesicles by different nanocarriers or vectors. As liposomes have been used as artificial cell models since the 1970s, numerous reviews and protocols with<sup>[94–96]</sup> and without<sup>[97,98]</sup> calcein are available, which we like to refer to. In

this section, only studies with calcein as a reporter and directly related to endosomal escape will be discussed to illustrate the liposomal features that can be exploited for the investigation of the specific characteristics of endosomal escape (Table 2).

In general, typical leakage experiments with encapsulated calcein involve the addition of the investigated nanocarrier to a dispersion of vesicles (Figure 4). Upon permeabilization of the lipid bilayer, the released calcein is diluted in the outer buffer. In the

**Table 2.** Investigation of calcein release from model vesicles.

Nanocarrier	Vesicle type <sup>a)</sup>	Lipids <sup>b)</sup>	Calcein concentr. mM	Incubation conditions buffer, pH, temperature, time	Ref.
Polymer	SUV	DHP, PC, Chol	40	• 10 mM phosphate, pH 7.4, 25 °C or 65 °C, 20 min	[101]
	LUV	PC, PG	80	• 10 mM HEPES + glucose, pH 5.8–7.6, up to 60 min	[102]
		PC	200	• 10 mM Tris-HCl, 100 mM NaCl, pH 10, 25 °C, up to 60 min	[103]
Peptide	LUV	PC, PE, BMP, Chol	60	• in: 10 mM NaH <sub>2</sub> PO <sub>4</sub> , 100 mM NaCl, pH 7.4 out: 10 mM NaH <sub>2</sub> PO <sub>4</sub> , 100 mM NaCl, pH 5.5, (or pH 7.4) RT, 60 min	[104–106]
		PC, PE, BMP, PG	70	• 5 mM NaH <sub>2</sub> PO <sub>4</sub> , 100 mM KCl, pH 7.4, RT, 60 min	[107]
		PC, PE, BMP, Chol, PA, PG	60	• 10 mM phosphate, 100 mM NaCl, pH 7.4, RT, up to 20 min, 60 min	[108]
		PC, PE, BMP, PI	70	• 10 mM NaH <sub>2</sub> PO <sub>4</sub> , 100 mM NaCl, pH 5.5, RT, 60 min	[109]
	PC, Chol	100	• PBS, pH 7.4, up to 30 min • in: 375 mM NaOH, 50 mM NaCl, pH 7.4 out: 200 mM NaCl, 20 mM citrate, pH 7.4/5, up to 60 min	[110] [111]	
	GUV	PC, PE, BMP, PG	70	• 10 mM phosphate, 100 mM NaCl, pH 7.4, RT, up to 20 min, 60 min	[108]
		PC, PG, Chol	50	• in: 130 mM NaCl, 20 mM Na <sub>3</sub> PO <sub>4</sub> out: 130 mM KCl, 20 mM K <sub>3</sub> PO <sub>4</sub> , pH 7, 4 h	[112]
Peptide/polymer	LUV	PC	40	• 10 mM NaH <sub>2</sub> PO <sub>4</sub> , pH 7.4, 5 min	[113]
		PC, Chol	90	• in: 137 mM HEPES, pH 7.4 out: 137 mM HEPES, pH 7.4 or 137 mM sodium citrate buffer, pH 5.0; 37 °C, 60 min	[29]
Peptide/liposome	LUV	PC, Chol	90	• 5 mM HEPES, 150 mM NaCl, pH 7.4, RT, 60 min	[114]
		PC, PS, Chol	40	• in: 1 mM EDTA, out: PBS or citrate/phosphate, pH 7.4/5.5, 37 °C 30 min	[115, 116]

<sup>a)</sup> SUV—small unilamellar vesicle (30–100 nm), LUV—large unilamellar vesicle (100 nm–1 µm), GUV—giant unilamellar vesicle (1–200 µm) <sup>b)</sup> In different ratios. Only types of phospholipids are distinguished, fatty acids can vary. DHP—dihexadecyl phosphate, PC—phosphatidylcholine, Chol—cholesterol, PE—phosphatidylethanolamine, BMP—bis(monoacylglycerol)phosphate, PG—phosphatidylglycerol, PA—phosphatidic acid, PI—phosphatidylinositol, PS—phosphatidylserine.

case of a gradual leakage, also calcein that remains entrapped is diluted. Thereby, self-quenching is reduced, and the fluorescence increases. There are two calcein release assays in artificial vesicles: The reduced self-quenching can be monitored via the fluorescence intensity and normalized to the maximal fluorescence reached by lysis of the remaining liposomes. Alternatively, the fluorescence lifetime and amount of free and entrapped dye can be determined. Typically, leakage is examined after 1 h incubation time. However, studying the time course of leakage over several hours can indicate certain leakage mechanisms.<sup>[99,100]</sup>

The model vesicles can roughly be classified according to their size into small unilamellar vesicles (SUV, 0.02–0.1 µm), large unilamellar vesicles (LUV, 0.1–1 µm) and giant unilamellar vesicles (GUV, 1–200 µm).<sup>[117]</sup> However, the size of the lipid vesicles only matters for comparison purposes. In the surveyed studies, mostly LUVs and GUVs have been investigated, which have too small membrane curvature to result in packing defects. More importantly, identical leakage mechanisms can appear different in vesicles of different sizes.<sup>[118]</sup> LUVs are commonly prepared by solvent-free self-assembly (Figure 4). For this, thin lipid films are obtained from organic solutions containing all lipid components. The films are rehydrated with an aqueous calcein buffer, followed by multiple freeze-thaw cycles,<sup>[102,105,108,110]</sup> and repeated extrusion through polycarbonate membranes with pore sizes of 100 nm,<sup>[101,102,104–106,108,109,113]</sup> or larger.<sup>[110,115]</sup> The outer buffer with free dye is exchanged via size exclusion chromatography (SEC) or centrifugation protocols.<sup>[114]</sup> GUVs can be obtained

by swelling of the dried lipid film in the desired buffer,<sup>[119,120]</sup> sometimes involving a polymer gel.<sup>[108]</sup> Electroformation can also be utilized, but GUVs obtained this way might suffer from artefacts when using charged lipids and calcein might also interfere.<sup>[121,122]</sup>

Not only the size, but more importantly the membrane composition is known to change during endolysosomal maturation (see as well Introduction).<sup>[9]</sup> These changes in composition inspired investigations of different lipid compositions containing BMP.<sup>[104–110]</sup> For instance, the group of J. P. Pellois tested different variants of the CPP TAT with liposomes containing BMP and/or other lipids and found that liposomal leakage occurred only in presence of BMP, but not if other anionic phospholipids such as phosphatidylglycerol (PG) or phosphatidic acid (PA) were incorporated.<sup>[104–106,108,109]</sup> Their further investigations included the simple binding between TAT variants and lipid and the endosomal escape in HeLa cells by analyzing the fluorescence distribution pattern (punctate vesicular or broad cytosolic) of the tetramethylrhodamine (TMR) the TAT variants were labeled with.<sup>[105,109]</sup> In these assays, the liposomal leakage/endosomal escape was concentration dependent and showed similar optimal concentrations for the respective TAT variant indicating that the results of the methods correlate well. Moreover, Pellois and co-workers also demonstrated that the incubation with anti-BMP antibodies inhibits the leakage/escape, both in liposomes and in cells.<sup>[108,109]</sup> The influence of the changing cholesterol content on the leakage of further peptides

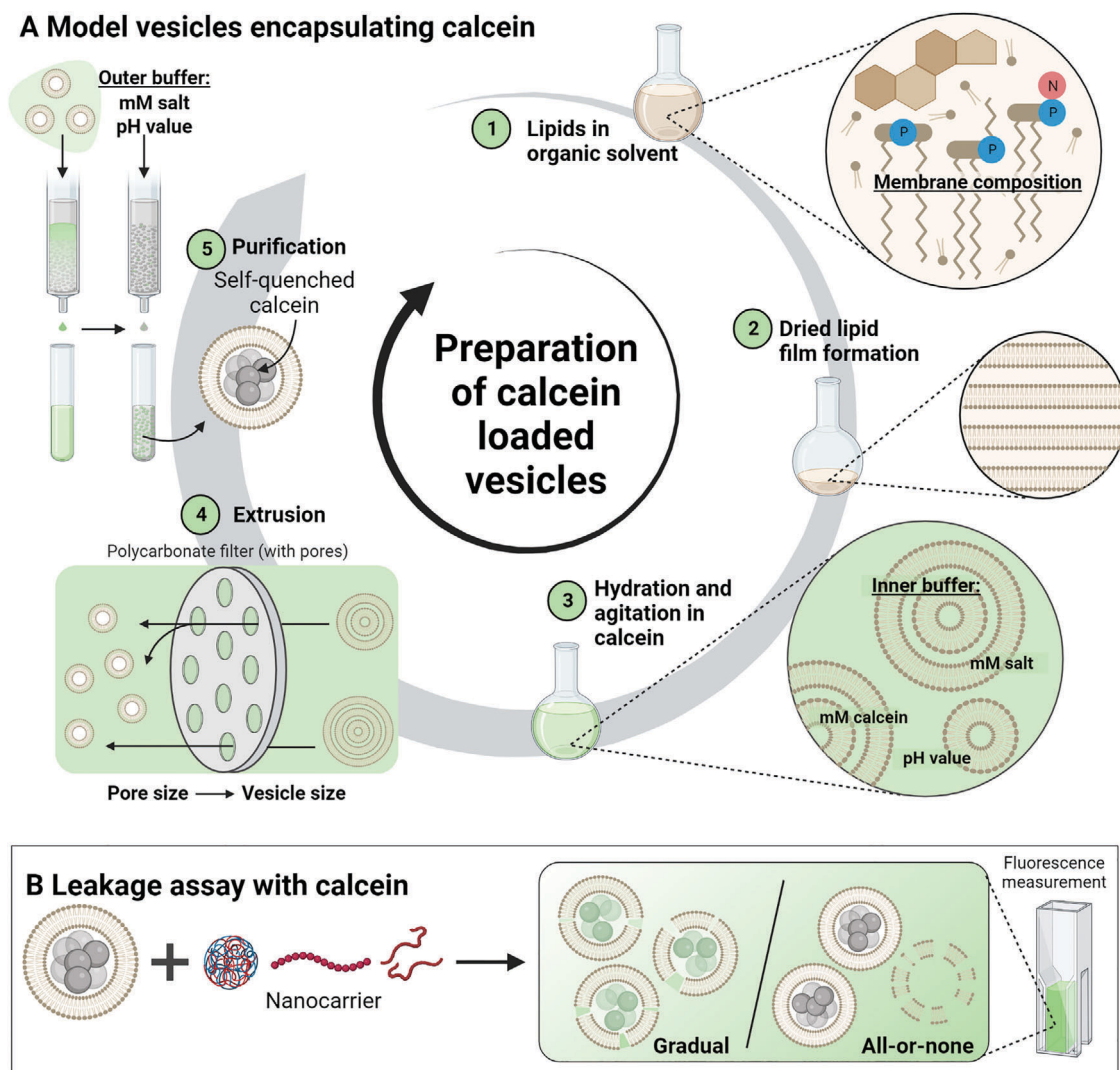


**Figure 4.** Preparation and calcein leakage from model vesicles. A) The model liposomes (LUVs) can be modified at different steps to mimic different properties of the endolysosomal pathway. B) Upon mixing of the liposomes with different nanocarriers, the release of calcein can be determined and characterized regarding the release mechanism (for example, gradual or all-or-none, transient or continuous). Adapted from “Liposome Preparation via Thin Film Hydration” (2022) by BioRender.com. Retrieved from <https://app.biorender.com/biorender-templates>.

was studied similarly,<sup>[111]</sup> demonstrating the potential of experiments with model liposomes to address specific questions more precisely.

Another aspect relevant for the design of leakage experiments in LUVs is the endolysosomal acidification process that can be mimicked by the appropriate pH value of the buffers. Changes in pH can lead to a change in the degree of charge not only of the tested nanocarrier but also of the anionic phospholipids, which can be exploited to design pH-responsive nanocarriers and lipidic drug delivery systems.<sup>[16,29,111,115,116]</sup> To correctly reflect the role of the endolysosomal acidification, the appropriate, isosmotic buffers, and salts have to be used for vesicle preparation, purification, and incubation. In most cases, phosphate buffers are employed, although concentrations and the type of added salt can vary significantly. For instance, Pellois and co-workers used an intra-liposomal pH of 7.4 to mimic the cytosol and an extra-liposomal pH of 5.5 to mimic the endolysosomal lumen.<sup>[104–106,109]</sup>

By contrast, Sarkar et al. used HEPES buffer (4-(2-hydroxyethyl)-1-piperazineethanesulfonic acid) to investigate calcein leakage of triblock copolymer micelles by varying the pH range from 5.8 to 7.6 outside the liposomes.<sup>[102]</sup> Furthermore, glucose was added to balance the different osmotic pressures inside and outside the liposomes, whereas other studies mostly used NaCl or KCl for compensation. If very high calcein concentrations (>70 mM) are required, also the weak solubility of calcein at low pH values has to be considered which requires the use of basic buffers (e.g., Tris-HCl pH 10)<sup>[103]</sup> for the hydration of the lipid film. Additionally, also a Na<sup>+</sup>/K<sup>+</sup> gradient can be applied to liposomes to mimic conditions present in nascent endosomes,<sup>[123]</sup> as Rangasamy et al. have shown with LUVs composed of PC, PG, and Chol with a sodium inside-buffer and a potassium outside-buffer mimicking high intra-liposomal Na<sup>+</sup>-concentrations and high cytosolic K<sup>+</sup>-concentrations, respectively.<sup>[112]</sup>

Despite the large variations in the experimental procedures limiting comparability of results, the calcein release from model vesicles represents a straightforward method to mimic selected aspects of endosomal escape in a controlled environment independent of the complex cellular processes. Nevertheless, membrane models, other conditions and procedures as well as theoretical concepts are still being advanced to further optimize the transferability of the results to experiments in cells.<sup>[61,124]</sup> For example, some studies chose an incubation temperature of 37 °C instead of room temperature.<sup>[115,116]</sup> This corresponds to the cellular environment and, together with the choice of fatty acid chains, may have an impact on the membrane fluidity of liposomes.<sup>[117,125]</sup> Furthermore, mimicking the exact membrane composition of endolysosomal organelles including different fatty acids and associated proteins is very complex and can only gradually be approached. To increase the similarity to natural lipid compositions, also naturally derived vesicles can be utilized. They can be obtained either via chemically induced cell blebbing followed by harvesting of the resulting GUVs, or by the rehydration of total lipid extracts from different cells/tissues.<sup>[126]</sup> The advantages and relevance of natural lipid compositions are limited by the uncertainty of their lipid composition, which is rather similar to the plasma membrane, or by missing asymmetry in the lipid distribution over the membrane. Nevertheless, these improvements are invaluable in filling the gap between mechanistic conclusions from simplified model studies to the biological behavior in cells.

To investigate vesicle compositions more comparable to endolysosomes, exosomes can be isolated from the cell culture supernatant since they originate from the multivesicular endosome (see also Figure 9) and also comprise the characteristics of different cell types.<sup>[127,128]</sup> While they are difficult to load with hydrophilic molecules such as calcein directly,<sup>[129]</sup> the nonfluorescent derivative calcein AM can be used instead. Calcein AM can diffuse into the exosomes and is subsequently converted to calcein by the esterases contained therein.<sup>[130]</sup> One minor limitation is that the high calcein concentrations required for the full information range encoded in self-quenching behavior cannot be reached. A similar approach is also utilized to examine the leakage of calcein AM from red blood cells upon perturbation of their plasma membrane by different nanocarriers.<sup>[88,131,132]</sup> Another aspect which has rarely been considered so far, is that nanocarriers in cellular endolysosomal organelles escape from the inside to the outside of the organelles, whereas they have to take the opposite way in assays using model vesicles. This could have an impact on the apparent leakage since the concentration gradient of the entrapped nanocarrier is reversed and the asymmetric membrane composition is not reproduced correctly. Furthermore, osmotic swelling as hypothesized for the proton-sponge mechanism cannot be modeled.

Strikingly, the calcein-based methods can be slightly modified in various ways, to not only examine the occurrence of calcein release from these model vesicles, but also the mechanism of the release. Here, we will only summarize assays using calcein, even though they might be based on calcein-free variants and there are calcein-free alternatives mentioned elsewhere.<sup>[196]</sup>

There are many postulated release mechanisms that can be classified in different aspects. One way is to distinguish transient leakage from continuous leakage.<sup>[133]</sup> Transient leakage occurs

fast upon interaction of the nanocarrier and the membrane and stops thereafter. Most commonly, this behavior is explained by the asymmetry stress mechanism,<sup>[134–136]</sup> or an involvement of membrane fusion in leakage (see below).<sup>[108,137]</sup> Continuous leakage, on the other hand, will happen through stochastically reoccurring leakage events or pores, thus slowly continues and affects the sample over several hours.<sup>[99,133,138]</sup> These types of pore formation kinetics can be distinguished for example by visualizing GUVs by confocal microscopy and acquiring time-resolved images, which allows for a direct optical monitoring of the leakage process in individual vesicles.<sup>[108,112,139–141]</sup> The large number of LUVs in a sample cuvette can also be exploited, when leakage is monitored over time. This allows for the same distinction of transient or reoccurring leakage.<sup>[99,142]</sup>

Release mechanisms can also be classified according to the number of pores or other leakage events affecting a given artificial vesicle.<sup>[118,143]</sup> In all-or-none leakage, rare leakage events are distributed heterogeneously over the artificial vesicle population. While the entire dye has been released through these strong events from some vesicles, others are not affected at all. In contrast, many weak pores or defects need to occur much more often in an individual artificial vesicle to cause detectable leakage. These events are distributed homogeneously over all vesicles and cause gradual or graded leakage. In artificial model vesicles, this behavior can be distinguished indirectly by measuring the concentration of entrapped dye, for example. In all-or-none behavior, the dye that is still entrapped was not diluted, while in gradual leakage, the entrapped dye dilutes gradually. For determining this, the relation of the calcein concentration to the extent of its self-quenching and hence the fluorescence-lifetime can be exploited.<sup>[60,118,144,145]</sup>

Furthermore, release mechanisms might involve additional effects such as membrane fusion of vesicles in models or intracellular vesicles in cells. For example, an interesting approach relies on the chelation property of calcein with divalent cations such as Co<sup>2+</sup> or Cu<sup>2+</sup>, which allows to investigate if calcein release occurs via the fusion of vesicles. Different vesicles are combined, some being loaded with EDTA (or divalent ions) and the others loaded with a mix of calcein and divalent ions (or calcein alone). Upon fusion of these vesicles, the fluorescence intensity increases (or decreases) due to the fluorescence (de)quenching.<sup>[101,114,146]</sup> If transferred to endolysosomal vesicles, these methods could provide valuable information on the endosomal escape mechanism.

#### 4. Calcein Release Studied within Cells

In Section 4, we revise calcein as a marker for studying endosomal escape. As a general procedure of all considered experiments, the dye (encapsulated or not) is first taken up by cells via endocytotic pathways. In this stage, a dotted pattern is often found in fluorescence microscopy since the fluorescence of the dye is often only partially quenched at the given concentrations. If appropriate experimental conditions are chosen with respect to calcein concentration, self-quenching in combination with the acidic pH is sufficient to reduce the fluorescence intensity of calcein in endosomes. In the next stage, i.e., with occurrence of an endosomal leakage event, calcein rapidly diffuses and dilutes into the neutral cytosol, which microscopically causes not only



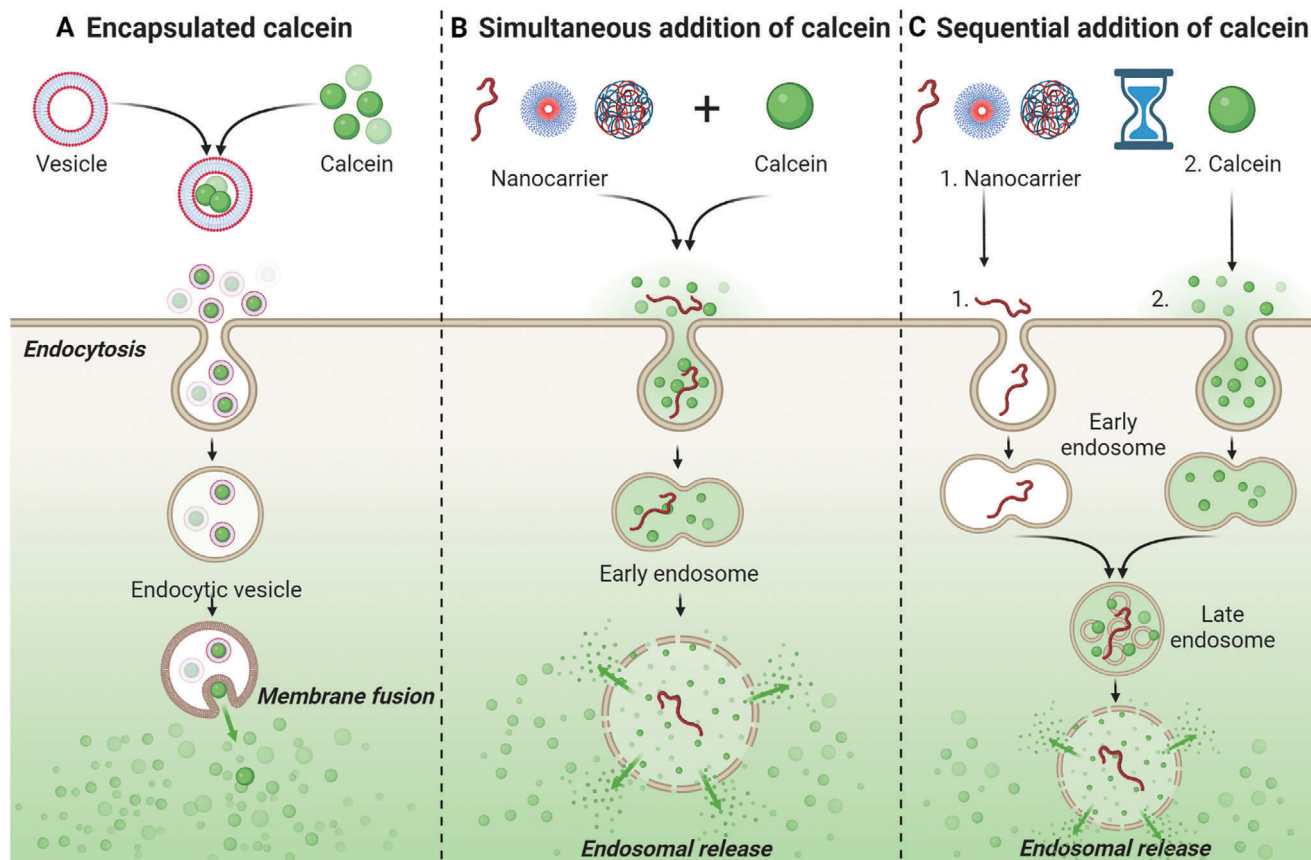


**Figure 5.** Types of calcein addition. The type of calcein addition is primarily determined by the type of nanocarrier (peptides/polymers, dendrimers, or nanoparticles). In the case of simultaneous addition, calcein can either be A) encapsulated in the nanostructure (often using self-quenching concentrations) or B) added to the cell culture medium at the same time as the agents. C) Sequential addition is also possible. In most cases, the cells are preincubated with the nanocarrier and calcein is added afterward.

a more diffuse fluorescent signal, but may also lead to a significant increase in intensity, if appropriate conditions are chosen initially.<sup>[147]</sup>

In this way, calcein has been used to evaluate the endosomal escape efficiency of various nanocarriers. Thereby, the escape has been investigated in a range of different cell lines, with experimental settings varying in terms of media composition, calcein concentration, incubation time, type of calcein addition as well as cell analyses. The type of calcein addition can be categorized into encapsulated and nonencapsulated or simultaneous and sequential addition and is described in Section 4.1-4.2 (Figure 5).

#### 4.1. Release of Encapsulated Calcein within Cells

In this approach, the investigated nanocarriers are able to encapsulate calcein at self-quenching concentrations within their hydrophilic interior. These nanostructures often consist of amphiphilic lipids forming liposomes similar to the model vesicles described above (Table 3). To facilitate drug delivery via endosomal release, modified lipids or lipids with advantageous properties are included, e.g., phosphatidylethanolamine (PE), cholesteryl hemisuccinate (CHEMS), or 1,2-dioleoyl-3-trimethylammonium propane (DOTAP).<sup>[148–154]</sup> Thereby, ioniz-

able lipids can facilitate endosomal escape via membrane fusion due to the formation of nonbilayer structures (hexagonal H<sub>II</sub> phase) with (naturally present) anionic phospholipids. Neutral fusogenic helper lipids such as unsaturated PE can further enhance the endosomal escape by their cone-like shape also favoring the membrane lysis via formation of nonlamellar intermediates.<sup>[155–157]</sup> Furthermore, synthetic variants of liposomes, polymersomes, formed by amphiphilic block copolymers have been investigated regarding their endosomal escape.<sup>[158–160]</sup> Combinations of lipids and polymers,<sup>[161–163]</sup> peptides, and liposomes<sup>[164]</sup> or completely different nanostructures, such as hollow capsules<sup>[67]</sup> have also been studied.

In general, the incubation times varied within a wide range, from 10 min to 4 days which could be related to varying kinetics between the different nanocarriers regarding endocytosis, material-cell interactions and endosomal escape. Long incubation times, e.g., could be related to the incorporation of molecules, such as polyethylene glycol (PEG)-chains that shield the surface of the nanocarrier and may interfere with a fast and efficient endosomal escape.<sup>[129,165]</sup>

The applied calcein concentrations in the nanostructures exhibited greater variation than those reported for the model liposomes, which may be attributed to the different preparation methods. Most of the polymer- and/or lipid-containing

**Table 3.** Investigation of calcein release from vesicles inside cells.

Nanocarrier	Polymers/lipids <sup>a)</sup>	Lipid composition mol%	Calcein concentr. <sup>b)</sup> mM	Cells <sup>c)</sup>	Incubation time	Analysis <sup>d)</sup>	Ref.
Liposome	PE:PHC, PC	8:2	60 (0.3)	L929 in PBS + 16 mM D-glucose	1.5 + 2 h	Quant.	[154]
	CHEMS:PE/PC	4:6	50	RAW264.7 in D10	1 h	Qual., stabil.	[148]
	CHEMS:PE:PEG-PE:Chol	21:43:6:30	40	Hs578t in D10, HG	15 min	Qual., stabil., FC	[149]
	PEG-PE:PC:Chol	6:47:47				Qual., stabil., FC	
	CHEMS:PE (:PEG-PE/PC)	4:6 (:0.06)	80	Differentiated THP-1 in R10	4 h	Qual., stabil., FC	[150]
	CHEMS:PE (:PEG-PE/PC/PS/PG)	4:6 (:0.3/6/4/4)				Qual., FC	[151]
Polymersome	CHEMS:PE:PEG-PE/PEG-Hz-CHEMS:PC:Chol	2:4:0.5:2:2	80	Mia-Paca 2	1, 2 h	Qual.	[152]
	DOTAP:PEG-PE:PC:Chol	1:0.25:4.8:2.3	60	HeLa in D10, HG	4 h	Qual., stabil.	[153]
	DOTAP:PEG-PE:PC:Chol:PE	1:1.3:1.9:9.6:1.8				Qual., stabil.	
Polymer/lipid	PEG-SS-PPS	—	100	J774A in D10	10, 60, 120 min	Qual.	[158]
	PEG- <i>b</i> -PPS	—	200	mouse dendritic cells in D	6, 12, 24 h	Qual.	[159]
	PEG- <i>b</i> -PPS	—	30	RAW264.7 in D	2 h	Qual., stabil.	[160]
Peptide/liposome	Suc-poly(glycidol) + PC	—	200	CV-1 in D10	3 h	Qual.	[161]
	PEtOx:CHMC + Chol, PC	—	60	HeLa in D10	1, 4 h	Qual., stabil., FC, LC	[162]
Other	DOX-PLGA + DMAB + PC	—	0.008*	MCF-7, HL-60 in R	15, 60, 240 min	Qual., FC	[163]
	(GALA)-His-Z <sub>HER2</sub> -BNC + PC, Chol, PG	—	105	SKBR3 in R10	1 + 5–47 h	Quant., LC	[164]
Exosome coated MOF-NP	Gold NP + PSS, PAH	—	4.8**	MCF-7 in D10, HG	over night	Quant., LC	[67]
	Exosome coated MOF-NP	—	1**	HeLa in D	2, 3, 4 d	Quant. stabil., LC	[129]
	MSN-PVP-PEG	—	1**	HeLa or KB in D10-F12	18 h	Qual., LC	[165]

<sup>a)</sup> Types of phospholipids by headgroup are mentioned. Fatty acids can be different, for PC and PE they were mostly dioleoyl or distearyl. **BNC**—bio-nanoparticle, **CHEMS**—cholesterol hemisuccinate, **CHMC**—cholesterol hemisuccinate, **Chol**—cholesterol, **DMAB**—dimethyldodecylammonium bromide, **DOTAP**—1,2-dioleoyl-3-trimethylammonium propane, **DOX**—doxorubicin, **HZ**—hydrazine, **Hz**—hydrazine, **MOF**—metal-organic framework, **MSN**—mesoporous silica nanoparticles, **NP**—nanoparticle, **PAH**—poly(allylamine), **PC**—phosphatidylcholine, **PE**—phosphatidylethanolamine, **PEG**—poly(ethylene glycol), **PEtOx**—poly(2-ethyl-oxazoline), **PG**—phosphatidylglycerol, **PHC**—palmitoyl homocysteine, **PLGA**—poly(lactic-co-glycolic acid), **PPS**—poly(propylene sulfide), **PS**—polystyrene, **PSS**—poly(styrenesulfonate), **PVP**—poly(2-vinylpyridine), **Suc**—succinylated. <sup>b)</sup> Grey shade indicates capsule preparation other than thin film rehydration or reverse phase evaporation. \*—converted based on information from the original publications. \*\*—concentration of capsule loading solution. <sup>c)</sup> **D**—DMEM, **D10**—DMEM + 10% FCS, **F12**—Ham's F12 medium, **HG**—high glucose (4.5 g L<sup>-1</sup>), **R**—RPMI, **R10**—RPMI + 10% FCS. <sup>d)</sup> **FC**—flow cytometry, **LC**—loading capacity/encapsulation efficiency, **qual.**—qualitative microscopy, **quant.**—quantitative image analyses, **stabil.**—stability against changes in environment.

structures were assembled via the already mentioned thin film hydration<sup>[148–154,158–162,164]</sup> usually resulting in high encapsulation efficiencies.<sup>[94]</sup> Thus, the calcein concentration within the polymersomes/liposomes is assumed to be similar to that used to rehydrate the thin film. However, some vesicles were prepared by more complex procedures and the actual amount of calcein within the nanocapsules was determined afterward.<sup>[67,129,165]</sup> Nevertheless, endosomal escape can still be detected with low (non-quenching) calcein concentrations as a change from a punctate fluorescence pattern to diffuse cytosolic fluorescence. Illes and co-workers described another interesting approach using metal-organic frameworks (MOF) to encapsulate calcein first in nanoparticles and then coating these with exosomal membranes derived from HeLa cells. This resulted in a strong shielding from the immune system and high calcein release from both, the exosome coated MOF and the endosome following 4 days of incubation in HeLa cells.<sup>[129]</sup>

Moreover, high (quenching) calcein concentrations inside the nanocarrier can be used to determine the stability of the nanocarrier similar to the method for the calcein release from artificial liposomes, by changing the ambient conditions, such as temperature,<sup>[148,149,153]</sup> serum content,<sup>[148,153]</sup> or pH-value.<sup>[129,149,150,162]</sup> In case of low calcein concentrations, also a calcein diffusion method (Franz cell diffusion) was used. The released calcein diffuses into a buffer without the nanocarrier which is separated by a dialysis membrane allowing for the discrimination between fluorescence originating from inside the nanocarrier and from released calcein in the solution.<sup>[94,129]</sup> Therefore, encapsulating nanocarriers allow for both, a general investigation within the natural environment (cells), and a detailed investigation of one specific feature of the endosomal escape within only one approach (stability of the nanocarrier).

#### 4.2. Simultaneous and Sequential Addition of Nanocarrier and Calcein as Sensor

The calcein assay is influenced by the nature of the nanocarriers and how it is performed, particularly with respect to the simultaneous presence and concentrations of the two substances (calcein and material) in the endosome. Calcein, as a small molecule, is rapidly taken up by cells, while nanocarriers may take longer to accumulate in the endosome, depending on their size and charge. Often, the nanocarrier and calcein are added simultaneously to the cells (Table 4), without mixing the two components beforehand.

Cationic polymers are often considered as synthetic gene transporters and nanocarriers to facilitate endosomal escape. The most studied polymeric gene transporters include PEI and poly(2-(dimethylamino)-ethylmethacrylate (PDMAEMA), whose endosomal release has also been investigated in several studies with calcein. PEI represents the commercial gold standard and is particularly interesting for the study of calcein release not only because of the controversial proton-sponge hypothesis. Bonner et al. tested different PEI architectures (crosslinked, linear, branched) and found endosomal escape in 75% of cells using the calcein assay if a crosslinked PEI variant was applied, which showed no toxic effects at this concentration and incubation time.<sup>[173]</sup> Vermeulen et al. investigated the endosomal escape

mechanism of linear PEI (JetPEI) and performed the calcein release assay in cell lines differing in endosomal size. They conclude that endosomal release can be promoted by smaller endosomes and an undisturbed buildup of osmotic potential. (Table 5).<sup>[111]</sup> Another well-known polymer is PDMAEMA as it is easily applied for a variety of nanocarriers and enables endosomal release of calcein.<sup>[169,175]</sup> This was demonstrated in fibroblasts and dendritic cells with different nanoparticle compositions, where calcein was added sequentially (after treatment with the polymer) or simultaneously with the polymer.<sup>[178,185–188]</sup> By inhibiting endosomal escape with bafilomycin A1, Wong et al. showed that acidification of the endosomes is crucial for release of calcein.<sup>[188]</sup> However, the large number of studies on vinyl polymers such as PDMAEMA do not yield clear correlations, which can also be attributed to the different investigation methods. Therefore, no final conclusion can be drawn about the release mechanism.

Due to its wide application and good availability, it is not surprising that different calcein concentrations and incubation times were used to study the endosomal escape of nanocarriers (Figure 6). Concentrations from 10  $\mu\text{M}$  to 3.21 mM were reported to study systems codelivering calcein,<sup>[167,170,191]</sup> with the majority of studies applying concentrations between 161 and 322  $\mu\text{M}$ .<sup>[168,173,177–186,190,192]</sup>

Using a calcein concentration of 161  $\mu\text{M}$ , Deshpande et al. have shown that poly(*N*-isopropylacrylamide nanogels with poly- $\epsilon$ -lysine can release calcein in cervical cancer cells.<sup>[168]</sup> Similar concentrations were used to study nanoparticles with hydrophobic components. Su and co-workers showed that pH-responsive polyaminoester nanoparticles with lipid shells induce highly efficient endosomal escape in dendritic cells at a calcein concentration of 240  $\mu\text{M}$ .<sup>[180]</sup> Wannasarit and colleagues were able to induce a poly(lauryl methacrylate-co-methacrylic acid)-mediated calcein release in three different colorectal adenocarcinoma cell lines using a calcein concentration of 322  $\mu\text{M}$ .<sup>[181]</sup> Calcein concentrations in a similar range have also been shown to be useful for studying CPPs.<sup>[184]</sup> As an example, Salomone and colleagues showed that a fusion peptide from the arginine-rich TAT motif with additional residues of cecropin-A and melittin can efficiently release calcein within 30 min with a calcein concentration of 250  $\mu\text{M}$ .<sup>[183]</sup> However, endosomal escape could also be detected with significantly lower calcein doses of 40  $\mu\text{M}$  or less. In HEK cells, calcein release was detectable with concentrations  $\leq 40$   $\mu\text{M}$  applying differently structured polyvinyl polymers and culture conditions.<sup>[169,171,175,176]</sup> Calcein concentrations in this lower range were also successfully used in leukemia cells and human prostate cancer cells to show escape induced by polyamidoamides and a PDMAEMA-containing micelle.<sup>[174,175]</sup> Jones et al. showed that PAA (poly(2-alkylacrylic acid) can deliver calcein to the cytosol by disrupting endosomes.<sup>[167]</sup> For this purpose, they co-incubated human myelomonocytic cells in complete medium with the polymers and calcein concentration of 3.21 mM for 30 min. In contrast to this, Ren et al. investigated receptor-mediated endosomal escape in human lymphoblastic leukemia cells in serum-containing medium by incubating the cells with 25  $\mu\text{M}$  calcein for 6 h.<sup>[193]</sup> As can be seen from the experimental set-up in these two studies, the calcein concentration and incubation time for efficient release detection are mutually dependent. The two studies also differed in the type of microscopy conducted (confocal or

**Table 4.** Investigation of calcein release with simultaneous addition of vector and calcein in vitro.

Type of carrier <sup>a)</sup>	Nanocarrier <sup>b)</sup>	Delivery of <sup>c)</sup>	Cell line	Calcein concentr. $\mu\text{M}$	Incubation conditions	Analysis <sup>d)</sup>	Ref.
Oligomers	Oligo(ethanamino) amides	pDNA	DU145	803	Growth medium + 10% serum, 3.5 h	Quant.	[166]
Linear polymers	Poly(2-alkylacrylic acid)s	pDNA	U937 (Jurkat)	3214	Growth medium + 5% serum, 30 min	Quant. + FC	[167]
	Poly( <i>N</i> -isopropylacrylamide)	siRNA	Hela, MG-63	161	Growth medium + 10% serum, 4 h	Quant.	[168]
	Poly(aminoethyl-methacrylate)s	pDNA	HEK	25	Opti-MEM, 4 or 4 + 20 h	Quant.	[169]
	PDMAEMA	—	U937, (Jurkat)	3214	Growth medium + 5% serum, 30 min, 48 h	Quant.	[170]
	Polyacrylamides, I-PEI	pDNA	HEK 293T	40	Growth medium + 10% serum + HEPES, Opti-MEM, 4 h	FC	[171]
	Polypiperazines, I-PEI	Dextran, BSA, RNase A, EGFP	HEK 293T	40	Opti-MEM, 16 h	Quant. + kinetics, FC	[172]
	(crosslinked) PEI	pDNA	KB	241	Opti-MEM, 2 h	Quant.	[173]
Dendritic polymers	Poly(amidoamine)	pDNA	DU145	25	Opti-MEM, 4 h	Quant.	[174]
Micelles	PDMAEMA-containing shell, PEI	pDNA	HEK 293T, K562	40	Growth medium + 10% serum + HEPES, 1, 4, 24 h	FC	[175]
	PDMAEMA-containing shell, I-PEI	pDNA	HEK 293T	40	Growth medium + 10% serum + HEPES, 1, 4, 24 h	Quant.	[176]
Nanoparticles	Core: PDEAMA, shell: poly(aminomethyl-methacrylate)	Proteins	Dendritic cells	241	Growth medium + 10% serum, 1 h	Quant.	[177]
	PLGA/PDMAEMA-co-PAA-BMA blend particles	—	DC2.4	321	Growth medium + 10% serum + HEPES, 4 h	Fixed, qual.	[178]
	Polyaminoester particles with lipid shell	Dextran	DC2.4	240	Growth medium + 10% serum + HEPES, 1 h	Fixed, quant.	[179]
	Graft of poly(lauryl methacrylate-co-methacrylic acid) on acetylated dextran	mRNA	CT-26	321	Growth medium (+ 10% serum), 1 + 3 h	Qual., FC	[180]
	Org./inorg. Nanoparticles with poly(phenol tannic acid) and metal ions	—	MDA-MB-231	241	Growth medium + 10% serum, 4 h	LTR, qual.	[181]
CPPs	Arginine-rich TAT with residues of cecropin-A and melittin	EGFP-TAT fusion protein, dextran, pDNA	Hela, CHO-K1, HUVEC	250	According to cell manufacturer's instructions, 30 min	Bafi, qual.	[182]
	Poly(acrylamide-co-methacrylic acid) nanogels with peptides	NPs	SW-48	161	Growth medium + 2% serum, 4 h	Quant. + kinetics, FC with threshold	[183]

<sup>a)</sup> **CPPs**—cell-penetrating peptides. <sup>b)</sup> **BMA**—butylmethacrylate, **PAA**—2-propylacrylic acid, **PDEAEMA**—poly(2-(diethylamino)ethyl methacrylate), **PDMAEMA**—poly(2-(dimethylamino)ethyl methacrylate), **PEI**—poly(ethyleneimine), **PLGA**—poly(lactic-co-glycolic acid), **RNase A**—ribo-nuclease A, **TAT**—trans-activator of transcription. <sup>c)</sup> **BSA**—bovine serum albumin, **EGFP**—enhanced green fluorescent protein, **mRNA**—messenger RNA, **NPs**—nanoparticles, **pDNA**—plasmid DNA, **siRNA**—small interfering RNA, **TAT**—trans-activator of transcription. <sup>d)</sup> **bafi**—bafilomycin-A1, **FC**—flow cytometry, **LTR**—LysoTracker Red. **Qual.**—qualitative microscopy, **Quant.**—quantitative image analyses.

**Table 5.** Investigation of calcein release with subsequent calcein addition in vitro.

Type of carrier	Nanocarrier <sup>a)</sup>	Delivery of <sup>b)</sup>	Cell line	Calcein concentr. $\mu\text{M}$	Incubation conditions	Analysis <sup>c)</sup>	Ref.
Linear polymers	JetPEI	pDNA	Hela, ARPE-19, A549, H1299	3000	Growth medium + 10% serum, 15 + 15 min	Quant. + FC	[11]
Nanoparticles	PDMAEMA- <i>b</i> -PEG PEG- <i>b</i> -PDEAEMA	— Ovalbumin	3T3 MEFs WT NIH/3T3	161 161	Growth medium + 10% serum, 2 + 2 h Growth medium + 10% serum, 2 + 2 h	Quant. Quant.	[188] [185, 186]
Peptides	Crosslinked PLGA/PEI particles Cytotransmab, TAT	BSA, SOD —	NIH-3T3 Hela	50 $\mu\text{g}/\text{dish}$ 150	Growth medium + 10% serum, 2 h + 30 min Serum-free medium, 4 + 2 h	Qual. Inhibitors, fixated, quant.	[189] [190]
	Polymer/cyclic peptide conjugate	—	HEK 293	146	Growth medium + 10% serum, 16 h + 30 min	Quant.	[113]

<sup>a)</sup> **PDMAEMA**—poly[2-(diethylamino)ethyl methacrylate], **PDMAEMA**—poly[2-(dimethylamino)ethyl methacrylate], **PEG**—poly(ethylene glycol), **PEI**—poly(ethylenimine), **PLGA**—poly(lactic-co-glycolic acid), **TAT**—trans-activator of transcription. <sup>b)</sup> **BSA**—bovine serum albumin, **pDNA**—plasmid DNA, **SOD**—superoxide dismutase. <sup>c)</sup> **Qual.**—qualitative microscopy, **quant.**—quantitative image analyses.

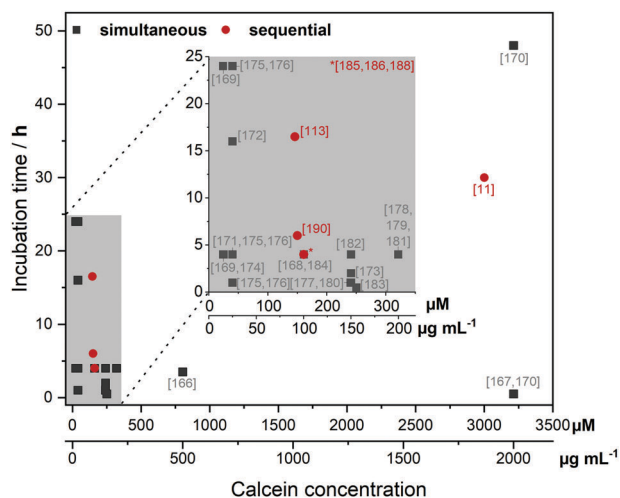


**Figure 6.** Concentrations and incubation times in experimental setups of calcein release. Different research groups have applied a range of different calcein concentrations and incubation times, whereas the assay has also differed in the type of calcein addition (simultaneous or sequential) as well as the nanocarriers and cell lines used.

nonconfocal) and their analyses (qualitative or quantitative image analyses).

Overall, a successful endosomal escape can be detected with different assay parameters optimized for each investigated carrier material, medium, and cell type (Figure 6). The broad varieties in these settings hardly allow to derive any specific trends from the yet given set of experiments found in literature. Indeed, our screening of literature reported data further raised the question, whether significantly different experimental procedures to studying endosomal release efficiency may even lead to different conclusions for similar systems. In this regard, we also like to refer to Section 5 and our final conclusions at this point.

### 4.3. Analytical Methods

The analysis of the calcein release assay can be performed in a variety of ways, depending on the problem to be addressed. The requirements for the analysis of the assay vary from attention to detail (accurate spatial and/or temporal resolution of the intracellular signal) to statistical significance of the data. To address the diverse requirements, the different analytical methods and their applications and limitations are discussed in the following (Figure 7).

In most studies, confocal microscopy has been shown to be a very powerful tool, even more useful than epifluorescence microscopy as the subcellular distribution of calcein can be elucidated.<sup>[169]</sup> For this purpose, also z-stacks can be prepared.<sup>[168,178,179]</sup> Primarily, live cell microscopy is used, also allowing kinetic studies.<sup>[172,183]</sup> Less commonly, cells are studied after fixation.<sup>[178,190]</sup> Fixation with subsequent permeabilization may complicate the interpretation of the calcein assay due to false positive results as a result of fixation artifacts. Besides, the subcellular distribution and fluorescence intensity of the calcein signal have been analyzed quantitatively.<sup>[67,129,154,168,173,174,177,188]</sup>

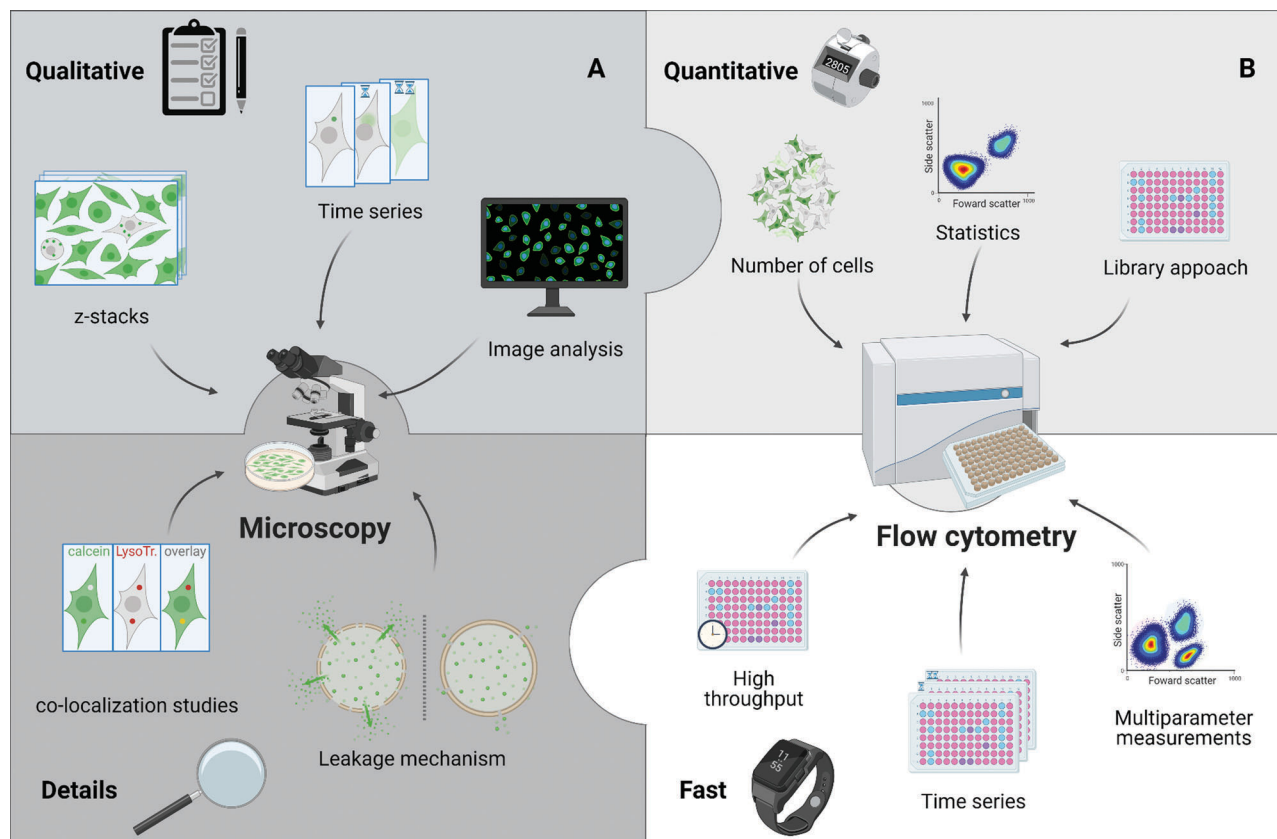


**Figure 7.** Analysis techniques of the calcein release assay. The predominant analytical technique for the calcein release assay is microscopy, as it provides spatial (and in the case of live cell microscopy, temporal) resolution of the fluorescence signal. The primarily qualitative conclusions can also be supplemented by statistically more robust conclusions through the use of image analysis techniques. For rapid quantitative measurements, flow cytometry can also be used to increase the statistical power of the data.

It is possible to count the cells with punctate and diffused calcein signal manually,<sup>[185,186]</sup> but a more effective approach relies on the use of various image analysis software, where regions of interest and/or thresholds are defined for an automated analysis.<sup>[166,169,170]</sup> The acquisition of many cells, e.g., with the help of montages, is also desirable for statistical significance. Colocalization studies with acidic compartments by acidotropic dyes can be conducted and may provide further information about the efficacy of calcein release, with lower colocalization indicating more efficient escape.<sup>[179]</sup> The Manders' coefficient is mainly used for this purpose. It quantifies the degree of colocalization between two fluorophores based on their absolute intensities within a pixel and is rather sensitive to background changes.<sup>[194,195]</sup> It should further be kept in mind that these dyes or also the investigated nanocarriers are usually weak bases increasing the pH value in endolysosomal compartments following longer incubation times which could alter the endosomal escape or the colocalization behavior. Furthermore, the fluorescence of calcein can be quenched at very low pH values inside the lysosome. Another very interesting approach was shown by Connor and Huang already in 1985 who established a calibration curve of calcein using a microscope photometer so that the cytosolic concentration of calcein within L929 cells was quantified.<sup>[154]</sup>

Furthermore, high-throughput methods based on flow cytometry are also used to quantify the calcein release, with higher cellular fluorescence intensities generally indicating released calcein compared to control cells with punctate fluorescence.<sup>[11,149–151,162,163,171,175,183]</sup> Again, appropriate thresholds must be defined for the fluorescence intensity of escape-positive cells. Microscopic and flow cytometric methods can also be combined, which provides more robust insights about endosomal escape.<sup>[167,183]</sup> Because microscopic studies allow spatial (and in the case of live cell microscopy, temporal) resolution of the calcein signal, release events can be measured unambiguously, with varying degrees of attention to detail. Microscopy is still the most commonly used technique but is comparatively time consuming and can only provide statistical information if a large number of cells are analyzed. For statistically robust results, flow cytometry is a faster complementary method, but it cannot spatially resolve the calcein signal within a cell. For fast statistically robust results, flow cytometry is a complementary method, but it cannot spatially resolve the calcein signal within a cell. In the best case, both methods are used in a complementary manner to provide a detailed picture of any potential escape. Although, both analytical techniques ideally coincide in the number of escape-positive cells in order to provide reliable results, deviations nevertheless might occur for example due to the applied thresholding.<sup>[172]</sup>

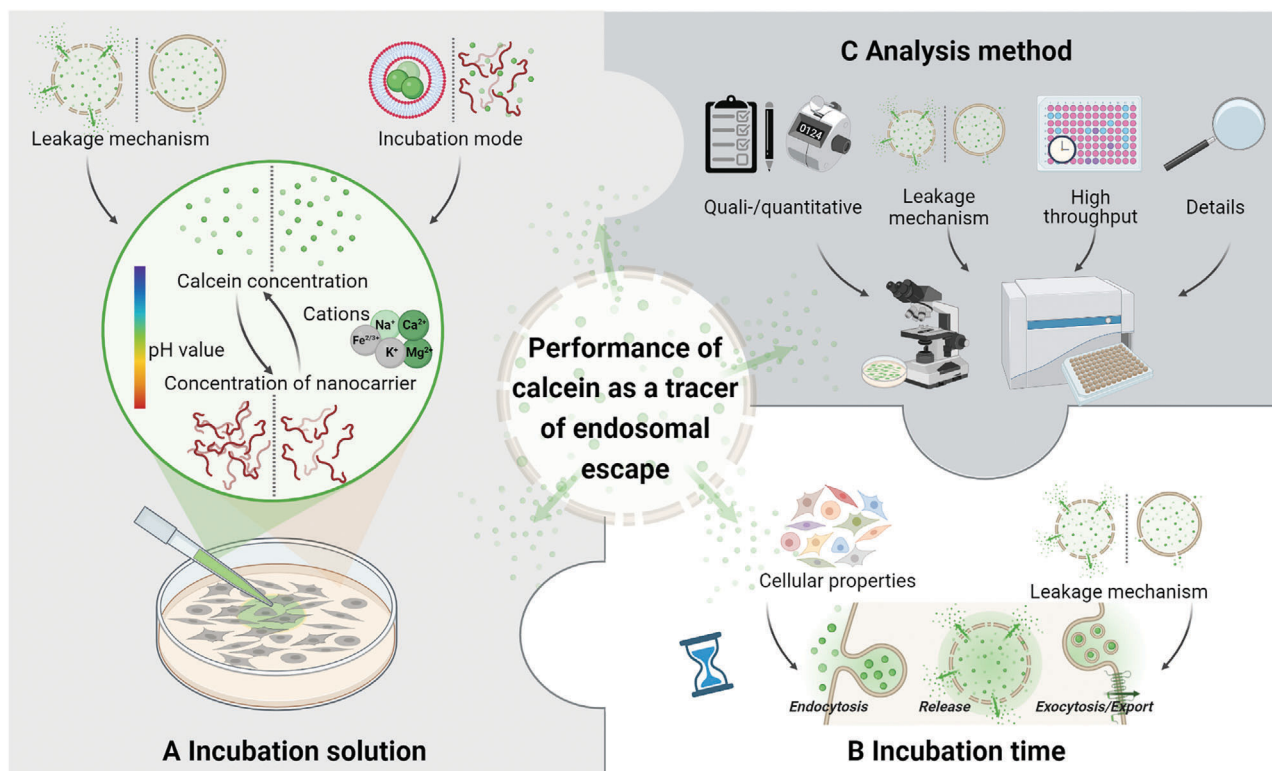


**Figure 8.** Factors determining the performance of the calcein release assay within cells. When planning the parameters of the assay, i.e., incubation solution, incubation time, and analysis method, the influence of different factors needs to be considered, e.g., the leakage mechanism of the nanocarrier, the incubation mode, cellular properties, and the requirements of the desired readout.

## 5. Potential Pitfalls of the Calcein Release Assay in Cells

Calcein has been extensively used to investigate endosomal escape of various types of nanocarriers within cells. However, the performed methods show differences in several aspects which demonstrates the complexity as well as the robustness of the assay. In general, it can be concluded that the performance of calcein as an indicator for endosomal escape depends on three main parameters which should be considered when planning a calcein release assay and will be discussed in this section: i) incubation solution, ii) incubation time, and iii) the analysis method (Figure 8). Regarding the calcein leakage assay with model vesicles, experimental parameters affecting liposomal leakiness have recently been reviewed elsewhere, e.g.,<sup>[94,117]</sup> and are therefore not considered further.

### 5.1. Physicochemical Factors Relevant for the Calcein Solution

As described before, three main factors influence the calcein fluorescence and should therefore be considered when thinking about the composition of the calcein solution: pH value, calcein concentration and the presence of cations (Figure 8A). However, the pH value is only of interest for the preparation of the calcein stock solution due to the pH dependent solubility of calcein.

Since the calcein release assay is based on the change in the fluorescence pattern upon endosomal escape (punctate endolysosomal to diffuse cytosolic) which also leads to an increase in the

fluorescence intensity within the cytosol, the calcein concentration is of major importance. A wide range of calcein concentrations has been applied by different research groups, demonstrating the robustness of the calcein release assay. The applied concentrations can roughly be related to the incubation mode of calcein, either encapsulated (self-quenching concentrations) or in simultaneous or sequential incubation with the nanocarrier (<3.5 mM calcein). Higher (self-quenching) concentrations could lead to an increase in the fluorescence intensity difference between endolysosome and cytosol and, hence, an easier detection of endosomal escape. However, dequenching of calcein upon endosomal escape (i.e., nonfluorescent endosomes indicative of quenched calcein fluorescence before the release) has only been observed in one study applying 146  $\mu$ M calcein.<sup>[113]</sup> In the other studies, mostly diffusion of calcein into the cytosol rather than dequenching was measured. Only in the case of calcein encapsulated at self-quenching concentrations into the nanocarriers, at least a dequenching of calcein released from the nanocarrier within the endolysosomes could be assumed. Nevertheless, higher concentrations of the small molecule calcein can also increase the osmotic pressure inside the endolysosomes promoting endosomal escape of materials using proton sponge mechanisms which might not occur otherwise.<sup>[37]</sup> Controls comprising treatment with high concentrations of calcein alone, or high calcein concentrations plus a nonreleasing substance equimolar to the investigated nanocarrier could help preventing false positive results. Furthermore, the chelation of calcium ions at high calcein concentrations could be problematic for the cells. To increase the

difference in the fluorescence intensity between endolysosomes and cytosol, also other factors can be adjusted such as the incubation time of calcein (shorter, subsequent to the nanocarrier) or the measurement settings in microscopy (optimal for the bright cytosolic fluorescence).

When choosing calcein concentrations for *in vitro* investigations, also the mode of calcein release by the nanocarrier is of importance. Although the reviewed studies often addressed the calcein release but not the mechanism so far, the results can again be influenced by the concentration of the nanocarrier. As an example, the combination of a nanocarrier gradually releasing calcein with too low concentrations of calcein could lead to the observation of no calcein leakage, which would be different at higher calcein concentrations. Therefore, a concentration-dependent calcein release could enable the investigation of gradual calcein release and may provide insights into the endosomal escape mechanism. Moreover, also time-resolved measurements at short intervals using microscopy can indicate the mode of calcein release (transient/continuous, gradual/burst) which has been shown already, e.g., with photoactivatable nanocarriers.<sup>[67,160,165]</sup> For this type of nanocarriers it is rather easy due to the rough determination of the release time point by the time of photoactivation, whereas for other nanocarriers some luck is required to image the right cell in the right moment. Nevertheless, we think this effort might improve the assay and provide further mechanistic insights.

Regarding the presence of cations, it should be considered that these may interact differently with calcein at various pH values and concentrations, very well illustrating the mutual dependence of these factors. Although the influence of different ions on the calcein fluorescence was already the topic of the earliest calcein studies, the conditions present in the calcein release assay to study endosomal escape inside cells can be more complex making it difficult to draw conclusions. A calibration curve of calcein in the respective buffer composition and/or cell culture medium as well as the inclusion of a corresponding control without the nanocarrier can help in visualizing the influence of ions in the applied buffers or cell culture media. Since nanocarriers for gene delivery are often cationic, they could interact with the calcein also electrostatically and influence its fluorescence intensity. This fact should further be considered for the design of the experiments, in particular regarding either a premixing of nanocarrier and calcein or their sequential addition. However, studies on potential interactions are seldom reported and the different addition modes of calcein and nanocarrier are rarely compared within a publication.

## 5.2. Biological Factors Relevant for the Incubation Time

Consideration of various parameters is particularly relevant when choosing the incubation time (Figure 8B). On the one hand, the uptake of the nanocarrier into the cell matters. On the other hand, the intracellular fate of the applied calcein should also be regarded, in particular if longer incubation times are studied. To visualize endosomal escape, calcein and the nanocarrier have to be present in the same compartment. Hu et al. examined this factor in their study and were able to verify the importance of the simultaneous presence of calcein and the delivering core-shell par-

ticles within the endolysosome for the investigated system. When calcein and the core-shell particles were added simultaneously, endosomal escape was successfully reported by calcein release. However, when the cells were first treated with calcein and then, after a washing step, the release particles were added, no endosomal escape was observed, but might have occurred unnoticed,<sup>[187]</sup> suggesting a rapid transport of calcein into, though, and out of the cell.

Since there is no evidence that calcein is metabolized within cells, conclusions about the intracellular fate of calcein might be drawn based on the fluorescence and its temporal and spatial changes. Thus, a punctate fluorescence pattern within cells incubated with calcein alone indicates an endocytotic uptake mechanism (Figure 9A). With regard to the calcein release assay, it should be considered that different cell types can exhibit different endocytosis rates for different (macro)molecules,<sup>[196,197]</sup> and might therefore require different incubation times to take up similar amounts of calcein or the nanocarrier. Although the details of endocytosis in different cell lines were not investigated for calcein so far, they have been shown for different nanocarriers.<sup>[11,175,198,199]</sup> Considering more quantitative measurements (flow cytometry), the normalization of the calcein release induced by any nanocarrier to a control sample (cells treated with calcein only) can be used to attenuate cell type dependent endocytosis rates of calcein.<sup>[11,171,172,175]</sup> In addition to the different endocytosis rates of the nanocarrier, the nanocarrier itself can have an impact on the endocytosis rate of calcein which is however not as easy to determine and therefore difficult to take into account. Nevertheless, one way to compensate for at least different endocytosis rates of the various nanocarriers is to report the calcein release in relation to the uptake of the nanocarrier.<sup>[150,151,172,176]</sup>

Interestingly, a decrease of the overall calcein fluorescence intensity in the cytosol was observed upon increasing incubation times with different polymers and cell lines.<sup>[169,175]</sup> Such observations hint toward a calcein excretion mechanism from the cytosol (Figure 9B). Since calcein AM is intracellularly converted into calcein upon esterase activity in viable cells, conclusions can be drawn from studies with multidrug resistant (MDR) cells and calcein AM. In these studies, calcein has been shown to be ATP-dependently exported from the cytosol by the multidrug resistance protein (MRP) belonging to the ATP binding cassette transport proteins,<sup>[200,201]</sup> whereas the calcein AM itself has been shown to be exported via the multidrug transporter 1 (MDR1) encoded P-glycoprotein.<sup>[202,203]</sup> Furthermore, cytosolic calcein can be exported within exosomes, microvesicles, or via gap junctions to other cells, which can be derived from studies utilizing calcein AM as a tracking label, e.g., for extracellular vesicles derived from calcein AM loaded cells.<sup>[204–206]</sup> Regarding the calcein efflux via gap junctions, a cell type dependency was observed when measuring the inward diffusion of calcein within spheroids of different cell lines which were preloaded with calcein AM.<sup>[207]</sup> The influence of the cell type on calcein efflux was further demonstrated using different prostate cancer cells and bone marrow endothelial cells. The results revealed a halving of intracellular calcein fluorescence already 6 h after calcein AM loading of the cells.<sup>[208]</sup>

Additionally, the calcein which is not released from endolysosomes can be expected to either end up in the lysosome, where its fluorescence might for example be quenched due to the



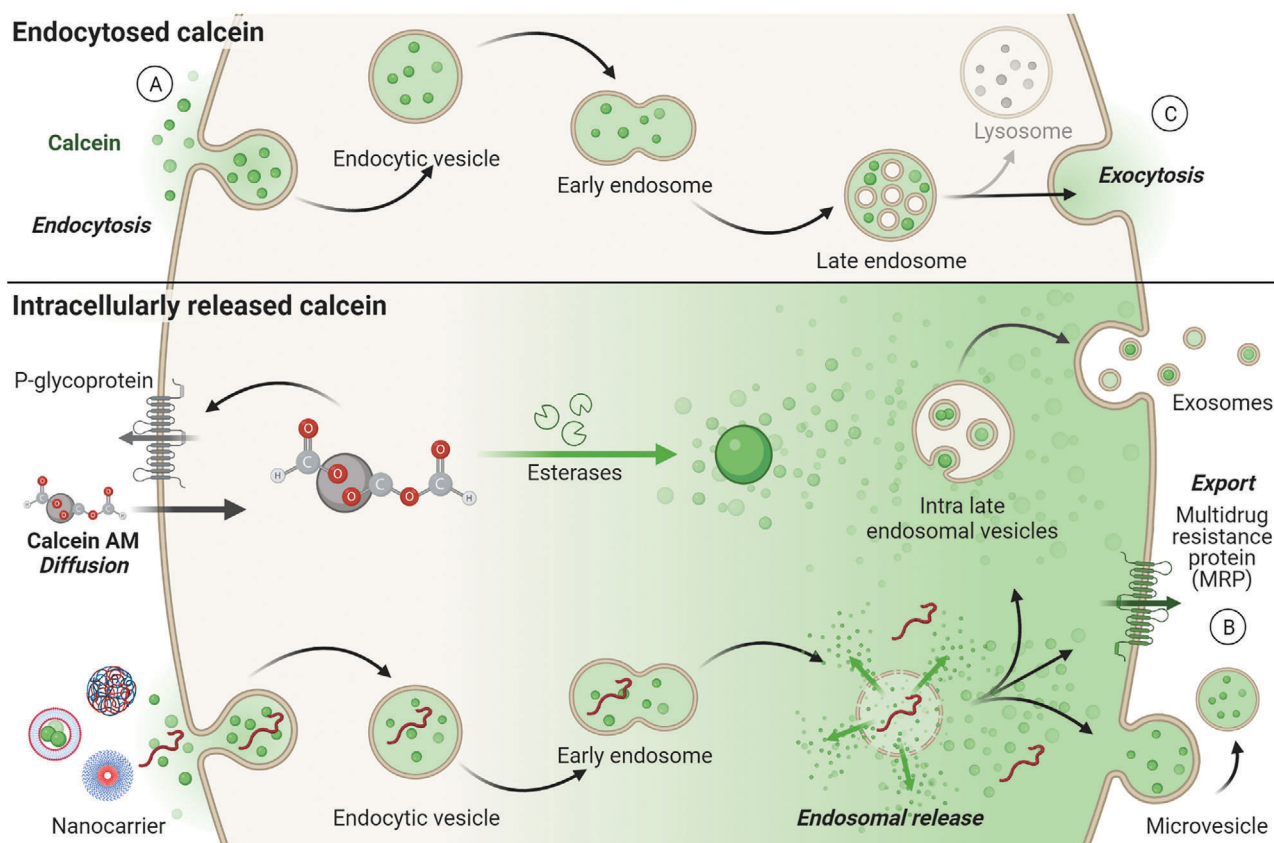


**Figure 9.** Intracellular pathways of calcein. A) Punctate fluorescence patterns within cells point toward an endocytotic uptake mechanism of calcein. B) Cytosolic/released calcein can be exported via the multidrug resistance protein, within microvesicles as shown in studies of cells loaded with calcein AM or in exosomes via the uptake into intra late endosomal vesicles. C) Regarding the excretion of endocytosed calcein, exocytosis is a hypothesis for calcein not released from endolysosomes. Adapted from “Endocytic Pathway Comparison (Layout)” and “Endocytic Pathway with Macropinocytosis and Phagocytosis” (2022) by BioRender.com. Retrieved from <https://app.biorender.com/biorender-templates>.

decreased pH value, or to be exported via exocytosis, since cells are known to dispose redundant, nondigestible molecules (Figure 9C).<sup>[127]</sup> Over time, this can also lead to a decreased intracellular calcein concentration ready to be released from endosomes which in turn can vary between different cell types. However, the accuracy of this assumption remains an open question, since the intracellular pathway of calcein, more importantly its kinetics and cell line dependencies, have not been investigated in detail so far. Nevertheless, this information could provide more insights into the calcein release assay including hints on how the assay should be planned and should therefore be thoroughly investigated.

A delayed addition of calcein (sequential incubation) might circumvent potential interferences of excretion mechanisms with nanocarriers requiring longer incubation times due to low endocytosis rates,<sup>[113]</sup> which could possibly result in misleading conclusions. If calcein is initially encapsulated within the nanocarrier (e.g., in liposomes), at least the degradation and/or exocytosis of calcein seem to be of limited importance, as the nanocarrier might disturb the endolysosomal maturation process and might protect the encapsulated calcein. Hence, the incubation time mainly depends on the time required for the nanocarrier to escape the endolysosome. In some studies, calcein release was observed following four days of incubation,<sup>[129]</sup> or even following

incubation with the nanocarrier encapsulating calcein for 1 h and medium for further 47 h.<sup>[164]</sup> This points toward slow uptake or endosomal escape kinetics.

All in all, the incubation time should be chosen long enough to allow i) a sufficient amount of calcein and nanocarrier inside the endolysosomes and ii) intracellular fusion of the organelles along the endolysosomal pathway, in case calcein and the nanocarrier were taken up by different organelles. In case of nanocarriers encapsulating calcein, the incubation time only has to be adapted to the former one. For comparison purposes, not only the uptake and excretion rates of calcein and the nanocarrier should be considered, but also the differences between cell types.

### 5.3. Factors Influencing the Accuracy of the Measurement

As described in the preceding section, different analytical methods have been utilized to characterize the calcein release within cells qualitatively or even quantitatively with different degrees of detail. When deciding which method to perform, (confocal) microscopy is preferred, due to a straightforward (and more reliable) discrimination of endocytosed and released calcein. Continuous advancement in technology allows images to also be quantified and processed using high-throughput analysis. Moreover, kinetic

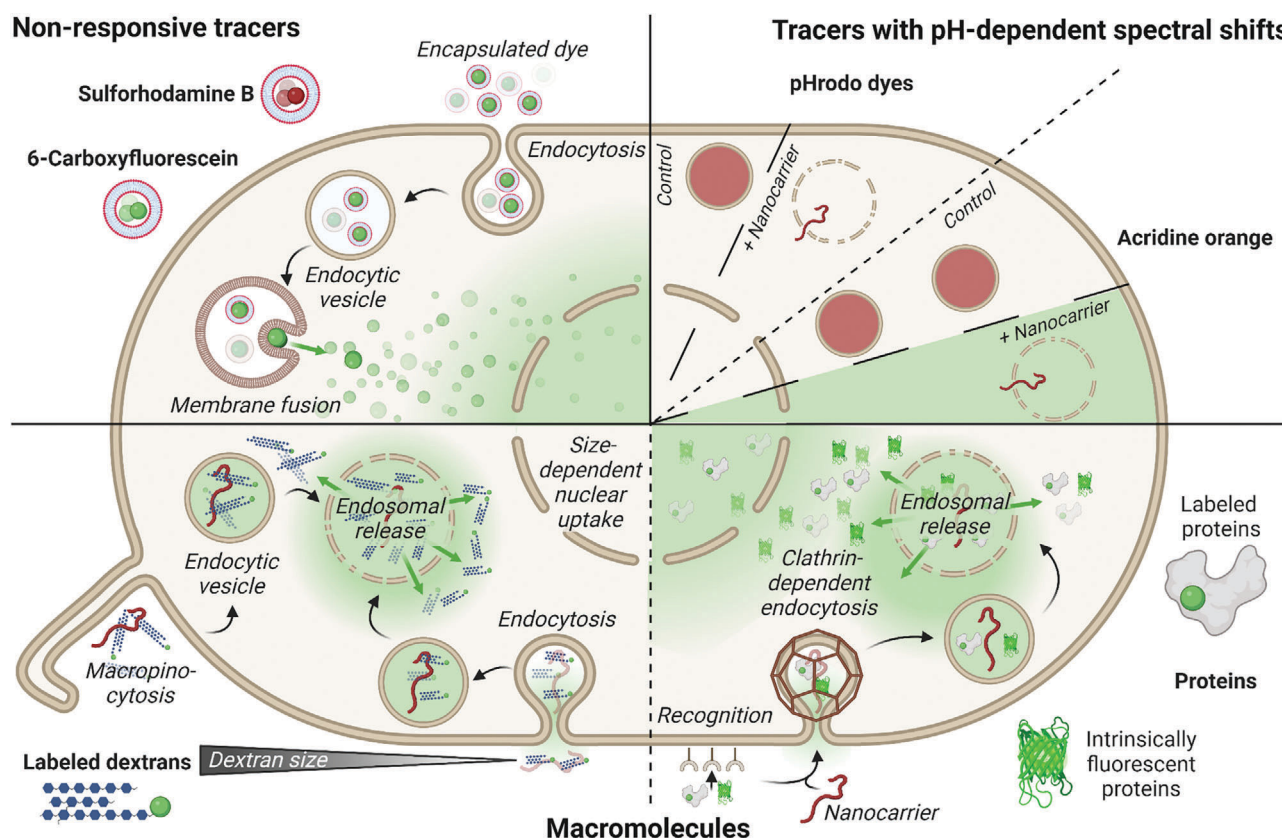


**Figure 10.** Complementary methods to the calcein release assay. In addition to calcein, other tracers, such as sulforhodamine B or 6-carboxyfluorescein can be encapsulated in vesicles to determine their release capabilities in cells. Tracers with pH-dependent spectral shifts, such as pHrodo or acridine orange can also be of interest, as they indicate the pH in their environment through changes in fluorescence. Besides small molecules, macromolecules such as dextrans or proteins are intriguing, as their size and complexity provide additional information about the escape.

investigations can be performed, which can lead to conclusions regarding the escape mechanism. Nevertheless, flow cytometry is the method of choice if more reliable statistics (fast analysis of >10 000 cells possible) are required, which would still be very tedious using confocal microscopy even if advanced image analysis software is used. However, there are certain pitfalls to be aware of and, in some cases, it should be considered more as a screening method that requires verification by microscopy. The latter becomes particularly important if the nanocarrier might alter the endocytosis rate of the cells leading to variations in fluorescence intensity within the endosomes, but not the cytosol. As only the overall fluorescence intensity per cell is detected in flow cytometry, this analysis alone would result in a false positive outcome compared to a control without the nanocarrier. On the contrary, a nanocarrier which induces only limited calcein release from endosomes can also hardly be detected but could suffice for transfection in the actual application. Therefore, it would lead to a false negative result due to the limited overall increase of fluorescence intensity within the cytosol which is overlaid by that of the endosomes. This issue has to be kept in mind in microscopy as well. In particular, acquisition settings which are optimized for the rather bright endosomes might not allow an identification of a graded or weak release. In general, it is advisable to combine several methods for determining calcein release, to enable quantitative as well as qualitative analysis.

## 6. Complementary Methods

The calcein release assay is a model for studying the release of cargo from nanocarriers. However, the carriers are loaded with different drug molecules that may have properties other than calcein, such as size, charge, and hydrophilicity. Therefore, the release of calcein from endosomes may not reflect the drug delivery potential of the nanocarrier. Ultimately, the calcein release experiment should be complemented by studies on the release of other model substances and drug molecules (Figure 10). In these cases, release from the carrier and endosomal permeabilization should also allow passage and release into the cytosol.

Besides calcein, other dyes are frequently used for dequenching assays in artificial vesicles, such as 6-carboxyfluorescein and sulforhodamine B. The recent review by Nasr and colleagues provides information on the use of these fluorophores for the study of liposomal membrane integrity.<sup>[94]</sup> These dyes are also inexpensive and easily accessible but have drawbacks as well. For example, the fluorescence of 6-carboxyfluorescein is strongly pH-dependent in the physiologically interesting pH range from the extracellular space to early endosome, whereas calcein is less sensitive in this regard.<sup>[58,94,209]</sup> Although the fluorescence intensity of sulforhodamine B is entirely pH-independent in the physiological relevant pH range,<sup>[210]</sup> its higher self-quenching concentration is rather disadvantageous.

The review by Martens et al. provides more information on other methods for studying endosomal escape in cells, as well as an overview of escape mechanisms.<sup>[37,96]</sup> This section focuses on methods that can be used complementary and provides comparisons to the calcein release assay. Sulforhodamine B can also be used inside cells as calcein analog to study endosomal escape.<sup>[210]</sup> However, it has been suggested that sulforhodamine B distributes less rapidly within the cell than calcein,<sup>[67]</sup> which may delay accurate timing of the endosomal escape event and could be disadvantageous in live cell microscopy.

In addition to the above mentioned chromophores, more specific indicators can be used which change their fluorescence in dependence of pH and, thus, provide further insight into the endosomal escape process.<sup>[5]</sup> Both, dyes that are quenched in a pH-dependent manner and those that shift in their excitation/emission wavelength are of interest. An interesting example are the commercially available, pH-sensitive pHrodo dyes (rhodamine derivatives), which show little to no fluorescent signal at neutral pH but are highly fluorescent in acidic environments.<sup>[211,212]</sup> These properties render the uncharged, membrane-permeable dyes ideal candidates for use as pH indicators in endosomal escape investigations when covalently bound to an endocytosed macromolecule. Consequently, a limited or impeded acidification of endosomes can be monitored by the absence of fluorescence in comparison to a control experiment, which allows to evaluate for example the pore formation in treatment with a nanocarrier by microscopy or cytometry.<sup>[113]</sup> Another interesting alternative is the membrane-penetrating, acidotropic, and metachromatic dye acridine orange. When cells are treated with acridine orange, the dye penetrates the membrane and distributes within the cell entering also any present endolysosomes. In the acidic endosomal milieu, acridine orange becomes protonated and is then no longer able to penetrate the cell membranes, which eventually leads to an accumulation in lysosomes. At the resulting higher concentrations in the lysosomes, acridine orange forms red fluorescent dimers, trimers, and oligomers,<sup>[213]</sup> which can be observed as red fluorescence, if the endo/lysosomes remain intact. Release of protonated acridine orange, e.g., by permeabilization of endosomes in the presence of any nanocarrier, results in deprotonation of the dye in the cytosol and thus in strong green cytosolic fluorescence of the homogeneously distributed monomer, which can be analyzed microscopically or by flow cytometry.<sup>[167,214]</sup> The strong concentration-dependent difference in the spectra of the dye, therefore, allows a clear distinction between cytosolic and endosomal fluorescence, i.e., differentiation between uptake and endosomal escape. To remove diffusing acridine orange, cells must be washed thoroughly both immediately after addition of acridine orange as well as before each analysis. It represents an elegant method in addition to investigations with calcein. However, acidotropic dyes such as LysoTracker or acridine orange might delay the lowering of pH in the endosome because they accumulate to high concentrations in acidic endosomes where they scavenge protons. Depending on the basicity of the nanocarriers relative to the acidotropic dyes used, protonation of the nanocarriers may also be delayed.

All complementary methods for calcein release discussed so far provide information on the occurrence of small pores, because of the size of the marker dye. However, in the evaluation of nanocarriers for biomedical applications, it is also of interest

if larger compounds or macromolecules can be released. Thus, other methods can be combined with the release of the small molecule calcein to evaluate the escape mechanism and delivery efficiency of a drug regarding biomedical applications. Calcein release is frequently studied in the context of nucleic acid transfection with cationic polymers. Often, calcein escape efficiency is correlated with pDNA transfection, independent of the used nanocarrier.<sup>[166,169,171,173–175]</sup> However, this correlation does not hold true in all cases. For example, Vermeulen and coworkers investigated the endosomal escape mechanism of JetPEI polyplexes, a linear PEI derivative,<sup>[111]</sup> and tried to correlate the release of calcein or labeled oligonucleotide according to a previously published procedure with the transfection efficiency.<sup>[6]</sup> Interestingly, a calcein release was observed in far more cells than the transfection and therefore does not correlate well, but the oligonucleotide release appeared to be a more reliable indicator for efficient transfection. The authors conclude that endosomal leakiness for small molecules can be induced by membrane destabilization due to the interaction with cationic polyplexes, hindering an effective buildup of osmotic pressure due to ion flux across this disturbed membrane and thus preventing the endosomal burst and escape of any macromolecules. Thus, investigations of calcein release may provide further indications about the mechanism of endosomal escape in addition to its efficacy.

If calcein release is studied in comparison to the escape of macromolecules of different sizes, a conclusion can be drawn about the size of the membrane defect that has occurred. For such studies, polysaccharides can be used such as dextrans, which have a rather rapid diffusion rate through the cytosol despite their different sizes. This favors a temporal determination of the escape event.<sup>[67]</sup> Ogris and colleagues used a FITC-labeled dextran (10 kDa), which allowed them to study the release of melittin-modified PEI polyplexes. In this case, the fluorescence of the FITC is enhanced upon release due to the increase in pH.<sup>[215]</sup> In another example, Zhan and colleagues<sup>[179]</sup> measured the release of various dextrans by blend particles featuring a PDMAEMA domain in comparison to calcein. They incubated dendritic DC2.4 cells simultaneously with calcein and dextrans of different sizes (4–2000 kDa), respectively.<sup>[179]</sup> Their study showed that endosomal release of compounds was not depending on the composition of the blend but on the size of the sensor molecule, whereas the smaller ones are released more easily. In addition to calcein release, Salomone et al. also investigated the release of different sized dextrans (3–40 kDa) by CPPs and found endosomal release.<sup>[183]</sup>

In addition to polysaccharides, peptides, and proteins can also be used as markers to study endosomal escape and place even greater demands on the nanocarrier due to their 3D structure.<sup>[172]</sup> Fluorescent proteins such as R-phycoerythrin (R-PE, 240 kDa) or EGFP (27 kDa) can also be used to study endosomal release. Although the endosomal uptake of these proteins without additional treatment with an uptake-inducing material is low, the mechanism of endosomal escape of the same material can be studied in more detail with fluorescent proteins. Since these proteins undergo a loss of fluorescence along the endolysosomal pathway due to denaturation, the presence of fluorescent signal inside the cytosol indicates an escape from the early endosome very robustly. Kopp and colleagues delivered R-PE into four different cell lines using calcium phosphate nanoparticles as

delivery materials.<sup>[216]</sup> Labeled proteins can also be used to investigate endosomal escape, but unlike intrinsically fluorescent proteins, the timing of the endosomal escape event cannot be investigated with labeled proteins since denaturation of the protein has no influence on the fluorescence intensity of the dye. Also, a positive signal does not necessarily indicate a complete release of the entire protein with its intact 3D structure. Here, too, a combination with other methods is meaningful. Nevertheless, labeled bovine serum albumin (BSA) is a suitable and easily available candidate, since it is efficiently taken up by endocytosis and can be detected more quickly than other complex proteins after the escape event due to its moderate diffusion speed. Diffusion in the cytosol is slower than for a small molecule like calcein, because the higher molar mass and the more complex structure of the protein result in comparatively slower diffusion.<sup>[67,172]</sup>

Actual transfection, i.e., the delivery of genetic material to its site of action, can also serve as evidence of endosomal release. Depending on the type of genetic cargo, different read-outs are used. In the case of pDNA transfection, protein expression provides very clear evidence that endosomal release of the plasmid must have been successful. However, the intensity of protein expression does not necessarily correlate with the rate of release. Rather, protein expression in this case indicates a successful overcoming of the nuclear barrier in addition to various other aspects. In the case of successful delivery of RNAs, either protein expression (mRNA) or silencing (e.g., siRNA) may indicate successful delivery, depending on the cargo. In either case, successful delivery (measurable as expression or knockdown) represents a global read-out that demonstrates the functionality of the genetic cargo.

## 7. Conclusion and Perspectives

Initially being developed for the detection of multivalent ions, calcein has without doubt become a working horse in the analysis of lipid membrane leakage in cells as well as in artificial liposomes. In particular, the detection of escape events from endo-/lysosomal compartments after cellular uptake renders this simple molecule a powerful tool in the investigation of diverse nanocarriers such as cell entry vectors or membrane destabilization agents. Its unique set of properties (i.e., a high charge density due to the multiple carboxylic acid groups, a low toxicity, a high extinction coefficient, and quantum yield, the self-quenching at increased concentrations, and a low sensitivity toward changes in pH) hinders undesired membrane penetrations, allows its detection in even low concentrations, enables a broad applicability in relevant physiological environments, and most importantly facilitates the detection of release events, respectively. On top, calcein is affordable for most researchers worldwide, since the straightforward synthetic access keeps costs low compared to many other complex sensor dyes used in biology or pharmacy. Its application further appears straightforward, since no additional chemical modifications are required, and simple coincubation is sufficient to monitor intracellular release events.

Nevertheless, various aspects should be kept in mind when planning experiments with calcein as reporter, since several pitfalls might deteriorate sensitivity, affect outcomes, or entirely lead to false interpretations of the data. The presence of multivalent ions or unintended interactions with nanocarriers (e.g., cationic polymers) can, among other factors, impact fluorescence

intensities, and have to be assessed prior to the experiments. Further down the road, additional difficulties may arise from the incubation conditions, the incubation time, or most of all the analysis of a potential escape. In particular, individual methods, such as microscopy or flow cytometry measurements, may underestimate or overrate escape events, respectively, if not carefully analyzed and compared to suitable controls. Due to all these different parameters affecting the outcome of the calcein release assay, it is hardly possible to suggest one specific protocol valid for different nanocarriers and cell lines. Generally, it can be recommended to start with testing different calcein concentrations and incubation times for each nanocarrier and cell line individually, not only for finding the appropriate concentrations and times but also for obtaining more information on the release mechanism. It is also overall advisable to combine several methods to investigate the calcein release assay, in order to facilitate not only a qualitative but also a quantitative analysis. For example, a combination of fluorescence-activated cell sorting and downstream microscopy or fluorescence correlation spectroscopy could be interesting to confirm the correlation between the different fluorescence intensities of the cells and the subcellular distribution of the fluorescent dye but has not yet been reported for calcein. Furthermore, live cell imaging is favorable due to the possibility to acquire more detailed information on the release mechanism (gradual/burst, transient/continuous).

Besides this individual optimization of experiments, a more global challenge resides in the comparability of datasets across various studies and particularly across different research groups. Of course, each nanocarrier or vector might require a specific set of conditions to effectively induce endosomal escape, which is further related to different analysis methods or assay parameters optimized for the respective system. Differences arise from the employed cell lines, the applied medium, or the potency and toxicity of the nanocarrier. The application of significantly different conditions might ultimately lead to different conclusions for similar or even the same nanocarriers. Fundamental understanding of key factors influencing endosomal escape however require that experimental setups allow a certain degree of comparison between results obtained in different laboratories worldwide. A minimum step toward a better comparability is in our opinion a comprehensive and detailed description of the experimental conditions including the initial preparation of the calcein solution, the incubation times with calcein and/or the applied nanocarrier, the incubation conditions and media, as well as the analytical methods. Moreover, also the not-optimal concentrations and incubation times measured during the assay establishment could be indicated in supplementary materials or made accessible on open data platforms. Ideally, any future study on this matter should maintain reasonable ranges of concentration for calcein,<sup>[5]</sup> which avoids the appearance of artifacts in the measurements, and include control experiments with established and commercial nanocarriers for comparability.<sup>[217]</sup> We are convinced that all research groups would benefit from such measures.

In a long-term perspective, certainly more advanced sensors will gain growing interest and complement the calcein release assay. Interesting candidates include among others pH-sensitive dyes, which allow for an additional readout of the increasing acidification during endosome maturation. Dye modified macromolecules or proteins of various sizes further allow more

detailed conclusions on the release process, since far larger pores or a burst of the compartments are required to release these molecules. The application of specific proteins or attached ligands might even facilitate to select specific uptake routes and gain information on the influence of different entry pathways. In addition, the application of fluorescent proteins represents a promising approach to verify a release prior to any degradation processes along the endo-/lysosomal pathway, which is crucial if the delivery of active enzymes is for example considered. Dyes that react in the presence of certain enzymes may also be of interest.<sup>[218]</sup> Combined with knowledge of the processes along the uptake pathway, a timing of release could become accessible.

The calcein assay nonetheless remains a basic, but potent method, which represents a straightforward entry into the analysis of potential release events, and it might not yet have revealed its full potential. If the nanocarrier is investigated with different calcein concentrations and at different incubation times, conclusions could be drawn about the release mechanism. For instance, distinguishing continuous release over time from more concerted, transient release, or distinguishing the individual release events as gradual or all-or-none. Furthermore, the excretion of released calcein from the cytosol might be detected. However, for such detailed conclusions, a more thorough understanding of the intracellular processing/trafficking/transport (rate) of calcein (in different cell lines) are required. Also, the combination with complementary sensor molecules or dyes promises to reveal a deeper understanding of the responsible processes for release or a more quantitative evaluation of efficacies. The continuous developments in fluorescence imaging, might provide additional insight into the cellular release mechanism (graded leakage vs. all-or-none leakage mechanism) based on the increasing knowledge derived from artificial liposomes. Furthermore, the model liposomes allow for the detailed investigation of the nanocarrier's performance in response to a specific feature of endosome maturation (change in pH or membrane composition), which certainly does not reflect the complex cellular environment but can give at least a hint on the release mechanism.

Overall, we are convinced that the calcein assay, if planned carefully and ideally combined with additional methods, will remain an essential tool in the characterization of release from lipid compartments in cells and a key toward a more fundamental understanding of the mode of action of many nanocarriers. The presented review hopefully inspires further groups to apply this assay and provides a sufficient database for efficient cross-correlations, which holds the potential to reveal key features relevant for the design of future nanocarriers.

## Acknowledgements

F.H-P. and F.R. contributed equally to this work. The authors gratefully acknowledge the Bundesministerium für Bildung und Forschung (BMBF, Germany, No. 13XP5034A PolyBioMik); the German Research Foundation (DFG) for generous funding within the Emmy-Noether Programme (Projekt ID: 358263073); German Research Foundation (DFG, ID: 415894560); and the support by the DFG-funded Collaborative Research Centre PolyTarget (SFB 1278, Project A05, B01, Z01, Project ID: 316213987). The figures were created with BioRender.com, which was also provided by the SFB 1278.

Open access funding enabled and organized by Projekt DEAL.

## Conflict of Interest

The authors declare no conflict of interest.

## Keywords

calcein release, endosomal escape, leakage, method comparison, polymer-membrane interactions, pore formation

Received: April 27, 2022

Revised: July 19, 2022

Published online: August 17, 2022

- [1] M. J. Mitchell, M. M. Billingsley, R. M. Haley, M. E. Wechsler, N. A. Peppas, R. Langer, *Nat. Rev. Drug Discovery* **2021**, *20*, 101.
- [2] V. Sanna, M. Sechi, *ACS Med. Chem. Lett.* **2020**, *11*, 1069.
- [3] P. Foroozandeh, A. A. Aziz, *Nanoscale Res. Lett.* **2018**, *13*, 339.
- [4] S. Behzadi, V. Serpooshan, W. Tao, M. A. Hamaly, M. Y. Alkawareek, E. C. Dreaden, D. Brown, A. M. Alkilany, O. C. Farokhzad, M. Mahmoudi, *Chem. Soc. Rev.* **2017**, *46*, 4218.
- [5] K. Deprey, L. Becker, J. Kritzer, A. Pluckthun, *Bioconjugate Chem.* **2019**, *30*, 1006.
- [6] Z. ur Rehman, D. Hoekstra, I. S. Zuhorn, *ACS Nano* **2013**, *7*, 3767.
- [7] A. T. Dinh, C. Pangarkar, T. Theofanous, S. Mitragotri, *Biophys. J.* **2007**, *92*, 831.
- [8] T. Merdan, K. Kunath, D. Fischer, J. Kopecek, T. Kissel, *Pharm. Res.* **2002**, *19*, 140.
- [9] J. Huotari, A. Helenius, *EMBO J.* **2011**, *30*, 3481.
- [10] S. R. Pfeffer, *Nat. Cell Biol.* **1999**, *1*, E145.
- [11] L. M. P. Vermeulen, T. Brans, S. K. Samal, P. Dubruel, J. Demeester, S. C. De Smedt, K. Remaut, K. Braeckmans, *ACS Nano* **2018**, *12*, 2332.
- [12] M. E. G. de Araujo, G. Liebscher, M. W. Hess, L. A. Huber, *Traffic* **2020**, *21*, 60.
- [13] A. El-Sayed, H. Harashima, *Mol. Ther.* **2013**, *21*, 1118.
- [14] H. D. Gallala, B. Breiden, K. Sandhoff, *J. Neurochem.* **2011**, *116*, 702.
- [15] J. Gruenberg, *Traffic* **2020**, *21*, 76.
- [16] F. Hullin-Matsuda, T. Taguchi, P. Greimel, T. Kobayashi, *Semin. Cell Dev. Biol.* **2014**, *31*, 48.
- [17] T. Kobayashi, M. H. Beuchat, J. Chevallier, A. Makino, N. Mayran, J. M. Escola, C. Lebrand, P. Cosson, T. Kobayashi, J. Gruenberg, *J. Biol. Chem.* **2002**, *277*, 32157.
- [18] H. Schulze, K. Sandhoff, *Cold Spring Harbor Perspect. Biol.* **2011**, *3*, a004804.
- [19] I. M. S. Degors, C. Wang, Z. U. Rehman, I. S. Zuhorn, *Acc. Chem. Res.* **2019**, *52*, 1750.
- [20] M. Durymanov, J. Reineke, *Front. Pharmacol.* **2018**, *9*, 971.
- [21] M. P. Stewart, A. Lorenz, J. Dahlman, G. Sahay, *Wiley Interdiscip. Rev. Nanomed. Nanobiotechnol.* **2016**, *8*, 465.
- [22] A. Ahmad, J. M. Khan, S. Haque, *Biochimie* **2019**, *160*, 61.
- [23] T. Bus, A. Traeger, U. S. Schubert, *J. Mater. Chem. B* **2018**, *6*, 6904.
- [24] O. Boussif, F. Lezoualc'h, M. A. Zanta, M. D. Mergny, D. Scherman, B. Demeneix, J. P. Behr, *Proc. Natl. Acad. Sci. USA* **1995**, *92*, 7297.
- [25] R. V. Benjaminsen, M. A. Matthebjerg, J. R. Henriksen, S. M. Moghimi, T. L. Andresen, *Mol. Ther.* **2013**, *21*, 149.
- [26] P. Midoux, M. Monsigny, *Bioconjugate Chem.* **1999**, *10*, 406.
- [27] B. Singh, S. Maharjan, T.-E. Park, T. Jiang, S.-K. Kang, Y.-J. Choi, C.-S. Cho, *Macromol. Biosci.* **2015**, *15*, 622.
- [28] N. D. Sonawane, F. C. Szoka, A. S. Verkman, *J. Biol. Chem.* **2003**, *278*, 44826.
- [29] A. M. Funhoff, C. F. van Nostrum, M. C. Lok, J. A. Kruijtzter, D. J. Crommelin, W. E. Hennink, *J. Controlled Release* **2005**, *101*, 233.

- [30] A. Akinc, M. Thomas, A. M. Klibanov, R. Langer, *J. Gene Med.* **2005**, 7, 657.
- [31] A. Kichler, C. Leborgne, E. Coeytaux, O. Danos, *J. Gene Med.* **2001**, 3, 135.
- [32] Z. ur Rehman, D. Hoekstra, I. S. Zuhorn, *ACS Nano* **2013**, 7, 3767.
- [33] M. L. Forrest, D. W. Pack, *Mol. Ther.* **2002**, 6, 57.
- [34] T. Bieber, W. Meissner, S. Kostin, A. Niemann, H.-P. Elsasser, *J. Controlled Release* **2002**, 82, 441.
- [35] R. Mo, Q. Sun, N. Li, C. Zhang, *Biomaterials* **2013**, 34, 2773.
- [36] I. Richard, M. Thibault, G. De Crescenzo, M. D. Buschmann, M. Lavertu, *Biomacromolecules* **2013**, 14, 1732.
- [37] T. F. Martens, K. Remaut, J. Demeester, S. C. De Smedt, K. Braeckmans, *Nano Today* **2014**, 9, 344.
- [38] E. Xu, W. M. Saltzman, A. S. Piotrowski-Daspit, *J. Controlled Release* **2021**, 335, 465.
- [39] S. L. Y. Teo, J. J. Rennick, D. Yuen, H. Al-Wassiti, A. P. R. Johnston, C. W. Pouton, *Nat. Commun.* **2021**, 12, 3721.
- [40] N. I. Zahaf, A. E. Lang, L. Kaiser, C. D. Fichter, S. Lassmann, A. McCluskey, A. Augspach, K. Aktories, G. Schmidt, *Sci. Rep.* **2017**, 7, 41252.
- [41] S. Schmidt, M. J. Adjobo-Hermans, R. Wallbrecher, W. P. Verdurmen, P. H. Bovee-Geurts, J. van Oostrum, F. Milletti, T. Enderle, R. Brock, *Angew. Chem., Int. Ed. Engl.* **2015**, 54, 15105.
- [42] N. Milech, B. A. Longville, P. T. Cunningham, M. N. Scobie, H. M. Bogdawa, S. Winslow, M. Anastasas, T. Connor, F. Ong, S. R. Stone, M. Kerfoot, T. Heinrich, K. M. Kroeger, Y. F. Tan, K. Hoffmann, W. R. Thomas, P. M. Watt, R. M. Hopkins, *Sci. Rep.* **2015**, 5, 18329.
- [43] B. C. Evans, R. B. Fletcher, K. V. Kilchrist, E. A. Dailing, A. J. Mukalel, J. M. Colazo, M. Oliver, J. Cheung-Flynn, C. M. Brophy, J. W. Tierney, J. S. Isenberg, K. D. Hankenson, K. Ghimire, C. Lander, C. A. Gersbach, C. L. Duvall, *Nat. Commun.* **2019**, 10, 5012.
- [44] H. Du Rietz, H. Hedlund, S. Wilhelmson, P. Nordenfelt, A. Wittrup, *Nat. Commun.* **2020**, 11, 1809.
- [45] H. Diehl, J. L. Ellingboe, *Anal. Chem.* **1956**, 28, 882.
- [46] H. Diehl, *Anal. Chem.* **1967**, 39, A30.
- [47] A. J. Hefley, *Ph.D. Thesis*, Iowa State University **1967**.
- [48] Richard Markuszewski, *Ph.D. Thesis*, Iowa State University **1976**.
- [49] D. B. Martin, *Ph.D. Thesis*, Iowa State University **1977**.
- [50] J. W. Furry, *Ph.D. Thesis*, Iowa State University **1985**.
- [51] R. W. Sabnis, in *Handbook of Biological Dyes and Stains*, John Wiley & Sons, Inc., Hoboken, NJ **2010**, p. 71.
- [52] H. Diehl, *Calcein, Calmagite and o, o'-Dihydroxyazobenzene. Titrimetric, Colorimetric, and Fluorometric Reagents for Calcium and Magnesium*, G. Frederick Smith Chemical Company, Columbus, OH **1964**.
- [53] B. Walter, *Ann. Phys.* **1888**, 270, 316.
- [54] B. Walter, *Ann. Phys.* **1889**, 272, 502.
- [55] B. Walter, *Ann. Phys.* **1889**, 272, 518.
- [56] R. F. Chen, J. R. Knutson, *Anal. Biochem.* **1988**, 172, 61.
- [57] J. N. Weinstein, S. Yoshikami, P. Henkart, R. Blumenthal, W. A. Hagins, *Science* **1977**, 195, 489.
- [58] T. M. Allen, L. G. Cleland, *Biochim. Biophys. Acta* **1980**, 597, 418.
- [59] D. A. Kendall, R. C. MacDonald, *Anal. Biochem.* **1983**, 134, 26.
- [60] H. Patel, C. Tscheka, K. Edwards, G. Karlsson, H. Heerklotz, *Biochim. Biophys. Acta* **2011**, 1808, 2000.
- [61] S. Salassi, F. Simonelli, A. Bartocci, G. Rossi, *J. Phys. D: Appl. Phys.* **2018**, 51, 384002.
- [62] S. Hamann, J. F. Kiilgaard, T. Litman, F. J. Alvarez-Leefmans, B. R. Winther, T. Zeuthen, *J. Fluoresc.* **2002**, 12, 139.
- [63] K. E. Roberts, A. K. O'Keefe, C. J. Lloyd, D. J. Clarke, *J. Fluoresc.* **2003**, 13, 513.
- [64] A. Andersson, J. Danielsson, A. Graslund, L. Maler, *Eur. Biophys. J.* **2007**, 36, 621.
- [65] R. Imamura, N. Murata, T. Shimanouchi, K. Yamashita, M. Fukuzawa, M. Noda, *Sensors* **2017**, 17, 1630.
- [66] G. Dorrington, N. P. Chmel, S. R. Norton, A. M. Wemyss, K. Lloyd, D. Praveen Amarasinghe, A. Rodger, *Biophys. Rev.* **2018**, 10, 1385.
- [67] N. Brkovic, L. Zhang, J. N. Peters, S. Kleine-Doepke, W. J. Parak, D. Zhu, *Small* **2020**, 16, e2003639.
- [68] W. Bae, T. Y. Yoon, C. Jeong, *PLoS One* **2021**, 16, e0247326.
- [69] D. F. H. Wallach, T. L. Steck, *Anal. Chem.* **2002**, 35, 1035.
- [70] R. M. Straubinger, K. Hong, D. S. Friend, D. Papahadjopoulos, *Cell* **1983**, 32, 1069.
- [71] F. C. Szoka, K. Jacobson, D. Papahadjopoulos, *Biochim. Biophys. Acta* **1979**, 551, 295.
- [72] C. B. Billesbolle, C. M. Azumaya, R. C. Kretsch, A. S. Powers, S. Gonen, S. Schneider, T. Arvedson, R. O. Dror, Y. Cheng, A. Manglik, *Nature* **2020**, 586, 807.
- [73] N. Oku, D. A. Kendall, R. C. Macdonald, *Biochim. Biophys. Acta* **1982**, 691, 332.
- [74] A. Ali, Q. Zhang, J. Dai, X. Huang, *BioMetals* **2003**, 16, 285.
- [75] B. B. Hasinoff, *J. Inorg. Biochem.* **2003**, 95, 157.
- [76] F. Thomas, G. Serratrice, C. Beguin, E. S. Aman, J. L. Pierre, M. Fontecave, J. P. Laulhere, *J. Biol. Chem.* **1999**, 274, 13375.
- [77] H. B. Li, F. Chen, *Fresenius' J. Anal. Chem.* **2000**, 368, 501.
- [78] J. Körbl, F. Vydra, R. Přebil, *Talanta* **1958**, 1, 281.
- [79] J. H. Eggers, *Talanta* **1960**, 4, 38.
- [80] A. M. Escarilla, *Talanta* **1966**, 13, 363.
- [81] G. M. Huitink, H. Diehl, *Talanta* **1974**, 21, 1193.
- [82] G. M. Huitink, D. P. Poe, H. Diehl, *Talanta* **1974**, 21, 1221.
- [83] D. H. Wilkins, *Talanta* **1960**, 4, 182.
- [84] I. D. Johnson, in *Molecular Probes Handbook: A Guide to Fluorescent Probes and Labeling Technologies*, 11th ed. (Ed: I. D. Johnson), Life Technologies Corporation, Carlsbad, CA **2010**, p. 833.
- [85] D. Thomas, S. C. Tovey, T. J. Collins, M. D. Bootman, M. J. Berridge, P. Lipp, *Cell Calcium* **2000**, 28, 213.
- [86] A. B. Harkins, N. Kurebayashi, S. M. Baylor, *Biophys. J.* **1993**, 65, 865.
- [87] E. S. Kaneshiro, M. A. Wyder, Y. P. Wu, M. T. Cushion, *J. Microbiol. Methods* **1993**, 17, 1.
- [88] D. Bratosin, L. Mitrofan, C. Palii, J. Estaquier, J. Montreuil, *Cytometry A* **2005**, 66, 78.
- [89] K. I. McConnell, S. Shamsudeen, I. M. Meraz, T. S. Mahadevan, A. Ziems, P. Rees, H. D. Summers, R. E. Serda, *J. Biomed. Nanotechnol.* **2016**, 12, 154.
- [90] S. Neri, E. Mariani, A. Meneghetti, L. Cattini, A. Facchini, *Clin. Diagn. Lab. Immunol.* **2001**, 8, 1131.
- [91] G. Drin, S. Cottin, E. Blanc, A. R. Rees, J. Temsamani, *J. Biol. Chem.* **2003**, 278, 31192.
- [92] R. Lichtenfels, W. E. Biddison, H. Schulz, A. B. Vogt, R. Martin, *J. Immunol. Methods* **1994**, 172, 227.
- [93] A. Nitsch, L. Haralambiev, R. Einkenkel, D. O. Muzzio, M. T. Zygmunt, A. Ekkerkamp, M. Burchardt, M. B. Stope, *In Vivo* **2019**, 33, 1767.
- [94] G. Nasr, H. Greige-Gerges, A. Elaissari, N. Khreich, *Int. J. Pharm.* **2020**, 580, 119198.
- [95] S. Dutta, B. G. Watson, S. Mattoo, J. C. Rochet, *Bio-Protoc.* **2020**, 10, e3690.
- [96] S. Guha, J. Ghimire, E. Wu, W. C. Wimley, *Chem. Rev.* **2019**, 119, 6040.
- [97] A. Akbarzadeh, R. Rezaei-Sadabady, S. Davaran, S. W. Joo, N. Zarghami, Y. Hanifehpour, M. Samiei, M. Kouhi, K. Nejati-Koshki, *Nanoscale Res. Lett.* **2013**, 8, 102.
- [98] S. Chatterjee, D. K. Banerjee, in *Liposome Methods and Protocols* (Eds: S. C. Basu, M. Basu), Humana Press, Totowa, NJ **2002**, p. 3.
- [99] A. Stulz, A. Vogt, J. S. Saar, L. Akil, K. Lienkamp, M. Hoernke, *Langmuir* **2019**, 35, 16366.
- [100] W. C. Wimley, K. Hristova, *Aust. J. Chem.* **2019**, 73, 96.
- [101] I. Tsogas, D. Tsiourvas, G. Nounesis, C. M. Paleos, *Langmuir* **2006**, 22, 11322.

- [102] Y. Sarkar, S. Roy, R. Majumder, S. Das, D. V. Bhalani, A. Ray, S. K. Jewrajka, P. P. Parui, *Soft Matter* **2020**, *16*, 798.
- [103] J. L. Thomas, H. You, D. A. Tirrell, *J. Am. Chem. Soc.* **1995**, *117*, 2949.
- [104] J. Allen, K. Najjar, A. Erazo-Oliveras, H. M. Kondow-McConaghy, D. J. Brock, K. Graham, E. C. Hager, A. L. J. Marschall, S. Dubel, R. L. Juliano, J. P. Pellois, *ACS Chem. Biol.* **2019**, *14*, 2641.
- [105] D. J. Brock, L. Kustigian, M. Jiang, K. Graham, T. Y. Wang, A. Erazo-Oliveras, K. Najjar, J. Zhang, H. Rye, J. P. Pellois, *Traffic* **2018**, *19*, 421.
- [106] K. Najjar, A. Erazo-Oliveras, D. J. Brock, T. Y. Wang, J. P. Pellois, *J. Biol. Chem.* **2017**, *292*, 847.
- [107] K. Sudo, K. Niikura, K. Iwaki, S. Kohyama, K. Fujiwara, N. Doi, *J. Controlled Release* **2017**, *255*, 28385674.
- [108] D. J. Brock, H. Kondow-McConaghy, J. Allen, Z. Brkljaca, L. Kustigian, M. Jiang, J. Zhang, H. Rye, M. Vazdar, J. P. Pellois, *Cell Chem. Biol.* **2020**, *27*, 1296.
- [109] A. Erazo-Oliveras, K. Najjar, D. Truong, T. Y. Wang, D. J. Brock, A. R. Prater, J. P. Pellois, *Cell Chem. Biol.* **2016**, *23*, 598.
- [110] Z. Qian, A. Martyna, R. L. Hard, J. Wang, G. Appiah-Kubi, C. Coss, M. A. Phelps, J. S. Rossman, D. Pei, *Biochemistry* **2016**, *55*, 2601.
- [111] S. M. Van Rossenberg, K. M. Sliedregt-Bol, N. J. Meeuwenoord, T. J. Van Berkel, J. H. Van Boom, G. A. Van Der Marel, E. A. Biessen, *J. Biol. Chem.* **2002**, *277*, 45803.
- [112] L. Rangasamy, V. Chelvam, A. K. Kanduluru, M. Srinivasarao, N. A. Bandara, F. You, E. A. Orellana, A. L. Kasinski, P. S. Low, *Bioconjugate Chem.* **2018**, *29*, 1047.
- [113] J. C. Brendel, J. Sanchis, S. Catrouillet, E. Czuba, M. Z. Chen, B. M. Long, C. Nowell, A. Johnston, K. A. Jolliffe, S. Perrier, *Angew. Chem., Int. Ed. Engl.* **2018**, *57*, 16678.
- [114] E. Mastrobattista, G. A. Koning, L. van Bloois, A. C. Filipe, W. Jiskoot, G. Storm, *J. Biol. Chem.* **2002**, *277*, 27135.
- [115] A. El-Sayed, I. A. Khalil, K. Kogure, S. Futaki, H. Harashima, *J. Biol. Chem.* **2008**, *283*, 23450.
- [116] A. El-Sayed, T. Masuda, I. Khalil, H. Akita, H. Harashima, *J. Controlled Release* **2009**, *138*, 160.
- [117] E. Rideau, R. Dimova, P. Schuille, F. R. Wurm, K. Landfester, *Chem. Soc. Rev.* **2018**, *47*, 8572.
- [118] S. Braun, S. Pokorna, R. Sachl, M. Hof, H. Heerklotz, M. Hoernke, *ACS Nano* **2018**, *12*, 813.
- [119] A. Jesorka, O. Orwar, *Annu. Rev. Anal. Chem.* **2008**, *1*, 801.
- [120] P. Walde, K. Cosentino, H. Engel, P. Stano, *ChemBioChem* **2010**, *11*, 848.
- [121] H. Stein, S. Spindler, N. Bonakdar, C. Wang, V. Sandoghdar, *Front. Physiol.* **2017**, *8*, 63.
- [122] J. Steinkuhler, P. De Tillieux, R. L. Knorr, R. Lipowsky, R. Dimova, *Sci. Rep.* **2018**, *8*, 11838.
- [123] C. C. Scott, J. Gruenberg, *BioEssays* **2011**, *33*, 103.
- [124] T. Shimanouchi, H. Ishii, N. Yoshimoto, H. Umakoshi, R. Kuboi, *Colloids Surf., B* **2009**, *73*, 156.
- [125] N. Wang, M. Chen, T. Wang, *J. Controlled Release* **2019**, *303*, 130.
- [126] L. Wang, N. Hartel, K. Ren, N. A. Graham, N. Malmstadt, *Environ. Sci.: Nano* **2020**, *7*, 963.
- [127] G. Raposo, W. Stoorvogel, *J. Cell Biol.* **2013**, *200*, 373.
- [128] C. Zivko, G. Fuhrmann, P. Luciani, *Biochim. Biophys. Acta, Gen. Subj.* **2021**, *1865*, 129559.
- [129] B. Illes, P. Hirschele, S. Barnert, V. Cauda, S. Wuttke, H. Engelke, *Chem. Mater.* **2017**, *29*, 8042.
- [130] W. D. Gray, A. J. Mitchell, C. D. Searles, *MethodsX* **2015**, *2*, 360.
- [131] I. Sovadinova, E. F. Palermo, R. Huang, L. M. Thoma, K. Kuroda, *Biomacromolecules* **2011**, *12*, 260.
- [132] S. K. Zhang, L. Gong, X. Zhang, Z. M. Yun, S. B. Li, H. W. Gao, C. J. Dai, J. J. Yuan, J. M. Chen, F. Gong, Y. X. Tan, S. P. Ji, *J. Gene Med.* **2020**, *22*, e3259.
- [133] W. C. Wimley, K. Hristova, *Aust. J. Chem.* **2020**, *73*, 96.
- [134] S. Esteban-Martin, H. J. Risselada, J. Salgado, S. J. Marrink, *J. Am. Chem. Soc.* **2009**, *131*, 15194.
- [135] H. Heerklotz, *Biophys. J.* **2001**, *81*, 184.
- [136] S. Shi, A. M. Markl, Z. Lu, R. Liu, M. Hoernke, *Langmuir* **2022**, *38*, 2379.
- [137] S. T. Yang, E. Zaitseva, L. V. Chernomordik, K. Melikov, *Biophys. J.* **2010**, *99*, 2525.
- [138] C. Mazzuca, B. Orioni, M. Coletta, F. Formaggio, C. Toniolo, G. Maulucci, M. De Spirito, B. Pispisa, M. Venanzi, L. Stella, *Biophys. J.* **2010**, *99*, 1791.
- [139] I. Plaza-Ga, V. Manzaneda-Gonzalez, M. Kisovec, V. Almendro-Vedia, M. Munoz-Ubeda, G. Anderluh, A. Guerrero-Martinez, P. Natale, I. Lopez Montero, *J. Nanobiotechnol.* **2019**, *17*, 108.
- [140] Y. Tamba, M. Yamazaki, *Biochemistry* **2005**, *44*, 15823.
- [141] N. Fuertes, A. J. Garcia-Saez, S. Esteban-Martin, D. Gimenez, O. L. Sanchez-Munoz, P. Schuille, J. Salgado, *Biophys. J.* **2010**, *99*, 2917.
- [142] S. G. Hovakeemian, R. Liu, S. H. Gellman, H. Heerklotz, *Soft Matter* **2015**, *11*, 6840.
- [143] A. S. Ladokhin, W. C. Wimley, S. H. White, *Biophys. J.* **1995**, *69*, 1964.
- [144] H. Patel, C. Tscheka, H. Heerklotz, *Soft Matter* **2009**, *5*, 2849.
- [145] B. Apellaniz, J. L. Nieva, P. Schuille, A. J. Garcia-Saez, *Biophys. J.* **2010**, *99*, 3619.
- [146] D. A. Kendall, R. C. MacDonald, *J. Biol. Chem.* **1982**, *257*, 13892.
- [147] D. F. Wallach, T. L. Steck, *Anal. Biochem.* **1963**, *6*, 176.
- [148] C. J. Chu, J. Dijkstra, M. Z. Lai, K. Hong, F. C. Szoka, *Pharm. Res.* **1990**, *7*, 824.
- [149] E. Ducat, J. Deprez, A. Gillet, A. Noel, B. Evrard, O. Peulen, G. Piel, *Int. J. Pharm.* **2011**, *420*, 319.
- [150] V. A. Slepishkin, S. Simoes, P. Dazin, M. S. Newman, L. S. Guo, M. C. Pedrosa de Lima, N. Duzgunes, *J. Biol. Chem.* **1997**, *272*, 2382.
- [151] S. Simoes, V. Slepishkin, N. Duzgunes, M. C. P. de Lima, *Biochim. Biophys. Acta, Biomembr.* **2001**, *1515*, 23.
- [152] M. Kanamala, B. D. Palmer, H. Ghandehari, W. R. Wilson, Z. Wu, *Pharm. Res.* **2018**, *35*, 154.
- [153] P. Enzian, C. Schell, A. Link, C. Malich, R. Pries, B. Wollenberg, R. Rahmzadeh, *Mol. Pharmaceutics* **2020**, *17*, 2779.
- [154] J. Connor, L. Huang, *J. Cell. Biol.* **1985**, *101*, 582.
- [155] C.-J. Chu, F. C. Szoka, *J. Liposome Res.* **1994**, *4*, 361.
- [156] X. Cheng, R. J. Lee, *Adv. Drug Delivery Rev.* **2016**, *99*, 129.
- [157] P. R. Cullis, M. J. Hope, *Mol. Ther.* **2017**, *25*, 1467.
- [158] S. Cerritelli, D. Velluto, J. A. Hubbell, *Biomacromolecules* **2007**, *8*, 1966.
- [159] E. A. Scott, A. Stano, M. Gillard, A. C. Maio-Liu, M. A. Swartz, J. A. Hubbell, *Biomaterials* **2012**, *33*, 6211.
- [160] A. E. Vasdekis, E. A. Scott, C. P. O'Neil, D. Psaltis, J. A. Hubbell, *ACS Nano* **2012**, *6*, 7850.
- [161] K. Kono, T. Igawa, T. Takagishi, *Biochim. Biophys. Acta* **1997**, *1325*, 143.
- [162] H. Xu, W. Zhang, Y. Li, F. F. Ye, P. P. Yin, X. Yu, M. N. Hu, Y. S. Fu, C. Wang, J. Shang de, *Pharm. Res.* **2014**, *31*, 3038.
- [163] Z. Li, B. Li, M. Wang, M. Xie, H. Shen, S. Shen, X. Wang, X. Guo, M. Yao, Y. Jin, *J. Mater. Chem. B* **2013**, *1*, 1466.
- [164] Y. Nishimura, K. Takeda, R. Ezawa, J. Ishii, C. Ogino, A. Kondo, *J. Nanobiotechnol.* **2014**, *12*, 11.
- [165] S. Niedermayer, V. Weiss, A. Herrmann, A. Schmidt, S. Datz, K. Muller, E. Wagner, T. Bein, C. Brauchle, *Nanoscale* **2015**, *7*, 7953.
- [166] U. Lachelt, P. Kos, F. M. Mickler, A. Herrmann, E. E. Salcher, W. Rodl, N. Badgujar, C. Brauchle, E. Wagner, *Nanomedicine* **2014**, *10*, 35.
- [167] R. A. Jones, C. Y. Cheung, F. E. Black, J. K. Zia, P. S. Stayton, A. S. Hoffman, M. R. Wilson, *Biochem. J.* **2003**, *372*, 65.
- [168] S. Deshpande, S. Patil, N. Singh, *ACS Omega* **2018**, *3*, 8042.

- [169] A. K. Trutzschler, T. Bus, M. Reifarth, J. C. Brendel, S. Hoepfener, A. Traeger, U. S. Schubert, *Bioconjugate Chem.* **2018**, *29*, 2181.
- [170] R. A. Jones, M. H. Poniris, M. R. Wilson, *J. Controlled Release* **2004**, *96*, 379.
- [171] F. Richter, L. Martin, K. Leer, E. Moek, F. Hausig, J. C. Brendel, A. Traeger, *J. Mater. Chem. B* **2020**, *8*, 5026.
- [172] F. Hausig, F. H. Sobotta, F. Richter, D. O. Harz, A. Traeger, J. C. Brendel, *ACS Appl. Mater. Interfaces* **2021**, *13*, 35233.
- [173] D. K. Bonner, X. Zhao, H. Buss, R. Langer, P. T. Hammond, *J. Controlled Release* **2013**, *167*, 101.
- [174] D. K. Bonner, C. Leung, J. Chen-Liang, L. Chingozha, R. Langer, P. T. Hammond, *Bioconjugate Chem.* **2011**, *22*, 1519.
- [175] F. Richter, P. Mapfumo, L. Martin, J. I. Solomun, F. Hausig, J. J. Frietsch, T. Ernst, S. Hoepfener, J. C. Brendel, A. Traeger, *J. Nanobiotechnol.* **2021**, *19*, 70.
- [176] F. Richter, K. Leer, L. Martin, P. Mapfumo, J. I. Solomun, M. T. Kuchenbrod, S. Hoepfener, J. C. Brendel, A. Traeger, *J. Nanobiotechnol.* **2021**, *19*, 292.
- [177] Y. Hu, T. Litwin, A. R. Nagaraja, B. Kwong, J. Katz, N. Watson, D. J. Irvine, *Nano Lett.* **2007**, *7*, 3056.
- [178] K. K. Tran, X. Zhan, H. Shen, *Adv. Healthcare Mater.* **2014**, *3*, 690.
- [179] X. Zhan, K. K. Tran, L. Wang, H. Shen, *Pharm. Res.* **2015**, *32*, 2280.
- [180] X. Su, J. Fricke, D. G. Kavanagh, D. J. Irvine, *Mol. Pharmaceutics* **2011**, *8*, 774.
- [181] S. Wannasari, S. Q. Wang, P. Figueiredo, C. Trujillo, F. Eburnea, L. Simon-Gracia, A. Correia, Y. P. Ding, T. Teesalu, D. F. Liu, R. Wittanapataptee, H. A. Santos, W. Li, *Adv. Funct. Mater.* **2019**, *29*, 1905352.
- [182] J. Chen, J. Li, J. Zhou, Z. Lin, F. Cavalieri, E. Czuba-Wojnilowicz, Y. Hu, A. Glab, Y. Ju, J. J. Richardson, F. Caruso, *ACS Nano* **2019**, *13*, 11653.
- [183] F. Salomone, F. Cardarelli, M. Di Luca, C. Boccardi, R. Nifosi, G. Bardi, L. Di Bari, M. Serresi, F. Beltram, *J. Controlled Release* **2012**, *163*, 293.
- [184] J. R. Clegg, J. A. Sun, J. Gu, A. K. Venkataraman, N. A. Peppas, *J. Controlled Release* **2021**, *329*, 1162.
- [185] N. Kongkatigumjorn, S. A. Smith, M. Chen, K. T. Fang, S. L. Yang, E. R. Gillies, A. P. R. Johnston, G. K. Such, *ACS Appl. Nano Mater.* **2018**, *1*, 3164.
- [186] N. Kongkatigumjorn, C. Cortez-Jugo, E. Czuba, A. S. Wong, R. Y. Hodgetts, A. P. Johnston, G. K. Such, *Macromol. Biosci.* **2017**, *17*, 1600248.
- [187] Y. Hu, P. U. Atukorale, J. J. Lu, J. J. Moon, S. H. Um, E. C. Cho, Y. Wang, J. Chen, D. J. Irvine, *Biomacromolecules* **2009**, *10*, 756.
- [188] A. S. Wong, S. K. Mann, E. Czuba, A. Sahut, H. Liu, T. C. Suckama, T. Bickerton, A. P. Johnston, G. K. Such, *Soft Matter* **2015**, *11*, 2993.
- [189] M. Galliani, C. Tremolanti, G. Signore, *Nanomaterials* **2019**, *9*, 652.
- [190] J. S. Kim, D. K. Choi, J. Y. Shin, S. M. Shin, S. W. Park, H. S. Cho, Y. S. Kim, *J. Controlled Release* **2016**, *235*, 165.
- [191] G. Rong, C. Wang, L. Chen, Y. Yan, Y. Cheng, *Sci. Adv.* **2020**, *6*, eaaz1774.
- [192] D. Adams, A. Gonzalez-Duarte, W. D. O'Riordan, C. C. Yang, M. Ueda, A. V. Kristen, I. Tournev, H. H. Schmidt, T. Coelho, J. L. Berk, K. P. Lin, G. Vita, S. Attarian, V. Plante-Bordeneuve, M. M. Mezei, J. M. Campistol, J. Buades, T. H. Brannagan, 3rd, B. J. Kim, J. Oh, Y. Parman, Y. Sekijima, P. N. Hawkins, S. D. Solomon, M. Polydefkis, P. J. Dyck, P. J. Gandhi, S. Goyal, J. Chen, A. L. Strahs, S. V. Nochur, M. T. Sweetser, P. P. Garg, A. K. Vaishnav, J. A. Gollob, O. B. Suhr, *N. Engl. J. Med.* **2018**, *379*, 11.
- [193] K. Ren, Y. Liu, J. Wu, Y. Zhang, J. Zhu, M. Yang, H. Ju, *Nat. Commun.* **2016**, *7*, 13580.
- [194] E. M. M. Manders, F. J. Verbeek, J. A. Aten, *J. Microsc.* **1993**, *169*, 375.
- [195] K. W. Dunn, M. M. Kamocka, J. H. McDonald, *Am. J. Physiol.: Cell Physiol.* **2011**, *300*, C723.
- [196] B. Alberts, A. Johnson, J. Lewis, P. Walter, M. Raff, K. Roberts, *Molecular Biology of the Cell*, 4th ed., International Student Edition, Routledge, England **2002**.
- [197] S. Kumari, S. Mg, S. Mayor, *Cell Res.* **2010**, *20*, 256.
- [198] Q. Xia, J. Huang, Q. Feng, X. Chen, X. Liu, X. Li, T. Zhang, S. Xiao, H. Li, Z. Zhong, K. Xiao, *Int. J. Nanomed.* **2019**, *14*, 6957.
- [199] H. Shin, M. Kwak, T. G. Lee, J. Y. Lee, *Nanoscale* **2020**, *12*, 15743.
- [200] M. Essodaigui, H. J. Broxterman, A. Garnier-Suillerot, *Biochemistry* **1998**, *37*, 2243.
- [201] N. Feller, H. J. Broxterman, D. C. R. Wahrer, H. M. Pinedo, *FEBS Lett.* **1995**, *368*, 385.
- [202] L. Homolya, Z. Hollo, U. A. Germann, I. Pastan, M. M. Gottesman, B. Sarkadi, *J. Biol. Chem.* **1993**, *268*, 21493.
- [203] Z. Hollo, L. Homolya, C. W. Davis, B. Sarkadi, *Biochim. Biophys. Acta, Biomembr.* **1994**, *1191*, 384.
- [204] V. B. Cismasiu, L. M. Popescu, *J. Cell. Mol. Med.* **2015**, *19*, 351.
- [205] K. A. Sinclair, S. T. Yerkovich, P. M. Hopkins, D. C. Chambers, *Stem Cell Res. Ther.* **2016**, *7*, 91.
- [206] S. Strassburg, N. W. Hodson, P. I. Hill, S. M. Richardson, J. A. Hoyland, *PLoS One* **2012**, *7*, e33739.
- [207] T. M. Achilli, S. McCalla, J. Meyer, A. Tripathi, J. R. Morgan, *Mol. Pharmaceutics* **2014**, *11*, 2071.
- [208] F. L. Miles, J. E. Lynch, R. A. Sikes, *J. Biol. Methods* **2015**, *2*, e29.
- [209] S. A. Smith, L. I. Selby, A. P. R. Johnston, G. K. Such, *Bioconjugate Chem.* **2019**, *30*, 263.
- [210] W. Viricel, A. Mbarek, J. Leblond, *Angew. Chem., Int. Ed. Engl.* **2015**, *54*, 12743.
- [211] N. J. Dolman, J. A. Kilgore, M. W. Davidson, *Curr. Protoc. Cytom.* **2013**, *12*, Unit 12.30.
- [212] M. Ogawa, N. Kosaka, C. A. Regino, M. Mitsunaga, P. L. Choyke, H. Kobayashi, *Mol. BioSyst.* **2010**, *6*, 888.
- [213] M. G. Palmgren, *Anal. Biochem.* **1991**, *192*, 316.
- [214] R. Kandil, Y. Xie, R. Heermann, L. Isert, K. Jung, A. Mehta, O. M. Merkel, *Adv. Ther.* **2019**, *2*, 1900047.
- [215] M. Ogris, R. C. Carlisle, T. Bettinger, L. W. Seymour, *J. Biol. Chem.* **2001**, *276*, 47550.
- [216] M. Kopp, O. Rotan, C. Papadopoulos, N. Schulze, H. Meyer, M. Eple, *PLoS One* **2017**, *12*, e0178260.
- [217] N. Bono, F. Ponti, D. Mantovani, G. Candiani, *Pharmaceutics* **2020**, *12*, 183.
- [218] C. R. Drake, D. C. Miller, E. F. Jones, *Curr. Org. Synth.* **2011**, *8*, 498.





**Franziska Hausig-Punke** studied nutrition sciences (B.Sc.) and molecular nutrition (M.Sc.) at the Friedrich Schiller University Jena. Since 2017, she conducts her Ph.D. in the research group of Dr. Johannes C. Brendel at the Jena Center for Soft Matter (JCSM) at Friedrich Schiller University Jena. She complements the chemically oriented research group with her strong biochemical background and focuses on the biological characterization of polymers for biomedical applications from all sides. Her dissertation explores the overcoming of the endosomal membrane by pH-responsive polymers for intracellular delivery of biopharmaceuticals.



**Friederike Richter** studied nutrition sciences (B.Sc.) and molecular nutrition (M.Sc.) at the Friedrich Schiller University in Jena. After her graduation in 2017, she started as a Ph.D. student in the junior research group of Dr. Anja Traeger at the Friedrich Schiller University in Jena. Her research focuses on the biological in vitro investigation of tailor-made synthetic polymers and cationic polymer micelles for gene delivery.



**Maria Hoernke** conducted her Ph.D. research on amyloid formation at the Max-Planck-Institute of Colloids and Interfaces in Potsdam. After receiving her Ph.D. (2012), Maria joined Gothenburg University (Sweden) where she obtained a Marie Curie IEF fellowship for protein structural dynamics investigated by time resolved X-ray scattering and surface-sensitive infrared spectroscopy. Since 2015, she continues her academic activities at Freiburg University (Germany) where she now leads an independent team funded by the German Research Foundation (DFG) and the Daimler and Benz Foundation. She is an expert in biophysical chemistry of lipid membranes in response to peptides, proteins, or polymers.



**Johannes C. Brendel** studied chemistry at the University of Bayreuth (Germany) and received his Ph.D. in 2013 on his studies of semiconducting polymers. From 2014 to 2016, he worked at the University of Warwick (UK) and the Monash Institute of Pharmaceutical Sciences (Australia) as a postdoctoral researcher funded by the German Research Foundation (DFG). In 2016, he established an independent research group at the Friedrich Schiller University Jena (Germany) which became funded within the Emmy Noether Programme in 2017. His research interests include the design of reactive monomers, the synthesis of well-defined polymer architectures, and their self-assembly into complex nanostructures.



**Anja Traeger** studied biochemistry with a focus on genetics (Bayreuth, York) and received her Ph.D. in biotechnology (Bayreuth) in 2011, where she investigated polymers for cellular delivery. Afterward, she moved to the Friedrich Schiller University Jena to do her habilitation under the supervision of Prof. U. S. Schubert after a research stay with Prof. K. Kataoka (Tokyo). In 2017, she received funding for her independent research group through the BMBF NanoMatFutur program. Her applied research focused on well-defined copolymers for gene delivery and interaction of polymer-based materials with cellular membranes for endosomal escape.